

# PROCEEDINGS 1983 SYMPOSIUM ON BUOY TECHNOLOGY

PROCEEDINGS 1983 SYMPOSIUM ON BUOY TECHNOLOGY

GC  
41  
S96  
1983





---

# **PROCEEDINGS 1983 SYMPOSIUM ON BUOY TECHNOLOGY**

**International Hotel**

**April 27-29, 1983**

**New Orleans, Louisiana**



**LIBRARY**

**APR 15 2005**

National Oceanic &  
Atmospheric Administration  
U.S. Dept. of Commerce

**Sponsored by:**

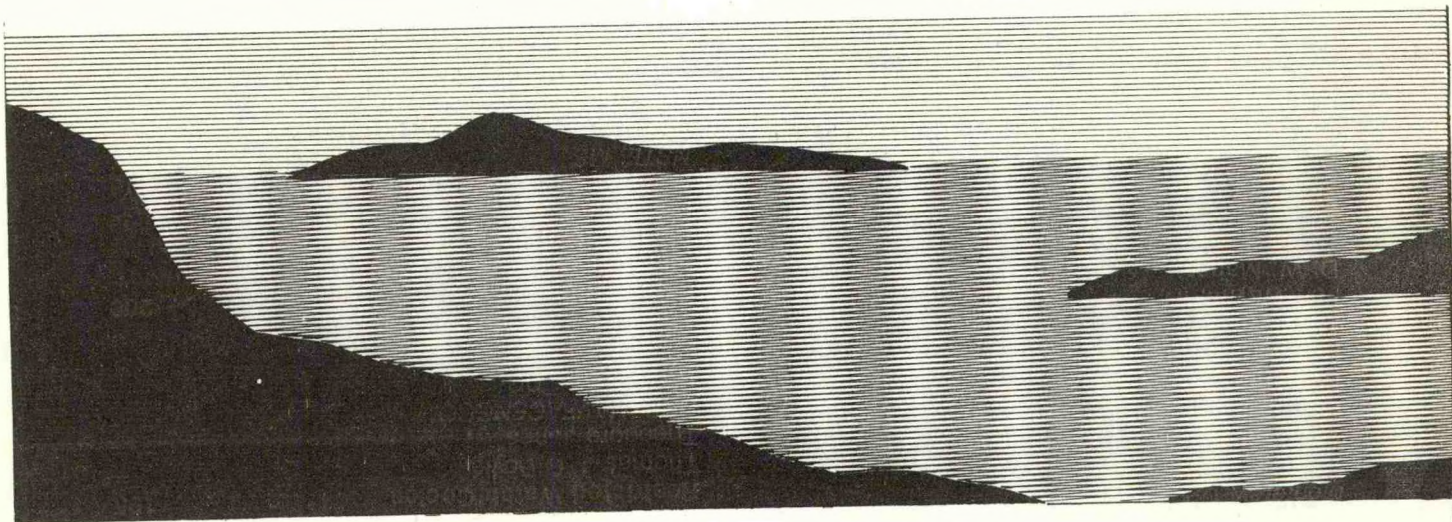
**THE MARINE TECHNOLOGY SOCIETY  
GULF COAST SECTION  
AND  
THE NOAA DATA BUOY CENTER**



---

GC  
41  
.S96  
1983





---

Published by:

The Marine Technology Society, Gulf Coast Section  
Building 2204  
NSTL, MS 39529

Responsibility for the contents rests upon the authors, and  
not upon the Marine Technology Society, Gulf Coast Sec-  
tion or its members.

Copies of this Record may be purchased from the Marine  
Technology Society. Order from:

---

MARINE TECHNOLOGY SOCIETY  
1730 M STREET N.W.  
WASHINGTON, DC 20036

All rights, including translations, are reserved by the Marine  
Technology Society. Abstracting is permitted with men-  
tion of source. Request for republication should be ad-  
dressed to the Marine Technology Society.

Copyright 1983 by the Marine Technology Society.

Printed in the USA.



---

# CHAIRMAN'S MESSAGE

Less than a year ago, the officers of the recently formed Gulf Coast Chapter of the Marine Technology Society were discussing a technical meeting on drifting buoys. At nearly the same time, during OCEANS '82, others of us were discussing a general buoy meeting. One had not been held since 1976. A quick survey of interest and the need decided the issue; forces were joined, and the 1983 Buoy Technology Symposium was born. A committee was formed (see elsewhere in these Proceedings) and eventually the meeting was held 27-29 April in New Orleans, the week preceding the Offshore Technology Conference in Houston. The reason for the latter was the hope that more international interest would be attracted to our meeting.

For whatever reason, it was truly an international meeting, as representatives of 8 other countries from

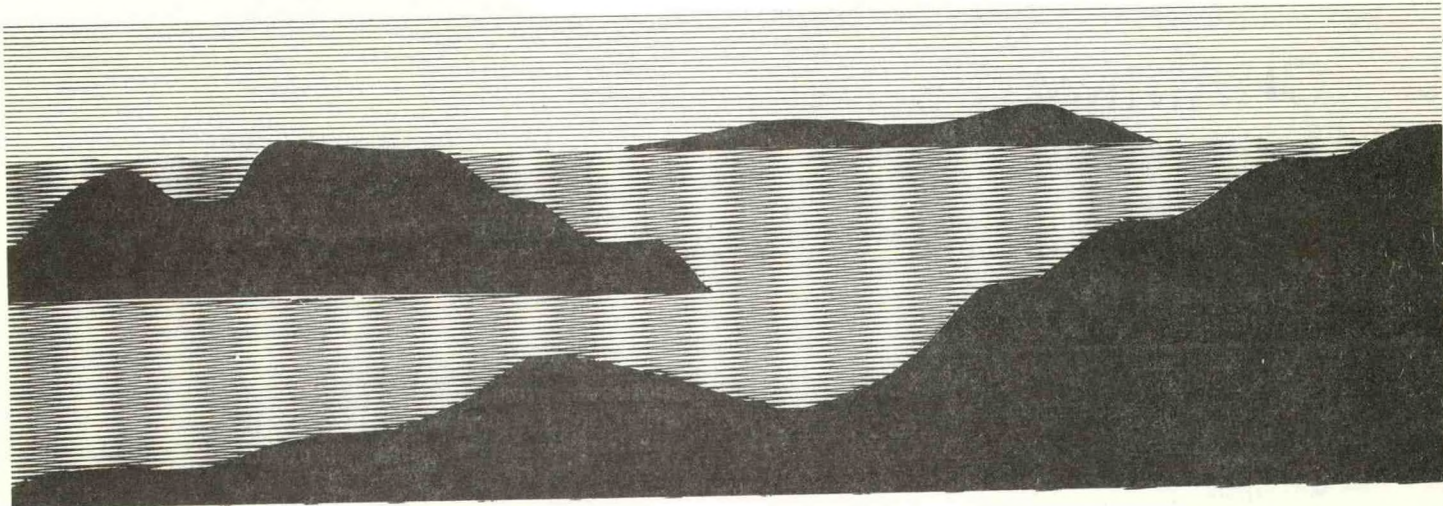
as far as Australia joined in the symposium. Almost 200 registered, and more than 50 papers were presented. The purpose of these proceedings is to record this update of the literature in regard to Buoy Technology.

My thanks go to the committee that organized and ran the symposium, especially the contingent from the University of Southern Mississippi, who is also responsible for the publishing of these Proceedings. Without authors who have faithfully reduced their thoughts to the written word, this volume would not be possible. Thank you and the session chairmen for producing interesting and lively sessions. With the high interest shown in this sometimes mundane subject, we are encouraged to plan a sequel in the not-as-distant future as was the case in the past.



William O. Rainnie, Jr.  
Symposium Chairman and Chairman of the  
MTS Buoy Technology Committee





---

## **PARTICIPATING ORGANIZATIONS**

**THE MARINE TECHNOLOGY SOCIETY (MTS)  
GULF COAST SECTION**

**NOAA DATA BUOY CENTER**

**MTS BUOY TECHNOLOGY  
UNIVERSITY OF SOUTHERN MISSISSIPPI**

---

## **SYMPOSIUM COMMITTEE MEMBERS**

**William O. Rainnie**  
Symposium Chairman

**Rudolph Hollman**  
Chairman, MTS Gulf Coast Section

**Frank Wilem**  
Vice Chairman, MTS Gulf Coast Section

**Stan Raffa**  
Secretary, MTS Gulf Coast Section

**Hendrik Daman**  
Treasurer, MTS Gulf Coast Section

**Keith Kaulum**  
Immediate Past Chairman,  
MTS Gulf Coast Section

**Myron Webb**  
Symposium Coordinator

**Stewart Nelson**  
Publicity

**W. Brett Wilson**  
Program Chairman, Drifting Buoys

**James Elkins**  
Program Chairman, Moored Buoys

**A. J. Oberkirch**  
Finances

**R. H. Canada**  
Special Events



# TABLE OF CONTENTS

## SESSION I: GENERAL

CHAIRMAN: W. O. Rainnie, NDBC,  
NSTL, MS

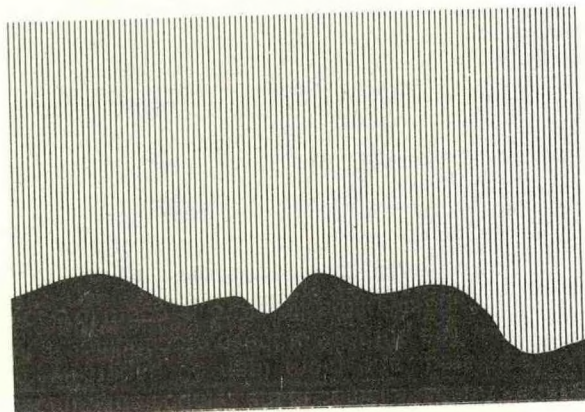
<b>The ARGOS Data Collection and Platform Location Space System: Oceanographic Applications</b> .....	1
R. Rosso Service ARGOS Toulouse, France	
<b>Integrated Communications in Buoy Systems</b> .....	6
Ed Mellinger Al Bradley Woods Hole Oceanographic Inst. Woods Hole, MA	
<b>A System for Data Acquisition in the Ocean Environment</b> .....	11
Don R. Howe W. H. Serstad Magnavox, Fort Wayne, IN R. L. Erichsen NDBC NSTL, MS	
<b>Coherent Digital Data Acquisition System</b> .....	20
Scott Daubin Daubin Systems, Inc. Key Biscayne, FL	
<b>Hydrodynamic Performance Evaluation of a Newly Developed Kevlar Rope Fairing</b> .....	25
Darrell Milburn Naval Ocean Research and Development Activity NSTL, MS	
<b>High Performance Deep Sea Surface Buoy Mooring</b> .....	32
Richard C. Swenson John Selleck Norman Dennis Naval Oceanographic Office NSTL, MS	

## SESSION II: ENVIRONMENT

CHAIRMAN: David Shields  
Naval Civil Engineering Laboratory  
Port Hueneme, CA

<b>Open Ocean Wave Buoy Comparisons in the North Atlantic</b> .....	41
Robert Bachman Edward Foley Susan Bales David Taylor Naval Ship Research and Development Center Bethesda, MD	
<b>An Analysis of Bureau of Land Management (BLM) Buoy Winds and Sea Heights Off the Southeast Atlantic Coast</b> .....	49
Michael Koziara Weather Service Forecast Office West Columbia, SC	
<b>High Resolution Directional Wave Spectra Using the FFT Digital Band Pass Filter Method</b> .....	55
Edward C. Brainard, II ENDECO, Inc. Marion, MA	
<b>Nondirectional Wave Measurements With the USCG Aid to Navigation Buoy</b> .....	62
Joseph Murphy University of New Orleans New Orleans, LA	
<b>The Statistics of Cross Spectra Applied to Waveheight Directional Spectral Measurement</b> .....	65
Donald E. Barrick Belinda Lipa Ocean Surface Research, Inc. Boulder, CO	





### SESSION III: MOORED BUOYS

CHAIRMAN: Richard C. Swenson  
Naval Oceanographic Office  
NSTL, MS

**The Use of NOMAD Hulls as Severe Environment Buoys** ..... 72  
G. L. Timpe  
NDBC  
NSTL, MS

**Moored Data Buoy on Shallow Water** ... 79  
W. C. M. Van Dijk  
*Rijkswaterstaat, The Netherlands*

**The NOAA Data Buoy Center's Utilization of NOMAD Buoy Hulls** ..... 96  
John Holmes  
*Computer Sciences Corporation*  
Donald Windham  
NDBC  
NSTL, MS

**Operational Uses of a Small, High-Capability Databuoy** ..... 100  
M. S. Martin  
Marex  
*Isle of Wight, United Kingdom*

**Air-Sea Heat and Momentum Fluxes from Moored Buoys** ..... 105  
R. E. Payne  
R. T. Nowak  
*Woods Hole Oceanographic Inst.*  
*Woods Hole, MA*

**The LOTUS Discus Mooring** ..... 108  
P. R. Clay  
*Woods Hole Oceanographic Inst.*  
*Woods Hole, MA*

### SESSION IV: DRIFTING BUOYS

CHAIRMAN: E. G. Kerut  
NDBC  
NSTL, MS

**Drifters: A Lagrangian Buoy Development Program** ..... 114

Robert Heinmiller  
*Omnet, Inc.*  
*Boston, MA*  
James McWilliams  
NCAR  
*Boulder, CO*

**Free Drifting RELAYS Buoy Systems** ... 118  
R. G. Walden  
H. O. Berteaux  
*Woods Hole Oceanographic Inst.*  
*Woods Hole, MA*

**Drifting Buoy Developments at the French Meteorological Office** ..... 124  
Pierre Blouch  
Francois Fusey  
*Centre Oceanologique de Bretagne*  
*Brest, France*

**Drifting Buoys in Support of Marine Meteorological Services** ..... 131  
Glenn Hamilton  
NDBC  
NSTL, MS

**Great Lakes Satellite-Tracked Current Drifters** ..... 138  
R. L. Pickett  
A. H. Clites  
J. E. Campbell  
*Great Lakes Research Laboratory*  
*Ann Arbor, MI*  
R. Partridge  
NDBC  
NSTL, MS

**Keynote Address** ..... 144  
James Winchester, Assoc. Admin.  
NOAA  
*Washington, DC*



## SESSION V: ENVIRONMENT

CHAIRMAN: E. G. Kerut  
NDBC  
NSTL, MS

- Storm Wave Characteristics in the Gulf of Mexico** ..... 147  
Ming-Yang Su  
Mark Bergin  
*Naval Ocean Research and Development Activity*  
NSTL, MS

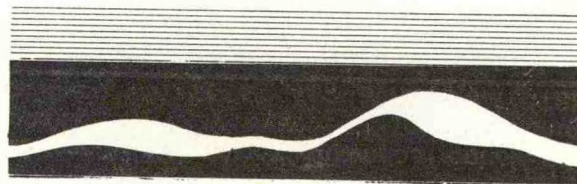
- Comparison of NDBC Wave Spectra with Output of the Fleet Numerical Oceanography Center Operational Global Spectral Ocean Wave Model** ..... 153  
Sheldon Lazanoff  
*Science Applications, Inc.*  
Monterey, CA  
Jack Kaitala  
*Fleet Numerical Oceanographic Center*  
Monterey, CA

- The Wave Data Analysis Function as Performed in Data Acquisition and Telemetry Systems** ..... 163  
Roland C. Fritts  
*Magnavox*  
Fort Wayne, IN  
D. W. Mahar  
USCG  
NDBC  
NSTL, MS

- An Analysis of Short Pendulum Heave Sensors** ..... 167  
Marshall D. Earle  
Richard W. Longman  
*Marine Environments Corp.*  
Manassas, VA

- On-Site, High Accuracy Navigation Utilizing Moored Buoys** ..... 176  
Corydon Pierson, Jr.  
*Buoy Technology, Inc.*  
Concord, NH

- NDBC Wave Measurement Activities and Plans** ..... 182  
Kenneth E. Steele  
NDBC  
NSTL, MS



## SESSION VI: MOORED BUOYS

CHAIRMAN: Darrell Milburn  
Naval Ocean Research and Development Activity  
NSTL, MS

- Semi-submersible Buoy for Stormy Seas** ..... 189  
Alan C. McClure  
Ivan Kirschner  
*Alan C. McClure Assoc., Inc.*  
Houston, TX

- A Design Procedure for Moorings With Restricted Watch Circles** ..... 195  
Thomas J. O'Boyle  
Theodore Jones  
*CHESNAVFACENGCOM*  
Washington, DC

- The Atom '79 Mooring Motion Experiment** ..... 200  
Kim Saunders  
Albert Green  
Fred Hamrick  
*Naval Ocean Research and Development Activity*  
NSTL, MS

- Long Term Sensor Platforms** ..... 210  
David Shields  
A. T. Maris  
L. A. Vega  
*Naval Civil Engineering Laboratory*  
Port Hueneme, CA

- Seismic Data Acquisition SPAR Buoy in the North Sea** ..... 224  
C. W. A. Browitt  
T. Turbitt  
*Institute of Geological Sciences*  
Edinburgh, United Kingdom

- Development of a Barely-Subsurface Deep Ocean Mooring** ..... 231  
Narender Chhabra  
John M. Dahlen  
*Charles Stark Draper Lab*  
Cambridge, MA



## SESSION VII: DRIFTING BUOYS

CHAIRMAN: Ronald P. Kozak  
NDBC  
NSTL, MS

### On Collecting Operational Meteorological Data from the Northeast Pacific Ocean With the ARGOS System . . . . . 241

R. E. Vockeroth  
D. Oracheski  
*Atmospheric Environment Service  
Toronto and Edmonton, Canada*

### Operational Uses of TIROS Oceanographic Drifters by the International Ice Patrol (1978-1982) . . . . . 246

Alan Summy  
Iain Anderson  
*International Ice Patrol  
Governors Island, NY*

### Kinematic and Dynamical Calculations from Lagrangian Measurements: Recent-Theoretical Advances . . . . . 251

James K. Lewis  
A. D. Kirwan  
R. E. Whitaker  
*Science Applications, Inc.  
Bryan, TX*

### The Computation of Kinematic Parameters for a Warm Core Ring Using Drifting Buoys . . . . . 255

R. E. Whitaker  
A. D. Kirwan  
James K. Lewis  
*Science Applications, Inc.  
Bryan, TX*

### The Kinematics and Geometry of a Gulf of Mexico Warm-Core Ring as Determined by Drifting Buoys . . . . . 259

R. E. Whitaker  
A. D. Kirwan  
James K. Lewis  
*Science Applications, Inc.  
Bryan, TX*

### An Operational Sea Ice Management System Based on Lagrangian Data from Ice Drifters . . . . . 260

James K. Lewis  
Warren Denner  
R. E. Whitaker  
*Science Applications, Inc.  
Bryan, TX*

## SESSION VIII: ENVIRONMENT

CHAIRMAN: Stanley Hecker  
MS/AL Sea Grant Consortium  
Ocean Springs, MS

### A General Automatic Profiling System for Great Lakes Applications . . . . . 265

F. E. Roy  
*Canada Centre for Inland Waters  
Burlington and Ontario, Canada*

### Aspects of the Instrumentation, Deployment, and Performance of 2.5 M Diameter Wave-Following Meteorological Data Buoys . . . 272

R. E. W. Pettifer  
M. J. Kerley  
D. J. Painting  
*Meteorological Office  
Bracknell, United Kingdom*

### Sensitivity of Surface Wind Stress to Uncertainties in Sensor Outputs of an Atmospheric Profiling System . . . . . 278

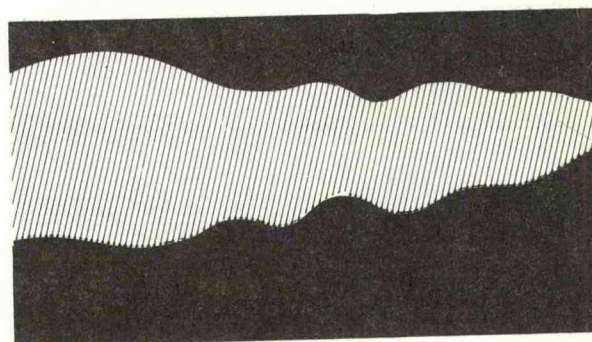
Fred Hilder  
*Naval Ocean Research and Development Activity  
NSTL, MS*

### Comparative Spectrum Analyses of Surface Wind Stress Field Based on NDBC Buoy Winds and FNOC Wind Analyses . . . . . 281

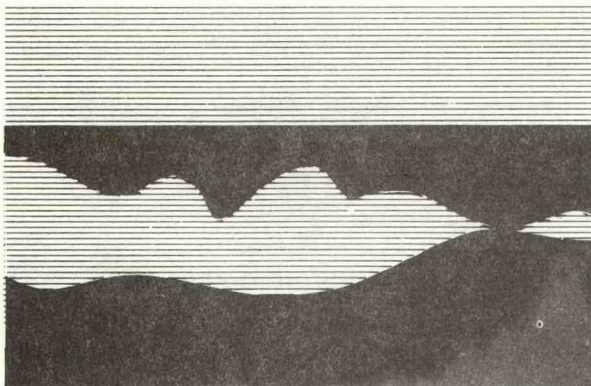
Michele Rienecker  
Christopher Mooers  
*Naval Postgraduate School  
Monterey, CA*

### Performance of the Aids-to-Navigation Buoy Environmental Sensor System . . . . . 286

Eduardo Michelena  
NDBC  
George Prine  
Frank Donovan  
*Computer Sciences Corp.  
NSTL, MS*







## SESSION IX: MOORED BUOYS

CHAIRMAN: Kim D. Saunders  
Naval Ocean Research and  
Development Activity  
NSTL, MS

### ENDECO Type 1033 Directional Wave and Current Telemetry System ..... 292

Paul Cronan  
William Gonsalves  
ENDECO, Inc.  
Marion, MA

### Moored Buoy Developments at EERM ... 299

Vladislav Klaus  
Centre Nationale De La  
Recherche Meteorologique  
Toulouse, France

### Successful Design and Handling Techniques for Tz Cables Used by NDBC During 1982 ..... 304

B. F. Case  
John Holmes  
Computer Sciences Corp.  
W. L. Beacht  
NDBC  
NSTL, MS

### Norwegian Operational Data Buoys in North- East Atlantic Waters ..... 309

Jan Stromme  
Bergen Ocean Data  
Bergen, Norway

### Cost-43—A Co-operative European ODAS Experiment ..... 315

R. E. W. Pettifer  
Meteorological Office  
Bracknell, United Kingdom

## SESSION X: DRIFTING BUOYS

CHAIRMAN: John O. Anderson  
Polar Research Laboratory  
Santa Barbara, CA

### Progressive Development of the CASID Buoys ..... 318

W. G. Large  
James McWilliams  
NCAR  
Boulder, CO  
P. P. Niiler  
Scripps Inst. of Oceanography  
La Jolla, CA

### Hybrid Time Domain Model for Drifting Buoy Motion ..... 324

John Nath  
Robert Hudspeth  
Oregon State University  
Corvallis, OR

### The Added Mass Coefficients of Several Ver- tically Axisymmetric Drifting Buoys ..... 334

Jieh Lee  
Computer Sciences Corp.  
NSTL, MS

### Slippage Errors and Dynamic Response of Four Drogued Buoys Measured at Sea ..... 338

John M. Dahlen  
Narender Chhabra  
Charles Stark Draper Lab  
Cambridge, MA

### Utilisation of Wave Energy to Enhance Station Keeping Capability of Free Drifting Buoys ..... 363

G. de F. Retief  
FPJ Muller  
University of Stellenbosch, South Africa

### Advances in Drifting Buoy Technology Utiliz- ing a Flexible Design Approach ..... 368

John O. Anderson  
Walter P. Brown  
Polar Research Laboratory  
Santa Barbara, CA



---

## **SESSION X: DRIFTING BUOYS (CONTINUED)**

### **The Disappearance of the Alaskan Gyre: The Anomalous Tracks of North Pacific Buoys 1981-1983 ..... 373**

W. J. Emery  
*University of British Columbia  
Vancouver, B.C., Canada*  
T. C. Royer  
*Inst. of Marine Sciences  
University of Alaska  
Fairbanks, AK*  
R. W. Reynolds  
*Climate Analysis Center  
NWS/NOAA  
Washington, DC*

## **PAPERS SUBMITTED BUT NOT PRESENTED**

### **Coherent Reception of HF Drifting Buoy Signals ..... 399**

Zhengxu Qian  
*Institute of Oceanology, Academia Sinica  
Qingdao, China*

### **Calculation of Statics of Subsurface Moored Buoy System ..... 403**

Song Minghang  
*Institute of Oceanographic Instrumentation  
National Bureau of Oceanography  
Tianjin, China*

### **SYMPOSIUM PARTICIPANTS LIST ..... 411**



# AUTHOR INDEX

Anderson, I. ....	246	Longman, R. W. ....	167
Anderson, J. O. ....	368	Mahar, D. W. ....	163
Bachman, R. ....	41	Martin, M. S. ....	100
Bales, S. ....	41	Maris, A. T. ....	210
Barrick, D. E. ....	65	McClure, A. C. ....	189
Beacht, W. L. ....	304	McWilliams, J. ....	318
Bergin, M. ....	147	Mellinger, E. ....	6
Berteaux, H. O. ....	118	Michelena, E. ....	286
Blouch, P. ....	124	Milburn, D. ....	25
Bradley, A. ....	6	Minghang, S. ....	403
Brainard, E. C. II ....	55	Mooers, C. ....	281
Browitt, C. W. A. ....	224	Muller, F. P. J. ....	363
Brown, W. P. ....	368	Murphy, J. ....	62
Campbell, J. E. ....	138	Nath, J. ....	324
Case, B. F. ....	304	Niiler, P. P. ....	318
Chhabra, N. ....	231,338	Nowak, R. T. ....	105
Clay, P. R. ....	108	O'Boyle, T. J. ....	195
Clites, A. H. ....	138	Oracheski, D. ....	241
Cronan, P. ....	292	Painting, D. J. ....	272
Dahlen, J. M. ....	231,338	Payne, R. E. ....	105
Daubin, S. ....	20	Pettifer, R. E. W. ....	272,315
Denner, W. ....	260	Pickett, R. L. ....	138
Dennis, N. ....	32	Pierson, C., Jr. ....	176
Donovan, F. ....	286	Prine, G. ....	286
Earle, M. D. ....	167	Qian, Z. ....	399
Emery, W.J. ....	337	Retief, G. de F. ....	363
Foley, E. ....	41	Reynolds, R. W. ....	373
Fritts, R. C. ....	163	Rienecker, M. ....	281
Fusey, E. ....	124	Rosso, R. ....	1
Gonsalves, W. ....	292	Roy, F. E. ....	265
Green, A. ....	200	Royer, T. C. ....	373
Hamilton, G. ....	131	Saunders, K. ....	200
Hamrick, F. ....	200	Selleck, J. ....	32
Heinmiller, R. ....	114	Serstad, W. H. ....	11
Hilder, F. ....	278	Shields, D. ....	210
Holmes, J. ....	96,304	Steele, K. E. ....	182
Howe, D. R. ....	11	Stromme, J. ....	309
Hudspeth, R. ....	324	Su, M. ....	147
Jones, T. ....	195	Summy, A. ....	246
Kaitala, J. ....	153	Swenson, R. C. ....	32
Kerley, D. J. ....	272	Taylor, D. ....	41
Kirschner, I. ....	189	Timpe, G. L. ....	72
Kirwan, A. D. ....	251,255,259	Turbitt, T. ....	224
Klaus, V. ....	299	Van Dijk, W. C. M. ....	79
Koziara, M. ....	49	Vega, L. A. ....	210
Lazanoff, S. ....	153	Vockeroth, R. E. ....	241
Large, W. G. ....	318	Walden, R. G. ....	118
Lee, J. ....	334	Windham, D. ....	96
Lewis, J. K. ....	251,255,259,260	Whitaker, R. E. ....	251,255,259,260
Lipa, B. ....	65	Winchester, J. ....	144



# THE ARGOS DATA COLLECTION AND LOCATION SATELLITE SYSTEM : OCEAN APPLICATIONS

Raymond ROSSO

SERVICE ARGOS - C.N.E.S.  
18 AV. EDOUARD BELIN - 31055 TOULOUSE CEDEX FRANCE

## ABSTRACT

The availability of the ARGOS satellite system for locating low power transmitters and collecting transmitted data have made possible the achievement of a large number of oceanographic study programs at relatively low cost. The FIRST GARP GLOBAL EXPERIMENT (1979-80) amply demonstrated the advantages and capabilities of the system, from the point of view of both international (W. M. O. and I. O. C.) and national organizations (N.O.A.A.,...). Up to 54 different organizations from 12 different countries have already been using the ARGOS system for oceanography : ARGOS is becoming one of the W. M. O.-I. O. C. recommended data collection systems for the 80's.

Spatiales) for France. All three of these organizations signed a memorandum of understanding concerning the ARGOS System in December 1974. The System's main mission is to provide an operational environmental data collection service for the entire duration of the NOAA TIROS-N program, i.e. from 1978 to 1987 at least. The ARGOS system is administered by Service ARGOS which is located in Toulouse, France and is part of the French space agency, Centre National d'Etudes Spatiales (CNES). The frequency band used (401 MHz) is reserved for environmental purposes, so that programs using the ARGOS system must be related to environmental studies, and be accepted by the joint NOAA-NASA-CNES ARGOS Operations Committee. Details on the various administrative procedures which must be followed may be obtained by contacting Service ARGOS at the address given above.

## CONTENTS

### 1. BACKGROUND

### 2. CURRENT STATUS

- 2.1. ARGOS data collection and location system
- 2.2. ARGOS data collection platforms
- 2.3. ARGOS current applications

### 3. FUTURE PROGRAMS

### 4. CONCLUSIONS

#### 1. BACKGROUND

The ARGOS System was primarily designed for the location (also called "positionning") of fixed and mobile platforms and for the collection of environmental data measured from these platforms.

The system is the result of a bilateral cooperation program between NASA (National Aeronautics and Space Administration) and NOAA (National Oceanic and Atmospheric Administration), for the United States, and CNES (Centre National d'Etudes

#### 2. CURRENT STATUS

##### 2.1. ARGOS data collection and location satellite System

The ARGOS System can be considered as comprising four "segments" :

- 1 - the set of all user's platforms, or, more correctly, the set of all user PTTs (Platform Transmitter Terminals), irrespective of whether these are mounted on buoys, balloons, animals, ships, or land-based stations,
- 2 - the ARGOS on-board equipment package that is included in the payload of the NOAA TIROS-N series of satellites,
- 3 - the ARGOS telemetry data receiving and communication network plus the Argos data processing center at Toulouse,
- 4 - the ARGOS data distribution system (also physically located at Toulouse) which distributes results to all system users.

##### 2.1.1. Platform transmitter terminals (PTT's)

The basic characteristics of ARGOS PTTs can be summarized as follows :



- transmission frequency : 401.650 MHz.
- message repetition period (i.e. interval between successive transmitted messages) : 40 to 60 seconds for location-type PTTs, 100 to 200 seconds for data-collection-only type PTTs,
- useful message length : 32 to 256 bits,
- mean power requirement : approximately 200 mw.

The accuracy of PTT's positions obtained with ARGOS depends on the stability of the transmitter but is usually better than 1 km with currently available commercial transmitters. To avoid interference between PTT's a registration procedure must be followed, in which each PTT is given a unique identification code by Service ARGOS. Similarly, transmitters for use with the system must meet certain technical criteria and be approved by Service ARGOS. A detailed list of manufacturers supplying ARGOS certificated PTT's may be obtained by contacting Service ARGOS.

#### 2.1.2. On-board equipment

The space segment of the ARGOS System consists of two satellites in polar orbits. The satellites presently performing this function are NOAA-6 (launched in June 1979) and NOAA-7 (launched in June 1981). The on-board Data Collection System (DCS) receives the messages transmitted by PTTs within its coverage. The processing performed by the DCS consists in the identification of the PTT and the recording of the time of the message reception, of the data contained in the message and the measurement of the doppler shift on the received signal. There are normally two satellites in operation, which means that a minimum of 4 positions per day are obtained from a PTT in equatorial regions, and up to 28 positions per day in polar areas. In temperate latitudes 8 positions per day are typically provided. These are not equally spaced in time due to the fact that the angle between the orbital planes of the two satellites is approximately 60°, rather than the 90° which would give equal spacing of the data.

#### 2.1.3. Ground reception and processing

Each time one of the satellites passes over one of the three telemetry receiving stations ( Wallops Island, Virginia, USA ; Gilmore Creek, Alaska, USA ; Lannion, France) all the recorded data are transmitted to that station. All ARGOS data received from the satellites are then sent via the National Earth Satellite Service and the NOAA Meteorological Operations Center at Suitland, Maryland, to the ARGOS Data Processing Center at Toulouse where the following processing tasks are performed :

1. decoding of the received PTT's messages and conversion of data into physical units,
2. very accurate computation of the satellites

orbits,

3. computation of PTT's position from orbital data and doppler shifts,
4. storage of all these processing results on computer files.

#### 2.1.4. Data distribution

Depending on the requirements of the PTT user, there are several ways in which the data collected by the ARGOS system may be obtained. The resulting data are available to the user on computer compatible tapes or printouts on a monthly or fortnightly basis. They are also available in computer files accessible by telephone, telex, or data transmission networks, within 4 hours after the time of transmission. Data ordered according to an appropriate format for the transmission from PTT to satellite, may be distributed automatically over the Global Telecommunications System (GTS) operated by the World Meteorological Organization (WMO). The data processing service is operated on a cost recovery basis, with charges based on the number of days for which transmissions are received for each PTT plus the costs of data delivery. For 1983 the standard rate is 140 French Francs per PTT day, plus 8 FF per day for access to the computer files, and 560 FF for each magnetic tape containing data from one experiment and sent outside the European Postal Union. Government and other non-profit users may reduce their costs by participating in the ARGOS Joint Tariff Agreement, which involves payment of a fixed cost covering all PTT's usage up to a certain global maximum. Users requiring data within times shorter than a few hours after transmission have also the possibility of receiving the data directly from the satellite. Each transmission is rebroadcast by the satellite as soon as it is received, so that anyone with a suitable receiver within radio range of the satellite can receive the data. Such receivers, or Local User Terminals (LUTs) are already being operated by some agencies, and one also is operated in Toulouse by Service ARGOS : its received data are available on the standard data files within less than 30 minutes after the time of transmission. Although positions can be determined from the information received by a LUT, the accuracies achieved so far are measured in tens of kilometers, much worse than those obtained through Service ARGOS's standard processing.

#### 2.2. ARGOS Data Collection Platforms

In oceanology, ARGOS PTTs are used on two basic types of platforms :

1. moving platforms : drifting buoys, ships, ice buoys,



## 2. fixed platforms : moored buoys.

### 2.2.1. Drifting buoys

Most of drifting buoys follow similar basic designs. The most common consists of a cylindrical spar buoy with a conical floatation collar in the region of the water line. The batteries, PTT and other electronics are located inside the spar, which may be of metal or plastic material, and the antenna is located in a fibreglass reinforced plastic cone or cylinder at the top. Commercially available buoys built along such lines have demonstrated good reliability under all ocean conditions. The standard designs have not yet fully exploited the possibilities for simple, small lightweight buoys which are permitted by the low power requirements of the ARGOS PTT's.

With care in the design, construction and handling of the buoy and its components, lifetimes of a year or more are not unusual. Of the 368 buoys deployed for the FGGE, 263 continued to transmit for more than 6 months, 177 for more than a year, and 56 for more than 18 months.

In almost all cases the main interest of oceanographers has been in the buoy tracks, even though many of the buoys were equipped with other sensors. Data from buoys equipped with drogues in the upper mixed layer is considered to be an accurate measure of the currents in that layer. However, the drogues do not last as long as the buoys, so that there has been considerable interest in interpreting the data from buoys without drogues. Rather surprisingly, the movements of such buoys are not obviously dominated by the wind, to the extent that, for some buoy types, it is difficult to tell from the buoy track whether or not a drogue is attached to the buoy. Although most drifting buoys have been launched from research vessels or other scientifically oriented ships, many have been deployed by normal commercial vessels, including container ships. A number have also been launched from aircraft, with no apparent degradation of their performance.

### 2.2.2. Ships

Today some 7 000 ships, termed V.O.S. (Voluntary Observing Ships) transmit irregularly meteorological and oceanographic data messages : one weak link of the current system is the radio-transmission of the observations from ship to shore. ARGOS offers the possibility of significantly improving the efficiency of the system with a minimum of change in current procedures. Instead of transmitting the collected data by radio, the ship crewmembers feed the data into an ARGOS manual PTT, which retransmits automatically and continuously these data towards the satellite. The capability of such terminals to withstand the stresses of a shipboard environment has been demonstrated without failure on several ships equipped by Service ARGOS PTT's.

### 2.2.3. Ice buoys

Ice buoys have been used extensively in Arctic regions to track iceberg movements and the ice edge, with a view of evaluating the risks of collision with drilling platforms and ships. Commercially icebuoys are currently available with different modes of deployment : helicopter, light aircraft or parachute. Such buoys are equipped with low temperature electronics and lithium batteries so that they can operate at arctic surface temperatures (down to - 50° C) For very accurate positioning of icebergs, ice buoys can be equipped with a satellite navigation receiver which provides the buoy position: the ARGOS PTT is only used nominally to transmit the computed position, but is also helpful as a back up positioning system in case of failure of the primary NAVSAT system.

### 2.2.4. Moored buoys

Diverse requirements for environmental data at specific locations over large intervals of time resulted in the need to moor buoys to the ocean floor. In early moored buoys most of the data were recorded on-board, to be recovered during visits. Unfortunately most of the recorded data were often lost in consequence of recorder failures or impossibility to locate and retrieve the buoy. Furthermore these moored buoys were often very large buoys, carrying advanced environmental sensors : losing such buoys was both very costly and dangerous for the maritime navigation. For these reasons the use of ARGOS PTT's was favored for positioning the buoy and transmitting some data (as back up of wide band telemetry systems).

Moored buoys of very different shapes are currently in use in experimental and operational programs using ARGOS, including the following shapes : boat, sphere, cylinder, discus.

## 2.3 ARGOS current applications

Ocean data are of interest not only in oceanography proper but also in related sciences as meteorology, climatology, glaciology, marine biology and also in ocean industries like offshore, fishing and transportation activities.

### 2.3.1. Observed parameters

The ocean parameters which has been observed via ARGOS can be divided into ocean parameters and atmospheric parameters. Each of these two categories can be subdivided into many classes depending on the scientific domain concerned : physics (temperature, pressure), dynamics (waves, wind), chemistry (salinity, pollution) and biology.

The sensors which have been extensively used first with ARGOS DCP's have measured sea surface temperature and barometric pressure. A large experience were acquired during the FGGE were



more than 300 ARGOS buoys were deployed using these sensors. However accurate pressure data is still difficult to achieve and even more difficult to verify over the life of the buoy. Measurement of the water temperature near the surface (SST) is a very standard practice on ARGOS DCP's : the true accuracy of these measurements is still difficult to assess due to SST sensors having different time constants and being placed at different depths.

Much work has been done to develop sensor systems for measuring water temperature below the surface: the main technological problem has been the mechanical design of the connection between the ARGOS buoys and the temperature sensors. Many manufacturers have built to date thermistor chains up to 150 m which have survived several months at sea : efforts to extend this depth are continuing. Other physical parameter including air temperature, wet bulb temperature, air sea temperature difference, ambient acoustic noise have received only experimental developments on ARGOS DCP's.

Wave measurements (wave amplitude, direction, spectra) have also been made from ARGOS DCP's : commercially available wave measuring buoys equipped with ARGOS PTT's can be used either in a mooring mode or a free drifting mode. The measurement of wind speed and wind direction have also received some attention. The main technological problem is to find a reliable anemometer which will support the marine environment. Another problem is to interpret the data, often acquired at a level below the height of the wave crests.

Concerning the measurement of ocean currents (velocity and direction, at various depth), the information is generally deduced from drifting buoys tracks computed by the ARGOS system.

### 2.3.2. Present ARGOS programs

Presently oceanographic programs using ARGOS are involving users of twelve different countries : USA, Canada, FRG, Norway, France, Australia, Japan, South Africa, U.K., India, Portugal, Netherland. These programs concern all oceans (Indian, Arctic, Antarctic) and seas.

More detailed informations about these programs can be found in the different ARGOS users conference proceedings, which can be obtained by contacting Service ARGOS.

The three last conferences were held in :

- San Francisco, California, october 28/29, 1981
- Paris, France, april 20/22, 1982
- Annapolis, Maryland, december 13/15, 1982

The present status (as of April 15, 1983) of ARGOS ocean DCP's is summarized in the table 1.

### 3. FUTURE PROGRAMS

Aside from operational meteorological arrays, the only foreseen large scale program is the World Climate Research Program (WCRP) recommended to the worldwide scientific community. This new program scheduled for the period 1985-90 will aim at the analysis of the impact of oceanic phenomena on the world climate. This is a joint meteorology-oceanography program where the study of very slowly varying oceanographic phenomena (involving periods of several years) will be given pride of place. This is in contrast to the GARP program which studied similar phenomena but only over a period of a few weeks.

One of the key systems available for the study of the oceans during the latter part of this decade is, of course, the ARGOS System since it is the only one of its type that will be fully operational during that period and which also meets the requirements of the preliminary programs. Furthermore, the quality of the services offered has been widely recognized.

The CAGE experiment will take place in the North Atlantic and will study heat exchanges between the atmosphere and the ocean. Among other facilities, this program will use 300 buoys in an effort to understand the annual and longer term variations in these heat exchanges. These buoys will be separated from one another by 200 km.

This experiment is comparable to the FGGE but the number of parameters measured will be greater and the sensors used more advanced. In particular sensors will be available for measuring insolation, wind speed, humidity, and the difference between the air and surface water temperatures. The WOCE (World Ocean Climate Experiment) experiment, which is also part of the WRCF program, is expected to use some 500 buoys during the period 1985-90. The aim of this experiment, which will be worldwide in coverage, is to improve our understanding of planetary climatological processes over time periods ranging from several weeks to several decades.

### 4. CONCLUSIONS

The increasing number of oceanographic programs making use of the ARGOS System and the general recognition of its operational qualities by the oceanographic and meteorological communities would appear to justify the hopes held by Service ARGOS that the System will be widely used during the coming decade for coordinated international programs such as WRCF. It is of course true that a continuous and centralized service covering data collection, platform location, the distribution of results is essential to the on-going development of the techniques that enable us to improve our understanding of marine environment. One of the attractive features of the current situation is that the ARGOS System provides global coverage, so that the



same DCP may be used anywhere in the world. It also means that DCP's which drift out of the area of interest of their original deployer may still be used by anyone willing to pay the cost of the tracking. The most important feature of the ARGOS system is that even the most remote areas are covered, where the rarity of data makes observations most valuable. In order to be sure of the future availability of this systems, DCP's users must continue to make their needs known to the agencies planning and operating the ARGOS System.

ARGOS OCEAN DCP's STATUS

(AS OF APRIL 15, 1983)

PLATFORMS COUNTRY	DRIFTING BUOYS	SHIP TERMINALS	ICE BUOYS	MOORED BUOYS	TOTAL
U.S.A.	67	4	10	42	123
CANADA	21	-	7	2	30
F.R.G.	26	-	-	-	26
NORWAY	19	-	-	3	22
FRANCE	10	3	-	4	17
AUSTRALIA	7	-	1	-	8
JAPAN	7	-	-	-	7
SOUTH AFRICA	6	-	-	-	6
U.K.	3	-	-	2	5
INDIA	3	-	-	-	3
PORTUGAL	2	-	-	-	2
TOTAL	171	7	18	53	249

TABLE 1



# INTEGRATED COMMUNICATIONS IN BUOY SYSTEMS

Ed Mellinger and Al Bradley

Woods Hole Oceanographic Institution  
Department of Ocean Engineering  
Woods Hole, MA 02543

## Abstract

Buoy systems designed for oceanographic research have traditionally employed underwater sensors distributed along a mooring line some kilometers in length. The sensor packages have evolved as autonomous data acquisition units, each equipped with local processors, data recorders, and power supplies. Emerging applications, including event driven sampling schemes and satellite data collection systems, will require a more general system architecture capable of bringing distributed sensor data to a central point for analysis and/or relay to shore. In this paper we describe an adaptation of the shipboard Serial ASCII Instrumentation Loop (SAIL) system architecture to the underwater environment. Necessary additions to the existing SAIL protocol are discussed, and an implementation of an underwater SAIL based system is described.

## Introduction

Several converging trends in the design and application of ocean instrumentation are presently providing both the need and the means for implementing new observational techniques. Considering research applications first, three areas of interest may be identified. First, new and more complex experiments are being proposed which require in situ compression or analysis of data from widely spaced sensors. An example would be an adaptive sampling system which responds in real time to the occurrence of a specific event, such as a seismic event or presence of an internal wave. These and other "smart" observational systems generally require an integrated sensor array linked to a central processor responsible for overall experiment control.

A second emerging application area concerns remote systems which return data to the user through specialized communication links, in real or near real time. Examples include satellite data collection systems (ARGOS, GOES/DCS), terrestrial radio channels, and some types of acoustic telemetry. In these systems, data must be collected at a central point prior to relay to ship or shore.

The third research "application" is the practical need to reduce the end user cost of designing and deploying custom instrument systems geared to specific experiments. A more flexible approach might be the creation of a library of sensor modules designed around a common interface scheme. A set of such modules could

be easily configured into a special purpose instrument system, and imbued with the intelligence necessary to perform specific observational functions by a general purpose central controller programmed for that specific experiment.

Ongoing developments in instrument technology have now placed within reach the ability to create systems with the capabilities outlined above. The most obvious of these developments is the ubiquitous microprocessor in its role as controller and data processor. Equally important is the decreasing complexity (or at least chip count) of microprocessor based systems, and the declining cost, energy consumption, and cubic volume per function which has resulted.

A second major advance in technique is the development and acceptance of data communication standards such as RS-232 and Ethernet [1], and specifically the development of methods well suited to the task of interconnecting the elements of a general purpose instrument system. Foremost among these is IEEE-488 (GPIB) [2], applicable to laboratory instrument systems. Unique shipboard requirements have led to the development of the Serial ASCII Instrumentation Loop (SAIL) protocol [3], for similar applications in shipboard data acquisition systems. The foundation for these and other data communications activities is the increasing power of descriptive tools used to characterize data communications systems. Models such as the Open System Interconnect (OSI) developed by the International Standards Organization [4] define concepts which allow communications systems for specific applications to be designed and optimized with a high degree of precision.

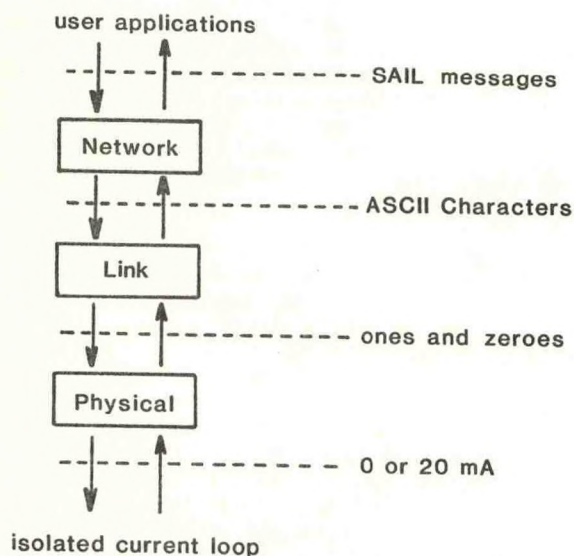
The convergence noted between research applications and instrument technology suggests an integrated approach to buoy system communications. Within a general purpose buoy system a number of potentially useful local communication pathways may be identified. Examples include communications between instruments along a sea cable, between instruments on a surface float or within a pressure case, and, before deployment, between the instrument system and its shipboard support equipment. This diversity can be handled by identifying the common features of each communication task and then partitioning the overall task into "layers" which generalize the specific features of each task. This partitioning, which is based on the OSI model mentioned previously, allows us to define a family of data links sharing many common features, and hence much common hardware and software.



We can now proceed to a statement of the task confronting ocean instrument designers: the need to create a method whereby diverse kinds of oceanographic instruments can be joined into complex systems which are greater than the sum of their parts. Needed is the "library" of instrument modules mentioned above, the observational systems in which to apply them, and most of all the common language which ties these elements together by allowing modules from different designers to work within the same system. In short, we need a data communication standard. As a working proposal, in the remainder of this paper we suggest an adaptation of the SAIL standard, currently in use for shipboard data acquisition. We present it as a trial solution, and not as a fait accompli or a ready made answer. We seek to initiate a discussion within the ocean instrument development community, with the goal of eventually creating a functional standard which is usable by all.

### SAIL Overview

Structure The SAIL data communications standard was originally proposed by Mesecar and Vito [5] as a technique for interfacing sensor systems to data loggers aboard research vessels. The standard defines a digital message interface between intelligent sensor modules and a central system controller. It is a member of the same "addressable devices on a bus" protocol class as IEEE-488, and hence is well suited to the role of linking general purpose instrument modules into special purpose instrument systems. Three separate levels or "layers" may be identified within the present version of the standard, as shown in Figure 1. The physical layer provides for point to point transmission of logical ones and zeroes, by means of a ground isolated 20 mA half duplex current loop passing through each device in the system. The link layer defines the format for information exchange on the loop by specifying that the ones and zeroes of the physical layer be formed into serial asynchronous ASCII characters



**Figure 1**  
SAIL Architecture

transmitted at rates of 110 to 9600 baud. The network layer provides the logical framework within which complete messages, composed of ASCII characters, may be exchanged between devices on the loop.

The network layer specifies that each module on the loop have a unique address through which it is accessed by the loop controller. The address, sent only by the controller, may be any unique character sequence preceded by the ASCII "#" character. Upon receiving its address from the controller, the module enters the "open" or addressed state. In this state it may return data messages to the controller, receive data or command messages from the controller, or perform other functions specific to its application. All loop data transfers are initiated by the controller; no mechanism is provided to allow a module to "interrupt" the controller. The network layer provides a number of auxiliary functions for loop initialization and synchronization, including a special command for dynamically varying the loop baud rate. The standard deliberately refrains from attempting to define the nature and format of messages passed on the loop, as such standardization carries the risk of outlawing potentially useful techniques not presently considered.

Applications Current loop SAIL (SAIL/CL), as outlined above, has been in use since 1978 in a number of applications. Aboard ships, it has proven to be a flexible means for configuring both general and special purpose data acquisition systems [6,7]. SAIL has also been extensively applied as a pre-deployment control and test interface on a variety of microprocessor based ocean instruments, replacing the limited (and often inaccessible) control panels employed previously. In this application, an operator at a CRT terminal can address any of several instruments on a loop and perform test and configuration procedures, without opening any pressure housings. The instruments under test may be located anywhere aboard ship, or alternatively, in any of several laboratory buildings. The isolated current loop physical layer has proven effective and reliable in the high EMI ship environment. Unfortunately, power consumption for the 20 mA loop itself approaches 100 mW per device connected, ruling out a straightforward application of SAIL to communications within deployed underwater instrument systems.

Proposed Extensions We propose two low power signalling techniques for addition to the physical layer of the SAIL standard, leaving the link and network layers essentially unchanged. The first is intended for long haul (up to 8 km) communications between instrument packages on full ocean depth sea cables, and can also be adapted to short range acoustic and radio links. The second recognizes the need for short range (less than 10 m) communications between adjacent sensor modules on a buoy or within a pressure case. Both signalling schemes mimic the logical-OR, half duplex nature of the 20 mA loop. A diagram of the SAIL architecture incorporating these additions is shown in Figure 2.

### Cable Communications Subsystem

The long haul cable communications subsystem must meet several specific requirements relating to ocean instrument systems. The principal need is for a low to medium speed digital data channel capable of operating in the 110-1200 bit/sec range. The channels involved have a restricted bandwidth due to cable capacitance in the



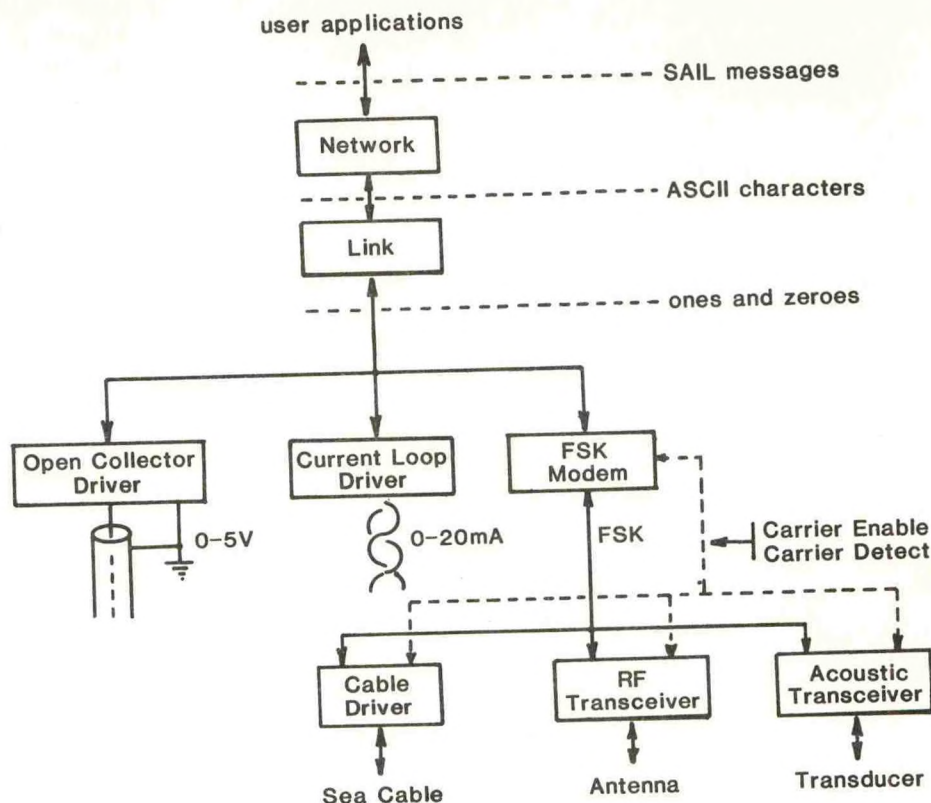


Figure 2  
Extended SAIL Architecture

50-150 pF/meter range and cable length of up to 8,000 m. The communication channel must have a multidrop (party line) format to support a bus type multiple instrument configuration, and specifically to support the half duplex, logical-OR format of the SAIL standard. In some situations a DC path may not exist through the channel, and in others it may be desirable to multiplex the data channel with the instrument power supply onto a single two-conductor cable. Most importantly, the cable communication subsystem must have small size, low power consumption, and high reliability suitable for ocean instrumentation applications.

A number of approaches to the communications system design have been considered, and undoubtedly others should be investigated in the future. Baseband (i.e. square wave) data with AC power distribution enjoys simple power conversion but suffers from high power losses in cable shunt capacitance. Amplitude modulated (carrier keyed on-off) data with DC power distribution leads to the simplest modem design but is sensitive to long term changes in signal amplitude, such as caused by seawater leaks in a cable jacket. The technique with the best all-around performance is frequency modulated (FSK) data, with DC power distribution where applicable. This well known technique fits easily into restricted bandwidths, achieves excellent error rate performance, and leads to a simple, efficient hardware realization, potentially single-chip. SAIL systems using FSK we term "SAIL/FSK".

The telecommunications industry standard for 1200 baud half duplex modems is the Bell type 202; this in-place standard is suitable for the SAIL environment. The 202 is a voice channel modem using FSK frequencies of 1200 Hz (mark) and 2200 Hz (space), and will operate with asynchronous data at any rate up to 1200 baud. High speed modems (and promised modem chips from several vendors) may effectively utilize the full channel rate where required. Low speed (110-300 baud) modems using the 202 signalling frequencies are very simple to implement and may coexist with high speed devices on the same channel under the SAIL network protocol.

Fig 3 is a block diagram of a simple (7 IC's) low speed modem developed at Woods Hole Oceanographic Institution (WHOI) to test the SAIL/FSK concepts. Presently 202-incompatible, it will be modified to use 202 frequencies in the near future. FSK carriers are enabled only during data transmission to allow multiple access to the cable channel and to keep standby power consumption at 2 mW per modem. Active (transmitting) power consumption is a function of the capacitive load presented by the cable, amounting to approximately 10 mW per 1000 m of cable for the 150 pF/m cable presently in use. The modem circuit has operated successfully at 600 baud, and has a measured raw error rate of  $10^{-5}$  at 300 baud.

The FSK technique successfully emulates the 20 mA loop used in present SAIL communications, but requires minor additions to the SAIL protocol for transparent communication. These include the following:



- 1) SAIL devices must enable the FSK carrier roughly one character time before data is transmitted, and disable the carrier one character time after transmission is complete.
- 2) SAIL devices must ignore any signals received in the absence of a carrier on the channel.
- 3) SAIL devices must incorporate a fail-safe timeout on the FSK transmitter to prevent "stuck-on" failures from disrupting the entire cable channel.

With these changes implemented, the FSK scheme allows SAIL techniques to be applied to long distance underwater communication. The FSK signals can also be sent over short range RF and underwater acoustic channels using the same format. The FSK signals are not intended for long distance RF or acoustic links, where more sophisticated modulation techniques must be employed.

#### Local Communications Subsystem

The second addition to the SAIL physical layer is intended for short distance local communication within a single mooring platform, such as between meteorological sensors on a surface buoy. In this environment, a multiple access channel is still required, but communication system overhead (power consumption and complexity) must be minimal. A simple two wire, open collector link meets these requirements and permits communication up to 10 meters with zero standby power drain. The bus is pulled to 5 V through a resistor suitable for the baud rate and cable involved; 5 V is defined as a mark, 0 V as a space, and 2.5 V as the transition threshold. This nearly trivial link (dubbed SAIL/OC) allows the full SAIL protocol to be retained for local communications between intelligent, low parts count sensor modules.

#### Applications

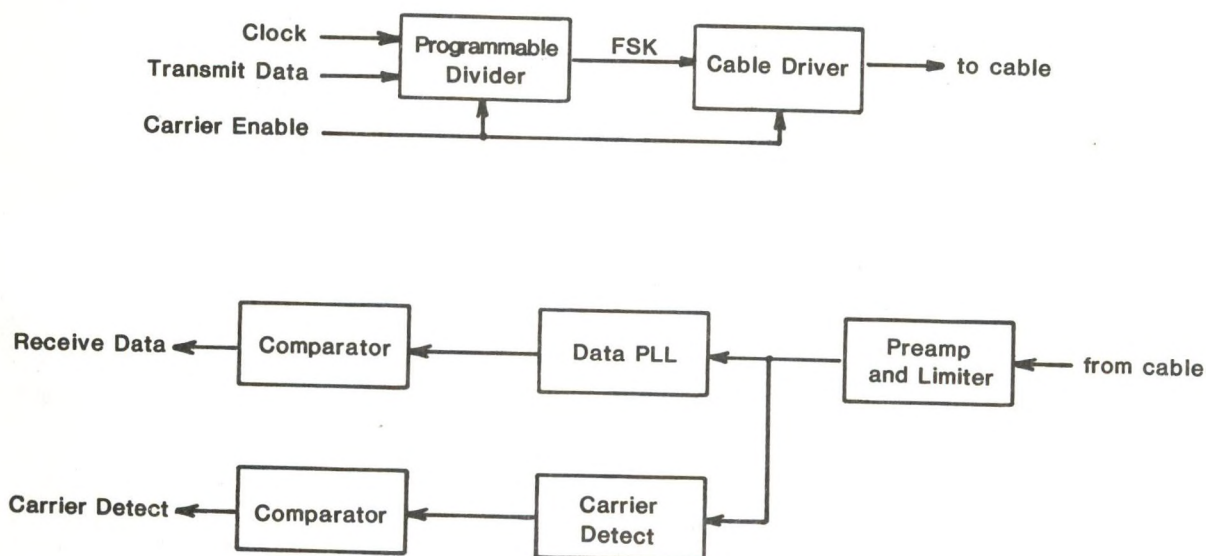
The first application of the extended SAIL standard is the NASA sponsored RELAYS (REal time Link Acquisition and Yare System) instrument platform presently under development at WHOI. This system, shown in Fig. 4, is a satellite linked surface drifter with a subsurface cable reaching 1000m into the ocean interior. Sensor systems planned for deployment on this cable include pressure/temperature modules, cable inclination/tension modules, current sensors, and a SOFAR float receiver. SAIL/FSK is used for communications between sensor modules on the cable and the 1805 microprocessor based system controller in the surface float; SAIL/OC will provide future integration of local meteorological sensor data. Acquired data is relayed to shore via the ARGOS satellite data collection system. Pre-deployment checkout and configuration is done via a standard SAIL current loop, and via a short range UHF radio link using SAIL/FSK immediately after launch. Initial full scale system tests are scheduled for September 1983.

#### Conclusions

The advantages of instrument systems built around general purpose communications links include:

- availability of real time data from all sensors;
- system control over sensor sampling parameters;
- elimination of redundant recorders and power supplies; reduced cost and weight;
- straightforward system configuration and reconfiguration; no controller hardware changes to support new sensors.

In this paper we have proposed the SAIL system



**Figure 3**  
Experimental FSK Modem



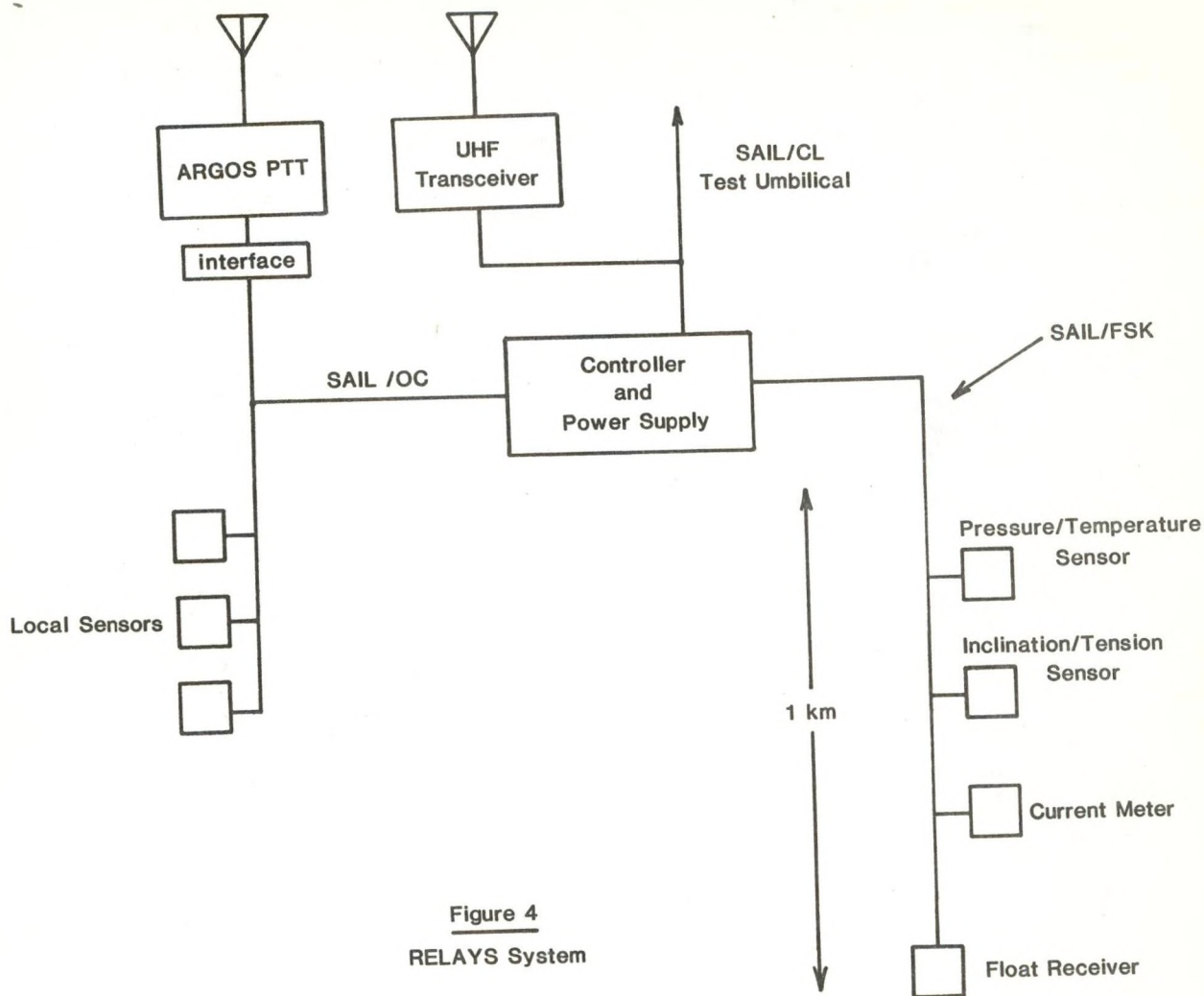


Figure 4  
RELAYS System

architecture as a candidate for instrument system communications, and have presented two extensions to the basic SAIL signalling method for implementing these communication links. It is our hope that instrument system designers will explore the possibilities of the SAIL approach in relation to their system requirements, and in so doing further expand the hardware and software basis on which other SAIL users may build. The present support of SAIL assures potential users that many of their basic data acquisition needs may already have been met by equipment developed elsewhere. Solving basic problems once and only once allows individual users to focus on particular problems posed by their applications, and assures them that the solutions which they develop will be useful to other members of the oceanographic community at large.

#### Acknowledgements

Support for this research has been provided by the National Aeronautics and Space Administration, Oceanic Processes Branch, under grants NAGW-265 and NAG-5-281. This is Woods Hole Oceanographic Institution contribution number 5345.

#### References

1. Metcalfe, R. M. and Boggs, D.R., Ethernet: Distributed Packet Switching for Local Computer Networks, Comm ACM vol. 19 no.7, July 1976.
2. Institute of Electrical and Electronics Engineers (IEEE), IEEE Standard Digital Interface for Programmable Instrumentation, IEEE Standard 488-1978, November 1978, 83 p.
3. UNOLS Technology Assessment Committee, Serial ASCII Instrumentation Loop, UNOLS TAC-81-1, 1981.
4. International Organization for Standardization (ISO), Reference Model of Open System Interconnection, Document no. ISO/TC97/SC16 N277, June 1979.
5. Mesecar, R., and Vito, J., A Partitioned Data Communications System, Exposure vol. 6 no. 3, July 1978. (Oregon State University ocean technology newsletter)
6. Peal, K.R., and Mellinger, E.C., A Standardized Shipboard Data Acquisition System, Proceedings IEEE Oceans, September 1981, pp 287-291.
7. Mesecar, R., and Dillon, W., Serial ASCII Instrumentation Loop for Marine Research Application, Proceedings IEEE Oceans, September 1981, pp. 296-300.



## A SYSTEM FOR DATA ACQUISITION IN THE OCEAN ENVIRONMENT

D.R. Howe, Magnavox Electronic Systems Company, Fort Wayne, Indiana

R.L. Erichsen, NOAA Data Buoy Center, NSTL Station, Mississippi

W.H. Serstad, Magnavox Electronic Systems Company, Fort Wayne, Indiana

### ABSTRACT

The Coastal Marine Automation Network (C-Man) collects and reports meteorological and oceanographic data from ocean buoy platforms and from coastal shore locations.

This data is reported through the Geostationary Operational Environmental Satellite (GOES) in a standardized format defined by the National Weather Service for distribution on their network without further modification.

The actual collection and reporting process is accomplished by the Data Acquisition Control and Telemetry (DACT) system being developed under the auspices of the NOAA Data Buoy Center. This platform has been designed to be easily converted for use in either the buoy or shoreside configuration.

This paper will describe these various features of the DACT system and how it fulfills the operational requirements of data acquisition in the ocean environment.

### 1. INTRODUCTION

The Coastal Marine Automated Network (C-MAN) is a system to provide around-the-clock weather observations from a network of data collection platforms located at headland shore sites, offshore fixed platforms, and Large Navigational Buoys (LNB's). Measurements made and reported from these sites are designed to meet the requirements of the National Weather Service. The program is being implemented by the NOAA Data Buoy Center.

The data collected by the automatic systems are processed on-site and reported in a directly readable WMO-format message. The communications link to the remote unattended stations is by means of the Geostationary Operational Environmental Satellite (GOES). As a supplement to the GOES, certain headlands stations also have direct access by means of a dial-up telephone link. In these cases, data may be accessed directly by means of a remote terminal equipped with a telephone modem. Typical operational installations are shown in Figures 1-1 and 1-2.

The primary emphasis of this paper is to describe the data collection system and techniques utilized on the LNB's. It should be pointed out that the actual hardware for these data collection systems

has been standardized for all of the C-MAN applications and differs only in the particular sensors installed and in the specific plug-in modules used.

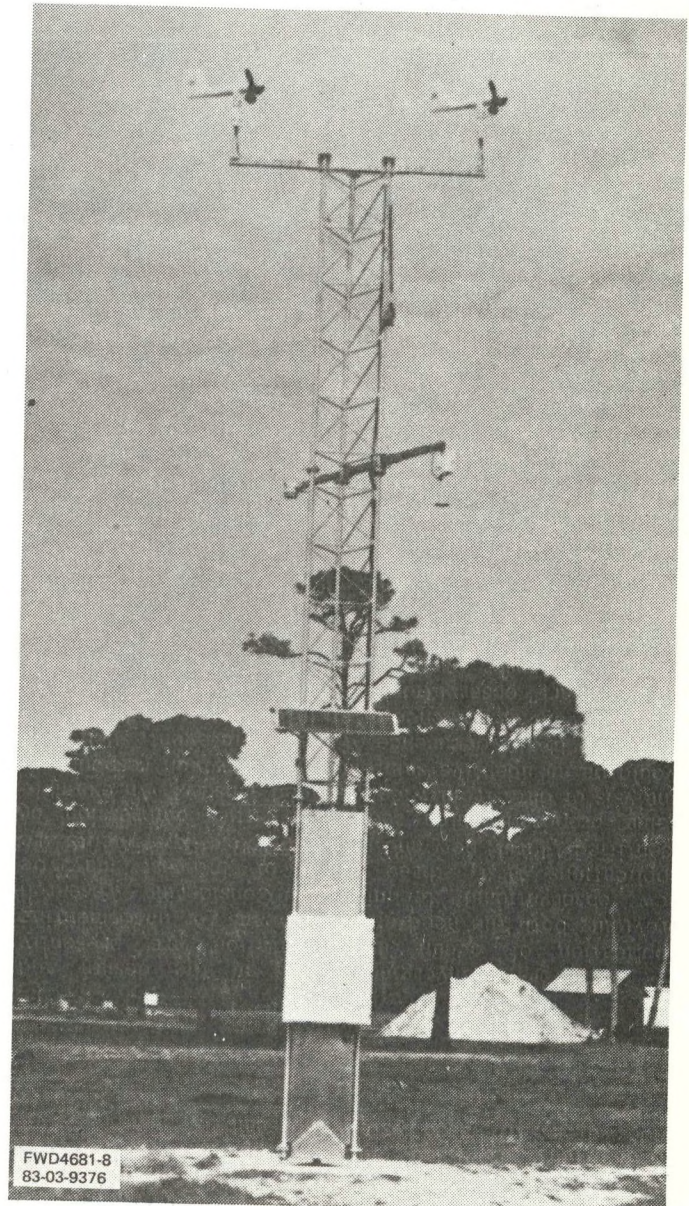


Figure 1-1. Fixed DACT Installation





Figure 1-2. Large Navigation Buoy

This data collection and reporting system is called the Data Acquisition Control and Telemetry (DACT) system. In order to readily accommodate a wide variety of sensor and processing requirements, the DACT has been designed to be modular in both hardware and software. A major portion of this flexibility is provided by the software intensive nature of the data collection system. Specialized test sets or standard RS-232 terminals may be used to enter a series of operating parameters to facilitate the specific field application requirements.

Of prime consideration in the design of an unattended system such as this is the system reliability and the variation in operating environments. Where equipment is located in relatively inaccessible locations and in particular buoy systems, reliability and maintenance philosophy have a direct bearing on the long term cost of ownership. Realizing the importance of these factors, NDBC has implemented an extensive Test and Evaluation phase.

The development program resulted in the delivery of four prototype systems. These systems are undergoing field evaluation; two of these have been installed at sites in New York and Florida and a third is to be installed on an LNB in the San Francisco area. An additional system is being operated at NDBC. The initial production program is underway with deliveries starting in May.

The following discussion will elaborate on the more salient features of this program with particular emphasis on the buoy applications.

## 2. SYSTEM CONFIGURATION

As indicated previously, the modularity and flexibility of the DACT system permit a wide variety of configurations. The block diagram of Figure 2-1 illustrates a typical LNB application.

As shown in this diagram, redundant wind sensors are typically used. The sensor complement consists of devices for wind speed and direction, buoy heading, barometric pressure, air temperature, and ocean temperature.

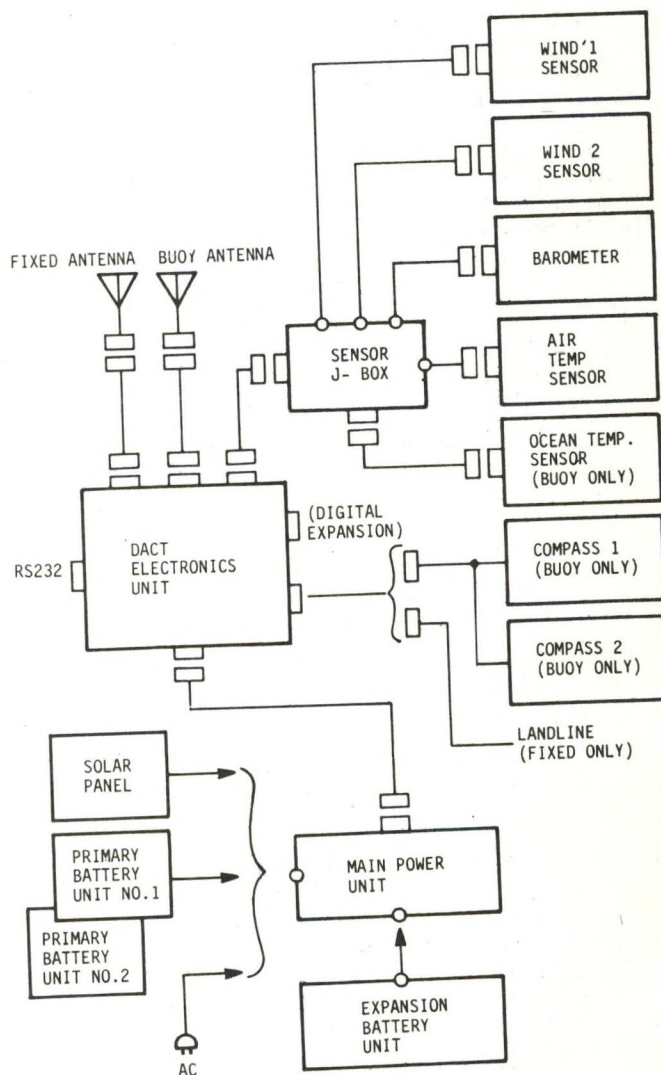


Figure 2-1. DACT System Components

A sensor junction box permits ready adaptation to each installation and also permits the addition of other type sensors at any time. Separate antenna inputs are provided for fixed (land-based) and buoy applications. In this particular case, the buoy system would use a 40-watt GOES transmitter in conjunction with an omni-directional antenna. A fixed location would use a 10-watt transmitter with a directional antenna.

The power system for a buoy would typically be secondary gel-cells charged from primary batteries.



Alternate power sources such as solar panels and 110-volts AC can be readily accommodated in the fixed installations.

Should field service be required, any component of the system can be disconnected and a new unit substituted without requiring any special calibration in the field.

By the use of a portable test set (or terminal), the system operating parameters can be easily changed in the field. Use of the test set also permits operating checks to be performed.

An indication of the measurement parameters is given in Figure 2-2. This list includes those parameters presently implemented in the DACT system and those parameters considered candidates for expansion.

The battery voltage and charge current are internal housekeeping functions and are provided to give an indication of power system status. One feature should be noted in the measurement of battery volt-

age. This sample is taken during the time when the transmitter is on and when the load on the battery supply is the greatest thus giving a worst-case type of reading.

In establishing the measurement criteria for a particular installation, the user may select the following sample options:

- (1) Enable or disable individual sensors
- (2) Select single sample or averaging
- (3) Acquisition intervals
- (4) Acquisition duration
- (5) Second-order correction coefficients for sensor inputs of the form  $ax^2 + bx + c$ .

Except for a few specific cases, such as waves and precipitation, individual samples are taken once per second during the acquisition period.

MEASURANDS	REPORTED DATA	MINIMUM REPORTING RANGE	MINIMUM REPORTING RESOLUTION	MINIMUM TOTAL SYSTEM ACCURACY
Battery Status	Battery Voltage	0 to 15V	0.1V	5% Rdg.
Charger Status	Charging Current	0 to 4A	0.01A	5% Rdg.
Air Temperature	Air Temperature	-50° to +50°C	0.1°C	±1.0°C
Sea Surface Temperature	Sea Surface Temperature	-50° to +50°C	±1.0°C	±1.0°C
Wind Direction	True Wind Direction	0° -360°	10°	±15° True (±10° Desired)
Wind Speed	Avg. Wind Speed	0-120 kts	1.0 kt	±2.0 kts or 5%
	Peak Wind Gust	0-160 kts	1.0 kt	±2.0 kts or 5%
Barometric Pressure	Altimeter Setting Indicator	900 to 1100 mb	0.1 mb	±1.0 mb
Dew Point	Dew Point Temperature	-31° to +86°F	1.0°F	-31° to -11°F: ±4°F -10° to +29°F: ±3°F +30 to +86°F: ±2°F
Waves	Wave Period (T)	3 to 30 sec	1 sec	±1 sec
	Significant Wave Height ( $H_{1/3}$ )	0 to 66 ft	1.0 ft	±1.5 ft
	Peak Wave Height	(TBD)	1.0 ft	(TBD)
Tide	Tide Level	(TBD)	0.1 ft	(TBD)
Precipitation	Cumulative Precipitation	0 to 9.99 in	0.01 in	±0.02 in or 4%
Sector Visibility	Visibility Range	0 to 8 Statute mi		0 to 3 mi: ±10% 3 to 8 mi: ±1 mi

Figure 2-2. DACT Measurement Parameters



Air temperature and sea surface temperature utilize a tri-element thermilinear component resulting in a linear variation of resistance with temperature.

The wind speed is derived from the analog output of an impeller driven magneto. Wind direction is resolved from the output of a potentiometer indicating the vane direction. To determine actual wind direction in a buoy installation, this output is processed in conjunction with the output of a buoy heading compass. Additional processing is required to correct for magnetic hull anomalies and to accommodate the zero-crossing phenomenon.

Barometric pressure is sensed by means of a temperature-compensated variable-capacitance pressure transducer. The pressure port is of special design to reduce the pressure errors contributed by wind flow across the port.

A Wave Measurement System is currently under development which is contained on a plug-in module. Details of this measurement system are covered in a paper entitled "The Wave Data Analysis Function as Performed in Data Acquisition and Telemetry Systems" presented in Session V of this Symposium.

The collected sensor data is processed, converted to engineering units, formatted into the proper message, and then transmitted.

The transmitted message is coded in ASCII and may be read directly without additional processing. The message format is in compliance with Federal Meteorological Handbook No. 2.

The system components making up a DACT for a buoy installation are shown in Figure 2-3. The most significant differences from a fixed installation are the use of an omni-directional antenna, compass, water temperature sensor and a 40-watt amplifier for the GOES transmitter.

### 3. DACT FEATURES

The inside view of the DACT Electronics Unit (DEU), shown in Figure 3-1, gives an indication of the modular construction of the unit. Plug-in modules facilitate the configuring of the DEU for specific applications. For example, the land-line modem can be removed, a Wave Analyzer module inserted in a spare slot, and a 40-watt RF amplifier mounted to the lid. This would reconfigure the DEU from a fixed headlands station to a buoy system. Spare card slots are provided for additional sensor conditioning modules.

The enclosure is fitted with an RFI gasket on the lid which also provides a pressure seal. A pressure inlet and a pressure release valve allow purging of the enclosure with dry nitrogen.

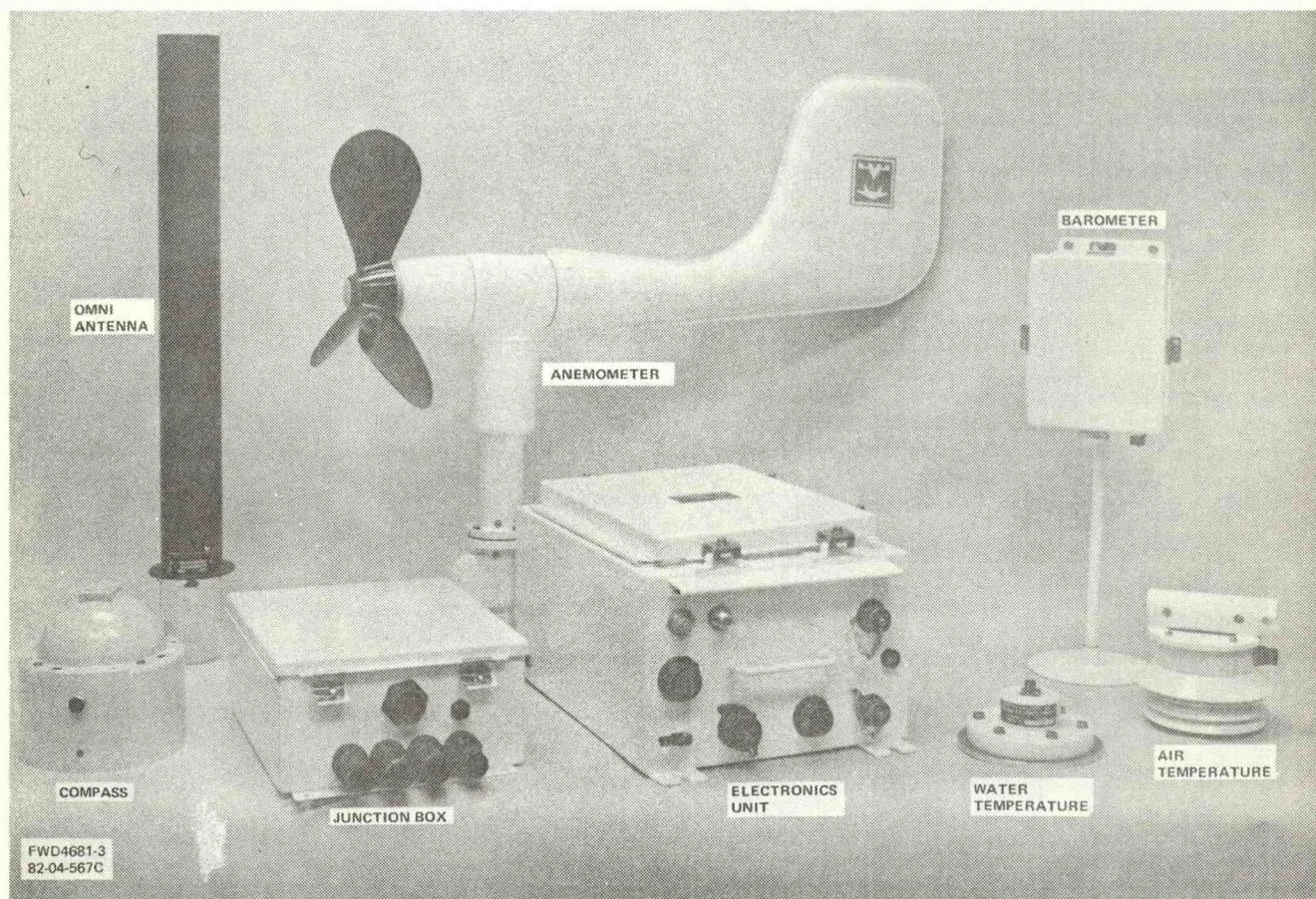


Figure 2-3. Buoy DACT System



The 10-watt GOES transmitter is a synthesized dual channel unit. Any of the GOES channels can be selected prior to deployment by means of switches mounted under the access cover on the transmitter.

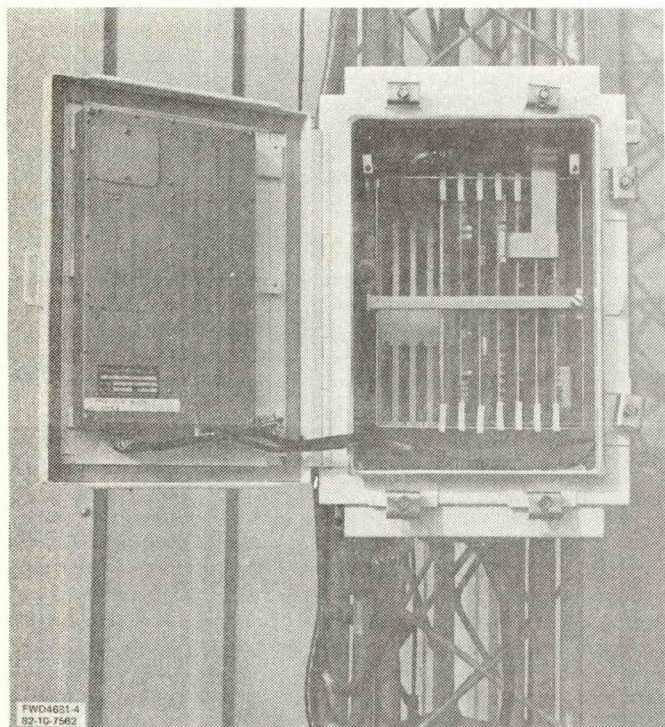


Figure 3-1. DACT Electronics Unit

One of the two preset channels is selected by software for normal transmission of synoptic data. Inherent in the software is also the ability to select either the long or short standard GOES headers on the transmitted message.

The set of selectable operating parameters which are entered by means of the test set or a terminal are stored in a set of Electrically Erasable PROMS. This feature allows entry of these parameters at the user's base site. The system may be disconnected for transportation to a field site, reconnected and initialized without having to enter the variable parameters in the field. This mode of operation is not the method normally used by NDBC since the field installers possess the necessary skills to accomplish this at the time of deployment.

Many functions available to the user by means of the RS-232 port on the DEU include:

- Enter parameters
- Read data
- Initiate a single sample acquisition
- Message transmit
- Data transmit
- Read clock
- Set clock
- Turn transmitter on or off
- Perform diagnostic tests
- List parameters
- Compose message.

Since it may not be desirable to have all of these functions available to every user, particularly over the land line, four levels of access code are provided. When accessing the system, a code must be entered. The particular code entered will automatically determine what functions are available to that user.

As a part of the general maintenance philosophy, built-in diagnostic tests are included in the system. Running of the complete set of tests requires the use of a sensor simulator in the test set to provide precise inputs for evaluation. A list of these tests is as follows:

- RAM Memory Test
- EPROM Test
- System Power Test
- Synthesizer Lock Test
- Sync Clock Test
- EAROM Memory Test
- Digital Port Test
- A/D Converter Test
- Multiplexer Test
- RTC Test (Real Time Clock)
- WDA Test (Wave Data Analyzer).

A single command will cause these tests to be run and a pass/fail indication will be readout on the terminal. In certain cases, additional information is provided. For example, if any of the four digital ports fail, the port and failure will be read out in the following format:

S-A=A5A5H R-A=0000H

The "S" means SENT. The "A" designates the failed port and may be A, B, C, or D. The A5A5H indicates the Hex data that was sent to the port. The "R" means RECEIVED. The "0000H" indicates the Hex data read from the port.

As configured for the C-MAN installations, the DACT system provides spare sensor input channels for expansion. A list of the sensor inputs is shown in Figure 3-2.

It should be noted that the values for analog channels 1 through 14 may be modified by a second-order equation of the form  $ax^2+bx+c$ . The values for a, b, and c may be entered by means of the test set or terminal. This permits great flexibility in the processing of a wide range of sensor inputs.

A 16-bit bidirectional digital port is provided with the capability of addressing four different devices. The specific utilization of this port is controlled by software.

A switch-closure type of digital input is implemented as an interrupt function. Potential use of this type of input might be a tipping bucket rain gage for example. This type of input would allow continued data collection independent of the normal data acquisition periods.

Two serial digital inputs are currently used to monitor the rate input from the compasses on the buoy systems.



ANALOG CHANNELS (16)			
CHANNEL	FUNCTION	INPUT	REMARKS
0	Battery Voltage	0-15V	$ax^2 + bx + c$
1	Spare	0-5V	
2			
3			
4			
5			
6			
7	Spare	0-5V	$ax^2 + bx + c$
8	Wind Dir A	0-5V	
9	Wind Dir B	0-5V	
10	Wind Sp A	0-20V	
11	Wind Sp B	0-20V	
12	Air Temp	Thermistor	
13	Ocean Temp	Thermistor	
14	Baro Press	0-10V	
15	Charger Current	0-0.1V	

DIGITAL CHANNELS			
(1)	16-bit parallel	- 4 addresses	- bidirectional
(1)	Switch Closure	- (Rain Gage)	- Interrupt
(2)	Serial Digital	- Rate	- Compass A & B
(1)	RS232		

Figure 3-2. Sensor Input Ports

Various uses for the RS-232 port of the DEU have been discussed. The primary purpose being to have access to the system by means of an external terminal.

#### 4. SOFTWARE

The software intensive nature of the DACT system is evident when considering that approximately 28K bytes of code are utilized in the current application. Organization of the software is in modules to facilitate changes, deletions, and additions. The Structure Chart in Figure 4-1 illustrates this approach.

Most of the software to control the NSC800 micro-processor is written in PL/M. The part not written in PL/M is written in Assembly language. The portions of the program in Assembly are the floating point algorithms and the software modules that link the floating point software with the PL/M source code. The program is stored in a set of Erasable Programmable Read Only Memories (EPROM's).

The DACT software is structured so the DACT can "time share". The three main functions of the DACT software are transmitting data, acquiring and processing data, and providing a user interface to the DACT system. The DACT software accomplishes this by continuously polling software flags which control the operation of the system. These flags are polled in the routine called SYSTEM CONTROL, whose relationship with the rest of the DACT software is illustrated in the Structure Chart.

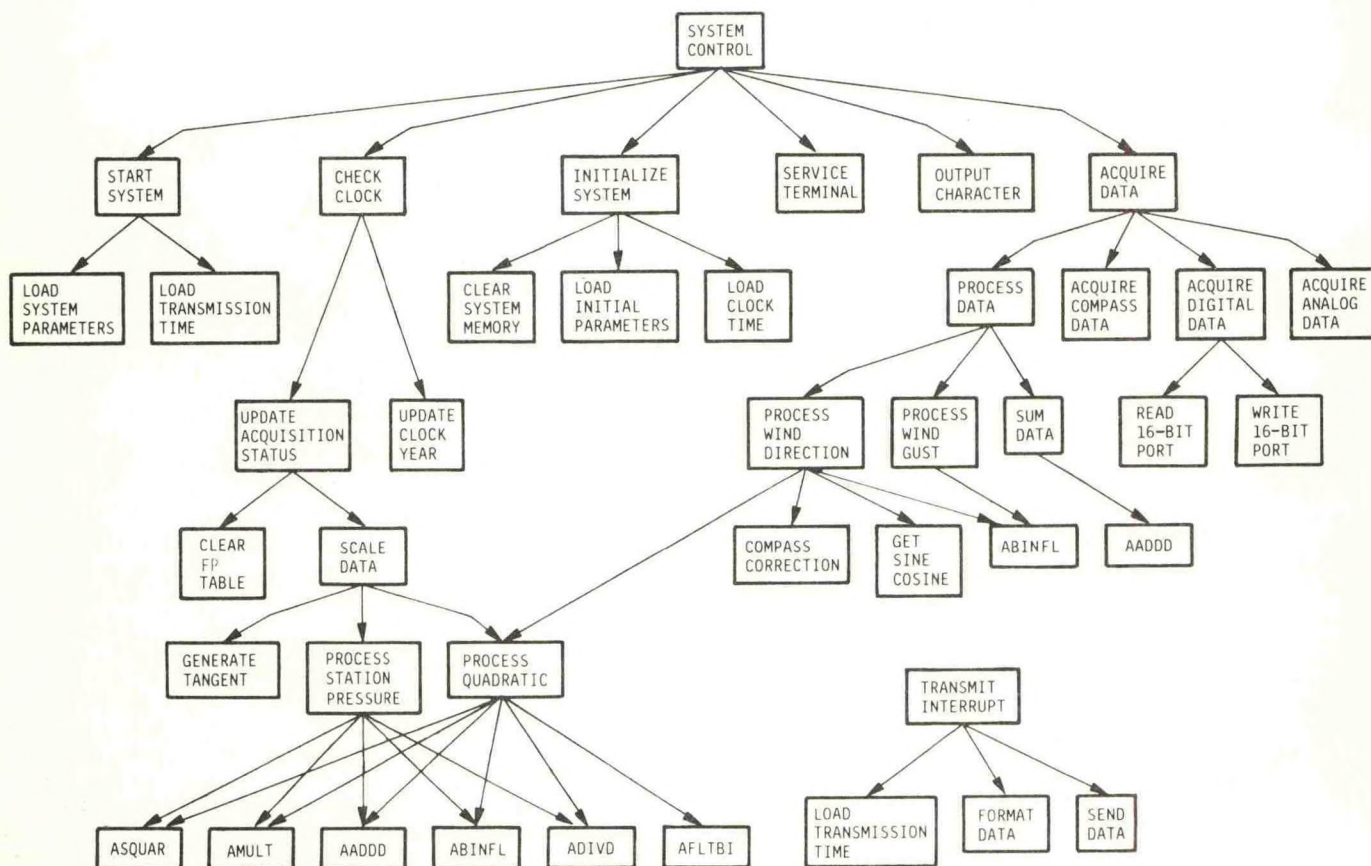


Figure 4-1. System Control, Structure Chart



The DACT Unit processes data as floating point numbers to achieve the best possible accuracy for each calculation. However, because some of the data from the sensors (wind direction and compass) is inter-related, special processing must be done to get the most accurate results.

For most of the analog sensors, the data is collected as a 12-bit sample, converted to floating point, either summed with or moved to the floating point data table, averaged, scaled, and then stored ready for formatting into a data message. The exception to this order of processing is wind direction. Wind direction inputs must be scaled, then combined with compass inputs to give a corrected wind direction. This value is then broken into its sine and cosine components. These values are converted to floating point numbers and then stored. When wind direction values are processed at the end of the acquisition cycle, the floating point numbers are converted to binary and the tangent is taken of the two components to give a wind direction in degrees. All sensor data is processed even if a sensor is not to be included in the output message.

The DACT Unit has a special algorithm that corrects for compass errors due to magnetic deviations caused by the metal buoy hulls. This algorithm is second-order linear fit of compass input data to a set of programmable input parameters. The user goes through a process of "spinning" the buoy and using the DACT to determine a set of correction parameters. These correction parameters are in the form of maximum, minimum, and zero positions, with deviation amplitudes of a 360° set of compass inputs. The DACT processes these inputs by doing an approximation of a sine wave to find the correction values. The sine wave that the data is collected from is generated by a linear fit of the maximums, minimums, and zero points, as well as a linear correction for inflection points of the linear fit (see Figure 4-2).

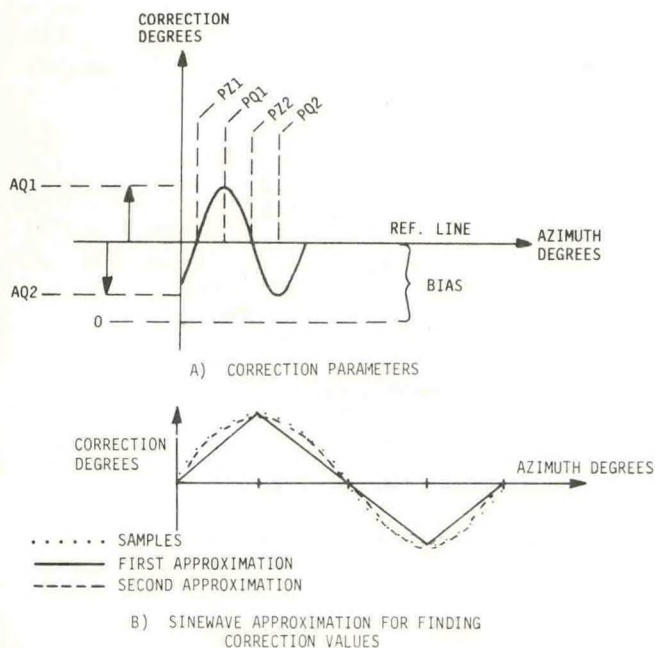


Figure 4-2. Compass Corrections

## 5. TEST SETS

To support the general maintenance philosophy, two types of test sets were provided on the DACT program: 1) the Field Test Set designed to be carried to the deployment site, and 2) the Bench Test Set (see Figure 5-1) for use at the maintenance facility. The two units are very similar, with the primary difference being the inclusion of an RF capability in the bench system.

The major components of the test sets are:

- RS-232 terminal with an LCD readout
- Hard copy printer
- Sensor simulator
- RF receiver for monitoring transmitted messages and measuring RF output power
- Telephone modem.

The RS-232 terminal contains a full ASCII keyboard, a 40-character readout and provides two-way communication with the DEU for the inputting of commands and variable parameters. Echoing of the input functions and the reading of outputs is possible by the two-line, 40-character LCD display. This unit also contains internal RAM memory with a capacity for 1600 characters.

A hard copy of the inputs and outputs of the DEU is available by selecting the built-in printer.

The sensor simulator provides known inputs for checking of the DEU functions. Five sets of simulated inputs may be selected for wind speed, barometric pressure, air temperature, sea surface temperature, and the analog channels. Four selectable input values are provided for the wind-vane angle and for the buoy heading.

Testing of the 16-bit parallel port is accomplished by the bidirectional transfer of simulated data with the appropriate handshaking and verification that valid transfers occurred. This test is done for each of the four possible port addresses.

The RF section of the Bench Test Set receives its input directly from the transmitter output of the DEU. The RF power meter provides a visual indication of the transmitter power output and once the test set receiver has achieved RF lock an LED indicator will light. A digital readout will indicate which of the GOES channels the DEU is transmitting on.

The received signal is demodulated and monitored for MLS sync, address and data. Once MLS sync is detected, the address and data are formatted for display on the LCD readout and printer.

Verification of the land-line communication mode is accomplished by means of the modem in the test set. The required ring signal is generated by the test set which activates the modem in the DEU. Communication is then established and the terminal is used to issue commands and receive responses over the modem.



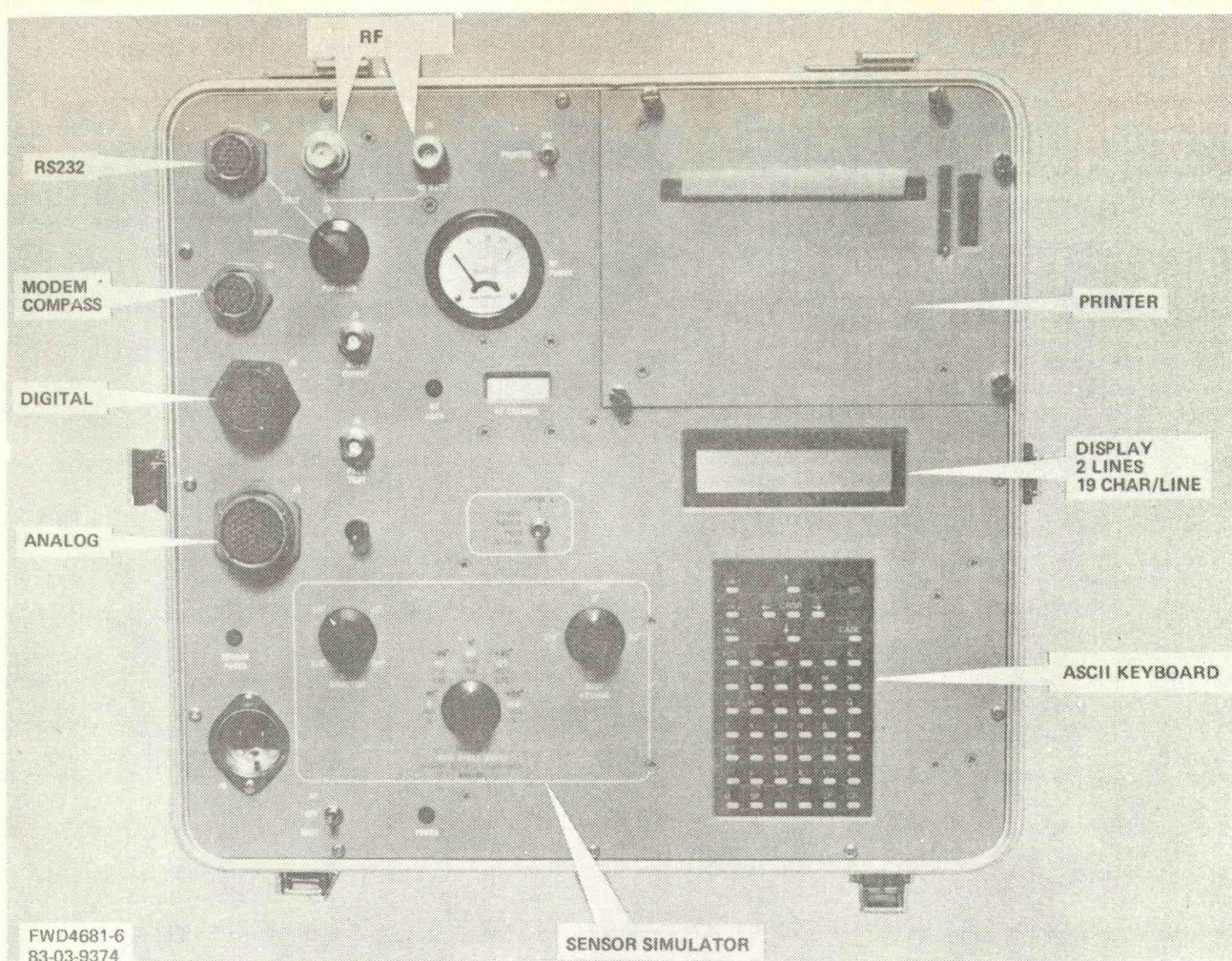


Figure 5-1. DACT EMI Test Summary

## 6. TEST PROGRAM

An inherent part of the test program is an extensive test requirement to verify the design and the hardware. During the prototype phase, a series of one-time tests were conducted which relate to proving of the design concepts. In addition, acceptance type tests were performed. These tests are carried forward to the production phase.

The test requirements are categorized into seven areas, namely:

- Design Proof
- Transportation and Handling
- EMI
- Temperature
- Functional
- 300 and 600-Hour Operational
- NDBC Field Evaluation.

The Design Proof tests are essentially tests to verify the implementation of certain design concepts and were performed on the first prototypes and the first production units of both configurations. There are 24 separate tests in this category and include such items as; system operation after a 20-day discharge of the batteries, EAROM non-volatile

ity, verification of the gust algorithm, and verification of the elevation correction algorithm to barometric pressure.

The Transportation and Handling tests consist of simulating shipping and handling conditions and determining their effects on the DACT equipment. The three specific areas are vibration, impact, and bench handling. A functional test is performed before and after being subjected to these tests. The procedure is specified in EIA Standard RS-414-A.

EMI tests were performed to determine the conducted and radiated susceptibility characteristics of the DACT. These tests included all of the major system components including sensors. A summary of these tests and the results are shown in Table 6-1. As a result of these tests, the barometric pressure transducer will incorporate special EMI features to eliminate potential susceptibility to RF fields at the operational sites.

Temperature tests are run at  $-40^{\circ}\text{C}$  and at  $+50^{\circ}\text{C}$ . Cycling is based on a 3-hour linear change to reach the desired temperature and a 3-hour soak at that temperature. A complete functional test is then performed.



Table 1. DACT EMI Test Summary

METHOD	TEST DESCRIPTION	INTERFERENCE TEST LEVELS	RESULTS
CS01	Conducted Susceptibility Tests at selected frequencies within the Range of 30 Hz to 50 kHz (+12 VDC Power Lead)	MIL-STD-461A Notice 1 Limits	Not Susceptible
CS02	Conducted Susceptibility Tests at selected frequencies within the range of 50 kHz to 400 MHz (+12 VDC Power Lead)	MIL-STD-461A Notice 1 Limits	Slight Susceptibility in Data Acq Mode @ 1.2288 MHz when interference signal was 0.4V above spec limit.
CS06	Conducted Susceptibility Tests using 6 to 10 PPS Spikes on +12 VDC Power Lead	MIL-STD-461A Notice 1 Limits	Not Susceptible
RS03	Radiated Susceptibility Tests - Electric Field, at selected frequencies within the range of 10 kHz to 10 GHz	6 V/M	Baro Pressure Susceptible Data Acq Mode @ six frequencies
CS01 CS02 CS06	Conducted Susceptibility Tests (above) repeated on the 115 VAC Charger Input High Lead	MIL-STD-461A Notice 1 Limits	Not Susceptible

of the equipment parameters and further detailed testing of system components continues. This extensive test program provides the basis for determining changes and enhancements to be incorporated before declaring the DACT system to be fully operational.

The normal Functional Test performed on every unit consists of 22 separate tests and provides a very comprehensive check of the system hardware and software. Portions of this test are run with the actual sensors and portions are run with simulated inputs. All communications modes are verified; GOES, telephone modem, and RS-232 terminal.

After successfully completing the foregoing tests, an on-the-air operational test is performed. This consists of placing the system in an operational configuration and transmitting through the GOES communications link. All of the prototype systems and the first two production systems were operated in this "hands-off" mode for a period of 600 hours. All remaining systems are operated for 300 hours.

After delivery of the four prototype systems to NDBC, a field evaluation program was initiated where the systems were tested under various actual and simulated field conditions. Extensive monitoring



# COHERENT DIGITAL DATA ACQUISITION SYSTEM (CODDAS)

Scott C. Daubin

Daubin Systems Corporation  
104 Crandon Blvd., Suite 315  
Key Biscayne, Florida 33149

## ABSTRACT

The Coherent Digital Data Acquisition System (CODDAS) is a compact, low power, light weight, low cost, modular underwater acoustic data acquisition system which performs the functions of (1) transient (shot) recognition, (2) spectral analysis, (3) time series sampling and (4) coherent demodulation. It records the processed data of these functions digitally on magnetic tape. The small size and weight of the instrument (7 in OD by 72 in LOA cylinder, 129 lbs in air, fully loaded) greatly simplify deployment and recovery, and expand the number of possible deployment platforms. CODDAS can be configured as a stand alone unit or as an element in an array of units, operating coherently. A Rockwell 6502 microprocessor, under stored program control, provides total operational flexibility to suit the needs of the user. 8 bit A/D sampling produces 42 dB of dynamic range in each gain state; four program controlled gain states, overlapped by 30 dB produce a total system dynamic range of 76 dB. The physical and data acquisition characteristics of CODDAS are presented.

## 1. INTRODUCTION

The Coherent Digital Data Acquisition System was developed in response to the requirement for an adaptable, modular, low cost instrument, contained in a small, light weight, air-droppable package. Although CODDAS can record any type of time series data, provided it is convertible to an electrical signal, it has proved its cost effectiveness in underwater acoustics research. Even though the data capacity of the CODDAS digital cassette recorder is less than 1% of that of the analog recorders of its predecessor instruments (ACODAC, PAR, VDABS), the advantages of a completely digital system are compelling; these include the handling ease resulting from the small size and weight and the complete operational adaptability provided by software control.

Design work on CODDAS began in 1980; it was first employed at sea in 1981. CODDAS has evolved from the Mod 0 unit (cylinder, 12 in dia by 48 in long, 265 lbs air wt) to the Mod 1 unit (cylinder, 7 in dia by 54 in long, 129 lbs air wt). The physical characteristics of the Mod 1 unit are shown in Table 1.

Table 1

CODDAS MOD 1 PHYSICAL CHARACTERISTICS

### DIMENSIONS:

OD . . . . .	7.00 in
ID . . . . .	5.75 in
L(CYL) . . . . .	54.00 in
LOA . . . . .	72.00 in

### WEIGHT:

#### WEIGHT IN AIR

IPV . . . . .	51 lbs
FITTINGS . . . . .	10 lbs
PAYLOAD	
BATTERY . . . . .	48 lbs
RECORDER . . . . .	5 lbs
ELECTRONICS . . . . .	7 lbs
MISC . . . . .	8 lbs
TOTAL PAYLOAD . . . . .	68 lbs
TOTAL WEIGHT IN AIR . . . . .	129 lbs
DISPLACEMENT IN SEA WATER . . . . .	76 lbs
WEIGHT IN SEA WATER . . . . .	53 lbs
MAXIMUM OPERATING DEPTH . . . . .	20,000 ft 6,100 m
IPV MATERIAL . . . . .	7075-T6 Al
BATTERY CAPACITY . . . . .	2,400 wh 100 ah @ 24 v

## 2. DATA ACQUISITION FUNCTIONS

CODDAS performs any combination of the data acquisition functions described below. Whether or not the function is implemented, and the values of the processing parameters, are under total software control.

o Transient Recognition and Recording - CODDAS recognizes the onset of a transient event, e.g. the signal from an underwater explosion, and without losing any data from the event, records a time series of the event 256 to 12,032 samples long.

o Spectral Analysis and Recording - CODDAS computes an N-point FFT of the ambient background at a predetermined repetition period, P, then averages S of these spectra prior to recording. The spectra can either be complex spectra or power spectra. Transient arrivals interrupt and preempt the spectral analysis.



• Time Series Reception and Recording - CODDAS receives and records a time series of data, varying in length from 256 to 12,032 samples.

• Coherent Demodulation and Recording - CODDAS derives and records the complex demodulates of a narrow band signal whose center frequency is  $\frac{1}{4}$  the sampling frequency.

• Internal Calibration - CODDAS conducts an internal calibration at a predetermined periodic interval. During this calibration a series of DC voltages at the system input place the system in each of its 4 gain states.

• Coherent Interunit Processing - By working on a common time base, a number of CODDAS units process data coherently.

The data acquisition characteristics of CODDAS Mod 1 are outlined in Table 2.

Table 2

#### CODDAS MOD 1 DATA ACQUISITION CHARACTERISTICS

Number of Input Channels . . . . . 1 to 16

Typical Processing Parameters:

Sampling Rate . . . . . 800 Hz

Low Pass Filter Cutoff Frequency . . 300 Hz

Rejection Rate . . . 45 dB/oct

Standard Time Series Duration . . 15.04 sec

Tape Length . . . . . 450 ft

Recording Density . . . . . 800 bpi

Number of Recording Channels . . . 4

Total Recording Capacity . . . . 15x10<sup>6</sup> bits

Power Spectral Resolution Options:

. . . 12.5, 6.3, 3.1, 1.6 Hz

Gain State Ranges:

State No.	Acoustic Level (dB re $\mu$ Pa)		CODDAS Input Level (dB re volt)		Dynamic Range (dB)
	Max	Min	Max	Min	
23	133	92	-01	-42	41
22	122	80	-12	-54	42
21	109	68	-25	-66	41
20	99	57	-35	-77	42
0A	133	57	-01	-77	76

Recording Space Requirements:

KBytes No/Tape Steps

450 ft Tape . . 1,875 1(450) 4,320,000

300 ft Tape . . 1,250 1(300) 2,880,000

Standard Time Series:

. . 12.664 170(450) 25,328

. . 12.664 113(300) 25,328

Power Spectrum (256 point, 16 bit resolution):

. . 0.589 3,667(450) 1,178

. . 0.589 2,444(300) 1,178

Typical Mission Profiles:

Duration (Days)	1	1	5	5	10	10	30	30
No. Calib. . .	4	4	20	20	40	40	120	120
No. Shots . .	166	161	150	107	130	85	50	-
No. Spectra .	0	96	0	480	0	960	0	1075

Figures 1 and 2 show examples of a transient time series and an averaged power spectrum of the ambient noise, respectively.

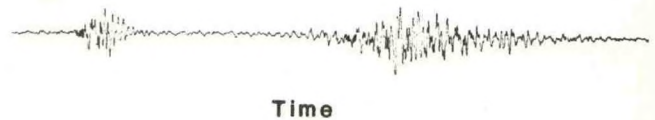


Figure 1 - CODDAS Transient Time Series Segment

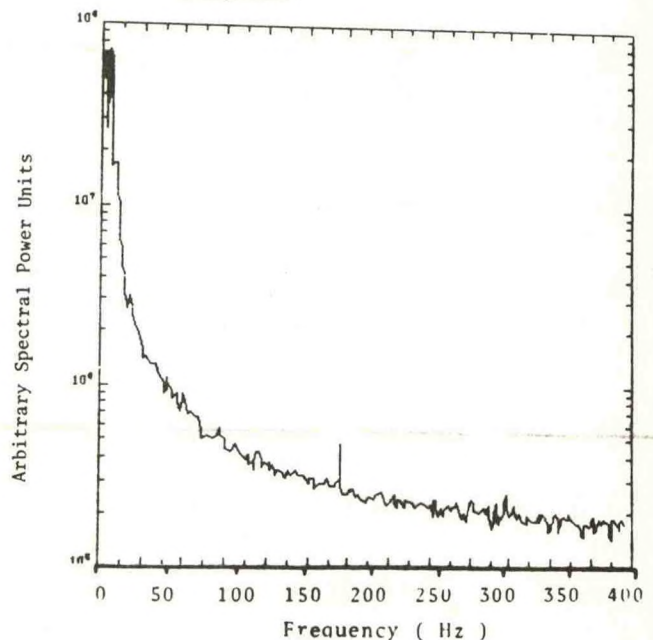
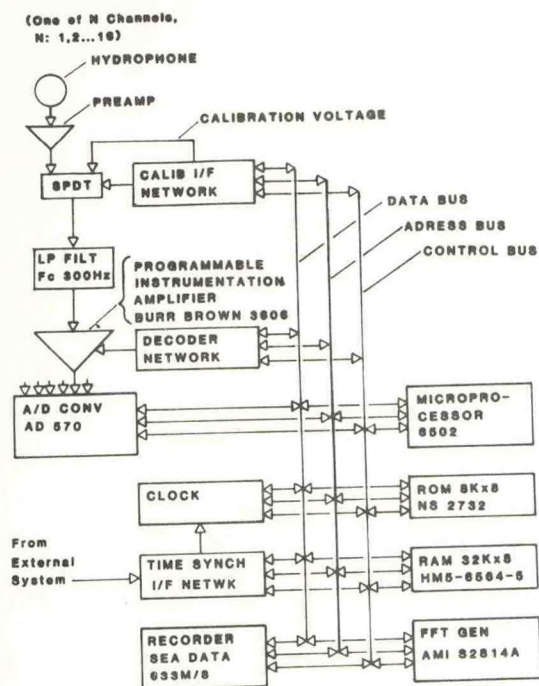


Figure 2 - CODDAS Power Spectrum  
(From 23 512 Pt. FFTs  
Averaged, 1.56 Hz Res.)

### 3. SYSTEM DESCRIPTION AND OPERATION

Figure 3 shows a functional block diagram of CODDAS Mod 1. Signals arriving from 1 to 16 hydrophones (or other sensors) are processed via the input low pass filter, the gain ranging amplifier, are digitized by an 8-bit A/D and are temporarily held in RAM. For each 256 or 512 point time series, the system (1) determines the average absolute value of the signal and thereby makes a decision as to what gain state is to be set for the reception of the next 256 or 512 point time series, and (2) based on the average energy in the most recent 128 measured points, compared with the energy of previous 128 points, makes a decision as to whether a transient has arrived. If the decision is "no", the measured points are





**Figure 3 - CODDAS Mod 1**  
**Functional Block Diagram**

wiped out, if they are not to be used for a scheduled power spectral computation, or other purpose. If the decision is "yes", the time series is accumulated until typically 12,032 points have been logged. At 800 Hz, that process requires 15.04 seconds. When one of the two buffers is filled with 12,032 data points, the data are written to tape. During the writing process, which requires approximately 57.83 seconds, data can continue to be accepted and stored in the second buffer. A 450 foot cassette tape, recording at a density of 800 bpi, can hold up to 170 of such data files.

Gain ranging is required because the dynamic range of the 8 bit A/D is only 42 dB and the required dynamic range for acoustic research is about 76 dB (minimum signal, 57 dB re  $\mu\text{Pa}$ ; maximum signal, 133 dB re  $\mu\text{Pa}$ ). Four gain states are provided, with an approximately 30 dB overlap. In each recorded time series data file of 12,032 data points, the first data record is the header record, which contains time and date and the gain state code of each 256 or 512 point time series in the file.

The AMI S2418A chip computes a 32 point FFT. By combining these mini-spectra according to an internal butterfly algorithm, the chip produces FFT's of N points ( $N = 32, 64, 128, 256$  or  $512$ ), containing N real coefficients and N imaginary coefficients. In generating a power spectrum each corresponding pair of real and imaginary points are squared and summed. This function is implemented external to the S2814A chip, but will be accomplished internally in follow-on chips. A

512 point FFT thus produces a 256 point power spectrum. At an 800 Hz sampling frequency this spectrum will extend to 400 Hz, with a resolution of 1.56 Hz. These coefficients are in linear energy units and may be averaged together before writing to tape.

Coherent demodulation requires sampling at a rate four times the center frequency of the line to be processed. If this function is to be implemented, the signal first passes through a narrow bandpass filter, not shown in Figure 3. The sampling time series is polarized as follows:  $+-+--+$  etc. All odd samples are averaged to produce the coincident component and all the even samples are averaged to produce the quadrature component. The effective processing bandwidth is the inverse of the averaging time.

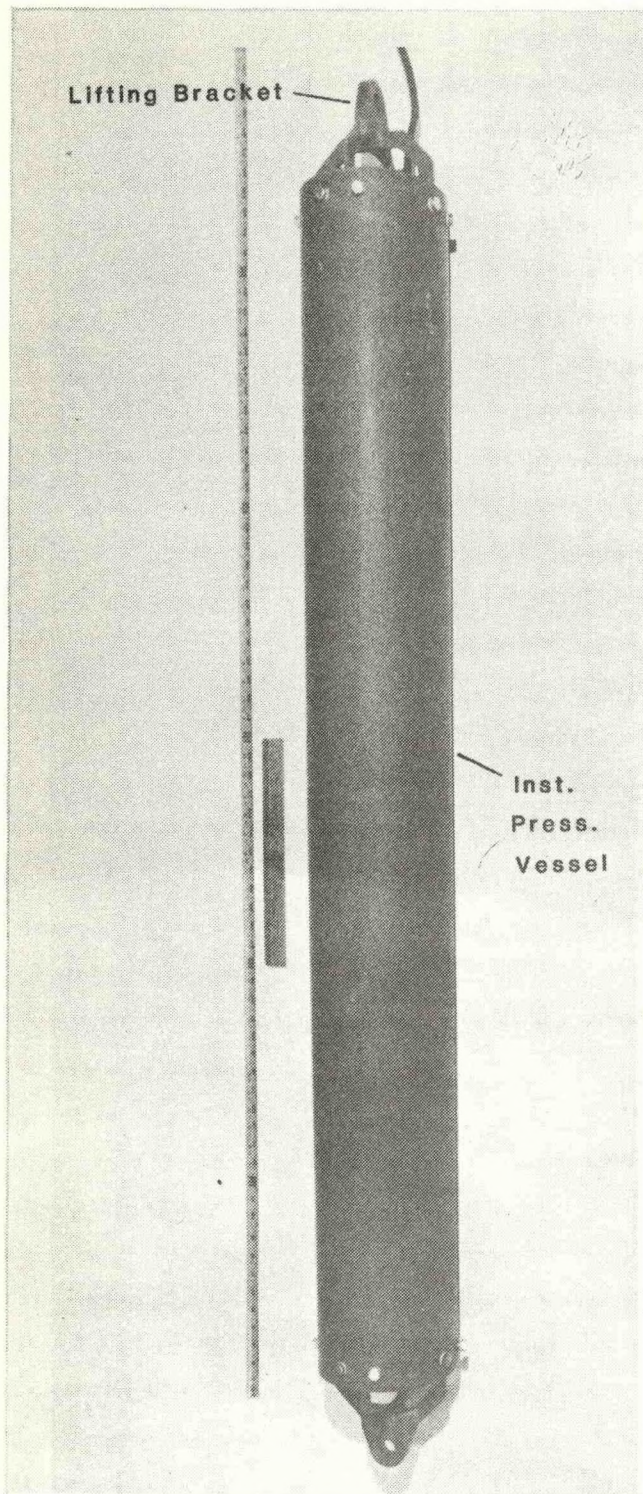
Coherent interunit processing requires that the clocks in each CODDAS unit be synchronized to at least  $3^\circ$  in phase at the highest frequency to be processed. At 300 Hz, this represents a maximum drift of  $27.8 \mu\text{sec}$ . A 36 kHz synchronizing signal ties together all CODDAS units operating coherently. The Time Synchronizing Interface Network Board measures the times of positive axis crossings of this 36 kHz signal and from this produces synch pulses which maintain the clock within the drift limits.

#### 4. MECHANICAL

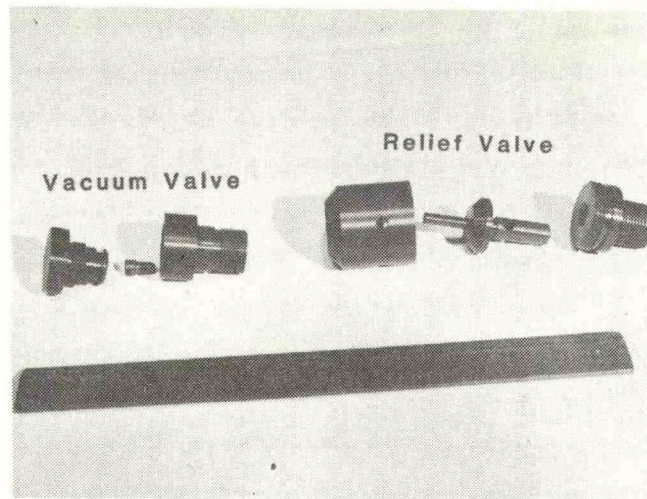
Figure 4 shows the assembled CODDAS Mod 1. In this arrangement, the hydrophone is mounted externally. In another configuration option, the hydrophone may be attached directly to the CODDAS unit, interior to the lifting bracket. CODDAS is intended to be integrated directly in the mooring. The lifting bracket, which is designed for a tensile load of 3,750 lbs with a safety factor of 4, places no load on the end caps. A relief valve, shown in Figure 5, located on the lower end cap of the IPV, protects personnel and equipment from any buildup of internal pressure due to battery outgassing. Evidence of relief valve actuation is immediately apparent by extension of the guide stem beyond the valve housing. Prior to deployment, the units are pumped down to a vacuum of about 28 in of Hg, then backfilled with dry nitrogen to about 15 in of Hg. This serves two purposes: (1) ability to hold a vacuum insures watertightness and (2) dry internal atmosphere prevents condensation at the cold depths of the ocean, thus protecting electronics. Vacuum connections are made at the vacuum valve, an exploded view of which is shown in Figure 5.

Figure 6 shows the details of the lifting bracket and end cap, assembled on the upper end of CODDAS. Figure 7 shows the upper portion of the electronics frame. The tape transport and electronic board socket connectors are evident. Mechanically the basic electronics are divided into seven boards: the analog board, A/D board, CPU board, RAM board, FFT board, tape I/F and timer board and clock board. If Coherent Interunit Processing (CIP) is to be implemented, an additional board, Time Synch I/F Network board, is used. The top of the main battery space is also seen.

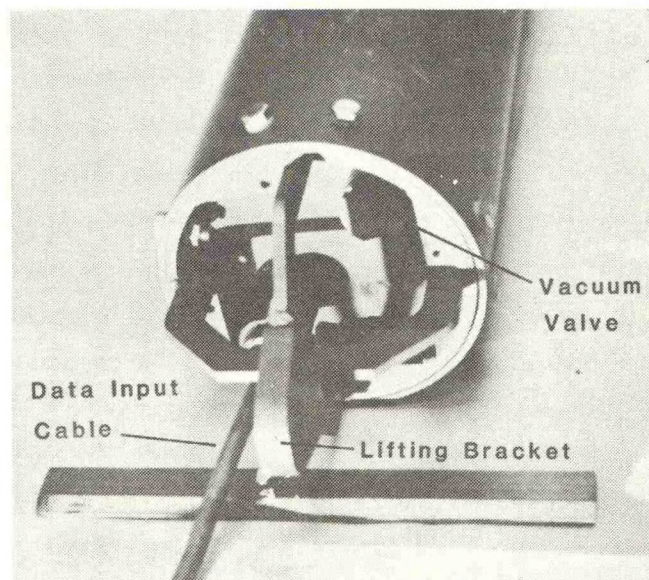




**Figure 4 - CODDAS Mod 1  
Mechanical Assembly  
(Ext. Hyd.)**

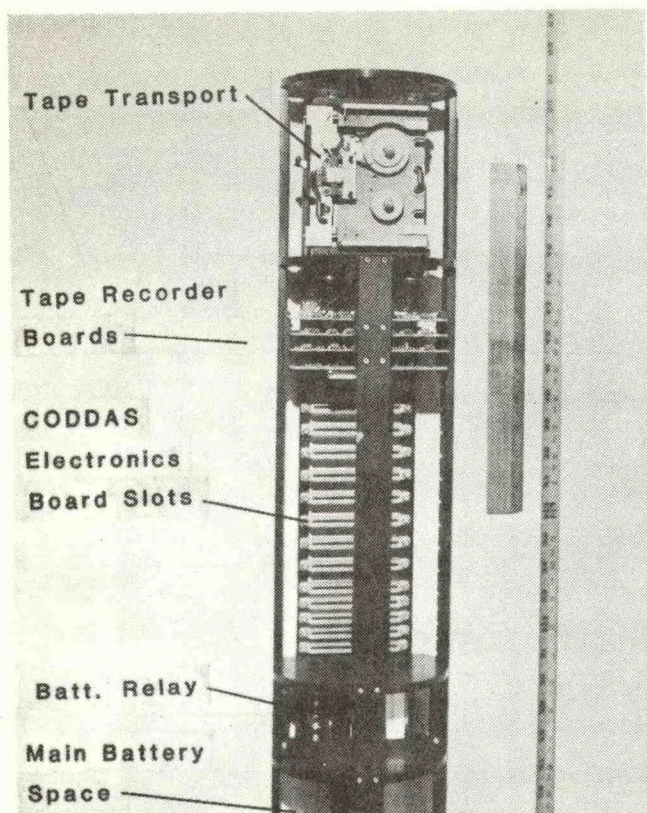


**Figure 5 - Vacuum & Relief Valves**



**Figure 6 - CODDAS Mod 1  
Mechanical Assembly  
(Ext. Hyd.)  
Upper End Details**





**Figure 7 - Coddas Mod 1  
Electronics Frame (Upper End)**

#### 5. DEPLOYMENT

Due to its compact size and light weight, Coddas can be deployed from small craft as well as larger vessels. It can also be packaged for air deployment. Coddas is designed for handling in the field by personnel unskilled in electronics. The internal clock operates from its own battery and requires no setting or synchronization at sea. To prepare the system for deployment, the technician merely has to remove a shorting connector in the hydrophone input cable and attach the hydrophone connector in its place. This starts the Coddas program, which provides a predetermined time delay before data processing commences; this time delay allows for the deployment time and settling time of the system. Should deployment be aborted, replacement of the shorting connector resets the program.

Coddas was developed under the auspices of the SEAS project of the Naval Ocean Research and Development Activity, under Office of Naval Research Contract No. N00014-77-C-0147.



# HYDRODYNAMIC PERFORMANCE EVALUATION OF A NEWLY DEVELOPED KEVLAR ROPE FAIRING

Darrell A. Milburn

Naval Ocean Research and Development Activity  
Ocean Technology Division  
NSTL Station, Mississippi 39529

## ABSTRACT

The strumming and drag performance of a newly developed Kevlar rope fairing have been determined experimentally. In one experiment, faired and unfaired rope samples of the same diameter were towed with one end free to obtain their normal and tangential drag coefficients. Results of the experiment are plotted versus Reynolds number and show that the fairing increases cable drag substantially. In another experiment the ropes were towed with a heavy, streamlined body attached. By comparing their resonantly excited tension fluctuations, it is found that the fairing reduces flow-induced cable vibrations significantly. Strum suppression effectiveness of the fairing has also been confirmed through acoustic measurements made at sea.

## INTRODUCTION

Marine cables exposed to ocean currents are subjected to periodic transverse and longitudinal motions caused by vortex-induced forces. This phenomenon, called strumming, can reduce cable fatigue life, increase cable drag, and cause measurement errors in attached sensors--especially hydrophones. Experimentally, it is well known that strumming can be reduced or suppressed altogether by attaching devices to the cable [2]. This, in turn, has led to the development of various types of devices. Some examples, which are more commonly referred to as fairings, are shown in Figure 1. A hydrodynamic evaluation of these and other types of fairings is available in [4] and [5].

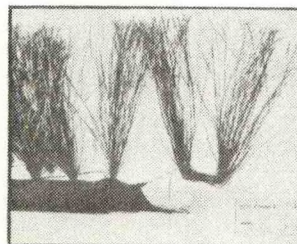
In this paper a more recent fairing, developed by Wall Industries, Inc., is described. Because of its simplicity, low cost, and potential durability, it was selected for test and evaluation.

To answer the question about its hydrodynamic performance, two experiments were conducted in the high speed tow basin at the David Taylor Naval Ship Research and Development Center. One experimental objective was to determine the strum suppression effectiveness of the fairing, and the other to measure the effect of the fairing on cable drag. The results of those experiments are contained herein. Presentations also include the theoretical basis of each experiment and a description of the experimental setups and procedures.

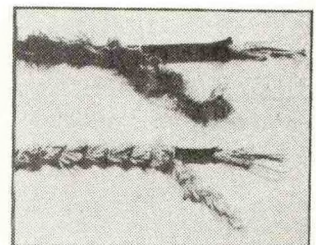
## TEST SAMPLES: A DESCRIPTION

The fairing developed by Wall Industries, Inc., is shown in the photograph of Figure 2. Basically, it consists of loops of nylon yarn which are stitched to the rope jacket. The stitching runs continuously along the jacket on three nearly parallel lines about 120 degrees apart. Two of the three stitch lines can be seen in the photograph. The length of the loops varies between 1 and 1-1/2 times the rope diameter.

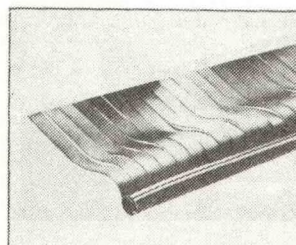
Two 30.8 m long rope samples were available for the experiments: One was faired, the other was not. Both have about a 7.9 mm (5/16 inch) diameter and are a Kevlar Miniline construction. Miniline is a registered trademark of Wall Industries, Inc., and Kevlar a registered trademark of E.I. DuPont de Nemours and Company. The Kevlar strength member in each rope is covered with a tightly braided, polyester jacket. A short length of each sample is shown in Figure 2.



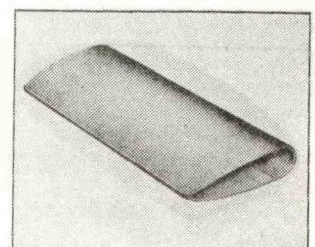
FRINGE



BRISTLE (TOP) AND BRUSH



RIBBON



STREAMLINED, CLIP-ON TYPE

Figure 1. Various types of cable fairings.



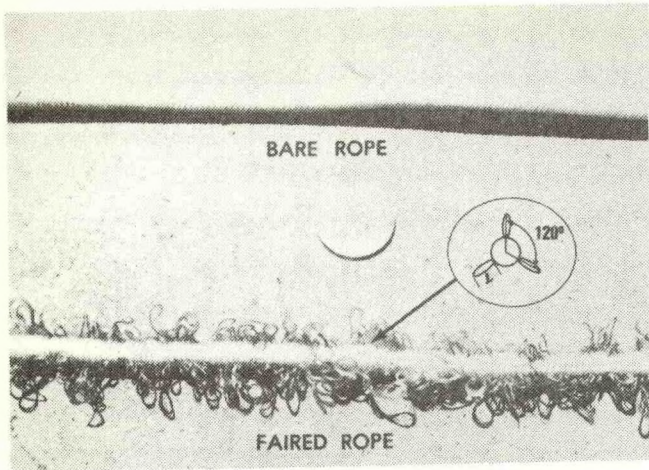


Figure 2. Photograph of Kevlar rope samples. A cross-sectional view of the faired rope is shown encircled.

### CABLE DRAG EXPERIMENTS

**Towing Theory.** The cable drag experiments are based on a two-dimensional, steady-state model of a cable subjected to fluid flow. The model, as developed by Pode [3], assumes that all forces and the cable are coplanar. It also assumes that flow is constant and uniform with depth, and that the cable is inextensible and perfectly flexible.

Under these conditions, the equilibrium equations of the tow cable are given by [1,3,6] as

$$T \frac{d\phi}{ds} = -F_n + w \cos \phi \quad (1)$$

and

$$\frac{dT}{ds} = F_t + w \sin \phi \quad (2)$$

Here  $T$  is cable tension,  $w$  is cable weight per length,  $\phi$  is cable angle, and  $s$  is a measure of cable length. Parameters  $F_n$  and  $F_t$  are the hydrodynamic loading functions. For round cables they are defined [1,6] as

$$F_n = 1/2 \rho C_n d (V \sin \phi)^2 \quad (3)$$

and

$$F_t = 1/2 \rho C_t \pi d (V \cos \phi)^2 \quad (4)$$

where  $\rho$  is fluid density,  $d$  is cable diameter, and  $V$  is flow speed. The terms  $V \sin \phi$  and  $V \cos \phi$  are, respectively, the flow speed components normal and tangential to the cable. Normal drag coefficient is represented by  $C_n$  and tangential drag coefficient by  $C_t$ .

In this approach the drag coefficients are considered as functions of the following velocity component Reynolds numbers,  $R_n$  and  $R_t$ :

$$C_n \propto R_n = d V \sin \phi / \nu \quad (5)$$

and

$$C_t \propto R_t = d V \cos \phi / \nu \quad (6)$$

where  $\nu$  is the kinematic viscosity of the fluid.

When a uniform cable is towed without attached bodies, its configuration is a straight line [3]. Thus,  $d\phi/ds = 0$  and equation (1) can be recast using equation (3) as

$$C_n = (w \cos \phi_c) / (1/2 \rho d V^2 \sin^2 \phi_c) \quad (7)$$

where  $\phi_c$  is called the critical angle [3]. On substituting equation (4) into equation (2) and integrating the result from  $s=0$  to  $L$ , the equation for the tangential drag coefficient becomes

$$C_t = T^*(1 - w \sin \phi_c / T^*) / (1/2 \rho \pi d V^2 \cos^2 \phi_c) \quad (8)$$

Here,  $T^* = T_1/L$  where  $L$  is cable length and  $T_1$  is cable tension at the tow point  $s=L$ . At sufficiently high speeds, cable angle will become small enough and cable tension large enough so that  $\cos \phi_c \approx 1$  and  $w \sin \phi_c / (T_1/L) \approx 0$ .

**Setup and Procedures.** The cable and environmental characteristics in equations (7) and (8) will be known. Thus, for a given towing speed an experimental measure of cable angle and towing tension will provide values of the cable drag coefficients. This suggests one experimental setup. But to minimize errors, however, two experiments were conducted: One to determine values of  $C_t$  versus  $R_t$ ; and the other to determine values of  $C_n$  versus  $R_n$ . Both are illustrated in Figure 3.

In the tangential drag experiment, each 30.8 m long sample was freely towed at constant speeds of 0.515 m/s (1.00 knots) to 2.575 m/s (5.00 knots) in increments of 0.515 m/s. For each speed, or run, voltage output from a tensiometer located at the tow point was recorded. Three sets of runs were made for each rope sample. After completing this experiment, each sample was cut to obtain a 6.1 m long piece. These shorter length samples were then freely towed at constant speeds of 0.129 m/s (0.25 knots) to 0.515 m/s in increments of 0.129 m/s. This series of runs comprised the normal drag experiment. Because of the slower speeds, shorter cable lengths were required to prevent dragging on the bottom of the tow tank. In the normal drag experiment the towed samples were photographed through an observation window located in the tow basin wall to obtain a measure of their towing angles. Such photographs were not taken in the tangential drag experiment.

In both experiments the rope samples were secured to the towing strut with a piece of string. Therefore, orientation of the fairing to the flow is not known. To minimize boundary effects, the tow point on the strut was submerged about 0.3 m. Speed of the tow carriage was adjusted to within  $\pm 0.5$  cm/s of that desired, and water temperature was measured to



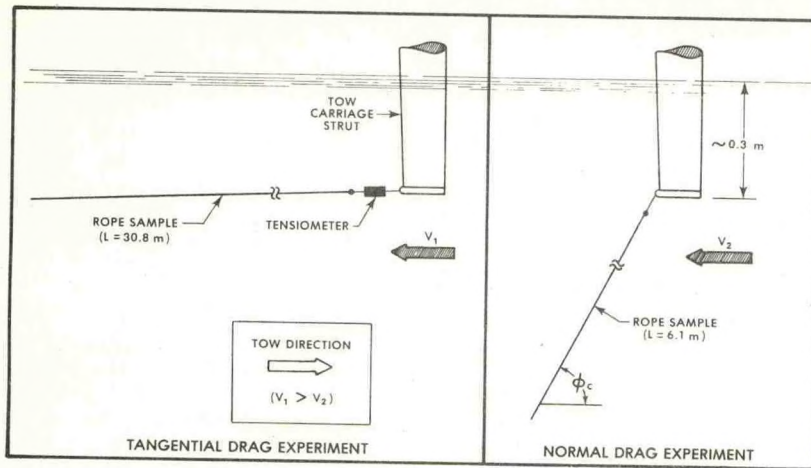


Figure 3. Experimental setup for the cable drag measurements.

determine water density and kinematic viscosity. Rope samples were thoroughly soaked before conducting the experiments to insure a stable cable weight.

Diameter, length and weight of each rope sample were accurately measured. Because entrapped air was a potential source of error, each rope sample was weighed while wet at predetermined time intervals. After their weights stabilized, samples were removed and allowed to dry. This procedure was repeated three times to obtain an error estimate based on the standard deviation of the measurements.

The procedure for calculating the cable drag coefficients can now be outlined. Values of normal drag coefficient are first determined from equation (7). With  $C_n$  known equation (7) is used to calculate the critical angle for each towing speed used in the tangential drag experiment. These results and the corresponding tension measurements are then used to calculate tangential drag coefficients from equation (8).

**Discussion of Results.** No appreciable, if any, rope vibration was observed during the drag experiments. Each sample also appeared to tow in the vertical plane defined by the directions of tow and gravity. Figure 4, which is comprised of the photographs taken during the normal drag experiment, gives the measured critical towing angles. And Table 1 gives the measured characteristics of the rope samples.

The bare rope was found to fit a straight line reasonably well for each tow speed. This was not the case for the faired rope, however. Instead, the shape of the faired rope was best fit by two straight line segments at the three lowest tow speeds. This can be seen in Figure 4, and is probably caused by non-uniform orientation of the fairing to the flow. If so, then the normal drag coefficient and, hence, cable angle would vary along the rope. Despite the cause, however, the effect was significantly reduced at 0.515 m/s. This might be expected since equation (1) shows that angular changes are inversely proportional to the cable tension which increases with towing speed.

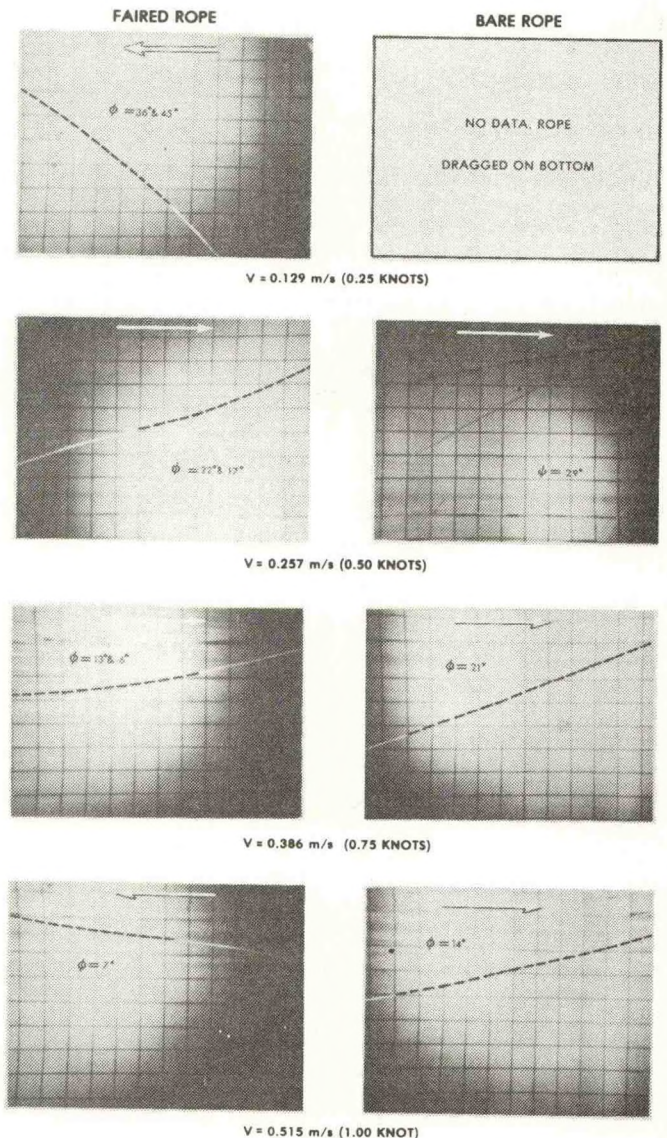


Figure 4. Photographs of rope samples freely towed in the normal drag experiment. Note the dotted lines mark the cable shape.



Table 1 --- Measured Rope Sample Characteristics

Characteristic	Bare Rope	Faired rope
Diameter, mm	8.3	7.8
Weight in water, N/m	0.108	0.098
Mass, kg/m	0.055	0.050
Length, m		
• Normal drag exp.	6.1	6.1
• Tang. drag exp.	30.8	30.8

A normal drag coefficient was calculated for each angle given in Figure 4. Hence, each segment of the bilinear-shaped faired rope is treated as a freely towed rope. The computed normal drag coefficients are plotted against Reynolds number in Figure 5. The solid line curve shown is an experimentally derived relationship for a perfectly smooth, circular cylinder. Because the bare rope is not perfectly smooth, it is not surprising to find that its data lies above the solid line. The three data points for the bare rope suggest a normal drag coefficient of 1.5 for Reynolds numbers between 950 and 1300. A dependence on Reynolds number is also suggested.

Normal drag coefficient data for the faired rope shows a negative gradient somewhat similar to the Vandiver and Pham data shown in Figure 5. The

Vandiver and Pham data is for the fringe fairing shown in Figure 1, and is given to show the effect of fairing angle of attack on normal drag coefficient. For Reynolds numbers between 550 and 850 the centroid of the data suggests a normal drag coefficient of about 3.6. This is nearly 2-1/2 times greater than that of the bare rope. Such a comparison, however, does not consider the effect of increased drag caused by a strumming bare rope. In particular, Griffin et al. [2] give data that shows the effective normal drag coefficient for a vibrating bare rope can be 1-1/2 to 3 times greater than that of a non-strumming bare rope.

Figure 5 also gives the computed tangential drag coefficients plotted against Reynolds number. Theoretically derived data for a perfectly smooth and rough circular cylinder are also given for purposes of comparison. It can be seen that the bare rope data lies between these two curves as expected. The tangential drag coefficient data for the faired rope exhibits a dependence on Reynolds number. This dependence is not apparent for the bare rope data which varies between 0.007 and 0.009. Such dependence is probably due to the fairing. The tangential drag coefficients given for the faired rope are, depending on Reynolds number, about 4 to 10 times greater than those of the bare rope.

**Experimental Error.** The method used to measure normal drag coefficients is simple and comparatively inexpensive. But with these advantages come several drawbacks. First and foremost is the experimental

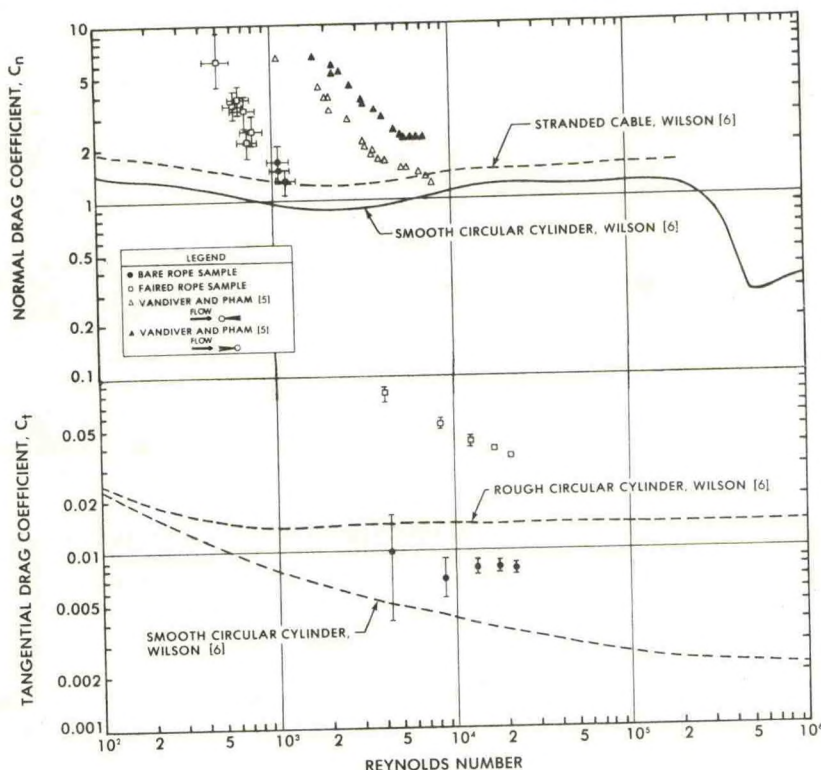


Figure 5. Drag coefficients versus Reynolds number.



error. This error is indicated in Figure 5 for each data point. The most significant error comes from the error in the measurement of cable angle. To examine this effect, differentiate equation (7) while holding constant  $\rho$ ,  $d$ , and  $V$  which were accurately measured. Dividing the resulting equation by equation (7) then gives

$$\frac{\Delta C_n}{C_n} = \frac{\Delta W}{W} + \alpha_1 \Delta \phi_c \quad (9)$$

where  $\Delta$  is the variational symbol and  $\alpha_1$  is a function of critical angle, plotted in Figure 6.

The variation found in the measured quantities are  $w = \pm 0.05 w$  and  $\phi_c = \pm 1^\circ$ . Therefore, the error contribution due to cable weight is about 5%. Error contributions due to cable angle can be estimated from Figure 6. For example, a  $45^\circ$  angle contributes a 5% error and a  $6^\circ$  angle about a 33% error.

Another drawback of the method is the narrow range of Reynolds numbers over which normal drag coefficients can be measured for these lightweight cables. Not knowing the angle of attack of the fairing to the flow and the questionable validity of the

sine-squared relationship, given in equation (3), for shallow towing angles are some other drawbacks.

Errors in the tangential drag coefficients are best explained by the following sensitivity relation

$$\frac{\Delta C_t}{C_t} = \alpha_2 \frac{\Delta T_1}{T_1} + \alpha_3 \frac{\Delta W}{W} - \alpha_4 \Delta \phi_c \quad (10)$$

which was derived in the same manner as equation (9). Here  $\alpha_2 = 1 + \alpha_3$  and  $\alpha_3$  and  $\alpha_4$  are functions of critical towing angle. Plots of  $\alpha_3$  and  $\alpha_4$  are given in Figure 6 and show that errors due to variations in cable weight and angle become small at shallow towing angles. Towing speed for the bare rope sample is given by the dashed-line curve in Figure 6.

#### CABLE STRUMMING EXPERIMENT

**Approach.** The plan here is to resonantly excite the two test samples by vortex shedding. This is done by matching the natural frequency of the test samples with their vortex shedding frequency. Then, by comparing their resonant response, an evaluation of the fairing is obtained.

The experimental setup is illustrated in Figure 7. Such an arrangement is intended to approximate a taut cable fixed at both ends. To accomplish this, the mass of the attached body shown must be large compared to that of the cable. In the setup shown, body mass is about 180 times greater than the cable mass. The body is also streamlined to reduce drag, and therefore cable catenary. Rope sample length is 4.5 m, a maximum based on the depth of the tow tank.

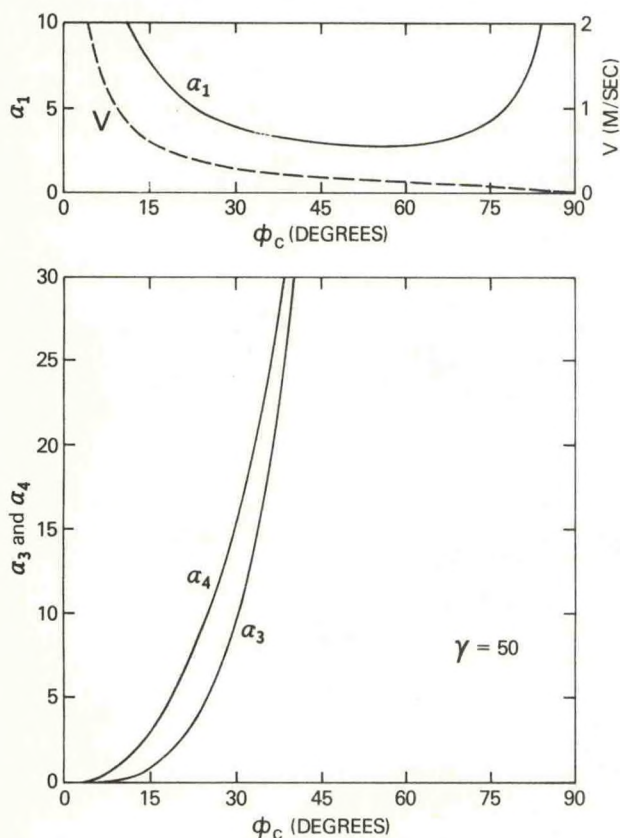


Figure 6. Sensitivity relation coefficients versus towing angle. The dash-line curve gives tow speed estimates for the bare rope sample.

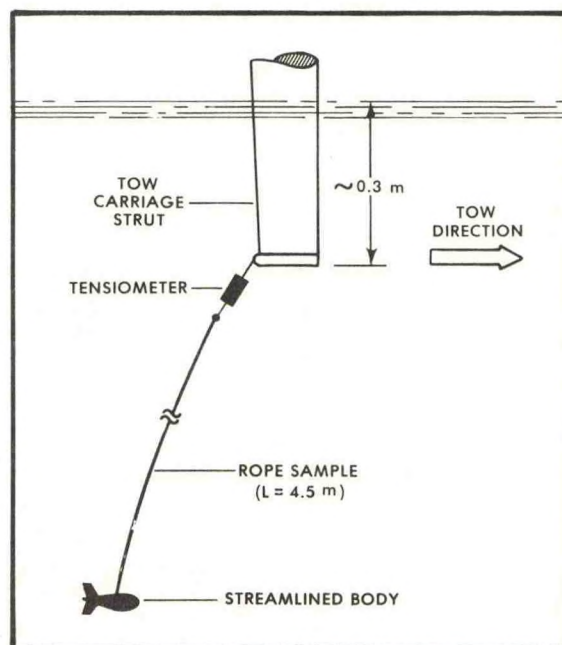


Figure 7. Experimental setup for the cable strumming measurements.



Experimental studies have shown that the natural frequencies  $f_k$  of a taut cable are reasonably estimated from the classical string equation

$$f_k = (k/2L) (T_1/M)^{1/2} \quad (11)$$

where  $k$  is the vibration mode number,  $T_1$  is the average cable tension and  $M$  is the virtual mass of the cable (mass plus added mass). If a periodic force is applied to the cable or its supports, then the cable will oscillate, after the decay of transients, at the excitation frequency. And if the frequency of the applied force coincides with the natural frequency of the cable, then resonance occurs.

There now remains the question of estimating the frequency of vortex shedding. It is well known [2] that the vortex shedding frequency  $f_s$  from a circular cylinder positioned normally to the flow is given by

$$f_s = S V/d \quad (12)$$

where  $S$  is the Strouhal number,  $d$  is the cylinder diameter, and  $V$  is flow velocity. The value of  $S$  is about 0.2 for Reynolds numbers between 400 and  $10^5$ . Towing speeds which might produce resonance in the bare rope were estimated by setting  $f_s = f_n$  and solving for  $V$ .

Because vortex shedding produces periodic side forces in the cross-flow direction, it is usual to think of vibrations normal to the incident flow. But there is also an in-line component of periodic force which has frequency  $2f_s$  and is proportional to the square of the transverse cable displacement [2]. In

the experiment in-line force was measured since it was simpler than measuring transverse cable displacement. This was accomplished by attaching a tensiometer at the tow point shown in Figure 7.

To obtain the tension measurements, the towing carriage was slowly accelerated from 0 to 2.6 m/s (5 knots) and then slowly decelerated to rest. During this run, tension fluctuations and carriage speed were simultaneously recorded on a strip chart recorder. Two sets of runs were made for each rope sample.

**Resonant Response Characteristics.** Resonance in both rope samples appeared to start at about 0.1 m/s. At about 0.2 m/s tension amplitudes in both reached peak values: About 12 N for the bare rope and 4 N for the faired rope. Tension fluctuations in both were nearly sinusoidal with about a 9 Hz frequency, which indicates a resonant lock-in phenomenon. This suggests a strumming frequency of about 4-1/2 Hz and about a 40% reduction in strumming amplitude for the faired rope.

As speed was increased from 0.2 to 1.6 m/s, the bare rope responded at three higher resonant cable vibration modes: The second mode with a 14 Hz strumming frequency at about 0.8 m/s; the third mode with a 19-1/2 Hz strumming frequency at about 1.1 m/s; and, the fourth mode with a 27 Hz strumming frequency at about 1.6 m/s. The tension fluctuations for these modes were not as steady as those found for the first mode. This can be seen in Figure 8 where selected tension fluctuation data are shown. At speeds above 1.6 m/s the tension fluctuations and frequencies of the bare rope were severe, indicating that the natural vortex shedding frequency is outside the wake synchronization range.

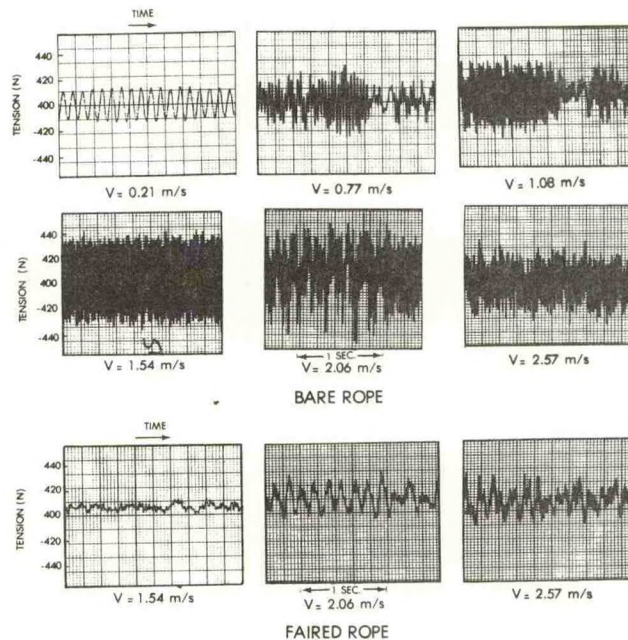


Figure 8. Tension fluctuation data for the rope samples.



In contrast, the faired rope did not respond resonantly at any of the higher cable vibration modes. Instead, at speeds above 0.2 m/s, its tension fluctuations were irregular and much less severe as shown in Figure 8. It is conjectured that the fairing increases damping and disrupts the spatial coherence of the vortices. If so, then wake synchronization and strumming would be suppressed.

The strum suppression effectiveness of the fairing has also been confirmed through acoustic measurements recently made at sea.

#### CONCLUSIONS

The fairing tested is an inexpensive and effective method of reducing strumming in Kevlar ropes and cables. Based on the cable drag experiments, the fairing increases cable drag substantially. In particular, the tangential drag coefficient of the faired rope is, depending on Reynolds number, about 4 to 10 times greater than that of a bare rope. Also, the faired rope's normal drag coefficient is about 2-1/2 times greater than that of a nonstrumming bare rope for Reynolds numbers between 550 and 850.

#### ACKNOWLEDGMENTS

The preparation of this paper and the experimental work was supported by the SEAS Program Management Office at the Naval Ocean Research and Development Activity, C.E. Stuart Program Manager. The writer also wishes to thank Ms. P. Harris for her computational assistance.

#### REFERENCES

1. Casarella, M. J. and M. G. Parsons, "A Survey of Investigations on the Configuration and Motion of Cable Systems Under Hydrodynamic Loading," MTS J., v. 4, July-Aug. 1970, pp. 27-44.
2. Griffin, O. M. et al., "The Strumming Vibrations of Marine Cables: State of the Art," Civil Engineering Laboratory, Port Hueneme, CA, Tech. Note N-1608, May 1981, 179 pp.
3. Pode, L., "Tables for Computing the Equilibrium Configuration of a Flexible Cable in a Uniform Stream," David W. Taylor Naval Ship Research and Development Center, Carderock, MD, Report 687, Mar. 1951, 223 pp.
4. Rispin, P. et al., "An Evaluation of Several Techniques for Reducing Cable Strum," David W. Taylor Naval Ship Research and Development Center, Carderock, MD, Report SPD 732-01, Nov. 1977, 57 pp.
5. Vandiver, J. K. and T. Q. Pham, "Performance Evaluation of Various Strumming Suppression Devices," Massachusetts Institute of Technology, Cambridge, MA, Rpt. No. 77-2, Mar. 1977, 105 pp.
6. Wilson, B. W., "Characteristics of Anchor Cables in Uniform Ocean Currents," Texas A&M University, College Station, TX, Tech. Rpt. No. 204-1, Apr. 1960, 157 pp.



# HIGH PERFORMANCE DEEP SEA SUBSURFACE BUOY MOORING

R. Swenson  
J. Selleck  
N. Dennis

U. S. NAVAL OCEANOGRAPHIC OFFICE  
NSTL STATION  
BAY ST. LOUIS, MISSISSIPPI 39529

This paper describes the upgrading of NAVOCEANO's Moored Acoustic Vertical Array (MAVA) buoy system for long term deployments in deep water requiring exacting sensor depth placement. Array cable and mooring line length along with minimum array deflection were critical in the design. Described is the technique used to determine the array and mooring line component lengths to one part in one thousand along with assessing the optimum cable strum suppression technique and measuring its associated drag coefficient. Moor performance is analyzed as a function of component selection, drag coefficient and current profile.

Improvements which result in less logistic support, ease of operation, and lower procurement and maintenance costs are also described. Ample precedence is cited for the use of the technology base from which this design is derived.

## INTRODUCTION

The Naval Oceanographic Office's (NAVOCEANO) Moored Acoustic Vertical Array (MAVA) is utilized to acquire acoustic data in ocean. This subsurface mooring consists of a data acquisition capsule, a vertical array of hydrophones, buoyancy, and mooring components. It is deployed by the anchor last method and recovered by activation of an acoustic release. Deployment depths range from a few hundred meters to 6000 meters and duration from a few days to several months. The two units at NAVOCEANO have been deployed approximately twenty-five times over the past several years in various parts of the world's oceans.

The buoys and these arrays are design replicas of the Naval Underwater System Center's Moored Acoustic Buoy (MABS).<sup>1</sup> The three MABS units have been deployed approximately seventy-five times. This makes a total number of deployments for this class of buoy near 100 without a single loss nor an observed fishbite. The design is of a 1972 vintage which capitalized on early developments in Kevlar ropes and cables.<sup>2</sup>

A measurement requirement consisting of repetitive three-month deployments over a two-year period with exacting sensor placement near the surface in deep water necessitated a redesign of the array and mooring system. Central in this design was pre-

dictability in array length and deflection due to ocean currents along with consideration of corrosion, logistics, deployment ease, reliability and economics.

## SYSTEM DESCRIPTION

The principle element of MAVA is the subsurface buoy, Figure 1, consisting of a syntactic foam flotation collar, an Instrumentation Pressure Vessel (IPV) which contains a 14-channel tape recorder and signal conditioning and timing electronics, and a lead acid battery pack.

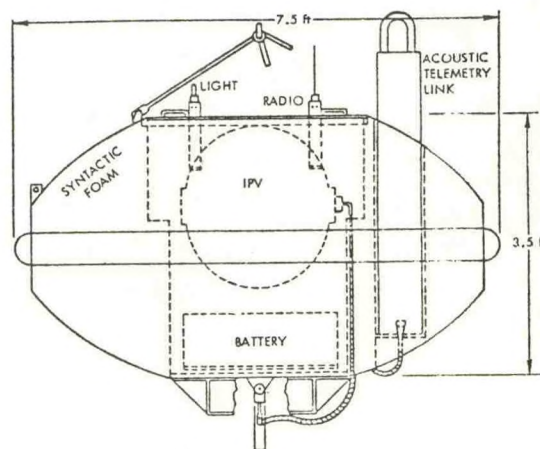


FIGURE 1. MAVA BUOY

The flotation collar produces 1200 pounds of net buoyancy and protects the IPV during deployment and recovery. The 28-inch diameter spherical IPV is sized as small as possible for weight, depth, handling and reserve buoyancy considerations. This fail-safe, robust buoy design has proven its utility. The principle disadvantage is a 4000-pound air weight. However, this is acceptable for "A" frame handling aboard the NAVOCEANO ships.

The original mooring design placed the buoy at the top of the hydrophone array, Figure 2.



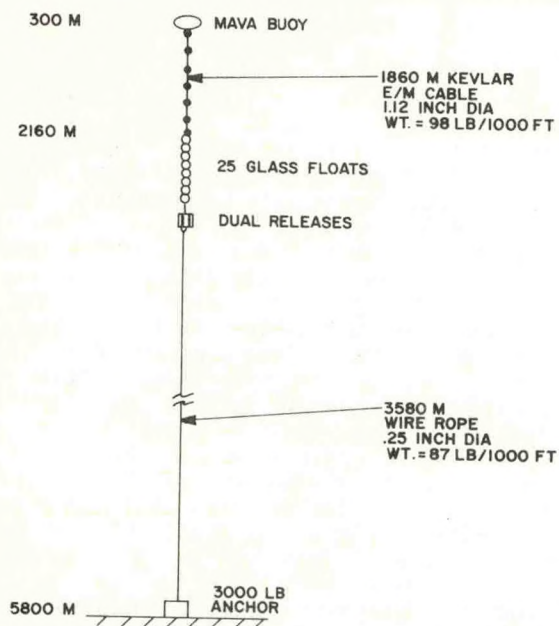


FIGURE 2. ORIGINAL MAVA MOORING

The array consisted of either twelve conductor triads arranged around a central strength member<sup>3</sup> or sixteen triads grouped in fours in four parallel Kevlar cables. Each design was held together with a braided jacket and was equipped with a high drag fringe fairing. Both were approximately one inch in diameter and weighed 0.10 and 0.13 pounds per foot in water respectively. The first design required hydrophones to be attached to the side of the cable whereas the second allowed the hydrophones to be inserted coaxially between the four cables in specially designed cages. Both required considerable care in handling and bending.

Based on the explicit requirement for number and placement of hydrophones, the most significant design change made to MAVA was to locate the buoy within the aperture of the array, Figure 3, and thus reduce the amount of copper conductors required to reach each hydrophone. This allowed the use of a six-conductor, Kevlar-reinforced cable with a breaking strength of 12,000 pounds, a 0.43 inch diameter and a mere 0.02 pounds per foot in water weight. Two hydrophones were supported five hundred meters above the buoy by one cable while two more were supported five hundred and one thousand meters below the buoy by another. An additional two were placed twenty-five meters above the buoy with a short length of cable. This arrangement reduced the array frontal area by 62% and reduced the weight from six hundred pounds to one hundred pounds.

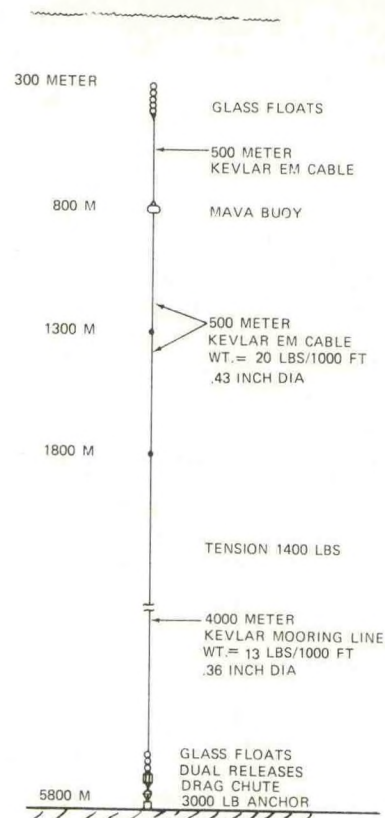


FIGURE 3. RECONFIGURED MAVA MOORING

Array makeup was simplified by procuring cable in premeasured five hundred meter lengths complete with special Hood stopper end fittings, Figure 4.

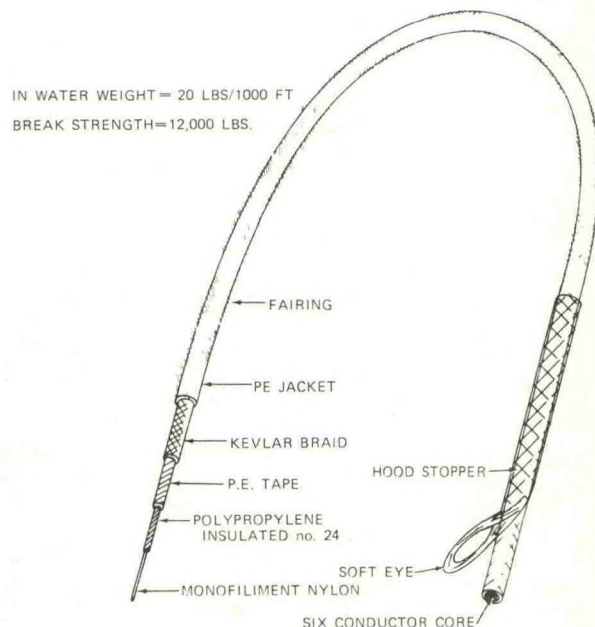


FIGURE 4 - KEVLAR EM CABLE



Hydrophones were placed in special in-line cages which were held in short four rope grommets and shackled eye-to-eye into the array cable section. The only metal parts were 5/16 inch thimbles and shackles used for this purpose. Since these are isolated from other metal hardware, corrosion is minimized. This arrangement provided the added feature that the array could be bent under load, thereby alleviating handling concerns. Array cable cost was reduced from \$43,750 to \$7,800 and availability was significantly improved. Other benefits achieved were modularity, simplicity, placement of the major buoy away from the more hazardous sea surface and increased mooring stiffness.

The requirement to place a sensor at 300 meters in a 5,800 meter water depth implied the use of steel cable for mooring wire. Traditionally, this gives the necessary length predictability. Utilizing the original configuration, Figure 2, 3,580 meters of 1/4 inch diameter wire rope would be required. This length would have an in-water weight of 1,017 pounds which in turn would require twenty-five 17-inch diameter glass floats to maintain moor tension. In addition, this cable would have to be jettisoned each time the mooring is recovered. It would be impractical to recover the wire rope since approximately fifteen more glass floats would have to be provided at the bottom to return the lower end of the cable to the surface. This would also necessitate 750 pounds of additional anchor weight.

These problems were avoided by utilizing Kevlar mooring lines. This would seem the obvious choice except for the uncertainty in predicting the stretched length. Braided lines utilizing a 10° braid angle with a tight braided jacket were used to minimize stretch. The lines were pre-stretched on an airport runway to 1,500 pounds tension and then relaxed to 1,000 pounds for ten minutes. Length was determined with an electronic distance meter to better than one part in one thousand. Constructional stretch removed by this process was approximately 0.3 percent. Lengths of 500, 100, and 50 meters were marked under tension and terminated with Hood type eye splices for subsequent assembly into the mooring.

The electromechanical cables were of the same construction and underwent the same stretching process. However, due to the compressibility of the conductor core, 1.5 percent constructional stretch was removed and 0.6 percent elastic stretch remained at 1,000 pounds tension.

When stretch length measurements were compared with slack length measurements made previously with a tape measure, a 0.7 percent error in the slack measurements was discovered. Had only the calculated elastic stretch of 0.25 percent been used along with these erroneous tape measured lengths, the moor would have been approximately 30 meters too long at a line tension of 1000 pounds. Thus, the extra precaution of pre-tensioning for length measurement and marking was warranted.

Given precise length prediction of the mooring lines, attention was then focused on the predictability of moor deflection due to ocean currents in an effort to achieve depth stability. Since force on the moor is directly proportional to the cable's drag coefficient and to the square of the current velocity, a factor of two errors on each would err the force by a factor of eight. Obviously, for long term remote buoy moorings, one must design for the worst case. The calculations were difficult, however, due to lack of knowledge of the ocean currents at the deployment site and uncertainty about the drag coefficient of the strum suppressed cable which utilizes a special fringe type fairing. Strum suppression was necessary in this case to minimize cable noise on this acoustic measurement system. Published data, 4, 5, 6, 7 indicated that the normal drag coefficient could be highly variable and larger than three. Thus, it was apparent that strum suppression fairings must be evaluated to discover one which minimizes drag and is predictable in the range of interest. This will be addressed later.

Although the described changes to the MAVA mooring and array were very attractive, they certainly could not be introduced into an operational NAVOCEANO measurement system without citing ample precedence. The Versatile Experimental Kevlar Array (VEKA),<sup>8</sup> designed by the principle author, has established a creditable technology base utilizing a variety of cables and array configurations. This system, shown in Figure 5, is utilized by the R&D community to support acoustic experiments and has been deployed approximately twenty-five times over a five-year period in various configurations. The cables, end fittings, fairing and handling procedures now adopted by MAVA were developed under the VEKA program.

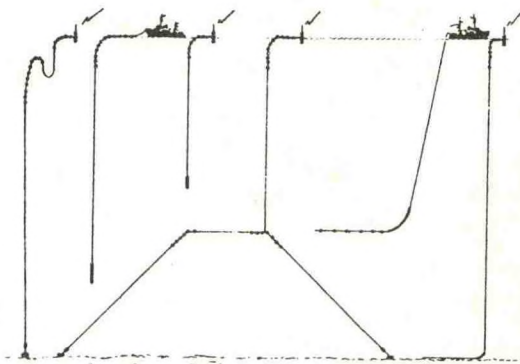


FIGURE 5. VEKA CONFIGURATIONS



## OPERATIONAL SCENARIO

Due to the smaller, lightweight cable which allows hand deployment and eases sensor handling, significant simplifications were made in the operational scenario. The deck winch formerly used to wind the array was eliminated by simply coiling the array cable and mooring line into a tank fashioned from livestock watering tanks, Figure 6.

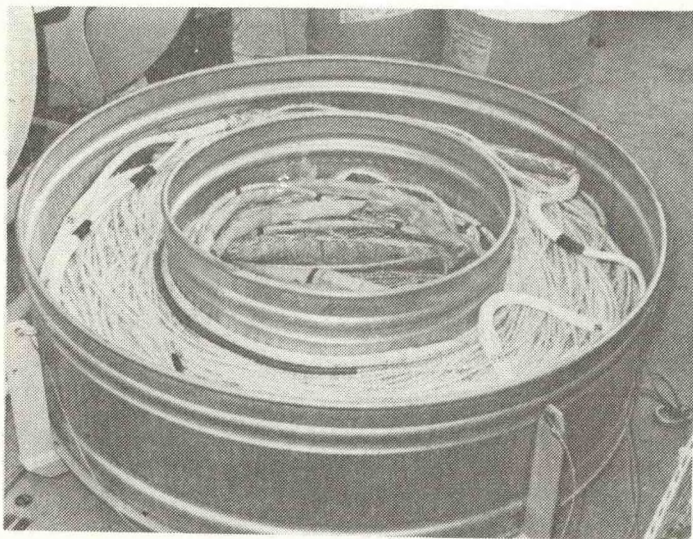


FIGURE 6. MAVA ARRAY AND MOORING LINE COILING TANK

This had the added advantage of permitting total array assembly and water bath testing prior to leaving port. This enhances reliability and reduces personnel requirements at sea.

To deploy the mooring, the top floats are overboarded followed by the lightweight array cable. This is payed out by hand, on demand, from the tank as the ship proceeds into the weather at approximately one knot. When the buoy is reached, it is lifted into the sea with the "A" frame and capstan. The lift line is left attached to the buoy for subsequent recovery. The remainder of the array and the mooring line follow until the anchor is reached. This is then overboarded for free fall to the sea floor, thus completing the mooring in approximately three hours.

Recovery is initiated by activating an acoustic release to jettison the anchor. Sufficient floats near the bottom raise the lower end of the lightweight mooring line to the surface for recovery in reverse order. This reloads the system to meet its repetitive deployment requirement. The mooring line and array cable haul-in is assisted by a single "V" puller, clamped onto the ship's capstan, Figure 7. The cable is coiled back into its tank by hand and the hydrophones are made available for calibration in preparation for redeployment for the next three month measurement period.

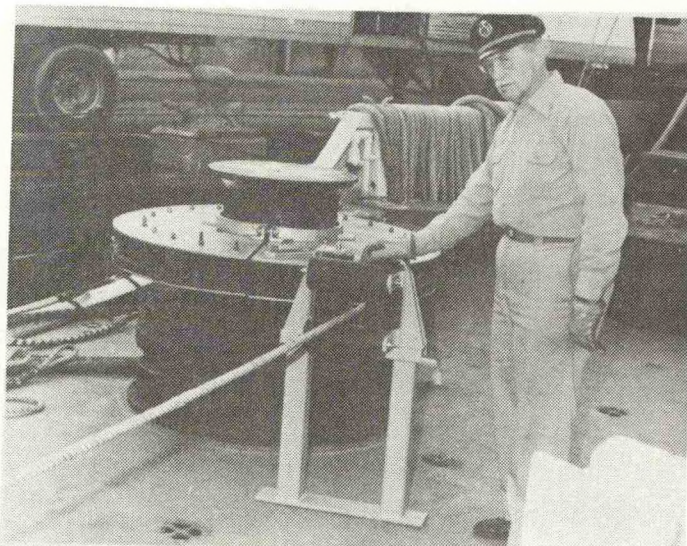


FIGURE 7. CAPSTAN ATTACHABLE "V" PULLER

## CABLE STRUM SUPPRESSION

The objective of this effort was not to do R&D on cable strumming, but rather to establish a measured cable drag coefficient for a three row yarn type fairing to be used on the MAVA cable. Although significant information existed in the literature<sup>9</sup> on cable strumming and drag, there was nothing with the required accuracy for the MAVA mooring analysis for this type of faired cable. Note that this mooring must be faired along its total length to reduce radiated strum noise. Thus, it was mandatory that a practical, low cost and acoustically effective fairing design be found which had an established drag coefficient.

The approach used was simply to braid over neutrally buoyant plastic rods with candidate fairing samples which varied in yarn type, density and length. The fairing was formed during the braiding process by inserting yarn into the braid. The rods were one-half inch in diameter. Samples eight, four and three feet in length were used to test each of the types of yarn fairing shown in Figure 8. Comparisons were made by measuring the drag forces on the samples as they were towed horizontally in a tow tank. The rigidity of the solid plastic rods enabled the samples to be towed orthogonally by simple harnesses of small diameter thread attached to the sample as illustrated in Figure 9.

The set of rods with braid but without fairing (identified as number one in Figure 8) was not observed to strum at a one-fourth knot but did begin strumming severely as the speed of the tow carriage was raised to one-half knot and above. This onset of strumming agreed with test results on various cables reported by Nowak.<sup>10</sup>



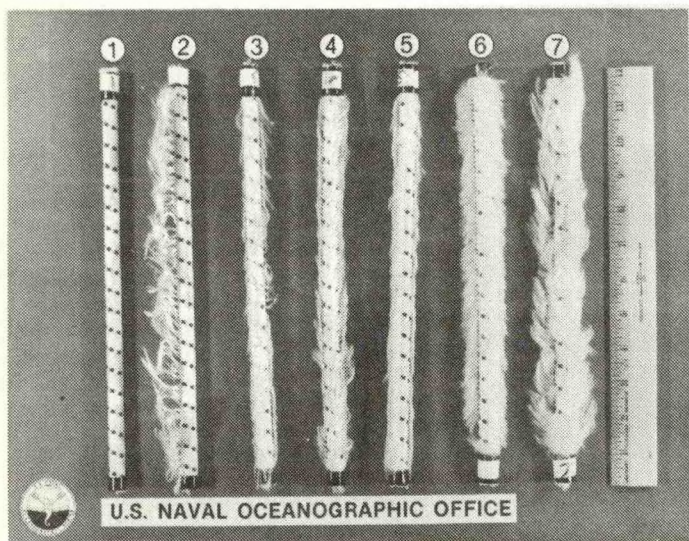


FIGURE 8. FRINGE FAIRING SAMPLES

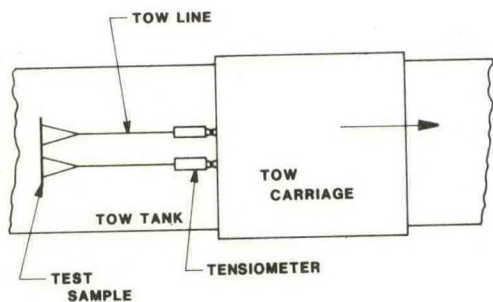


FIGURE 9. HORIZONTAL TOW ARRANGEMENT

On the other hand, samples four through seven of triple line fairing eliminated rod strum at speeds up to  $3\frac{1}{2}$  knots in the series of towed tests on three and four foot lengths. Results were found to be unchanged if rubber cords were inserted into the towing line which stretched fifteen feet under maximum tensiometer load. Thus, the strong statement can be made that even when the faired rods (four through seven) were towed under minimal constraint in any direction, the rods did not strum. The behavior of the normal drag coefficients of several of triple-line fairings is shown in Figure 10. The bare rod exhibited the expected non-strumming drag coefficient of 1.2 at less than one-half knot. This increased to 2.5 at two knots while strumming. However, this measurement technique is questionable for strumming members.

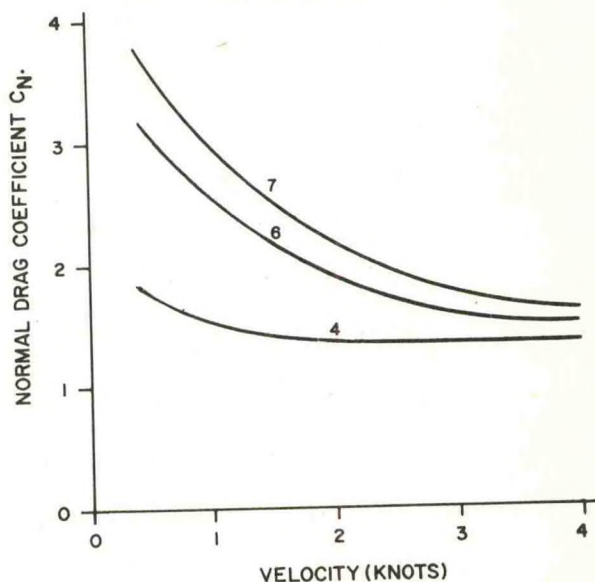


FIGURE 10. NORMAL DRAG COEFFICIENT  $C_N$

The tangential drag of the fairing samples was determined by simply measuring the tow force of the samples as they were towed longitudinally down the tank, Figure 11.

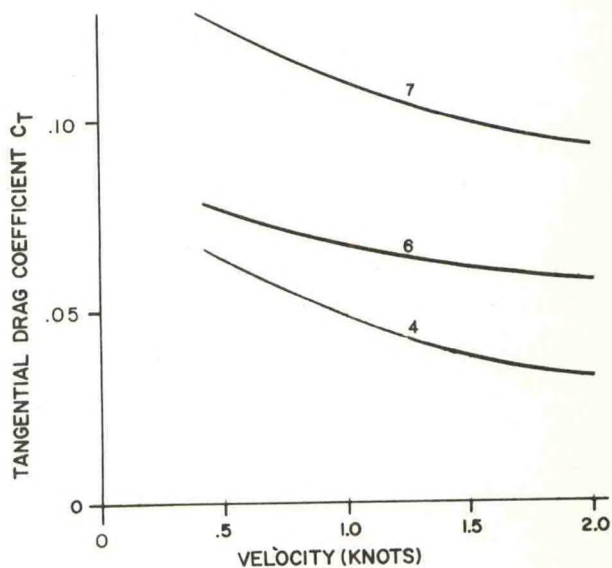


FIGURE 11. TANGENTIAL DRAG COEFFICIENT  $C_T$



A final series of tests was addressed strictly toward further substantiation of the anti-strumming properties of types four and seven of the triple-line yarn fairings. The tests were not addressed to determining drag coefficients. For these tests, a thirty-pound lead sinker with low drag was suspended by the eight foot test samples and towed at various speeds up to five knots as shown in Figure 12.

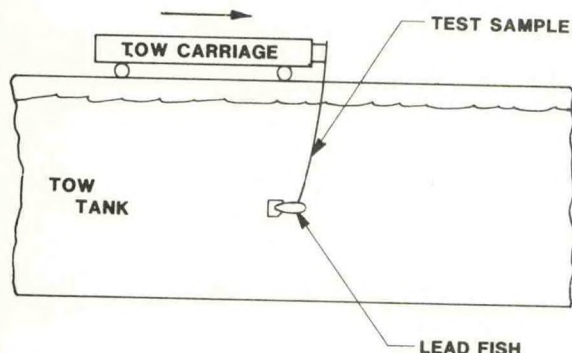


FIGURE 12. VERTICAL TOW ARRANGEMENT

The type four and type seven faired rods exhibited no observable strumming whatsoever. On the other hand, the unfaired rod did not strum at a one-fourth knot but commenced strumming at a one-half knot and continued up to five knots. This confirmed the results of the earlier towed tests.

The conclusions drawn from these tests were: (1) sample number two which was faired with only one line of yarn may exhibit directional properties;<sup>11</sup> (2) sample number three equipped with three rows of light yarn exhibited an increase in drag above one knot; (3) samples five, six and seven all decreased in drag for the velocities measured but had high initial values. Sample number four was chosen because of its initial  $C_D$  value of 1.7 at 0.5 knots which decreased to 1.3 at 3.5 knots and because it is practical in an operation sense. This three row fairing has a 1260 denier nylon yarn,  $1\frac{1}{2}$  cable diameters long, spaced seven per inch (every third braid pick). It effectively suppresses strumming and thus, acoustic noise, and provides a predictable drag which can be used with confidence in mooring analysis.

#### MOORING ANALYSIS

The steady-state performance of both the original and the reconfigured MAVA moorings was analyzed using a subsurface mooring analysis program developed at Woods Hole Oceanographic Institute.<sup>12</sup> The primary goal of the analysis was to determine the deflection characteristics of each configuration. Other goals were to determine tensions throughout the moorings, buoyancy requirements, and forces acting on the anchors.

The two moorings were modeled in 5,800 meters of water. The uppermost hydrophone in each configuration was to be placed at a depth of 300 meters.

Two steady-state, unidirectional current profiles were considered. The first subjected the moorings to a 0.2 knot uniform current from 500 meters depth to the bottom. In the second, a worst case current of 0.5 knot was used. Both profiles have a 1.0 knot surface current which decays linearly to the respective velocities at 500 meters.

The drag coefficients used in the analyses were selected after reviewing numerous publications on cable strumming and drag. A coefficient of  $C_D = 1.8$ , reported by Alexander<sup>13</sup> for bare cable, was used for the wire rope. For the original electro-mechanical (E/M) cable which has a helical fringe fairing,  $C_D$  was chosen to be 4.0. This choice was based on test results reported on similar types of cable.<sup>5,6</sup> In the reconfigured design, the mooring line and the E/M cable were both assigned a  $C_D$  of 1.7. This is substantiated by the in-house measurements discussed previously.

The results of the analyses are presented graphically in Figure 13. Table I gives specific results which quantitatively show the improved performance. As expected, the reconfigured mooring design shows significantly less deflection for a given current profile than does the original design. This is due primarily to the reduced frontal area and lower  $C_D$ 's of the mooring line and E/M cable in the new configuration.

The reduced deflection is important because the behavior of the mooring under actual conditions is now more predictable. As seen in the table, vertical excursions of the hydrophones have been reduced by 80 to 90 percent. Horizontal excursions, while not as critical as vertical excursions, have been reduced by 50 to 65 percent. This means that the hydrophones will be much closer to the desired operating locations in the water column. Also, deviations from nominal positions due to changing currents will be much lower.

Another benefit of reducing the deflection is the decrease in horizontal force on the anchor. The table shows a significant reduction in this force for the new configuration. Thus, a lighter weight anchor can be used to hold the mooring in position.

Finally, in a deep moor, it is highly unlikely that the current will be coplanar along the entire length of the moor. Thus, the analysis represents the worst case situation and better depth stability for the sensors can be expected.



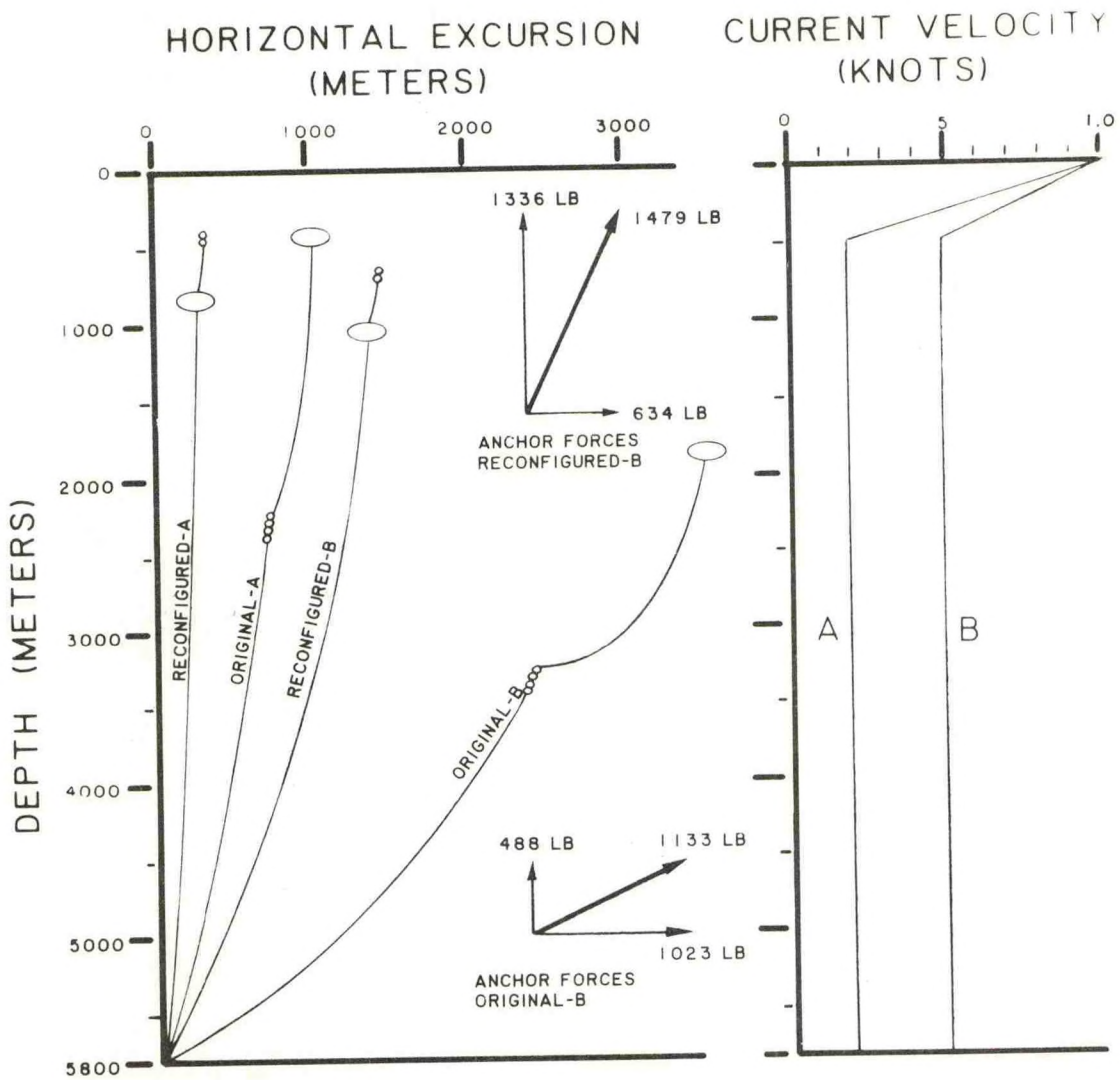


FIGURE 13. MAVA DEFLECTION CURVES



	ORIGINAL DESIGN		RECONFIGURED DESIGN	
	<u>.2 KNOT</u>	<u>.5 KNOT</u>	<u>.2 KNOT</u>	<u>.5 KNOT</u>
Normal Frontal Area (meters <sup>2</sup> )		85.1		59.1
C <sub>D</sub> , E/M Cable		4.0		1.7
C <sub>D</sub> , Mooring Line		1.8		1.7
Horizontal Force at Anchor (pounds)	315	1023	130	634
Line Tension at Anchor (pounds)	982	1133	1492	1479
Line Inclination at Anchor (Degrees from vertical)	19	65	5	25
Vertical Excursion (meters)				
Uppermost Hydrophone	116	1564	12	250
Lowermost Hydrophone	85	1089	10	232
Horizontal Excursion (meters)				
Uppermost Hydrophone	1040	3577	340	1484
Lowermost Hydrophone	753	2511	264	1280

TABLE I. RESULTS OF MOORING ANALYSIS

#### CONCLUSIONS

Significant improvements were made in the NAVO-CEANO's acoustic measurements system, MAVAS, by adopting technology developed by the Navy-supported VEKA program. Quantitative achievements were reductions in array frontal area by 62%, weight by 83%, cost by 82%, added buoyancy by 56% and array deflection by 87%. More important, but harder to qualify, were favorable impacts on deployment ease, required deck gear, logistics, repair, reliability and required support personnel. Most important, however, had these changes not been made, the sensors could not have been held at the desired location throughout the three month measurement periods. Also, the lower phones would have been subjected to noise produced by the conventional mooring line.

This effort has produced a high performance mooring which will predictably and efficiently place and hold sensors quietly in the desired location in the deep ocean. An additional bonus was the evaluation of several cable strum suppressing candidates which lead to the selection of a fairing for moored systems with minimal drag and an established drag coefficient.

Finally, this mooring should continue to establish precedence for this technology which can be utilized by the ocean community in general.

#### ACKNOWLEDGEMENTS

The authors thank Dr. Charles M. Alexander of the Naval Ocean Research and Development Activity for his helpful suggestions which resulted in a simple technique to measure the drag force on these cables. Also, to Messrs. Alec Hood and Tom Yale of Wall Rope, Inc., for inventing and developing the "Fringe Fairing Machine" and for many other contributions in developing and producing these mooring components.



## REFERENCES

1. King, Peter K. and Swenson, Richard C., "The Moored Acoustic Buoy System (MABS)", MTS Journal v. 10 n. 8 October-November, 1976.
2. Swenson, Richard C., "The Cable Development Program for Suspended Sensor Applications", Naval Underwater Systems Center, New London Laboratory, September, 1975.
3. Bower, Grant R., "Technical Note, Center Strength, Mava Array", Naval Oceanographic Office, NSTL Station, Bay St. Louis, MS, April, 1981.
4. Milburn, Darrell A. and Rispin, Paul, "Hydrodynamic Test and Evaluation of a Newly Developed Kevlar Rope Fairing", Naval Ocean Research and Development Activity, NSTL Station, MS, December, 1981.
5. Meggitt, D., Kline, J. and Pattison, J., "Suppression of Mooring Cable Strumming", Proceedings of the Eighth Ocean Energy Conference, Paper IB5, Marine Technology Society: Washington, DC, 1982.
6. Kline, Jeffrey, Brisbane, Arthur, and Fitzgerald, Edward, "A Study of Cable Strumming Suppression", October, 1980, Technical Report No. 249, Civil Engineering Laboratory, Naval Construction Battalion Center, Port Hueneme, CA.
7. Vandiver, J. K., and Pham, T. P., "Performance Evaluation of Various Strumming suppression Devices", MIT Ocean Engineering Department Report 77-2, March, 1977.
8. Swenson, Richard C., Gholson, Norman H., and Rumpf, Robert R., "VEKA/FLIP Variable Depth Horizontal/Vertical Array", Marine Technology Society Journal, Vol. 4 - No. 1, 1980.
9. Griffin, O. M., Ramberg, S. E., Skop, R. A., Meggitt, D. J., and Sergev, S. S., "The Strumming Vibrations of Marine Cables: State of the Art", TN No. N-1608, Civil Engineering Laboratory, Naval Construction Battalion Center, Port Hueneme, CA, May, 1981.
10. Hays, Dr. E. E., Nowak, Richard T., and Boutin, Paul R., "Strumming Tests of Two Faired Cables", Woods Hole Oceanographic Institution, Woods Hole, MA, October, 1975, Unpublished manuscript.
11. Chey, Y. H., "Strum and Drag Measurement of Underwater Cables", General Electric Co., TM 990-2014, June, 1975.
12. Moller, Donald A., "A Computer Program for the Design and Static Analysis of Single-Point Sub-surface Mooring Systems" NOYFB Technical Report, Woods Hole Oceanographic Institution, Woods Hole, MA, June 1976, Unpublished Manuscript.
13. Alexander, C. M., "The Complex Vibrations and Implied Drag of a Long Oceanographic Wire in Cross-Flow", Ocean Engineering, Vol. 8, 379-406; 1981.



# OPEN OCEAN WAVE BUOY COMPARISONS IN THE NORTH ATLANTIC

by

Edward W. Foley, Robert J. Bachman and Susan L. Bales

David W. Taylor Naval Ship  
Research and Development Center  
Bethesda, Maryland 20084

## ABSTRACT

An evaluation was conducted during May 1982 for the purpose of comparing the performance of three wave buoys. The evaluation was conducted from the Dutch oceanographic research vessel TYDEMAN in the North Atlantic. The three buoys used in the evaluation were: 1) an ENDECO Corporation Type 956 buoy owned by the David Taylor Naval Ship Research and Development Center (DTNSRDC), 2) a WAVEC buoy under development by the Datawell Corporation, and 3) a disposable buoy designed and built by Delft University. All buoys used a telemetry link to transmit measured data to recording instrumentation on TYDEMAN. Although the three buoys represent different design approaches to the wave surface measurement problem, the measurement derived energy point spectra and significant wave heights showed good agreement.

## 1. INTRODUCTION

For some years, the U.S. Navy has measured ocean waves during full-scale ship trials in the open ocean. These measurements were generally taken to quantify the prevailing wave environment in order to better interpret the measured ship responses. During the 1970's, wave measurements were generally made using the well known Datawell Corporation WAVERIDER buoy.

While much valuable information has been derived from these measurements, their application has only been partially successful. The deficiency has been that no wave directional data were available (except by visual estimates). This has made it difficult if not impossible to correlate measured full-scale ship responses with those derived in towing tanks or by numerical prediction using empirical/theoretical models.

In 1980, the U.S. Navy initiated a research program with the objective to provide the ship designer with a substantially improved wave spectral model. The approach was to develop algorithms for predicting realistic seaways throughout

the Northern Hemisphere. The new model was to permit the simultaneous representation of both locally generated wind seas and swell from decaying or distant storms. While the emerging results of this program are reported elsewhere (References 1,2,3,4 and 5), it became clear that new measurement techniques would be required to evaluate the new wave spectral model.

The most crucial new parameter requiring measurement was wave directionality. Several techniques were briefly explored with the constraint that the wave measuring device must be deployable from a variety of ship sizes and configurations. Some of the possibilities included hull-mounted radars, discus buoys, using the ship itself as a sensor, and overflying/remote sensors. Within the available time and economic constraints, it was determined that a fairly small roll/pitch buoy might provide a sufficient first order measurement of wave directionality (e.g., for evaluation of wave spectral hindcasts and forecasts which are being synthesized into the new ship design model).

This paper highlights the early experience gained by deploying such a buoy that has been manufactured by the ENDECO Corporation. Results are compared against a "standard" wave acceleration buoy and another prototype directional sensing buoy. While the directional data results are not yet available, the point spectral data provide an important seaway comparison.

## 2. INSTRUMENTATION

The instrumentation used during the May 1982 TYDEMAN trial consisted of various equipment supplied by Datawell Corporation, Delft University and the US Navy (DTNSRDC). Each organization basically supplied a wave buoy, recording instrumentation, and a small computer for analysis.

The Datawell Corporation supplied their new WAVEC buoy for the trial as shown by the photograph of Figure 1. The buoy was considerably larger and heavier than the other buoys although exact dimensions and weight are not known to these authors. The accelerometer, pitch-roll sensors,



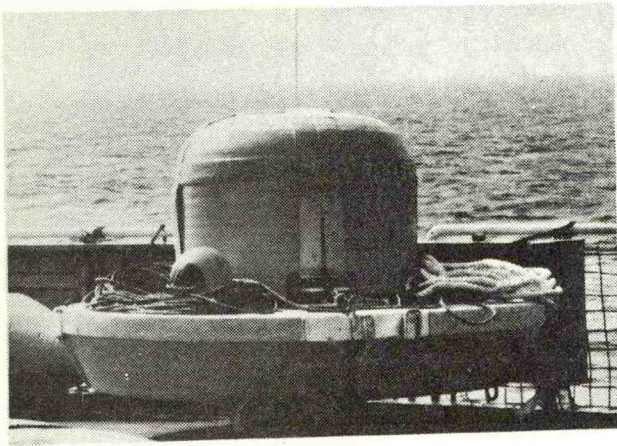


Figure 1. Datawell WAVEC Buoy

batteries, instrumentation and telemetry equipment were all housed within a container approximately the size of a standard 55 gallon drum. Attached to this drum was a specially constructed flotation collar which gives the buoy its required discus shape. The buoy can thus be correctly described as a slope following discus buoy. The buoy also has a spherically shaped dome structure, visible in the photograph, which aids in preventing capsizing.

The Delft University supplied a wave buoy of university design for the trial. This buoy was designed to be of minimal cost and yet still be a reliable instrument for adequate measurement of waves (of sufficient length and size to affect vessel motions). For purposes of this paper it is referred to as the Disposable Buoy or the Delft Buoy. The Disposable Buoy is shown in Figure 2.

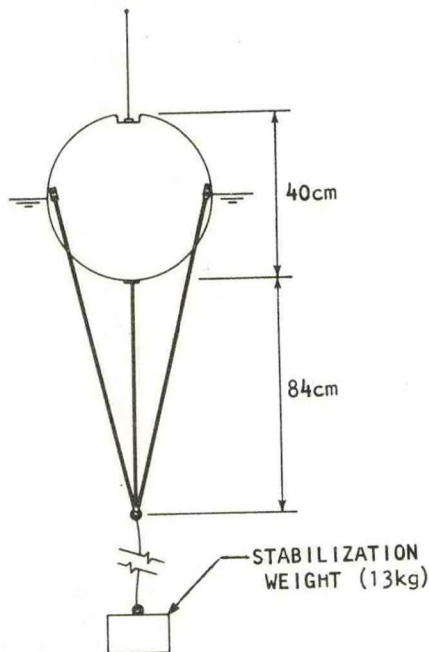


Figure 2. Delft Disposable Buoy

The buoy sphere is built using a fiberglass construction and contains rechargeable batteries, a fixed vertical accelerometer, electronics, and an FM transmitter. The accelerometer signal is not double integrated onboard the buoy, as might be expected from a more expensive buoy.

Reference 6 describes the buoy and its use, sometimes as a disposable instrument, during several sea trials. A complete description of the buoy is given in Reference 7. However, the basic hydrodynamic stabilization of the fixed vertical accelerometer can be understood by observing Figure 3. The rigid tripod tail of the buoy (length

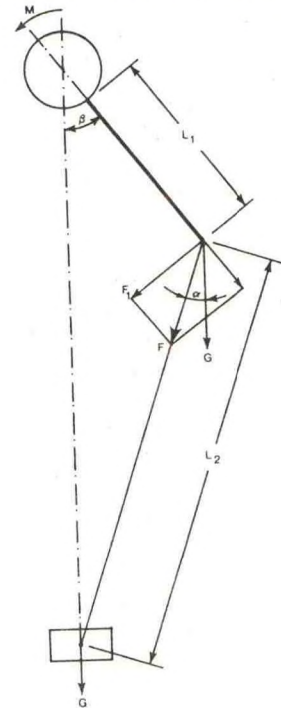


Figure 3. Stabilization Diagram

$L_1$ ) has a weight  $G$  attached to it by a steel cable of length  $L_2$ . A wave induced moment  $M$  would result in a buoy tilt of  $\beta$  degrees. In this condition, an erecting moment of  $F_1$  times  $L_1$  would be obtained, where  $F_1$  is the perpendicular resolution of the wire tension. During this trial, a wire length of 40 meters was used such that  $L_2$  can be assumed to be much greater than  $L_1$  and thus the angle  $\alpha$  approaches zero. Therefore, the erecting moment can be expressed as:

$$F_1 \cdot L_1 = L_1 \cdot G \cdot \sin \beta$$

This rather simple method for vertical stabilization of the accelerometer seemed to function very well with no tilting of the sensor observable.

DTNSRDC deployed an ENDECO Corporation Type 956 Directional Buoy during the trial. This buoy is the result of development work at the University of Rhode Island as well as ENDECO Corporation and has been the subject of several papers, see References 8, 9 and 10. The Type 956 buoy was also deployed during the ARSLOE experiment as reported



in Reference 11. The configuration of the buoy is shown in Figure 4. The sphere of the buoy (fiber-glass) houses the electronics, transmitter, and

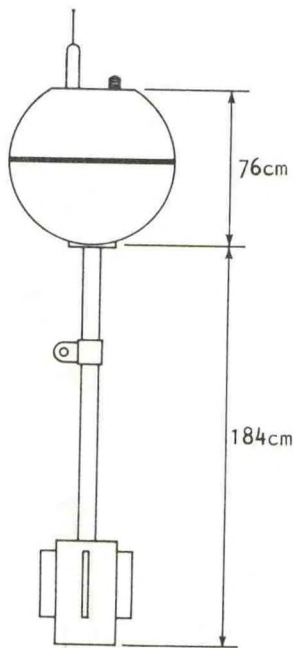


Figure 4. ENDECO Type 956 Buoy

batteries for the buoy, while the lower pendulum assembly (PVC and stainless steel hardware) houses the pitch-roll sensors and accelerometer. The pendulum assembly acts as a moment arm to tilt the buoy in response to the orbital motion of the incident wave field. This buoy has thus been referred to as an orbital following buoy. Because of its inherently stable design, the Type 956 buoy is not subject to the capsizing problems associated with the discus slope following buoys.

The signals from the buoys were recorded in analog form using Honeywell Model 5600 recorders. This ensured the reliable recording of the data in spite of problems encountered with the computer systems. Delft University and Datawell Corporation employed Hewlett - Packard micro computer systems, while DTNSRDC used a Digital Equipment Corporation micro computer system for the purpose of digital data collection and analysis.

### 3. TRIAL DESCRIPTION

The wave measurement trial was conducted aboard the Dutch oceanographic research vessel Hr.Ms. TYDEMAN. TYDEMAN is a 90 meter open ocean research vessel equipped with various cranes and winches necessary for general oceanographic research. The design of the vessel and expertise of its crew made a relatively routine procedure of launching and recovering the various wave buoys. The trial consisted of several buoy launches at various locations along a meandering transit route

from Den Helder, Netherlands to Santa Cruz de Tenerife in the Canary Islands. The transit route is shown in Figure 5 along with an indication of

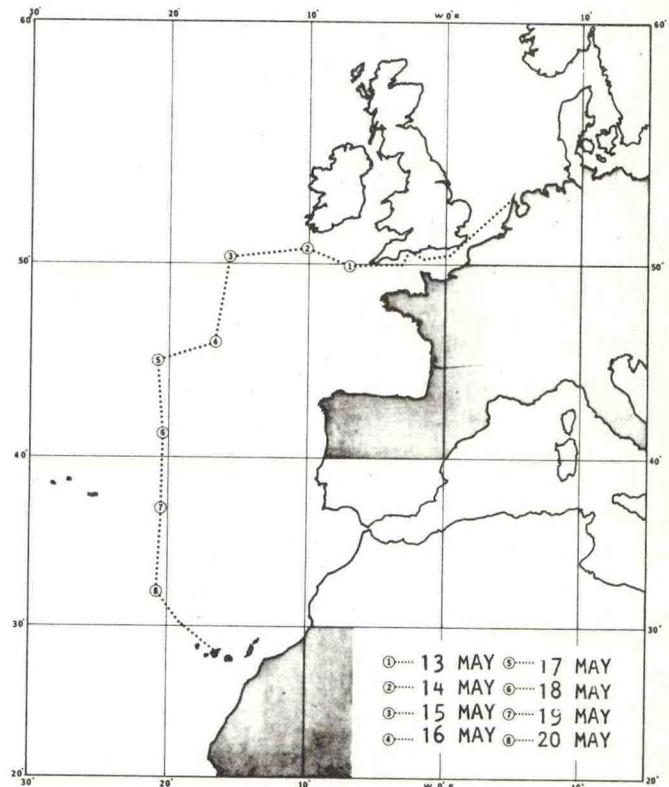


Figure 5. TYDEMAN Transit Route

the locations where data were collected. The route was determined in part by analysis of daily wave forecasts received from the US Navy's Fleet

Numerical Oceanography Center (FNOCC) in Monterey, California. During the trial, the FNOCC forecasts were examined approximately every twelve hours in order to identify regions of greater wave activity. When possible, the course of the ship was altered to steam towards those regions.

A typical day's operations began with an early morning launch of the three wave buoys. The ship then conducted course keeping maneuvers to evaluate the seakeeping characteristics of the vessel while the buoys free floated from the site of the launch. Near midday, the ship maneuvers were temporarily halted, and the buoys located, retrieved and then, relaunched. This was necessary in order to keep the three buoys in a reasonable proximity to one another since they had varying drift rates. The WAVEC buoy had by far the highest drift rate due to the large sail area of the styrofoam cap. The ENDECO and Delft buoys stayed closer together with the ENDECO drifting slightly more than the Delft. After collecting data during the afternoon with the ship conducting maneuvers once again, the buoys were relocated and retrieved prior to darkness. Thus, wave data were collected in a nearly continuous fashion throughout the daylight hours. During the night, the ship transited and sometimes adjusted course



to encounter more severe weather as located by the wave forecasts.

#### 4. DATA ANALYSIS TECHNIQUES

The heave data measured by the buoys were analyzed in two ways. First, the data measured by each of the three buoys were reduced and analyzed by a single technique. This allowed comparison of the buoys by eliminating differences in analysis techniques. Second, the heave data measured by the ENDECO buoy were analyzed using three different techniques to produce spectral estimates. In the first analysis technique, the Delft University utilized an autocorrelation method. In the second technique, DTNSRDC analyzed the data using the digital band-pass filter technique supplied by ENDECO Corp. In the third technique, DTNSRDC applied its own power spectral density analysis to the heave data. The signal from the ENDECO buoy was sampled at a rate of one per second over a period of 30 minutes during each collection run. Each data record was truncated to a total of 1024 samples.

The details of the Delft University's analysis technique are not well known by the authors of this paper, but the analysis utilizes a standard "Blackman-Tukey" method for computing the power spectral density function via its Fourier transform relation to the autocorrelation function. The analysis uses a number of filterweights on the order of 100. The frequency resolution in this analysis is 0.101 radians per second.

The ENDECO analysis edits the data by eliminating spikes and floating the data about their mean. The analysis then transforms the data into the frequency domain using the fast Fourier transform (FFT). Next, a bandpass filtering method is performed before inverse transforming the data. This analysis does not apply a weighting function to the heave data. The frequency resolution in the analysis is 0.063 radians per second.

The analysis employed by DTNSRDC also uses an FFT algorithm. A full cosine data window is applied to reduce the side-lobe leakage and a 50 percent overlap is performed on the record segments. The overlap allows 15 segments, of 128 samples each, to be ensemble averaged. The 15 segments provide a statistical bandwidth of 0.101 radians per second with 30 degrees of freedom.

#### 5. RESULTS AND DISCUSSION

The comparison of data from the three buoys was facilitated by using a single method of analysis. Since Delft University was provided with data records from the WAVEC buoy and the ENDECO buoy, Delft had the opportunity to analyze the heave data of all three buoys. In addition to the buoy comparisons made using the Delft

analysis, two additional analyses were applied to particular data sets to observe differences in analysis techniques.

For the purposes of examining the differences in analysis techniques, the three previously described techniques were applied to a common set of data. The data chosen was the heave signal from the ENDECO buoy. The spectral energies determined by the analyses were then compared for Runs 25, 30, and 31, see Figures 6, 7, and 8, respectively.

The Delft analysis produces greater total wave energy, as reflected in the significant wave height,  $(\bar{\zeta}_w)_{1/3}$ , than the ENDECO and DTNSRDC analyses in Runs 25 and 30; but in Run 31, the Delft analysis accounts for less energy than the other two. In the first two runs, the Delft analysis produces higher spectral densities than the others at the spectral peaks. In the third run, the spectral densities agree well around the peak but vary in the higher frequencies.

In Run 25, the primary spectral peaks for all the analyses occur at about 0.78 to 0.81 radians per second. The shift of the peak in the ENDECO analysis is probably due to the different frequency bandwidths used. All analyses indicate a second energy peak in the neighborhood of 0.63 radians per second.

The spectra agree best in Run 30. The significant wave heights and the spectral densities above 0.9 radians per second are almost identical. The frequencies at the primary peak and the secondary peak agree between the Delft and the ENDECO analyses if the shift in the frequency bandwidth is considered, with the spectral densities produced by the ENDECO analysis slightly below that of the Delft analysis in this region. The frequencies of the primary and secondary peaks, as produced by the DTNSRDC analysis, are reversed compared to the other two analyses. The spectral densities in this region are also less than that produced by the Delft analysis.

The energy peak in Run 31 is very similar for the three different analyses in the frequency range of about 0.63 to 0.70 radians per second. A smaller second peak is also present at about 0.88 radians per second. In the region above 1.0 radians per second, all three analyses differ. The energy produced by the Delft and DTNSRDC analyses follow the same trend, with the DTNSRDC analysis showing more energy. The ENDECO analysis follows a different trend, but tends to agree in showing more energy in the higher frequency region than the middle region.

In each of the three runs, the primary energy lies within the range of about 0.5 to 1.0 radians per second. Although the spectral densities vary across the frequency range for each run of the ENDECO and DTNSRDC analyses, the total energy is virtually the same. The total energy produced by the Delft analysis varies with respect to the other two analyses. In the three runs considered, the Delft analysis indicates a total energy



greater than the other two analyses in one run, a similar total energy in another run, and a lesser total energy in the third run. This is probably due to each digital record of a particular run, used by the Delft analysis, being different from the digital record shared by the ENDECO and DTNSRDC analyses, for that particular run. In one run, the spectral densities agree in the lower frequency range, whereas in another run, the spectral densities agree in the higher frequency range. In a third run, the spectral densities do not agree, but follow the same trend. It therefore appears that no single analysis is consistently better than the others.

The three buoys were compared, as previously mentioned, using Delft University's autocorrelation technique. This analysis was carried out during the course of the trial and a comparison of significant wave heights obtained for selected runs are shown in Figure 9. The comparisons are in general favorable, however some variation can be noted for some of the data. For instance, data on the morning of the 13th and the afternoon of the 18th indicate more disparity than the other recordings. But again, the lack of any discernable trends indicates that the variations are probably due to measurement technique (radio interference, recording bias, buoy separation etc.) rather than an error in the buoy signal. Additionally, spectral comparisons are given for the same three runs previously examined (Runs 25, 30 and 31). These comparisons are shown in Figures 10, 11, and 12, respectively.

The spectral peak energy measured in Run 25 varied between buoys. The peak frequency ranged from 0.69 radians per second for the WAVEC buoy to 0.84 radians per second for the Delft buoy, with a frequency of 0.78 radians per second for the ENDECO buoy. The comparisons of the peak energy measured in Run 30 and Run 31, agree better than in Run 25. In both Run 30 and Run 31, the peak frequency for all three buoys was 0.64 radians per second. The poorer comparison for Run 25 may in part be explained by the fact that the data was recorded at the end of the day with the buoys at a maximum separation distance. Runs 30 and 31 were early morning recordings with a minimum separation.

The spectral densities vary among the buoys in Run 25, but the dominant energies agree within the same frequency range. The variation of significant energy among the buoys is larger than for the other two runs. This is probably due to spatial separation between the buoys. Both the ENDECO and the Delft buoys show double peaks in their energies, indicating dominant energy found in nearby frequency bands. The center frequencies of the two buoys roughly agree at the peaks. The WAVEC buoy interprets the dominant energy as being in a single peak located at a frequency between that of the double peaks of the other two buoys. In the low frequency range, the Delft buoy shows some energy that is not indicated by the other two buoys. This may have been introduced in the analysis and double integration routines. Throughout the rest of the frequency range the

energies are similar. The Delft buoy shows the greatest energy, followed by the WAVEC buoy, and then by the ENDECO buoy.

The shape of the spectra are similar in Run 30, but with less energy indicated by the ENDECO buoy. All three buoys measured the dominant energy in the same frequency range. The spectral densities for the Delft and WAVEC buoys are greater than the ENDECO buoy at the peak frequency, while all the densities above 0.75 radians per second agree. In this run, the WAVEC buoy shows the greatest energy, followed by the Delft buoy and then the ENDECO buoy.

Excluding the unfiltered energy located in the low frequency range for the Delft buoy, the shapes of the spectra in Run 31 are similar. Again, the three buoys measured the dominant energy within similar frequency ranges. A secondary region of energy is picked up by all buoys around a center frequency of about 1.6 radians per second. The Delft and ENDECO buoys agree in spectral density at their peak frequency, but the ENDECO buoy shows this energy across more than one frequency band. In this run, the ENDECO buoy and the Delft buoy indicate spectral densities greater than the WAVEC buoy at the peak, but are reversed at the higher frequencies. The Delft buoy shows the greatest energy, followed by the ENDECO buoy and then the WAVEC buoy.

The comparisons of the buoys were made for runs in mild to moderate sea conditions. Generally, the wave spectra compared well. In one run, one of the buoys did not match the other two in density, at the peak frequency. In another run a different buoy did not match the other two in density at the peak. This indicates a variation not particular to the type of buoy. The frequencies of the peak energy of all the buoys agree as do the basic shapes of all the spectra. The energy measured by the Delft buoy was greater than the other two buoys in two of the runs where the extra energy was found at low frequencies. If this energy is not considered, the total energies measured by the buoys is more similar.

When comparing the buoys using the same analysis technique, there appears to be no consistency in variation among the buoys. They all produce similar results, but no buoy exhibits a systematic spectral bias greater or less than the other.

## 6. CONCLUDING REMARKS

This paper has presented a comparison of point spectra measured in the North Atlantic Ocean with three relatively new buoy designs. Due to differing intended applications for the buoys, they differ significantly in their designs. In spite of this, the measured significant wave heights compared reasonably well. Some individual differences between spectral energy plots were noted, however no consistent pattern could be dis-



cerned. The differences in the spectral plots were of no more consequence than the differences found between three different analysis techniques.

Evaluation of the directional data and software analysis techniques (provided by ENDECO) is ongoing. A subsequent publication will show the results of this evaluation along with a comparison of the FNOC forecasts to the measurements taken in-situ during the trial. It is hoped that a Comparison of the directional results of the ENDECO buoy, and Datawell WAVEC buoy can also be included.

Following the TYDEMAN trials, the ENDECO buoy was used in another trial onboard the USNS Hayes under the joint sponsorship of the Naval Research Laboratory (NRL) and DTNSRDC. Participating in this trial effort were representatives of the British Institute of Oceanographic Sciences with a cloverleaf directional buoy. Also, representatives of NRL utilized two types of radar to demonstrate their potential for sensing directional wave data. These data should provide additional comparisons for evaluating the ENDECO performance and will be the subject of future publications.

#### 7. ACKNOWLEDGEMENTS

The work reported herein was sponsored by the Naval Material Command/Naval Sea Systems Command Exploratory Development Surface Wave Spectra for Ship Design Program.

Clearly, the work could not have been carried out without the kind cooperation of the Royal Netherlands Navy, Exchange Agreement No. MWDEA N-65-TN-4803.

In particular, the expert coordination provided by Dr. Ir. J.M. Dirkzwager of the Ministerie Van Defensie permitted the trial to take place, and he is gratefully acknowledged for his insight into the benefit of such cooperative efforts. Additionally, the high degree of professionalism of the Delft University team under the leadership of Prof. Ir. J. Gerritsma contributed greatly to the technical success of the work. The assistance of Mr. M. Buitenhok, Mr. J. Ooms, and Mr. P. de Koning is greatly appreciated. Mr. Gerritsen of Datawell is also acknowledged for his assistance and stimulating discussion throughout the trial.

The wave forecasts radioed by FNOC were extremely helpful in planning the ship's route and the efforts of LCDR. Maas are particularly appreciated.

And finally, the officers and crew of the TYDEMAN, under the able leadership of CAPT A.P.H.M. Lempers, are gratefully acknowledged for their continuing assistance and hospitality throughout the trial.

The responsibility for all statements of fact and opinion rests with the authors.

#### 8. REFERENCES

1. Cummins, W. E. and S. L. Bales, "Extreme Value and Rare Occurrence Wave Statistics For Northern Hemisphere Shipping Lanes," Proceedings of the Society of Naval Architects and Marine Engineers STAR Symposium, June 1980.
2. Bales, S.L., W.T. Lee and J.M. Voelker, "Standardized Wave and Wind Environments For NATO Operational Areas," David W. Taylor Naval Ship Research and Development Center Report No. SPD-0919-01, July 1981.
3. Cummins, W.E., S.L. Bales and D.M. Gentile, "Hindcasting Waves For Engineering Applications," Proceedings of the International Symposium on Hydrodynamics in Ocean Engineering, The Norwegian Institute of Technology, August 1981.
4. Bales, S.L., W.E. Cummins and E.N. Comstock, "Potential Impact of Twenty Year Hindcast Wind and Wave Climatology on Ship Design," Marine Technology Vol. 19, No. 2, April 1982.
5. Bales, S.L., "Designing Ships to the Natural Environment," Naval Engineers Journal Vol. 95, No. 2, March 1983.
6. Gerritsma, J., "Results of Recent Full Scale Seakeeping Trials," Technische Hogeschool Delft, Laboratorium Voor Scheepshydraumica report no. 495, March 1980.
7. Buitenhok, M. and J. Ooms, "An Updated Design of a Disposable Wave Buoy," Technische Hogeschool Delft, report no. 463, May 1978.
8. Middleton, F.H., L.R. LeBlanc, and M. Czarnecki, "Spectral Tuning and Calibration of a Wave Follower Buoy," Eight Annual Offshore Technology Conference, paper no. OTC 2597, May 1976.
9. Middleton, F.H., L.R. LeBlanc, and W. Sternberger, "Wave Direction Measurement by a Single Wave Follower Buoy," Tenth Annual Offshore Technology Conference, paper no. OTC 3180, May 1978.
10. Brainard, E.C., "Wave Orbital Following Buoy," paper presented at Marine Technology '80 Conference (not in the transactions), October 1980.
11. LeBlanc, L.R. and F.H. Middleton, "Storm Directional Wave Spectra Measured with a Single Buoy," Oceans '82 Conference, Sept. 1982.



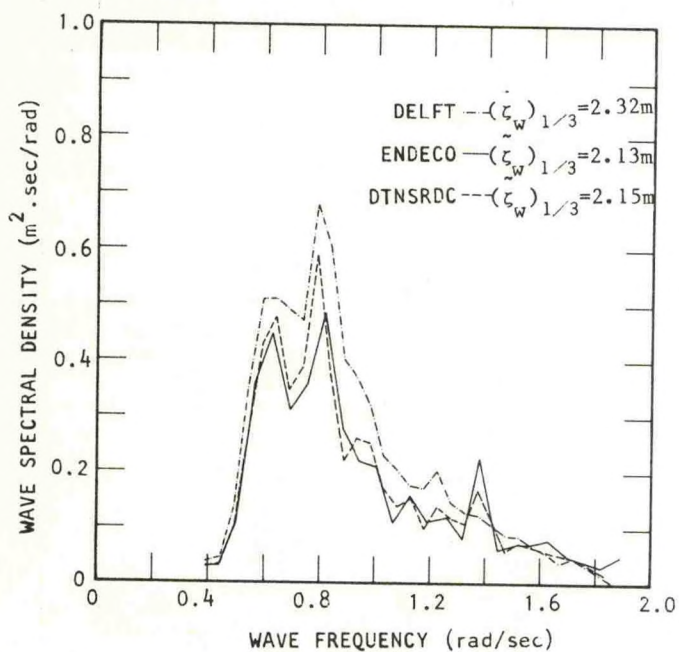


Figure 6. Spectral Comparisons of three Analyses Using the ENDECO buoy for Run 25

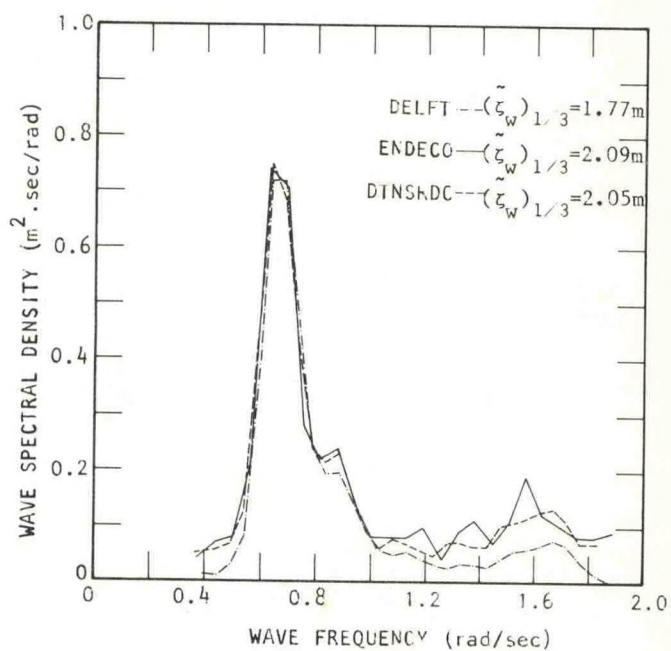


Figure 8. Spectral Comparisons of Three Analyses Using the ENDECO Buoy for Run 31

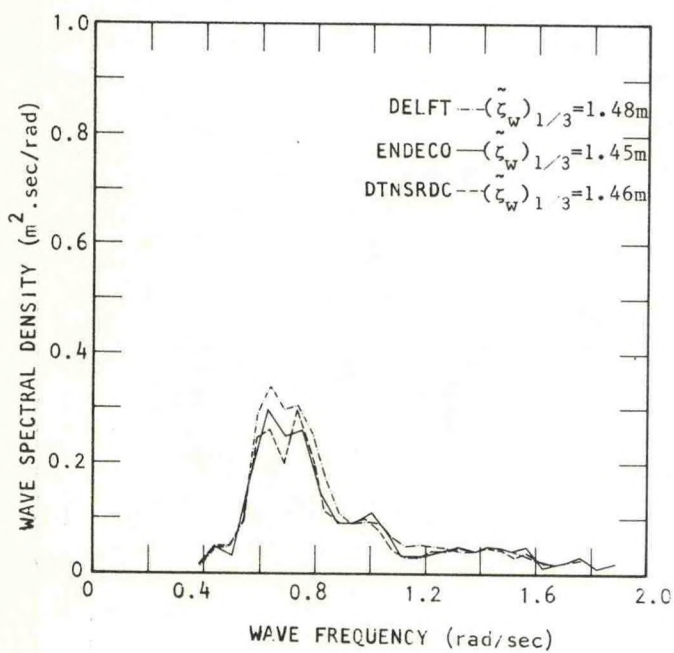


Figure 7. Spectral Comparisons of Three Analyses Using the ENDECO Buoy for Run 30

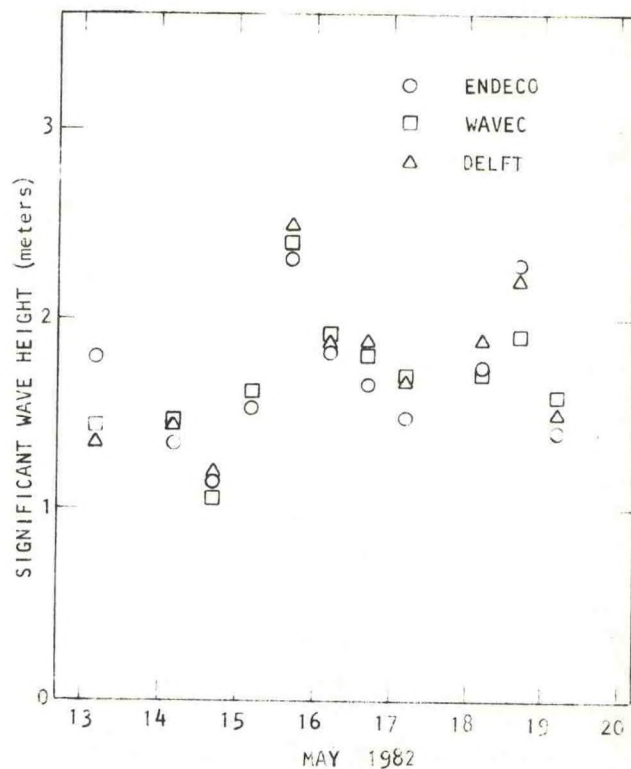


Figure 9. Significant Wave Height Comparisons Using the Delft Analysis Procedure



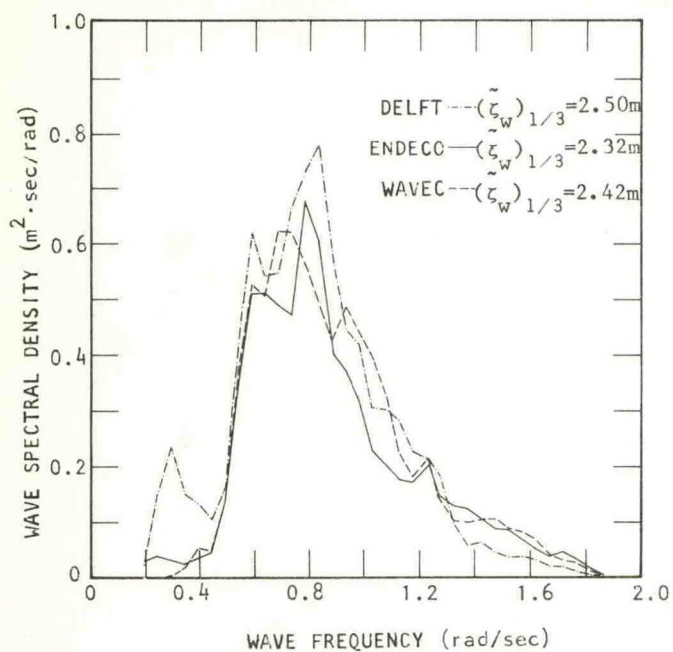


Figure 10. Spectral Comparisons of Three Buoys Using the Delft Analysis for Run 25

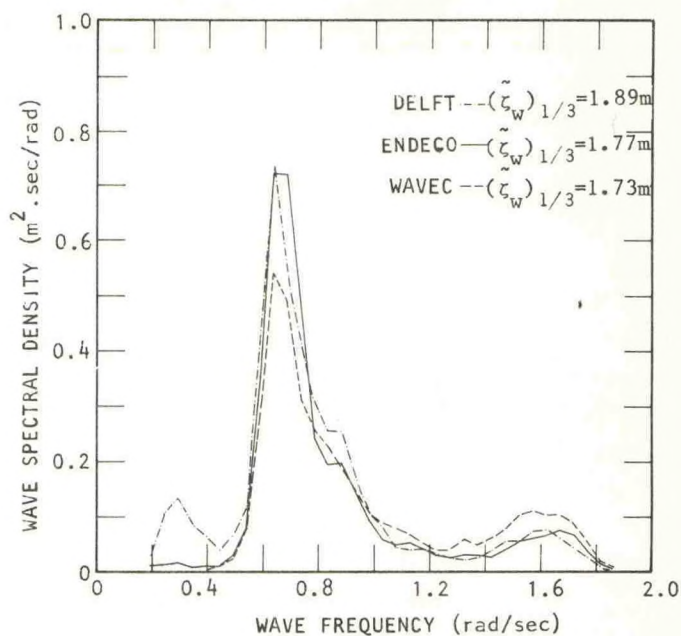


Figure 12. Spectral Comparisons of Three Buoys Using the Delft Analysis for Run 31

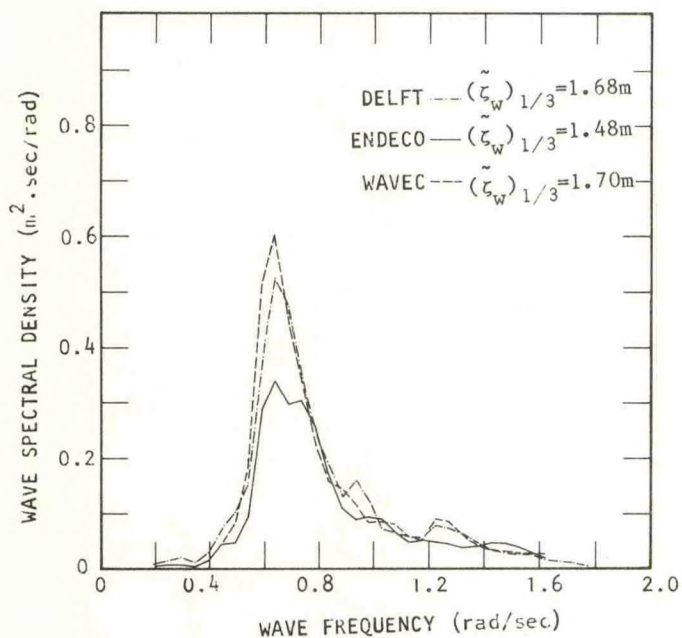


Figure 11. Spectral Comparisons of Three Buoys Using the Delft Analysis for Run 30



AN ANALYSIS OF BUREAU OF LAND MANAGEMENT (BLM) BOUY WINDS AND SEA HEIGHTS  
OFF THE SOUTHEAST ATLANTIC COAST

1  
Michael C. Koziara

National Weather Service Forecast  
Office, NOAA  
West Columbia, SC 29169

ABSTRACT

Bureau of Land Management (BLM) bouy wind and sea height data are examined for two locations off the southeast Atlantic coast. 1200 GMT reports were extracted from January through March and July through September, 1981 and January through June, 1982. Wind roses are constructed for eight compass points and two wind speed intervals. In addition, frequency diagrams of wind speed and sea heights are derived. Strong northwest to northeast winds are prevalent during the winter while light southwest flow occurs during the spring and summer. Average seas varied between one and 1 1/2 meters during the spring/summer and winter seasons, respectively.

percentage of observations available by season ranged between 72 and 83 percent (Table 1).

Table 1. Percentage of available wind and sea height observations from Bureau of Land Management (BLM) bouys 41004 (32.6 N, 78.7 W) and 41005 (30.4 N, 80.1 W) at 1200 GMT during January through March (winter), 1981/1982; April through June (spring), 1982; and July through September, 1981.

Bouy	Period	Wind	Sea Height
41004	Winter 1982	83	82
41005	Winter 1981	73	78
41004	Spring 1982	76	77
41005	Spring 1982	77	77
41005	Summer 1981	72	--

2. METHOD

Wind roses are constructed for eight compass points and two wind speed intervals (i.e., 0 to 15 and 15 to 30 knots) to show the frequency of occurrence of these components. In addition, frequency diagrams of wind speed (in 5 knot classes) and sea heights are derived.

3. RESULTS

A. Wind

1. Winter

Overall, the wind roses in Figs. 2 and 3 show that northwest and northeast winds are most common with frequencies in the 20 to 30 percent range. In contrast, winds from the north and southwest through east occur with frequencies of 10 percent or less. The majority of wind directions had "weak" speeds in the 0 to 15 knot range; while most of the west and northeast winds fell into the "strong" 15 to 30 knot class. Moreover, Figs. 4 and 5 indicate that the bulk of the wind speeds fell into the 10 to 20 knot range and that speeds in excess of 25 knots are rare.

1. INTRODUCTION

Real time Bureau of Land Management (BLM) bouy wind and sea height data are examined for two locations off the southeast Atlantic coast. The first BLM bouy, 41004, was located at 32.6 N, 78.7 W (about 75 nautical miles east-southeast of Charleston, SC); the second, 41005, was stationed at 30.4 N, 80.1 W (around 75 nautical miles east-northeast of Jacksonville, FL) (Fig. 1).

1200 GMT reports were extracted from the periods January through March/July through September, 1981 and January through June, 1982. The observations were grouped into three month seasons for the purposes of determining mean behavior and to facilitate interseasonal comparisons. The seasons are defined as follows: winter covers the months January through March; spring, April through June; and summer, July through September. The

1

Current Affiliation: National Weather Service  
Forecast Office, NOAA  
Slidell, LA 70458



The prevailing northwest to northeast flow is associated with air flowing out of continental polar (cP) anticyclones centered in the midwest and northeast U. S., respectively. Furthermore, the lack of any significant easterly component implies that the mean cyclone path is well to the northwest and north of the study area.

The lack of data prevented any north versus south comparisons within a given year. However, inter-annual differences were found. In particular, there was a greater incidence of "strong" west and northwest winds in 1981 than 1982. In addition, northeast winds occurred with less regularity in 1981 than in the following year. These differences are due to a shift in the mean position of the cP anticyclone from the Midwest to the Northeast during this time period.

## 2. Spring and Summer

"Weak" southwest flow dominates the study area during these seasons (Figs. 6 - 11). The Bermuda anticyclone is responsible for the mean flow; frontal intrusions into the region are rare. However, the summer of 1981 had a high occurrence of northeast winds caused by repeated intrusions of "back door" cold fronts (Fig. 8).

Year to year comparisons are not possible due to the lack of data; however, these differences are believed to be small. Finally, there did not seem to be any significant difference in the behavior between the north (41004) and south (41005) bouys during the warm seasons.

## B. Sea Heights

Sea heights average around 1 1/2 meters in the winter and around one meter during the spring (Figs. 12 - 15); while seas in excess of 2 1/2 meters are uncommon but are more apt to occur in the winter. These differences are probably due to the comparative strength of the winter over the spring synoptic pattern.

As stated previously, lack of sufficient information in both winters prevented any meaningful north versus south comparisons. Surprisingly, there was little change in the sea height characteristics for the two winters (Figs. 12 versus 13). Finally, sea heights tended to be slightly higher at the south (41005) than at the north (41004) bouy during the spring of 1982.

## 3. CONCLUSIONS

"Strong" northwest to northeast winds are prevalent during the winter while "light" southwest flow occurs in the spring and summer. The frequent intrusions of cP anticyclones into the Midwest and Northeast are responsible for the mean winter flow while the Bermuda anticyclone determines the basic wind behavior during the spring and summer.

Average seas varied between one and 1 1/2 meters during the spring/summer and winter seasons, respectively.

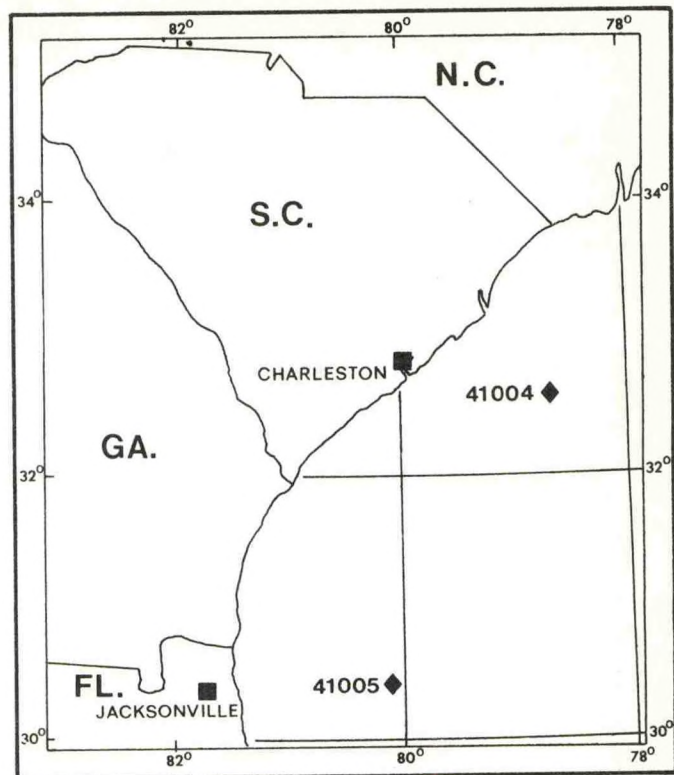


Fig. 1. Location of Bureau of Land Management (BLM) bouys in the study area. Bouy 41004 is at 32.6 N, 78.7 W; Bouy 41005 is at 30.4 N, 80.1 W.

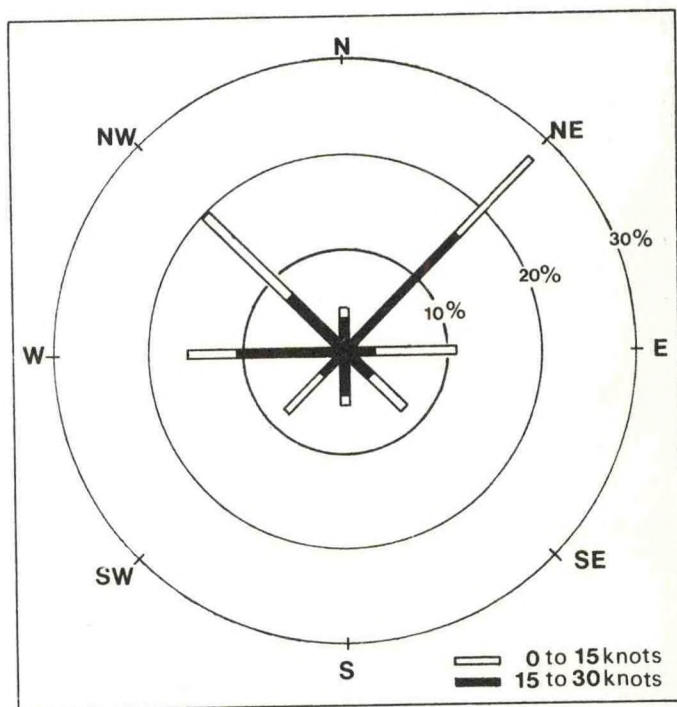


Fig. 2. Wind Rose for bouy 41004. 1200 GMT, January through March (winter), 1982. 75 cases



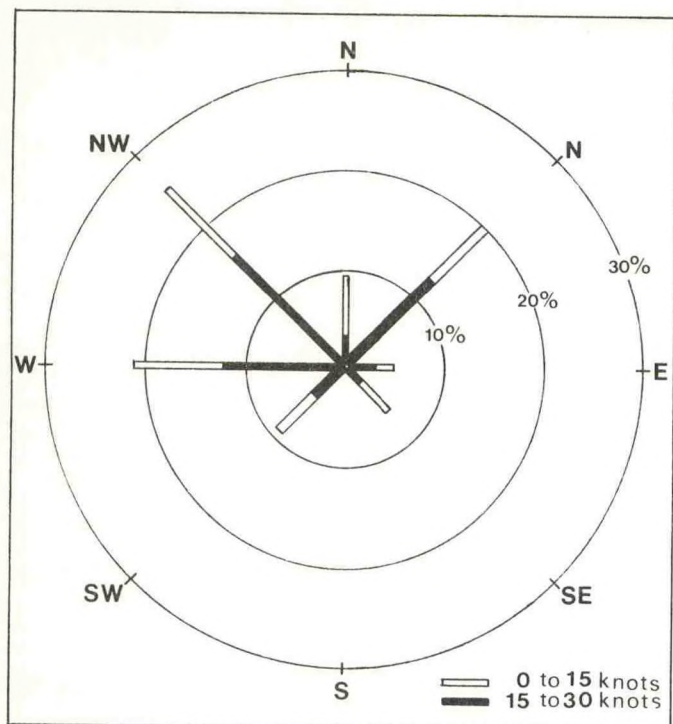


Fig. 3. Wind Rose for bouy 41005. 1200 GMT, January through March (winter), 1981. 66 cases

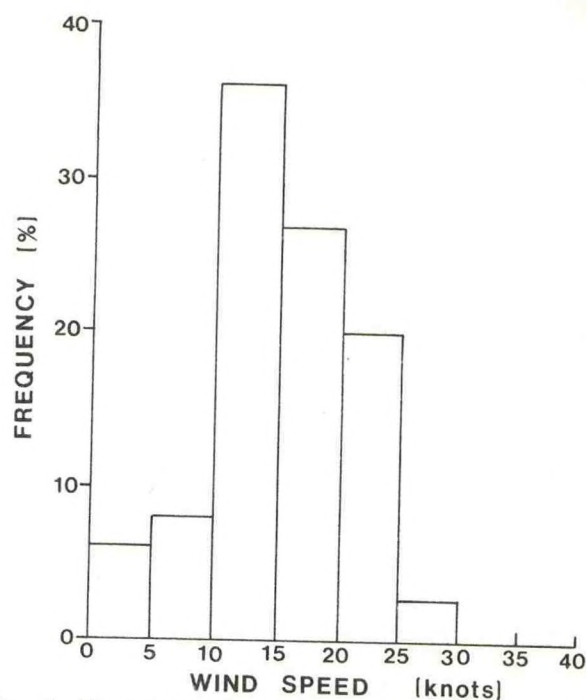


Fig. 5. Wind Speed Frequency Diagram for bouy 41005. 1200 GMT, January through March (winter), 1981. 66 cases

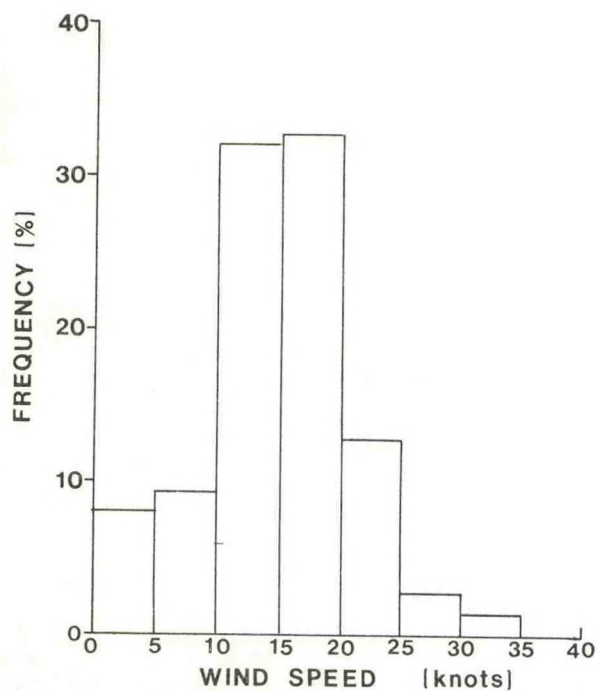


Fig. 4. Wind Speed Frequency Diagram for bouy 41004. 1200 GMT, January through March (winter), 1982. 75 cases

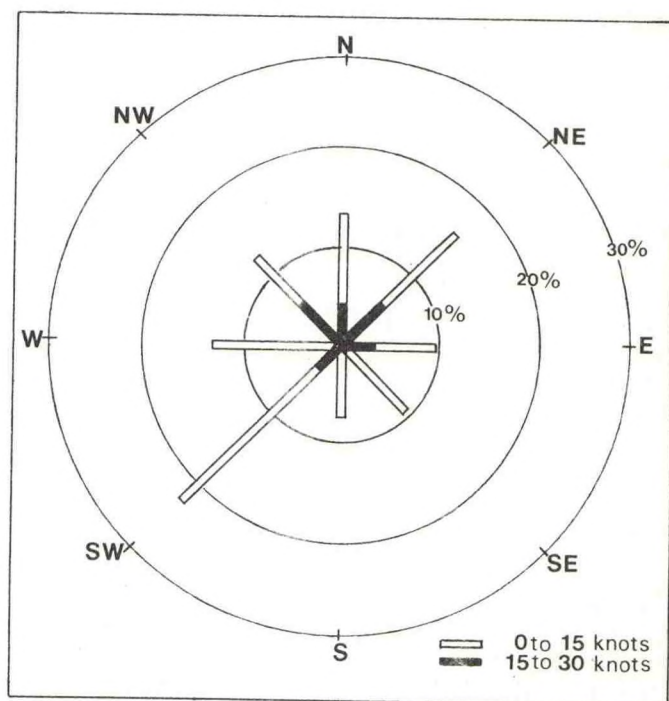


Fig. 6. Wind Rose for bouy 41004. 1200 GMT, April through June (spring), 1982. 69 cases



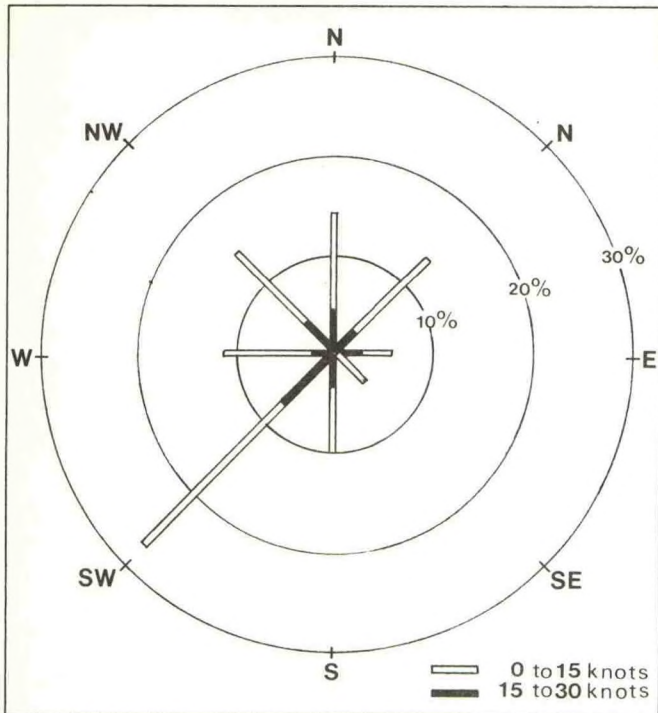


Fig. 7. Wind Rose for bouy 41005. 1200 GMT, April through June (spring), 1982. 70 cases

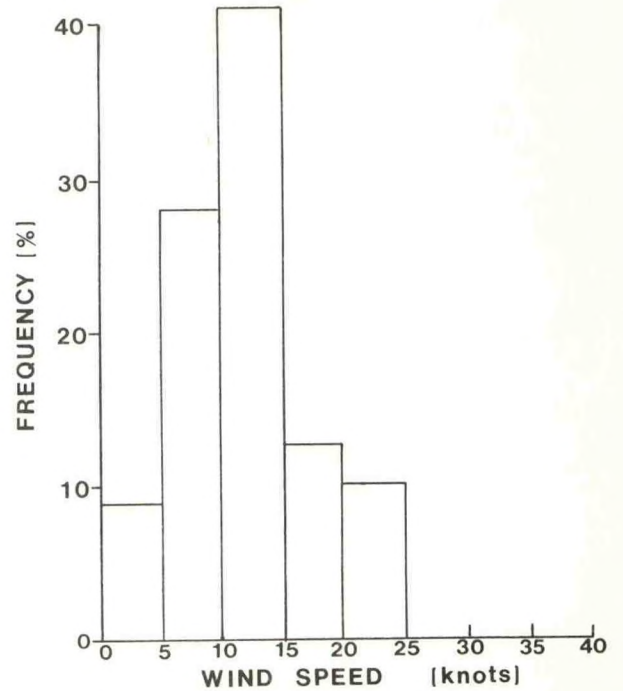


Fig. 9. Wind Speed Frequency Diagram for bouy 41004. 1200 GMT, April through June (spring), 1982. 69 cases

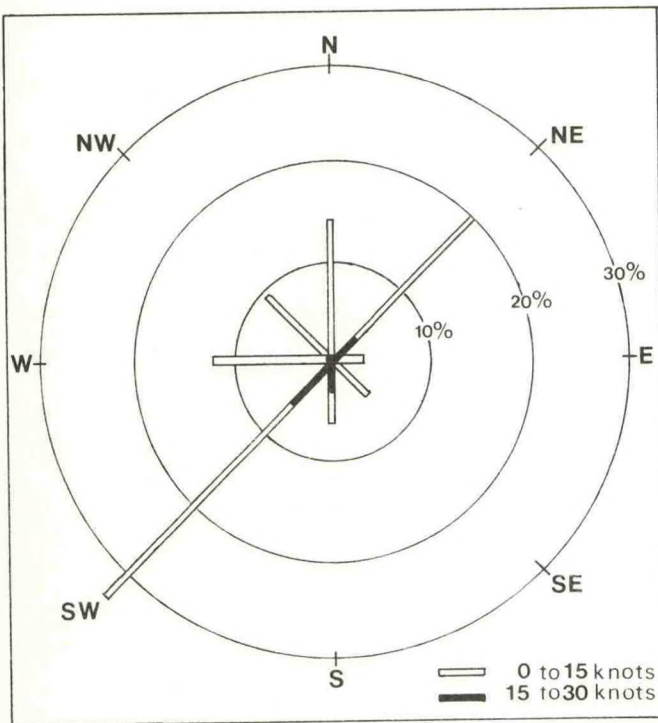


Fig. 8. Wind Rose for bouy 41005. 1200 GMT, July through September (summer), 1981. 66 cases

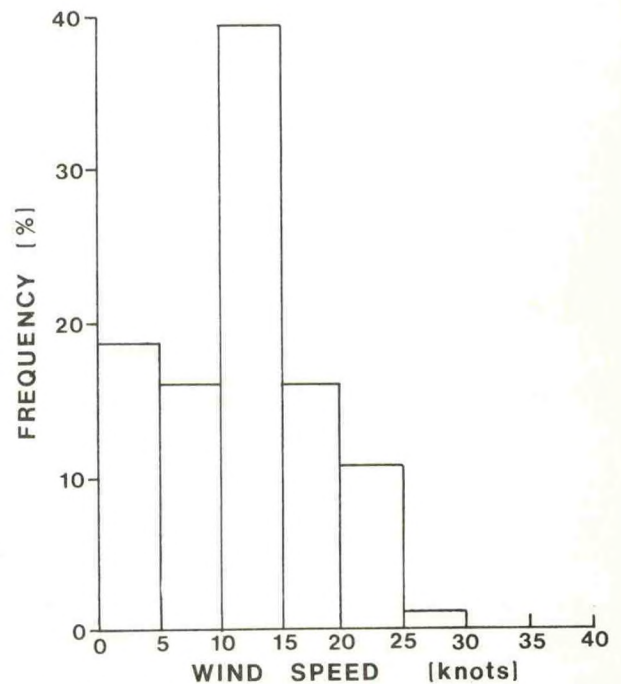


Fig. 10. Wind Speed Frequency Diagram for bouy 41005. 1200 GMT, April through June (spring), 1982. 70 cases



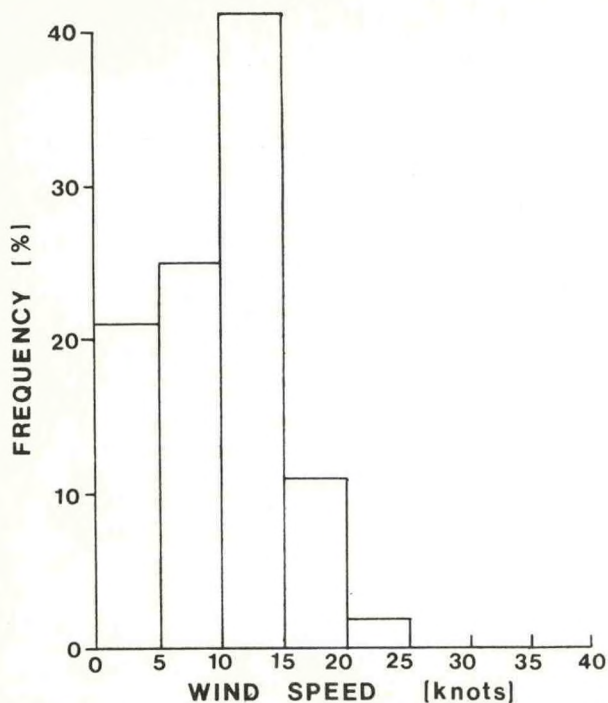


Fig.11. Wind Speed Frequency Diagram for bouy 41005. 1200 GMT, July through September (summer), 1981. 66 cases

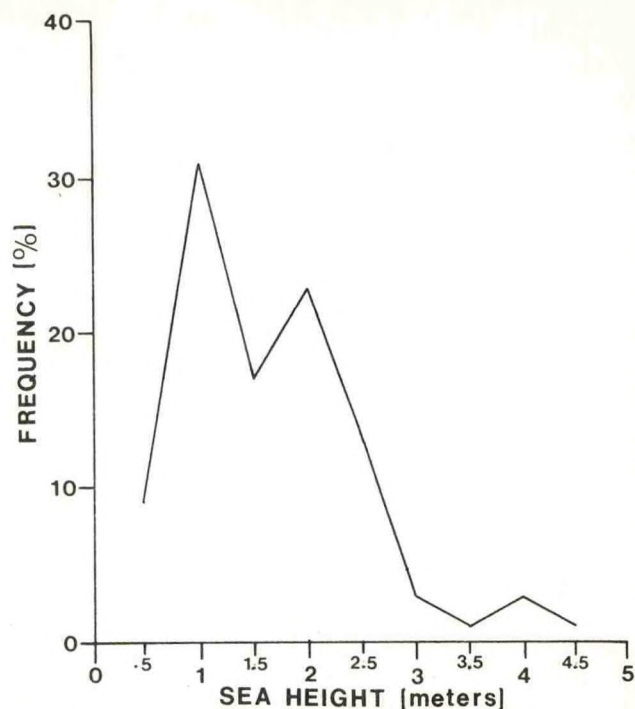


Fig.13. Sea Height Frequency Diagram for bouy 41005. 1200 GMT, January through March (winter), 1981. 70 cases

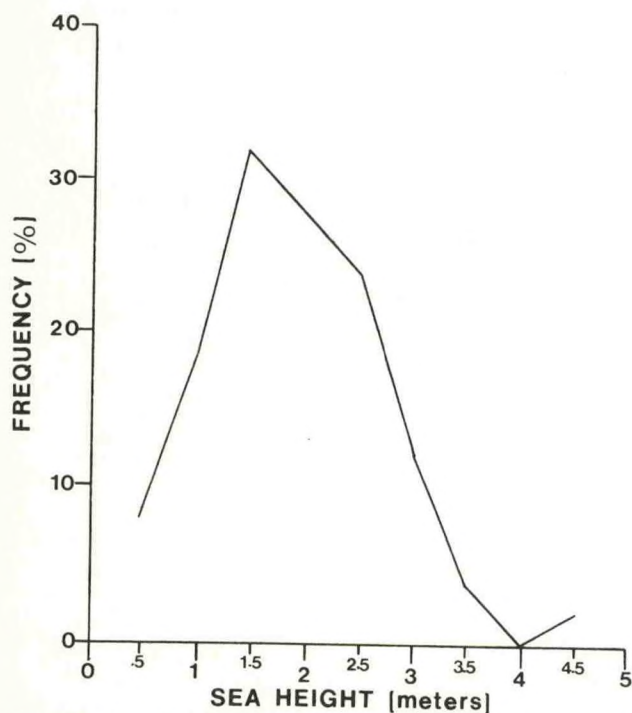


Fig.12. Sea Height Frequency Diagram for bouy 41004. 1200 GMT, January through March (winter), 1982. 74 cases

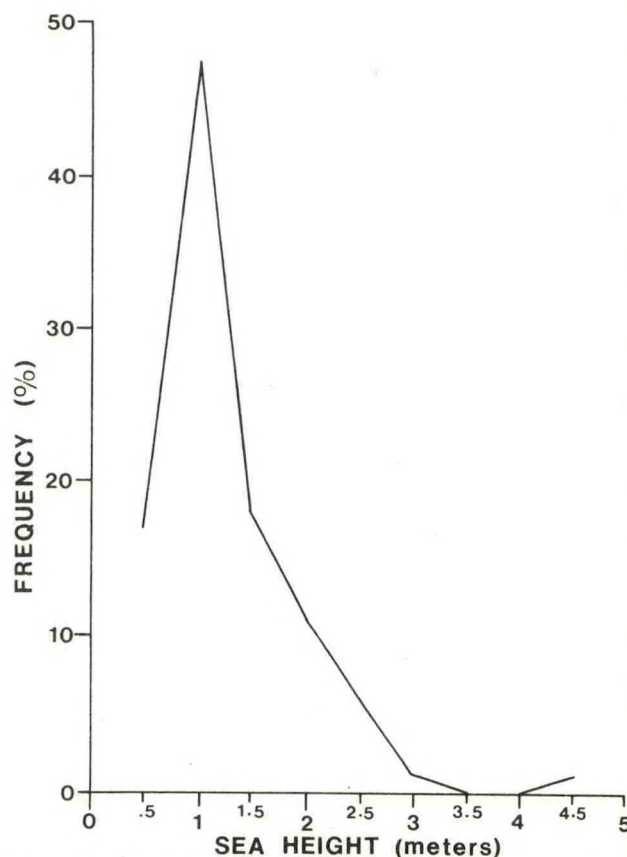


Fig.14. Sea Height Frequency Diagram for bouy 41004. 1200 GMT April through June (spring), 1982. 70 cases



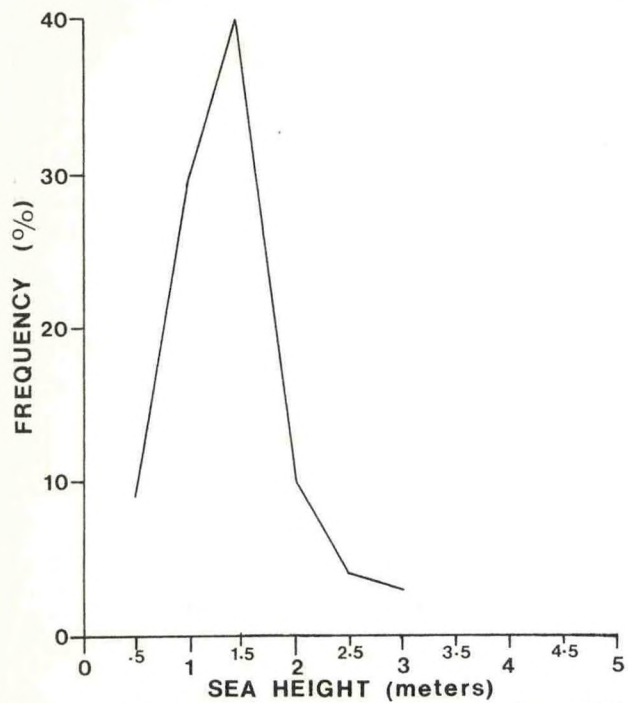


Fig.15. Sea Height Frequency Diagram for bouy 41005.  
1200 GMT, April through June (spring), 1982.  
70 cases



# HIGH RESOLUTION DIRECTIONAL WAVE SPECTRA USING THE F.F.T. DIGITAL BAND PASS FILTER METHOD

Edward C. Brainard II

ENDECO, INC.  
Marion, MA 02738

## ABSTRACT

The Longuet-Higgins and the newly developed Fast Fourier Transform (F.F.T.) Digital Band Pass Filter Method are reviewed. The algorithms used in each method are discussed. The directional resolution of the methods are analyzed using actual outputs from a rotating arm calibration system. Comparisons of actual sea data are presented showing the marked directional resolution improvement obtained using the F.F.T. Digital Band Pass Filter Method.

The implications of the new high resolution techniques are important relative to their impact on structural analysis, sediment transport and ship design. Previous techniques have provided directional resolutions within  $111^\circ$  for narrow band wave energy. The new technique provides directional resolution less than  $20^\circ$  for similar conditions.

## 1. INTRODUCTION

At the present time, directional spectra computed from a single buoy follow the cross spectral techniques by Longuet-Higgins, et al.<sup>1</sup> This technique represents a unique, ingenious and efficient mathematical method to compute directional spectra, mean wave direction and a spreading coefficient. However, the computational outputs contain considerable smoothing of the data and provide unrealistic reporting of the real world.

The increasing interest of petroleum companies to operate in more severe and deeper outer continental shelf areas has developed the need for higher resolution wave directional spectra. The data is essential to predict structure performance and can play an important role in the design of a cost-efficient project.

Panicker<sup>2</sup> outlines analysis techniques including Direct Fourier Transform Method, Parameterized Estimation Method, Amplitude and Phase Detection Technique, Discrete Wave Train Analysis and Data Adaptive Techniques which include the Maximum Likelihood Method and Maximum Entropy Method. Long, et al.,<sup>3,4</sup> describes additional development of adaptive statistical techniques for computing high resolution spectra from a Pitch/Roll buoy.

All the above methods, when applied to buoy applications, use continuous data strings from heave, pitch and roll and rely on a known and predictable phase relationship between the measure-

ment of heave and slope, but the finite dimensions of buoys generate unpredictable phase lags when operated in different sea conditions and under varying mooring conditions caused by varying depth and current. These unpredictable phase lags, as well as nonlinear wave conditions, introduce directional errors into the directional spectra. The development of the F.F.T. Band Pass Filtering Method has evolved to minimize these directional errors and provide an efficient computational method to provide high resolutions directional spectra.

## 2. LONGUET-HIGGINS METHOD

Cross Spectral methods using buoy heave, pitch and roll in this intercomparison use the Longuet-Higgins<sup>1</sup> method. The technique was adapted to the ENDECO Type 956 Directional WAVE-TRACK<sup>TM</sup> Buoy using techniques described by LeBlanc, et al.<sup>5</sup> Reduction of negative energy and side lobes computed in the directional spectra were minimized using weighting coefficients described by LeBlanc, et al.<sup>6</sup>

The generalized expression used in computation of directional spectra was:

$$E(f, \theta) = \frac{1}{2} a_0 + .781 (a_1 \cos \theta + b_1 \sin \theta) + .348 (a_2 \cos 2\theta + b_2 \sin 2\theta)$$

The computations were carried out using the following specifications:

Sampling Interval:	1 sec
Number of Data Points:	1024
Frequency Band:	.03 to .3 Hz
Frequency Bandwidth:	.01 Hz
Number of Frequency Bands:	28
Number of Frequency Components within Band:	10
Degrees of Freedom within the Band:	20

## 3. F.F.T. BAND PASS FILTERING METHOD

The ENDECO F.F.T. Band Pass Filtering Method uses the Cooley & Tukey<sup>7</sup> Fast Fourier Transform to digitally filter the heave, pitch and roll time series data into bands of .01 Hz bandwidth.

Figure 1 shows a simplified flow chart of the data processing technique. See specifications above which are followed during typical processing.

Initially, all of the heave data is checked for spikes, adjusted for proper units and normalized about the mean. The heave data is read into



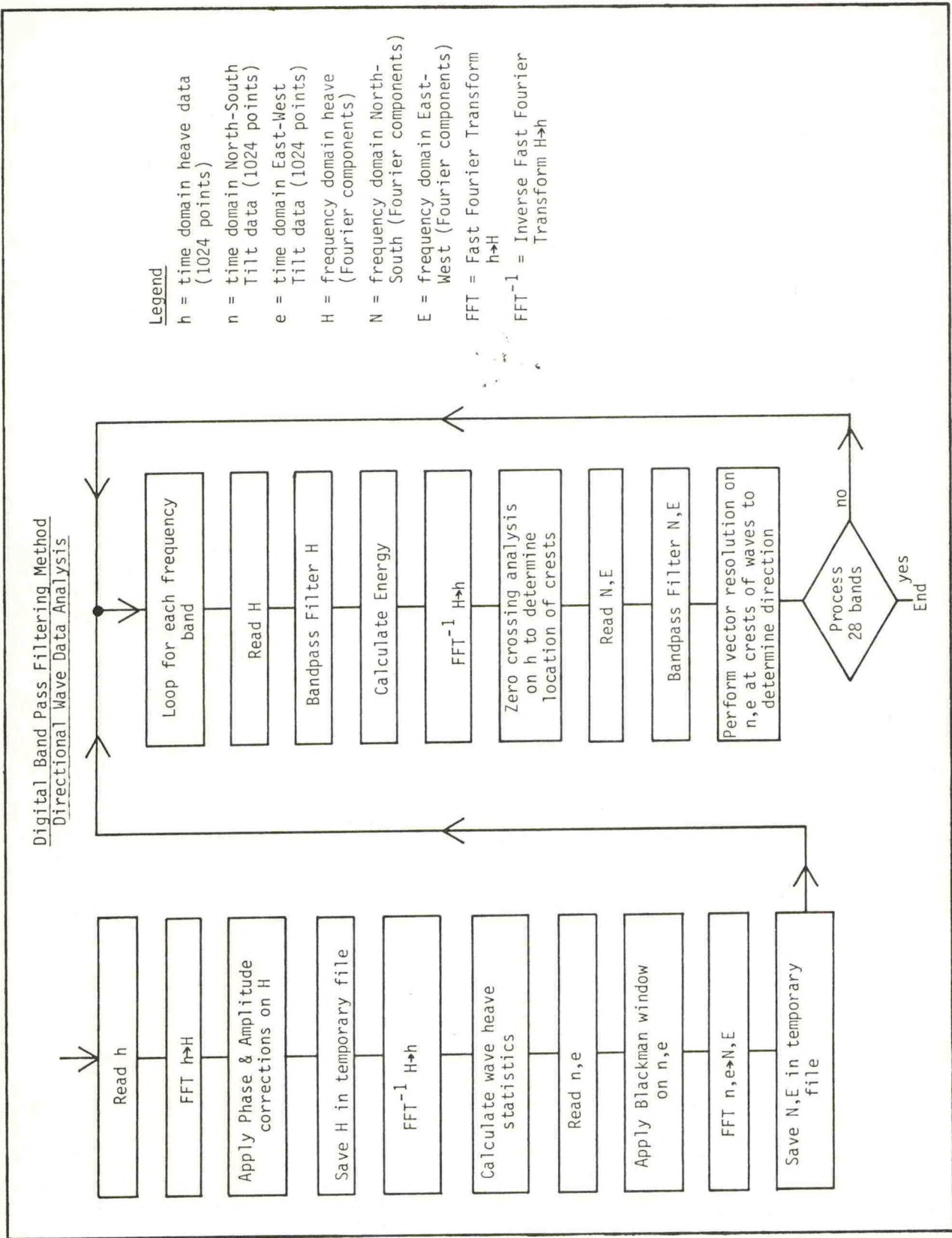


Figure 1. Flow Chart of ENDECO F.F.T. Band Pass Filtering Method



the F.F.T. routine and converted to the frequency domain. The data is corrected for phase and amplitude errors and inverse transformed to give a new time series which more accurately represents the actual wave train monitored by the WAVE-TRACK buoy. Zero up-crossing wave statistics are performed on the corrected heave data to give significant wave height, profile of the maximum wave, etc.

At this point, the North-South and East-West Tilt data are checked for spikes, adjusted for proper units, normalized about the mean and the Blackman window is applied. The F.F.T. is used to transform the data into the frequency domain. Phase and amplitude corrections are made.

Now the heart of the processing begins and is repeated sequentially for each frequency band. The heave data is read and the F.F.T. is used as a band pass filter. This is achieved by setting all the frequency components to zero except those in the desired band. Then the components are inverse transformed to generate a heave data string in the time domain which only contains the frequency components of the desired band. Zero up-crossing analysis is carried out on the filtered heave data to determine the time of the crest of each wave. The data is stored.

The North-South and East-West Tilt data in the frequency domain are read and are similarly band pass filtered using the F.F.T. similar to the heave data. At each wave crest of the heave data, the two tilt components are sampled. A vector computation provides an instantaneous direction at the wave crest for each wave.

$$\theta = \tan^{-1} \left( \frac{T_{E-W}}{T_{N-S}} \right)$$

Where

$\theta$  = Instantaneous direction  
 $T_{E-W}$  = Tilt (East-West)  
 $T_{N-S}$  = Tilt (North-South)

This value,  $\theta$ , is multiplied by the square of the wave height to provide weighting of the direction relative to the energy of that wave and added into an accumulator. After processing the data string, the weighted mean and standard deviation are computed. Simultaneously, a matrix consisting of a joint distribution of .01 Hz resolution frequency bands from .03 to .3 Hz and 10 degree direction bands from 000° to 360° is developed. At each wave crest, the square of the RMS wave height is summed with the appropriate element of the 36 element directional array. After all of the wave crests have been analyzed, the values in each directional element are normalized by the number of waves in the frequency band. The end result is a directional variance spectrum of the sampled data.

Figure 2 provides a simplified representation of the processing of narrow bandwidth data from the three channels. Note that a phase error of 90° between heave and tilt will not introduce a directional error as long as the tilt signals are resolvable from noise.

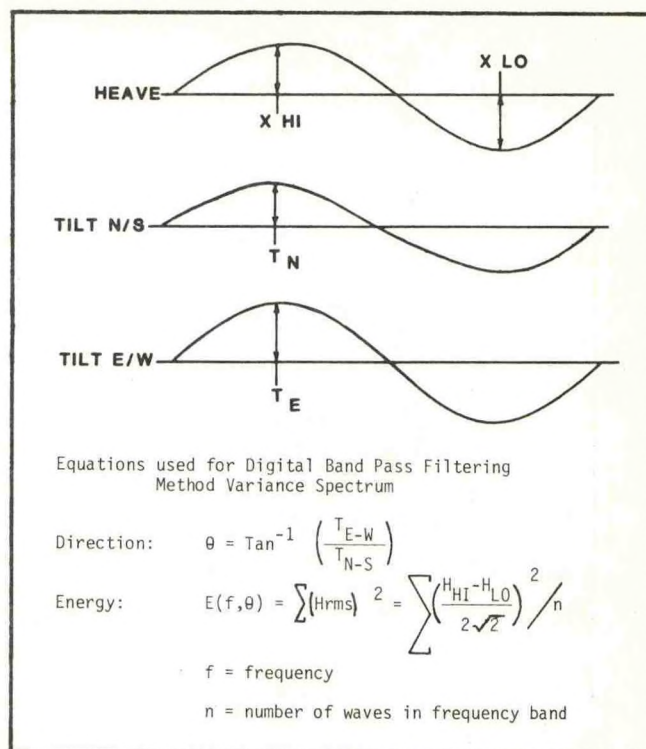


Figure 2. Analysis of Heave,  $T_{N-S}$  &  $T_{E-W}$  Data (.01 Hz Bandwidth) to Determine Mean Direction, Standard Deviation and Directional Spectra.

#### 4. COMPARISON OF ROTATING ARM SPECTRA

Even though the development of the F.F.T. Band Pass Filtering Method and the modifications of the Longuet-Higgins Method were carried out using mathematically simulated data, final comparison of the methods was performed using data generated from the rotating arm device shown in Figure 3. Using data from this source aids in more closely approaching the real world and sometimes reveals overlooked characteristics of the buoy and software system. Since the ENDECO Type 956 Directional WAVE-TRACK Buoy permits the easy removal of the sensor package from the buoy, the rotating arm can be designed with minimum size, weight and cost.

Data was taken with the arm rotating at nearly constant frequency and fixed in direction during the sampling interval. The output thus represents a unimodal spectrum at one frequency and direction, even though direction may not sit precisely in the center of a specific band.

Figure 4 shows the directional spectra for inputs at constant frequency of .07 Hz from 000° to 360°. The high resolution of the F.F.T. Band Pass Filter Method is clearly evident as compared to the Longuet-Higgins Method. At the mean direction, the F.F.T. Band Pass Filter Method shows 17 times greater energy in the peak direction band.



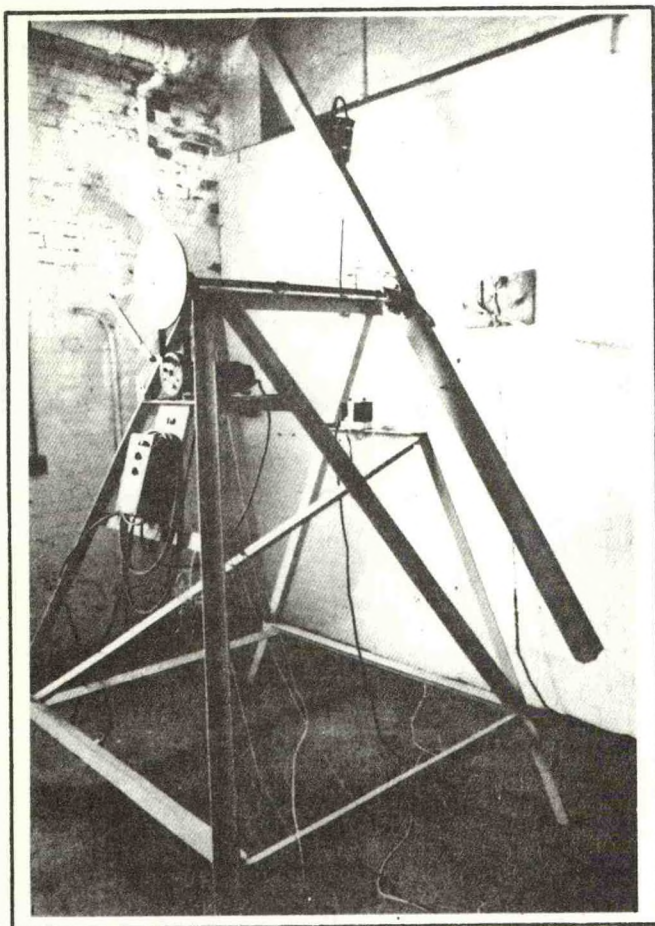


Figure 3. ENDECO Rotating Arm WAVE-TRACK Calibration System

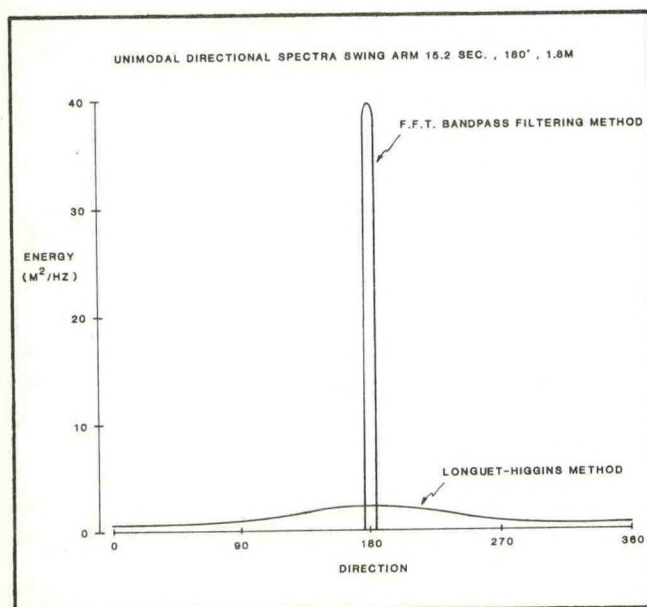


Figure 4. Swing Arm Unimodal Directional Spectra Using Two Methods of Processing

## 5. HALF POWER BANDWIDTH

The theoretical half power bandwidth of the Longuet-Higgins Method using weighting coefficients of 0.781 and 0.348, as recommended by LeBlanc<sup>6</sup>, is 111°.

The half power bandwidth for the F.F.T. Band Pass Filter Method is influenced by the width of the directional bins used during the processing. In the case of this analysis, 10° width bins have been used.

An exact intercomparison of the directional resolution of the two different methods is difficult since the processing methods are radically different. Based on the equivalent bandwidth concept of a signal spectrum, the approximate half power bandwidth or resolution is 20° for the F.F.T. Band Pass Filter Method using 10° width directional bins.

Figure 5 shows four cases of hypothetical unimodal spectra of narrow bandwidth. Case A shows all the energy concentrated at the center of the 0° bin of 10° bandwidth. Case B shows the energy shifted +5°. In this case, 50% of the energy will fall in each of the 0° to +10° bins. Case C shows the similar result as the energy is shifted to -5° from Case A. Case D shows the resultant of directional shifting of ±5° which fall into directional bins +10° and -10°. Since the bin bandwidth is 10°, the resultant half power resolution is 20°.

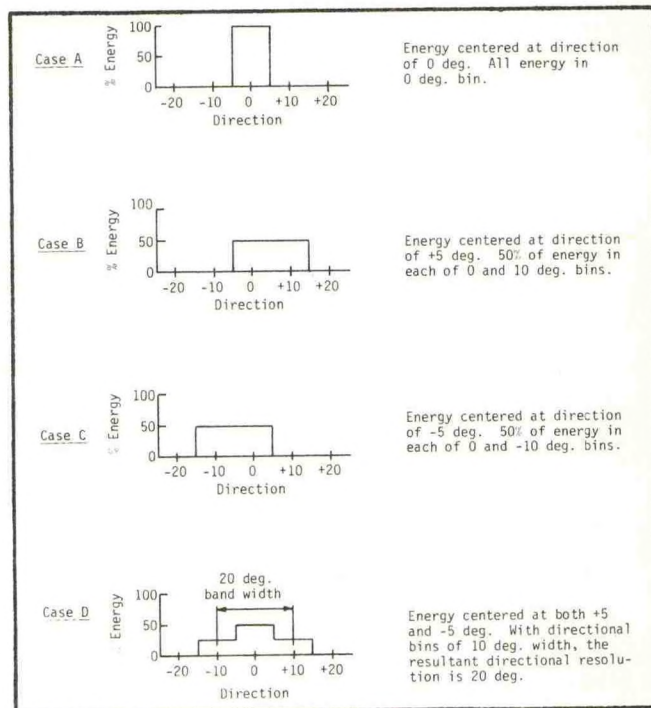


Figure 5. Bandwidth of F.F.T. Band Pass Filtering Method Using 10° Directional Bins



In summary, the directional resolution of the F.F.T. Band Pass Filter Method is:

$$\text{Resolution} = 2 (\text{Bin Width}) = 20^\circ$$

Thus, a reduction in bin width will result in greater directional resolution down to the point where the limit is the resolution of the buoy hull hydrodynamics and the sensor resolution. The sensor resolution is the limiting factor in this case. It is  $\pm 1.4^\circ$ .

#### 6. COMPARISON OF ARSLOE DIRECTIONAL SPECTRA

Figure 6 shows a directional spectra table at 1115 hours on October 25, 1980, near the peak

of the storm experienced in the ARSLOE experiment reported by Szabados<sup>8</sup>. This data was processed using the Longuet-Higgins Method. Figure 7 shows the same data processed using the F.F.T. Band Pass Filter Method. The data was purposely taken from a time during the storm where narrow frequency band spectra was present. During the early stages of the storm, the spectra would vary from broad to narrow as the conditions of wind and current changed. This particular condition of narrow frequency spectra shows that the real world does have conditions approaching those generated on the swing arm used during the testing of the buoy.

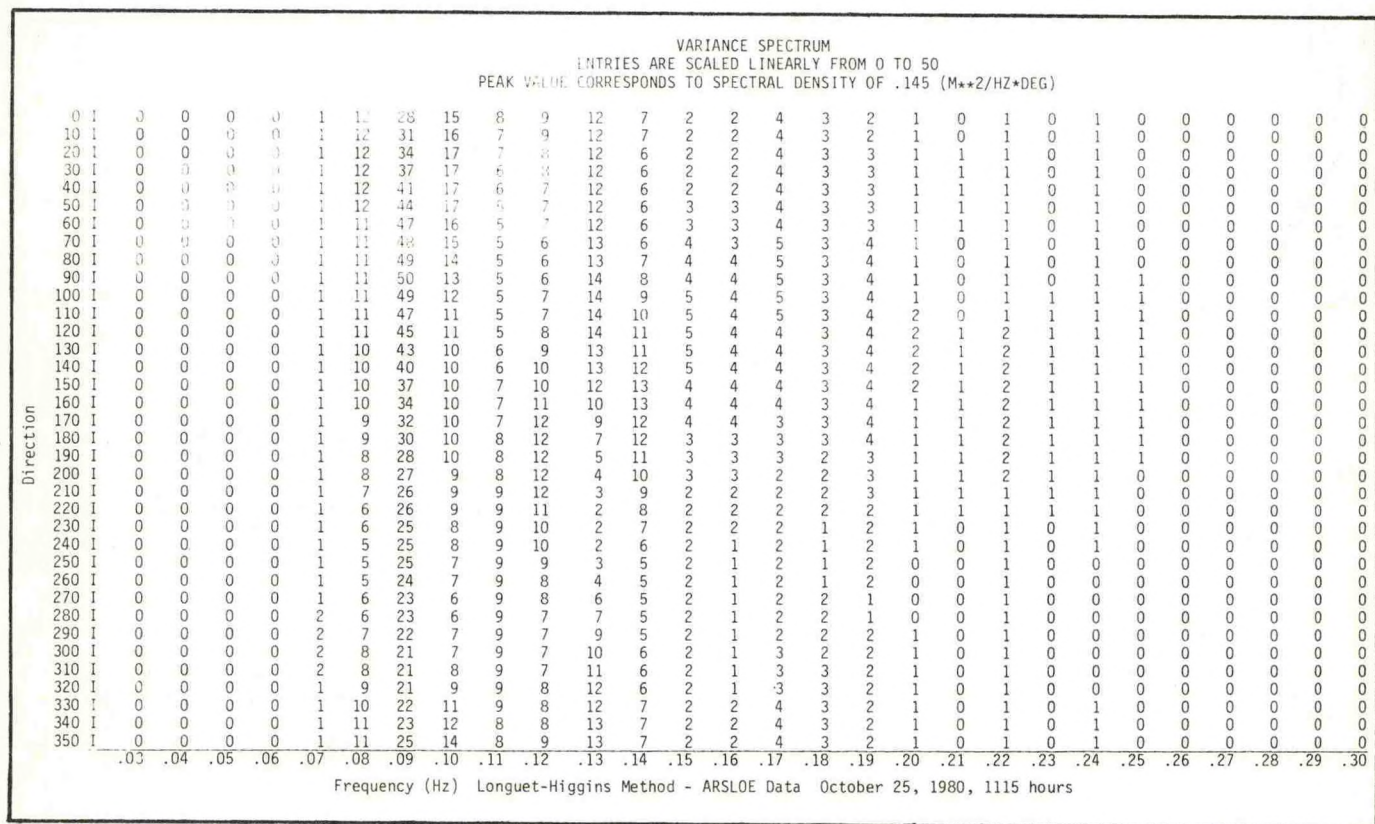


Figure 6. ARSLOE Data from ENDECO Type 956 Directional WAVE-TRACK Buoy at 1115 hours, October 25, 1980 Near Peak of Storm Using Longuet-Higgins Method



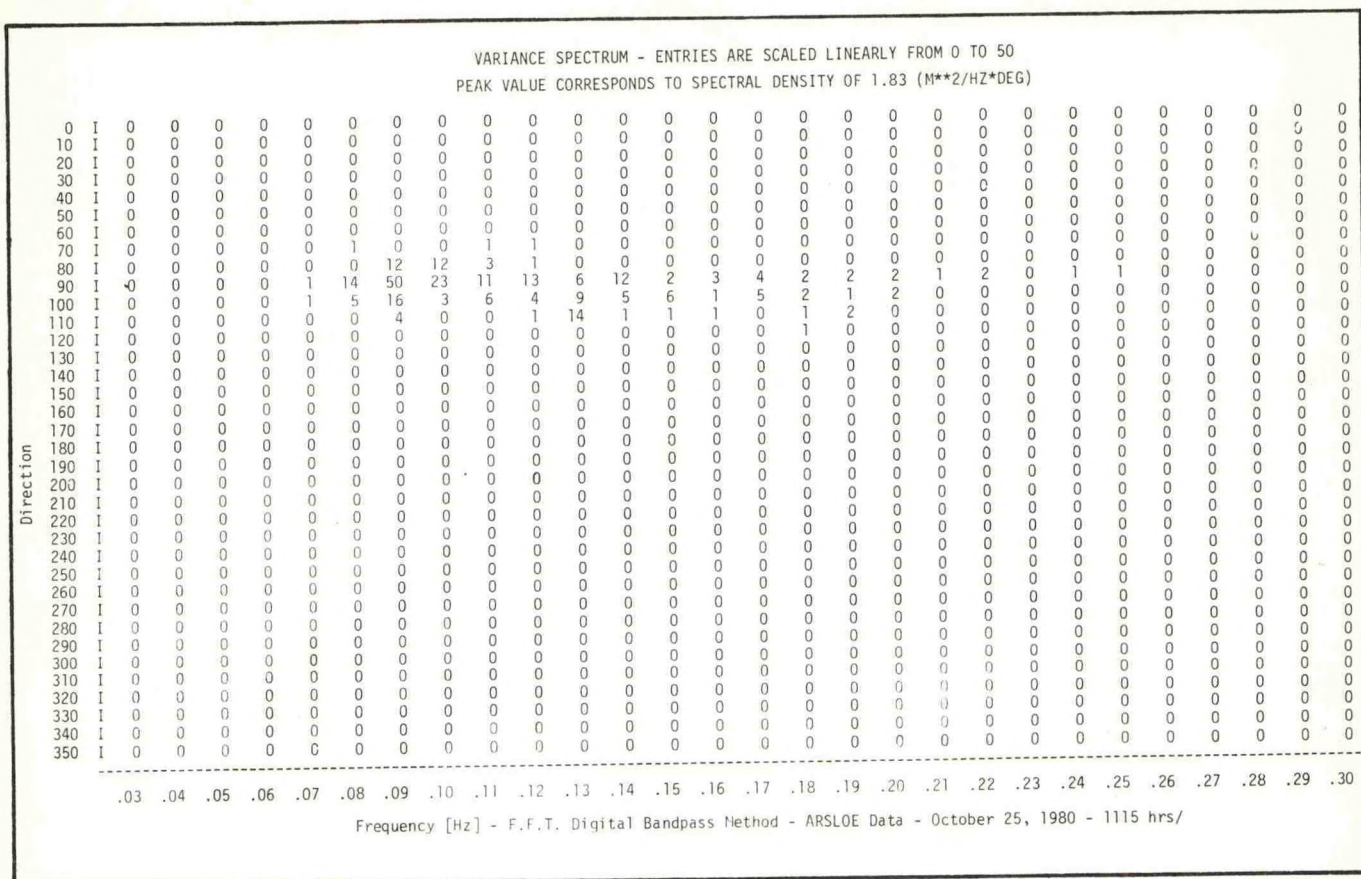


Figure 7. ARSLOE Data from ENDECO Type 956 Directional WAVE-TRACK Buoy at 115 hours, October 25, 1980 Near Peak of Storm Using F.F.T. Band Pass Filtering Method

Figure 8 shows a graph of the directional spectra at the frequency of peak energy using the two methods at 1115 hours October 25, 1980. The spreading of the Longuet-Higgins Method is quite apparent. The band-widths of these two spectra are 195° and 15°. The difference in peak energy is 1262%.

## 7. STATISTICAL REVIEW OF METHODS

Figure 9 shows the heave spectra from the ENDECO WAVE-TRACK Buoy derived from the Longuet-Higgins Method of analysis of the buoy heave channel. Also shown is the heave spectrum derived by summing the energy in each frequency column of the F.F.T. Digital Band Pass variance spectrum and using the following formula to determine energy in each frequency band:

$$E(f)_{\text{Total}} = \left( \frac{\sum E(f)}{50} \right) (a)(b)$$

Where

$E(f)$  = Energy in each bin

$a$  = scale factor ( $M^2/HZ \times \text{Deg}$ )

$b$  = bin width = 10°

Also shown are the 90% confidence limits computed for the spectrum from the traditional Longuet-Higgins auto spectral method. The 90%

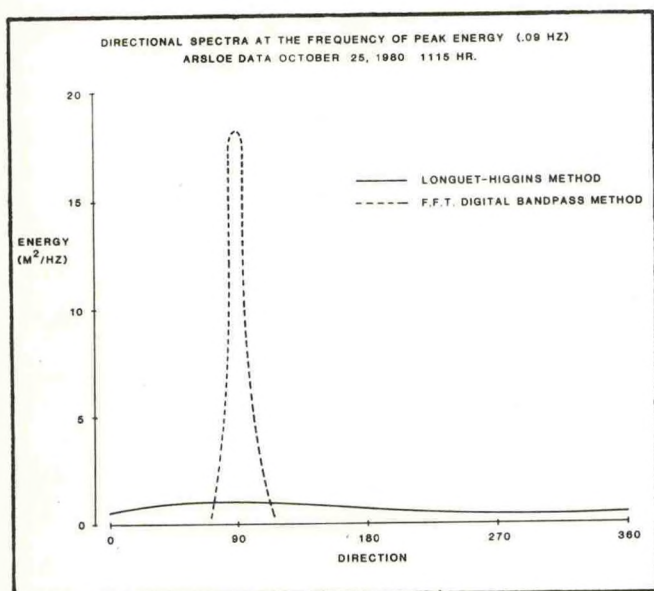


Figure 8. Directional Spectra at the Frequency Peak Energy (.09 Hz) Using the Two Methods at 1115 hours, October 25, 1980



confidence limits are calculated using the relationship:

$$\frac{\chi^2 E'(f)}{\chi^2_{\gamma;0.05}} \leq E(f) < \frac{\chi^2 E'(f)}{\chi^2_{\gamma;0.95}}$$

Where

$\gamma$  = degrees of freedom (twice the Fourier components in each band)

$E'(f)$  = calculated spectral energy density

$E(f)$  = True spectral energy density

$\chi^2$  = values are obtained from a Chi-Square distribution table or from the equation below:

$$\chi^2_{\gamma;0.05} = \left[ 1 - (2/\gamma) + 1.645(2/\gamma)^{1/2} \right]^3$$

$$\chi^2_{\gamma;0.95} = \left[ 1 - (2/\gamma) - 1.645(2/\gamma)^{1/2} \right]^3$$

From Figure 9 it is clear that the F.F.T. Band Pass Filter Method produces variance spectra which closely follow within the 90% confidence limits of the traditional Longuet-Higgins auto spectral method.

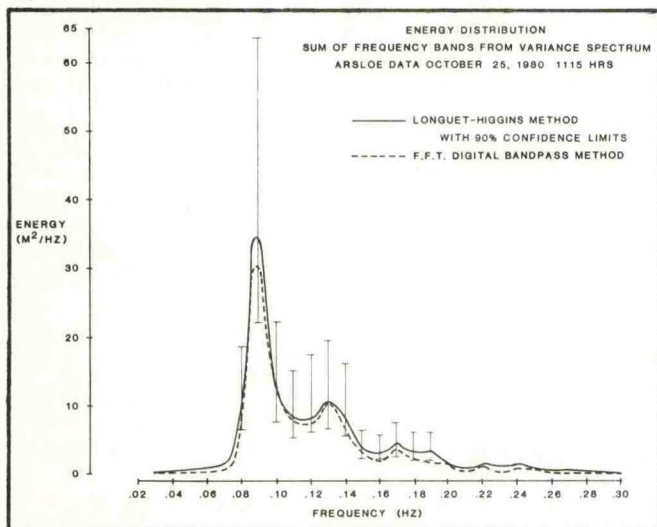


Figure 9. Heave Spectra from Conventional F.F.T. Heave Spectral Analysis and Similar Spectrum Derived from F.F.T. Band Pass Filtering Method by Summing Matrix Energy at Each Frequency

## 8. CONCLUSION

A new method for generating high resolution directional spectra has been presented. This method is immune to system phase errors of up to  $\pm 90^\circ$  which may be caused by buoy hydrodynamic responses or electronic and system processing phase shift. The system is also insensitive to the buoy tilt response.

A typical storm situation encountered at the 1980 ARSLOE experiment has been processed using the Longuet-Higgins and the F.F.T. Band Pass Filter Methods during a period showing unimodal conditions with low wave crest dispersion. The

results show a difference of 1262 between the values of maximum energy density at the peak frequency with half power bandwidths 1300% greater for the Longuet-Higgins Method than the F.F.T. Band Pass Filter Method.

The F.F.T. Band Pass Filter Method is suggested for use in directional wave analysis at critical events due to its considerably higher directional resolution and immunity from system phase and amplitude errors.

## 9. ACKNOWLEDGEMENTS

I wish to acknowledge the assistance and encouragement of the following individuals: Dr. Marshall Earle, Marine Environments Corp., Dr. Chi Hau Chen, Southeastern Massachusetts University, and Edward C. Brainard III of ENDECO, INC.

I also wish to thank NOAA/NOS, Wave Climate Group, Dr. Ledolph Baer, for the use of ARSLOE data from the ENDECO Type 956 Directional WAVE-TRACK Buoy.

## 10. REFERENCES

1. D. E. Cartwright, M. Longuet-Higgins, and N. D. Smith, "Observations of Sea Waves Using the Motions of a Floating Buoy," *Ocean Wave Spectra* (U. S. Naval Oceanographic Office, May 1961).
2. N. N. Panicker, "Review of Techniques for Directional Wave Spectra," *Procedures of the International Symposium on Ocean Wave Measurement & Analysis* (New Orleans, LA., September 1974).
3. K. Hasselman and R. B. Long, "A Variational Technique for Extracting Directional Spectra from Multi-Component Wave Data," *Journal of Physical Oceanography* Vol. 9, No. 2 (March 1979).
4. R. B. Long, "The Statistical Evaluation of Directional Spectrum Estimates Derived from Pitch/Roll Buoy Data," *Journal of Physical Oceanography* Vol. 10, No. 6 (June 1980).
5. L. R. LeBlanc and F. H. Middleton, "Pitch-Roll Buoy Wave Directional Spectra Analysis, Measuring Ocean Waves," *Proceedings of a Symposium and Workshop on Wave-Measurement Technology* (Washington, D. C., April 1981).
6. L. R. LeBlanc and F. H. Middleton, "Storm Directional Wave Spectra Measured with a Single Buoy," *Marine Technology Society, Oceans 82*, (September 1982).
7. J. W. Cooley and J. W. Tukey, "An Algorithm for the Machine Calculation of Complex Fourier Series," *Math Comput.* Vol. 19, pp. 297-301 (April 1965).
8. M. W. Szabados, "Intercomparison of the Offshore Wave Measurements during ARSLOE," *Marine Technology Society, Oceans 82*, September 1982.



NONDIRECTIONAL WAVE MEASUREMENTS  
WITH THE USGS AID TO NAVIGATION BUOY

Joseph E. Murphy

University of New Orleans  
New Orleans, LA 70148  
(Consultant to Computer Sciences Corporation)

ABSTRACT

During late January 1982, a USGS Aid to Navigation Buoy, Type 8-26, configured with a wave measurement system was deployed simultaneously with a modified Datawell Waverider buoy, each capable of reporting through the GOES system. This experiment provided 73 pairs of power spectral densities, significant wave heights, and wave periods. Using the Waverider spectra as ground-truth, a computer program provided estimates of the USGS buoy hull power transfer function. Results of this calibration will be presented, as well as a comparison of wave data obtained with the USGS buoy and a large discus hull during the same experiment. A resonance in the USGS buoy hull near 0.35 Hz reported elsewhere is confirmed.

1. INTRODUCTION

This report describes the analysis of wave data acquired during experiments performed in August 1981 and January 1982 to assess the feasibility of using an ANBESS hull (U.S. Coast Guard Buoy, Type 8-26) to make nondirectional wave measurements. During the August 1981 experiment, an ANBESS hull and OTP (Ocean Test Platform, a 12-meter concrete discus buoy) were deployed simultaneously at site 42007 (30.1N latitude, 88.9W longitude) near Panama City, Florida. These two buoys were configured with WDA systems described elsewhere.<sup>1</sup> Sixty-four pairs of wave displacement power spectral densities were obtained in the first experiment and used in the initial analysis. In the January 1982 experiment at the same site, three buoys were deployed: ANBESS, OTP, and WRANSAC. The third buoy was developed by the NOAA Data Buoy Center (NDBC) as a calibration standard. It is a modified Datawell Waverider buoy system capable of reporting through the GOES UHF system in near real time. Comparison spectra from any of the larger buoys and the 0.9-meter diameter WRANSAC are used to estimate the hull power transfer function (PTF) of the former. This second experiment in January 1982 yielded 74 spectral pairs (ANBESS/WRANSAC) for use in the subsequent analysis.

2. WAVE DATA COMPARISON: AUGUST 1981 EXPERIMENT

Wave data from an ANBESS hull and OTP were first acquired during the August 1981 experiment at site 42007. These data were processed with the recently modified version of the computer program BTFFIT which is described in Reference 2. Sixty-four pairs of wave displacement power spectral densities were available for the analysis. This experiment could not yield accurate estimates of the ANBESS hull PTF because OTP had not been calibrated, although the general behavior of its hull PTF could be estimated from experience with other 12-meter discus buoys.<sup>3</sup>

Using the 64 spectral pairs between 0.16 Hz and 0.40 Hz it was found that the correlation coefficient varied from a low of 0.676 at 0.36 Hz to a high of 0.928 at 0.19 Hz. Moreover, the BTFFIT calibration showed that both the least squares estimate and the fourth order technique for the hull PTF's have a resonant behavior centered on 0.35 Hz. These preliminary results are shown in Figure 1.

3. WAVE DATA ANALYSIS: JANUARY 1982 EXPERIMENT

During late January 1982 three buoys, ANBESS, OTP, and WRANSAC were simultaneously deployed at site 42007. The data obtained were used to calibrate both OTP and ANBESS. The OTP/WRANSAC calibration using the BTFFIT program utilized a total of 521 spectral pairs with significant correlation from 0.08 Hz up to 0.50 Hz. Because of a power failure, the ANBESS/WRANSAC calibration was limited to a total of 74 spectral pairs. These showed significant correlation from 0.10 Hz up to 0.50 Hz.

New hull PTF's for ANBESS and OTP derived from the BTFFIT calculations were used to process the data from the January 1982 experiment a second time. Specifically, wave displacement power spectral densities, significant wave heights and wave periods were calculated from the original ANBESS and OTP data after correcting for hull PTF's.



Using the 74 coincident data sets available, the wave heights compared as follows:

Mean wave height (ANBESS)	0.956 meter
Mean wave height (OTP)	0.866 meter
Mean wave height difference	0.090 meter
Wave height correlation	0.904

Figure 2 illustrates how the significant wave heights obtained from the two buoys tracked one another during the experiment.

Similarly, using the same 74 coincident data sets, the wave periods were compared with the following results:

Mean wave period (ANBESS)	4.715 sec
Mean wave period (OTP)	4.824 sec
Mean wave period difference	0.109 sec
Wave period correlation	0.804

The estimates for the ANBESS hull PTF's used in this second set of calculations for wave displacement power spectral densities, wave heights and wave periods were taken to be the geometric mean of the least squares and fourth order technique estimates. These are given in Figure 3. Using the 74 pairs of coincident wave displacement psd's, the average correlation coefficient (from 0.11 Hz to 0.50 Hz) was 0.769.

In the second experiment using the WRANSAC psd's as ground-truth, the 74 spectral pairs gave estimates of the ANBESS hull PTF showing a much sharper resonance at 0.35 Hz. The resonant frequency and sharpness of the curve agrees with the earlier results of Price.<sup>4</sup>

#### 4. DISCUSSION AND CONCLUSIONS

Data acquired in August 1981 from ANBESS and OTP show significant correlations between their power spectral densities; using the OTP as a reference, the data indicated a resonance associated with the ANBESS hull at 0.35 Hz.

Simultaneous deployment of ANBESS, OTP and WRANSAC in January 1982 allowed improved estimates to be made of the OTP hull PTF and the ANBESS hull PTF. The resonant behavior of the ANBESS hull was confirmed. Using these new hull PTF's corrected values of significant wave heights and wave periods obtained with ANBESS and OTP compared very well. The agreement of their wave displacement power spectral densities was not outstanding, but considering the limitation of 74 ANBESS/WRANSAC spectral pairs for the calibration, it was good. Between 0.11 Hz and 0.50 Hz, the average correlation coefficient of the psd's was 0.769.

The ANBESS hull can be used to acquire nondirectional wave data. Under the sea-state conditions of January 1982, it provided accurate estimates of significant wave heights and waver periods, and useful estimates of wave displacement psd's. The latter should improve with additional data. The resonant behavior at 0.35 Hz is reproducible and can be accounted for in the calibration procedure.

#### ACKNOWLEDGEMENTS

This paper was prepared under subcontract to the Computer Sciences Corporation, NSTL, with funding provided by the NOAA Data Buoy Center. Mr. Kenneth E. Steele of NDBC and Mr. Henry T. E. Coolidge of CSC participated in technical discussions of the work presented here, and their comments and suggestions are gratefully acknowledged.

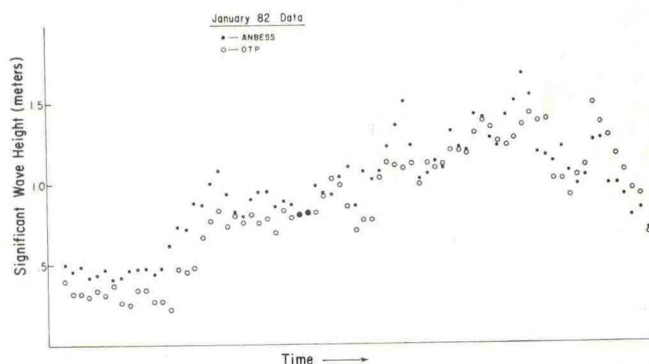


Figure 1. August 1981 ANBESS/OTP Calibration

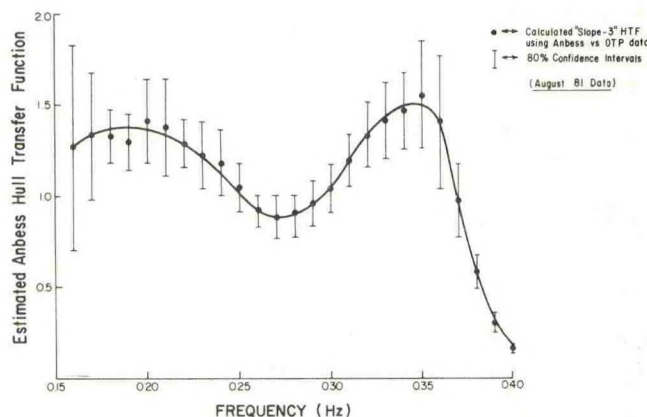


Figure 2. January 1982 ANBESS-OTP Wave Heights



Table 1. ANBESS Hull Calibration

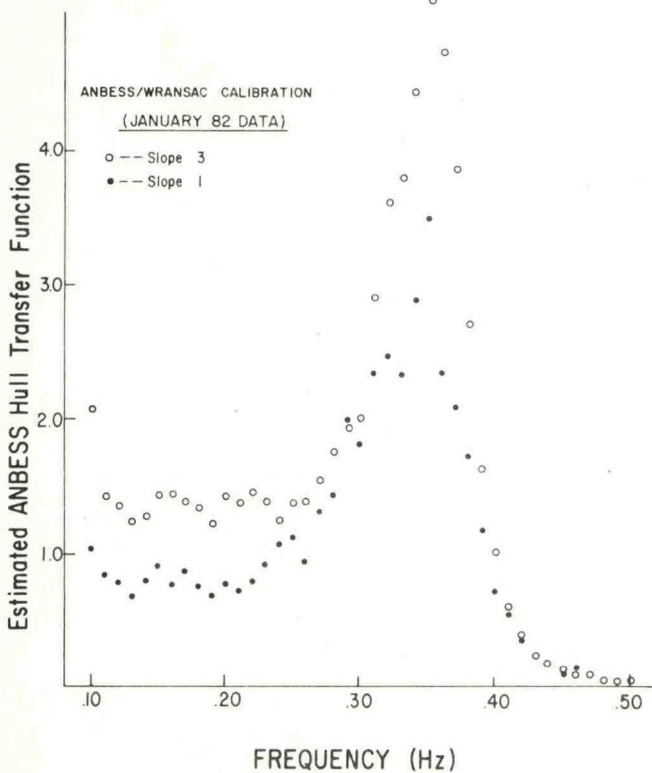


Figure 3. ANBESS Hull Filtering Function

## REFERENCES

1. Steele, K. E., Smoyer, R. H. Jr., and Ward, S. P., "Real time wave measurement systems," WMO Technical Conference on Automation of Marine Observations and Data Collection, Hamburg, West Germany, September 7-11, 1982.
2. Murphy, J. E. and Steele, K. E., "Uncertain Wave Spectra: Calibrating Large Buoys for Wave Measurements," MTS-IEEE OCEANS 82 Conference Report, Washington, DC, September 20-22, 1982.
3. Murphy, J. E., "NDBO Large Discus and NOMAD Buoy Calibrations with WRANSAC," Proceedings of the MTS-IEEE OCEANS 79 Conference, San Diego, CA, September 17-19, 1979.
4. Price, D., "Buoy Response Amplitude Operators Obtained from Step Response Tests," Offshore Technology Conference, Houston, TX, May 3-6, 1976.

Freq (Hz)	Pts.	Corr Coeff	H(LLS)	H(FOP)
0.11	26	.790	0.832	1.409
0.12	37	.836	0.761	1.351
0.13	42	.765	0.666	1.224
0.14	49	.738	0.787	1.263
0.15	62	.704	0.910	1.433
0.16	69	.549	0.761	1.421
0.17	68	.635	0.861	1.379
0.18	66	.620	0.741	1.333
0.19	66	.616	0.676	1.204
0.20	69	.706	0.781	1.399
0.21	70	.634	0.706	1.380
0.22	71	.580	0.780	1.442
0.23	71	.592	0.920	1.367
0.24	62	.871	0.068	1.215
0.25	66	.839	1.109	1.375
0.26	65	.670	0.924	1.379
0.27	72	.765	1.316	1.542
0.28	70	.809	1.439	1.745
0.29	67	.799	1.980	1.919
0.30	72	.821	1.805	2.000
0.31	72	.791	2.337	2.891
0.32	73	.742	2.461	3.603
0.33	73	.746	2.326	3.792
0.34	73	.822	2.897	4.423
0.35	72	.823	3.490	5.167
0.36	73	.761	2.350	4.723
0.37	73	.763	2.070	3.847
0.38	73	.744	1.719	2.686
0.39	73	.737	1.163	1.613
0.40	73	.770	0.723	0.999
0.41	73	.832	0.527	0.594
0.42	72	.862	0.342	0.371
0.43	73	.838	0.248	0.232
0.44	73	.827	0.171	0.158
0.45	73	.691	0.089	0.109
0.46	73	.844	0.111	0.074
0.47	73	.854	0.071	0.049
0.48	73	.815	0.041	0.034
0.49	73	.772	0.026	0.022
0.50	71	.835	0.020	0.016



# THE STATISTICS OF CROSS SPECTRA APPLIED TO WAVEHEIGHT DIRECTIONAL SPECTRAL MEASUREMENT

Donald E. Barrick and Belinda J. Lipa

Ocean Surface Research  
1131 Cranbrook Ct 165 Harcross Rd  
Boulder CO 80303 Woodside Ca 94062

## ABSTRACT

The optimal estimation of wave directional parameters with maximum likelihood depends on the availability and use of a covariance matrix among the Fourier angular coefficients at each wave frequency. The known statistics of the sea surface permits the derivation of this covariance matrix in terms of the cross spectra between the instrument outputs. It is then shown how the data covariance matrix, simply obtained from the information already transmitted to shore from data buoys, is used with maximum likelihood to estimate desired parameters and their statistical uncertainties.

## 1. INTRODUCTION

Pitch/roll buoys, wavestaff arrays, current meters moored near the surface, and bottom-deployed pressure sensors are examples of *in situ* instruments used to derive information about waves and their directional properties on the ocean surface. Longuet-Higgins et al. <1> have established the accepted method of describing quantitatively the directional wavefield, or waveheight directional spectrum, in terms of the heave and slope sensors on a pitch/roll buoy; from the cross spectra among the three instruments, five angular Fourier series coefficients at each wave frequency are obtained that represent the directional waveheight distribution. Deployment of operational discus buoys based on these methods is underway in the U.S. <2> and other countries. The difficulty of user interpretation of a table of Fourier angular coefficients vs wave frequency has led to the desire for more obvious

descriptors of the directional wavefield, such as significant waveheight, dominant wind-wave or swell direction and period, and a measure of the wave angular spread.

The sea surface height to lowest order is a Gaussian random variable, and attempts to measure its mean parameters with a finite number of samples (or finite observing period) will therefore include some statistical uncertainty. Likewise, calibration procedures for the instruments on these buoys that involve responses to waves will produce system transfer functions that can contain statistical uncertainties resulting from the random wavefield. Although error estimates (or confidence limits) are available for waveheight and the non-directional spectrum based on its chi-squared probability density, uncertainties in the other Fourier coefficients and directional spectral descriptors have not yet been obtained. Ultimately, operational systems should

routinely provide outputs of statistical uncertainties along with each parameter measured. Long <3> introduces the subject of model fitting with statistical wave measurement.

In this paper we outline a procedure for estimating statistical uncertainties in all derived wave directional parameters, based on maximum-likelihood and linear error-propagation methods; we have used these methods successfully for measurements of ocean surface parameters (such as currents) with CODAR <4>. The heart of this procedure involves the use of a covariance matrix that contains cross spectral element products. Numerical computations are expedited by deriving and using the statistical properties of these cross spectra that originate from the Gaussian waveheight and waveslope



signals; these statistics are extensions of the familiar chi-squared distribution. The next section presents and discusses the essential statistical properties of these cross spectra. The subsequent section examines the Fourier-coefficient covariance matrix derived therefrom. Section 4 then shows how this covariance matrix is used along with maximum likelihood to estimate the uncertainties in all parameters desired from the pitch/roll buoy.

## 2. STATISTICS OF CROSS SPECTRA

For many years it has been recognized that the (digital) Fourier transform of a simple waveheight time series (for example, the double-integrated accelerometer output from a Waverider heave buoy) has real and imaginary parts at each frequency point that to very good approximation are: (i) zero-mean Gaussian random variables with equal variances; (ii) are statistically independent of each other; (iii) are inherently statistically independent of values at every other frequency point (i.e., discounting time-series finite window effects). This leads to a nondirectional power spectrum that is chi-squared with two degrees of freedom; when K independent power spectra are added (averaged) together, the result is also chi-squared, with 2K degrees of freedom. From tables of this well-known distribution, rms uncertainties and/or confidence limits of the waveheight nondirectional spectrum are readily obtained at each frequency point. In addition, since the square of rms or significant waveheight is proportional to the sum of all power spectral points, waveheight uncertainties are also available from the chi-squared nature of the sum/integral of the spectral values.

Pitch/roll wave buoys, however, provide the waveheight directional spectral Fourier angular coefficients in terms of cross spectra among the heave and slope sensors. In addition, simpler descriptors of the waveheight directional spectrum are often desired, such as the dominant wave or swell direction. The optimal method for the extraction of such parameters is maximum likelihood; use of this method along with linear error

propagation theory can also provide estimates of statistical uncertainties in all derived parameters, as will be described subsequently. Before such methods can be applied, however, a knowledge of the statistical distribution of cross spectra is required in order to obtain the necessary covariance matrices. As with the chi-squared distribution for the nondirectional spectrum, the statistical distribution of these cross spectra can be determined from the Gaussian nature of ocean waves. Because this has not been done, we present and discuss the cross-spectral statistical properties relevant to pitch/roll buoy analysis.

In what follows, we assume cross spectra have been (digitally) calculated, and have already been corrected for relevant hull, sensor, and electronic transfer functions, so that they are truly proportional to heights and slopes of the waves at the given spectral point. If K independent cross-spectral values at a given point are available, we assume they have been averaged (added) together, just as was done for the power spectrum. Now let us define the nonvanishing real or imaginary part of a given cross spectral value between instrument "α" and instrument "β" as  $\kappa_{\alpha\beta}$ , indicating that K independent values are averaged to obtain this point. (When the left subscript, K, is omitted, we understand infinite-ensemble average.) If the two subscripts are equal, we of course are dealing with the power spectrum, which we already know is chi-squared with 2K degrees of freedom. For the pitch/roll buoy, since height and slope of a wave are in quadrature, we know <1> that the nonvanishing co and quad spectral elements that  $P_{\beta}$  represents are

$$C_{11}, C_{22}, C_{33}, Q_{12}, Q_{13}, C_{23}.$$

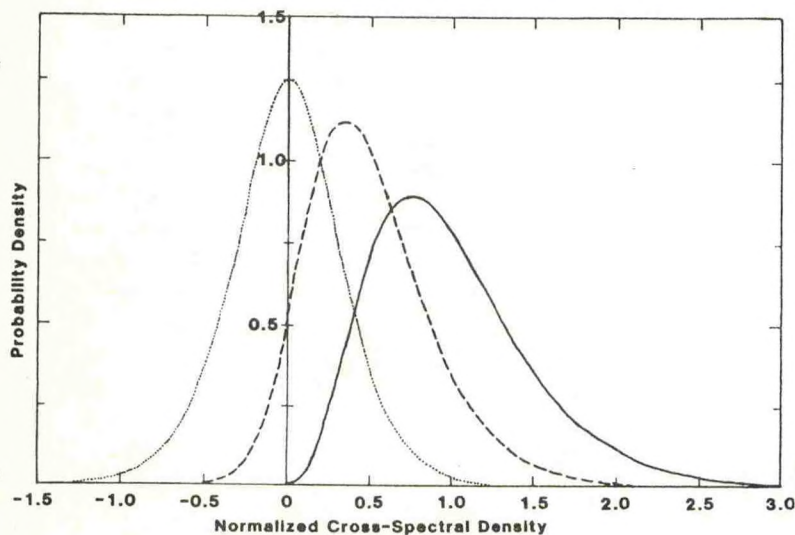
First we determine and discuss the probability density of the nonvanishing quantities,  $\kappa_{\alpha\beta}$ . This is obtained from the joint Gaussian probability density function of the real and imaginary parts of the sensor voltages comprising the cross spectrum. Because of its simplicity of form, we show here the characteristic function of the probability density function for the cross spectral element,  $\kappa_{\alpha\beta}$ ; this is merely its Fourier transform over variable w. We used the fact



that the K values averaged together were statistically independent.

$$\Phi_{\kappa_{\alpha\beta}}(w) = \frac{1}{(1 - i \frac{w P_{\alpha\beta}}{2K} + (\frac{w}{2K})^2 (P_{\alpha\alpha} P_{\beta\beta} - P_{\alpha\beta}^2)) K}$$

In this expression,  $P_{\alpha\alpha}$ ,  $P_{\beta\beta}$ , and  $P_{\alpha\beta}$  are the infinite-ensemble averages of all possible permutations of the nonvanishing cross spectra among instruments  $\alpha$  and  $\beta$ . (The order of subscripts is interchangeable.) Notice that when  $\alpha = \beta$ , the characteristic function is seen to reduce to that for the familiar chi-squared distribution, whose density is readily available. For a general cross spectrum, however, the probability density, although we have derived it elsewhere in closed form, is not a simple expression. Therefore we do not present it here, but rather, show curves of the density for the case  $K=4$ . We consider three cases:



(i) when the correlation between the instruments is unity (e.g., for  $P_{\alpha\beta}^2 = P_{\alpha\alpha} P_{\beta\beta}$ , solid curve); (ii) where the correlation coefficient is 1/2 (dashed curve); (iii) where the correlation is zero (dotted curve). We show the density for  $P_{\alpha\beta} > 0$  ( $P_{\alpha\beta}$  turns out to be the mean or centroid of the density function); this quantity can be and often is negative. Notice that for perfect correlation (for which the density reduces to chi-squared), the random variable must always be positive.

Now we present the covariance (i.e., second moment) for the K-sample-averaged

nonvanishing cross spectral elements  $\kappa_{\alpha\beta}$  and  $\kappa_{\gamma\delta}$ . This is

$$\text{Cov}(\kappa_{\alpha\beta} \kappa_{\gamma\delta}) = \frac{1}{2K} (P_{\alpha\gamma} P_{\beta\delta} + P_{\alpha\delta} P_{\beta\gamma})$$

Again, the quantities that appear on the right refer to the infinite-ensemble averages of the cross spectra. Also, any (or all) of the subscripts referring to a given instrument can be the same as any other. Thus, for example, when all subscripts are the same, we have the familiar variance of the power spectrum, which is chi-squared with  $2K$  degrees of freedom, expressed in terms of the square of its mean and decreasing inversely with the number of samples,  $K$ . In general, all covariances of cross spectra decrease inversely with  $K$ , which is reassuring.

To illustrate how these relationships are applied, let us consider three cross-spectral covariances for the pitch/roll buoy as examples. We employ the conventions of Longuet-Higgins et al. (1), where subscripts 1,2,3 refer to height, East slope, and North slope, respectively. Then the covariances between the following three K-sample-averaged, nonvanishing pairs are obtained from the above general result:

$$\text{Cov}(\kappa_{C_{11}} \kappa_{C_{22}}) = \frac{1}{K} Q_{12}^2$$

$$\text{Cov}(\kappa_{C_{11}} \kappa_{Q_{12}}) = \frac{1}{K} C_{11} Q_{12}$$

$$\text{Cov}(\kappa_{C_{23}} \kappa_{Q_{12}}) = \frac{1}{2K} (C_{23} Q_{12} + C_{22} Q_{13})$$

Three important points are worth remembering from the results discussed in this section:

i) All cross-spectral covariances fall off inversely with  $K$ , the number of independent samples in the average, just as happens for similarly averaged power spectra. Since the Fourier angular coefficients of the waveheight directional spectrum are made up of linear combinations of instrument cross spectra, their covariances (to be examined in the next section) can be expected to fall off also inversely with  $K$ .

ii) The purpose of deriving the theoretical expressions for covariances of cross spectra is to expedite drastically their computation from the data. Although the K-sample covariances are given in terms of infinite-ensemble-averaged quantities, satisfactory estimates are



obtained by using the K-sample values of the cross spectra in the covariance equations. The alternative to using these theoretical expressions with the data would be to compute estimates of all 36 covariances among the 6 buoy cross spectra from the K separate instrument FFTs, a much more time and memory-consuming procedure. (The validity of the theoretical expressions have in fact been verified in this manner from CODAR data.) For NOAA's wave data buoys as they presently operate, this latter procedure is not possible because only sample-averaged Fourier angular coefficients are computed on board and transmitted to shore. In either case, however, the accuracy is the same.

iii) The figure for sample-averaged cross-spectral densities for K=4 illustrates an important point crucial to subsequent reduction of maximum likelihood to least-squares. Even with as few as K=4, the probability densities in all cases already remarkably resemble the Gaussian bell shape; this is also predicted by the Central Limit Theorem of statistics, but it is surprising that it occurs here for as few as four samples. For usual buoy operation over 15-20 minute observing periods, K is typically either 16 or 32, so that the resulting probability will be indistinguishable from Gaussian for all practical purposes. Therefore, the Gaussian assumption for the K-sampled cross-spectral data samples made later is established here.

### 3. COVARIANCE MATRIX FOR FOURIER ANGULAR COEFFICIENTS

Longuet-Higgins et al. <1> express the first five Fourier angular coefficients at each wave frequency in terms of the corrected instrument co and quad spectra that are nonzero; we use their nomenclature and normalizations here. Since the Fourier coefficients,

$$a_0, a_1, b_1, a_2, b_2$$

are linear combinations of these cross spectra, the covariances of K-sample-averaged Fourier coefficients are determined in a straightforward fashion from the K-sample-averaged cross spectra using the equations of the preceding section. There are 25 elements in this covariance matrix, and it is given in Table I.

There are two reasons why this covariance matrix is important. If the user plans to go no further than the K-sample-averaged Fourier coefficients at each wave frequency as his/her data product, then the diagonal elements of this matrix are the variances in the five angular coefficients; their square roots are therefore their rms uncertainties. Confidence limits can be established for the coefficients if these are preferred; for K greater than four, the probability densities are sufficiently close to Gaussian (as established in the preceding section) that this distribution can be used for the confidence limits <5> instead of the

$$\frac{1}{2K} \begin{bmatrix} a_0^2 + b_2^2 - a_2^2 & a_0 a_1 + b_1 b_2 - a_1 a_2 & 4a_1 b_1 & a_0 b_1 + b_1 a_2 + a_1 b_2 & 2b_2 a_2 \\ a_0 a_1 + b_1 b_2 - a_1 a_2 & b_1^2 + a_0(a_0 - a_2)/2 & 2b_1 a_0 & b_1 a_1 + a_0 b_2/2 & b_1 a_2 + a_1 b_2 - a_0 b_1 \\ 4a_1 b_1 & 2b_1 a_0 & 2a_0^2 & 2a_0 a_1 & 2(a_1^2 - b_1^2) \\ a_0 b_1 + b_1 a_2 + a_1 b_2 & b_1 a_1 + a_0 b_2/2 & 2a_0 a_1 & a_1^2 + a_0(a_0 + a_2)/2 & a_0 a_1 + a_1 a_2 - b_1 b_2 \\ 2b_2 a_2 & b_1 a_2 + a_1 b_2 - a_0 b_1 & 2(a_1^2 - b_1^2) & a_0 a_1 + a_1 a_2 - b_1 b_2 & a_0^2 + a_2^2 - b_2^2 \end{bmatrix}$$

TABLE I. Covariance matrix among the Fourier angular coefficients from a pitch/roll buoy. The data values  $z_1, z_2, z_3, z_4, z_5$ , in this matrix represent the coefficients  $b_2, b_1, a_0, a_1, a_2$ , in this respective order.



more complicated but exact probability discussed previously.

The second reason why this covariance matrix is useful is for the determination of other parameters of the waveheight directional spectrum. Here, the basic data values will now be taken as the K-sampled Fourier coefficients. Their covariance matrix,  $C_2$ , as shown below, is used both in the determination of the desired parameters themselves, as well as in their uncertainties.

#### 4. MAXIMUM LIKELIHOOD AND THE COVARIANCE MATRIX FOR PARAMETER EXTRACTION

Often parametric descriptors of the waveheight directional spectrum are desired that are much simpler to understand and less voluminous in nature than the five Fourier angular coefficients at each wave frequency. Certain of these parameters are readily obtained directly from the coefficients. For example, the nondirectional spectrum is identically equal to  $a_0$  vs wave frequency, and its uncertainty is immediately obvious from its chi-squared distribution. Likewise, significant waveheight is proportional to the square root of the area under the nondirectional spectrum, and its uncertainty also follows from the chi-squared spectral statistics. The dominant spectral period, defined as the centroid of the nondirectional spectrum, is also directly obtained, along with its uncertainty  $\langle 5 \rangle$ .

Two additional parameters are usually desired from a pitch/roll buoy (the parameters discussed above are available from a simple heave buoy like the Waverider): dominant wave direction and angular spread at each wave frequency. The technique we offer here is a departure from past methods, and before we begin, let us examine these past methods and their deficiencies. Longuet-Higgins et al.  $\langle 1 \rangle$ , and many others  $\langle 6 \rangle$ , employ a convenient model for unimodal angular wave patterns of the form

$$g(\theta) = \frac{1}{2\pi} A(s) \cos^s\left(\frac{\theta - \theta_0}{2}\right)$$

where  $A(s)$  is a normalizing constant such that

$$\int g(\theta) d\theta = 1.$$

In this model,  $\theta_0$  represents the dominant wave direction and  $s$  is a measure of the angular spread.  $\theta_0$  is readily obtained as the arctangent of the ratio of  $b_1$  to  $a_1$ . However, it is also equal to half the arctangent of the ratio of  $b_2$  to  $a_2$ . Since we are dealing with noisy data, each of these equations will give a different estimate for dominant wave direction. Which is better? Or should the two be averaged? Or is a weighted average of the two better (by some at best rather arbitrary formula)? Or perhaps the estimate from the second harmonic ratio should be ignored, because everyone "knows" that second harmonics are always less reliable than first harmonics? Whatever method is used, what is the resulting statistical uncertainty in the dominant wave direction? And finally, does this model really describe the data, i.e., is the wavefield at this frequency unimodal, or is there a swell component present from another direction along with the wind waves? Maximum likelihood offers the accepted, objective basis for deriving optimal estimates of the desired parameters, determining their uncertainties, and answering the question as to whether the model assumed actually describes the data.

A concise statement of the maximum likelihood principle involves the joint probability density of the measured, noisy data (in our case, the K-sample-averaged Fourier angular coefficients), that explicitly includes the true means for these data values. These true means are known expressions that contain the parameters of the model we feel will describe the data. If the noisy data values are measured and hence known, and we want to determine the parameters for our model, maximum likelihood proves that the optimum values for these parameters are those that maximize this joint probability function. If the data values are sufficiently close to Gaussian (as we



showed they are for K-sampled pitch/roll buoy Fourier coefficients), then maximizing this joint Gaussian probability density (with nonzero correlations or covariances among the data values) is identical to minimizing the argument of the Gaussian exponential, which is a least-squares sum containing the inverse of the data covariance matrix as weights in the terms of the sum.

Let us express this in matrix form. Let  $\mathbf{Z}_n$  be the measured data values (in our case, Fourier angular coefficients) whose exact values if there were no noise or error would be the model values  $y_n(\bar{r})$ , in terms of several parameters,  $\mathbf{r}_m$ , where we represent these parameters as a vector,  $\bar{r} = [r_1, \dots, r_M]$ . We assume we know the form of the model we want, but do not know the values of the parameters that make it best fit the data. Assume there are N pieces of data  $\mathbf{Z}_n$ , and M values of unknown parameters  $\mathbf{r}_m$ . For the problem to have a unique solution, of course, N must be greater than M. Again, if we use our example and model, we have four *directional* angular coefficients and two parameters (dominant wave direction,  $\theta_0$ , and spreading parameter, s). Furthermore, there is a simple closed-form expression for the model that fits each coefficient (i.e., the  $\mathbf{Z}_n$ , which in our case represent  $b_2, b_1, a_1, a_2$ ) in terms of the two parameters  $\theta_0$  and s; this is given in Eqs. (21-23) of <6>. Now, define the N-element column vector with elements  $\epsilon_n$ , as the differences between the data values and the model:

$$\epsilon_n = \mathbf{Z}_n - y_n(\bar{r}).$$

Then our least-squares formulation of maximum likelihood involves minimizing the sum of the squares of these deviations, expressed in matrix form as

$$I(\bar{r}) = \epsilon \mathbf{C}_z^{-1} \epsilon \rightarrow \min$$

where  $\mathbf{C}_z$  is the NxN covariance matrix among the data values. The parameters  $\mathbf{r}_m$  are found that minimize this sum. If the model is linear in all or some of the parameters  $\mathbf{r}_m$ , these can be solved for and/or eliminated using simple matrix algebra. If, as is the case here, the model is nonlinear in some parameters, they are found either by a grid search over the parameter ranges for the mini-

mum, or by efficient versions of multi-dimensional root finders.

After optimum estimates of these parameters  $\mathbf{r}_m^*$  are obtained in this manner, estimates of their uncertainties are found by combining least-squares with linear error propagation theory <7>. The only assumption required is that the fluctuation in the data values about their mean, or optimal values, is small. This is certainly the case here because of the large number of independent samples, K, in the original cross-spectral data averages (i.e., 16 or 32). Then the covariance matrix  $\mathbf{C}_p$  (which is MxM) for the derived parameter values is

$$\mathbf{C}_p = (\mathbf{E}^T \mathbf{C}_z^{-1} \mathbf{E})^{-1}$$

where

$$E_{nm} = \frac{dy_n}{dr_m}$$

with  $E_{nm}$  being the elements of an MxN matrix,  $\mathbf{E}$ , and the original covariance matrix of the data  $\mathbf{C}_z$  and its inverse being NxN. (Superscript "T" denotes matrix transpose; "-1" is the matrix inverse.) The differential matrix  $\mathbf{E}$  is known; the differentiations are performed on the model elements  $y_n(\bar{r})$  in terms of the parameters  $\mathbf{r}_m$ , and the parameter estimates obtained previously are used in these differentials. For the case we have been considering, the square roots of the two diagonal elements of  $\mathbf{C}_p$  would then be the rms uncertainties in the dominant wave direction,  $\theta_0$ , and spread factor, s.

One remaining question can now be answered using our least-squares formulation of maximum likelihood: how well did the model we assumed actually fit the data? Or might another model fit it better? This question is answered objectively using the chi-squared test from statistical inference (chi-squared being used differently here than in the K-sample-averages discussed previously). With the inverse of the covariance matrix weighting the terms of the least-squares sum, the value of the sum at the minimum should be close in magnitude to N-M if the model fits the data well <7>. To use the chi-squared test, a significance level  $\xi$ , (usually small) is chosen and



the value of the sum at the minimum compared with the fractile  $X^2_{(1-\xi)}$  for  $N-M$  degrees of freedom (found in standard statistical texts, <7>). If the sum is considerably larger, the model is not fitting the data well, and another ought to be tried and the same test applied.

Although probably not desired on a routine, operational basis, maximum likelihood also allows detailed studies of the contours of constant level for the least-squares sum around its minimum value; these contours can be related through the F-test <7> to confidence limits on the derived parameters.

## 5. CONCLUSIONS AND RECOMMENDATIONS

The theoretical covariances and their statistical properties for cross spectra lead to the covariance matrix for the Fourier angular coefficients of the directional spectrum from a pitch/roll buoy. This matrix is very important in the extraction and interpretation of directional information. In their own right, the square roots of the diagonal elements of this matrix are the rms uncertainties of the angular coefficients; these uncertainties decrease inversely with the square root of the number of samples averaged, just as for the nondirectional spectrum. The validity of the theoretical covariance matrix has been verified experimentally; this expression therefore can and must be used rather than computing it from each data sample because the latter procedure is not within the realm of present onboard processors.

The extraction of parameters that describe directional properties of the wave-field should in the future be done using maximum likelihood techniques; these methods are universally accepted by the scientific community as the optimal way to invert and interpret noisy geophysical data. This method requires the use of the data covariance presented here, both for the extraction of the desired parameters (e.g., dominant wave direction and directional wave spread), as well as for the estimation of uncertainties in these quantities.

## ACKNOWLEDGMENTS

This work was supported in part under Subcontract No. CSC/ATD-83-C-511 from Computer Sciences Corporation, a prime contractor to NOAA's National Data Buoy Office.

## REFERENCES

- <1> M.S. Longuet-Higgins, D.E. Cartwright, and N.D. Smith, "Observations of the Directional Spectrum of Sea Waves Using the Motions of a Floating Buoy," Ocean Wave Spectra, Prentice-Hall:New York, 1963, pp 111-132.
- <2> K.E. Steele, E.L. Burdette, and A. Trampus, "A System for the Routine Measurement of Directional Wave Spectra from Large Discus Buoys," Proceedings of the MTS-IEEE Oceans '78 Conference, Washington, D.C., 1978.
- <3> R.B. Long, "The Statistical Evaluation of Directional Spectrum Estimates Derived from Pitch/Roll Buoy Data," J. Physical Oceanography, Vol. 10, 1980, pp 944-952.
- <4> B.J. Lipa and D.E. Barrick, "Least-Squares Methods for the Extraction of Surface Currents from CODAR Crossed-Loop Data: Application at ARSLOE," IEEE J. Oceanic Engr., 1983, in press.
- <5> D.E. Barrick, "Accuracy of Parameter Extraction from Sample-Averaged Sea-Echo Doppler Spectra," IEEE Trans. Antennas Propagat., Vol. AP-28, 1980, pp 1-11.
- <6> D.E. Barrick and B.J. Lipa, "A Compact Transportable HF Radar System for Directional Coastal Wave Field Measurements," Ocean Wave Climate, M.D. Earle and A. Malahoff, eds., Plenum:New York, 1979, pp 153-201.
- <7> P.R. Bevington, Data Reduction and Error Analysis for the Physical Sciences, McGraw-Hill:New York, 1969.



## THE USE OF NOMAD HULLS AS SEVERE ENVIRONMENT BUOYS

G. L. Timpe, LT USCG

NOAA Data Buoy Center  
National Space Technology Laboratories  
NSTL Station, MS 39529

### ABSTRACT

In the past, the NOAA Data Buoy Center (NDBC) had used 12-m and 10-m discus-shaped buoys on their severe environment stations in the North Atlantic and Pacific Oceans, and had restricted the 6-m boat-shaped Navy Oceanographic Meteorological Automatic Device (NOMAD) buoys to less severe locations. However, the phenomenon of the large discus buoys capsizing in steep, breaking waves has led to a re-evaluation of this practice. In 1979, a NOMAD buoy was moored next to a 12-m discus buoy on a North Pacific station, in an effort to test both the survival of the hull and the quality of its transmitted data. The success of this experiment, coupled with NDBC's continued good experience with the hull and the economic advantages of using a smaller buoy, has led to the recent recertification of the NOMAD buoy for use on severe environment stations. This paper covers the NOMAD buoy's background, the details and results of the North Pacific test, and the basis for recertification of the NOMAD as a severe environment buoy.

### INTRODUCTION

Of all the components in a moored buoy system, the buoy's hull is the most critical. The hull is the platform that supports the other buoy subsystems. It provides the volume for the electronics, power system, and sensors. The hull's buoyancy must be sufficient to support the total system weight plus the maximum expected mooring and environmental loads. The hull must be designed to withstand wind drag, current drag, translational and rotational inertial forces, hydrostatic pressure, and forces transmitted to the hull by the mooring. The hull should be designed so that the forces that it transfers to the mooring are minimized. In addition, the motions of the hull should also be minimized so as not to adversely affect the sensor and antenna performance. If the hull is to survive and operate in its design environment, it must have a sufficient metacentric height, and it should possess a righting moment over a wide range of buoy inclinations.

There are a number of different hull types that can be used: toroid, spherical, spar, discus, and boat-shaped. The type of hull used in a given moored buoy system is best determined by a trade-off study between the factors of type of application, environmental conditions expected, hull type performance characteristics, and cost. On NDBC's

data buoy network, there are three hull types principally used. These are the 12-m and 10-m diameter steel discus-shaped buoys, which displace 90,000 kg and 52,000 kg respectively, and the 6-m boat-shaped NOMAD buoy which displaces 8,700 kg.

### DISCUS BUOY DEVELOPMENT

The development of large discus-shaped buoys originated in the early 1960's, when the Office of Naval Research (ONR) contracted the Convair Division of General Dynamics (GD) Corporation to generate the design of a general purpose oceanographic telemetry buoy [1,2]. The design criteria called for the survival of the buoy in the following environmental conditions: current velocity of 5 m/s, 18 m breaking waves, wind velocity of 75 m/s, and an ice loading of 26 mm on all exposed surfaces. Model tests were conducted on 10 candidate hull forms to measure the drag characteristics and response of each. In 1965, the study concluded that the 12-m, 90,000 kg discus buoy was the best choice for such an application. As a result, the 12-m "monster buoy" was developed. This 12-m design was the basis for at least four buoys built by ONR in the late 1960's, and for six buoys built by NDBC in the early 1970's. In 1973, cost constraints prohibited the construction of additional 12-m hulls by NDBC. A compromise between cost and survivability was made and the size of the buoys was scaled down to 10-m [3]. NDBC currently has two types of 10-m discus hull in use; the original 10-m hull designed by GD in 1973, and a value-engineered version of that buoy, developed in 1978.

### NOMAD DEVELOPMENT

In 1946, the U.S. Navy's Bureau of Ships initiated a project with the David Taylor Model Basin (DTMB) and the National Bureau of Standards (NBS) to develop an automatic weather-station buoy [4]. The resultant buoy design, whose general form was based on the earlier "Roberts buoy," was the NOMAD. The first NOMAD buoy, NOMAD-1, was built in 1952 to the specifications prepared by DTMB [5]. After a period of testing in Chesapeake Bay and off the Maryland Coast, the buoy was moored in the Gulf of Mexico, at position 25°N 90°W, in September 1958. The buoy occupied this station (off and on) until early 1964 [6,7]. Between 1961 and 1971, 20 additional NOMAD buoys were constructed, the majority of these for the Naval Air Systems Command (NAVAIR). The buoys were operated in a wide range of locations, with favorable results. In the early 1970's, there was a realignment of the U.S. Navy's



buoy program. NAVAIR's NOMAD program was discontinued, and the Naval Underwater Systems Center (NUSC) took custody of the program's hardware.

In 1974, NUSC transferred three NOMAD buoys to NDBC to support offshore oil lease studies in the Gulf of Alaska. This was followed by the transfer of five additional NOMAD buoys to NDBC in 1975. Since that time, NDBC has acquired 15 of the original 21 NOMAD buoys built, 14 of which are still in its active buoy inventory. From 1974 to late 1976, NDBC used NOMAD buoys exclusively in its short-term acquisition program in relatively nearshore environments. In late 1976, NDBC started using NOMAD buoys on its long-term National Weather Service (NWS) stations. However, as before, the NOMAD buoys were restricted to nearshore and less severe locations, with the larger 12-m and 10-m discus hull's used exclusively on the severe sites in the North Atlantic and Pacific Oceans.

### NOMAD BUOY CHARACTERISTICS

The NOMAD buoy is a boat-shaped hull 6-m long, 2.9-m wide, and 2.1-m in depth. In its deployed configuration, the buoy displaces 8,732 kg (with 2,971 kg of that being ballast) and has a reserve buoyancy of 8,845 kg. With the exception of the prototype, all NOMAD hulls are constructed of 5086 marine alloy aluminum. The buoy carries redundant wind and air temperature sensors on a mast at the 5-m level. The buoy's barometric pressure sensor, sea surface temperature sensor, and one-dimensional wave spectrum sensor are located inside the hull. The buoy is attached to its mooring by a triangular yoke, transversely positioned between two vertical legs, approximately 2.5-m back from the bow of the buoy. The yoke is free to rotate in the fore and aft plane, but restrained from any movement (translational or rotational) in the transverse direction. This arrangement results in a low-drag hull that has the directional response of turning into the waves, wind, and current. When these environmental forces are not coplanar, the preferential orientation of the hull is dependent on its draft and the relative magnitude of the environmental forces. The buoy exhibits drag characteristics, and heave and pitch responses that are similar to those exhibited by discus-shaped hulls. However, as in most boat-shaped hulls, the NOMAD's buoy lively roll response is a problem area. Fortunately, the buoy's low natural period of roll minimizes the possibility of roll amplification, and the directionality of the hull/mooring system reduces the probability of the NOMAD encountering the potentially dangerous beam seas that create the most excessive roll motions. Because of its smaller size, the NOMAD buoy exhibits greater motion in a seaway than the large discus hulls. However, the buoy's directional response of turning into the seas, apparently has prevented the capsizing problems that have plagued the 10-m discus buoys.

The NOMAD hull form was one of the buoy types analyzed by GD in the ONR data buoy study conducted in the early 1960's. The NOMAD hull had drag characteristics and pitch response comparable to the large discus buoy. However, there were apparently three reasons for its elimination from further con-

sideration in the study. First, there was a preference for a symmetrical hull shape. (It was believed then that a symmetrical hull could produce far better wave data.) Second, the NOMAD buoy had excessive response in the roll mode which could result in potentially high signal losses in its HF transmission of data. Third was the problem of the buoy's relatively small volume. The twin propane-generators being considered at that time for the buoy power system required a buoy with an estimated enclosed volume of 70 m<sup>3</sup> [2], four times the enclosed volume of the existing NOMAD buoy.

NDBC has had good experience with the NOMAD buoy. The use of CMOS technology that has drastically reduced the power requirements of the buoy, coupled with the use of UHF satellite communications, have eliminated, for NDBC's use, the ONR study's original objections to the buoy. The hull has proven to be reliable, easy to handle, and extremely seaworthy.

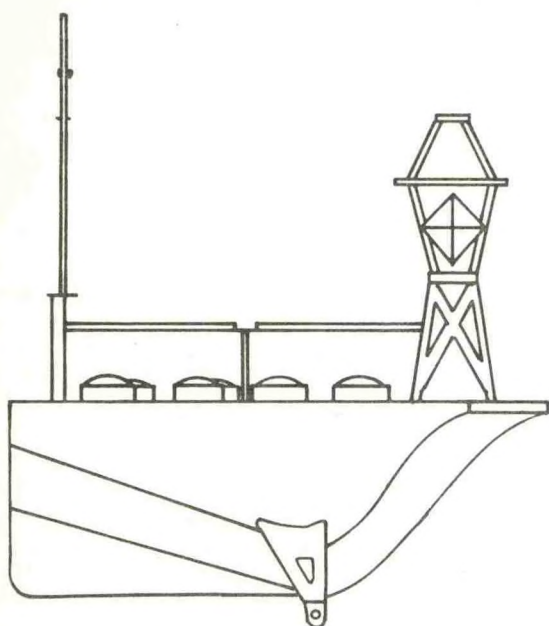
There are two different configurations of NOMAD buoys used by NDBC. The first of these is the original design developed by the U.S. Navy. These buoys are fabricated from 10-mm (3/8-in.) thick aluminum plates. The other configuration is the second generation NOMAD buoy designed by NDBC in the early 1980's. The buoy's exterior lines are identical to the original NOMAD; however, its structural design was value engineered to reduce its fabrication cost. The value-engineered (VE) NOMADs are constructed with 13-mm (1/2-in.) thick deck and side plates, and 16-mm (5/8-in.) thick bottom and transom plates [8,9]. Because of the structural redesign, the location of the VE NOMAD's vertical center of gravity (VCG) is lower than that of the original NOMAD design. As a result, the VE NOMAD buoy's transverse stability is improved over that of the original design [10] (see Figure 1).

### CAPSIZING STUDIES

Since 1977, five of NDBC's discus buoys have capsized during severe storms [3,11]. In 1977, two 10-m discus hulls capsized while moored in the Pacific. In 1979, a 12-m buoy broke its mooring and capsized while adrift northeast of Bermuda. In 1980, another 10-m buoy capsized while moored in the North Pacific. Then in 1981, a 5-m buoy capsized while moored off the coast of South Carolina. From NDBC's point of view, the frequency of the capsizings was a great concern. In addition to the time and expense of recovering, righting, and refurbishing the capsized buoy, there was concern about the resultant loss of meteorological data. As a result, in the late 1970's, several studies into the capsizing problem were initiated.

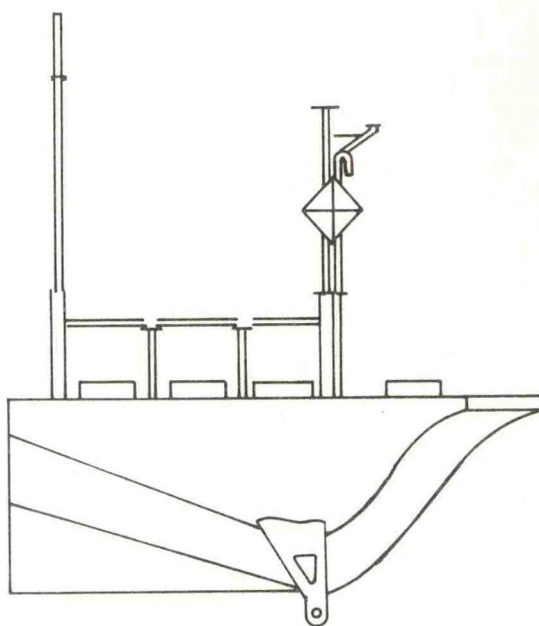
Initially, the environmental conditions associated with each of the capsizings were collected and compared [11,12]. In most of the capsizings, the environmental conditions were associated with cold front passages and were remarkably similar. As a result of this comparison, it was postulated that the capsizings occurred when strong, gusty winds created high, short-period waves. High, steep, breaking seas resulted when these high-frequency





USN STYLE NOMAD

HULL WEIGHT	4536 kg
DEPLOYED WEIGHT	8732 kg
METACENTRIC HEIGHT	.38 m
VERTICAL CENTER OF GRAVITY	1.44 m
ROLL PERIOD	3.8 sec
PITCH PERIOD	2.5 sec
Kxx	1.95 m
Kyy	1.17 m



VALUED ENGINEERED NOMAD

HULL WEIGHT	4264 kg
DEPLOYED WEIGHT	8732 kg
METACENTRIC HEIGHT	.52 m
VERTICAL CENTER OF GRAVITY	1.29 m
ROLL PERIOD	3.5 sec
PITCH PERIOD	2.4 sec
Kxx	1.25 m
Kyy	1.93 m

Figure 1. Physical Characteristics of NDBC's NOMAD Buoys

waves were superimposed on the existing long-period wave field.

In 1978 and 1979, Hoffman Maritime Consultants conducted two studies into the survivability of discus buoys [13,14]. Using hindcast techniques, comparative capsizing probabilities were evaluated for different buoy sizes at a number of locations. These studies recommended the use of larger discus buoys on severe sites in the North Atlantic and Pacific. In fact, the later study concluded that buoys as large as 15-m were needed to survive capsizing on several of the severe stations in the North Pacific.

In conjunction with these other efforts, Nath and Chester [15] examined the performance of the discus buoys in steep waves. Their study attempted to predict the reliability of discus buoys for use in engineering planning purposes. These reliability estimates were determined using a combination of laboratory scale model tests, data from actual buoy capsizings, and ocean wave statistics. The result was a joint probability density function relating a wave steepness parameter ( $\kappa$ ) and a wave height parameter ( $\eta$ ), where  $\eta = H_s/D$  ( $H_s$  is the significant wave height, and  $D$  is the buoy's diam-

eter). It was found that, in general, a discus buoy will only capsize in breaking waves that are large relative to the buoy's diameter. In such a sea state, the values of  $\eta$  and  $\kappa$  are both high, and the probability of the buoy capsizing is increased. The study concluded that in the Northeast Pacific Ocean, the wave climate includes a high percentage of large breaking waves and the resultant reliability of the 10-m discus buoys in that area is relatively low.

In 1978, the Naval Architecture Firm of Gibbs & Cox was contracted to conduct a study into ways of improving the stability of 10-m discus hulls [16]. This study considered the effects of increasing the buoy's diameter, lowering the hull's center of gravity, and increasing the buoy's draft. The study concluded that the most economic way of improving the buoy's stability would be through the use of solid ballast in lieu of the liquid ballast presently used. Designs were formulated for a solid ballast system; however, budget constraints have prohibited any buoy from being modified. Serious questions remain about whether such a solid ballast system would actually improve the buoy's resistance to capsizing.



In late 1978, NDBC sponsored a "Severe Environmental Buoy Workshop" to examine the discus buoy's capsizing problem and look at possible solutions [3]. The workshop concluded that the construction of large 15-m discus buoys was not an economic solution to the problem. Instead, it was agreed that 12-m hulls should be used on all severe sites, and if 10-m hulls are used on such sites, they should be equipped with solid, in lieu of liquid, ballast. The use of other hull forms as severe environment buoys was also discussed, and in this context, it was suggested that NDBC test the NOMAD buoy in a severe environment. While it was generally agreed that a NOMAD buoy could physically survive in a severe environment, areas of concern centered on the buoy's lively roll response, and on the use of sensors located at the 5-m level. It was postulated that severe weather or icing could easily damage the sensors, and that the quality of the data (especially wind speed and direction) would be affected by the excessive roll motions of the hull.

#### NORTH PACIFIC TEST

On October 16, 1979, a NOMAD buoy (6N06) was moored in 2,700 m of water, approximately 2 km from a 12-m

hull (12D01) occupying station 46005. This station, 500 km west of Astoria, Oregon, was the site of the first 10-m hull capsizing in January 1977. The purpose of this deployment was (1) to test the survivability of a NOMAD buoy in a severe environment, (2) to test the survivability of the sensors mounted at the buoy's 5-m level, and (3) to determine the quality of the acquired data using the data from the nearby 12-m buoy as a baseline (see Figure 2).

The 12-m buoy was equipped with a UDACS meteorological payload. The standard parameters of wind speed and direction, sea level barometric pressure, air temperature, and sea surface temperature were measured. The payload sampled all these parameters eight times a second, and computed averages for 8.5 minutes every hour. In addition, the buoy was equipped with a wave spectrum analyzer (WSA), which measures values of wave height, wave period, and one-dimensional wave spectrum. These parameters were measured continuously for a sampling period of 8.5 minutes each hour.

The NOMAD buoy was equipped with a Magnavox Phase II meteorological payload. This payload sampled wind vector components once every second, sea level

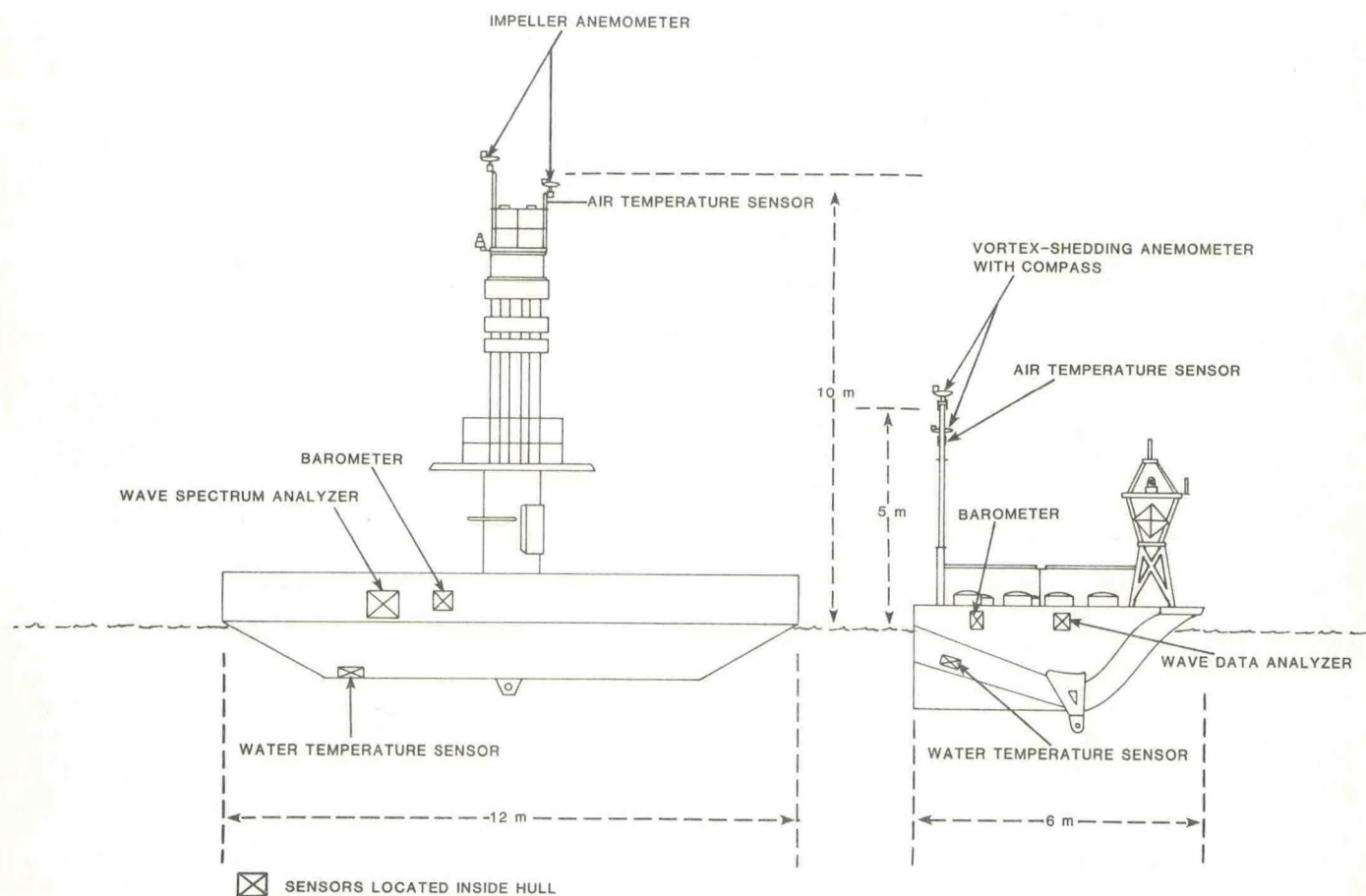


Figure 2. Component Diagram of Buoys Used in the North Pacific Test



pressure and air temperature every 4 seconds, sea surface temperature once (sensor has a 10-minute time constant), and then computed 10-minute averages prior to transmission. In addition, the NOMAD buoy was equipped with the more advanced wave data analyzer (WDA). The WDA measured values of wave height, wave period, and one-dimensional wave spectrum over a sampling period of 20 minutes, each hour.

During the period of the test, two severe storms passed through the area. During one of these occasions, significant wave heights as high as 7 m were recorded under conditions similar to those associated with the 10-m capsizing in 1977. Thus, a wide range of comparison data was available. Unfortunately, the data comparison was complicated by a number of factors: comparison of wind data measured at two different levels, use of two different payloads with different sampling periods, comparison of wave data measured by two different wave sensors, and comparison of sea surface temperature measured at 1 m (12-m hull) with that measured at 0.5-m (NOMAD). In spite of these problems, the data comparison was generally good. The correlation between the values of wind direction measured by the two buoys was satisfactory, with 68% of the data within  $\pm 10^\circ$ , and the majority of the differences greater than  $\pm 10^\circ$  were associated with low wind speed. The wind speed comparison initially appeared disappointing. However, once the values were corrected for the differences in sensor height between the two buoys, the corrected speed measurements agreed, with approximately 75% of the data within 1 m/s or 10%. The barometric pressure comparison was excellent, with air temperature and sea surface temperature less satisfactory but still within the acceptable range. The biggest problem in the data comparison was with the wave measurements. Throughout the testing period, the wave heights measured by the NOMAD buoy were consistently higher than those measured by the 12-m hull. It was postulated that this discrepancy could have resulted from two factors. First, the differences may have been caused by the use of two different wave measurement sensors. Second, the differences may have been a result of inaccuracies in calibration of the hull's transfer function. After an analysis of these two potential problems area, it was generally believed that the maximum error resulting from the method of hull calibration was 0.5 m, and it was concluded that the bulk of the differences resulted from use of two different sensors. The WSA used on the 12-m buoy was NDBC's first generation wave sensor, and they have subsequently been replaced on all operational buoys with the more sophisticated WDA.

The experiment ended ahead of schedule on January 7, 1980, when the mooring on the NOMAD buoy failed and the hull went adrift. The buoy was recovered, and in June 1980, it relieved hull 12D01 on station 46005. The NOMAD buoy was deployed independently on that station until November 24, 1981. During that time, NOMAD hull 6N06 measured significant wave heights of 10.1 m and wind speeds of 23.4 m/s, conditions higher than any encountered by 12-m and 10-m buoys previously on that station. After recovery of the buoy in November 1981, the buoy was

extensively inspected. The only hull damage evident was minor corrosion damage to the hull's bulkheads caused by the spillage of the liquid electrolyte from the buoy's battery power system.

In addition to the information obtained in the North Pacific test, two other sources provide an insight into the NOMAD buoy's severe weather performance: (1) the NOMAD buoy's numerous documented encounters with hurricanes, and (2) the NOMAD buoy's past record of deployments.

In their 25 years of use, NOMAD buoys have encountered hurricanes on many occasions. In September 1960, the center of Hurricane Ethel passed over NOMAD 1 at position  $25^\circ\text{N } 90^\circ\text{W}$  [16]. Throughout the storm and after, the buoy continued sending coherent, correct data. In September 1961, Hurricane Carla passed directly over NOMAD 1 [17]. Its winds were estimated at 51 m/s with gusts over 64 m/s. During the storm, weather induced leaks caused the failure of the barometer and wind speed sensor; however, no hull damage occurred and the remaining sensors continued sending data. In September 1979, a NOMAD buoy on station 42003 ( $26^\circ\text{N } 86^\circ\text{W}$ ) was directly in the path of Hurricane Frederic as it moved into the Gulf of Mexico with estimated winds of 54 m/s [18]. The buoy remained on station and delivered 83% of its meteorological data and 72% of the wave data during the storm. In addition, NOMAD buoys have had fringe encounters with Hurricane Betsy in September 1975, Hurricane Anita in August 1977, and with Hurricane Babe in September 1977, all without recorded hull or sensor damage [19].

The NOMAD buoy's past record of deployments also provide a key to the buoy's performance. In spite of the stipulation that NOMAD buoys be restricted to less severe locations, the environmental conditions on many of these stations were more severe than expected (see Table 1). Between 1976 and 1979, NOMADs were deployed at five sites where Hoffman's hindcast studies recommended using 15-m discus hulls [20]. The buoys occupied these stations for a total of 3,715 days without a hull failure. During the same time period, NOMADs were deployed at three sites that Hoffman's studies concluded were severe enough to warrant use of 12-m discus hulls [20]. NOMAD buoys occupied these stations for a total of 1,260 days, again without a hull failure.

#### NOMAD RECERTIFICATION

With the results from the North Pacific test in, a study was conducted to look at additional considerations that may result from the use of the NOMAD hull as a severe environment buoy [19]. This study concluded that the lower transportation and maintenance costs associated with the NOMAD buoy resulted in a considerable economic advantage. The NOMAD buoy, because of its relatively small size and weight, can be transported overland by rail or truck. Once the buoy is at its port of embarkation, the hull can be lifted onboard the deploying vessel and carried to its deployment site. This greatly reduces the time, cost, and amount of ship-time required for each deployment. A much larger degree of flexibility is also provided in planning



Table 1. Summary of NDBC's Use of NOMAD Buoys

STATION NUMBER	LAT °N	LONG °W	HULL RECOMMENDED BY THE HOFFMAN STUDIES		PERIOD NOMAD BUOY ON STATION	DAYS ACTUALLY ON STATION (TILL 1 NOV 82)
			1978	1979		
41002	32.3	75.3	10D	10D	8/82-PRESENT	82
41003	30.3	80.4	10D	10D	10/78-1/82	832
41005	31.7	79.7	10D	10D	3/79-1/82	965
41006	29.3	77.3	*	*	5/82-PRESENT	159
42001	25.9	89.7	*	*	5/77-8/79	738
42003	26.0	86.0	*	*	11/76-8/80	1283
44001	38.7	73.6	10D	12D	7/78-10/79	471
44002	40.1	73.0	10D	10D	10/75-10/80	1542
44003	40.8	68.5	10D	15D	3/77-PRESENT	1868
45001	48.0	87.6	*	*	5/79-PRESENT	799
45002	45.3	86.3	*	*	9/79-PRESENT	729
45003	45.3	82.8	*	*	5/80-PRESENT	604
45004	47.2	86.5	*	*	4/80-PRESENT	567
45005	41.7	82.5	*	*	6/80-PRESENT	620
45006	47.3	90.0	*	*	6/81-PRESENT	323
45007	42.7	87.1	*	*	7/81-PRESENT	374
45008	44.3	82.4	*	*	9/81-PRESENT	263
46001	56.0	148.0	12D	15D	6/82-PRESENT	131
46002	42.5	130.3	12D	15D	9/82-PRESENT	45
46005	46.1	131.0	12D	12D	10/79-11/81	603
46007	59.2	152.7	12D	15D	6/77-6/79	713
46008	57.1	151.7	12D	15D	5/78-2/79	255
46009	60.2	146.8	12D	15D	9/77-10/79	689
46012	37.4	122.7	12D	12D	11/80-PRESENT	620
46022	40.8	124.5	12D	10D	1/82-PRESENT	290
46023	34.2	120.7	12D	10D	4/82-PRESENT	209
46025	33.6	119.0	12D	10D	4/82-PRESENT	195
51001	23.4	162.3	12D	10D	2/81-PRESENT	629
EB33	58.5	141.0	12D	12D	10/74-4/76	489
EB43	59.8	142.0	12D	12D	8/76-9/77	299
EB35	55.3	157.0	12D	15D	8/76-3/77	180

\*HOFFMAN STUDIES NOT APPLICABLE TO THESE SITES.  
EXPANSION ON WORK BY PALMER, 1982 [20]

the logistics of the hull's deployment. In contrast, the 12-m and 10-m discus buoys must be towed from the port of embarkation to station and back. All this at a considerable cost to the limited resource of ship time. The maintenance costs associated with the NOMAD buoy are also much less than those of the discus buoys, principally because of the buoy's smaller size and its aluminum construction. In fact, the cost of the discus hulls biannual refurbishments are approaching, and are in some cases greater than, the construction costs of a new NOMAD buoy. In 1982, because of these considerations, NDBC recertified the NOMAD buoy for use on severe environment stations.

#### FUTURE PLANS

NDBC has used NOMAD buoys as part of their ocean data buoy network since 1974, and in general, their performance has been commendable. As a result of this, NDBC is planning a 100% increase in the number of NOMAD buoys in its inventory. Five VE NOMADs were fabricated and delivered to NDBC in 1982. Currently, a second series of 10 VE NOMAD buoys is being constructed, with delivery in 1983 and 1984. This will bring the total number of NOMAD buoys in NDBC's inventory to 29. It is anticipated that these additional buoys will be used in a number of applications. They will allow an expansion of the existing network, provide for the increased use of NOMAD buoys on severe environment stations, enable the retirement of some of NDBC's older 12-m hulls, and in addition, the increased number of available buoys will allow the stationing of spare hulls on the east, west, and Gulf Coast to act as "swing buoys," and as a result, reduce station downtime [20].

Development of a directional wave data capability for NDBC's buoys had been under way since late 1976. The system, based on the work of Lonquet-Higgins, Cartwright and Smith [21], was originally developed for use on symmetrical discus buoys. Studies have recently been initiated to determine the feasibility of producing directional wave data from a boat-shaped NOMAD buoy equipped with a similar system. If these studies prove successful and the NOMAD hull can produce valid directional wave information, the NOMAD would then possess the full range of data gathering characteristics possessed by the larger discus hull.

No inference is made that NOMAD buoys will replace the large discus buoys. As stated before, selection of a hull type is a matter of trade-offs. The discus buoys are a proven design with many advantages: a 10-m sensor height, large weight and volume margins, and in most conditions they are extremely stable platforms. Compared to this, the NOMAD buoy has 5-m sensors, is severely volume constrained, and is a stable but lively hull. However, it has been shown that in many applications, especially on severe environment stations, survivability and cost constraints favor the use of NOMAD buoys.

#### REFERENCES

1. Anonymous, "Development of an Ocean Data Station Telemetry Buoy Progress Report," General Dynamics Corp., Report No. GD/C-65-018, May 1965.
2. Devereaux, Robert S. and Feenan D. Jennings, "The Monster Buoy," Geo-Marine Technology, April 1966.
3. Anonymous, "Final Report of the NDBO Severe Environment Buoy Workshop," NDBO Report No. F-200-1, July 1979.
4. Ebner, Roland A., "The Development of a Buoy for Meteorological Set AN/SMT-1 and the Ground Tackle for Anchoring," David Taylor Model Basin Report No. C-454, December 1951.
5. Anonymous, "Buoy for Meteorological Set AN/SMT-1, Assembly and Details," David Taylor Model Basin Drawing No. S-10703, September 1951.
6. Hakkarinen, William, "The World of NOMAD-1," Marine Technology Society Buoy Technology Conference Proceedings, March 1964.
7. Hakkarinen, William, "Sea Operations with the NOMAD Buoy," (private correspondence) May 1969.
8. Basci, M., H. Yeh, and M. Chi, "NOMAD Buoy Value Engineering," Chi Associates, June 1980.
9. Timpe, G. L., and W. O. Rainnie, Jr., "Design of a Value-Engineered (VE) NOMAD Buoy," NDBO Report No. F-250-3, July 1982.



10. Anonymous, "Results of the Inclining Experiments Conducted on NOMAD hulls, 6N02 and 6N16," NDBO Report No. F-221-6, May 1982.
11. Hamilton, Glenn D., "Severe Buoy Wave Conditions," in press, Mariners' Weather Log, 1982.
12. Hamilton, Glenn D., "Buoy Capsizing Wave Conditions," Mariners' Weather Log, Vol. 24, No. 3, May-June 1980.
13. Anonymous, "An Evaluation of the Capsizing Behavior of Discus Buoys at Several Locations," Hoffman Maritime Consultants, Inc., Report no. 7883, July 1978.
14. Anonymous, "Assessment of Buoy Stability and Wave Climatology at All Existing and Proposed Buoy Locations," Hoffman Maritime Consultants, Inc., Report No. 79121, December 1979.
15. Nath, J. H. and S. T. Chester, Jr., "Steep Wave Spectrum Relations and Buoy Reliability," Report to NDBO, January 1979.
16. Anonymous, "Improvement Study in the Survivability of 10-Meter Production Environmental Buoys," Report No. 18581 (1-389), April 1978.
17. Marcus, Sydney, O., Jr., "Evaluation of NOMAD-1 Data for Meteorological and Oceanographic Applications," Marine Technology Society Buoy Technology Conference, March 1964.
18. Johnson, Andrew, Jr., and S. Renwick, "Buoy Observations During Hurricane Frederic," NDBO Report No. F-170-5, May 1981.
19. Johnson, Andrew, Jr., and S. Renwick, "Buoy Observations During Hurricanes Anita and Babe," NDBO Report No. F-170-2, August 1978.
20. Palmer, R. S., Jr., "Swing Buoy Study," NDBO Report No. F-221-8, June 1982.
21. Longuet-Higgins, M. S., D. E. Cartwright, and N. D. Smith, "Observations of the Directional Spectrum of Sea Waves Using the Motions of a Floating Buoy," Proceedings of the International Symposium on Ocean Wave Spectra, Prentice Hall, 1963.



# MOORED DATA BUOY ON SHALLOW WATER.

W.C.M. van Dijk

MINISTRY OF TRANSPORT AND PUBLIC WORKS  
HYDRAULIC DIVISION - COASTEL AND MARITIME DISTRICT.

## ABSTRACT.

The mooring systems of data buoys are designed for deep waters. Therefore, a new design had to be developed to meet the standards required for the shallow water in the North Sea. Calculations have been made and tests carried out in the Delft Hydraulics Laboratory. Physical tests were performed at a location SW of the Isle of Wight (UK) and in the North Sea. The final design of the mooring system is presently in use at one location of the network of survey stations in the North Sea.

## 1. INTRODUCTION.

To meet the demands for data from the North Sea, a network consisting of fixed locations (platforms and piles) and moored buoys has been set up by the government. (fig. 1)

At several of the locations Datawell waverider-buoys are being used to obtain wave information. However these have the following disadvantages:

- they are vulnerable, inter alia to collisions, there is a considerable wastage;
- only the vertical water movement can be measured;
- the transmission in the 27 - 30 Mhz band causes problems.

For operational activities and study, more quantities per location such as wind, airpressure, tide and others are needed. For this purpose an other type of buoy is necessary. An investigation in Europe into an available type led to the selection of a Marex databuoy, which is a sensor platform that was small enough to follow the wave contours accurately and also stable enough to measure windspeed at a level of 10m above MSL. (fig. 2). However, this buoy had no mooring system available for the shallow waters in the North Sea (depth 20 - 45m below MSL).

Marex designed several mooring systems, which were tested both near the Isle of Wight and in the North Sea near the platform "Meetpost Noordwijk" (MPN) (measuring station Noordwijk).

In addition, tests were carried out in wave flumes in the Delft Hydraulics Laboratory and calculations were made on the influence of the mooring on the behaviour of the buoy during waveriding. The results have led to a final design for shallow water.

## 2. STANDARDS REQUIRED FOR THE MOORING.

A mooring system of a databuoy that would ride the waves and measure the windvelocity and direction in tidal currents (3knts), waves ( $H = 10m$ ) and the water-depth (20m below MSL) has to meet the following requirements:

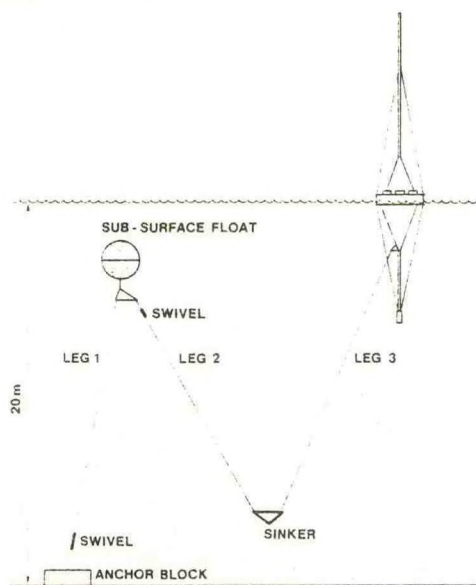
- it needs sufficient elasticity (spring);
- a life span of at least one year;
- an ability for rapid and easy deployment (slack water period is less than 1 hour), requiring only a 1-point mooring system;
- free rotation round the anchor block (the tidal current changes twice a day).

In addition it was necessary to examine if it was possible to connect a signal cable along the mooring in order to obtain tidal values from a sensor in the anchor block.

## 3. DESIGN OF THE BASIC CONFIGURATION.

Considering the afore mentioned demands and hydraulic conditions, it is clear that a direct line between the anchor block and the buoy would provide not the desired solution. It was impossible to use a similar rubber line with the same elastic characteristics as was used for Datawell waveriders, because of the forces exerted on this line. The elastic properties of expansion and contraction of the rubber line have been translated in a "concertina" model. The mooring forces and the total loads on the basic configuration as shown in the figure on top of the next page were determined in a mechanical model. At the same time a first impression was gained of the movements of the different mooring components, such as the subsurface float and the sinker (fig. 3 and 4). However, in this model, all the components of the mooring system are in phase but, as it appeared later, this is not always true in practice.





basic configuration mooring 1.

At the Delft Hydraulics Laboratory (DHL), the influence of the sinker on the buoy movement was calculated, based on the linear wave theory and a static model. By means of the Morrison formula, the resistance which the sinker meets during the movement, and the force it exerts on the buoy were calculated. It appeared from the calculations that the influence is less than 5%. Research into the dynamic behaviour of the buoy under different current and wave conditions requires a very expensive model. In practice the above approximation yields good working results.

The configuration referred to above was tested at a location SW of the Isle of Wight at a water-depth of 20m below MSL, with a tidal current of up to 2 knots and a windforce ranging from 4 - 7 on the Beaufort Scale. During the 3-weeks test period, 4 inspections were carried out by divers. The conclusions from the diving reports were as follows:

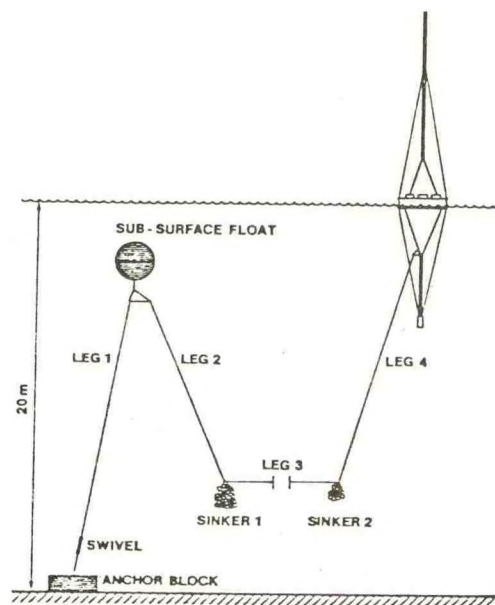
- snatch loads occurred on the legs 1 and 2 due to the wave attack on the subsurface float.
- spring was lacking in the system (in the 2 knots tidal current the system is nearly completely expanded)
- contact occurred between the subsurface float and the data buoy.

As a result of these experiences, leg 1 and leg 2 were kept apart by a 30m long nylon rope and the sinker was replaced by two smaller ones. The intention of these modifications was:

- to increase the horizontal component of the mooring tension at the buoy so that the mooring could sustain higher current loads (fig.5)
- to minimise the wave induced tensions in the legs 1 and 2. This would greatly reduce the fatigue loading in these legs;
- to minimise the risk of the data buoy hitting

the subsurface buoy during slack water.

The figure below shows the basic mooring configuration with the modifications that were carried out before a second test period.



basic configuration mooring 2.

During a subsequent 3-weeks test period, the buoy was subjected to two heavy storms of force 9 and 10 respectively. Two diving surveys carried out during this period yielded the following information:

- the spring characteristics had improved;
- heavier sinkers and more buoyancy of the subsurface float would be required because of the stronger tidal currents in the North Sea.

Leg 3 was made of a nylon rope because it had to be flexible enough to permit unhampered floating of the buoy with the change of direction of the tide and to prevent it touching the sea bed as this could have caused scoring and hooking behind the anchor block.

#### 4. MODEL TESTS WITH DIFFERENT MOORING SYSTEMS.

In the wave and wind flumes of the DHL, the following systems have been tested under differing wave- and current conditions.

- a. 1-point mooring system, with variations in:
  - length of the legs;
  - weight of the sinkers and their position in the mooring.
- b. 2-point mooring system, with variations:
  - length of the legs;
  - weight of the sinkers and their position in the mooring.
- c. 1-point mooring system with legs 2, 3 and 4, as one floating line.



The basic configuration of the systems mentioned is reproduced in fig. 6 a, b and c.  
The test were carried out with the following model scales:  
length scale  $n_l = 40$ , timescale and velocity scale  $n_t = n_v = \sqrt{40} = 6,3$ .

Scheme of the hydraulic conditions:

flume I : - 1m wide  
- regular waves

mooring type	$H_s$ m	$T_m$ s	V m/s	$\alpha$ degrees
a, b and c	2 and 4,7	8 and 11	0, 0,6 and 1,2	0 and 180

Flume II : - 2m wide  
- irregular waves

mooring type	$H_s$ m	$T_m$ s	V m/s	$\alpha$ degrees
b	4,8 and 8,4	8 and 9	1,2	0, 30, 60 and 90

$H_s$  = significant wave height.

$T_m$  = mean wave period.

V = mean velocity of the current.

$\alpha$  = angle between the model and the direction of the current.

#### Results of the tests:

It appeared that with:

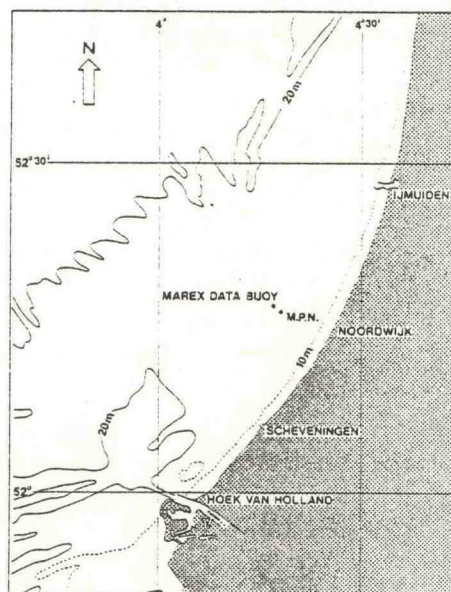
- type a: - during slack water, low tidal currents and waves contact was made between sinker 1 and leg 1 which might cause damage;  
- the movement of the subsurface float were often contrary to those of the buoy;  
- all the variations applied to the basic design decreased the elasticity in the system.
- type b: - there was no contact between the mooring parts;  
- the distance between anchor blocks is very important. It should be correct to 5 meters;  
- all the variations applied to the basic design decreased the elasticity and increased the contact between the mooring components.
- type c: - as a result of the rapid changes in the forces exerted on the mooring line due to the wave movement the buoy was subjected to short, heavy snatches and started rotating;  
- the buoy is pulled under the water surface if it is attacked by a wave.

#### Conclusions:

- the influence of the waves is greater than the influence of the currents;
- the weights of the sinkers can not be determined accurately;
- the lengths of the legs can be determined rather accurately;
- type b gives too many problems in practice;
- type c with the floating line does not meet the requirements;
- it was decided to proceed with type a, the 1-point mooring system.

#### 5. PROTOTYPE TESTS IN THE NORTH SEA.

The Marex data buoy has been deployed near the Meetpost Noordwijk (MPN) at a distance of ca. 800m (as shown in the figure below).



location Marex-MPN.

The waterdepth was 18m below MSL the tidal range 1,90m, and the tidal current 3 knots. This particular location was chosen for the following reasons:

- the measurements taken from the platform (wind-sensors and wavestaff) could be compared with those from the buoy (windsensors and waverider-sensor);
- the transmission of the buoy could be incorporated in the transmission path of the platform, so that transmission and data registration could not cause problems;
- the possibility to keep the buoy under observation.

During two periods, March - Aug. 1980 and Jan. - Oct. 1981, the buoy was deployed. Between those periods, and after the last one, modifications were carried out on the mooring.



The mooring configuration at the beginning of the first test period is shown in fig. 7.

The buoy and its mooring system have been considered for the following aspects:

- manageability;
- behaviour of the mooring;
- quality of the wind and the wave data.

#### A. Manageability.

For the deployment procedure of the buoy and its mooring a ship with a big working deck and a 5 - 10 ton crane was required. The deck was used to lay out the mooring components in order to connect the various components and for the deployment procedure itself. The heavy crane was used to deploy the buoy, the sinkers and the anchor block. The deployment took no longer than half an hour at the slack water period. After the deployment the buoy was pulled away from the ship by an inflatable rubber boat. In this way, the mooring lines were played out in the water so that the legs could not become tangled.

Work on the buoy (changing modules and testing sensors) and in the mast (checking and changing sensors) can be done when the maximum wave height of 80-90 cm is not exceeded.

The recovery of the buoy and the mooring took about 3/4 hour.

#### B. Behaviour of the mooring.

During each test period the mooring was inspected by divers. These inspections were done with a video camera via which instructions could be given to the diver.

The inspection during the first period showed:

- a crack in the signal cable and serious damage over its full length;
- damage to the signal cable and sensorhousing in the anchor block due to the contact between the sinker 1 and leg 1;
- near destruction of the anodes and more corrosion in leg 1 than anticipated.

After the first test period the mooring was recovered and subsequently modified (fig. 8). These modifications comprised, inter alia, the improvement of:

- the connection between the signal cable and the other mooring components;
- an added protection of leg 1.

In addition a truck tyre was fitted around the sinker 1 so as to provide gentler contact with leg 1, whereas different components were reinforced.

The inspection during the second test period showed:

- the signal cable had undergone the same damage as before, caused in particular by the contact between the sinker 1 and leg 1;
- damage to the triangle, caused by the movement of the subsurface float, due to the wave attack on the subsurface float;
- no marine growth over the first 5m of leg 3 due to the contact of leg 3 with leg 1.

#### C. Quality of the wave parameters.

From the buoy and the Meetpost Noordwijk wave parameters have been calculated from simultaneous measurement series each lasting 20 min., a sample frequency of 2 Hz and a measurement frequency of 1 per hour. By means of the Fourier transformation the spectral parameters were obtained. The following selection of parameters have been compared:

H1/3 = the average of the highest 1/3 part of the wave heights;

Hmax = the maximum zero up-crossing wave height;

GGT = the average zero-crossing wave period;

Mo = the total variance spectral density;

TE1 = the sum of the high frequency part of the total energy between 0 - 0.2 Hz (0 - 5 s);

TE2 = the sum of the frequency part of the total energy between 0.2 - 0.1 Hz (5 - 10 s);

TE3 = the sum of the frequency part of the total energy between 0.1 - 0.03 Hz (10 - 30 s).

For these parameters, the correlation coefficients are calculated from the time series of 20 min.

H1/3 : 0,985	GGT : 0,871	TE1 : 0,966	TE3 : 0,950
Hmax : 0,887	Mo : 0,977	TE2 : 0,969	

The graphs of H1/3, GGT and Mo are given in fig.9. In the fig. 10 and 11 two examples of various density spectra with a high and low value of Mo and H1/3 are shown. In those graphs a good resemblance is shown between the various spectra shapes. At the same time, it is clear that waves with a period  $\geq 0.5$  Hz can not be measured by the buoy.

The conclusion of this comparison is that the buoy yields good quality wave data.

#### D. Quality of the wind parameter.

The wind velocity and the wind direction were measured over time periods of 10 min., with a sample frequency of 0.5 Hz and a measurement frequency of 1 per hour. The parameters were obtained by average vector determination.

A correlation calculation gave the following coefficients

- wind velocity : 0.892
- wind direction : 0.886.

Both graphs are shown in fig. 12a and b.

The conclusion can be made that the buoy yields good wind data.

### 6. FURTHER DEVELOPMENTS.

The experiences obtained from handling the buoy and the mooring, as well as from the diving reports and the damage to the mooring shown were incorporated into the new configuration of the mooring.

The main modifications were:

- no signal cable along the mooring lines;
- sinker 1 was replaced by a bundle of chains, so that the unavoidable contact between the sinker 1 and leg 1 will be as gentle as possible;
- an insulating tube covers the first 5m of leg 3 so as to avoid tangling with leg 1 during the turning of the tide.



- the anchor block was replaced by a bundle of chains as a result of which the fluctuating forces in leg 1 will be reduced;
- increasing the length of leg 3 to 45m due to the greater water-depth.

The buoy has been deployed at the location ELD (fig. 1) since September 1982.

The water-depth at the location is 26m below MSL. With 11,5m long leg 1 the subsurface float will now be out of the reach of the direct wave attack. Less damage to the triangle can be expected.

With those changes, the data buoy has withstood several storms up to wind force 12, and max. wave heights up to 12m.

Nevertheless, for this type of mooring, the most dangerous situation will occur when there is none or hardly any current and small waves.

#### 7. SIGNAL-STRAIN CABLE.

From the prototype tests, it appeared that it was impossible to fasten a signal cable along the mooring lines. As alternative could be to use a signal-strain cable consisting of a keflar string twined with signal wires which would be encased by a p.v.c. steel re-inforced cover. The disadvantages of such a cable are however:

- the large radius of the curve of the cable and its "memory" which will determine the behaviour and manageability of the mooring lines;
- connection of the sinkers;
- high costs of development and manufacture of a relatively short cable.

Due to the last mentioned item the plan has not been implemented.

#### 8. CONCLUSIONS.

From the calculations, the model tests in the Delft Hydraulics Laboratory and the prototype tests near the Isle of Wight and on the North Sea, the following conclusions can be drawn:

- a. the 1-point mooring system meets the standards, as described in par. 2 under the hydraulic conditions of the North Sea, when it is deployed at a minimum water-depth of 25m below MSL. It is not possible to connect a signal cable along the mooring lines when materials, such as chain and nylon rope are used for those lines.
- b. the 2-point mooring system is technically the best system but too complicated for practical use.
- c. the 1-point mooring system, with a floating line separating the subsurface float and the buoy, does not meet the standards.



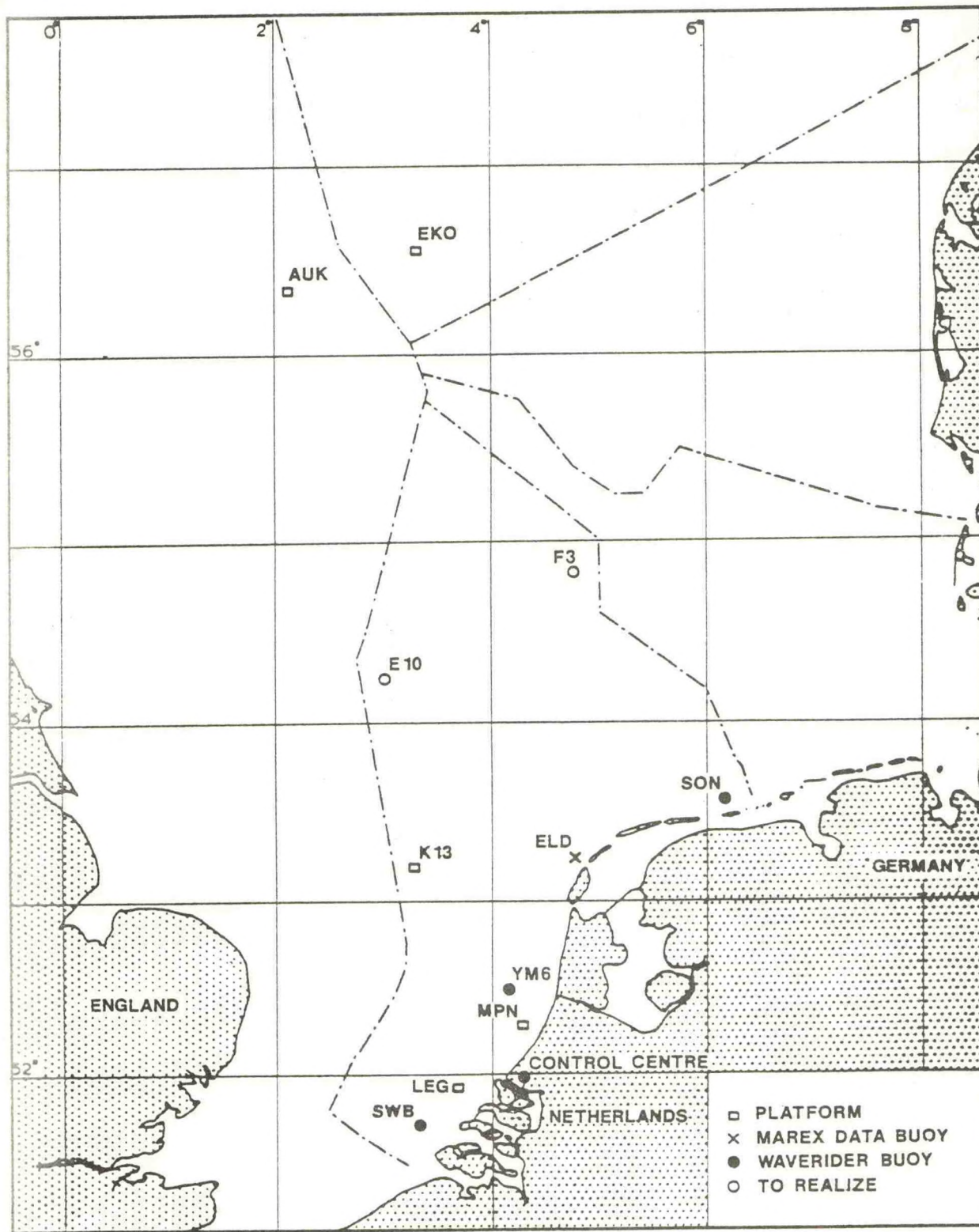


FIG.1 LOCATIONS NETWORK OF SURVEY STATIONS IN THE NORTH SEA



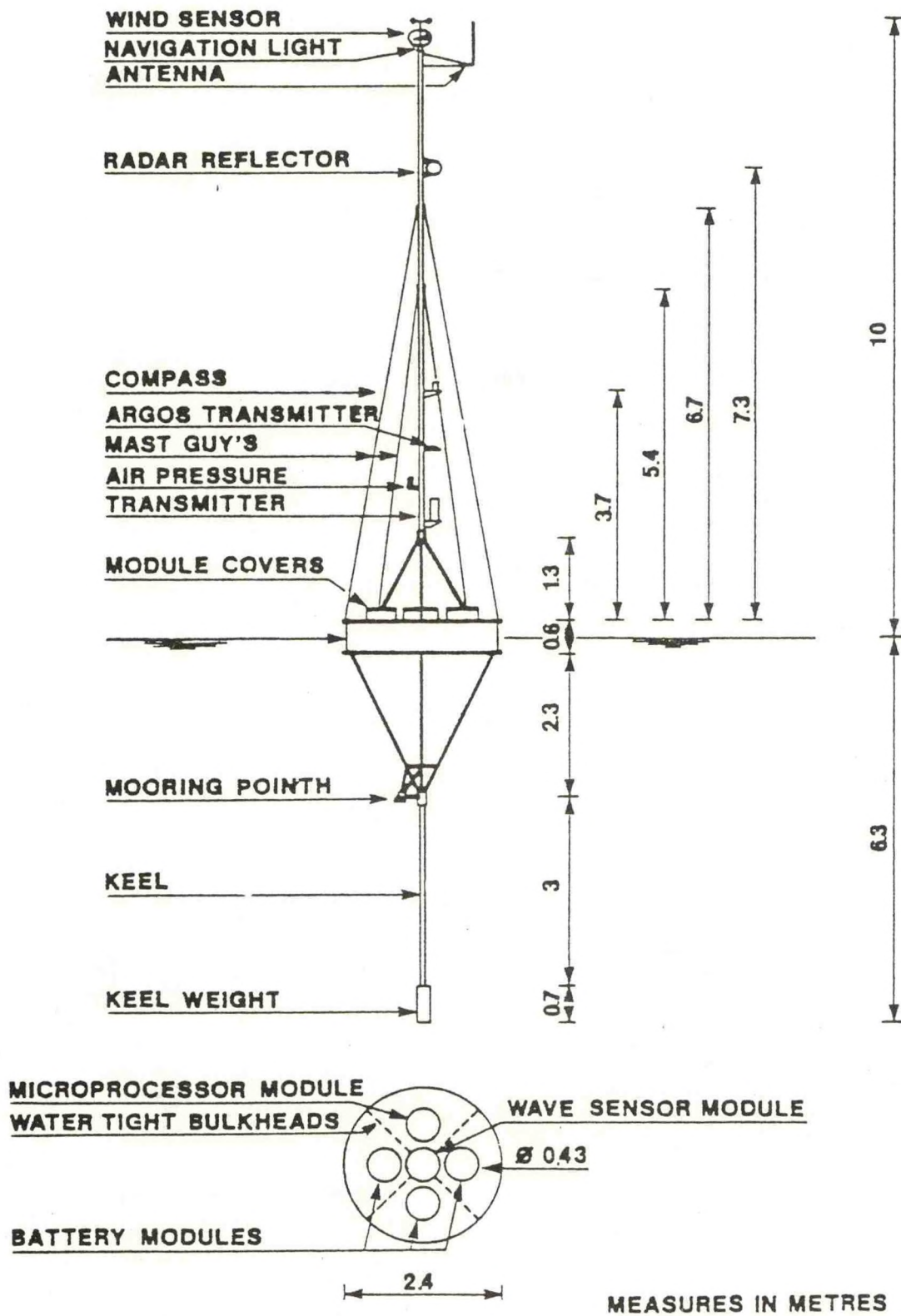


FIG. 2 MAREX DATA BUOY



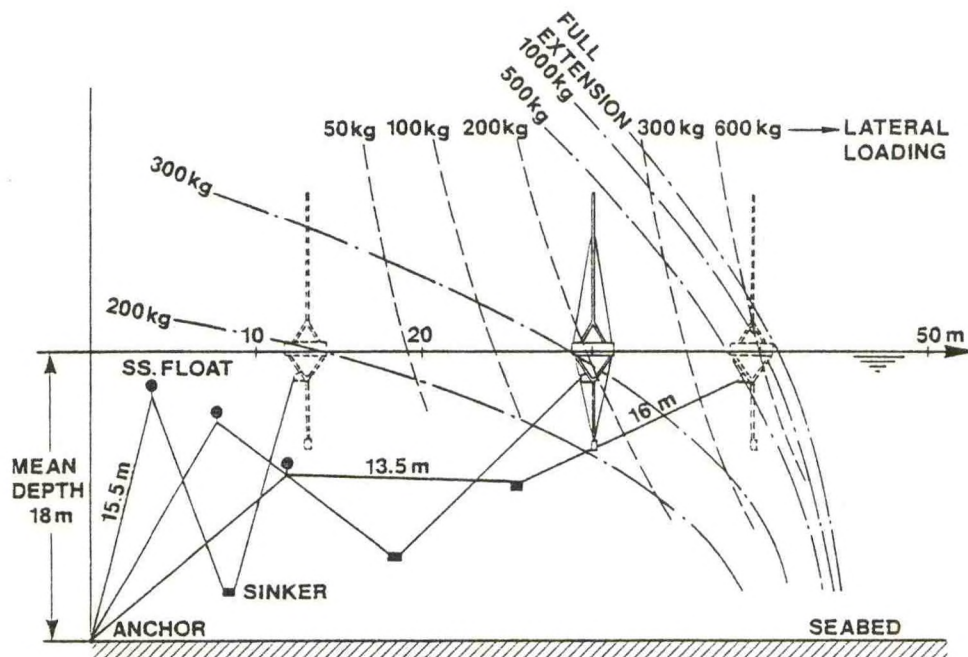
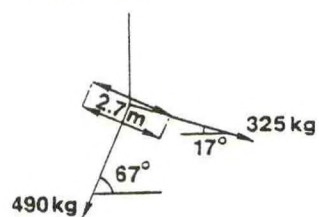
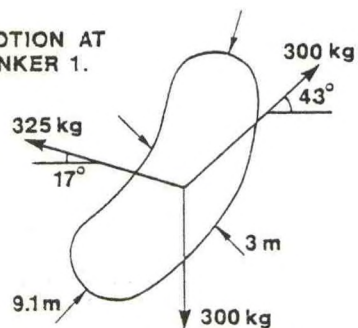


FIG. 3 MOORING CONFIGURATION 1  
MOORING TENSIONS (MECHANICAL MODEL).

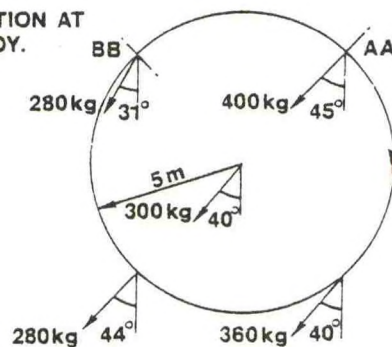
MOTION AT  
SUB SURFACE BUOY.



MOTION AT  
SINKER 1.



MOTION AT  
BUOY.



MOTION AT  
ANCHOR.

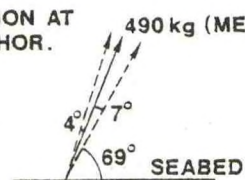


FIG. 4 MOORING CONFIGURATION 1. BASIC MOVEMENTS (MECHANICAL MODEL).



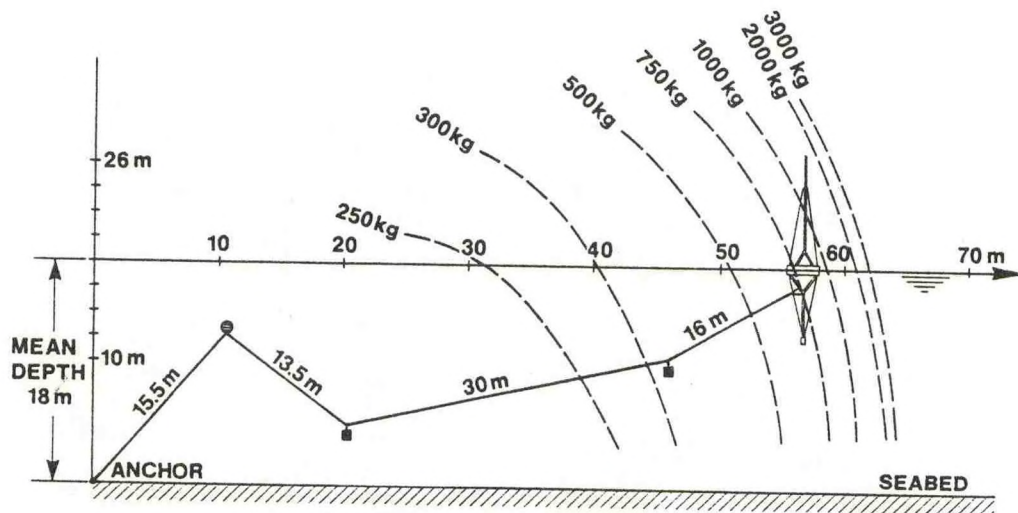


FIG. 5 MOORING CONFIGURATION 2  
MOORING TENSIONS (MECHANICAL MODEL).

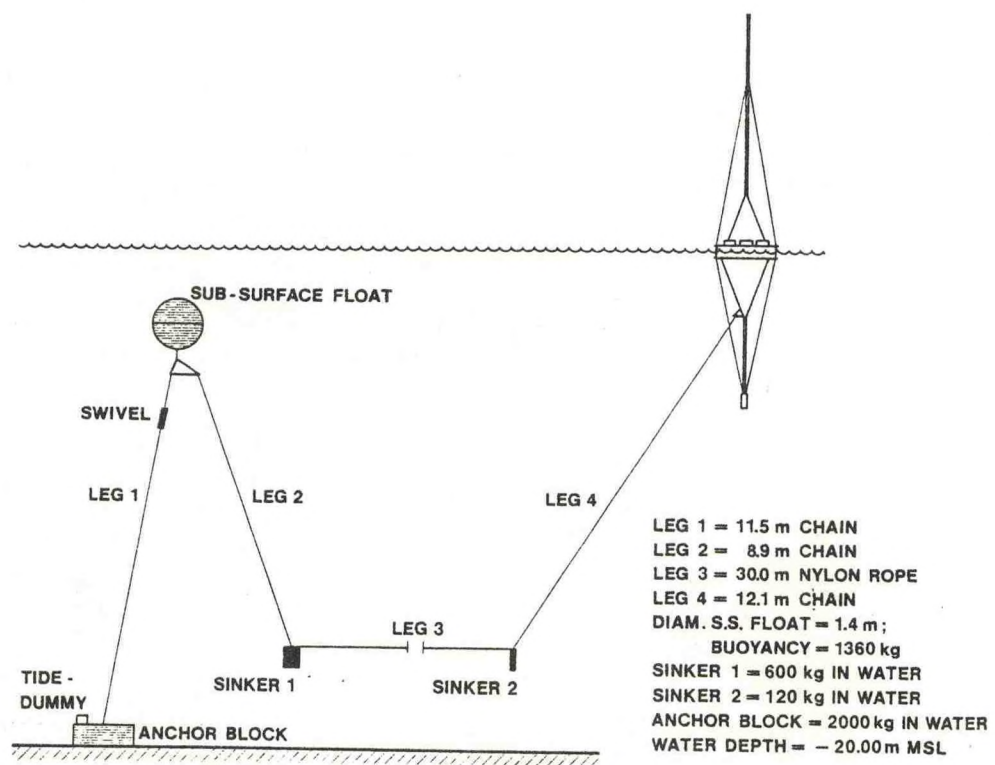


FIG. 6a 1-POINT MOORING SYSTEM  
BASIC CONFIGURATION



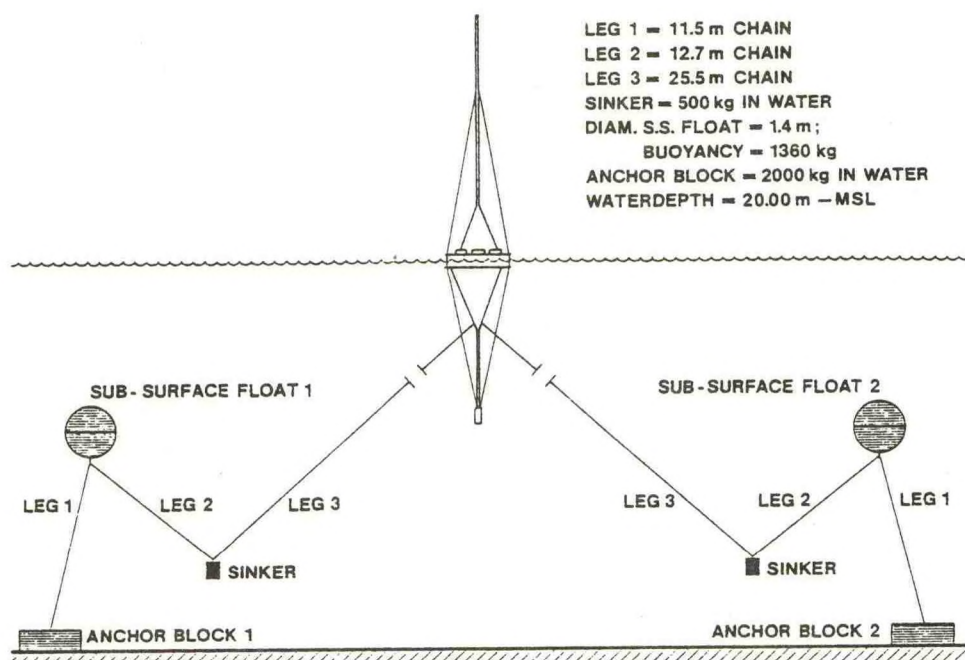


FIG. 6b 2-POINT MOORING SYSTEM  
 BASIC CONFIGURATION

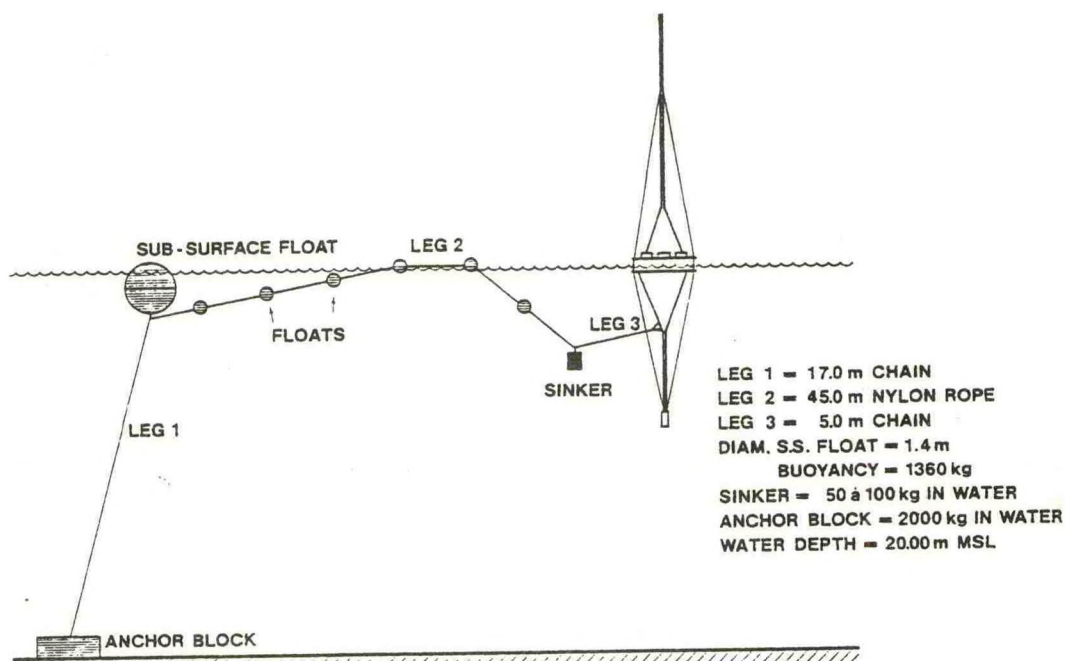


FIG. 6c 1-POINT MOORING SYSTEM WITH FLOATING LINE  
 BASIC CONFIGURATION



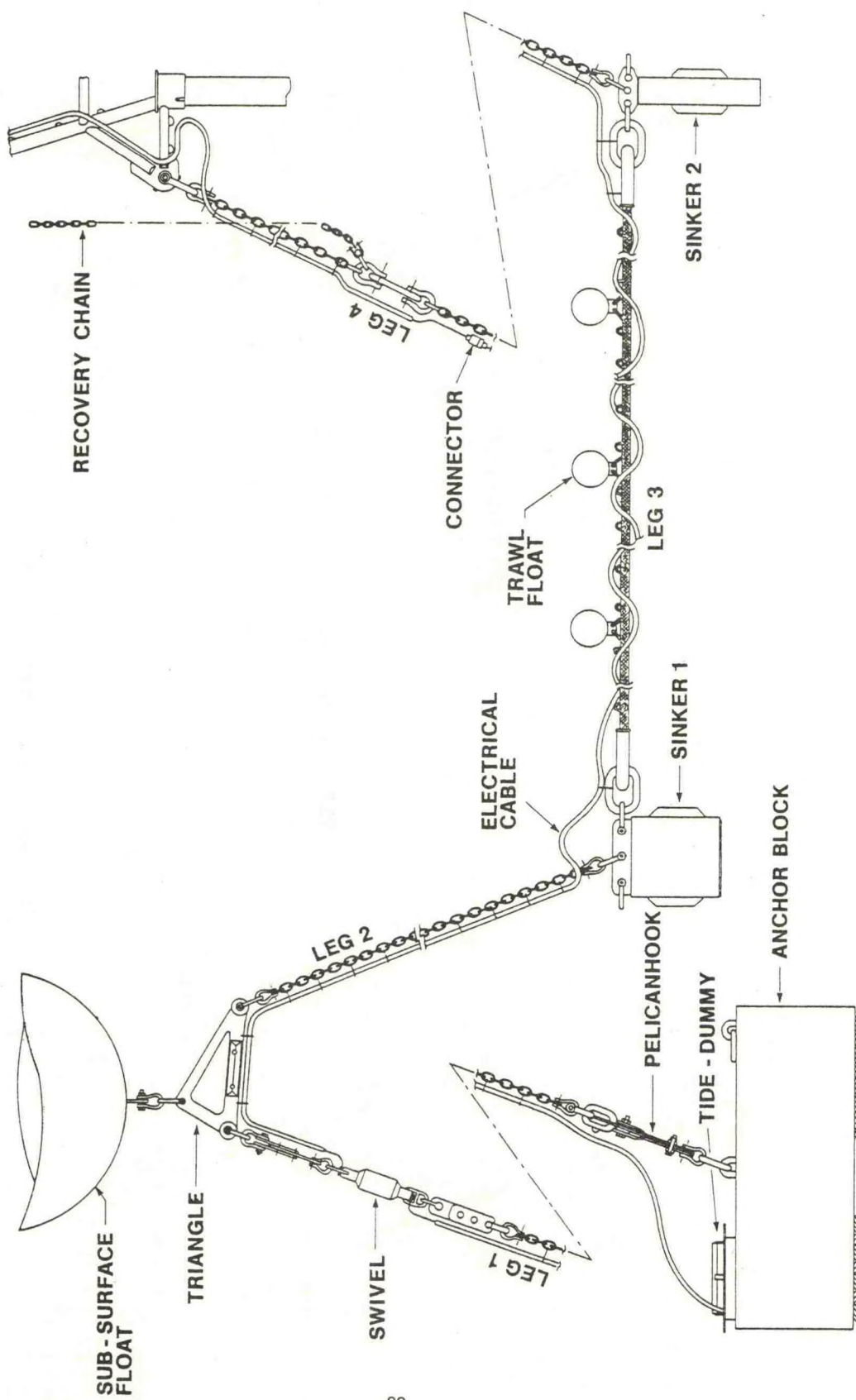


FIG. 7 MOORING SYSTEM FOR LOCATION M.P.N. TEST PERIOD ( 1980. )



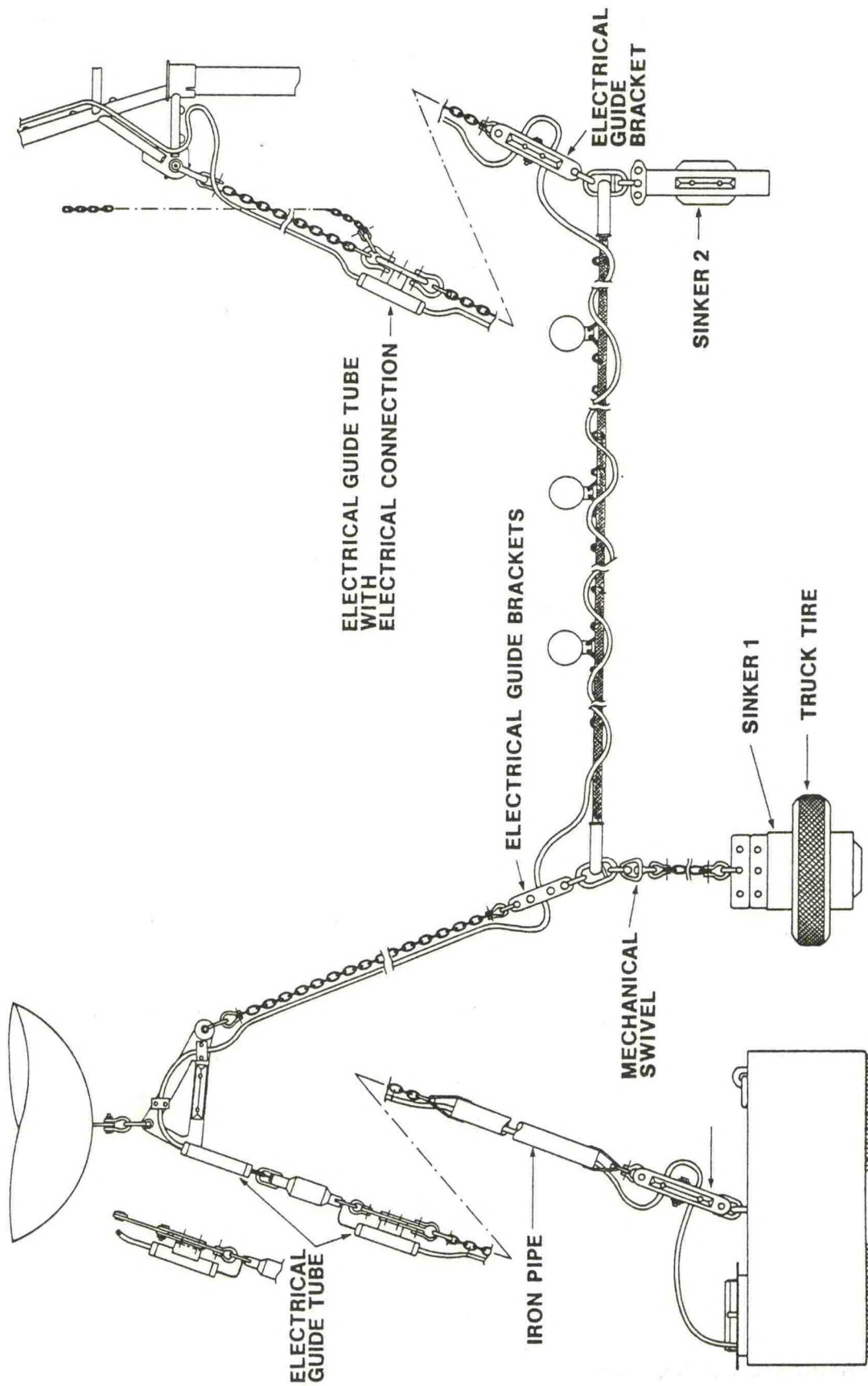


FIG. 8 MODIFICATION MOORING SYSTEM LOCATION M.P.N. (1981)



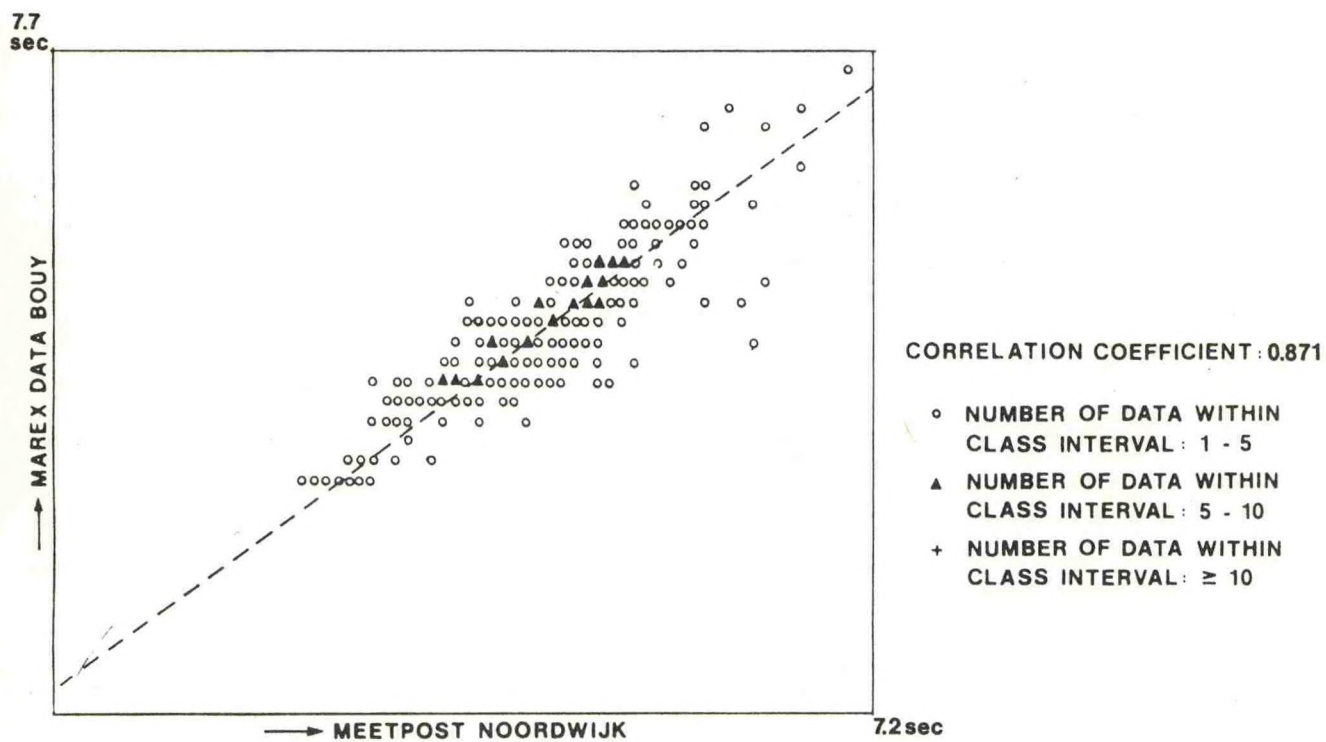


FIG.9a ORTHOGONAL CORRELATION GGT

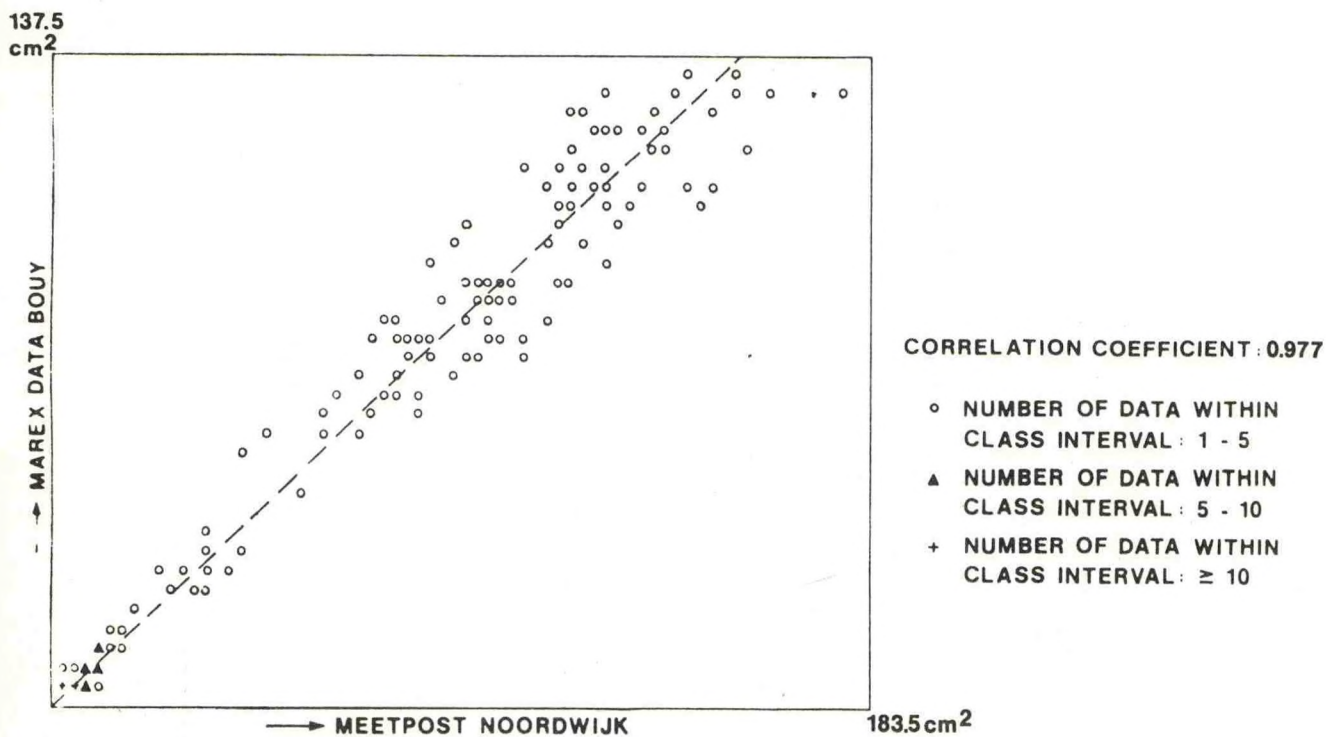


FIG.9b ORTHOGONAL CORRELATION Mo



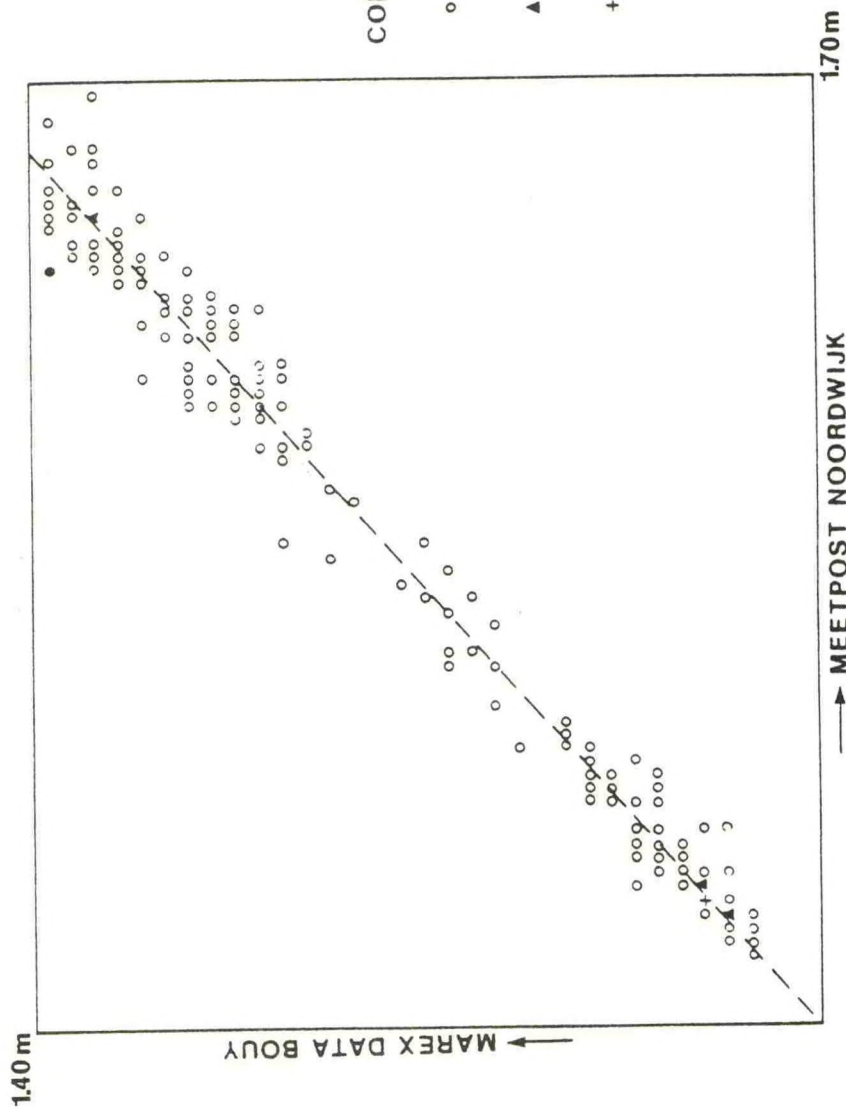


FIG. 9<sup>c</sup> ORTHOGONAL CORRELATION  $H^{1/3}$



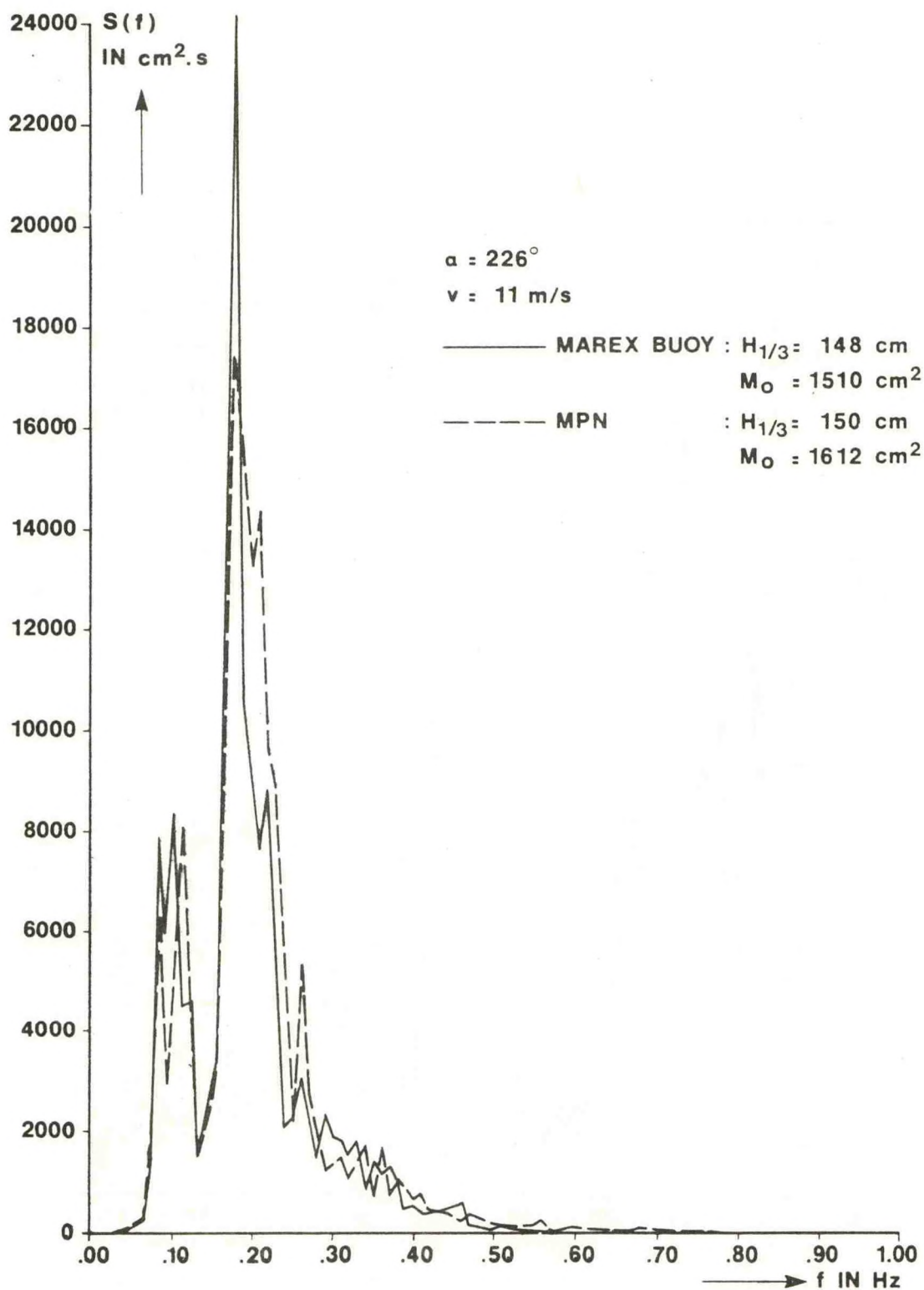


FIG. 10 ENERGY DENSITY SPECTRUM  
 MAREX DATA BOUY AND MEETPOST NOORDWIJK .



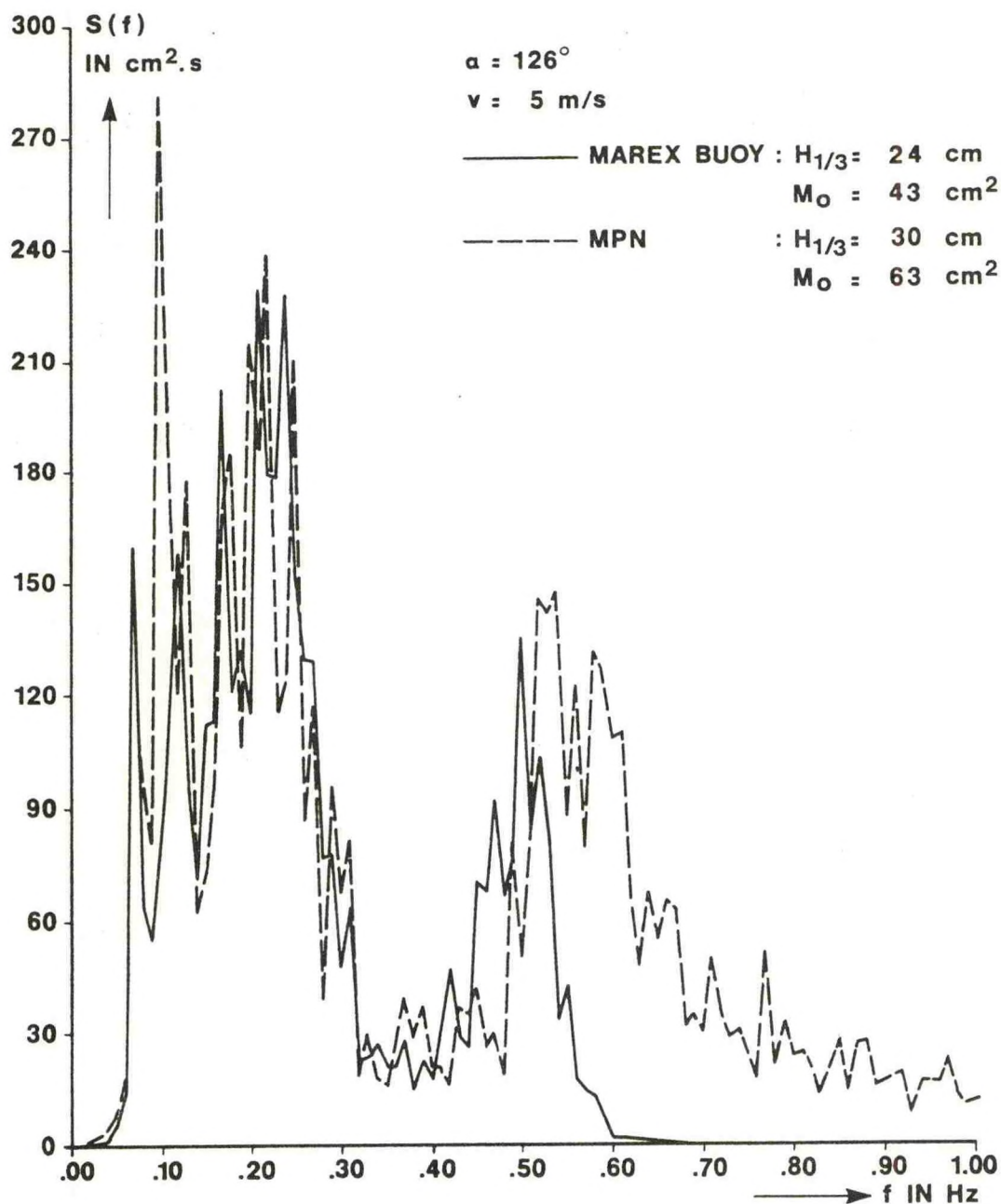


FIG. 11 ENERGY DENSITY SPECTRUM  
 MAREX DATA BOUY AND MEETPOST NOORDWIJK.



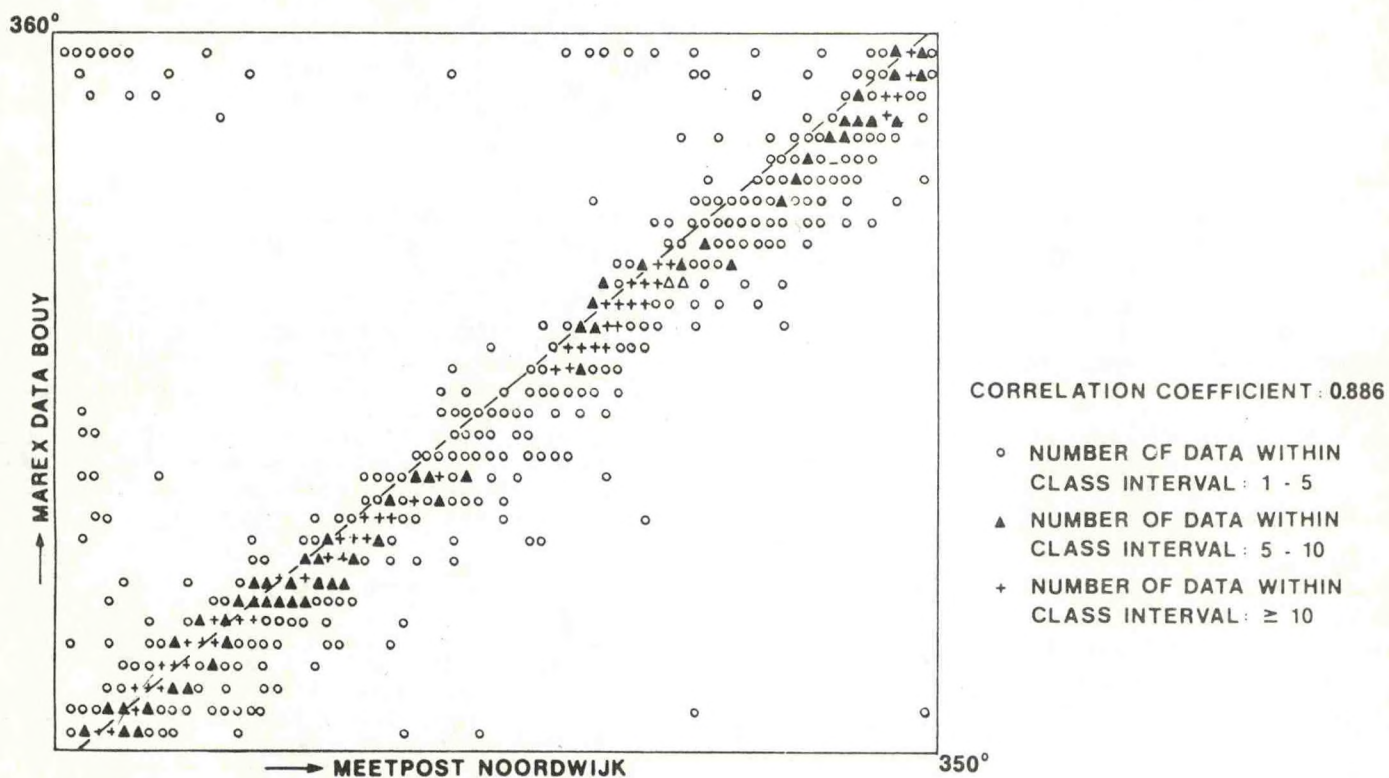


FIG.12 ORTHOGONAL CORRELATION WINDDIRECTION

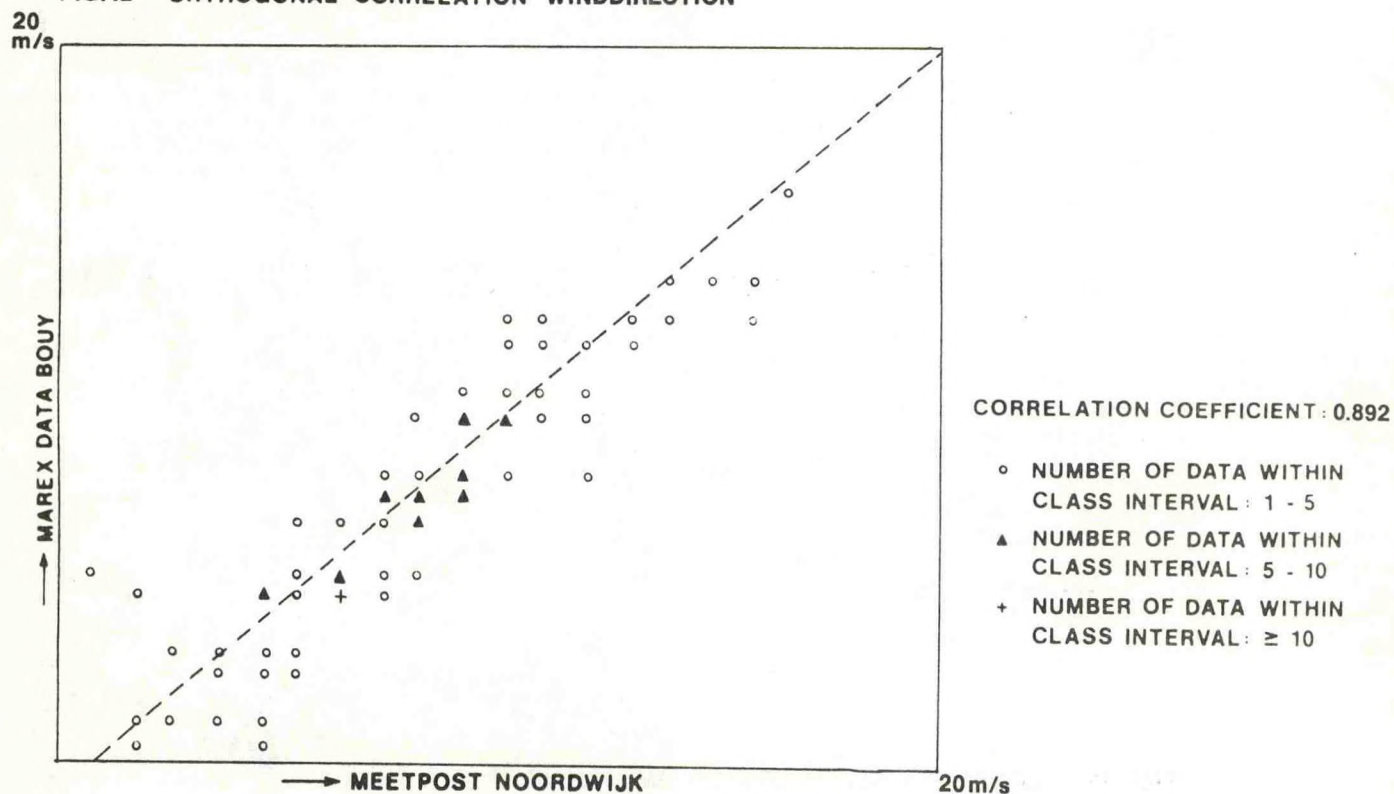


FIG.13 ORTHOGONAL CORRELATION WINDVELOCITY



## THE NOAA DATA BUOY CENTER'S UTILIZATION OF NOMAD BUOY HULLS

Don Windham

and

John Holmes

NOAA Data Buoy Center  
National Space Technology Laboratories  
NSTL Station, MS 39529

### ABSTRACT

The NOMAD Buoy has been in use since 1955. These buoys, which were constructed mostly of aluminum, were all retired by 1970. This history of the buoys during the 1970s and early 1980s recounts the problems of obtaining the available old buoys and the project to construct new value-engineered NOMAD hulls for the NDBC buoy fleet.

### INTRODUCTION

The authors make no claim to any thought or effort that went into the concept and design of the Naval Oceanographic Meteorological Automatic Device (NOMAD) buoy hull. In fact, both had early reservations as to whether or not it would serve as an acceptable ocean instrument platform. In all honesty, those reservations may have resulted from unpleasant experiences with the hulls that had nothing to do with their suitability for use as ocean weather stations. Mr. Holmes first became acquainted with the buoy in the mid-fifties when he was tasked to design a suitable mooring, and he is not anxious to discuss the merits of that design to any great degree. His silence may come from the buoy's apparent reluctance to being tied as described in Mr. William Hakkarinen's 1964 paper entitled "The World of NOMAD-1." Mr. Windham's nodding acquaintance came in the early seventies when he moved into the oceanographic instrument world after several years in aerospace. His introduction was made by reading the many available articles in the MTS proceedings prompted by the fact that the NOAA Data Buoy Center (NDBC) was negotiating for some of the old excess hulls. His first intimate experience came in May of 1977 when he and two contract engineers changed out a failed navigation warning light installed on a NOMAD buoy. The task was completed after about 2 hours of frustrating work, 10 skinned knuckles, two barked shins, several bruises on various body appendages, a pair of torn trousers, and several hundred swear words. This heroic effort was accomplished while the NOMAD was set on a concrete hardstand at the Cape May, New Jersey, Coast Guard Base. From these early experiences wouldn't you know that their first choice for this paper title was "I Hate NOMAD Buoys," but it seems that series may be copyrighted already.

After revealing biased personal thoughts regarding the use of these hulls fueled by their early experiences, it may seem strange that they would

Computer Sciences Corporation  
National Space Technology Laboratories  
NSTL Station, MS 39529

attempt a paper on the subject. However, after reading Mr. Hakkarinen's paper and talking with many people who had used the hulls, it became apparent their early aversions were the same as most everyone else who used the hulls. Since both authors strongly agree that personal feelings have to be set aside in the pursuit of scientific truth, it was decided to recount what NDBC records show with astounding clarity--it works and it works well.

### BACKGROUND DISCUSSION

When ashore the plump, semi boat-shaped aluminum NOMAD hull, with its stainless steel mooring yoke tied up at the front, gives most instrument people a case of nerves. Negative thoughts seem to take over, many of which if true can be serious limitations. Some of these areas of concern are amplified when the buoy is placed in the water (see Figure 1). Its low profile allows the sensors to be awash during any sea state other than flat calm and also affects the high frequency data band radio signals, its response to wave and currents is semi-directional, and its known wild heaving motions are devastating to underwater cable connections. Other questions were its size (reserve buoyancy)--how could it support the mooring line weight and have enough space for an adequate power system yet be kept small enough to handle?

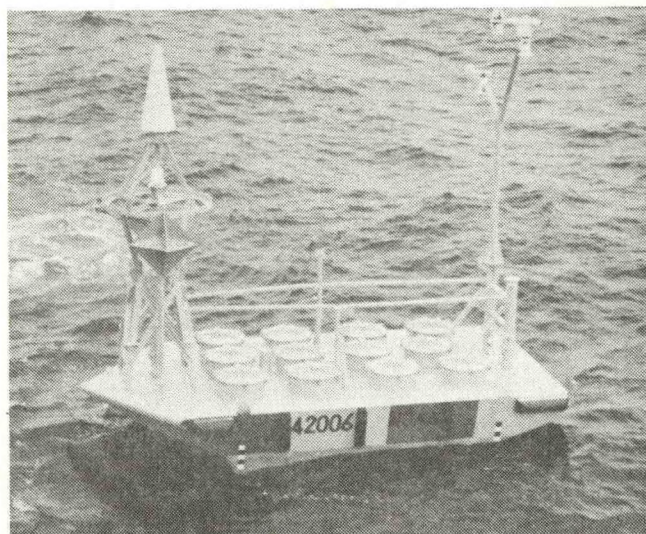


Figure 1. NOMAD Buoy



The development of a synthetic mooring line overcame the limitations on mooring weight. The development of high-power density batteries completely alleviated the bulky power system problem, and now ballast has to be added even when a 2-year battery supply is installed in the hull. These early problems could have been overcome two decades ago by increasing the 6m x 2.9m x 2.1m dimensions, but an increase would have taken it out of the truck transportable category and placed it into the same expensive transportation grouping with the large discus buoys.

The data systems were the major limiting factor on any early buoy. Their large physical size and high-power requirements would not fit into any small long-life buoy. The susceptibility of the old vacuum tube electronics to the wild accelerations of the NOMAD caused even further complications. Extensive efforts at solving these problems resulted in many successful short deployments. Outstanding craftsmanship was evident in the mid-fifties systems still in place in some of the buoys acquired by NDBC. Those early systems were timed by precision Navy chronometers wound by stepping relays, powered by heavy banks of lead acid batteries. These were completely shock mounted. Other efforts at improvement included development of a 10-year Strontium 90 power supply and several versions of wind-powered generators. Even if all these efforts were successful due to the obvious meticulous work performed, the data transmission problems were enormous.

Many of these engineering problems had not been resolved at the inception of the old National Data Buoy Project (now NDBC), so the decision to use large discus buoys was made. The escalating costs of these systems kept the concept of smaller, lower-cost systems alive within NDBC and eventually culminated in the marriage of the small NDBC satellite data system and the NOMAD hull.

As early as 1972, NDBC was exchanging communications with the Navy regarding their possible use of excess NOMAD hulls. In 1973, NDBC requested that the Naval Underwater Systems Laboratories lend them some of the hulls, but no action resulted. Then in May of 1974, after several months of discussion, a loan agreement was finally consummated for three of the hulls. About 2 weeks later, tentative agreement for five additional hulls was reached and NDBC was in the NOMAD business with eight good hulls.

After some initial success (high points will be discussed later), NDBC realized that their compact data system, powered by high-density batteries installed in a NOMAD buoy hull, was indeed an excellent system. When Coast Guard Warrant Officer Walter L. Carr was assigned as the NDBC Logistics Officer in 1976, he was given a high-priority project--find all the old NOMAD hulls and get them for NDBC if possible. His assignment led to lots of telephone calls, many letters, and several trips to check the numerous places a NOMAD buoy might be. Mr. Carr succeeded in finding and obtaining seven more NOMAD hulls including one from the museum at the Washington Navy Yard. He investigated rumors about several more which included one sunk off the

west coast and one in the Azores Islands. The one rumored to be in the Azores later turned up in Lisbon, Portugal, but attempts to obtain it have not been successful. Several of the rumors proved to be true, but some of these buoys were smaller sizes. Three two-third sizes and a couple of half sizes were picked up by NDBC. In dockside tests these proved to be unseaworthy. The largest one is currently being used in a fixed outdoor exhibit at the National Space Technology Laboratories Visitors' Center in Bay St. Louis, Mississippi.

After the successful integration of the excess Navy NOMADS into NDBC's operational network, a simple design using the same hull shape and dimensions was completed by NDBC in 1980. Five of these value-engineered (VE) buoys were contracted for and delivered by 1982. All five were fitted with data systems and are now in active service. NDBC recently signed an agreement with the Coast Guard Shipyard in Curtis Bay, Maryland, for 10 more of the VE hulls. Delivery is expected to begin in early 1983.

#### HISTORICAL HIGHLIGHTS OF NOMAD UTILIZATION

Immediately after the transfer of the first Navy excess NOMAD hulls to NDBC in 1973, one was shipped to the Magnavox plant, Fort Wayne, Indiana, where it was outfitted with their successful version of the Limited Capability Buoy (LCB) payload and a 6-month power supply. It was then shipped to Juneau, Alaska, where it was deployed in the Prince William Sound about 70 nautical miles from Ocean Cape. The deployment was made by NDBC and Coast Guard personnel working from the Coast Guard Buoy Tender PLANETREE in mid-October of 1974. The LCB payload measured wind speed and direction, air pressure, air temperature, and surface water temperature. These data were transmitted through a high-frequency data link to the Coast Guard/NDBC receiving station at San Francisco, via land line to the Coast Guard operated NDBC receiving station at Miami, Florida. It was then preprocessed for routing to NDBC and the various data users every 3 hours. Even though this complex data link was by nature troublesome, the 6-month deployment was considered highly successful, furnishing much needed continental shelf data for the Bureau of Land Management's oil exploration studies. This project launched the highly successful NOMAD buoy/small data system marriage and a long era of cooperation with the Department of the Interior.

This buoy was removed from its station in May of 1975, refurbished, and redeployed at the same position in July of 1975. It went adrift in early 1976, was retrieved by the Coast Guard, reworked, and redeployed in August of 1976. At about this same time, a second NOMAD was deployed in the Gulf of Alaska, and a third was deployed off the New Jersey Coast. This third NOMAD deployment put NDBC into NOMAD utilization in both major oceans. They were limited to continental shelf locations, and the payloads were unpredictable due to the complex high-frequency data link in use, but all were considered successful.



In late 1976, a fourth NOMAD was deployed on Georges Bank off the New England Coast and another in Cook Inlet, Alaska. With the increasing number of NOMAD buoys came the problems that sometimes were associated with their wild bucking motions. One mooring system in Alaska became so entangled it did not set properly, and the buoy was recovered after dragging anchor several miles. Attempts at designing an all-chain mooring that could not be easily cut by vandals did not work out because of corrosion problems resulting in failure. These were very exciting days for NDBC. One of the Alaskan buoys broke its mooring in late 1976, took on some water, but was recovered by the Coast Guard. It was reworked and redeployed in early 1977, but this seemed to be the harbinger of things to come as the buoy off the New Jersey Coast also went adrift. After several mooring failures, the early version of a position-fixing system operating through a satellite was added. The fact that a major system failure in the HF data system could not be repaired at sea caused further complications because the earlier versions had to be retrieved and brought ashore for repairs. Even with those early problems, the NOMAD capability was needed by NDBC and the failures were worked around because of the demand for continental shelf data.

In early 1978, the NOMAD moored in Cook Inlet, Alaska, broke its mooring, drifted the full length of the Shelikof Straits, and went aground on the southwestern portion of Kodiak Island. An attempted recovery in March by their USCGC SEDGE was aborted after a tow line parted. A second attempt in May had to be aborted due to bad weather. The buoy was finally recovered by a commercial tug out of Kodiak, but major hull pitting corrosion had occurred where the buoy was buried in the sand. It appeared to have been set up by the aluminum hull and the stainless steel yoke after one of the yoke insulators was broken. This buoy is still in service, but it is limited to freshwater deployments.

A significant plateau in the use of the NOMAD hull was reached on July 12, 1978, at 5:15 p.m. eastern standard time when the USCGC HORNBEAM deployed the first NOMAD with a UHF satellite reporting data system installed. One of the authors, Mr. Windham, had the privilege of being on this deployment some 45 miles southeast of Cape May, New Jersey. This ushered in a system that truly could stay on station for years rather than months, and the expected 100% data received goal could be realized. But the little beast didn't "play easy to get" again as the new data system ceased transmitting July 15 after less than 3 days on station. It was apparently another victim of the wild bucking motion of the buoy. Another goal was reached very quickly, the replacement of a failed payload at sea, when a new unit was installed placing the buoy back in service July 27. Thus, some 25 years after the first NOMAD buoy was deployed its utilization as a working ocean data platform that could remain for several years on station was finally a reality!

In August of 1978, another Gulf of Alaska NOMAD mooring failed and it went aground on a very rocky beach of Montague Island. Investigations revealed

the hull would probably be destroyed if simply dragged off the beach by a tug, so other arrangements had to be made. This was accomplished in November of 1978 by a U.S. Army flying crane out of Fort Richardson, Alaska, and the buoy was placed back in service. Several other mooring failures have occurred and routine retrievals have been made but the moorings have held under most circumstances. One recent incident involved a NOMAD off the California coast when an apparent poacher shot a seal on the buoy, damaged the deck, and shot one strategic hole in the hull near the waterline. This resulted in the buoy filling partially with water and destruction of the power system. But the buoy and electronics survived this incident, and the buoy is being repaired at NSTL for further service.

In 1979, NDBC, at the request of the National Weather Service, initiated a network of weather reporting buoys in the Great Lakes. This has grown into a total of eight buoys that remain on station only during the summer months. They are removed each fall, and the hulls are placed in winter storage at a nearby shore station. This deployment cycle is necessary because of the ice formation in the winter that could destroy and sink the buoys. In fact, several late retrievals have been very difficult because of ice buildup on the old familiar tower-type forward masts. A new mast design for the buoys susceptible to ice buildup is utilized on the lakes buoys; therefore, the deck configuration and appearance are somewhat changed from those that have been in service since the early days.

In November of 1979, NDBC deployed a NOMAD near one of the deep ocean 12-m discus buoys about 200 nautical miles west of Astoria, Oregon. The purpose of this double station was to study the survivability of the hull and its data system and to compare the data with that from the large discus buoy. This study demonstrated that the data compared favorably with that from a large discus buoy. This study indicated that one of the major restrictions to NOMAD utilization could be lifted, and the decision to procure more NOMAD hulls was then made.

Of the 15 NOMADs obtained by NDBC from the Navy and other sources, 14 are still in service as of this date. The only loss occurred in October of 1980 when the buoy east of Atlantic City went adrift. It was tracked by its satellite locating system as it swung south and entered the Gulf Stream, which immediately started it north/northeast at about 20 knots per day. No Coast Guard vessel could be freed from other missions, and attempts at obtaining help from other sources failed. The buoy, tracked for several weeks, was reported sighted several times by various ships, but no retrieval has been made to date. Some diehards in NDBC believe the durable little monster may show up again even at this late date.

## CONCLUSIONS

The NOMAD buoy is becoming the workhorse of the NDBC network as evidenced by the recent procurement of the VE NOMADs. If these late procurements are



as durable as the old Navy hulls, the "Wild Bucking Beasts" (as named by a USCG buoy tender captain over two decades ago) will be around many more years. Through these almost three decades that the NOMAD has been in use, it should have proven to many observers that appearance, semi-scientific judgment, and other personal feelings are not a reliable way of evaluating performance, utility, and longevity of a device. The experience has been very informative to the authors who hope that this paper may prove to be of use in some of the readers' scientific pursuits.

#### BIBLIOGRAPHY

1. Hakkarinen, William, "The World of NOMAD-1," Marine Technology Society Buoy Technology Conference Proceedings, March 1964.
2. Anonymous, Selected articles from the "NOAA Data Buoy Technical Bulletin" published November 1974 through December 1977.
3. Anonymous, Selected Material from Correspondence Archives of NOAA Data Buoy Center, January 1973 through December 1982.
4. Carr, Walter L. CWO USCG, Personal File and Notes, July 1976 through June 1979.
5. Anonymous, The Encyclopedia of Oceanography I, Reinhold Publishing Corporation, 1966.
6. Timpe, G. L., "The Use of NOMAD Hulls as Severe Environment Buoys," MTS/NDBC 1983 Symposium on Buoy Technology, April 27-29, 1983.
7. Timpe, G. L. and W. O. Rainnie, Jr., "Development of a Value-Engineered NOMAD Buoy," Proceedings of the MTS-IEEE OCEANS 82 Conference, Washington, DC, September 1982.



# OPERATIONAL USES OF A SMALL, HIGH-CAPABILITY DATABUOY

M.S. Martin

MAREX LIMITED, ENGLAND

## Abstract

In the early 1970's the expanding program of offshore oil exploration in the UK North Sea created the need for oceanographic and met. data for the area. Several long-term data collection programs were run based on weatherships, but increasing costs meant that databuoys (always a good idea) would be the best basis for such studies.

This paper is concerned mainly with operational aspects of a databuoy designed to fill that need.

The buoy system hardware is described briefly first, but the main detail is concerned with descriptions of different operations world wide each with its own hardware mix, data handling arrangements and duration requirements.

The aim is to point up the diversity of user requirements and to make some assessment of future developments.

## Assessment

### Basic Buoy System

The design brief for this databuoy was for a platform able to obtain data of a similar type and accuracy to that from a weathership. The buoy should follow the surface in order that an accelerometer could be used for wave profile measurement, and stability should be such that winds could be measured at 10m elevation.

It should be small enough to be deployed and recovered by ships of convenience and should operate for extended periods on sites of up to 1000m water depth.

The layout of the buoy to meet these criteria is shown.

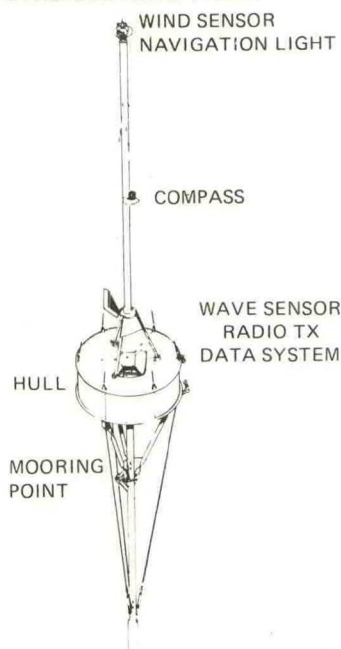


Figure 1 — GA of buoy

The hull is 3m dia, the overall length is 17m and the all-up weight is 1500Kgs. Batteries and Electronic systems are contained in water tight modules which can be exchanged while the buoy is on station, and the data acquisition system on-board is based on a CMOS micro.

Some more hardware detail will be given in the appropriate sections.

## USAGE

Metoccean data is required for both design purposes and for actual operations, by engineers, oceanographers and operators. To quantify these needs, they range from long-term accumulation of raw data for subsequent analysis through to instant figures, frequently updated, for an operation lasting only a few hours.

Data Processing differs for each end of the spectrum, according to prior usage in that particular specialism, and so do all aspects from mobilisation to maintenance.

This range can be illustrated by examples of various operations.

### 1. Wave direction measurement off W. Scotland

This project involves the investigation of the wave direction climate for a wave energy program run by Department of Energy.

Several different systems have been devised for wave direction measurement, but there is not yet a consensus on analysis methods nor a familiarity in handling the results.

The specification calls for raw data on heave, pitch, roll and heading to be accumulated on shore for later analysis.

Hence the buoy performance criteria are:

- to follow the wave slope
- to transmit all the data ashore
- to last 6 months plus on station

This is an example of a system with no instantly usable display onshore, apart from housekeeping.

The standard hull/keel combination has a roll period of some 4.5 secs and this is reduced to 1 second by decoupling the ballast weight and reducing the mast height and weight.

This also reduces initial tilt stability to allow accurate wave slope following.



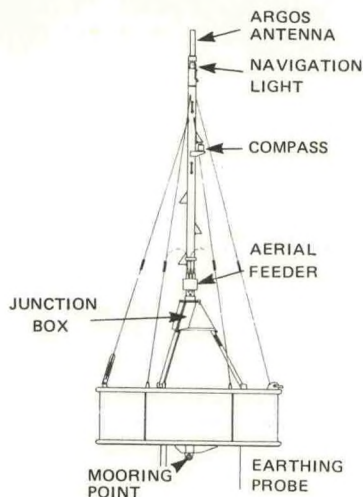


Figure 2 — Wave direction buoy

The data link range is 20 miles and each message consists of 19,200 values which are transmitted in blocks at 300 baud over a phase modulated HF radio link to a recording shore station.

Operational criteria are:

- no gaps in the data
- 2 year project

This means that a spare buoy is to be held in readiness for deployment and that housekeeping data transmitted by the buoy must be perused regularly.

A proposal to send housekeeping data by satellite was not taken up and arrangements have been made to monitor the shore station in order to check the buoy data system is functioning correctly.

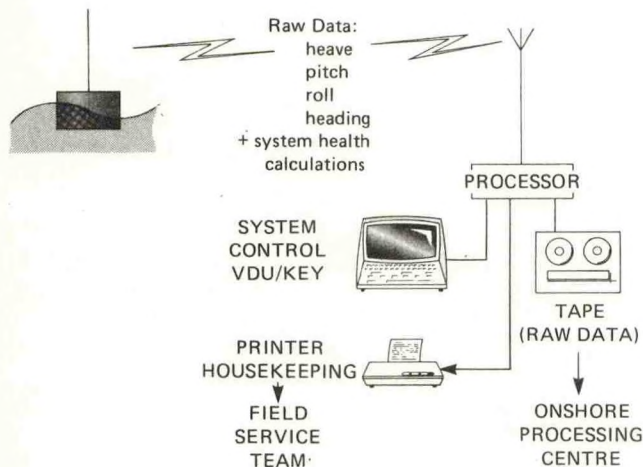


Figure 3 — data path

In future, wave directional analysis will be used more frequently as engineers and operators become familiar with results and acquire a feel for achievable accuracies. The results will be used directly and as inputs to computer-based systems designed to assist in, say, platform manoeuvring and emplacement operations where wave trains and their energy are important forcing functions.

Assuming that a consensus is reached on a method of reducing the data, the computation required on board the buoy will be fairly extensive. There will be ever a need for more capable, low power drain processors for buoy data systems.

## 2. Bering Sea

This involved placing 4 metocean buoys in a remote offshore area north of the Aleutians to evaluate the feasibility of exploration and drilling operations. Economic decisions would be based on metocean statistics which in turn determine the design of the drilling units and platforms.

The buoys had to send back data with the best achievable reliability, over a 1 year period with no servicing visits scheduled, due to the remoteness of the site.

Data measured were:

Winds  
Waves  
Air temperature  
Barometric pressure

One dimensional heave spectra and threshold — selected raw data were required.

The buoys were fitted with a standard suite of met. sensors, with a duplicate wind sensor pair as back up.

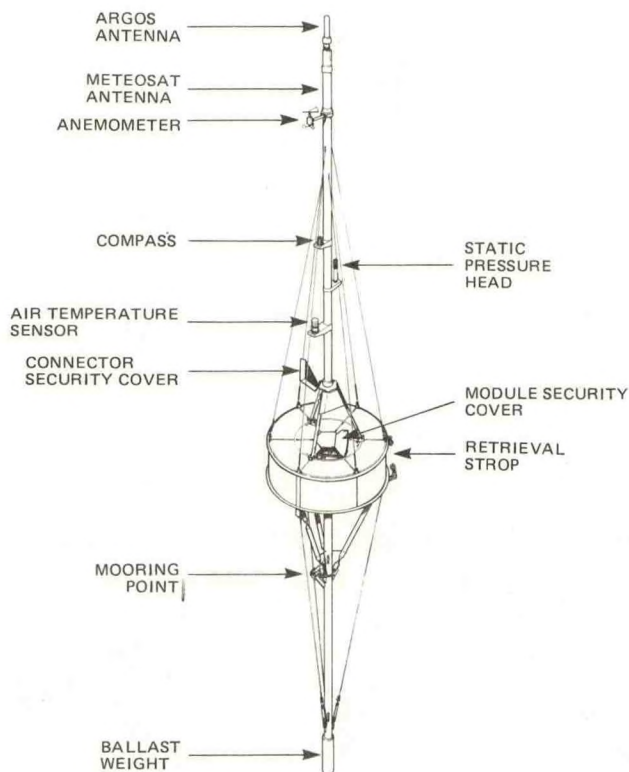


Figure 4 — Buoy G.A.

Data links were also duplicated, with ARGOS and GOES transmitters being fitted.

The neat coaxial mounting of the 2 antennae is shown.



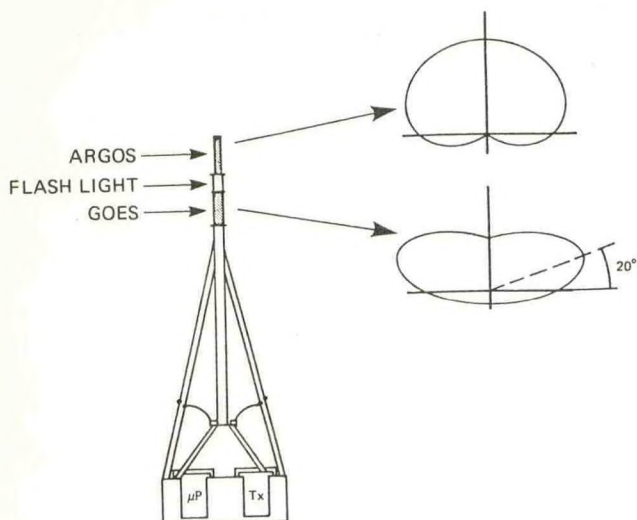


Figure 5 — antenna detail

Omnidirectional transmission patterns in azimuth were necessary as each buoy rode to a single point mooring.

Operational criteria were:

- 1 year plus on-site life
- no servicing
- deployment by ship of convenience
- client would designate operators
- 2 water depths

The client was clear on all the data processing required and this led to a condensed message for which the power budget allowed multiple transmission to improve integrity of the data link.

Housekeeping data was used to assist archiving only, since the only operational use for it was to monitor performance of the on-board raw data logger.

Good communication between the English hardware manufacturer and the U.S. operator was maintained in the mobilising phase, leading to a practice assembly, commissioning and deployment exercise at the U.S. shore base before moving to site.

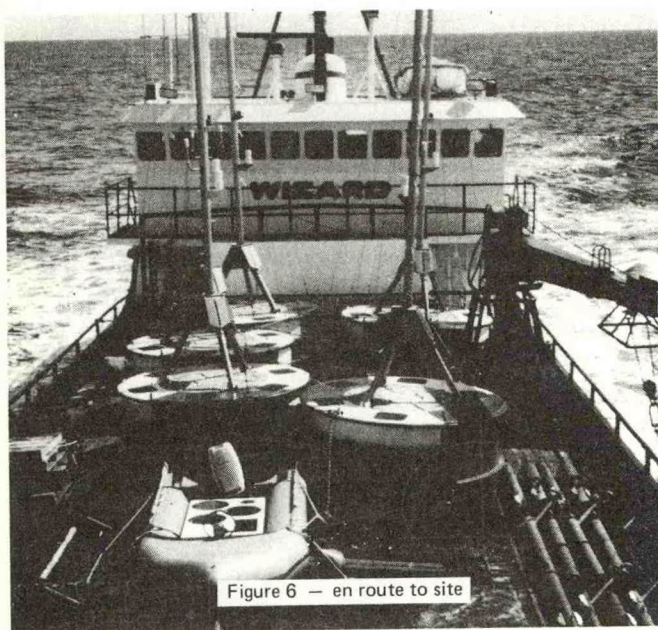


Figure 6 — en route to site

Setting the electronics to work and assembling the mooring kit correctly were both vital to achieve the long term reliability required and such training and familiarisation should be allowed for in an operational budget.

Moorings were designed to minimise chafe and long term corrosion, and no failures occurred.

### 3. Brunei

This offshore area is more benign, but the economics of platform designs to exploit the offshore reservoirs demand accurate metocean measurements. The area is near a typhoon belt and the ratio of extreme-to-normal events is higher than for most areas.

Besides the logging of wave data, these buoys are used as the primary source of data for weather forecasting for the area and instant availability of data ashore is of first importance.

There are 2 buoys on sites near oilfields, one on each boundary of the offshore area. Offshore operations there are based on prevailing local conditions, so accuracy and continuity of data are (as ever) important.

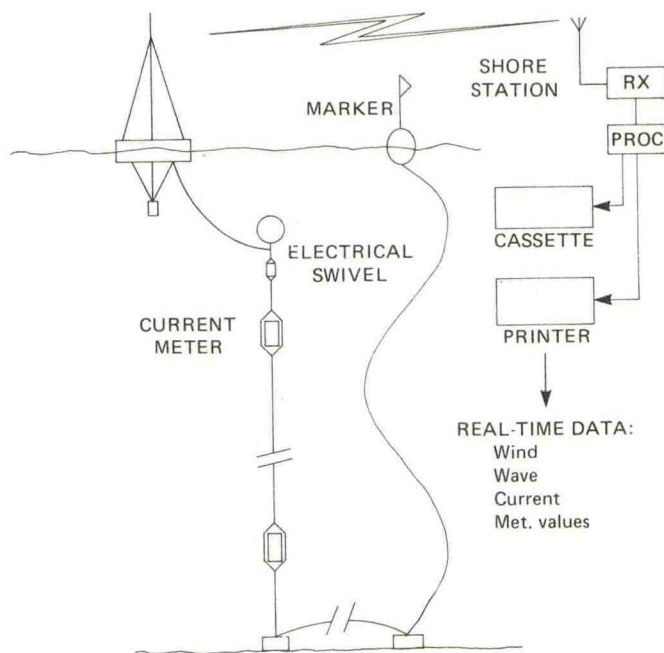


Figure 7 — buoy system

The buoys measure met ocean values, including currents. The unpredictability of currents in the area make real time display of current values on shore important, and the buoy processor controls current measurement through a hard-wired sub sea data link.



These links each contain an electrical load bearing swivel which passes commands, data and power through at separated frequencies, and has proved reliable in service over several years in tropical salt water.

Operators are provided on a full time basis by the manufacturer in order to ensure continuity of data. A spare buoy with extra sub assemblies is held in readiness ashore, and a maintenance-by-replacement policy is adopted. This involves maintaining accurate shore station records of housekeeping data transmitted and a thorough knowledge of the buoy system field performance. This has led to the systematised maintenance procedure essential for continuity as operators are changed at the end of their tours.

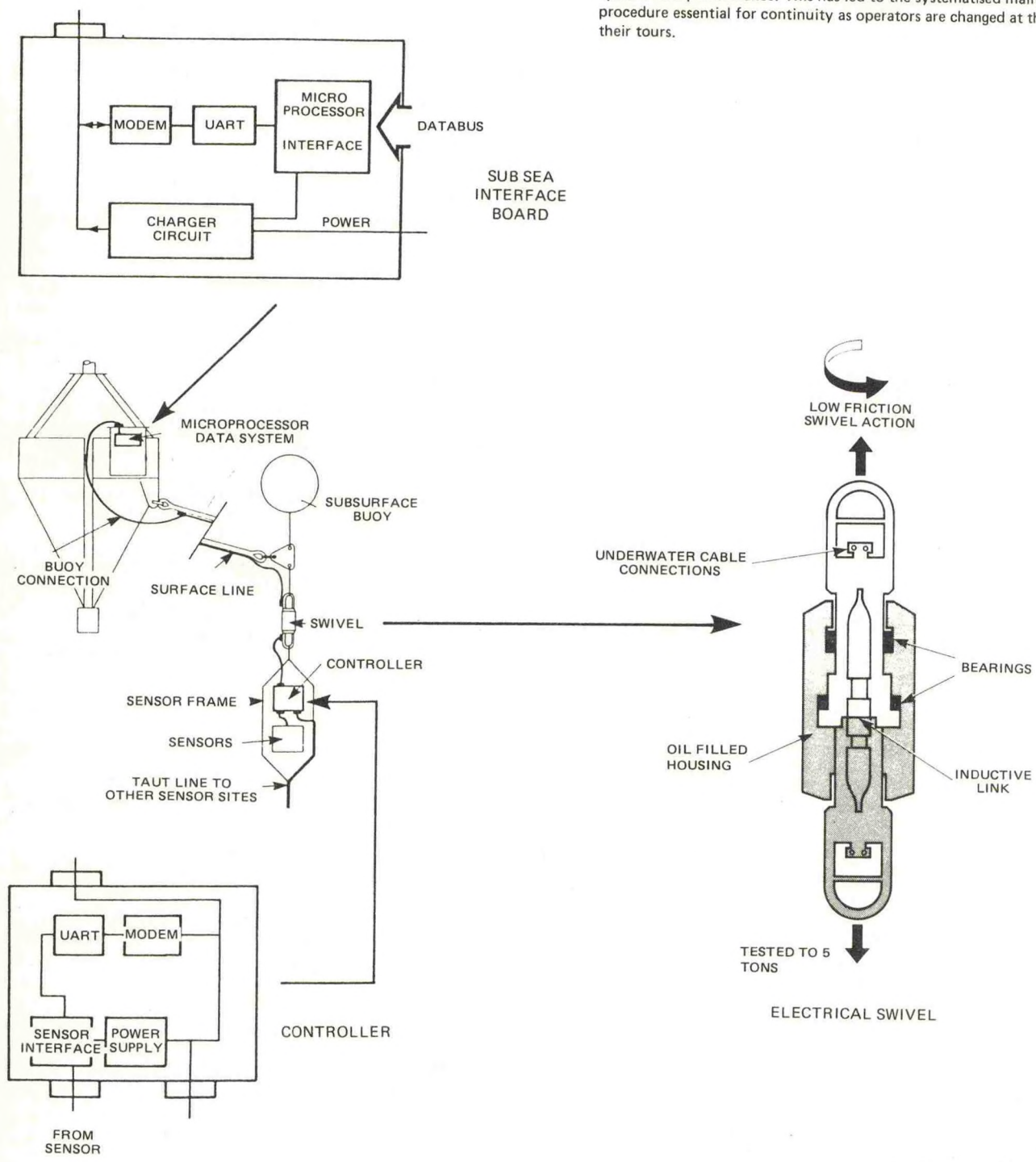


Figure 8 — sub sea communication system

The data is of interest to many sectors of the clients workforce ashore, and the shore station has repeaters at various points as well as archiving data on magnetic tape.



#### 4. Kuwait and Egypt

These two buoy systems are similar in that they measure wind, wave current and tide and display the results onshore in real time.

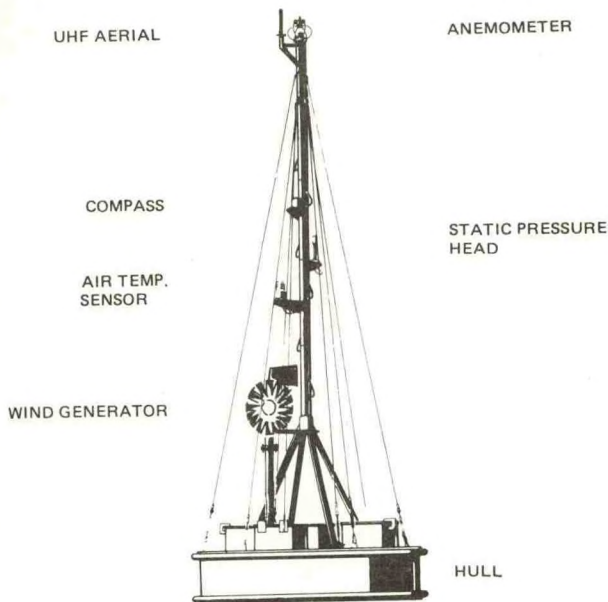


Figure 9 — buoy with wind generator

The data transmission is UHF (line of sight) from a jetty and an SBM respectively and their purpose is solely to control offshore tanker movements. Currents in each case are unpredictable and if operational results warrant it, a study will be carried out on ways of achieving uninterrupted tanker loadings.

In this example the order of events is reversed — operational results may lead to environmental studies.

#### 5. North Sea — Hutton TLP deployment

This buoy measures wind, wave spectra, surface current, and presents results in real time.

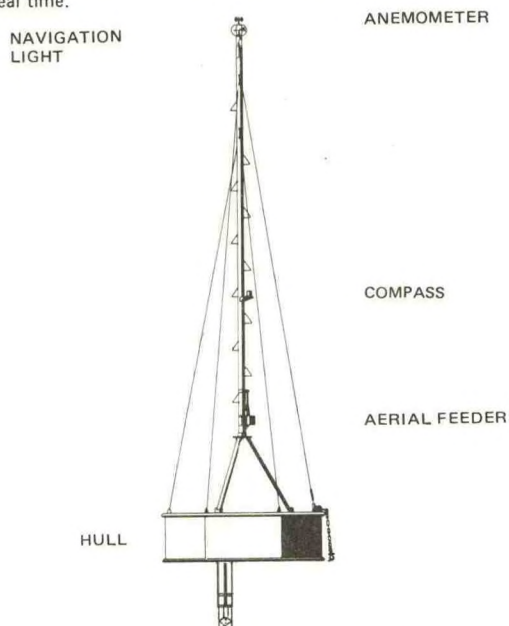


Figure 10 — buoy with surface current meter

It will be used during the mating and tow-out phases of the platform, solely for checking on prevailing conditions. Each phase has designated go/no go conditions for wave and current and update time must be as fast as possible so that trends can be resolved and related to the time constants of the hull and deck manoeuvres.

A logging option is provided for a second phase, where the buoy stays alongside the deployed platform to provide environmental data to correlate with platform motion values.

However the emphasis in the specification is on rapid computation of spectra to allow the fastest possible update of displayed data.

#### Conclusions

The applications described above range from solely long term logging of raw data for design purposes to solely short term displays of processed data, with rapid update, for controlling time — critical operations.

If there is a single common factor throughout, it is reliability. A buoy of this size and capability cannot really be classed as disposable in that a site cannot be sown with a number of buoys in order to ensure results from at least one.

The cost of even a straightforward boat charter to repair a buoy will probably exceed the cost of hardware replaced and will have adverse effects on the credibility of the databuoy as a long-term device.

Processing requirements have to suit oceanographers, marine engineers and structural engineers and must follow advances in computational techniques in these fields. This means that a greater, not a lesser, processing load will probably be presented to the buoy operator in the future.

A further aspect is that instant availability of data is nearly always desirable, whether for reasons of system checking or for consumption by the user — another case for powerful on-board processor.

Instant availability of data allows it to be used as a direct (or a monitored) input to time dependent processes like platform monitoring.

Databuoys will always be able to utilise those advances in electronics primarily slated for other technologies. Oceanographers and engineers can only benefit from seeing and using the data thus made available to them.



# AIR-SEA HEAT AND MOMENTUM FLUXES FROM MOORED BUOYS

Richard E. Payne and Richard T. Nowak

Woods Hole Oceanographic Institution, Woods Hole MA 02543

A new instrument package for deployment on moored buoys is described which was designed to record, and transmit via satellite, the parameters required for estimating air-sea momentum and heat fluxes. An analysis of the errors inherent in the derived fluxes is given.

$Q_S$  can be measured directly,  $\alpha$  can be estimated from  $Q_S$  and sun altitude and declination (Payne, 1972). It is difficult to measure  $Q_B$  from a ship and probably next to impossible from a buoy. Fortunately, in the tropics, where SEQUAL is located, the long wave radiation flux is fairly small and uniform. We will have to rely on indirect estimates for this term.

Momentum flux, or wind stress, and sensible and latent heat fluxes can be estimated by means of the bulk aerodynamic formulae:

$$\tau = \rho_a C_D U^2$$

$$Q_E = a_{E E} C_{E E} (g_o - g) U$$

$$Q_H = a_{H p} C_{H p} (T_o - T) U$$

## 1. INTRODUCTION

Several experiments recently proposed require estimates of the fluxes of momentum and heat between the atmosphere and the sea surface over broad areas of the ocean and over long periods of time. At present, the only feasible way to do this is to record observations of appropriate parameters from buoys. We report on a sensor and data recording and transmission package which was developed for deployment on moored toroidal surface buoys in the Seasonal Equatorial Atlantic (SEQUAL) experiment.

## 2. MOMENTUM AND HEAT FLUXES

The net heat flux across the sea surface is given by:

$$Q = Q_S (1 - \alpha) - Q_B - Q_E - Q_H$$

where  $Q$  is the short wave solar radiation flux,  $\alpha$  is the albedo,  $Q_B$  is the long wave radiation exchange,  $Q_E$  is the latent heat flux and  $Q_H$  is the sensible heat flux.

where the symbols have the usual meanings. Recent investigations of the drag and exchange coefficients have improved our ability to estimate these quantities taking into account atmospheric stability and variations in wind velocity (see, for example, Large and Pond, 1982, Byrne, 1982).

A sufficient number of measurable physical parameters which will allow us to estimate all but long wave radiation is solar radiation, wind speed and direction, air temperature, and temperature, relative humidity, and barometric pressure. Part of our development work has been to identify and test a set of commercially available sensors which will measure these parameters with sufficient accuracy and be robust enough to withstand the rigors of 6 month mid ocean deployments.

## 3. SENSORS AND SENSOR ACCURACY

Solar radiation is measured with an Eppley differential thermopile pyranometer. Basic sensor accuracy is 3% but buoy motion and salt particles on the glass envelope probably degrade this to 5-10%. We have not found either effect to be particularly serious in a few previous deployments.

Wind speed and direction are measured with an R. M. Young Model 5102 integral propeller-vane



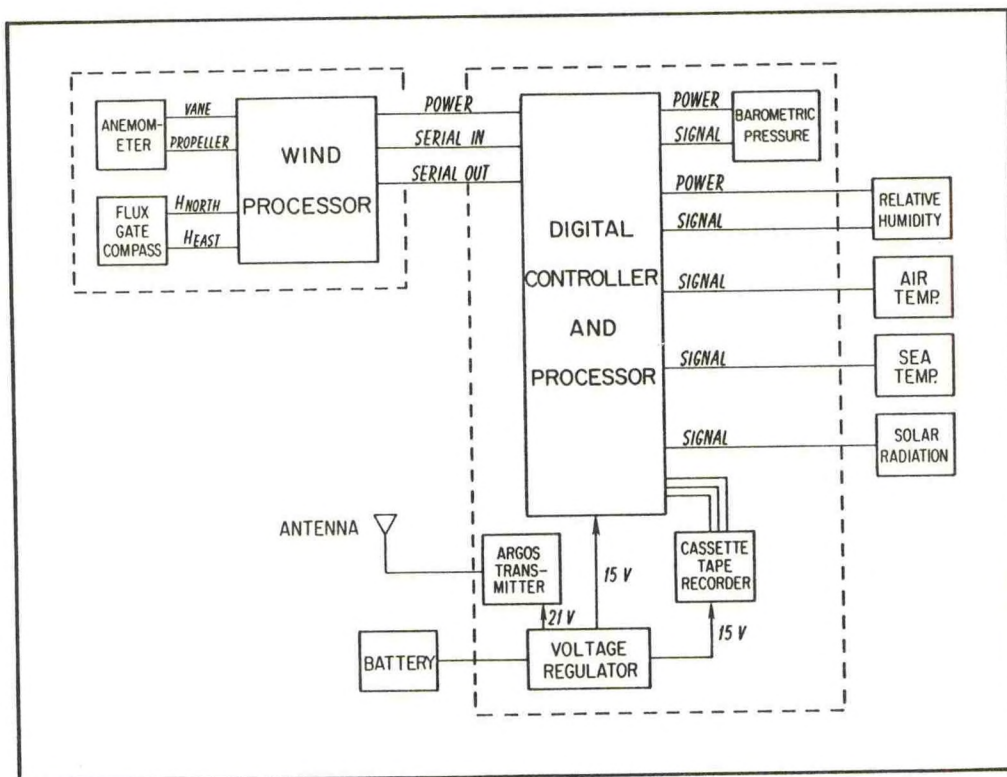


Figure 1. Block diagram of meteorological recorder

anemometer and instrument orientation with a flux gate compass. The molded plastic helicoidal propeller has a distance constant of 3.3 m and the vane has delay distance 1.3 m and damping ratio 0.27 making this a reasonably sensitive combination. A four month deployment off the California coast last summer showed it to be reasonably rugged and reliable. Past experience has shown us that it is essential to vector average the wind at high frequency to avoid aliasing by the buoy motion (Weller *et al.*, 1983). This is accomplished by a microprocessor located with the anemometer and compass. The wind processor appears in Figure 1. The digital electronics will be described later in this paper. Accuracy of the vector averaged wind speed is probably better than 3%.

Air and sea temperatures are both measured with thermistors potted in Delrin tubes. In addition, the air temperature thermistor is housed in a radiation shield to protect it from solar radiation. The first deployment used a W.H.O.I.-built version of a shield designed by Prof. G. C. Gill of the University of Michigan. Later deployments will probably use another version of the same design built by R. M. Young Co. The shield will keep solar heating of the air temperature thermistor to no more than 0.1°C under most conditions. Uncertainty in the sea temperature measurement is about 0.05°C.

The Väisälä Humicap Model 14U sensor is used for measuring relative humidity. Through laboratory calibrations we have found that repeatability and stability over 6 months is at least as good as  $\pm 2\%$  RH. The sensor is enclosed in a sintered brass filter with 37 $\mu$  pore size to prevent salt particles from reaching it. Later this year we will attack the problem of preventing salt buildup on this shield.

For barometric pressure measurements we are using the Paroscientific Digiquartz Model 215-AS-002 transducer together with an omnidirectional port designed by G. C. Gill to minimize the dynamic effects of the wind. At trade wind speeds the port limits dynamic effects to a few tenths of a millibar.

#### 4. DIGITAL ELECTRONICS

At about the time we began the design of the digital electronics, a new set of microprocessor boards became available which were based on the NSC-800 microprocessor chip, a low power version of the Z-80 with the full Z-80 instruction set. The board manufacturer, Onset Computer Corporation, also implemented a new bus which features the capability of putting each of the boards into a sleeper mode in which they consume much less power. The combination of this ability and the high speed of the NSC-800, 2 MHz,



leads to an average power consumption close to what it would be with an RCA 1802, our original choice. The advantage is the rich and flexible instruction set.

Of the boards produced by the Onset Computer Corporation, we are using: The CPU-800 containing the NSC-800 CPU, 1K of RAM, 22 I/O lines, an EPROM, and a voltage regulator; the ADC-32, a 32 channel A to D converter; The ACR-10, a combination UART and math board; The MOR-800 containing a real-time clock and a 4 channel A to D converter; and Onset's motherboard and breadboards.

Figure 1 is a block diagram of the system. The propeller-vane anemometer, compass, and wind processor are mounted as a single unit. Once per propeller revolution (30 cm of air) the wind processor reads the compass and vane, computes an east and north component and adds it to the east and north component sums in memory. Meanwhile the digital controller and processor is sampling and averaging inputs from the other sensors. Once per recording interval, typically 15 minutes, the controller sends the averages to the Sea Data digital tape recorder. In addition, once per hour it sends hourly averages to the ARGOS transmitter (Polar Research Laboratory ADAP 901) which transmits that set of values every 60 seconds for the following hour. Timing of both microprocessors is set by the controller.

We have made a major commitment to these instrument packages. The two already set on SEQUAL moorings will be replaced in August for the second six month deployment; one will be set on a LOTUS (Long Term Upper Ocean Study) mooring just before this meeting; we have proposed to set three more on moorings in the equatorial Pacific in October as part of the Tropic Heat experiment.

#### 5. HEAT AND MOMENTUM FLUX ACCURACY

Accuracies of heat and momentum fluxes vary with measurement conditions but we can estimate them for typical tropical oceanic conditions.

With an uncertainty of 10% in drag coefficient and 3% in wind speed, momentum flux can be estimated to about 12%.

Albedo is small, 6-10% during most of the day and 6% averaged over the whole day, and it can be estimated quite accurately. Uncertainty in the shortwave radiation absorbed by the ocean, then, is that of the solar radiation measurement, 5-10%. Daily absorbed radiation totals on the equator are, then about  $5800 \pm 460 \text{ W hr m}^{-2}$ .

Sensible heat flux over the tropical Atlantic averages about  $240 \text{ W hr m}^{-2}$  per day. With 10% uncertainty in exchange coefficient, average air-sea temperature difference  $1.0 \pm 0.1^\circ\text{C}$ , and average wind speed  $4.0 \pm 0.1 \text{ m s}^{-1}$ , the daily total sensible heat flux is  $240 \pm 40 \text{ W hr m}^{-2}$ .

Mean latent heat flux is about  $2160 \text{ W hr m}^{-2}$  per day. With uncertainties of  $0.1^\circ\text{C}$

in air temperature,  $0.05$  in sea temperature, and 3% in relative humidity (the largest contributor) in addition to the uncertainties in exchange coefficient and wind speed, the mean daily latent heat flux is about  $2160 \pm 325 \text{ W hr m}^{-2}$ .

Long wave radiation balance within two degrees latitude of the equator is about  $960 \pm 240 \text{ W hr m}^{-2}$  per day.

The components of heat flux into the ocean, then, are:

Short wave solar radiation	$5810 \pm 460 \text{ W hr m}^{-2}$
Long wave radiation flux	$-960 \pm 240$
Latent heat flux	$-2160 \pm 330$
Sensible heat flux	$-240 \pm 40$

These uncertainties are good enough for some investigations but in order to improve heat balance estimates in the tropics we should work on improving measurements of solar radiation, although these measurements may be better than our somewhat pessimistic assessment, and relative humidity, or some other measure of atmospheric water content. For the latter we must wait for the invention of a new sensor, preferably one which measures bulk properties of the air.

#### 6. ACKNOWLEDGMENTS

The work described here was funded by a National Science Foundation grant OCE 8 22061.

#### 7. BIBLIOGRAPHY

- Byrne, H. M., 1982: The variation of the drag coefficient in the marine surface layer due to temporal and spatial variations of the surface wind and sea state. Ph.D. dissertation, University of Washington.
- Large, W. B., and S. Pond, 1982: Sensible and latent heat flux measurements over the ocean. *J. Phys. Ocean.*, **12**, 464-482.
- Payne, R. E., 1972: Albedo of the sea surface. *J. Atmos. Sci.*, 959-970.
- Weller, R., R. E. Payne, W. G. Large, and W. Zenk, 1983: Wind measurements from an array of oceanographic moorings during JASIN 1978. *J. Geophys. Res.*, submitted.



# The LOTUS Discus Mooring

Peter R. Clay

WOODS HOLE OCEANOGRAPHIC INSTITUTION  
Woods Hole, Massachusetts 02543

## ABSTRACT

The Woods Hole Oceanographic Institution has been involved in a Long Term Upper Ocean Study (LOTUS) for the past three years. The goal of the project is to obtain a continuous two year record of atmospheric data combined with current and temperature measurements in the upper water column. An engineering test stage of two years preceded the experiment during which time much was learned and incorporated in later operational moorings. Two of four moorings in the experiment were heavily instrumented. This paper discusses the initial surface mooring design, subsequent changes and finally some of the engineering data obtained.

## 1.0 INTRODUCTION

The Long Term Upper Ocean Study (LOTUS) is an experiment at the Woods Hole Oceanographic Institution designed to acquire a continuous set of current and temperature data in the upper water column over a two year period. This data acquisition began in May 1982 with the deployment of four moorings instrumented with current meters, thermistor chains and engineering instrumentation. A two year engineering test stage preceded the May 1982 deployment. In the test stage two surface moorings were set sequentially, LOTUS 1 and LOTUS 2, in order to better evaluate the feasibility of the experiment. Table 1 summarizes the type and time of the LOTUS surface moorings deployed to date.

LOTUS MOORING NO.	TYPE OF MOORING	DEPLOYMENT DATE	RECOVERY DATE	REMARKS
LOTUS 1	1st Engineering	May '80	Aug. '80 Sept. '81	Parted after 120 days on station
LOTUS 2	2nd Engineering	May '81	Sept. '81	Fully recovered after 120 days on station
LOTUS 3	1st Scientific	May '82	Oct. '82	Fully recovered after 171 days on station
LOTUS 4	2nd Scientific	Oct. '82	Mar. '83 Apr. '83	Parted after 108 days on station

TABLE 1

### Summary of LOTUS Surface Mooring Deployments

This paper summarizes the initial design characteristics of the surface mooring, traces its evolution to the present design, and discusses problem

areas encountered and subsequent solutions.

## 2.0 LOTUS 1

The LOTUS site is 34° North and 70° West in the North Atlantic approximately 300 miles (556 km) East of Cape Hatteras. Water depth is 5368 meters and the bottom is relatively flat. Proximity to the Gulf Stream and its meanders is remote, although Gulf Stream cold eddy activity has been noted.

The first LOTUS surface buoy, LOTUS 1, used a proven mooring design developed in the 1960's at the Woods Hole Oceanographic Institution<sup>1,2</sup>. Figure 1 shows the initial engineering version of the mooring. A 12' (3.7 m) aluminum discus buoy, with a three part rigid bridle, provided the buoyancy for a string of instruments which included a current meter, tensiometers, thermistors and other engineering instruments which were connected by either chain or torque balanced wire rope. Below the instrumentation, wire rope extended down to the lower limit of the fishbite zone (2000 meters). Plaited eight strand nylon connected the rest of the mooring to the backup recovery system made of thirty-five 17" (43 cm) glass balls attached to a length of chain some 30 meters off the bottom<sup>3</sup>. A large clump and Danforth anchor provided holding power for most current conditions.

One design objective was to maintain a small watch circle even in the presence of a Gulf Stream cold eddy. Assumed design current profiles are shown in Figure 2. The geometry of the mooring and the resulting stresses along the line were computer predicted<sup>4</sup>. Scope and mooring components were adjusted until satisfactory results were obtained. Scope has been traditionally defined as the total unstretched mooring line length divided by the depth. Including the effects of anchor launch which stretches the mooring line before anchor impact yields a more realistic definition of scope. Permanent elongation due to the anchor launch transient has been measured to be as much as 12% in 3/4" (1.9 cm) nylon. As designed LOTUS 1 had a scope of .93 using the traditional definition whereas, in fact, its stretched length after anchor bottoming was approximately equal to the water depth.

After approximately four months, the LOTUS 1 mooring parted resulting in the loss of the discus buoy. Upon arrival at the mooring site, it was



determined acoustically that both the top instrument cluster and backup recovery system did not provide sufficient buoyancy to bring the mooring to the surface. Instead, the flotation ascended to a depth of 1500 meters and remained there. Dragging operations over three separate attempts finally retrieved the mooring in pieces. Similar recovery operations are described in Refs. 5 and 6.

After recovery the failure point was found to be the master link at the termination below the VMCM as shown in Figure 1. One glass ball was missing from the back-up recovery system and one instrument case had imploded when the instrument cluster settled to the bottom. The marginal reserve buoyancy due to added weight and reduced buoyancy resulted in a very limp mooring. A computer simulation study<sup>7</sup> showed complete loss of reserve buoyancy with a barotropic current of 20 cm/sec. The limp subsurface mooring bows downward laying more line on the bottom as the current increases.

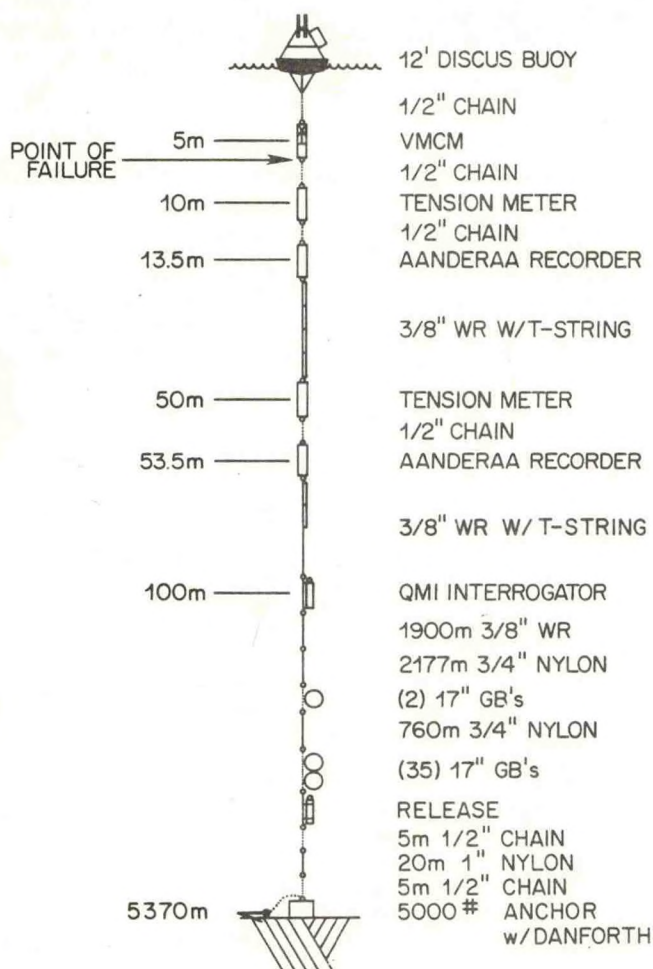


Figure 1 LOTUS 1 Engineering Discus Mooring

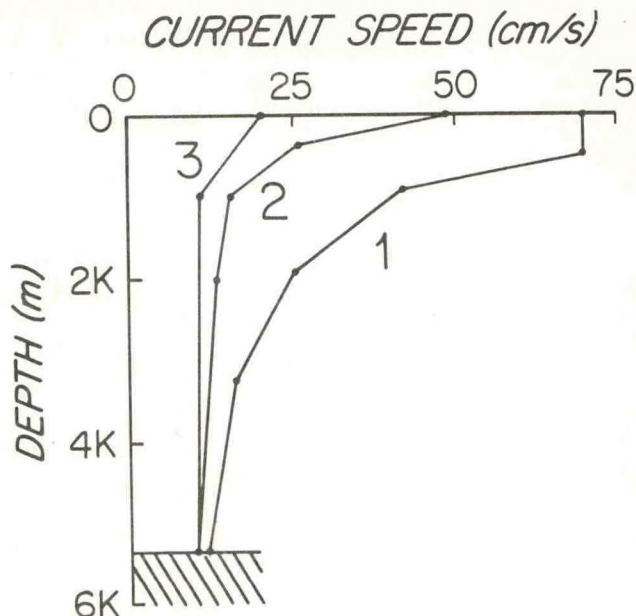


Figure 2 Design Current Profiles

As Figure 3 shows, the vertical component of tension decreases from 80# to zero at 20 cm/sec current at which time the mooring meets the bottom at an angle of 90° from the vertical. In other words as long as a current of 20 cm/sec existed, the mooring would not come to the surface.

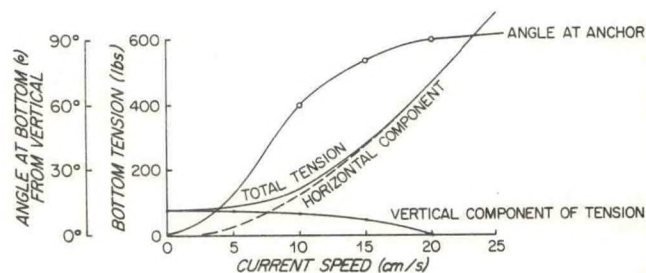


Figure 3 Back-up Recovery Computer Study

The LOTUS 1 mooring parted because a ½ inch (1.3 cm) galvanized master link failed. These links are made of an alloy steel which were proof tested and then galvanized. The probable cause of failure was identified by metallurgical analysis to be liquid metal embrittlement. This type of failure was due to the link being hot dipped galvanized after being stressed during the proof test operation. We have since replaced these alloy links with plain carbon steel galvanized pear links for all mooring applications.



### 3.0 LOTUS 2

After the loss of the LOTUS 1 surface buoy, a new buoy was designed and built, Figure 4. The changes resulted in a smaller, but stronger, 10' (3 m) hull which could be more readily deployed from the small OCEANUS class research vessels. Six watertight compartments surrounding an internal instrument well were pressure tested prior to filling with two pound density closed cell polyurethane foam. The bulkheads separating the hull compartment, being structural components, also served as attachment points for both lifting bales and the rigid bridle legs, thus distributing the loads evenly over various components of the hull.

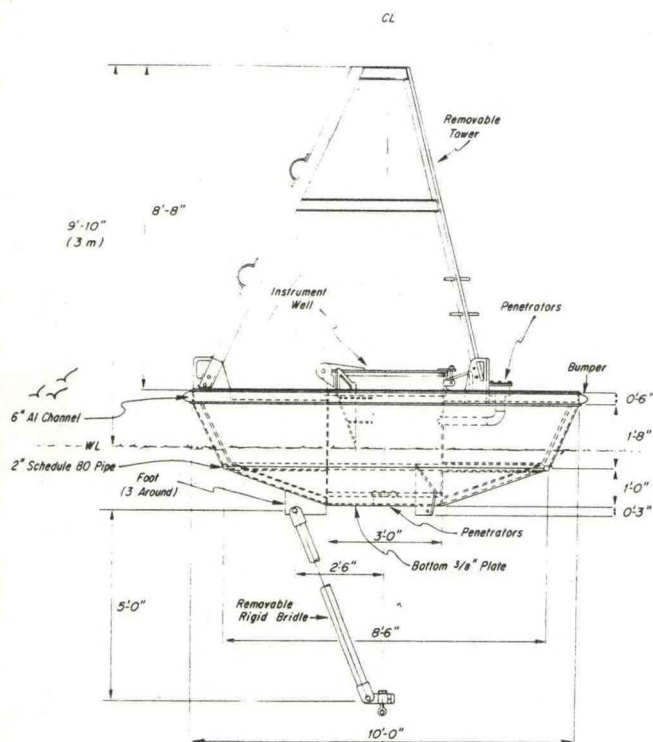


Figure 4 10 ft. Discus Buoy

The bridle attachment points were situated to provide a good base upon which the buoy could rest when stored without its bridle. Buoy tilt when lifting from the pick-up bale was designed so that the lifting line would clear the tower and its delicate instruments. Figure 5 depicts the buoy going over the ship's rail with the mooring line attached to the rigid bridle.

The rigid bridle has been in use for some time on Woods Hole's surface buoys. It provides a strong righting moment when combined with a heavy weight below. The heavy weight is made up of 2000# (906 kg) of instrumentation, chain, and wire rope.

A steel spider at the lower end of the bridle contains a telemetering tensiometer and the mooring

line connection. Chafe and wear at this connection have always been a problem on surface moorings. Shackles in bales tend to wear rapidly at the attachment point. A steel universal joint was designed to transfer this motion smoothly and reduce wear. Delrin bushings were used to isolate the stainless steel tensiometer connection from the universal joint. The shackle connection at the other end of the universal joint was rotated 90° to provide true universal action.

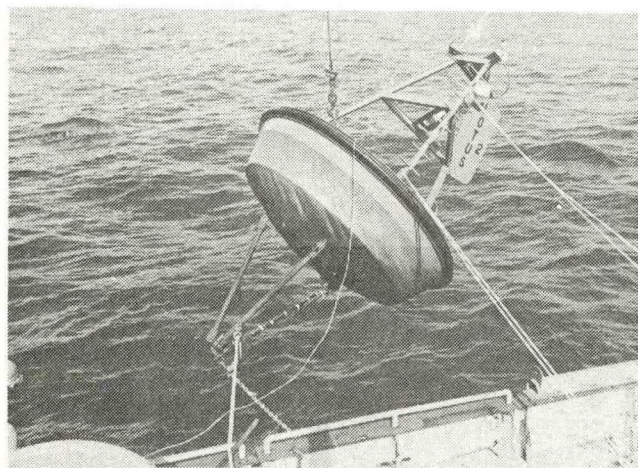


Figure 5 10 ft. Discus Buoy Deployment

In addition to a stronger buoy and a better connection, the mooring was further refined to accommodate the increased weight and drag introduced by additional instrumentation (Figure 6). In order to reduce the load on the buoy the lower 1650 meters of 3/8" (1 cm) wire rope previously used was replaced with 5/16" (.8 cm). Table 2 describes some of the important mooring parameters as computer calculated both with and without currents. Maximum buoy tension of 3960# (1794 kg) occurs with profile #1 with an associated horizontal excursion of 3448 meters. With no current this tension is reduced to its minimum of 2009# (911 kg). High horizontal holding power is intentionally not designed into the mooring anchor system - no Danforth or flukes are used. Under strong current situations, this allows the anchor to drag rather than to increase the tension and cause the buoy to submerge. Using a coefficient of friction of .5 for a clump anchor system, calculations show the anchor to begin dragging at a current profile slightly less than profile #1. Corresponding tension at the anchor is 4700# (2131 kg) at an inclination of 17° from the vertical with a horizontal component (drag) of 1400# (634 kg), and a vertical component of 4500# (2038 kg). The 7000# (3171 kg) anchor resists the vertical component, but the horizontal component just exceeds its holding power, so dragging may occur.

Upon recovery of LOTUS 2 tests were performed on the 3/4" (2 cm) nylon extending from 2000 meters to the bottom. It was found that degradation of up to 20% in the upper shots had occurred, presumably due to over two million tension cycles



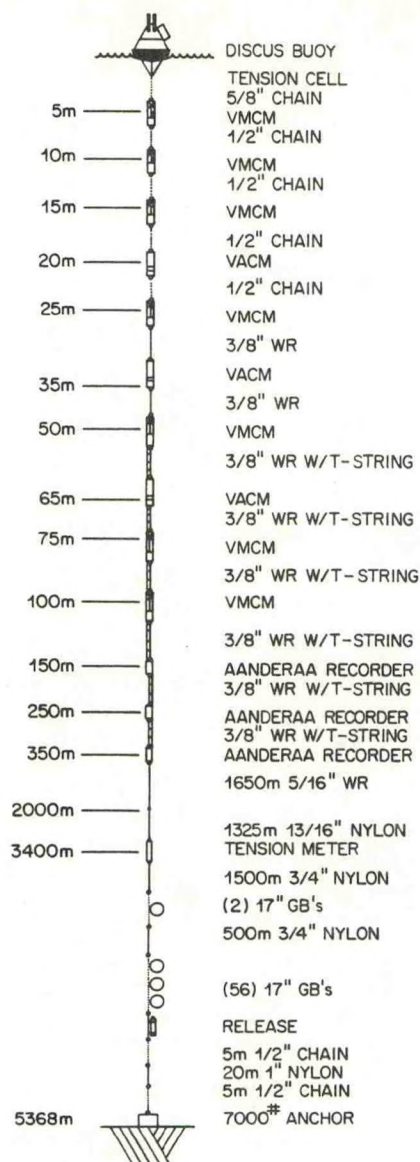


Figure 6 Typical Scientific Mooring

in six months. Figure 7 shows the decrease in degradation with depth or length along the nylon. Tensiometers placed along the mooring line have showed that large dynamic loads are transferred along the wire rope sections with very little attenuation. It is the nylon that takes the abuse absorbing the shock resulting from wave excitation. The figure shows that the upper 1000 meters of nylon experiences the most loss of strength. Beginning with LOTUS 3, the top section of 3/4" (2 cm) nylon was replaced with a 1000 meter shot of 13/16" (2.1 cm) nylon to reduce the amount of degradation. Post-recovery tests on the 13/16" (2.1 cm) nylon have shown no significant degradation implying that the larger diameter stronger rope is not influenced adversely by the transmitted dynamics.

Beginning with LOTUS 2 satellite telemetry via the ARGOS system was added to the buoys. Data tele-

LOCATION AND CHARACTERISTIC	ZERO CURRENT	CURRENT PROFILE NUMBER		
		3	2	1
BUOY TENSION	2009# (911 kg)	2148# (974 kg)	2278# (1033 kg)	3960# (1796 kg)
BUOY EXCURSION	0	1881 m	2454 m	3448 m
WIRE TENSION	976# (443 kg)	1115# (506 kg)	1246# (565 kg)	2936# (1331 kg)
NYLON TENSION	278# (127 kg)	414# (189 kg)	560# (255 kg)	2305# (1045 kg)
ANCHOR TENSION	3000# (1361 kg)	3074# (1394 kg)	3183# (1444 kg)	4728# (2145 kg)
DRAG AT ANCHOR	0	164# (74 kg)	257# (117 kg)	1374# (632 kg)

Table 2 Computer Design Characteristics

metered included tension, position, sea and air temperature, barometric pressure, wind speed and direction, battery voltage and water level in the buoy well. Since LOTUS 2 this data has been received daily by telephone and compared to expected performance. At the end of the month a listing is obtained with all data points received during that month. On an average, about ten satellite passes occur daily with a maximum of ten separate transmissions per pass.

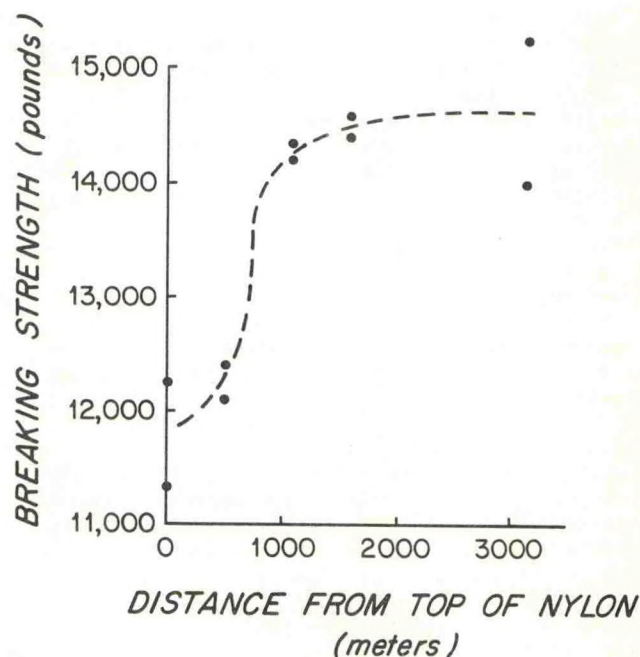


Figure 7 Nylon Degradation

Figure 8 shows the telemetered buoy positions for LOTUS 2 as calculated by the ARGOS tracking system. The buoy moves around its anchor position within an average maximum watch circle of 5 km. The smaller motions are due to system errors ( $\pm 1$  km), tidal effects and inertial oscillations. Large-scale motion is fairly slow with complete watch-



circle rotation taking as long as a month or more to complete.

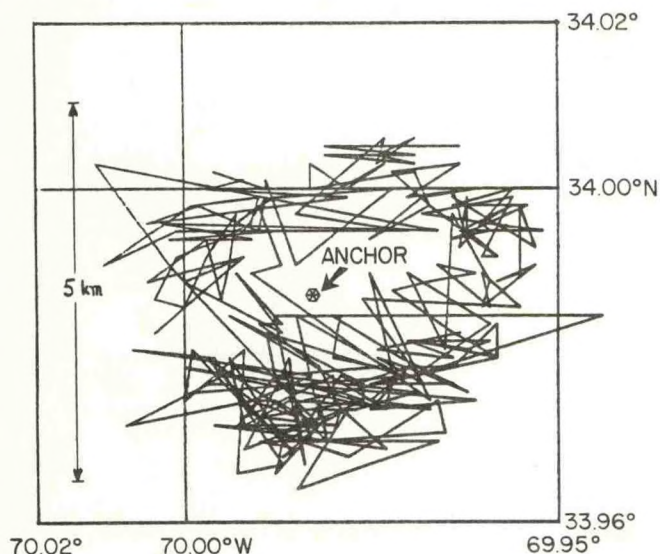


Figure 8 LOTUS 2 Telemetered Buoy Positions

#### 4.0 LOTUS 3

LOTUS 3 was deployed in May 1982, and remained on station for the intended six months. It was the first of four projected scientific deployments. Figure 6 shows the mooring schematic. Very few design changes were incorporated in this mooring except for the greater number of instruments in the upper water column. Ten current meters were placed within the top 100 meters with the majority being vector measuring current meters (VMCM's). Three 100 meter thermistor chains with recorders at the lower ends extended from 50 meters to 350 meters. Upon recovery in October 1982 very little chafe or degradation was found anywhere in the mooring system. The isolation/universal link worked well as did the larger 13/16" (2.1 cm) nylon in the top 1000 meters of synthetics.

Mooring performance, although not yet confirmed with complete current data agrees well with the computer design simulation. Complete current information to the bottom will become available in April 1983 when the three subsurface moorings set at the LOTUS site are recovered.

From the data obtained to date, however, much has still been learned. Maximum tensions experienced occur during anchor launch with values reaching 5500# (2495 kg) at the buoy. Portions of two tension records made at 10 and 3400 meters depth are shown in Figure 9. The data shows a peak tension at launch of about 5000 pounds (2495 kg) at the upper instrument and 3400# (1542 kg) at the deeper instrument. The energy absorption effect of the nylon is evident in the deeper record which shows the attenuation of tension variations due to waves.

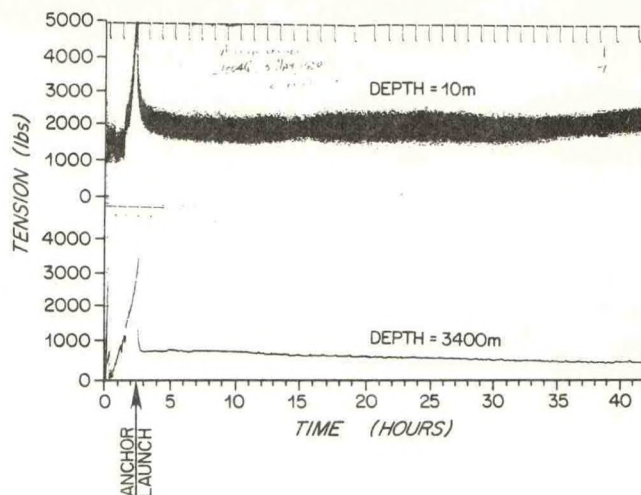


Figure 9 Tensiometer Records (10 m and 3400 m)

Figure 10 shows the top (5 m) current meter speed over a 20 day period during which a cold eddy passage was experienced on June 4, 1982. An eyeball average shows a general increase in speed over the preceding week with a likewise increase in diurnal amplitudes. The second curve is the tension at the buoy as telemetered and the bottom curve the tension at a tensiometer at 3400 meters depth. The increase in tension with the approaching eddy is evidenced by all curves as is the double hump during its passage. The decrease in amplitude variations with depth is again evidenced in these curves. Fluctuations of plus and minus 1000# (454 kg) are typical about the mean tension anywhere along the wire rope section of the mooring. The bottom tension curve follows the same shape as the upper curve's mean with an offset of about 1200 pounds at lower activity levels and 2000 pounds at times of maximum tensions.

#### 5.0 LOTUS 4

The second scientific mooring, LOTUS 4, was deployed in October 1982 with an intended duration of six months. Tracking both LOTUS 3 and LOTUS 4 buoys showed motions similar to LOTUS 2 with daily horizontal motions of approximately 300 meters and a maximum deflection of 2.5 kilometers. Telemetered tension and position data on LOTUS 4 compares favorably with previous results implying that repetition in design has been achieved.

LOTUS 4 went adrift on February 22, 1983, and began drifting to the west-southwest at an average speed of about .25 knots. Daily tracking by satellite permitted its eventual recovery by the R/V KNORR on March 9, 1983. Average tension at the buoy of 1500 pounds indicated that failure must have occurred in the 5/16" wire rope section. This large tension applied on the rigid bridle kept the buoy upright, thus allowing tracking to continue and making recovery feasible.



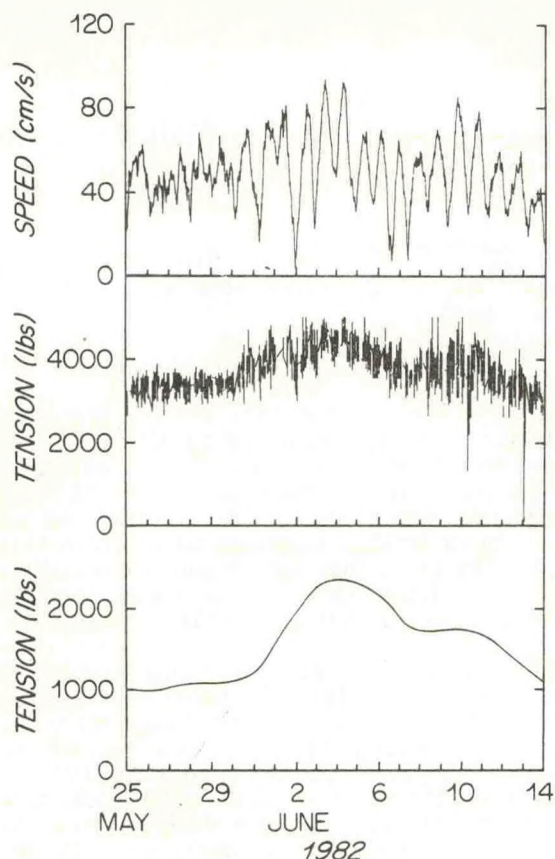


Figure 10 Current and Tension Records

#### 6.0 CONCLUSIONS

The LOTUS discus mooring has gone through numerous design changes since the initial setting in 1980. With the failure of LOTUS 1 and its subsequent recovery by dragging, it was determined that back-up recovery should provide buoyancy for imploded instrument cases as well as failure up to the bridle. A significant excess buoyancy (400# (181 kg) in this case) is required to permit recovery using reserve buoyancy in currents over about 40 cm/sec. Master links which are galvanized after stressing can fail as the LOTUS 1 recovery and other tests proved. These links were replaced with pear links which are not susceptible to liquid metal embrittlement. The design of a universal joint eliminated the wear problem at the buoy-to-mooring connection. A stronger, but smaller discus buoy was designed, built, and tested in six month deployments at sea with good results. Degradation, in the high energy synthetic section resulted in the replacement of the top 1000 meters of nylon with a larger size which takes the abuse without loss in strength. Computer design calculations agreed with data obtained<sup>7</sup> and will be further evaluated upon obtaining complete current information in May 1983.

Satellite telemetry was beneficial in that mooring tensions and positions were monitored daily and compared with expected maximums and minimums. Telemetry also helped in the recovery of LOTUS 4 which went adrift and would have been lost

otherwise. Complete instrument string recovery was possible including the failed mooring component which proved to be the 5/16" wire rope.

#### ACKNOWLEDGEMENTS

The author wishes to thank Robert Walden and Henri Berteaux for their assistance in preparing the manuscript. Also, thanks are due to the Woods Hole Oceanographic Institution Graphic Arts Department, and the secretarial services of Charlotte Muzzey.

This work was funded by the Office of Naval Research under Contract N00014-76-C-0197; NR 083-400.

This paper is Woods Hole Oceanographic Institution Contribution No. 5354..

#### REFERENCES

1. R. G. Walden and N. N. Panicker, "Performance Analysis of Woods Hole Taut Moorings", Woods Hole Oceanographic Institution No. 73-31, June 1973.
2. R. H. Heinmiller and R. G. Walden, "Details of Woods Hole Moorings", Woods Hole Oceanographic Institution No. 73-71, October 1973.
3. H. O. Berteaux and R. H. Heinmiller, Jr., "Back-Up Recovery of Deep Sea Moorings", Marine Technology Society Journal, Vol. 7, No. 3, pp. 16-20, May-June 1973.
4. H. O. Berteaux, and N. K. Chhabra, "Computer Programs for the Static Analysis of Single Point Moored Surface and Subsurface Buoy Systems", Woods Hole Oceanographic Institution No. 73-22, March 1973.
5. R. H. Heinmiller and D. A. Moller, "Failure of a Moored Array in a Gulf-Stream Eddy", Marine Technology Society Journal, Vol. 8, No. 8, pp. 35-38, August 1974.
6. M. A. Paige, P. J. Heuser, L. A. Lindquist, C. R. Mayoral and J. H. Selleck, "A Surface Recovery Technique for Deep Moored Vertical Arrays", Naval Oceanographic Office, No. TR-278, August 1981.
7. D. A. Moller, "A Computer Program for the Design and Static Analysis of Single-Point Subsurface Mooring Systems: NOYFB", Woods Hole Oceanographic Institution No. 76-59, June 1976.
8. R. P. Trask, M. G. Briscoe and N. J. Pennington, "Long Term Upper Ocean Study (LOTUS), A Summary of the Historical Data and Engineering Test Data", Woods Hole Oceanographic Institution No. 82-53, December 1982.



## DRIFTERS: A LAGRANGIAN BUOY DEVELOPMENT PROGRAM

by

Robert Heinmiller  
Omnet, Inc.  
70 Tonawanda Street  
Boston, MA 02124

James McWilliams  
National Center for Atmospheric Research  
P.O. Box 3000  
Boulder, CO 80303

### ABSTRACT

DRIFTERS is a cooperative engineering and scientific program to advance the technology and understanding of measurement systems on drifting buoys to meet the needs of scientific programs planned for the latter half of the 1980's.

The program includes the development in parallel of two measurement systems, an inexpensive, near-surface Lagrangian drifter and a heat content and surface flux drifter. Each of these has a number of components. These systems will, insofar as possible, be inexpensive, long-lived, expendable, modular in their measurement capabilities, aircraft deployable, and capable of communicating their data and location through satellites.

### 1. INTRODUCTION

DRIFTERS is a cooperative engineering and scientific program to advance the technology and understanding of measurement systems on drifting buoys. There is a demonstrable scientific need for improvements upon existing systems, if we are to be able to carry out some of the ambitious experiments on ocean circulation and ocean-atmosphere interaction being planned for the latter part of this decade.

The program is funded by the National Oceanic and Atmospheric Administration (NOAA), the National Aeronautics and Space Administration (NASA), and the Office of Naval Research (ONR).

A number of scientific and engineering activities are taking place explicitly within the DRIFTERS program. In addition, DRIFTERS expects to draw on many efforts taking place outside of the immediate group.

### 2. THE SCIENTIFIC NEED

A number of experiments are in the planning stages for the next decade aimed at determining

the state of the upper ocean, its low frequency variability, and its relationship with heat and momentum fluxes between the ocean and atmosphere. While remote sensing techniques from space can reasonably be expected to contribute in several important ways during this period it is clear that many important variables will remain inaccessible from space, and an affordable in situ capability will be needed.

Traditional uses of drifting buoys in oceanography have largely been confined to making estimates of horizontal currents. However, data interpretations have, of necessity, been imprecise, due to lack of reliable calibrations. There is the further physical complication of large vertical shear in even low-frequency currents near the surface. The horizontal complexity of currents is also great, both near the surface and at depth.

Thus, a sequence of regional deployments of large numbers of well-calibrated Lagrangian drifters which resolve currents at different depths near the surface should lead to important advances in our understanding of the general circulation of the oceans, both on the mesoscale and larger. Depth resolution will be obtained by a combination of surface drifters, drogued drifters, Doppler current profilers, and SOFAR floats. The existence of several Lagrangian buoy systems, each aimed at a different set of parameters or part of the water column, will allow the design of customized experiments, each using a different mix of the available technology.

A less traditional use of drifting buoys can be illustrated by an experiment planned for the second half of the decade: a study of the tropical Pacific upper ocean heat, mass, and momentum budgets and the Southern Oscillation.

The tropical Pacific is, more than anywhere else, the site of energetic, large-scale, low-frequency (e.g., seasonal and interannual) variability with large correlations between ocean and atmosphere, related to potentially predictable climate variations around the globe. Because of the remoteness of this area, the tropical and south Pacific phenomena are not well described. In this context, buoy systems can provide valuable measurements of four types: ocean circulation, ocean heat, air-sea fluxes,



and atmospheric surface circulation. Reliable, inexpensive, unattended systems are needed, which would form the nucleus of an ocean observing system.

Ocean circulation measurements from drifting buoys have their greatest potential value in the possibilities they offer for the resolution of the four dimensionally complex structure of the South Pacific and Equatorial current system. They can be deployed in large numbers by relatively inexpensive means in remote locations such as these, either from ships-of-opportunity or from aircraft. Near surface measurements are needed to observe the wind-driven boundary layer mass transports, and, particularly away from the Equator, deeper measurements are needed for the geostrophic gyre and mesoscale eddy currents. For the latter, SOFAR floats using an acoustic relay system are probably the most appropriate technique. Drifters provide not only local current measurements but also by their trajectories a direct indication of particle transport and diffusion if the drifter Lagrangian characteristics are sufficiently good.

### 3. THE DEVELOPMENT PROGRAM

Working within the context of the scientific plans outlined above, DRIFTERS will concentrate primarily on the development of two measurement systems, an inexpensive, near-surface Lagrangian drifter and a heat content and surface flux drifter. Each of these has a number of components, as enumerated below. These systems will, insofar as possible, be inexpensive, long-lived, expendable, modular in their measurement capabilities, aircraft deployable, and capable of communicating their data and location through satellites. The scientific components of the program will guide the measurement objectives of the systems, collaborate in the calibration and interpretation of the measurements, and plan the experiments in which these systems will be used.

Other related efforts being carried out by DRIFTERS participants include: evaluation of historical drift buoy data; development of a depth-cycling submerged general circulation drifter; the development of a wave-zone drifter; and computer modelling of the upper ocean.

Organizationally, DRIFTERS is composed of a steering group of engineers and scientists. The participation of a group of committed scientists is crucial to the success of the program. This group is involved in the development effort: in the evaluation (or re-evaluation) of the user specifications (for sensors, data handling subsystems, buoy platforms, and the overall buoy systems); in field testing of prototypes; in the evaluation of buoy performance and data; and in the identification of new areas where

development is desirable.

The engineering efforts take place in individual projects at several institutions, but with enough overall coordination to provide communication and cross-fertilization between areas.

### 4. THE LOW-COST DRIFTER (LCD)

Work being carried out by a group led by John Dahlen at the Charles Stark Draper Laboratories will use existing surface drifting buoys as starting points toward the eventual goal of a less expensive, smaller, more accurately Lagrangian, and better calibrated system. Future scientific experiments may comprise as many as several hundred such buoys. In these quantities the cost of both the buoy and the deployment are important factors in the feasibility of the experiments. Reducing these costs will involve the use of less expensive transmitter/locators, solar power, and smaller, lighter hulls and simplified drogues for air deployment.

In addition, it is scientifically necessary for the Lagrangian drifter to be well calibrated in its water following characteristics. Indeed, much of the engineering effort will focus on the trade-off between, on the one hand, an approach to "perfect" Lagrangian behavior and, on the other hand, a clear understanding of the degree and nature of the departures from such behavior in varying oceanic conditions. Miniaturization of the surface elements, symmetrization of the drag elements, and mechanical decoupling of the connecting elements are means of reducing spurious motions due to wind and wave driving or due to ocean current shear. A first, and probably continuing, step in this development is agreement between the engineers and scientists as to the meaning of near-surface current measurements in various contexts.

It is assumed that, for the majority of the experiments envisioned, location fixing is only necessary at intervals of a week or more. This may permit the use of a simple, low profile antenna, leading in turn to a smaller float with less freeboard. The antenna will actually be awash much of the time, providing location data only at random intervals. Obviously, the achievable data rates must be carefully evaluated as a function of sea state.

Experience indicates that (depending on how the scientific problem is defined) a simple rope drogue can be just as effective as more elaborate "point" drogues, such as parachutes or "window shades". In addition to being easy to model and understand, such a drogue offers operational simplicity and ruggedness.



The LCD is expected to make use of a lower-cost satellite transponder currently under development at the Goddard Space Flight Center.

Based on these ideas, present design configurations for the LCD include a small (approximately 50 centimeter diameter) ellipsoidal plastic float, low profile antenna (possibly a printed circuit on the inside upper surface of the float), solar power, and rope drogue with no more than a stabilization weight on the end. Sensors for additional quantities such as ocean surface temperature will be included as options if they do not compromise the primary objective.

Such a buoy might be packaged for shipping and deployment in a tube 0.5 meter in diameter and a meter long. The container can be designed to dissolve or break away in the water. The packaged buoy might be deployed from aircraft with a minimal drag chute to slow it down. The per-buoy cost of the LCD will be somewhat dependent on the cost of the transponder. We anticipate a total cost sufficiently low to allow deployment in large quantities in general circulation experiments.

#### 5. HEAT CONTENT AND SURFACE FLUX DRIFTER (FLUX)

The heat content and surface flux drifter (the Flux Buoy) is under development by a group led by Dr. William Large, at the National Center for Atmospheric Research. This buoy system is to be a highly modular one to allow a wide variety of configurations in different scientific uses. It is based upon a general purpose sensor line and a data logger/processor. The modular sensors of the system will include ocean thermistors, current meters, pressure sensors, hydrophones, and sensors for atmospheric pressure, wind speed and direction, temperature, humidity, and perhaps solar short-wave radiation. The passive current following characteristic of this buoy system are of secondary concern. We expect that the development of this buoy system will take advantage of several parallel development efforts: the Relays system, the self-contained Doppler log, and meteorological sensor developments.

Relays is a drifting system which, in addition to collecting measurements of its own, will relay SOFAR float signals to a shore station via satellite. The system is being developed by a group headed by Dr. Robert Chase at Woods Hole Oceanographic Institution. (A report on the Relays system is being given by others at this Symposium.) Two components of the Relays system are a central data logger/processor and a general purpose sensor cable. The processor is expected to have the flexibility to collect, process, and telemeter a wide variety of information, including data from sensors on the cable and acoustic data from the SOFAR floats. We anticipate that the processor and cable developed for Relays will be easily adaptable to

the Flux Buoy. Several of the participants in Relays are members of DRIFTERS, which will insure transferability at the appropriate time.

A self-contained Doppler log is also under development, under the guidance of Dr. Russ Davis at Scripps Institution of Oceanography. Mounted on a drifting buoy or its cable, such a log will give a detailed profile of relative flow. This makes possible the calibration of the Lagrangian performance of the drifter as part of its engineering evaluation, as well as an operational measurement capability.

Development and testing of a suitable collection of sensors is underway. Some sensors are under development outside the context of the group, and we will stay in close touch with these efforts. Meteorological sensors for temperature, humidity, pressure, radiation, and wind stress will be evaluated and selected to meet the scientific goals of DRIFTERS.

Of particular interest is the measurement of wind stress and precipitation from subsurface ambient acoustic data. Since it is wind stress that is of inherent interest, rather than speed, this promising technique could eliminate the need for mechanical wind speed sensors, always one of the less reliable sensors in long-term deployments. Similarly, precipitation is a difficult measurement to make from a drifting buoy by conventional means.

Several scientific experiments planned by DRIFTERS scientists for the 1983-1986 period using existing buoy systems (the CASID/PRL buoys) will also be utilized for field testing of the Flux Buoy and its various subsystems.

By making the Flux buoy system modular (and therefore adaptable to a variety of experiments) and by going to the commercial sector (see Section 4), we expect that the result will be a less expensive measurement system than comparable existing air-sea interaction buoys.

#### 6. PROGRAMMATIC CONSIDERATIONS

Given the locations and size of the scientific experiments being contemplated (see below), deployment logistics and costs will be a major factor in the use of drifting buoy systems. The option of air deployment will be designed into each of the buoy systems under development. This option will not, of course, be exercised in all experiments. There have been several successful air deployment efforts in other contexts. The ADOMS system and the NDBO/PRL/Coast Guard effort are examples. We expect to adopt features of these systems, not to do new development in this area, except as needed to adapt to the specific buoy systems in which we are interested.



The same considerations, as well as the scientific sampling requirements, dictate that the buoys remain operational for as long as possible. We are aiming at minimum two-year lifetimes for each system.

If the tools which we propose to develop are to be utilized widely, the technology must be made available to the scientific community. For many forms of technology, elaborate support facilities are needed which individual scientists cannot be expected to provide. The DRIFTERS group will address the transfer of the technology both to the commercial sector and to some form of operational facility.

Oceanography does not have a good record in moving techniques and instruments into the commercial sector for marketing and further development. Specialized designs and the need for elaborate logistic support are among the reasons for this. Small potential markets and high overhead (both for the producer and for the customer) make many oceanographic measurement systems unattractive to the private sector.

We will address ourselves to this problem as part of the overall development effort. In particular, for the flux buoy, our objectives of flexibility, modularity, and broad scientific applicability, if achieved, should expand the potential market for a given buoy system. In the case of the Lagrangian buoy system, we anticipate that the development of a low cost system, capable of deployment in large enough numbers to meet the needs of anticipated experiments in the next decade, will similarly make such a buoy system attractive.

We further intend to plan for the transfer of the technology to be developed by DRIFTERS by investigating the possibility of an operational facility to which many scientists may come to have experiments carried out. We have no prejudice on the need for, the form of, or the site of such a facility. Thus we do not propose to establish one during the early stages of development, although a plan for meeting future operational requirements is needed within a few years.

We believe that some combination of commercial sector production of buoys and components, in combination with an established operational capability, can insure the availability of drifting measuring systems to the scientific community in the next decade and beyond.



# Free Drifting RELAYS Buoy Systems

R. G. Walden and H. O. Berteaux

WOODS HOLE OCEANOGRAPHIC INSTITUTION  
Woods Hole, Massachusetts 02543

## ABSTRACT

A description follows of a free drifting buoy system (RELAYS) capable of receiving acoustic signals from SOFAR floats and of measuring oceanic parameters from the surface down to the depth of the SOFAR sound channel (1100 m). Data acquired are processed on board the buoy and transmitted for distribution via the ARGOS system using two NOAA polar orbiting satellites. System analysis, component design, and system evaluation are presented with emphasis on the mechanical aspects of the system.

## 1. INTRODUCTION

Oceanographic measurements obtained from satellite instrumentation are two dimensional and limited to the ocean surface. To expand the utilization of satellite technology in support of oceanographic research, a NASA sponsored program was initiated in 1981 by the Woods Hole Oceanographic Institution. The principal objective of the RELAYS (Real-time Link and Acquisition Yare Systems) program is to acquire and relay through satellite linkage long term measurements of the interior ocean properties.

In its simplest form a RELAYS system consists of a surface buoy housing the data processing and satellite communication electronics and a long instrumented cable for gathering and transmitting data from various depths. Data acquisition can be made with the help of sensors mounted on the cable or through hydrophones receiving acoustic signals from remote sources.

Free drifting RELAYS buoys represent an expansion of the drifters used in the last decade<sup>1,2,3</sup>. They will permit a broader spectrum of measurements, made over a larger depth range. As an example, a network of free drifting RELAYS, instrumented to measure water temperature, pressure, and relative flow, can provide the temporal and three dimensional sampling needed for a better description and understanding of ocean meso and large scale dynamics. Another attractive possibility is to use free drifting RELAYS to receive acoustic signals from SOFAR floats. These floats, with a signaling range of up to 2500 kms, follow the ocean currents prevailing at their deployment depth<sup>4</sup>. A knowledge of their successive positions relative to the known position of two or more RELAYS can be

used to construct the float trajectories. These in turn can be used to describe deep oceanic circulation.

The first engineering prototype of a RELAYS free drifting system has been built and tested at sea. This paper reviews the system objectives, the analysis, the design, the fabrication and the evaluation of this prototype, placing emphasis on the mechanical aspects of the system. The electronic subsystem is described in a companion paper<sup>5</sup>. The paper concludes with a short review of future efforts.

## 2. PROTOTYPE SYSTEM OBJECTIVES

In its first phase, the objectives of the RELAYS program were to design, build, and test a free drifting buoy system capable of receiving acoustic signals from SOFAR floats and of measuring oceanic parameters from the surface down to the depth of the SOFAR sound channel (1100m). The data thus acquired was to be processed on board the buoy and transmitted for distribution via the ARGOS system using two NOAA polar orbiting satellites. Data and buoy position were to be received several times a day. The system had to survive open ocean conditions with a useful life of at least two years.

## 3. SYSTEM MECHANICAL ANALYSIS

The three different candidate systems considered for the application are depicted in Figure 1.

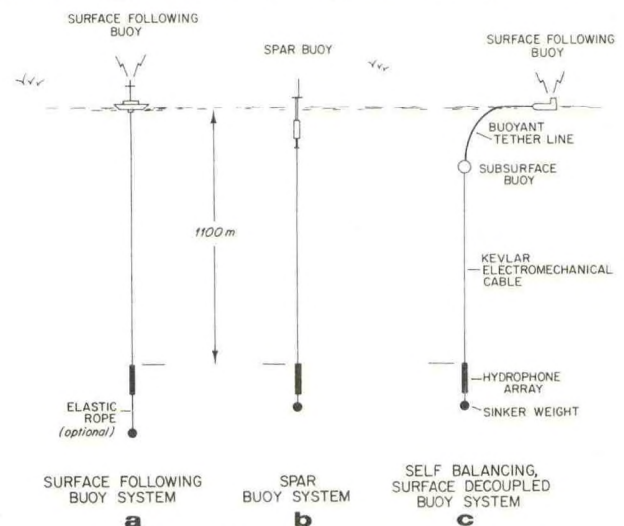


Figure 1 RELAYS Candidate Buoy Systems



In the first and simpler one the cable is directly attached to a surface following buoy. This is the approach followed in many drifters equipped with a short instrument line. As the cable length increases so do the chances for cable relaxation and snap loads. Furthermore excessive motion of the hydrophone array would also be a drawback. The second system uses a spar buoy to decouple the cable from surface excitation. Unfortunately most spar buoys, unless of large size and mass, rapidly become surface followers as wave period and amplitude increase<sup>6</sup>. This approach thus does not appear to be practical. In the third configuration a subsurface buoy, supporting most of the cable, hydrophone, and sinker weight, is connected to a surface following buoy with a length of buoyant cable. When properly ballasted, the sinker weight pulls the subsurface buoy away from surface wave activity, leaving approximately half of the buoyant cable on the surface. As waves pass by a certain amount of this floating cable is momentarily pulled under. Because of the small buoyancy provided per unit cable length, the forces acting on the submerged part of the system are small. As a result large waves produce only small cable tension fluctuations and small hydrophone displacements. The price to pay in this approach is increased system complexity.

The response to waves and currents of candidate configurations 1a and 1c was investigated with the help of computer models. This analysis provided the rationales for the selection of the RELAYS prototype configuration. It also provided useful quantitative information for the prototype design.

**Dynamic Analysis.** It is well known that cables hanging from heaving ships or buoys become slack if their upper end is forced to fall faster than their lower end can sink<sup>7</sup>. This temporary cable relaxation may permit kinks to form and snap loads to occur. These in turn would cause accelerated cable failure. Consequently, the prime purpose of the dynamic analysis was to develop and exercise simple computer models which would reveal the presence of slack conditions and could quantify the peak tensions resulting from any snap loading.

The first and simplest RELAYS buoy system to be analyzed consisted of a surface following buoy, a Kevlar electromechanical cable, the hydrophone array, and a sinker weight to hopefully keep the cable taut at all times. The length of the cable was 1100 meters, its diameter 0.45 inch (1.14 cm) and its strength 6000 lbs (2725 kg). Weight of sinkers considered ranged from 100 lbs (45 kg) to 2000 lbs (900 kg). Following the approach described in<sup>8</sup>, a single degree of freedom spring-mass system with nonlinear damping was used to model this buoy configuration. In this model the masses of the E/M cable, the hydrophone, and the sinker are lumped at the lower end of the cable. The upper end is forced to follow a prescribed sinusoidal vertical displacement. Two equations of motion are used to compute the ensuing displacement of the lumped mass. The first applies as long as the tension in the cable remains positive. When the cable becomes slack the "free flight" equation prevails. Using this model the response

of this first RELAYS configuration to waves with amplitudes ranging from three ft (1 m) to 40 ft (12 m) and periods ranging from 2.5 seconds to 40 seconds was investigated. Slack conditions followed by large snap loads were detected in most cases studied. These results clearly demonstrated the vulnerability of this configuration, the main problem being the stiffness of the Kevlar cable.

Inserting a length of elastic rope (nylon, natsyn rubber) between the hydrophone and the sinker weight could provide enough compliance to suppress cable slackness and reduce tension peaks. To assess the validity of this approach, this soft spring configuration was modeled as a two degrees of freedom spring-mass system. In this model the first mass lumps the cable and the hydrophone array, the second being the virtual mass of the sinker. The substantial longitudinal drag of the E/M cable is applied to the first mass. The model is depicted in Figure 2a. Here again the upper

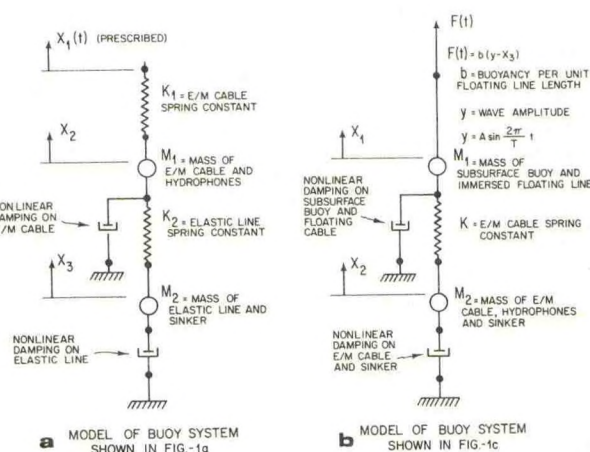


Figure 2 Math Models

end of the cable follows a prescribed sinusoidal vertical displacement. This model was exercised to investigate the response of some 40 combinations of compliant ropes and sinker weights to waves of 10 and 20 feet (3 and 6 m) amplitudes with periods ranging from 5 to 30 seconds. Only those systems with sinker weights in excess of 600 lbs (270 kg) were found to be free of slack conditions when acted on by 10 ft (3 m) waves. When doubling the amplitude of the waves, a minimum sinker weight of 1500 lbs (725 kg) was required to prevent cable relaxation. Hydrophone motion remained large in all cases. These results placed severe doubts on the practicality of using a surface following configuration for the RELAYS prototype.

Clearly the large displacement of the cable upper end had to be reduced to keep sinker weights and resulting tensions within reasonable and safe limits. The surface decoupled configuration depicted in Figure 1c was introduced for this purpose. This configuration was modeled with the two degrees of freedom system shown in Figure 2b. This model was exercised on a number of systems using several combinations of sinker weights and tether cable buoyancy. In all cases studied,



sinker displacements were but a small fraction of wave amplitude, typically a foot (0.3 m) or less for 10-20 ft (3-6 m) waves. Fluctuations of E/M cable tensions due to dynamic excitation were also found to be small, typically less than 10% of the static mean due to sinker immersed weight. Cable slack conditions could not be detected. This last configuration thus appeared very attractive, and was retained as the best candidate for further analysis.

**Static Analysis.** The effects of steady state currents on this self-balancing and surface decoupled configuration were studied next. Of concern was the possibility of shear currents producing a large catenary in the free hanging E/M cable. The hydrophone array could then be displaced upwards, perhaps way above its intended deployment depth. The subsurface buoy could also rise close to the surface and be subjected to wave action. Conversely large amounts of floating cable could be pulled under. The wave isolation mechanism that this buoyant cable provides would then be lost. To investigate these possibilities, the equilibrium geometry of representative buoy systems subjected to various current profiles was computer calculated. Effects that tether line buoyancy and sinker weight had on the depth of the subsurface buoy and the hydrophone array were systematically evaluated. Results from this sensitivity study revealed that current shear of the type shown in Figure 3 produces a depressor effect on the upper part of the

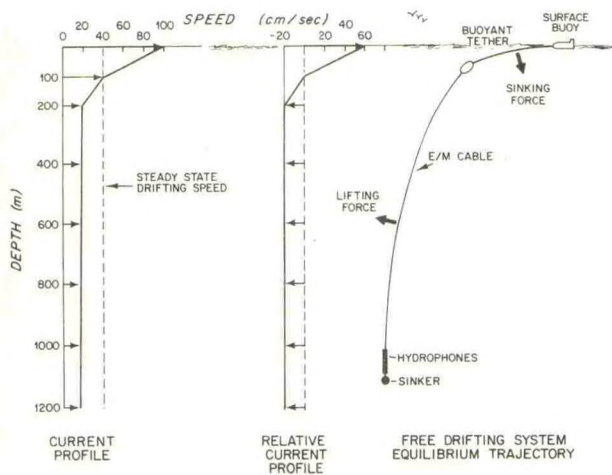


Figure 3 Free-Drifting System Trajectory

free hanging cable, whereas the lower part experiences lift forces. If the integrated depressor effect exceeds the total lift, then some of the line floating on the surface is pulled under to provide the additional buoyancy required. On the other hand, if the lift effect predominates then some of the floating cable is pushed back to the surface. The amount of line pushed back or pulled under depends on current shear intensity, buoyancy provided per unit of length of the floating line, and sinker weight. For example, it was found that a combination of high shear, light sinker and slightly buoyant line would force the float and the entire buoyant line to be on the surface.

Conversely a strongly buoyant cable combined with a heavy sinker would minimize the effects produced by strong shear currents. Of course these last features are undesirable from the dynamic point of view, large buoyancy leading to more wave excitation and heavy sinker weight translating into high cable tension.

#### 4. PROTOTYPE DESIGN AND DEVELOPMENT

To satisfy the objectives previously mentioned and implement the encouraging results obtained in the analysis just discussed, the RELAYS prototype configuration depicted in Figure 4 was devised.

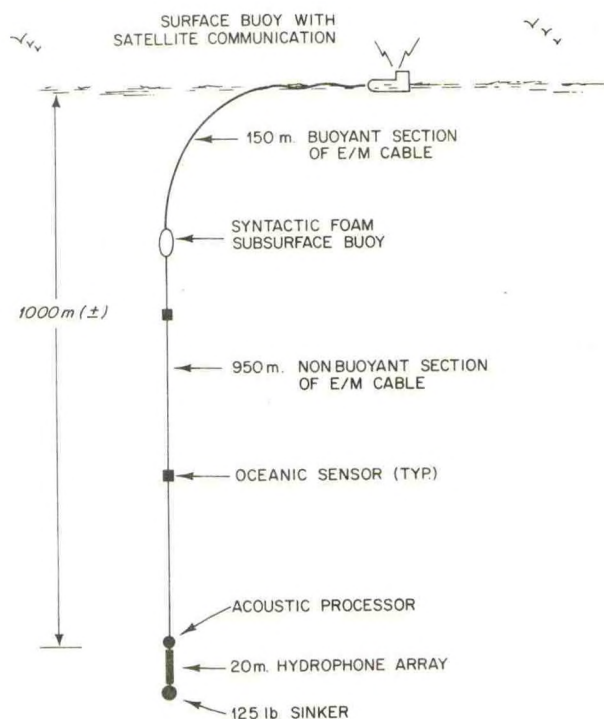


Figure 4 1st RELAYS System Configuration

This system uses a low profile surface buoy which contains the data processor, satellite communications equipment, and antenna with necessary batteries. The electromechanical (E/M) cable connecting the buoy to the hydrophone array is made of two parts, a buoyant section 150 m long at the top with the remaining 1000 m negatively buoyant. A discrete buoyancy element is placed at the end of the buoyant portion of the cable. Oceanographic sensors are inserted at discrete intervals along the cable length. The acoustic processor, hydrophone array and sinker are attached to the lower end of the E/M cable. The system buoyancy is adjusted so that approximately 75 m of buoyant cable floats on the surface. This configuration produces very small tension variations in the cable due to surface waves and small hydrophone wave induced displacements. The filtering and compliance introduced by the floating portion of the cable are responsible for this effect and additionally minimize the load variation on the



buoy. The buoy is shown in Figure 5.



Figure 5 RELAYS Buoy

### System Components

**Surface Buoy.** The surface buoy (Figure 6) is much like a floating log, tethered at its bow and heavily ballasted. This configuration provides a rugged, sea-kindly construction, presenting a small cross section area to waves yet having a reasonable righting moment. The hull is 2.5 meters long, one meter wide, and 0.6 meter high.

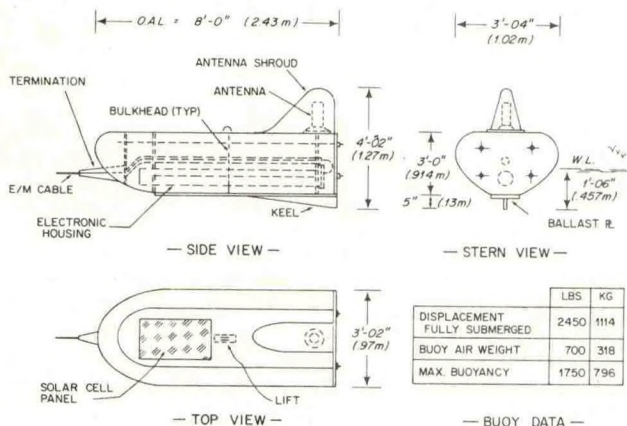


Figure 6 RELAYS Buoy Details

The buoy weighs 700 pounds (320 kg) with a water line approximately at mid-hull. It has a small keel to increase stability. The hull has four bulkheads held in place by four longitudinal rods. An instrument case (filament wound fiberglass) extends nearly the length of the hull above the keel. A PVC pipe runs from the bow tether point to the after bulkhead as a conduit for the E/M sensor cable which then feeds into the instrument case via a waterproof connector. Polyurethane foam with a density of 2 lbs/cu ft (0.3 gm/cc) fills all spaces between the bulkheads and forms the bow

shape. A fiberglass covering over the foam provides a strong rugged surface. The antenna is mounted aft on top of the buoy. Its fiberglass shroud helps the buoy to maintain orientation into the wind. Solar panels can be mounted on the float deck to supply charging current to the batteries.

**Cable.** Desirable features for the electro-mechanical cable connecting the surface buoy to the hydrophone array included: three electrical conductors, materials which would bond well to polyurethane, jacketing material to resist fish-bite, lightweight in water, 150 m of the total 1150 m to be positively buoyant, and adequate strength to account for cable degradation due to fatigue. The cable, shown in Figure 7, was jointly designed with Blake Wire and Cable Co., Torrance, CA.

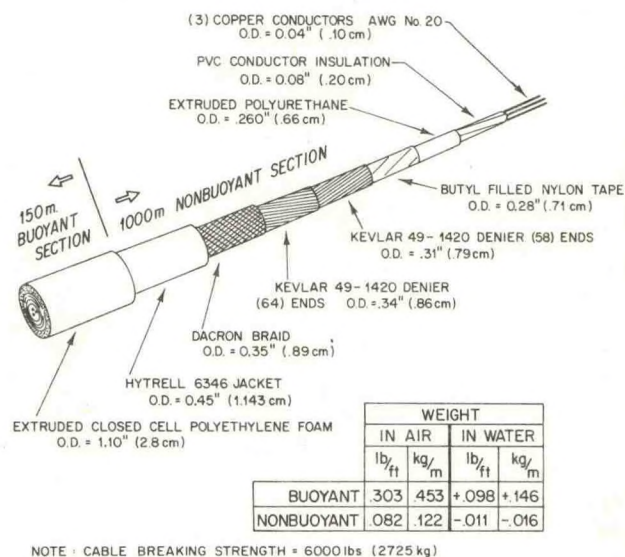


Figure 7 Cutaway of Electromechanical Cable

The conductors are made of number 20 AWG copper wires, insulated with PVC, and covered with polyurethane. This permits excellent bonding, both to the polyurethane and the PVC at terminations. The strength members are Kevlar 49 in two contra-helical layers. The jacket is extruded Hytrel 6346, a material which we have found to provide a fair amount of fishbite protection. The non-buoyant section of the cable (1000 m long) weighs .011 lbs/ft (.016 kg/m), in sea water. Its outside diameter is 0.45 in (1.143 cm). The remaining 150 m is foamed to an outside diameter of 1.1 inch (2.8 cm) with closed cellular polyethylene foam. This section has a buoyancy of .098 lb/ft (.145 kg/m). The cable has a rated breaking strength of 6000 lbs (2.700 kg).

**Cable/Buoy Termination.** The E/M cable attaches to the bow of the buoy by means of a special polyurethane boot. This point in the system undergoes continual flexing due to surface waves. Repeated flexural loading will cause failure of the Kevlar strands due to abrasion and



rupture of the copper conductors, particularly if the stresses are concentrated in a small area. RELAYS uses a tapered polyurethane boot to distribute the stresses due to bending over a large distance along the cable, and provides some additional compliance. The conical outside section is made of a low durometer (Shore A-70) polyurethane which flexes well and has excellent fatigue properties. A plug of higher durometer polyurethane (Shore D-80) is cast around the Kevlar fibers and the electrical conductors within the boot. This plug maintains the cable mechanical strength and provides a watertight electrical termination. The boot is depicted in Figure 8.

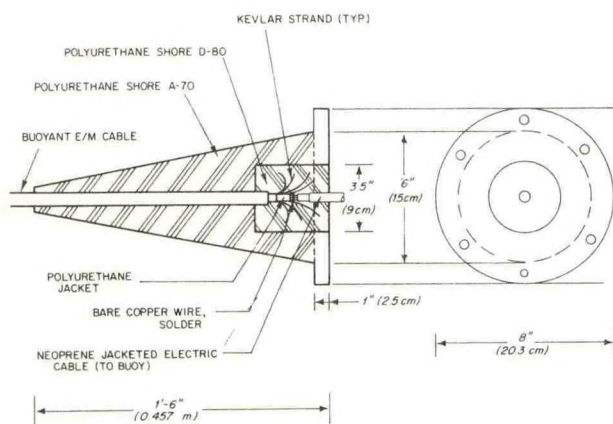


Figure 8 Tether Boot

**Cable/Sensor Terminations.** All sensors are attached in line to the E/M cable. Figure 9 shows details of a typical cable termination. The E/M cable is anchored within the stainless steel end piece with polyurethane (Shore D-80 durometer). A bond is achieved to the cable jacket, Kevlar fibers, conductor insulation and the stainless steel end piece. A boot of more flexible polyurethane (Shore A-70 durometer) is molded around the outside of the cable and end piece to reduce

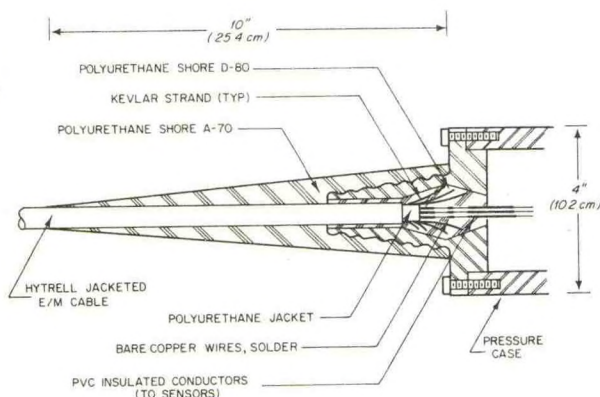


Figure 9 Typical Sensor-to-Cable Connection

bending stress in the cable. The conductors are water-blocked before entry into the pressure case.

**Subsurface Buoy.** The subsurface buoy attached at the lower end of the buoyant cable section provides 150 lbs (68 kg) of buoyancy. It is made of two halves bolted around the cable. Material is composite syntactic foam with a density of 20 lb/cu ft (.5 g/cc).

**Sinker.** A streamlined sinker with an immersed weight of 125 lb (57 kg) is attached to the lower end of the hydrophone array. The sinker pulls the cable taut and keeps the array nearly vertical in the presence of shear currents.

## 5.0 TEST AND EVALUATION

Components of the system were tested in the laboratory and off the dock preparatory to a sea test of the complete system. The termination designs were tested for strength and water-tight integrity at proof pressure. The cable weight and buoyancy was measured. Water absorption of the foamed cable was determined at design pressure. The hull was trimmed and ballasted in the water off the dock.

The system was tested at sea to:

- observe its sea-keeping characteristics
- observe amount of buoyant cable on the surface
- determine the hydrophone depth as a function of current shear to confirm the computer simulation
- measure the dynamic changes in tension at the hydrophone array and above the sinker weight
- test communications with the satellites.

The system was launched with little difficulty north of the Bahamas in 2000 meter water depth. A tension/pressure recorder was inserted between the hydrophone array and sinker weight to measure changes in tension due to surface excitation and changes in the depth of the array with current shear. The sinker end was deployed first from the vessel and the non-buoyant electromechanical cable payed out. The subsurface float was attached at the beginning of the buoyant cable and this cable then payed out. The buoy was placed in the water last.

The system appeared to come into equilibrium in about 30 minutes at which time 32 meters of buoyant cable were on the surface. The following day, presumably under different shear current conditions, 62 meters were on the surface. The buoy rode well in 8 to 12 ft (2.5 to 3.5 m) waves orienting itself into the wind and surface current.

A section of the tension/pressure record is shown in Figure 10. The pressure record shows the hydrophone array sinking to 1080 meters as the system settles out after deployment of the buoy. Inspection of the tension record shows large dynamic fluctuations during cable pay-out, ship motions being transmitted to the lower end of the



cable. A dramatic decrease in these fluctuations is evident when the buoy is put in the water and is no longer attached to the ship. Motions of the buoy due to surface waves likewise appear to be completely filtered and not present at the hydrophone array.

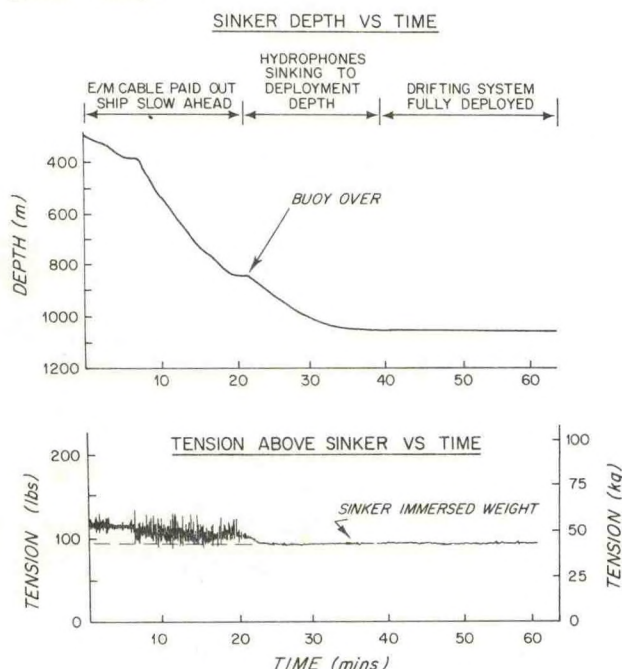


Figure 10 Tension/Depth Record

## 6.0 CONCLUSIONS

Conceptual RELAYS drifting buoy systems have been analyzed and a candidate design selected. The system chosen employs a rugged small surface buoy to which is attached a long sensor cable tethered to the bow with a short length floating on the surface. This approach reduces the dynamic loads on the buoy due to waves and also minimizes sensor motions. The complete system was tested at sea and observed for a period of 24 hours. The buoy rode well, pointing into the seas and wind. The hydrophone array at the bottom of the sensor cable remained stationary at 1080 meters with no observable motions from surface waves which were judged to be 8 to 12 ft (2.5 to 3m) in height. Excellent communications with the satellite were established in spite of considerable platform motion.

Two more systems are being prepared which will contain pressure/temperature sensors. These systems will be deployed in 1984 to permit a long-term evaluation. Eventually the buoy and cable will be packaged for air-drop deployments.

## ACKNOWLEDGEMENTS

The authors wish to thank Messrs. Peter Clay, Patrick O'Malley and Matthew Gould for their efforts as members of our RELAY team. We acknowledge the excellent support at sea provided by the officers and crew of the R/V CAPE FLORIDA. We appreciate the secretarial support provided by Mrs. C. Muzzey.

This development was supported by the National Aeronautics and Space Administration (NASA) through Grants NAGW-265 and NAG 5-281.

## REFERENCES

1. J. M. Hall and E. G. Kerut, "Development of a Meteorological and Oceanographic Drifting Buoy System", IEEE J. Oceanic Eng. OE-1: 56-69 (1975).
2. P. L. Richardson, R. E. Cheney and L. A. Mantini, "Tracking a Gulf Stream Ring with a Free Drifting Surface Buoy", Journal of Physical Oceanography 7:580-590 (1977).
3. G. R. Cresswell, "Satellite-Tracked Buoys in the Eastern Indian Ocean", Proceedings 14th International Symposium, Remote Sensing Environment, San Jose, Costa Rica, 1:531-535 (1980).
4. D. Webb, "SOFAR Buoys for Polymode", MTS Ocean's 77 Conference Record, Los Angeles, October 1977.
5. E. Mellinger and A. Bradley, "Integrated Communications in Buoy Systems", Proceedings MTS/NDBC 1983 Symposium on Buoy Technology, April 27-29, 1983.
6. D. Shields, "NCEL Ocean Platforms Seminar Technical Note", in preparation, NCEL Port Hueneme, CA, June 1983.
7. A. Driscoll, "Handbook of Oceanographic Winch, Wire and Cable Technology", (Chapter 7. H. O. Berteaux Equipment Lowering Mechanics). Graduate School of Oceanography, University of Rhode Island, Kingston, RI., (1982).
8. J. Goeller and P. Laura, "A Theoretical and Experimental Evaluation of Impact Loads in Stranded Steel Cables during Longitudinal Excitation", Department of Mechanical Engineering, Themis Program Report 70-2, Catholic University of America. (1970).

This paper is Woods Hole Oceanographic Institution Contribution No. 5353.



# DRIFTING BUOY DEVELOPMENTS AT THE FRENCH METEOROLOGICAL OFFICE

Pierre BLOUCH and François Xavier FUSEY

Direction de la Météorologie  
Etablissement d'Etudes et de Recherches Météorologiques  
CMM/MS Centre Oceanologique de Bretagne BP 337 29273 BREST CEDEX FRANCE

## ABSTRACT

The French Meteorological Services have been developing small drifting buoys for several years which transmit their data by satellite. We are here presenting a new type of buoy which in particular measures the wind in a simple and efficient way. Three of these buoys were tested during an experiment in the North-East Atlantic. They were accompanied by more simple buoys drogued at 1,000 meters. Some of the results of this experiment are presented and in particular an attempt to study the response of the drift of the buoys to the wind.

## 1. INTRODUCTION

The use of drifting buoys to increase the number of meteorological observations in certain remote areas, tends to be more and more used by the meteorological offices of certain countries including the french one. The measurements are useful firstly for improving the analysis of certain fields which are indispensable in producing accurate weather forecastings and secondly as "sea truth" for validating and parameterizing the calculation of algorithms of satellite measurements.

Besides the previous advantages, the use of drifting buoys equally allows studies of Ocean-Atmosphere interactions as in the correlation between the drifts of the buoys and the wind measured by them.

After the good results obtained by MARISONDE B's during the F.G.G.E. [1][2] measuring sea surface temperature and atmospheric pressure, the E.E.R.M. (\*) has developed new buoys called MARISONDE G's which in addition measure the force and the direction of the wind. These buoys, like their predecessors are not very expensive relatively (about \$ 15,000).

## 2. DESCRIPTION OF THE MARISONDE G

To evaluate wind direction, two possibilities were open to us. One consisted of equipping the buoy with a compass and a direction

anemometer; the other, of directing the buoy into the wind using a profiled mast. The first system, which on the one hand being more expensive because it requires a double-reading (compass and direction anemometer) and a sophisticated electronic integration, and on the other hand being more fragile, is used only on the moored buoys. The second system has been developed for the drifting buoys MARISONDE G's (fig.1).

The buoy's hull is composed of a fibre glass armoured polyester tube equipped with a biconical float encircled with an elastomere protective belt. The electronic circuits and the energy source are placed inside. The inferior part of the buoy hull is equipped with a roll damping disc.

The whole system is topped with a tail unit allowing the rotation of the buoy under the wind's influence. This tail unit includes an anemometer and an air intake for the air pressure sensor.

Overall length of the buoy : 4.20 m  
Diameter of the float : 0.54 m  
Total weight (ballast included) : 120 kg

Light and easy to handle, the buoy can be launched with ease without any technical preparation. The ballast, composed of a chain ensures a good vertical stability which is necessary for the transmission to the satellite.

Therefore the sensors aboard the buoy are :

- a temperature probe which consists of a copper resistance (sensitivity 10 ohms per °C, 2330 ohms at 0°C, resolution 0.1 °C) placed through a stainless steel pipe at thirty centimeters below the floating line.

- an air pressure sensor composed of an aneroid cap and located in the center of the buoy. This sensor which is one of the first marine instruments developed for the buoys has been shown itself very reliable during the F.G.G.E. experiment in 1978 (accuracy  $\pm 0.5$  mbar, resolution 0.1 mbar). The connection with the atmosphere is done through a standpipe by the air intake located at the top of the buoy.



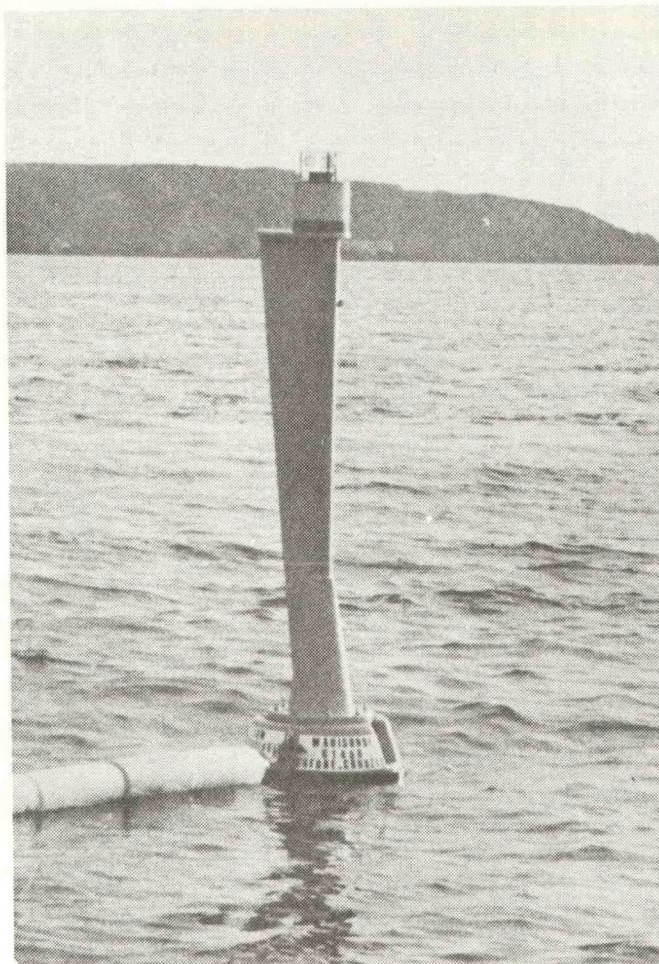
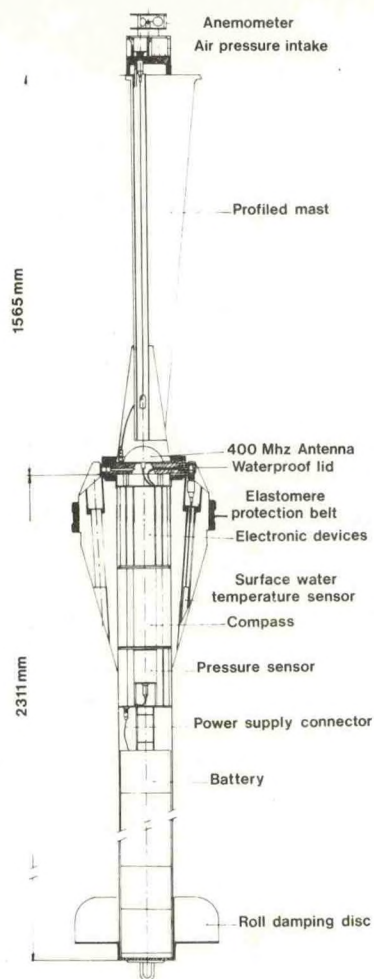


Fig. 1 MARISONDE G Sketch-plan and photo

- a cap anemometer designed at CERAM (\*). It gives a number of turns proportional to the wind speed.

- a compass of the flux-meter type which measures the magnetic field components relatively to the buoy.

The electronic unit, based on a microprocessor type computer, is designed to accept further equipments such as a bathythermic line. The atmospheric pressure is an average on 60 seconds and the electronic unit gives the tendency on three hours.

The measurement of wind in direction and speed is an average on 256 seconds. It must be noted that the wind direction is also mechanically filtered by the roll damping disc.

(\*) E.E.R.M. Etablissement d Etudes et de Recherches Météorologiques.

(\*) CERAM Centre de Recherches Atmosphériques de Magny-les-hameaux.

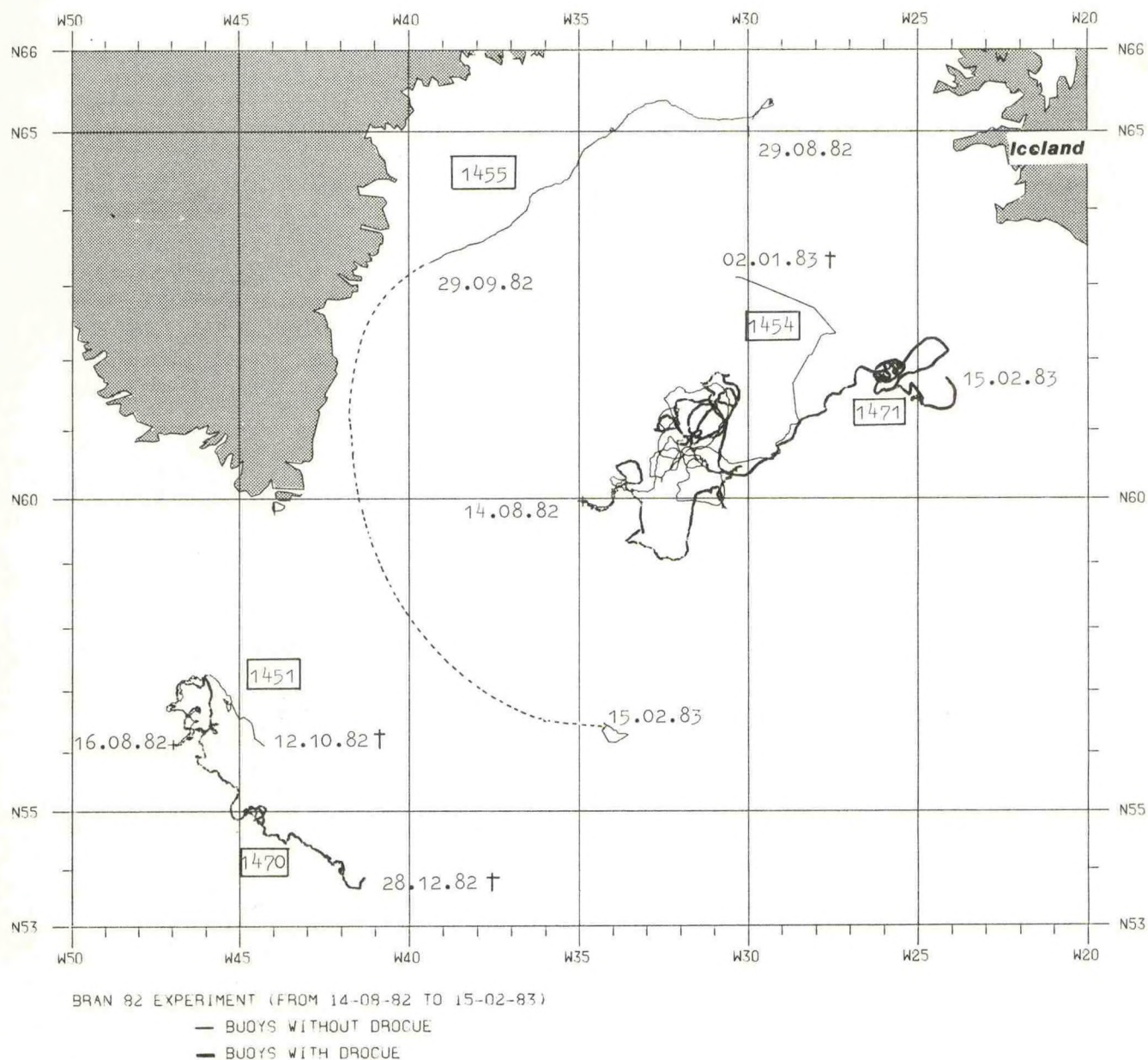
DIRECTION DE LA METEOROLOGIE - FRANCE

Tests in a wind tunnel, then at sea, have shown that the buoy was correctly directed under the wind's influence.

The rhythm of measurements may be programmed before the launching (every hour or at synoptic hours only). The data are collected and stored after digitalization by the circuitry set (CADOM) which finally sends all the information to the transmitter, including battery voltage data for technological checking in a condensed 64 bits message. The transmission which lasts 440 ms is repeated every 60 seconds. Data collection and location of the buoys are obtained through the ARGOS system.

The whole equipment is supplied with energy through lithium batteries of 60 Ah under 19.2 volts which allow three months autonomy at sea with a rhythm of acquisition of one measurement every three hours and one transmission every minute. The hull of the buoy can accept 6 batteries of this type which means the buoy can have a functional life of up to 18 months.





### 3. PRESENTATION OF BRAN 82 EXPERIMENT

This experiment was the first where MARISONDE G's were used. It followed on from BRAN 80 during which 4 MARISONDE B's were drifted eastwards from the 30th western meridian (launching between 50 and 58°N) [3] [4] [5].

The initial goal of this type of experiment is to show that the use of a network of buoys can increase the meteorological cover of the oceans without too high a cost. The region chosen for this experiment is in fact poor in observations but on the other hand interesting as far as "depression crossings". The launching of buoys (2 MARISONDE B's and 3 MARISONDE G's) was done thanks to the crews of two

Icelandic ships contacted by the Icelandic Meteorological Office, serving under COST 43.

The deployment was as follows:

65°N - 30°W	MARISONDE G 1455	(64523)
60°N - 35°W	MARISONDE G 1454	(64522)
	MARISONDE B 1471	(64521)
56°N - 47°W	MARISONDE G 1451	(62592)
	MARISONDE B 1470	(62591)

A network of buoys used for meteorological ends is more interesting if the buoys do not drift too quickly (risk of being wrecked on a coast). In the interest of studying the means of slowing down the drift of buoys, the MARISONDE B's were fitted with drogues at a depth of 1,000 meters. (fig. 2)



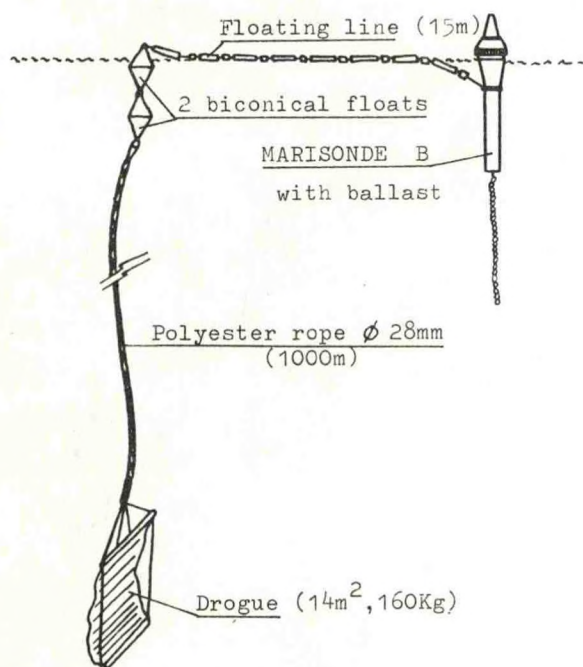


Fig. 2 MARISONDE B with its drogue at a depth of 1,000 meters.

The trajectories are shown on the map on the previous page. The MARISONDE G's carry out their measurements at synoptic hours, the MARISONDE B's every 15 minutes. During the experiment, the reception station for satellite data of LANNION, using the direct slow transmission of the ARGOS system, decodes the results and transmits them on the GTS in the form of a SHIP FM 13 message. The ARGOS department in TOULOUSE for its part, transmits the data of MARISONDE B's in the form of a DRIBU message after processing, that is to say 3 to 6 hours after the data has been received at LANNION.

Yet, the orbits of the satellite NOAA 6 and NOAA 7 mean that, for the MARISONDE G's the data of 21 h are never received by LANNION in direct transmission and only 29 % of the data of 0 h are received.

#### 4. STUDY OF THE TRAJECTORIES

We immediately observe a strong resemblance between the drift of the drogued buoys and the undrogued ones. Drifters 1451 and 1470, launched on 82/08/16 were directed towards the south-east at the rate of 7.5 and 5 cm/s respectively after doing a loop northward. Buoy 1451 stopped working on 82/10/12 probably due to a broken mast. Buoy 1470 stopped on 82/12/28 for unknown reasons.

Drifters 1454 and 1471, launched on 82/08/14 were drifted towards the north-east at the rate of 15 and 12 cm/s respectively after having made many loops around a mean location 61°N-32°W. Buoy 1454 stopped working on 83/01/02, and buoy 1471 continues to function normally.

Buoy 1455, launched on 82/08/29, was drifted along the coast of east Greenland towards the south-west at an average speed of 27 cm/s. It stopped transmitting on 82/09/29 probably through a rupture of the mast, but has since recommenced transmission as from 83/01/15 with just the sea surface temperature functioning normally. The antenna being at the foot of the mast, the rupture of it, does not necessarily mean a break in transmission. The lack of reception from the buoy, observed some days after a breakdown in the measurement of the wind (rupture of the mast) could be explained by the presence of water covering the antenna. When the water disappears, reception starts up again.

The data recorded by the ARGOS service at TOULOUSE and relayed to us, gives us about 8 to 10 locations a day in this area and about 94 % of meteorological synoptic data. We calculated the average velocities of drift of the buoys at synoptic hours using positions interpolated every 3 hours (cubic spline). After having checked that the wind directions were coherent, we carried out comparisons between the wind and the drift, buoy by buoy. The drogued buoys were not too far from the MARISONDE G's dropped at the same places (less than 200 km), we compared their drift with the wind measured by the latter.

Thus, using the undrogued buoys, we tried to determine the surface current response to the wind. However, we are aware that the MARISONDE G's have a wind resistance which is not negligible : 37 % of their surface area is above water but only 16 % is more than 35 cm above the floating line. In the case of drogued buoys, we tried to determine if the buoys kept or did not keep their drogue.

The speed histograms show that the MARISONDE B's are not as fast as the MARISONDE G's (fig.3) but the difference is so small and can perhaps be attributed as much to the weaker wind resistance of these buoys as to the presence of drogues. The speed of the MARISONDE G's and B's are respectively 2.1 and 1.6 % of the wind speed.

The spectral analysis show that our data clearly display the inertial waves (fig.4). The analysis of the wind velocities and atmospheric pressure, compared with those of the drift of the buoys tend to show that a link exists between atmospheric phenomena of meso-scale structure and the movements of the buoys. The periods for which significant energy peaks for the different variables can be observed, are at 80, 200 and 300 hours (fig. 5).

Then, we tried to compare the directions



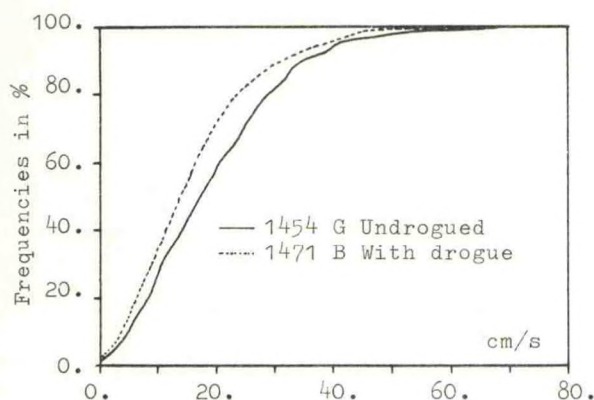


Fig. 3 Cumulative frequencies of drifter velocities.

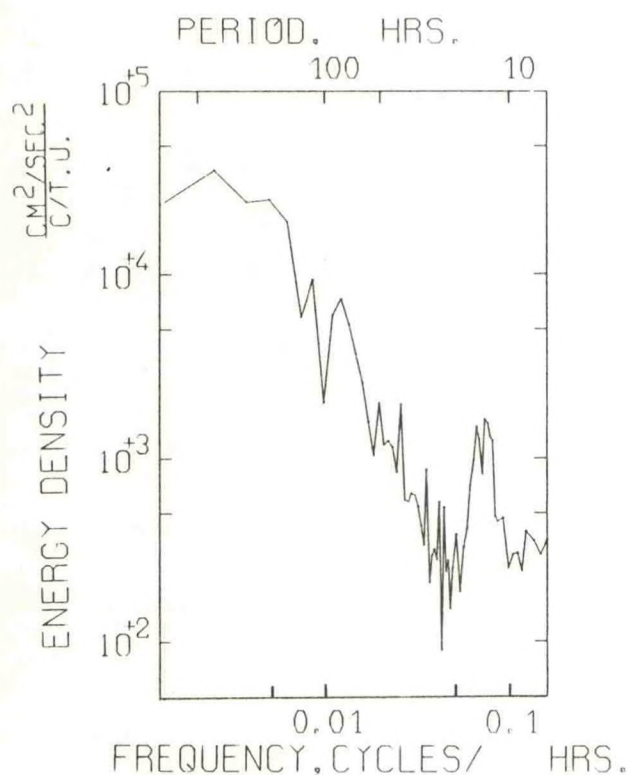


Fig. 4 Total spectrum of drifter velocities Buoy 1454 (3 pieces with 135 estimates per piece)

taken by the buoys in relation to wind direction. As a preliminary, we filtered the vectors of the movement of the buoys using a Hanning filter with a cutoff period of 36 hours in order to break free the inertial waves.

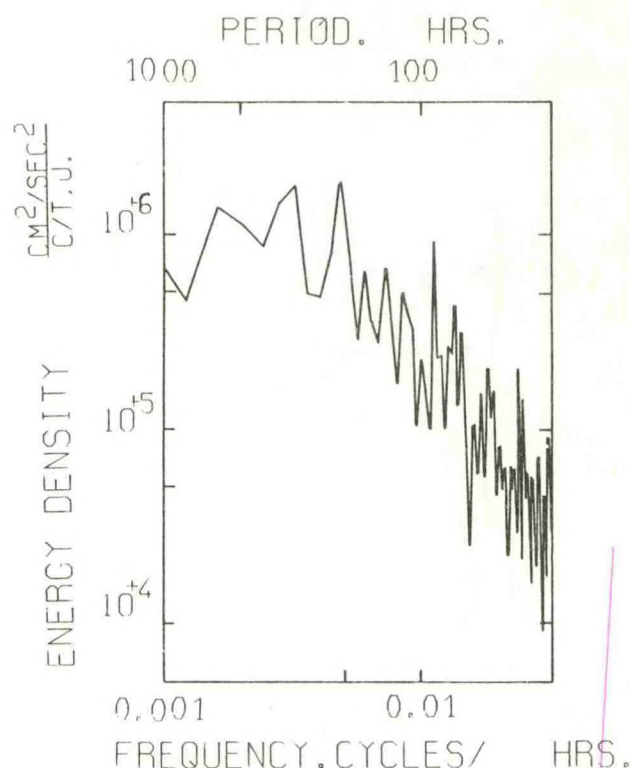


Fig. 5 Total cross-spectrum between drifter and wind velocities - Buoy 1454 (1 piece with 810 estimates)

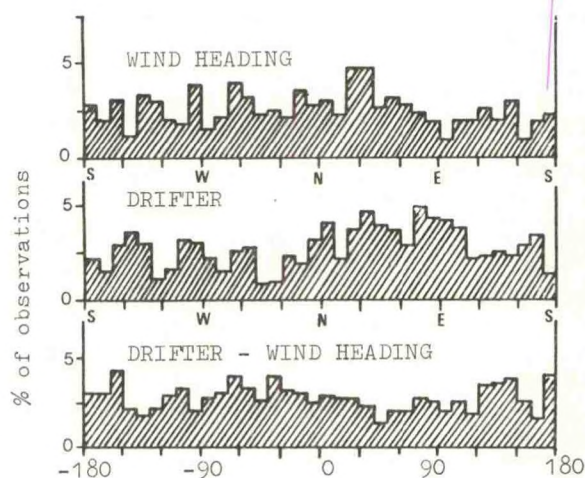


Fig. 6 Composite histogram of wind heading, drifter heading and the drifter heading less the wind direction (1454).

Figure 6 shows that the deviations between the wind and the buoy direction are almost evenly distributed conversely to that which could have been expected. However, the distribution of the averages of these deviations, according to the divisions of wind directions presents an



interesting structure unspite of the high values of the standard deviations (in order of 100 degrees) (fig.7) : for winds blowing from the north to those blowing from the south-west passing through those from the east, the deviation is in the region of 20 degrees.

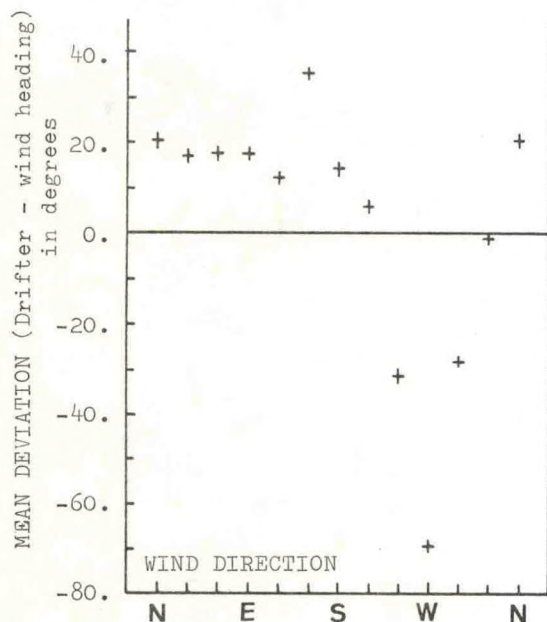


Fig. 7 Variation of mean deviations as function of the wind direction. (1454)

Taking up the works of KIRWAN et al. [6] again, we tested two methods of regression between the wind vectors  $\vec{V}$  and the vectors of the buoys movement  $\vec{C}$ . The first method consists of testing a linear theory of which the form is :

$$\vec{C} = A \cdot \vec{V} + \vec{C}_g$$

The coefficients of the matrix A and the components of the vector  $\vec{C}_g$  which can be regarded as the geostrophic current, are calculated by a least squares method. The second method consists of testing a law of the Ekman + Stokes type. The direct drift of the buoy due to the effect of the wind on the superstructures, which is assumed to be linear, is included in the drift effect of Stokes.

The Ekman drift is of a quadratic type and forms a certain angle with the wind direction. The equation of the law is in the form :

$$\begin{cases} U = (a_{11} \cdot U_a + a_{12} \cdot V_a) \cdot M_a + b_1 \cdot U_a + U_g \\ V = (a_{21} \cdot U_a + a_{22} \cdot V_a) \cdot M_a + b_2 \cdot V_a + V_g \end{cases}$$

$$\text{with } M_a = (U_a^2 + V_a^2)^{1/2}$$

U and V are the components of the vector of the buoy's movement.  $U_a$  and  $V_a$  are the components of the wind vector.

The coefficients  $a_{ij}$  and  $b_i$  and the components  $U_g$ ,  $V_g$  of the vector "geostrophic current"  $\vec{C}_g$  are calculated by a least squares method.

The two methods were tested in the aggregate and then for periods of ten days. The results were not very satisfactory. In fact, the coefficients of correlation are of little significance if the equivalent number of independent vectors is introduced to calculate the significant thresholds.

In conclusion to this study, it seems that the zone studied presents a strong geophysical oceanic turbulence and although it shows similar characteristics to those of atmospheric turbulence as far as the peaks of kinetic energy density are concerned, the two are not directly linked. Simple theories such as the ones we tested cannot be applied.

The presence of the drogues in such an area in order to slow down the drift of the buoys does not appear to be indispensable, given the slow aggregate speeds of the undrogued buoys 1451 and 1454 (4 cm/s) and the very similar behaviour of the drogued buoys.

## 5. CONCLUSION

The BRAN 82 experiment has allowed us to establish that the principle of the measurement of the wind by a buoy orienting itself in the wind holds good. The short life of the MARISONDE G's means we have to revise the solidity of the mast which appears to be the principal cause of the breakdown of the buoys.

Another deployment of 3 MARISONDE G's in the Tropical Atlantic is anticipated in the current 1983 within the framework of the FOCAL experiment. The sea conditions being less severe in this area, we hope that the life cycles of the buoys will be longer.

A modified MARISONDE G is currently being studied. In addition to the existing sensors, it will have a bathythermic line made up of about ten sensors distributed to a depth of 150 meters. A new deployment of MARISONDE G's with reinforced masts is anticipated in the BRAN zone for 1984.

## ACKNOWLEDGMENTS

We would like to thank the Icelandic Meteorological Office for its assistance in the drifter deployment and particularly Mr. Flosi SIGURDSSON. We would also like to thank the crews of the GODAFOSS and the HAFTHOR.



- 1 PETIT M. et al. , Projet MARISONDE 3<sup>ème</sup>  
dossier, Direction de la Météorologie  
France, 1982
- 2 DANIAULT N. , Contribution à l'étude des  
trajectoires des bouées dérivantes de  
la FGGE, ARGOS users conference PARIS,  
April 1982, 43-52
- 3 KLAUS V. , Results obtained with drifting  
buoys developed at EERM and a drifting  
network in North Atlantic, Proceedings  
WMO Technical Conference on automation  
marine obs. and data collection  
HAMBURG, September 1981, 149-156
- 4 KLAUS V. , Bouées météorologiques dévelop-  
pées à l'EERM , ARGOS users conference  
PARIS, April 1982, 85-93
- 5 KLAUS V., BLOUCH P. , Bouées météorologi-  
ques dans l'Atlantique, Poursuite des  
expériences, La Météorologie N°28,  
March 1982, 33-37
- 6 KIRWAN A. D. , Mc NALLY Jr.G. , PAZAN S.  
and WERT R. , Analysis of Surface Cur-  
rent Response to wind, Journal of Phy-  
sical Oceanography 9, March 1979,  
401-412



## DRIFTING BUOYS IN SUPPORT OF MARINE METEOROLOGICAL SERVICES

Glenn D. Hamilton

NOAA Data Buoy Center  
National Space Technology Laboratories  
NSTL Station, MS 39529

### ABSTRACT

Drifting buoys have been very effective in improving weather analyses and forecasting in data-sparse marine areas during the Global Weather Experiment and other test studies. The World Meteorological Organization has recognized this potential and has called for the implementation of operational drifting buoy programs for regional and global purposes.

This paper discusses drifting buoy operations, applications, measurement parameters, telemetry, processing, and dissemination; and examines optimum drifting buoy networks and operating procedures which, when implemented, could greatly increase marine data coverage and improve global and regional weather analysis and forecasting.

### INTRODUCTION

Drifting buoy data have been very effective in improving weather analyses and forecasting in data-sparse marine areas during the Global Weather Experiment and other test studies. The World Meteorological Organization has recognized this potential and has called for the implementation of operational drifting buoy programs for regional and global purposes.

To fully implement these programs and utilize the capabilities of drifting buoys, numerous aspects need to be considered such as past performance, communications and processing schemes, measurement parameters required, and optimum buoy networks.

### THE OPERATIONAL DRIFTING BUOY PROGRAM DURING THE GLOBAL WEATHER EXPERIMENT

The two main objectives of the Global Weather Experiment (also called the First GARP Global Experiment--FGGE) were: to obtain a better understanding of atmospheric motion for the development of more realistic models for extended range forecasting, general circulation studies, and climate; and to assess the ultimate limit of predictability of weather systems.

Figure 1 shows a schematic picture of the drifting buoy developed by the U.S. for FGGE. The U.S. deployed 66 buoys in the Southern Hemisphere during the experiment: 48 were deployed by ships and 18

by aircraft (Figure 2). The buoys measured barometric pressure and sea surface temperature and communicated via TIROS-N polar orbiting satellites [1]. The transmitted data are stored by the satellite, together with sufficient information about the buoy transmission, to permit determination of buoy position. Figure 3 shows some of the tracks of the U.S. buoys. The major acquisition, processing, and dissemination functions are shown in a data-flow block diagram in Figure 4. All the data are collected at the control data acquisition stations in Gilmore, Alaska, and Wallops Island, Virginia. The received and detected data are sent to the spacecraft operational control center in Suitland, Maryland, for preliminary processing. The data are then transmitted to the Centre National d'Etudes Spatiales (CNES), an agency of the French government in Toulouse, for processing by Service ARGOS. Processed data are then disseminated as appropriate. Meteorological data are disseminated worldwide over the Global Telecommunications Service (GTS).

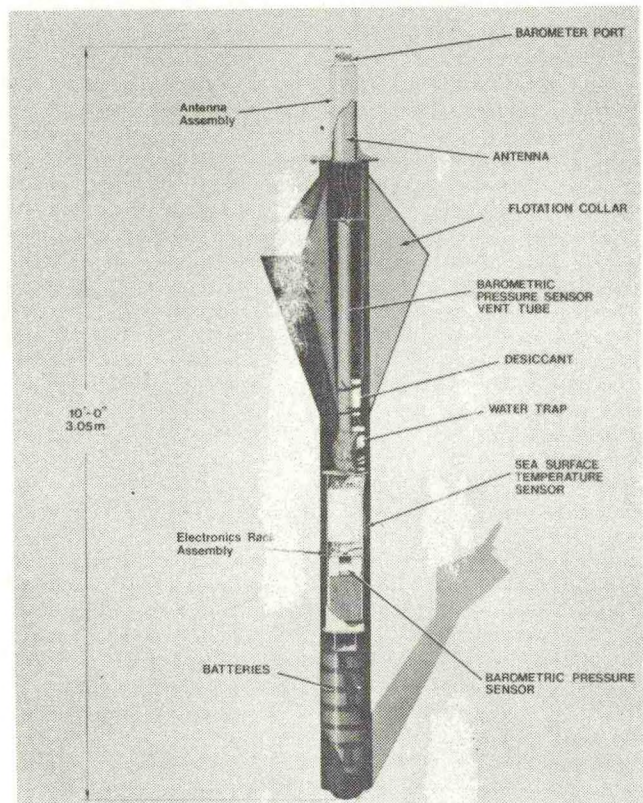


Figure 1. FGGE Meteorological Drifting Buoy



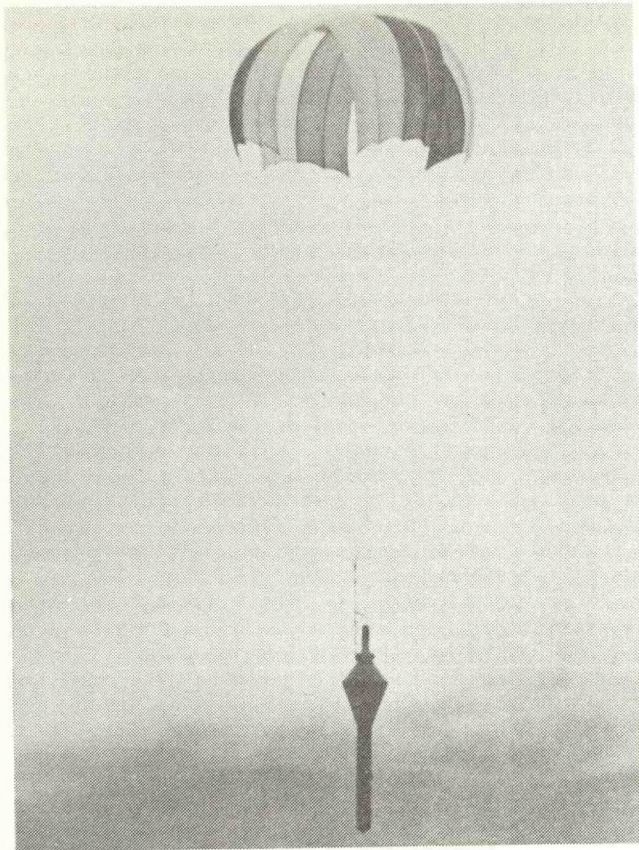


Figure 2. Air-Drop Drifting Buoy

A total of 313 drifters from all countries were deployed in the Southern Hemisphere during the FGGE period, and data from the buoys were sent over the GTS four times a day [2]. The lifetime of the buoys proved to be longer than expected and had an average life of 196 days. Some buoys transmitted valid data for over a year. During the two special observing periods, sea surface temperature and atmospheric pressure data were used by meteorological centers in Melbourne, Washington, and Bracknell (U.K.) among others, while oceanographic data were generated from these basic data at Washington and Ottawa.

There was a significant beneficial impact on Southern Hemisphere forecast operations because of the extra data available in near-real time during FGGE. This conclusion was substantiated both by performance statistics in 1979 versus previous years, and by many case studies of synoptic events by Australian and New Zealand meteorologists.

The enhanced data base was well utilized for a better understanding of the large-scale fluctuations which control the weather from day to day. Implications of FGGE on the design of future Southern Hemisphere observing and analysis/forecast systems were considerable. Data assimilation experiments indicated that the enhanced surface pressure network provided by drifting buoys is indispensable for an ongoing realistic numerical analysis/forecast cycle with minimum manual intervention--some-

thing which hitherto had never been feasible in the Southern Hemisphere.

It was generally agreed by those who used the data from drifting buoys that:

- Surface pressure analyses, particularly in the southern oceans, were improved greatly
- The improved analyses resulted in a much improved quality of forecasts in the area
- Sea surface temperature data were available in sufficient quantity to permit the preparation of 5-day period maps for the first time
- Trajectory information should permit research into sea surface circulations in the southern oceans in the future.

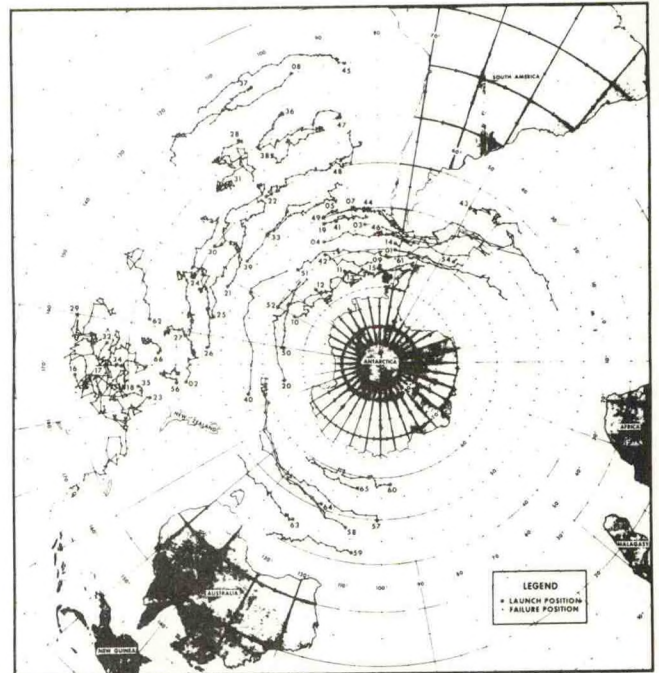


Figure 3. U.S. FGGE Drifting Buoy Tracks as of November 5, 1979

#### IMPACT OF DRIFTING BUOY DATA ON WEATHER ANALYSIS AND FORECASTING DURING THE STORM TRANSFER AND RESPONSE EXPERIMENT (STREX)

Twenty-three U.S. and Canadian buoys were deployed in the Northeast Pacific as part of the Storm Transfer and Response Experiment (STREX). Their initial disposition is shown in Figure 5. Sea level pressure (SLP) and sea surface temperature (SST) observations were transmitted by all buoys, and some also measured wind speed, air temperature, and subsurface temperature. Drifting buoy data received by the NOAA-6 or TIROS-N satellites were tape recorded and/or relayed immediately to a Local User Terminal (LUT) in Canada. The LUT in Edmonton processed immediate transmissions, and the resulting reports were placed on various circuits including the West Coast Marine Circuit (WCMC). Service ARGOS in France processed the recorded data and placed the resulting reports in the GTS network.



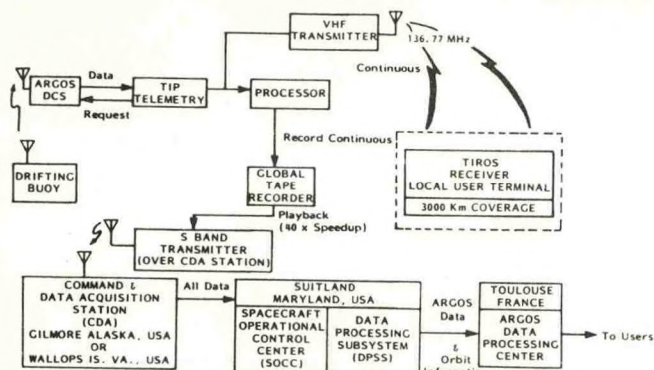


Figure 4. Data Flow for Drifting Buoy System

The NOAA Data Buoy Center (NDBC) contracted with Ocean Data Systems, Inc., (ODSI) for a study: "The Impact of Drifting Buoy Data on Weather Analysis and Forecasting" [3]. ODSI's subsidiary, Global Weather Dynamics, Inc. (GWDI), received data from both the GTS and WCMC data circuits and routinely used the STREX drifting buoy observations in local (fine-mesh) analysis models.

The GWDI Message Switching System (MMS) time tagged and archived all data bulletins received from STREX drifting buoys and from ships at sea. The National Meteorological Center (NMC) also evaluated receipt times of drifting buoy observations at NMC. Receipt time delays for drifting buoy and ship reports are compared in the following table:

COMPARISON OF RECEIPT TIME DELAYS AT ODSI AND NMC FOR DRIFTING BUOY BULLETINS AND CONVENTIONAL SHIP REPORTS

DELAY STATISTICS (hours)	ODSI			NMC	
	BUOYS VIA LUT	BUOYS VIA GTS	SHIPS ALL CIRCUITS	BUOYS VIA LUT	BUOYS VIA GTS
MEAN	0.68	3.02	4.19	0.51	3.20
STANDARD DEVIATION	0.55	1.44	3.31	NA	NA
MINIMUM	NA	NA	NA	0.12	0.90
MAXIMUM	NA	NA	NA	3.73	12.77

NMC PERFORMS FOUR BASIC NUMERICAL ANALYSES: (1) LIMITED FINE MESH (LFM) AT H + 2:00 HOURS, (2) OPERATIONS AT H + 3:45 HOURS, (3) OPTIMUM INTERPOLATION (OI) AT H + 4:30 HOURS, and (4) FINAL AT H + 9:30 HOURS WHERE H REFERS TO STANDARD SYNOPTIC OBSERVATION TIMES. BASED UPON ODSI TIME TAGS, DATA AVAILABILITY FOR THESE NMC ANALYSES WOULD BE AS FOLLOWS:

PERCENT DATA AVAILABLE FOR NMC ANALYSIS CYCLES AS INDICATED BY ODSI RECEIPT TIMES

	NMC ANALYSIS CYCLE			
	LFM H+2:00*	OPERATIONAL H+3:45	OI H+4:30	FINAL H+9:30
BUOYS VIA LUT	98	100	100	100
BUOYS VIA GTS	24	79	91	99
SHIPS (all circuits)	29	57	66	88

\*TIMES ARE HOURS AFTER SCHEDULED SYNOPTIC OBSERVATION TIME (H).

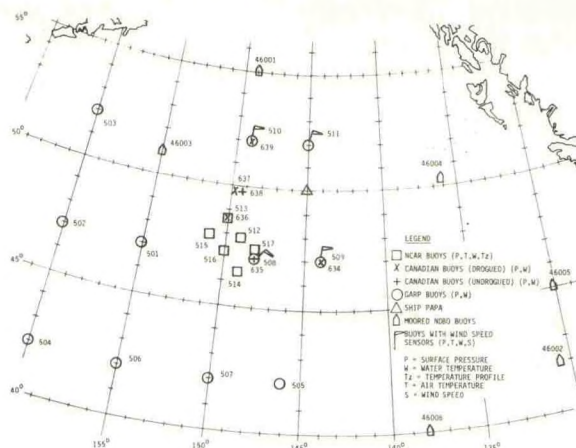


Figure 5. STREX Observing System

Buoy drift plots were prepared for the STREX period for both drogued and undrogued buoys. Buoy observations were compared with three different numerical analyses which were derived with and without the benefit of drifting buoy observations. Comparisons were made between sea surface temperature analyses and values reported by the STREX buoys. Wind speeds from both moored and drifting buoys were compared with winds derived for numerical analyses.

The following major conclusions were drawn from this study:

- The STREX array was not ideal for operational impact evaluation but still clearly demonstrated the potential benefit of drifting buoys to operational analysis and prediction
- All buoys should be drogued to minimize drift
- Sea surface temperature values were generally excellent
- Wind speed values were systematically low because of the anemometer height
- Sea level pressure, sea surface temperature, and wind speed reports from good drifting buoys have accuracies comparable to those reported by NDBC moored buoys
- Data timeliness of drifting buoy reports received via a LUT is completely acceptable for operational analysis and prediction. Data timeliness via Service ARGOS on the GTS was generally not acceptable. Reliable drifting buoy reports processed by a LUT should be introduced into GTS main line trunks no later than 1 hour after observation time
- The two satellite interrogation schemes used during STREX led to data gaps at certain synoptic times. Any operational network design should seriously consider satellite orbit configurations. It is most important to retrieve drifting buoy observations at night when ship reports are relatively sparse due to the single radio operator problem.



## POTENTIAL EFFECTIVENESS OF DRIFTING BUOY DATA FOR MARINE WEATHER ANALYSIS AND FORECASTING ON A GLOBAL AND REGIONAL BASIS

The use of drifting buoys during FGGE and STREX has clearly shown their value to weather analysis and forecasting. Large marine areas of the world are essentially void of data, and potential use of systems such as drifting buoys represents a significant increase in available environmental reports over the ocean.

An analysis of the world's fleet activities by the U.S. Coast Guard showed that on an average, 21,000 vessels were actually at sea on a given day [4]. Statistics for January 1973 compiled at the U.S. National Climatic Center showed that 31,774 ship reports were collected from the world's oceans and that only 9,160 ship observations, or 29 percent, were collected in real time. In the tropical zone, 9,491 ship weather reports were collected in non-real time and only 1,730, or 15 percent, were received in real time. In the Southern Hemisphere, 816 observations were collected in non-real time and 323 messages, or 22 percent, were received in real time. This emphasizes the low percentage of ships at sea actually reporting and stresses the need for alternative data sets such as drifting buoy networks.

The World Meteorological Organization (WMO) requirement for a global horizontal resolution of observations is 1000 km over oceanic areas. The resolution and frequency requirement for regional networks is 300 km four times daily [5]. Figure 6 shows areas with reporting coverage for a 300-km

spacing criterion of surface observations. Obviously, the reporting coverage would be larger if more ship reports were received in real time. Nevertheless, it is clearly evident that oceans, in particular, are lacking in numbers of observations.

Drifting buoy data are used in both numerical and conventional surface analyses, and the density of buoys should be such that the depiction of weather systems and intensity of storms can be adequately defined. Clearly there must be a trade-off between desired spacing and the resources available.

Voluntary observing ships frequently do not report weather observations during nighttime hours, and drifting buoy reports become of even greater significance during this period. Consideration must be taken of times and coverages of satellite reception of buoy data to minimize gaps in data delivery because of satellite transit tracks.

### OPTIMUM NETWORKS FOR OPERATIONAL WEATHER ANALYSIS AND FORECASTING

Under contract for the NOAA Data Buoy Center, Ocean Data Systems, Inc., conducted a study [6] for the following purposes:

- Determine optimum drifting buoy networks in both the Northeast Pacific and Northwest

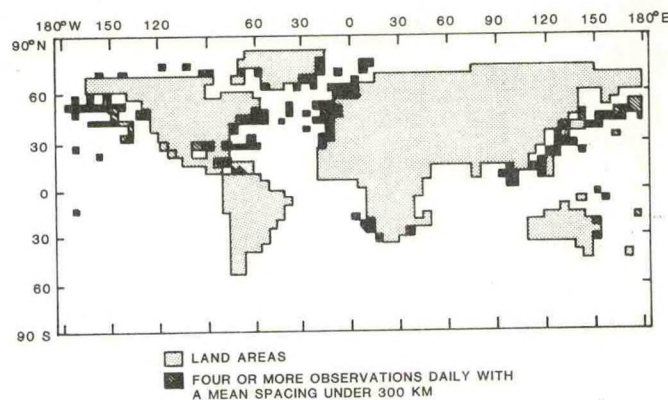


Figure 6. Areas with Adequate Coverage for a 300-km Spacing Criterion

Atlantic Oceans, taking into account not only numerical modeling considerations, but also support to commercial fishing and shipping activities

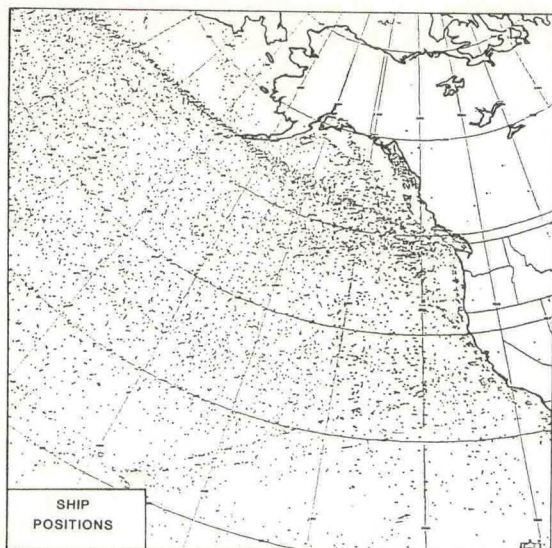
- Devise deployment strategies for achieving these networks. This includes analysis of buoy trajectories from the STREX data and studies of surface currents from the literature to determine buoy "seeding" points
- Devise algorithms for determining cost effectiveness of buoy deployment taking into account factors such as ship or airplane time, routing and costs, staging areas, scheduling, and seasonal factors.

An area like the Northeast Pacific or Northwest Atlantic would fall into the regional category, for which WMO recommends an observational network with a 300-km spacing. This corresponds to one observing station for each nine square degrees of surface area. If the Northeast Pacific is defined as encompassing the area from the west coast of the U.S. to the international date line, and from 25°N to the southern coast of Alaska, then it occupies about 1300 square degrees. About 130 observing stations would then be required to cover this area, using the spacing recommended by WMO. For the Northwest Atlantic, the numbers are comparable as the area of interest may extend from 20°N to 60°N and from 30°W to the east coast of the U.S. The two regions together would thus require about 260 buoys. At the cost of \$7500 per buoy, this represents an initial investment of nearly \$2,000,000. This cost and the additional replacement cost are so high as to be prohibitive. The WMO recommended spacing cannot be met by drifting buoys alone.

There are many ships at sea at any one time that report weather data, and this can be seen in the composite plot shown in Figure 7 which shows the positions of the ships when they reported weather data at 00Z for a 67-day period for November 11, 1980, through January 19, 1981 in the Northeast Pacific. The major shipping lanes are clearly evident. However, the coverage for just 1 day shows considerable data void areas at 12Z (Figure 8) which is nighttime in the Northeast Pacific.

Even with the ship reports in addition to drifting buoys, it is still not economically feasible to maintain a consistent 300-km spacing, especially in



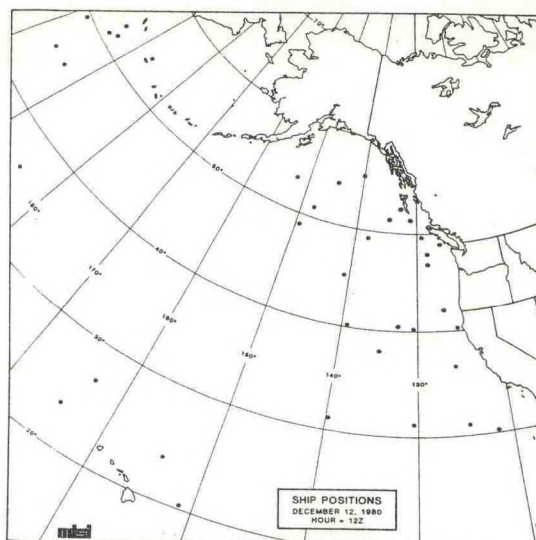


**Figure 7. Ship Positions (Dots) at the Time Weather was Reported for the Northeast Pacific. This is a Composite Figure Covering 67 Days (14 November 1980 through 19 January 1981) and is for the 00Z Synoptic Time.**

the Pacific. If the spacing is increased to 500 to 600 km outside of shipping lanes, the required number of buoys can be substantially reduced. A network of 24 buoys in each region, when combined with ship reports, would give adequate coverage. Some of the smaller-scale weather features will be missed in the weather analyses and forecasts with this larger spacing, but in most cases the overall effect would not be serious. It is worth noting that during FGGE, the buoy spacing was 250-500 km in active weather regions and 500-700 km in less-active regions. For this total of 48 buoys, it might be expected that three to four of them would fail and have to be replaced each month. Although this replacement rate is still higher than desired, it should be attainable.

The recommended buoy arrays, based on the above considerations, are shown in Figures 9 and 10 for the Northeast Pacific and Northwest Atlantic Oceans, respectively. The two-dimensional arrays are made up of staggered linear arrays spaced 8° in longitude and 4° in latitude, thus producing a nearly square grid tilted at 45° to the latitude and longitude circles. This grid widens out in distance toward the equator although the longitude spacing in degrees remains constant. The meteorologically more-active higher latitudes are therefore better covered than the calmer lower latitudes. The spacing is 512 km at 55°N latitude and 599 km at 25°N.

In these figures, the major shipping lanes are shown as the stippled areas. In the case of the Northwest Pacific, the shipping lanes are well defined and have thus been avoided in setting up the buoy grid. For the Northwest Atlantic, however, the shipping lanes from the U.S. to Europe are poorly defined and consequently it would be inappropriate to avoid them.



**Figure 8. Ship Positions (Dots) for the Northeast Pacific on 1 Day (12 December 1980) at 12Z**

The buoys would likely be deployed in stages as they became available rather than all at once. They should therefore be deployed in such a way as to build the recommended arrays in a manner most useful for weather analysis and forecasting. These partial arrays should favor the higher latitudes as these are more meteorologically active. In the case of the Northwest Atlantic, one lower-latitude buoy should be deployed early to help cover the area frequented by tropical cyclones.

#### **DRIFTING BUOY DATA TELEMETRY SYSTEM FOR REGIONAL APPLICATIONS**

As discussed earlier, transmission of buoy data through the ARGOS system is untimely with respect to making the data available for weather forecasting purposes. Clearly, alternative means of communication need to be considered.

As one of several components of a new meteorological data system for the Northeast Pacific Ocean, the Canadian Atmospheric Environment Service (AES) undertook in the spring of 1979 to use FGGE-type drifting buoys and the ARGOS data collection system on the NOAA satellites to reduce gaps in the coverage of surface data obtained from voluntary observing ships and moored buoys. To obtain the buoy data in "real time" for meteorological analysis (1 hour or less), an ARGOS Local User Terminal (LUT) capability was developed by adding decoding and location computation facilities to the S-band (1698 to 1717 MHz) HRPT (High Resolution Picture Transmission) weather satellite receiving station installed in the AES Arctic Weather Centre in Edmonton, Alberta. Vockeroth and di Cenzo [7] summarizes the experience of the AES with LUTs and is used extensively in this section.

The 1 to 4 hours normally required to collect and distribute meteorological reports via the principal telemetry readout stations and the ARGOS centre in Toulouse can be reduced to about 30 minutes by processing the real-time data receivable from the satellites when they are within the common field of



view of the data platform and a LUT. This gain in the timeliness of the reports provided by a LUT is achieved at the expense of a lower daily number of reports, a more-limited reception area, and less-accurate locations if these are computed at the local station.

To add platform positions to reports produced at a LUT, two methods may be used. A recent previous position reported by CNES may be used, or the position may be computed at the LUT itself if it is suitably equipped. For rapidly moving platforms, on ships or balloons, only the latter method is suitable; it is being used at Edmonton and is to be used in the Toronto station also. Good platform locations normally require data reception for 6 or more minutes in a given orbit. This reduces the limiting range of platform locations below that of data reception. The location procedures used in the Edmonton LUT result in random location errors of about 1% of the distance between the moving platform and a fixed location reference transmitter. In the Pacific target area, this results in errors up to 30 km, but smoothing techniques permit these errors to be reduced to 10 km or less for slow-moving platforms. This is adequate for meteorological mapping. For shipboard platforms such averaging techniques cannot be used, and it is intended to use suitably located reference transmitters to reduce such location errors to acceptable levels in the near coastal areas. It is noteworthy that the CNES location reports have a mean error of 0.5 km or less.

#### DEVELOPMENTAL SYSTEMS

Over open ocean areas in the vicinity of tropical cyclones there are very few surface observations

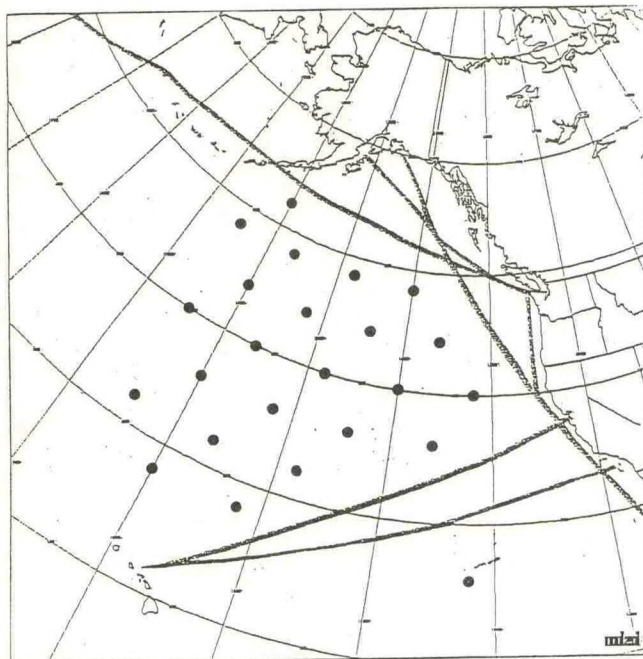


Figure 9. The Recommended Array of 24 Drifting Buoys for the Northeast Pacific. The Stippled Areas Show the Major Shipping Lanes.

reported as ships tend to avoid the severe weather. To provide additional reports, NDBC and the U.S. Navy have developed a program to deploy drifters along the projected track of a storm. Figure 11 shows a sample plan to deploy the buoys on the 30-kn wind radius of a theoretical storm. At present, plans to air deploy six buoys by USAF Weather Reconnaissance WC130 aircraft in the Western Pacific and Atlantic/Gulf of Mexico during the 1983 storm season are being made. These buoys are anticipated to provide vital, and otherwise unattainable, information on intensity and movement of tropical cyclones.

In an effort to provide additional measurements of significant meteorological parameters, developmental programs are being undertaken. For example, Figure 12 shows an experimental drifting buoy which is being tested to provide air temperature, barometric pressure, wind speed and direction, and water temperature.

Drifting buoys have the potential and are "coming of age" in providing an extremely important set of weather observations to data-sparse marine areas to assist forecasters in better defining weather systems and improving storm warnings and forecasts.

#### SUMMARY

1. Drifting buoys have improved weather analysis and forecasting capabilities in data-sparse marine areas.
2. Cost-effective networks of drifting buoys with spacing of 500 to 600 km can be deployed, which will give adequate coverage for weather patterns.

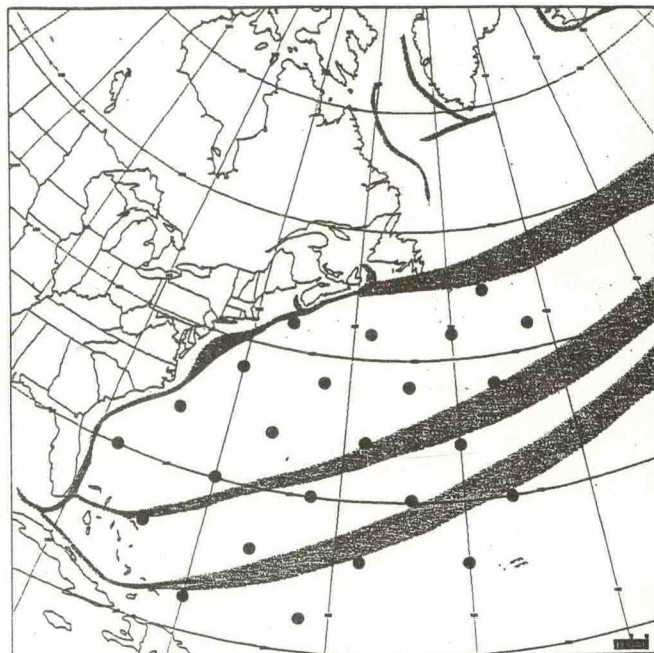


Figure 10. The Recommended Array of 24 Drifting Buoys for the Northwest Atlantic. The Stippled Areas Show the Major Shipping Lanes.



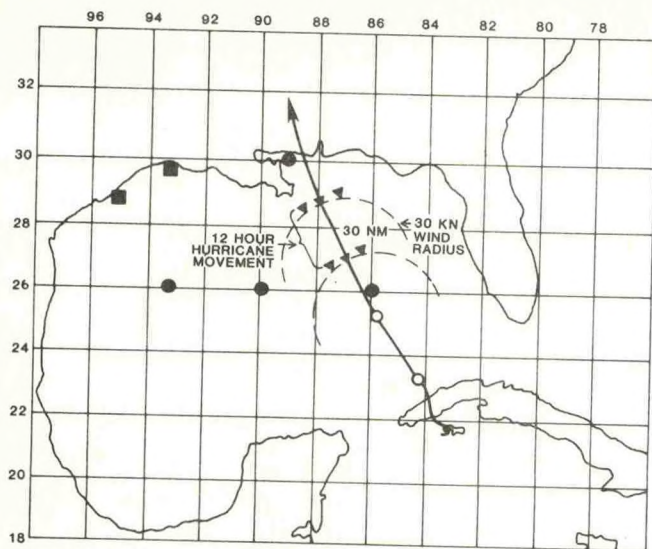


Figure 11. Proposed 1982 Hurricane Drifting Buoy Experiment (Track of Hurricane Frederic)

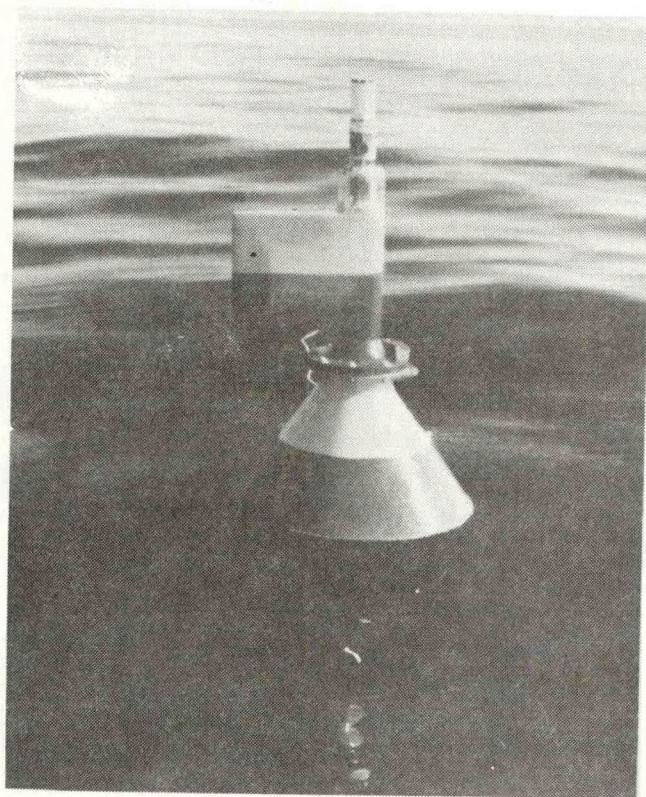


Figure 12. Wind Measuring Drifting Buoy

3. Local User Terminals provide a means to obtain drifting buoy data in a timely manner.
4. Drifting buoys have a tremendous potential for providing a complete set of vital meteorological observations.

#### REFERENCES

1. Kerut, E. G. "Development of Drifting Buoy Systems for Oceanographic and Meteorological Applications," OCEANS '80 Proceedings.
2. World Meteorological Organization, "Critical Review of the FGGE Drifting Buoy System," 1979.
3. Ocean Data Systems, Inc. (ODSI), "The Impact of Drifting Buoy Data on Weather Analyses and Forecasts in the Northeast Pacific," 1981.
4. World Meteorological Organization, "Satellite Data Requirements for Marine Meteorological Services," WMO-No. 548, 1980.
5. World Meteorological Organization, Technical Regulations, WMO-No. 49.
6. Ocean Data Systems, Inc., (ODSI), 1982, "Design and Cost of Operational Drifting Buoy Networks for Weather Analysis and Forecasts."
7. Vochereth, R. E., di Cenzo, C. S., 1982, "Collecting Meteorological Reports with the ARGOS System," ARGOS Users Conference, Annapolis, MD, December 1982.



## GREAT LAKES SATELLITE-TRACKED CURRENT DRIFTERS

R. L. Pickett\*, R. M. Partridge†, A. H. Clites\*, and J. E. Campbell\*

\*Great Lakes Environmental Research Laboratory

†National Space Technology Laboratories

### ABSTRACT

Satellite-tracked current drifters proved to be a valuable tool for monitoring near-surface currents in the Great Lakes. Position accuracy tests conducted at four land locations around the lakes showed that errors were less than 1 km, and did not vary with latitude, longitude, transmitter age, or battery condition. Wind drift was estimated to be 0.7% and was verified with dye and oil spills. Various drogue configurations did not alter drifter tracks. Drifter recovery was aided by the design of a 10-km range, portable radio direction-finder. A replaceable battery module and armor plating enabled reuse of the drifters. Lake Michigan tracks to date show strong northward currents in the east, southward currents in the west, and meandering currents near the middle of the lake.

### INTRODUCTION

The Great Lakes, the world's largest freshwater supply, are surrounded by intense concentrations of men and machines. Sixty percent of the Canadian population and 15% of the U.S. population live there. Thirty million people drink the water, and the United States alone withdraws 25 billion gallons of water daily for generating electricity, drinking, sewage treatment, and industry. As a result of these uses and their related transportation requirements, there are now more contaminants per unit volume of water in the Great Lakes than in the ocean.

Petroleum is the most common toxin shipped on the lakes. Each year its transportation results in an average of about 10 spills with volumes greater than 100 gallons (Keillor, 1980). Chemical industries represent another source of toxins. From 1973 to 1979, there were an average of about 27 chemical spills per year in Great Lakes' waters. The major chemicals were sulfuric acid, hydrochloric acid, toluene, xylene, ammonia, naphthalene, phenol, and styrene. As in the case

of oil, most chemicals were spilled in the inter-connecting channels (Bower and Myll, 1980).

These problems led to a Joint Water Quality Agreement in 1978 that stated, "The Government of Canada and the Government of the United States of America. . . continue to be concerned about the impairment of water quality on each side of the boundary to an extent that it is causing injury to health and property on the other side. . ." The agreement also noted that current data were needed to determine toxin pathways and to prevent the spread of pollutants (International Joint Commission, 1978).

One method for meeting these current data requirements is to observe objects moving with the water. The earliest study (Harrington, 1894) used drift bottles to estimate Great Lakes currents. Although cheap to use, drift bottles cannot reveal current speeds and path details. These disadvantages were overcome by tracking drifters with ships. Next, RADAR reflectors and radio transmitters were added to ship-tracked drogues to increase detection range (see reviews by Monahan and Monahan, 1973; International Joint Commission, 1975). Finally, a communication system was developed that allowed drifters to be tracked by satellite. The early satellite-tracked versions were handmade and had position errors of 5 km (Kirwin et al., 1976 in the ocean; Mortimer, 1977 in lakes).

Satellite tracking has advantages over conventional techniques. Expensive ships are not required for monitoring, accurate positions are available every few hours, and large numbers of drifters can be tracked simultaneously. The only disadvantage is cost (\$5,000 U.S. per drifter).

The four satellite-tracked drifters used in these tests were manufactured by Polar Research Laboratory in Santa Barbara, California. This particular model, one of several commercially available types, consists of a 35 kg surface unit, a 1 m length of nylon line down to a chain yoke and a weighted 1 m x 4 m nylon window shade type drogue or sea-anchor (see Fig. 1). This arrangement is designed to measure currents about 4m below the water surface (at the drogue center). The surface unit consists of a fiberglass antenna shroud on top of a 0.2 m diameter, 1 m long,



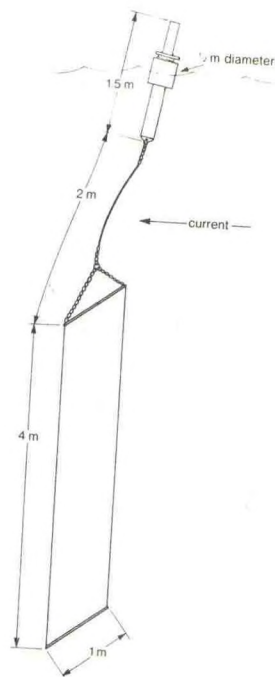


Figure 1. Sketch of satellite-tracked current drifter. Each drifter consists of a 35 km surface unit containing the transmitter and battery pack, a nylon line down to a chain yoke, and a weighted nylon window shade type drogue.

aluminum cylinder. Surrounding the top of this cylinder is a foam-filled, fiberglass covered, flotation collar. Inside the cylinder is a 400 MHz transmitter that sends a 0.4 s burst every minute. In the bottom of the cylinder are 72 alkaline D-cell batteries that provide a six-month life. The units transmit to TIROS satellites, and position is determined by Doppler shift via the ARGOS system.

Results from the tests of these four drifters suggest that the units have position errors less than 1 km, have a 0.7% wind drift, and can be easily refurbished and reused. They appear to be valuable for mapping current pathways and understanding and predicting spill movements.

#### TESTS

##### Position Accuracy

Before the drifters were used in the Great Lakes, their positioning accuracy in this region was measured. Also variations in this accuracy with latitude, longitude, transmitter age, battery condition, tilt angle, and shielding were tested. Finally, how frequently positions were obtained was established.

Table 1 shows results relating to the first two tests. Standard deviations of position errors are given for new drifters, used drifters, and used drifters with new batteries. Position errors were random and unbiased and ranged from 0.1 to 0.6 km. Variations between individual drifters were as large as variations due to other causes. When units were laid on their sides or strongly shielded, as for example aboard ship, the positions obtained were still as accurate, but about one third of the positions were missed. In summary, nothing was found that degraded drifter positional accuracy.

In the Great Lakes region, an average of 7 positions per day (range 6 to 1) were obtained. The receiving system was down on about 1 day in 5 resulting in the loss of some positions. To minimize the effects of these down times an automatic dial-up and recording computer terminal was used to repeatedly interrogate the system.

In addition to missed positions, there was also a delay in receiving positions. This delay was critical when a drifter was headed into high surf or rocky coasts. The elapsed time from a satellite overpass until a position was available on the receiving system ranged from 3 to 12 hours,

Table 1.

Drifter Position Errors  
(standard deviations in km)

##### A. New Drifters

Position	Type Error	Drifter serial #				Number Observations
		3386	3387	3388	3389	
43.308°N	Lat.	0.3	0.2	0.3	0.2	30
83.707°W	Long.	0.3	0.3	0.4	0.2	
	Total	0.5	0.4	0.5	0.3	
43.223°N	Lat.	0.2	0.2	0.4	0.1	13
86.341°W	Long.	0.3	0.3	0.4	0.2	
	Total	0.4	0.3	0.6	0.2	
45.563°N	Lat.	0.2	0.2	0.3	0.2	22
84.672°W	Long.	0.2	0.2	0.4	0.2	
	Total	0.3	0.3	0.5	0.2	
43.006°N	Lat.	0.4	0.1	0.2	0.1	4
82.422°W	Long.	0.1	0.1	0.2	0.1	
	Total	0.5	0.2	0.3	0.1	

##### B. After 5 Months of Use

43.308°N	Lat.	---	0.2	0.3	0.2	27
83.707°W	Long.	---	0.3	0.2	0.2	
	Total	---	0.3	0.4	0.3	

##### C. After Battery Replacement

43.308°N	Lat.	---	0.2	0.2	0.1	25
83.707°W	Long.	---	0.2	0.2	0.2	
	Total	---	0.3	0.3	0.2	



averaging 4 hours in the morning and 6 hours in the evening.

### Tracking

One advantage of drifters over moored current meters is that a drifter's path indicates where waterborne material actually goes. Hence spill, search and rescue operations, and sediment transport problems can be studied directly. Another advantage is that very weak currents can be measured by tracking over long time periods.

A disadvantage of drifters is wind motion. Antennas or RADAR reflectors sticking above the water act like sails that cause the drifter to move downwind. Wind motion can either be estimated and removed in data processing, or minimized by using larger drogues and smaller antennas.

Dye was used to confirm this wind motion. Repeated tests showed that the drifters slowly leave a dyed area of water. In a typical test the drifter would move about 10 m downwind from a dye patch in 3 hours. Since both the drifter and the dye moved 2 km during that time, the apparent windage was about 10m per 2 km or 1/2%.

This slippage can also be estimated theoretically (Kirwin et al., 1974). The first step consists of measuring the water drag and air drag areas of the drifters. The ratio of these areas turned out to be 25:1 for the drifters used in these tests. Following the Kirwin et al. technique, this ratio leads to a 0.7% wind effect. Thus the drifter should move downstream with 99.3% of the water speed and downwind with 0.7% of the surface wind speed. Surface wind speed is less than reported wind speed which is usually observed at 10 m above the surface. Nevertheless, this estimated windage is similar to estimates from the dye studies described above. Once this windage is known precisely, it can be used to correct observed drifter paths to estimate true water parcel paths.

### Drogue Tests

Along with the above tests, drogue modifications were tried. The standard window shade drogue was tested against a cruciform (cross-shaped) drogue with the same weight and area, and against a drifter with no drogue. These modifications, in turn, were compared to dye and oil patches.

These drogue tests showed no significant differences between window shade and cruciform drogues (Fig. 2). Both types moved slightly downwind from dye patches, and both types were quickly left upwind by oil slicks.

However, when drogues were removed, the surface unit tracked oil slicks quite well. One unit stayed near the center of an oil slick moving at  $0.5 \text{ m s}^{-1}$  during a 3-hour test. Hence, drifters with no drogues appear useful for tracking oil spills.

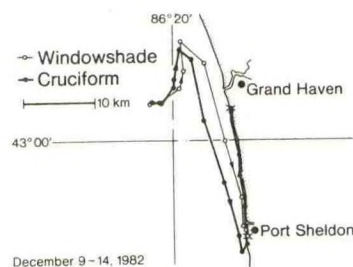


Figure 2. Comparison of window shade and cruciform drogues. Two drifters differing only in drogue shape (same drogue weight and cross-sectional area) followed similar deep water paths in Lake Michigan for 5 days. The window shade unit moved slightly faster (dots are at approximately 6h intervals) and ran aground sooner. The cruciform snagged bottom in the surf zone and went north with the longshore current.

Another drogue test consisted of altering drogue depths. These tests were performed by simply increasing the length of line from the surface unit to the chain yoke. Since Great Lakes winter currents are barotropic, changing drogue depth should not significantly alter their paths. Comparisons of 4 and 9 m depths (center of drogue) confirmed these uniform currents (Fig. 3) and suggest these drifters can be easily modified to monitor currents at various depths (e.g., to study thermocline shear in summer).

### Launching and Recovery

The drifters were ruggedly made since they were designed to be dropped by parachute. However, ship launchings were used in these tests to allow monitoring above and below water. The units were simply slid overboard. After initial

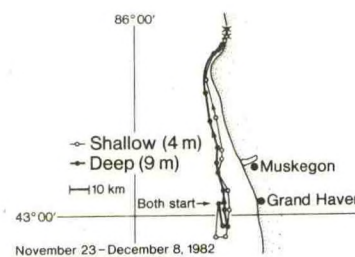


Figure 3. Comparison of shallow and deep drogues. Two drifters differing only in depths of their window shade drogues (center of drogue was at 4 m and 9 m below surface) followed similar paths in Lake Michigan for 2 weeks (dots are at 1 day intervals). They started south for a day, then turned north for the rest of the period.



tests, a Great Lakes car ferry was used to launch the units on a routine lake crossing.

Although launching was simple, recovery was complicated. The first drifter came ashore after one month during  $20 \text{ m s}^{-1}$  winds and 5 m seas. Owing to the position delays described above, the unit was destroyed by the surf before it could be located.

The solution to this delay problem was the design and construction of a portable locator unit. The resulting radio direction-finder consisted of a modified UHF-TV antenna, a miniaturized 400 MHz receiver, a lantern battery, and earphones. By scanning the horizon with the antenna, a drifter's transmission could be heard. Relative location angle could be determined at ranges up to 10 km from ship or shore. This device allowed quick recovery of a drifter headed for shore during a storm or in a rocky area. Also this locator allowed quick recovery and resetting of drifters for localized studies (e.g., mapping a river plume).

Recovery also entailed on-site repair. Necessary materials (fiberglass kits, insulation spray foam, hardware) could all be easily obtained locally. Spare quick-connect battery packs were made up in advance for easy battery replacement. For winter use in ice-infested waters, an aluminum armor was riveted over the vulnerable fiberglass and foam flotation collar. Finally, since surf pounding occasionally caused units to leak, six dessicant bags were fitted in empty spaces around the transmitter to minimize water damage.

#### DRIFT TRACKS

On 15 September 1982, four drifters were placed on the east side of southern Lake Michigan. On 1 February 1983, three of these original four were reset on the west side of central Lake Michigan. Positions have been received regularly. Path lengths have ranged up to 900 km and the units have washed ashore in 1 to 3 months. The median current speed from all tracks was  $.17 \text{ m s}^{-1}$  and 99% of the speeds were less than  $.55 \text{ m s}^{-1}$ . These speeds are comparable to those observed with moored current meters in Lake Michigan surface waters (Saylor, et al., 1980).

The long-term drifter movement suggests strong northward currents off the eastern shore, southward currents off the western shore, and slow meandering currents near the middle of the lake (Fig. 4). On an intermediate (3-5 day) time scale, the tracks show changes that result from changing winds modifying the lake's circulation. On a still shorter time scale, the tracks show clockwise inertial circles (sample in Fig. 5). These inertial circles are always present, are only a few kilometers in diameter, and thus do not show up in the larger scale of Fig. 4.

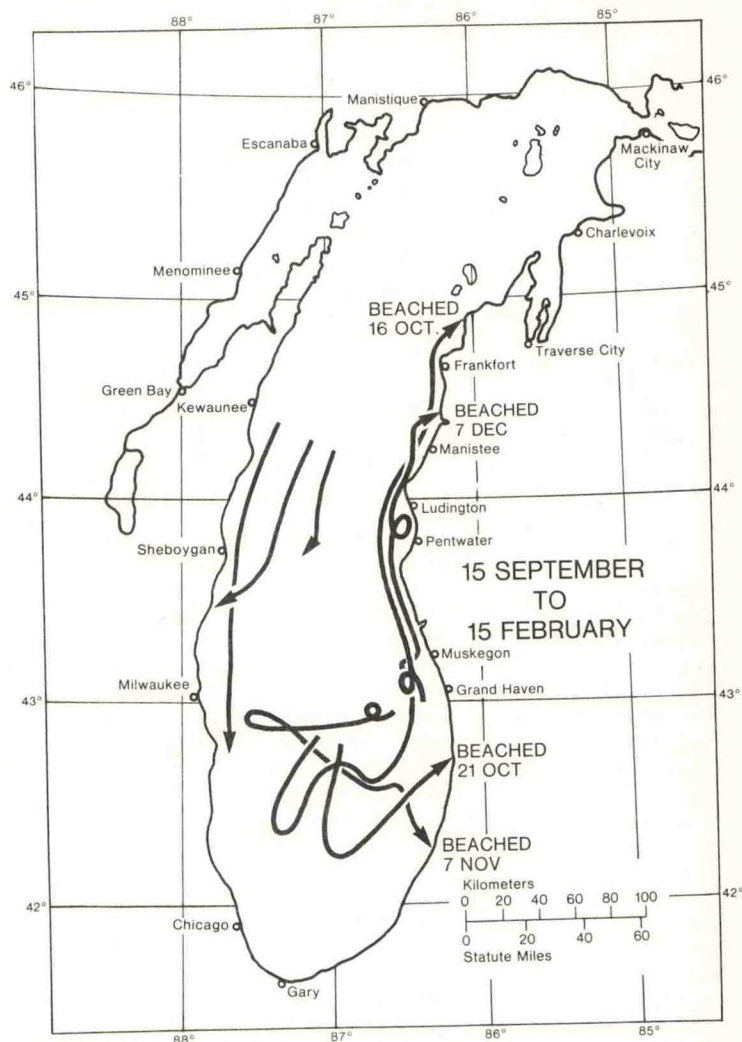


Figure 4. Drifter paths from 15 September 1982 to 15 February 1983. On 15 September four drifters were placed in the southeast region of Lake Michigan. As they beached, they were repaired and on 1 February 1983 three of the four were reset on the west side of central Lake Michigan. Net movements to date suggest northward currents off the eastern shore, southward currents off the western shore, and meandering currents in the middle of the lake.

#### CONCLUSIONS

Satellite-tracked current drifters have two disadvantages. The first is cost. As demand for the devices increases, longer production runs and more competing manufacturers should result in lower costs. In the meantime, an effective cost-cutting strategy in the Great Lakes is recycling. Damage can be repaired, armor added, batteries replaced, and the units reused to significantly reduce the cost per track.



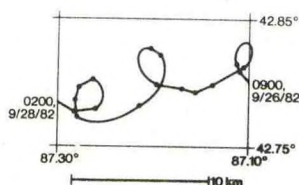


Figure 5. High resolution section of drifter path in Lake Michigan's southern basin. Path details reveal clockwise inertial circles with 17.4 hour period and about 2 km diameters. In this case, circles are superimposed on a mean west drift.

The other disadvantage is wind drift. This can be minimized by either correcting observed tracks for wind or increasing the drogue area. Either method would appear to work.

These drifters also have advantages. They can show where waterborne material actually goes and can measure very weak currents. Best of all they are easy to use. A "smart" computer terminal can dial up the ARGOS system, record and edit positions, calculate statistics, and plot tracks for a large number of drifters.

In summary, satellite-tracked current drifters are valuable for monitoring current paths, and understanding and forecasting spill movements in the Great Lakes. For example, Fig. 6 shows the mean winter circulation of Lake Michigan derived from a forecasting model (Pickett, 1980). Note that both the model and the observed tracks in Fig. 4 show strong northward currents on the

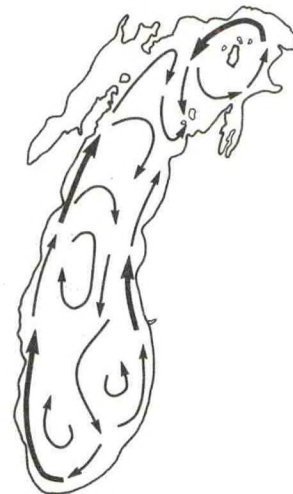


Figure 6. Model mean winter circulation of Lake Michigan (from Pickett, 1980). Comparisons of Figs. 4 and 6 show agreement off the east shore where both tracks and model show northward currents (bold model arrows indicate stronger currents). Mid-lake eddies in the southern basin are also confirmed by the drifter tracks. However, the model's strong northward mean current off the western shore has not been confirmed to date.

#### REFERENCES

- Bower, J.M., and J. Myll 1980. Vessel related spills of toxic chemicals on the Great Lakes: Likely locations and types of chemicals. Great Lakes Environmental Planning Study Contrib. #29, Great Lakes Basin Commission, Ann Arbor, Mich. 15 pp.
- Harrington, M.W. 1894. The currents of the Great Lakes. *U.S. Weather Bur. Bull. B.* 23 pp.
- International Joint Commission. 1975. Workshop on the feasibility of remote tracking of drogues and other instruments drifting in coastal waters. IJC Regional Office, Windsor, Ontario. 135 pp.
- International Joint Commission. 1978. Great Lakes water quality agreement of 1978. IJC, Ottawa, Ontario. 52 pp.
- Keillor, J.P. 1980. The hazards of tank ships and barges transporting petroleum products on the Great Lakes. *Coastal Zone Manage. J.* 8:319-336.
- Kirwin, A.D., G. McNally, M.S. Chang, and R. Molinari. 1974. The effect of wind and surface currents on drifters. *J. Phys. Oceanogr.* 5:361-368.
- Kirwin, A.D., G. McNally, and J. Coehlo. 1976. Gulf Stream kinematics inferred from a satellite-tracked drifter. *J. Phys. Oceanogr.* 6:750-755.
- Monahan, E.C. and E.A. Monahan. 1973. Drogues, drags, and sea anchors. Tech. Rept. No. 36. Univ. of Mich. 21 pp.
- Pickett, R.L. 1980. Observed and predicted Great Lakes winter circulation. *J. Phys. Oceanogr.* 10:1140-1145.



Saylor, J.H., J.C.K. Huang, and R.O. Reid. 1980.  
Vortex modes in southern Lake Michigan. J.  
Phys. Oceanogr. 10:1814-1823.

Mortimer, C.H. 1977. One of Lake Michigan's  
responses to the sun, the wind, and the  
spinning earth: The thermal bar. Forum  
1977, Lectures in Celebration of the 20th  
Anniversary of the Establishment of the  
University of Wisconsin-Milwaukee.



## HISTORY OF DATA BUOY DEVELOPMENT SINCE 1970

An Address by  
Associate Administrator James W. Winchester  
Before  
Buoy Technology Symposium  
New Orleans, Louisiana  
April 28, 1983

### INTRODUCTION

It's a pleasure to be here today. As you probably know, I once wore the hat that Jerry McCall now wears, so I am pleased to have had a hand in the early development of buoy technology. Also, it's good to be back looking at familiar faces and hopefully learning whether or not the issues have changed over the last few years.

Unfortunately, I am not able to keep abreast of what is happening to buoy technology, but in my present position with President Reagan's Administration, I am proud of the fact that the NOAA Data Buoy Center is an outstanding example of a successful government/industry partnership. As you know, the President has consistently stated that government's role is to assist industry in providing jobs and promoting our national economy, instead of trying to compete with industry and/or imposing unreasonable constraints on corporations and businesses. In addition to establishing an effective governmental/industrial relationship, the record clearly shows that the NOAA Data Buoy Center has been the leader in utilizing buoy technology to develop a product that has worldwide acceptance as an efficient, cost-effective data acquisition system. I take some personal pride in helping to establish and implement the NDBC concept of engineering systems development, and I assure you that other NOAA elements responsible for oceanic and atmospheric programs are being required to adopt a similar government/industry partnership type of operation.

### HISTORY

The need for a data buoy program came out of a well-established national requirement to acquire near real-time environmental data from oceanic and marine areas. The buoy programs that had been conducted by several different agencies over a period of years had not been able to satisfy that requirement. Components were fragile, and the systems were unreliable. So, a National Data Buoy Development Project was formed in 1968, and it was transferred to NOAA when the agency was formed in 1970. NOAA's first buoy program was essentially an engineering evaluation. The results of these evaluations soon showed that past buoy systems had not been successful because the designs were too complex and system costs were excessive.

In 1973-1974, we redirected the program. We established specific buoy mission objectives, simplified the buoy system designs, and established system reliability and cost goals. We managed the program, but we gave the job of meeting the various technical and cost requirements to industry, without a lot of red tape and government interference. We did not try to set up a group of government employees in a laboratory to carry out the development and demonstration of the equipment. Our first program was called the Prototype Environmental Buoy (PEB for short). The buoys in the PEB network performed well, and have continued to work effectively. Over the years, the NOAA moored buoy designs have been modified from those of the initial PEB designs, but the moored buoy network is still the major contributor of weather and sea-surface observational data from the near-shore marine areas. Buoys now provide about 10% of all surface weather observational data.

The moored buoy program was primarily intended to support weather forecasting. The PEB was not intended to respond to all bona fide data buoy users. Many oceanographic and special study needs, such as those involved in the climate program, were specifically not addressed by PEB. It was expected that add-on capability for certain of the later moored buoys and special buoys for particular purposes would be required. In response to part of the broader missions for buoys, simple drifting buoys and special polar buoys were developed to support some oceanographic, Arctic, and a few special research programs. The Global Atmospheric Research Program (GARP) Atlantic Tropical Experiment (GATE), the First GARP Global Experiment (FGGE), the Arctic Ice Dynamics Joint Experiment (AIDJEX), and the Equatorial Pacific Ocean Climate Studies (EPOCS) were specifically supported by drifting buoys. Ocean wave-measuring systems and other oceanographic capabilities were also developed as add-on systems for moored buoys. These capabilities were installed on moored buoys where they were needed most. Many of these programs are still under way and, in some instances, will require more developmental effort in the future. A family of buoys has now come into the inventory. Each of which has made its own contribution to increasing knowledge of the ocean's environment and behavior, and has led to further buoy improvements.



## PRESENT STATUS

After 10 years of operational experience, the costs of moored data buoy electronics have been greatly reduced and system reliability has been improved significantly. Data buoys now provide the standards for marine environmental data, especially weather and wave data. Data buoy observations and reports are the standard to which other marine information, such as ship and other occasional reports, are compared. Buoy observations have become vital to coastal and marine weather forecasting. When the reports are not received, operational weather forecasters make their views known. This is a good sign. It demonstrates the confidence that these users show in buoy data, and the important role buoys play.

Probably, the most significant information from the moored data buoy network is near real-time data on the intensity of storms at sea. Satellite data cannot provide these precise surface details, and ships often do not report weather observations, especially at night. Also, whenever possible, ships avoid storms at sea, but moored buoys, on the other hand, make observations regularly and report the weather--good or bad. This capability is appreciated not only by weather forecasters but by scientists as well. Today, the Interior Department's Minerals Management Service supports about as many buoys in the Pacific as does NOAA. All are operated by NOAA, however. The Department of Energy is also a strong data buoy or data buoy system supporter. Even the public is aware of data buoys. Last year, there was an attempt to eliminate two buoys from networks in both the Atlantic and Pacific. The general opposition to that proposal was heard all the way to Congress. The proposition was promptly dropped.

Drifting buoys initially made their mark in support of major scientific studies. However, in the Global Weather Experiment in 1979, and later in the Storm Transfer and Response Experiment (STREX), drifting buoys were also proven to be reliable and useful to operational weather forecasters as well as to oceanographers. I have heard that some of the oceanographic STREX drifting buoys "saved the day" winter before last, when a developing low in the Gulf of Alaska "crashed" the National Meteorological Center (NMC) forecast model. Reports from a few drifting buoys operating to support what was termed an "experiment" were used to characterize the storm situation sufficiently well to permit an adequate analysis of its intensity. After that event, the drifting buoy reports were closely watched.

So, there is now increasing utilization of drifting buoys for meteorological purposes. At the same time, drifting buoys are being used in the oceanographic studies, air/sea interaction studies, and even in pollution monitoring programs. Numerous agencies, including NOAA, the Marine Minerals Service, Navy, and NASA are using drifting buoys routinely, or experimenting with them on specific projects. Even the Agency for International Development (AID) is evaluating their use. These buoys have become effective working tools which can be deployed on global scales and which can acquire surface meteorological data, as well as ocean temperature measurements to a depth of several hundred meters. Drifting buoys had already shown promise in EPOCS and FGGE for making Lagrangian measurements of surface and subsurface ocean currents. Further work is planned to further develop and refine the current measurement capabilities of these buoys.

## FUTURE PROGRAMS

The future prospects for buoys and buoy technology is much brighter today, I believe, than it was during the late sixties when the national buoy program was formed. Users have now accepted buoys as an effective data collection and dissemination system. This was not true in the 1960s. Also, the scope of activity can be applied to various automated environmental observing and reporting systems. Since increasing costs of people observers are forcing automation of the observing and reporting functions not only at sea but also on land as well, the application of buoy technology will be extended to other environmental observing missions. Even at airports and other locations where people must be present, it probably is cost effective to automate the observation and reporting functions. Data buoy technology and the results of buoy development programs will be utilized for many land-based systems.

Even with the buoy improvements and network expansions to date, not all buoy requirements are being satisfied. Coastal populations are also increasing faster than those in most other areas. Offshore areas near the coastline are seeing more and more commercial and recreational activity. All of these trends point to emphasis on more precise and timely marine offshore and coastal weather and wave forecasts. To improve forecasts, additional observations are needed. A variety of different observing and reporting systems may contribute to the data collection programs that are likely to be employed, but buoy technology will probably be involved.

The role of drifting buoys can be expected to expand as well. International, as well as national, interest has been aroused by the potential of drifting buoys. New classes of drifters may be needed. As the requirements become more clearly identified, further development will be needed. The use of drifting buoy tracking technology is also used in nonbuoy applications and may expand.



## SUMMARY

In many respects, data buoys, buoy technology, and buoy program management techniques have become timely issues. Developments using satellite tracking and data relay have come in a timely manner. Innovative new potentials being offered by engineers are being adopted by users. Buoy systems are being bought, deployed, and used effectively. Buoy technology is also a cost-effective approach for numerous other automated environmental observing programs. This is being recognized and applied in several programs. The attendance at this symposium attests to the interests in buoys.

The management techniques and approaches that have been followed by NDBC in its buoy programs are also being used in other areas which result in cost savings to the American taxpayer. In summary, the potentials of these technical and management concepts are exciting and are beginning to be recognized. Buoy efforts are paying off, and the future of the buoy work looks bright.



# STORM WAVE CHARACTERISTICS IN THE GULF OF MEXICO

Ming-Yang Su and Mark T. Bergin

Naval Ocean Research and Development Activity  
NSTL Station, MS 39529

## ABSTRACT

Four statistical characterizations of ocean storm waves are presented and discussed:

- a) probability distributions of surface displacement;
- b) joint distribution of wave heights and periods;
- c) spectral bandwidth dependence of wave groups; and
- d) extreme wave groups.

From these evidence is found of the existence of strong nonlinear gravity wave instabilities.

## 1. INTRODUCTION

A serious threat to the operation of ocean environmental data buoys is that of wave action in storm seas. Frequently the greatest forces imposed on buoys in storm conditions are from waves rather than wind or currents, and are sometimes the cause of buoy capsizing (Hamilton, 1980). Obviously knowledge of the statistical description of storm seas is of importance in the design and deployment of buoys. At present, three environmental buoys deployed for the National Weather Service by NDBO are in service in the Gulf of Mexico.

In this paper is presented a summary of a comprehensive statistical analysis of storm seas in the Gulf of Mexico. Four main categories of wave characteristics considered here are (a) probability distributions of sea surface displacements; (b) joint and marginal distributions of wave heights and periods; (c) properties of wave groups; and (d) extreme wave groups. Dependence of these statistical characterizations on the bandwidth of the associated power (variance) spectra is emphasized in this investigation; bandwidth is parameterized by the spectral peakedness,  $Q_p$  (Goda, 1970), defined as:

$$Q_p = \frac{2}{m_0} \int_0^{\infty} f [E(f)]^2 df$$

where  $m_0$  is the zeroth moment of the power spectrum,  $E(f)$ ;  $f$  being the frequency. The sea surface elevation data utilized in this investigation were from measurements made by wave staff gauges mounted on an offshore oil platform in the Gulf of Mexico; water depth at the platform was 340 feet. A consortium of eight oil companies

sponsored the data collection during the years 1969 through 1971 (Ward, 1974). Nearly six hundred data records, each twenty minutes in length and with significant wave height,  $H_s \geq 2$  m (giving nearly 120,000 individual waves) is used. Included in the data set are recordings made during the passage of three hurricanes near the platform.

Several new features in the statistical analysis are noted that have not been previously reported in available publications. These features are attributed to manifestations of the nonlinear nature of finite-amplitude gravity waves, and have been under study in recent years (Su, 1982a, b and Su et al., 1982).

## 2. PROBABILITY DISTRIBUTIONS OF SURFACE DISPLACEMENT

The ocean surface can roughly be approximated by a stationary superposition of many wave components with different frequencies and random phases and propagation directions. Hence, from the Central Limit Theorem, the probability distribution of surface displacement  $P(\zeta)$  (where  $\zeta$  is the normalized surface displacement) should be nearly Gaussian. This basic theoretical expectation was confirmed from field data computations first by Kinsman (1960) (see also Phillips, 1977). Also, it was shown that the  $P(\zeta)$  was slightly skew towards negative  $\zeta$ , and could be fit better by the Gram-Charlier distribution as first proposed by Longuet-Higgins (1963). More recently Haver (1980) computed  $P(\zeta)$  for eight wave records obtained from rough seas in the North Sea; he concluded that all but one case was well represented by a Gaussian distribution. In general, our computations of  $P(\zeta)$  from Gulf of Mexico storm recordings agree with those of Haver. Furthermore, we have computed the  $P(\zeta)$  for three ranges of  $Q_p$ : (a)  $1.0 \leq Q_p < 2.0$ , (b)  $2.0 \leq Q_p < 3.0$ , and (c)  $3.0 \leq Q_p < 4.5$ . From these a weak dependence of  $P(\zeta)$  on  $Q_p$  was noted; the degree of skewness toward negative  $\zeta$  increasing with larger  $Q_p$ . This skewness is rather small even for the higher range of  $Q_p$  as evident in Figure 1 ( $3.0 \leq Q_p < 4.0$ ). Figure 2 gives  $P(\zeta)$  computed from five wave records made during Hurricane Camille, with  $H_s$



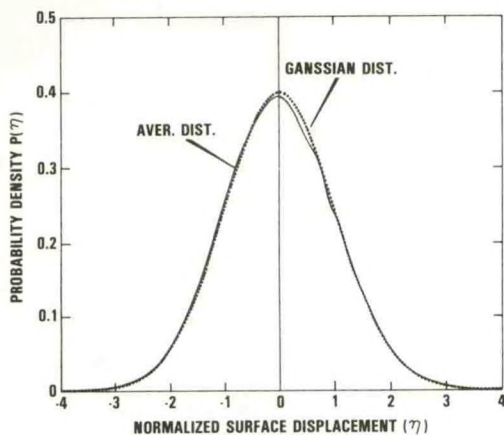


Fig. 1. The probability distribution of surface displacement,  $P(\eta)$ , for  $3.0 \leq Q_p \leq 4.0$ .

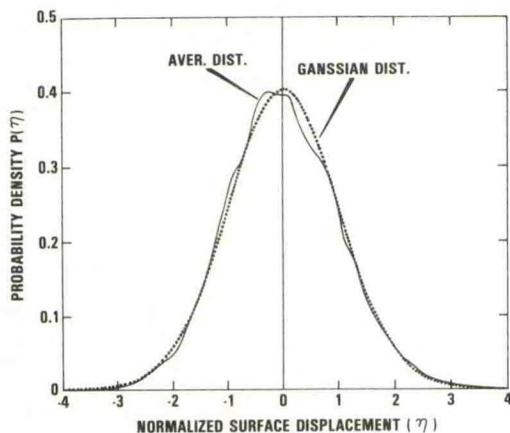


Fig. 2. The probability distribution of surface displacement,  $P(\eta)$ , computed from five wave records during Hurricane Camille, with  $H_s$  ranging from 9.6 to 13.7 m.

ranging from 9.6 to 13.7 m. Here a larger deviation of the measured  $P(\eta)$  from a Gaussian distribution is seen, with the major portion of the deviation occurring for  $|\eta| < 1.5$ , i.e. for higher frequency waves.

Quantitative measures of departure from a Gaussian distribution are the skewness ( $K_3$ ) and kurtosis ( $K_4$ ), defined as (Phillips, 1977):

$$K_3 = \frac{\overline{\eta^3}}{(\overline{\eta^2})^{3/2}}$$

$$K_4 = \frac{(\overline{\eta^4} - 3\overline{\eta^2}^2)}{2(\overline{\eta^2})^2}$$

Table 1 lists the average  $K_3$  and  $K_4$  from our computations together with those of Haver (1980) and, Huang and Long (1980, from the data of Kinsman, 1960).

The best agreement among the three cases was found to be between the Haver work and the present study, both of which are based on storm sea situations. Note that the waves of Kinsman's data were formed at low wind speed and short fetch.

### 3. JOINT DISTRIBUTION OF WAVE HEIGHTS AND PERIODS

The joint distribution,  $P(H,T)$ , of height,  $H$ , and period,  $T$ , of individual waves is an important statistical descriptor of sea state for many marine engineering purposes. Integrating  $P(H,T)$  with respect to  $T$  and  $H$  provides a direct computation of the marginal distributions of wave height,  $P(H)$ , and wave period,  $P(T)$ . The zero up-crossing method was used to derive individual waves from continuous sea surface elevation records.  $H$  and  $T$  are crest-to-trough wave height and wave period, normalized by, respectively, the r.m.s. of surface displacement and the average zero up-crossing period of each twenty minute record.

Figure 3 shows the joint distribution of height and period for all recordings with  $H_s \geq 2$  m. The equal density contour lines reveal a characteristic 'oyster shell' shape, with a mode (maximal density) located near  $H = 1.0$  and  $T = 0.505$ . For  $H > 4.0$  the  $P(H,T)$  is roughly symmetric about  $T = 1.28$ . This  $P(H,T)$  is found to be in good agreement with that presented by Cavanie et al. (1976) based on nearly 28,000 storm waves from the North Sea.

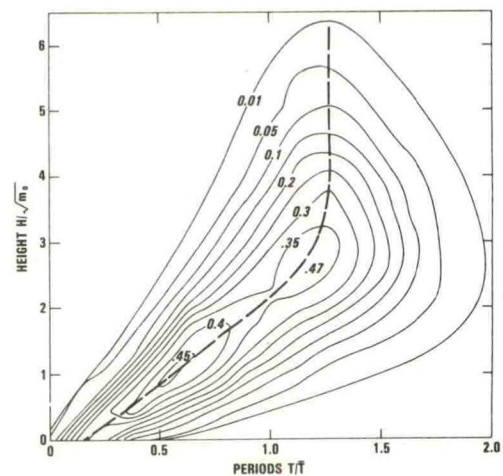


Fig. 3. The joint distribution of heights and periods for all recordings with  $H_s \geq 2$  m.

Table 1  
Skewness ( $K_3$ ) and Kurtosis ( $K_4$ ) of the  
Probability of Surface Displacement  $P(\eta)$

$Q_p$	Present Study (1983)				Kinsman (1960)	Haver (1980)
	1.0-4.5	1.0-2.0	2.0-3.0	3.0-4.5		
$K_3$	0.49	0.027	0.068	0.071	0.18	0.093
$K_4$	0.052	0.086	-0.039	-0.069	0.03	0.045



Figure 4 is the joint distribution of height and period for records with  $Q_p \geq 3.0$ , i.e. for more narrow spectra. Overall the shape of the  $P(H,T)$  contours is a narrower 'oyster shell' than Figure 3. A feature not, to our knowledge, recognized before is the second maximum appearing near  $H = 3.0$  and  $T = 1.2$ . In contrast, the  $P(H,T)$  for  $Q_p < 2.0$ , i.e. for wider spectra, is found to have broader contours and contain only one maximum.

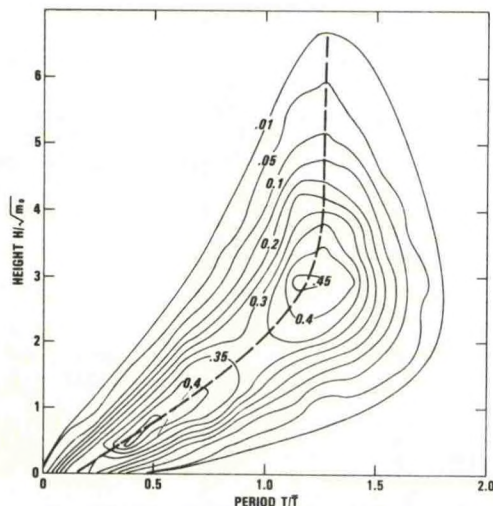


Fig. 4. The joint distribution of heights and periods  $P(H,T)$  for records with  $Q_p \geq 3.0$ .

The marginal distribution of wave period,  $P(T)$ , for various  $Q_p$  ranges is given in Figure 5. For  $Q_p \leq 2.0$   $P(T)$  is nearly symmetric about  $T = 1.0$ ; as  $Q_p$  increases the peak becomes progressively more skew toward  $T > 1.0$ . This asymmetry of  $P(T)$  about  $T = 1$  is also evident in the statistics presented by Cavanie et al. (1976), Goda (1978),

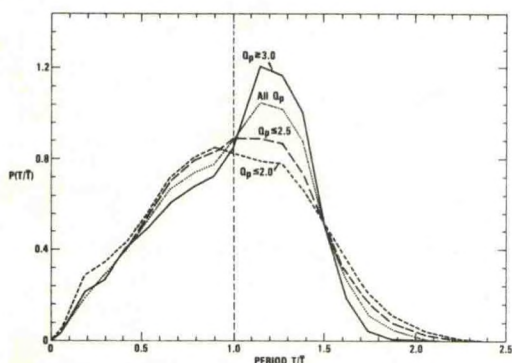


Fig. 5. Marginal distribution of wave period  $P(T)$  for various ranges of  $Q_p$ .

Kjeldsen and Myrhang (1979). Theoretical predictions of  $P(T)$  made by Longuet-Higgins (1975) and Cavanie et al. (1976), based on the assumption of a random linear Gaussian process, yield symmetric (Longuet-Higgins) or nearly symmetric (slightly skew toward  $T < 1$ , Cavanie et al.) distributions. Currently there is no theory available capable of explaining either the bi-modal characteristic of  $P(H,T)$  for narrow spectra, or the associated asymmetry.

The marginal distribution of wave heights,  $P(H)$ , has been computed for various ranges of  $Q_p$ . All are found to be quantitatively representable by a Rayleigh distribution, as has been frequently noted in the literature. As such they are not included here. See Forrestal (1978) and Longuet-Higgins (1980) for discussions on the  $P(H)$ .

#### 4. PROPERTIES OF WAVE GROUPS

A wave group is defined here to be a contiguous sequence of individual zero up-cross waves, all heights of which exceed the significant wave height,  $H_s$ . Direct observations indicate that higher waves occur more frequently in groups than singly. There are several methods that may be employed to quantitatively express the extent of wave 'groupiness'; we shall present several such measurements emphasizing their dependence on the spectral peakedness,  $Q_p$ .

In Figure 6 is presented the one-lag and two-lag correlation coefficient of successive wave heights. The coefficients ( $R_1$  and  $R_2$ ) are defined by:

$$R_n = \frac{1}{R_o(M-n)} \sum_{j=1}^{M-j} (H_j - \bar{H})(H_{j+n} - \bar{H})$$

where  $M$  is the number of individual waves in a given wave height record, and  $\bar{H}$  is the average

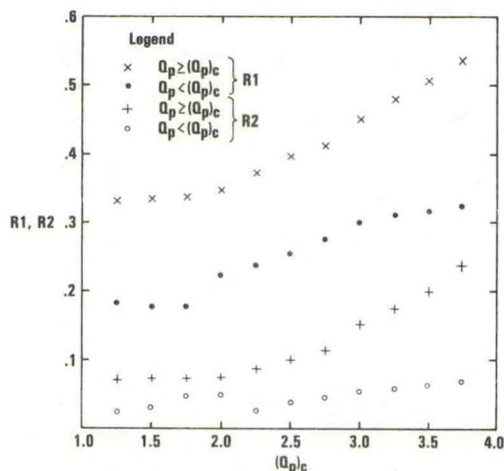


Fig. 6. The one-lag and two-lag correlation coefficients of successive wave heights,  $R_1$  and  $R_2$  for various ranges of  $(Q_p)_c$ .



wave height for the record. Both  $R1$  and  $R2$  are seen to be highly dependent on  $Q_p$ ;  $R1$  increasing from 0.18 to 0.54 as  $Q_p$  varies from 1.0 to 3.5, and  $R2$  increasing from 0.02 to 0.24 over the same range of  $Q_p$ .

The average number of successive individual waves exceeding the significant wave height is designated as  $\bar{L}_1$ , the mean group length. Variation of  $\bar{L}_1$ , with the spectral peakedness parameter is given in figure 7. Over the spectral range examined  $\bar{L}_1$  increases from about 1.3 to 1.7 as  $Q_p$  increases. In other words, two waves with height  $H > H_s$  are more likely to succeed one another in narrow spectra situations.

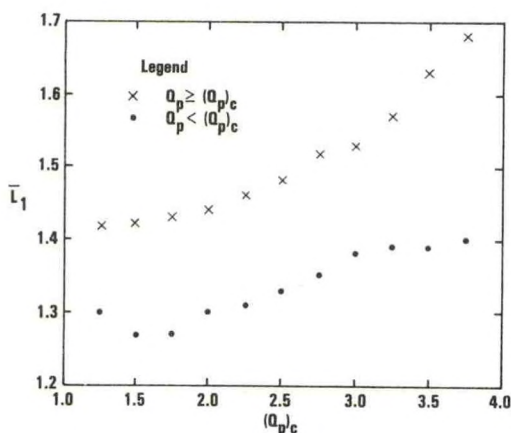


Fig. 7. The variation of the average mean group length,  $\bar{L}_1$ , vs. various ranges of  $(Q_p)_c$ .

Figure 8 gives the variation of the group length probability distribution for various ranges of  $Q_p$ . From these computations it is evident that for larger  $Q_p$  a higher likelihood exists that longer wave groups will be formed. Included on

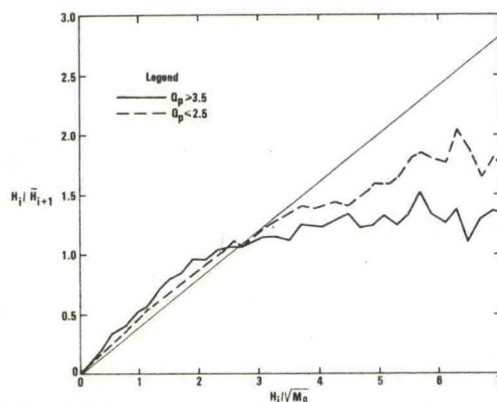


Fig. 8. The variation of the probability distribution of the group length  $P(L_1)$  for various ranges of  $Q_p$ .

The figure is the distribution derived under the assumption that successive waves are statistically independent and have wave heights following the Rayleigh distribution (Goda, 1970 and Rye, 1974). It is apparent from these curves that successive ocean waves do not exhibit independence.

Another measure of wave groupiness is the joint distribution of successive wave heights,  $P(H_i, H_{i+1})$ . For brevity we decline to show  $P(H_i, H_{i+1})$  but, instead, the conditional variation  $H_i/H_{i+1}$  vs.  $H_i$ , where  $\bar{H}_{i+1}$  is the average height of the wave immediately following some particular wave,  $H_i$ . For statistically independent successive waves this relationship would be linear. In the computations of  $P(H_i, H_{i+1})$  made with the ocean data (Figure 9) it is seen that wave records with smaller  $Q_p$  are more nearly linear, while for larger  $Q_p$  ( $\geq 3.5$ ) there is a considerable deviation from linearity for  $H_i > 4.0$ . That is, higher waves have a stronger successive wave height dependence, this tendency intensified with narrowing spectral bandwidth (increasing  $Q_p$ ).

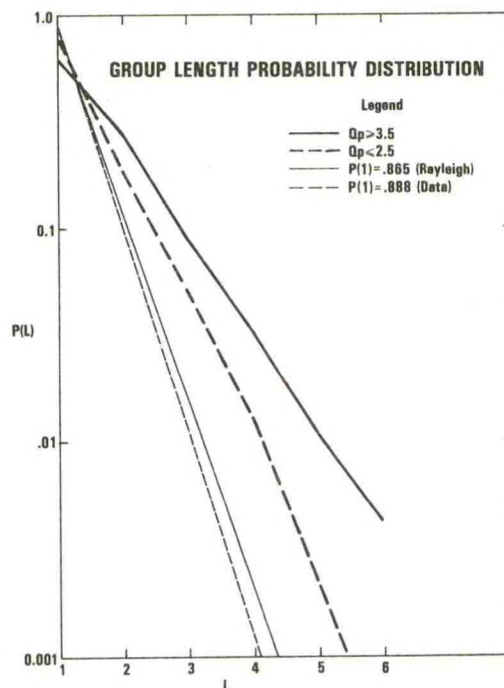


Fig. 9. The conditional variation of  $H_i/H_{i+1}$  vs.  $H_i/\bar{H}_0$  for various  $Q_p$ .

A more detailed discussion of wave group characteristics based on the Gulf of Mexico storm data has been given previously (Su, Bergin and Bales, 1982). In particular it was noted that no essential differences in wave group characteristics are evident when the wave growth and decay stages are compared, in contrast to a previous finding by Rye (1974).



## 5. EXTREME WAVE GROUPS

The extreme wave group (EWG) is a concept that combines the previously separately considered wave groups and extreme waves. We consider the EWG to be a more pertinent structural response parameter in certain situations. The EWG is defined as the wave group containing the largest wave height over some prescribed period of wave measurement (twenty minutes in this study). For convenience we express the EWG symbolically by:

$$W_i, \quad i = 0, \pm 1, \pm 2, \pm 3.$$

Where  $W_0$  is the wave with the largest wave height, the three negative subscripts indicating the waves immediately preceding  $W_0$  and the positive subscripts the waves immediately following  $W_0$ . The associated wave heights, periods, and steepnesses are expressed as  $H_i$ ,  $T_i$  and  $ak_i$

(steepness,  $ak_i$ , defined as the product of wave amplitude,  $1/2H_i$ , and wave number  $k_i$ ).

The averages of  $H_i$ ,  $T_i$  and  $ak_i$  for the extreme wave groups are given in Table 2. Note that:

- $\overline{H_{-1}}, \overline{H_{+1}}$  ( $\approx 3.8$ ) and  $\overline{H_0}$  ( $\approx 6.32$ ) exceed  $\overline{H_2}$ ,  $\overline{H_3}$  and,
- $\overline{T_{-1}}, \overline{T_0}, \overline{T_{+1}}$  ( $\approx 1.34$ ) exceed  $\overline{T_2}, \overline{T_3}$  ( $\approx 1.1$ ).

Also, it is noted that the average wave height  $\overline{H_i}$  equals 2.51 for the entire data set.

Table 2  
Statistics of Extreme Wave Groups  
( $H_s > 2$  m, All  $Q_p$ )

i	-3	-2	-1	0	1	2	3
$\overline{H_i}$	2.50	2.74	3.83	6.32	3.88	2.67	2.41
$\overline{T_i}$	1.04	1.10	1.32	1.35	1.34	1.12	1.03
$\overline{ak_i}$	.159	.139	.130	.194	.126	.145	.141

The concave upward shape of the envelope of  $\overline{H_i}$  ( $i = 0, \pm 1, \pm 2, \pm 3$ ) implies that the EWG cannot be the result of a beat phenomenon due to the linear superposition of two sinusoidal waves of slightly different wavenumber. Note that  $\overline{ak_0}$  (0.194) is much larger than  $ak$  (0.15), while  $\overline{ak_{-1}}$  (0.13) and  $\overline{ak_{+1}}$  (0.126) are smaller than  $ak$ . The average  $ak$  for  $W_{-1}, W_0$  and  $W_1$  is, however,  $(0.13 + 0.19 + 0.126) = 0.15 = \overline{ak}$ . The above statistics imply that the extreme wave group consists of only three consecutive waves,  $W_{-1}, W_0$ , and  $W_1$ , in the mean. These features of the EWG wave parameters,  $\overline{H_i}, \overline{T_i}$  and  $\overline{ak_i}$  have striking similarities to the characteristics of wave groups resulting from strong nonlinear dynamics observed in laboratory experiments (Su, 1982b).

## 6. CONCLUDING REMARKS

We have presented a short summary of four statistical characterizations of storm wave data collected in the Gulf of Mexico. Of these, the joint distribution of wave heights and periods, and the extreme wave groups contain evidence of the strongly nonlinear behavior of ocean waves in storm seas. It is felt that many wave groups may be attributed to instability-induced modulation rather than to the generally accepted classical linear beats phenomena. More extensive analyses and results on storm waves shall be reported in the future.

## 7. ACKNOWLEDGEMENT

We are indebted to the eight oil companies headed by Shell Development Company for making available to us the wave data analyzed in this paper. We would like to thank Dr. A.W. Green for his helpful suggestions in improving the first manuscript.

## 8. REFERENCES

- Cavanie, A. M. Arhan and Ezraty. 1976. A statistical relationship between individual heights and periods of storm waves. BOSS '76, pp. 354-360.
- Forristall, G.Z. 1978. On the statistical distributions of wave heights in a storm. J. Geophys. Res. 83, pp. 2353-2358.
- Goda, Y. 1970. Numerical experiments on wave statistics with spectral simulation. Rept. Port and Harbour Res. Inst., Vol. 9, No. 3, pp. 3-57.
- Goda, Y. 1978. The observed joint distributions of periods and heights of sea waves. Coastal Engineering Conf., 1978. pp. 227-246.
- Hamilton, G.D. 1980. Buoy capsizing wave conditions. Marine Weather Log. 24(3), pp. 165-175.
- Haver, S. 1980. Analysis of uncertainties related to the stochastic modelling of ocean waves. Report. The University of Trondheim, Division of Marine Structures.
- Huang, N.E. and S.R. Long. 1980. An experimental study of the surface elevation probability distribution and statistics of wind-generated waves. J. Fluid Mech., 101, pp. 179-200.
- Kinsman, B. 1960. Surface waves at short fetch and low wind speed - a field study. Chesapeake Bay Institute, John Hopkins Univ. Tech. Rep. No. 19.
- Kjeldsen, S.P. and D. Myrhaug. 1979. Formation of wave groups and distributions of parameters for wave asymmetry, VHL Report No. STF 60 A79044, River and Harbour Laboratory, Trondheim.



10. Longuet-Higgins, M.S. 1963. The effect of nonlinearities on statistical distributions in the theory of sea waves. *J. Fluid Mech.*, 17, pp. 459-480.
11. Longuet-Higgins, M.S. 1975. On the joint distribution of the periods and amplitudes of sea waves. *J. Geophys. Res.* 80, pp. 2688-2694.
12. Longuet-Higgins, M.S. 1980. On the distribution of the heights of sea waves: some effects of nonlinearity and finite bandwidth. *J. Geophys. Res.* 85, pp. 1519-1523.
13. Phillips, O.M. 1977. The Dynamics of the Upper Ocean. Cambridge University Press.
14. Rye, H. 1974. Wave group formation among storm waves. *Proc. 14th Coastal Engineering Conf.*, Vol. 1, pp. 164-183.
15. Su, M.Y. 1982a. Three-dimensional deep-water waves. Part 1. Experimental measurement of skew and symmetric wave patterns. *J. Fluid Mech.*, 124, pp. 73-108.
16. Su, M.Y. 1982b. Evolution of groups of gravity waves with moderate to high steepness. *Phys. Fluids*, 25, pp. 2167-2174.
17. Su, M.Y., M. Bergin, P. Marler and R. Myrick. 1982. Experiments on nonlinear instabilities and evolution of steep gravity wave trains. *J. Fluid Mech.*, 124, pp. 45-72.
18. Su, M.Y., M. Bergin and S. Bales. 1982. Characteristics of wave groups in storm seas. *Proc. Ocean Structural Dynamics Symposium '82*. Corvallis, Oregon, pp. 118-132.
19. Ward, E.G. 1974. Ocean Data Gathering Program - An Overview. *Offshore Tech. Conf.*, pp. 771-780.



COMPARISON OF NDBO WAVE SPECTRA WITH OUTPUT OF THE FLEET NUMERICAL OCEANOGRAPHY  
CENTER OPERATIONAL GLOBAL SPECTRAL OCEAN WAVE MODEL

Sheldon Lazanoff<sup>1</sup>  
Jack Kaitala<sup>2</sup>

<sup>1</sup> Science Applications, Inc., 205 Montecito Avenue, Monterey, CA 93940

<sup>2</sup> Fleet Numerical Oceanography Center, 40 Dept., Monterey, CA 93940

ABSTRACT

Fleet Numerical Oceanography Center (FNOC) has been using the Spectral Ocean Wave Model (SOWM) since 1974 to produce Northern Hemisphere real-time operational wave spectral analyses and forecasts to 72 hours. The SOWM outputs are transmitted to both Navy and civilian users.

A new Global SOWM (GSOWM), which is scheduled to replace the SOWM, is presently undergoing operational evaluation. GSOWM wave spectra need to be compared to wave spectra transmitted in real time from the NOAA Data Buoy Center (NDBC) wave buoys in order to determine if the GSOWM has skill. Some examples are shown. Wind velocities which are the forcing functions of the GSOWM are being compared to wind velocities from the buoys. The FNOC verification plan is discussed. Comparisons between NDBC and GSOWM one-dimensional wave spectra are shown. A discussion of potential problems is presented.

1. INTRODUCTION

Since 1974 FNOC has been using the SOWM to produce real-time operational deep-water two-dimensional wave spectral analysis/forecasts in the Northern Hemisphere (Lazanoff and Stevenson, 1974).<sup>1</sup> The SOWM was originally developed under the direction of Professor Willard J. Pierson. The SOWM output is available to both navy and civilian users. For example, two private meteorological/oceanographic forecasting firms routinely use SOWM data as integral parts of their oceanographic forecasts.

The SOWM is scheduled to be replaced by a newer global SOWM (GSOWM) which is beginning to undergo operational evaluation at FNOC. The significant differences between the SOWM and GSOWM are listed in Table 1. The GSOWM, as a computer model, is expected to produce more accurate analyses and forecasts than the SOWM but this has not been clearly demonstrated. Comparisons between the GSOWM, SOWM and buoy wave spectra are required to determine which model produces more accurate output. The buoys which will be used for comparison are shown in Figure 1. The proximity of the coast to

buoys 46010, 46011, and 46012 will be considered when using their output. In this paper some comparisons between GSOWM and NDBC buoy wave spectra will be shown.

Wind inputs to the GSOWM will be compared to the wind velocity measured by the buoys since any wave analysis/forecasting model, no matter how sophisticated, can only be as accurate as the input to the model. Wind velocity and frictional wind speed are the only inputs to the SOWM and GSOWM. At FNOC the wind data are obtained by following the sequence of events shown in Figure 2. Prior to January 1983 an atmospheric primitive equation model (PEM) developed at the Naval Postgraduate School was used for computing the required input to the planetary boundary layer (PBL) wind model. Now FNOC uses the new Navy Operational Global Atmospheric Prediction System (NOGAPS), developed by Professor Arakawa of UCLA and adapted for navy use by the Navy Environmental Prediction Research Facility (NEPRF), to produce the meteorological fields. Although specific differences between the two atmospheric models will not be discussed, one point must be considered in terms of wave model accuracy. The developers of NOGAPS have proven that NOGAPS, as a meteorological model, is more accurate than the PE model which will be reflected in the accuracy of the GSOWM or SOWM. These idiosyncrasies need to be identified. For example, the study of Osburn (1972)<sup>2</sup> demonstrated that the phase speed of the low pressure systems propagated by the PE model was too slow. This type of information will be acquired for NOGAPS.

The point of the above discussion is to illustrate that the evaluation of the GSOWM cannot be limited to comparing wave spectra. The wind input to the wave models need to be analyzed in context to the atmospheric model which provided the initial input.

2. WIND INPUT

In the past long term comparisons between the wind data derived from the PE model and accurately measured wind data were not done. Several studies have been done for short time periods. Friehe and Pazan (1978)<sup>3</sup> compared FNOC wind fields to data from a buoy located at 35°N, 155°W for the time period of 18 October 1974 to 19 November 1974. Friehe and Pazan computed a mean square difference



of 6.9 m/s between buoy and FNOC computed wind speeds so that the difference in buoy and computed wind speeds did not exceed 2.6 m/s with 68% confidence. The average difference in wind direction was approximately  $3^{\circ} \pm 20^{\circ}$ . These comparisons were only for one point and could not be generalized to other points.

The intent of FNOC is to do long-term comparisons between the GSOWM wind data and the buoy winds. Comparisons such as shown in Figures 3 and 4 will be done on a continuing routine basis. The buoy winds are corrected to 19.5 m which is the height of the computed GSOWM winds. For this study the GSOWM winds were computed for neutral stability. In the future the winds will be corrected for air-sea stability. This is important because for a given wind speed, waves grow faster and larger in unstable conditions than in stable conditions. As of this writing a total of 72 comparisons were made for 7 buoys. The total mean difference between the buoy wind speeds and the GSOWM wind speeds is -1.33/sec. The RMS spread is 2.85 m/s. The mean difference between buoy and the GSOWM wind directions is  $4^{\circ}$  with a RMS spread of  $34^{\circ}$ . If the five largest differences (greater than an absolute value of  $70^{\circ}$ ; none of the other differences were greater than  $43^{\circ}$ ) in directions are removed, the mean difference remains basically the same but the RMS spread reduces to  $22^{\circ}$ .

Obviously, it is difficult to make conclusions from such a small sample; however, some points can be made. After removing the five largest differences in wind direction comparisons, the mean directional difference and RMS spread seems to indicate that the atmospheric model is generally moving the surface pressure systems at the correct phase speed and the pressure systems have the proper shape. This is probably not true when the differences were large. Four of the large differences occurred for buoy 46004 which is located at 50.9N, 135.9W. Since as seen in Figure 1, buoy 46004 is located in the open ocean near buoy 46003, located at 46.1N, 131.0W, whose directions compared much more favorably to the GSOWM wind direction, further investigation is required before the source of the problem can be determined.

In the cases where the wind directions compared favorably, it is quite obvious that the GSOWM wind speeds are consistently higher than the buoy wind speeds. Even correcting for stability, the GSOWM wind speeds would remain high. Regression lines are plotted on Figures 3 and 4 to indicate how the buoy wind speeds can be used to correct the analyzed GSOWM wind speeds for individual grid points. Our plan is to adjust the roughness length used in the GSOWM wind model. This will make the correction uniform for the entire model and will take stability into account.

One interesting point that we discovered in preparing this paper is that the buoy wind data, unlike other sources of wind data, are not being adjusted correctly for stability and anemometer height in preparation

for input into the FNOC atmospheric analysis models. The omission apparently first occurred when the buoy message format was changed several years ago. An effort is now being made to correct this oversight.

### 3. WAVE SPECTRAL COMPARISONS

The original intent of this paper was to show a statistical comparison between buoy wave spectra and GSOWM wave spectra; however, several problems occurred which have limited this portion of the study. The problems include the installation of the operational GSOWM on a new state-of-the-art vector computer and the installation of a new operational atmospheric analysis/forecasting model on the new computer. The operational GSOWM had been programmed for the CDC CYBER 203 computer which was located at FNOC. The CYBER 203 computer and its system software were replaced by a CYBER 205 computer and new system software at the end of 1982. Errors in the new system software have impeded the implementation of the GSOWM on the CYBER 205 computer. Changing from one operational atmospheric model (PEM) to another (NOGAPS) also caused delays. As of this writing the final preparations of placing the GSOWM in an operational evaluation mode on the computers are being completed. Several test runs have been made. Examples of real-time comparisons between GSOWM and NDBC wave spectra are shown in Figures (5) and (6). The comparisons were made after two time steps (6 hours). Since the GSOWM was initiated with zero wave energy in each case, there was insufficient time to allow low frequency energy to propagate throughout the grid system. This is readily obvious in Figures (5) and (6). The wind wave portion of the spectra compare quite favorably when the wind speeds are comparable as seen in Figure 5. The wind wave spectra do not compare favorably when the wind speeds are not comparable as seen in Figure 6.

FNOC plans to do these types of comparisons on a continuous real-time basis for all available buoy data. FNOC will compare significant wave heights, model periods, and spectral shapes. The spectral shapes will be used to evaluate the wind wave growth algorithms and swell energy propagation calculations.

### 4. CONCLUSIONS

The GSOWM will undergo operational evaluation for a 3-6 month period. The NDBC buoys provide the major source of comparative wind and wave data. After the GSOWM winds have been adequately adjusted to match the buoy winds, then the wave spectra will be compared. If it can be proven that the GSOWM is superior to the SOWM as an analysis/forecasting model, then the GSOWM will replace the SOWM as the FNOC operational model. Even after the GSOWM is operational, the comparisons will continue to be made on a real-time basis so that confidence limits can be developed for the forecasts. Also, the comparisons will be used to indicate areas where the GSOWM can be improved. As buoy two-dimensional wave spectra become available, these data will be used for comparison.



Finally, at the present time there aren't any next generation wave models being developed within the navy system to replace the GSOWM. By obtaining long-term comparisons Navy researchers will have some indication as to which direction they should be headed in the development of new wave analysis/forecasting models.

#### 5. REFERENCES

1. Lazanoff, S. and N. Stevenson. An Evaluation of a Hemispheric Operational Wave Spectral Model, Fleet Numerical Oceanography Center Technical Note 75-3, June 1975.
2. Osburn, J. An Evaluation of 36-hour forecasts of Small Scale Disturbances (SD) at 500 mbs for Nov 1971, Fleet Numerical Oceanography Center Internal Communication, January 1972.
3. Friehe C. and S. Pazan. Performance of an air-sea interaction buoy, Journal of Applied Meteorology, pp 1488 - pp 1497, October 1978.



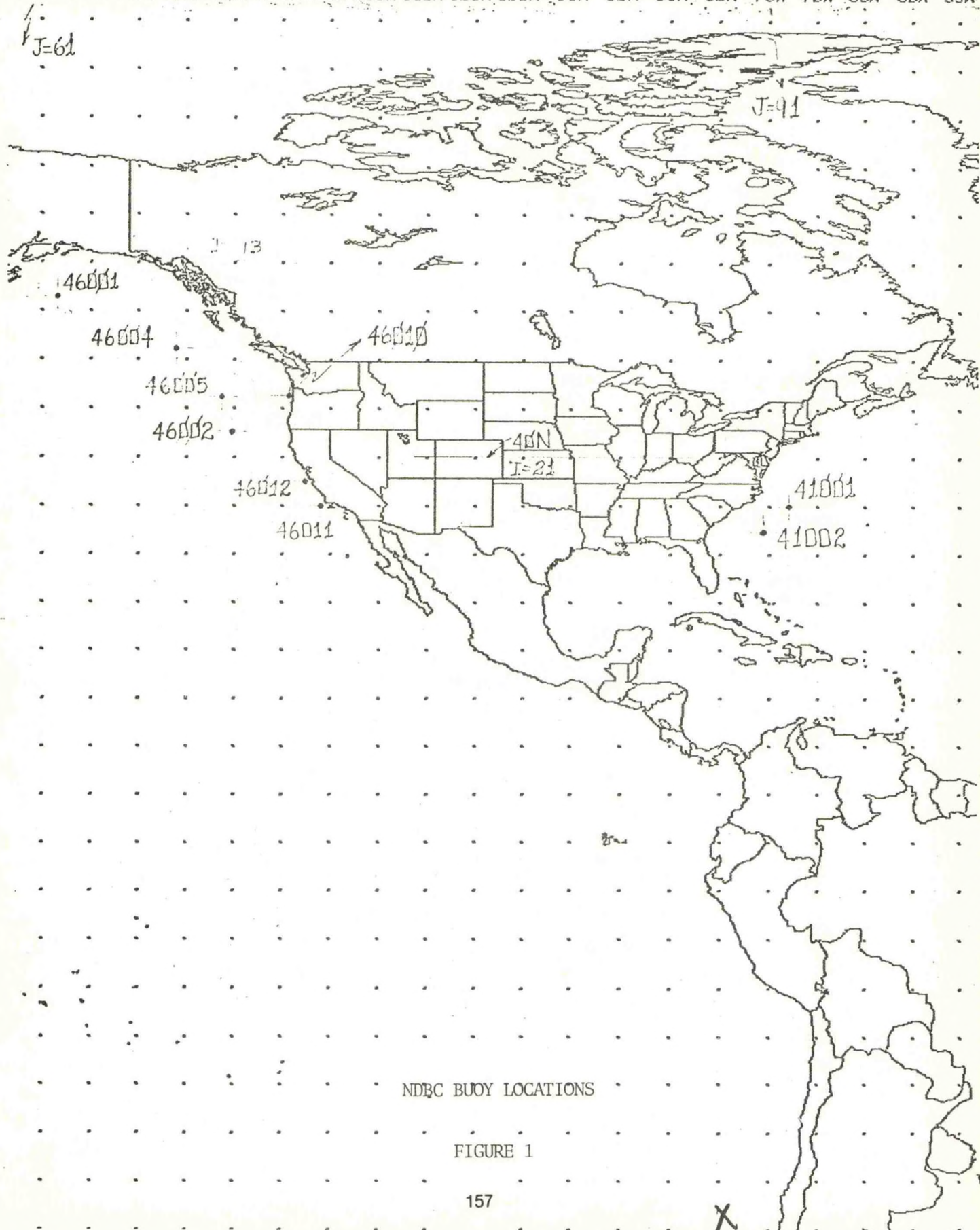
	SOWM	GSOWM
PBL WIND INPUT	EVERY 6 HOURS	EVERY 3 HOURS
MODIFIED MILES-PHILLIPS GROWTH EQNS	YES	YES
GROWTH LIMITED BY PIERSON- MOSKOWITZ FULLY DEVELOPED SPECTRA	YES	YES
WAVE ENERGY DISTRIBUTED BY SWOP MECHANISM DURING GROWTH CYCLE	OVER 6 DIRECTIONS	OVER 12 DIRECTIONS
WAVE-WAVE INTERACTION TERM OR OTHER NON-LINEAR TERMS	NO	NO
WAVE SPECTRA REPRESENTATION	15 FREQUENCIES BY 12 DIRECTION (30° DIRECTION BANDS)	15 FREQUENCIES BY 24 DIRECTION (15° DIRECTION BANDS)
TIME STEP	3 HOURS	3 HOURS
GRID SYSTEM	ICOSAHEDRAL GNOMONIC PROJECTION	SPHERICAL GRID
MESH LENGTH	100-180 NAUT. MILES	2.5° BY 2.5°

DIFFERENCES BETWEEN SOWM AND GSOWM

TABLE 1



150W 145W 140W 135W 130W 125W 120W 115W 110W 105W 100W 95W 90W 85W 80W 75W 70W 65W 60W 55W



NDBC BUOY LOCATIONS

FIGURE 1



	OLD FNOC SYSTEM	NEW FNOC SYSTEM
<u>SYSTEM</u>	<u>NORTHERN HEMISPHERIC</u>	<u>GLOBAL</u>
1. Atmospheric Analysis	FNOC Surface Pressure Marine Winds FNOC Upper Air -	FNOC Surface Pressure Marine Winds NOGAPS Upper Air PBL
2. Atmospheric Forecast	PEM Surface Pressure Upper Air -	NOGAPS Surface Pressure Upper Air PBL
3. Marine Boundary Layer Analysis and Forecast	PBLNH Surface Fluxes Winds	GSCLI Surface Fluxes Winds
4. Wind-Wave Model	SOWM	GSOWM

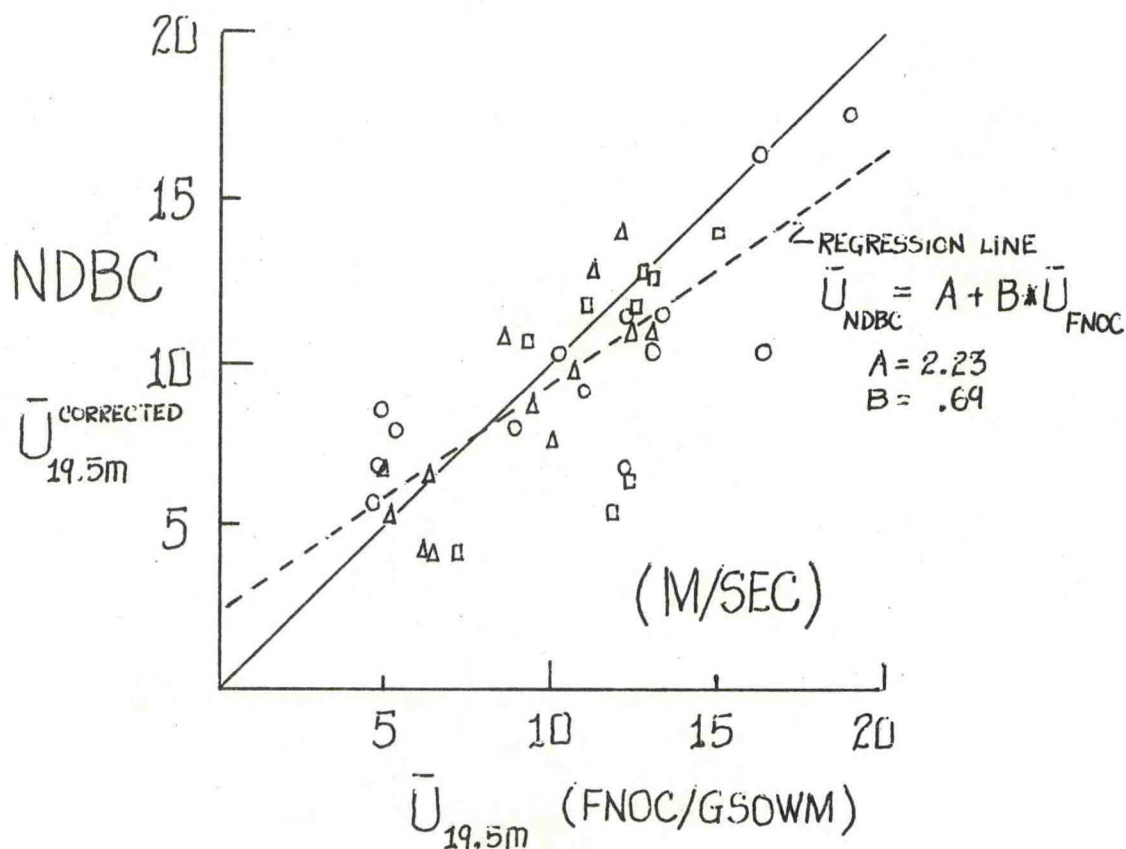
PBLNH - Planetary Boundary Layer, Northern Hemisphere  
GSCLI - Global Surface Contact Layer Interface

FNOC WIND-WAVE MODEL SYSTEMS:  
A Sequential Tabulation of Principal Components

FIGURE 2

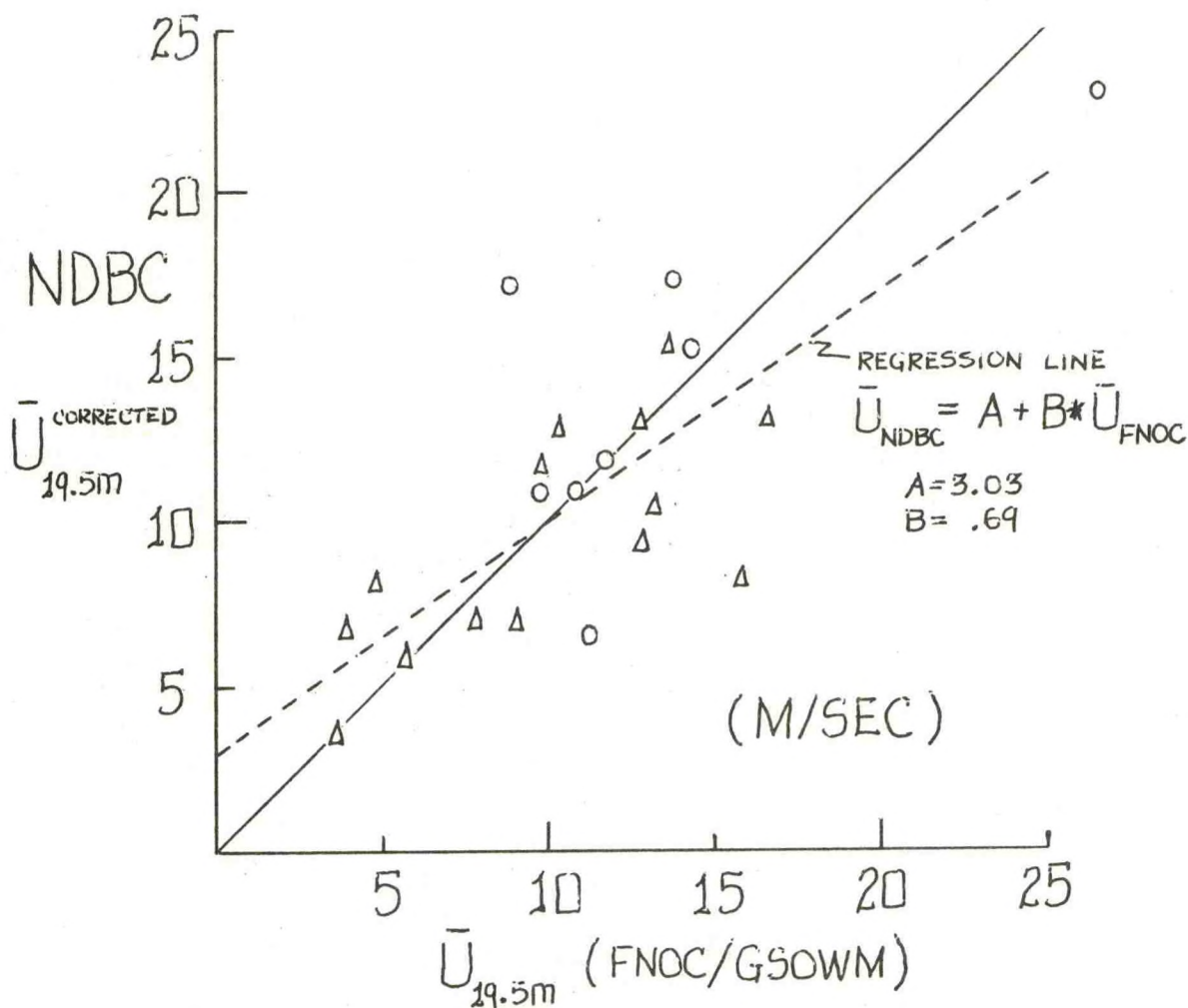


Symbol	NDBC	Samples
○	46002	14
△	46004	13
□	46005	9





Symbol	NDBC	Samples
o	41001	8
Δ	41002	14



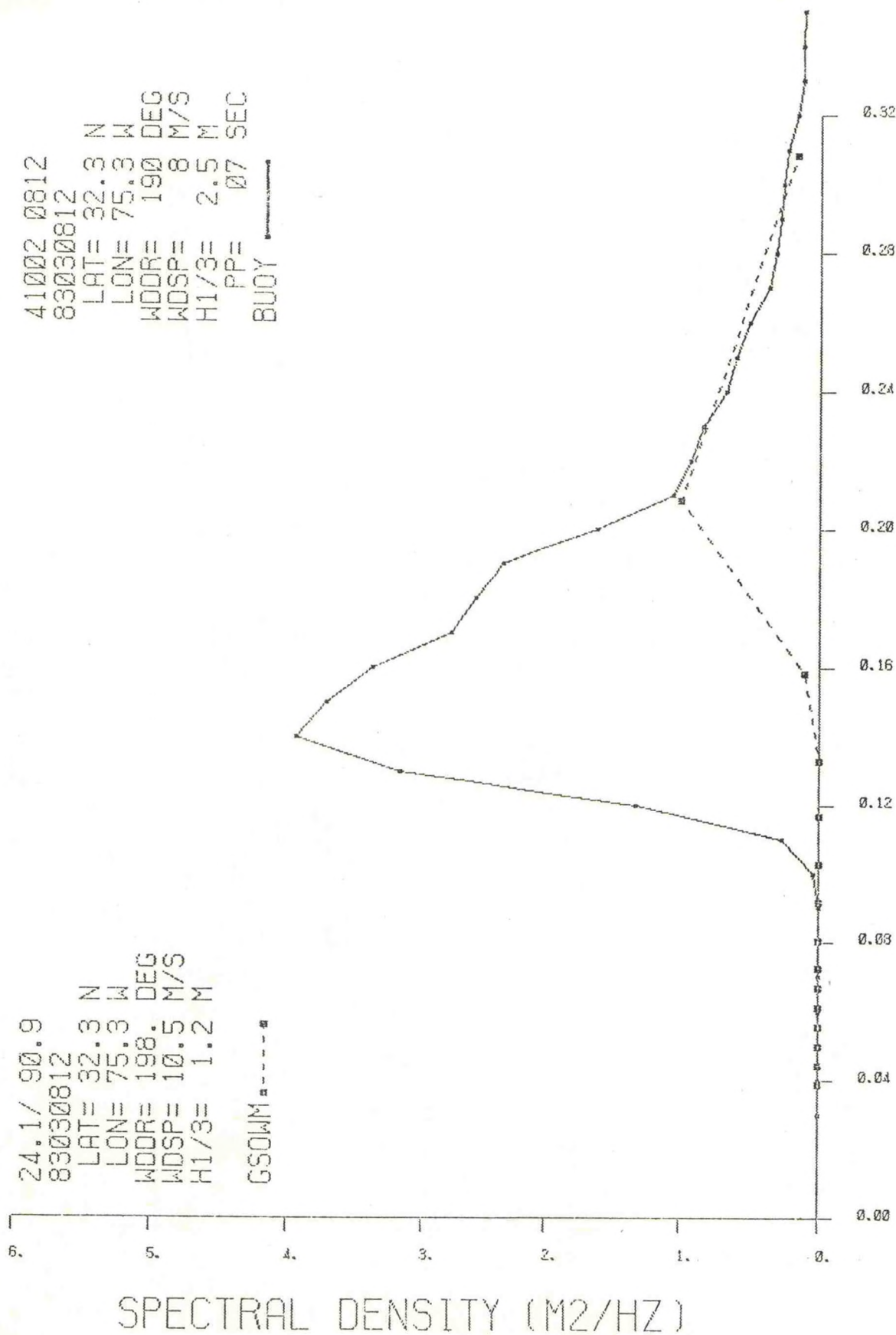
PLOT OF NDBC WIND SPEEDS (CORRECTED TO 19.5 METER ANEMOMETER HEIGHT) vs  
 FNOG 19.5 METER GSOWM WINDS FOR 2 DEEP WATER BUOYS  
 EAST OF THE GULF STREAM  
 Samples Drawn from the Period: 19 Nov 82-7 Mar 83

FIGURE 4



24.1/ 90.9  
 83030812  
 LAT= 32.3 N  
 LON= 75.3 W  
 WDR= 198. DEG  
 WDSP= 10.5 M/S  
 H1/3= 1.2 M  
 GSOWM -----

41002 0812  
 83030812  
 LAT= 32.3 N  
 LON= 75.3 W  
 WDR= 190 DEG  
 WDSP= 8 M/S  
 H1/3= 2.5 M  
 PP= 07 SEC  
 BUOY -----



WAVE SPECTRAL COMPARISON

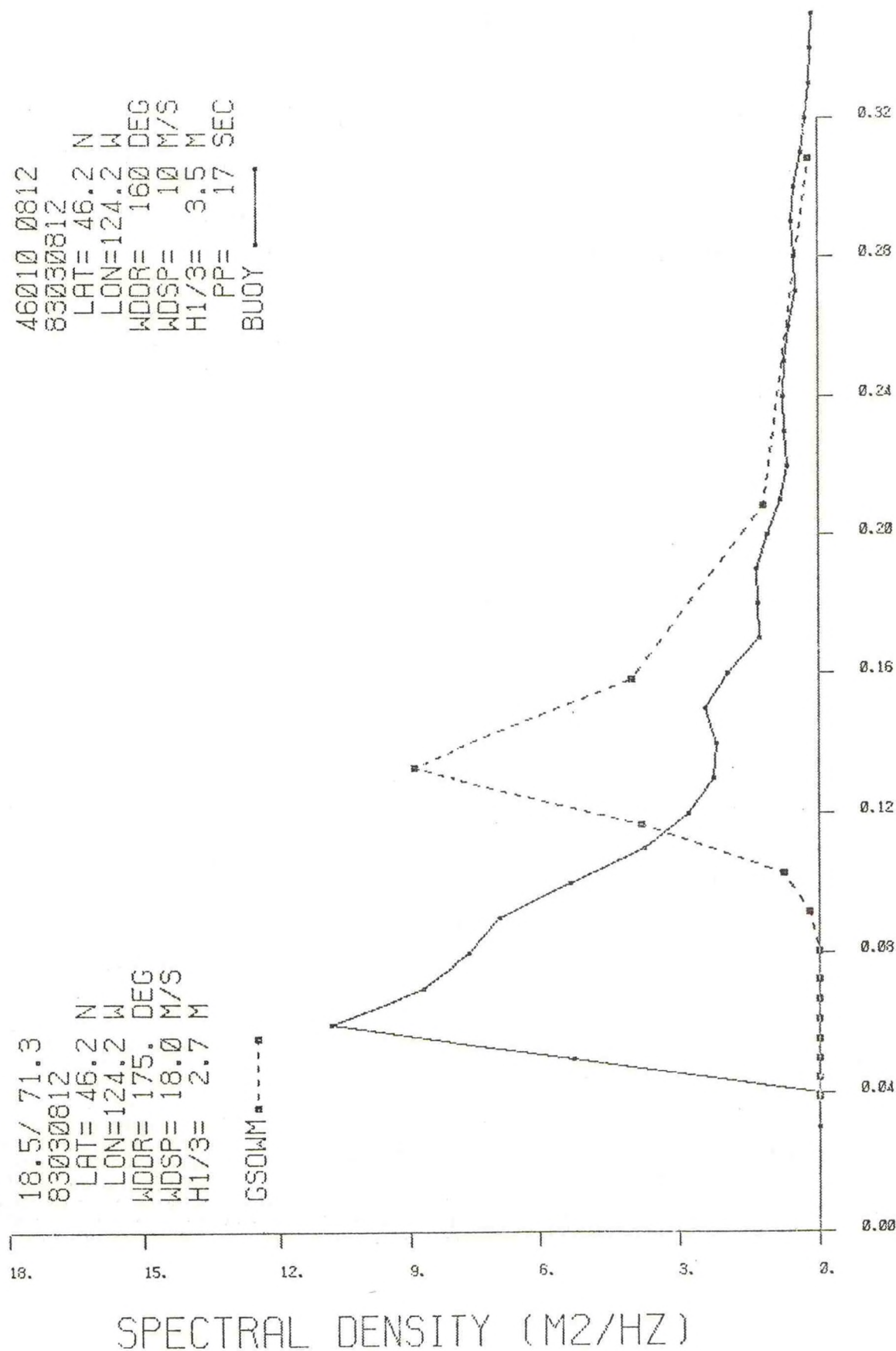
FIGURE 5



18.5/ 71.3  
83030812  
LAT= 46.2 N  
LON=124.2 W  
WDR= 175. DEG  
WDSP= 18.0 M/S  
H1/3= 2.7 M

GSONW ---■---

46010 0812  
83030812  
LAT= 46.2 N  
LON=124.2 W  
WDR= 160 DEG  
WDSP= 10 M/S  
H1/3= 3.5 M  
PP= 17 SEC  
BUOY ---



FREQUENCY (HZ)

WAVE SPECTRAL COMPARISON

FIGURE 6



# THE WAVE DATA ANALYSIS FUNCTION AS PERFORMED IN DATA ACQUISITION AND TELEMETRY SYSTEMS

Roland C. Fritts, Magnavox Electronic Systems Company, Fort Wayne, Indiana  
Commander Dennis W. Mahar, United States Coast Guard, NOAA Data Buoy Center, NSTL Station, Mississippi

## ABSTRACT

Magnavox Electronic Systems Company (MESOC) is presently involved with the development of a Wave Data Analyzer (WDA) function to be implemented in the Data Acquisition Control and Telemetry (DACT) systems. The wave data analysis function is basically partitioned in the DACT System in the following manner:

- (1) A 6-pole butterworth filter function is performed on the WDA card.
- (2) The data is digitized by the DACT analog to digital converter and passed to the WDA card.
- (3) The WDA card performs a direct, FFT based spectrum analysis of the displacement data and calculates values of wave height, wave period, and other required data.
- (4) The WDA card presents the processed data to the main processor in the DACT System at regular intervals to be formatted for output.
- (5) The DACT will include this data in modem and transmitted data messages on request or at regular synoptic intervals.

This paper contains a detailed description of the means of data collection, data processing, and data formatting for the WDA function in the DACT System.

## INTRODUCTION

The Wave Data Analyzer (WDA) function as implemented in Data Acquisition Control and Telemetry (DACT) systems has a dual purpose. The DACT/WDA systems will provide general wave information to the National Weather Service as well as specific wave information to be used by the scientific community. Figure 1 is a block diagram of the DACT/WDA function.

The DACT System is a weather data collection platform which has been developed for NOAA Data Buoy Center (NDBC). This device collects weather data at regular intervals, formats the data in ASCII, and transmits the data via satellite. If the DACT System is installed on or close to land, and has a land line, then the weather data can be accessed via telephone.

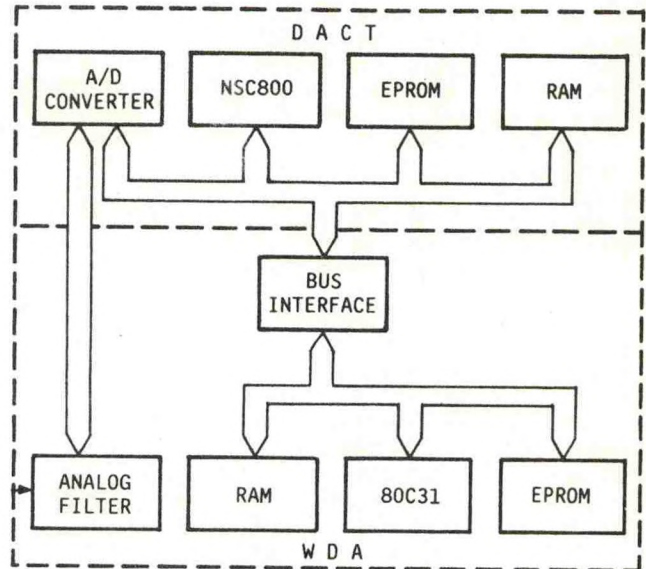


FIG. 1. DACT/WDA Functions

The DACT System is user programmable. The user can enable/disable sensor inputs, adjust scaling values, set or read the DACT time, change the transmit time, change the data acquisition characteristics, and command system self-tests from a terminal connected to the DACT's RS-232 input. If the DACT System is connected to a land line, then these functions can also be accessed via the telephone.

The WDA card is a plug-in option to the DACT System which will enable the system to collect and process wave data. The output of the WDA card will be specific wave characteristics as well as spectral density information. The spectral density information that will be outputted will be the power spectrum estimates for frequencies from 0.03 to 0.40 Hz in 0.01-Hz increments. To generate the output data, the WDA card will be collecting wave information in a 0 to 0.5-Hz bandwidth at a 2.56-Hz sample rate. This data will be FFT processed in overlapped, 256 sample data blocks. The specific wave characteristics (peak wave height, significant wave height, and wave period) will be generated from the spectral density output.



The card has programmable features. The WDA card can be programmed with different lengths of data averaging and to process data from different buoy hull types. The WDA card can also be enabled or disabled as a programming feature.

The DACT System can also initiate a Built-in-Test (BIT) function within the WDA card which tests itself and returns the test status to the DACT for display.

#### WDA REQUIREMENTS

The method of implementation of the WDA function within the DACT System was driven by several special requirements. One of the requirements is that the hardware to implement the WDA function could only use one card slot within the DACT System. This requirement prompted the utilization of the DACT's data collection capabilities to collect and digitize the data for the WDA card. This eliminated the need for an A/D converter and support logic to be included on the WDA card. Another requirement of the WDA function is that it produce spectral information with the same or better accuracy than WDA systems presently in operation. However, WDA systems presently in operation process the wave data using an autocovariance estimation technique and pass the autocovariance data (via transmitter) to a larger computer system for further processing. The DACT/WDA function is required to use an FFT processing approach and perform all of the processing within the DACT System. With all the processing done in the DACT System, the processed wave information received from the DACT, by either land line or satellite, would be ready for use by the NWS without further processing. The WDA function was also to be implemented such that expansion of the WDA function to a Directional Wave Data Analyzer (DWDA) function could be implemented without major changes to the basic data collection and processing structures.

#### ANALOG FILTERING

The DACT System receives analog signals from the wave sensor (Wave Staff or accelerometer) via the sensor junction box. The analog signal enters the DACT Electronics Unit (DEU) and the WDA card where it is passed through a 6-pole Butterworth low-pass filter to reduce the effect of aliasing on the sampled data. This filter has a -3 dB cutoff point at 0.5 Hz, after which it drops off at a rate of -120 dB/decade. The filtered analog signal is then scaled to a range acceptable to the analog bus, and passed to the A/D conversion card where it is converted to digital form.

#### PARALLEL PROCESSING

The WDA microprocessor has four parallel processing functions. The microprocessor can perform a data collection timing function, a data storage function, a data processing function, and a processed data transfer function in parallel. This is achieved by using the interrupt structure of the microprocessor to initiate the data storage, data transfer, and data collection timing function while the data processing function operates in the main processing loop of the WDA microprocessor.

Even though these processes can operate in parallel, activities within one process do initiate other parallel processes. The data collection timing function initiates the data storage function. When the data storage function determines that a new set of data points have been stored, it initiates the data processing function. When the data processing is complete, it initiates the processed data transfer function. The data collection timing function cycles continuously while the WDA card is enabled. The other functions are initiated on demand. Figure 2 illustrates WDA parallel processing timing.

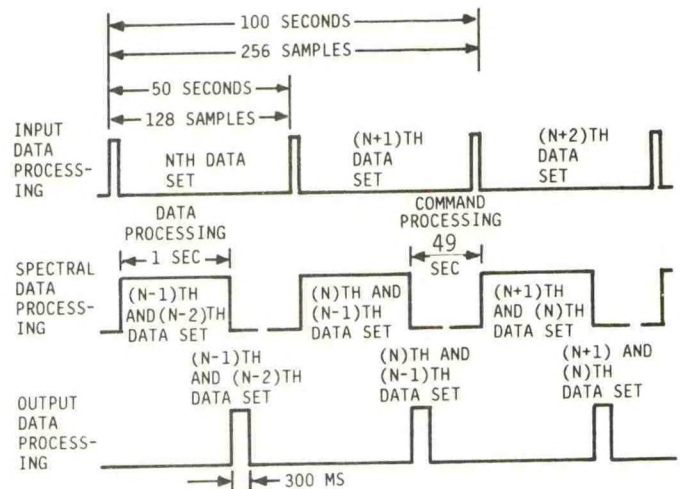


FIG. 2. WDA Processing Timing

#### DATA COLLECTION TIMING FUNCTION

The WDA microprocessor (Intel 80C31) has two built-in timers. One of the timers is used to implement the data collection timing function. Each time the timer counts down an interrupt is issued to the WDA microprocessor.

The WDA microprocessor counts the countdown cycles; and when an appropriate number of cycles has occurred, it sends an INTR signal to the DACT microprocessor. The INTR signal is issued to the DACT microprocessor at a 2.56-Hz rate. This signal causes the DACT microprocessor to digitize the analog wave sensor information and pass the digitized data to the WDA microprocessor. The WDA microprocessor resets its counters and timers and cycles through the timing process again.

The DACT microprocessor has one function which is of higher priority than digitizing analog wave signals. This is the satellite transmission control function. While the DACT microprocessor is performing this function, it will not honor data collection interrupts from the WDA microprocessor. Since breaks in the collection of the digitized wave data will cause generation of invalid spectral density information, the WDA microprocessor must detect these breaks in the data collection and not process data through these breaks. The WDA microprocessor data collection timer function de-



tests when wave data collection has discontinued. When this break in wave data collection is detected, the WDA microprocessor will reset its data storage pointers so that, when the wave data collection resumes, the WDA microprocessor will process a contiguous set of wave data.

#### DATA STORAGE FUNCTION

The data storage function is initiated by digitized wave data being transferred from the DACT microprocessor to the WDA microprocessor. The WDA microprocessor counts and stores the data in a table. When the WDA microprocessor detects that it has 128 new data points and 256 contiguous data points, it resets its data counter and sets a flag to initiate data processing on the 256 contiguous data points. The data storage table is 512 data points in length so that the data collection process can continue while the data processing function uses the last 256 data points.

#### DATA PROCESSING

When the WDA processor determines that it has received 128 new data points, it initiates the data processing function. The data processing function will perform several operations on the data before it is formatted for output. The following operations are performed on the raw wave data:

1. The new 128 samples and the last 128 samples are weighted by a Hanning Window. This is a simple multiplication of a table of raised cosine values with each of the 256 points. Windowing and overlap of data segments is used to increase the number of degrees of freedom of the spectral density estimates to be calculated. The number of degrees of freedom depends on the type of data window used, the amount of processing, overlap used, the number of points in the FFT, and the total number of data points used. The equation for degrees of freedom is given by

$$\text{Degrees of Freedom} = A \cdot N / L$$

where: A is a coefficient whose value is determined by the type of window, the amount of overlap, and the number of points used in the FFT. N is the total number of data points processed and L is the number of points in each FFT segment. The parameter A has a value of 3.79 when a 256-point FFT is used with a Hanning Window and 50% overlap.

2. A 256-point FFT is performed on the windowed data. The output of the FFT is 256 complex pairs of data points.

3. The spectral densities are generated for each frequency of interest by summing the squares of the real and complex components.

4. The spectral densities from this processing interval and the previous processing intervals are averaged to produce an average set of spectral densities. The number of processing intervals to be averaged is programmable via the DACT System. The WDA microprocessor may be programmed to average 17,

23, 29, or 35 sets of spectral densities which represent 15, 20, 25, or 30 minutes of data collection.

5. The averaged spectral densities are then converted from acceleration to displacement (this operation is not performed in the case of a wave staff sensor). The displacement spectral densities are generated using the following equation:

$$SDd(n) = SDA(n) * (2 \pi F_n)^{-4}$$

where:  $F_n$  is the frequency of interest,  $SDd(n)$  is the spectral density in terms of displacement, and  $SDA(n)$  is the spectral density in terms of acceleration. A table of the values of  $(2 \pi F_n)$  will be stored in EPROM.

6. The average spectral densities are corrected for known buoy noise and power transfer function. The WDA microprocessor can be programmed to process data from acceleration sensors mounted on four different buoy hulls or a wave staff. The buoy hulls it can accommodate are the Nomad, 10-meter, 12-meter, and E-buoy hulls. The correction is performed with the following algorithm:

$$CSD(n) = SDA(n) - NC(n)/PTF(n)$$

where:  $CSD(n)$  = Corrected Spectral Density  
 $SDA(n)$  = Spectral Density Average  
 $NC(n)$  = Noise Correction  
 $PTF(n)$  = Power Transfer Function.

This correction is performed on each of the frequencies of interest. The noise correction values  $NC(n)$  and the power transfer function values  $PTF(n)$  for each buoy hull type and wave staff are stored as tables in WDA EPROM memory.

7. The WDA microprocessor then calculates the wave period from the frequency of highest average spectral density. The wave period information is stored in units of seconds as prescribed by NWS formats.

8. The significant wave height is calculated from the spectral information and stored in units of 1/2 meters as prescribed by NWS formats. The significant wave height ( $H_{1/3}$ ) is calculated using the following equation:

$$H_{1/3} = 4 \sqrt{(0.01) \left( \sum_{m=0}^{40} S_m \right)}$$

where: 01 is the spectral density resolution, and  $S_m$  ( $m = 0$  to 40) are the specific spectral densities.

9. The peak wave height is calculated from the spectral information and is stored in units of 1/2 meters as prescribed by NWS formats.

10. The spectral data is formatted in ASCII and stored for output.



11. Data quality words are formatted for output. The content of these words are not defined at this time, but will be used in future development of WDA processing.

12. The formatted data is loaded into the WDA microprocessors output queue and passed to the DACT microprocessor, via the digital bus, to be placed in the output data message. The format of the spectral data is illustrated by figure 3.

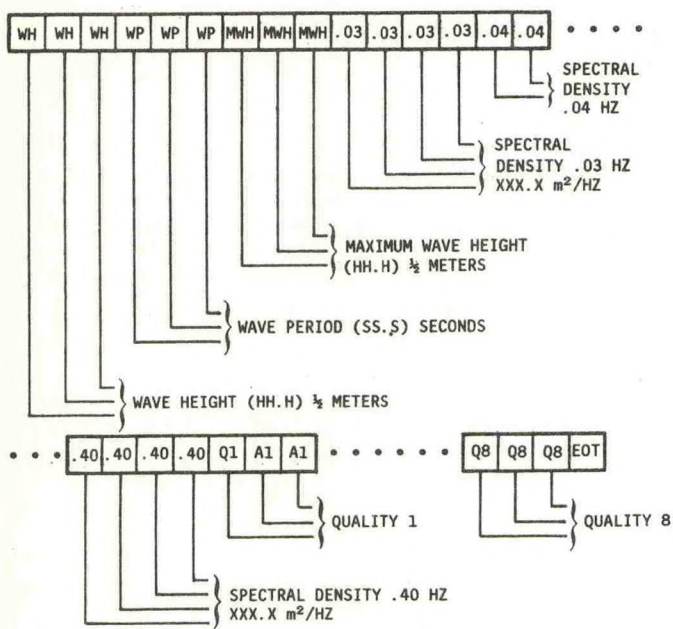


FIG. 3. Format of Spectral Data

## TRANSMISSION OF WAVE DATA

The DACT microprocessor receives new wave data from the WDA card every 50 seconds. However, it only saves the last wave data received during the MET data acquisition interval. This is done so that the wave data to be transmitted or accessed via modem corresponds in time to the MET data information to be transmitted.

The wave period, significant wave height, and peak wave height are transmitted in the special NWS format as well as part of the spectral information which is transmitted after the NWS formatted message.

## REFERENCES

Welch, Peter D., "The Use of Fast Fourier Transforms for the Estimation of Power Spectra: A Method Based on Time Averaging Over Short, Modified Periodograms," IEEE Trans. Audio Electroacoustic, Vol. AU-15 pp. 70-73, June 1967.

Steele, K.E. and M. Earle, "The Status of Data Produced by NDBO Wave Data Analyzer Systems," Proceedings of the MTS-IEEE Oceans '79 Conference, San Diego, California, September 17-19, 1979.



# AN ANALYSIS OF SHORT PENDULUM HEAVE SENSORS

Marshall D. Earle and Richard W. Longman\*

Marine Environments Corporation  
10629 Crestwood Drive  
Manassas, Virginia 22110

## ABSTRACT

Theory for accelerations measured by short pendulum devices on wave following buoys is developed. The theory includes wave slope effects, horizontal and vertical wave acceleration effects, and viscosity and buoyancy effects when short pendulums are suspended in fluids to provide damping. Based on the theory and numerical calculations, short pendulum devices do not provide acceleration measurements that are better than those provided by strapped-down accelerometers on wave slope following buoys. As a result of buoyant forces acting on short pendulums that are suspended in fluids and finite amplitude wave effects that become more important for steep waves, short pendulum devices actually provide poorer measurements of buoy vertical accelerations than strapped-down accelerometers on wave slope following buoys.

## 1. INTRODUCTION

Buoy wave measurements involve double integration of buoy vertical acceleration records to provide buoy heave. Difficulty in vertically stabilizing accelerometers by inexpensive and low power consuming approaches is a problem for wave measurement buoys. One approach is use of strapped-down accelerometers to measure buoy acceleration perpendicular to the deck of a wave slope following buoy. This approach is used by the National Oceanic and Atmospheric Administration (NOAA) Data Buoy Center (NDBC) and effects of this approach on NDBC measurements have been quantified.<sup>1</sup> Strapped-down accelerometers cause low frequency noise in wave displacement spectra. Use of NDBC hull responses and data processing techniques shows that strapped-down accelerometers produce significant wave height errors that are generally less than 5% but that effects on low frequency swell measurements may at times be substantial. The work described here was performed to determine if short pendulum accelerometer devices might be improvements over strapped-down accelerometers.

A number of mechanical devices have been proposed to approximately measure buoy vertical accelerations at reasonable cost. One device is a single axis accelerometer which measures acceleration along the axis of a short (1 to 10 cm) pendulum. The pendulum is usually suspended in an oil filled enclosure to provide damping. As a result of its short length, the pendulum has a short natural period. The rationale for this type

of device is that the pendulum will not respond to buoy motion, particularly horizontal accelerations, at wave periods that are much longer than the period of the short pendulum. Hence, the pendulum might be expected to remain nearly vertical so that only buoy vertical accelerations would be measured by the accelerometer. However, if a short pendulum is mounted on a wave following buoy, the pendulum tends to align itself perpendicular to the wave surface as often stated (e.g. Reference 2). This behavior is expected from physical reasoning because the bob of a short pendulum is equivalent to the water particles that form the sea surface. Thus, use of a short pendulum device would be equivalent to use of a strapped-down accelerometer to measure accelerations perpendicular to the deck of a buoy that aligns itself with wave slopes. However, complications occur for large values of wave slopes and for short pendulums suspended in fluids which cause a buoyant force.

This paper describes characteristics of accelerations measured by short pendulum devices. Equations of motion for a damped short pendulum with its pivot point moving as if on a wave following buoy are developed and analytically solved for special cases. For more general cases of wave motion, these equations are solved numerically. Short pendulum deflections from an earth-fixed vertical and comparisons of accelerations along the pendulum axis to actual vertical accelerations serve as the basis for evaluation of the short pendulum measurement approach. Comparisons are also made between accelerations measured by a short pendulum device and accelerations measured by a strapped-down accelerometer with its axis perpendicular to the deck of a wave slope following buoy.

## 2. EFFECTS OF HORIZONTAL ACCELERATIONS

### A. Undamped Case

When a pendulum is suspended from a point undergoing wave motion, horizontal wave accelerations are the primary cause of deflections of the pendulum from an earth-fixed vertical. Vertical wave accelerations produce a time varying effective gravitational force on the pendulum as the pendulum's support point moves up and down. The effectiveness of a short pendulum accelerometer device can be substantially evaluated by analytical solutions to the equations of motion for a simple pendulum suspended from a support

\*Also with: Department of Mechanical Engineering  
Columbia University, New York, N.Y. 10027



point which is moving horizontally in a manner similar to horizontal wave motion.

A sinusoidal wave component is given by

$$\xi = a \cos(kx - \sigma t) \quad (1)$$

where  $a$  is wave amplitude,  $k$  is wave number,  $x$  is horizontal position,  $\sigma$  is radian wave frequency ( $2\pi/\text{period}$ ), and  $t$  is time. The horizontal displacement of a point moving with the sea surface about its equilibrium position is given by

$$x_1 = -a \sin(kx - \sigma t) \quad (2)$$

and the wave slope is given by

$$\xi_x = -ak \sin(kx - \sigma t) \quad (3)$$

At an arbitrary  $x$  position given by  $x = 0$ , these equations become

$$\xi = a \cos(\sigma t) \quad (4)$$

$$x_1 = a \sin(\sigma t) \quad (5)$$

$$\xi_x = ak \sin(\sigma t) \quad (6)$$

where the horizontal motion of the support point is given by Equation (5).

The equation of motion for the undamped case is developed from Lagrange's equation which is given by

$$\frac{d}{dt} \left( \frac{\partial L'}{\partial \dot{\theta}} \right) - \frac{\partial L'}{\partial \theta} = 0 \quad (7)$$

$$L' = T - V \quad (8)$$

where  $T$  is kinetic energy and  $V$  is potential energy which are given by

$$T = \frac{1}{2} m \left( a^2 \sigma^2 \cos^2 \sigma t + L^2 \dot{\theta}^2 + 2aL\dot{\theta} \cos \theta \cos \sigma t \right) \quad (9)$$

$$V = mgL (1 - \cos \theta) \quad (10)$$

Here,  $m$  is the mass of the pendulum bob,  $L$  is the length of the pendulum which is treated as not having mass,  $\theta$  is the angular displacement of the pendulum from the vertical,  $\dot{\theta}$  is the angular velocity of the pendulum and the other parameters are as previously defined. For the kinetic energy, the first term represents kinetic energy associated with the movement of the support point, the second term represents kinetic energy associated with the velocity of the bob relative to the support, and the last term represents kinetic energy associated with the scalar product of the velocities of the bob and the support point. The equation of motion is given by

$$\ddot{\theta} + \frac{g}{L} \sin \theta = \left( \frac{a}{L} \right) \sigma^2 \sin \sigma t \cos \theta \quad (11)$$

For small angles,  $\theta$ , this equation becomes

$$\ddot{\theta} + \frac{g}{L} \theta = \left( \frac{a}{L} \right) \sigma^2 \sin \sigma t \quad (12)$$

which has the steady-state solution

$$\theta = \frac{(a/L) \sigma^2}{g/L - \sigma^2} \sin \sigma t \quad (13)$$

There is also a transient solution that depends on the initial conditions at  $t=0$  but this solution is not of interest when a short pendulum device is used to measure waves.

For short pendulums,  $g/L$  is much larger than  $\sigma^2$  so that

$$\theta \approx \frac{a \sigma^2}{g} \sin \sigma t \quad (14)$$

Since  $\sigma^2 = gk$  for deep water waves, Equation (14) becomes

$$\theta \approx ak \sin \sigma t \quad (15)$$

which is identical to Equation (6). This result shows that a short pendulum deflects from the vertical by an amount equal to the wave slope. An accelerometer attached to a short pendulum and that measures acceleration parallel to the length of the pendulum would measure the same accelerations as a strapped-down accelerometer that measures acceleration perpendicular to the deck of a wave slope following buoy.

## B. Damped Case

Effects of horizontal wave accelerations can be studied for a damped simple pendulum by use of the Rayleigh dissipation function given by

$$R = \frac{1}{2} c \dot{\theta}^2 \quad (16)$$

where  $c$  is a damping coefficient. The damped case is of interest because an undamped short pendulum could resonate if there is any buoy-caused excitation at the pendulum's natural frequency. For the damped case, Lagrange's equation is given by

$$\frac{d}{dt} \left( \frac{\partial L'}{\partial \dot{\theta}} \right) - \frac{\partial L'}{\partial \theta} = - \frac{\partial R}{\partial \dot{\theta}} \quad (17)$$



where  $L'$  is as previously defined. The equation of motion is given by

$$\ddot{\theta} + \frac{c}{mL^2} \dot{\theta} + \frac{g}{L} \sin \theta = \frac{a}{L} \sigma^2 \sin \sigma t \cos \theta \quad (18)$$

Multiplication by  $mL$  shows that the drag force on the pendulum bob is  $(c/L)\dot{\theta}$ .

In this paper, the pendulum bob is considered as a sphere moving in a viscous fluid. The drag force on a sphere moving with velocity,  $v$ , is given by

$$F_{\text{drag}} = 6\pi r \mu v = 6\pi r \mu L \dot{\theta} \quad (19)$$

where  $r$  is the radius of the sphere and  $\mu$  is the fluid viscosity. Since this drag force equals  $(c/L)\dot{\theta}$ ,  $c$  is given by  $6\pi r \mu L^2$ .

For small angles,  $\theta$ , the equation of motion is

$$\ddot{\theta} + \bar{c} \dot{\theta} + \frac{g}{L} \theta = \frac{a}{L} \sigma^2 \sin \sigma t \quad (20)$$

where

$$\bar{c} = \frac{c}{mL^2} = \frac{6\pi r \mu}{m} \quad (21)$$

The steady-state solution for small angles is given by

$$\theta = \frac{(a\sigma^2/L) \sin(\sigma t + \gamma)}{\left(\left(\frac{g}{L} - \sigma^2\right)^2 + \bar{c}^2 \sigma^2\right)^{1/2}} \quad (22)$$

where

$$\gamma = -\pi/2 + \tan^{-1} \left( \frac{g/L - \sigma^2}{\bar{c}\sigma} \right) \quad (23)$$

These equations show that the amplitude and phase of deflections from an earth-fixed vertical are dependent on both wave frequency and fluid viscosity. If fluid viscosity changes substantially with temperature, a short pendulum device could have a time-varying sensitivity to horizontal wave accelerations.

If the maximum magnitude of Equation (22) is less than the deflection,  $a\sigma^2/g$ , selection of fluid viscosity could enhance performance of a short pendulum device. This criterion is

$$\frac{(a/L)\sigma^2}{\left((g/L - \sigma^2)^2 + \bar{c}^2 \sigma^2\right)^{1/2}} < \frac{a\sigma^2}{g} \quad (24)$$

which is equivalent to

$$\bar{c} > (2g/L)^{1/2}, \mu > (2g/L)^{1/2} \frac{m}{6\pi r} \quad (25)$$

when  $g/L$  is considerably larger than  $\sigma^2$ . Because a short pendulum has a high value of  $g/L$ , a very high viscosity is needed to produce sufficient damping to decrease angular deflections. As an example, for  $r = 5$  cm,  $L = 10$  cm, and  $m = 50$  grams, the viscosity must be greater than 7.4 poises. Even heavy machine oil has a viscosity of approximately 7 poises. Use of a high viscosity fluid also introduces other problems when the container that holds the fluid and short pendulum is tilted as it moves with a wave following buoy. The container, fluid, and pendulum will all tend to move as a unit and the deflection of the pendulum will approximately correspond to the wave slope.

The condition for critical damping is given by

$$\bar{c} = 2(g/L)^{1/2} \quad (26)$$

so that for typical viscous fluids short pendulum devices are underdamped. For short pendulums with  $\bar{c}$  less than or equal to the critically damped value and  $g/L$  much greater than  $\sigma^2$ , Equations (22) and (23) become

$$\theta \approx ak \sin \sigma t, \gamma \approx 0^\circ \quad (27)$$

Values of  $\theta$  are actually negligibly greater than  $ak$ . Thus, a single axis accelerometer with its axis parallel to a critically damped or underdamped short pendulum would measure the same accelerations as a strapped-down accelerometer on a wave slope following buoy.

The derivations have so far not considered the buoyant force acting on the pendulum bob if the pendulum is suspended in a fluid. As a result of the fluid displaced by the pendulum bob, there is an upward buoyant force that reduces the effective gravitational force that acts to maintain the pendulum in an approximately vertical position. Buoyant forces can be considered by reduction of the value of  $g$  in Equation (10). The value of  $g$  (now the effective acceleration due to gravity) in the denominators of Equations (14) and (22) will now be less than the value of  $g$  (the actual acceleration due to gravity) used for  $\sigma^2 = gk$  in the numerators of these equations so that a short pendulum device will have angular deflections from the true vertical that are larger than the wave slopes. If a short pendulum is designed so that its mass is much larger than the mass of fluid that it displaces, buoyant effects are small and use of a short pendulum device remains equivalent to use of a strapped-down accelerometer on a wave slope following buoy.

### 3. EFFECTS OF HORIZONTAL AND VERTICAL ACCELERATIONS

#### A. Equation of Motion

Both horizontal and vertical wave accelerations



can be considered by movement of a short pendulum's support point in circles corresponding to orbital wave motion. For a sinusoidal wave component given by Equation (1), the motion of the support point is given by

$$a \sin(\sigma t) \hat{x} + a \cos(\sigma t) \hat{z} \quad (28)$$

where  $\hat{x}$  and  $\hat{z}$  are unit vectors in the horizontal and vertical directions. The kinetic energy,  $T$ , and the potential energy,  $V$ , are given by

$$T = \frac{1}{2} m \left( a^2 \sigma^2 + L^2 \dot{\theta}^2 + 2aL\dot{\theta}\sigma \cos(\theta + \sigma t) \right) \quad (29)$$

$$V = mg (a \cos \sigma t - L \cos \theta) \quad (30)$$

where interpretation of the kinetic energy terms is similar to that for Equation (9). The potential energy term now includes a contribution as a result of the vertical motion of the support point. By use of Lagrange's equation, Equation (17), with the Rayleigh dissipation function, the equation of motion is found to be

$$\ddot{\theta} + \bar{c}\dot{\theta} + \frac{g}{L} \sin \theta = \frac{a\sigma^2}{L} \sin(\theta + \sigma t) \quad (31)$$

where  $\bar{c}$  is defined by Equation (21). For small angles,  $\theta$ , the equation of motion becomes

$$\ddot{\theta} + \bar{c}\dot{\theta} + \left( \frac{g}{L} - \frac{a\sigma^2}{L} \cos \sigma t \right) \theta = \frac{a\sigma^2}{L} \sin \sigma t \quad (32)$$

Comparison of this equation to Equation (20) shows that the vertical motion is equivalent to a time-varying effective gravitational acceleration. The relationship,  $\sigma^2 = gk$ , shows that the time-varying part of the effective gravitational acceleration is smaller than the actual gravitational acceleration by the factor,  $ak$ , which is the wave slope. When  $ak$  approaches zero, Equation (32) approaches Equation (20) which applies to horizontal motion of the pendulum's support point. Thus, effects of vertical accelerations are second order effects.

Equation (31) was solved numerically to provide results later described. Numerical solutions have the advantage of not requiring any assumptions in solving Equation (31) which is a nonlinear second order differential equation. An improved Euler method (e.g. Reference 3), which is a second order Runge-Kutta method, was used to numerically integrate Equation (31). The time step,  $h$ , was 0.01 sec. The truncation error for this method is proportional to  $h^3$  and was negligible. A small time step is desirable not only to reduce truncation error but also because the time step should be small compared to the natural period of the short pendulum. Numerical solutions include a transient solution which

depends on initial conditions and a steady-state solution which is independent of initial conditions. Numerical integrations were carried-out for a sufficiently long time to provide steady-state solutions independent of initial conditions.

## B. Measured Acceleration

The acceleration measured by a single axis accelerometer attached to a short pendulum with its measurement axis parallel to the length of the pendulum is obtained by resolving the acceleration of the pendulum bob to provide the acceleration component parallel to the pendulum length. Considering that the accelerometer would also measure deviations from  $g$  given by  $g(1 - \cos \theta)$  yields

Measured acceleration (pendulum) =

$$g(1 - \cos \theta) + L\dot{\theta}^2 - a\sigma^2 \cos(\sigma t + \theta) \quad (33)$$

The first term is caused by a time varying measurement of the acceleration due to gravity. The second term is a centripetal acceleration term. The last term is caused by the time varying tilt of the accelerometer relative to the horizontal and vertical wave accelerations. The actual vertical acceleration is given by

$$\text{Actual vertical acceleration} = -a\sigma^2 \cos(\sigma t) \quad (34)$$

The acceleration measured by a strapped-down accelerometer on a wave slope following buoy is given by

Measured acceleration (strapped-down) =

$$g(1 - \cos \beta_x) - a\sigma^2 \cos(\sigma t + \beta_x) \quad (35)$$

where  $\beta_x$  is the wave slope. As  $\theta$  approaches the wave slope, accelerations measured by a short pendulum device approach those measured by a strapped-down accelerometer. As  $\theta$  approaches zero, accelerations measured by a short pendulum device approach the actual vertical acceleration. Values of  $\theta$  are given by solutions to Equation (31).

## 4. NUMERICAL CALCULATIONS

Numerical solutions to Equation (31) permit evaluation of short pendulum devices for the general case of a damped pendulum subject to horizontal and vertical wave accelerations. Computer simulations for a range of single component wave conditions were made for an ENDECO (Marion, Massachusetts) short pendulum accelerometer (Type 13-10-18830) which is an example of a short pendulum device. This device was not designed for use on wave slope following buoys and was used for analysis to include actual physical characteristics of a short pendulum device and to evaluate the general usefulness of such devices if used on wave slope following buoys. Calculations with different physical



characteristics show that the results are not very sensitive to characteristics of a particular short pendulum provided that the pendulum has a large value of  $g/L$ , where  $g$  is the effective gravitational acceleration and  $L$  is the pendulum length.

The ENDECO device is a sphere which is supported by a small chain link to form a short physical pendulum which is suspended in an oil filled container. A single axis accelerometer with its measurement axis oriented toward the support point is within the sphere. Except for the space taken up by the accelerometer, the upper half of the sphere is filled with lead and the lower half is free flooding to the oil. This design shortens the pendulum by placing the pendulum center of mass in the upper hemisphere of the sphere. The effective length of the pendulum is approximately 2.4 centimeters and the viscosity of the oil is approximately 2.0 poises. The total mass enclosed by the sphere is approximately 500 grams and the oil displaced by the sphere is approximately 100 grams. Although the pendulum is considerably underdamped, theory and numerical calculations show that critical damping would only slightly change the pendulum's performance.

Numerical calculations were made for sinusoidal wave components with periods of 5, 10, 15, and 20 seconds and amplitudes of 1, 5, 10, and 15 meters provided that the wave slope,  $ak$ , was less than the maximum value, approximately 0.5, associated with wave breaking. Values of  $ak$  ranged from 0.01 to 0.40. Numerical results agree with theory for special cases such as small slopes. Figures 1 and 2 illustrate angular deflections from the vertical and wave slopes for two wave cycles corresponding to  $ak=0.04$  (a typical value) and  $ak=0.40$  (a high value). The short pendulum has angular deflections a small amount greater than the wave slopes for  $ak=0.04$ . Differences between short pendulum angular deflections and wave slopes increase with wave slope and become substantial for  $ak=0.40$ . Figures 3 and 4 show actual vertical accelerations, short pendulum measured accelerations, and strapped-down accelerometer measured accelerations for the  $ak=0.04$  and  $ak=0.40$  cases. All accelerations are similar for  $ak=0.04$ , but both the pendulum measured and strapped-down measured accelerations have significant errors for  $ak=0.40$ . In addition, the pendulum measured accelerations are poorer than the strapped-down accelerations. As explained by theory, errors for both types of measurements increase and the pendulum measured accelerations become worse compared to the strapped-down accelerometer measured accelerations as wave slopes increase. While the differences in the figures may not appear large, the nonlinear nature of Equations (33) and (35) describing the acceleration measurements causes excess low frequency noise and modification of wave displacement spectra when a spectrum of wave components is measured in the manner described by Reference 1 for strapped-down accelerometers. Spectral effects of short pendulum devices and strapped-

down accelerometers would be similar as a result of the general equivalence of these two types of measurements with short pendulum device effects being somewhat worse than strapped-down accelerometer effects. The numerical calculations show that a short pendulum device is less satisfactory than a strapped-down accelerometer on a wave slope following buoy which in turn is less satisfactory than a vertically stabilized accelerometer.

## 5. CONCLUSIONS

Based on the developed theory and numerical calculations, short pendulum devices do not provide acceleration measurements that are better than those provided by strapped-down accelerometers on wave slope following buoys. This behavior occurs as a result of higher order wave slope effects and buoyant forces acting on short pendulums that are suspended in fluids. However, differences between the two types of measurements may not be significant for some applications. The results, which show the general equivalence of the two types of measurements, are not very sensitive to characteristics of the short pendulum provided that the pendulum remains short. This paper does not address the usefulness of short pendulum devices with buoys that do not follow wave slopes. The usefulness of short pendulum devices for such buoys depends on the responses of such buoys to waves. The developed theory and numerical techniques are useful for evaluating the effectiveness of other types of pendulum devices for wave measurements.

## 6. ACKNOWLEDGEMENTS

This work was supported by NDBC under Computer Sciences Corporation (CSC) subcontract to Marine Environments Corporation. Ms. Kathryn Bush programmed the numerical integration procedure and assisted in the overall study. Useful advice was provided by Mr. Kenneth E. Steele, of NDBC, and Mr. Henry T.E. Coolidge, of CSC.

## 7. REFERENCES

1. Earle, M.D. and Bush, K.A., Strapped-Down Accelerometer Effects on NDBO Wave Measurements, Proceedings Oceans 82, IEEE and MTS, Washington, D.C., 1982, 838-848.
2. Tucker, M.J., The Accuracy of Wave Measurements Made with Vertical Accelerometers, Deep Sea Research, 1959, 185-192.
3. Dorn, W.S. and McCracken, D.D., Numerical Methods with Fortran IV Case Studies, Wiley and Sons, New York, N.Y., 1972.



Figure 1. Comparison of Short Pendulum Angular Deflections from the Vertical and Wave Slopes for Sinusoidal Waves with a Typical Wave Slope,  $ak=0.04$ .

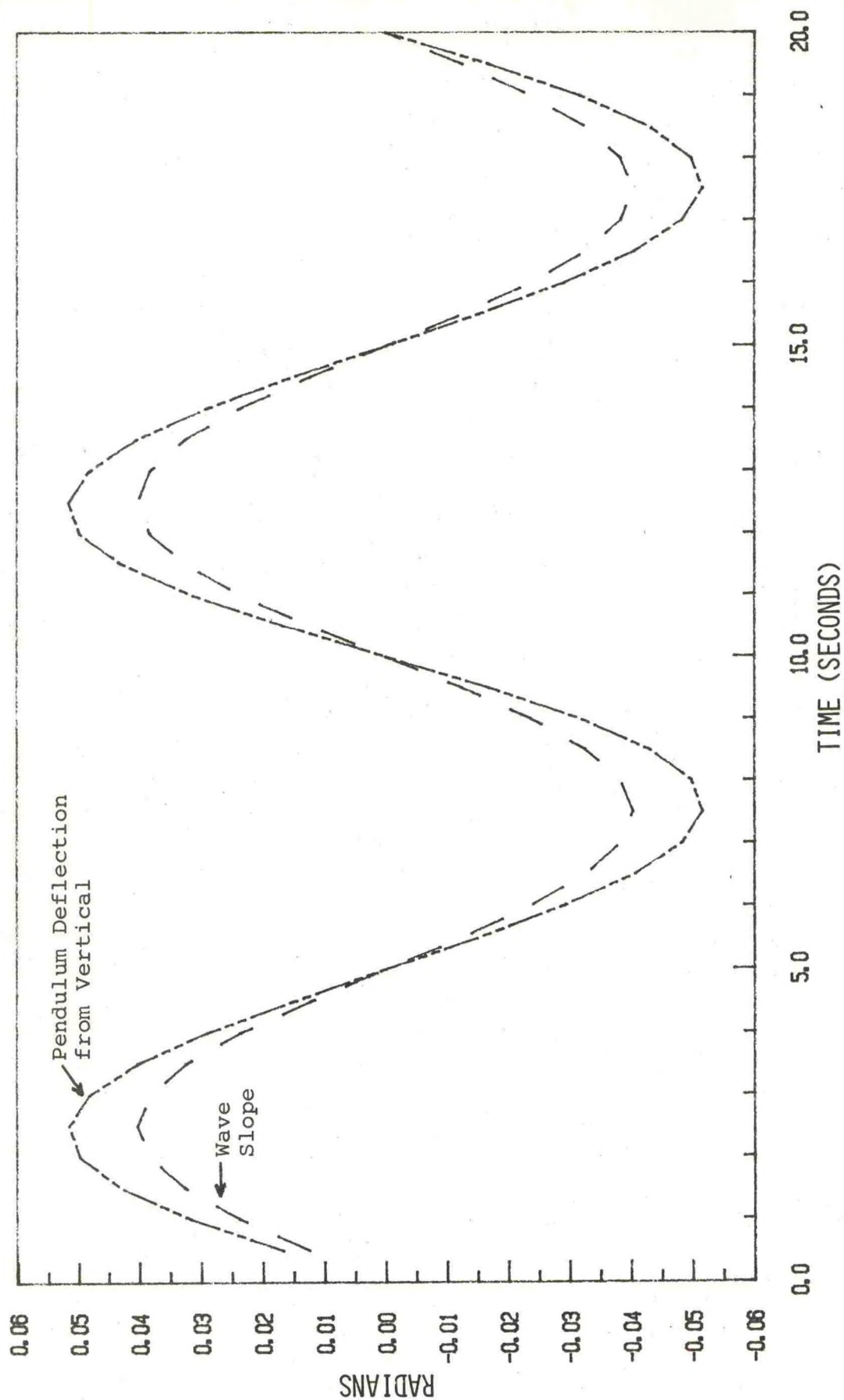




Figure 2. Comparison of Short Pendulum Angular Deflections from the Vertical and Wave Slopes for Sinusoidal Waves with a High Wave Slope,  $ak=0.40$ .

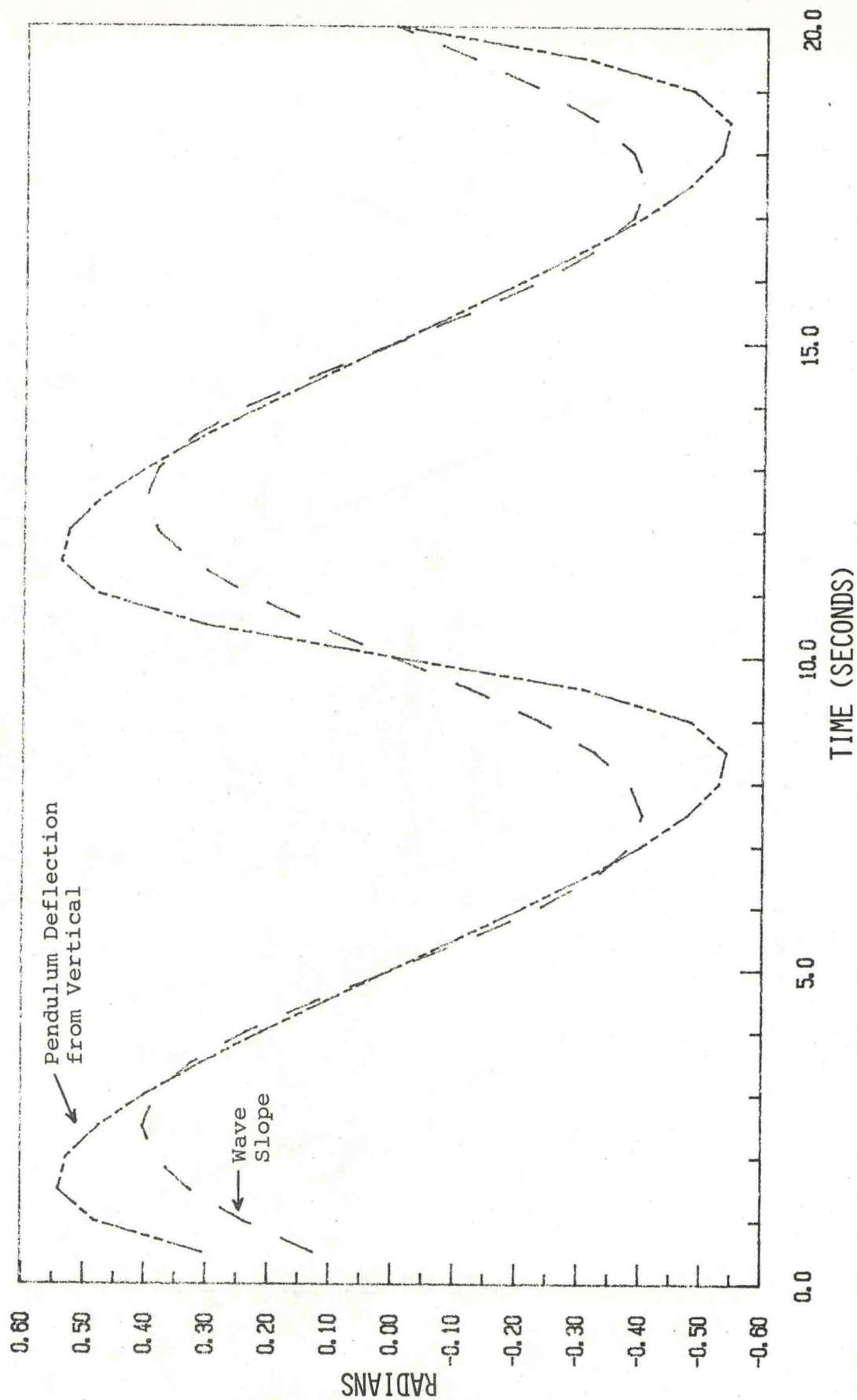




Figure 3. Comparison of Actual Vertical Accelerations, Short Pendulum Measured Accelerations, and Strapped-Down Accelerometer Measured Accelerations for Sinusoidal Waves with a Typical Wave Slope,  $ak=0.04$ . The pendulum measured accelerations are slightly worse than the strapped-down accelerometer measured accelerations.

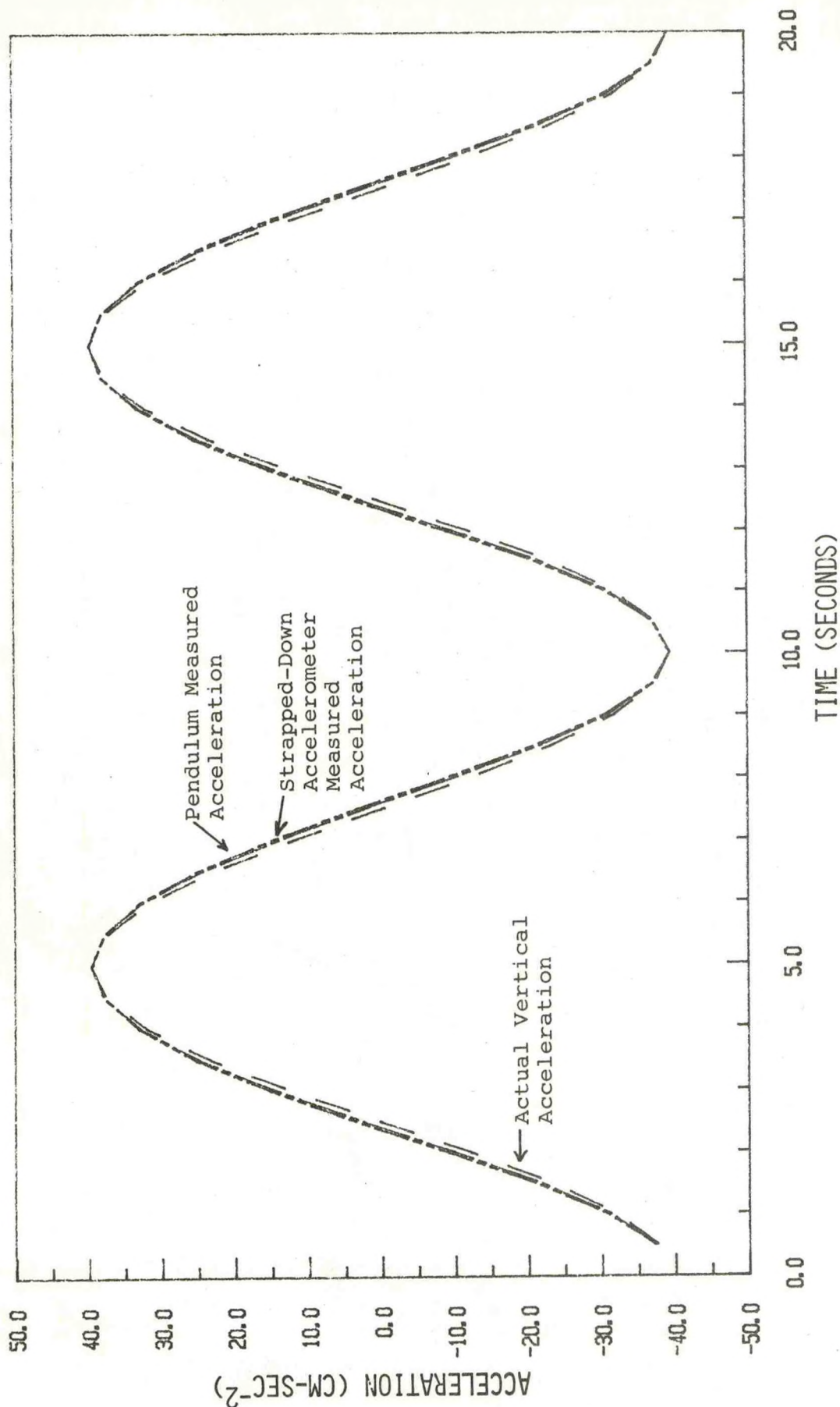
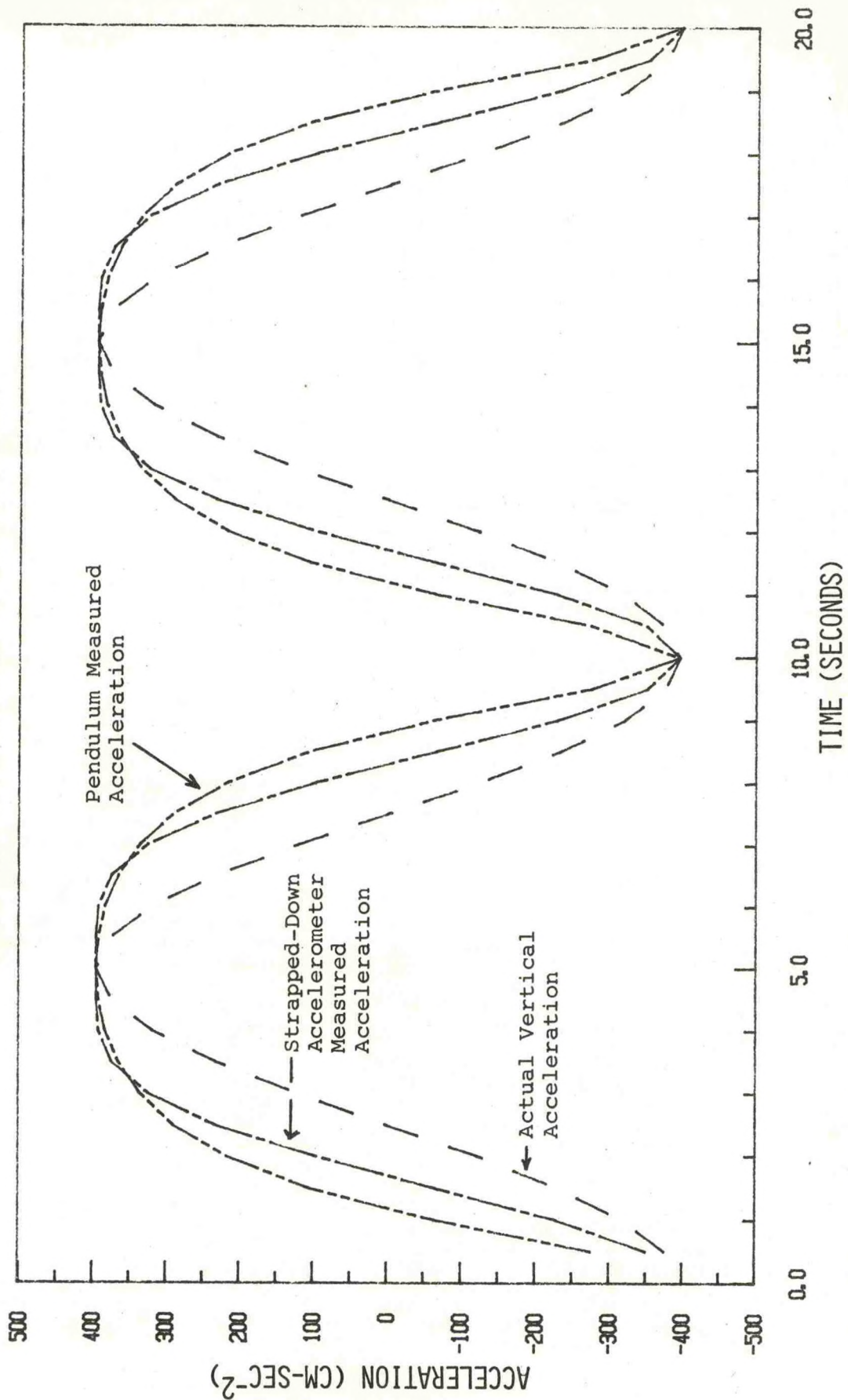




Figure 4. Comparison of Actual Vertical Accelerations, Short Pendulum Measured Accelerations, and Strapped-Down Accelerometer Measured Accelerations for Sinusoidal Waves with a High Wave Slope,  $ak=0.40$ . The pendulum measured accelerations are worse than the strapped-down accelerometer measured accelerations.





# ON-SITE, HIGH ACCURACY NAVIGATION UTILIZING MOORED BUOYS

Corydon B. Pierson, Jr.

Buoy Technology, Inc.  
Concord, NH 03301

## ABSTRACT

As oil exploration moves further into frontier areas, conventional shore based navigation becomes hard pressed to meet exploration requirements. Utilizing elastically tethered, taut moored surface buoys with electrical power generation capabilities of up to 120 watts, navigation base stations can be placed on-site, optimizing signal availability and coverage. Mooring techniques vary from simple single point moors to compound tri-leg moors. The results of a parametric analysis performed to identify mooring configurations as a function of current and water depth are presented which limit the surface buoy total horizontal excursion to 10 meters. On-board electrical power generating systems based on propane fueled thermoelectric generators are presented. The use of high energy density lithium batteries as an alternative energy source is discussed.

## 1. INTRODUCTION

Navigational accuracy requirements for offshore geophysical exploration are continuing to tighten as activities move into deeper waters. Buoy Technology, Inc. (BuoyTec) has previously demonstrated the successful utilization of taut moored buoys to extend navigation coverage far beyond the range of shore stations in frontier programs off Newfoundland, Canada (1), (2), (3) and more recently in the Bering Sea off the State of Alaska.

Interest in further exploration of the Gulf of Mexico, Western Australia and Eastern Canada in water depths exceeding 200 meters has necessitated investigation of mooring techniques other than simple single point taut moors in order to restrict total horizontal excursions of the surface buoy to 10 meters. BuoyTec's finite element computer program was used to perform a parametric analysis which

established the maximum water depth verses water currents for three mooring configurations.

Power requirements for state-of-the-art medium to long range radio positioning systems typically require between 50 and 100 watts of continuous power. This power level is sufficiently large, eliminating all but the highest density energy sources. Currently, propane fueled thermoelectric generators are employed on the buoys, however, advances in technology make lithium batteries a possible alternative.

## 2. COMPUTER SIMULATION

BuoyTec's computer program, STATMOOR is a finite element program written in BASIC for the Apple II computer. The mathematics of the finite element portion of the program are given in reference 4. STATMOOR, written as an interactive program, was modified for this study to perform the simulations in a serial fashion without manual intervention. In this manner, the program was initiated at the end of the workday and allowed to run overnight, with the computational results ready for review the next morning. STATMOOR performed over 400 simulation runs of three different single point mooring configurations. The objective was to identify the mooring configuration required as a function of water depth and current in order to limit the total horizontal excursion of the surface buoy to 10 meters, Figure 1.

As water depths increase beyond 100 meters, maximum total buoy excursions of 10 meters (equivalent to buoy watch circle radius of 5 meters) become significantly less than the 5 to 10 per cent of water depth specified for BuoyTec's simple single point taut moors as illustrated in Figure 2. This simple single point mooring configuration is referred to as Class I in this study.



The station keeping ability of the surface buoy is a direct result of the high tension in the elastic mooring array. As the buoy moves horizontally away from a point directly above the anchor, a restoring force develops in the mooring array which tends to bring the buoy back over the anchor. Figure 3 illustrates this concept. Forces which tend to move the equilibrium position of the buoy off station are produced principally by water currents and to a lesser extent, wind.

As a consequence of having to maintain surface buoy excursions within an absolute displacement regardless of water depth, alternate mooring techniques are required. These techniques provide the effect of placing an "artificial seafloor" nearer to the water surface. By providing this artificial seafloor, station keeping capabilities of the surface buoy once again approach the 5 to 10% specification when referenced to this artificial seafloor.

Artificial seafloors can be generated by at least two methods. First, for moderate depths and water currents, subsurface buoyancy provided by a low drag buoy can be utilized to reduce the horizontal displacement of the portion of the mooring array below the elastic tethers, as shown in Figure 4. This mooring configuration is referred to as the CLASS II configuration. As water depths and/or current profiles increase, a very stable artificial seafloor can be provided by a tri-moored subsurface buoy, Figure 5. This mooring configuration is referred to as CLASS III.

The computer simulation focused on Class I and II moors, water depths ranging from 100 to 520 meters and surface currents ranging between 25 and 75 centimeters per second (0.5 to 1.5 knots). Figure 6 illustrates the normalized current profile used in this study.

### 3. SUMMARY OF COMPUTER SIMULATION

Based on the normalized current profile given in Figure 6, Figure 7 presents a plot of selected output from the computer simulation runs. This figure identifies the mooring class required, as a function of water depth and surface current, to limit the total surface buoy excursion to less than 10 meters. Utilizing the vast amount of data obtained from the computer runs, other mooring classification curves

could be plotted for any total surface buoy excursion up to 20 meters. The flexibility of the simulation program STATMOOR, will allow tailoring the computer generated current profile to fit actual profiles when they are available.

Table 1 was derived from Figure 7 and illustrates the maximum water depth limit for Mooring Class I and II subjected to surface currents of 25, 38 and 50 cm/s, respectively.

As illustrated in Figures 7, the amount of subsurface buoyancy directly affects the station keeping performance of the mooring, as well as the logistical requirements for the system. Determination of the optimum size of the subsurface buoy depends on the depth desired for installation of the navigation buoy.

Tri-leg moors have been shown to provide very stable subsurface moors (5), (6). Although this study did not include complex trimoors, the minimum depth and current limits defining their operational threshold were determined as shown in Figure 7.

The extended range available from moored buoys is illustrated in Figure 8 for the Gulf of Mexico. Shown in this figure is the estimated signal coverage from Cubic Western's ARGO positioning system. In actual field operation in the Bering Sea, signal ranges from the buoys have been measured in excess of 700 km (7).

TABLE 1 MAXIMUM WATER DEPTH IN METERS TO MAINTAIN A TOTAL BUOY EXCURSION LESS THAN 10 METERS

MOORING CLASS	SURFACE CURRENT		
	25 cm/s	38 cm/s	50 cm/s
CLASS I	300	160	95
CLASS II 8000 NT	380	185	100
CLASS II 35000 NT	>520	310	140
CLASS III	>520	>310	>140



#### 4.0 ON BOARD ELECTRICAL POWER GENERATION

The maximum regulated electrical power presently available on BuoyTec's navigation buoy is approximately 110 watts. This electrical power is produced by an internally mounted, water cooled thermoelectric generator (TEG) fueled by propane (Figure 9). Use of the TEG as the power source necessitates providing adequate paths for combustion air and exhaust gas and also a means for replenishing the propane fuel supply contained within the buoy. Substituting batteries for the TEG as the electrical power source simplifies the buoy hull construction by elimination of the air supply and exhaust stacks, remote propane refueling hose and all associated gas plumbing fixtures.

The energy density of high performance lithium batteries approaches the overall energy density of the propane fueled TEG's presently employed in the buoys, Table 2. Lithium thionyl chloride batteries were chosen for further investigation based on their potentially high energy density and recent advancements made in manufacturing these batteries. The following table illustrates the energy density of lithium thionyl chloride batteries manufactured by the ALTUS CORPORATION.

TABLE 2 ENERGY DENSITY OF LITHIUM THIONYL CHLORIDE BATTERIES AND PROPANE FUELED THERMOELECTRIC GENERATOR

MODEL	ENERGY DENSITY Wh/lb
1400 Ah Battery	180
2000 Ah Battery	200
8000 Ah Battery	215
THERMOELECTRICS	225

#### 5. SUMMARY OF ELECTRICAL POWER SOURCES

The energy density of the lithium thionyl chloride battery compares favorably with that of the propane fueled TEG. Table 3 compares the weights and service intervals of the two energy sources.

TABLE 3 WEIGHT (lbs) AND SERVICE INTERVAL (days)  
TEG/PROPANE VS. LITHIUM THIONYL CHLORIDE

POWER SOURCE	SYSTEM WEIGHT	LITHIUM MODULE WEIGHT	SERVICE INTERVAL	
			50 W	110 W
TEG/PROPANE	759	N/A	60	30
1400 Ah	240	30	28	12.7
2000 Ah	312	39	40	18.2
8000 Ah	1000	125	160	72.7

Figure 10 projects the operational costs of the TEG/propane and lithium battery systems. This figure illustrates that due to the very high cost of the batteries, the principal means of achieving battery system costs comparable to the TEG/propane system is to reduce the dependence on a support vessel. A reduction in dependence on a support vessel may indeed be achievable with the battery system since the buoy is now a simpler design and sealed from the moisture elements, consequently, system reliability is increased. How much of a reduction in vessel support can be achieved remains to be determined from operational experience.

#### 6. REFERENCES

1. Pierson, C. B., Jr., "A High-Precision Radio-Positioning Offshore Navigation Buoy," SEA TECHNOLOGY, March 1982, pp. 35-39.
2. Chappell, P. and Wesson, H., "High-Accuracy Navigation for Long-Range Offshore Geophysical Exploration," Texas Instruments, Inc., (unpublished manuscript), 1981.
3. Gay, J. and Wyman, D., "Precise Positioning for Detailed Geophysical Exploration," Proceedings of the Institute of Navigation, October 27-29, 1982, pp. 105-110.
4. Berteaux, H., BUOY ENGINEERING, John Wiley & Sons, New York, 1976.
5. Savage, G. and Hersey, J., Editors, "Project Seaspidar," Woods Hole Oceanographic Institution, Report No. 68-42, (unpublished manuscript), 1968.
6. Walden, R. and Berteaux, H., "Design and Performance of a Deep-Sea Tri-Moor," Proceedings of Marine Technology Conference, September 23-25, 1974, pp. 31-96.
7. Personal conversation with oil company executives, Fall 1982.



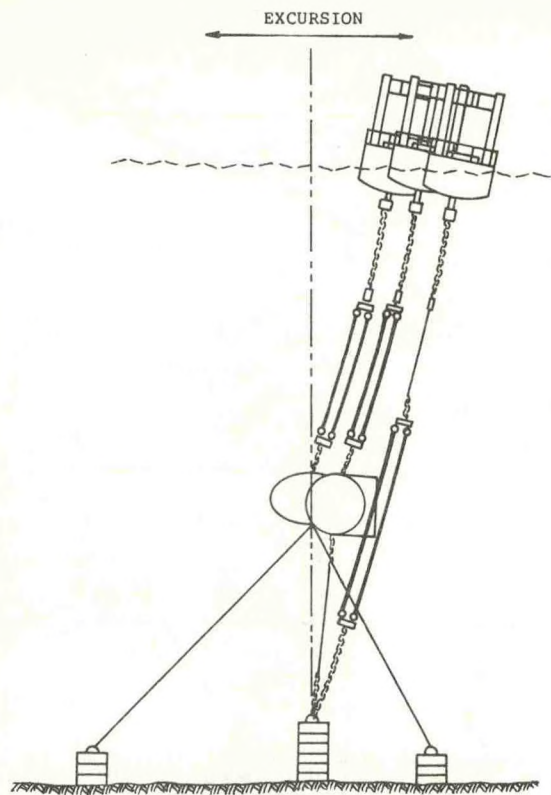


Figure 1 Illustration of buoy excursions

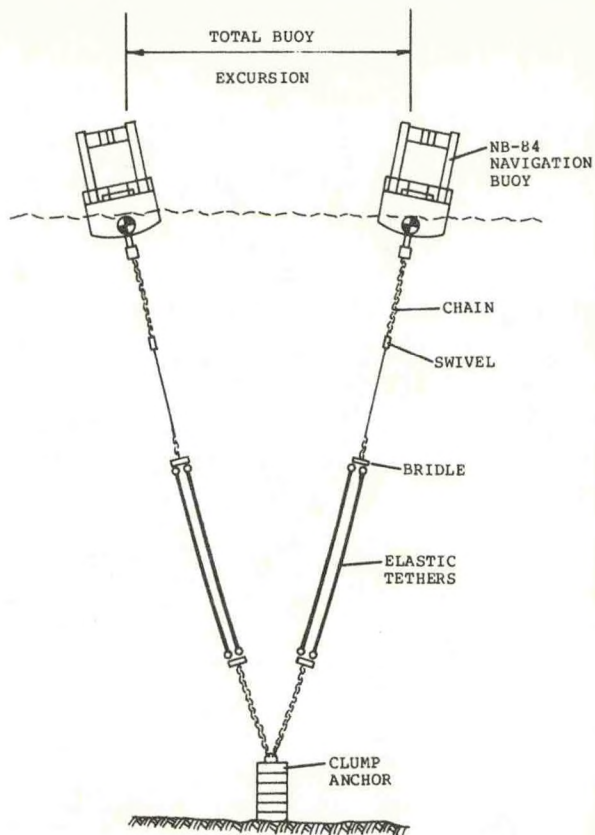


Figure 2 Class I Configuration

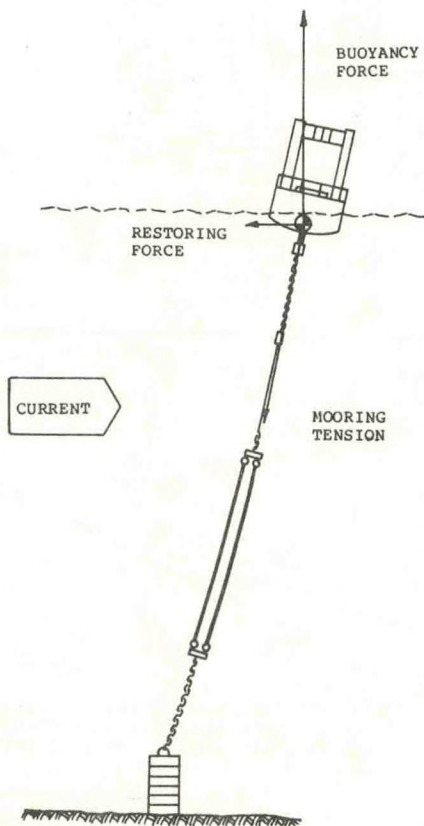


Figure 3 Typical forces acting on buoy

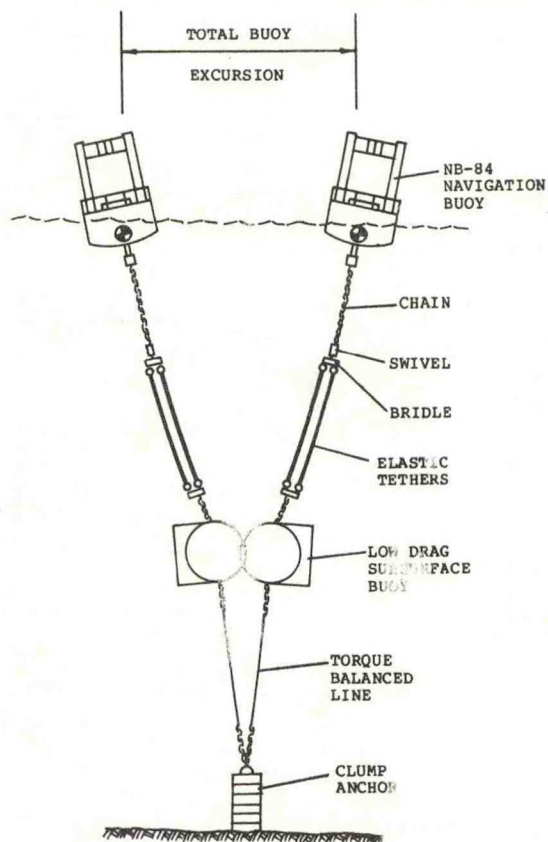


Figure 4 Class II Configuration



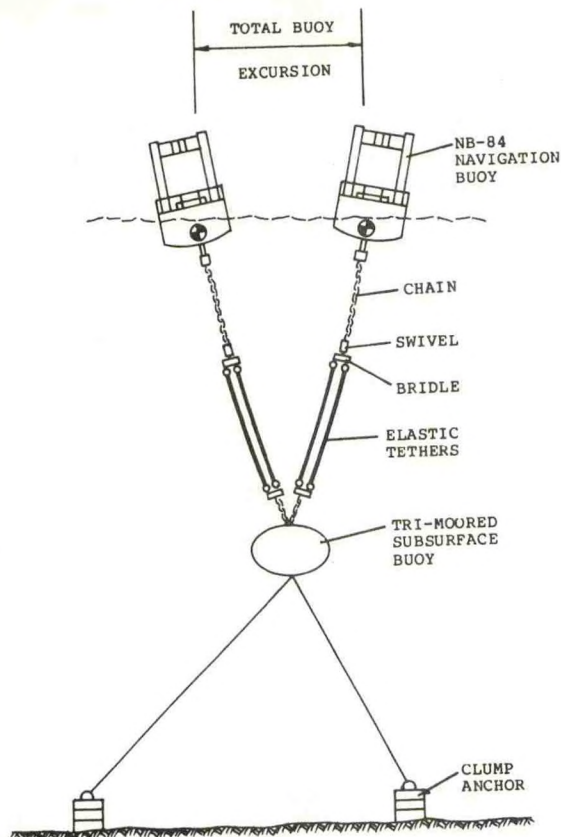


Figure 5 Class III Configuration

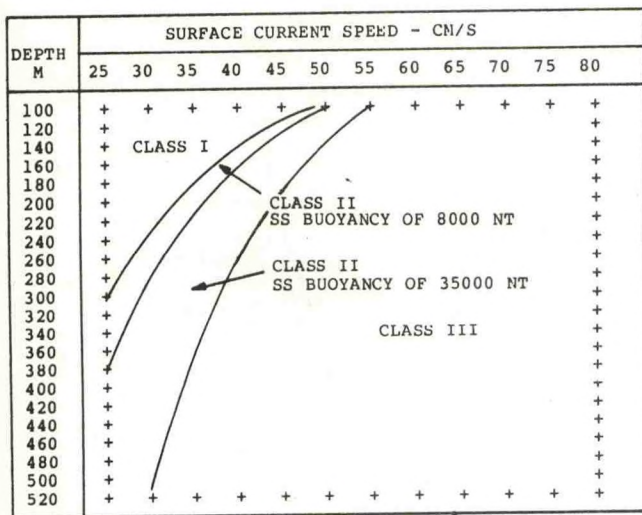


Figure 7 Mooring class required to maintain a total buoy excursion less than 10 meters

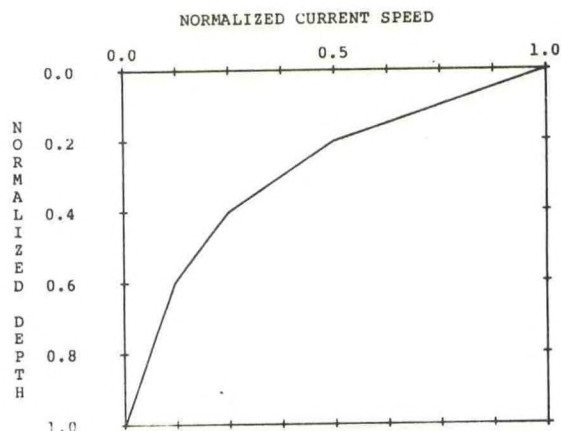


Figure 6 Normalized current profile

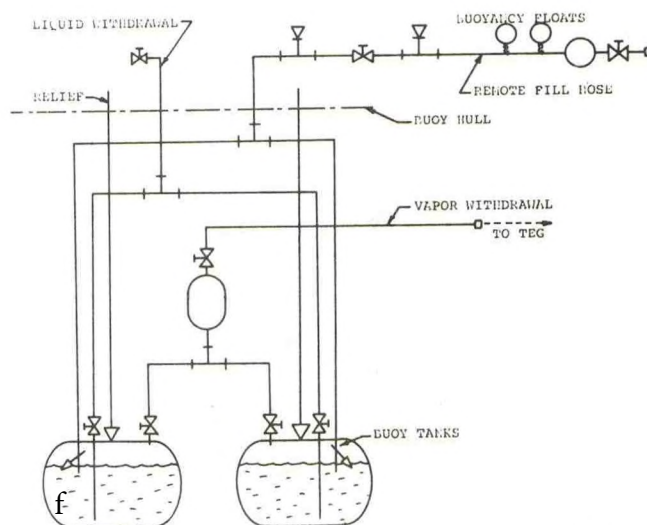


Figure 9 Simplified plumbing schematic for the NB-84 Buoy

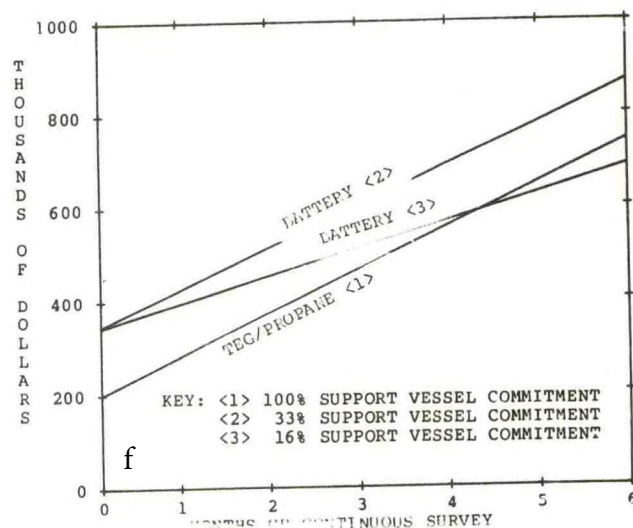


Figure 10 Comparison of the estimated operating costs of the battery systems



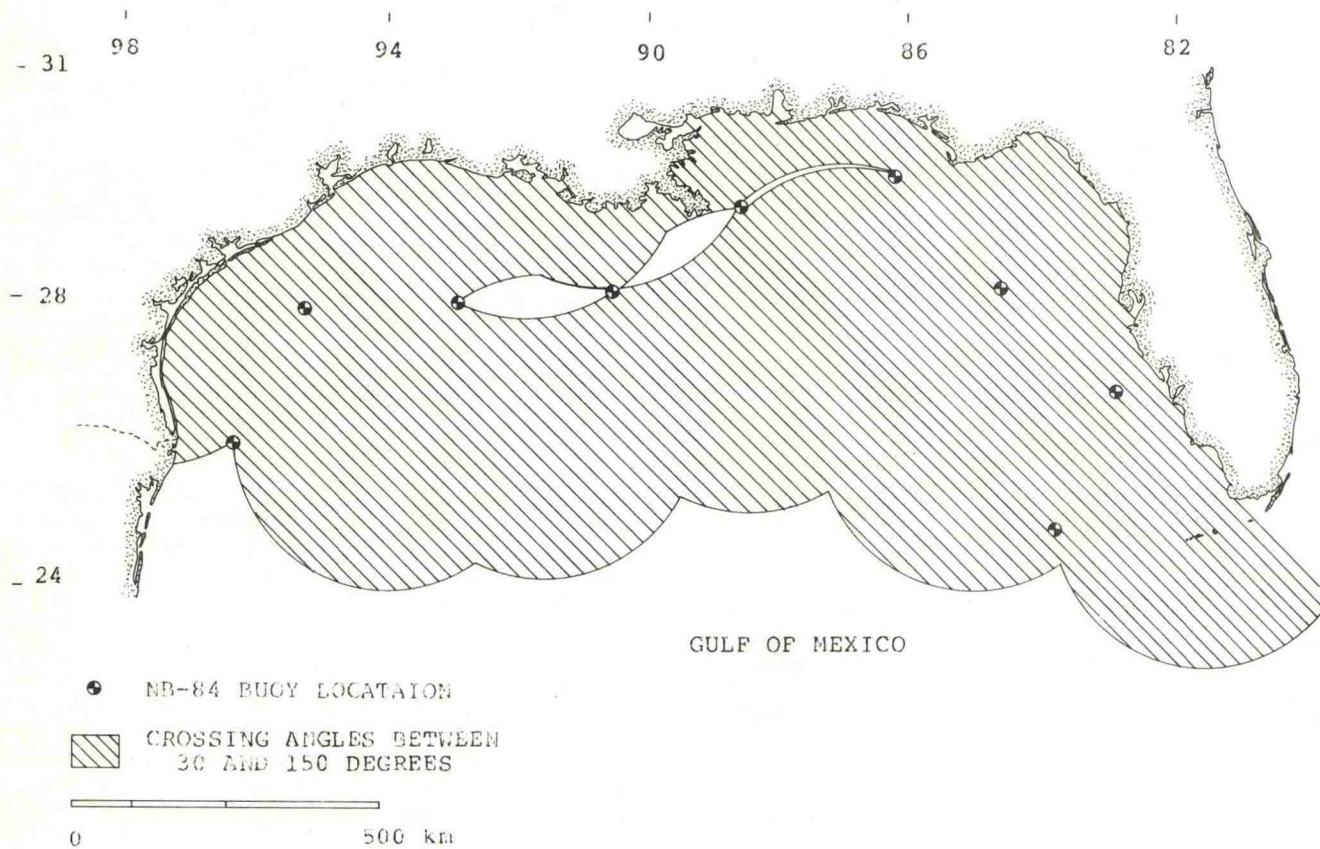


Figure 3 Navigation coverage of the Gulf of Mexico available from buoys



NDBC  
WAVE MEASUREMENT ACTIVITIES AND PLANS

K. E. Steele

NOAA Data Buoy Center  
National Space Technology Laboratories  
NSTL Station, MS 39529

**ABSTRACT**

This paper provides an overview of NDBC wave measurement activities in the recent past, with particular emphasis on FY 1982. FY 1983 activities under way or about to be initiated are also described, and plans for FY 1984 or beyond are projected.

**INTRODUCTION AND BACKGROUND**

Wave measurement activities at the NOAA Data Buoy Center (NDBC) have several related objectives. First, there is the development and field verification of techniques for the measurement of useful wave data from marine platforms. A second objective that follows from field verification is the procurement and deployment, by NDBC operational divisions, of reliable measurement systems for the routine acquisition of wave data from many sites in the ocean. To ensure that acceptable data result, a third objective is the development and application of calibration and data quality procedures to these operational measurement systems. Ultimately, the objective is simply to produce satisfactory data for users.

Such data are useful to a variety of government and nongovernment users, prominent among which is the U.S. National Weather Service (NWS). Another large user needing near-real-time data is the U.S. Navy. It needs data to verify, improve, and support its wave prediction models, which produce fleet marine forecasts (Ref. 1). Those engaged in ship routing also need near-real-time data, as do some offshore construction and oil exploration companies.

Among the large uses needing data, but with a less critical real-time requirement, is the U.S. Army Corps of Engineers (COE). Among its concerns are harbor protection and coastal engineering. The COE, those studying air-sea interactions, and those developing improved wave prediction models, have need of data sets acquired at more than one location, over some time period, and comprising a variety of environmental conditions. To meet such needs with current technologies, networks of reliable, routinely operating, wave-measuring buoys are needed.

Efforts to meet these data needs have been under way at NDBC for some time. The first experimental systems were deployed in 1973 and 1974 (Ref. 2, pages 1, 18). Another system, the first to be used

in quantity by NDBC, was the "Wave Spectrum Analyzer (WSA)" system first deployed in 1975 (Ref. 2, pages 28, 39). This analog system for observing and reporting nondirectional wave spectra was produced and used operationally at 10 ocean sites over a 4-year period. In 1976 and 1977, a digital nondirectional "Wave Data Analyzer (WDA)" was developed, tested in the laboratory, installed in a buoy, and demonstrated at sea (Ref. 2, pages 49 and 61). Analyses (Ref. 3, page 1) indicated that the quality of WDA data was superior to that of the WSA and earlier systems. Also, the electronics in the WDA system were more reliable than those of the WSA. Accordingly, WSA systems were phased out of service and replaced by WDA systems.

During this same period, a Geostationary Operational Environmental Satellite (GOES)-reporting Waverider Analyzer Satellite Communicator (WRANSAC) was developed (Ref. 2, page 80). It combined a conventional 0.9-meter diameter Waverider with a WDA and a satellite transmitter. The hull of this Waverider is a heave surface follower over a wide range of frequencies. In 1978, it was initially used to calibrate and quality-check systems on two WDA-equipped larger hulls, which filter wave spectra at the higher frequencies of interest (Ref. 2, page 111). Systematic evaluations of simultaneous data taken by WRANSAC and WDA-equipped buoy systems resulted in improved estimates of the hull wave transfer function on the boat-shaped Naval Oceanographic and Meteorological Automatic Device (NOMAD) and 12-meter discus hull configurations (Ref. 3, page 11). Geometrical scaling applied to the improved 12-meter discus transfer function allowed a better estimate of the hull transfer function for the 10-meter discus hulls to be made (Ref. 3, page 6).

Development of the capability for near-real-time reporting of directional wave spectra from NDBC buoys began in 1976 (Ref. 2, pages 94 and 103). The feasibility of the original concept was demonstrated in 1977 aboard a 12-meter diameter discus buoy deployed in the Atlantic off Jacksonville, Florida. Further development of directional wave measurement capability followed in 1978 with the deployment of the same large hull in the Gulf of Mexico near Panama City, Florida (Ref. 3, page 29). This configuration included improvements in the system hardware and software, and has been called the Experimental Environmental Research Buoy (XERB).



A calibration capability was established for this improved system through arrangements with the Naval Coastal Systems Center (NCSC) at Panama City. Directional wave data from three NCSC wavestaffs located on the "Stage I" tower some 10 miles out in the Gulf of Mexico from Panama City were taken for comparison to similar data from the 12-meter XERB buoy moored under test a few hundred meters from the tower (Ref. 4, page 45). The XERB was deployed at this site for a year, then refurbished and relocated to a site off Cape Hatteras, North Carolina. During the winter of FY 1981, XERB provided directional wave data to support the Atlantic Remote Sensing Land Ocean Experiment (ARSLOE), sponsored by the National Ocean Survey (NOS) Coastal Waves Program (CWP) and U.S. Army Corp of Engineers (COE).

The by-year descriptions of NDBC activities below are categorized into nondirectional, and directional, wave measurement systems

## FY 82 ACTIVITIES

### NONDIRECTIONAL WAVE MEASUREMENT SYSTEMS

DACT Nondirectional WMS Development--Development was initiated in FY 1982 for a new nondirectional wave measurement system (WMS) suitable for use with the Data Acquisition Control and Telemetry (DACT) payload (Ref. 5), which is now being built for NDBC under contract. This new WMS, a replacement for the now-aging WDA systems, will comprise the latest in energy-efficient CMOS hardware and sophisticated software. As a part of the DACT, it is expected to operate aboard a variety of fixed and moored marine platforms, including NDBC deep ocean hulls, exposed headland piers and breakwaters, and U.S. Coast Guard (USCG) Large Navigational Buoys (LNBs). Its low power consumption will allow use aboard hulls with limited battery space, such as the USCG Aids-to-Navigation (ATON) hulls and low-cost coastal buoys. During FY 1982, a concept for a sophisticated DACT WMS was formulated, documented (Ref. 6), and considered for development. However, a less complex system concept was finally adopted as a near-term goal. This compromise was made to meet a pressing operational requirement for an inexpensive system that can operate with buoys or wavestaffs.

### Improvement of Hull Transfer Function Determination

Methods--Several years ago, NDBC developed a method for determining heave hull transfer functions (Ref. 3, page 11). In this method, narrow band (0.01 Hz) heave spectra, from a system mounted aboard a hull not equally responsive to all frequencies of ocean waves, were fitted to corresponding spectra measured by some ground-truth system such as the small surface following WRANSAC buoy, or a wavestaff. At each frequency, a least squares fit of hull spectra to ocean spectra was performed to determine the power-filtering function of the hull. A computer program was implemented to apply the method. The resultant frequency dependent filter function was then installed in a calibration data base at the National Meteorological Center (NMC) and used to correct operational wave data (Ref. 3, page 1).

This system has been used and has worked well, but the least-squares fit is not an ideal choice because it ignores the rather large variations in the "correct" spectra arising from environmental variability. During FY 1982, NDBC completed implementation and testing of a new algorithm that does not ignore the larger environmental variability associated with larger spectral values. This new approach was applied to LNB (Ref. 4, page 31) and ATON spectra acquired in past years, and to the 12-meter discus concrete Ocean Test Platform (OTP, located at site 42007 in the Gulf of Mexico) and ATON (Ref. 7) data acquired in FY 1982. The OTP is a buoy close to shore and to NDBC that is used to test marine equipment. The new method generally produces smoother measured filtering functions and thus appears to be clearly superior to the old.

ATON Hull Performance Testing--If ATON hulls are to be instrumented in the future with conventional NDBC nondirectional wave measurement systems such as the DACT, the hull with its conventional mooring must have a predictable response to wave motion in all environments in which it might be used. During FY 1982, and ATON hull was instrumented with an operational WDA system. It was then moored and operated for a short period at the site of the OTP in the Gulf of Mexico. As a measure of the true sea, data from the small surface-following WRANSAC buoy were acquired simultaneously from the same site. Determination of the ATON hull transfer function indicated that, for the relatively light sea states occurring during the deployment, such a hull instrumented with an NDBC conventional nondirectional wave measurement system would be capable of producing wave height, wave period, and spectral data of a quality acceptable to the NWS and many other users of wave data (Ref. 7).

### Determination of OTP Hull Power Transfer Function

The ATON/WRANSAC test described above was executed at the deployment site of the OTP so that WRANSAC data could be used as well for the calibration of the conventional WDA system aboard the OTP. The OTP is a 12-meter diameter concrete discus hull in 15 meters of water, so its filtering characteristics were not necessarily expected to be identical to those of other 12-meter hulls. Analysis of OTP/WRANSAC data with the new algorithm produced a hull-transfer function for the OTP hull which was significantly different from that of conventional steel hulls measured in deeper water. This new transfer function should lead to improved spectra, wave height, and wave period data from the OTP, which will facilitate future field testing at the OTP site.

Evaluation of WDA Heave Sensor System--All WDA systems produce data from the electrical analog of a linear accelerometer, the axis of which is aligned with the hull vertical at all times. Ideally, the accelerometer should instead remain vertically stabilized in the earth frame of reference. For some years, NDBC has been concerned with the question of just what errors are introduced into wave height, wave period, and spectra by the fixed-accelerometer arrangement. In 1978, a comparative analysis of field-measured data taken from



a single hull with both types of systems aboard was sponsored by NDBC (Ref. 2, page 87). It detected no significant difference in those parts of the spectrum where non-negligible real sea energy existed. But the light sea states that prevailed during this test left the question only partially resolved.

During FY 1982, NDBC contracted for the development and application of a computer model to simulate the sensor's motion and the performance of operational measurements in a wide range of sea states (Ref. 4, page 17). The simulation included tilting motions as well as vertical and horizontal accelerations at the mean horizontal position of the hull. The results indicated that, although the significant wave height and period are in error by at most 5 percent, heave spectral values at low frequencies can be in error by greater amounts when swell is present. These errors were traceable to spurious energy appearing at each frequency due to the true spectral energies interacting with the strapped-down accelerometer effects. Thus, larger real spectra produce larger apparent noise levels. NDBC low-frequency noise corrections have been designed to cope with large sea states, and thus are excessive for many, more common, sea states. Accordingly, small swells in the presence of typical wind driven seas tend to be obscured.

The use of a short pendulum mounting for the accelerometer to eliminate the effects of strapping down was also investigated through the simulation, but it was found not to be a solution (Ref. 8). A cursory review of what has been proven about the popular Datawell heave sensor led to no immediate conclusion that this expensive, heavy, and bulky sensor necessarily provides the true vertical acceleration of the hull on which it is mounted, when that hull is subjected to the motions of the real environment. In FY 1982 there was no apparent certain solution found to the need for an accurate sensor system for hull heave acceleration, and further investigation was planned for FY 1983.

Development of Displacement Time-Series Measurement Techniques--For some applications, users need wave displacement time-series data. But vertical acceleration of the hull is the basic measurement aboard buoys, and it is a nontrivial problem to produce an accurate reproduction of the source displacement. One difficulty is that phase and amplitude alterations occurring in the double integrator circuits of the Datawell and similar heave sensors distort the time series coming from the sensor. During FY 1980, NDBC funded the development, under contract, of techniques for the numerical double integration of the accelerometer output. A simulation was programmed in which acceleration, mathematically derived from a postulated realistic displacement time series record, was used to reconstruct the original displacement. This simulation demonstrated (Ref. 9) that, for properly selected parameters (sampling rates, etc.), accurate hull displacement records can be produced from acceleration. During FY 1982, this simulation effort was extended to investigate the potential deleterious effects of DC drifts in the accelerometer outputs. Results (Ref. 10) showed that steps must be taken in the onboard data

processing to protect against the effects of drifts that could occur. These techniques for numerical double integration, when perfected, are intended for use in future operational systems.

## DIRECTIONAL WAVE MEASUREMENT SYSTEMS

XERB Performance Evaluation--During FY 1982, performance of the directional wave measurement system deployed aboard the XERB during the FY 1981 ARSLOE was evaluated. It was found to be generally satisfactory, although some needed design corrections and improvements were identified (Ref. 4, pages 53 and 57).

Redesign of DWDA Azimuth Angle Algorithm--The algorithm (Ref. 4, page 37) used in the XERB directional wave measurement system to calculate hull azimuth angle is not suitable for use aboard NDBC operational discus hulls, where large induced as well as fixed magnetic fields sometimes prevail. During FY 1982, the algorithm was redesigned to take account of both fixed and induced fields, tested with field measured data, and its capability to produce accurate azimuth angles verified. The algorithm also was installed in the new DWDA systems during FY 1982.

Improvement of Testing Capability for Directional Wave Measurement Systems--During FY 1982, NDBC procured a second "simple" sensor simulator, a copy of another unit procured earlier. In this system, magnetometers outputs are simulated by DC voltages dependent on hull azimuth but not on pitch and roll. Although it doesn't simulate the effect of wave motion on the output of the magnetometer, this simulator does accurately construct voltages that would come from heave, pitch, and roll sensors mounted on a perfect-surface-following hull oriented at a specified fixed azimuth angle and subjected to a specified pure wave train. These two sensor simulators were used in DWDA (Ref. 4, p. 75) and PDWDA testing in FY 1982.

Delivery of New DWDA Systems--Four new DWDA systems conditionally passed Factory Acceptance Tests in FY 1982, but delivery was delayed to allow the contractor time to implement needed changes identified in the tests and in the evaluation of XERB performance. The needed changes arose from magnetic differences between the XERB hull and NDBC operational hulls, and from deficiencies in certain components of the system that did not meet specifications. These systems were subjected to thorough testing with the simple sensor simulator just described, and results (Ref. 4, page 75) were excellent. However, a satisfactory level of system reliability was not achieved in FY 1982.

Field Testing of the PDWDA System--A second field test of the so called "Prototype Directional Wave Data Analyzer (PDWDA)" system at site 42007 in the Gulf of Mexico was completed in FY 1982. This system includes a pitch/roll directional wave measurement system mounted in a 3.65-meter diameter discus hull, an onboard data processing system, and a transmitter system for relaying data to shore through GOES (Ref. 4, pages 63 and 71). During the



field test, the system functioned for approximately 1 month. Much of the data appeared to be quite good, but a malfunction in the Datawell heave sensor channel contaminated portions of the data. Since the principal goal of testing was to achieve solid reliability in field operations, the buoy was returned to NDBC in late FY 1982 for refurbishment with a goal of attaining high reliability for the electronics and sensors before further testing.

Instrumentation of the NCSC Stage I Platform for Directional Wave Measurements--During FY 1982, NDBC instrumented the NCSC Stage I tower at Panama City with three Baylor wavestaffs, contributed by the NOAA/NOS Coastal Waves Program. The outputs of these wavestaffs are transmitted via NCSC radio telemetry from the tower to an NDBC electronics system located at the NCSC laboratories in Panama City. This electronics system contains algorithms that transform the Baylor outputs into those of simulated heave, pitch, and roll sensors mounted aboard a fictitious perfect-surface-following buoy located at the site of the wavestaffs. These equivalent buoy sensor outputs are then fed into a directional wave measurement system, and GOES-reporting payload, of the type that was used aboard XERB in the ARSLOE. The data telemetered to GOES by this system appear to be coming from a buoy, thereby allowing all of the capability for teletype relay of buoy data, calibration of buoy systems, and data quality checking to be applied to the tower measurements.

## FY 83 ACTIVITIES

### NONDIRECTIONAL WAVE MEASUREMENT SYSTEMS

Design and Fabrication of a DACT WMS--During FY 1983, the design, fabrication, integration, and testing of a new nondirectional wave-measurement system for use with the DACT payload has been initiated under NDBC contract (Ref. 11). This new nondirectional wave measurement system will consist of a single board incorporated into the DACT itself, and will operate with either buoy-mounted accelerometers or wavestaffs. It will provide, in near-real time through teletype in ASC II, significant wave height, wave period, peak wave height, and wave spectral values at various frequencies. In wavestaff applications where telephone access to the DACT is available, the system can be interrogated in real time for measurements no older than a few minutes. First field tests and application of the system are expected in late FY 1983.

Determination of E-Buoy Hull/Mooring Performance for Wave Measurements--For future routine marine meteorological measurements, NDBC plans to make use of a small aluminum 3-meter diameter "E-buoy," the basic design of which was developed at the Woods Hole Oceanographic Institute. As part of the field testing of the E-buoy hull, a conventional WDA system is being included with the payload to test the heave surface following characteristics of the hull. Wave spectra are being acquired from both the OTP and the (co-located) E-buoy, to determine the mechanical filtering characteristics of the E-buoy hull/mooring. The same techniques used to evaluate the ATON hull/mooring are being applied.

Preliminary results indicate that there should be no serious problems in making nondirectional wave measurements from an E-type hull.

Sensor Systems Evaluations--Definite progress was made in FY 1982 in analyzing the effects of using strapped-down accelerometers. But there continues to be some uncertainty about the measurements from both fixed and vertically stabilized (supposedly) sensor systems that are actually being used aboard NDBC hulls. A correct understanding of the behavior of heave, pitch, and roll sensors aboard floating platforms is essential to the achievement and quantification of data quality, and the reduction of sensor sizes and costs. Reductions in sensor size translate into further cost reductions, since hull-size reduction is limited by sensor size. NDBC is performing further analyses and field tests in FY 1983 towards the goal of a thorough understanding of heave, pitch, and roll sensors.

The FY 1983 effort includes two parallel activities. Some resources are being devoted to the search for an alternative to the Datawell HIPPI heave sensor. But since there is no obvious alternative, and since those sensors already in inventory and must be used unless and until an alternative is found, a larger fraction of resources will be devoted to evaluating the performance of the Datawell sensor. Such evaluation is to establish system measurement accuracies, which should serve as a baseline for judging alternative systems as well as satisfying user needs for data-quality information.

Noise Correction Level Improvements--Some years ago, NDBC empirically determined that acceleration spectrum energy levels, at low frequencies where no sea energy was expected, appeared to grow with either sea state or wind speed. A fixed noise-level correction function, which was high and rose linearly with decreasing frequency below 0.12 Hz, was adopted. It has been used to correct the acceleration spectral data produced by operational WDA systems, which are fed by strapped-down accelerometers. In FY 1982 it was determined, by simulating the motion, that these rising "noise" levels probably result from the accelerometer being strapped down (Ref. 4, page 17). During FY 1983 the simulation is being used to develop sea state dependent noise-correction levels, which should improve the sensitivity of existing operational WDA systems and/or planned DACT wave measurement systems.

Field Measurement Support for the Coastal Waves Program (CWP)--In mid-FY 1983, NDBC expects to begin providing engineering and operational support for the buoy field measurement activities of the NOAA Coastal Waves Program (Ref. 12), administered by the National Ocean Survey (NOS). Anticipated activities in FY 1983 are the retrieval of 4 buoys now at sea off the upper Atlantic Coast of the United States, replacement of power supplies, and the redeployment of the buoys.

### DIRECTIONAL WAVE MEASUREMENT SYSTEMS

Deployment of the New DWDA Systems--If satisfactory reliability can be achieved, one of four new DWDA



systems will be installed aboard a 10-meter diameter discus hull at the National Space Technology Laboratories (NSTL) where NDBC is located. This system will include the latest algorithm refinements, and is intended to produce entirely satisfactory data for operational applications. This buoy will first be moored adjacent to the NCSC Stage I tower for calibration and data-quality checking during a 1- to 2-month period. Thereafter it is likely to be deployed at another site, probably in the Gulf of Mexico. Another of the new DWDA systems is to be installed aboard a 10-meter discus hull in the Pacific. The planned deployment site for the first Pacific DWDA is 46024, near San Pedro, California. One of the four units will be held as a spare, and one used aboard a NOMAD hull, as next described.

Test and Evaluation of DWDA System Mounted on a NOMAD Hull--The planned common use of boat-shaped NOMAD hulls (Refs. 13, 14) in NDBC measurement networks makes it highly desirable that directional wave spectra be measurable from NOMAD hulls. Although the asymmetries of the hull may lead to degradation of data quality in comparison to that from a discus, the relatively small size of the hull suggests that the NOMAD hull may be a heave/slope surface follower, with respect to both amplitude and phase, in the frequency range of interest to users. If it is, and if the higher frequency pitch/roll motions are merely linearly superimposed motions, then a DWDA system may work well enough for operational purposes on a NOMAD hull. Accordingly, NDBC plans to instrument a NOMAD with one of the new DWDA systems in FY 1983, and to test and evaluate it at sea against some standard. Plans are not complete at this time, and depend on the availability in FY 1983 of a NOMAD hull for this purpose.

Refinement of System Testing Capability for Directional Wave Measurement Systems--During FY 1983, NDBC is having built, under contract, a signal generator that will not only accurately simulate the outputs of onboard heave, pitch, and roll sensors, but also those coming from a magnetometer mounted on surface-following discus hull. Furthermore, the two present (Ref. 4, page 75) systems can simulate only one pure wave train, whereas this new system can simulate two in different directions. The surface following discus motions simulated will include rotations of the hull in azimuth angle. In addition, the simulator will be capable of simulating Baylor wavestaff outputs. This new equipment will improve capability to prove the proper functioning of the quite complex DWDA, PDWDA, and Baylor wavestaff-based directional wave measurement systems.

Continued Operation of the NCSC Stage I Directional Wave Measurement System--In FY 1983, the Baylor wavestaff measurement system mounted on the NCSC Stage I tower is to be used to functionally evaluate, calibrate, and quality check both the PDWDA system mounted on the 3.65-meter discus hull, and the new DWDA system mounted on a 10-meter discus hull. At present, NDBC intends to operate the existing directional wave measurement system aboard the Stage I tower through the end of FY 1983, after which it is likely to be removed sometime in FY

1984 due to the questionable future of the tower, which has been found to have possible structural weaknesses.

Installation of an Atlantic Fixed Platform DWDA System--Due in part to the questionable future of the NCSC Stage I tower, NDBC intends in FY 1983 to instrument an Atlantic coastal tower with a directional wave measurement system based on wavestaffs, and similar to that of the Stage I tower. The USCG Chesapeake Light Station near Virginia Beach is an attractive choice, and an investigation of the technical and operational feasibility of its use is under way at this time (April 1983).

The system design for the Atlantic platform will be somewhat improved over that of the present NCSC system. Whereas the NCSC system assumes a plane surface for the wave, the new system will transform wavestaff time series directly into the frequency domain. This improved method will be installed and tested at NCSC before installation in the Atlantic.

A directional wave measurement system located on the Chesapeake Light Station will serve many purposes. NDBC directional and nondirectional wave-measuring buoys prepared for deployment in the Portsmouth/Norfolk area can be calibrated and/or data quality checked against the fixed platform system by making brief stops at the tower on the way to deployment. When the particular buoy is to provide scientific-quality data, longer stops and post-deployment checks can be performed.

The Chesapeake Light Station is in the vicinity of the present deployment sites for the Coastal Waves Program (CWP) wave measuring buoys. Thus it may be useful in contributing data to the model developments envisioned by the CWP. Since the tower transmitted data appear to be coming from an operational buoy, directional wave data can be routinely reported to NWS as required, particularly during hurricanes or other critical storm conditions. The site is conveniently located for overflights of aircraft instrumented for the testing of remote sensing systems designed for use aboard satellites and aircraft. Furthermore, the site is conveniently located to support the testing of Coastal Ocean Dynamics Application Radar (CODAR), a radar remote sensing system designed for near-water-surface mountings. An important function served by NDBC buoy and tower-based systems is the provision of accurate in situ data for radar remote sensing systems, which potentially can provide cost-effective worldwide measurements in future years.

Finally, a tower installation of this type will provide a focal point for future multi-system experiments similar to ARSLOE. Whichever fixed site in the Atlantic is selected for the installation, it promises to provide continuous hourly directional wave data of very high quality to be used for a number of purposes at a reasonable expenditure of resources.

Continued Testing of the PDWDA--The refurbishment of the PDWDA system aboard a 3.65-meter discus was begun in FY 1982 and completed in October 1982. Refurbishment included the end-to-end testing of



the new azimuth-angle measurement system in the presence of controlled hull, pitch, and roll angles as large as 20°. Results were excellent, but have not yet been published.

Since refurbishment, the buoy has been shipped overland to Panama City and deployed near the NCSC Stage I tower some 10 miles offshore at approximately 30 meters water depth. Unfortunately, early reports from the buoy showed that there was no voltage on the heave sensor channel, for reasons as yet unknown. All other elements of the system appear to be operating normally. Bad weather and infrequently-available logistic support have thus far prevented repair or retrieval of the buoy. It is the intent of NDBC to bring the buoy to dock-side, replace the heave sensor, and redeploy the buoy next to the tower for a 1- to 2-month period. Preliminary calibration and data quality checks of the system against the Baylor wavestaff system on the Stage I tower will be performed promptly. Data will later be subject to in-depth analysis with more sophisticated data-analysis tools that are being developed in FY 1983. If PDWDA performance is reliable and accurate during the Stage I deployment, the buoy will be returned to NSTL, an already-fabricated anticapsizing system installed, and the buoy redeployed at a severe environment site, probably that of the Chesapeake Light Station. The buoy is designed to right itself and resume reporting in case of capsizing. The severe environment tests will be designed primarily to demonstrate that a small mobile discus can be effectively used to measure directional spectra in environments so severe as to capsize it from time to time.

Development of Formal Directional Wave Data Inter-comparison Techniques--To take full advantage of the quality ground-truth data provided by fixed platform systems, formal methods for the calibration and data quality checking of one directional wave measurement system against another (the standard) are being developed in FY 1983. These methods will then be applied both to data acquired at the NCSC Stage I tower and data acquired at the Atlantic fixed installation in late FY 1983 and in subsequent years. To the extent possible, the intercomparison methods will be generalized to allow their application to the comparison of radar remote-sensing systems to in situ systems.

## FUTURE ACTIVITIES, FY 1984 AND BEYOND

### NONDIRECTIONAL WAVE MEASUREMENTS

Implementation of First DACT WMS--It is expected that a breadboard DACT wave measurement system capable of operating with wavestaffs and aboard buoys will be tested in the field in late FY 1983. A production prototype design should be complete in late FY 1983 or early FY 1984, and field testing should begin soon thereafter. Performance evaluations will be funded in FY 1984, and perhaps 20 of these wave measurement subsystems will be procured for use with operational DACT systems. The performances separately with fixed platform wavestaffs, and aboard hulls of various sizes and shapes, will be evaluated as soon as possible. Improved algorithms for noise correction and new algorithms for

maximum wave height, under development in FY 1983, may be incorporated in FY 1984.

Preliminary Design, Advanced DACT WMS--The first DACT WMS design, intended to accommodate wavestaffs and buoys, will not be capable of operating with pressure transducers. In addition, it will not measure peak wave height from the time series record. These capabilities are not being attempted in the design of the first DACT wave measurement system because of the difficulty, delay, and cost of meeting these requirements. The tentative plan is to prepare in FY 1984 a preliminary design for an advanced DACT WMS that will meet these additional requirements. However, before a design is prepared a thorough review of the origins of these requirements, and of alternate means for meeting NWS data requirements, will be performed.

Development of Drifting Buoy WMS Concept--In past years, NDBC has considered the development of a wave measurement system suitable for use on drifting buoys--meaning, disposable. But an expendable system that produces useful data could never be conceived. Technologies continue to improve, however, and there may now be a way. During FY 1984, NDBC plans to review the possibilities of a suitable WMS for drifting buoys.

Evaluation of the ATON Hull Performance in a Severe Environment--The ATON hull evaluations begun in FY 1982 are not being continued in FY 1983 due to a shortage of needed equipment. This equipment is expected to become available in FY 1984, and testing will resume. NDBC expects to test a properly instrumented ATON hull in a severe environment to verify that the good performance evidenced in light sea states in FY 1982 extends to all sea states.

### DIRECTIONAL WAVE MEASUREMENT SYSTEMS

Heave/Pitch/Roll Sensor Improvements--The apparent unavailability on the market of a satisfactory pitch/roll sensor is the most pressing technical problem related to wave measurements. A compact, reliable, inexpensive, power efficient, accurate, and proveably accurate pitch/roll sensor for use on buoys is needed. A closely related, but somewhat less critical, problem is the apparent unavailability of a satisfactory heave sensor. It is somewhat less critical because, were a good pitch/roll sensor available, triaxial accelerometer outputs could be used to calculate the true vertical heave of the hull. Solutions to these problems would improve the quality of measured data, reduce the cost and size of sensors, facilitate at-sea installation of measurement equipment, make possible waves measuring buoys that are small, flexible, and cost effective, and (through cost reductions) expand the applicability of directional wave measurement systems. If better sensors are not found in FY 1983, the search will continue in FY 1984.

Concept Formulation for a DACT Directional WMS--During FY 1984, a design concept for a directional wave measurement system to be used with the DACT will be formulated. This concept should be consistent with installation aboard smaller hulls, and produce directional data for routine operational use by the NWS.



Operation of DWDA Systems--If satisfactory system reliability can be achieved, at-sea performance evaluation of the new DWDA systems are planned for FY 1984. The design and construction of these units will be evaluated, and critical deficiencies corrected. Documentation will be completed and reviewed for accuracy and thoroughness.

Evaluation of NOMAD DWDA System Performance--Some time will be required to evaluate the performance of a DWDA system mounted on a NOMAD hull, after data begin to come in. The evaluation begun in FY 1983 will continue in FY 1984. The expectation is that ground-truth comparison data will be acquired, and comparison systems developed in FY 1983 will be applied to evaluate performance.

Operate Fixed Platform Calibration Facility--There will continue to be a need for a fixed platform directional wave measurement system, to serve as a source of accurate directional wave data. Therefore NDBC plans to continue the operation of the Atlantic facility, integrated in FY 1983, for the multiple applications previously listed.

Use of the PDWDA System--Technical difficulties prevented full use of the PDWDA as a research tool in FY 1982 and FY 1983. Nevertheless, all elements of the system except the heave sensor have been operating at sea for several months, and there appears to be no reason why the system should not operate reliably in the future. NDBC expects to be able to use this buoy in FY 1984 to test new wave measurement concepts for small as well as large buoys.

### CONCLUSIONS

The technical breakthrough that would most advance buoy wave measurements is the identification or development of a pitch/roll sensor ideally suited for small hull mountings. Such would lead to increased data productivity at lower cost.

Of continuing concern to NDBC is the difficulty of achieving reliability for directional wave measurement systems in an operational environment. The complexity of these systems makes their operation difficult, even on a moderate scale. Calibration, data-quality evaluation, and system maintenance procedures must be improved and made routine. If this can be achieved, the goal will be to expand somewhat the percentage of buoys in NDBC networks with directional capability.

### ACKNOWLEDGMENTS

This survey draws upon work being performed by various elements of NDBC, Computer Sciences Corporation, and other contractors. Numerous individuals contribute, and it is hoped that the cited references assign credit fairly. Particular thanks are due Ms. Sandi Stanic, who prepared numerous versions of the text (in response to fluid conditions), and Ms. Leigh Schaumburg, who edited it.

### REFERENCES

1. Lazanoff, Sheldon and Jack Kaitala "Comparison of NDBC Wave Spectra with Output of the Fleet Numerical Oceanography Center Operational Global Spectral Ocean Wave Model," MTS/NDBC Symposium on Buoy Technology, April 27-29, 1983.
2. "Summary of NDBO Wave Measurement Development Activities," NDBO Report No. F-344-1, September 1978.
3. "Progress Report for NDBO Wave Measurement Systems Development Activities During 1978-1979," NDBO Report No. F-344-2, July 1979.
4. "Progress Report for NDBO Wave Measurement Systems Development and Field Testing (1980-1982)," NDBO Report No. F-344-3, September 1982.
5. Howe, Don, "A System for Data Acquisition in the Ocean Environment," MTS/NDBC 1983 Symposium on Buoy Technology, April 27-29, 1983.
6. Steele, K. E., "Design Consideration for Wave Systems Suitable for Use with C-MAN Environmental Systems," NDBO Report, January 1982.
7. Murphy, Joseph, "Nondirectional Wave Measurements With the USCG Aid to Navigation Buoy," MTS/NDBC 1983 Symposium on Buoy Technology, April 27-29, 1983.
8. Earle, Marshall D., "An Analysis of Short Pendulum Heave Sensors," MTS/NDBC 1983 Symposium on Buoy Technology, April 27-29, 1983.
9. Earle, Marshall D. and Kathryn A. Bush, "Acceleration to Displacement Conversion in the Frequency Domain," Marine Environments Corporation Report 80-7-W, July 1980.
10. Earle, M. D. and K. A. Bush, "Analysis of Low Frequency Noise Effects on Double Integration of Acceleration," Marine Environments Corporation Report 82-4-W, February 1982.
11. Fritts, Roland C., "The Wave Data Analysis Function as Performed in Data Acquisition and Telemetry Systems," MTS/NDBC Symposium on Buoy Technology, April 27-29, 1983.
12. "Program Development Plan for the NOAA Coastal Waves Program," NDBO Report No. F-344-4, November 1980.
13. Timpe, G. L., "The Use of NOMAD Hulls as Severe Environment Buoys," MTS/NDBC Symposium on Buoy Technology, April 27-29, 1983.
14. Holmes, John and Donald Windham, "The NOAA Data Center's Utilization of NOMAD Buoy Hulls," MTS/NDBC Symposium on Buoy Technology, April 27-29, 1983.



## SEMI-SUBMERSIBLE BUOY FOR STORMY SEAS

by Alan C. McClure and Ivan N. Kirschner

Alan C. McClure Associates, Inc.

The semi-submersible buoy, consisting of an open lattice of tubular members, has been shown to possess excellent durability in severe sea conditions. For applications requiring a steady platform, such as data telemetry, the semi-submersible is particularly suitable.

The paper describes the inherent characteristics of this class of buoy and compares them with those of other widely used buoys. Designs for two buoys of different size and application are presented as examples of the semi-submersible buoy.

### INTRODUCTION

The semi-submersible buoy was conceived as a solution to a need for a large, stable, reliable operating base in exposed sea areas. The semi-submersible is most appropriate in open ocean locations in the range of about 100 000 lb to 500 000 lb displacement. A distant cousin of the familiar semi-submersible drilling rig, the buoy utilizes some of the same principles. Natural periods of motion are designed to be greater than those of waves normally encountered. The buoy operates, in its design operating weather, in wave periods below its resonance where response is minimal. Very little vertical or angular motion results from waves in this regime; therefore, this is a desirable characteristic for a buoy to be used as a beacon, a microwave relay station, or as a stable reference point in the ocean. Its indifference to waves makes it less than ideal as a wave detector but other characteristics render the semi-submersible an excellent general purpose oceanographic station.

Figure 1 presents a typical configuration of a three-column semi-submersible buoy. This design has been developed for the Defense Systems Division of Cubic Corporation for use in an overwater Air Combat Maneuvering Instrumentation range (tacts/ACMI). This system consists of an array of five buoy-mounted remote electronic units which relay data from maneuvering aircraft to a master station. The data are processed in real time by a multiple CPU mini-computer for monitoring and reconstruction of tactical aircraft training exercises. The particular

geographical location requires remote antenna heights of 75 feet above the water, hence the relatively large buoy.

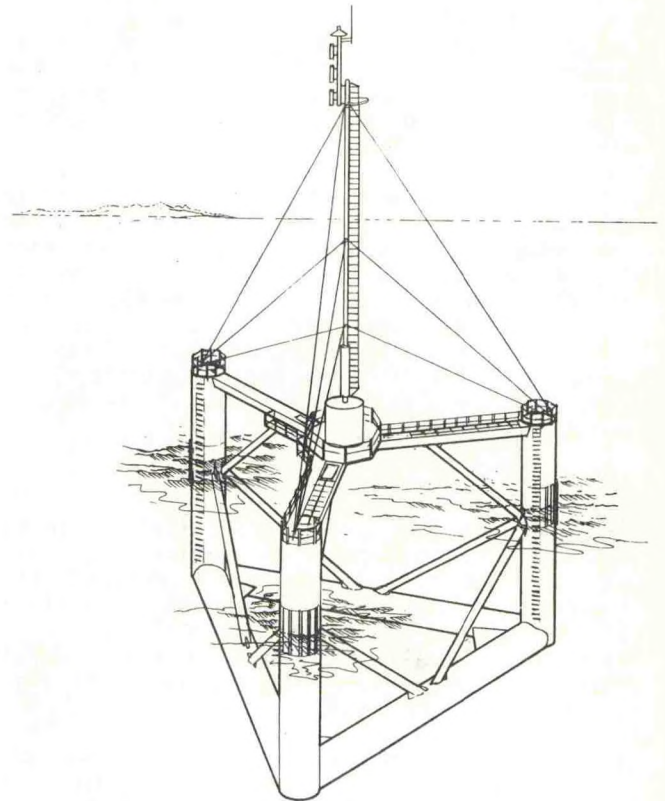


Figure 1: Typical Configuration of a Semi-Submersible Buoy

### FEATURES OF A SEMI-SUBMERSIBLE BUOY

#### Structure

The semi-submersible buoy consists of an open lattice of tubular members. It is highly transparent to waves, allowing waves to pass through the structure with little effect on either motions or structural loading. Conversely, the structure has little effect on the imposing wave.



The main structure is composed of tubular members and box beams. The columns intersect at their lower ends with horizontal tubular elements which run between the columns. At their upper end, the columns intersect with horizontal box beams which run to the center of the triangle defined by the column centers. In a smaller version of the design, tubular members are used in place of the box beams for ease of construction.

In order to obtain minimum motion and minimum response to waves, the design must be more open than the designs of semi-submersible drill rigs. That is, the elements must be more slender in relation to their spacing. Any reasonable number of columns may be used; however, we believe that the minimum number of columns (three or four) results in a more economical structure. The cross-sectional shape of the columns may also be varied. However, simple cylindrical or tubular members are easy to construct, and provide the required characteristics of strength and rigidity. Many of the elements can be made of standard pipe, further reducing costs.

A structure made entirely of cylindrical tubes will have very low damping, probably too low for optimum performance. Therefore, it is necessary to incorporate some flat plate elements in the structure. As shown in Figure 1, the flat plates also serve the purpose of corner gusset plates to increase the rigidity of the structure. Diagonal members stiffen the structure as required but participate only to a minor degree in the dynamic performance of the buoy.

#### Ballasting

For convenience in moving from building site to operating site, the buoys are built so that they may be towed at a shallow draft at which the lower cylindrical members will be at the surface of the water. This not only reduces towing resistance but also increases the stability so that they may be towed at higher speeds than would otherwise be possible.

Water ballast is then used to bring the buoy down to its operating draft. This is accomplished by an old submarine trick. The buoy is first very carefully and accurately ballasted in a calm water location using solid ballast to bring it to a predetermined level. Upon reaching the operating location, the water ballast tanks are opened and completely flooded to bring the buoy to the proper draft. There is thus no adjustment needed at the operating site. This not only saves time, but also makes it possible to perform careful adjustment of the weight distribution in calm water near the building site. Adjustment at the operating site would be extremely difficult because of waves and wind.

Figure 2 on the following page shows the typical deployment of a semi-submersible buoy.

The use of solid ballast also makes it possible to adjust the vertical center gravity of the buoy to obtain the desired angular motion and stability characteristics.

Buoyant spaces in the lower cylinders and columns may be foam-filled to minimize the possibility of sinking in case of damage, cracks, or leaks in the structure.

#### Mooring

Two mooring systems have been developed for the buoys. In some cases a single point mooring is satisfactory and is certainly less expensive than a multipoint mooring. Where the watch circle must be restricted, or antenna orientation is a consideration, a multipoint mooring is required, which in most cases is a three-point mooring corresponding to the three columns of the buoy. For a three-point mooring, lines may be attached to padeyes located on the columns at an optimum point below the waterline. In this position, forces of wind and current are balanced so that the mooring system has negligible effect on the inclination of the buoy. In the cases where a single-point mooring is called for, a center structure has been provided so that the mooring attachment point can be about half way between the baseline and the waterline. This enables the mooring load point to be close to the center of pressure of wind and current. The buoy has sufficient stability so that heel due to wind and current is fairly small.

#### Motion Characteristics:

The buoy is designed to remain relatively stationary even in very severe waves. The limits of minimum motion are defined by:

- (1) wave height, when the crest or trough intersects the upper or lower buoyant members of the buoy, and
- (2) wave period approaching the heave natural period of the buoy.

With regard to the wave height limitation, a typical large buoy design has 15 feet of clearance from still water to the upper structure. Assuming the wave crest is 60% of wave height, the buoy will behave linearly in waves up to about 25 feet in height. This eliminates the possibility of large motion in all but severe storm conditions.

An important advantage of a semi-submersible buoy of this type is the ability of the designer to tune the natural motion response periods to the expected sea spectrum conditions.

The buoy design shown has a natural period in heave of about 14 seconds, which is greater than most ocean swells. In the buoy designs developed to date, heave damping is relatively large to



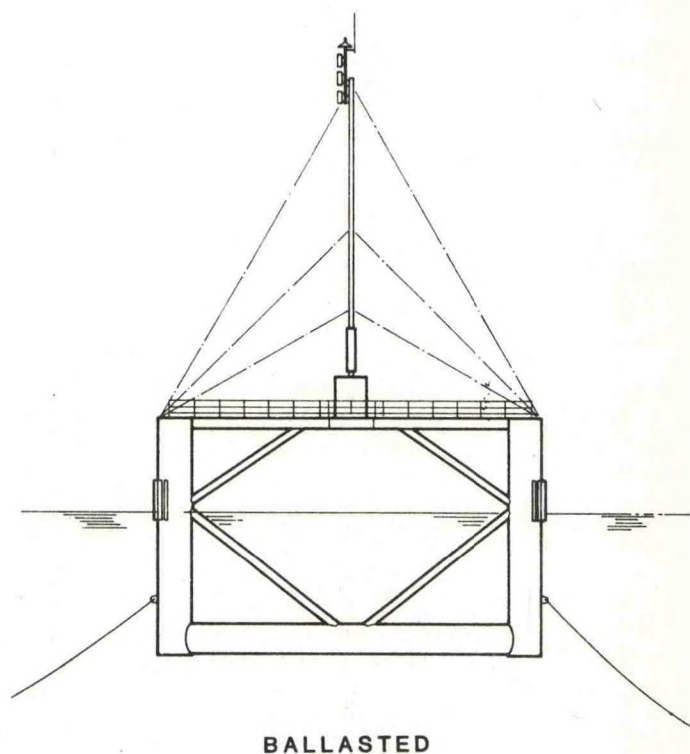
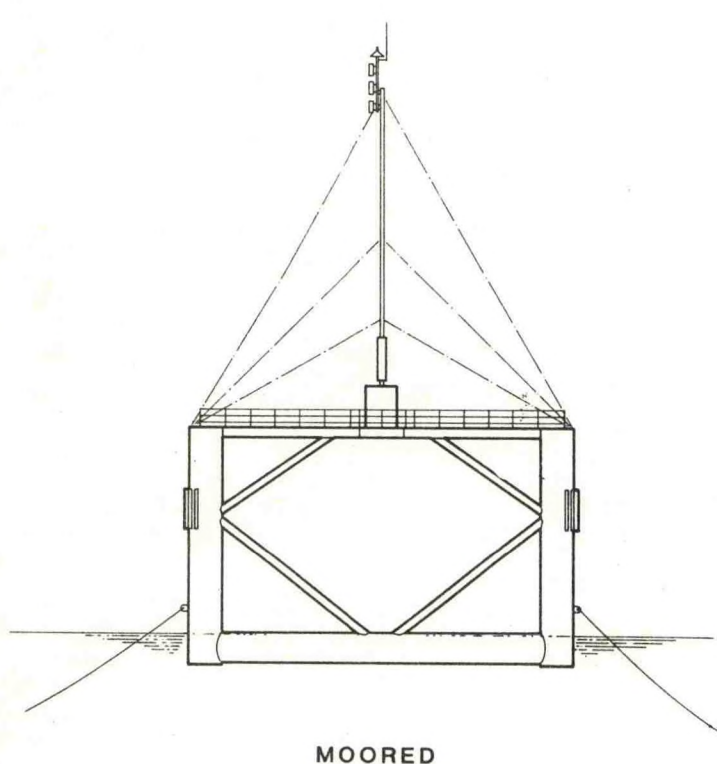
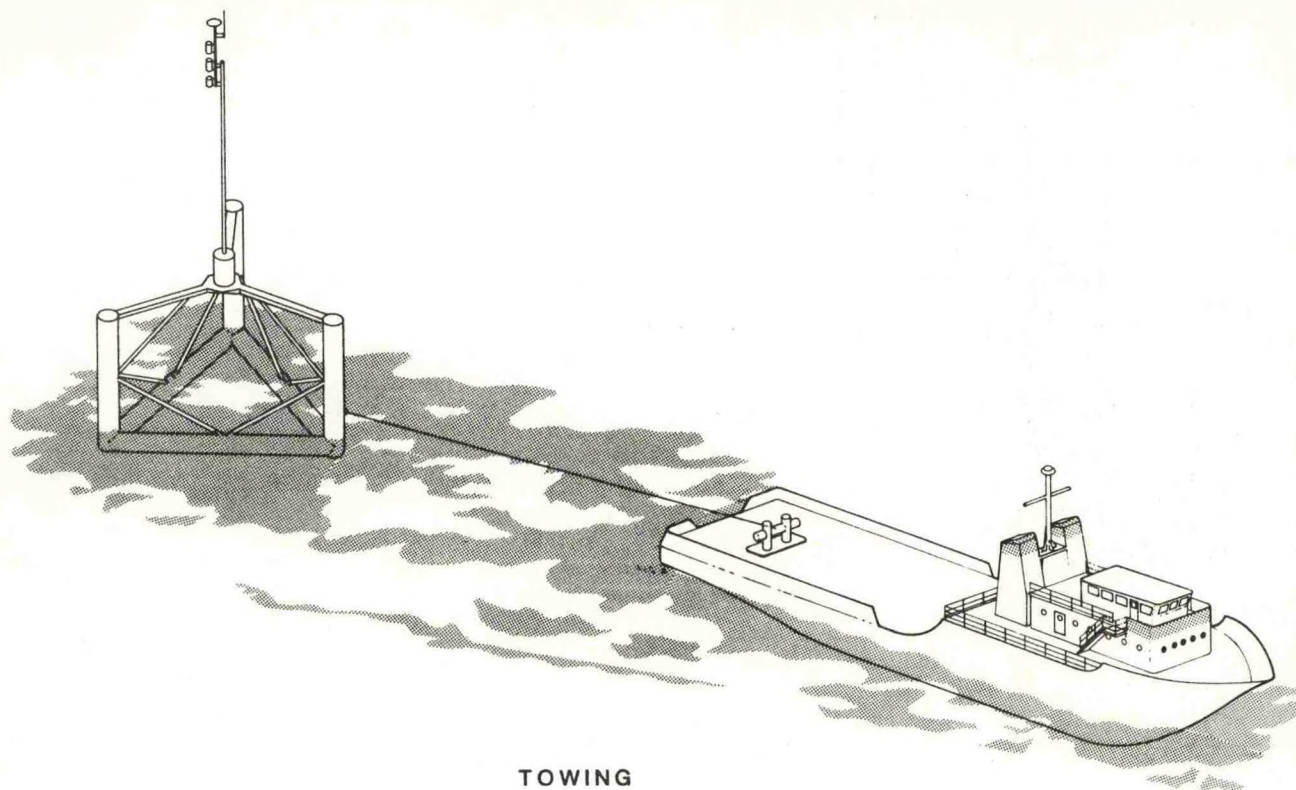


Figure 2: Ballasting Procedure of a Semi-Submersible Buoy

The buoy is towed to its operating site at a shallow draft. With the lower hulls just intersecting the waterline, the stability and towing

resistance of the buoy are optimum. The buoy is then moored and ballasted.



control motion in unusually long waves. The natural periods of angular motion are characteristically longer than the heave period.

A vessel's natural period in heave is dependent on the mass, the added mass, and the waterplane area. The natural periods in roll and pitch are dependent on the mass, the added mass, the radii of gyration, and the metacentric height in the plane of motion. Knowing the nature of the sea in the area of deployment, the designer can choose appropriate periods of motion and vary the parameters on which the periods of motion depend in order to achieve these periods.

#### Stability:

Aside from its favorable motions characteristics, the principal advantage of the semi-submersible buoy is its range of stability. It has only one stable position: upright. By varying the placement of the solid ballast in the buoy the metacentric height can be easily varied.

Hydrostatic curves for a buoy of 500 000 pounds displacement are shown in Figure 3. Such a buoy is positively stable to an angle of 180 degrees. In other words, were the buoy to be overturned, it would right itself.

#### Survival:

Buoy failure can occur from structural failure, capsizing, flooding, mooring failure, and equipment failure. Each of these hazards has been considered during design of the buoy in order to maximize reliability of the entire system.

The stability phase of the design includes calculation of the hydrostatic characteristics of a chosen geometry. From these calculations a hydrostatic curve sheet is produced, similar to the one shown in Figure 3. This information is used to place upper limits on the vertical center of gravity to insure positive stability in the upright condition. Detailed designs include calculation of the stability for all angles of heel to insure that the buoy is stable in all conditions.

Model tests have been performed for a buoy of 500 000 lb displacement. The model was subjected to large breaking waves. It is interesting to note that it was not possible to capsize the buoy, while disc buoys capsized repeatedly in the same waves.

The environmental forces due to wind, waves, and current are predicted for each design. This information is used to calculate the primary bending moment on each major element of the buoy to insure sufficient strength. Local stress is diminished by providing continuity of structure at all critical joints, and by sufficiently stiffening the columns, and the lower and upper hulls. Gussset plates are provided at the ends of

the diagonal cross braces in order to more evenly distribute the stress at the joints. The damping plates at the intersection of the lower hulls provide additional rigidity.

The most vulnerable parts of the buoy are the handrails and gratings. The handrails are wire rope supported by angle bars, and are thus easily replaced. The gratings are fashioned from commercially available materials hooked to the supporting structure, and are also easily replaced.

Ample cathodic protection and protective coatings are provided to reduce the degradation of the structure by corrosion.

The semi-submersible buoy is designed so that all spaces below the waterline are either ballasted with sea water or foam-filled. Even if a leak in the hull envelope were to develop, there would be no voids to fill except the ballast tanks, which are normally full in the operating condition. All spaces above the waterline are either sealed, foamed, or drained. Thus the possibility of the buoy's sinking is negligible.

The mooring system is designed to reduce the possibility of failure. Chain segments are included at the top and bottom of each line to resist damage both at the surface (i.e. by fishing lines or boat propellers) and on the seabed (by chafing or hanging up). The line which makes up the middle segment of each mooring line is chosen for good strength and stretch characteristics. Anchors are chosen based on their high holding power.

All calculations concerning the mooring system are based on the extreme environmental conditions for the area of deployment. Thus the possibility of failure of the mooring system is minimized.

The operating equipment on board the buoy is quite simple. Outfit typically consists of sealed, solid-state electronic equipment, marine batteries, and solar panels.

The ballast system consists of piping and valves. The horizontal lengths of piping are angled downward for proper drainage. All piping is supported by sleeves welded to the structure. Provision is made for proper venting and drainage of all spaces.

Davits are provided on the larger buoys for purposes of installing and replacing equipment. These are supported in sockets and are removable. The delicate parts of the ballast air system are also removable. These parts may thus be stored in a safe place on board the buoy tender or on shore.

The favorable motions of the buoy and the simplicity of the outfit combine to reduce the possibility of equipment failure.



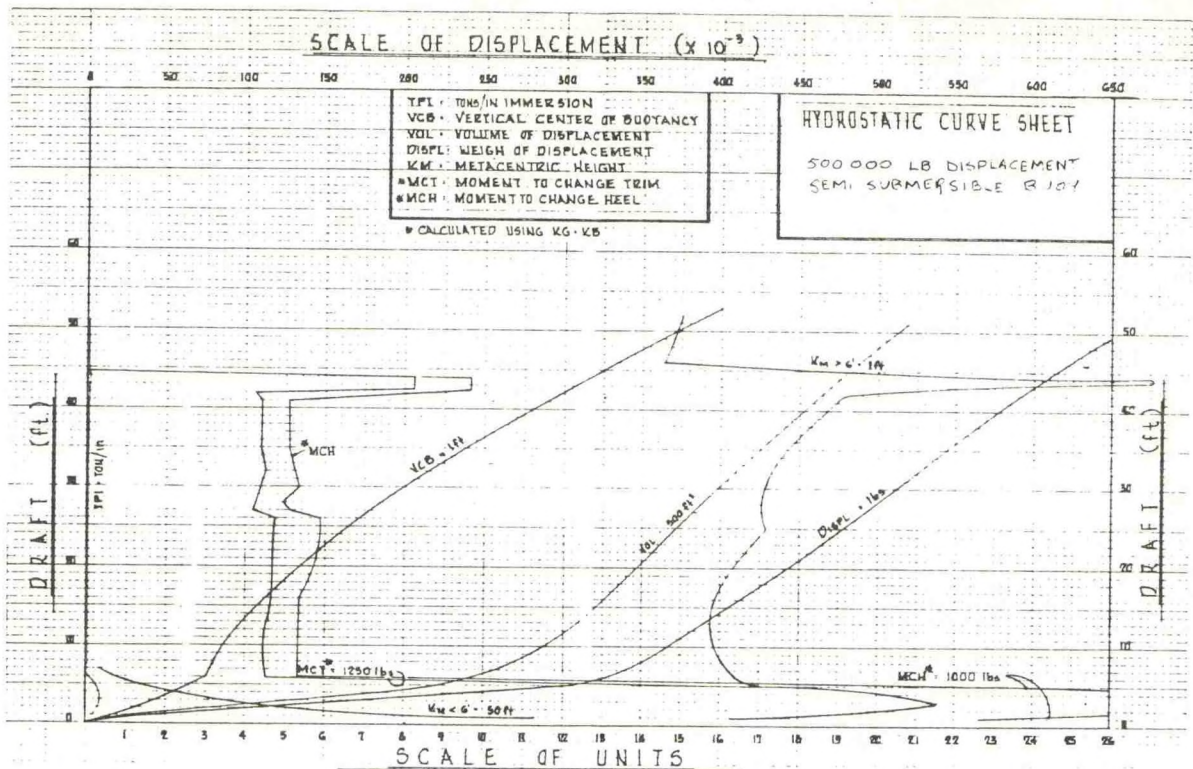


Figure 3: Hydrostatic Curve Sheet for a 500 000 lb Displacement Semi-Submersible Buoy

#### COMPARISON WITH OTHER CONFIGURATIONS

Other types of buoys which have been used or have been proposed for deep sea applications are circular disc buoys, vertical spars, spars with a large buoyant chamber, and a modified boat-shaped buoy. Each type of buoy has its own area of application and particular desirable characteristics. The salient features of the semi-submersible buoy are that it tends to be stationary in a seaway, has great resistance to capsizing or overturning in severe conditions such as breaking waves or high winds, and imposes low forces on the mooring.

Disc type buoys tend to follow the wave surface very closely rendering them satisfactory for measurement of wave amplitude. On the other hand, a number of disc buoys have capsized in service or have broken loose from their moorings, indicating less than desirable survivability in severe weather.

Spar buoys have been used for navigation purposes in shallow water. They have the ability to remain reasonably upright in most conditions but may show very large angles of inclination in certain combinations of wind and current and have very large vertical heave motions at certain wave frequencies. Like the semi-submersible, the spar buoy will not capsize and also does not follow the wave surface.

The semi-submersible is an ideal solution to the need for an inexpensive stable platform at a remote ocean location. Two such applications are described in the following section.

#### APPLICATIONS

##### Offshore air combat maneuvering range:

All buoy designs to date have been used to relay data telemetrically. The Air Force tests its aircraft by means of a maneuvering range, consisting of strategically located antennae which track the aircraft in their maneuvers and relay the data to a shore-based computer. This information is then used to critique and improve tactical aircrew's training.

Because the marine environment provides for low interference, both in the transmission of data and in the testing of the aircraft, an offshore air combat maneuvering range is ideal.

In order to achieve sufficient antenna height, a tall mast is needed. To make calibration of the antennae possible, it is necessary to mount the antennae on a very stable platform. A semi-submersible buoy is very suitable for this application, because it is quite stable and has a large resistance to wind heel.

A typical range consists of five semi-submersible buoys deployed on a circle of thirty miles



diameter. Each buoy houses the tracking, calibration, and relay antennae, as well as electronic support equipment, batteries, and solar panels.

#### Seismic data relay station:

Another application of the semi-submersible buoy is in the relay of seismic data from the seabed to a shore-based station. One configuration has been designed wherein a monitor on the sea floor relays data to a semi-submersible buoy via a cable. The buoy supports mast-mounted antennae and the powering equipment (batteries and solar panels) required to relay the data ashore.

#### Other applications:

One configuration which has been proposed but not designed would be used to collect oceanographic data. Such a system might consist of an array of wave-following buoys relaying wave data to a semi-submersible buoy which would, in turn, relay the data ashore. Instrumentation mounted on the semi-submersible master buoy would collect other data such as atmospheric, subsea, physical and biological data.

The semi-submersible buoy might also be used as any of a variety of navigational aids.

#### Conclusions:

Using known principles, the semi-submersible buoy represents a non-developmental floating vessel having a number of desirable properties for a wide range of applications. It is characterized by steadiness in a seaway, high reliability, and moderate cost. The concept lends itself primarily to the larger buoy sizes. Designs have been prepared for buoys of 100 000 lb to 500 000 lb operating displacement for open ocean service. Smaller buoys would be practical in sheltered locations.

#### ACKNOWLEDGEMENTS

The authors and Alan C. McClure Associates, Inc. gratefully acknowledge the participation of Cubic Corporation, and in particular Mr. James Parsons and Mr. Charles Whitney in development of the semi-submersible buoys.



# A DESIGN PROCEDURE FOR MOORINGS WITH RESTRICTED WATCH CIRCLES

by Thomas J. O'Boyle and Theodore P. Jones

Ocean Engineering and Construction Project Office  
Chesapeake Division, Naval Facilities Engineering Command

## ABSTRACT

This paper demonstrates a rational process for the design of moorings which require restricted watch circles. A systematic approach relating buoy deflection, water depth, anchor drag, leg pretension and other physical parameters is presented. The result is a pretensioned mooring which meets the performance requirements of a reduced watch circle and allows for the unknown anchor drag distances which arise from the geotechnical uncertainties of the site.

This approach has been successfully used by the Navy to design and install moorings for ammunition barges in Puget Sound, WA. It is not covered in standard Navy mooring design manuals, nor is it detailed in other port facilities design texts. Previous methods have not addressed the relationship between anchor drag and pretension forces. This method is an invaluable aid to the designer of a restricted watch circle mooring since it can easily be coded for a hand held calculator or a computer.

## 1. INTRODUCTION

The Officer in Charge of Construction, Naval Facilities Engineering Command, TRIDENT (OICC, TRIDENT) was tasked to provide three fleet moorings on the west side of Indian Island, Puget Sound, Washington. These moorings were Phase I of a total of six moorings to be installed at the Naval Undersea Warfare Engineering Station (NUWES), for securing YC and YFN ammunition barges. Due to unusual site characteristics and the tight positioning constraints of the Explosive Safety Quantity Distances (ESQD) it was imperative that the moorings be implanted in precise locations and that the mooring circles swept by the anchored barges be of minimal dimensions. See Figure 1.

In June 1978, OICC TRIDENT requested that the Ocean Engineering and Construction Project Office, Chesapeake Division, Naval Facilities Engineering Command (CHESNAVFACENGCOM, FPO-1) perform a design review and determine the installation options for the first three moorings (Phase I). The remaining three moorings were to be designed in FY82 and installed in FY83. The moorings were designed to be permanent installations and hold the barges in

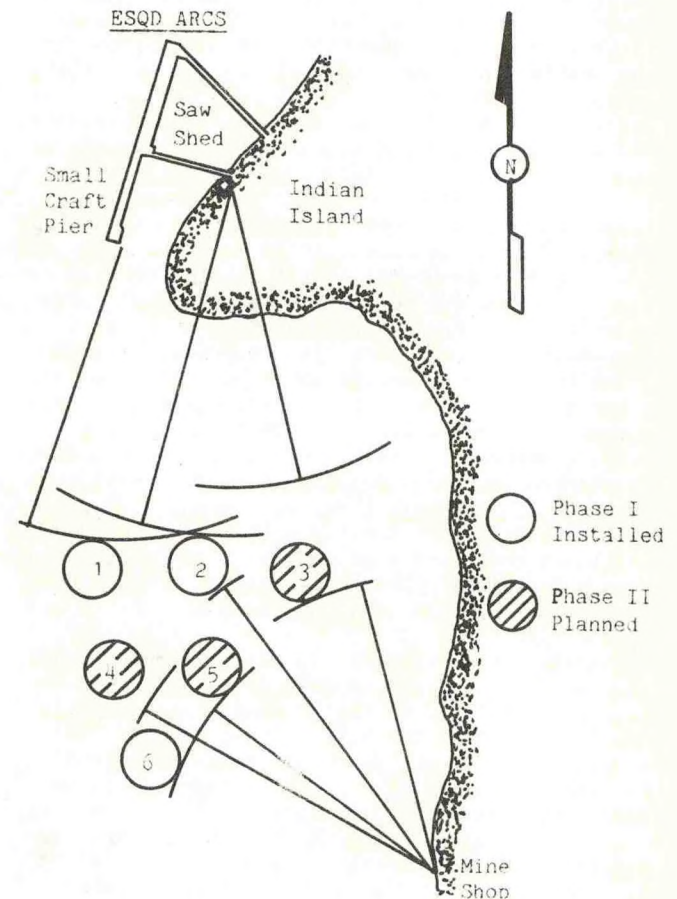


Figure 1

a 100 mph wind with a nominal 2 knot current resulting in a 12 kip design load. The mean low water depths at the Phase I mooring locations varied slightly around 90 feet and the available bottom data indicated approximately 90 feet of zero blow count material below the mud line.

Prior to requesting that FPO-1 perform a design review, OICC TRIDENT procured the mooring materials based on the available information (90 feet of water plus 90 feet of zero blow count material).



In brief, the problem was to design a mooring for 90 feet of water using only the material already procured that could be accurately and cost effectively installed and, when under full design load, would have a buoy watch circle of 50 feet or less.

## 2. PHASE I

We wanted the final design for Phase I to remain as close as possible to a standard fleet mooring design, such as found in the Navy's Design Manual, NAVFAC-DM-26 (July 1968). See Reference 1. All the Naval Public Works Centers (PWC) that install and service the existing fleet moorings use DM-26 as their guide. The PWC riggers are familiar with the configurations and connections of the standard mooring types. Also, the installation procedure would be familiar to PWC deck personnel and could be accomplished using Government assets. The installation would be safer than if a unique design was used. The main disadvantage of using the standard design for this installation was the large watch circle that is associated with a long riser. This large watch circle would be in excess of the allowable 50 foot maximum. The mooring configuration options we considered were: (a) a two point mooring; (b) a telephone-type mooring; (c) a free-swinging, shortened riser mooring. The two point (bow-stern) mooring would restrict the barge movement the greatest, but would require the procurement of more material. The telephone-type mooring brings all the anchor legs up to the buoy. This arrangement reduces the watch circle efficiently, but in this water depth, results in excessive weight in the water column. The buoys available on island were not large enough to support this much weight. The free-swinging mooring configuration was chosen as the best option.

A standard free-swinging riser-type mooring would have a buoy watch circle greater than 70 feet in this water depth. We had to modify this configuration to reduce the watch circle and keep the vertical load on the buoy low enough to maintain at least 18 inches of freeboard under a no load condition. We decided to achieve this by putting a pretension on each leg at the ground ring. See Figure 2. This pretension would be generated by lifting the ground ring a distance from its standard position near the bottom, thus creating a catenary in each leg.

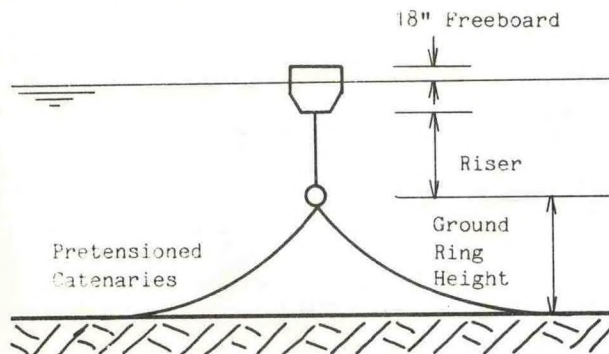


Figure 2

To aid in the numerous calculations, we used a programmable TI-59 calculator for Phase I. Because the programs written on the TI-59 could only handle one horizontal force applied to a catenary at a time, several preliminary loads had to be calculated before the final catenary model could be used. This final model simulated the mooring as a single leg made up of the ground chain and riser. The pretension applied to the ground ring and the calculated environmental horizontal load on the buoy were combined and applied at the buoy only.

The first calculations determined the vertical force needed to lift one end of a ground leg. We made the following assumptions:

1. the projected horizontal distances from the anchor to the ground ring remained constant for each series of vertical forces we applied,
2. the anchor did not move for each series of vertical forces,
3. the chain laid flat on a level bottom,
4. the chain started out straight and tight from the anchor to the ground ring,
5. the chain did not sink below the mud line, and
6. all the load was applied to a single leg.

To account for the unknown anchor drag distance in this zero blow count material, we shortened the projected horizontal catenary length in increments. We created a "synthetic riser" equal in length to the increment we removed. See Figure 3. The combined length of the synthetic riser and the chain on the bottom at zero load equalled the same constant for each anchor drag distance. Figure 4 shows the vertical load due to a single leg at equilibrium for a range of anchor drag distances and ground ring heights.

The vertical force calculation for a single leg was multiplied by 3 to determine the combined effect of all of the legs. We added a nominal riser weight to calculate the total vertical load on the buoy. This allowed us to remove many trivial cases from further consideration. The vertical force on the buoy had to be investigated for the full tidal range. We assumed the ground ring height would vary from +10 feet to -3 feet about its position at MLLW. For example, if the ground ring was 30 feet off the bottom at MLLW, the vertical load on the buoy was calculated for a ground ring height of 40 feet to check for overloading at high tide.

The relationship between the horizontal pretension force at the ground ring and the ground ring height for various anchor drag distances is given in Figure 5. These values are crucial in the final deflection model for the system.



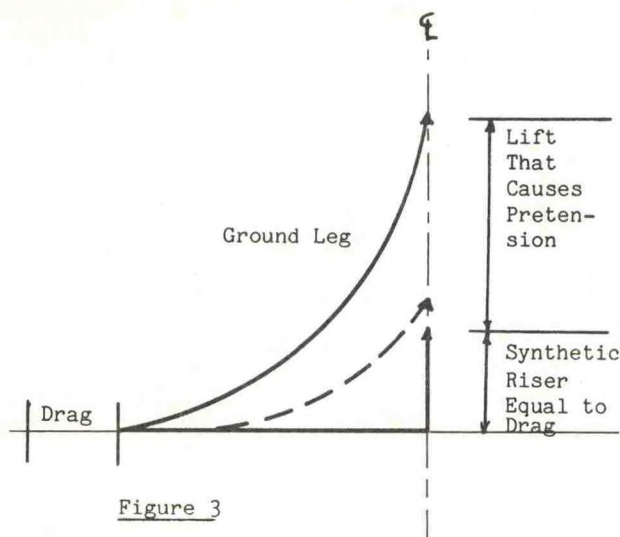


Figure 3

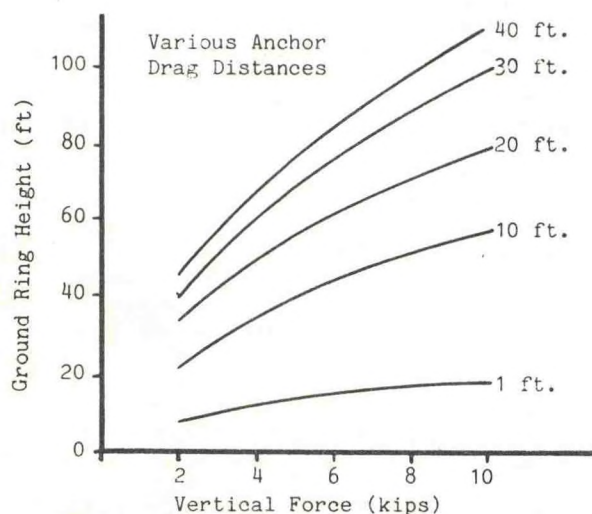


Figure 4

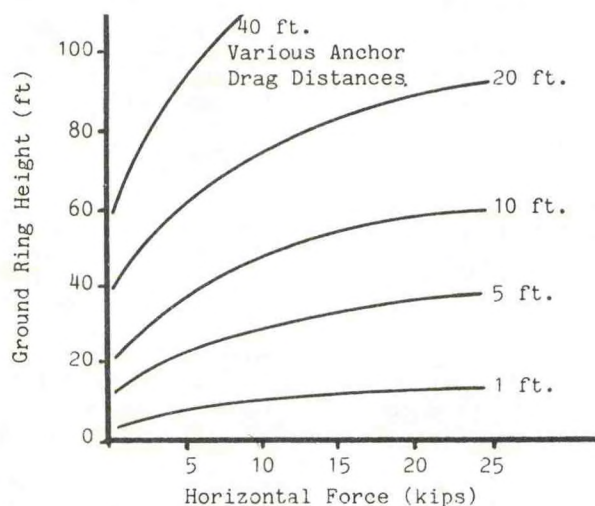


Figure 5

As mentioned previously, the TI-59 calculator can handle only one horizontal force applied to the catenary at a time. The model we used combined the pretension load on the ground ring and the horizontal load on the buoy and applied this load to the catenary at the water's surface. We checked the effect on the accuracy of the deflection calculation due to the combination of the two applied loads as follows. First, the deflection of a catenary formed by only the chain from ground ring to anchor was calculated for a horizontal force equal to the pretension plus surface horizontal forces for a water depth equal to the ground ring height. Second, the catenary was modified to include the riser from ground ring to surface, the same load was applied at the surface and the deflection of the ground ring was determined. These two deflections were approximately the same. This method resulted in a conservative watch circle estimate because the weight of the suspended chain from the other two legs was neglected. This weight would tend to reduce the watch circle.

Using the above model, we calculated the mooring's displacement from its no load position for a range of buoy loads. We plotted the results of these calculations on two sets of curves. The first curves showed Horizontal Displacement versus Horizontal Force. The horizontal force plotted was only the force at the buoy, not the combined force used for the displacement calculations. The second set showed Horizontal Displacement versus Total Vertical Force on Buoy. We used these curves to decrease the number of acceptable candidates by illustrating which configurations would result in vertically overloading the buoy at full deflection. This was not the same requirement as the 18 inch freeboard minimum at no load.

We then combined the information from the above curves into a set of final design curves. For each reasonable ground ring height, we plotted Anchor Drag versus Horizontal Displacement for various water depths and the associated riser lengths. The final design curves illustrated the critical anchor drag distances where: (a) the ground chain became slack below the ground ring; (b) there was excessive vertical force on the buoy, and; (c) there was excessive horizontal deflection of the buoy. The best ground ring height and riser length could then be chosen based upon the maximum anchor for all tidal depths.

During the design phase of this project, a detailed site survey was conducted of the mooring area, and the bathymetry confirmed a flat bottom. The sub-bottom profiles indicated the same type of material was present at all the mooring locations, but could not give any indication of the soil strength. Several Vibracores were taken in the area and showed a greenish gray organic material. The only indication of soil strength was obtained during an anchor pull test; the anchor remained on the upper layer of the mud after free-falling through the water column. A line secured to the crown measured the same as the water depth. These field findings strengthened our basic design assumptions and ensured an accurate design.



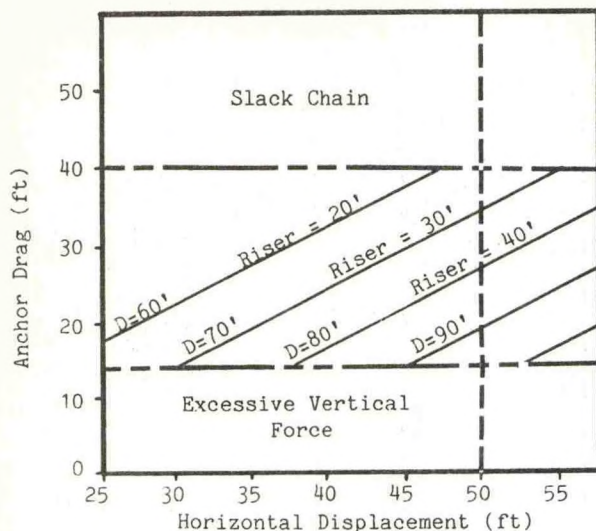


Figure 6

To avoid problems during installation, we kept the design of all three moorings identical. The design called for a three leg riser type mooring. Each ground leg was 430 feet long and was spaced 120' apart horizontally. Each riser was 35 feet long, placing the ground ring 40 feet below the surface. This constant riser length simplified the rigging. We calculated that each mooring would have a watch circle within the 50 foot maximum. The design allowed the following anchor drag tolerances: (a) each anchor would slip at least 15 feet, thus avoiding an excess vertical force on the buoy; (b) each anchor could slip up to approximately 30 feet and the mooring would still have less than a 50 foot watch circle.

The installation method was developed simultaneously with the design to ensure that the installation was feasible and that the assumptions made in the design would not be violated. The following scenario was used to install these moorings. Each buoy was fitted with a 45 foot section of chain that could be removed and a 35 foot riser which were attached to the ground ring. Each leg was laid out on the bottom from the ground ring toward a pre-positioned marker buoy. Each anchor's flukes were welded fully open and control lowered using a crown line so the flukes were pointed down. After all three legs of one mooring were installed, each anchor and chain was pulled radially outward using the crown line. This ensured that the chain was straight and tight. After this pull was accomplished, the buoy was lifted up high enough to allow the 35 foot riser to be secured to the deck and then the 45 foot piece of chain was removed. During the lifting operation the load was measured on a dynamometer secured between the buoy and the crane's hook. Using a graph of the Ground Ring Height versus Total Vertical Force, the approximate average anchor slip was determined. Then with this approximate value of anchor slip, the appropriate Anchor Drag versus Horizontal Displacement curve was used to get an approximate watch circle. This field prediction of

the watch circle size was made by the engineer on site to see if it would be necessary to reset the anchors and try again. Each mooring's predicted watch circle fell below 50 feet and no anchor resetting was needed. The final step in the installation was to lower the buoy back into the water with the 45 foot chain section removed.

Unlike all standard Navy fleet moorings, these unique moorings were put through an acceptance test. A tug was secured to each buoy and a dynamometer measured the load applied in the line. The load was brought up to the design load and with this load held constant, the tug pulled approximately toward each anchor. The buoy displacement was noted using transits. The result was an average watch circle of 35 feet.

### 3. PHASE II

The same site characteristics and positioning constraints placed on the first three moorings held for these. As seen in Figure 1, these remaining moorings were bounded by the installed three. Also, the materials for Phase II were procured and on site. The 50 foot maximum watch circle at the same design load was still the main design criteria.

Phase II differed from Phase I in that the hardware was a smaller size, the placement of these three was more restricted due to the previously installed moorings and the number 3 mooring was to be installed on the side of a sloping bottom. Despite these differences the same concept was chosen.

For Phase II the TI-59 calculator was replaced by a catenary mooring program written to our specification by Presearch Inc. See Reference 2. The program is coded for a TEKTRONIX 4081 interactive graphic terminal in FORTRAN. This program has the graphic capabilities of displaying both an elevation view and a load-deflection curve for a mooring leg. The leg can have up to three different materials and two sinkers. Our program is flexible and can be used to analyze a catenary with a single leg or a compound leg using a spider plate or equalizer. Also, the program can do the analysis of a mooring on an inclined bottom. This program made it possible to drastically reduce the time required to perform the iterative calculations.

The material procured for Phase II included 9,000 pound Navy stockless anchors with stabilizers. The behavior of this particular anchor was known because the Naval Civil Engineering Laboratory (NCEL), Port Hueneme, California had performed several anchor holding experiments at Indian Island. See reference 3. This exact anchor type was one of the types used by NCEL. The data from these pull tests was used to better predict the anchor drag distances and anchor holding capacities.

Moorings number 4 and 5 were analyzed using the same procedure as in Phase I. The unknown anchor drag distance resulting from lifting the ground ring made this parametric study necessary. Like-



wise, a parametric study was done for mooring number 3 but, because of the sloping bottom, each leg had to be investigated separately.

In November 1982, we conducted a bottom investigation at mooring site number 3. This investigation consisted of a team of divers swimming down the slope and trying to push a rod into the bottom at predetermined locations. The maximum penetration was approximately one foot. A grab sample from below the loose mud revealed a sandy silt bottom. Two of the mooring's three anchors will be placed in this soil and the third anchor will be in mud.

The final design for all three remaining moorings followed a similar procedure as before. Special consideration was given to the effect of the different bottom soils and slope on the movement of mooring number 3's anchors. The fluke angles will be set to sand on two of the three anchors for mooring number 3.

At this time it is anticipated that we will use a similar installation scenario as in Phase I. This has not been finalized and depends on vessel availability.

#### 4. CONCLUSION

The Navy's successful installation and acceptance test of the three moorings in Phase I proves this procedure of shortening the riser to reduce the watch circle to be effective. The installation procedure is a critical factor to consider to ensure the results are as designed. This method also results in accurate positioning of the mooring.

The design procedure can easily be accomplished with a hand held calculator such as the TI-59. However, a computer aided mooring design program such as our's saves considerable time and effort during the iterative calculations.

#### 5. REFERENCES

1. Naval Facilities Engineering Command, Harbor And Coastal Facilities Design Manual, NAVFAC DM-26, July 1968, Chapters 6 and 7.
2. Presearch Incorporated, Fleet Mooring Leg Design Program Documentation, Vol. 2, User Documentation, FPO-1-82(33), performed for Ocean Engineering and Construction Project Office, Chesapeake Division, Naval Facilities Engineering Command, under contract N62477-81-C-0025, December 1982.
3. Taylor, R.J., Conventional Anchor Test Results At San Diego and Indian Island, Technical Note 1581, Civil Engineering Laboratory, Naval Construction Battalion Center, July 1980, pg. 151.



## THE ATOM '79 MOORING MOTION EXPERIMENT

Kim David Saunders  
Albert W. Green  
Fred C. Hamrick\*

Naval Ocean Research and Development Activity  
Oceanography Division, Code 331  
NSTL Station, Mississippi 39529

### ABSTRACT

The trajectory of a densely instrumented, single point, tautline, subsurface oceanographic mooring was tracked using acoustic transponders and pressure recorders. The results of analyses of current, temperature, pressure, current meter orientation, and acoustic records show that translational mooring motions contributed relatively small errors in current measurements. Greater errors were introduced by uncompensated azimuthal speed response variations in the current meters. The spectral slopes of the errors were found to be the same as those of the measured currents. The observed mooring trajectory was compared with the results of a numerical dynamical model that was forced by the observed currents. Significant differences between the simulation and the observations were found.

### INTRODUCTION

Single-point, tautline moorings are the type most commonly used in oceanographic work. Their wide-spread use stems from the relative ease of deployment and recovery, and from the lower costs compared with multi-point moorings. Although it has generally been assumed that mooring motion contributes little effect in current or temperature measurements, this assumption has not been directly verified.

In this paper, we describe the results of mooring motion measurements and the effects on current measurement errors; we also compare the results of attempts to simulate the observed mooring motions using a numerical dynamical model.

Previous work of this type has been limited in duration and dynamic range of the forcing. Two previous investigations are similar to the present work. The first, conducted in 1972 (Chhabra et al., 1974), consisted of a single point, tautline mooring with two vector averaging current meters (VACMs) at 500 and 1018 m in a depth of 5450 m. The mooring was tracked using an acoustic transponder system. Chhabra (1977) used a dynamical model to correct current measurements for effects of mooring motion.

\*Computer Sciences Corporation  
NSTL Station, MS 39529

The second experiment, which had a duration of only 12.2 hours, was conducted within the Barking Sands acoustic tracking facility in Hawaii (Walden et al., 1977). The mooring contained five VACMs, one temperature-pressure recorder, and two Niskin-type current meters. During this experiment, the currents were weak.

A numerical model that can accurately simulate the observed mooring trajectory is important, since it could eliminate the need for acoustic tracking systems. Unfortunately, these earlier experiments were carried out in regions of weak currents, so the dynamic range of the forcing was small.

The present work was motivated by interests in accurately measuring current fluctuations in the high-frequency, high-wavenumber regime of internal gravity waves. At frequencies above 1 cycle per hour, the current fluctuations in the natural internal wave continuum are small (nominally less than 1 cm/sec, r.m.s.); consequently, we considered that mooring motions of the same magnitude and frequency might be a significant source of noise. The results of earlier work did not furnish a reliable guide to estimating the extent of this potential noise problem, so we attempted to design an experiment that could give accurate estimates of motion-induced errors in current measurements. The configuration of this mooring is described in section 2. ATOM is the acronym used throughout this paper, as this was an Acoustically Tracked Oceanographic Mooring. In section 3, we describe the structure of the experiment, the results and the comparisons between the observed mooring motions, and the numerical model. Section 4 contains discussions of the sources of mooring motion induced errors and the differences between the model and the observation.

### EXPERIMENTAL DESIGN

#### A. Variables and Instrumentation

The experiment was designed primarily to observe the high-frequency, high-wavenumber portion of the current and temperature spectrum in the upper ocean. The mooring motion study was secondary. As such, the bulk of the current meters--13 NBIS Acoustic Current Meters (ACM)--were placed in a dense vertical array near the top of the mooring. The remainder of the current meters--eight EG&G Vector Averaging Current Meters (VACM)--were placed



above and below the dense ACM section. The nominal depths (for zero current) of the current meters are shown in Figure 1; four Temperature/Pressure Recorders (T/P) were placed on the mooring to measure the vertical excursions of the mooring.

**FINAL CONFIGURATION FOR ATOM '79**  
(Acoustically Tracked Oceanographic Mooring)

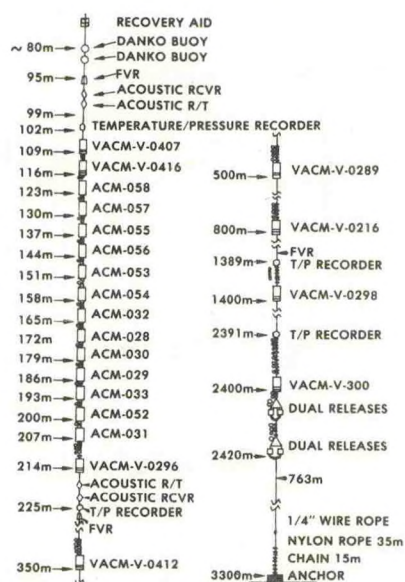


FIGURE 1. Schematic configuration of the ATOM '79 mooring

The acoustic tracking instrumentation was supplied and operated by Dr. Robert Spindel of Woods Hole Oceanographic Institution. Two sets each of pulsed acoustic travel time tracking and Doppler tracking instruments were placed in the mooring at the design positions shown in Figure 1.

The operation of the Doppler tracking system is described in Porter et al. (1973) and Spindel et al. (1978). The combined system is described in Spindel et al. (1976). One pair of pulsed and Doppler tracking recorders was placed just above the dense current meter array and another just below it. Three acoustic transponders with CW beacons were implanted on the sea floor after the mooring was deployed.

#### B. Site Selection

The mooring was deployed in the central Gulf of Mexico at 25°48.33'N, 89°44.65'W. This location was chosen because of several important features: the proximity of a NOAA data buoy equipped with meteorological and surface wave sensors; the bottom was relatively flat; and, historically, this was a region of low currents. The last condition was desired to avoid excessive mooring motion and to provide a "typical" background for studying high-frequency processes.

During the period of the experiment, the first two site selection criteria were satisfied, but the last was not. When the mooring was deployed, a strong flow, on the order of 2-3 knots (1-1.5 m/s) to the northwest was present. This was either an unusual westerly excursion of the Loop Current or an eddy recently separated from that current.

The primary effect of the strong current on the experiment was to deflect the mooring considerably more than had been anticipated. The actual depths of the instruments were about 100 m deeper (at least initially) than the design depth. The deeper excursions of the mooring resulted in over-ranging of the pressure sensors, which caused the loss of vertical position data during these periods. Figure 2 shows the time series of pressure at the upper T/P recorder.

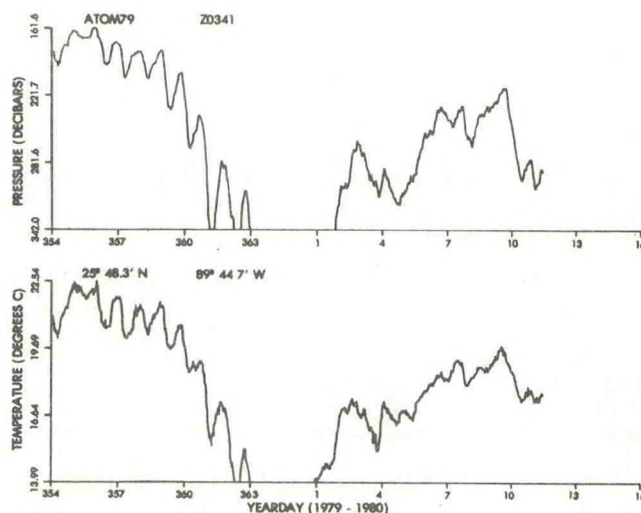


FIGURE 2. Time series of pressure at the upper T/P sensor

#### C. Data Processing

The T/P recorders sampled pressure and temperature every two minutes, recording the samples on a digital cassette tape. This was read and translated at the C.S. Draper Laboratory, and the results were returned to us on a 9-track digital tape.

Plots of temperature and pressure appeared to show a strong correlation (Fig. 3). The correlation coefficient is -0.97. We derived a linear fit between the pressure at the upper T/P recorder and the temperature at the uppermost ACM, and used this relation to estimate the pressure history at the T/P recorder from the ACM temperature history.

The horizontal positions of the mooring were measured at 30-minute intervals using two acoustic pulsed tracking systems. Two out of three transponders failed by January 8, 1980. The lower recording unit ran from the time of deployment until the transponder failure, while the upper unit overwrote



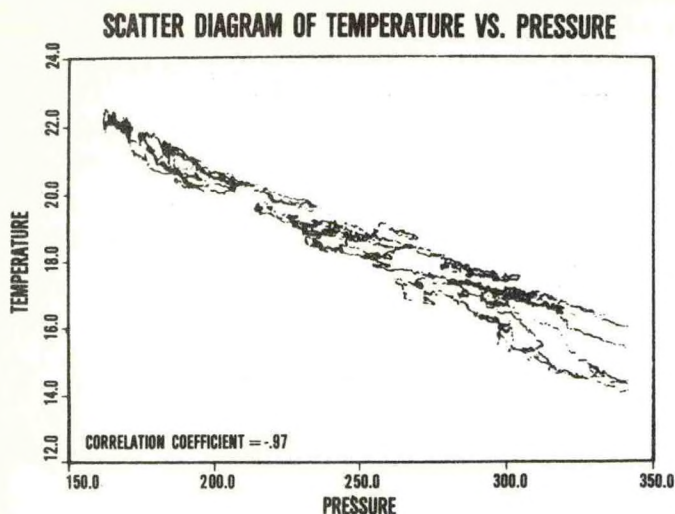


FIGURE 3. Scatter diagram of temperature vs. pressure

the beginning of the tape, leaving only data after December 28, 1979. The Doppler systems sampled data every 30 seconds.

Because of beacon/transponder problems, there were usually only two good paths from which to determine the instrument position. Therefore, the depths of the acoustic units were extracted from recorded pressure data or from estimates of depth derived from ACM temperature and T/P correlations. Missing position data were interpolated linearly.

The current meter records (including temperatures) were translated from the original cassette data tapes to engineering units, and edited for spikes and time offset errors. Standard processing was performed on the data to produce statistics, spectra (including cross spectra) and plots (Saunders et al., 1980).

## RESULTS

### A. Observed Currents

The currents observed at the upper acoustic current meter (Fig. 4) are typical of the currents observed at the other current meters in the upper 150 m of the mooring.

These currents were, on the average, directed toward the west-northwest ( $293^\circ$  magnetic) at a speed of 0.44 m/s, with a standard deviation of about 0.07 m/s. The maximum speed was 0.63 m/s in the direction of  $309^\circ$  magnetic. This maximum speed occurred about January 2, 1980. The minimum speed was about 0.25 m/s in a westward direction on December 22 and again on December 25.

The rotary spectra of the currents at the upper ACM (Fig. 5) exhibit a clockwise peak at the inertial frequency, while the spectrum falls off approximately as  $f^{-2}$  at higher frequencies. There appears to be a slight tendency toward flattening at the higher frequencies.

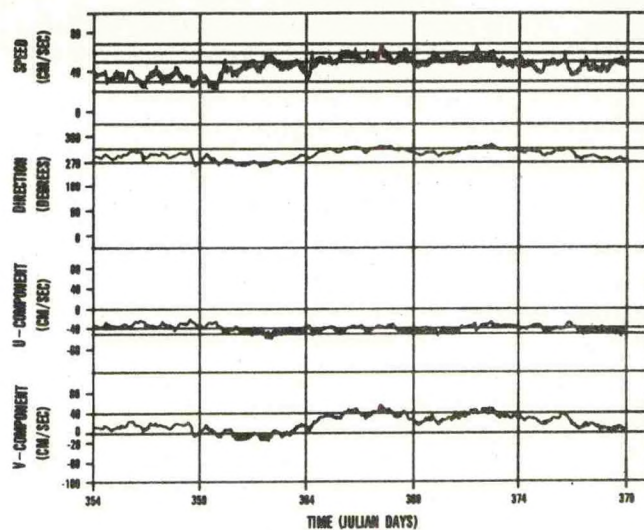


FIGURE 4. Currents observed at the upper ACM

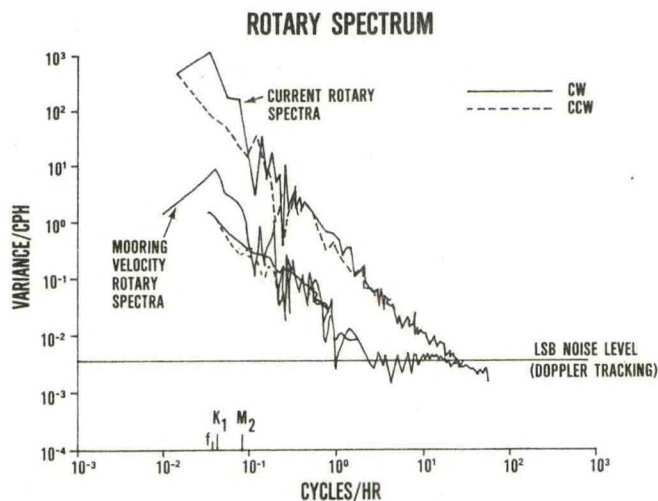


FIGURE 5. Rotary spectra of currents at the upper ACM

### B. Observed Mooring Motions

The greatest horizontal excursion of the mooring occurred on January 2, coinciding with the period of maximum current. The minimum excursion occurred on December 22 during a period of low current. The average speed of the mooring was 0.0038 m/s with a standard deviation of about 0.0026 m/s. The mooring speed, direction, and velocity component plots are shown in Figure 6.

The rotary spectra of the mooring velocities derived from both the acoustic travel time and Doppler systems are plotted in Figure 5, along with the current spectra for comparison. The amplitudes of the mooring velocity spectra are below those of the currents at all frequencies and fall off at the same rate at frequencies below about 2-3 cycles per



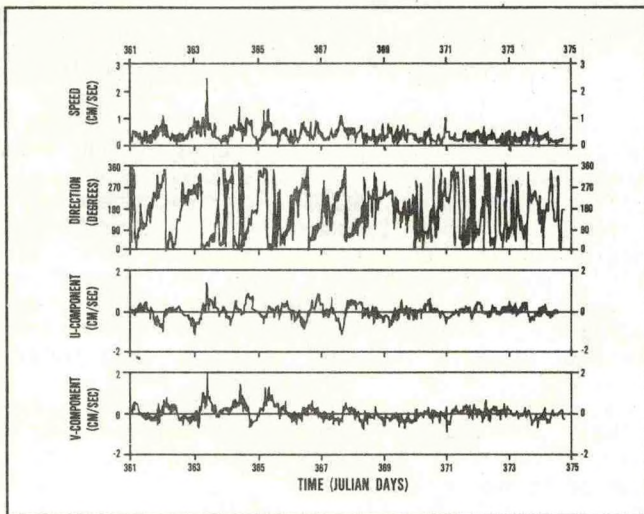


FIGURE 6. Time series of mooring velocity components

hour. At higher frequencies the Doppler spectra become flat at a level approximately the same as that of the current spectra at the Nyquist frequency (this flattening appears to be an instrumental artifact).

Azimuthal variations in current meter speed response will introduce errors in the measured current as the mooring twists about its local tangent vector. The directional speed response of the VACM has been reported in Woodward and Appell (1973). The directional response of the ACM (Fig. 7) has been studied by Saunders (1980), who found that extreme errors as large as +8% of the ambient current speed may be present for certain orientations

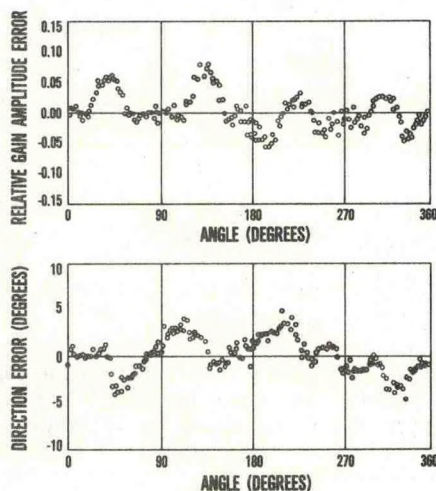


FIGURE 7. Directional response of the NBIS Acoustic Current Meter

of the current meter case with respect to the flow. For example, with a current of 0.5 m/s, errors up to 0.04 m/s might be expected.

This estimate is unduly pessimistic, as most situations are not worst case, and this estimate makes no reference to the spectral distribution of the directional speed response errors. The ACM records the case orientation once for every eight current and temperature samples (in the case of the ATOM '79 experiment, once every eight minutes). From the case orientation data, we have computed the relative direction of the current with respect to the case (Fig. 8). Using an approximate directional speed response function obtained as an

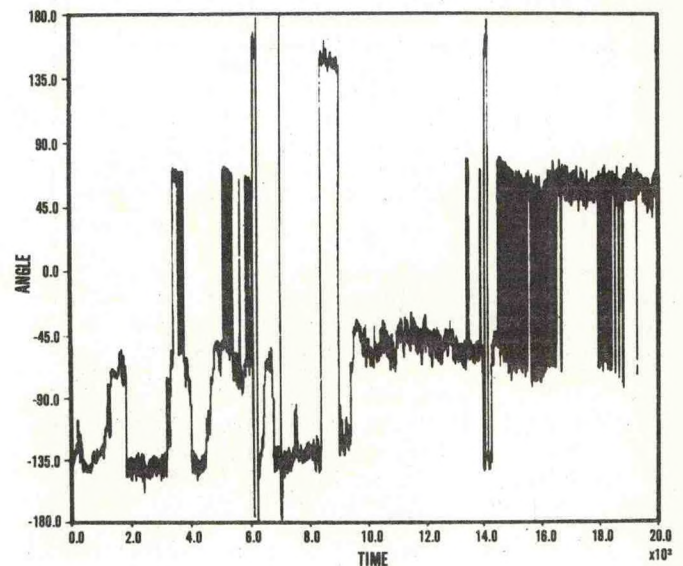


FIGURE 8. Time series of case orientation

average of the measured response functions from several ACMs (Saunders, 1980), the time series of the directional errors was computed for both velocity components. The r.m.s. error was 0.0116 m/s, with a standard deviation of 0.0058 m/s. This is about three items as large as the errors due to translational motions.

Spectra of the horizontal errors were computed and are plotted in Figure 9 with the current spectra plotted for reference. Because the sampling interval was eight minutes, the Nyquist frequency for this comparison is 3.75 cycles per hour. Below this cutoff, the spectra of the errors in each velocity component fall off with approximately the same power law and well below the current spectra. The level of the directional error spectra is higher in most bands than that of the translational error spectra.

### C. The Numerical Mooring Motion Model

Models of the response of flexible cable to a moving fluid have been in development since at least 1918 (Casarella and Parsons, 1970). The basic method for these models has not changed greatly,



## ROTARY SPECTRUM

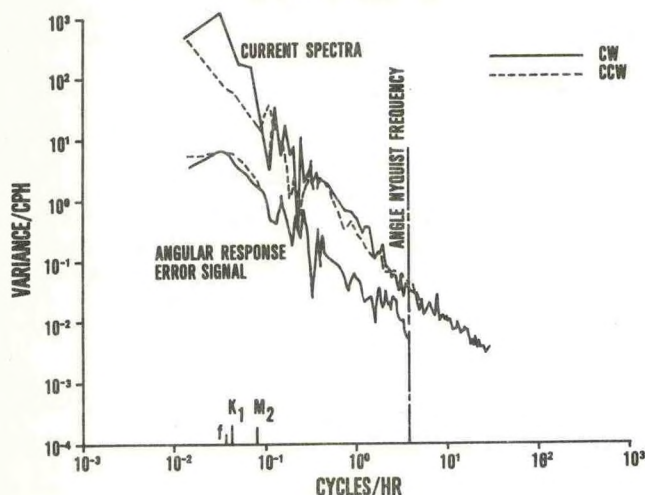


FIGURE 9. Angular error response spectra compared with corresponding current spectra

the primary advances being in the introduction of dynamics and three-dimensional forcing and response, which were made possible by the recent advent of high-speed digital computers.

To simulate the mooring motion, we chose what we believed to be the best numerical mooring motion model available. This model was developed by N.K. Chhabra of the C.S. Draper Laboratory, and has been used for a variety of current meter moorings (Chhabra, 1973, 1974, 1976, 1977; Chhabra et al., 1974). This model incorporates three-dimensional forcing and response with dynamic effects.

Besides the currents, which force the motion of the mooring, the other key parameters in the model include the buoyancies, areas, and drag coefficients of the mooring elements. For the dynamic response, the virtual masses of the elements are also needed. Of these parameters, the drag coefficients are perhaps the least well known.

The principal error in the proper choice of drag coefficient is probably due to strumming effects. The effective drag coefficient is a function of the amplitude of the strumming (Every et al., 1982). Skop and Rosenthal (1980) proposed a formula for this effect, giving the amplified drag coefficient as a function of the Reynolds number. Experiments by Alexander (1981) indicate that the Skop and Rosenthal formula may overestimate the drag coefficient for Reynolds numbers of about 7000-12000 (the range of his measurements). He found that in this range, the drag coefficient was approximately constant with a value of 1.791 with a standard deviation of 0.020. We chose, at least as a starting point, to use 1.8 as our initial drag coefficient for the wire rope mooring elements.

The drag coefficients for other mooring components were taken from Pattison et al. (1977) where available. Some of the mooring elements had peculiar shapes, and the drag coefficients for these

were not known. A value of 1.5 was assumed for these components.

While analyzing the current records, we found that the coherence between pairs of current meters was very low for frequencies above 1 cycle per hour. This was true, even for pairs of current meters separated by as little as 7 m. Because of the low coherence at high frequencies, there was little to be gained by sampling the currents at rates higher than once every 30 minutes. We therefore low-pass filtered the current records with a 30-minute cutoff. These records were used as the forcing for the model. This also had the beneficial effect of reducing the time needed for each model run.

The currents were input at each current meter position and were linearly interpolated between meter positions.

The observed and predicted time series of the positions of a point on the mooring corresponding to the position of the lower acoustic recorder are plotted in x (east), y (north), and z (vertical) components in Figures 10 and 11. The deviations of these positions from the observed positions are plotted in Figure 12.

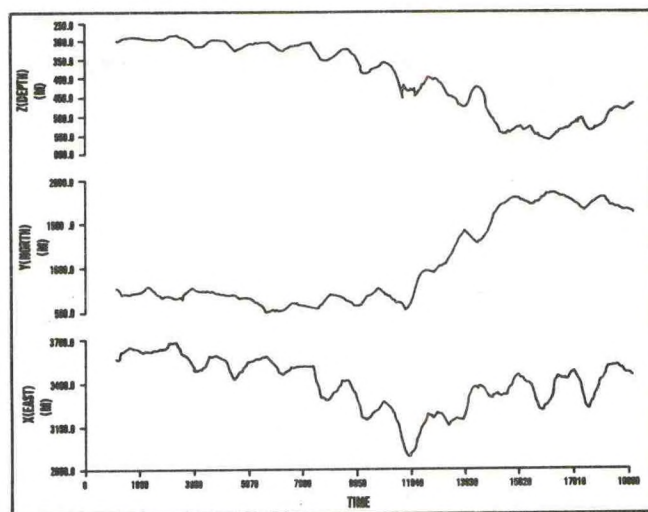


FIGURE 10. Plot of the x (east), y (north) and z (depth) positions of a point on the ATOM '79 mooring corresponding to the lower T/P recorder as observed

To quantify the comparison between the model and the observations, we have adopted the use of a norm, similar to that used by Allender et al. (1977), defined by

$$N_T = \frac{\sum_{i,k} \int_0^T W_{i,k} [\phi_i^{10}(t, \vec{x}_k) - \phi_i^{1m}(t, \vec{x}_k)]^2 dt}{\sum_{i,k} \int_0^T W_{i,k} [\phi_i^{10}(t, \vec{x}_k)]^2 dt}$$



where

$w_{i,k}$  are weights,  $\phi' \equiv \phi - \frac{1}{T} \int_0^T \phi dt$ .

$$\phi_i^0(t, \vec{x}_k)$$

denote observed variables and

$$\phi_i^m(t, \vec{x}_k)$$

denote the variables predicted by a model.

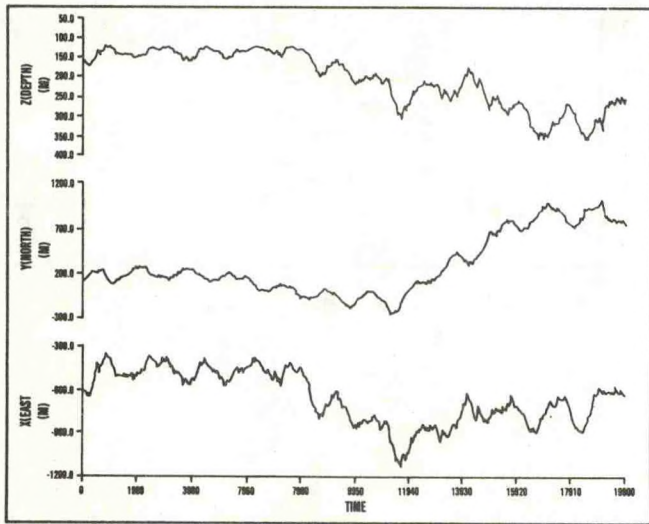


FIGURE 11. Plot of the x (east), y (north) and z (depth) positions of a point on the ATOM '79 mooring corresponding to the upper T/P recorder as predicted by the Chhabra model

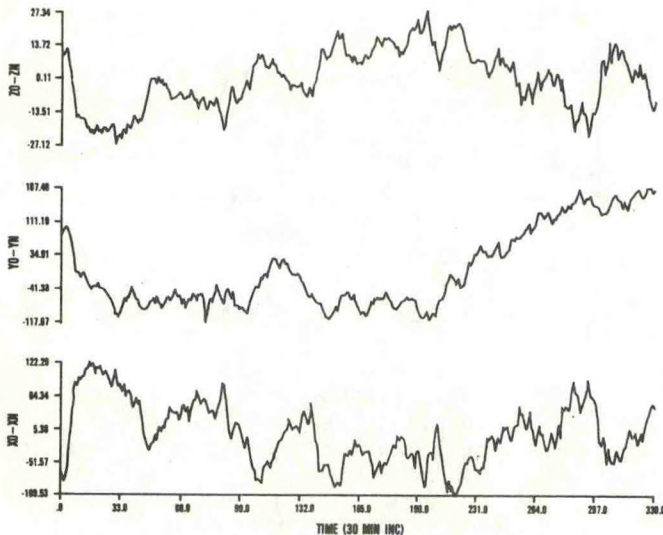


FIGURE 12. Plots of position differences between model predictions and observed positions for the same place on the mooring as that used for Figures 20 and 21

This norm is zero when there is perfect agreement between the model and observations and one when a null prediction is as good as that of the model. If the norm is greater than one, the model is worse than a null prediction. The norm for the prediction shown in Figure 11 was 0.45.

As a further test of the model, we computed the spectrum of the predicted mooring velocities (Fig. 13). This spectrum has a very different behavior than that of the observed mooring velocities, exhibiting a flat to rising tendency with frequency.

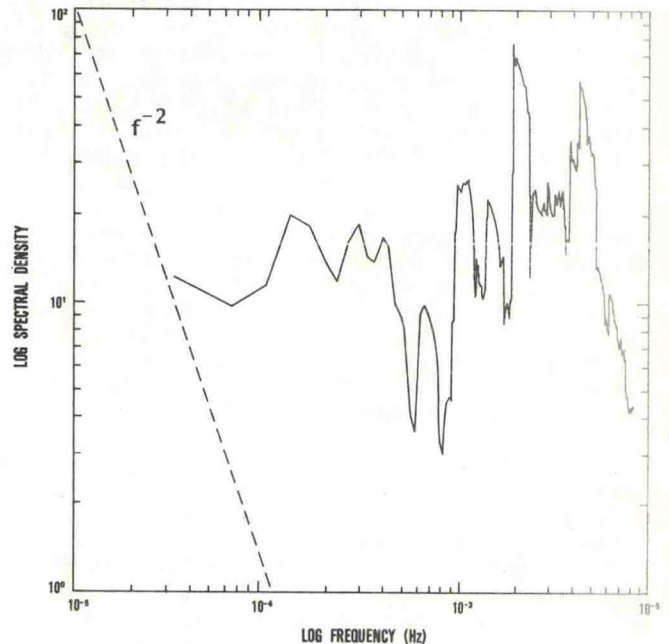


FIGURE 13. U-velocity spectrum of the mooring, estimated by the Chhabra model

## DISCUSSION

In the previous section, we found that

- The current errors due to mooring motion were a small fraction of the current, and that the r.m.s. fluctuation of the errors were small in relation to the r.m.s. fluctuations of the current.

- The random orientations of the current meters with respect to the flow, coupled with the imperfect horizontal speed response was the largest source of error.

- The translational motion of the mooring produced errors about a third as large as those due to rotational motion of the meters.

- The spectrum of the translational error velocity was of similar shape to and less than that of the current.

- The attempt to model the mooring motion using a well-accepted model was unsuccessful in accounting for a large amount of the variance of the



the mooring motion, and produced mooring velocities that had a different spectral shape than that of the current.

In this section we will consider the correction of errors caused by instrument rotations, the cause of the observed translational mooring velocity spectral shape and the feasibility of replacing acoustic tracking of moorings by numerical models using the observed currents to estimate the forcing function.

In principle, correcting the rotationally induced mooring motion error should be simple. All that is required is a good knowledge of the horizontal current meter speed response and the time history of the case orientation. In practice, the correction, particularly after the data have been collected, is difficult. The difficulty arises from a generally poor knowledge of the horizontal response, the rate of sampling of the case orientation, and the averaging method used in processing the current data as they are being collected. These problems can be overcome by careful calibration and redesign of the sampling and averaging methods used in the current meters. An alternative is to redesign the current meters to improve the horizontal response. While difficult, neither of these techniques appears insuperable.

If we assume that the error due to horizontal response can be sufficiently reduced, then we can attempt to eliminate the second source, the translation of the instruments. In the ATOM '79 experiment, we found that the r.m.s. fluctuations of the mooring translational velocities were about 2.6 mm/sec. These are small errors and, in many situations, may be ignored. However, there are some classes of experiments that are critically affected by these relatively small errors. In those cases errors must be corrected or clearly quantified.

There has been some question regarding the contribution of the translation motion error at higher frequencies. We will attempt to set this question to rest before proceeding to the problems of numerical simulation.

It is important to note that forcing frequencies corresponding to peaks in the velocity spectra have little influence on the mooring response in other frequency bands. For example, consider a forcing current of the form  $u = \sin \omega t$ , for which the drag force will be  $D = |\sin \omega t| \sin \omega t$ . The Fourier series expansion of the drag force is

$$D = -\frac{8}{\pi} \sum_{n=1}^{\infty} \frac{1}{n(n^2-4)} \sin n\omega t, \quad n \text{ odd.}$$

The coefficients decay as  $n^{-3}$ . The effect on the spectrum would therefore appear as  $n^{-6}$ . As this is a much faster decay than the typical current spectrum which falls off as  $\omega^{-2}$ , the effect would be simply to modify the spectral level, but not the slope. It might be conjectured that if a velocity time series possessing a continuous spectrum were utilized, the only effect on the spectral shape of the operator  $O(u) = |u|u$  would be to adjust the

level, but not the shape of the spectrum. Figure 14 presents the spectrum of the east component ( $u$ ) of observed currents at the upper current meter on the ATOM mooring while Figure 15 shows the spectrum of  $|u|u$ . Both spectra have almost precisely the same slope, confirming the conjecture made above.

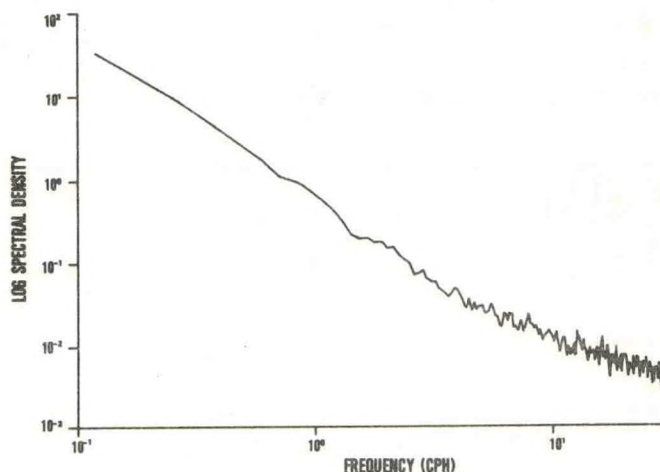


FIGURE 14. Spectrum of the  $u$  component of velocity

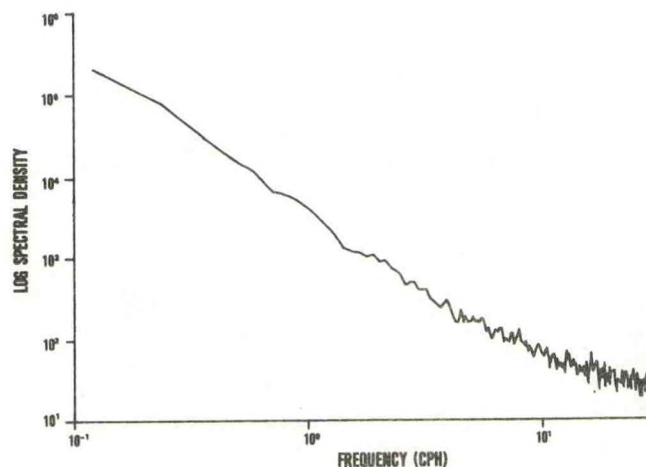


FIGURE 15. Spectrum of  $u \sqrt{u^2 + v^2}$

Spindel et al. (1978) have reported spectra of mooring positions that fell off as  $\omega^{-4}$ . This is consistent with our observations, which show the spectrum of the mooring velocity to fall off as  $\omega^{-2}$ . There is some question, however, why the mooring responds in such an apparently linear manner to what appears to be an inherently nonlinear process.

To gain insight into the physics of the mooring motion, we will consider the motion of a simple inverted pendulum, driven by a randomly fluctuating velocity superimposed on a steady flow.



For simplification, we linearize the equations of motion by assuming that the mean flow is an order of magnitude greater than the fluctuating component of the flow, such that each of the velocity components does not change sign. The data from Figure 4 shows this to be a reasonable assumption for the case of the ATOM mooring.

The equations of motion for a very simple system may be written (Skop and Rosenthal, 1980):

$$M \ddot{x} + \frac{1}{\rho} \rho C_D A (\dot{x} - U) |\dot{x} - u| + \frac{B}{L} x = 0,$$

where

$M$  = the virtual mass of the system,  
 $\rho$  = the density of the fluid,  
 $C_D$  = the drag coefficient,  
 $B$  = the buoyancy,  
 $L$  = the length of the mooring wire,  
 $A$  = the area of the mooring elements,  
 $U$  = the imposed fluid velocity.

If we assume that  $U = U_0 + u$ , where

$$U_0 \gg u,$$

we may linearize the equation of motion obtaining

$$x = x_0 + x'$$

$$M \ddot{x}' + \rho C_D A U_0 \dot{x}' + \frac{B}{L} x' = \rho C_D A U_0 u$$

Simple scaling arguments show that the acceleration term is negligible, leaving as the first-order equation

$$\dot{x}' + \frac{B}{\rho C_D A U_0 L} x' = u$$

We then take the Fourier transforms of both sides of the equation, multiply by the complex conjugates and average, obtaining the following relation between the spectrum of the current,  $S_{uu}$  and that of the mooring velocity  $S_{mm}$ :

$$S_{mm}(\omega) = \frac{\omega^2 S_{uu}(\omega)}{\lambda^2 + \omega^2}$$

where

$$\lambda = \frac{B}{\rho C_D A U_0 L}$$

To see if this linearization were applicable to the actual case with two degrees of freedom with nonlinearity, we constructed a time series in  $U$  and  $V$ . The spectrum of  $U$  is shown in Figure 16. An average velocity component of 0.5 m/s was added to each fluctuating component and the resultant vector time series used to drive a numerical integration of the full equations of the motion for the simple inverted pendulum. The spectrum of the  $U$ -component of the mooring is shown in Figure 17. The spectra are separated at low frequencies, but converge to one another at high frequencies.

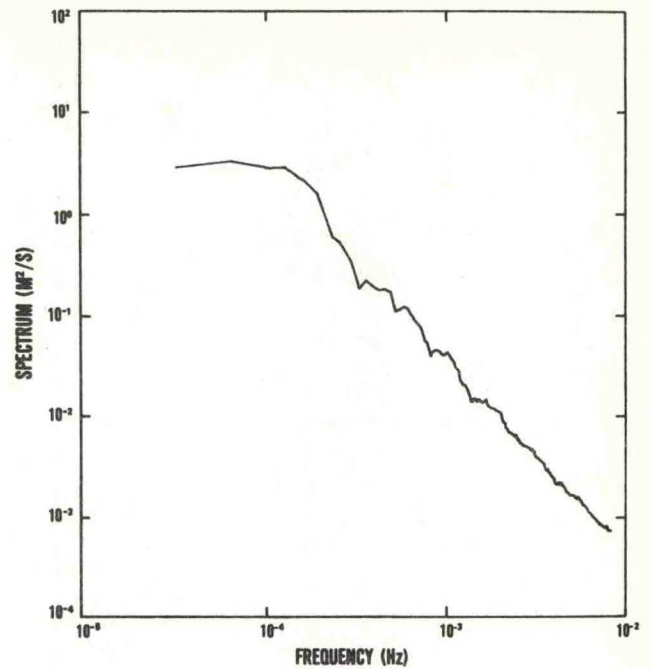


FIGURE 16. Spectrum of input velocity to the simple mooring motion model

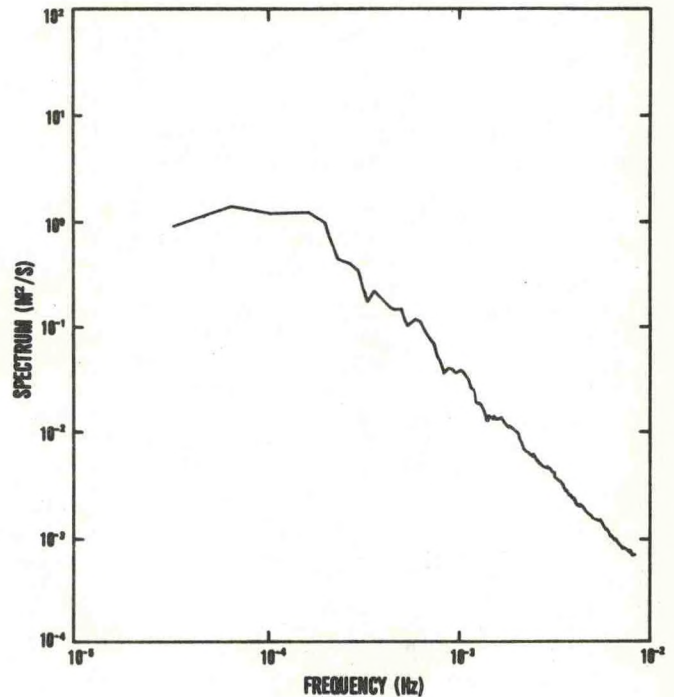


FIGURE 17. Spectrum of the mooring x-component velocity response

It thus remains to explain why the spectra of the observed mooring motions are smaller at all frequencies than those of the currents.



The model proposed by Skop and Rosenthal assumed that the velocity was a linear function of depth. This implies that for their model to be realistic at all frequencies, the velocities at all depths must be coherent and in phase for all frequencies up to the natural frequency of the mooring. Our observations have shown that for periods shorter than about one hour, the velocity coherence drops to essentially zero over distances of 7-14 m. It would therefore be naive to assume that their model can apply for the higher frequencies. Furthermore, one would expect to see a considerable attenuation of the mooring motion in the higher frequency bands. This is precisely what is observed. The flattening in Figure 5 is attributed to instrument sampling noise, as discussed earlier.

The translational motion was not as serious as the combined effects of torsional motions coupled with the nonperfect horizontal response of the current meter. This problem need not be serious, as it can be considerably reduced by proper calibration of the current meter and more rapid sampling of the case orientation. It may also be possible to improve the directional response of the current meter by simple mechanical modification.

Instrumenting a mooring to determine the mooring motion is expensive. If a numerical model can adequately simulate the mooring's response to the current forcing, then it would be cost effective to use the model to obtain hindcasts of the motion based on the observed currents. One of the primary goals of the ATOM experiments was to determine whether it was feasible to accomplish this modeling using existing models.

The Chhabra model SSD31 was used as our paradigm. We found that the value of the norm used as a measure of accuracy of the model was 0.45.

We must address the question of whether this departure of the model performance from the observed mooring motions was particular to this model or would be repeated in any other state-of-the-art model. The second choice is probably correct. We have found that the currents become incoherent at frequencies above 1 cycle per hour at separations of only 7-14 m. Because of the sparse sampling of currents on most moorings, some type of interpolation must be made over regions of the mooring where there are no measurements. The interpolation introduces a false coherence to the signal in these regions, producing an incorrect response of the mooring line to the current. We suggest that this problem might be overcome by an interpolation method that preserves the spatial-temporal coherence structure of the flow while reproducing the flow at the measurement points.

A secondary cause of error in all existing models is the value of the drag coefficient used for the mooring line under strumming conditions. This is an area where more research is required if accurate mooring motion models are to be effective.

## CONCLUSIONS

We summarize the discussion with these conclusions:

- The error due to neglecting mooring motion is small in all frequency bands, so this error should be considered for only very sensitive experiments.

- Certain classes of current meters possess imperfect horizontal speed responses that can cause relatively large errors in the measured current. Improved data recording methods or meter designs can eliminate this source of error.

- After current errors caused by meter case rotations, translational motions of the mooring are the largest source of error. Because of difficulties in applying numerical models to simulate these motions (due to a probable combination of unresolved current structure and model design), acoustic tracking for sensitive experiments is recommended.

## REFERENCES

- Alexander, C.M. (1981). The complex vibrations and implied drag of a long oceanographic wire in cross-flow. *Ocean Eng.*, v. 8, 379-406.
- Allender, J.H., M.J. Berger, and K.D. Saunders (1977). Preliminary verification of numerical circulation models for Lake Michigan. Symposium on Modeling of Transport Mechanisms in Oceans and Lakes, Manuscript Report Series No. 43, 47-58, Marine Sciences Directorate, Department of Fisheries and the Environment, Canada.
- Casarella, M.J. and M. Parsons (1970). Cable systems under hydrodynamic loading. *J. Mar. Tech. Soc.*, v. 4, 27-44.
- Chhabra, N.K. (1973). Mooring mechanics - a comprehensive study, Vol. 1. C.S. Draper Laboratory, Inc., Report R-775.
- Chhabra, N.K. (1974). Verification of a computerized model for sub-surface mooring dynamics using full scale ocean test data. *Proc. Mar. Tech. Soc.*, Tenth Ann. Conf., 69-80.
- Chhabra, N.K. (1976). Mooring mechanics - a comprehensive computer study, Vol. 2. C.S. Draper Laboratory, Inc., Report R-1066.
- Chhabra, N.K. (1977). Correction of vector-averaging current meter records from the MODE-1 central mooring for the effects of the low frequency mooring line motion. *Deep Sea Res.*, v. 24, 279-287.
- Chhabra, N.K., J.M. Dahlen, and M.R. Froidevaux (1974). Mooring Dynamics Experiment - determination of a verified dynamic model of the WHOI intermediate mooring. C.S. Draper Laboratory, Inc., Report R-823.



Every, M.J., R. King, and D.S. Weaver (1982). Vortex-excited vibration of cylinders and cables and their suppression. Ocean Eng., v. 9, 135-157.

Porter, R.P., R.C. Spindel, and R.J. Jaffee (1973). CW beacon system for hydrophone motion determination. J. Acous. Soc. Am., v. 64, 1691-1679.

Saunders, K.D. (1980). Horizontal response of the NBIS acoustic current meter. Proc., OCEANS '80, IEEE Pub. No. 80CH1472-7, 220-225.

Saunders, K.D., A.W. Green, and M. Bergin (1980). A comprehensive graphical representation of data obtained in the Acoustically Tracked Oceanographic Mooring (ATOM) experiments. NORDA Tech. Note 85, Naval Ocean Res. and Dev. Activity, NSTL Station, Miss.

Skop, R.A. and F. Rosenthal (1980). Some new approximation techniques for mooring system design.

In: Near Surface Ocean Experimental Technology Workshop Proceedings, 33-39, Naval Ocean Res. and Dev. Activity, NSTL Station, Miss., R.C. Swenson and R.S. Mesecar (co-chairmen).

Spindel, R.C., R.P. Porter, W.H. Marquet, and J.L. Durham (1976). A high resolution pulse-Doppler underwater acoustic navigation system. IEEE J. of Ocean Eng., v. OE-1, 6-13.

Walden, R.G., C.C. Collings, Jr., P.R. Clay, and P. O'Malley (1977). Validation of the DOCMS intermediate mooring. Woods Hole Oceanogr. Inst., Report WHOI-77-53 (unpub.).

Woodward, W.E. and G.F. Appell (1973). Report on the evaluation of a vector averaging current meter. NOAA Tech. Memo. NOAA-TM-NOIC-1.



## LONG TERM SENSOR PLATFORMS

D. R. Shields,<sup>a</sup> A. T. Maris<sup>b</sup> and L. A. Vega<sup>b,c</sup>

NAVAL CIVIL ENGINEERING LABORATORY,<sup>a</sup> Port Hueneme, California 93043  
GIANNOTTI & ASSOCIATES, INC.,<sup>b</sup> Berkeley, California 94703

### ABSTRACT

This paper presents results of a parametric study on generic discus, spar, semisubmersible and vertically moored semisubmersible platforms. Eighteen platforms and their physical characteristics are presented. The frequency domain models used to obtain the platforms' responses are summarized. Each platform's RAOs and selected rms responses are presented. This information may be used as an aid in the selection of an optimum platform type (of the size range studied) for conceptual and preliminary studies. Construction cost estimates are presented for the generic platforms based on the \$/pound of steel.

### INTRODUCTION

The Naval Civil Engineering Laboratory (NCEL) has the Navy wide responsibility for research and development related to moored floating platforms and fixed surface and subsurface ocean structures. Requirements have been documented for the need to develop technology which will provide reliable and economical long term (6 to 20 years) stable-unmanned ocean platforms for deepwater deployment (up to 7,000 feet).<sup>26</sup> NCEL, under sponsorship of the Naval Facilities Engineering Command, has several efforts underway which will: develop, modify, integrate, and validate computer models for predicting moored platform motions; provide candidate platform configurations which will meet operational motion requirements and survivability requirements a minimum cost; and provide long term synthetic mooring components.

One intended Navy use of ocean platforms is for Tactical Aircrew Combat Training Systems (TACTS).<sup>16</sup> A series of ocean platforms having microwave antennas and other associated equipment are used to form an offshore TACTS range. The Navy presently has one such range in the Atlantic Ocean, and the Air Force has similar ranges in the Gulf of Mexico and in the Mediterranean Sea. The Navy's range uses three leg conventional pile-founded steel jacket

structures located in water depths of less than 150 feet. The Air Force uses a hybrid structure composed of a single vertical steel cassion with a steel gravity base mat foundation in the shallow coastal waters of the Gulf of Mexico. In the Mediterranean Sea the Air Force presently employs trimoored 10-meter discus buoys in water depths of 900 feet, 2,700 feet, 6,100 feet and 7,400 feet.<sup>4</sup> These trimoorings have encountered some problems and six line failures resulted from evidently being broken by trawlers or draggers.<sup>2</sup> The Air Force is also planning to install an Air Combat Maneuvering Instrument (ACMI) range off Okinawa using trimoored three column semisubmersible platforms in water depths of 2,600 to 10,600 feet.<sup>13</sup>

An outline has been provided for the format of guidelines and data base representation which would enable a preliminary selection of an ocean platform for a given site and operational requirements.<sup>15</sup> In response to this outline an extensive review of existing technical literature on the performance data of generic ocean platforms as well as computer aided analyses to develop additional performance data was prepared.<sup>7</sup> The results of the computer aided analyses are the primary subject of this paper.

### GENERIC FLOATING PLATFORMS

In deepwater, which for the purpose of this paper shall be taken as water depths exceeding 500 feet, it is generally conceded that some type of moored floating platform will offer the most economic alternative for the Navy when small deck payloads are being considered. These platforms may be described by their buoy shape configurations and are classified as wave following, deep immersion and open framed. The various types of each are presented in Table 1.

Wave following configurations which have large waterplane areas and small displacements tend to follow waves in both heave and slope. The wave slope ( $\alpha_w$ ) is expressed as

$$\alpha_w = \frac{\pi H_w}{L_w} \quad (1)$$

where  $L_w$  = wave length

$H_w$  = wave height

<sup>c</sup>Presently with EG&E Washington Analytical Services.



Wave following configurations which have large displacements will follow the wave amplitude but not the slope. Deep immersion configurations have small water plane areas and relatively large displacements. The small water plane allows this shape to be nearly transparent to the wave which works in conjunction with the large displacement resulting in their motions being reasonably decoupled from the wave surface profile. A comprehensive review of discus and spar buoys has been presented by Berteaux.<sup>22</sup>

Generic platform shapes of these various buoy configurations were used in this investigation. The purpose was to develop information describing the platforms' performance to a given ocean environment for use in preliminary selection. It is recognized that the performance could be improved through refinements such as damping plates and heave tuning of spars.<sup>25</sup> The results of pertinent studies should be used in the design phase for optimization of the platform.<sup>1 9 11</sup>

The generic platforms selected for this investigation are the discus and spar buoy depicted in Figure 1, and the semisubmersible and vertically moored semisubmersible depicted in Figure 2. The vertically moored semisubmersible concept is commonly referred to as a tension leg platform (TLP) by the offshore petroleum industry. However, the TLPs of the offshore industry will have displacements two orders of magnitude greater than are anticipated for Navy range applications. The first full scale drilling and production TLP to be built, the Hutton TLP by Conoco, has a displacement of 63,300 tons.<sup>14</sup> Another major difference is that the offshore petroleum industry's TLPs at present have selected high strength tubular members as the first choice for tension leg elements, because they are considered to have advantages of both good corrosion resistance and good fatigue resistance.<sup>6</sup> The handling systems required on a TLP to install and tension these tubular tension leg elements is quite large, complex and heavy. A detailed description of the Hutton TLP-system and an extensive general review of TLP mooring technology are available.<sup>24 23</sup> Two major problems with this type of TLP mooring system for Navy applications are: (1) the platform size would need to be increased to accommodate the tension leg element handling system, and (2) in water depths of 6,000 feet, the weight of the tension leg element would become excessive. Therefore a tensioned mooring is preferred which would utilize wire or synthetic rope to minimize the size of the platform.

The TLP concept for a range platform is one which has an anticipated displacement of less than 750 tons and utilizes wire or synthetic rope as tension leg elements. To distinguish this platform concept from the behemoth TLP, the term vertically moored semisubmersible is used in this paper. Presently in vogue is the generic term compliant platform (e.g., guyed and articulated towers and TLPs) which is taken to mean a platform type which is constrained for

the vertical displacements of heave and rotations of pitch and roll, and is compliant for the lateral displacements of surge and sway and rotation of yaw. Therefore, if one was so disposed he might wish to think of compliant buoy systems as buoys having highly tensioned moorings which result in the previously described motions.

## NUMERICAL MODELS

Discus and spar buoys were modeled using the National Oceanic and Atmospheric Administration Data Buoy Center (NDBC) program developed by Sargent et al.<sup>21</sup> This is a frequency domain model which solves for the buoy responses of heave, pitch and surge.

The equations of motion are

$$m \ddot{\Sigma} = F_i + F_d + F_h + F_m + F_w \quad (2)$$

where  $m$  = mass of the hull

$\ddot{\Sigma}$  = any rectilinear displacement

$F_i$  = hydrodynamic inertial force

$F_d$  = damping force

$F_h$  = hydrostatic restoring force

$F_m$  = mooring force

$F_w$  = wave force

The comprehensive development of this mathematical model and its experimental and analytical verification are available from NDBC.<sup>8 10</sup> For the analysis presented in the paper the buoys were modeled as unmoored buoys. However, several moored spar and discus buoys were modeled with a single point mooring and while some effect was observed it was judged that the mooring system did not significantly impact the RAOs or response.<sup>7</sup>

Semisubmersible and vertically moored semisubmersible platforms were modeled using the SPFOR preprocessor program of ROTECF.<sup>19</sup> This program performs a linearized analysis of the motion response of a stable ocean platform made up of a space frame assembly of slender cylindrical members.<sup>18</sup>

The platform is treated as a rigid body having six degrees of freedom for which the linear differential equations of motion are

$$\sum_{j=1}^6 \left[ (m_{ij} + a_{ij}) \ddot{x}_j + b_{ij} \dot{x}_j + c_{ij} x_j \right] = F_i e^{i\omega t} \quad \dots i = 1, 2, \dots, 6 \quad (3)$$



where  $m_{ij}$  = mass, moments of inertia, and products of inertia of the structure

$a_{ij}$  = added mass and acceleration coupling force coefficients

$b_{ij}$  = linearized damping force coefficients

$c_{ij}$  = restoring force coefficients which include hydrostatic and mooring forces

$F_i$  = external exciting force amplitude

The fluid force per unit length for a member is computed as though the structure were stationary in its mean position and is given by

$$\vec{F} = - \iint_S p \vec{n} ds + \frac{\rho D}{2} C_D \vec{u}_n \left| \vec{u}_n \right| \quad (4)$$

$$+ \frac{\pi \rho D^2}{4} C_a \vec{a}_n$$

where  $p$  = pressure at a point on the member surface given by the linearized Bernoulli equation for the incident wave system

$\vec{n}$  = unit outward surface normal vector

$ds$  = element of peripheral arc length of cylinder cross section

$\rho$  = density of fluid

$D$  = diameter of member

$C_D$  = quadratic drag coefficient for flow normal to the member centerline

$\vec{u}_n$  = component of resultant velocity normal to the centerline of the member

$C_a$  = added mass coefficient

$\vec{a}_n$  = component of resultant acceleration normal to the centerline of the member

The first term of Equation 4 is the Froude-Krylov force, the second term the drag force and the third term is the added mass force. The Morison equation may be thought of as a simplification of Equation 4 where the Froude-Krylov force is included in the third term and is approximately correct for its intended application to stationary cylinders.

The quadratic drag force in Equation 4 is replaced by an equivalent linear drag force

$$C_D \vec{u}_n \left| \vec{u}_n \right| \cong C_{DL} \vec{u}_n \quad (5)$$

where  $C_{DL}$  = linearized drag coefficient

For the case of regular waves the equivalent linear drag coefficient is given as<sup>3</sup>

$$C_{DL} = C_D \frac{8}{3\pi} u_o \quad (6)$$

where  $u_o$  = amplitude of the periodic fluid velocity

An iterative technique for replacing  $u_o$  in Equation 6 with the amplitude of the oscillatory resultant normal velocity is given by Burke and discussed by Paulling et al.<sup>5 20</sup>

The program can analyze the platform as either free floating or moored. In the case of a tensioned vertical mooring the restoring force in a mooring leg is given by

$$F_n = \frac{T_n}{L_n} x_n \quad (7)$$

where  $n$  = mooring leg

$T_n$  = tension in mooring leg

$L_n$  = length of mooring leg

$x_n$  = displacement of mooring leg platform end

#### COMPUTER SIMULATION OF PLATFORM RESPONSE

A data base was developed for platform performance for the generic discus, spar, semi-submersible and vertically moored semisubmersible using the two previously described computer programs. The characteristics of each platform are presented in Table 2. Payloads of 600 and 6,000 pounds located at either 30 or 100 feet above MWL were used for the platforms.

Once the transfer function (response amplitude operator) is obtained the response to a random seaway may be computed. The spectral density of a linear response is given by

$$S_R(w) = \left| T(w) \right|^2 S(w) \quad (8)$$

where  $S(w)$  = spectral density function of the random seaway

$T(w)$  = complex transfer function

The rms value of the response, assuming a Gaussian distribution of the time history, is



$$T_{rms} = \sqrt{\int_0^{\infty} S_R(\omega) d\omega} \quad (9)$$

Other statistical measures such as the average of the highest  $1/\eta$  peaks are proportional to the rms. The following table gives these coefficients of proportionality for the average of the highest  $1/\eta$  peaks.

$\eta$	C
3	2.0
10	2.54
100	3.34

Regular wave excitation at 20 frequencies was provided to allow pitch/roll and heave response amplitude operators (RAOs) to be developed. The excitation for the discus and spar buoys was modeled by the ISSC two parameter spectrum given by

$$S(\omega) = 345 H_s^2 T (\omega T)^{-5} \exp[-630 (\omega T)^{-4}] \quad (10)$$

where  $S(\omega)$  = one sided half amplitude spectral density function ( $\text{ft}^2\text{-sec}$ )

$\omega$  = frequency (rad/sec), ( $\omega = 2\pi f$ )

$T$  = mean period (sec)

$H_s$  = significant wave height (ft)

The excitation for the semisubmersible and vertically moored semisubmersible was modeled by the Bretschneider two parameter spectrum given by

$$S(f) = 5 \left( \frac{H_s}{4} \right)^2 f_o^{-1} \left( \frac{f_o}{f} \right)^5 \exp \left[ \frac{-5}{4} \left( \frac{f_o}{f} \right)^4 \right] \quad (11)$$

where  $S(f)$  = one sided half amplitude spectral density function ( $\text{ft}^2/\text{Hz}$ )

$f$  = frequency (Hz), ( $\omega = 2\pi f$ )

$f_o$  = frequency of peak of spectrum (Hz) =  $1/T_o$

$H_s$  = significant wave weight (ft) =

$$4 \sqrt{\int_0^{\infty} s(f) df}$$

Both of these spectra are commonly used in ocean engineering applications when no fetch limitation is required. The following values are used

as input to both of the spectral models used in determining the platform's response.

H (ft)	ISSC T(sec)	Bretschneider $f_o$ (sec)
8	5.5	6.5
16	7.8	9.2
32	11.1	13.0

All platform responses presented in these analyses, with the exception of the vertically moored semisubmersible, are for unmoored floating platforms. The assumption for using unmoored platforms is that a slack mooring with a scope several times the water depth provides virtually no restraint on the high frequency wave induced responses. Obviously, this would not apply to platforms which were taut moored or when the mass of the mooring lines was large enough to impact the platforms response. Steady wind and current forces are not included in the analyses. A maximum significant wave height of 32 feet was selected because, with the small size of the platforms studied, linear analysis results above this point would not yield accurate results. Also not considered in these analyses were drift forces,<sup>12</sup> dynamic coupling between the platform and mooring system, and unsteady hydrodynamic effects. These analyses were limited to water depths between 100 and 7,000 feet. The lower limit is required due to a lack of validated analytical models for shallow water and the upper limit by existing operational experience.

The semisubmersible hull used in this study utilizes 4 pontoons as opposed to the familiar catamaran configuration used by drilling semisubmersibles. Since the drilling semisubmersible must spend time in transit from one site to another, the catamaran hull is required for improved hydrodynamics during transit. This is not a consideration for a semisubmersible which is permanently stationed at one site. Because of the use of 4 pontoons the response to both head and beam seas are equal. The response to quartering seas was not investigated in this study.

For analysis of the semisubmersible a  $C_D$  of 0.7 and  $C_a$  of 1.0 were selected as representative average values. These values were also used for the vertically moored semisubmersible whose mooring was modeled using a spring constant of 12,000 pounds/feet in a water depth of 600 feet.

Heave and pitch/roll RAOs for discus, spar and semisubmersible platforms are presented in Figures 3 through 8. Heave and surge RAOs for the vertically moored semisubmersible are presented in Figures 9 and 10. The rms response are given in Table 2 for each significant wave height used.



The following general conclusions are for platforms with characteristics similar to those of this paper and are not intended to be representative of those platforms in applications which are not similar. The general conclusions drawn from the RAOs and calculated rms responses and information covered in the literature review on platforms<sup>7</sup> are as follows:

- Discus buoys generally follow wave contours and exhibit relatively short natural pitch/roll periods which are on the order of 2 to 8 seconds for a range of platform GM values from 2 to 20 feet.
- Twenty to 30 foot diameter discus buoys with low gyradii (5 to 10 feet) generally follow wave contours and exhibit relatively short natural pitch/roll periods which are on the order of 2 to 4 seconds for a range of platform GM values from 15 to 25 feet (e.g., D-3, D-4).
- Discus buoys with large gyradii (15 to 30 feet) and GM values between 10 and 20 feet generally exhibit peak pitch/roll RAO responses on the order of 4 times the wave slope with natural periods between 5 and 7 seconds (e.g., D-1, D-2, D-5).
- Constant cross section cylindrical spar buoys can exhibit relatively large heave and pitch amplitudes since their natural periods fall in the range of 10 and 20 seconds, respectively, and significant amounts of energy exist in waves of these periods.
- The 25-foot-diam cylindrical spar (SP-4) is seastate limited to  $H_s \sim 16$  feet. Above this sea state, high<sup>s</sup> wave energy exists at frequencies corresponding to the spar heave natural frequency and the spar experiences extreme angular and vertical motions.
- Spars using two cross sections with a small waterplane increase the spar natural periods above 25 seconds and allow the spar to avoid these excessive motion conditions.
- To provide a spar with reasonable response characteristics, the spar waterplane area was reduced with the use of a spar mast with a diameter of 2 to 5 feet and mass distribution significantly adjusted to increase the heave natural period above 30 seconds (e.g., SP-1, SP-2, SP-3 (Shape A, Figure 1)). This provided natural heave and pitch/roll periods required to operate in severe seas.

- Semisubmersible platforms (45 feet wide by 45 feet long) with GM values from 0.5 to 3.5 feet and gyradii from 20 to 30 feet exhibit natural pitch/roll periods between 15 and 45 seconds with rms pitch/roll amplitudes generally below 3 degrees. Rms heave amplitudes are generally below 10 feet in seas up to  $H_s$  of 32 feet. These analyses considered semisubmersibles down to only 45 by 45 feet as a practical minimum size. A 30-foot wide by 30-foot long by 1.5-foot column diameter semisubmersible investigated did not have sufficient stability to support a reasonable payload.
- Vertically moored semisubmersibles must have draft and freeboard significantly greater than a semisubmersible to accommodate large waves and set down.
- Vertically moored semisubmersibles analyzed exhibit low pitch/roll and heave motions as expected. Surge/sway natural periods exceed 30 seconds and heave natural periods are on the order of 3 to 6 seconds. To operate in seas greater than about  $H_s = 16$  feet, the columns must be tall<sup>s</sup> enough to accommodate passing waves, thus preventing excessive deck wetness or pontoon emergence.
- The design of vertically moored semisubmersibles carrying a 6,000-pound payload is primarily governed by environmental loading instead of payload requirements as in the case of the previous platforms. Due to their principle of operation, the vertically moored semisubmersible considered herein should be limited to depths greater than 200 feet.

#### PLATFORM CONSTRUCTION AND INSTALLATION COST DATA

Published cost data are in general incomplete, relevant only to thousand-ton payload platforms and give only cost trends between various platform types and subsystems. Since construction and deployment procedures for small instrument platforms are significantly different from large platforms, direct use of these published data would be inappropriate. Therefore, cost data developed here use a unit-price method and cost indexing based on the 1982 shipyard and steel fabrication data shown in Table 3. "Installed payload cost" includes the cost of platform construction and installation. Cost data indicate that platform and installation costs range from 20 to 100% of construction costs. For some offshore oil platforms, the installation costs equal the cost of construction. Construction costs do not include the



design effort. Table 3 shows the results of the literature search and buoy manufacture cost survey.

The trends in data indicate that construction unit-price decreases with displacement. For example, in considering discus buoys, the construction unit-price of 50,000 pounds displacement is about 40% higher than the price for 200,000 pounds displacement. For displacements larger than 200,000 pounds, the data appear to indicate a limiting value of  $\sim 2$  \$/lb (Gulf of Mexico). However, due to the scatter in data obtained, no definite conclusion can be drawn. There is also a trend in the total cost as a function of geographical location resulting from the differences in environmental loading (therefore, design) and labor. Moreover, construction unit-price for platforms built in Northern Europe (North Sea application) is twice the value of comparable design for the Gulf of Mexico (3 \$/lb versus 1.5 \$/lb). In addition, installation unit-price in the Gulf is also less than in the North Sea.

#### CONCLUSION

The work presented here provides a summary of platform characteristics, RAOs, and response which will allow for a preliminary selection of the most economically optimum platform meeting a user's requirements. These user's requirements may be termed "platform operability," that is, how does the platform meet the mission requirements. Using the RAOs and the wave statistics for a given site an estimate may be derived about the expected amount of exceedance that the platform responses will be greater than the mission requirements can tolerate. Thus trade-offs in operability and cost may be performed.

Future work to be conducted by NCEL will include the coupling of frequency and time domain platform models with NCEL's dynamic cable analysis program SEADYN.<sup>17</sup> A comprehensive development plan for long term sensor platforms is presently being formulated at NCEL for a 4-year R&D program to begin later this year. This program will concentrate on the size of platforms discussed in this paper.

#### ACKNOWLEDGMENTS

The authors are grateful to the Naval Facilities Engineering Command and the Naval Civil Engineering Laboratory for permission to publish this paper.

#### REFERENCES

1. Angelides, D. C., C. Chen, and S. A. Will. "Dynamic response of tension leg platform," in Proceedings of the Third International Conference on Behavior of Off-Shore Structures, Cambridge, Mass., 1982. Chrysostimos Chrysostomidis and Jerome J. Connor, ed., Hemisphere Publishing Corp, 1982.

2. Asworth, C. "An application of synthetic line for permanent deep water mooring," Presentation summaries, Synthetic Line Workshop II, Groton, Conn., Jun 1982. Kenneth R. Bitting, ed. United States Coast Guard and Naval Underwater Systems Center, Groton, Conn.

3. Blagoveshchensky, S. N. Theory of ship motions, vol. 1. Dover, New York, N.Y., 1962.

4. Blough, J. V. BTOT-SD2-81-11: ACMI mooring system life expectancy study. Bell Technical Operations Texton, Armament Division. Eglin AFB, Fla., Feb 1981.

5. Burke, B. G. "The analysis of motions of semisubmersible drilling vessels in waves," Society of Petroleum Engineers Journal, Sep 1970.

6. Dunn, F. P. "Deepwater drilling and production platforms in non-arctic areas," in Proceedings of a Symposium, Outer Continental Shelf Frontier Technology, Washington, D.C., Dec 1979. Washington, D.C. Marine Board, Assembly of Engineering, National Research Council, National Academy of Sciences, Washington, D.C., 1980.

7. Naval Civil Engineering Laboratory. Technical Memorandum No. 44-82-06: Ocean platform selection guidelines, task 2: Data base assessment by Giannotti and Associates, Inc. Port Hueneme, Calif., Jul 1982.

8. NOAA Data Buoy Center. Report NDBC 6113.1: Static and dynamic analysis of a moored buoy system, by Theodore R. Goodman, Paul Kaplan, Theodore P. Sargent, and James Bentson. NSTL Station, Miss., Apr 1972.

9. Horton, E. G., L. B. McCammon, J. P. Martha, and J. R. Paulling. "Optimization of stable platform characteristic," in Proceedings of the Offshore Technology Conference, Houston, Texas, 1972. (OTC Paper No. 1553)

10. NOAA Data Buoy Center. Report NDBC 6113.1: Experimental and analytical studies of buoy hull motions in waves, by Paul Kaplan, Alfred I. Raff, Theodore P. Sargent. NSTL Station, Miss., Apr 1972.

11. Kim, C. H. and J. A. Mercier. "Analyses of multiple-float-supported platforms in waves," Ninth Symposium on Naval Hydrodynamics. Office of Naval Research, Paris, France, 1972.

12. Lundgren, H., S. E. Sand, and J. Kirkegaard. "Drift forces and damping in natural sea states: A critical review of the hydrodynamics of floating structures," in Proceedings of the Third International Conference on Behavior of Off-Shore Structures, vol. 2, Cambridge, Mass., 1982. Chrysostimos Chrysostomidis and Jerome J. Connor, ed., Hemisphere Publishing Corp, 1982.



13. McClure, A. C. and I. Kirschner. "Semi-submersible buoy for stormy seas," presented at the 1983 Symposium on Buoy Technology, Marine Technology Society, New Orleans, La., 1983.

14. Mercier, J. A.. "Evolution of tension leg platform technology," in Proceedings of the Third International Conference, on Behavior of Off-Shore Structures, Cambridge, Mass., 1982, (unbound paper). Chrysostimos Chrysostomidis and Jerome J. Conner, ed., Hemisphere Publishing Corp, 1982.

15. Naval Civil Engineering Laboratory. Unpublished Report: Ocean platform selection guidelines," by C. Moore, L. Vega, and T. Ward. Port Hueneme, Calif., Sep 1981.

16. North, D. M. "Navy air combat program gives fleet pilots realistic training," Aviation Week and Space Technology, Oct 18, 1982.

17. Palo, P., D. Meggit and W. Nordell. "Dynamic cable analysis models," in Proceedings of Offshore Technology Conference, Houston, Texas, 1983. (OTC Paper No. 4500)

18. Paulling, J. R. "Wave induced forces and motions of tubular structures," Eighth Symposium on Naval Hydrodynamics, sponsored by the Office of Naval Research, Pasadena, Calif., 1970.

19. Johns Hopkins University Applied Physics Laboratory. Contract Report: Theory and user manual for OTEC C. W. pipe programs ROTECF and SEGPIP, by J. R. Paulling. Baltimore, Md., Jul 1980. (Contract No. N00024-78-C-5384)

20. Paulling, J. R. and E. E. Horton. "Analysis of the tension leg platform," Society of Petroleum Engineers Journal, Sep 1971.

21. NOAA Data Buoy Center. Report NDBCM 6113.2: Computer program documentation report: buoy-cable dynamics program, by Theodore P. Sargent, Alfred I. Ruff, and James Bentson. NSTL Station, Miss., Apr 1972.

22. Naval Civil Engineering Laboratory. Technical Note N-\_\_\_\_: NCEL ocean platforms seminar, by D. R. Shields. Port Hueneme, Calif., (in preparation)

23. \_\_\_\_\_. Technical Memorandum No. 44-83-05: OTEC mooring technology, by D. R. Shields, R. L. Wendt, and B. A. Johnson. Port Hueneme, Calif., Dec 1982.

24. Tetlow, J. and M. Leece. "Hutton TLP mooring system," in Proceedings of the Offshore Technology Conference, Houston, Texas, 1982. (OTC Paper No. 4428)

25. Tucker, M. J. "The heave response of a spar buoy," Ocean Engineering, vol 9, no. 3, 1982.

26. Civil Engineering Laboratory. Technical Memorandum No. 44-80-5: Long-term sensor platforms - a milestone zero report, by T. M. Ward, D. R. Shields, D. A. Vidal and R. T. Hudspeth. Port Hueneme, Calif., Aug 1980.

Table 1. Buoy Shape Configurations

Wave Following	Deep Immersion	Open Framed
Toroid (S)*	Cylindrical Spar	Space Frame Spar
Discus (S)	Augmented Spar	Semisubmersible
Cone (L)	Conical Spar	
Sphere (L)		
Boat Hull (I)		

\*Corresponds to displacement: Large (L), Intermediate (I), Small (S)



Table 2. Platform Characteristics

Platform No.	Discus					Spar				Semisubmersible				Vertically Moored Semisubmersible				
	D1	D2	D3	D4	D5	SP1	SP2	SP3	SP4	SM1	SM2	SM3	SM4	T1	T2	T3	T4	T5
Length/Breadth (ft)	20	20	20	30	30	8.6	8.6	8.6	25	45	45	45	60	45	45	45	60	60
Diameter (ft)						3	3	2										
Upper Diam (ft)						100	110	100	100	34.3	50	34.3	40	34.3	50	34.3	40	120
Depth (ft)	4.0	4.0	4.0	6.0	6.0	50	60	50										
Depth (Lower) ft						80	90	80	70	24.3	40	24.3	30	24.3	40	24.3	30	70
Draft (ft)	1.33	2.0	1.33	2.0	2.0	6,000	6,000	600	6,000	6,000	6,000	600	6,000	6,000	6,000	600	6,000	6,000
Payload (lb)	6,000	600	600	6,000	6,000	42,658	68,254	42,658	600,000	65,400	170,600	65,400	212,500	65,400	170,600	65,400	212,500	327,200
Structural Weight (lb)	19,300	32,600	19,300	54,100	67,100													
Ballast (lb)	1,500	7,000	6,900	30,400	17,000	151,342	162,375	148,656	1,600,000	34,800	162,300	40,200	163,600	10,800	138,300	16,200	139,600	153,600
$\Delta$ (long tons)	11.97	18.94	11.97	40.40	40.40	89.29	105.6	85.67	982	47.41	151.3	47.41	170.6	47.41	151.3	47.41	170.6	228.0
Payload (ft above WL)	30	100	30	30	100	30	100	30	30	30	100	30	100	30	100	30	100	100
KG	8.45	3.2	2.2	3.9	9.0	26.95	28.87	24.43	32.15	9.3	13.2	6.7	11.1	9.3	13.2	6.7	11.1	41
GM	11.0	10.4	17.2	25.2	20.1	.77	3.71	1.83	2.86	0.6	1.1	3.3	2.3	0.6	1.1	3.3	2.3	
$K_{xx} = K_{yy}$	14.9	12.6	5.0	8.6	26.4	23.35	44.7	19.35	23.43	22.4	30.8	18.8	28.6	22.4	30.8	18.8	28.6	76.6
RMS Pitch (deg)																		
$H_S$ (ft) = 8	35.9	28.8	6.1	8.1	32.3	-.03	-.04	-.06	-.07	.76	.11	.91	.66	0.14	0.63	0.12	1.27	
$H_S$ (ft) = 16	40.8	32.6	7.3	9.1	48.5	2.4	1.5	7.2	12.5	1.4	.23	1.6	1.3	0.18	0.55	0.14	2.45	.73
$H_S$ (ft) = 32	43.3	34.0	8.5	10.5	54.7					2.2	0.4	3.0	2.1	0.20	0.48	0.16	1.12	
RMS Heave (ft)																		
$H_S$ (ft) = 8	2.1	2.1	2.1	2.1	2.4	.65	.65	.65	2.5	.65	.31	.65	.35	.06	.14	.06	.27	--
$H_S$ (ft) = 16	4.1	4.1	4.1	4.1	4.1	1.4	1.2	1.6	10.8	1.7	1.2	1.7	1.5	.10	.24	.10	.47	.28
$H_S$ (ft) = 32	8.1	8.2	8.1	8.2	8.2	3.8	3.9	4.6	17.1	6.5	10.6	6.5	6.3	.13	.31	.13	.60	.48
RMS Surge (ft)																		
= 8	5.6	1.6	0.6	0.5	3.1	0.5	0.4	0.5	0.8	0.8	0.6	0.8	0.6	.75	.6	.75	.6	--
= 16	6.2	2.5	1.2	1.1	4.5	1.8	1.4	1.7	2.3	2.4	2.1	2.4	2.1	2.5	2.1	2.5	2.1	3.22
= 32	6.6	3.0	2.6	2.5	5.2	4.9	3.6	4.9	5.6	6.2	5.6	6.2	5.8	6.3	5.7	6.3	5.9	9.86



Table 3. Platform Cost Factors

Literature and Shipyard Survey

Platform Type	Cost/lb Constr. (\$/lb)	Constr. & Install. Construction	Remarks (lb)
<u>Summary</u>			
Spar	$2.65 \pm .50$	$1.25 \pm .15^a$	$\Delta = 68,000 \pm 15,000$
Discus	$2.65 \pm .20$	$1.25 \pm .15^a$	$\Delta = 73,000 \pm 20,000$
Semi	$2.60 \pm 1.00$	$1.25 \pm .15^a$	$\Delta = 171,000 \pm 50,000$
TLP		$1.75 \pm .15$	No data available
Fixed Tower	$2.65 \pm 1.55$	$1.75 \pm .15$	
General	$2.75 \pm .55$		Shipyard Prices • Drag Embedment Anchors: 1 \$/lb • Wire Rope and Chain ~ 0.50 \$/lb

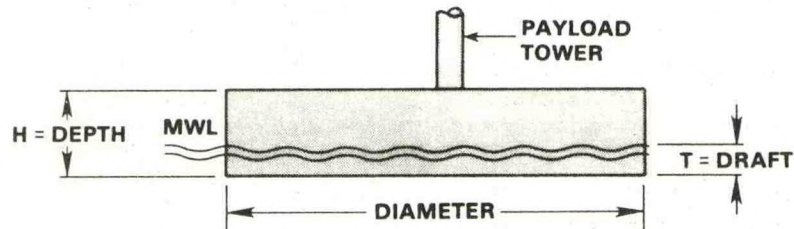
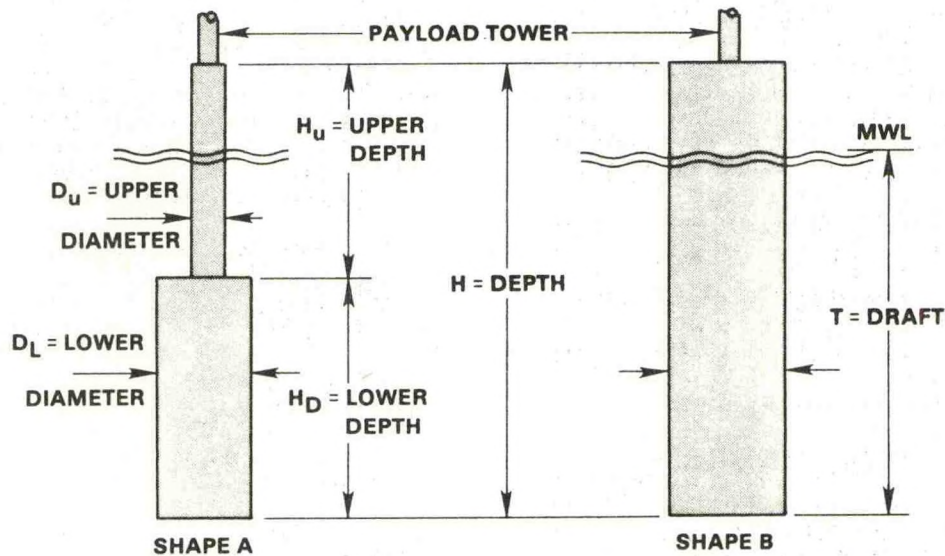
<sup>a</sup>Single point mooring**PRINCIPAL DIMENSIONS GENERIC DISCUS BUOYS****PRINCIPAL DIMENSIONS GENERIC SPAR BUOYS**

Figure 1. Generic discus and spar buoy.



Principal Dimensions Generic  
Semisubmersible & Vertically  
Moored Semisubmersible Buoys

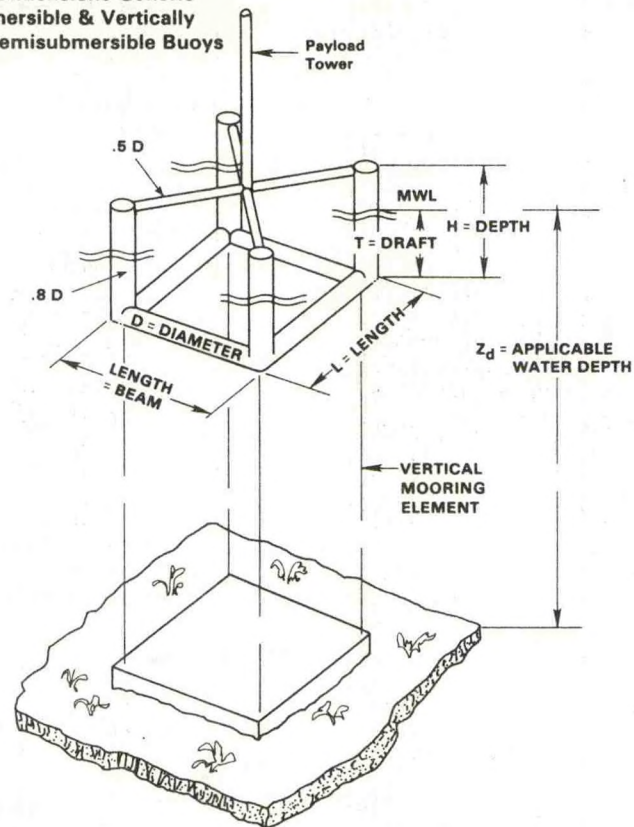


Figure 2. Generic semisubmersible buoy.

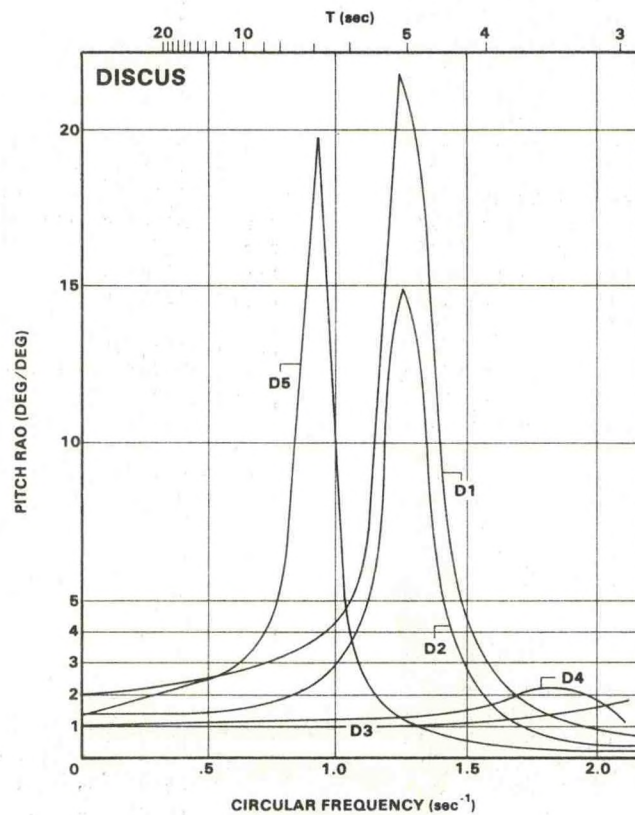


Figure 3. Discus pitch RAOs.



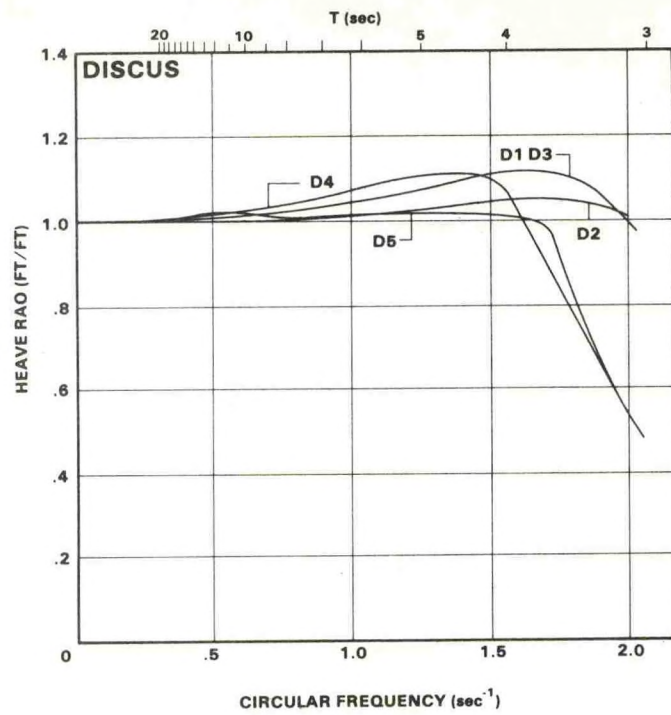


Figure 4. Discus heave RAOs.

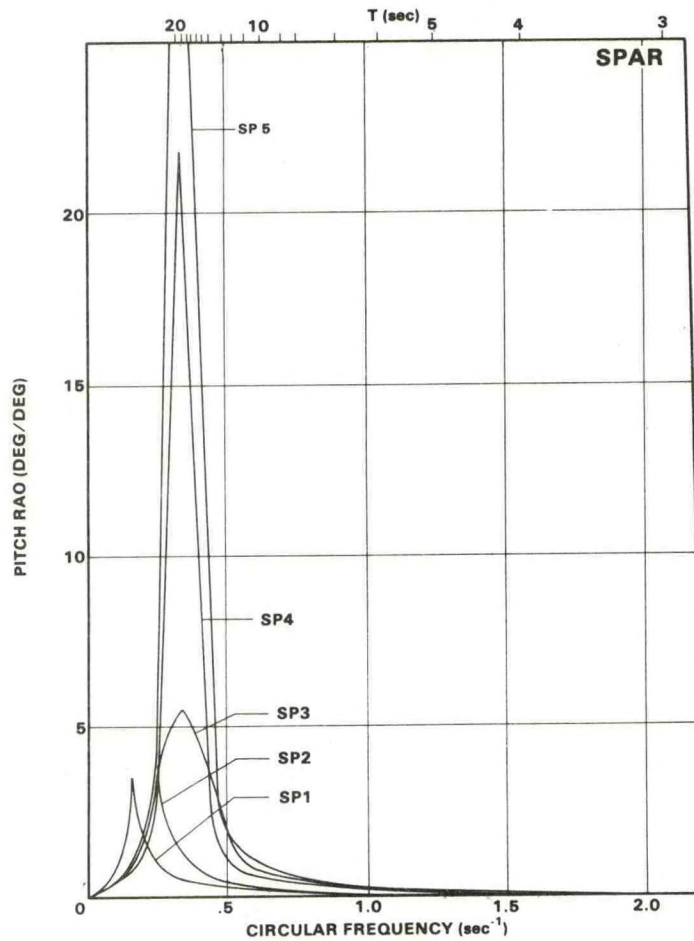


Figure 5. Spar pitch RAOs.



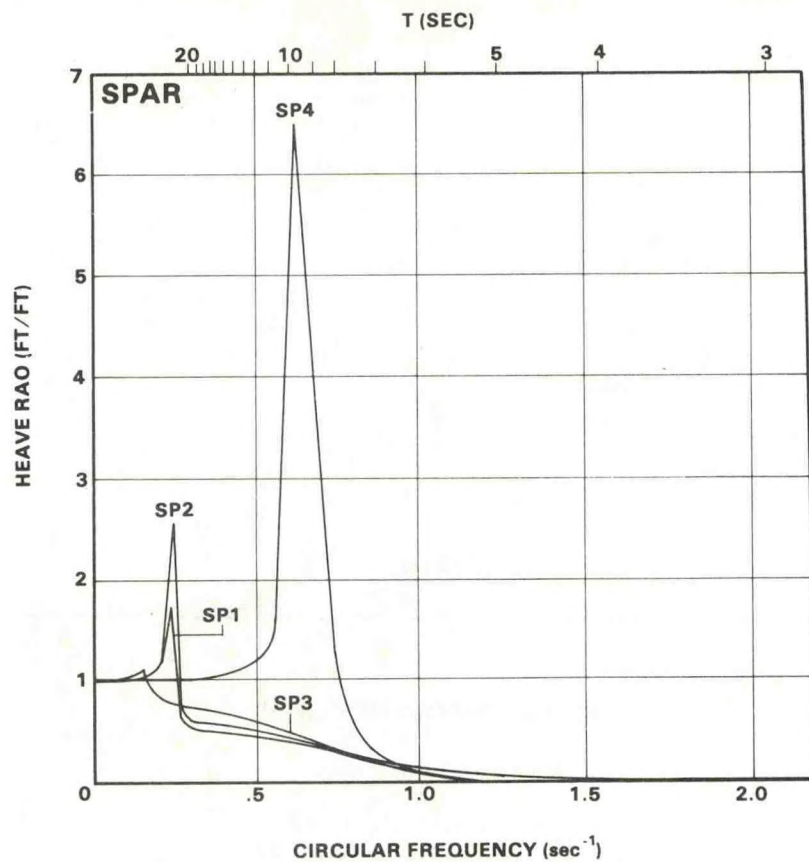


Figure 6. Spar heave RAOs.

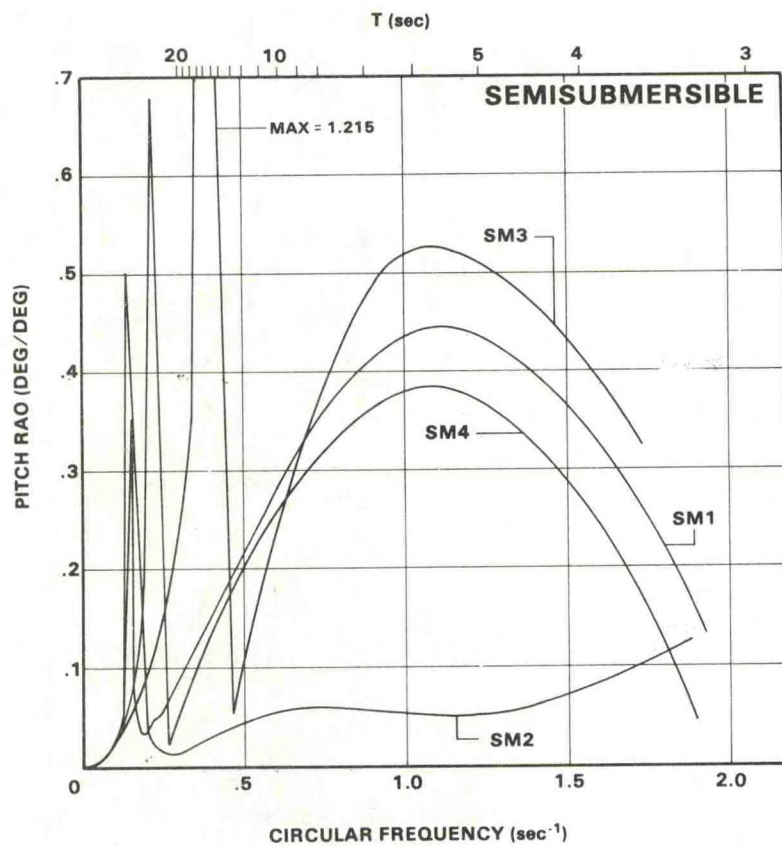


Figure 7. Semisubmersible pitch RAOs.



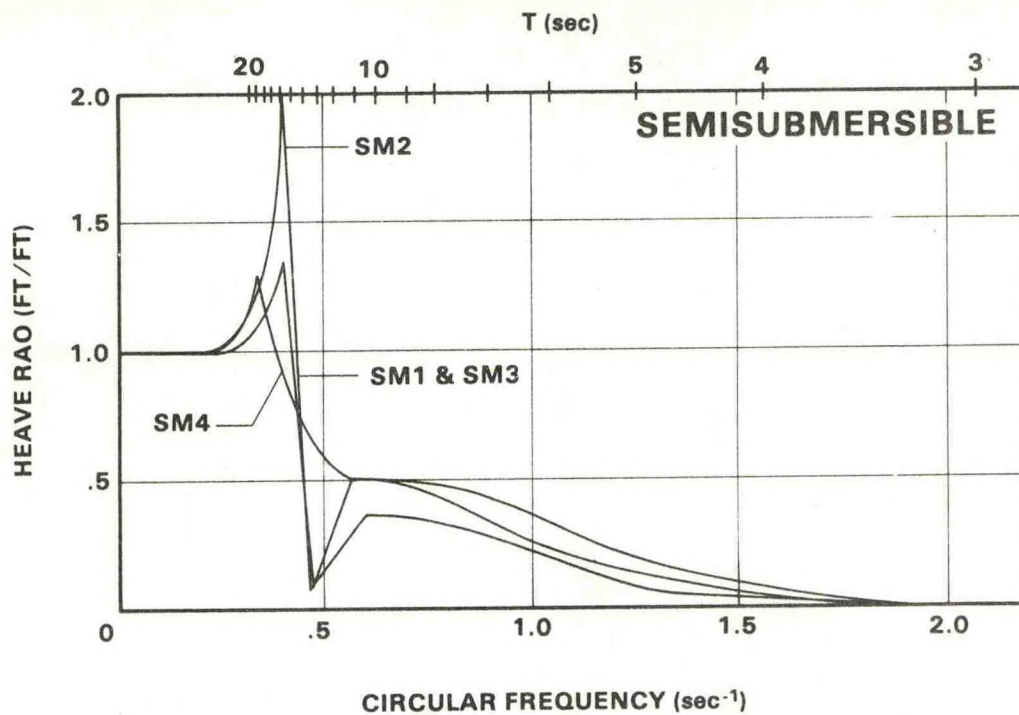


Figure 8. Semisubmersible heave RAOs.

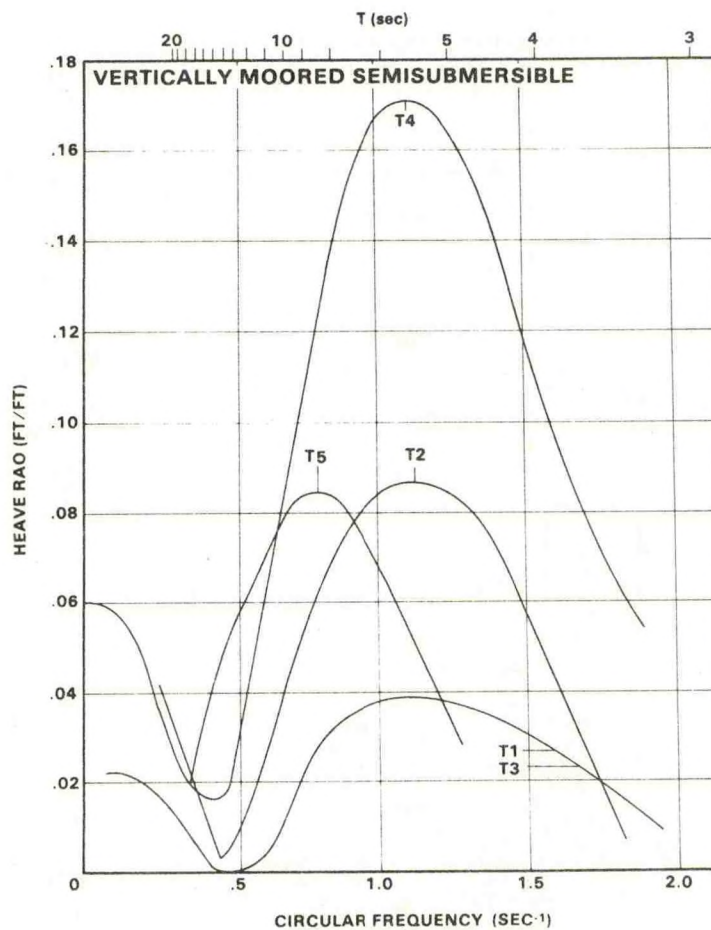


Figure 9. Vertically moored semisubmersible heave RAOs.



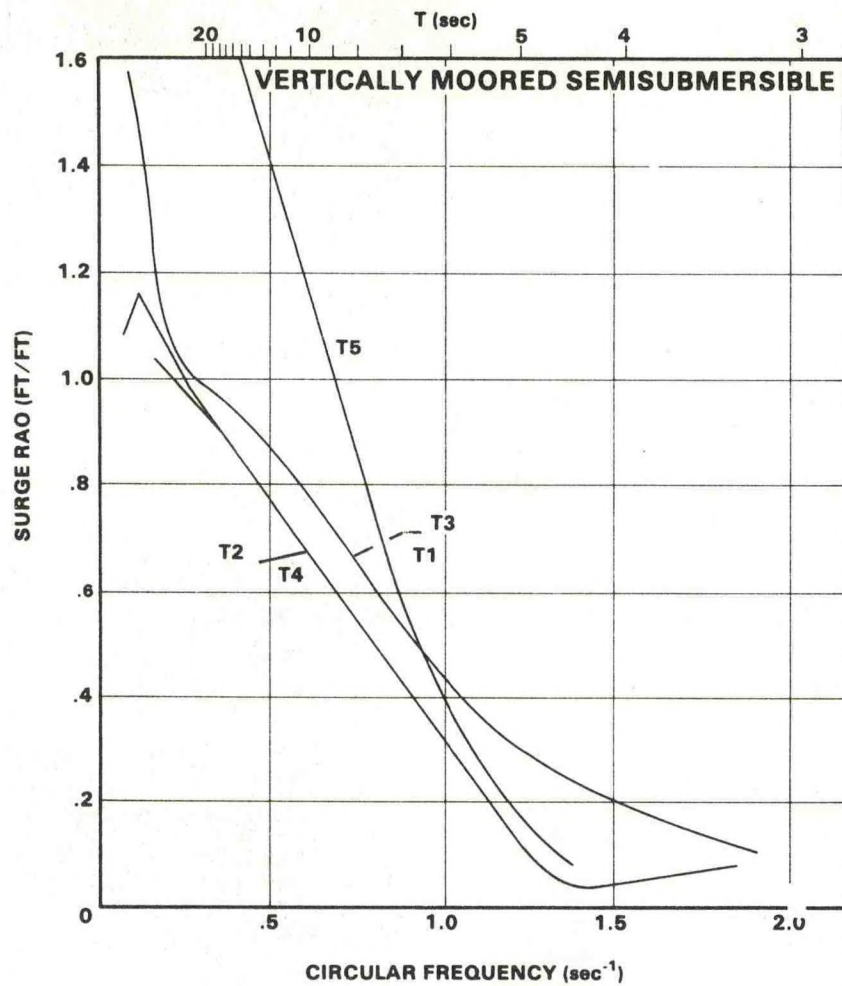


Figure 10. Vertically moored semisubmersible surge RAO.



# SEISMIC DATA ACQUISITION SPAR BUOY IN THE NORTH SEA

C W A Browitt and T Turbitt

Institute of Geological Sciences  
Murchison House, West Mains Road  
Edinburgh, EH9 3LA, UK

## APPLICATION

In 1979, the Institute of Geological Sciences and UK Department of Energy embarked on a programme of North Sea earthquake monitoring in order to establish correlations between seismicity and geological structure, and to improve the assessment of seismic risk to oil-field installations. On land, instrumental coverage of the area has been extended (Figure 1) and data exchange with neighbouring countries (particularly Norway) has been enhanced. To obtain accurate epicentres and depths of foci for earthquakes in the middle of the North Sea, local stations are needed which, for this application, means sea-bottom seismographs.

## CHOICE OF SYSTEM

Vibration noise levels on oil production platforms prevent their use for mounting seismometer transducers. Short-term noise tests conducted along 5 km profiles away from the concrete platforms Brent D and Statfjord A and in platform-free areas of the North Sea, show that noise reduces to background levels over a distance of approximately 2 km (Turbitt et al., 1983).

To improve the chances of successful data acquisition on a continuous basis, a philosophy of minimum technical innovation was adopted for the programme. It was proposed to house standard slow-running FM tape recorders on an oil platform

(Beryl A) and create a data-link from a sea-bed package 2 km away. It was hoped that by placing the instruments close to the platform a degree of policing against interference by shipping would be achieved.

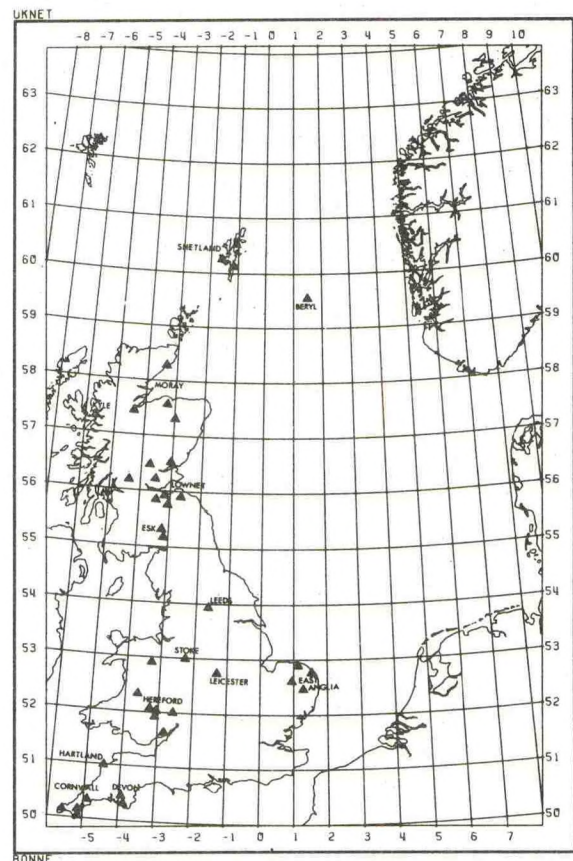


Figure 1. The UK seismograph network of the Institute of Geological Sciences.



The sea-bed instrumentation comprises an orthogonal set of Geotech S500 seismometers, which do not require levelling, and a Graseby hydrophone connected to Earth Data amplifier modulator units. The devices are housed in a 100 cm x 25 cm mild steel cylindrical pressure vessel with a wall thickness of 0.8 cm. The package, with the instruments, weighs 200 kg in air and about 125 kg in water. It is bolted to a 50 kg steel cradle fabricated from angle iron to provide stability and improve coupling to the sediments. Where dissimilar metals could not be avoided direct contact has been prevented by using polyacetal bushes. The bandwidth of the system (0.5 - 16 Hz) is appropriate for local earthquake monitoring.

The connection of sensors to recorders using an acoustic link was discounted owing to the difficulty in attaching a receiver and signal cable to the oil platform, the high power requirements and uncertainties in effectiveness at the required data rates in a noisy environment. A long underwater cable-link was rejected because of the difficulty and cost of protecting it through the wave action zone and the vulnerability to ship's anchors and trawling. The data-link problem was, therefore, reduced to selecting a suitable platform between the instrument package, on a short cable, and a UHF radio link to the recorders on the oil platform. The use of low power radio-links for seismic data transmission is standard technology and is used at ranges up to 100 km on land in the UK.

#### SPAR BUOY DESIGN

There appear to be three general problems in maintaining a moored buoy on station for a long period of time:

- i) Constant motion at the mooring points wears them out;
- ii) Sinking following ship collision;
- iii) Deliberate interference by ship's personnel.

In addition, there are specific difficulties in the Beryl area of the North Sea owing to the concentration of shipping and the hostile environment (Table 1).

TABLE 1

Environmental criteria - 50 year recurrence based on DEN guidance notes for Beryl field.

Wave height:	29.00 m max
Wave period:	15.50 sec
Wind (hourly mean)	
10 m above surface:	38.00 m/sec
Wind (3-sec gust)	
10 m above surface:	52.00 m/sec
Current - surface:	1.22 m/sec
Current - sea-bed:	0.61 m/sec
Storm surge:	0.60 m
Spring tide range:	1.50 m

Of several designs examined, the Havron Engineering taut-moored spar buoy was selected as most likely to survive and provide cable protection, battery capacity and stable radio transmission. It was considered that a relatively large system would enhance survivability and dimensions were established on the basis of environmental criteria, response and the maximum which could be deployed with a standard oil supply vessel.

The system is shown schematically in



Figure 2 with pictorial illustrations in Figures 3 and 4. The buoy is 30 m long with a mast extending 10 m above mean sea-level and a weight in air of 9 tonnes. The slender top section not only improves the dynamics of the buoy in response to wave motion but also presents a small target and low inertia for ship collision. The main buoyancy tanks have internal bulkhead seals and are below 10 metres from mean sea-level which prevents damage in a collision.

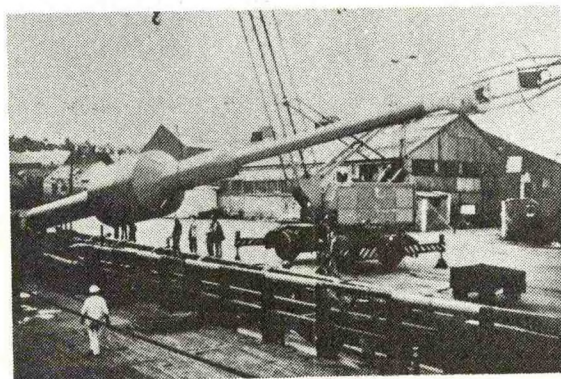


Figure 3. Spar buoy being loaded onto the crash rail of a supply boat.

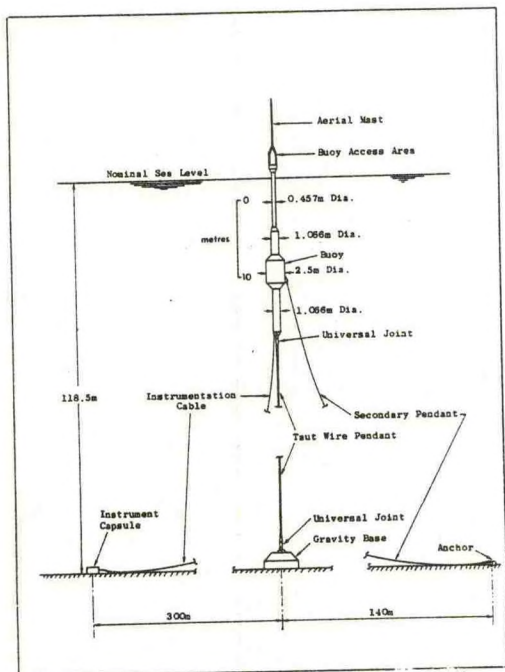


Figure 2. Sketch of the spar buoy system.

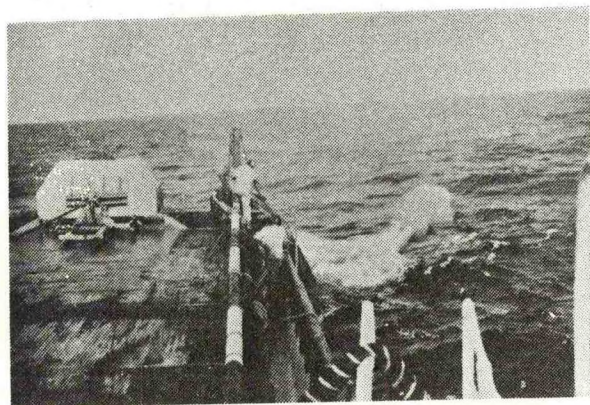


Figure 4. Gravity base and spar buoy during deployment.



A taut-wire pendant secures the bottom of the buoy to a concrete gravity base weighing 45 tonnes in water (80 tonnes in air) through universal joints. At these coupling points there is provision for link plates to accommodate small variations in the water-depth which is plumbed immediately before installation. A secondary pendant connected to a 1 tonne anchor forms a catenary mooring which prevents spinning.

The instrument package is placed at a distance of about 300 m to avoid vibration noise generated by the buoy itself. The electrical cable which has a 4 tonne working load enters the buoy well below the air-sea interaction zone and is ducted to the instrument chamber above mean sea-level. The termination electronics, two UHF radios and a battery voltage monitor are housed here above a 7 m suspended string of zinc-carbon cells which power the system for one year. End-fed dipoles are fed by cables potted in hydraulic hose and strapped to the mast.

A bilge pipe extends to the bottom of the battery compartment to permit the evacuation of water following a ship collision or ingress through the hatch when work is undertaken in marginal conditions. Air bottles are connected to a Schrader valve in the hatch cover to blow the bilges.

A navigation light, mounted on the mast, was originally powered from the main battery source. It is, however, vulnerable to damage and potential shorting of the power lines and has been redesigned to be independently powered from batteries housed on the mast.

Buoy motion model tests predict the maximum tilt of the system to be  $8^{\circ}$  in response to an 18 m, 16 sec period wave and  $12^{\circ}$  in response to the 50-year recurrence wave (Table 1). Gravity base

stability calculations performed by Lloyds Register show that in severe conditions (50-year wave):

- i) Positive contact will be maintained between the base and the soil;
- ii) A factor of safety of 1.5 against bearing failure will be achieved on a soil with properties corresponding to a soft clay (with undrained shear strength of  $0.53 \text{ tf/m}^2$ ) or a very sandy silt (with angle of friction of  $26.2^{\circ}$ ).
- iii) Sliding failure is less critical than bearing failure.

Although a specific site investigation was not made, the general soil properties of the area satisfy ii), above.

#### DEPLOYMENT

An oil rig supply boat was used for deployment as these vessels have the heavy duty winches necessary for the 80 tonne gravity base and the deck length to accommodate the buoy.

The gravity base was winched on to a steel cradle and held by sea fastenings and the 75 mm lowering wire attached to the ship's main winch. The main pendant was connected from the top of the concrete block to the bottom of the buoy which was secured along the ship's crash rail.

When on station the subsidiary anchor was connected to the spar buoy and lowered to the sea-bed and its lowering wire left buoyed off. The ship steamed upwind whilst the buoy was lowered over the side and allowed to stream astern (Figure 4). The concrete base was lowered over the stern, a smooth entry



being achieved with the aid of the self-tipping cradle. As the base approached the sea-bed, the buoy was drawn towards the stern by the main pendant and eventually assumed a vertical attitude over the block. The subsidiary anchor prevented the buoy coming into contact with the stern. It was subsequently picked up and moved to the south to allow the seismometer package to be deployed to the north, and adequate tension applied to prevent rotation of the buoy.

A tripod mast with antennae, navigation light and connecting cables was erected later.

The sea-bed instrumentation package was deployed at a line-measured distance of 300 m from the buoy using a small boat to define the position. Following the laying and transfer of the electrical cable to the spar buoy, it was inserted through the internal pipe from the base of buoy using divers.

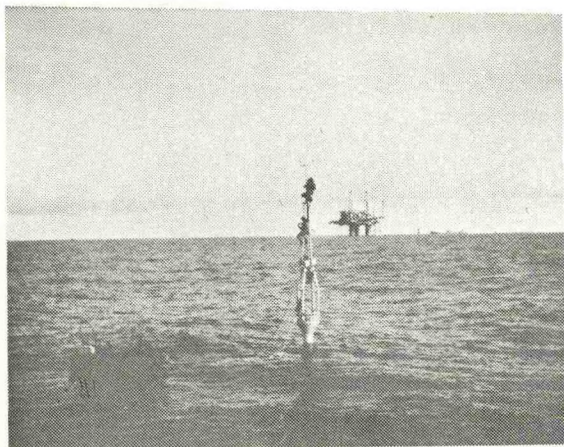


Figure 5. The spar buoy installed 2 km from the Beryl Alpha production platform to which data is transmitted by UHF radios.

## PERFORMANCE

The operational performance of the system is summarised below:

- i) July 1980 - spar buoy deployed.
- ii) October 1980 - seismometer package and buoy instrumentation installed. Owing to adverse weather conditions only part of the battery complement was loaded.
- iii) December 1980 - batteries exhausted and data flow ceased.
- iv) February 1981 - buoy holed in a ship collision, battery chamber flooded and package and electrical cable lost.
- v) May 1981 - repairs effected and new package laid.
- vi) May to December 1981 - continuous data recovery. There was no down time despite severe gales in November.
- vii) 21 December 1981 - the battery voltage monitor indicated that a complete discharge occurred in a period of a few minutes.
- viii) March 1982 - a surface inspection indicated a fault in the electrical cable and that a diving operation was required.
- ix) May 1982 - a diving inspection showed that the subsidiary anchor wire had become twisted around the main pendant fouling the electrical cable. This was probably due to a break on the sea-bed which is likely to have been caused by ship-ping. Repairs were effected and the sea-bed package recovered in



working condition. It showed no corrosion after the one year immersion.

- x) May 1982 through April 1983 - continuous data recovery.

The diving inspection in September 1982 showed that there was negligible wear on the main pendant and its mooring points at the buoy. The subsurface parts of the buoy were in good condition after 26 months in the sea. Above the surface, the galvanised and painted mast, the cables and antennae showed no deterioration but the painted mild steel deck, tubulars and handrail had rusted. These areas were repainted.

The two most significant problems encountered have been apparently caused by shipping. Both incidents occurred in the winter when speedy diagnosis and rectification were hindered by the adverse weather conditions prevalent in the northern North Sea during this season.

Since the first partial commissioning of the sea-bed instruments in October 1980, the system has operated successfully for 72% of the time. In the period from May 1981, when the first full load of batteries was installed, to the present (April 1983), recording has been achieved for 85% of the time.

The seismological performance is illustrated in Figure 6. This seismogram shows the 3 seismometer and 1 hydrophone record from a small local earthquake. It was not detected on land.

During the summer months the records are frequently contaminated by air gun seismic profiling (Figure 7) which militates against any attempt to use an event-triggered recording system.

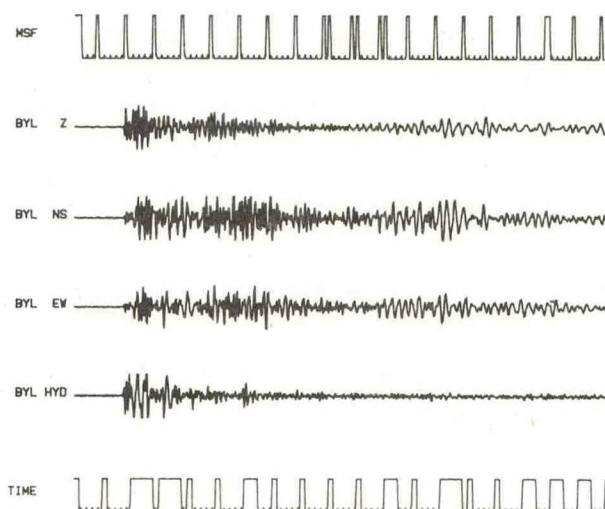


Figure 6. Beryl seismometer and hydrophone records of a small magnitude local earthquake on 18 May 1982.

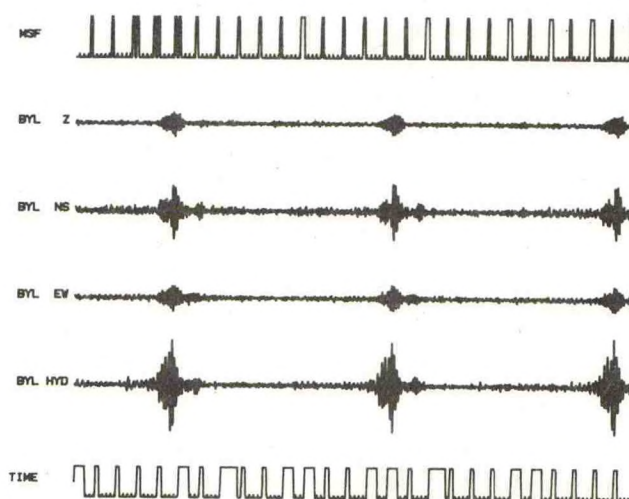


Figure 7. Air gun signals recorded on the Beryl seismograph in the passband 3 to 15 Hz, 13 May 1982.



# ACKNOWLEDGEMENTS

We are indebted to Mobil North Sea for logistic support on and around the Beryl Alpha production platform. The work is supported by the Natural Environment Research Council and the Department of Energy and is published with the approval of the Director of the Institute of Geological Sciences (NERC).

# REFERENCES

- Avedik, F. and Renard, V., 1973. Seismic refraction on Continental shelves with detectors on sea floor, *Geophys. Prospecting*, 21, pp. 220-228.
- Browitt, C.W.A., 1979. Seismograph networks of the Institute of Geological Sciences, UK, *Phys. Earth and Planet. Interiors*, 18, pp. 127-134.
- Cranford, M.D., Johnson, S.H., Bowers, J.E., McAlister, R.A. and Brown, B.T., 1976. A direct-recording ocean-bottom seismograph, *Bull. seism. Soc. Am.*, 66, pp. 607-615.
- Francis, T.J.G., Porter, I.T., Lane, R.D., Osborne, P.J., Pooley, J.E. and Tomkins, P.K., 1975. Ocean bottom seismograph, *Marine Geophys. Res.*, 1, pp. 195-213.
- Higley, P.D. and Joyal, A.B., 1978. New mooring design for a telemetering offshore oceanographic buoy, *Oceans '78*, Washington DC, Marine Tech. Soc., pp. 10-17.
- Houliston, D.J., 1978. A frequency multiplexing transmission system, *Inst. Geol. Sci.*, GSU Report No. 95.
- Myatt, J., Penn, A.W. and Poole, M.J., 1971. Isotope powered thermoelectric generators, Fourth United Nations International Conference on the Peaceful Uses of Atomic Energy, Geneva, 1971, A/CONF. 49/P/487, pp. 1-7.
- Rusby, J.S.M., Hunter, C.A., Kelley, R.F., Wall, J. and Butcher, J., 1978. The construction and offshore testing of the UK Data Buoy (DBI Project), *Oceanology International*, 1978, pp. 64-80.
- Sinha, M.C., 1978. Stresses and deformations in cylindrical pressure vessels, Department of Geodesy and Geophysics Univ. Cambridge Report, pp. 1-15.
- Smith, W.A. and Christie, P.A.F., 1977. A Pull-Up Shallow Water Seismometer, *Marine Geophys. Res.*, 3, pp. 235-250.
- Sutton, G.H., Kasahara, J., Ichinose, W.N. and Byrne, D.A., 1977. Ocean bottom seismograph development at Hawaii Institute of Geophysics, *Marine Geophys. Res.*, 3, pp. 153-177.
- Turbitt, T., Browitt, C.W.A., Morgan, S.N., Newmark, R. and Petrie, D.L., 1983. Instrumentation for North Sea seismic data acquisition. In: A.R. Ritsema and A. Gurbinar (eds.), *Seismicity and Seismic Risk in the Offshore North Sea Area*, pp. 155-157.



## DEVELOPMENT OF A BARELY-SUBSURFACE DEEP OCEAN MOORING

Narender K. Chhabra and John M. Dahlen

C.S. Draper Laboratory Inc.  
Cambridge, Mass.

### ABSTRACT

A deep ocean mooring was developed to support the Draper Laboratory Profiling Current and CTD Meter (PCM) and other oceanographic instruments in planned upper ocean experiments. Four moorings with engineering test instrumentation, have been set and recovered in Equatorial Pacific and North Atlantic experiments during the past two years. In both North Atlantic deployments engineering data were gathered concurrently with PCM operations. These moorings were set in 5366 m depth with their subsurface floats at ~ 20 m depth. The equatorial moorings were set in 4350 m depth with their subsurface floats at 14 m and 8 m depth. Long-term survival (13 months) and biological fouling protection have been demonstrated. Mooring response to a broad range of waves and currents has been measured. Occasional large excursions and axial oscillations must be considered for applications involving fixed instruments. The PCM is immune to these effects.

### MOORING DESIGN

A mooring was designed to support the Draper Laboratory Profiling Current and CTD Meter (PCM)<sup>6</sup> in planned upper ocean experiments. In January 1981 it was deployed during PEQUOD\* for five days with engineering instrumentation to measure its response to currents and surface waves. It was then redeployed and left for a 13-month life test. Two additional deployments with the PCM and engineering instrumentation were carried out during LOTUS<sup>†</sup>. The task of data analysis and evaluation of the test moorings is complete and documented<sup>1</sup>.

#### Design Requirements

The primary requirements to be satisfied by a near-surface mooring for the PCM are:

1. Provide a taut, non-magnetic guideline for the PCM to roll upon between a top stop close to the surface and a bottom stop 200-300 m deep.
2. Function satisfactorily for at least one year unattended.
3. Provide buoyancy distribution to permit backup mooring recovery and PCM survival in the event of any single line or buoy failure.

\*PEQUOD: Pacific Equatorial Ocean Dynamics program (0°, 145°W)

†LOTUS : Long Term Upper Ocean Study (34°N, 70°W)

4. Minimize dynamic excitations of the mooring line below the PCM bottom stop so that conventional fixed current meters placed between this point and the bottom may attain acceptable accuracies.
  5. Avoid extreme dynamic excitations of the PCM guideline in order to prevent undue wear, fatigue, or PCM accuracy degradations.
  6. Reduce low frequency horizontal and vertical excursions sufficiently to obviate the need for correction of current meter records.
- There are two conventional approaches to our mooring design problem. One is to moor a surface buoy from which the guideline may be suspended. The other is to moor a subsurface buoy just below the sea surface and let the upper portion of the mooring line serve as the guideline. The surface mooring approach entails serious problems: high development and hardware cost (to resolve and combat fatigue problems); vandalism; collision, possible guideline/mooring line entanglement; and large dynamic errors in fixed current meters (below the PCM) which will heave due to surface wave excitation of the buoy. Neither is the subsurface mooring approach devoid of problems, among which are: difficulty of implantment such that the top float is near its target depth; drag from strong currents which pull down the top float, depressing the maximum height attainable by the PCM; and possibly significant dynamic errors in fixed current meters which heave due to surface wave forces on the subsurface buoy. Experience warned us to avoid the surface mooring approach and to concentrate instead on the more manageable subsurface design.

#### Design Concept

Our design approach was as follows: A high tension subsurface mooring extends from the PCM bottom stop to the bottom. The buoy on top of this mooring provides an anchor point for a medium tension mooring/guideline extending up to another buoy just below the surface. The upper line serves as the PCM guideline while the lower line holds fixed instruments at any desired levels. A problem setting the top float close to its target depth by an anchor last deployment arises because of uncertainties in mooring length and ocean depth at the anchor drop site. For the ocean tests conducted to date we chose to "brute force" this problem by careful measurements of the actual full-length mooring line under tension, selection of a relatively flat-bottomed implantment site, and accurate measurements of the ocean depth, taking into consideration the fall-back of the anchor. For future experiments we are hoping to incorporate



a "Trimmer" into the line. Here the top float would be targeted below nominal depth to allow for the worst length and depth errors; then after implantment the "Trimmer" would pay out just enough line to allow the top float to rise to its optimum depth.

The problem of drag from strong currents and consequent top float depression has been attacked by designing a taut mooring which is stable by virtue of its great buoyancy and minimum diameter, high-strength mooring line. Our design tool is a computerized model developed at the Draper Laboratory under ONR sponsorship<sup>2,3</sup>. The results of our analysis, indicated good stability can be obtained at reasonable cost, however experimental verification was required because of uncertainty in the drag of a line strumming in high velocity flow. Depression of the top float limits the height attainable by the PCM, but it does not affect accuracy since the PCM has the vertical mobility to sample at all prescribed depths below the top float.

The problem of wave-dynamic excitation of the mooring line was analyzed using another computerized model also developed at Draper under ONR sponsorship<sup>4,5</sup>. The computer simulations were promising for the assumed moorings and environment. They lead us to expect small enough response that the line below the PCM will be a suitable platform for fixed current meters, thereby enhancing the cost effectiveness of the mooring. Experimental verification was again required because of uncertainty in the knowledge of the environment.

There are two major reasons for designing a two-part mooring. First, using a relatively small float (~ 1000 lbs buoyancy) at the top of the guideline results in a moderate tension just 16% of guideline breaking strength. A large margin of safety is thus provided in the line which must withstand fatigue due to strumming and the surface wave field. The main line below the PCM bottom stop is tensioned to 50% of its breaking strength. Second, the top float receives the pressure and viscous drag forces imparted by the wave field, and the smaller this float the smaller the wave-frequency stresses in the guideline, and the smaller the vertical oscillations induced in the main mooring line.

We would like to see wave oscillations below the main floatation attenuated to less than 2 cm/sec. Larger oscillations of the guideline above this point can be tolerated by the PCM by virtue of its mechanical decoupling from axial line motion and its electronic smoothing of current probe signals.

#### MOORING CONFIGURATIONS TESTED

Four versions of the mooring design have been set and recovered in PEQUOD and LOTUS sites during the past two years. A fifth version is presently installed at the LOTUS site. Differences in the five versions are listed in Table I. This table lists the duration of the experiments, major components characteristics, and the location of the engineering instrumentation. Figure 1 is a schematic drawing of the latest version (PCM Zeta) recovered from the LOTUS site.

DESIGNATION ITEM	PEQUOD MOORINGS		LOTUS MOORINGS		
	DYNAMIC TEST	LIFE TEST	PCM EPSILON	PCM ZETA	PCM ETA
DURATION	Jan 81 5 days	Jan 81- Feb 82	May 81- Sept 81	May 82- Nov 82	Apr 83- Aug 83
MAIN FLOATATION	41" Steel sphere 20-17" GBs	41" Steel sphere 20-17" GBs	41" steel sphere 25-17" GBs	2 @ 48" steel spheres	1 @ 41" 1 @ 48" steel spheres
WIRE SIZE	1/4"	1/4"	1/4"	5/16"	1/4"
FORCE VECTOR RECORDERS*	#1 @ 63m #2 @ 126m #3 @ 256m #4 @ 273m	NONE	#1 @ 30m #3 @ 210m #4 @ 1232m	#1 @ 32m #3 @ 187m	#3 @ 183m
TEMPERATURE PRESSURE RECORDERS*	1 @ 22m	1 @ 22m 1 @ 250m 1 @ 270m	1 @ 28m	1 @ 30m	1 @ 28m
RECOVERY BUOYANCY	33 GBs	33 GBs	35 GBs	95 GBs	78 GBs
ANCHOR AIR-WEIGHT	4350 lbs	4800 lbs	4760 lbs	9000 lbs	7000 lbs

\* All instruments except the Life Test TPRs recorded in a burst mode.

TABLE 1 - DIFFERENCES IN FIVE VERSIONS OF THE MOORING DESIGN



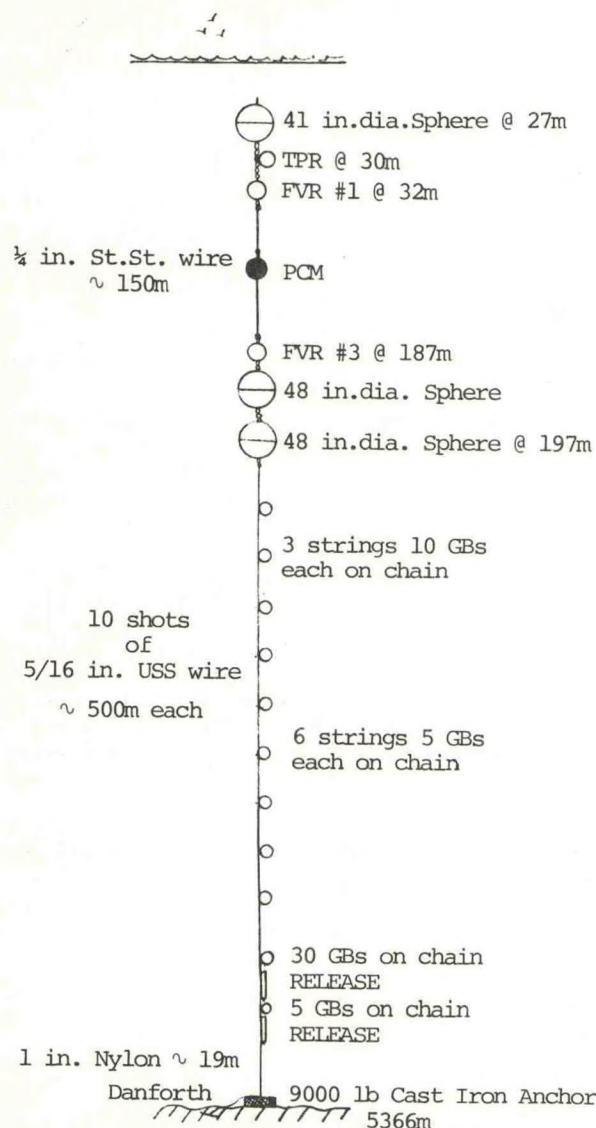


FIG 1 - PCM ZETA MOORING CONFIGURATION

#### PEQUOD Dynamics Test

The first test mooring with engineering instruments on it was set for five days at the PEQUOD site. The mooring was set in 4350m depth with its subsurface float at 14m depth. A total of four Force Vector Recorders (FVRs measuring accelerations, pressure and tension) and one Temperature/Pressure Recorder (TPR measuring pressure and temperature) recorded data at various points along the mooring in a burst mode (1.875 s intervals for 8 minutes) every 64 minutes in order to determine the high frequency behavior of the mooring. Of the four FVRs, there are two different configurations of sensors. The two lower FVRs (Nos. 3 and 4) use a load cell to measure tension, a pressure transducer to track depth and an accelerometer oriented with its input axis (z) parallel to the mooring line to monitor mooring line axial oscillations. The two upper FVRs (Nos. 1 and 2) differ in that they substitute a strumming monitor for the pressure measurement.

To monitor strumming perpendicular to the mooring line, the outputs from two orthogonal accelerometers (x and y) are multiplexed into a bank of three filters whose outputs are in turn multiplexed to an RMS-to-DC converter. Finally, the output of the converter was digitized and recorded. The need for the RMS measurement becomes obvious when one considers the sampling rate and quantity of storage needed to record an 8 minute time history of an input whose frequency could be as high as 40 Hz. The choice of the filter breakpoints were based on an analysis of the expected wave inputs and vortex-induced strumming for a current regime between 25 and 150 cm/sec. Wave inputs all fall below ~1Hz. The FVR itself simulating the PCM might shed vortices between ~ 1 and ~ 6 Hz, where as the mooring line would shed between ~ 6 and ~ 40 Hz. Further details on the mooring instrumentation including an estimate of the system accuracies can be found in reference 1.

#### PEQUOD Life Test

The first test mooring described above was redeployed one day after its initial recovery in January 1981 and recovered thirteen months later in February 1982. It carried three TPRs designed to monitor its long term stability. The two recorded parameters, pressure and temperature, are sampled and accumulated every 30 s, with the resultant accumulation recorded every 32 minutes. This mooring provided data on mooring degradation and survival capability.

#### LOTUS Tests

Three similar moorings were deployed at the LOTUS site (5366m depth). These moorings provided platforms for an operational PCM (PCM Epsilon, PCM Zeta and PCM Eta). The engineering instrumentation inserted in these moorings (Table I) operated in a burst mode where each sensor channel was sampled every 1.875 s for a duration of 4 minutes, with a burst repetition period of 1024 minutes (~ 17 hrs). Configurations of sensors in the TPR and the FVRs were the same as in the PEQUOD experiment.

The first (PCM Epsilon) LOTUS mooring was configured almost exactly like the PEQUOD moorings. This mooring experienced unacceptable vertical excursions\* during a short period of time when high currents from a gulf stream ring pushed the mooring down as much as 180m. Mooring depression statistics show them to be less than 54m, 95% of the time. These depressions were considered excessive and a stiffer mooring was designed for the PCM Zeta deployment. Tension in the main mooring was increased by using 5/16 in. wire instead of the 1/4 in. Main floatation was provided exclusively by steel spheres which have lesser drag per unit buoyancy than the glass balls. The PCM Eta version which is presently installed is a more economical design. The main mooring line diameter is reduced to 1/4 in. from 5/16 in. and a lighter anchor is used which makes this version easier to deploy. Mooring excursions would increase but were calculated to be  
 \*PEQUOD life test mooring, recovered after the PCM Epsilon mooring, also had unacceptable vertical excursions.



a lot lower than the PCM Epsilon mooring excursions. Comparison of the mooring excursions for the PEQUOD life test and the three LOTUS moorings is presented later in this paper. For future versions syntactic foam floatation would be considered for replacement of the steel spheres. Syntactic foam floatation is more expensive and slightly larger but will reduce the need for large numbers of glass balls (needed for backup buoyancy in case of steel sphere failures) and hence will require a lighter anchor.

#### TEST RESULTS

Average; peak-to-peak; and standard deviation of depth measurements for all bursts of the TPR inserted near the top of the PEQUOD dynamic, PCM Epsilon and PCM Zeta moorings are presented in Figures 2 through 4. Depth variations (6.4 hour average) measured by the TPR inserted at the 250m depth of the PEQUOD life test mooring are presented in Figure 5.

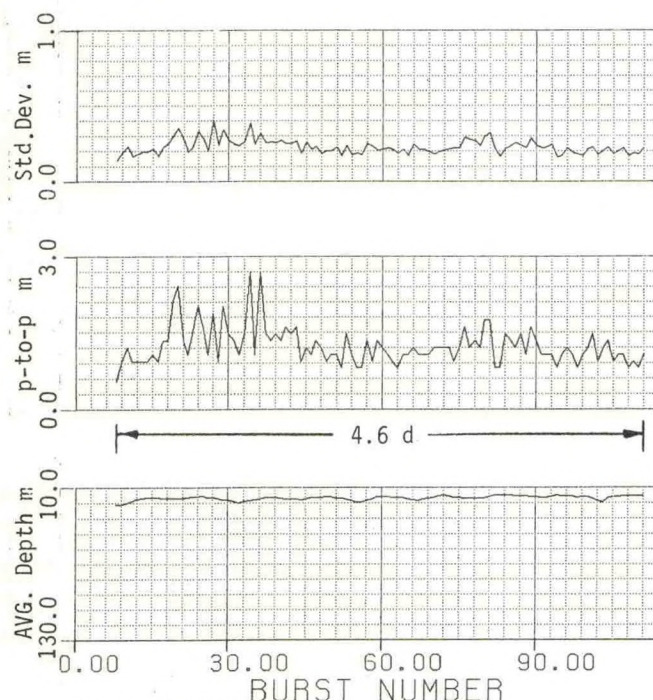


Fig 2 - PEQUOD Dynamics Test Mooring - TPR data

#### Deployment Accuracy

Minimum depths of the four moorings, derived from TPR measurements, are compared with their target depths in the following Table II. The setting errors are small enough for our purpose and can be traced to some combination of the following sources: a) Poor knowledge of ocean depth at the anchor impact point; and b) Errors in length measurement or stretch estimates (probably less than 5m).

#### Survival

The PEQUOD Life Test Mooring was in place between

Experiment	Water Depth (m)	Target Depth Top (m)	Minimum Depth Top (m)	Diff. m
PEQUOD Dynamic	4350	20	14	-6
PEQUOD Life Test	4350	20	8	-12
PCM Epsilon	5366	25	21	-4
PCM Zeta	5366	27	20	-7

Table II

28 Jan 81 and 19 Feb 82, surviving 387 days of the equatorial Pacific near-surface environment. All components from the top of the guide line downward were recovered in good condition. However some of those at shallower levels fared rather badly.

The most serious result was the complete loss of the Temperature/Pressure Recorder which was clamped to a tension rod in line just below the top subsurface float. Apparently the combination of wave excitation and over-hanging moment of the T/PR caused the hole in the clamp insulating bushing to wear to almost twice normal size allowing the T/PR and clamp to slide downward along the tension rod, stopping against the lower shackle. It eventually broke free.

Corrosion of the galvanized steel tension rod was much greater than usual probably due to the clamp failure but not sufficient to seriously weaken the rod. The bottom three of the four 5/8" galvanized steel safety shackles connecting this tension rod

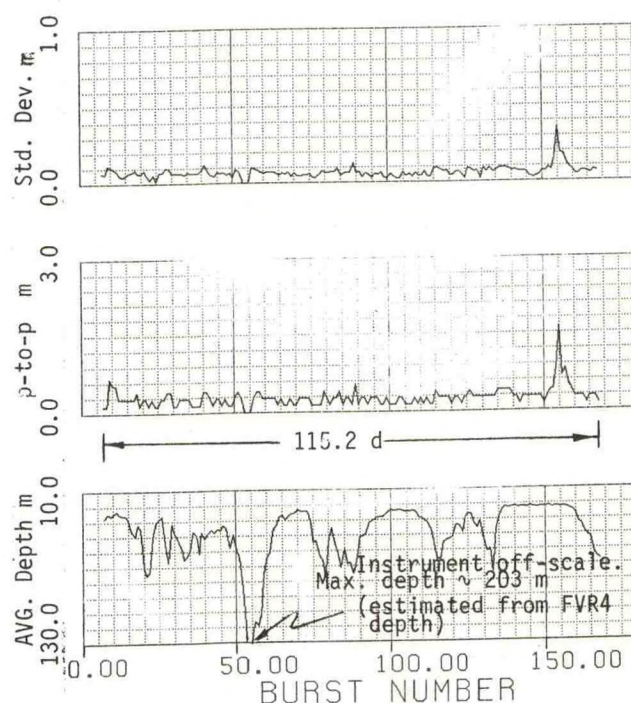


Fig 3 - PCM Epsilon Mooring TPR data



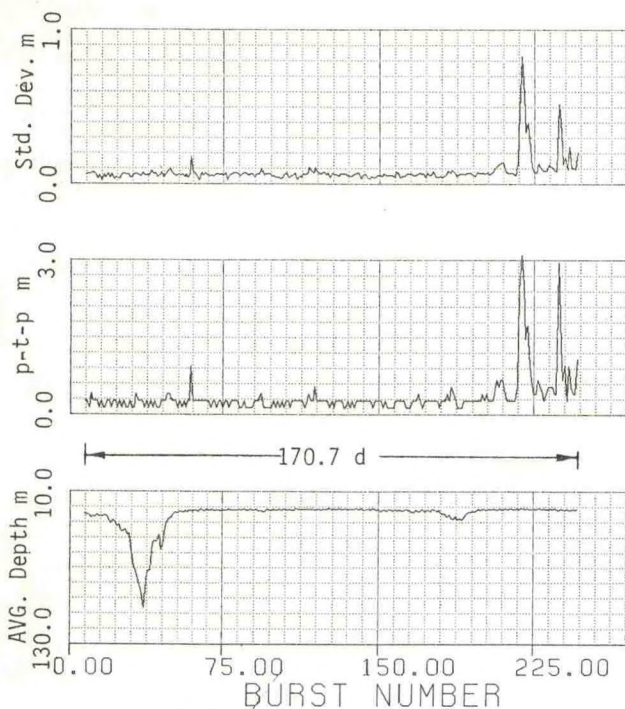


Fig 4 - PCM Zeta Mooring -  
TPR data

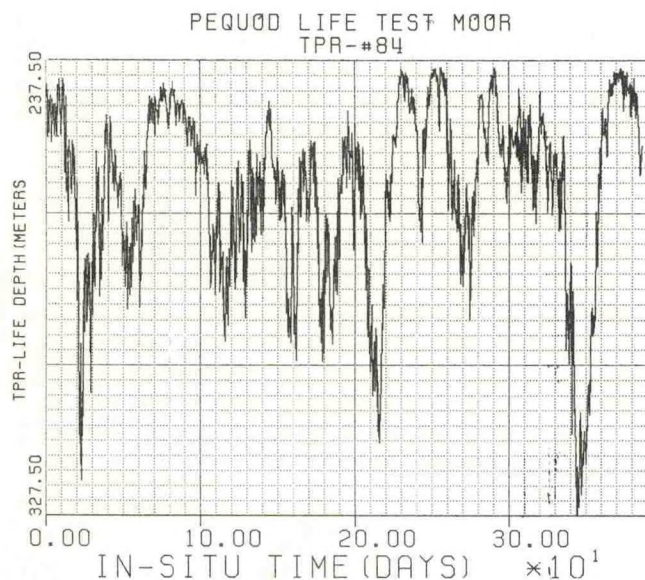


Fig 5 - TPR Data - Each Point is 6.4 hr  
Average

as a series element of the mooring were also damaged by corrosion. These shackles had been secured with nuts and 316 stainless steel cotter pins during deployment, as is usual practice, but on recovery the cotter pins and nuts were missing and even the threads on the bolts were partially corroded away. Additional severe corrosion was seen on these shackles' eyes and bolts and on the 5/8" shackle immediately above the guideline. The

bottom link of the 1/2" proof coil chain was corroded where it touched this shackle.

We were pleased to find no significant bio-fouling. The top mooring float was quite clean although there was some blistering of the manufacturer's undercoat. The dark red antifouling paint\* has also shown similar success when applied to tide gages deployed in tropical lagoons and to the PCM in near-surface experiments. There was some slime on the guideline but no "grass" or animal life that might interfere with the operation of the PCM. (The PCM rollers normally discourage marine growth anyway.)

One of the most uncertain factors in the survival of the mooring was the durability of the terminations on the stainless steel guideline. Although there is a wealth of experience on, and therefore confidence in, galvanized fittings swaged on to 3 x 19 galvanized wire rope, there was little information available on the long-term survival of stainless steel assemblies. The terminations used were designed using mil-standard dimensions, machined from type 304 stainless steel, and swaged onto the guideline wire using a "LOCOLOC" manual swaging machine. Particular attention was paid to isolating dissimilar metals and to sealing interfaces to prevent crevice corrosion. The wire/termination joint was tightly wrapped and reinforced with alternate layers of vinyl electrical tape, glass-fiber tape, and "Scotchkote" sealant to form a stiff, waterproof boot. Neither of the guideline terminations showed any corrosion or indication of possible failure.

One 5/8" shackle on each of the two lower T/PRs (250 meter depth) was found, upon recovery, to have been secured inadvertently with a cadmium-plated steel cotter pin rather than the usual 316 stainless steel pin. Although the pins had some surface rust they were intact and the shackles secure.

The condition of the remainder of the mooring was excellent and essentially no different from that of a standard intermediate mooring upon recovery after one-year immersion.

The galvanized marine hardware above the guideline should be changed. One approach is to replace it with hardware of non-corrosive materials. If galvanized fittings are used, they should be much larger (3/4" nominal size) and have clamp-on zinc anodes and non-metallic locking devices or insulated stainless cotter pins. Proof coil chain should have its factory-applied zinc coating (which is notoriously thin) stripped and be hot-dip regalvanized.

The condition of the moorings recovered from the LOTUS site was excellent. There was no significant corrosion or fouling in deployments lasting up to six months.

\*Gloucester 515 Special Red A.F. Paint  
(70.2% Cuprous Oxide)



## Axial Mooring Velocities

An accelerometer measures the component of  $\vec{f}$  (specific force  $\equiv$  nongravitational vector force on instrument  $\div$  mass of instrument) along its input axis.

$$\vec{f} = \vec{a} - \vec{g}$$

where  $\vec{g} \equiv$  local gravity vector

and  $\vec{a} \equiv$  instrument linear acceleration vector

We make the reasonable assumption that, for the duration of a burst (480 or 240 seconds), the variation in the component of  $\vec{g}$  along the input axis of the accelerometer is negligible compared with the variation of  $\vec{a}$  then:

$$f_z(t) = a_z(t) - g_z$$

where  $z$  is the input axis direction. Since the mean of  $a_z(t)$  is zero  $g_z$  is given by the mean of  $f_z(t)$  (measured signal). Having obtained  $a_z(t)$ ; it can be integrated once to give  $v_z(t)$  (instrument linear velocity) and integrated twice to give  $d_z(t)$  (instrument linear displacement).

$a_z(t)$ ,  $v_z(t)$  and  $d_z(t)$  were calculated via discrete fourier transform techniques for various FVRs and bursts. Calculations for FVR No. 1, burst No. 27, PEQUOD experiment are presented below. For details of these calculations see reference 1. As shown in that reference, a simple integration of the acceleration signals gave velocity and displacement plots which had low-frequency fluctuations suggesting unreasonable results. For example; the FVR No. 1-burst No. 27-PEQUOD experiment displacement plot had a peak-to-peak  $z$  displacement of greater than 48m during the eight minute burst. As seen from Figure 2, the TPR (located close to FVR No. 1) shows a peak-to-peak vertical displacement\* of less than two meters. These low-frequency fluctuations in the calculated velocities and displacements were removed by neglecting fourier components having frequencies lower than 0.017Hz (60 s period). These final plots are presented in Figure 6. The peak-to-peak  $z$ -displacement of  $\sim 2$ m present in Figure 6 corresponds to the 2m peak-to-peak vertical displacement of TPR seen in Figure 2.

Standard deviations of the time-plots of acceleration, velocity and displacement (like the one's presented in Figure 6) are listed for some FVRs and bursts in Table III. Standard deviations of the axial velocities of the moorings show a range of 1cm/sec to 18cm/sec. To show how energetic the listed bursts were compared to the rest of the experiments; burst percentiles (based on  $z$ -accelerometer data), mooring top depth and experiment duration is also listed.

### Measurements of Mooring Strumming

FVR1 rms measurements for the PCM Epsilon mooring

\*The TPR depths include the effect due to dynamic pressure from surface waves.

are presented here. Figure 7a is the rms channel of FVR-1 burst No. 155. The plot is of raw count versus time and shows how the accelerometers and filters were sequenced. The annotations along the top of the plot give the accelerometer channel and filter for that instant of time. The second point after an accelerometer had been switched is marked on the plot. The annotations along the 50 count line give the conversion factors between count numbers and g's. A count of fifty is equal to 0.034, 0.032, 0.017, 0.021, 0.023, and 0.081 g depending on the accelerometer channel and filter for that instant of time. The rms values suggest a

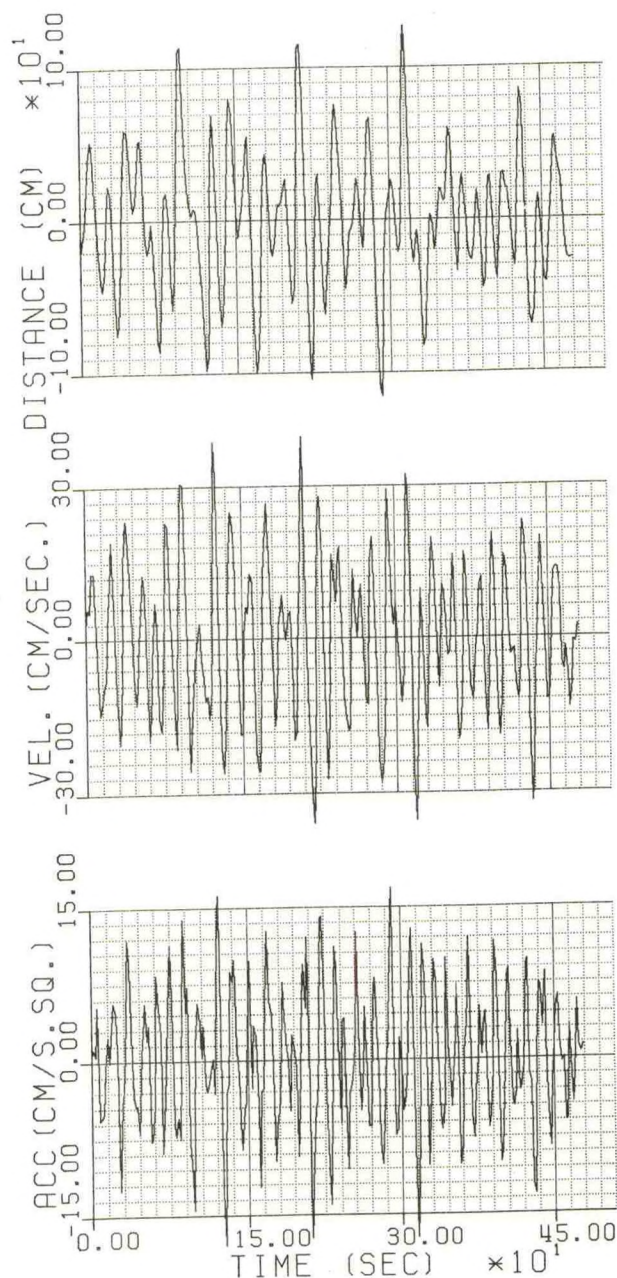


Fig 6 - Acceleration, Velocity and Displacement of FVR1 PEQUOD Dynamics Test - Burst 27



EXPERIMENT	Burst No.	PERCENTILE* Burst %age	DOMINANT PERIOD (s)	SYSTEM	$\sigma_a$ cm/sec <sup>2</sup>	$\sigma_v$ cm/s	$\sigma_d$ cm
PEQUOD -5 Days -480 s Bursts -Top @ 14m	27	54	17	FVR1	6.65	15.19	47.11
				FVR3	5.88	12.76	33.54
PCM EPSILON -115 Days -240 s Bursts -Top @ 21m	54 (max depth)	87	15	FVR1	3.93	6.33	17.26
				FVR3	0.53	1.00	3.10
	155 (max wave)	99	15	FVR1	9.53	18.41	38.58
				FVR3	8.36	16.55	35.03
PCM ZETA -171 Days -240 s Bursts -Top @ 20m	64	65	14	FVR1	2.20	3.34	6.87
				FVR3	2.25	3.18	5.31

\* Percentage of Bursts with Standard Deviations of Accelerometer Signals less than the Burst Studied.

TABLE III - Integration of Accelerometer Signals Via Fourier Transform Techniques

large oscillation in the 0 - 1.6 Hz filter and a small vortex oscillation (2 - 45 Hz). In a 50 cm/sec current; the vortex frequency for the body (FVR) is  $\sim 2$  Hz and for the mooring line is  $\sim 13$  Hz. The large horizontal oscillation ( $\sim 0.07$  g, rms) in the 0 - 1.6 Hz filter seems to be due to wave frequencies.

For comparison, the rms channel of FVR-1 during burst No. 54 is presented in Figure 7b. This burst occurred on the 38th day, when the maximum excursions were experienced and hence marks the time when the mooring was subjected to the maximum currents. It is during these high currents that a mooring is most susceptible to high frequency strumming. Figure 7b shows large horizontal oscillation ( $\sim 0.15$  g, rms) due to vortex shedding in the mooring (6 - 45 Hz filter). This is the oscillation felt in the FVR which is a reasonable simulation of what the PCM might feel.

#### Low Frequency Excursions

Low frequency excursions of the PEQUOD dynamic test, PEQUOD life test, PCM Epsilon, and PCM Zeta moorings were presented in Figures 2 through 5. PEQUOD dynamics test was for five days and excursion data from it was uninteresting. PEQUOD life test and PCM Epsilon moorings were almost exactly the same and both experienced excessive vertical excursions. This mooring design had a large number of glass balls up at the 250m depth which contributed a substantial portion of the mooring drag. PCM Zeta and Eta moorings are stiffer.

Performance of the PCM Zeta mooring under various currents is compared with PCM Epsilon mooring in Figure 8. The horizontal scale on this figure is the velocity in cm/sec and the left vertical scale

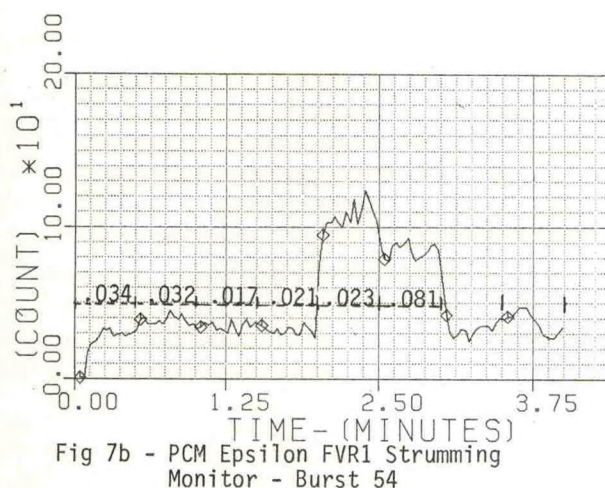
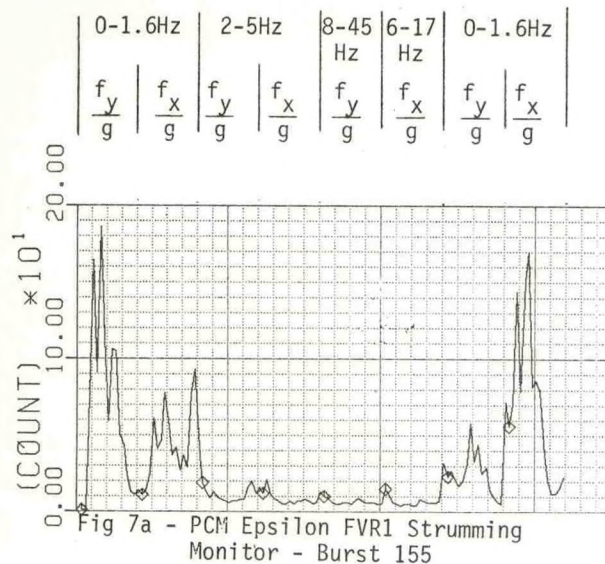
is the depression (m) of the mooring top. The two solid curves are obtained from computer simulations<sup>2</sup>.

The right vertical scale is derived from PCM Epsilon measurements (Figure 3). It shows the percentage of time the mooring experienced depressions less than a certain given value. For example; 95% of the time PCM Epsilon mooring's top had depth excursions less than 54m. Using the solid calculated curve of PCM Epsilon mooring we obtain a velocity value of 53 cm/sec for a depth excursion of 54m. Hence if our calculations and assumptions of current profile shape were exact, 95% of the time the current was less than 53 cm/sec. To test the accuracy of our calculations and assumptions about the current profile shape; we plotted onto Figure 8 some points derived from simultaneous measurements of currents by the PCM and depth by the TPR. Comparison between the measured data and the calculated curve is good even though a very crude assumption of current profile, being constant between 0 and 650m and zero below 650m, was made. This current profile shape is based upon profiles taken in gulf stream rings.

For a current of 53 cm/s, PCM Zeta mooring top's depth excursion is 13m (Figure 8, calculated curve). It can be concluded from this analysis that, assuming the current environment for PCM Zeta is similar to the one experienced by PCM Epsilon, whereas 95% of the time PCM Epsilon mooring top's depth excursion was less than 54m, it would be less than 13m for the PCM Zeta mooring top.

How did the PCM Zeta mooring do? TPR depth data from PCM Zeta was analyzed. Figure 9 presents the percentage of time mooring top depression was below a certain value. Data from PCM Zeta as well as





PCM Epsilon is presented. It is clear from this figure that the PCM Zeta mooring had far less depth excursion than the PCM Epsilon mooring. A curve showing the estimated PCM Zeta excursions is plotted in addition to the measured data. This curve is derived from curves presented in Figure 8 and assumes 1) that the PCM Zeta current environment was the same as the PCM Epsilon current environment and 2) that the current profile has a certain fixed shape (constant between 0 and 650m depth; zero below 650m). The estimated and the measured curves match well except near the high excursion end of the curves. This discrepancy is most likely due to higher currents during PCM Zeta than were experienced during PCM Epsilon. Estimated excursions of the PCM Eta mooring are superimposed on the PCM Epsilon and PCM Zeta moorings excursions presented in Figure 9.

#### Wave Response

Computer simulations of the wave-dynamic excitation of the PEQUOD mooring line were run. For each simulation, a single gravity wave of different time-period and a 1.52m amplitude along with a measured current profile was used as the input forcing.

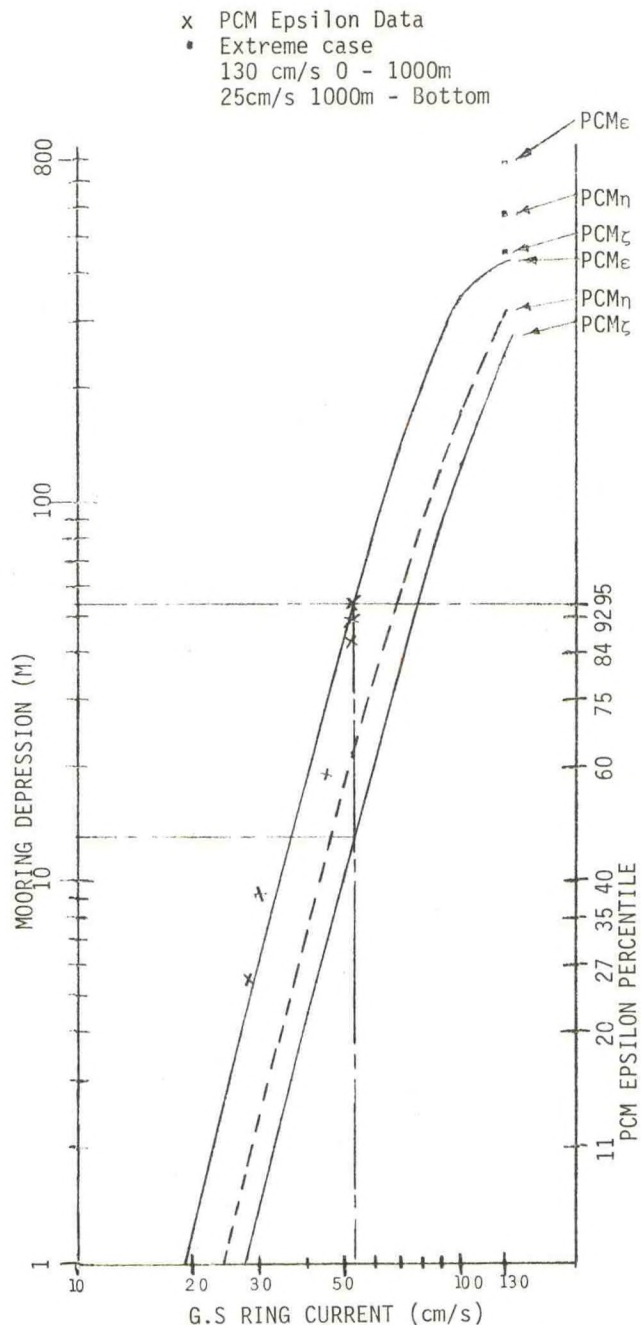


Fig 8 - Calculated Depression of PCM Mooring Top vs Gulf Stream Ring Current (0-650m depth)

Six sensor signals were simulated. These were 1) TPR81 depth\*, 2) FVR4 depth\*, 3) FVR1 tension, 4) FVR4 tension, 5) FVR1 z-accelerometer, and 6) FVR4 z-accelerometer. In addition, mooring velocity at the FVR4 location was also calculated. Details of these simulations are presented in reference 1.

Results of the computer simulations listed above were compared with measurements for a possible model validation. Procedure chosen for this \*Depth is calculated from simulation of the pressure at these locations and includes the contamination due to surface wave dynamic pressure.



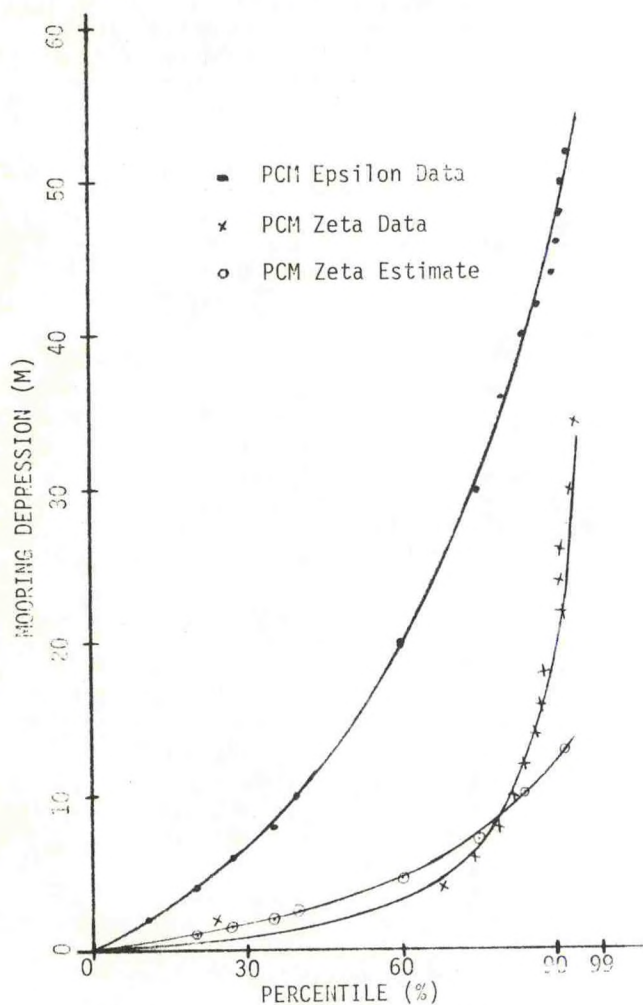


Fig 9 - Excursion Comparison

comparison is as follows: Power spectral density plots for burst 27 measurements of the six sensor signals simulated above were calculated. Square root of the power at a given frequency is the standard deviation of the harmonic corresponding to that frequency. Standard deviations of all harmonics for the six sensor signals were computed. Two ratios of these standard deviations are presented as a function of frequency in Figures 10 and 11. Ratios presented are 1) FVR1 tension/FVR4 tension; and 2) FVR4 z-specific force/FVR4 tension. Superimposed on these ratios are the simulated values for these ratios. The comparisons are good.

#### CONCLUSIONS

Test results presented in this paper show that we have the ability to deploy barely-subsurface moorings in deep water ( $\sim 5000\text{m}$ ) by the anchor-last deployment. Our success to date has been accomplished by constraining our deployments to areas having smooth, gradually sloping bottoms which can be surveyed just prior to deployment. A slight

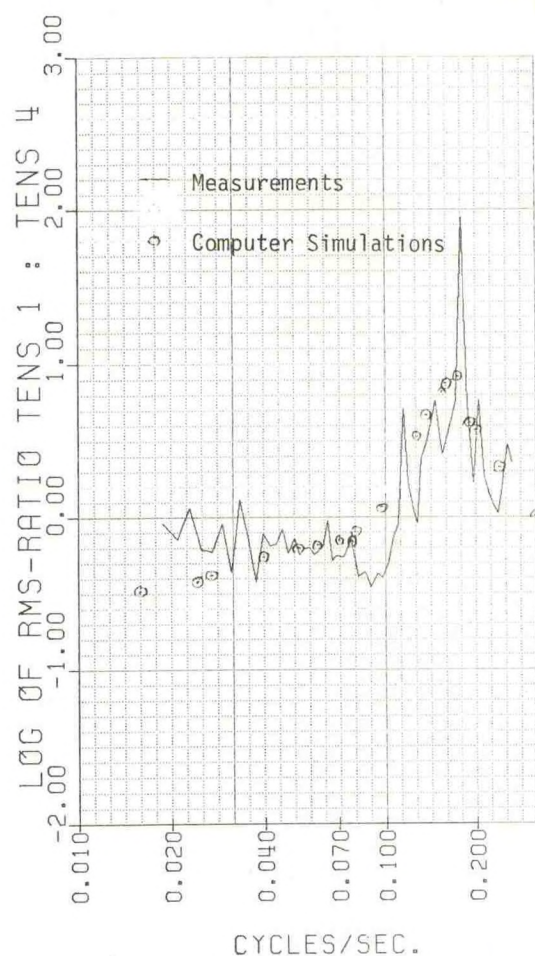


Fig 10 - Ratio of FVR1 Tension and FVR4 Tension

bottom slope, uncertainties in line length and stretch, and variable currents all conspire to put the top float so deep that scientific goals are jeopardized or so shallow that the hardware as well as the goals will be lost. The obvious solution to this problem is to incorporate a line payout device in the mooring so that after initial setting the line may be lengthened as required to raise the top float to its desired level.

Test results also show the ability of this mooring to survive for at least thirteen months in an upper ocean equatorial environment.

Calculations of vertical mooring velocities from accelerometer measurements show that points near the top of the mooring oscillated axially with a standard deviation of roughly between 3-6 cm/sec during North Atlantic deployments and 15 cm/sec during Pacific Equatorial deployments for most of the time. The velocities were larger in the Pacific deployments because the mooring was closer to the surface. PEQUOD life test and PCM Epsilon moorings experienced excessive vertical excursions. Stiffer moorings were designed for PCM Zeta and



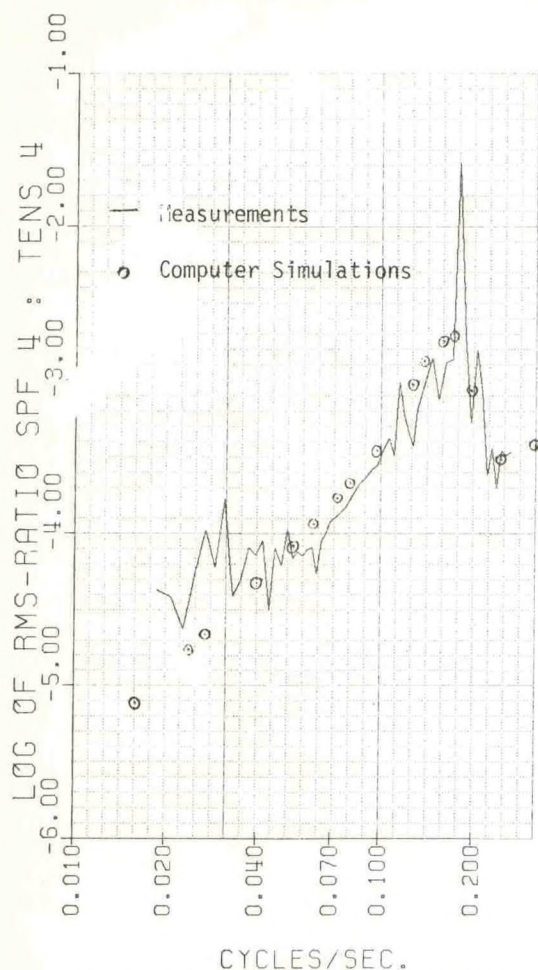


Fig 11 - Ratio of FVR4 z-specific Force and FVR4 Tension

PCM Eta experiments. Excursion data from PCM Zeta mooring looks encouraging. Occasional large excursions and axial oscillations must be considered for applications involving fixed instruments. The PCM is immune to these effects.

Computer simulations of the mooring motions and tensions in the mooring line give good comparisons with the recorded measurements. In the model validation studies, no effort was made to improve the mathematical models.

#### ACKNOWLEDGMENT

The mooring development reported herein was supported by the National Science Foundation, through the PEQUOD program, and by the Office of Naval Research, through the PCM/LOTUS PROGRAM. Draper Laboratory personnel who made especially valuable contributions to this development work include: Richard Araujo, Carmen Martorella, Robert Reid, James Scholten, John Shillingford, and Matti Soikkeli. Kay Hall typed this paper. M.I.T. Professor Charles Eriksen, the science program Principal Investigator, provided much valuable

guidance and assistance. Finally we wish to acknowledge the excellent support provided by the crews and scientific parties aboard the R/V. T. G. Thompson (Jan/Feb 81 and Feb/Mar 82 cruises) and the R/V Oceanus (four LOTUS cruises between May 81 and Nov 82).

#### REFERENCES

1. Araujo, R.K.; N.K. Chhabra; J.M. Dahlen and R. W. Reid (1983) Development of a Deep-Ocean Mooring for an Upper Ocean Profiling Current and CTD Meter, C.S. Draper Laboratory, Inc. Report R-1634, in preparation.
2. Chhabra, N.K. (1974) Verification of a Computerized Model for Subsurface Mooring Dynamics Using Full Scale Ocean Test Data. Proceedings MTS Tenth Annual Conf., Sept. 1974.
3. Chhabra, N.K. (1977) Correction of Vector-Averaging Current Meter Records from the MODE-1 Central Mooring for the Effects of Low-Frequency Mooring Line Motion. Deep-Sea Research, 24, 279-287, March 1977.
4. Chhabra, N.K. (1979) Dynamics of a Tethered Spar Buoy System - Validation Using Full Scale Ocean Test Data. Presented and Published in the Proceedings of the Specialty Conference Civil Engineering in the Oceans IV, ASCE, San Francisco, Sept. 1979, pp-208-223.
5. Chhabra, N.K. (1982) 1976 Mooring Dynamics Experiment - Verification of Dynamic Model of a Surface Mooring, C.S. Draper Laboratory, Inc., Report R-1567, Nov. 1982.
6. Eriksen, C. C.; J. M. Dahlen and J. T. Shillingford, Jr. (1982) An Upper Ocean Moored Current and Density Profiler Applied to Winter Conditions Near Bermuda, Journal of Geophysical Research, Vol. 87, No. C10, pp 7879-7902, Sept. 20, 1982.



# ON COLLECTING OPERATIONAL METEOROLOGICAL DATA FROM THE NORTHEAST PACIFIC OCEAN WITH THE ARGOS SYSTEM

R.E. Vockeroth and D. Oracheski

Atmospheric Environment Service  
Toronto and Edmonton, Canada

## ABSTRACT

The collection of real-time meteorological reports from drifting buoys in the northeast Pacific Ocean through an ARGOS direct readout station in Edmonton, Alberta is described, and some possible alternatives are reviewed.

## 1. INTRODUCTION

With reception from all points on the earth six or more times per day and with the capability to determine the position of moving data platforms, the ARGOS system with instruments operating on two NOAA Polar orbiting satellites is particularly suited to the collection of data from drifting buoys. Since January 1980, the Atmospheric Environment Service of Canada (AES) has conducted trial operations of drifting buoys in the northeast Pacific Ocean, and has been receiving their data through an ARGOS Direct Readout Station (DRS) in Edmonton, Alberta (di Cenzo, 1981). Figure 1 shows the computed mean number of daily receptions by the NOAA satellite and by the Edmonton DRS, and the actual number of receptions per day at Edmonton from seven trial buoys in February, 1982. However, it has become evident that the time of data availability, relative to the standard meteorological data collection times, is as important as the number of reports obtainable per day. Using system specifications provided by Service ARGOS (1978), and experience from the operation of the Edmonton station (Vockeroth, Beale and Stauder, 1983) the frequency and timing of the data reports that could be expected from meteorological data buoys in the northeast Pacific Ocean have been examined.

## 2. METEOROLOGICAL DATA COLLECTION

To be most useful in the operational meteorological analyses that are used to produce the large majority of weather forecasts, data should be measured as near as possible to

the standard synoptic reporting times: 0000Z, 0600Z, 1200Z and 1800Z (Coordinated Universal Time, UTC, formerly called Greenwich Mean Time, GMT) and should be received in the meteorological offices within one hour of these times. Data measured or received at other times are more difficult to assimilate in most operational procedures, and therefore of less value.

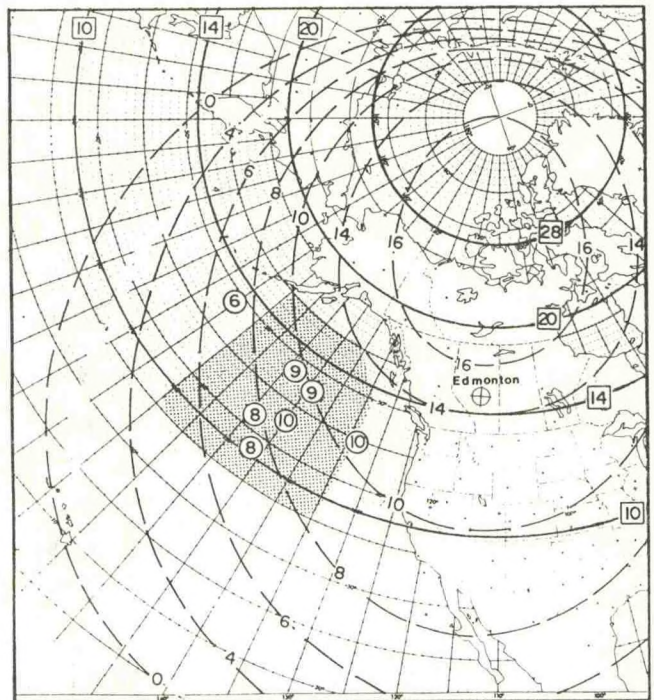


Figure 1 Reception ranges and frequencies for ARGOS data platforms.

Legend:

Meridional Circles - Calculated number of daily reports via Service Argos in Toulouse

Dashed lines - Calculated number of daily reports via Edmonton DRS

Small Circles - Sample daily number of buoy receptions via Edmonton

Shaded Area - Proposed data-buoy field.



As currently operating in the two NOAA satellites, the ARGOS system can obtain data six times per day from platforms near to the equator, and up to 28 times per day from platforms within 15° of the earth's poles. Such frequent data coverage can be provided globally when the reports are stored in the satellites, and then relayed to the ARGOS Data Centre in Toulouse, France. This data route requires two to four hours to collect, process and issue reports to the Meteorological Telecommunications System (GTS). Direct readout stations can receive the same reports from only a limited area, but can distribute them to regional forecast offices and to the GTS in about 30 minutes.

By plotting the ground tracks of the satellite orbits that pass within telemetry range of the data buoys and of direct readout stations, the daily frequencies and times of data collection can be studied (Vockeroth and di Cenzo, 1982). In this study the coverage of the ARGOS data system was computed with a Caltech Seatrack graphical calculator, using overlays developed by the principle author, and the following parameters:

- A mean satellite orbit period of 101.6 minutes. The actual periods were 101.19 minutes for NOAA 6 and 102.0 minutes for NOAA 7 in December, 1982.
- Equator crossing times at the published nominal times. NOAA 6 was 3.63 minutes later and NOAA 7 was 5.04 minutes earlier on 21 December, 1982.
- Limiting buoy and satellite telemetry transmission ranges of 2,800 km and 3,100 km respectively. The actual effective reception ranges of the buoy and the satellite transmissions, determined from the data recovery at the Edmonton DRS, extend from 2,700 km to 3,400 km, apparently depending upon atmospheric refraction effects.
- A minimum data reception time of 3 minutes at the DRS, so that at least three of the buoy transmissions, at 55 second intervals, can be received, and the data reliability can be assessed.
- A 110 minute interval, from 75 minutes before to 35 minutes after the nominal synoptic hour, selected to optimize both the availability and timing of meteorological reports for the standard synoptic analyses.

### 3. DATA RECEPTION FROM THE NORTHEAST PACIFIC

Using the parameters defined above, data reception was assessed over the northeast Pacific Ocean area shown in Figure 2. A proposed buoy network location (Kerut, 1982) is shown in this figure, as well as the satellite transmission

reception limits for the DRS at Edmonton (EG), and for hypothetical readout stations at Gilmore Creek, Alaska (GC) and at Kauai (KA) in the Hawaiian Islands. These 3100 km range circles appear as ellipses on the map projection that was used. Four typical satellite orbit tracks, each close to a standard synoptic time, are also shown in this figure.

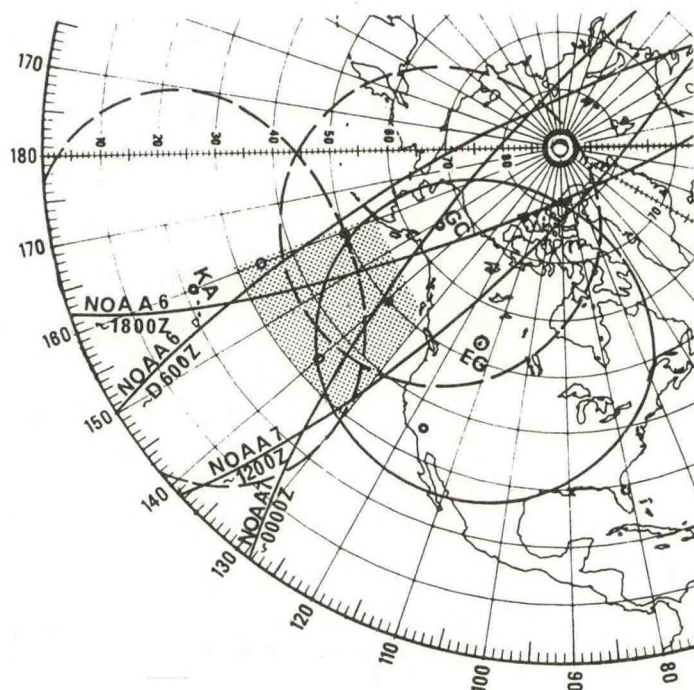
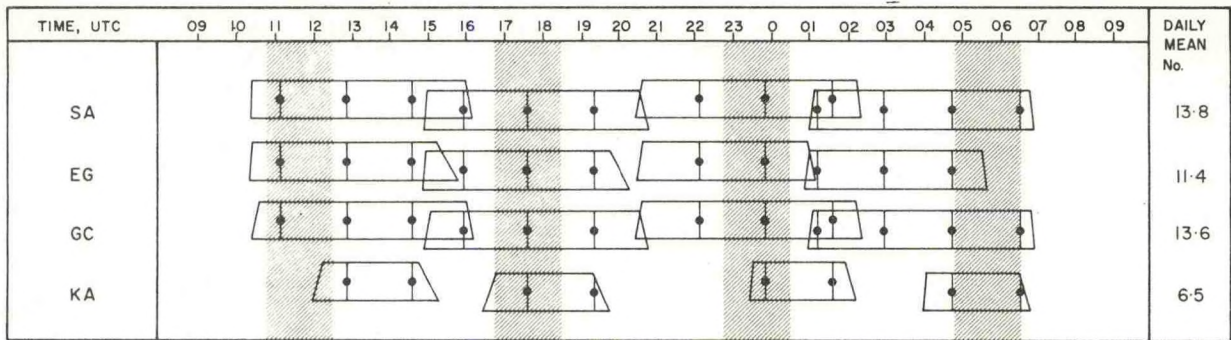


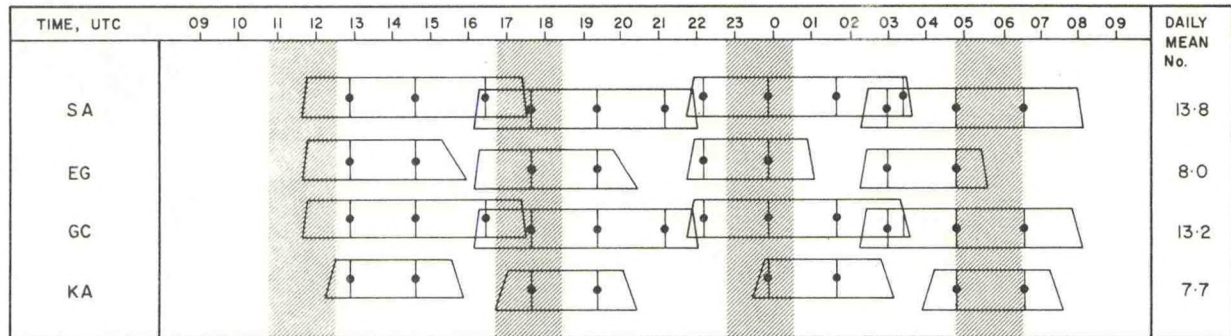
Figure 2 Map of the NE Pacific Ocean showing the normal maximum range of receiving satellite data transmissions at Edmonton (EG), Gilmore Creek (GC), and Kauai (KA). Four typical satellite orbits, each close to a standard synoptic time, and the locations of the four buoys in Figure 3, are also shown.

Figure 3 shows the data reception time limits, and typical satellite orbit times for buoys at four representative locations within the proposed network. The base line of each time window shows the normal earliest and latest reception times, and the top edge shows the time limits for orbits with reception durations of three or more minutes. Actual receptions will be at approximately 102 minute intervals within the indicated time windows. Reception times are earlier by about 24 minutes per day for NOAA 6 and 12 minutes per day for NOAA 7, and thus have repetition cycles of approximately 4.25 and 8.5 days respectively. The time windows designated SA show the intervals during which data could be obtained through the Service ARGOS data centre in Toulouse, France, i.e. the limits of data reception set by the orbits of the two NOAA satellites.

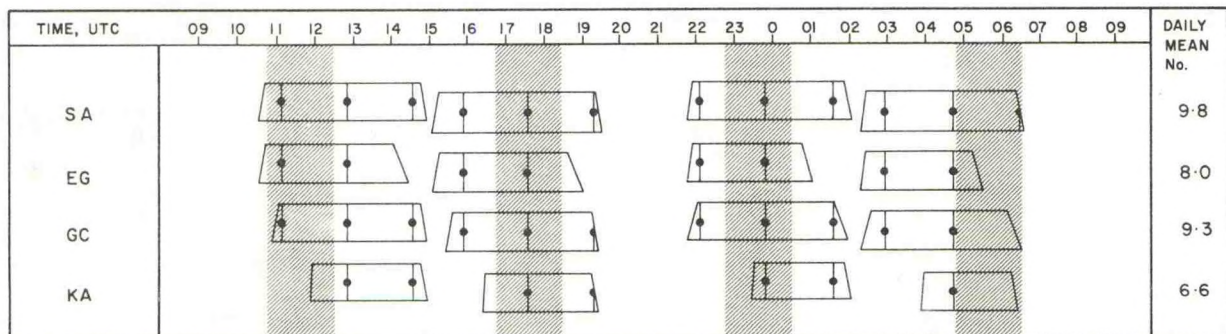




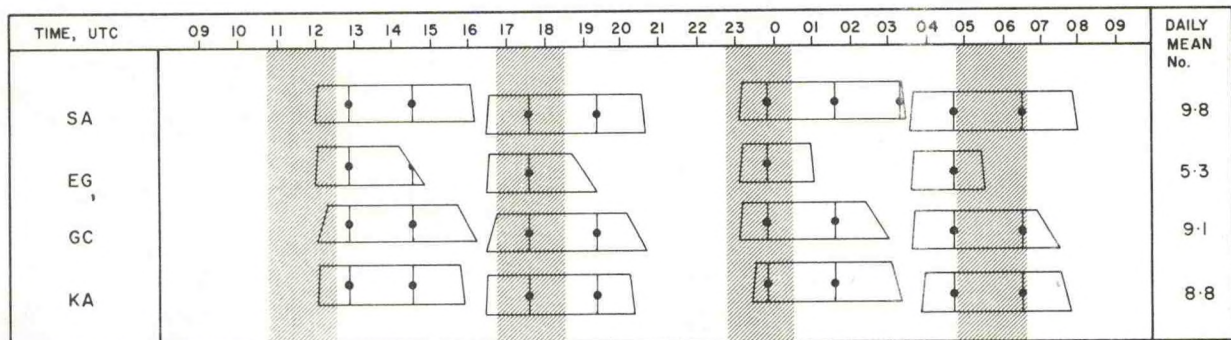
BUOY AT 50°N 140°W



BUOY AT 50°N 160°W



BUOY AT 35°N 140°W



BUOY AT 35°N 160°W

Figure 3 - Reception time windows for buoys at 4 positions. The shaded bands show the proposed optimum time bands for synoptic meteorological reports. Typical satellite orbit times for NOAA 6 and NOAA 7 are indicated by the symbol: ♦



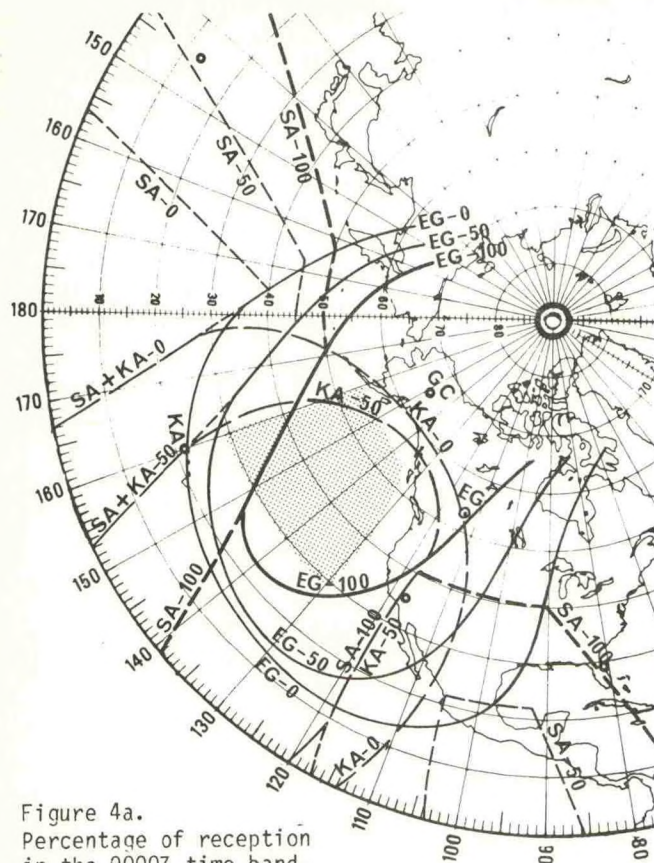


Figure 4a.  
Percentage of reception  
in the 0000Z time band.

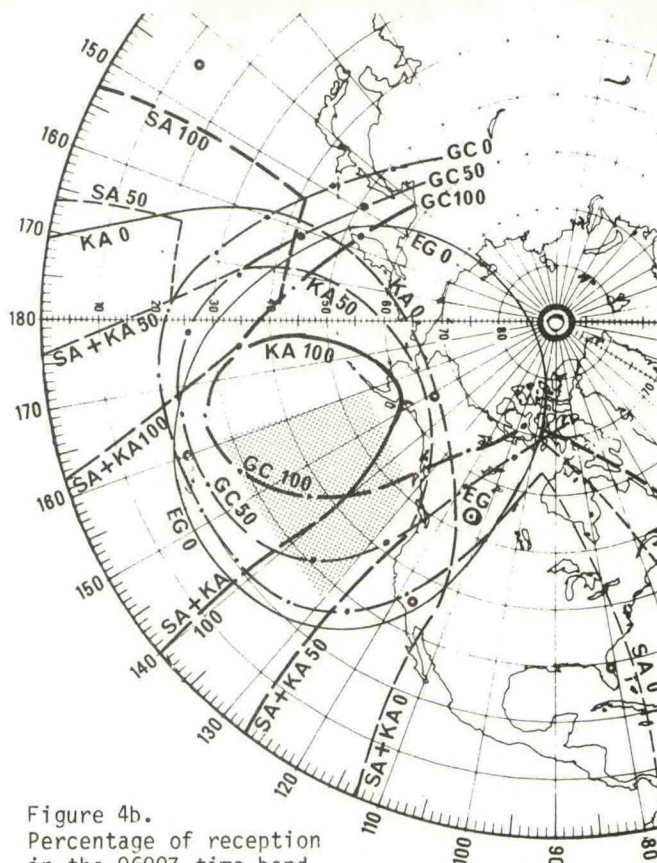


Figure 4b.  
Percentage of reception  
in the 0600Z time band.

Figure 4 - Data reception in the NE Pacific in percentage of days that reports could be received from buoys in the delineated areas by each of four data routes. See text for definition of the time bands.

The computed time windows for Edmonton (EG) show that the DRS there can potentially receive all of the reports that the current NOAA/ARGOS system can provide from these four locations in the defined 1200Z, 1800Z, and 0000Z time bands. On the other hand, it is evident that Edmonton can receive only a small part of the reports in the 0600Z synoptic band, while stations at Gilmore Creek and/or Kauai would be able to receive practically all of these data. This type of analysis can help in the study of means for offsetting a lack of reports in any of the time bands. Examination of Figure 3 shows that while Edmonton can not normally receive reports from the four sample buoy locations in the defined 0600Z time interval, reports could be received regularly from three of them between 0325Z and 0515Z, and for 90% of the time also from 35°N 160°W. In considering the availability of operational reports, it should be realized that the primary function of the Edmonton DRS is to provide AVHRR images from the NOAA satellites, and also that it collects reports from buoys in the Arctic Ocean as well as from the Pacific. When these tasks conflict, the actual data collection from an area may fall below the potentials described in this paper.

To illustrate in another way the potential of the NOAA/ARGOS system for collecting data from the northeast Pacific area, reception percentage contours for each of the four defined synoptic time intervals were plotted on a map of the area. The lines on the maps in Figure 4 marked SA 100, EG 100, KA 100, etc., show the areas within which Service ARGOS, the Edmonton DRS, or a station at Kauai could provide a report from each platform operating in the outlined area 100 days out of 100. Similarly, the contours marked 50 show the limits of data reports 50 days out of 100. The contours marked 0 show the limits beyond which data reception cannot normally be expected.

#### 4. SUMMARY

The locale of the proposed buoy network in the northeast Pacific is well served by the current NOAA/ARGOS data collection system, and also by the DRS at Edmonton. By comparison, as Figure 4 shows, relatively few meteorological reports could be obtained at the synoptic times from the low and mid-latitudes in the area near the 180th meridian. (Similar data gaps, at the four principle synoptic times, occur at the 0° and the two 90° meridians).



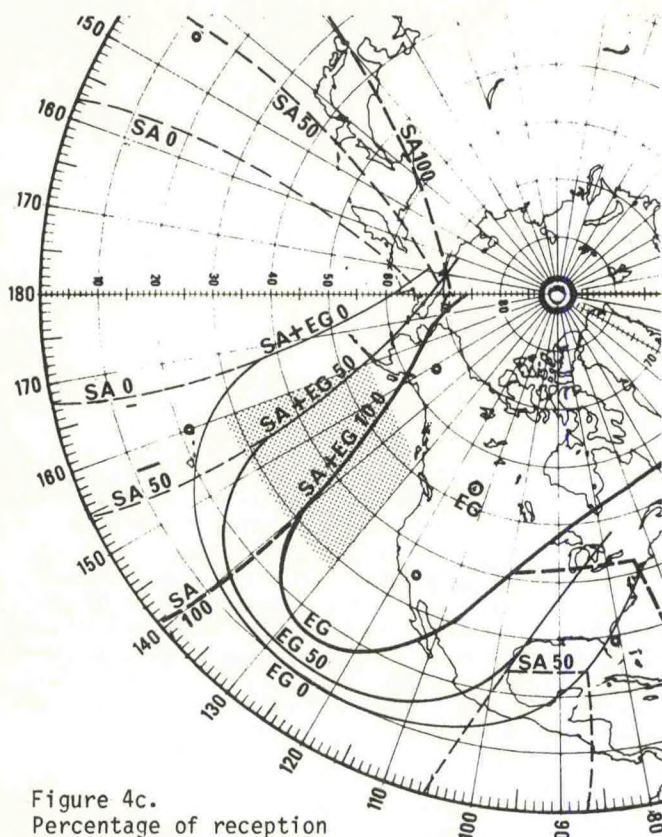


Figure 4c.  
Percentage of reception  
in the 1200z time band.

Figure 4 - Continued: Legend:

100% daily reception   
 50% daily reception   
 Outer limit of reception

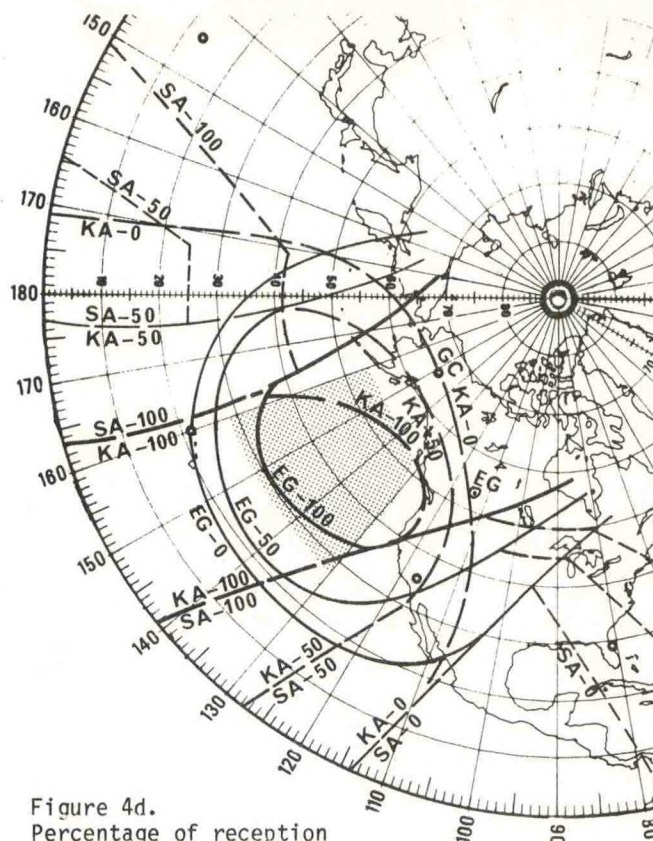


Figure 4d.  
Percentage of reception  
in the 1800z time band.

Service ARGOS, SA   
 The Edmonton DRS EG   
 Gilmore Creek GC   
 Kauai KA

It is also evident that contrary to our expectations before making this study, direct readout stations in Hawaii or Alaska would add relatively few meteorological synoptic time reports to those that can be received at Edmonton from the proposed north-east Pacific buoy field. A station in Hawaii would extend the reception area far southward, and would give both better 0600Z coverage and backup reception to the Edmonton station. Similarly a station in Alaska would add the 0600Z reports missed by Edmonton from the North Pacific and also from the Arctic Ocean. Only with the addition of a third ARGOS satellite in a suitable orbital plane could full coverage of the Pacific Ocean be provided. Conversely, the loss of a satellite in the current NOAA 7 orbit would remove the 0000Z and 1200Z coverage of the northeast Pacific. This would greatly reduce the value of this type of buoy network as a means of filling in data-sparse areas, and negate its use in offsetting the well-known shortage of reports from voluntary vessels at 1200Z in this area.

## 5. REFERENCES

- di Cenzo, C.S., 1981; The Edmonton data collection platform processing and locating facility. ARGOS Workshop, San Francisco, October.
- Kerut, E.G., 1982; Drifting buoy studies for weather applications. ARGOS Users Conference, Annapolis, December 13-15.
- Service ARGOS, 1978; Users Guide - Satellite based data collection system, Toulouse, France.
- Vockeroth, R.E., H.T. Beale, and M. Stauder, 1983; Real time data networks using drifting buoys. Proceedings, AMS/CMOS 5th Symposium on Meteorological Observations and Instrumentation, Toronto, April 11-15.
- Vockeroth, R.E. and C.S. di Cenzo, 1982; Collecting meteorological reports with the ARGOS system. ARGOS Users Conference, Annapolis, December 13-15.



OPERATIONAL USES OF TIROS OCEANOGRAPHIC DRIFTERS BY THE INTERNATIONAL ICE PATROL  
(1978 - 1982)

Alan D. Summy  
Lieutenant Commander, USCG

Iain Anderson  
Lieutenant (jg), USCG

Commander, International Ice Patrol  
Governors Island  
New York, NY 10004

ABSTRACT

Since 1978, International Ice Patrol (IIP) has been using Tiros Oceanographic Drifters (TODs) to obtain real time sea current information in the areas of high iceberg activity south of 52°N. The TODs are air dropped from a USCG C-130 aircraft while on a routine ice reconnaissance flight. Aircraft deployment allows the TODs to be placed over a large region at a minimum of cost and time. The TODs were all equipped with window shade drouges tethered 10 meters below the surface, drouge tension sensors, sea surface temperature (SST) sensors, and battery voltage monitors. All sensor information and positions are collected by SERVICE ARGOS in Toulouse, France and relayed to the IIP via computer link. A series of programs were developed to compute total drift vectors from the TOD data. These vectors were converted into a "quasi-geostrophic" data base which could be used to modify the existing historical geostrophic currents in the IIP region either temporarily or permanently.

1. INTRODUCTION

The International Ice Patrol (IIP), a mission of the United States Coast Guard, is tasked by law and international treaty to observe and report on icebergs in the vicinity of the Grand Banks of Newfoundland. The purpose being to inform the entire maritime community of the extent of the iceberg danger region. The icebergs encountered in the North Atlantic originate primarily from the calving of glaciers along the west coast of Greenland. The Labrador Current carries the ice southward along the eastern edge of the Grand Banks, where it becomes a danger to ships transiting the North Atlantic Ocean (figure 1). The period of ice danger usually extends from March through July, with a yearly average of about 325 bergs drifting south of 48°N. During the period of ice danger, the IIP twice daily issues an ice bulletin indicating the southern and eastern limits of all known ice in the Grand Banks region. The bulletin contains predicted positions of the southern and eastern most icebergs.

Since the formal inception of the IIP (following the sinking of the RMS TITANIC) by the 1914

Safety of Life at Sea Conference (SOLAS), the methods used to accomplish its tasks have evolved with advances in technology. Visual reconnaissance has been the major source of information on iceberg location since World War II. IIP is presently evaluating a Side Looking Airborne Radar (SLAR) system for iceberg detection. The SLAR will allow IIP to make reconnaissance flights virtually regardless of the on-scene weather. Until the SLAR is proven, visual sightings will be used as the primary method of iceberg observations.

The persistence of fog in the Grand Banks region can prevent visual observations of ice for periods of more than two weeks. To fill in the gaps between visual observations, a method for predicting the drift of icebergs was needed. Since 1979, the IIP has been using a computer model to predict the drift of icebergs. (For details of the model see Mountain, 1980.) The forces included in the drift model are the Coriolis force, wind drag, water drag, and a gravitational component due to the sloping sea surface. Wave forces on icebergs are ignored. The two environmental forcing factors responsible for drifting the icebergs are the geostrophic and wind driven currents.

The wind driven current in four layers is calculated by solving a time dependent Ekman equation forced by the local wind history. The wind

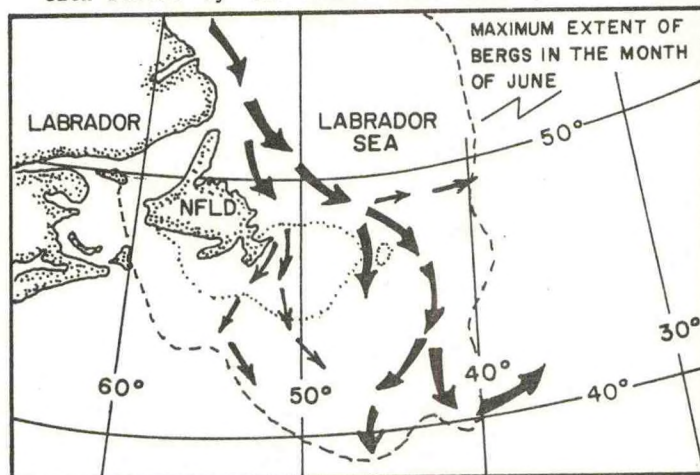


Figure 1

General paths of icebergs in the Grand Banks region.



field used as the forcing factors are received twice daily from Fleet Numerical Oceanographic Center (FNOC), Monterey, CA. The wind information is received in a 1° latitude by 2° longitude grid.

In 1978, an historical geostrophic current field for the IIP region of the North Atlantic was created by averaging all available standard hydrographic sections. Until recently, IIP has had no choice but to consider the current field static when, in reality, the region is somewhat dynamic. The field is stored in a 20' latitude by 20' longitude field except in the region of the Labrador Current where the field is 20' latitude by 10' longitude. A method was needed to modify this historical field both on a temporary and permanent basis. The cost and availability of ship time for a long term project is prohibitive. The solution chosen was the use of TIROS Oceanographic Drifters (TOD's). The TOD is classed as a La Grangian drifter; that is a buoy whose position is used to track the movement of a near surface water mass. The TOD is "coupled" to the water mass by a "window shade" drogue on a 10m tether (figure 2). The TOD's allow for the acquisition of real time geostrophic current information at a relatively reasonable cost.

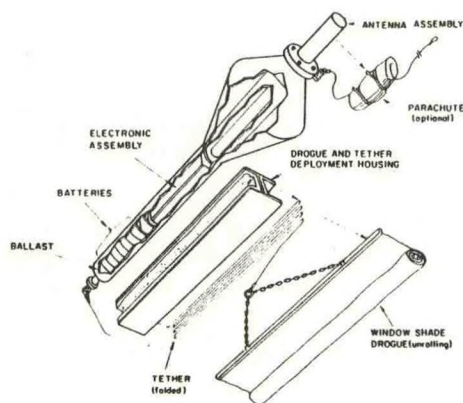


Figure 2

TIROS Oceanographic drifter (TOD)

## 2. DEPLOYMENT

Since 1978, IIP has deployed 27 TOD's in the Grand Banks region of the North Atlantic. The sites of TOD deployment are dependent upon the location of iceberg concentrations along the general paths of iceberg movements (figure 1). In experiments to test the IIP drift model, a TOD will be deployed next to a tagged iceberg. This will allow us to tune our model to reduce our error.

IIP has two methods of TOD deployment. TODs will be deployed occasionally from U. S. Coast Guard icebreakers transiting the region. The TOD is then deployed in a manner similar to a current meter string, except the TOD can be lowered into the water. The majority of the TODs deployed by IIP have been air dropped from a Coast Guard C-130 aircraft from an altitude of about 1000 feet. Only 1 of 27 TODs deployed in this manner have failed to deploy correctly.

## 3. DATA ACQUISITION AND OPERATIONAL USE

The TODs deployed by the IIP are all equipped with positioning packages, sea surface temperature (SST) sensors, battery voltage monitors, window shade drogues, and drogue tension monitors. All of the sensor information and positions are collected from the TIROS series satellites by SERVICE ARGOS in Toulouse, France. SERVICE ARGOS processes the position information and sends it and the coded sensor information to the National Earth Satellite Service where it can be picked up by U.S. users via a telephone-terminal link. The International Ice Patrol accesses this file daily to pick up all drifter positions which were received over the past 24 hours. During the last season we averaged approximately 10 positions per buoy per day. The positions are at random times so there is no set schedule that one can plan on for evenly spaced data.

A program was written to analyze this random (in time) data so that it could be evaluated at regular synoptic hours. The program takes in all of the buoy data and computes the sum of all times and distances entered. It then fits a cubic spline curve to the data. From this curve it can then interpolate values of position and velocity for each of the synoptic hours. What is returned by the program is a position (LAT, LONG) and velocity in U and V components. The next step in the program is to correct these computed velocity components for the effect of the wind generated current.

The IIP wind product is picked up from the FNOC computer by telephone link and recorded on magnetic tape. The wind information is then loaded into the PRIME 750 computer for access by the suite of ICEPLOT programs. After receiving the interpolated buoy velocities and positions the program calls subroutine EKWIND which computes the Ekman current for a given position from the information in the wind file. The below equations are used to compute the U and V Ekman components:

$$\text{STRESS} = \text{CDA} * \text{WINDSPD}^2 \quad (1)$$

where CDA = density of air x drag coefficient =  $1.875 \times 10^{-6}$

$$\begin{aligned} \text{EKU} &= \text{EKU} + \text{DEK} * \text{STRESS} * \text{SIN}(\text{WIND}) \\ \text{EKV} &= \text{EKV} + \text{DEK} * \text{STRESS} * \text{COS}(\text{WIND}) \end{aligned} \quad (2)$$

where DEK is a computed value of wind decay factor for EKMAN current at a given latitude and WIND is wind direction plus a rotation factor due to latitude. Decay and rotation factors are explained rigorously in Mooney's (1978) Technical Report.

The above solution of the EKMAN equations is based on a 96 hour wind history. The components (EKU, EKV) of the wind driven current are now subtracted from the U and V components that were calculated from the buoy drift data to create a "quasi-geostrophic" current.

$$\text{Corrected } U_{\text{comp}} = U_{\text{buoy}} - \text{EKU} \quad (3)$$

$$\text{Corrected } V_{\text{comp}} = V_{\text{buoy}} - \text{EKV} \quad (4)$$



The new values are then written onto a new file and saved for the ICEPLOT program.

The ICEPLOT program is the key to our operation. This program models the movement of icebergs by application of forces due to wind drag, water drag, Coriolis force, and a gravitational force due to the slope of the sea surface. The model was developed by Dr. M. D. Mountain of the U. S. Coast Guard Oceanographic Unit in 1978. IIP produces forecasts of iceberg locations in the North Atlantic and broadcasts this information twice daily. Since aerial reconnaissance is very weather dependent, the need for a prediction model is obvious.

The key to the ICEPLOT model is the solving of four equations simultaneously. The four equations which describe the drift of icebergs are:

$$\frac{dx}{dt} = U \quad (5)$$

$$\frac{dy}{dt} = V \quad (6)$$

$$\frac{dU}{dt} = fV - fV_g + \frac{\left[ \frac{1}{2} \rho_a C_{D_a} A_a W^2 \sin \phi + \sum_{i=1}^4 \frac{1}{2} \rho_w C_{D_w} A_i (E_i - U) S_i \right]}{M} \quad (7)$$

$$\frac{dV}{dt} = fU - fU_g + \frac{\left[ \frac{1}{2} \rho_a C_{D_a} A_a W^2 \cos \phi + \sum_{i=1}^4 \frac{1}{2} \rho_w C_{D_w} A_i (N_i - V) S_i \right]}{M} \quad (8)$$

As one can see in equations (7) and (8) the model is a four layer model so that by calculating water drag in layers we can allow different sizes of icebergs to be considered. Figure (3) shows a graphic illustration of how this is done.

#### WATER DRAG CALCULATION

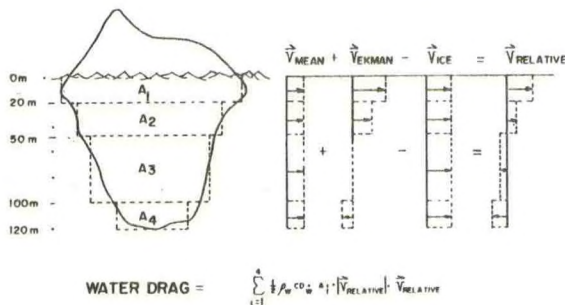


Figure 3

Method for calculating Water Drag in layers.

Where the buoy data comes in to play is to help us add a real time modifier to the terms  $U_g$  and  $V_g$  in equations (7) and (8). Up until last season the model used a historical current file with no input of real time data. Now the program analyzes those areas of the IIP region through which buoys have passed by fitting a two-dimensional least squares spline through the new current data and the historic data. The spline fit is based on an assignment of nodes to each historical data point. The area analyzed for evaluation is based on a nine node grid, i.e. one in each direction from that node chosen as center point. If there is no new data between two nodes, there will be no residuals and thus the historic current structure in that area would be preserved. However, if new data did exist then a weighted average process is completed and a new velocity vector is used for that area.

The weighted average works as shown below in equation (9).

$$\text{Modified } V_{\text{comp}} = \frac{\text{corrected } V_{\text{comp}}(wf) + \text{Historical } V_{\text{comp}}}{2} \quad (9)$$

where (wf) = weight factor which can range from 0 to 999.

The modified currents are then used to compute the iceberg drift trajectory. If over the next week no new buoy data is received for the effected area then a relaxation takes place that will relax the value for speed and direction back half way to the original historic value and all the way back at the end of a second week with no new modification data.

It should be noted at this point that there are several restrictions to this program:

- 100 input positions per buoy is maximum number that program will handle;
- 100 days is maximum time span for any one buoy;
- all positions must be entered in order of increasing time.

The other use made of data obtained from the drifting buoys is the comparison of FNOC's SST product with the temperature we receive from the Sea Surface Temperature Sensor on each buoy. Although only having a point valve, the temperature from the buoy gives us a real time value that can be used to compare the SST values produced by FNOC for that buoys particular region. As summer comes on these temperatures also allow us to see when the buoy has become entrained in a warm or cold eddy or moved into or across the Labrador current. During such an occurrence one may see a temperature change of up to ten degrees over a 24 hour period.

Starting this season SST has become even more important as it is now being input into an iceberg



deterioration model. If the model proves itself it will be moved into the ICEPLOT routines and become an integral part of the overall model.

#### 4. COLLECTED TOD DATA USE

The general paths icebergs take on their journey from the Labrador Sea to their eventual destruction in the warm waters of the Gulf Stream do not change. Therefore several of the 27 TODs deployed by IIP along these paths have travelled through the same geographical region. With several TODs travelling through the same region, it is possible to evaluate, and modify if necessary, the historical geostrophic currents of that region.

The criteria selected for making permanent changes to the historical geostrophic current field were: (1) a minimum of five TOD tracks passing through the same  $1^\circ$  latitude by  $1^\circ$  longitude rectangle; and (2) the speed and direction of the TOD's through each rectangle selected must have been reasonably similar. The time of year of the TODs passage was not a factor since the current field used by IIP is independent of time. We feel this selection method should eliminate those differences caused solely by eddies or other short term ocean features.

The validity of certain regions of the IIP historical current field have come under suspicion from the differences between computer predicted iceberg positions and those of actual sightings. The most prevalent area in which this occurred was north of the Flemish Cap. Three  $1^\circ$  latitude by  $1^\circ$  longitude rectangles met the criteria described above for consideration for making permanent changes to the current field.

The three rectangles selected were between  $48^\circ$  and  $49^\circ$  north and  $46^\circ$  and  $49^\circ$  west (figure 4). TODs from 4 different years passed through this area and are included in figure 4. We made some fairly drastic changes to the current file, changing some directions by  $180^\circ$  and/or increasing velocities by up to one order of magnitude. Some of the examples of the changes made are shown in Table 1. The above changes were made in January 1983. This iceberg season should give us a chance to evaluate the changes we've made. We will be also conducting a hydrographic cruise this June that will include the area where changes to the current file were made. This will be used as an added check to the above method of changing the historical current field.

The TOD tracks that we have collected are also useful in determining general circulation patterns in the IIP region. The general tracks of the TODs, and hence the icebergs, in the IIP region appear to be topographically steered (Shuhay 1981). The collected data suggests that objects being drifted south by the Labrador Current will follow one of three paths as they near the Flemish Cap area. If the object is outside of the 2000 meter contour then it will likely be spun off to the east and then to the northeast as it passes north of the Flemish Cap. From here it will enter the eastward flowing North Atlantic drift removing the object

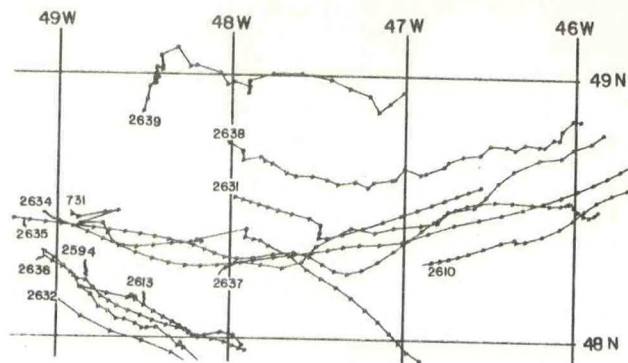


Figure 4

All TOD tracks through the area where the historical current field was modified permanently.

from the IIP area. If the object is between the 200 and 500 meter contours then it will most likely continue south through the pass between the Grand Banks and the Flemish Cap in the main stream of the current. If the object is between the 1000 and 2000 meter contours, it will most likely be swung off too the northeast and then pass south around the Cap (figure 5). These findings are consistent with the flow pattern described by Petrie and Anderson (1983). The placements of this years TODs was designed to further test this observation.

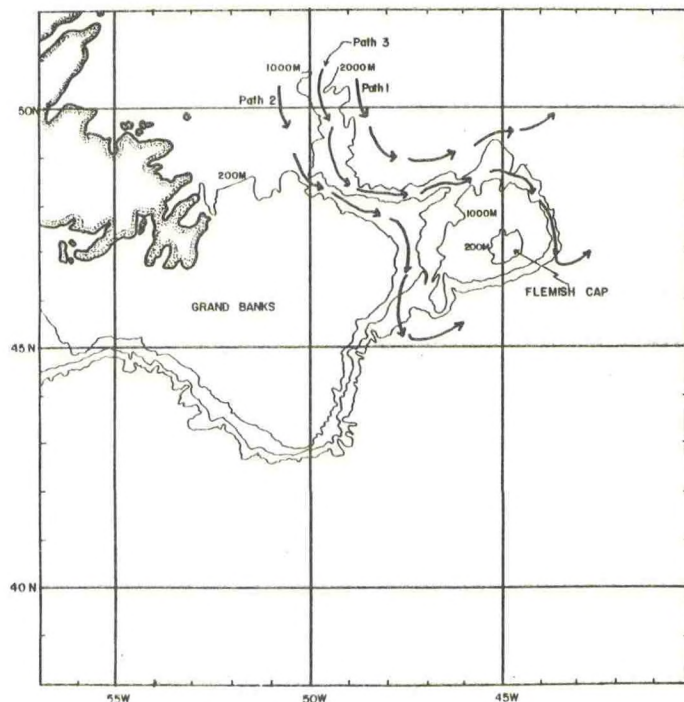


Figure 5

General bathymetrically guided paths of drifting objects around the Grand Banks region.



## 5. SUMMARY

We have found that the TODs provide us accurate information and much timelier measurements at a reduced cost compared to shipborne hydrographic surveys. Deployment by aircraft allows TODs to be deployed, and hence information gathered, in a rapid manner. With the increase in satellite technology, we hope to be able to improve the accuracy of our model by adding more real time environmental information.

## 6. ACKNOWLEDGEMENTS

We would like to thank Michael Lee for his assistance in drawing the figures and Steven Cooper for typing this paper. Our thanks to Commander, International Ice Patrol for making this paper possible.

## 7. REFERENCES

Mountain, R. G. (1980) "On Predicting Iceberg Drift", U. S. Coast Guard Oceanographic Unit, Cold Regions Science and Technology, Vol 1, pp 273-282.

Mooney, K. A. (1978) "A Method for Manually Calculating the Local Wind Current", U. S. Coast Guard Oceanographic Unit Technical Report 78-2.

Shuhy, J. L. (1981) "Oceanographic Conditions on the Grand Banks During the 1981 International Ice Patrol Season", Report of the International Ice Patrol Service in the North Atlantic Ocean, Season of 1981, Coast Guard 188-36, Bulletin No. 36 (unpublished as of this date).



# KINEMATIC AND DYNAMICAL CALCULATIONS FROM LAGRANGIAN MEASUREMENTS: RECENT THEORETICAL ADVANCES

James K. Lewis

A. D. Kirwan

R. E. Whitaker

Science Applications, Inc.  
4348 Carter Creek Parkway  
Bryan, Texas 77801

University of South Florida  
Department of Marine Science  
St. Petersburg, Florida 33701

Science Applications, Inc.  
4348 Carter Creek Parkway  
Bryan, Texas 77801

## ABSTRACT

Analytical solutions are presented for model equations from which vorticity  $\zeta$ , divergence  $D$ , normal deformation rate  $N$ , and shear deformation rate  $S$  are calculated from drifting buoy data. The solutions show that methods previously used in calculating these differential kinematic parameters (DKP) were incorrect. Also, the time interval  $t$  between buoy position fixes must be  $\leq 6$  h for typical oceanic conditions and  $\leq 24$  h for pack ice. For time intervals  $> t$ , the equations for calculating the DKP become non-linear.

Interpretations of the DKP are reviewed and two techniques for dynamical analyses are presented. The use of a vorticity equation is seen to require  $\zeta$ ,  $D$ , the curl of the wind stress, and the vertical thickness  $H$  of the medium marked by a cluster of buoys. Analytical solutions to the equations of motion also require  $H$  and give buoy motion as the sum of time-damped inertial oscillations.

## 1. INTRODUCTION

Any movement may be broken down into the five basic motions of translations, rotation  $\zeta$  (vorticity), divergence  $D$ , normal deformation rate  $N$ , and shear deformation rate  $S$ . These last four differential kinematic parameters (DKP) are important since they describe relative motion within a given material. By tracking transponders in water, on ice, or in sediments, one may determine the kinematic characteristics of the region in question. This information may then be used in monitoring real-time conditions, studying dynamics, developing predictive models, and establishing design specifications (e.g. for structures on ice or in unconsolidated sediments).

Drifters clustered in small regions of the ocean have been used to infer characteristics of horizontal shears. A model frequently used for this purpose was developed by Molinari and Kirwan (6) and Okubo and Ebbesmeyer (8). The model is of the "local" variety. In essence, it is a Taylor's expansion for the velocity of the  $i^{\text{th}}$  drifter in the cluster relative to some moving origin:

$$u_i = [(D+N)x_i]/2 + [(S-\zeta)y_i]/2 + f_i \quad (1)$$

$i=1, \dots, n.$

$$v_i = [(S+\zeta)x_i]/2 + [(D-N)y_i]/2 + g_i$$

Here the coordinates of drifter  $i$  with respect to the origin are  $x_i$  and  $y_i$ , and  $f_i$  and  $g_i$  represent the sum of the higher order non-linear terms in the expansion as well as random turbulent motion. From the statistical standpoint,  $f_i$  and  $g_i$  represent random deviations from the model. In an absolute frame, the cluster is being translated at the absolute velocity of the origin.

In (1), the velocity gradients across the parcel have been expressed in terms of the DKP:

$$D = \partial u / \partial x + \partial v / \partial y \quad (\text{divergence})$$

$$\zeta = \partial v / \partial x - \partial u / \partial y \quad (\text{vorticity})$$

$$S = \partial v / \partial x + \partial u / \partial y \quad (\text{shearing deformation rate})$$

$$N = \partial u / \partial x - \partial v / \partial y \quad (\text{normal or stretching deformation rate}).$$

## 2. SOLUTION TECHNIQUES

Previous studies have estimated the DKP by determining the  $u_i$ ,  $v_i$ ,  $x_i$ , and  $y_i$  from absolute position data and then employing least squares (6, 8, 5). These procedures assumed that the independent variables in the least squares equations (drifter velocities and positions) were determined independently. This assumption is never true, but the analysis presented in this paper provides a means of overcoming this short-coming by making explicit use of appropriate solutions to (1). To this end, note that equations (1) are coupled, first order differential equations for the present position of the  $i^{\text{th}}$  drifter. The forms of the analytical solutions for these equations are crucially dependent on the frequency parameter

$$\gamma^2 = N^2 + S^2 - \zeta^2. \quad (2)$$

There are three classes of solutions depending on different values of  $\gamma^2$  (see 7 for a discussion). All three can be expressed in the form



$$x_i(t) = X_i H(t) + Y_i J(t) (S-\zeta)/\gamma + ((S-\zeta)/\gamma) \cdot \int_0^t g_i(t-\beta) J(\beta) d\beta + \int_0^t f(t-\beta) H(\beta) d\beta \quad (3)$$

$$y_i(t) = X_i J(t) (S+\zeta)/\gamma + Y_i K(t) + ((S+\zeta)/\gamma) \cdot \int_0^t f_i(t-\beta) J(\beta) d\beta + \int_0^t g_i(t-\beta) K(\beta) d\beta.$$

The  $X_i$  and  $Y_i$  are the coordinates of the  $i^{\text{th}}$  drifter at time  $t = 0$  relative to the local origin at that time.

The forms for the  $H$ ,  $J$ , and  $K$  functions depend upon  $\gamma^2$  (Table 1). When the sum of squares of the shear and normal distortion exceed the squared vorticity ( $\gamma^2 > 0$ ), then the drifter displacements will increase exponentially with time (for  $D=0$ ).

For  $\gamma^2 = 0$ , the solution predicts that the drifter displacements will grow linearly with time (aside from the divergence term). Finally, for  $\gamma^2 < 0$ , the solution shows that the drifter trajectories (relative to the origin) form ellipses (for  $D=0$ ).

It should be noted that, for appropriately short times (i.e.  $Dt/2$  and  $\gamma t/2 \ll 1$ ) and constant  $f_i$ 's and  $g_i$ 's, all cases reduce to the approximate linear form:

$$x_i = X_i + t [X_i (D+N)/2 + Y_i (S-\zeta)/2 + f_i] \quad (4)$$

$$y_i = Y_i + t [X_i (S+\zeta)/2 + Y_i (D-N)/2 + g_i].$$

This equation says that the present position relative to the moving origin is obtained by adding to the previous relative position the displacements due to the random velocity and to the velocity induced by the average rotation, divergence, and distortion of the cluster during the time interval. We may rewrite the first equation in (4) as

$$\frac{x_{t_1} - x_{t_0}}{t} = \left[ \frac{D+N}{2} \right] x_{t_0} + \left[ \frac{S-\zeta}{2} \right] y_{t_0} + f_i \quad (5)$$

where  $t = t_1 - t_0$ ,  $(x_{t_0}, y_{t_0}) = (X, Y)$  for the  $i^{\text{th}}$  drifter, and  $(x_{t_1}, y_{t_1}) = (x, y)$  for the  $j^{\text{th}}$  drifter.

The form of (5) typically used in previous studies

$\gamma^2$	$H(t)$	$J(t)$	$K(t)$
$> 0$	$e^{Dt/2} (\cosh \gamma t/2 + (N/\gamma) \sinh \gamma t/2)$	$e^{Dt/2} \sinh \gamma t/2$	$e^{Dt/2} (\cosh \gamma t/2 - (N/\gamma) \sinh \gamma t/2)$
$= 0$	$e^{Dt/2} (1 + N t/2)$	$(t e^{Dt})/2$	$e^{Dt/2} (1 - N t/2)$
$< 0$	$e^{Dt/2} (\cos \gamma t/2 + (N/\gamma) \sin \gamma t/2)$	$e^{Dt/2} \sin \gamma t/2$	$e^{Dt/2} (\cos \gamma t/2 - (N/\gamma) \sin \gamma t/2)$

Table 1 Definitions of the  $H$ ,  $J$ , and  $K$  functions. Here  $\gamma$  represents the magnitude of  $[N^2 + S^2 - \zeta^2]^{1/2}$ .

was

$$\frac{x_{t_2} - x_{t_0}}{2t} = \left[ \frac{D+N}{2} \right] x_{t_1} + \left[ \frac{S-\zeta}{2} \right] y_{t_1} + f_i \quad (6)$$

where the DKP values were those at time  $t_1$  and the left hand side of (6) was an estimate of the relative  $u$  speed at time  $t_1$ , with  $t_2 = 2(t_1 - t_0)$  (5). Thus, the analytical solutions show that the previous solution techniques did not employ the correct forms of the Taylor's expansions.

These analytical solutions provide information concerning three important factors:

a) The solutions give us a system of equations in which the only independent variables are position and random velocity. This eliminates the problem of having two independent variables (position and velocity) that are not determined independently.

b) The solutions give the correct form of the Taylor's expansion to calculate the DKP. This form is quite convenient in that it does not require position fixes at a constant time interval.

c) The solutions show that the equations in (4) can be used only for time intervals  $t$  between position fixes such that

$$Dt/2 \text{ and } \gamma t/2 \ll 1.$$

For typical values of oceanic DKP, the above restriction implies a time interval of  $t \leq 6$  h while on ice one must have  $t \leq 24$  h.

The last factor is important in that, if  $t$  is not small enough, the versions of (4) become nonlinear, (see Table 1). To solve for the DKP in this case requires iterative techniques.

### 3. DKP INTERPRETATION AND APPLICATION

Kirwan (3) has provided physical interpretations of the DKP:

- $\zeta$  - the change in the orientation of a cluster (without a shape or size change),
- $D$  - the change in the size of a cluster (without an orientation or shape change),
- $N$  - the change in the shape of a cluster due to forces acting normal to the sides of the cluster (without a size or orientation change), and
- $S$  - the change in the shape of a cluster due to forces acting parallel to the sides of the cluster (without a size or orientation change).



A simplified physical picture given by the model equations is that an individual drifter's velocity is composed of a mean translatory velocity of the cluster, plus a velocity induced by the rotation, divergence, and distortion of the cluster, plus a random or turbulent velocity. The mean cluster velocity is attributed to large-scale (relative to cluster size) motions, the induced velocity to cluster-scale motions, and the random component to the small-scale turbulent field. The scale of these latter motions is assumed to be much less than of the cluster.

The physical processes represented by the time histories of  $\zeta$  and  $D$  may be used to study dynamics through the use of the vorticity equation obtained from the curl of the equations of motion for a parcel of thickness  $H$  and density  $\rho$ :

$$\dot{\vec{U}} + f \vec{k} \times \vec{U} = -g \nabla \eta + (\vec{\tau}_S - \vec{\tau}_B + \nabla \vec{\tau}_I) / (H\rho) \quad (7)$$

where

$\vec{U}$  is velocity in the horizontal plane,

$\dot{\vec{U}}$  is material time rate of change of  $\vec{U}$ ,

$\vec{\tau}_S$  is stress exerted by the atmosphere on the upper surface of the parcel,

$\vec{\tau}_B$  is stress exerted on the lower surface of the parcel,

$f$  is the Coriolis parameter,

$g$  is acceleration due to gravity,

$\eta$  is the horizontal surface anomaly,

$\vec{k}$  is the unit vector in the vertical direction, and

$\vec{\tau}_I$  is the internal horizontal stress vector.

The curl of (7) gives

$$(\zeta + f) + (\zeta + f) D = \text{curl}_Z (\vec{\tau}_S - \vec{\tau}_B + \nabla \vec{\tau}_I) / (H\rho). \quad (8)$$

The time histories of buoy positions,  $\zeta$ , and  $D$  allow us to calculate the LHS of (8) as a function of time. We see that the thickness  $H$  over which  $\zeta$  and  $D$  are representative must be known if we are to determine components of the RHS of (8). If one can estimate  $H$  and calculate curl

$\vec{\tau}_S$  using information such as wind data, then all the terms in (8) may be calculated as a function of time by assuming

$$\vec{\tau}_B = KR\vec{U}. \quad (9)$$

In (9),  $K$  is a linear drag coefficient and  $R$  is one minus the ratio of  $|\vec{U}|$  to the speed of the material under the parcel. In this case, (8) may be rewritten as

$$H\rho [(\zeta + f) + (\zeta + f)D] - \text{curl}_Z \vec{\tau}_S + KR\zeta = \text{curl}_Z (\nabla \vec{\tau}_I). \quad (10)$$

Thus, all the terms on the LHS of (10) can be calculated and the effect of the internal horizontal stress may be determined as a residual. In this way, one may study parcel motion dynamically using the time variations in the balance of vorticity.

Another method of using the DKP is studying dynamics involves analytical solutions to (7) in which we assume  $\nabla \vec{\tau}_I = 0$  and  $\vec{\tau}_B = KR\vec{U}$ . The solutions to (7) with these assumptions are

$$\begin{aligned} U_{x,t} &= e^{-\Gamma t} [U_{x,0} \cos ft + U_{y,0} \sin ft] \\ &+ \int_0^t e^{-\Gamma \gamma} [\tau_{s,x} \Big|_{t-\gamma} \cos f\gamma \\ &+ \tau_{s,y} \Big|_{t-\gamma} \sin f\gamma] d\gamma / (H\rho) \\ U_{y,t} &= e^{-\Gamma t} [U_{y,0} \cos ft - U_{x,0} \sin ft] \\ &+ \int_0^t e^{-\Gamma \gamma} [\tau_{s,y} \Big|_{t-\gamma} \cos f\gamma \\ &- \tau_{s,x} \Big|_{t-\gamma} \sin f\gamma] d\gamma / (H\rho) \end{aligned} \quad (11)$$

where  $\vec{U}_0$  is the velocity of the parcel at  $t=0$  and  $\Gamma = KR/(H\rho)$ .

Assuming that  $R > 0$ , the physical interpretation of (11) is that the net translation of the parcel is the sum of time-damped inertial oscillations. Because of the Coriolis effect, both direction components of the parcel over any time period are influenced by both components of  $\vec{\tau}_S$ . However, the drag of the material against the bottom of the parcel reduces the influence of any instantaneous  $\vec{\tau}_S$  as time passes. In order to carry out correlation studies between  $\vec{\tau}_S$  and  $\vec{U}$ , the relationship in (11) indicate that  $\vec{\tau}_S$  and  $\vec{U}$  must be well defined over the inertial period in order to carry out the time integration process.

We may wish to simplify (11) by estimating the time  $t$  required such that  $e^{-\Gamma t} = 0.1$ . For  $t$ 's of this value or larger, the damping term reduces the contributions of the various kinematics to  $\leq 10\%$  of their original values. Using a ratio parameter of  $R = 0.5$  and various values for the drag coefficient (2,4), we find that a maximum value for  $t$  is approximately 11 hours. Thus, by having  $\sim 12$  hrs of surface stress data, the theoretical relationships between the parcel kinematics and the forcing functions may be estimated by

$$\begin{aligned} U_{x,t} &\doteq \int_0^{12 \text{ hrs}} e^{-\Gamma t} [\tau_{s,x} \Big|_{t-\gamma} \cos f\gamma \\ &+ \tau_{s,y} \Big|_{t-\gamma} \sin f\gamma] d\gamma / (H\rho) \\ U_{y,t} &\doteq \int_0^{12 \text{ hrs}} e^{-\Gamma t} [\tau_{s,y} \Big|_{t-\gamma} \cos f\gamma \\ &- \tau_{s,x} \Big|_{t-\gamma} \sin f\gamma] d\gamma / (H\rho). \end{aligned} \quad (12)$$

Thus, if  $H$  is known and  $\nabla \vec{\tau}_I = 0$ , one may predict the translation of a parcel using forecasted surface stresses,  $\vec{\tau}_S$ . If  $H$  is known but  $\nabla \vec{\tau}_I \neq 0$ , we may study the time-integrated effects of  $\nabla \vec{\tau}_I$  by



subtracting the parcel velocity predicted by (12) from the parcel velocity as determined by buoys.

For the case in which  $H$  is unknown and  $\vec{v}_{T_I} = 0$ , we may divide  $\vec{U} \cdot H$  as calculated using surface stresses in (12) by the parcel velocity as determined by buoys in order to estimate the parcel depth  $H$ .

We may use (12) to calculate the DKP induced by surface stress for conditions such that  $\vec{v}_{T_I} = 0$ :

$$\begin{aligned} D &= \int_0^{12 \text{ hrs}} e^{-I\gamma} \left[ \vec{v}_{T_S} \Big|_{t-\gamma} \cos f_\gamma \right. \\ &\quad \left. + \text{curl}_z \vec{\tau}_S \Big|_{t-\gamma} \sin f_\gamma \right] d\gamma / (H\rho) \\ \zeta &= \int_0^{12 \text{ hrs}} e^{-I\gamma} \left[ \text{curl}_z \vec{\tau}_S \Big|_{t-\gamma} \cos f_\gamma \right. \\ &\quad \left. - \vec{v}_{T_S} \Big|_{t-\gamma} \sin f_\gamma \right] d\gamma / (H\rho) \\ N &= \int_0^{12 \text{ hrs}} e^{-I\gamma} \left[ N_w \Big|_{t-\gamma} \cos f_\gamma \right. \\ &\quad \left. + S_w \Big|_{t-\gamma} \sin f_\gamma \right] d\gamma / (H\rho) \\ S &= \int_0^{12 \text{ hrs}} e^{-I\gamma} \left[ S_w \Big|_{t-\gamma} \cos f_\gamma \right. \\ &\quad \left. - N_w \Big|_{t-\gamma} \sin f_\gamma \right] d\gamma / (H\rho) \end{aligned} \quad (13)$$

where the normal and shear deformation rates of the surface stress are represented by  $N_w$  and  $S_w$ ,

respectively. We see that the Coriolis effect results in the DKP being a function of two differential motion parameters of the wind stress.

Once again, for instances such that  $\vec{v}_{T_I} \neq 0$ , the difference between the predicted DKP and the DKP determined from buoys is the time-integrated effect of  $\vec{v}_{T_I}$ .

#### 4. SUMMARY

Theoretical analyses are presented which lead to greater insights into the calculation, interpretation, and application of the differential motion of drifting buoys. The DKP can be calculated using the linear equations in (4) only when the time interval  $t$  between successive position fixes is such that  $t \ll 2/D$  and  $t \ll 2/\gamma$ . This restriction for typical oceanic DKP gives  $t \leq 6$  h. Typical ice DKP gives  $t \leq 24$  h. However, smaller time intervals may be required to study the correlations between the kinematics of a parcel and the surface stresses on the parcel [see equations (12) and (13)]. This is a result of the Coriolis effect.

Drifting buoy data may be used to study dynamics using either the vorticity equation (10) or the analytical solutions to the equations of motion given in (12) and (13). The vorticity equation requires an estimate of the depth  $H$  over which the calculated vorticity and divergence are representative. This depth, along with the curl of the surface stress, allows one to calculate the effect of the internal horizontal stresses  $\vec{v}_{T_I}$  as

a residual. The analytical solutions to the equations of motion may also be used to calculate the effect of the internal horizontal stresses as a residual. Moreover, the individual relationships for the DKP given in (13) allows one to determine to what degree  $\vec{v}_{T_I}$  affects each of the DKP. If it is ascertained that  $\vec{v}_{T_I}$  has little effect on a particular parameter then buoy and wind data may be used in the parameter expression in (13) to solve for the representative depth,  $H$ .

#### ACKNOWLEDGEMENT

This research was sponsored by the Bureau of Land Management under contract No. NA-81-QA-C-148 and contracted under Dr. Glenn Hamilton of the NOAA Data Buoy Center.

#### REFERENCES

- Defant, A., *Physical Oceanography*, Vol. 1, Pergamon Press, Oxford, 1961, 729 pp.
- Heaps, N. S., Development of a three-dimensional numerical model of the Irish Sea. Rapp. P. -V. Réun. Cons. int. Explor. Mer, 167, 1964, 147-162.
- Kirwan, A. D., "Oceanic velocity gradient." J. Phys. Oceanogr., 5.4, 1975, 729-735.
- Langleben, M. P., Water drag coefficient at AIDJEX station Caribou. In *Sea Ice Processes and Models* (R. S. Pritchard, ed.), Univ. of Wash. Press, Seattle, 1980, 464-471.
- Lewis, J. K. and A. D. Kirwan, "Analysis of horizontal shear data." Final Report, NRL, contract N00014-81-C-2103, 1981, 63 pp.
- Molinari, R., and A. D. Kirwan, "Calculation of differential kinematic properties of the Yucatan Current from Lagrangian observations." J. Phys. Oceanogr., 5, 1975, 483-491.
- Okubo, A., "Dispersion of floatable particles in the vicinity of velocity singularities such as convergences." Deep Sea Res., 17, 1970, 445-454.
- Okubo, A., and C. C. Ebbesmeyer, "Determination of vorticity, divergence, and deformation rates from analysis of drogue observations." Deep Sea Res., 23, 1976, 349-352.



# THE COMPUTATION OF KINEMATIC PARAMETERS FOR A WARM CORE RING USING DRIFTING BUOYS

R. E. Whitaker

A. D. Kirwan

J. K. Lewis

Science Applications, Inc.  
4348 Carter Creek Parkway  
Bryan, Texas 77801

University of South Florida  
Department of Marine Science  
St. Petersburg, Fla. 33701

Science Applications, Inc.  
4348 Carter Creek Parkway  
Bryan, Texas 77801

## ABSTRACT

A technique is presented for computing the vorticity  $\zeta$ , divergence  $D$ , normal deformation rate  $N$ , and shear deformation rate  $S$  for drifters in a warm core ring. This technique is based on analytical solutions to the model equations for these differential kinematic parameters (DKP) in which vorticity dominates ( $\zeta^2 > N^2 + S^2$ ). A formulation is derived in which the center of expansion is the center of the ring rather than the centroid of a set of drifters. It is assumed that the drifter velocities and DKP are relatively constant during one period of rotation. The calculations give the interesting result that the ring DKP may be determined using only one drifter. It is shown that extrema from the drifter velocity records give the required number of variables to calculate the DKP. In addition, estimates of the velocity of the center of the ring can also be made.

## 1. INTRODUCTION

On 19 November 1980, the NOAA Buoy Office (NDBO) deployed three experimental buoys in the Gulf of Mexico. The purpose of the deployment was to determine the buoy's operational effectiveness for gathering near real-time meteorological and oceanographic data from data-sparse regions. A summary of the analysis of the engineering data is given in (1). In this paper, the buoy will frequently be referred to as a drifter.

The three drifters were deployed in a warm core ring which had been shed by the Loop Current. The drifters were deployed at approximately 24° 30'N and 92°W. All three drifters stayed in this feature through 17 April 1981. Since the drifters tracked the ring for such a long period, their trajectories contain considerable information on the existing currents and horizontal velocity gradients. These features are important considerations in the design for buoy array dispersion measurements in the open ocean for climate-related programs.

In this paper, we document the method developed to calculate the ring's vorticity  $\zeta$ , divergence  $D$ , normal deformation rate  $N$ , and shear deformation rate  $S$ . The basis of the model from which these differential kinematic parameters (DKP) were

calculated is given in (2). However, this basis can be derived from more general variational formulations for geophysical fluid dynamics (3,4).

## 2. FORMULATION

The velocity  $\vec{v}$  (components  $\tilde{u}$  and  $\tilde{v}$ ) for a buoy in a ring can be partitioned into two parts: a ring translation velocity  $\vec{U}$  and a rotational or swirl velocity  $\vec{u}$ . In component form

$$\tilde{u} = U + u \quad (1)$$

$$\tilde{v} = V + v.$$

Theoretical work (see 2) has shown that the relative trajectory of a parcel around a rotationally-dominated feature (i.e.  $\zeta^2 > N^2 + S^2$ ) is given by

$$\begin{aligned} x &= \{X [\cos \gamma t/2 + (N/\gamma) \sin \gamma t/2] \\ &\quad + Y ((S-\zeta)/\gamma) \sin \gamma t/2\} \cdot e^{Dt/2} \\ y &= \{X((S+\zeta)/\gamma) \sin \gamma t/2 + Y [\cos \gamma t/2 \\ &\quad - (N/\gamma) \sin \gamma t/2]\} \cdot e^{Dt/2} \end{aligned} \quad (2)$$

where  $(X, Y)$  is the position of the parcel relative to the ring center at time  $t = 0$ . Thus, the swirl velocity is obtained by differentiating (2) and writing the results in the form of

$$\begin{aligned} u &= A e^{Dt/2} \cos (P + \Gamma) \\ v &= B e^{Dt/2} \sin (P - \Gamma) \end{aligned} \quad (3)$$

where

$$A = A_x (\gamma/2)$$

$$B = B_y (\gamma/2)$$

$$P = \gamma t/2 + M + \pi/2$$

$$M = \frac{1}{2} \left\{ \tan^{-1} \left[ \frac{-(XN+Y(S-\zeta))}{\gamma X} \right] + \tan^{-1} \left[ \frac{Y_Y}{(X(S+\zeta)-YN)} \right] \right\}$$

$$\Gamma = \frac{1}{2} \left\{ \tan^{-1} \left[ \frac{-(XN+Y(S-\zeta))}{\gamma X} \right] - \tan^{-1} \left[ \frac{Y_Y}{(X(S+\zeta)-YN)} \right] \right\}$$

where  $A_x$  and  $B_y$  are the amplitudes of the velocity fluctuation. Equation (3) demonstrates clearly that the motion is periodic with amplitudes which increase or decrease exponentially in time depending upon whether there is horizontal convergence ( $D < 0$ ) or divergence ( $D > 0$ ). The period of the



motion is

$$T = 4\pi/\gamma \quad (4)$$

and there is a phase shift between the x and y components of  $2\Gamma + \pi/2$  radians.

### 3. RELATIONSHIP BETWEEN THEORY AND OBSERVATIONS

The quantities in the theory that are observed by drifting buoys are  $\hat{u}$  and  $\hat{v}$ . From these observations, we wish to calculate the DKP and ring translation velocities  $U$  and  $V$ . These 6 quantities can be calculated from values of each of the absolute velocities at three critical points, which are three successive extrema, and are indicated in Fig. 1.

There are three stages to the calculation given the six critical values of the absolute velocity. The first stage is to note  $\gamma/2$  and  $\Gamma$  along with the values of the absolute velocities. The  $\gamma/2$  quantity is readily determined by fixing the time between successive extreme for each component (there are separate  $\gamma/2$ 's for the  $\hat{u}$  and  $\hat{v}$

records). Then we use

$$\gamma/2 = \pi(1/(t_1 - t_0) + 1/(t_2 - t_1))/2$$

where  $t_i$  are the times of successive extrema.

The calculation of  $\Gamma$  is slightly more complicated. The following sequence has been developed from the theoretical expressions for the swirl velocity for an anticyclonic ring:

- For a  $\hat{u}_{\max}$  followed by a  $\hat{v}_{\min}$  or a  $\hat{u}_{\min}$  followed by a  $\hat{v}_{\max}$ ,  

$$2\Gamma = \pi/2 - (t_u - t_v) \gamma/2$$
- For a  $\hat{v}_{\min}$  followed by a  $\hat{u}_{\min}$  or a  $\hat{v}_{\max}$  followed by a  $\hat{u}_{\max}$ ,  

$$2\Gamma = -\pi/2 - (t_u - t_v) \gamma/2.$$

Note that for purely circular motion,  $2\Gamma = -\pi/2$ .

The second stage is the calculation of the swirl velocity amplitudes from (1) and (3), respectively. From the swirl velocities, it is possible to calculate the DKP from  $A$ ,  $B$  and  $\Gamma$ .

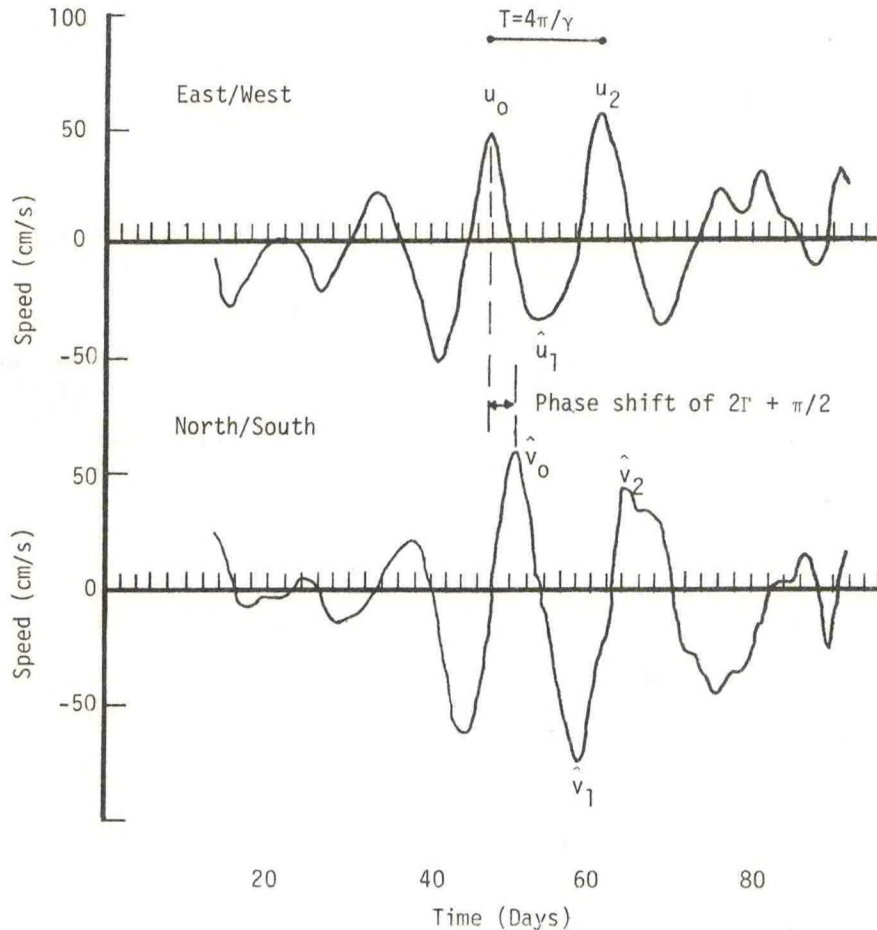


Fig. 1. The time histories of the absolute velocity components of a drifter in a Gulf of Mexico ring.



The procedure requires an iterative solution technique outlined in Fig. 2. The example is for the x (east/west) velocity component which has a starting time ( $t_0$ ) at a local maximum of the absolute velocity. The times when the x velocity is at the following minimum and maximum is  $t_1$  and  $t_2$ , respectively. The velocities at  $t_0$ ,  $t_1$ , and  $t_2$  are denoted by  $\hat{u}_0$ ,  $\hat{u}_1$ , and  $\hat{u}_2$ , respectively. Extension of this method to subsequent times and the y (north/south) velocity component is straight-forward.

From (1) and (3), the values of the absolute velocity at the critical times are

$$\hat{u}_0 = U + A \quad (5)$$

$$\hat{u}_1 = U - A e^{Dt_1/2} \quad (6)$$

$$\hat{u}_2 = U + A e^{Dt_2/2} \quad (7)$$

Eliminating D between (6) and (7) yields

$$\ln[(U - \hat{u}_1)/A] = (t_1/t_2) \ln[(\hat{u}_2 - U)A].$$

Solving for A gives

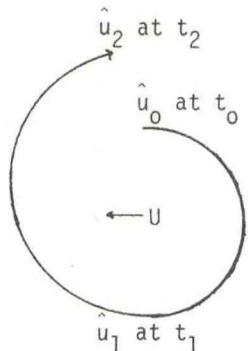
$$A = [(U - \hat{u}_1)^{t_2}/(\hat{u}_2 - U)^{t_1}]^{1/(t_2 - t_1)}. \quad (8)$$

By inserting (8) into (5), one obtains

$$U = \hat{u}_0 - [(U - \hat{u}_1)^{t_2}/(\hat{u}_2 - U)^{t_1}]^{1/(t_2 - t_1)}. \quad (9)$$

This last equation may be solved by iteration. Relaxation techniques result in the following iterative expression:

$$U_n = U_{n-1} + R \left[ \frac{\hat{u}_0 - [(U_{n-1} - \hat{u}_1)^{t_2}/(\hat{u}_2 - U_{n-1})^{t_1}]^{1/(t_2 - t_1)}}{(\hat{u}_2 - U_{n-1})^{t_1}} \right] \quad (10)$$



where the initial value of  $u$  is zero and the relaxation constant  $R$  is varied between 0.2 and 0.8 in order to produce convergence.

Once  $U$  is determined, (8) is used to calculate the swirl velocity magnitude  $A$ . Finally, the value for  $D$  is given by solving (6) or (7) for  $D$ .

Apart from the divergence terms, a constant of motion obtained from (2) and (3) is the angular momentum/unit mass. This is given by

$$v_y - u_x = L = (2/\gamma) A B \cos 2\tau. \quad (11)$$

Then the remaining DKP can be calculated from

$$\begin{aligned} \zeta &= (A^2 + B^2)/2L \\ S &= (A^2 - B^2)/2L \\ N &= -AB \sin 2\tau/2L. \end{aligned} \quad (12)$$

#### 4. CALCULATION OF DKP

To illustrate the sequence of calculations and the time intervals over which particular values of the DKP for a specific drifter apply, consider the following sequence of critical times:

$T_1$  - time of maximum  $u$

$T_2$  - time of minimum  $v$

$T_3$  - time of minimum  $u$

$T_4$  - time of maximum  $v$

$T_5$  - time of maximum  $u$

$T_6$  - time of minimum  $v$ .

Since the sequence of maxima and minima is periodic, it is not critical that the analysis start with a maximum  $u$ .

As explained in section 3, time  $T_1$ ,  $T_3$  and  $T_5$

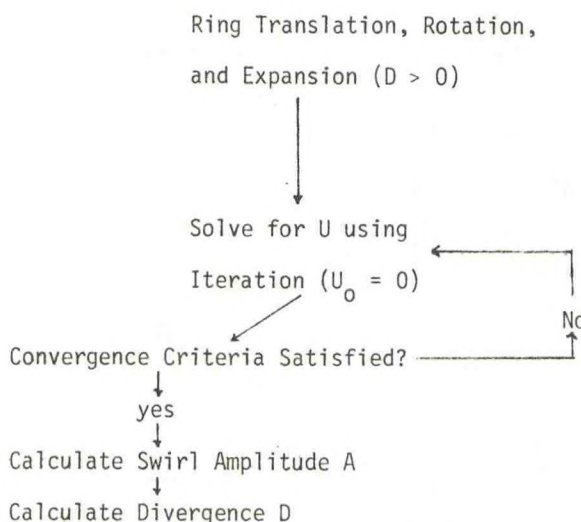


Fig. 2. An outline of the procedure for calculating the ring translation velocity, rotational velocity amplitude, and divergence based on the absolute motion of a buoy.



are used to calculate  $\gamma/2$  for  $u$  and times  $T_2$ ,  $T_4$ , and  $T_6$  are used to calculate  $\gamma/2$  for  $v$ . These times are also used to calculate the phase difference ( $2\tau$ ). Thus, there are phase differences for the sequences  $T_1 - T_3$ ,  $T_2 - T_4$ , etc. The calculation procedure provides an  $A$  and  $D$  for the time period  $T_1 - T_5$  and  $B$  and  $D$  for the time period  $T_2 - T_6$ . The calculations are then repeated for the next sequence of critical times, starting with  $T_2$  and ending with  $T_7$  (time of minimum  $u$ ).

From this it is seen that the  $A$  applies to the time period  $T_1 - T_5$  and  $B$  applies to the time period  $T_2 - T_6$ . Thus, we can consider the characteristic times for  $A$  and  $B$  as the respective midpoints of these intervals. Furthermore, there is an overlap of the time intervals,  $T_2 - T_5$ . The midpoint of this interval is used as the characteristic time for  $\zeta$ ,  $N$  and  $S$ . Note that this characteristic time deviates slightly from that of the divergence since this coincides with that of the amplitudes.

With the amplitudes, phase differences, and characteristic times thus determined,  $L$ ,  $\zeta$ ,  $N$  and  $S$  can be calculated in accordance with (11) and (12). After each calculation, the critical times are advanced by one and the calculations repeated. In this way, a time series of DKP can be constructed.

## 5. SUMMARY

A technique has been presented for calculating the kinematic parameters for a rotationally-dominated ocean feature ( $\zeta^2 > N^2 + S^2$ ) through the use of Lagrangian data. The technique was specifically detailed for application to a warm-core ring, but the basis should be applicable to other features such as Rossby waves, eddies, and topographic waves. Thus, drifting buoys could be used to determine the kinematics of such rotational features as a function of time and distance from the center of the feature. The most interesting aspect of this research is the capability of determining the kinematics using just one drifter.

## ACKNOWLEDGEMENT

This research was sponsored by the Bureau of Land Management under contract No. NA-81-QA-C-148. Data were supplied by Dr. Glenn Hamilton of the NOAA Data Buoy Center.

## REFERENCES

1. U. S. Department of Commerce, National Oceanic and Atmospheric Administration, TzD Buoy Operational Test and Evaluation Final Report, Computer Sciences Corp. and National Space Technology Laboratories, September 1981, 79 pp.
2. Lewis, J. K., A. D. Kirwan, and R. E. Whitaker, "Kinematic and Dynamical Calculations from Lagrangian Measurements: Recent Theoretical Advances." Presented at the 1983 Symposium on Buoy Technology, New Orleans, Louisiana, April 27-29, 1983, Sponsored by the Marine Technology Society and the NOAA Data Buoy Center.
3. Stephens, J. J., "A Variational Approach to Numerical Weather Analysis and Prediction." PhD Dissertation, Dept. of Meteor., Texas A&M University, College Station, Texas, 1965.
4. Stephens, J. J., "Variational Statement of Quasi-Static and Geostrophic Equilibria." *Die Beit.zur Physik der Atmosphäre*, 1967, 40, 3, 103-107.



THE KINEMATICS AND GEOMETRY OF A GULF OF MEXICO  
WARM-CORE RING AS DETERMINED BY DRIFTING BUOYS

R. E. Whitaker

A. D. Kirwan

James K. Lewis

Science Applications, Inc.  
4348 Carter Creek Parkway  
Bryan, Texas 77801

University of South Florida  
Department of Marine Science  
St. Petersburg, Fla. 33701

Science Applications, Inc.  
4348 Carter Creek Parkway  
Bryan, Texas 77801

ABSTRACT

NDBC deployed three drifters in a warm core ring in Northeast Campeche Bay during November 1980. The trajectories of these drifters through April 1981 are presented and discussed. These data sets provide for the evaluation of a sequence of absolute velocities over the record length. The kinematic parameters of the ring, as well as the swirl and translation velocities, were computed from the absolute

velocities. The histories of the kinematic parameters and the swirl and translation velocities are presented and discussed. The results from the three drifters show considerable consistency. Variations are most likely the result of changing kinematics with distance from the center of the ring. The computed evolution of the ring's shape and orientation are presented and discussed. Dynamics are considered using the ring vorticity and divergence in the vorticity equation. The time history of the residual of the vorticity balance is considered in relation to horizontal shear stresses and the curl of the wind stress.



# An Operational Sea Ice Management System Based on Lagrangian Data from Ice Drifters

James K. Lewis

Warren W. Denner

R. E. Whitaker

Science Applications, Inc.  
4348 Carter Creek Parkway  
Bryan, Texas 77801

Science Applications, Inc.  
205 Montecito Avenue  
Monterey, CA 93940

Science Applications, Inc.  
4348 Carter Creek Parkway  
Bryan, Texas 77801

## Abstract

Drifting buoys on ice can be used to calculate differential kinematic parameters (DKP) of vorticity  $\zeta$ , divergence  $D$ , normal deformation rate  $N$ , and shear deformation rate  $S$ . Real-time monitoring of sets of buoys in a region allows construction of two-dimensional pictures of regional DKP. Since kinematic ice features tend to move in patterns over the ice, these two-dimensional pictures can be used by operations personnel as a real-time warning system, much in the same sense as weather radar. In addition, theoretical developments indicate that wind stress and DKP measurements could allow estimates of the two-dimensional variations of ice thickness. The same theory indicates that 12 hrs worth of wind stress data are required to predict the various ice kinematic parameters.

The applied aspects of DKP monitoring in ice-infested waters are discussed and include ship routing, over-ice transportation, aircraft operations, drilling, and oil spill countermeasures.

## 1. INTRODUCTION

In order to design for specific conditions in an environment, one must determine the basic modes of motion in the environment, including differential motion. The four parameters of differential motion are vorticity  $\zeta$ , divergence  $D$ , normal deformation rate  $N$ , and shear deformation rate  $S$ . These differential kinematic parameters (DKP) are particularly important in an ice-infested environment due to the variations in sea ice loading that each variable causes.

By tracking transponders on ice, one may calculate the DKP of the ice in a real-time mode. (See 11 and 9 for a description of the technique for calculating DKP from drifting buoys.) This mode could be applied in a variety of ways, including real-time operational monitoring, development of ice movement prediction models, studying ice dynamics, and the initialization and verification of dynamic/thermodynamic ice models. In this paper, we briefly touch on the technical details of calculating the DKP using buoys on ice. Also, we discuss the implication of theoretical responses of ice to driving forces and the actual response as measured by buoys. Finally, we discuss the operational

requirements and basis for a sea ice management system which includes Lagrangian data from buoys drifting with the ice.

## 2. TECHNICAL AND THEORETICAL CONSIDERATIONS

Velocity gradients across a given parcel of ice may be expressed in terms of the DKP. The physical interpretation of these kinematic parameters are (see 3 and Fig. 1).

- $\zeta$  - the change in the orientation of an ice parcel,
- $D$  - the change in the size of an ice parcel,
- $N$  - the change in the shape of an ice parcel due to forces acting normal to the sides of the parcel, and
- $S$  - the change in the shape of an ice parcel due to forces acting parallel to the sides of the parcel.

Since drifting buoys can be used to calculate the DKP (10, 6, 4), one could use the buoy data in a real-time mode to construct a two-dimensional picture of the DKP over a region of interest. This information, supplemented with theoretical ice-wind relationships and observations of ridging and lead formation, could be used by operations personnel as a real-time warning system. In particular, the pattern of DKP variations could be used much in the same sense as weather radar since kinematic ice features tend to move in patterns over ice.

Lewis et. al (7) have shown that the theoretical relationships between ice motion and wind forcing/water drag are

$$U_{x,t} = e^{-\Gamma t} [U_{x,0} \cos ft + U_{y,0} \sin ft] + \int_0^t e^{-\Gamma y} [\tau_{s,x} \Big|_{t-y} \cos fy + \tau_{s,y} \Big|_{t-y} \sin fy] dy / (H\rho) \quad (1)$$

$$U_{y,t} = e^{-\Gamma t} [U_{y,0} \cos ft - U_{x,0} \sin ft] + \int_0^t e^{-\Gamma y} [\tau_{s,y} \Big|_{t-y} \cos fy - \tau_{s,x} \Big|_{t-y} \sin fy] dy / (H\rho)$$

where  $U$  is the ice velocity,  $\Gamma = KR/(H\rho)$ ,  $K$  is a linear water drag coefficient,  $R = 1 - |\vec{V}|/|\vec{S}|$ ,  $|\vec{S}|$  is the speed of the water under the ice,  $H$  is the ice thickness,  $\rho$  is the density of ice,  $\vec{\tau}$  is the



$D$  = Divergence  
(Area Change)

$N$  = Normal Deformation Rate  
(Shape Change,  $\frac{DA}{Dt} = 0$ )

$S$  = Shear Deformation Rate  
(Shape Change,  $\frac{DA}{Dt} = 0$ )

$\zeta$  = Vorticity  
(Orientation Change,  $\frac{DA}{Dt} = 0$ )

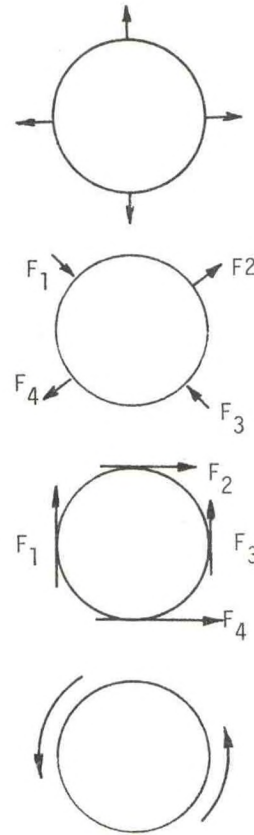


Fig. 1. Schematics of the physical interpretations of the DKP.

wind stress,  $f$  is the Coriolis parameter,  $t$  is time, and  $U_0$  is the ice velocity at  $t = 0$ . Equation (1) is the analytical solution to the primitive equations of motion in which surface height anomalies and internal ice stress are neglected. The height anomaly term has been found to be small even for relatively enclosed regions (12). However, the internal ice stress is a factor which cannot always be neglected.

Before we consider the utility of the equations in (1), we wish to simplify the expressions by determining the time  $t'$  such that  $e^{-\Gamma t'} = 0.1$ . For times greater than  $t'$ , the exponential damping term reduces the influences of  $\vec{U}_0$  and  $\vec{\tau}|_{t-t'}$  to  $\leq$

10% of their original values. The ratio parameter  $R$  was set to 0.5 (12,8), the ice thickness  $H$  was set at 4.0 m, and various values of the drag coefficient were used (5,1). The maximum  $t'$  calculated was approximately 11 h. Thus, by having approximately 12 h of wind stress data, the theoretical relationship between the ice motion and the forcing functions may be estimated by

$$U_{x,t} \doteq \int_0^{12 \text{ hrs}} e^{-\Gamma \gamma} \left[ \tau_{s,x} \Big|_{t-\gamma} \cos f_\gamma + \tau_{s,y} \Big|_{t-\gamma} \sin f_\gamma \right] d\gamma / (H\rho) \quad (2)$$

$$U_{y,t} \doteq \int_0^{12 \text{ hrs}} e^{-\Gamma \gamma} \left[ \tau_{s,t} \Big|_{t-\gamma} \cos f_\gamma - \tau_{s,x} \Big|_{t-\gamma} \sin f_\gamma \right] d\gamma / (H\rho).$$

There are two implications of the results shown in (2). First of all, we can form the DKP from (2) using the proper combinations of velocity gradients (see 7). These expressions are

$$D \doteq \int_0^{12 \text{ hrs}} e^{-\Gamma \gamma} \left[ \nabla \cdot \vec{\tau}_s \Big|_{t-\gamma} \cos f_\gamma + \text{curl}_z \vec{\tau}_s \Big|_{t-\gamma} \sin f_\gamma \right] d\gamma / (H\rho) \quad (3a)$$

$$\zeta \doteq \int_0^{12 \text{ hrs}} e^{-\Gamma \gamma} \left[ \text{curl}_z \vec{\tau}_s \Big|_{t-\gamma} \cos f_\gamma - \nabla \cdot \vec{\tau}_s \Big|_{t-\gamma} \sin f_\gamma \right] d\gamma / (H\rho)$$



$$N = \int_0^{12 \text{ hrs}} e^{-\Gamma_Y} \left[ N_W \right]_{t-Y} \cos f_Y + S_W \left[ \sin f_Y \right]_{t-Y} dY / (H_0) \quad (3b)$$

$$S = \int_0^{12 \text{ hrs}} e^{-\Gamma_Y} \left[ S_W \right]_{t-Y} \cos f_Y - N_W \left[ \sin f_Y \right]_{t-Y} dY / (H_0).$$

where  $N_W$  and  $S_W$  represent the normal and shear deformation rates of the wind stress, respectively. The relationships in (2) and (3) show us that each ice kinematic parameter is a function of two wind parameters:

$$\vec{U} = f_1 (\tau_{S,X}, \tau_{S,Y})$$

$$D = f_2 (\nabla \vec{\tau}_S, \text{curl}_Z \vec{\tau}_S)$$

$$\zeta = f_3 (\text{curl}_Z \vec{\tau}_S, -\nabla \vec{\tau}_S)$$

$$N = f_4 (N_W, S_W)$$

$$S = f_5 (S_W, -N_W).$$

The second implication arises from the fact that we have neglected internal ice stresses in our original relationships. Thus, the functions shown in (4) should be thought of as the theoretical free drift responses. The actual responses, those which are calculated from buoys drifting on ice, are

$$\vec{U} = f_1 + g_1 \text{ (internal ice stress)}$$

$$D = f_2 + g_2 \text{ (internal ice stress)}$$

$$\zeta = f_3 + g_3 \text{ (internal ice stress)}$$

$$N = f_4 + g_4 \text{ (internal ice stress)}$$

$$S = f_5 + g_5 \text{ (internal ice stress)}$$

where the  $g_i$  are the unknown time-integrated effects of the internal ice stress on each kinematic parameter. Thus, position and wind data from buoys drifting on ice may be used to calculate the actual  $\vec{U}$ ,  $D$ ,  $\zeta$ ,  $N$ , and  $S$  and also the  $f_i$ 's.

The relationships in (5) indicate that the difference between the actual kinematic parameters and the  $f_i$ 's will give us the internal ice stress effects. Of course, this can only be determined by knowing the ice thickness  $H$ . However, if the internal ice stress has little or no effect on one of the DKP (say, for example,  $\zeta$ ), then it may be possible to calculate the ice thickness by using (2) or (3) with wind data (for the RHS of the expressions) and buoy data (for the LHS of the expressions) and solving for  $H$ .

### 3. A SEA ICE MANAGEMENT SYSTEM

Any particular operation in ice-infested waters requires a variety of information with respect to present and future ice conditions. In addition, the format and extent of this information may be different depending on the type of operation and time of year. Thus, an operational sea ice

management system (OSIMS) must be configured to provide the required information on the appropriate time and space scales for a particular area for any specific operation. Table 1 shows information requirements for a variety of parameters related to short term forecasting.

A substantial component of an OSIMS could be a system of buoys drifting with the ice. The OSIMS could monitor in real-time the appropriate buoys for a required spatial scale at the required time intervals. The ice kinematics could be calculated in a real-time mode also, and this information can be used in various operations.

In order to have a complete OSIMS, one must have an operational ice movement and growth model (2). But all models of this sort (dynamic and thermodynamic) must be initialized and, at appropriate intervals, verified and updated as required. Drifting buoys could provide the initialization and verification with respect to ice motion in strategically important regions. In addition, if ice thickness can be determined, the buoys could also provide the initialization and verification for the ice growth.

Overall, the OSIMS would consist of drifting buoys, an ice movement and growth model, ice climatology, a system for information synthesis (e.g. recording critical values of the DKP for particular operations), and a display system for real-time monitoring of the ice kinematics. The display system would be used to construct a two-dimensional picture of each kinematic parameter over a given region. A CRT could be used to display a contoured plot of the parameters, and regions which have exceeded critical values would be shaded in a specific manner (e.g. color coded; Fig. 2). This would allow for the monitoring of the development, translation, and dissipation of critical regions, similar to weather radar systems.

The following are some of the operations for which buoys drifting on ice can be used:

- ship routing - in areas of maximum divergence, one finds ice that is under the least amount of internal pressure. Also, there are greater chances of open water in areas of greatest divergence. Thus, two-dimensional patterns of ice divergence can be used to determine the best through-ice transits for ship routing. In addition, if the ice thickness  $H$  can be predicted, ship routing can be aided by two-dimensional patterns of ice thickness and internal ice stresses.
- on-ice transportation and aircraft operation - in areas of maximum convergence, one expects to find less open water and greater ice pressure. Thus, on-ice operations could be planned in regions of maximum convergence.
- through-the-ice operations - for equipment that is placed through the ice, the compression, shear, and vorticity predictions could be used to indicate the type and magnitude of forces to which the



equipment is subjected.

- on-the-ice deformation - for systems placed on the ice, deformation rates would indicate the overall horizontal deformation that the systems must withstand.
- under-ice operations - relationships between buoy-indicated kinematics and pressure keels could be used to indicate the frequency, orientation, and size of ice keels.
- oil spill countermeasures - buoys could be used to track oil-contaminated ice while convergence/divergence regions could aid in planning cleanup operations.
- acoustic operations - regions of greatest ice deformation could be used to indicate areas with higher acoustic noise levels within the water column and characterize under-ice roughness to determine scattering losses related to acoustic propagation.

## REFERENCES

1. Heaps, N. S., Development of a three-dimensional numerical model of the Irish Sea. *Rapp. P. -V. Réun. Cons. int. Explor. Mer.*, 167, 147-162, 1974.
2. Hibler, W. D., A dynamic thermodynamic sea model. *J. Phys. Oceanogr.*, 9 (7), 815-846, 1979.
3. Kirwan, A. D., "Oceanic velocity gradients." *J. Phys. Oceanogr.*, 5 (4), 729-735, 1975.
4. Kirwan, A. D., J. K. Lewis, and R. E. Whitaker, Analysis of drifter dispersion by rings. Final Rept. for MMS contract NA-81-QA-C-148, 105 pp, 1983.
5. Langleben, M. P., Water drag coefficient at AIDJEX station Caribou. In *Sea Ice Processes and Models* (R. S. Pritchard, ed.), Univ. of Wash. Press, Seattle, 464-471, 1980.
6. Lewis, J. K. and A. D. Kirwan, "Analysis of horizontal shear data." Final Report, NRL, contract N00014-81-C-2103, 63 pp., 1981.

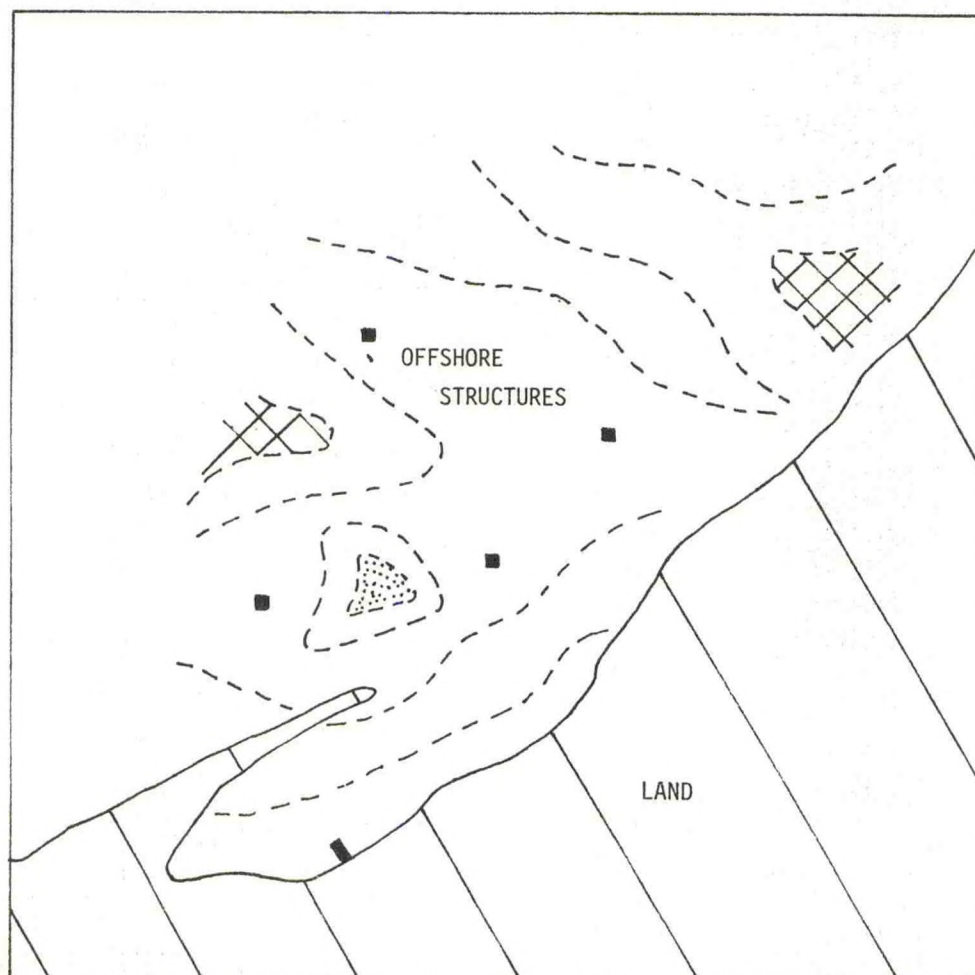


Fig. 2. An example of a contour plot for a kinematic parameter. Dashed lines represent the contours and cross mesh represents minima while dots represent maxima.



7. Lewis, J. K., A. D. Kirwan, and R. E. Whitaker, Kinematic and dynamical calculations from Lagrangian measurements: recent theoretical advances. Proceedings, MTS/NDBO Symposium on Buoy Tech., New Orleans, LA., 1983.
8. McPhee, M. G., An analysis of pack ice drift in summer. In *Sea Ice Processes and Models* (R. S. Pritchard, ed.), Univ. of Wash. Press, Seattle, 62-75, 1980.
9. Molinari, R., and A. D. Kirwan, "Calculation of differential kinematic properties of the Yucatan Current from Lagrangian observations." *J. Phys. Oceanogr.*, 5, 483-491, 1975.
10. Okubo, A., C. C. Ebbesmeyer, J. M. Helseth, and A. S. Robins, Reanalysis of the Great Lakes drogue studies data: final report. Mar. Sci. Res. Center, Stony Brook, N.Y., Spec. Rept. 2, 84 pp., 1976.
11. Okubo, A., and C. C. Ebbesmeyer, "Determination of vorticity, divergence, and deformation rates from analysis of drogue observations." *Deep Sea Res.*, 23, 349-352, 1976.
12. Udin, I. and A. Omstedt, Sea Ice-75 dynamical report. Res. Rpt. No. 16:8, Winter Navigation Res. Board, Swedish Administration of Shipping and Navigation, Finnish Board of Navigation, 32 pp, 1976.

Table 1. Requirements for observed parameters needed for short term sea ice forecasting.

PARAMETER	ACCURACY	SPATIAL COVERAGE (km)	TEMPORAL COVERAGE (days)
Drift			
Small Scale	50m/day	1	0.25
Regional Scale	1 km/day	5	1-5
Concentration	2-10%	10-25	1-3
Thickness	0.2-1 m	25-50	1-3
Edge	0.5-3km	1-10	1-3
Ridging			
Density (#/km)	10-50%	0.05-0.1	7-28
Orientation	10-30°	-	7-28
Height	1-5m	-	7-28
Lead-Orientation	10-30°	-	1-3
Fractional Area	10-50%	0.05-0.1	1-3
Fractional Area			
Type	5-10%	1-25	7-28



A GENERAL AUTOMATIC PROFILING SYSTEM  
FOR GREAT LAKES APPLICATION

F.E. Roy

National Water Research Institute  
Canada Centre for Inland Waters  
Burlington, Ontario, Canada L7R 4A6

ABSTRACT

The General Automatic Profiling System (GVAPS) developed by the National Water Research Institute, has been designed to collect fine resolution vertical profiles of current velocity and temperature in continuous time series over long time intervals. This type of data is of considerable value in depicting or visualizing the physical processes involved in vertical mixing phenomena in large lakes, and in the development and calibration of numerical models.

The system is described and some operational problems during its development are discussed, including the logistics of its deployment and its operational reliability. Samples of data showing the variability of velocity and temperature structure of lakes are presented.

INTRODUCTION

The detail study of mixing and advective transport processes in vertically stratified large lakes is a study in part of the dynamic vertical gradients of velocity, temperature and water chemistry properties. The study is obviously much enhanced if continuous time series of such vertical gradients can be observed at high spatial resolution and over time periods in the scale of major meteorological forcing events.

At the National Water Research Institute (NWRI), as at other similarly directed institutes, the majority of such profile data is obtained from fixed-string instrumentation moorings. These instrument systems have the disadvantage of poor spatial resolution which inhibits detail study of vertical processes, and of greatly increased cost through the increased number of instruments per mooring if higher resolution is sought.

The initial development by NWRI of an automatic profiling system had as the main objectives:

- the measurement of synoptic vertical profiles without the need for many fixed sensors to obtain the desired resolution of time and depth;
- the ability to carry a variety of sensors, i.e., physical, chemical, optical;

- high reliability for long periods of unattended operation;
- capability for shorebased or offshore operation, year round;
- ease of deployment and retrieval with existing support facilities.

The prototype configuration chosen was based on a bottom mounted winch connected through 1000 m of cable to a power supply and monitoring station on shore (Ward-Whate, 1977). This equipment was deployed in Kootenay Lake, British Columbia, in the fall of 1977 and spring of 1978.

The success of this operation reported by Hamblin & Kuehnelt (1980), encouraged the addition of an offshore capability. The present paper describes the General Vertical Automatic Profiling System (GVAPS) developed from the baseline experience with the Kootenay system.

DESCRIPTION

The GVAPS (Figure 1) comprises a single positively buoyant sensor vehicle carrying the instrument array, a bottom mounted winch, a moored power/monitor buoy, and a single surface to bottom cable combining the functions of mooring and communication to the bottom.

Sensor Vehicle

The sensor vehicle (Figure 2) described in detail by White (1980), is a general purpose platform upon which sensors may be mounted.

It contains a Sea Data Model 656-1 A/D converter which converts sensor analog outputs to serial digital format and transmits this data via the tether, winch and mooring cable to the recorder and data display in the power/monitor buoy.

The vehicle body is a cylinder 21.9 cm diameter by 1.1 m long with "O" ring sealed top and bottom bulkheads. Buoyancy and vertical stability are provided by a 69 cm syntactic foam split sphere clamped to the upper half of the body. Including tether cable attachment, the vehicle is 2 m long, has a mass of 104.4 kg, and a net positive buoyancy of 808 N.



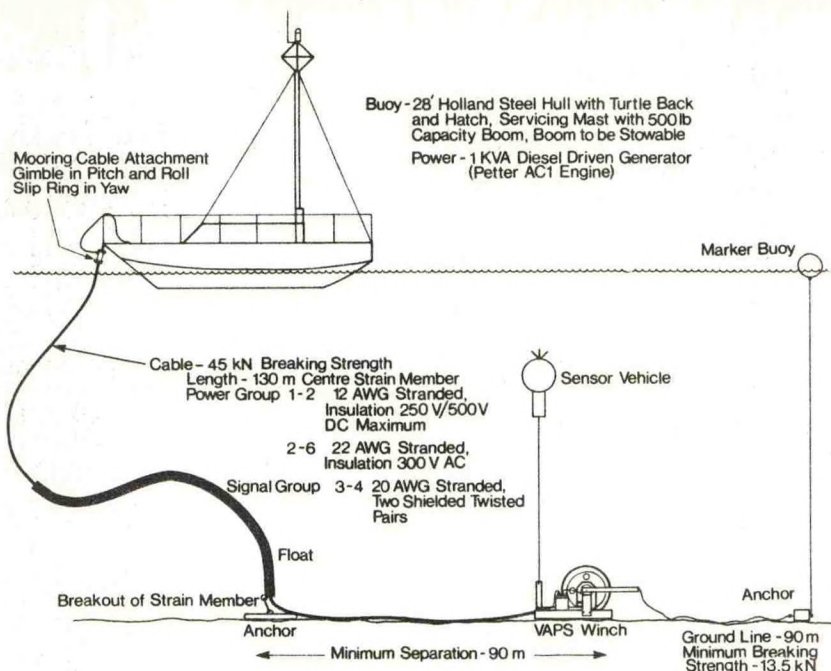


Figure 1. GVAPS Installation Configuration

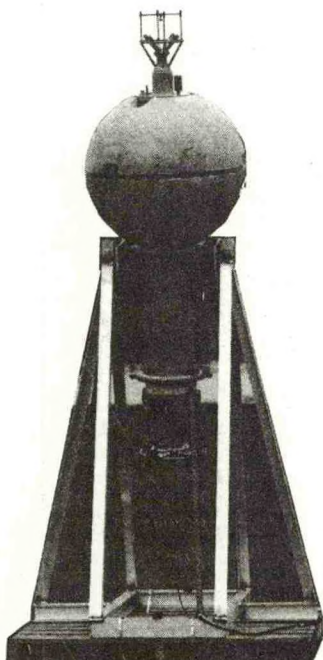


Figure 2. Sensor Vehicle in Transport Frame

The present sensor array is summarized in Table 1, and reflects studies of lake physics and sensor motion. Velocity and temperature sensors are duplicated on the bottom of the vehicle to place them within the bottom boundary layer of shallower lakes.

The primary sensors for depth, temperature, and current are mounted on the top bulkhead. The current sensor plane is 28 cm above the top of the sphere, and 20.3 cm above the depth sensor. The heading and tilt sensors are mounted inside the pipe section, approximately at the center of buoyancy of the vehicle. The duplicate temperature and current sensors are mounted on the bottom bulkhead, 170 cm below the depth sensor.

Due to the winch frame and the tether cable guide this places the lower current sensor plane about 1.31 m from the lake bottom.

#### The Winch

The winch (Figure 3) is designed for operation submerged in freshwater to depths of 200 m on bottoms ranging from hard rock to soft silty clay (bearing capacity 680 Pa). It comprises a welded aluminum channel base frame 125 cm x 200 cm, supporting a drum and slip ring, winch drive assembly, fairlead screw, and compensation air tanks.

The drum is grooved to accommodate 200 m of nominal 6 mm diameter tether cable in a single layer. A 6-circuit slip ring in an air pressure compensated housing is provided.

The winch drive assembly is an air pressure compensated housing containing a 186.5 W dc motor and speed reducer, motor speed feedback, profile limit switches, motor brake and sensor vehicle power supply. The bottom limit of the profile is manually set prior to deployment. The upper limit



TABLE 1  
INSTRUMENT ARRAY

Data Channel	Instrument	Manufacturer	Range	Resolution	Accuracy
1	Depth	Teledyne Taber Model 0200-008075-50	0-50 m	1.44 cm/bit	$\pm 0.5\%$ F.S. $\pm 1$ bit with modified transfer function
2	Temperature Upper	Rosemount Model 171 ED	0-25°C	12.1 m°C/bit	$\pm 50$ m°C
3	Current Upper X	Christian Michelsens Institute-Prototype- Reflected Beam	2-125 cm/s	2 cm/s	$\pm 10\%$ 2 cm/s
4	Current Upper Y	Christian Michelsens Institute-Prototype- Reflected Beam	2-123 cm/s	2 cm/s	$\pm 10\%$ 2 cm/s
5	Heading	Digicourse Model 101 Type 251 Interface	0-360°C	$\pm 1^\circ$	$\pm 3-6$
6	Vehicle Tilt X axis	Humphrey Model V 118-0402-1	$\pm 45^\circ$	$\pm 1^\circ$	
7	Vehicle Tilt Y axis	Humphrey Model V 118-0402-1	$\pm 45^\circ$	$\pm 1^\circ$	$\pm 1^\circ$
8	Temperature	Rosemount	0-25°C	12.1 m°C/bit	$\pm 50$ mZC
9	Current Lower X	Christian Michelsens Institute Prototype Direct Beam	2-250 cm/s	.13 cm/s/bit	10% 2 cm/s
10	Current Lower Y	Christian Michelsen Institute Prototype Direct Beam	2-250 cm/s	.13 cm/s/bit	10% 2 cm/s

is remotely set after deployment. For unattended operation the upper limit is typically set about 2 m below the surface to avoid damage from small boat passage or excessive wave motion, but may be re-set from the power/monitor buoy at any time for attended experiments.

The line speed of the winch is adjustable from 0.25 to 25 cm/s, within  $\pm 0.2\%$  of full speed.

#### Power/Monitor Buoy

The power/monitor buoy (Figure 4) is an extensively modified 8.5 m, double chine steel sailboat hull of about 3.5 tonnes, with a draft of 1.5 m. It contains a 1.5 kW diesel-electric plant (a Petter AC-1 single cylinder engine and Newage DBA rotating armature ac generator) with a 60 day fuel supply and winch control and data acquisition consoles. Auxilliaries include a navigation

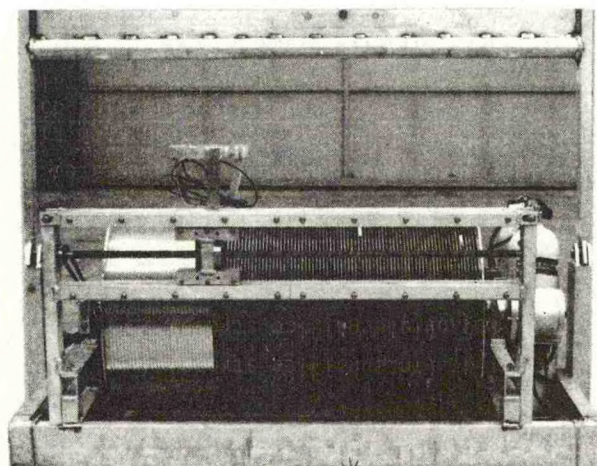


Figure 3. Winch



marker light, deck and interior lighting, a power distribution panel, and automatic fire suppression equipment. The hull has a ballasted keel and is fitted with a skeg and locking rudder. It has been found to tow stably at speeds of 7 to 9 kt in fair weather.

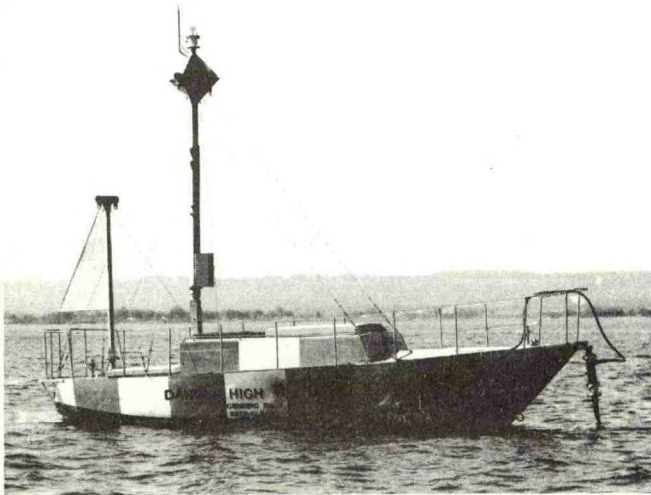


Figure 4. Power/Monitor Buoy

#### Mooring/Signal Cable

The function of the mooring/signal cable is to moor the buoy to the lake bottom, and to transfer power and data signals between the buoy and the winch/sensor vehicle. This cable comprises a helixed bundle of 22 conductors, water blocked and wrapped in mylar tape, then jacketed in PVC. This is then covered with two lays, torque balanced, of 7.5 mm plow steel open armor, again jacketed in PVC. The cable has a design break strength of 44.5 kN, is 22.3 mm in diameter, has a minimum bend radius of 380 mm, a mass of 740 g/m, and a weight in water of 3.42 N/m. This cable is supplied to us by South Bay Cable Division of Consolidated Products Ltd.

The surface end of the cable is fastened to the bow peak of the power buoy through a watertight swivel assembly containing a slip ring and a universal joint. The cable is thus isolated from yawing, rolling and pitching angular motions of the buoy. The cable termination to the swivel assembly is via a Preformed Marine Dyna-Grip with an underlay of lighter grip rods. Thus the grip is tapered to some degree, is about 2 m long, and gives a 90° bend on a radius of 1 m for a lateral load of 2660 N.

The anchor point of the cable is fabricated from a Preformed Marine Dyna-Grip Mid-Span Attachment, and shackled to a 3.4 kN railway wheel anchor with no provision for swivelling. We have chosen a mooring scope of about 2.5 times the depth in order to minimize vertical loads on the anchor.

To avoid tangling and cable snagging on bottom rocks, the lower half of the cable is buoyed to a slightly positive condition by attaching 20 N Grimsby floats at 5 m spacings.

Although we have had some success with this cable configuration in 60 m water depth, the form of the mooring is still a matter of some question and requires further experience to establish satisfactory reliability.

#### Data Acquisition System

The GVAPS Data Acquisition System is essentially a Sea Data Model 650 Data Logger separated into two parts. The Model 656-1 A/D Converter Package, is a 16 channel A/D converter and transceiver packaged for installation in the cylindrical sensor vehicle. The Model 656-2 Recorder is a transceiver and double cassette recorder packaged for rack mounting in the monitor buoy. The two packages are connected by a 4-wire set which carries two optically isolated, differential, 20 mA current loops, one for serial data, and one for shift pulses. These shift pulses synchronize data bit transmissions from the A/D converter in the sensor vehicle with the recorder operation in the surface buoy.

The A/D converter contains a rechargeable battery powered 6-day crystal clock and ON/OFF control logic based on the state of its 50 Vdc power input. Both the converter and recorder have sufficient energy storage to complete a data and time scan and write a file gap in the event of 50 Vdc power failure.

This feature is used to separate data into convenient files by using the profile upper limit switching to switch sensor vehicle power off for 13 s at the "beginning" of each down profile.

The A/D converter scan interval is switch selectable to 1, 2, 4 or 8 seconds. Both scan interval and clock reset are in the sensor vehicle, and not accessible once the vehicle is sealed and deployed. The clock auto-resets every six days while running.

Each 450 ft tape cassette has a capacity of 84,200 scans of time and 10 data channels. The twin cassettes on the recorder thus provide about 7.8 days data storage at the continuous rate of four seconds per scan typical of our operation.

On the surface buoy, in parallel with the 656-2 Recorder, is a Sea Data Model 17 Bit Display Box, and two Hewlett Packard 7100 B Strip Chart Recorders. The bit display box provides continuous display in binary form of the data stream being recorded. It also provides D/A conversion of any selected serial set of four data channels with  $\pm 5$  Vdc analog outputs for display on the chart recorders. This permits in situ evaluation of the GVAPS operation and the quality of the data being collected. This is valuable for trouble shooting, and for precise set up of profile timing and depth limits.



Ashore, the data tapes are read through a Sea Data Model 12A Reader and transcribed to a half inch computer compatible tape for bulk scaling conversion, editing, filing, and plotting of selected sequences. The Model 12A Reader may also be used in conjunction with an HP 9845 Desk Top to provide a quick look conversion of single profile data files in engineering units.

#### DEVELOPMENT

The initial trade-offs leading to the choice of a bottom winch configuration for this type of system are discussed by Ward-Whate (1977). The main reasons were the relative simplicity of control of the sensor vehicle profiling motion, isolation of the sensors from motions of surface or sub-surface support buoys, ability to profile up to the air-water interface and close to the bottom, and the relative ease of deployment. The main disadvantage is the power consumption of the winch.

The adoption of a surface buoy with a diesel-electric plant provides essentially unlimited power storage. Existing equipment without modification can easily meet a 60 day mission. Mission time can easily be extended by refuelling on site. As well, the buoy provides a comfortable work station for setting up and monitoring experiments and retrieving data cassettes, and ready access to the winch control and data display for altering mission profile if desired.

The choice of a commercially available sailboat hull was based on the cost saving over the design and construction of a special hull, and on the success reported by Dessureault et al (1982) with a similar hull evaluated as a data buoy vehicle.

The mooring/signal cable follows logically from the selection of a surface buoy approach.

#### Problems

There have been some development problems.

The winch has been redesigned to improve the reliability of its automatic control. A skeg and rudder were added to the power/monitor buoy for directional stability in tow. The buoy fuel system has been revised for easier cleaning and increased fuel supply pressure. There have been wiring connection fatigue failures on engine auxiliaries.

The most difficult task has been learning how to produce a survivable mooring cable. Moorings to date have been in shallow water, less than 60 m, with wave heights up to 1.5 m, and periods of four to six seconds.

The swivel assembly at the buoy was intended to reduce bending stresses at this point, and bypass the electrical conductors around the mechanical termination. Bending strain relief moulded into the cable termination to the swivel assembly proved inadequate. The inertial mass of the swivel assembly was still large enough to produce fatigue bending at this point (Figure 5). This

has been countered in the present cable by the 2 m long tapered strain relief described earlier. Survival of a 15 day deployment with two major storms off Cobourg, in Lake Ontario, has given encouragement, but satisfactory long term survivability has yet to be demonstrated.

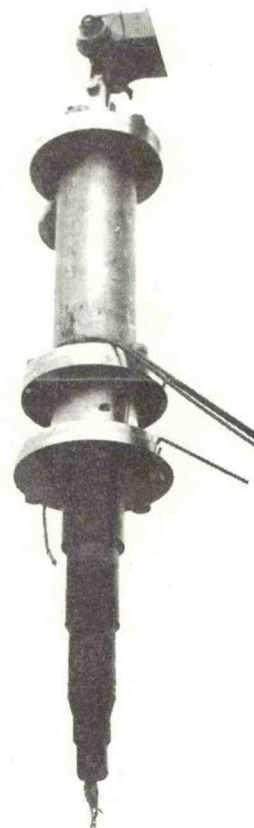


Figure 5. Fatigued Mooring Cable

#### DEPLOYMENT

The logistic support for system deployment in our operation comprises a 15 m, 36 tonne work boat for tow, and a 3 m by 6 m pontoon barge for transport and deployment of the winch, sensor vehicle and mooring cable. This barge has a hoisting frame and a 1 tonne capacity winch. The GVAPS components may be trucked to the closest near site shore facility or assembled for tow from the NWRI facility. A towing speed of 7 to 9 kts is used in calm sea. To date, the longest tow has been 168 km, Burlington to Cobourg on Lake Ontario.

The system is deployed by temporarily stern anchoring the power/monitor buoy upwind, backing the pontoon barge off laying out cable, lowering the anchor, backing off further laying the balance of mooring cable, and then lowering the winch and sensor vehicle in a single package.

The deployment operation takes about two hours, requires a calm sea with wave height not over 0.5 m, and four people.



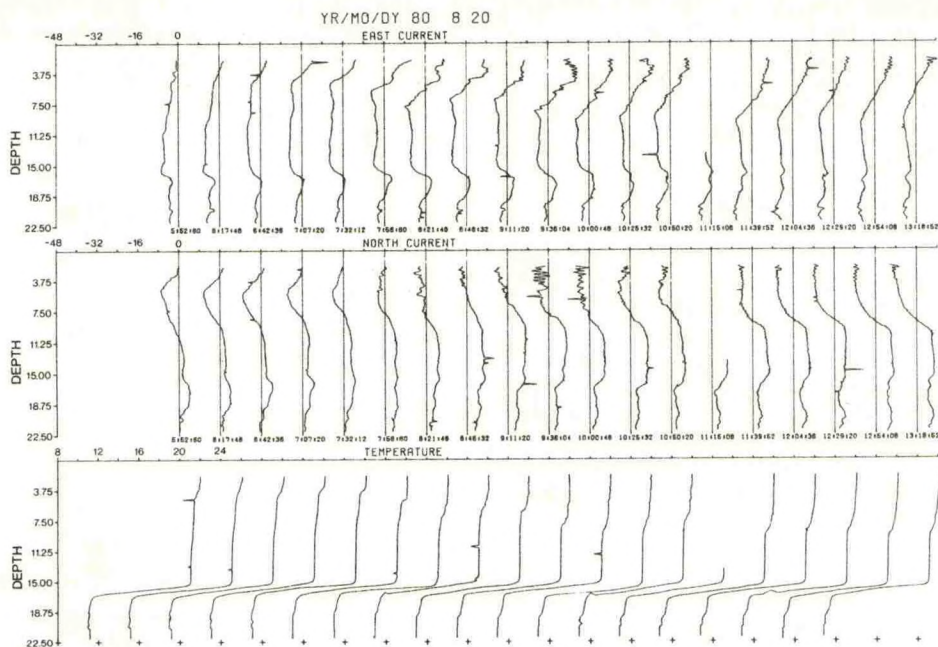


Figure 6. Sample GVAPS Data

## RESULTS

GVAPS has so far been operated in the central basin of Lake Erie (1980), Hamilton Bay, Lake Ontario (1981) and in Lake Ontario nearshore off Port Hope (1982). In spite of the developmental problems mentioned, a library of some 400 lake profiles and 2300 bay profiles have been recorded.

By way of illustration, Figure 6 shows a sequence of approximately 8-1/2 hours of observation taken in the Central Basin of Lake Erie on August 20, 1980. The station was located approximately mid-lake on a line between Erieau, Ontario, and Cleveland, Ohio. The sequence runs from 05:53 to 14:33 GMT and reflects the response to the passage of a squall line between 07:00 and 11:00. Hourly averaged wind rose from 3 m/s (5.8 kt) to 9 m/s (17.5 kt) from 07:00 to 08:00 and then fell back to 2.3 m/s (4.5 kt) again by 11:00 (Figure 7). The accompanying shift in the direction of wind, i.e., wind to rather than wind from, was from NNW at 06:00 to NEE at 08:00 with the peak wind, to SSE at 11:00 as the wind declined. After passage of the squall by 13:00, the wind was about 2 m/s (4 kt) towards NNW.

The profiler was operating between bottom + 1.3 m (about 21 m depth) to surface -2m, with a time interval of 24.6 minutes between profiles. The plot depicts east currents (+ to right), north current (+ to right) and temperature.

The dominant and relatively static features depicted are:

- a main thermocline at about 16 m with 21°C in the upper water or epilimnion and 11°C in the lower water or hypolimnion. This thermocline is very sharp with a thickness of about 1.5 m;

- a general movement of the epilimnion towards NNW, with remnants of SSE layer from 2 to 7 m left over from previous excitation.

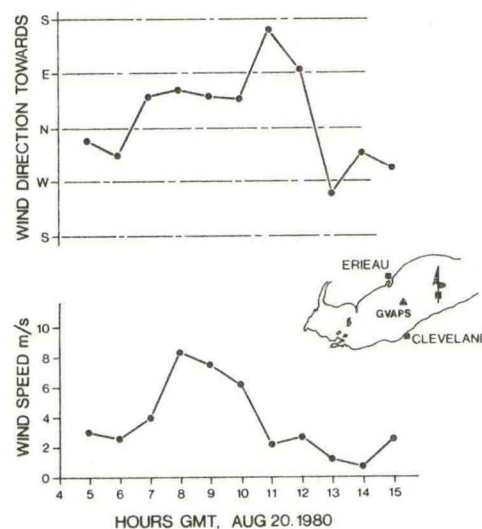


Figure 7. Erieau Wind Concurrent with the Data of Figure 6



The onset of the squall wind, rising from 3 to 9 m/s NEE between about 06:30 and 08:30 sets up a surface current east of 8 cm/s and a shear zone at about 5 m which descends to about 9 m by 10:00. The shift of wind direction to SEE after 10:00, as the wind strength declines, gives rise to an increasingly southern set to the surface current as the easterly component declines. By 12:00 the surface layer is moving almost opposite to the general epilimnion movement, and there is a clearly defined shear zone at the 9 m depth. The development of this shear or mixing zone and its progression down in to the epilimnion is clearly shown in the temperature profiles as a 1.5°C gradient from the surface to the 9m depth. The strength of the squall disturbance has not affected the thermocline. The time lag between the peak of the wind input at 08:00 and the maximum development of the surface mixed layer to 9m is about six or seven hours.

It is clear from this cursory examination, that GVAPS data can provide fresh insights into lake processes.

#### FUTURE DEVELOPMENTS

Our goals for the immediate future are to expand the measurement capability by adding sensors for Dissolved Oxygen and Transmissability and to demonstrate that the problems of mooring cable security and system unreliability have been resolved to the point where the equipment may be deployed on a routine basis.

To this end, the sensor vehicle will be fitted with a Yellow Springs Instrument (YSI) Model 5739 Dissolved Oxygen Probe. Although the response time of this type of instrument is slow, it should prove adequate with the low profiling speed and 4 second scan interval typical of the GVAPS operation. This probe is compatible with most requirements in shallow lakes and lake coastal areas where dissolved oxygen levels and their relationship to eutrophication are of concern.

It is relatively easy to obtain small devices to measure the light transmission through water at a single frequency. The output of such devices is inversely proportional to the absorptivity and reflectivity of particles in the water. This sort of information in several frequency bands can be used in conjunction with velocity, temperature, and dissolved oxygen to further study such things as the suspension and transport of materials in the bottom boundary layer, the extent of the boundary layer, the presence of turbid layers in the water column which may relate to oxygen take up or generation and so forth.

It is hoped that by the addition of these two sensing capabilities, correlations between physical, chemical and biological parameters in lakes may be found to further illuminate lake processes.

In the longer term, it is intended to develop a new generation GVAPS with a view to reducing the logistical requirements for its deployment and field support. Based on a review of mission goals, and improvements in electronics and in battery power sources, a fully submersible system of similar capability might be developed.

#### ACKNOWLEDGEMENTS

The author wishes to acknowledge the contributions of many from Engineering Services over the years, and the total team support extended by the Applied Physics and Systems Division and Technical Operations Division of NWRI in the development of GVAPS. The support of CSS SHARK during many field trials is also acknowledged.

#### REFERENCES

- Ward-Whate, P.M., 1977. A vertical automatic profiling system, Oceans '77 Conf. Record, p. 25B1-25B5, MTS-IEEE.
- White, B. 1980. EVAPS. Vehicle Handbook, ES 1086/1, NWRI, Unpublished.
- Hamblin, P.F. and R. Kuehnell, 1980. An evaluation of an unattended current and temperature profiler for deep lakes. Notes, Limnol. Oceanogr. 25(6), 1980, 1128-1141.
- Dessureault, J-G., J. Brooke, J.A. Elliott, 1982. The motion of a 9.1 m yacht hull buoy moored in open sea. Ocean Engineering, Vol. 9, No. 1, 1982, pp 65-97.



# ASPECTS OF THE INSTRUMENTATION, DEPLOYMENT AND PERFORMANCE OF 2.5 M DIAMETER WAVE-FOLLOWING METEOROLOGICAL DATA BUOYS

By R. E. W. Pettifer, M. J. Kerley and D. J. Painting

Meteorological Office, Bracknell, UK

## ABSTRACT

Over the past twelve years the Meteorological Office has been involved with the UK Directorate of Naval Oceanography and Meteorology in a programme of development, testing and deployment of two 2.5 m diameter toroidal wave-following data buoys and a 2.5 m diameter discus buoy.

This paper describes some of the problems addressed and the solutions developed for them in the realms of meteorological sensing, telecommunications, buoy deployment, mooring and maintenance.

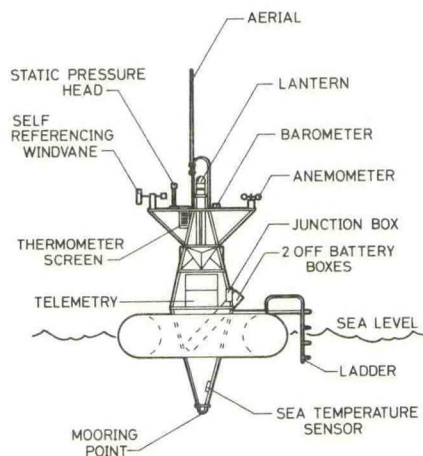


FIG. 1 THE 2.5 M DIA. TOROID BUOY, OBOE 1

## 1. INTRODUCTION

Over the past twelve years the Meteorological Office has been involved with the Department of Naval Oceanography and Meteorology in a programme of development and testing of two types of 2.5 m wave-following data buoys.

The two buoys we have used have been a fibreglass toroidal hull with a stainless steel tubular superstructure and shown in Fig 1 and, Fig 2, a Marex-type steel discus hull equipped with a 10m alloy mast.

Our present programme of development and operational deployment of ODAS grew from early attempts in which on-board data capture and a system life of a few weeks were acceptable. Present operational requirements are for real-time data capture and a minimum system life between service visits of six months.

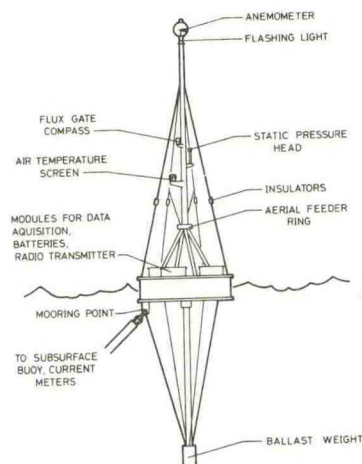


FIG. 2 THE 2.5 M MAREX-TYPE DISCUS BUOY

## 2. EQUIPMENT

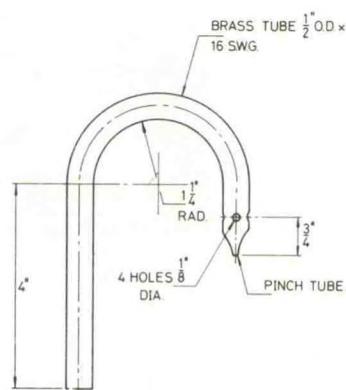
### 2.1 Power Supplies

In early work we employed, as the primary power source, lead-acid accumulators housed in brass cases. These accumulators gave insufficient power and were cumbersome to handle and were therefore abandoned. Air-depolarised batteries manufactured



by Le Carbone were tried but since the top of the buoy superstructure is only 2.5 m above the water, we experienced problems with water entering the battery containers through the vent pipe. We tried an alternative Le Carbone battery which did not require venting but these batteries did not meet the manufacturer's specification and failed after 2-3 months' deployment.

In spite of many attempts with alternative batteries of other types we were forced to return to air-depolarised cells and we eventually devised a technique for venting the batteries which has overcome the problem of the ingress of water. The vent tube was bent to form an inverted 'U', the end sealed and a number of small holes drilled around the perimeter of the tube for ventilation. This arrangement is shown in Fig 3: it has now been in continuous use for two years without failure on a buoy deployed in Lyme Bay.



VENT TUBE FOR AIR DEPOLARIZED  
BATTERIES

FIG. 3

The batteries are mounted in shallow glass fibre boxes about 47 cm x 13 cm x 161 cm with a neoprene rubber gasket seal beneath a flat lid which is retained by bolts screwed into captive nuts retained in the edge of the wall. The vent pipe is led through one end of the box and the power connections through the other via waterproof plugs and sockets. The boxes are then retained end-on in stainless-steel cages, partly below the waterline of the buoy for which they help to provide ballast (Fig 1).

The primary batteries, which are non-rechargeable and are replaced every six months, charge Nickel-Cadmium secondary batteries which provide a stable voltage source for the electronics.

## 2.2 Sensors

Our buoys are designed principally for meteorological purposes and the only oceanographic measurement which we regularly make is sea temperature. Considerable difficulty has been experienced in the quest for a satisfactory set of sensors and some of

these are discussed here. A more complete account has been given by Pettifer (1).

### 2.2.1 Wind Measurements

After testing several types of anemometer and wind vane we have settled upon the Porton Anemometer and Vane manufactured by Vector Instruments (Fig 4) and these have been used in our marine systems for the past six years with considerable success. They consume little power and in spite of their frail appearance have proved exceptionally reliable at sea for periods in excess of eight months. They have the great advantage of being lightweight and are therefore easily handled on board the buoy by service technicians who, by the use of quick-release clamps, can easily change either an anemometer or a vane whilst standing on the buoy hull.

The self-referencing version of the Porton wind vane has been found to be particularly useful since it overcomes the problem of alignment on the buoy and avoids the difficulty of interfacing vane readings with simultaneous compass readings.

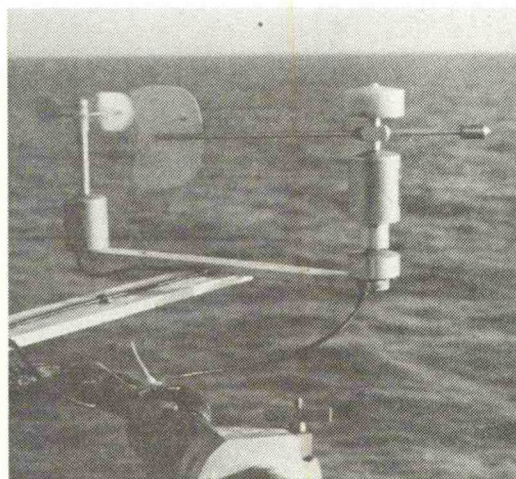


FIG. 4 THE PORTON ANEMOMETER AND  
SELF-REFERENCING WIND VANE

The performance of the wind sensors on the Lyme Bay ODAS is shown in Figs 5 and 6. Figure 5 shows a comparison between the wind direction measured on the buoy and, with a different type of sensor, at the Royal Naval Air Station (RNAS) Portland which is onshore about 2 miles north of the buoy location. In view of the considerable differences between these two sites the agreement between the two sets of data is very good. An equivalent wind speed comparison is shown in Fig 6 and the close agreement between the two instruments is clear. It is notable that the Portland measurements were made at the standard WMO exposure height of 10 m whereas the buoy anemometer and vane are only 2.5 m above the buoy deck level. This point is discussed more fully in Section 3.



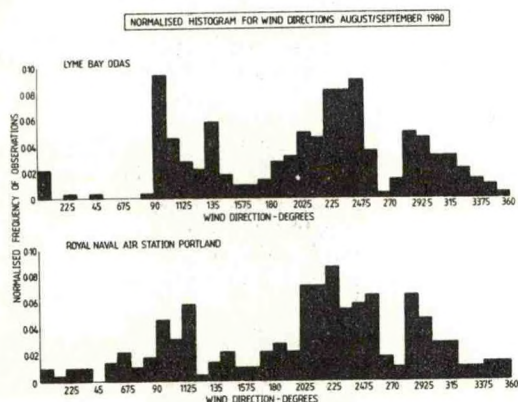


FIG. 5 COMPARISON OF WIND DIRECTION MEASURED ON OBOE IN LYME BAY AND THE ROYAL NAVAL AIR STATION PORTLA

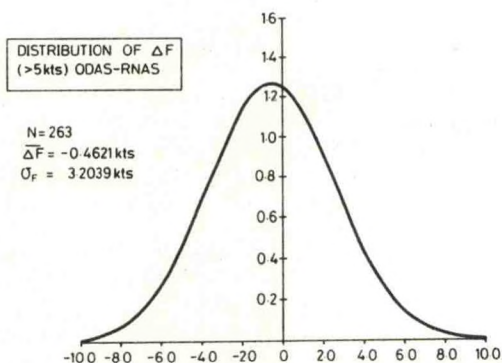


FIG. 6 COMPARISON OF WIND AND SPEED ON OBOE 1 IN LYME BAY AND THE ROYAL NAVAL AIR STATION PORTLAND

## 2.2.2 Pressure Measurements

Automatic pressure sensors suitable for use on buoys are mainly aneroid devices. Such devices may be made of a variety of metals but most of them have large temperature coefficients and a non-linear response. On some buoys, the temperature problem can be reduced by installing the device below the water line where the temperature range to which it is subjected is quite small, however even then temperature effects can be troublesome. For this application we have experienced considerable difficulties with commercially available pressure sensors, mostly associated with power consumption, calibration instability and radio frequency interference. However, a diaphragm pressure sensor, manufactured by Rosemount Inc., suitably packaged as shown in Fig 7, has been in satisfactory

operation on the Lyme Bay ODAS since mid 1980 and has since been introduced on several other of our marine systems. Its advantages are its high degree of tolerance to the mechanical shocks involved in buoy deployment and operation, freedom from RF interference, a negligible temperature coefficient between 5°C and 40°C and low power consumption.

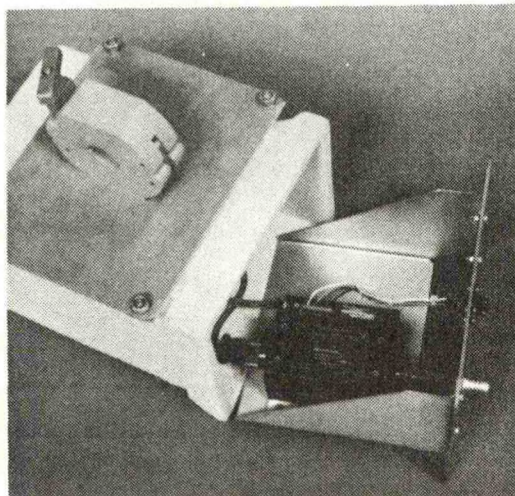


FIG. 7 THE ROSEMOUNT PRESSURE SENSOR AND ITS PACKAGE FOR OBOE 1

On ODAS it is not easy successfully to expose pressure sensors to the free, static air pressure and at the same time protect them properly from the effects of salt water. It is not satisfactory merely to connect the package to a simple vent tube, open to the atmosphere, because venturi effects will then result in quite incorrect results.

We have developed a static pressure head with no moving parts which is manufactured from plastic and is therefore suitable for use at sea. The head is connected by a simple pipe to the input port of the pressure sensor and is clamped to the buoy superstructure in a position exposed to the free air-stream. It is our experience that the design of such a static pressure head requires very careful optimisation if large pressure errors are to be avoided at high wind speeds. Some aspects of the performance of our static pressure head have been discussed by Foot et al (2). This design of static pressure head is now made under licence by Marex Ltd and is available from them.

Figure 8 shows the mean difference of reported pressure from RNAS Portland Meteorological Office and ODAS 2. During the period investigated, August-September 1980, wind speeds up to 25 kn occurred. For a pressure sensor mounted on a buoy which may be rising and falling by up to 10m or more it is difficult to establish a datum about which pressure readings are referred - usually accepted as mean sea level. Thus, the best that can probably be done is to sample the pressure over a period of time and compute some mean value from the readings



obtained. Sampling should preferably be at random intervals to avoid the possibility of coinciding with a particular wave period.

Although we do not go to the lengths of random sampling, we are confident that we can measure pressure reliably and consistently to better than  $\pm 1$  mb. Although this is only half the accuracy called for by the WMO guidelines, where there are no alternative sources, data of this quality are of very real value at least to the synoptic meteorologist.

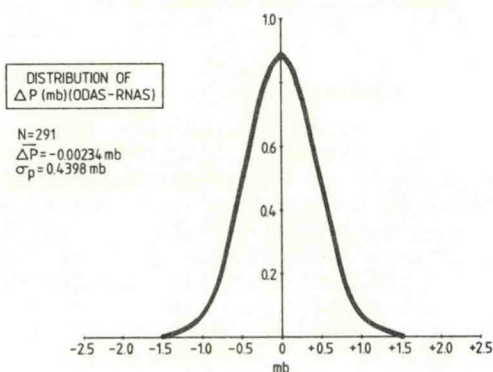


FIG. 8 COMPARISON OF PRESSURE MEASUREMENTS ON OBOE 1 AND THE ROYAL NAVAL AIR STATION PORTLAND

### 2.2.3 Humidity Measurements

Our work in this area has concentrated upon the use of hygroscopic polymers deposited on a plate and used as a substrate for a set of interleaved electrodes between which either the electrical resistance or capacitance is measured. There are several such sensors but the two with which we have had most success have been the PCRC-11 and the Vaisala Humicap. Salt is the major enemy and this type of sensor must have its surface protected from salt particles but, of course, must still be exposed to the ambient humidity. To achieve this we have adopted two techniques. The first is simply to enclose the sensor in an envelope of cellulose acetate attached to a frame into which the sensor is mounted. This arrangement is shown in Fig 9a and has been used with considerable success both on the UK National Data Buoy DB1 and on our 2.5 m buoy in Lyme Bay. The lifetime of these sensors protected this way has exceeded the routine service interval on both buoys.

The disadvantage of this technique is that the time constant of the PCRC when protected in this way is excessive, particularly at low temperatures (1). To overcome this difficulty a method was devised which enables us to deposit a film of cellulose

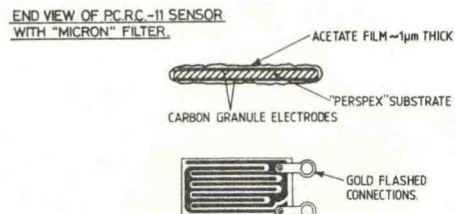
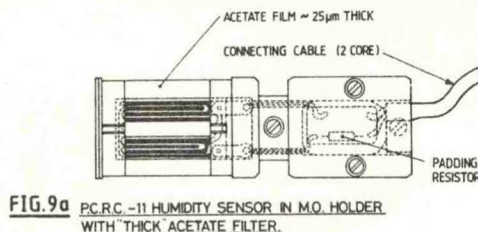


FIG.9b PCRC-11 HUMIDITY SENSOR.

acetate a few  $\mu\text{m}$  thick directly onto the sensor surface (Fig 9). Provided this film is free from pinholes it effectively prevents salt crystals from attacking the polymer, allows the water vapour to pass through to the sensor, does not affect the electrical resistance of the device and reduces the time constant to levels which are acceptable for synoptic meteorology. The accumulated salt can be successfully washed off the surface of the film without damage to the sensor. A device of this type was in constant use on the ODAS on Muckle Holm Island (Shetland) for two years and proved very successful. The difficulty of actually depositing the film on the sensor, however, made this method unattractive for routine use and we have now developed (3) a further technique in which the sensor is covered with a commercially-available PTFE-based fabric known as GORTREX. This fabric is obtainable in a variety of pore sizes and we have had good results with pores  $\sim 0.02 \mu\text{m}$  diameter. However, we may not as yet have optimized this parameter.

In order to expose the PCRC sensor and the standard electrical resistance thermometers which we use on ODAS for measuring air temperature we have developed a fibreglass radiation screen shown in Fig 10. The screen is fixed to the buoy superstructure by quick-release stainless-steel clamps at a point as far away from the effects of wave-splash as possible. The screen itself requires no maintenance apart from the routine removal of salt deposits but for simplicity a change of sensors is accomplished by changing the entire screen. This screen is made under licence by Marex who have recently also begun to manufacture the entire buoy electronics package and the shore station equipment required to interrogate it.

### 2.3 Data Recovery

Data recovery methods on our buoys are conventional. The inshore, toroidal buoys carry standard VHF transmitters and transmit at pre-timed intervals or on demand signalled by receipt of a telemetry tone sent by the shore station. This tone may be



generated by an operator at a remote teleprinter connected to the shore station by the public telephone network. These buoys do not carry on board microprocessors and the data are transmitted in engineering units. An on-line processor may be included in the shore station. The discus buoys, used at much greater distances from shore, carry either HF Piccolo systems or a DCP operating to one of the geostationary satellites. These buoys have on-board microprocessors and transmit in WMO meteorological code for direct insertion into the GTS.

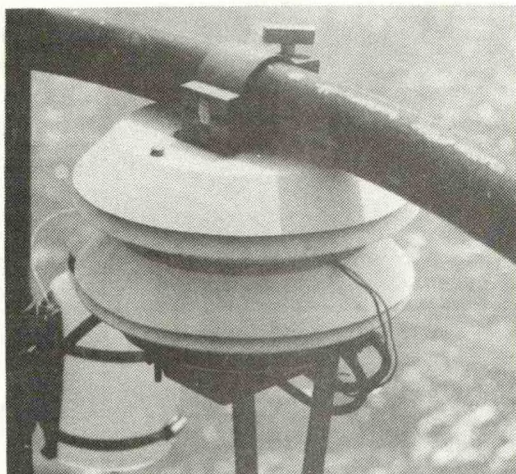


FIG. 10 THE ODAS RADIATION SCREEN

#### 2.4 Mooring and Deployment

The mooring methods we have used with 2.5 m buoys have depended mainly upon the location of the buoy site and its associated water depth. So far all our moorings have been of the single-point variety. Although the buoys successfully withstood mean winds of up to 45 kn, we have suffered mooring failures due to corrosion of a Tellurit compression fitting on a steel rope, inaccurate depth surveys in shallow tidal water which led to the buoys drifting onto mud banks at low tide, and abrasion at the clump weight fixing point due to lack of compliance in the system. The most frequent source of failure, however, has been damage from trawl wires which has resulted in the complete loss of one open ocean buoy which was cut adrift and eventually wrecked.

For shallow, inshore water deployments of the 2.5 m diameter toroid, we now use the mooring shown in Fig 11 which is of 18mm chain, 60m of which lie on the sea bed to give the necessary compliance to the rig. This mooring has survived mean winds of up to 60 kn in a continuous 18-month deployment. For our next open ocean deployment, due this month, we will use a type of three-point mooring which consists of a swivel attachment point on the buoy to which are shackled three lines, symmetrically placed around the buoy axis. The lines are combinations of 12 mm chain and 44 mm polypropylene rope. The mooring depth is 170 m.

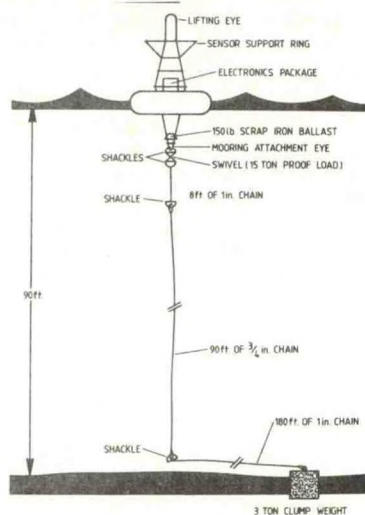


FIG. 11 THE LYME BAY MOORING

The most serious difficulty we have experienced with these deployments has been the damage caused to buoys and moorings by fishing vessels. This has extended to the complete removal of a buoy on one occasion and the total wreck of a buoy on another. Serious efforts are being made in Europe through agencies such as COST-43 to begin a campaign of education and co-operation aimed at overcoming this problem but success has been limited so far.

A lesson learnt from these experiences is that any but the most inshore buoys should carry an Argos location facility so that early warning is received that a buoy is off station and so that its subsequent movements can be monitored for recovery purposes.

### 3. THE REPRESENTIVITY OF DATA

However high the quality of the instrumentation used, however good its calibration, it is extremely easy to make poor meteorological measurements as a result of unrepresentative exposure. The World Meteorological Organization (WMO) lays down standard rules of exposure for meteorological instruments on land. However, to apply these to the case of ODAS can be both difficult and expensive and the question arises as to whether the rules are applicable to the case anyway.

For example, WMO regulations (4) state that the standard exposure height for wind instruments over level, open terrain is 10m. Clearly in the case of a data buoy the surface characteristics usually bear little resemblance to level terrain. Furthermore, the wind instrument is subject to change in level and to angle of attack on timescales comparable with the sampling interval required to generate say 10-minute mean values.

We believe that such effects may make the application of WMO exposure rules unrealistic and unnecessary for data buoys. This point has been discussed more fully by Fettiher (1) but by way of



illustration, Fig 12 shows the differences between the reported wind speeds from cup anemometers mounted at different heights above sea-level. These sensors were of different manufacture and on different buoys, a Norwegian semi-spar buoy and a Marex wave rider buoy, (Fig 2), moored about 2 km apart. The sensors were exposed at 2.5m and 10m respectively. Both sensors had previously been compared in the laboratory and the appropriate calibration corrections have been applied to these data.

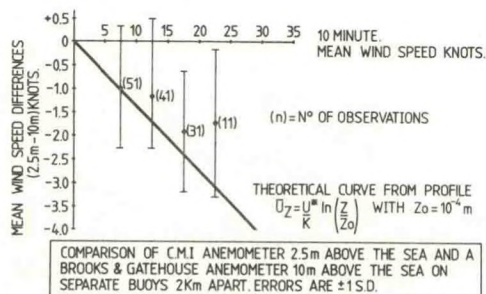


FIG. 12

It can be seen that the mean systematic difference is between 1 and 2 kn over the speed range 5-30 kn. At the high end of the range these differences are well below the expected value derived from the commonly-used logarithmic wind profile. This result is, perhaps, not surprising since no allowance is made for the errors in wind speed which arise from the motion of the buoy or from the dynamic characteristics of the sensors.

When all possible sources of error are taken into consideration, we believe that on a moored buoy we cannot expect to measure wind speed with confidence to better than 5 kn for speeds up to 30 kn irrespective of the exposure height of the sensor on the buoy. Furthermore, since the 10-minute mean sea-level is generally indeterminate for a buoy, it unnecessary for synoptic meteorological purposes, to expose wind sensors at heights approaching 10m on buoys. This is a very useful conclusion as it can lead to significant savings in capital costs of equipment during buoy design.

#### 4. CONCLUSION

We have concluded that given the present state of development of meteorological sensors, reliable and acceptably accurate measurements of wind speed, wind direction, temperature, humidity and pressure can be made automatically on moored ODAS of this type for continuous periods in excess of six months. The use of high (10m) masts for wind exposure is not required on these buoys and the general level of uncertainty in wind speed measurements made at about 2m above the (calm) sea is about  $\pm 5$  kn for

speeds up to 30 kn. For pressure the general level of uncertainty from these systems is about  $\pm 1$  mb provided the sensor is exposed through a carefully optimized static pressure head.

In general terms we have learnt that no sensor or system can be relied upon for use at sea unless it has been demonstrated to be reliable in that environment over periods comparable with the unattended operational period and that ease of handling, especially lightness and easy fixing, together with low power consumption are the most important physical attributes of a sensor given that it is meteorologically acceptable.

We believe that the high cost of adequate sea-bed surveys and the hire of vessels with suitable characteristics for buoy deployment are essential expenses which must be incurred if the risk of the loss of the capital investment in the buoy itself is to be reduced to acceptable levels. Equally, the cost of regular inspection of the ODAS mooring is an essential part of the routine maintenance burden which goes with operating such systems.

Finally, we are convinced that for every such deployment, other than very close inshore, the ODAS must be equipped with a satellite location beacon because, notwithstanding any care taken with the design and establishment of the mooring, the risk of the mooring being severed either deliberately or accidentally is very high.

#### 5. REFERENCES

1. Pettifer, R. E. W. 'Meteorological Sensors for Marine Systems' COST-43 Tech Doc No 46, Proc Seminar on ODAS and Related Topics, Bergen 1980.
2. Foot, J. S., Bond, F. S., and Pettifer, R. E. W. 'A Report on the Laboratory Comparison of Meteorological Sensors used on the Norwegian BS Buoy Trial at 60°N 5°W in Summer 1979' COST-43 Tech Doc No 38, Bergen 1980.
3. Clarke, C. S. and Painting, D. J. 'A Humidity Sensor for Automatic Weather Stations' Proc WMO/AMS/CMOS Fifth Symposium on Meteorological Observations and Instrumentation, Toronto 11-15 April 1983 (in press).
4. World Meteorological Organization Guide to Instrument and Observing Practices Fifth ed. 1981 §6.6 (in press).



# SENSITIVITY OF SURFACE WIND STRESS TO UNCERTAINTIES IN SENSOR OUTPUTS OF AN ATMOSPHERIC PROFILING SYSTEM

Fred A. Hilder

Naval Ocean Research and Development Activity  
Oceanography Division, OSTL  
NSTL Station, Mississippi 39529

## ABSTRACT

The sensitivity of the surface wind stress to uncertainties in the outputs of sensors in a proposed atmospheric profiling system is examined. Four sensors are assumed to be vertically deployed under a balloon in an unstable atmospheric surface layer over water. Typical heights above the water surface would be 3 m, 8 m, 20 m, and 50 m. A Gaussian random number generator is used to introduce rms errors in wind speed, temperature, and pressure. The rms error in wind stress is then calculated. As an example, using typical over-water values for wind speed and temperature under unstable conditions, for rms errors of 0.05 m/sec in wind speed, 0.01°C in temperature, and 0.05 mbar in pressure, the rms error in wind stress is 0.26 dyn/cm<sup>2</sup>. The importance of precision in an atmospheric profiling system is apparent.

## 1. INTRODUCTION

An atmospheric profiling system has been designed to determine the surface wind stress over the ocean. The wind stress is needed to determine the dependence and temporal variability between surface wind stress and microwave emissivity from the ocean. The profiling system is designed to simultaneously sample air temperature and wind speed at four different heights. The data set is transmitted continuously via an RF link to a receiving set where it is reproduced as analog output voltages. The proposed deployment of the system is shown in Figure 1. We believe we will fly the balloon at about 100 m, with the highest sensor at 50 m and the lower three at 20, 8, and 3 m.

An accuracy of 0.2 dyn/cm<sup>2</sup> in absolute wind stress determination is desired<sup>1</sup>. The specific question addressed in this paper is the sensitivity of the surface wind stress over water to uncertainties in the sensor outputs. In our profiling system, all four sensors output wind speed and air temperature. Additionally, the highest sensor outputs atmospheric pressure as a height determination. The heights of the lower three instruments are obtained by subtracting their distance along the tether line.

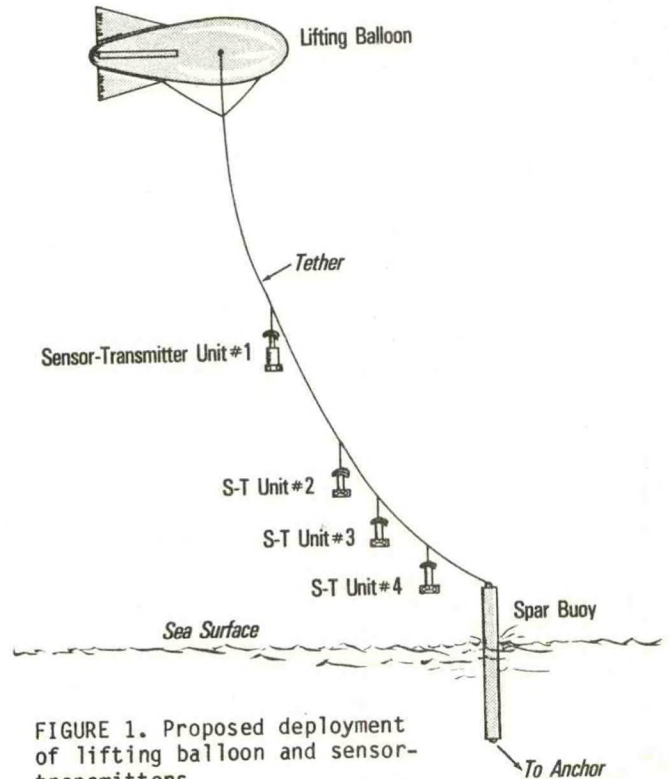


FIGURE 1. Proposed deployment of lifting balloon and sensor-transmitters.

## 2. PROCEDURE

The mathematical representation of the wind speed and temperature profiles follows the work of Paulson<sup>2</sup>. The basis for the representation is the similarity hypothesis of Monin and Obukhov. It is used to describe the mean wind speed and temperature as a function of height in the atmospheric surface layer. This layer is defined as the layer near the earth's surface in which the turbulent fluxes are approximately constant with height.

The basic equation to determine tangential wind stress is

$$\tau = \rho u_*^2 \quad (1)$$



where  $\tau$  is the tangential wind stress,  $\rho$  is air density, and  $u_*$  is the friction velocity. From the similarity hypothesis, we have

$$u = \frac{u_*}{k} [\ln(z/z_0) - \psi] \quad (2)$$

where  $u$  is the mean wind speed at some height  $z$ ,  $k$  is van Karman's constant,  $z_0$  is the roughness length, and  $\psi$  is the integrated nondimensional wind speed gradient. Eq. (2) may be written in the form

$$u = (u_*/k)(\ln z - \psi) - (u_*/k)\ln z_0 \quad (3)$$

Hence, if our representation is correct, observations of  $u$  plotted vs.  $(\ln z - \psi)$  will be linear. A straight line fit by the method of least squares to  $u$  vs.  $(\ln z - \psi)$  should yield an estimate of  $u_*$  and  $z_0$ .

As an example (Fig. 2) we have  $u$ , mean wind speed in m/sec, as the ordinate and  $(\ln z - \psi)$  as the abscissa with four data points and a least squares fit through the data.

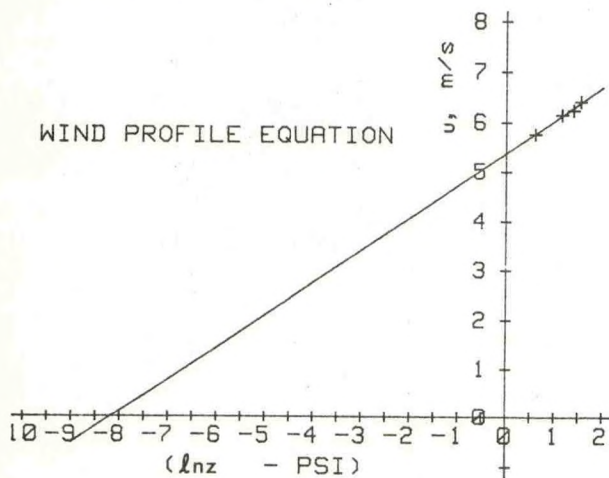


FIGURE 2. Mean wind speed ( $u$ , m/s) vs.  $(\ln z - \psi)$  with least squares fit to four data points.

Returning to Eq. (3), we have the factor  $\psi$ , which must be determined. We assume unstable conditions and from Paulson<sup>2</sup>

$$\psi = 2\ln[(1+x)/2] + \ln[(1+x^2)/2] - 2\tan^{-1}x + \pi/2 \quad (4)$$

where

$$x = (1 - 16 z/L)^{1/4} \quad (5)$$

In this development,  $L$  is the Monin/Obukhov length,  $z$  as before is the height and  $z/L$  is the gradient Richardson number,  $Ri$ . By definition,

$$Ri = (g/T)[\partial\theta/\partial z]/(\partial u/\partial z)^2 \quad (6)$$

where  $g$  is the acceleration of gravity,  $T$  is the mean temperature,  $\partial\theta/\partial z$  is the temperature gradient, and  $\partial u/\partial z$  is the wind speed gradient.

We face a problem in obtaining these gradients, i.e., the partial derivatives of the temperature and wind speed with respect to height, as the exact equations are not known. In fact, the equation of the wind speed with respect to height is what we are trying to determine. Paulson<sup>2</sup> uses an approximation method to determine these partial derivatives. He obtains thereby one gradient Richardson number which is applicable at the geometric mean height of the observation levels. For profiling systems with a maximum height of 10 m, e.g., on masts at sea, the error is probably not significant when compared to the uncertainty of the profile formulas. With our system having the highest sensor at 50 m, we used typical equations for temperature and wind speed vs. height. Specifically,

$$u = A \ln z + B z^{1/2} + Cz + D \quad (7)$$

$$\theta = Ez - 1/2 + F$$

where  $A$ ,  $B$ ,  $C$ ,  $D$ ,  $E$ , and  $F$  are constants to be determined by least squares fit to data. The partial derivatives  $\partial u/\partial z$  and  $\partial\theta/\partial z$  are then determined and the Richardson numbers obtained at each height.

As mentioned previously, the highest sensor outputs atmospheric pressure in addition to wind speed and air temperature. This pressure, when compared to surface pressure, is used to determine the height of the highest instrument. First, the recorded temperatures were converted to virtual potential temperatures using the dry adiabatic lapse rate and a moisture correction<sup>3,4</sup>. A relative humidity of 75% was assumed. Then, using the hydrostatic equation and the equation of state, the height of the highest sensor was determined. The ten revised mean data points (four temperature, four wind speed, and two pressure) are then used in a nonlinear least-squares program<sup>5</sup> to obtain the wind stress.

We now concern ourselves with the accuracy of the result. The sensors will have, of course, some instrument error. We introduce an error in temperature, wind speed or pressure, or in combination. The errors were Gaussian distributed by central limit theorem<sup>6</sup> in conjunction with the random number generator of the Hewlett-Packard 9826 computer system. (All the programming was done on the



HP 9826 (BASIC) computer system). Twenty-five runs were made for each error analysis. The mean, variance, and standard deviation of the wind stress were obtained. Results are shown in Tables 1 and 2.

### 3. RESULTS AND CONCLUSIONS

In Table 1 we show the resulting rms error in shear stress when an rms error is introduced in wind speed or air temperature at each sensor. No error is introduced in pressure, so the sensor heights remain fixed. The rms errors of 0.05 m/s in wind speed and 0.15°C in air temperature result in an rms error in shear stress just within the desired 0.2 dyn/cm<sup>2</sup> accuracy. A combined rms error of 0.05 m/s in wind speed and 0.01°C in air temperature results in an rms error of 0.23 dyn/cm<sup>2</sup> in shear stress.

In Table 2 we introduce errors in the pressure at the highest sensor. It should be noted that 1 mbar represents approximately 10 m in height. It is seen that the combined rms errors of 0.05 m/s in wind speed, 0.02°C in air temperature and 0.05 mbar in pressure result in an rms error of 0.26 dyn/cm<sup>2</sup> in shear stress.

The importance of precision in an atmospheric profiling system is apparent.

### REFERENCES

1. Goodman, R., J. Bailey, J. Gallagher, R. Kirk, R. Nagle, V. Noble, A. Pressman, and K. Van Sickle, Oceanographic remote sensing; a position paper. Naval Ocean Research and Development Activity, NSTL Station, Miss., 1979, 24 pp.
2. Paulson, C. A. The mathematical representation of wind speed and temperature profile in the unstable atmospheric surface layer. *J. Applied Meteor.*, 1970, 9:857-861.
3. Hess, S. L. An introduction to theoretical meteorology. Henry Holt & Co., N. Y., 1959, 362 pp.
4. Cardone, V. J. Specification of the wind distribution in the marine boundary layer for wave forecasting. New York Univ. Geophys. Sci. Lab. Rpt. TR-69-1, 1969, 137 pp.
5. Lybanon, M. Nonlinear least squares curve fit program. Computer Sciences Corp., NSTL Station, Miss. (unpublished), 1980.
6. Ruckdeschel, F. R. BASIC scientific subroutines, Vol. 1. Bytel/McGraw-Hill, Peterborough, N.H., 1981, 316 pp.

TABLE 1. Error (rms) in shear stress after 25 calculations using random Gaussian inputs. Data Set #1\*.

Wind Speed m/s	Introduced rms error Temperature °C	Pressure mbar	Resulting rms error in shear stress dyn/cm <sup>2</sup>
0.01	0	0	0.04
0.03	0	0	0.10
0.05	0	0	0.18
0.075	0	0	0.23
0.10	0	0	0.33
0	0.01	0	0.01
0	0.025	0	0.04
0	0.05	0	0.07
0	0.10	0	0.16
0	0.15	0	0.19
0.05	0.01	0	0.23

\*Sensor heights: 49.2 m, 8 m, 4 m, 2 m. (Temperature uncertainties do not significantly affect height of sensor #1.) Wind stress with basic data is 1.10 dyn/cm<sup>2</sup>.

TABLE 2. Error (rms) in shear stress after 25 calculations using random Gaussian inputs. Data Set #2\*.

Wind Speed m/s	Introduced rms error Temperature °C	Pressure mbar**	Resulting rms error in shear stress dyn/cm <sup>2</sup>
0	0	0.15	0.44
0	0	0.30	1.00
0.05	0.01	0.05	0.26
0.05	0.1	0.05	0.44
0.1	0.01	0.1	0.58

\*As uncertainties in the pressure are introduced, the height of the highest sensor varies in each calculation. The distance between sensors remains constant. Wind stress with basic data is 1.60 dyn/cm<sup>2</sup>.

\*\*0.1 mbar equates to about 1.0 m in height.



# COMPARATIVE SPECTRUM ANALYSES OF SURFACE WIND STRESS FIELDS BASED ON NDBC WINDS AND FNOC ANALYSES

by Michele M. Rienecker  
and  
Christopher N.K. Mooers

Department of Oceanography  
Naval Postgraduate School  
Monterey, CA 93940

Time series of surface winds from three NDBC buoys and two neighboring FNOC grid points in the Northeast Pacific are used to estimate time series of the wind stress for summer and winter regimes during 1977 to 1979. Through autospectral and cross-spectral analysis, a comparison of these wind stress series is made in the frequency domain. The energy levels of the FNOC autospectra are significantly higher than those of the spectra of a nearby buoy; however, the FNOC spectra are closer in energy level to the spatial average of the buoy spectra. Overall, the spectral shapes are similar. For periods longer than 10 days, the spectra from the FNOC analyses are shown to be coherent with spatially-averaged spectra of buoy data. In the short-period storm band, 3-to-10-day period, the FNOC spectra and buoy spectra of the wind stress components show moderate coherence.

## 1. INTRODUCTION

Surface wind analyses from Fleet Numerical Oceanography Center (FNOC) have been available on a coarse grid for more than a decade. These analyses have been used by oceanographers and meteorologists to estimate variables that are directly related to the atmospheric forcing of the ocean. In particular, the wind stress and wind stress curl are often calculated because of their relation to surface Ekman transports and Ekman suction/pumping, respectively. Since dense observational data sets are usually not available to provide estimates of these quantities, it is important to know how representative any analyses are of actual surface winds.

A comparison of winds computed by the National Marine Fisheries Service, using the FNOC pressure analysis, with those measured by buoys near the British Columbia Coast [5] shows that the computed winds are representative of measured winds only for periods longer than two days. Such a comparison should also be made for the FNOC analyses; previously only limited time domain comparisons have been made of the FNOC wind analyses with time series of wind observations north of 20°N [2]. A comparison of FNOC wind fields with data from buoys in the equatorial region has been made in the frequency domain [4] and statistically significant coherence was found only for signals with periods longer than 10 days. However, it is expected that the former FNOC analyses will be more representative of the wind fields of mid-latitude regions; the quality of these analyses needs to be checked

for more than one location and season. A convenient way to perform this cross-check is through spectrum analysis from which the time scales over which the FNOC wind analyses accurately represent the observed wind field may be determined. This paper explores, through a comparison of pressure and wind stress series as a function of frequency, the observations from three NDBC buoys and two FNOC grid points located in the Northeast Pacific, as shown in Figure 1.

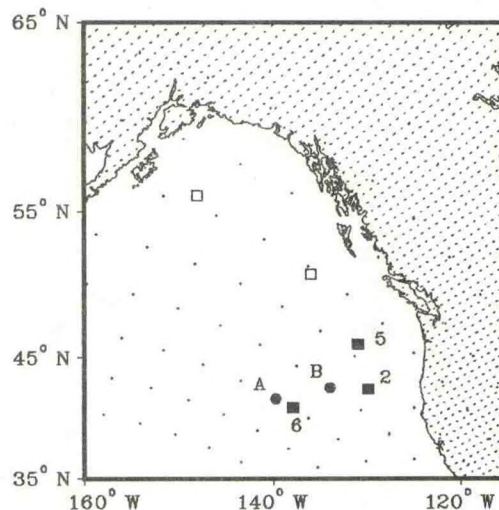


Figure 1: The locations of offshore NDBC buoys and FNOC grid points in the Northeast Pacific. The FNOC points (A and B) used in this analysis are indicated as ●, the buoys 46002 (denoted 2), 46005 (5) and 46006 (6) are shown as ■.

## 2. DATA PROCESSING AND ANALYSIS

The NOAA Data Buoy Center (NDBC) operates several Deep Ocean Moored Buoys in the Northeast Pacific. Three of these buoys, 46002 (at 42.5°N, 130°W), 46005 (at 46°N, 131°W) and 46006 (at 41°N, 138°W), are chosen for this analysis because of their simultaneous continuous records for summer and winter regimes in the time frame of January, 1977 to December, 1979. The moorings were initially 10m discus buoys, 46005 being replaced by a 12m discus buoy in August, 1978 and 46006, similarly, in August 1979. For these buoys, the wind and pressure sensors are located at approximately 10m



above the water and have an accuracy of 1mb (in a range 900 to 1000mb) in pressure, 1m/s (in a range 0 to 80 m/s) in wind speed and 10° (in a range 0 to 360°) in wind direction. The data are sampled every 1/8 sec and averaged over 8.5 min. An edited copy of three-hourly data which had been archived at the National Climatic Center (NCC) was provided by the Navy Detachment at NCC. Six-hourly values were extracted from the data set to compare with the six-hourly FNOG analyses.

FNOG provided pressure fields from their operational analysis and the global band analysis winds, which are calculated from the pressure fields using a gradient wind balance. The analyses are provided on a 63x63 grid on a polar stereographic projection of the Northern Hemisphere. The projection is true at 60°N, where the grid spacing is 381km, and the x-coordinate origin coincides with 80°W.

For comparison with the 10m buoy data, the FNOG winds, which are calculated at a height of 19.5m, are adjusted to the 10m level by an iterative scheme using a neutral flux-profile relationship [1]. The winds are also referenced to the north-south, east-west coordinate frame of the buoy winds. The pressure is adjusted to surface level, where the buoy data are provided, using the hydrostatic approximation.

Although buoy data are included in the FNOG analyses, they are blended with a "first-guess" field and ship observations. Here, these two wind series are considered to be quasi-independent. (There is a question as to whether or not the buoy winds which influenced the FNOG analyses during the years of this study were adjusted from the correct anemometer height to 19.5m (J. Kaitala, personal communication); further, it is not known whether or not the buoy data were included in the analyses since documentation of the data used is not available. Work is progressing at FNOG to upgrade the manner in which the buoy data influence the current analyses to reflect fully the quality of the buoy observations.)

The two FNOG points high-lighted in Figure 1 are chosen for the spectral analysis: one, denoted A, is closest to buoy 46006 which has relatively few missing data values for the three summers from 1977 to 1979; the other, denoted B, is chosen as a common point of comparison with the three buoys. Since the FNOG analysis is performed on a coarse grid, its results may be more representative of spatially averaged data and so a higher coherence with the average of the three buoys would be expected than in a comparison with a single buoy.

The time period May to July (Julian days 121 to 211) is chosen as being representative of a summer regime and 'uninterrupted' data (with gaps no longer than one day) are available for the three years for buoy 46006 and for 1978 and 1979 for 46002 and 46005. The winter regime is represented as November to January (Julian days 305 to 365 and 1 to 31) and 'uninterrupted' data are available for 1977/78 and 1978/79 for 46002 and 46005 and for 1977/78 for 46006. Unreasonable data values are removed from the file and any missing value is estimated by

linearly interpolating between the data values preceding and following the missing point. The wind stress is calculated according to the formula

$$\tau = c_D \rho |u| u,$$

where  $u$  is the velocity in m/s,  $\rho$  is the air density, taken as 1.225 kg/m<sup>3</sup>, and  $c_D$  is the drag coefficient chosen, according to [3], as

$$c_D = (0.75 + 0.067|u|) \times 10^{-2},$$

to give the stress in dyn/cm<sup>2</sup>. The spectral analysis is performed on the data with the mean and any trend removed. A cosine (Hanning) time weighting is applied to each time series before the fast Fourier transform is applied. The spectral estimates are averaged over three consecutive estimates and, in addition, ensemble-averaged if more than one realization (either from another year or another buoy, or both) is available. Hence, the minimum number of degrees of freedom available is 15 and the bandwidth is .08 cpd. The bandwidth does not change with ensemble-averaging.

### 3. RESULTS

Time series plots of the variables of interest reveal that fluctuations in the FNOG fields tend to be stronger than for the buoys. Even for the pressure field there are quite often differences of 10mb or more. Sample time series, with mean and trend removed, for buoy 46006 and FNOG point B during the 1977/78 winter are plotted in Figure 2. Time series (not shown) for a summer regime are similar, with the magnitudes of the fluctuations being smaller. Generally, the FNOG series lag those of the buoy by a few hours, sometimes more, which is consistent with the predominant propagation velocity of weather systems; the fields are more closely synchronized in summer. Apart from this phase difference, the sign of  $\tau_x$  and  $\tau_y$  (the stresses in the east-west and north-south directions, respectively) are usually the same, with the FNOG stresses generally larger.

Comparison of the plots of the summer autospectra for FNOG point A and buoy 46006, each ensemble-averaged over three years, and the plots for FNOG point B with the average of the three buoys, each ensemble-averaged over two years, show that spatial averaging, as expected, gives closer agreement between the two series, especially at the lower frequencies.

For the former case, shown in Figure 3, the spectral shape is sometimes different; this is particularly noticeable for the stress components at the lower frequencies. In the autospectral plots,  $\tau_x$  has been offset from its true value by one decade and  $\tau_y$  by three decades. The energy levels of the FNOG spectra are higher than those for the buoy. The pressure spectra could be considered to agree within their 95% confidence bands and are virtually identical at about 0.1cpd; however, the FNOG stress components most often have between three to ten times more variance at any frequency. For this point comparison, the coherence for the pressure is fairly high except at the highest frequencies. There is moderately significant coherence for  $\tau_x$  and  $\tau_y$  for periods of 3 to 10 days. Although for



$\tau_x$  there is high coherence at the 3-day period, where there is likely to be a strong, well-organized signal, except for this isolated frequency, the coherence tends to degrade to being not significantly different from zero for periods shorter than 5 days.  $\tau_y$  is coherent for all of the short-period storm band. For frequencies higher than 0.3cpd there are fewer coherent peaks for the stress than there were for pressure. There are generally large phase fluctuations at higher frequencies.

For the spatially averaged case in the summer regime, Figure 4, the autospectra are closer in energy and closer in shape at the lower frequencies. The spectra very nearly agree to within the 95% confidence band except for the noticeable differences in the short-period storm band. The coherence is higher for disturbances in the long-period storm band, 10-to-30 days, but it is lower in the short-period storm band than for the previous point comparison. The coherence for both  $\tau_x$  and  $\tau_y$  is low in the short-period storm band.

For the winter regime, Figure 5, when there is stronger variability in the fields, there is close agreement in the spectra for frequencies higher than 0.2cpd when FNOC point B is compared with an average over the three buoys; although there is still statistically significant differences in the energy levels for  $\tau_x$  and  $\tau_y$  at the lower frequencies. There are some very significant coherence peaks in the short-period storm band. The coherence for  $\tau_x$  again degrades at the higher frequencies in the short-period storm band; but for pressure and  $\tau_y$ , the coherence is higher at the high frequencies than was the case for summer.

#### 4. SUMMARY

Comparison, by cross-spectral analysis, of FNOC time series of pressure with those of three NDBC buoys reveals significant coherence at all but the highest frequencies. The coherence is significant for a wider band of frequencies in the spatially-averaged comparison than for the point comparison. For  $\tau_x$  and  $\tau_y$ , the FNOC spectra are more representative of a spatial average of the buoy spectra for the low frequencies. The coherence degrades more quickly with increasing frequency in this spatial average comparison than for the point comparison. In the short-period storm band, the FNOC stresses show moderate coherence with the stresses from a nearby buoy. At higher frequencies, the two series are only moderately coherent for isolated frequencies at which strong, well-organized signals may be expected. If high frequencies are simplistically associated with high wavenumbers, this lack of coherence may be associated with sub-grid scale variability which FNOC analyses cannot resolve and which the spatial average of the buoy spectra suppresses. The coherence for  $\tau_x$  degrades at high frequencies more rapidly than for  $\tau_y$  and this could have an impact on the quality of wind stress curl calculations and their comparisons. In 1982, FNOC changed its analysis model; the current wind analyses should also be evaluated if used to provide atmospheric forcing variables.

#### 5. ACKNOWLEDGEMENTS

We are grateful to Dr. R. L. Haney from the Meteorology Department at NPS for his comments and for kindly providing some six-hourly FNOC analyses

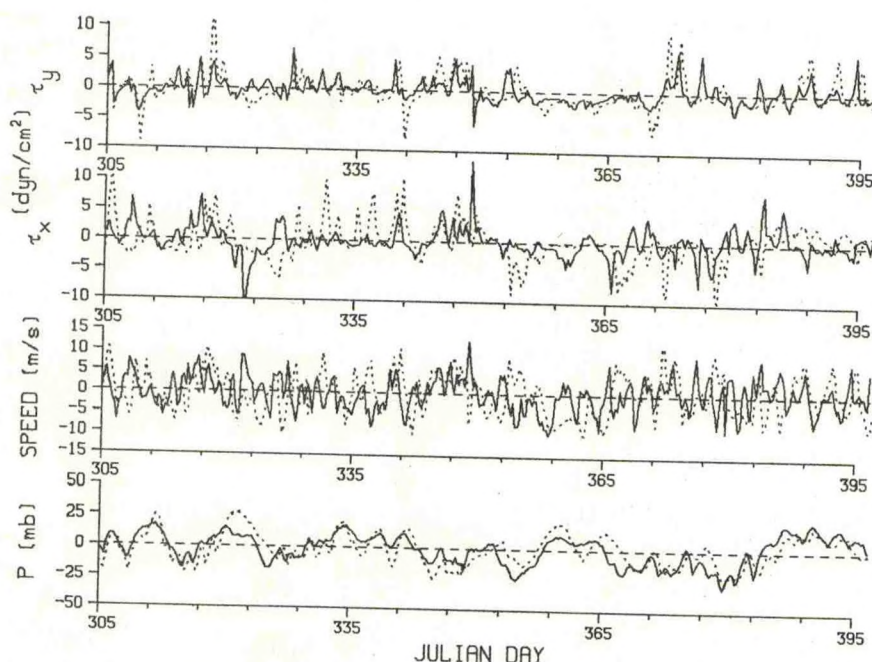


Figure 2: Time series plots of pressure, wind speed and stress components, with mean and trend removed, for FNOC point B, ..., and buoy 46006, —, during the 1977/78 winter regime.



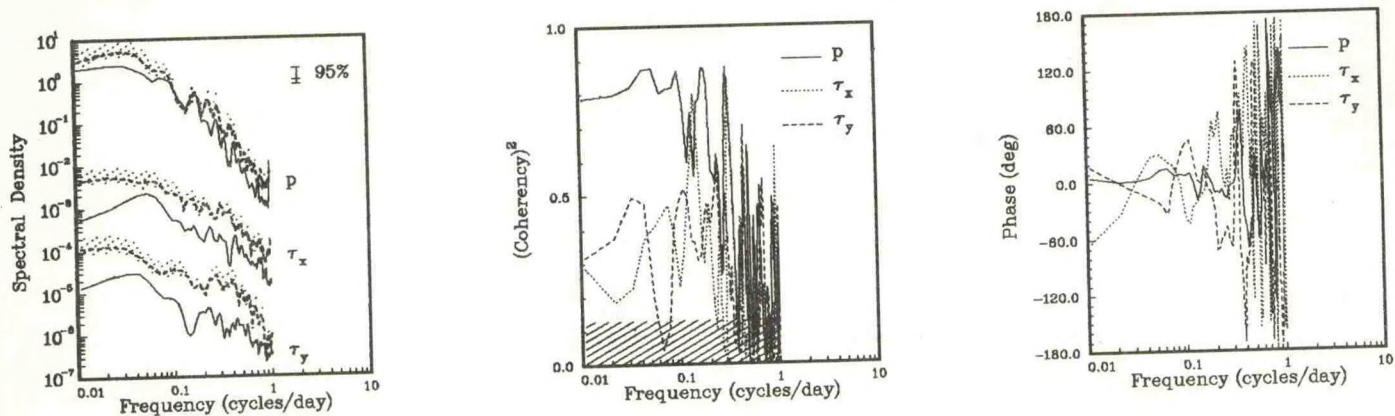


Figure 3: Comparison of FNOc point A and buoy 46006 in a summer regime through autospectral plots (---- FNOc and — buoy), (coherency)<sup>2</sup> and phase. The estimates are ensemble-averaged over 1977 to 1979. In the first diagram, the speckled region indicates the 95% confidence band for the FNOc autospectral estimates. There are 45 degrees of freedom. The units for the autospectra are:  $p$ , (mb)<sup>2</sup>/cpd;  $\tau_x$  and  $\tau_y$ , (dyn/cm<sup>2</sup>)<sup>2</sup>/cpd. Outside the cross-hatched region in the second diagram, the (coherency)<sup>2</sup> is non-zero with 95% confidence.

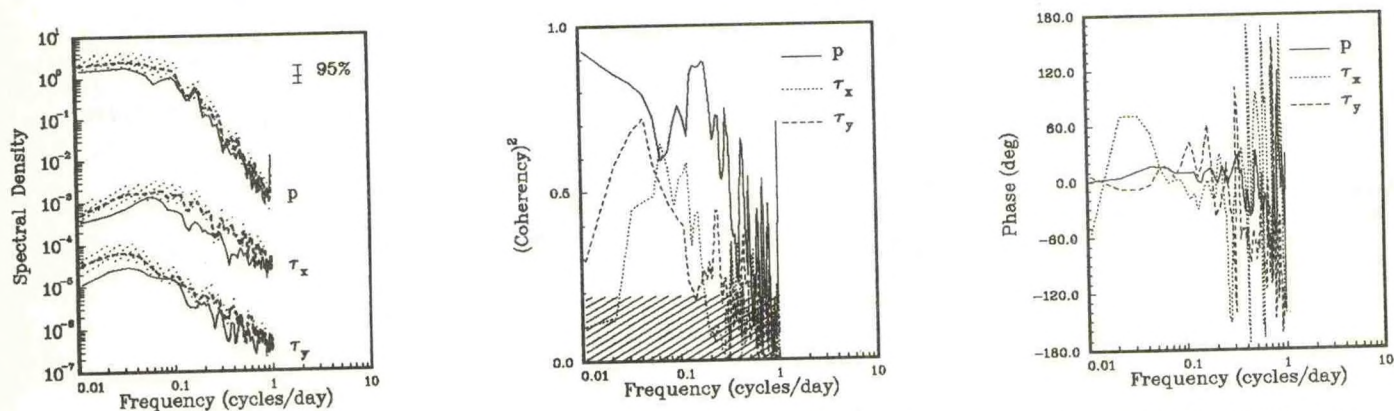


Figure 4: As for figure 3, but a comparison of FNOc point B and an average over buoys 46002, 46005 and 46006 for the summers of 1978 and 1979. There are 30 degrees of freedom.

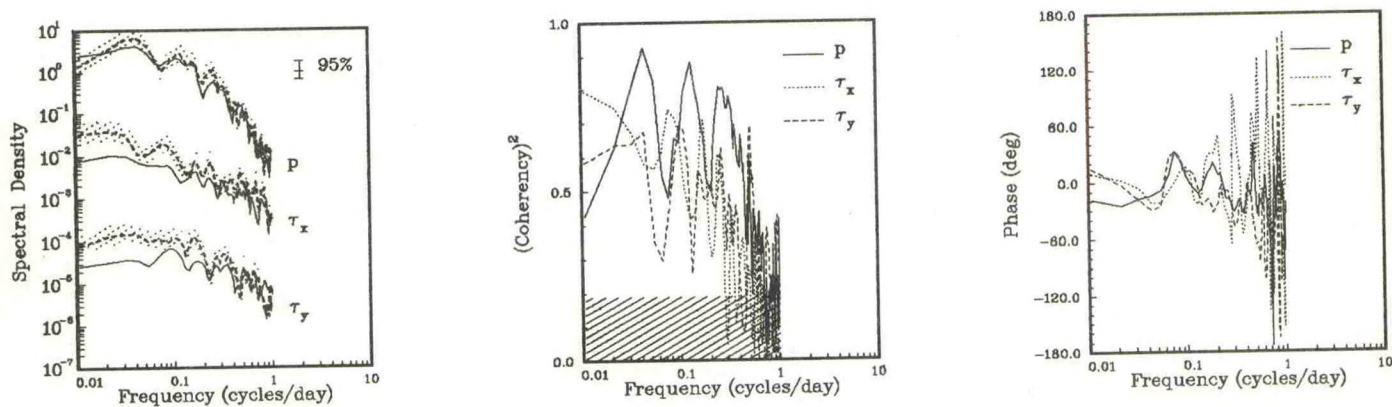


Figure 5: As for figure 4, but the buoy estimates are from 46006 in the winter of 1977/78 and from 46002 and 46005 in the winters of 1977/78 and 1978/79; there are 15 to 30 degrees of freedom, respectively.



which had not been available from the archives. We thank also Dr. J. Kaitala, FNOC, Mr. L. Clarke, FNOC and Mr. S. Lazanoff, SAI, for their useful comments and for their insights into FNOC analyses. Comments from Dr. D. Gilhousen, NDBC, were also appreciated. Computer time was provided by the W. R. Church Computer Center at the Naval Postgraduate School. This research is supported by the Physical Oceanography Program of the Office of Naval Research.

## 6. REFERENCES

- (1) Businger, J. A., J. C. Wyngaard, Y. Izumi and E. F. Bradley, 1971: Flux-profile relationships in the atmospheric surface layer. J. Atmos. Sci. 29, 181-189.
- (2) Friehe, C. A. and S. E. Pazan, 1978: Performance of an Air-Sea Interaction Buoy. J. Appl. Meteor. 17, 1488-1497.
- (3) Garratt, J. R., 1977: Review of Drag Coefficients over Oceans and Continents. Mon. Wea. Rev. 105, 915-929.
- (4) Pazan, S. E., T. P. Barnett, A. M. Tubbs and D. Halpern, 1982: Comparison of Observed and Model Wind Velocities. J. Appl. Meteor. 21, 314-320.
- (5) Thomson, R. E., 1983: A Comparison Between Computed and Measured Oceanic Winds Near the British Columbia Coast. J. Geophys. Res. 88, 2675-2683.



## PERFORMANCE OF THE AIDS-TO-NAVIGATION BUOY ENVIRONMENTAL SENSOR SYSTEM

Eduardo M. Michelena

NOAA Data Buoy Center  
National Space Technology Laboratories  
NSTL Station, MS 39529

George D. Prine and Frank J. Donovan

Computer Sciences Corporation  
National Space Technology Laboratories  
NSTL Station, MS 39529

### ABSTRACT

The design, laboratory testing, and at-sea performance of a unique environmental sensor system is discussed. This system was specifically constructed for use by the NOAA Data Buoy Center (NDBC) on an 8- by 26-ft Coast Guard Aids-to-Navigation buoy. The environmental variables measured are: wind velocity, atmospheric pressure, air temperature, and water temperature. The wind sensor package also incorporates a remote readout compass and supports the air temperature sensor's solar radiation shield, which is a new design.

The sensor suite is part of a complete meteorological and oceanographic data acquisition and telemetry system under evaluation at NDBC to determine the feasibility of instrumenting medium size Aids-to-Navigation buoys. The features of this system are described in general, and the salient operational advantages and performance defects identified by the continuing evaluation program are explained.

### INTRODUCTION

A great need exists for the acquisition and dissemination of meteorological data from over water in the nearshore regions. Such information is extremely useful to the National Weather Service (NWS) marine forecasters as well as to the operators of fishing and pleasure boats and to those persons engaged in general coastal shipping.

To fulfill this need, NDBC began a program in 1978 to determine the feasibility of deploying and operating a data acquisition and communication system aboard a relatively small buoy. A U.S. Coast Guard (USCG) Aids-to-Navigation buoy of medium size (8 feet in diameter by 26 feet overall height) was chosen as a platform for the remote measurement system. These 8- by 26-ft buoys are of standard USCG design and are routinely moored in many near-shore locations. Figure 1 shows the buoy on which the Aids-to-Navigation Environmental Sensor System (ANBESS), designed and built at NDBC, was designed and operationally tested.

The main electronic system and the battery pack that supplies all the electrical power for continuous operation is installed inside one of the two cylindrical compartments in the buoy's hull. Circular hatch covers keep water from entering the

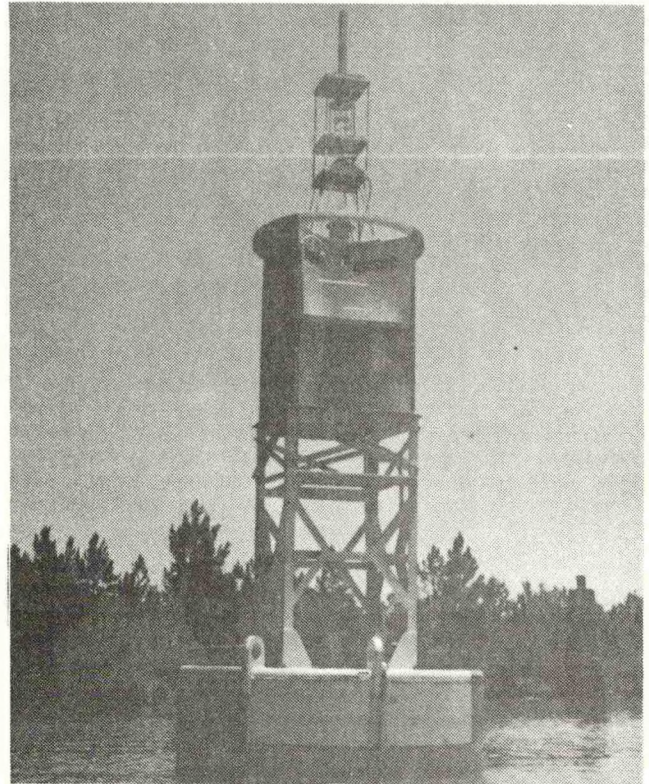


Figure 1. The 8- by 26-Ft U.S. Coast Guard Aids-to-Navigation Buoy

compartments, but the electronic equipment is also protected by its own container drum. Electrical cable penetrations to this container are airtight.

The ANBESS meteorological sensors are located on top of the buoy and are supported by a small tower structure which is attached to the buoy's main trunk by four legs. This arrangement is shown in Figure 2 where the thin support legs can be seen bridging over the navigation warning light and thus providing minimum visual interference.

The buoy configuration shown in Figure 1 was used to conduct all the at-sea tests of the meteorological variables measurement system. The first series of evaluations took place in the Gulf of Mexico off the coast of Mississippi, followed by another deployment of ANBESS in the Atlantic Ocean off the coast of Virginia. The data from these tests were relayed to shore via the Geostationary Operational





Figure 2. ANBESS Sensor Tower

Environmental Satellite (GOES) UHF radio telemetry link and simultaneously recorded using a magnetic tape unit on board the buoy.

#### DATA ACQUISITION UNIT

The entire package of data acquisition and radio communication electronics is assembled on one support chassis which in turn fits inside a protective metal drum. This container is a common 20-gal chemical storage drum with an airtight seal. Installation of the system in the 8- by 26-ft buoy requires first that one standard Coast Guard 2000 ampere-hour battery pack, the main electrical power source, be inserted into the buoy's hull compartment. The electronic enclosure is then placed over the battery pack, and finally the compartment's hatch is bolted shut.

The details of the design and specifications of the data acquisition unit are described in Baker et al. (1980). The electronic assembly consists of Motorola 6800 microprocessor systems for control, computation, data formatting, and data storage. A modified Handar Model 520A GOES Data Transmit Terminal (GDTT) is used to send the data message to GOES for relay to shore. An analog multiplexer and an analog-to-digital converter handle the sensor signals that are sampled by the acquisition system. Analog signal conditioning boards are used with those sensor signals that need modification before reaching the analog-to-digital converter.

The data system was programmed to acquire raw data from all the sensors at 1-sec intervals for a duration of 128 sec. Raw data values are then scalar averaged, formatted, converted to ASCII characters,

and transmitted to GOES. This complete data processing operation is continuously repeated on an hourly cycle. A special algorithm is used to combine the buoy heading information from a magnetic compass with the relative wind direction measured by the wind vane. The true wind direction results from this computation. Also calculated during each data acquisition period is a peak wind gust value, which is the maximum 8-sec sliding average of the wind speed samples.

All the raw data samples are stored on magnetic tape using a Data Electronics, Inc. (DEI) series CMID-3400S2 cartridge tape drive that is also installed in the electronic package. Recovery of this raw data permitted the detailed evaluation of sensor performance during the dynamic conditions that exist while the buoy is on station and routinely gathering meteorological data.

#### SENSORS

The ANBESS is capable of measuring, remotely reporting, and on-board recording the following environmental variables: wind speed, wind direction, air temperature, barometric pressure, and sea surface temperature. The air temperature sensor, the wind speed sensor, wind direction sensor, and magnetic compass needed to reference direction measurements to magnetic north are placed at the top of the buoy. A stainless steel (nonmagnetic) structure supports these meteorological sensors. An electronic barometer is used to measure the sea level barometric pressure. This sensor is located inside the electronic enclosure placed in the buoy's hull. Venting to the atmosphere outside the buoy is through a plastic breather tube that terminates in a pressure port located on the buoy's vertical centerline and just under the radar reflector area. The surface water temperature sensor is located just below the buoy's waterline and encapsulated in a sealed sleeve attached to the outside surface of the hull.

The meteorological sensor support tower is shown in Figure 2. The lower platform holds the Digicourse Model 101 magnetic compass. This compass has a Gray coded optical card that is viewed with a phototransistor and light-emitting diode array. The output signal is a serial pulse train of N+1 pulses where N is the compass (buoy) heading in degrees. Measurement resolution is 1 degree with a repeatability of +0.5 degrees (Digicourse, 1978). The compass corrector magnets and a heeling magnet placed under the compass body had to be adjusted to bring the buoy heading measurement error to within +5 degrees (worst case) when the compass was installed on the buoy.

The wind speed/wind direction/air temperature sensor package is placed on the intermediate platform of the support tower as shown in Figure 2. This package was assembled using a standard Model No. 6001 R. M. Young Company cup and vane wind sensors system but modified to fit inside an aluminum protective cage. The unmodified wind sensors are described in the instruction manual for the Model 6101 3-cup anemometer and the Model 6301 wind vane (Young, 1977). The wind speed analog output signal



is a DC voltage from a tachometer-generator. The nominal scaling is 0.105 VDC per m/s. The wind direction relative to the buoy is determined using a small wind vane that turns an electrical potentiometer transducer with a total nominal resistance of 1000 ohms and a gap of 8 degrees. Both the wind vane shaft and the shaft for the 3-cup wheel are supported by stainless steel ball bearings. External construction details of the wind sensors are shown in Figure 3. Note from this figure that the cup anemometer is installed in an inverted position. This orientation did not cause any problems in the operation of the sensor.

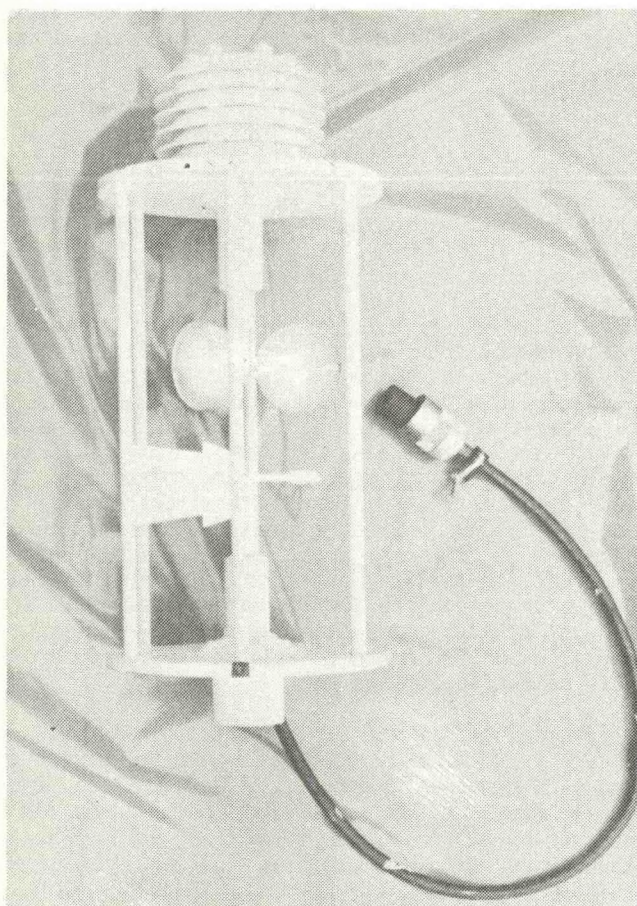


Figure 3. Meteorological Sensor Package

The air temperature sensor, located on top of the wind sensor protective cage, is in turn shielded from solar radiation by a multiple shade assembly. The temperature sensor itself, a Yellow Spring Instruments Model 44212 Thermilinear thermistor, is encapsulated in a Delrin sheath located in the center of the radiation shield. The shield is fabricated from vacuum-formed white plexiglass inverted cups. Details of the shield are given in a technical report by Gill (1979).

A protective cage was used for assembling the meteorological sensors to permit easier installation and removal of this package at sea. The cage's aluminum bars also keep buoy handling lines from tangling around the wind sensors. All intercon-

necting electrical wires from the individual sensors are routed through internal passages in the end plates and cage bars. These wires are terminated in a waterproof pigtail and connector as shown in Figure 3.

The general characteristics of the environmental measurements made by ANBESS are presented in the following table:

VARIABLES	REPORTING RANGE	REPORTING RESOLUTION
AVERAGE WIND SPEED	0 TO 30 M/SEC	1 M/SEC
PEAK WIND GUST (8 SEC/AVG)	0 TO 60 M/SEC	1 M/SEC
AVERAGE WIND DIRECTION	0° TO 360° TRUE	10° TRUE
SEA SURFACE TEMPERATURE	-5° TO +40°C	1°C
AIR TEMPERATURE	-30° TO +40°C	1°C
BAROMETRIC PRESSURE	900 TO 1100 MBAR	0.1 MBAR

### SENSOR CALIBRATIONS

The calibrations of the air and water temperature sensors and of the electronic barometer were performed at the test facilities of the National Space Technology Laboratories (NSTL). These sensors were not modified from their standard configuration when incorporated into the design of the ANBESS. The individual sensor calibrations only served to verify agreement with manufacturer's specifications.

The Yellow Spring Instrument (YSI) Model 44212 Thermilinear thermistor used in the air temperature sensor assembly was calibrated over the range from -40°C to +40°C. The difference between the actual and the indicated temperature values was less than +0.1°C as specified by YSI over the applied temperature range. The conversion equation for this sensor was also the one specified by YSI:

$$R(\text{ohms}) = -129.163 \times T(^{\circ}\text{C}) + 13698.23$$

The water temperature sensor, which uses a YSI 44202 Thermilinear thermistor protected by a metal sleeve, was checked over the temperature range -5°C to +40°C and found to be within +0.1°C of the value predicted by the manufacturer's conversion equation:

$$R(\text{ohms}) = -32.402 \times T(^{\circ}\text{C}) + 4593.39$$

The barometric pressure sensor, a Rosemount, Inc., Model 1201F1A3A1BSC56 was compared against a pressure standard over its operating pressure range from 900 to 1100 millibars at environmental temperatures from -10°C to +40°C. Calibrations showed that the measurement error was always less than +0.5 millibars when using the manufacturer's conversion equation:

$$P(\text{mb}) = 900 + 20 \times V(\text{volts})$$

Special care was taken with the wind speed and wind direction sensor calibrations. As mentioned earlier, the wind sensors were constructed by modifying a standard 3-cup anemometer and wind vane. Of



great interest was the modification of the air flow around the sensors caused by the protective cage.

All wind sensors calibrations were done in the NSTL wind tunnel. Both the effects of sensor tilt and of the orientation with respect to wind direction of the protective bars were investigated. The average calibration curve for the anemometer is shown in Figure 4. The straight line fitted to the data has a slope of 0.104 volts per m/s and passes through the coordinate origin. An average speed response value was used because, as may be observed in Figure 5, the speed output signal was found to be a function of the cage orientation with respect to the wind vector. The wake that forms behind the cage's bars affects the drag force produced by the wind on the individual cups of the 3-cup speed wheel.

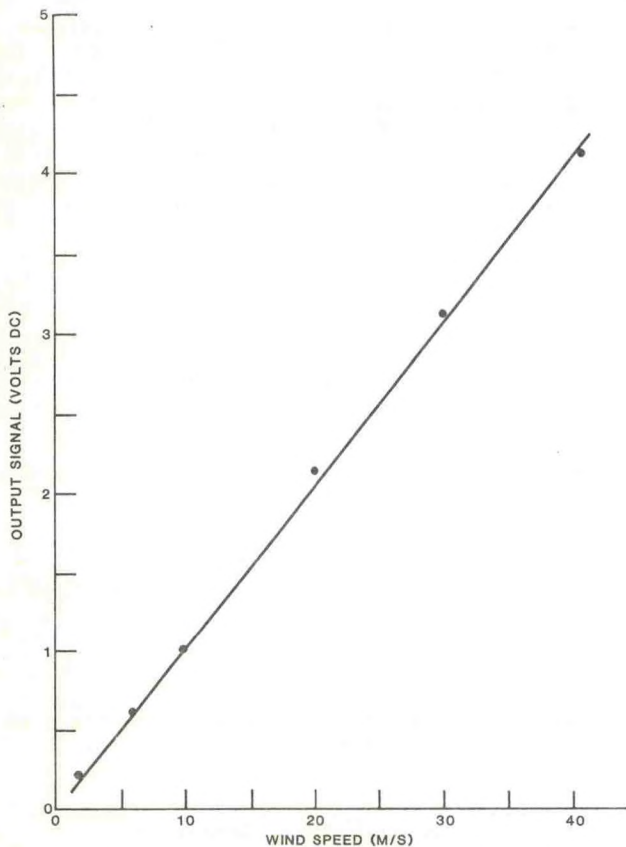


Figure 4. Wind Speed Sensor Calibration

The response of the wind vane to the protective cage orientation and to wind direction is presented in Figure 6. The straight line fitted to the calibration data is drawn through an average position relative to all the data points because of the undulations in the vane's angular response caused by flow interference. The slope of the straight line calibration approximation is 2.68 ohms per degree. Figure 6 also demonstrates that the 1000 ohm nominal resistance potentiometer has an actual electrical resistance range of 0 to 940 ohms and a gap of about 8 degrees.

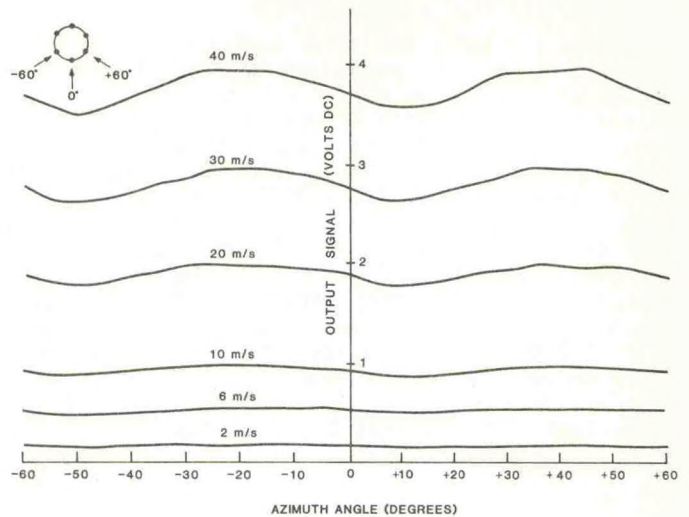


Figure 5. Wind Speed Sensor Angular Response

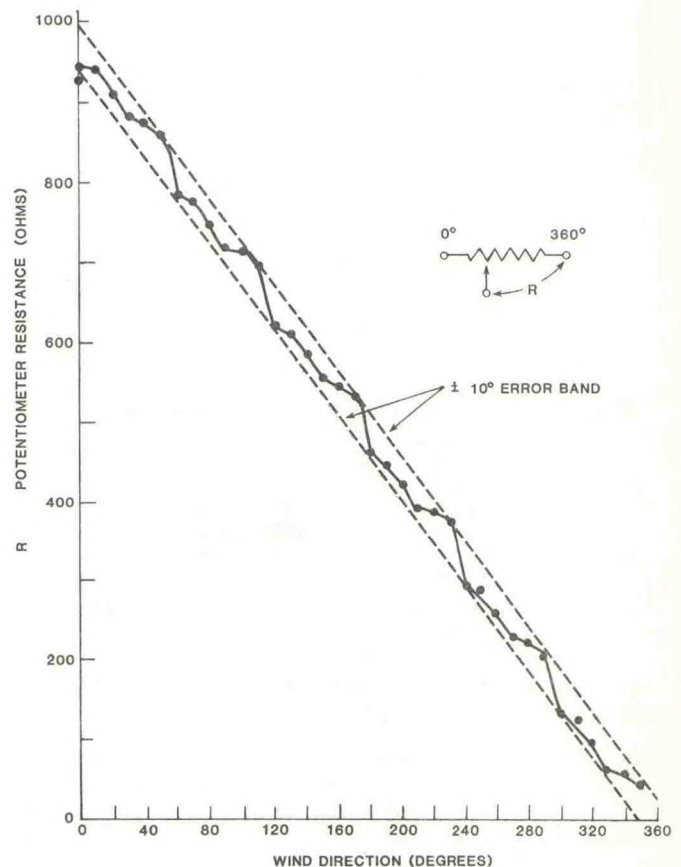


Figure 6. Wind Direction Sensor Calibration

#### EXTERNAL FACTORS

Although the laboratory calibrations of the ANBESS sensors demonstrate that highly accurate environmental measurements can be obtained, external factors due to the particular buoy installation introduce significant errors.



Incoming and reflected solar radiation can produce heating of the air temperature sensor and cause the measured value to be higher than the actual ambient air temperature. This effect was investigated for the solar radiation shield used on the ANBESS sensor package. Tests conducted in the University of Michigan wind tunnel (Gill 1979) demonstrated that solar heating will cause an air temperature measurement error of about  $+1.5^{\circ}\text{C}$  when the wind speed or ventilation is  $0.5\text{ m/s}$ . This temperature measurement error (heating error) decreases to less than  $0.5^{\circ}\text{C}$  for wind speeds greater than  $3.5\text{ m/s}$ . Figure 7 presents the upper limit of all temperature measurement errors as a function of wind speed for the ANBESS under the worst conditions of sun elevation angle and radiation intensity.

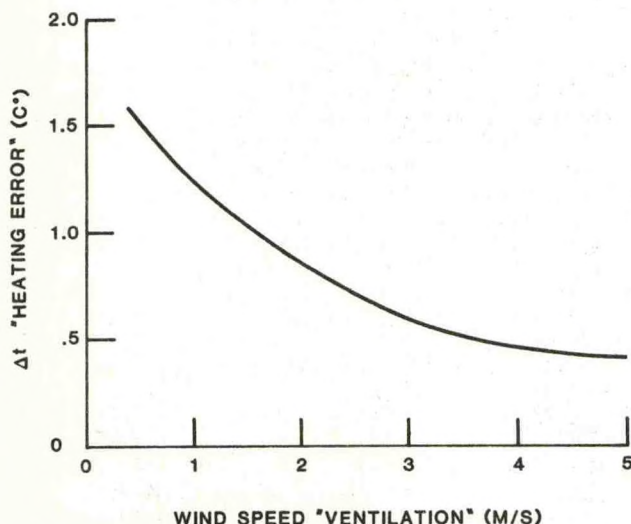


Figure 7. Effectiveness of the Solar Radiation Shield

The measurement of the wind velocity vector can best be accomplished with an ideal wind sensor that does not modify the air flow streamlines by its presence. This "transparency" is impossible to accomplish. The magnitude of several disturbing factors were determined for the ANBESS through a series of wind tunnel tests and by recording on magnetic tape consecutive data samples at 1-second intervals while the buoy was deployed.

By tilting the meteorological sensor package with respect to the axis of the wind tunnel, the effect of buoy pitch and roll on the wind measurement was simulated. These data indicate that for inclinations up to  $+15$  degrees into and away from the wind, the maximum measurement error expected is 3% of the actual wind speed. The error in wind direction for these same test conditions was insignificant.

For the wind measuring sensor, the greatest error producing external factor is the interference to the air flow by the vertical cage bars. This error is a function of wind direction azimuth angle as can be seen in Figures 5 and 6. The effect of relative wind direction on the speed measurement is an over or under estimation of the actual value by

as much as 6.5%. The wind direction measurement error as a function of relative azimuth angle was never greater than  $\pm 10\%$ . This can be seen in Figure 6 where the excursions in the wind direction calibration curve fall within the  $\pm 10\%$  error band for all angles.

Some measurement errors due to dynamic effect on the ANBESS are discussed in Garrard 1981. Fluctuations in the instantaneous wind speed measurement are highly correlated to buoy pitch and roll motion, but variations at the same period as the preferred heave oscillations of the buoy did not contaminate the record. Maximum differences between the 2-minute average wind speed and peaks in the wind speed records are, at worst, about 10%.

The wind flow around the barometric pressure inlet port was found to affect the pressure measurement. Figure 8 presents an example of this effect. The magnitude of the wind speed induced deviation found in the barometric pressure records obtained when the buoy was deployed has a maximum value of  $0.1\text{ mb}$  for the highest average wind speed case ( $15\text{ m/s}$ ). The testing of the screen type barometric pressure port installed on ANBESS is described in Greer et al. 1977.

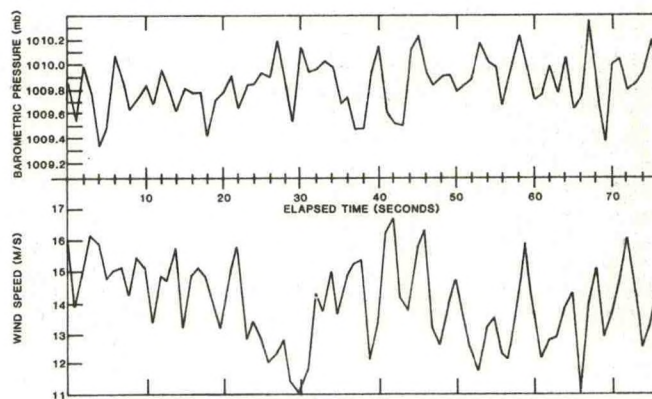


Figure 8. Effect of Wind Speed on the Pressure Measurement

## CONCLUSIONS AND RECOMMENDATIONS

The measurement and the reporting to a remote data dissemination facility of the atmospheric variables including wind speed, wind direction, barometric pressure, and air temperature as well as sea surface temperature were done on a routine basis for a period of 1 year. A modified 3-cup anemometer and a miniaturized wind vane, both placed inside a protective cage, can reliably measure the wind velocity vector at the top of an 8- by 26-ft U.S. Coast Guard Aids-to-Navigation buoy. Measurement errors for these variables are less than 10%. Barometric pressure measurements from ANBESS have a maximum error of  $\pm 1.0$  millibars. The air temperature measurement will be in error by less than  $0.5^{\circ}\text{C}$  as long as the wind speed is greater than  $3.5\text{ m/s}$ .



Changes in the design of the meteorological sensor package are needed to reduce the size of the support structure. This structure can be completely eliminated by integrating the meteorological sensors, the magnetic compass, and the satellite communication antenna into a single assembly. The pressure port used for the barometer should be of an improved design and should be relocated to the top of the buoy and also integrated into the sensor package.

More bars should be placed around the perimeter of the protective cage. Although a greater interference to the air flow will be created, a more uniform wind velocity sensor response will be obtained. Also a stronger cage will result as needed for a stand alone sensor package as recommended above.

#### REFERENCES

- Baker, Donald L., Raymond H. Canada, Jr., George D. Prine, 1981: The ANBESS Test Payload, Oceans 80 Conference Record, Institute of Electrical and Electronic Engineers, Seattle, WA.
- Digicourse, 1978: Electronic Magnetic Compasses, Depth Sensors and Support Equipment for Navigation, Seismography and Oceanography, Digicourse, New Orleans, LA.
- Gill, Gerald C., 1979: Development of a Small Rugged Radiation Shield for Air Temperature Measurements on Drifting Buoys, Technical Report made to NOAA Data Buoy Office, NSTL Station, MS.
- R. M. Young Company, 1977: Sensitive Wind Instruments Catalog, Traverse City, MI.
- Garrard, R. F., 1981: Preliminary Dynamic Error Analysis for the ANBESS Data Acquisition System: Unpublished Report to NOAA Data Buoy by Computer Sciences Corporation, NSTL Station, MS.
- Greer, J. H., Holmes, J. F., and Miles, R. T., 1977: Design and Testing of Barometer Inlets to Eliminate Wind Velocity Error in NOAA Data Buoy Installations. Instrument Society of American Conference, Niagara Falls, NY.



## ENDECO TYPE 1033 DIRECTIONAL WAVE & CURRENT TELEMETRY SYSTEM

Paul H. Cronan  
William D. Gonsalves

ENDECO, INC.  
Marion, MA 02738

### ABSTRACT

This paper presents the development of an integrated, directional wave and current monitoring system, capable of telemetering these data to a shore or ship-based receiving station. Current, temperature and conductivity data from up to three (3) modified ENDECO Type 174 Tethered Current Meters are transmitted via an acoustic link to a modified ENDECO Type 956 Directional WAVE-TRACK™ Buoy. Both wave and current meter data are then transmitted via an FM radio link, at selected intervals, to the receiver unit where a digitized RS-232-C output is available for immediate processing or recording. Complete software to provide near real-time reporting of directional wave spectra, current speed and direction, temperature, conductivity and salinity, is supplied as part of the Type 1033 System.

This system fulfills the need for an easily deployed (and moved) configuration that uses the ENDECO Tethered Current Meter design in conjunction with the Directional WAVE-TRACK Buoy for real time data in marine operations and scientific applications.

### 1. INTRODUCTION

The technology of oil exploration, offshore structures, and scientific research have a crucial need for accurate, reliable wave and current data. This system joins the proven ENDECO Type 956 Directional WAVE-TRACK Buoy with the standard Type 174 Tethered Current Meter via a slow-speed acoustic data link. These data are then telemetered to a shore or ship-based receiving station over an FM radio link for processing. Applications such as pipe-laying and rig operations can now use this data on a real-time basis for operational use.

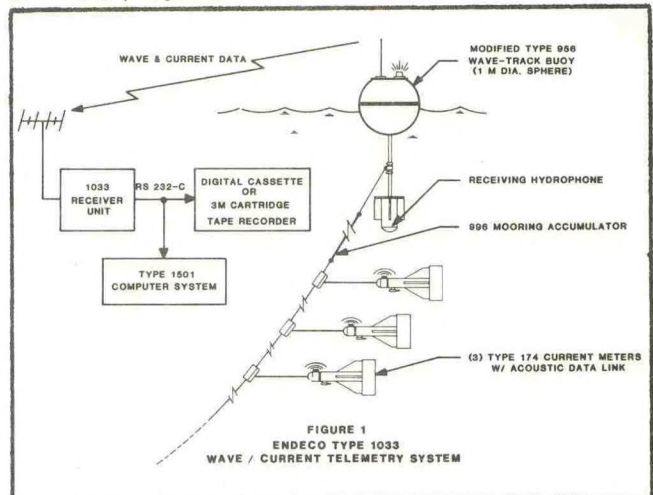
### 2. GENERAL DESCRIPTION

The ENDECO Type 1033 WAVE-TRACK and Current Data System provides a means of telemetering real-time directional wave data and near-real-time ocean current, temperature, and conductivity data to a shore or ship-based receiving station. Figure 1 shows the major system components and how they are deployed.

The three modified Type 174 Current Meters are easily attached to the mooring by means of a modified Cook clamp swivel device. These current meters measure speed, direction, temperature and conductivity, and telemeter this data via an

acoustic link to the surface mounted Type 956 Buoy.

The Type 956 WAVE-TRACK Buoy has been modified to include an acoustic data receiver and C-MOS memory system. Wave and current data are transmitted at predetermined intervals over an FM radio link to the receiver unit. The outputs from the Receiver unit (RS-232-C, 110 baud) can then be processed on an ENDECO Type 1501 WAVE-TRACK Data Processor or equivalent computer system using the specially developed Type 1033 software programs.



#### A. Offshore Equipment

The system is deployed as shown in Figure 1. All mooring components are designed and specified according to the site requirements based upon the following information:

- Water depth
- Expected current profile
- Expected wave conditions
- Bottom characteristics
- Tidal range
- Current meter depths

Current speed, direction, water temperature, and conductivity are monitored using a modified Type 174 Tethered Current Meter. This instrument's unique tether approach enables it to filter out erroneous data introduced by mooring motion or orbital motions in the water column. It is, therefore, well adapted to measure currents near the surface or at depths to 150 meters. The instrument utilizes a PVC pressure case and is



neutrally buoyant when deployed.

The modifications to the standard Type 174 Current Meter to enable its integration into the Type 1033 System consist primarily of the addition of an acoustic transmitter module and a longer pressure case to house this module. All functions of the standard Type 174 Current Meter are preserved including its self-contained magnetic tape recorder. These current meters may also be used as self-recording units by simply not energizing the acoustic module.

An upward-looking ring ceramic acoustic transducer is mounted on top of the current meter. The transducer is designed to produce a conical beam pattern which increases the effective acoustic power by approximately 6 dB. The acoustic signal-to-noise ratio at the receiving hydrophone has been calculated to be 12 dB minimum under worst case conditions. The doppler shift of the acoustic data signals, due to the relative motions between the transmitting and receiving hydrophone, is calculated to be less than  $\pm 100$  Hz. The acoustic receiver bandwidth of  $\pm 250$  Hz provides a conservative margin of safety to ensure that the received signal is well within the receiver bandwidth under the worst case conditions.

To reduce the effect of surface bubbles, the receiving hydrophone is placed in the base of the sensor package approximately 7 ft. below the surface. This feature, along with the high signal-to-noise ratio, shaped beam patterns, and conservative receiver bandwidth, ensures highly reliable acoustic data receiver system and a larger battery pack. The Type 956 Directional WAVE-TRACK Buoy provides an accurate measurement of wave direction and heave using an "inverted pendulum" design wave orbital following buoy. This technique uses a symmetrical, single point moored surface buoy monitoring system that provides complete wave directional spectra and wave energy information. The pitch, roll, direction and accelerometer instrumentation is located in a submerged pressure case; the electronics and battery power are located in the spherical surface buoy. The mooring cable attaches at the hydrodynamic balance point between the buoy and the submerged sensor package that acts as the "fulcrum" of the inverted pendulum. This configuration allows the buoy to move in phase with the orbital wave motion. A breaking wave will cause maximum tilt at the wave crest. Since this action is in tune with the expected motions of the buoy, it does not introduce errors.

#### B. Type 1033 Receiver

The ENDECO Type 1033 WAVE-TRACK and Current Data Receiver is a compact receiving unit designed to receive multiplexed FM signals from the Type 1033 WAVE-TRACK Buoy. It consists basically of a receiving antenna, coaxial cable, and the receiver unit. The receiver unit's primary function is to digitize the wave data, and convert both the wave and current meter data into an RS-232-C serial data stream. The RS-232-C output data can then be processed to obtain the required wave and current data or recorded for later use. Analog wave data signals are also provided for the user. The

receiver unit operates on AC power and is housed in an all-aluminum, rack-mounted enclosure.

#### C. Type 1501 WAVE-TRACK Data Processor (Optional)

The Type 1501 WAVE-TRACK Data Processor provides near real-time processing of the 8-bit binary data from the ENDECO Type 956 Directional WAVE-TRACK Buoy. The data processor utilizes an 8-bit Z80 based S-100 bus microprocessor operating at 4 MHz with 64K bytes of random access memory (RAM). In the standard configuration, two RS-232-C serial ports provide interface to the digitized output from the WAVE-TRACK receiver and to a terminal. The 80 column terminal operates at 300 baud. It provides a means to interface and control the Type 1501 WAVE-TRACK Data Processor and to obtain permanent written reports of wave statistics, maximum wave profile, energy spectra, directional information and current meter data.

The system is also provided with dual 8 inch double density floppy disc drives. Disc A provides the CP/M operating system, real-time clock and housekeeping software. In addition, the compiled FORTRAN IV version of the appropriate WAVE-TRACK and current meter software is resident on Disc A. Disc B is used for permanent storage of the data and the processed output from each data transmission. This processed output is identical to the file printed at the terminal after each processing.

The system is provided with a real-time clock which is set to the desired time and date using the terminal. The clock is provided with a rechargeable battery power source so that a power interruption does not require a reset of the clock for 4 days. The clock output is written on each processed file indicating the time at which data from the Type 1033 System is first received and the time at which the processing is completed.

The Type 1501 WAVE-TRACK Data Processor is a very flexible device. ENDECO, INC. can provide changes to the software by supplying new program floppy discs. This allows the end user to be immediately updated with the latest software without hardware modification.

Software is available to process the Type 1033 buoy output and provide the following outputs:

##### Wave:

- Number of wave processed
- Maximum period
- Mean period
- Period of maximum height
- Significant period
- Maximum height
- Height Variance
- Significant height
- RMS height
- Profile of maximum wave
- Tabulation of 28 frequency bands:
  - Energy density
  - Mean direction
  - Standard deviation
  - Direction spectra



#### Current Meter:

I.D. Number  
Time  
Speed  
Direction  
Temperature  
Conductivity

Additional features may be added to the processing software according to the customer's requirements.

## 2. FUNCTIONAL DESCRIPTION

### A. Offshore Equipment

Figure 2 is a diagram showing all the functional blocks of the Type 1033 Transmitter unit including the Current Meters and Transmitting Buoy. The system is configured to transmit ocean current data from three current meters attached to the mooring line along with directional wave information obtained from the surface instrumentation.

The outputs from the current meter sensors (speed, direction, temperature and conductivity), along with header, identification and transmission count data, are multiplexed and applied to the Universal Asynchronous Receiver Transmitter (UART) circuit. The UART converts the 8-bit parallel words into a serial data stream and adds stop, start, and parity bits. The digital data stream is then converted into Frequency Shift Keying (FSK) signals, amplified and transmitted via an acoustic link to the WAVE-TRACK Buoy every 2 minutes.

The acoustically transmitted data is formatted in the following manner:

- a. Identification word (4-bit byte)
- b. Transmission counter:
  - (1) 4-bit byte whose count will increment by 1 for each complete scan (i.e., every 2 minutes); it will count 0 through 15 and then repeat.
- c. Current Speed:
  - (1) 8-bit gray code word from an optical speed encoder
- d. Current Direction:
  - (1) 8-bit gray code word from a magnetic compass with an optical encoder
- e. Temperature:
  - (1) 8-bit binary word derived from a thermistor sensor
- f. Conductivity:
  - (1) 8-bit binary word inductive conductivity sensor

Waveform A (Figure 2) shows the acoustic data format transmitted from the current meters. Since the start, stop and parity bits have been added to each data word by the UART, 11-bits are required to transmit each 8-bit data word. Each five word data-scan, therefore, requires the transmission of 55-bits. Note that each current meter transmits two acoustic frequencies, one frequency representing a logic "0" and the other frequency a logic "1". Since the Type 1033 System has three current meters, 6 distinct acoustic frequencies are used. These frequencies are in the 20 to 36 kHz band with a minimum of 1 kHz spacing between

adjacent frequencies to avoid interference. The frequencies are programmable via dip switches located in the acoustic transmitting module. A relatively slow transmission rate of one 5 ms pulse per second allows the acoustic reverberation to diminish before the next one is transmitted. Every two minutes, each current meter will transmit a complete 5-word transmission sequence to the surface buoy. Since different acoustic frequencies are used, transmissions from three current meters can occur simultaneously without mutual interference. If desired, the 2-minute interval can be extended up to 10 minutes, which would significantly increase the battery life in the current meters.

The acoustic receiver, located in the surface buoy, amplifies the received signals detected by the hydrophone. The composite signal is then applied to band pass filters ( $\pm 250$  Hz bandwidth) where the signal is separated into the transmitted components (i.e.,  $f_1, f_2, f_3, f_4, f_5, f_6$ ). The FSK demodulator then reconstructs the transmitted binary data for each current meter. The binary data is then stored in C-MOS memory. Each memory is capable of storing in excess of sixty 5-word frames of acoustic data. Every 20 minutes the stored data is transmitted to shore and the memory erased. During the RF transmission cycle, current meter data stored in memory is shifted out at a 110 baud rate. This digital data stream (which already has the start, stop and parity bits) is converted into a FSK audio signal and transmitted over an FM radio link to the receiver unit.

The Directional WAVE-TRACK functional blocks are also shown in Figure 2. Wave heave is sensed using a force-balance Servo accelerometer whose output is double integrated to produce a voltage proportional to heave. Two orthogonal tilt sensors, in conjunction with an ENDECO Type 869 Flux Gate Compass and a coordinate resolver circuit, provide analog outputs of North-South and East-West Buoy Tilts proportional to the respective tilts. These 3 output signals (Heave, N-S Tilt, and E-W Tilt) drive three sub-carrier voltage controlled oscillators whose outputs are combined and transmitted to the Type 1033 Receiver Unit.

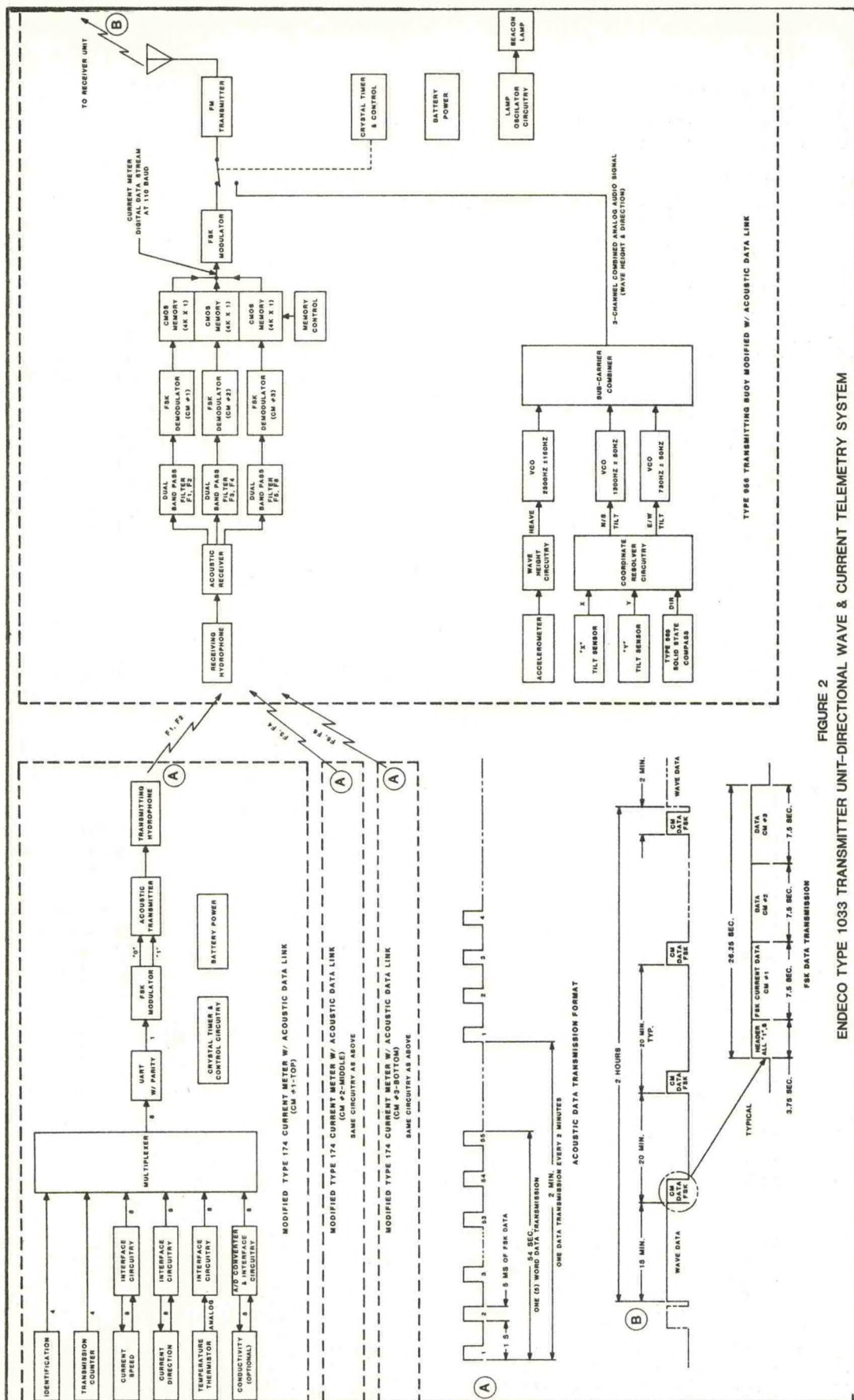
Figure 2, Waveform B, shows the combined wave and current meter transmission format. Note that all wave data is transmitted for an 18-minute duration every 2 hours. Also, the current meter data is transmitted digitally in a FSK format every 20 minutes at a data rate of 110 baud. Other transmitting intervals and durations can be selected by the user.

### B. Type 1033 Receiver Unit (Figure 3)

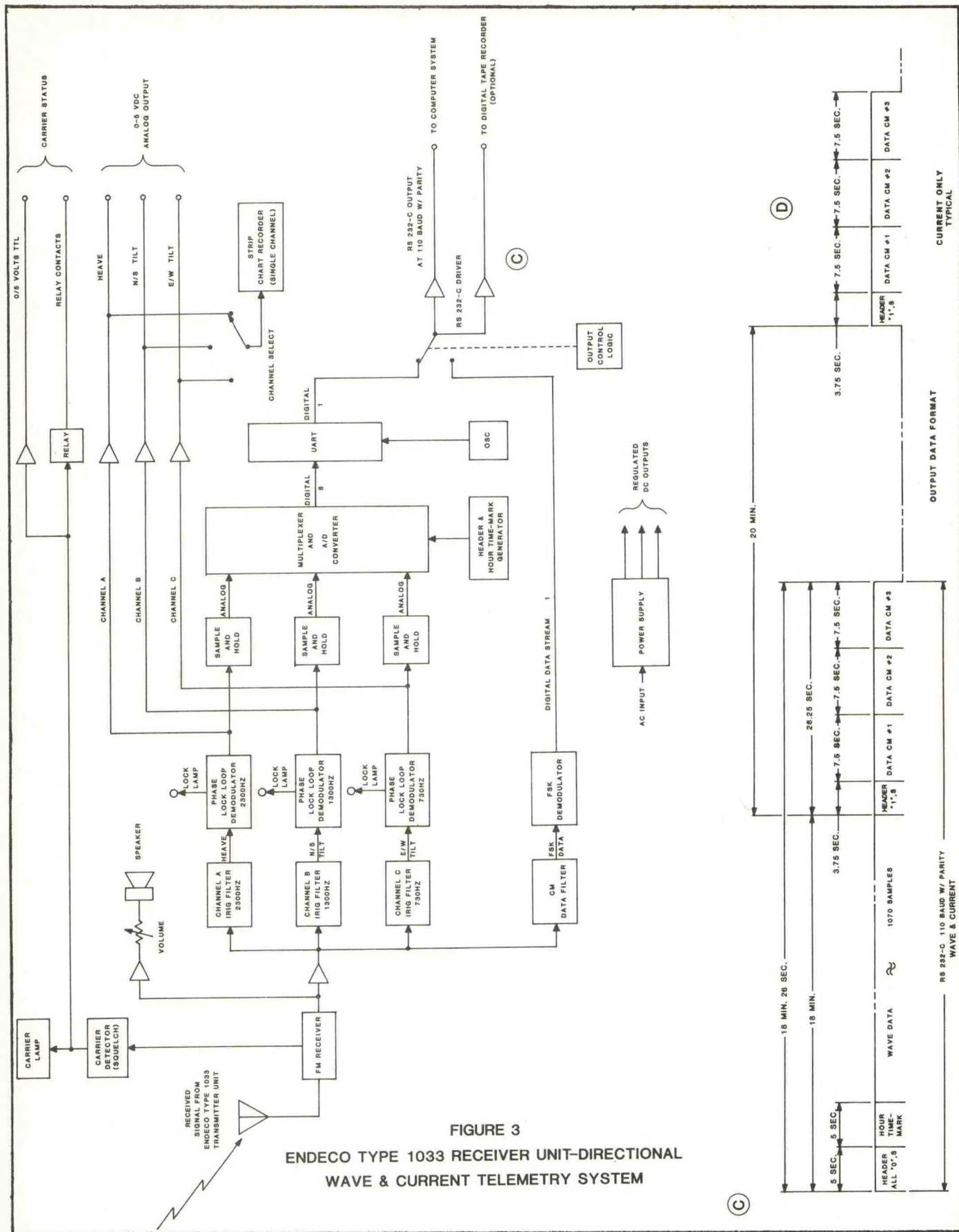
The Receiver Unit combines the functions of digitizing the 3 channels of wave data and decoding the FSK current meter data. It has the ability to discriminate between wave data and current meter data.

Wave data is separated into their respective channels using standard IRIG band pass filters. Phase lock loop demodulators provide additional noise rejection and perform a frequency-to-voltage conversion for each channel. The three channels











are sampled simultaneously at 1 second intervals with the sample and hold circuits. A multiplexer and A/D converter sequentially digitizes the held data into parallel 8-bit words, which are then converted into a serial data stream complete with stop, start and parity bits at a 110 baud rate by the UART. The data stream is then conditioned into an RS-232-C format for use by the processing or recording equipment. Note that wave data is preceded by a 5-second header of logic "0"'s followed by 5 seconds of hour time marks (see C, Figure 3). The logic "0" header allows the beginning of transmission to be positively identified. This is especially useful when recording the output data on a digital tape recorder which provides no separation between recorded transmissions.

Hour time marks are inserted immediately following the above header. The count will increment by one every hour (0-255) and then repeat. This feature is useful when the recording device does not provide a time mark. The time mark generator has a battery backup so that power interruptions will not affect the time data. Twenty-six seconds of current meter data follow the wave data. Logic circuitry will detect the presence of current meter data during the 3.5 second period of header information, thereby switching the input to the RS-232-C driver over into the current meter mode. Note that both the digitized wave data and the transmitted current meter data are at 110 baud rate (10 char/sec). The sequential digital outputs can now be easily processed to obtain the required time series or statistical data.

The output data formats of wave and current and wave only are shown in Figure 3, Waveforms C & D. The overall timing sequence is the same as that shown of the transmitting buoy (Waveform B, Figure 2).

### 3. TEST RESULTS

The Type 1033 System underwent a battery of tests at the ENDECO facility with emphasis placed on the reliability of the acoustic data link. Following the laboratory tests, sea tests were performed in the shallow waters of Buzzards Bay. The Type 1033 software was checked out by processing both live and simulated data. No acoustic transmission errors were observed during these system tests.

After further acceptance testing at the customer's facility, the Type 1033 System is scheduled to be deployed in mid-April 1983 to obtain real-time data for a pipe-laying operation.

### 4. SPECIFICATION SUMMARY

#### Current Meters - modified ENDECO Type 174

##### Sensor Specifications:

##### Current Speed

Sensor Type: Ducted Impeller  
Speed Range: 0-223.2 cm/sec (0-4.34 kt) @ 2 min. interval  
0-44.8 cm/sec (0-.87 kt) @ 10 min. interval  
Impeller Threshold: Less than 2.57 cm/sec (0.05 kt)  
Resolution: 0.4 percent of speed range

Speed Accuracy:  $\pm 3.0$  percent of Full Scale

##### Current Direction

Magnetic Direction: 0-360°

Resolution: 1.4°

Accuracy:  $\pm 7.2^\circ$  above threshold

##### Temperature

Sensor: Thermilinear thermistor

Range: -50 to +45°C

Accuracy:  $\pm 0.2^\circ\text{C}$  referenced to computer calibration

Resolution: 0.098°C

##### Conductivity

Sensor: Electrodeless probe

Range: 5 to 55 millimhos/cm (0-70 range optional)

Accuracy:  $\pm 0.55$  millimhos/cm

Resolution: 0.098 millimhos/cm

##### Acoustic Data Link Transmitter

Transducer Type: Ring ceramic

Frequency: 20 to 36 kHz

Source Level: 85 dB re 1  $\mu\text{bar}$  @ 1 m

Modulation: FSK

Pulse Length: 5 ms

Design Range: 1000 m

Power: Lithium batteries - 4 month life

##### Operating Environment

Operating Medium: Salt fresh or polluted water

Operating

Temperature Range: -50 to +45°C (23° to 113°F)

Maximum Depth: 152 m (500 ft)

##### Instrument Housing

Material: PVC plastic

Weight: 14 kg (31 lb) in air

Buoyancy: Approximately neutral

Dimensions: 85.1 cm (33.5 in) long x 40.6 cm (16 in) diameter

##### Transmitting Buoy

##### Acoustic Data Link Receiver:

Number of Channels: 3

Transducer Type: Ring Ceramic

Frequency: 20-36 kHz (factory set)

Modulation: FSK

Sensitivity: 10  $\mu\text{V}$

Output Signal: C-MOS compatible digital data

Memory Size: 4K x 1 channel (C-MOS)

##### Wave Buoy Instrumentation

Wave Height Range: 15 m (50 ft); 30 m (100 ft) optional

Wave Height

Resolution: 5.9 cm (2.3 in) for 15 m range  
11.7 cm (4.6 in) for 30 m range

Wave Period Range: 2-30 sec

Accelerometer

Linearity: Better than  $\pm 0.2$  percent

Wave Direction: 0-360° Conventional wave direction

Wave Direction

Resolution: 1.4° (8-bits)

Wave Direction

Accuracy:  $\pm 10.0^\circ$

Tilt Sensor Type: Differential Hg capacitance sensor with vertical reference

Buoy Tilt Range:  $\pm 45^\circ$  per axis



Buoy Tilt  
     Resolution: 0.35°  
 Buoy Tilt  
     Accuracy: ±4.0°  
 Compass: Dual axis flux gate (ENDECO Type 869 Solid State Compass)  
 Transmitting  
     Frequency: To be specified by customer  
 Transmitting  
     Power: 100 mW  
 Subcarrier  
     Frequencies:  
         Heave: 2300 Hz ±150 Hz  
         North-South: 1300 Hz ±50 Hz  
         East-West: 730 Hz ±50 Hz  
 Power: Lithium battery pack (6 month life)

Operating Environment  
 Operating Medium: Salt, fresh or polluted water  
 Operating Water  
     Temperature: -5° to +45°C (23 to 113°F)

Instrument Housing  
 Materials: Reinforced fiberglass and PVC plastic  
 Dimensions: 1.0 m (3.28 ft) diameter x 2.44m (8 ft) long plus antenna  
 Weight in Air: 100 kg (220 lb)

#### General Specifications:

RF Frequency: To be specified by customer  
 Sensitivity: Better than 1  $\mu$ V  
 Digital Outputs:  
     Format: RS-232-C at 110 baud (10 char/sec)

Wave Data  
     Digitizing Rate: 1.0 sec (others are selectable)  
 Current Data:  
     Start Indication: 3.75 sec of logic "1"'s  
     Header & Identification: 4-bit word  
     Frame Counter: 4-bit word  
     Speed, Direction, Temperature &  
     Conductivity: 8-bit word (each)

#### Environmental Limitations

Operating Temperature  
     Range: 0° to 40°C

#### Physical Characteristics

Material: 19" aluminum rack-mounted enclosure  
 Dimensions:  
     Height - 18 cm (7")  
     Width - 48 cm (19")  
     Depth - 38 cm (15")  
 Weight: 10 kg (22 lb)

#### 5. GENERAL REFERENCES

Middleton, F.H., LeBlanc, L.R. and Czarnecki, M.F., Spectral Tuning and Calibration of a Wave Follower Buoy, OTC No. 2697, 1976.

Longuet-Higgins, M.S., Cartwright, D.E., and Smith, W.D., Observations of the Directional Spectrum of Sea Waves Using the Motions of a Floating Buoy, Ocean Wave Spectra, May 1961.

Middleton, F.H., LeBlanc, L.R., and Sternberger, W.I., Wave Direction Measurement by a Single Wave Follower Buoy, OTC Proceedings, 1978.

Brainard II, E.C., Wave Orbital Following Buoy, MTS Proceedings, 1980.

#### ENDECO Data Sheets:

Type 1033 Directional Wave & Current System  
 Type 956 Directional WAVE-TRACK System  
 Type 174 Tethered Current Meter  
 Type 869 Solid State Compass  
 Type 996 Fail-Safe Mooring Accumulator  
 Type 1501 WAVE-TRACK Data Processor



## MOORED BUOY DEVELOPMENTS AT E.E.R.M.

Vladislav KLAUS

Direction de la Météorologie  
Etablissement d'Etudes et de Recherches Météorologiques  
CNRM, Avenue Eisenhower, 31057 TOULOUSE CEDEX, FRANCE

### ABSTRACT

After the realization of the small drifting MARISONDE B buoys used for the First GARP Global Experiment in 1978 and 1979, the project of fixed oceanic meteorological automatic stations appeared to be a logical step of development to EERM, mainly because of the observation network deficiencies over the oceans. This paper describes the present state of the fixed buoy program at EERM including the MARISONDE RC, the BOSCO and the wave buoy MARISONDE H.

### 1. THE MOORED WEATHER STATIONS PROGRAM

EERM realized its first attempt at a deep sea mooring with a MARISONDE B [6] 300 kilometers from Brittany in April 1979. This buoy, which had given very positive results during the First GARP Global Experiment (F.G.G.E.) as a drifting beacon, proved too fragile for an off-shore mooring. The sailors dragnets and the strokes of the surface movements caused in a short time damage on the line and on the buoy itself.

As a result, EERM resorted to a float of greater inertia and smoother movements not liable to raising by a fishery net. Parallely, developments on marine sensors have led to an evolved drifting spar buoy (MARISONDE C) which measures wind speed and direction, air temperature and pressure tendency in addition to the air pressure on sea surface temperature already designed on the FGGE MARISONDE B. Thus was created the MARISONDE RC which is a combination of the MARISONDE C version with a steel two tons biconical float R. The transmission is done through the ARGOS system [3] (Fig.1).

Six of these buoys have been manufactured for off shore permanent meteorological observations and local scientific experiments. Positive results have been obtained both with the pay-load and the holding of the line. Still, in remote areas such as ARMOR their size revealed too small for an efficient signalling and damages occurred due to collisions with ships.

In consequence, a 20 tons version called BOSCO has been designed in 1982, equipped with a doubled electronics and a modular setting. The improvements concern mainly the maintenance facilities on the open sea and the transmission through geostationary satellite, which will allow for real time exploitation for meteorological forecast. Sensors and processing are the same as on the MARISONDE RC.

#### 1.1 The MARISONDE RC

##### 1.1.1. General description (Fig.2)

The MARISONDE RC has a steel biconical structure (diameter 1.6 meters, height 5.5 m or 6.6 m with the lower hull) which contains on its axis a 20 cm diameter tube for the electronic and sensors unit fitting. Aerial measurements such as wind speed, wind direction and air temperature are taken 2.5 meters above the sea level.

This buoy, which can easily be conveyed on ground by standard vehicles, is also able to bear, due to its buoyancy (800 kg), the forces exerted by the mooring line. Thus we avoid any surface line easily destroyed by ships and sea turbulence.

The electronic unit is contained in a 2.3 m long cylinder topped by the sensors and the flash light platform (Fig. 1). It is fixed in the axial upper tube of the biconical structure.

##### 1.1.2. The electronics and the sensors

The energy is supplied by batteries, so the consumption reduction was one of the major tasks. The electronics is designed in the C-MOS type and the sensors are specially developed to endure the corrosion and turbulence of the marine environment, and to have the same precision and stability as the ground instruments. Annual consumption is 200 Ah under 16-24 volts for the whole electronics-transmitter-sensors system. The flash light is separate (90 Ah under 12 V). With lithium batteries, the energy supply needed for one year autonomy fills the 1.10 meters high lower part of the cylinder.



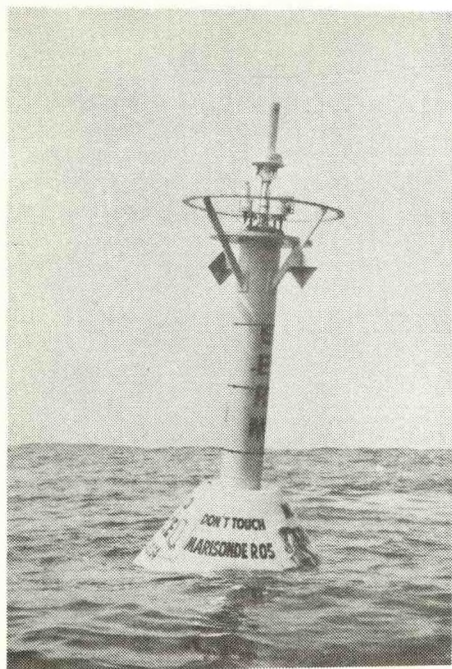


Fig. 1 - The MARISONDE RC on sea and cross-section of the electronic unit the wind sensors and the compass.

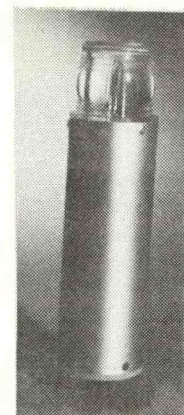
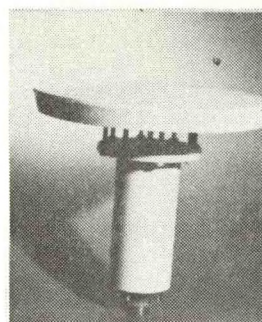
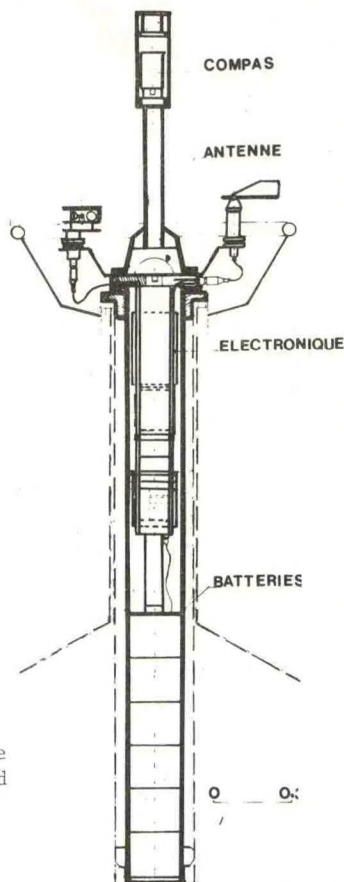


Fig. 2 -

The barometer (down left)  
The air temperature protection (up left)  
and the flash-light (up right)

The hourly renewed data, transmitted through the ARGOS system, are as follows :

- Last air pressure
- Last synoptic air pressure on a 3 hours basis (0-3-6 h etc...)
- Pressure tendency (difference of the two last synoptic pressure data)
- Sea surface temperature (at 70 cm under the sea level)
- Air temperature
- Wind speed (in knots)
- Wind direction
- House keeping parameter (battery voltage)

The data are sent every minute during 0.52 s in the form of a 401.65 MHz message allowing location through satellite and the daily checking of the buoy position.

#### a) The air pressure measurement [1]

The barometer is located in the hull above the batteries. It consists of an aneroid cap related to one face of a capacitor. The resulting capacity is converted into frequency (150 to 300 KHz for 920 to 1050 millibars) after 1 minute collection and then adjusted according to the inner temperature. The 3rd and 4th cards memorize the synoptic value and calculate the pressure tendency, bringing thus to the electronic unit called CADOM (Central d'Acquisition de Données Météorologiques) the three pressure digitized data. Accuracy is better than the 0.5 millibar value required by Meteorological Office.

The barometer is connected to the outer environment through an air intake located at the top of the mast.

#### b) The temperature measurements

For both the air and the water instruments, the sensor is a copper resistor (CUPROSWEM). Its resistance is 2330 ohms at 0°C and its sensibility 10  $\Omega$  /°C. Measurement is realized with a 1 mA continuous current sent during 0.2 second. The SST sensor, protected by a bronze cover, is located under the float at about 70 cm under the surface [6].

The air sensor fixed at the top of the mast has a plastic mushroom form protection against sun rays, sea reflections and rain. A 2 cm high space is preserved at the sensor level for natural ventilation.

Accuracy is 0.2°C for the SST and 0.5 for the air temperature sensors.

#### c) The wind measurements

The wind speed is measured through a light cap anemometer (0.610 kg) located on the mast. A special effort was made to preserve the micro ball-bearing water-tightness and to increase the lifetime up to 9 months. The physical value is obtained from the number of current variations induced by the passage of two rotative magnetic frames beside a fixed proximity detector.



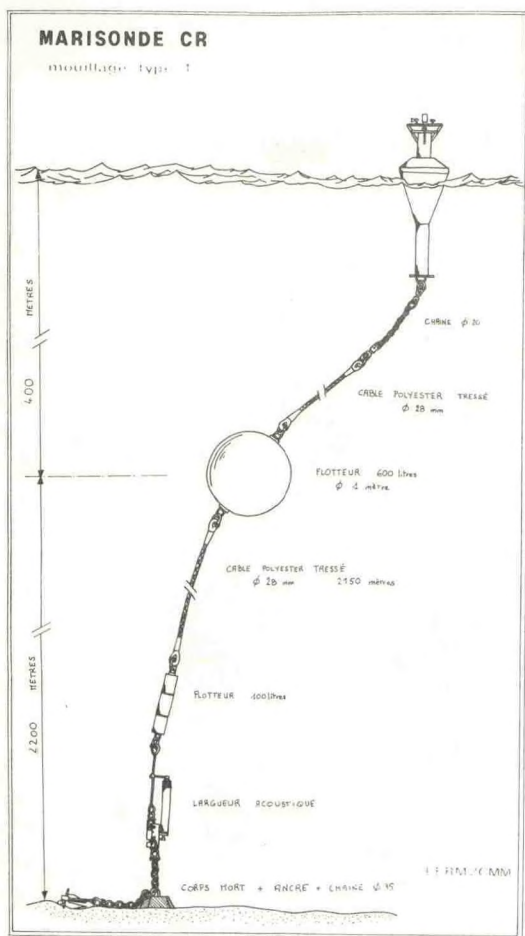


Fig. 3 - The MARISONDE RC mooring line (for 2600 m depth)

It is given in knots (0,5 m/s) after 512 seconds measurement.

The wind direction is measured with a pale anemometer and a flux-gate compass. The mean value is obtained from 128 data collections taken every 4 seconds : the initial data is added to the 127 differences sum between each of the 127 values and the initial one.

#### d) The electronics

Measurements chronology, conversion and digitalization are performed by the data collection and storage circuitry set (CADOM). MARISONDE RC deliver, according to ARGOS logic requirements, a 4 x 32 bits message including 1 x 32 bits for identification and location and 3 x 32 bits for data transmission.



Figure 4 - The MARISONDE RC deployment points

#### 1.1.3. The mooring technique (Fig. 3)

Several experiments in Atlantic Ocean (Point ARMOR 48°28'N, 12°35'W) have led us to a particularly reliable mooring line. It is mainly composed of a polyester 28 mm diameter rope tightened between the buoy and a 3 tons concrete anchor at the bottom. A subsurface 1.5 m diameter float (600 kg buoyancy) at 350 m depth lightens the line tension on the buoy and keeps the acoustic release above the bottom mud. With the taut line we avoid any damage from ships on the surface and increase the vertical stability of the buoy. Computer calculations have shown that maximum tension on the rope is 2 tons just under the buoy level for 15 meters wave height. The line is designed for a 12 tons maximum tension.

#### 1.1.4. The deployments and results

Several launchings have been performed since April 1979 with MARISONDE RC in Atlantic Ocean and Mediterranean Sea. The three first ones are semi-permanent meteorological observation stations (Fig. 4).



- ARMOR Atlantic 48°28'N, 12°35'W (April 79) [2]
- ALPEX 1 Mediterranean 43°N, 04°E (February 82)
- ALPEX 2 Mediterranean 42°N, 07°E (February 82)
- One equipment RC in Le Havre on the light buoy of the "PHARES ET BALISES".
- Two equipments RC in the Guinea Gulf : 0°N 04°W for the FOCAL EXPERIMENT (January 83-January 84).

The two first moorings on ARMOR broke after 2 months and 2 weeks respectively. The following ones, realized with the line described in I.1.3. stayed 9 months each before recovery. Damage from collision with ships occurred twice and on one occasion the float and the whole line have been recovered safe, but the electronics and sensor unit was stolen.

For long distance areas such as ARMOR, EERM has designed the bigger BOSCO buoy which hopefully should solve the problems encountered with the MARISONDE RC.

#### 1.2. The BOSCO buoy (Fig. 5)

In order to improve the observationnal continuity on the ARMOR point we have considered the possibility of a doubled equipment and easy repairs on sea. The BOSCO has a 3.6 meters diameter platform on which the elements are set in a modular way so that replacement on board could be easier. The structure was computed for small natural periodicities (3.0S and 3.5S for vertical movements and oscillations respectively).

The electronics uses a microprocessor, the barometer and the batteries are set in removable 40 cm long cylinder in tight closed boxes on the platform.

The sensors are located at 5 meters above the sea level and an active radar transponder will reduce collision probability. In addition to the ARGOS system, this buoy will be equipped with an ATMOS beacon transmitting 3 hourly data through the geostationary METEOSAT satellite.

The first prototype of BOSCO is tested in the Brest harbour (March 83) before operational mooring on the ARMOR point in summer 1983 for permanent meteorological observations. The results obtained with this buoy will determine whether in the next future such structures could be extensively adopted for the meteorological oceanic network. Beside these exploitation prospects, technological developments are being done for increasing the measurements capacities with sun radiation and subsurface temperature instruments. Investigations are in progress also to get energy supply from a hydraulic jack activated by the line tension periodical variations.

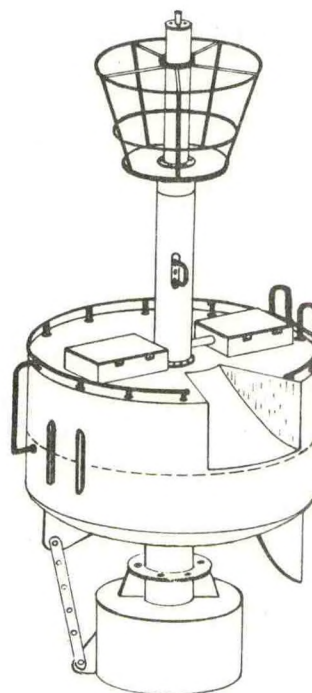
#### 2. THE WAVE BUOY MARISONDE H

Parallely with the big oceanographical buoys developed at CNEXO, EERM has realized a much simpler one for meteorological observations. The MARISONDE H is a hemispheric 1.2 m diameter buoy transmitting on real time the mean wave height and mean wave period values. [4]

Fig. 5 - The BOSCO buoy

### BOUEE " BOSCO "

(STRUCTURE)



Immersed up to the diametral plane with the help of a 90 kg ballast at the bottom of a 0.9 meter long rod fixed under the hemispheric structure, this buoy has been designed for a good vertical stability which allows precise vertical linear acceleration and a close link with the surface level, necessary for an accurate correlation between the buoy acceleration and the sea state. The natural periods are outside the wave period interval: 1.2, 2.1s for vertical movement and oscillations respectively. The total weight is 320 kg.

The sensor is a single accelerometer located in the center of the buoy near the floating level, it has been adapted directly from the pressure sensor of the other MARISONDE buoys. One of the two frames of the capacitor has been loaded for a better acceleration sensitivity.

A microprocessor collects every 0.5 s the frequency converted acceleration data during 10 minutes and then performs a double integration from which are computed the mean wave height and the mean wave period (H1/3 and T1/3). Measurements can be renewed every 15, 30, 60 or 180 minutes [5]

The data are sent through an ARGOS transmitter.



According to the measurements renewal periodicity, consumption of the MARISONDE H is 257, 162, 113 or 78 Ah (for measurements every 15, 30, 60 and 180 mn respectively).

A first prototype has successfully been tested on sea at Brest in February 1981. The structure was equipped with the accelerometer and a tape recorder collecting continuously the acceleration data. The definitive MARISONDE H1 with the microprocessor has been launched in the same area in June 1982 and good correlation has been observed with visual observation and wind measurements. A final validation test will be made in spring 1983 with another wave measurement instrument. (Fig. 7).

The second prototype, equipped with a 1.5 meters high mast sustaining wind speed and wind direction sensors, will be completed in spring 1983 (Fig. 6).

Several applications are already provided with the MARISONDE H. The first one is the synoptic assistance for the Meteorological sea state coast observation network, the equipment of which is becoming insufficient and obsolete. Several other drifting applications are in prospect for both scientific and operational uses. One of these is the validation of the ionospheric radar which collects data of the surface wind and the sea state through wave reflection on the ionospheric layers. Another prospective use is assistance for recovery operations of the European rocket first stage after launching in French Guyana.

#### LITTERATURE

1 BEAUREPAIRE M, A. FRAPPIER

"Le nouveau baromètre CAP 130 pour mesure de pression atmosphérique sur bouée ou station automatique"  
Note technique EERM N°75 Direction de la Météorologie - Juillet 1980.

2 FUSEY F.X.

"La bouée MARISONDE en phase opérationnelle"  
METMAR N°110 pp 5-15 - Direction de la Météorologie 1er trimestre 1981.

3 KLAUS V.

"Moored Automatic stations developed at EERM and modes of transmission"  
Proceedings WMO Conference on Automation of Marine observations and Data Collection - Report N°7 Hamburg, 7-11 September pp 95-102.

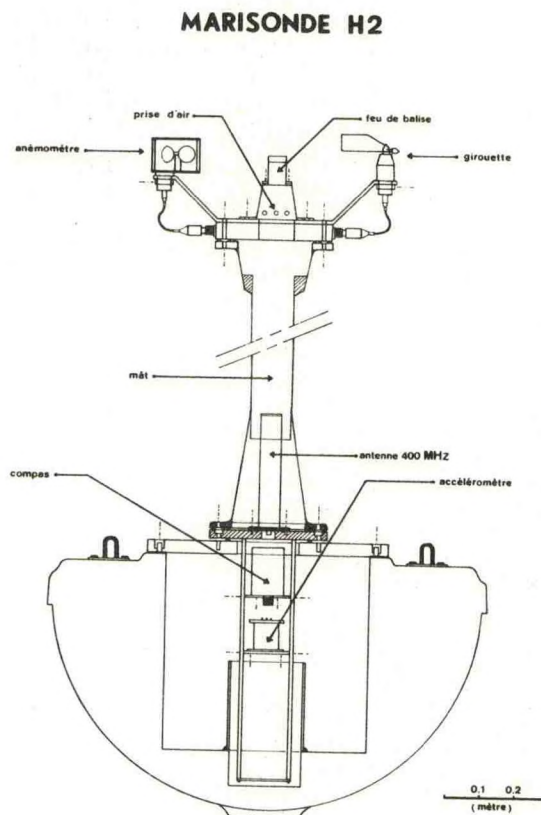
4 KLAUS V., A. PETITPA

"MARISONDE H - Etude de structure et premiers résultats".  
Note technique EERM N°92 - Direction de la Météorologie Février 1981.

5 QUINTY P.

"Définition d'un algorithme permettant, à partir des données accélérométriques, le calcul de deux paramètres significatifs de la houle et d'un calculateur embarquable utilisant cet algorithme".  
Thèse Docteur de 3ème cycle - Université Pierre et Marie Curie - Paris 6 - Novembre 1982.

Fig. 6 - The MARISONDE H2



- 6 THERY J.J., P. BOULY, M. BEAUREPAIRE  
"MARISONDE B, description série PEMG"  
Note technique EERM N° 41 - Direction de la Météorologie - Novembre 1979.

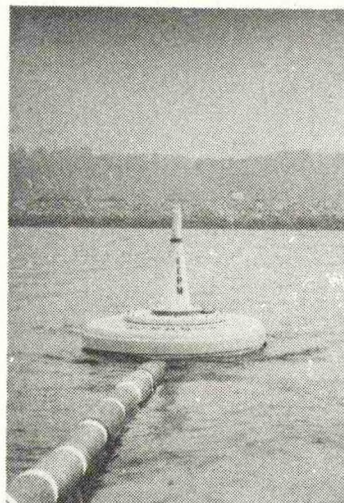


Fig. 7 -

The MARISONDE H 1  
on sea



# **SUCCESSFUL DESIGN AND HANDLING TECHNIQUES FOR Tz CABLES USED BY NDBC DURING 1982**

B. F. Case and J. F. Holmes

Computer Sciences Corporation  
National Space Technology Laboratories  
NSTL Station, MS 39529

W. L. Beacht

NOAA Data Buoy Center  
National Space Technology Laboratories  
NSTL Station, MS 39529

## **ABSTRACT**

This paper describes the methods and problems of deployment and retrieval of Tz (temperature measurement in the z direction) cables in the Gulf of Mexico and the Great Lakes. The methods of hull penetration (including materials and their use), cable design, strain reliefs, and the Kevlar strength members are discussed in detail. Projects results, including sample data, are also presented.

## **INTRODUCTION**

When the NOAA Data Buoy Center (NDBC) was organized in 1970, the data buoys were designed to take water temperature measurements at discrete depths using an aircraft data communication scheme. The data were transmitted by an inductive coupler and a single electrical wire in the mooring line. The system worked but was plagued with problems such as handling and data communications, and the Tz (temperature in the z direction) feature was "put on the back burner" until the buoys and data systems were made more reliable.

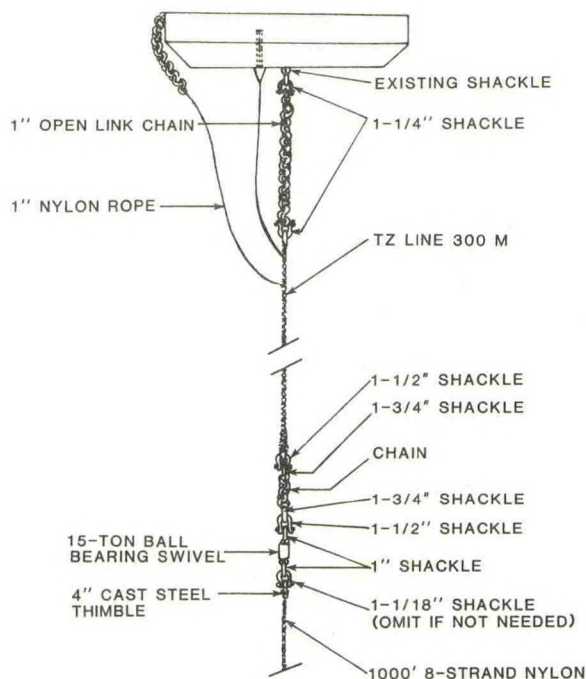
By 1976, the NDBC data buoys had produced many buoy years of reliable and accurate weather data. In 1976, the buoy office conducted a Temperature Measurement Conference and it was decided that NDBC should develop Tz lines and not some other type of measurement system such as profilers. In 1978, the Tz cable program was again set into motion with a simple and straightforward concept of the Tz measurement technique. The Tz Buoy Development Plan [1] was written. This plan called for an analysis of existing ocean temperature data collection systems. A total of 33 systems were investigated under this plan. Then in October of 1978, a system review was completed and the recommendations published in the report Ocean Temperature Measurement Systems [2] for moored buoys.

After a series of tests in late 1979, three cable designs immediately were recommended for further development:

- Integrated Tz System--where the Tz cable and mooring line are integrated into one line (Figure 1)
- Physically-Tied Tz System--where the Tz cable is tied at 20-ft intervals to the mooring line (Figure 2)

- Hang-Free Tz System--where a "short" Tz cable is hung off the stern of a NOMAD (boat-shaped) buoy (Figure 3).

The development of materials such as Kevlar and polymer molding compounds were becoming more widely used in the ocean engineering community. The Kevlar was used as low-stretch synthetic lines and the polymer moldings were used for waterproofing, strain, and stress reliefs. A decision was made to test these materials in two of the selected candidate Tz systems.



**Figure 1. Integrated Tz System**

## **SYSTEM DESIGNS AND DEPLOYMENT**

Because the Naval Ocean Research and Development Activity (NORDA) was instrumental in pioneering the use of Kevlar for a strength member in instrument arrays, they were contracted to develop the integrated Tz cable. The integrated Tz cable consisted of a mooring line integrated with an electrical cable. NORDA procured the integrated Tz cable from Wall Rope Co. with a torque balanced, braided, waxed Kevlar 29 strength member around 18 pairs of



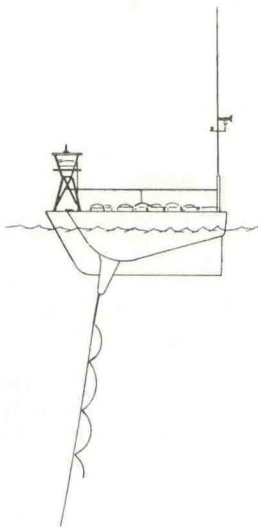


Figure 2. Physically-Tied Tz System

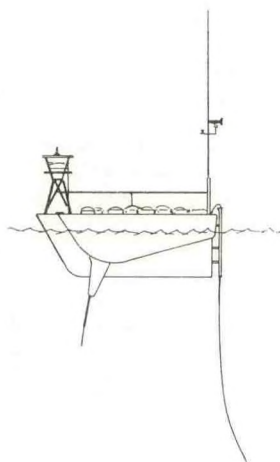


Figure 3. Hang-Free Tz System

polyurethane jacketed conductors. The individual conductors were insulated with polypropylene (see Figure 4 for detailed construction). At the desired intervals along the line, 12 YSI 44903, metal encapsulated thermistor assemblies were installed. The thermistor assemblies were encapsulated in the metal/polyurethane filled bullet-shaped housings to protect the thermistor beads and their leads from damage. To install the thermistor assemblies, the external covering of polyester braid was slit about 5 cm lengthwise at each thermistor location, and the Kevlar was separated enough to expose the central electrical conductors. A pair of conductors was cut, and a thermistor assembly was installed on the upper end of the conductor pair and inserted into a lubricated tygon tube inside the cable. At two locations, pressure transducers were installed using connectors. A

3-in. tufted nylon fairing was used for antistrumming protection. The length of cable used in the mooring system was terminated with dacron stoppers. The electrical cable penetrating the buoy hull was strain protected by a urethane stress relief "carrot" using a 6 to 1 scope and a durometer of 60. Several durometer urethane materials and shapes for the "carrot" and other strain and stress devices were tested before the final selections were actually accepted. The hull penetration was made through a standpipe using a 1-in. stainless steel threaded pipe embedded in the "carrot" as a securing and routing device (Figure 5) for the electrical cable.

Samples of this integrated cable design were break tested by the manufacturer, and extensive electrical tests were conducted by the contractor. After the thermistor assemblies were installed, a maximum load pull test was conducted by NDBC. After the integrated Tz cable satisfactorily passed these tests, it was calibrated in a large temperature pressure bath at NSTL.

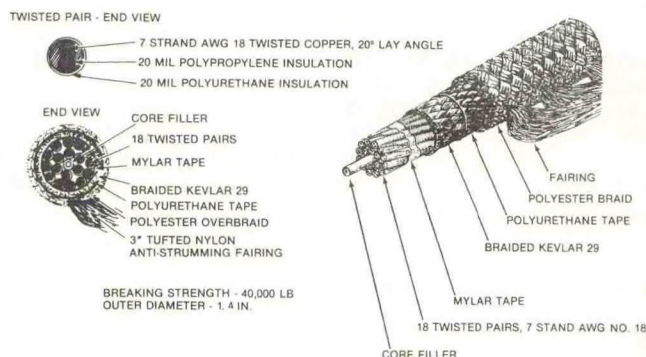


Figure 4. NDBC Integrated Thermistor Array

The next step was to integrate the Tz system into a modified 5-m discus buoy hull equipped with a General Service Buoy Payload (GSBP). The GSBP reported wind speed and direction, air temperature, surface temperature, and barometric pressure hourly. The buoy also was equipped with motion sensor packages for sensing rotation and wave action. With this hourly recorded data, logical conclusions could be drawn during the post deployment analysis.

After the integration checkout was completed, the system was disassembled and the buoy was placed in the NSTL canal so the at-sea deployment and recovery procedures could be completely rehearsed by the deployment team. The detailed deployment and recovery procedure had been written to cover each step of these complicated at-sea operations. Each step had been simplified as much as possible in the planning stage. This rehearsal debugged the deployment procedure and gave the deployment team confidence in their abilities. This procedure called for the team to assemble the middle and lower moorings, attach the integrated Tz cable to the



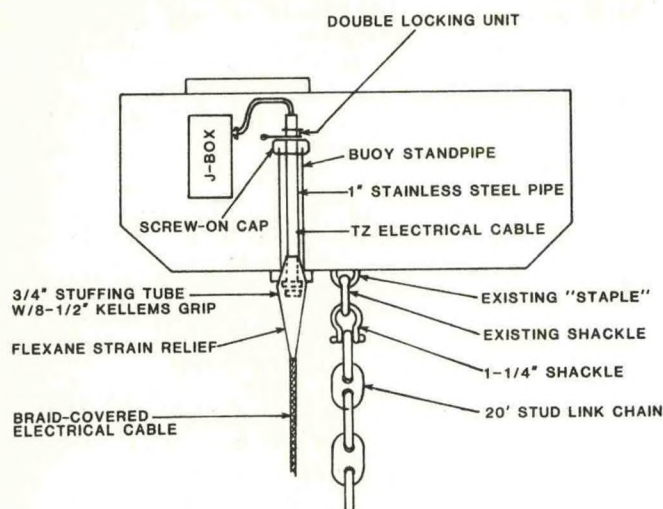


Figure 5. Standpipe with Carrot Seated

middle mooring, and figure 8 the cable on deck while enroute to the deployment location. Upon arrival, the deployment team would board the buoy and prepare it to accept the cable and mooring. Then the upper end of the Tz cable was passed from the ship to the buoy by tag line. When the upper end of the cable was secured on the buoy deck, a previously installed messenger line was attached and the electrical cable was lowered over the side of the buoy and pulled through the standpipe. This step also seated the "carrot" strain relief in the hull penetration standpipe. Once the "carrot" was seated and secured, the upper mooring was assembled on the buoy deck and lowered over the side of the buoy. The cable was connected electrically, and readings were made from each sensor to assure proper operation at this time. The buoy was closed and the deployment team returned to the ship. The remainder of the Tz cable, middle mooring, and acoustic release assembly was deployed by hand. The lower mooring was deployed by dropping the 6,000-lb clump anchor. Once the mooring was set and the sensors given time to stabilize, 3 hours of ground truth (XBT temperature profile) data were transmitted back to NSTL for comparison with the data received from the buoy via the satellite system.

During the 8 months that this system was deployed, one of two pressure sensors failed because of corrosion in the connector and five of the eight thermistors were out of tolerance because of water intrusion through the urethane potting and epoxy coating. However, the cable mechanically withstood the harsh Gulf of Mexico environment without damage for 8 months other than one area which was probably fishbite. This damaged area was removed and sent to Woods Hole Oceanographic Institute for study [3] and confirmed as a probable fishbite. This damage was located 865 ft down the line. The portion of line below the probable fishbite area was sent to Wall Rope Co. for strength test. The strength test proved that the portion of the cable that had not been disturbed and the lower termination were still

at the original break strength. The areas where the Kevlar had been disturbed had lost 1/5 of the original break strength [4]. This loss had been accurately predicted by the manufacturer. The upper 850 ft of cable was reterminated and has since been deployed with an inductively-coupled Tz system in the Gulf of Mexico.

The second Tz cable system to be described in this paper is the physically-tied Tz system designed for a Great Lakes NOMAD buoy. This system was put through the same design and predeployment tests as the integrated Tz cable. However, additional tests were required on the upper section of the electro-mechanical cable because of the swinging yoke assembly (Figure 6) used as the mooring attachment on the NOMAD hull. This assembly had presented challenging routing and stress problems in the design phase. Preliminary test results indicated a simple "torque tube" design would offer the best overall protection for the cable in this area. A test cable was fabricated and cycled 358,974 times on a simulated yoke assembly using the inexpensive "torque tube" routing and stress relief design. The test cable survived the stress test, and this proposed design was used on the deployed model.

The physically-tied cable was 50-m long with eight thermistors and two pressure transducers installed at discrete depths. The strength member was a 160-ft braided Kevlar rope terminated with eye splices at each end. The 16-conductor electrical Tz cable lashed to the strength member had a 1/4-in. wire rope coated with polyurethane for a core. The conductors were insulated with nylon coated PVC. The cable was water blocked with a putty material and waterproofed with a polyurethane extrusion. Eight thermistors and two pressure transducers were installed at discrete levels. The electromechanical cable was lashed to a torque-balanced Kevlar strength member every 20 ft. During the first deployment, an 18-in. loop was provided between each lashing to accommodate stretching and twisting. At alternate 20-ft. intervals,



Figure 6. Swinging Yoke Assembly



braided Dacron recovery slings were installed on the Kevlar strength member. The electromechanical cable was routed from the top of the Kevlar line termination along a 15-ft length of stud link chain to the buoy swinging yoke. A 42-in. loop was provided in the section to accommodate entry offset and twisting. This upper section of the electromechanical was whipped with 1/4-in. nylon coated with polyurethane for wear and stress relief.

Detailed deployment and recovery plans were written for each task and a rehearsal was conducted whenever possible before deployment. Because of the "torque tube routing" on the yoke, the system had to be assembled and installed completely before deployment. After the assembly and checkout on the ship's deck, the buoy was lowered into the water and towed away from the ship while the Tz line was hand lowered from the deck. The rest of the mooring was set by dropping the clump.

During the first season (1981), the system was deployed in Lake Michigan for 6 months. Two weeks before the scheduled December recovery, a catastrophic failure of five thermistors and one pressure transducer occurred during a severe winter storm. After recovery and during the initial failure analysis inspection, no damaged or serious wear areas could be located on the outer coverings of the cable assembly. But during a more detailed inspection, a small tear was found in the cable breakout stress relief mold at the 6-m level. The stress relief mold was removed, and the cable was carefully opened at this point. All broken wires were located in a 1-in. area at this location. All tests conducted indicated that this section should have a shorter twist loop and be more flexible to avoid future stress damage. The lashing did not provide the stress relief needed in this area. Since then a braided covering has been used as the stress relief. This section of cable was removed and replaced with a braided section that meets the new requirements. Also a more flexible stress relief wear protection material was installed. The stretch loops between the tie-points were also reduced to 2 inches. The Tz cable system was recalibrated and deployed for a second time in 1982 for a period of 9 months (March through November). During this second deployment, all temperature sensors operated the full 9 months and the only failure noted was a pressure transducer developed an intermittent problem. The recovery was conducted on December 8, 1982. During the post recovery failure analysis, no damage or excessive wear was noted. The assembly was recalibrated and has been redeployed for a third season without rework in 1983.

#### COMMONALITIES OF THE SYSTEMS

The two long-term successful deployments just described have several commonalities. Both Tz systems used Kevlar strength members, polymer molding compounds as major components, and extensive planning and testing preceded each deployment. The Kevlar fiber has proven to be an easy to handle, durable, and reliable low-stretch strength member. The Kevlar fabricated into a torque balanced rope was successful in transmitting the discus buoy rotation to an in-line swivel to avoid cable twist-

ing that would result in conductor breakage. The use of durable polymer compounds for stress relief and wear protection on areas where heavy fatigue had been experienced in earlier systems proved very successful.

#### DATA ANALYSIS

A graph illustrating the data obtained from buoy station 45007, which was moored in the middle of Lake Michigan east of Milwaukee at 42.7°N 87.1°W, is shown in Figure 7. The data are continuous from March 23, 1982, when the buoy was deployed to November 15, 1982, when the buoy was retrieved for the winter ice season. The display Figure 8 shows the temperature for each thermistor location, with #0 the surface water temperature down to #7 for the 47-m depth. The water depth is 161 m at the buoy location, and it is the low pocket for southern half of Lake Michigan.

On April 4, #7 temperature sensor began to show a general downward trend to a low of 0.5°C on April 18 when it started up and continued up until the passage of a storm on May 7 made the #7 sensor fall into a regular pattern for the rest of the year.

The actions of #7 could be explained this way: the warm weather of late March and early April melted the snow, which picked up the chemical fertilizers on the farming fields of central Michigan. This water emptied into Lake Michigan by the numerous streams and rivers on the east shore. The additional chemicals and the cold water made the mixture sink into the pocket below the Tz line, just reaching up to #7 sensor.

It should be mentioned that the temperature of maximum density for fresh water is +3.8°C, and for saltwater at 33 ppt, and the maximum density occurs at -1.3°C or the freezing point of saltwater. Therefore, the water with fertilizers (both phosphates and nitrates) in it will not rise to the lake surface as it goes below 3.8°C, but it will continue to remain in the pocket.

The storm on May 7 mixed the lake sufficiently to dissipate the fertilized waters throughout the lake and eliminate that anomaly. Chemical samples taken in the deep area in another year are expected to confirm or lay to rest the fertilizer theory.

Another point of interest is the temperature of the surface water, which remained low until June 23 when a sunny day heated it up so that it remained the warmest sensor until August 20 when it slowly began to go below the temperature of the 10-m sensor.

As for internal waves in the lake, the maximum activity during July can be seen at #1 and #2 or a depth of 10 to 14 m. While during late August and September, the internal waves or the thermocline had moved to #3 and #4 or 19 to 25 m, and in late September and October the thermocline had moved to #5 at 28 m. The last major movement of the lake was on October 20 when a fall storm passed over the lake mixing all the water to a temperature of 8 to 9°C.



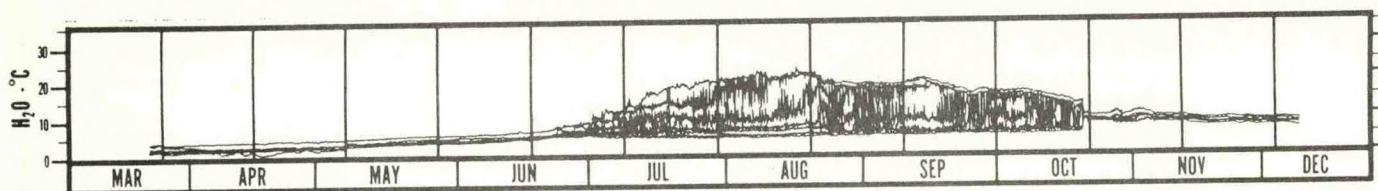


Figure 7. Data Obtained from Buoy Station 45007

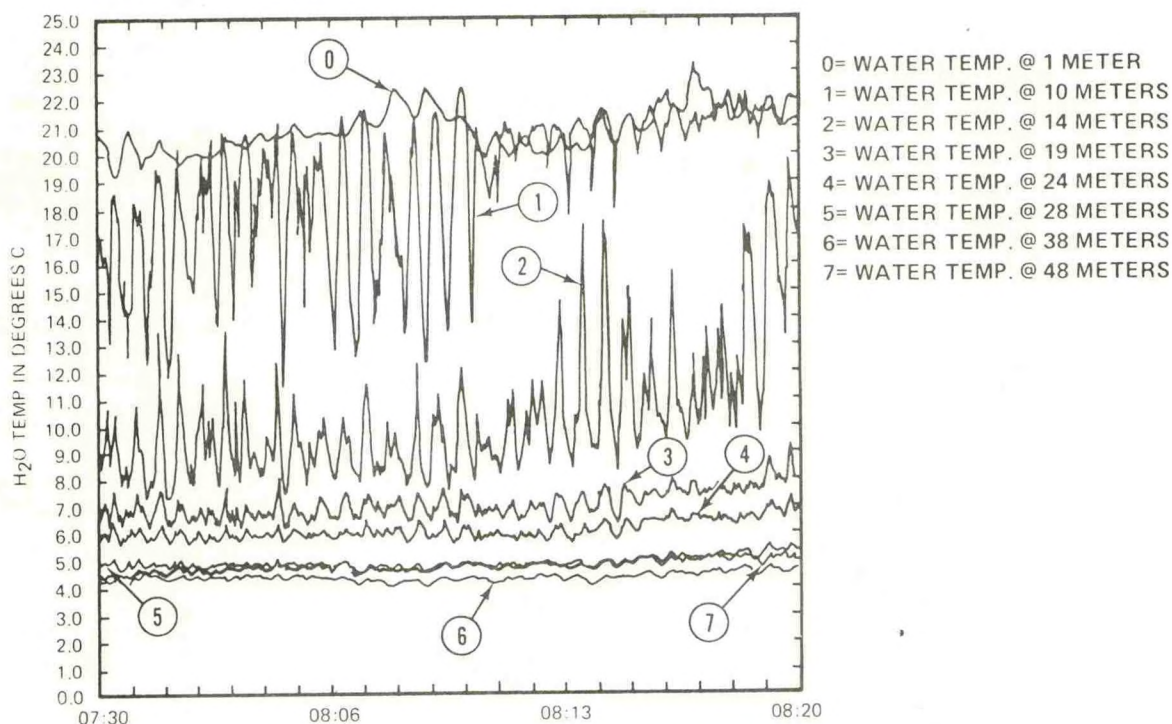


Figure 8. Temperature for Each Thermistor Location

About November 1, it appears the lake was trying to stratify again, but there was not enough residual energy in buoyancy in the cool water, 8 to 10°C, or enough time with no storm agitation to stratify the water. After November 7, the lake was preparing for its ice cover as the surface temperature was the lowest of the Tz string. During this time of year, the lake obtained its greatest oxygen ( $O_2$ ) content because any meteorological disturbance, i.e., wind or barometrical change, would mix the lake.

The data obtained by the integrated Tz system from buoy location 42009, moored southeast of Mobile, AL, in 3,300 ft of water are not illustrated in this paper but are available from NDBC. These data have many points of interest as did the physically-tied cable located in Lake Michigan. The correlation of meteorological data and bathymetrical data from the two deployments has proven very interesting.

#### CONCLUSIONS

Technology is presently available to design and fabricate an operational Tz system for worldwide deployment. The use of Kevlar fibers for strength members and polymer molding materials for stress and wear relief played an important role in the

success of these deployments. However, these successes would not have been possible without careful planning, extensive testing, and personnel training. This technology, coupled with the currently useful satellite data systems, can produce a continuum of data that will be invaluable to the scientific community. This data, as illustrated, may be acquired hourly for extended periods of time from any moored location. The system designs should be as simple as possible with careful considerations given to the ease of handling during deployment and recovery operations.

#### REFERENCES

1. "NDBO Tz Buoy Development Plan," Engineering and Science Services Laboratory Report, 1978.
2. "Ocean Temperature Measurement Systems for Moored Buoys," Engineering and Science Services Laboratory Report, October 1978.
3. Prindle, Bryce, "Cause of Damage to NDBO Station 42009 Tz Mooring," Woods Hole Institute Report, 1982.
4. Beacht, W. L. and B. F. Case, "Integrated Tz Line Test and Evaluation Final Report," NDBO Report, 1982.



# NORWEGIAN OPERATIONAL DATA BUOYS IN NORTH-EAST ATLANTIC WATERS

Jan A. Strømme

Bergen Ocean Data  
Bergen, Norway

## ABSTRACT

Moored, high capacity data buoys with onboard data processing and data transmission facilities are now operational on the continental shelf off Mid-Norway and in the North Atlantic. Two different buoy hulls are used; - the cylindrical buoy designed as a meteorological data collection platform, and the disc-shaped buoy designed for meteorological and oceanographic observations.

Instrumentation and sensors for the two types of buoy hull are interchangeable. The data acquisition system is based on an extensive use of CMOS microprocessors, and various types of radio communication systems are available. A shore-based data receiving station is included in the system.

Small, freely drifting buoys have come into increasing use in North-East Atlantic waters over the past few years. The buoys are a modified version of the drifting buoys deployed under FGGE, and report water temperature and barometric pressure via ARGOS to a local user terminal in NORWAY.

## 1. INTRODUCTION

In 1963 the first Norwegian experimental meteorological data buoy was deployed in open waters, and since then a long series of prototype buoys has been designed, built and tested in all weather conditions in the Norwegian Sea and North-East Atlantic. Most of this work has been carried out by the Norwegian Meteorological Institute (NMI) and Chr. Michelsen Institute (CMI), in cooperation with other Norwegian research institutes and industrial companies. Since 1976 moored data buoys have been operational on the continental shelf, collecting meteorological data and wave data, in particular for use by the oil industry. Mooring locations for the experimental as well as the operational Norwegian data buoys are widely distributed in the North Sea and the North-East Atlantic. Mooring depth varies from 100 m to more than 2000 m, and in most of the area wind speeds of

60 knots and wave heights of 20 to 25 m have been recorded. Operational data buoy systems which are currently in use in Norway comprise moored oceanographic and meteorological data buoys, free drifting buoys, shore-based receiving stations and automatic meteorological stations for the polar regions. This paper will very briefly discuss the various types of equipment used.

The Bergen Ocean Data company was formed to produce and market the data buoys and other equipment described below.

## 2. MOORED BUOYS

Two different buoy hulls have been designed and are now available; the cylindrical NORMET buoy and the disc-shaped NORWAVE buoy. Instrumentation and sensors for the two types of buoy hull are interchangeable.

The NORMET meteorological buoy is designed for use as a platform for meteorological observations. The first prototype was deployed in 1973 in the North Atlantic, and since then a number of buoys have been moored in those waters as automatic weather stations. Standard meteorological sensors for the NORMET buoys measure barometric pressure, air and sea surface temperatures and wind speed and direction. For data transmission the NORMET buoy is normally equipped with an HF radio transceiver and an ARGOS satellite transmitter. The NORMET buoy hull is made of non-magnetic stainless steel, glassfibre-reinforced polyester and polyurethane foam. A stabilizing structure with a ballast weight is bolted to the base of the hull. The data acquisition module and the battery bank are located in the inner tube of the buoy, with access through the top cover. Buoy diameter is 1.0 m, length of hull including stabilizing structure is 7.2 m and total weight is approx. 1300 kg.



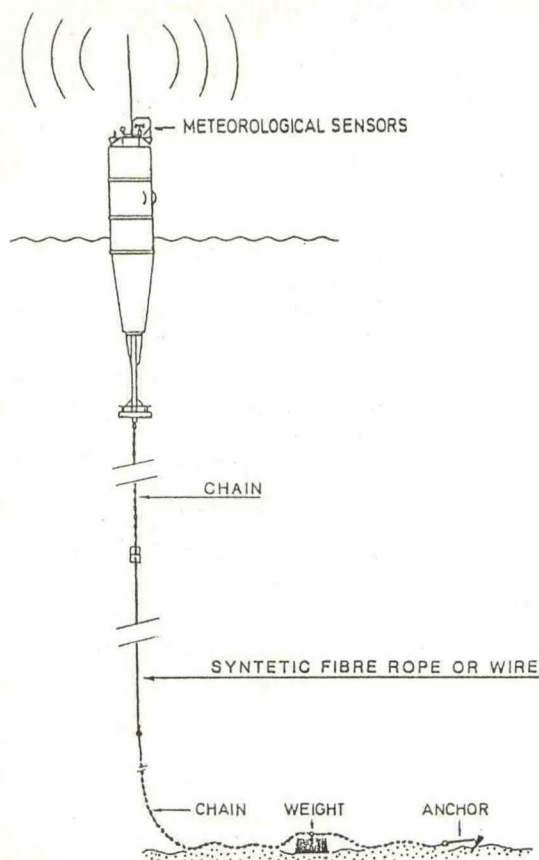


Figure 1. NORMET data buoy.

The NORMET data buoy is anchored by a semi-taut mooring line, consisting of chain, wire rope or synthetic fibre rope and a mooring weight and/or an anchor. The NORMET buoy ODAS 451 is now moored west of the Faeroes in 1500 m deep water and functions as an automatic weather station in the COST-43 project. The buoy reports met-data every three hours by HF radio to a receiving station located in Reykjavik, Iceland, and by ARGOS satellite telemetry to a local user terminal, LUT, in Oslo and via Service ARGOS.

The NORWAVE buoy is designed as a wave-following meteorological and oceanographic observation platform, and has been extensively used for climatological and wave directionality studies in the Norwegian Sea. The buoy provides the user with real-time data on wind, temperatures, barometric pressure, wave and other met-ocean observations. The buoy is provided with onboard processing and long-term data storage capabilities, and transmission of data to shore is provided via HF, VHF or UHF radio to a receiving station, or by means of low orbiting satellite telemetry. Construction materials of the NORWAVE buoy are non-magnetic stainless steel, glass-fibre-reinforced polyester and

polyurethane foam, chosen for long term durability in marine conditions.

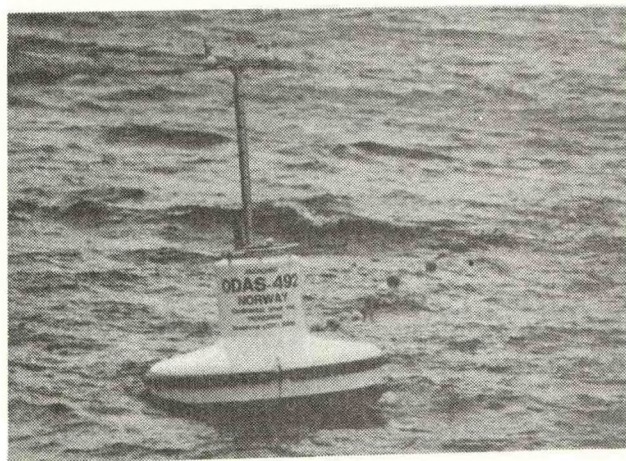


Figure 2. NORWAVE data buoy.

Meteorological sensors and the radio antenna are located in the sensor mast. The data acquisition module, battery pack and wave sensor are located in the instrument compartment. The buoy is provided with lifting hooks and fenders, and a steel substructure with ballast weight is bolted to the base of the hull. Buoy hull diameter is 2.75 m, total height of buoy including sensor mast and keel is approx. 6 m, while the total weight of buoy is 1300 kg.

Two different types of mooring systems have been used for the NORWAVE buoy. The first, shown in figure 3 consists of a floating mooring line, a subsurface buoy, a taut mooring line, mooring weight and anchor and chain. This mooring system leaves the buoy relatively free of frictional, inertial and elastic mooring line effects, and has proven to be very suitable when the buoy is used for wave directionality measurements. The taut mooring line can have oceanographic sensors attached to it. The mooring system described is the one most commonly used by Norwegian data buoys since 1979, and has been used in water depths up to 300 m. With only minor modifications, the mooring system can be used in water depths of 1000 m or more.

The mooring system is deployed by using the "buoy first - anchor last" method. For service the buoy can be recovered without lifting the mooring system. Since January 1980 data buoys of the NORWAVE type have been used in the ODAP program and moored in several locations on the Norwegian continental shelf, in particular in the areas off Mid-Norway. The buoy reports 3 hourly data via ARGOS satellite telemetry to a LUT at the NMI in Oslo.



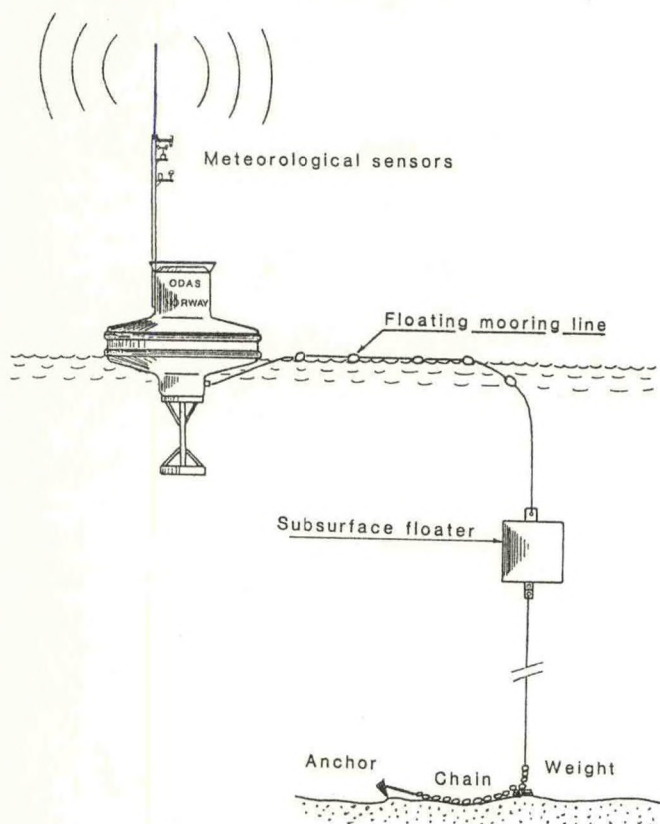


Figure 3. NORWAVE data buoy.

The reports include meteorological data for forecasting purposes and wave data for climatological studies. Wave directionality analysis are produced by an onshore computer from time series of buoy heave and tilt data stored on magnetic tape onboard. ODAP is a large multiyear oceanographic measuring programme covering the Norwegian continental shelf. The programme is financed jointly by Norwegian oil companies and governmental agencies and institutions; the Continental Shelf Institute, IKU, in Trondheim is in charge of all field activities.

### 3. SENSORS AND INSTRUMENTATION

#### Sensors.

Standard meteorological and oceanographic sensors for the NORWAVE and NORMET buoys are:

- \* Wind speed and wind direction sensors, including a north reference compass.
- \* Air temperature sensor.
- \* Barometric pressure sensor.
- \* Water temperature sensor.
- \* Wave sensor. (Heave sensor or heave pitch and roll sensor). NORWAVE buoy only.

The wave sensor is mounted on the vertical centre line of the buoy and close to the centre of buoyancy. The sensors listed have been selected because of their proven performance over many years on data buoys. Other sensors can be installed for sampling such parameters as relative humidity, sea water conductivity, temperature profile, current speed and current direction.

#### Data Acquisition.

Until recently the NORWAVE and NORMET buoys were provided with a data acquisition system which had been developed in the early 70's. This system was based on CMOS electronics and had a large data sampling capacity but very poor data processing capabilities. Last year a completely new design was introduced. This Data Acquisition System, DAC, is designed as a low-power system for applications in moored and free drifting data buoys and automatic weather stations for remote areas. The DAC is designed as a modular system and it is based on only two different types of electronic printed circuit boards, pcb. System block diagram is shown in figure 4. The first type of pcb is the Central Control Processor, CCP, located on a single Eurocard. The CCP contains the central processing unit, (an 8 bit CMOS micro-processor), EPROM and RAM memory, input/output circuits and the calendar. Only one CCP is required to operate the DAC. The CCP can communicate with different types of other equipment, such as the Sensor Interface Units, SIU, (unlimited number), magnetic tape recorder, ARGOS PTT, HF, VHF or UHF radio transmitter/receiver units, printer terminal or visual display unit, (for control and test purposes). The other type of pcb is the Sensor Interface Unit, which will process data from a particular sensor or group of sensors. Each SIU consists of two parts, the general part and the special part, both located on a single Eurocard pcb. The general part comprises a data acquisition system consisting of an 8 channel multiplexer, a 10 bit A/D converter, a single-chip CMOS  $\mu$ P, EPROM and RAM, input/output circuits and power regulators. The special part of the SIU gives room for all interfacing necessary between the sensor and the general part of the SIU. Each SIU is switched on by a signal produced by the task time-table on the CCP. Communication CCP - SIU is via the main communication bus on 8 bit ASCII format, 300 or 9600 baud. Sensors signals collected are processed in the  $\mu$ P of the SIU. The processing includes linearizing, averaging, temperature compensation, combining two or more signals, vector integration, adding of calibration data, scaling and parameter designation.



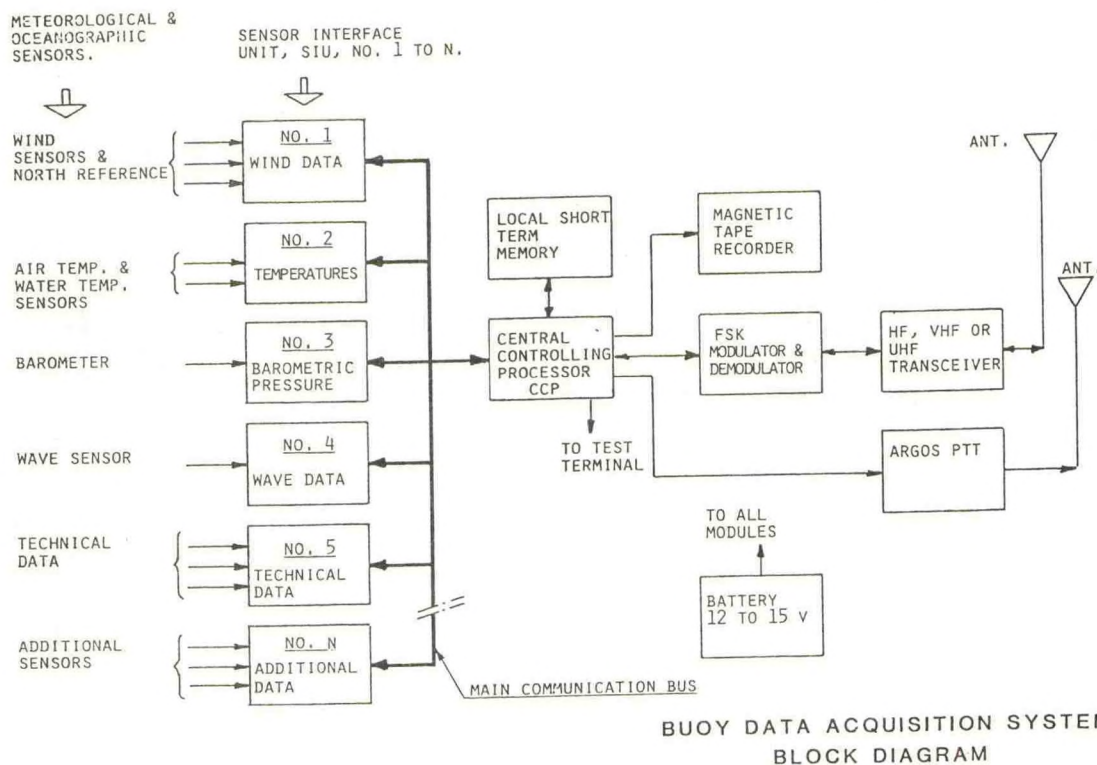


Figure 4.

For calibration and servicing purposes the SIU can be connected directly to a printer terminal or equivalent via the RS232 C or 20 mA current loop terminals.

#### Data transmission.

The NORWAVE and NORMET data buoys are provided with the following data transmission systems:

**HF radio link:** Single or two-way systems (for remote control), operating in one or more channels in the WMO/IOC-allocated ODAS radio frequency bands.

Range: approx. 2000 km.

Modulation: Two-tone FSK.

**VHF or UHF radio link:** Range up to 50 km. Single or two-way systems.

ARGOS low-orbiting satellite telemetry, including buoy positioning.

ARGOS telemetry is the system most often used in North Atlantic waters, whereas point-to-point communication on VHF/UHF or HF is preferred in areas where no local ARGOS ground station is available. Normally all data collected are pre-processed by the onboard computer before transmission to shore.

In addition, all raw and processed data can be stored onboard on a high-capacity cassette type magnetic tape recorder. Onboard storage of data is of particular interest in those cases where a non real-time and high data recovery rate capability is required, in cases where the amount of data is too large compared to the radio transmission capacity, or in cases where detailed analysis of data on an onshore computer is required. An example is onboard storing of the buoy heave, pitch, roll and heading data for further wave directionality analysis on the onshore computer.

#### 4. POWER SYSTEM

The NORWAVE and NORMET data buoys are powered by a single battery or a bank of battery modules. Each module is fitted with large carbon-zinc or lithium thionyl elements, wired up to give the required capacity and supply voltage. Typical battery lifetime is in the range of 9 to 15 months.



## 5. SHORE BASED RECEIVING STATION

The NORWAVE and NORMET buoys transmit data by HF or VHF/UHF radio to a NORLOG shore station. The shore station, which can receive data from a number of data buoys, can also operate as a transmitting station, making it possible to selectively interrogate and command one or more data buoys in a network.

The shore station comprises the following equipment:

- \* Radio antenna, directional or omnidirectional.
- \* HF, VHF or UHF radio transceiver.
- \* Data demodulator and modulator.
- \* Data processor.
- \* Digital magnetic tape recorder.
- \* Printer terminal.
- \* Power supply, with back-up battery.

A telephone modem for transfer of data via the public telephone network, and a visual display unit can be connected. The shore station is located in a standard 19" rack. Data received by the shore station are decoded in the FSK data demodulator/decoder, recognized, identified and processed by the data processor. The data processor software contains a bit comparison technique program used to eliminate any errors in the received data. Standard shore station output formats are:

Meteorological, oceanographic and technical data which are transmitted from the buoys at regular intervals, (i.e. every 3 hours) are displayed on a printer/VDU and recorded on magnetic tape in plain text, and in engineering units. Observation date and time are included. Standard signal format is ASCII, 300 baud, RS232 C.

```

ID: 0101 TXCODE: 22 TDATE: 190483 TTIME: 205000
NTX MDATE MTIME AIRT HUMD SEAT WVAW WSPM WGUS
002 190483 204900 22.3 65.6 20.6 145//// 19.2 24.4
HMEAN HSI6 HMAX TSIG TZ
1.70 1.90 3.40 5.10 4.70
INT1 BAT1 BAT2 POWF POWR ERRCODE PARITY CHECKSUM
21.4 14.3 3.4 10.2 1.8 015 0000 0000
BEXX
BUDY 23001 19214 99237 10585 46/// /1519 /0223
4//// 5//// 22200 00206 10504
  
```

Figure 5. Example on printout of data from the NORLOG shore station.

In addition the meteorological data and some of the oceanographic data are transformed by the data processor to the standard WMO Ship Code, and are displayed on printer/VDU and recorded on magnetic tape.

## 6. DRIFTING BUOYS.

Various types of drifting buoys have been deployed in North-East Atlantic waters and the Arctic regions since 1975. All use ARGOS for positioning and telemetry of data, and they have normally a low data acquisition and data processing capability. Some of the buoys are designed as expendable units, while other types are recovered and reused after service.

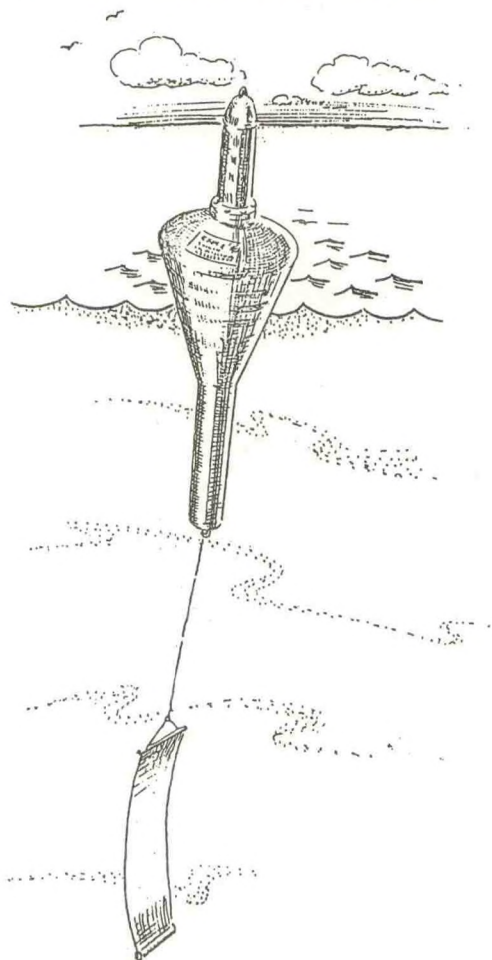


Figure 6. NORDRIFT. Meteorological drifting buoy.

The NORDRIFT buoy, which is the only drifting buoy discussed in this paper, is a modified version of the Norwegian drifting buoys deployed under the WMO FGGE experiment. The buoy is provided with sensors which measure barometric pressure and water temperature, and barometric pressure tendency is calculated by the onboard microprocessor before transmission of data via the ARGOS PTT. Sampling interval is user-programmable, and is normally 15 minutes for buoys deployed in the North Atlantic.



The data acquisition system is identical with that used in the large data buoys, but it contains fewer sensors (see figure 4 ). Additional sensors for sampling other parameters such as air temperature and temperature profile can however be installed. The battery pack consists of lithium thionyl elements, and typical lifetime is 12 months. The buoy hull is made of non-magnetic stainless steel tube, containing all electronics and the battery, and it has a conical float made of polyurethane foam with a glassfibre-reinforced polyester skin. In order to reduce drifting speed, the NORDRIFT buoys are provided with either a window-shade drogue or a long synthetic fibre rope with high drag coefficient and a piece of chain.

The NORDRIFT buoys and a few other types of drifting buoys are deployed in the North Atlantic under the ODAP program. The buoys are deployed by the Norwegian Coast Guard, and they are normally recovered for service and maintenance after 6 to 12 months in operation. The plan for drifting buoys in the ODAP program in 1983 includes 12 to 14 units at sea and a few ashore for service. The buoys report via ARGOS to a local user terminal at the NMI in Oslo. Data are used for weather forecasting, in particular for offshore oil activities on the Norwegian continental shelf.



## COST-43 - A CO-OPERATIVE EUROPEAN ODAS EXPERIMENT

R. E. W. Pettifer B.Sc., Ph.D.

Chairman COST-43

### ABSTRACT

COST is an acronym for Co-operation on Science and Technology which is a major European co-operative programme on a wide range of scientific and technical research subjects. The programme is progressed through a large number of independent Projects.

COST Project 43 is unique among the COST Projects in that it is governed by a full international agreement between the signatory states who contribute to a small common administrative fund which pays for a Technical Secretariat to act as a focal point and technical advice centre. The aim of the Project is to establish around the European continental shelf and adjacent ocean areas west to the 32° Meridian and east to the 12° Meridian and between the 44°N and 60°N parallels, an experimental network of "real-time" oceanographic and meteorological ocean data acquisition systems, ODAS.

The experimental programme has lasted four years and its structure, achievements and future will be discussed.

### 1. INTRODUCTION

COST is an acronym for Co-operation in Science and Technology and is the name of a European programme of co-operative ventures ranging over a very wide spectrum of scientific and technical activities from the processing of sewage sludge to the study of transport systems. The programme is divided into a large number of autonomous PROJECTS, each flagged with a number, which are managed by their own Management Committees. The Management Committee of a project is comprised of representatives of those nations desirous of being involved in that project.

COST-43 is one of these projects and has as its aim the establishment of an experimental network of ocean stations (ENOS) for the acquisition of real-time meteorological and oceanographic data in European waters from Spitsbergen to the Azores and from 32°W to the European Continent including the North Sea, the Baltic and the Western Mediterranean. Among COST projects, COST-43 is unique in that it is governed by an International Agreement and has a small central fund with which it supports a Technical Secretariat. The Project life is four

years from its formal inception in June 1979 and it therefore is due to come to an end in June 1983. However negotiations are now in progress to extend the Agreement for a further four years and it is hoped that these will soon reach a successful conclusion. Prior to the formal start of the Project, signalled by the ratification of the Agreement by seven of the Signatory States, there was a lengthy interim project phase which culminated in a technical conference in December 1978.

### 2. THE COST-43 PROGRAMME

The project originally consisted of a series of national contributions by the Signatory States to the Agreement (Denmark, Finland, France, Ireland,\* Norway, Portugal, Sweden and the United Kingdom, since joined by the Netherlands and Iceland). These programmes were ambitious but were offered on a non-committal basis and in the event have been modified in response to a general decrease in resources available for this work. Nevertheless, a substantial number of Ocean Data Acquisition Systems (ODAS) have been initiated under the aegis of the Project and a 2.5-fold increase in daily real-time ODAS data output has occurred in the European region as the result of COST-43 action. See Fig. 1. These data originate from 44 ODAS stations distributed as shown in Fig. 2. Between 20 and 25 of these stations are now operational, and all are fixed sites. In addition to these fixed deployments, a programme of drifting buoy deployment was carried out early in the Project in the Azores region and further such programmes have been or are being carried out in the mid-Atlantic, the Bay of Biscay and around Iceland and Norway.

A feature of the COST-43 activity has been the gradual increase in co-operation between the various nations in the project aimed at establishing as joint programmes tasks which are too large for individual national institutes to handle by themselves. Such joint ventures have been carried out by France and Portugal, by Norway and the U.K., by Finland and Sweden and again by Norway and the U.K. this time in conjunction with Iceland. Exploratory talks are now in progress to try to establish further joint programmes in the Eastern Atlantic and the N. Sea. A virtue of the COST-43 arrangement is that such joint programmes, involving relatively major commitments for individual institutes or organizations, can be accomplished under the terms of a simple letter of intent between the Heads of \*also Belgium and Spain



Establishments, backed by the force of the International Agreement. These joint programmes have led to the establishment of both experimental and operational ODAS. Current work of this kind is in the Baltic and in the North Eastern Atlantic where a joint Norwegian/U.K./Iceland operational buoy has been established.

In addition to the equipment programmes, COST-43 carries out an active liaison and technical administration rôle in conjunction with other bodies in Europe which are concerned with related maritime matters. The principal activity in this regard has been the design of a proposed new ODAS data code for use, at least on a regional basis, on the Global Trunk System of WMO. This code does not replace the existing DRIBU, SHIP, BATHY and TESAC Codes but compliments them by making provision for the report of the real-time synoptic meteorological and oceanographic data obtainable from fully instrumental automatic ODAS. The code proposal was recently well received at the Commission on Basic Systems of the WMO and, it is hoped, will soon come into regional use in Europe. It may well find a wider use in due course.

Further activity of this type has been addressed to the problems raised by Customs formalities associated with the return to the owner nation of ODAS equipment found drifting or washed ashore, the question of salvage payments, the sanctity of ODAS from interference and the establishment of an internationally acceptable set of ODAS markings and signals. Extensive discussions have been held with IMO, IOC, WMO and many other international agencies of this type to try to resolve these issues but although much progress has been made, no formally agreed outcome has yet been achieved for them.

It was an original intention of the COST-43 programme that considerable co-operation would be generated between the nations involved and especially between the institutes contributing to the various national programmes, to facilitate the deployment, recovery and service of ODAS on an opportunity basis. By close liaison through the Technical Secretariat it was hoped that ship time could be obtained from one institute for another of a different nation on the basis of opportunity in the margins of other national projects and as a general contribution to the COST-43 programme. This idea has not been a success. We have found that in general there is very little opportunity and when there is some, then there is very little margin! A lesson learned seems to be that an ODAS venture requires dedicated ship time and that these costs are very high. However, it is the case that individual nations, as their specific contribution to a particular ODAS venture, have provided opportunity ship time in the margins of other activity such as coastguard and naval duties and this has kept the cost of some of our projects in the realms of the possible.

### 3. THE COST-43 TECHNICAL SECRETARIAT

The activities of COST-43 are co-ordinated by a Technical Secretary or Project Leader who is the only full-time employee of the Project. The Secretariat is based in the Christian Michelsen Institute in Bergen, Norway and provides a technical advice and liaison facility to assist national programmes with technical problems, to establish links between the various national institutes involved and to provide a background force to keep the Project momentum up, particularly by initiating the negotiations for joint programmes. The Technical Secretariat publishes a series of COST-43 Technical Documents which cover such subjects as reports on sensor comparisons, an inventory of current ODAS, a bibliography of current ODAS literature, especially unpublished reports, and a file of equipment suppliers. Much of this information is difficult to obtain in a coordinated form by other means.

The Project has held two technical seminars. The first of these was held in Lisbon in 1978 the second in Bergen in 1980. The proceedings of both meetings were published as COST-43 Technical Documents. A final seminar for the present four-year period is to be held in June 1983 in Reading, England.

The annual report of the Project, published each year in three volumes, contains in the volume of Technical Annexes (Vol 2) up-to-date reports from each participating nation of the status of their ODAS programmes so far as they contribute to the Project. This document and all COST-43 Technical Documents are available on request and at a small charge from the Technical Secretariat.

### 4. THE FUTURE

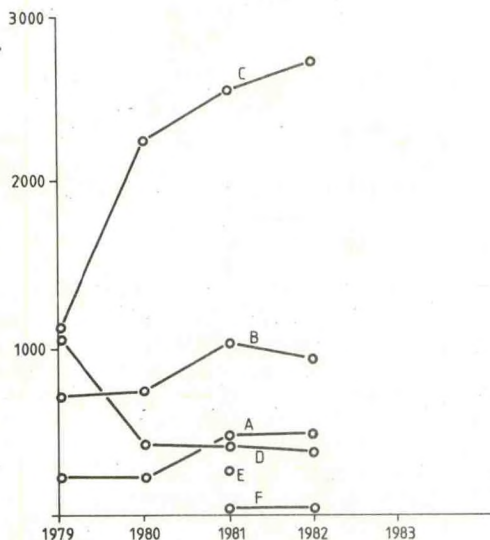
It seems clear that at least in the short to medium term there is little hope of establishing even the modest ODAS network aimed at by COST-43 unless the co-operation inherent in the Project can be continued. So far eleven nations have agreed in principle to continue with the work but not without considerable difficulty in finding the necessary funds. Even though the largest national contribution required did not exceed \$90,000 spread over four years, nevertheless, such is the economic climate that several nations with much smaller contributions than this found it hard to obtain promises of the necessary funding. However, subject to the actual signature of the Agreement, it does now seem likely that the Project will continue for a further four years.

In this time, we must seek to extend the co-operative activity, to generate more positive achievements and to demonstrate to those who have no inherent feel for the subject that there is both a real need for the data and only one realistic way to get it. An area in which COST-43 has been slow to move is in seeking co-operation to the West. Although the Western boundary is arbitrarily drawn at 32°W, this is not an absolute limit and there is no reason in principle why, for example, some COST-43 nations acting singly or together could not undertake



co-operation with oceanographic and meteorological programmes in the N. Atlantic which are generated from N. America and it is certainly true that an active dialogue between COST-43 and representatives of other large ODAS programmes would be of benefit to both sides.

Nº OF DATA/DAY



CATEGORY A: REAL TIME TRANSMISSION VIA GTS.  
 B: AVAILABLE FOR REAL TIME TRANSMISSION BUT NOT VIA GTS.  
 C: REAL TIME TRANSMISSION AT INTERROGATING TIMES.  
 D: NO REAL TIME TRANSMISSION.  
 E: AVAILABLE ON LISTING TAPE.  
 F: TRANSMISSION VIA SERVICE ARGOS.

FIG.1 COST 43 ODAS DATA PER DAY.

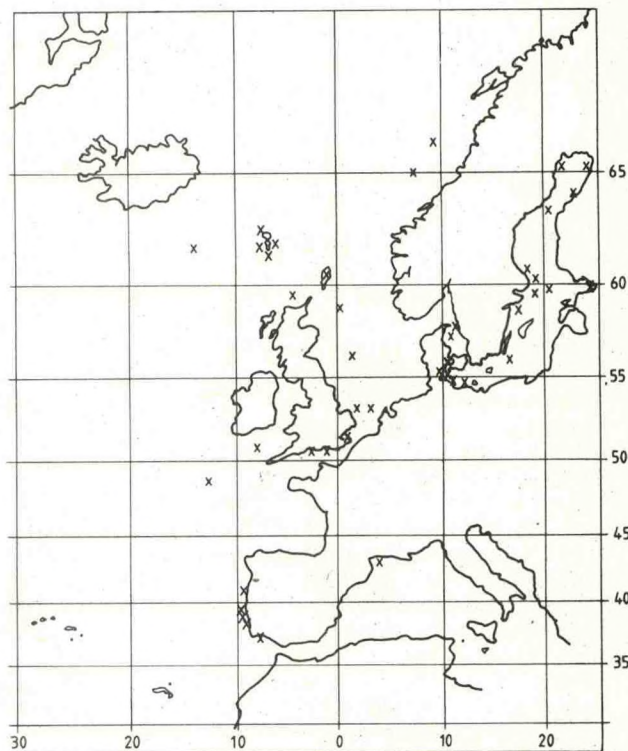


FIG.2. COST-43 ODAS AS AT JUNE 30th. 1982.

PLP 7/3/83

DRE No A 4/24104 Iss1 T7499

RPG T7499

ISS.1 A4/24103



## PROGRESSIVE DEVELOPMENT OF THE CASID BUOYS

W.G. Large and J.C. McWilliams  
National Center for Atmospheric Research

and

P.P. Niiler  
Scripps Institute of Oceanography

### ABSTRACT

The engineering developments and deployments of three generations of Climate Air-Sea Interaction Drifting (CASID) buoys are described. The first deployment of six CASID I buoys coincided with the Storm Transfer and Response Experiment (STREX) in the northeast Pacific during November and December 1980. Redesigns based on a failure analysis of these buoys led to the CASID II buoy, three of which were deployed in October 1981 back in the STREX area. Extensively analyzed data from these two deployments are presented, including calculations of changes in the upper ocean's heat content, estimates of the entrainment and advective heat fluxes, and crude reconstructions of the current profile. We show large mesoscale and year-to-year variability in the oceanic response to strong atmospheric forcing.

### 1. INTRODUCTION

The Climate Air-Sea Interaction Drifting, CASID, buoy has been developed over the past few years as a tool for investigating the processes that determine the upper ocean's thermal structure, and hence the sea surface temperature,  $T_s$ . Such studies in the north-east Pacific near Ocean Weather Station "PAPA" (50°N, 145°W) were conducted during the spring of 1970 (Denman and Miyake, 1973) and during the late summer of 1977 in the Mixed Layer Experiment, MILE, (Davis, de Szoeke, Halpern and Niiler, 1981, and Davis, de Szoeke, and Niiler, 1981). The first two CASID deployments, also near "PAPA" had the objective of extending these observations to the stormy late fall and winter months of 1980 and 1981, in conjunction with the Storm Transfer and Response Experiment, STREX. Many years of observations at "PAPA" show the sea surface temperature to decrease from an average of 13.2°C in late September to an average of 5.4°C by February. This cooling is composed of episodic (1°C/day) cooling events, associated with some but not all of the high wind periods, superimposed on a lesser general cooling trend.

During the first CASID deployment (26 October to 15 December, 1980) the upper ocean's thermal response to one storm was observed on horizontal scales of 50 to 300 km by the array

of 6 buoys. Subsequent events were seen completely by only one buoy, because of numerous failures of the others. A failure analysis following the recovery of 5 CASID I buoys led to several redesigns, which were incorporated into 3 second generation CASID II buoys. These buoys were deployed on 25 October, 1981, and an almost complete data set was returned. One buoy was recovered on 20 January, 1982, and a second in May, 1982, and both were found to be in excellent condition. The third buoy continued to report nearly all its data reliably beyond its designed lifetime of one year. The data from these buoys shows the evolution of the upper ocean's three-dimensional thermal structure over horizontal scales from 10 to 150 km.

The interpretation of the CASID I and II results is hampered somewhat by the lack of measurements of the local atmospheric forcing at each of the buoys. A third generation CASID III buoy, therefore, is being constructed with an air-sea flux measurement capability. Specifically wind velocity, air temperature and air humidity sensors are to be added. The first CASID III deployment was in April, 1983, in conjunction with the Long Term Upper Ocean Study, LOTUS near 34°N, 70°W. The objective was to investigate the establishment of the Sargasso Sea Seasonal Thermocline through successive construction and destruction of the daily thermocline.

### 2. CASID I AND II DEPLOYMENTS

Figure 1 is a sketch of the CASID I AND II buoys. The hull, is essentially the Polar Research Laboratory, PRL, hull developed for FGGE. Ten thermistors were spaced along the line, but clustered between 32 and 77m in order to resolve the deepening of the mixed layer. The two-dimensional shape of the line can be inferred from the pressure sensor data, giving the actual depth of each temperature measurement. All the temperatures and subsurface pressures were sampled every 43.7 seconds. The averages and variances of 256 samples (3.11 hours) were transmitted every 174.8 seconds for 6.22 hours. With this scheme all the CASID II transmissions were received from 4 to 18 times by service ARGOS receivers on the NOAA-6 and TIROS-N polar orbiting satellites. The antennae of CASID I buoys were more susceptible to submergence because there was less floatation and



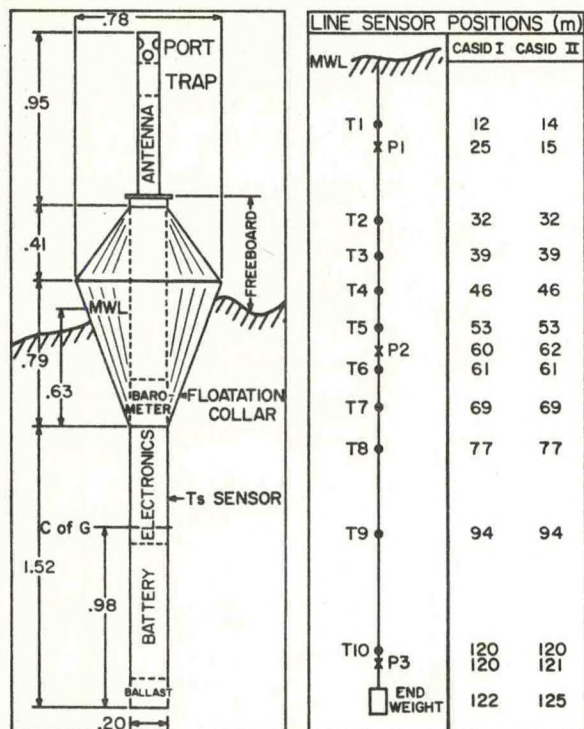


Figure 1: Sketch of the CASID I and II buoys, showing the mean water line, MWL, center of gravity, C of G and important components and dimensions of the hull (left panel). The right panels show the positions of the subsurface temperature and pressure sensors along the suspended line.

more vertical line drag, so that occasionally during a storm a 3.11 hour average or variance was never received and the data lost. Other major improvements in CASID II over CASID I were a more flexible and less abrasive line to hull connection and the barometer port and water trap assembly.

The resulting vast improvement in the sensor performance is shown in table 1. In CASID I only the sea surface temperature measurement was received reliably throughout the deployment. Only about one-half of all the measurements were reliable for more than two weeks. The CASID I design of the line to hull connection seems to have been very near to critical, since there is such large variation in when sensors failed due to conductors breaking at the connection. Fortunately, for 57 days, there is sufficient data from buoy S2 to calculate the upper ocean heat content. This calculation can only be done on all the buoys for about the first ten days, which is before most of the other components of STREX had begun.

In CASID II there was no serious data loss before E1 and E2 were recovered. Only the pressure sensor failures of E3 after 200 days prevents complete analysis of a 1 year time series from this buoy. The cause of the pressure sensor failures has been found and can easily be remedied. However, why the pre-launch PRL

	S2	S1	S3	N3	N2	N1	E1	E2	E3
Pa	8	21	7	23	10	21	*	*	*
Ts	*	*	*	*	*	*	*	*	*
T1	0	19	16	9	18	6	*	*	78
T2	57	12	20	9	22	13	*	*	*
T3	57	0	11	5	16	30	*	*	*
T4	57	22	20	11	5	11	*	*	*
T5	49	12	21	11	19	15	*	*	*
T6	58	23	21	9	20	30	0	*	*
T7	57	12	22	20	30	6	*	*	*
T8	42	22	7	6	18	8	*	*	*
T9	64	11	20	6	0	9	*	*	*
T10	59	7	7	0	21	0	*	*	100
P1	58	18	19	4	14	6	*	50	0
P2	31	8	19	12	13	10	4	*	>200
P3	28	8	7	7	33	0	*	*	>200
R	90	90	90	90	90		115	210	
A						150			>365
R=Recovered							A=Aground		

Table 1. Duration of reliable data from the CASID I and II sensors, in days following the deployment. Continuous reliable performance until recovery or running aground is denoted by a \*.

calibration seems to be biased by up to 1 decibar in CASID II and up to 9 decibars in CASID I is not yet understood.

The trajectories of the first 50 days of the CASID I and CASID II deployments, interpolated to 1 position every inertial period, are shown in figure 2. The 100km grid to the southwest joins the Julian day 300, 1980, positions of the CASID I buoys. The more northerly N buoys tended to diverge and move to the north compared to the more southerly S buoys, which tended to converge and move more to the east. The triangle near "PAPA" (50°N, 145°W) joins the Julian day 300, 1981, positions of the CASID II buoys. E1 and E2 were launched 20km apart and their motion is highly coherent, especially for the first 40 days. However, E3, launched only 30km north of E2 does not display coherent motion.

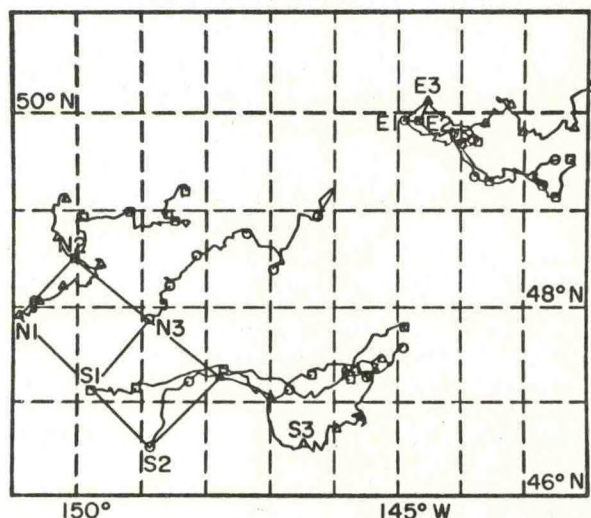


Figure 2: Trajectories of the CASID I and CASID II buoys, with symbols plotted every 10 days.



Table 2 shows the average speeds (net displacement/time) of the CASID I and II buoys. Over 10 days the speeds range from 1.2 to 11.4 km/day (12 to 114 km displacements), but over 50 days they only range from 2.9 to 7.4 km/day (145 to 370 km displacements). In general, the long lines acted as an effective drogue, slowing the buoys to about one-half the speed of undrogued

Period	1980					1981				
	N3	N2	N1	S2	S1	S3	E1	E2	E3	
300-310	4.5	4.9	2.9	8.8	5.0	6.4	8.2	5.8	7.3	
310-320	4.5	5.7	3.3	11.4	10.2	6.6	2.4	2.0	3.7	
320-330	6.4	5.3	8.8	8.2	10.2	4.3	5.3	4.9	3.7	
330-340	5.3	1.2	6.2	1.6	4.5	3.3	8.2	8.2	6.2	
340-350	8.2	3.3	4.9	5.5	9.0	7.3	3.3	4.9	6.2	
300-350	4.6	3.0	2.9	6.3	7.4	3.8	3.7	3.7	3.9	

Table 2: Average drift speeds of CASID I and CASID II buoys (km/day = 1.16 cm/sec).

buoys launched nearby in STREX. The CASID I array design was based on 22 drifter trajectories from the Anomaly Dynamics Study (Kirwan, et al., 1978). The buoys were to have arrived in the vicinity of "PAPA" in less than 50 days, but traveled more slowly than expected.

### 3. SEA SURFACE TEMPERATURE

The most important oceanic parameter in air-sea interaction is the sea surface temperature,  $T_s$ . It evolves in response to a variety of oceanic and atmospheric processes, the most important of which are: surface heat fluxes, horizontal heat advection, vertical heat advection and diffusion, and entrainment of colder thermocline water into the turbulent mixed layer. Decreases in  $T_s$  of about  $3.5^\circ\text{C}$  were observed between Julian days 300 and 350 in both the 1980 and 1981 deployments (figure 3). The time series show distinct cooling events superimposed on a general cooling trend with only occasional warming periods. Changes in  $T_s$  at buoys N1 and S2 show little coherence though the buoys were separated by only 100 - 300km. However the three E buoys, which were often separated by less than 50km display more coherent  $T_s$  traces.

In order to investigate the causes of the observed  $T_s$  evolution we consider the equation derived by Stevenson and Niiler (1983), when the depth of integration is the mixed layer depth  $h = -Z_m$

$$\frac{\partial T_s}{\partial t} + \vec{V}_c \cdot \nabla T_s = \frac{(Q_0 - Q_m) - (T_s - T_m)}{\rho c h} - \frac{(\partial h + \vec{V}_m \cdot \nabla h + W_m)}{\partial t} \quad (1)$$

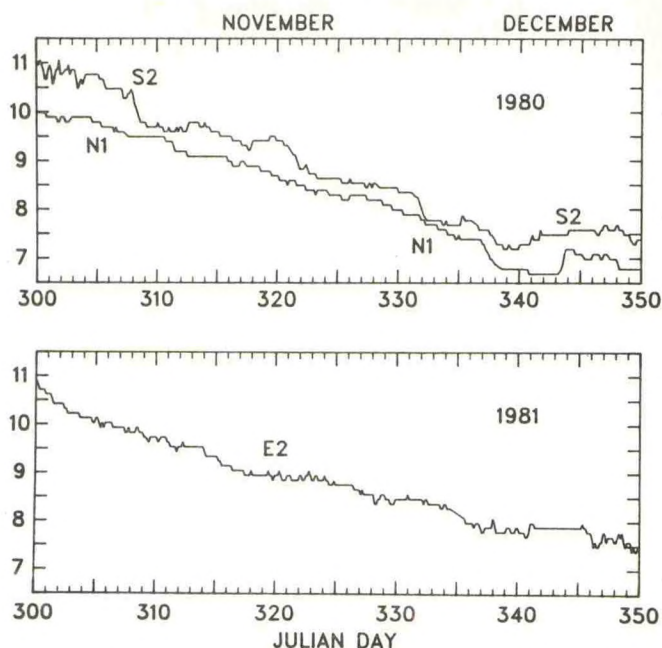


Fig. 3. Sea surface temperature ( $^\circ\text{C}$ ) time series from the CASID I and CASID II deployments.

where the temperature, currents and diffusive heat flux at the base of the mixed layer are  $T_m$ ,  $\vec{V}_m$ ,  $W_m$  and  $Q_m$ , respectively. The mixed layer has an average current  $\vec{V}_c$ , density  $\rho$  and heat capacity  $c$ . A small horizontal divergence term has been neglected in (1) (see Large et al (1983) for details). The left side of (1) is the total derivative following the flow at  $\vec{V}_c$ ,

$$\frac{DT_s}{Dt} = \frac{\partial T_s}{\partial t} + \vec{V}_c \cdot \nabla T_s = \frac{dT_s}{dt} + \vec{V}_r \cdot \nabla T_s, \quad (2)$$

where  $dT_s/dt$  is the temperature change seen by a buoy drifting with velocity  $\vec{U} = \vec{V}_c - \vec{V}_r$ .

The mixed layer current  $\vec{V}_c$  is required in order to evaluate the importance of the terms in (2). A procedure for crudely estimating  $\vec{V}_c$  from the vertical rise of either a bottom or mid CASID pressure sensor, R3 or R2, is detailed in Large et al. (1983). It is based on the assumption that the wave driven buoy hull and current driven line are essentially decoupled and that the latter is primarily responsible for the translational motion of the CASID systems. Simulations of a numerical model (Nath, 1976) at the NOAA Data Buoy Center, NDBC, seem to show hull motion reasonably well. However, the line simulations are strongly coupled to the wave driven hull, which is inconsistent with the line motion observed (figure 4). First the maximum observed R3 was less than 10m, much of which was likely caused by inertial period oscillations in R3, fig. 4. Even though the simulations were run without currents they show large vertical rises due to waves alone. Second, the simulated response to a 10m, 11 second linear wave has the entire line in nearly sinusoidal motion with a 5.4m amplitude (standard deviation 3.8m). In fig. 4 the upper and lower portions of the line do not move together and the standard deviation increases with depth.



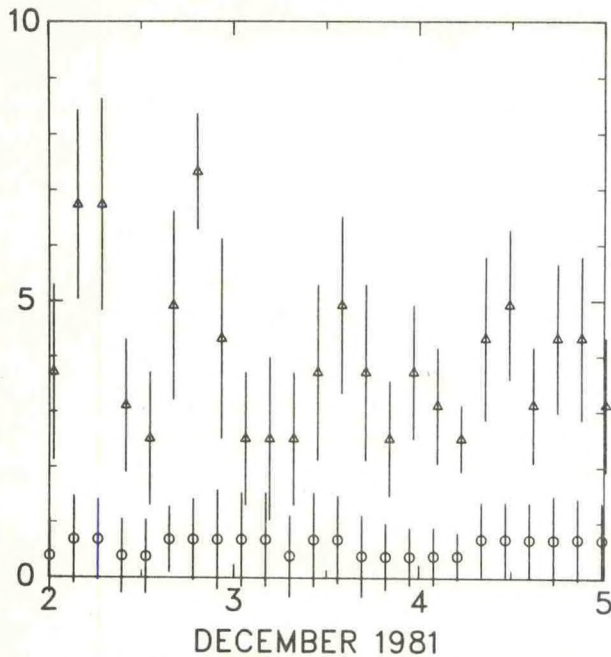


Fig. 4. Vertical rises of the CASID II bottom (triangles) and top (circles) pressure sensors R3 and R1, respectively in meters. Vertical bars extend  $\pm 1$  standard deviation.

A simple model of the current profile, consisting of three components is sketched in Fig. 5. A low frequency (relative to the inertial frequency) current,  $\vec{V}_c$ , is confined to and constant throughout the mixed layer. Another,  $\vec{V}_L$  is constant below  $Z = Z_m$  and assumed parallel to  $\vec{V}_c$ . These currents are primarily responsible for the mean buoy motion and for advecting heat in the horizontal. Finally there is a possibly strong inertial oscillation, which because of its rotational nature, contributes little to mean motions or heat advection averaged over several inertial periods,  $P_i$ . The inertial currents are modelled with a constant  $\vec{I}_c$  in the mixed layer and a constant  $\vec{I}_L$  below

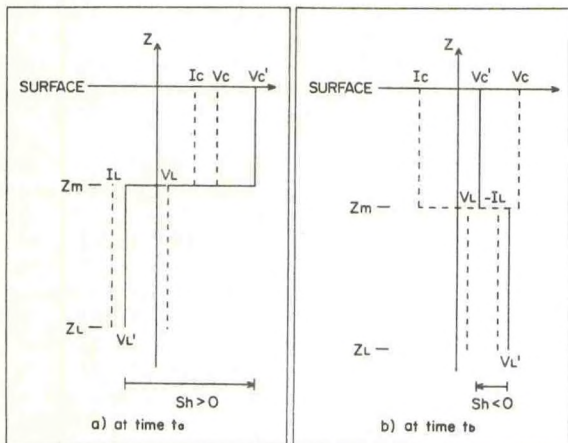


Fig. 5. Simple current model showing the mixed layer current  $\vec{V}_c$  and the inertial component  $\vec{I}_c$  a) parallel, time  $t_a$  and b) antiparallel, time  $t_b$ .

$Z = Z_m$ , which are always antiparallel. It follows that once every inertial period,  $\vec{V}_c$  and  $\vec{I}_c$  are aligned (time  $t_a$ , Fig. 7a) and that one-half a period before or after (time  $t_b$ , Fig. 7b) they are opposed. Even if inertial currents are present there is a two-dimensional current profile at least twice each inertial period:

$$\begin{aligned} V(z) &= V_c' = V_c \pm I_c \quad Z_m < Z < 0 \\ &= V_L' = V_L \pm I_L \quad Z < Z_m \end{aligned}$$

where the components are added at time  $t_a$  and subtracted at time  $t_b$  and  $I_c$  and  $I_L$  are of opposite sign.

For any two-dimensional profile, functional forms for the buoy's speed and the shape of line as given by R3 and R2 can be found. From the inverse functions a current profile can be constructed from observations of the buoy's trajectory, the mixed layer depth,  $Z_m$ , and the rise of any pressure sensor deeper than about 30 meters. Even crude estimates of low frequency currents in and below the mixed layer will be useful in calculating the horizontal advection of heat.

The contributions to  $T_s$  changes from the terms in (2) are shown in table 3. The overall averages of buoys S2 and E3 show the horizontal heat advection,  $\vec{V}_c \cdot \nabla T_s$  to be nearly 30% as large as the local rate of change,  $\partial T_s / \partial t$ ; a similar result to MILE. On these time scales the advection associated with the relative velocity is negligible. It becomes more important, but never dominant, as the time period shortens. Also on shorter time scales (Julian day 311 to 316.4) the horizontal advection can be nearly 70% as large as the local rate of change. The temperature decreases under  $DT_s/Dt$  need to be accounted for by the terms on the right of (1).

	$t_1$	$\frac{DT_s}{Dt}$	$\frac{\partial T_s}{\partial t}$	$\vec{V}_c \cdot \nabla T_s$	$\frac{dT_s}{dt}$	$\vec{V}_r \cdot \nabla T_s$
Buoy S2 1980	300.	-.34	-.37	.03	-.41	.07
	305.5	-.87	-1.13	.26	-.92	.05
	311.	-.16	-.51	.35	-.19	.03
	316.4	-.52	-.73	.21	-.54	.02
	321.9	-.41	-.56	.15	-.37	-.04
Inertial Periods	327.3	-.74	-.88	.14	-.72	-.02
Buoy S2 33 Days	300	-3.04	-4.18	1.14	-3.15	.11
Buoy E3 83 Days	300 1981	-4.19	-5.90	1.71	-4.19	0

Table 3. Integrals of the terms in equation (2) from time  $t_1$  in Julian days, showing the contributions in  $^{\circ}\text{C}$  to the observed changes in sea surface temperature.



During spring and summer (1) is balanced by the surface heat flux,  $Q_0$ . However, during STREX, estimates of  $Q_0$  following buoy S2 show it to account for only about  $0.5^\circ\text{C}$  cooling. From days 300 to 310 the ocean surface appears to be gaining heat, yet the sea surface temperature decreases. Even if the  $Q_0$  estimates are in error by a factor of 2, it is clear that surface heating is not the dominant term on the right of (1) during the fall and early winter.

Figure 6 shows the ocean temperatures at the S2 and E2 buoys. It is from these data that the remaining terms on the right of (1) are estimated. First  $h$  is taken just below the mixed layer depth, so that the average temperature from the surface to  $h$  is still nearly equal to  $T_s$ , and  $Q_m$  is small. The vertical heat advection resulting from  $W_m$  was estimated from vertical excursions of isotherms in the thermocline by Davis, DeSzoeke, Halpern and Niller (1983), who found that it was an important term in the mixed layer heat budget. The effect of  $W_m$  can most clearly be seen in the low frequency (15 day) E2 temperature trace at 70 meters. The magnitude of  $W_m$  is typically a meter on two per day, but occasionally it can be nearly 10m/day and a very important term. It frequently changes sign and over 50 days it is of less importance. The entrainment is described by  $\partial h / \partial t$  which tends to be positive since the mixed layer tends to erode downwards. Following day 330, 1980,  $h$  increases about 20m in only 5 days. Over 50 days it increases about 50 meters in 1980, but only about 30 meters in 1981. The  $W_m \cdot \nabla h$  term can be as much as 1m/day, but since  $h$  tends to decrease in the direction of flow  $V_m$ , this term tends to increase  $T_s$ .

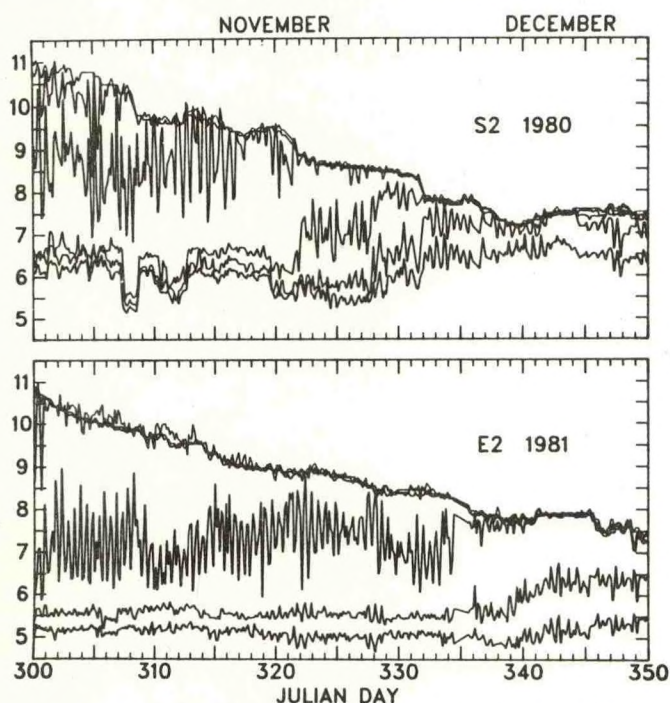


Fig. 6. CASID I and II ocean temperatures ( $^\circ\text{C}$ ) at the surface 40m, 50m, 70m, 90m and 110m depths.

In summary, the fall seasonal decrease in sea surface temperature seen in figure 3 appears to be due mainly to a sequence of episodic, storm induced, entrainment events. In addition there may be a general cooling trend due to surface heat fluxes and a net vertical advection of heat out of the mixed layer. It also appears as if the gradient in the mixed layer depth would tend to increase  $T_s$  slightly. On storm time scales the entrainment cooling may be either enhanced or greatly modulated by vertical advection. The CASID I observations suggest that the balance between these processes changes over horizontal scales less than 100 km, which is much less than the scale of atmospheric forcing.

#### 4. CASID III

The STREX experience revealed the value of local estimations of the surface fluxes of momentum and heat. These measurements are even more important in the LOTUS deployment of four third generation CASID III buoys, and therefore a suite of meteorological sensors has been added. A very attractive wind velocity measurement, that is being evaluated, is to derive a wind speed from the ambient acoustic noise at 4.3, 8.0 and 14.5 kHz obtained from a hydrophone attached to the CASID thermistor line at 120m depth. The noise measurements may also contain useful information on precipitation. The wind direction is then obtained from a compass inside the hull giving the hull orientation, which is aligned with the wind by a fin attached to a 2 meter tower atop the hull. In this way the wind velocity is obtained without placing sensors with moving parts in the hostile marine environment. Problems associated with buoy motion and the wind profile near the wave field are greatly diminished.

The 2m tower also supports temperature and humidity sensors housed in radiation shields. Sensor degradation and contamination is a familiar problem over the ocean. We have chosen sensors that at least show calibration stability in the laboratory, and are exploring various means of protecting them during LOTUS, namely sintered brass filters, porous membranes and cloth wrappings.

Nearby shipboard measurements of wind velocity, air temperature and humidity are the standards to which all the buoy measurements are to be compared. In addition the ability of the fin to track the changes in wind direction has been monitored by two propeller anemometers mounted at  $\pm 30^\circ$  angles to the horizontal direction of the fin. Any differences in the outputs of the two propellers reflect winds that are not aligned with the fin. The propellers also give a wind speed that can be used to continue checking the hydrophone derived speeds after the ship returned to port.



The CASID III hull and line remained as nearly identical as possible to the proven CASID II designs. In order to resolve the daily and seasonal thermoclines the thermistors were placed at 4, 6, 9, 12, 18, 26, 34, 44, 54 and 100 meters along the line. Since most sensors are higher than CASID II, the mid-pressure sensor was moved up to 46 meters. Two of CASID III buoys had digital barometers from Atmospheric Instruments Research Corp. instead of the usual Paros barometers. They are less than one-half the cost and output pressure directly in millibars from a microprocessor containing temperature coefficients. These barometers are not yet fully tested and the LOTUS deployment will aid the manufacturer in evaluating their at sea performance. The core LOTUS experiment is centered about a mooring with current meters distributed throughout the water column. The current meter records will allow the proposed scheme of inferring a current profile from the CASID data to be thoroughly evaluated and possibly improved.

#### ACKNOWLEDGMENTS

CASID buoy development could not have progressed to its present state without those through whose courtesy the CASID buoys have twice been launched and recovered. For these efforts we wish to thank Dr. J. Garrett, S. Huggett, C. de Jong and J. Love of the Institute of Ocean Sciences Patricia Bay, Canada and the officers and crews of CCGS Vancouver, CSS Parizeau and CFAV Endeavour.

#### REFERENCES

- Davis, R.E., R. deSzoeki, D. Halpern and P. Niiler, 1981: Variability in the upper ocean during MILE. Part I: The heat and momentum balances. *Deep-Sea Research*, 28, 1427-1451.
- Davis, R.E., R. deSzoeki and P. Niiler, 1981: Variability in the upper ocean during MILE. Part II: Modeling the mixed layer response. *Deep-Sea Research*, 28, 1453-1457.
- Denman, K.L. and M. Miyake, 1973: Upper ocean modification at Ocean Station PAPA: observations and simulation. *J. Phys. Oceanogr.*, 3, 185-196.
- Kirwan, A. D., G. McNally, B. Reyna and W. Merril, 1978: The near surface circulation of the eastern North Pacific. *J. Phys. Oceanogr.*, 8, 937-945.
- Large, W.G., J.C. McWilliams and P.P. Niiler, 1983: Surface drifting buoy observations of the ocean's thermal response during STREX. In preparation.
- Nath, J.H., 1976: Numerical model computer program, "Drifting Buoy System". NOAA Data Buoy Office, NSTL Station MS.
- Stevenson, J.W. and P.P. Niiler, 1983: Upper ocean heat budget during the Hawaii to Tahiti shuttle experiment. In preparation.
- Wilson, B., 1981: Selection of ballast and thermistor line end weight values for the STREX hull drifting buoy gulf of Alaska application. NOAA Data Buoy Office, NSTL Station MS.



# HYBRID TIME DOMAIN MODEL OF DRIFTING BUOY MOTION

by

John H. Nath, Professor, and Robert T. Hudspeth, Associate Professor

Department of Civil Engineering  
Ocean Engineering Program  
Oregon State University, Corvallis, Oregon

## ABSTRACT

The time domain numerical model predicts the motion of a spheroid buoy on surface water waves including the drift characteristics. The spheroid has a vertical axis of symmetry and the intersection of the body surface with a vertical plane that includes that axis describes an ellipse. The vertical axis of the ellipse may be greater than the transverse axis (spar buoy), or it may be much smaller (disc buoy). An axisymmetric Green's function program calculates the added mass and radiation damping coefficients. Laboratory model tests were conducted for program validation.

## 1. INTRODUCTION

The drifting buoy is an instrumented vehicle for measuring ocean phenomena. It is allowed to drift in order to record the measurements as a function of buoy position. It has sometimes been assumed that the motions and drift of a buoy-tether-drogue system are determined mostly by the currents. However, the accuracy of the system is not well-known and it is desired to develop methods for assessing them. If the effects from wind, waves and current can be assessed separately, they could be combined to predict the total motions. It is known that waves alone may provide considerable drift. The numerical model described in this paper attempts to predict the motion characteristics of spheroidal drifting buoys on two-dimensional waves.

The two most important parts to the problem are: 1) the prediction of the motion of the buoy in heave, pitch and surge due to periodic waves, and 2) the prediction of the water particle kinematics and dynamics in the near surface zone of the waves. This paper deals mostly with the first problem. The work includes a laboratory model study of three spheroidal buoys subjected to periodic waves.

Drifting buoys may be constructed in various shapes and it is felt that a wide range of shapes can be investigated through the spheroid. A spheroid is a volume which has a vertical axis such that any plane passing perpendicular to this vertical axis will describe a circle at the

intersection. A vertical plane which includes the vertical axis describes an ellipse at the surface intersection. If the vertical axis is much longer than the maximum horizontal diameter, a spar buoy is defined. If it is much shorter, a disc buoy results. When the two axes are equal, a spherical buoy is described. For the examples in this paper the buoys are ballasted so that the water line is at the spring line of the buoy (mid position).

This numerical model takes into account that the buoy will heave and pitch at its own natural frequencies in these motions on the surface of a wave, with respect to the moving water surface. In addition, the buoy will heave in accordance with the wave characteristics and the pitch will be influenced to some degree by the wave steepness. The acceleration and velocity effects within the upper regions of the wave, acting on the buoy, result in a net horizontal transport of the buoy. This numerical model uses an axisymmetric Green's function routine to predict the radiation damping and added mass coefficients for the buoy as it moves with respect to the moving wave surface. These components are combined with the ambient accelerations and velocities within the wave. It is assumed that the buoy characteristic length (usually the diameter) is small with respect to the wave length so that the diffraction effects can be ignored. Thus, a combination of potential flow effects, utilizing the Green's function methods, with a Morison equation approach, yields the total instantaneous force components acting on the buoy. These forces are used to determine the accelerations of the buoy in the three modes of motion with respect to local body coordinates. The accelerations are then transformed to the inertia coordinate system and the velocities and displacements of the buoy for the next time increment are determined by a suitable integration method.

This technique depends on determining the dynamics and kinematics of the water particle motions in the near surface layers of the wave. Very little information exists on measurements in this region of water waves. So far, reliance has been placed upon estimates of these quantities from a stretched linear theory and from the stream function theory.

## 2. THEORETICAL DEVELOPMENT

The objective of this work is to develop a predictor for the motion characteristics of a spheroid buoy on periodic waves. In addition, time



domain analyses can be made with random waves but they are quite expensive and are rarely attempted. The work is divided into three programs: one dealing with the physical characteristics, one for the added mass and radiation damping coefficients, and one for the general motion predictor.

#### i) Buoy physical characteristics

This program determines the center of gravity location (cg), the moment of inertia (I) about the center of gravity, the center of buoyancy, the metacentric height, and the coordinates of the buoy surface, which depend on the degree of discretization chosen by the user. The user determines the total weight, payload weight, the ratio between the vertical and horizontal axes and the total buoy volume. Much of this information is required as input information to the axisymmetric Green's function program.

#### ii) Axisymmetric Green's function program

This program computes the surge, heave and pitch response of the buoy in the frequency domain. It is based on assumptions of linearity. The user inputs the coordinates of the floating buoy surface for below the still water surface, and the other physical characteristics, plus the wave frequency. The output is the added mass and radiation damping coefficients for the three degrees of freedom of the buoy in this two-dimensional study, and the non-dimensional response amplitudes. By sweeping through several frequencies the resonant frequencies in heave and pitch can be determined. In part iii) it will be assumed that the buoy will heave and pitch at its natural periods in those motions, while it is also excited by the much longer period of the wave. Thus, it will heave with the wave period, with its own resonant periods superimposed.

The hydrodynamic coefficients for a free floating, vertically axisymmetric body of revolution that is harmonically oscillated in still water may be computed from the hydrodynamic pressure forces on the body. Herein all geometries are made dimensionless with the maximum radius,  $b$ . A definition sketch for many of the following terms is given in Fig. 1. For polar coordinates aligned with the body axes  $r^2 = x^2 + y^2$  and  $\theta = \tan^{-1}(y/x)$ . Dimensionless geometric and displacement variables are defined as  $r' = r/b$ ,  $z' = z/b$ ,  $X' = X_m/b = X_m \exp i\psi_m$  (where  $X_m$  are the body translations,  $m=1,2$ ).

For simple harmonic motion in otherwise still water the temporal dependence may be separated according to  $\exp -i\omega t$  in which the radian oscillations (wave) frequency is  $\omega = 2\pi/T$ , where  $T$  is wave period. The dimensionless wave number and wave frequency are defined by  $k' = 2\pi b/L$  and  $\nu' = \omega^2 b/g$ , in which  $L$  is the wave length and  $g$  is the acceleration constant. The restoring forces (moment) are nondimensionalized according to  $F'_{mj} = F_{mj}/\rho g b^3$  ( $j=1,2$ ) and  $M'_{m3} = M_{m3}/\rho g b^4$  [ $m=1,2,3$   $mj$  (surge, heave, pitch)] in which  $\rho$  is the fluid mass density. In addition,

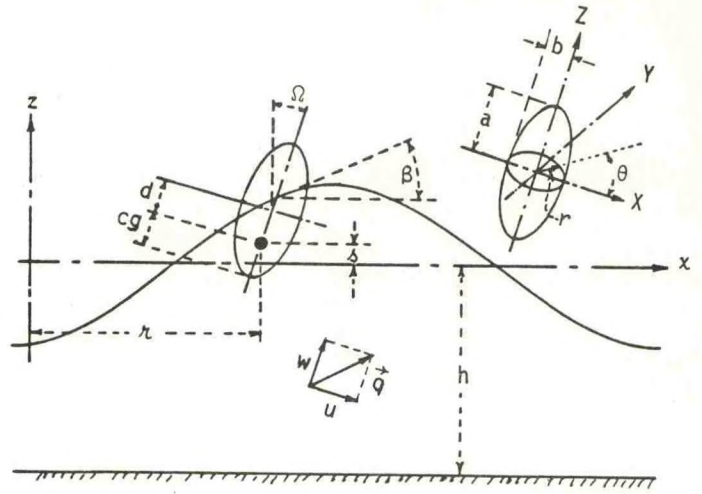


Fig. 1 Definition Sketch

$$F'_{mj} = - (b/g) (A'_{mj} \ddot{X}'_m + \omega N'_{mj} \dot{X}'_m); m=1,2; j=1,2,3 \quad (1a)$$

$$\text{and } M'_{3j} = - (b/g) (A'_{3j} \ddot{\Omega} + \omega N'_{3j} \dot{\Omega}); j=1,2,3 \quad (1b)$$

in which the over dot indicates  $\partial/\partial t$ , and the dimensionless added mass coefficients  $A'_{12} = A'_{21} = A'_{23} = A'_{32} = 0$  and the dimensionless radiation damping coefficients  $N'_{12} = N'_{21} = N'_{23} = N'_{32} = 0$ .

The dimensionless restoring forces and moments may be computed from the solutions to the radiation-wave force boundary value problems in which the rigid, axisymmetric body is oscillated in each mode of oscillation,  $m$ , in otherwise still water. The fluid motion resulting from these forced oscillations may be described by a scalar velocity potential which is assumed to be a linear sum of the potentials from each oscillation mode:

$$\phi(r, \theta, z, t) = R\ell(\exp -i\omega t \sum_{m=1}^3 X_m \phi_m) \quad (2)$$

where

$$\phi_m = i\omega b (\delta_{m1} + \delta_{m2} + b\delta_{m3}) \phi'_m; m=1,2,3 \quad (3)$$

where  $R\ell$  means "the real part of" and  $\delta$  is the Kronecker delta.

The dimensionless water particle velocity vector,  $\vec{q}$ , is defined by the negative gradient operator according to

$$\vec{q} = R\ell (-\vec{\nabla}\phi) \quad (4)$$

The linearized dimensional free surface elevation,  $\eta(r, \theta, t)$  for the radially radiating wave is computed from

$$\eta(r, \theta, t) = R\ell(\dot{\Phi}/g); \text{ at } Z = 0 \quad (5)$$

and the dimensional hydrodynamic component of pressure,  $p(r, \theta, z, t)$ , is given by

$$p(r, \theta, z, t) = R\ell(\rho \dot{\Phi}). \quad (6)$$



The dimensional restoring force may be computed from the hydrodynamic pressure according to the surface integral

$$F_{mj} = \int p n_m dS \quad (7)$$

The added mass and radiation damping coefficients are thus obtained from the scalar velocity potential,  $\phi$ , and by Eqs. 1, 6 and 7.

The boundary value problems for the dimensionless radiation wave potentials,  $\phi_m$ , required for the restoring forces for an oscillating body in still water (Eqs. (2 and 3) may be summarized from ref. (5) as (in the following the primes have been omitted from the dimensionless quantities for convenience)

$$\nabla^2 \phi_m = 0 \quad ; \quad |r| < \infty \quad ; \quad -h \leq z \leq 0 \quad (8a)$$

$$\frac{\partial \phi_m}{\partial z} = 0 \quad ; \quad z = -h \quad (8b)$$

$$\frac{\partial \phi_m}{\partial z} - v \phi_m = 0 \quad ; \quad z = 0 \quad (8c)$$

$$\frac{\partial \phi_m}{\partial n} = -B_m \quad ; \quad \text{on the surface } S(r, \theta, z) \quad (8d)$$

(all for  $m = 1, 2, 3$ )

in which the operator,

$$\nabla^2 = \frac{1}{r} \frac{\partial}{\partial r} \left( r \frac{\partial}{\partial r} \right) + \frac{1}{r^2} \frac{\partial^2}{\partial \theta^2} + \frac{\partial^2}{\partial z^2} \quad (8e)$$

provided that the radiation condition is given by

$$\lim_{r \rightarrow \infty} \sqrt{r} \left[ \frac{\partial}{\partial r} - i\kappa_m \right] \phi_m = 0 \quad (8f)$$

where  $\kappa_m$  are the eigenvalues.

The inhomogeneous boundary conditions for the radiation boundary value problems,  $B_m$ , are given by the following direction cosines:

$$\text{surge: } B_1 = n_1 \cos \theta \quad (9a)$$

$$\text{heave: } B_2 = n_2 \quad (9b)$$

$$\text{pitch: } B_3 = (r n_2 - (z-d) n_1) \cos \theta \quad (9c)$$

The dimensionless velocity potentials,  $\phi'_m$ , for the radiated waves are assumed to be given by a distribution of sources over the immersed surface area of the body according to the surface integral

$$\phi'_m(r, \theta, z) = \frac{1}{2\pi} \int f_m(R, \theta, Z) G(r, \theta, z | R, \theta, Z) dS(R, \theta, Z); \quad m = 1, 2, 3 \quad (10)$$

in which the dummy variables of integration  $(R, \theta, Z)$  represent points on the immersed surface of the axisymmetric spheroid. The Green's function,  $G(r, \theta, z | R, \theta, Z)$ , (or resolvent kernel) in Eq. (10) is given by the following eigenfunction expansion (6,9):

$$G(r, \theta, z | R, \theta, Z) = i\pi \sum_{n=1}^{\infty} Q_n(\kappa_n z) Q_n(\kappa_n Z) \cdot \sum_{\ell=0}^{\infty} (2-\delta_{\ell 0}) J_{\ell}(\kappa_n \{r\}) H_{\ell}^{(1)}(\kappa_n \{R\}) \cos \ell(\theta - \theta) \quad (11)$$

in which the orthonormal eigenfunctions are defined by

$$Q_n(\kappa_n \{z\}) = N_n^{-1} \cosh \kappa_n \left( \frac{z}{2} + h \right) \quad (12a)$$

and

$$N_n^2 = (4\kappa_n)^{-1} [2\kappa_n h + \sinh 2\kappa_n h] \quad (12b)$$

and the eigenvalues are computed from

$$v - \kappa_n \tanh \kappa_n h = 0 \quad (12c)$$

if  $\kappa_1 = k$  and  $\kappa_n = i\kappa_n$  for  $n \geq 2$ , and  $H_{\ell}^{(1)}$  is the Hankel function of the first kind of order  $\ell$ . The upper argument is to be used in the Bessel function if  $r \geq R$  and the lower argument otherwise.

The dimensionless source strength,  $f_m(R, \theta, Z)$  for each mode of oscillation in Eq. (10) is computed from the following surface integral equation (2):

$$\int f_m(R, \theta, Z) \frac{\partial}{\partial n} G(r, \theta, z | R, \theta, Z) dS(R, \theta, Z) = -2\pi B_m; \quad m = 1, 2, 3 \quad (13)$$

Expanding the dimensionless source strength,  $f_m$ , in a Fourier series in  $\theta$  and integrating analytically around the axisymmetric body of revolution reduces the surface area integral in Eq. (13) to a line integral along the boundary curve in the plane of axisymmetry. This line integral in the plane of symmetry may now be evaluated numerically by discretizing the boundary curve into  $J$  straight line segments and solving for the unknown source strength at the center of each segment; i.e.,

$$[a_{ij}][f_j]_m = [B_i]_m; \quad i, j = 1, 2, \dots, J \quad \text{for each } m = 1, 2, 3 \quad (14)$$

Convergence of the diagonal elements in Eq. (14) is slow due to the logarithmically singular behavior of the Green's function. Fenton (4) and



Isaacson (6) discuss the criteria used to truncate the infinite series for the evanescent eigenmodes in Eq. (11). However, both diagonal and off-diagonal elements must be treated separately in order to avoid the singular behavior of the modified Bessel function of the first kind in the off-diagonal elements.

Complex-valued matrix inversion algorithms are required in order to solve the simultaneous linear system of equations needed to determine the hydrodynamic added mass and radiation damping coefficients from the radiated wave restoring forces. Fenton (4) recommended using the Gauss-Seidel iterative method for the diffraction problem which gives the exciting forces on the body. Unfortunately, the Gauss-Seidel method will not converge for all cases and it is necessary to determine when this method will converge.

For each dynamic mode, it is necessary to first determine the most computationally efficient matrix inversion method to use by determining whether or not the matrix of coefficients is diagonally dominant (1,3). The maximum value of the ratio of the off-diagonal elements to the diagonal elements must be less than unity in order for the Gauss-Seidel iterative method to converge. If this criterion is not satisfied, Gauss elimination must be used.

### iii) Time domain model

This model is similar to the one described in (8). However, certain segments, or subroutines, have been completely changed with respect to the lumped mass systems and integration technique. The major change for the new work is the method used to calculate the forces acting on the buoy hull.

In summary, the lumped parameter, time domain model first calculates the discretized distribution of external and internal forces acting on the system at some instant in time, based upon the nodal coordinates and velocities. Runge-Kutta and predictor-corrector integration methods then predict the displacements and velocities at the completion of the next time increment, when forces can again be calculated. When there is no tether and drogue, the buoy constitutes the only lump in the system. This paper focuses on the numerical treatment for the buoy.

For the two-dimensional problem herein, the equations of motion for the buoy are assumed to be:

$$[A]\ddot{\{X\}} = [F]\{q\} + [N]\{\dot{\xi}\} + \{B\} + \{T\} + \{G\} + \{W\} + [V]\{\dot{\xi}|\dot{\xi}|\} \quad (15)$$

$$= R_1 + R_2 + R_3 + R_4 + R_5 + R_6 + R_7$$

where  $[A]$  is the dimensional effective mass matrix of the buoy,  $X$  is the displacement,  $[ ]$  indicates a square matrix,  $\{ \}$  indicates a column matrix,

and the seven force components of the right hand side of Eq. 15 are, respectively:

- $R_1$  = added mass, Froude Krylov
- $R_2$  = radiation damping
- $R_3$  = buoyancy
- $R_4$  = tether tension
- $R_5$  = gravity
- $R_6$  = wind drag
- $R_7$  = viscous damping (drag) .

The components of the individual matrices are:

$$[A] = \begin{bmatrix} \mu_{11} + A_{11} & 0 & A_{13} \\ 0 & \mu_{22} + A_{22} & 0 \\ A_{31} & 0 & \mu_{33} + A_{33} \end{bmatrix} \quad (16)$$

where:

$\mu_{11} = \mu_{22} = \text{buoy wt./g}$

$\mu_{33} = I$ , the mass moment of inertia about the center of gravity

$A_{ij}$  = dimensional added mass coefficients obtained from the axisymmetric Green's function program

$A_{22}$  = the value determined for the heave natural frequency

$A_{33}$  = the value determined for the pitch natural frequency

$A_{11}$  &  $A_{13}$  = the average of the values at the pitch and heave natural frequencies (there is no natural frequency in surge) and  $A_{13} = A_{31}$  ;

$$\ddot{\{X\}} = \begin{Bmatrix} \ddot{x} \\ \ddot{y} \\ \ddot{z} \\ \ddot{\Omega} \end{Bmatrix} \quad (\text{the 3 buoy accelerations}) \quad (17)$$

and

$$[F] = \begin{bmatrix} A_{11} + \delta_{11} & 0 & A_{13} \\ 0 & A_{22} + \delta_{22} & 0 \\ A_{31} & 0 & A_{33} \end{bmatrix} \quad (18)$$

where  $\delta_{11} = \delta_{22}$  = the displaced fluid mass (which varies with time). Herein the product of  $\delta$  and the water particle acceleration will be termed the Froude-Krylov force. The fluid accelerations in the body coordinates are



$$\{\ddot{q}\} = \begin{Bmatrix} \ddot{u} \\ \ddot{w} \\ \ddot{\beta} \end{Bmatrix} \quad (19)$$

where  $\ddot{u}$  and  $\ddot{w}$  are evaluated at the instantaneous center of buoyancy (centroid of the displaced volume) and  $\ddot{\beta}$  and  $\ddot{\beta}$  are evaluated where the water surface intersects the buoy centerline, and

$$[N] = \begin{bmatrix} N_{11} & 0 & N_{13} \\ 0 & N_{22} & 0 \\ N_{31} & 0 & N_{33} \end{bmatrix} \quad (20)$$

where  $N_{ij}$  = the radiation damping coefficients in dimensional form,  $N_{11}$  and  $N_{13}$  = the average of the values at the heave and pitch natural frequencies,

$N_{22}$  = value at the heave natural frequency,  $N_{33}$  = value at the pitch natural frequency and  $N_{13} = N_{31}$ .

The *relative* fluid velocities are

$$\{\dot{\xi}\} = \begin{Bmatrix} u - \dot{x} \\ w - \dot{z} \\ \dot{\beta} - \dot{\Omega} \end{Bmatrix} \quad (21)$$

where, for at least a first approximation,  $u$  and  $w$  are evaluated at the center of buoyancy;  $\dot{x}$  and  $\dot{z}$  are evaluated at the center of gravity of the buoy, whereas  $\dot{\Omega}$  represents the buoy pitch angular velocity. The characterization and usage of  $\beta$ ,  $\dot{\beta}$  and  $\ddot{\beta}$  is known to be experimental. The effectiveness of this characterization has not been fully evaluated at this time.

The buoyancy matrix,  $\{B\}$ , considers the degree of submergence, the angle of pitch and the water surface slope, to determine the  $x$  and  $z$  directed buoyancy forces and the (restoring) moment acting on the buoy hull.

The tether tension and gravity matrices are fairly self evident. For the wind force matrix,  $\{W\}$ , it is assumed that the time varying wind on the buoy can be described in some way. Often it is assumed to be constant. The wind acts on the exposed area with the tendency to tip the buoy and push it into the water, if on the leading side of the wave.

The remaining matrices are:

$$[V] = \begin{bmatrix} V_{11} & 0 & 0 \\ 0 & V_{22} & 0 \\ 0 & 0 & V_{33} \end{bmatrix} \quad (22)$$

where the  $V_{ij}$  are the drag factors, including the nondimensional drag coefficients, effective projected areas and fluid mass densities. Since a displaced volume moment of inertia could not be calculated for part of  $V_{33}$ , the buoy moment of inertia is used; and

$$\{\ddot{\xi}|\ddot{\xi}|\} = \begin{Bmatrix} (u-\dot{x})|u-\dot{x}| \\ (w-\dot{z})|w-\dot{z}| \\ (\dot{\beta}-\dot{\Omega})|\dot{\beta}-\dot{\Omega}| \end{Bmatrix} \quad (23)$$

The procedure for numerical modeling is to first select the buoy geometry from the needs of the mission and the results of program i) regarding the physical characteristics. Then the axisymmetric Green's function program is used to determine the added mass and radiation damping coefficients for the three degrees of freedom system. Several wave frequencies need to be introduced so that the resonant conditions in heave and pitch can be determined. For the surge direction, there is no natural frequency. Therefore, the coefficients used for that direction must be selected by judgment. Often they can be the averages of the values taken from the heave and pitch natural frequencies. Likewise, the off-diagonal values for the added mass and radiation damping coefficients can be determined from the averages of the values at the heave and pitch natural frequencies. All of this is an attempt to utilize constant added mass and radiation damping coefficients because the major effort here is to be able to numerically model the natural heave and pitch characteristics of the buoy about those natural frequencies while the action is superimposed upon waves that are relatively long (low frequency).

The next step is to introduce these coefficient values into the numerical model iii) for predicting the motion of the buoy on waves. The model includes considerations for tether and drogue, or it can be moored. Separate subroutines are developed so that if the tether and drogue are not required, those subroutines are not utilized.

### 3. LABORATORY AND NUMERICAL MODEL TESTS

Three axisymmetric buoy shapes were tested in the Oregon State University wave flume at the Wave Research Facility, (OSU-WRF). They were: a fat spar; a sphere; and a fat discus. The physical characteristics of the buoys are given in Table 1. There were three types of tests.



Table 1 Buoy physical properties

Buoy	a/b	2b (ft)	wt (lbs)	I (f-#-s <sup>2</sup> )	Cg (ft)	ADM22	ADM33
Spar	1.96	1.27	65.0	.450	.82	.7901	.2535
Sphere	1.00	1.58	65.0	.284	.53	.8904	.1227
Discus	0.49	1.99	63.0	.202	.41	1.1403	.1532

1) Impulse response tests were made in heave and pitch where, for the heave test, the buoy was lifted nearly out of the water and released. Super-8 mm movies were taken of the resulting motion to record the heave decay curve. For the pitch impulse response, the buoy was forcefully pitched over and allowed to pitch back and forth until it was still. A background grid was provided for quantifying displacements and rotations. Parallax was taken into account when necessary in the data reduction which was done with a stop frame analyzer. The numerical model was exercised in the same way. Sample heave and pitch impulse response curves for the spherical buoy are shown in Figs. 2 and 3. Table 2 gives a comparison of results for the natural periods. It is interesting to note that minor adjustments were made to the numerical model only for the viscous drag coefficients to get nearly equivalent damping between the numerical and physical models.

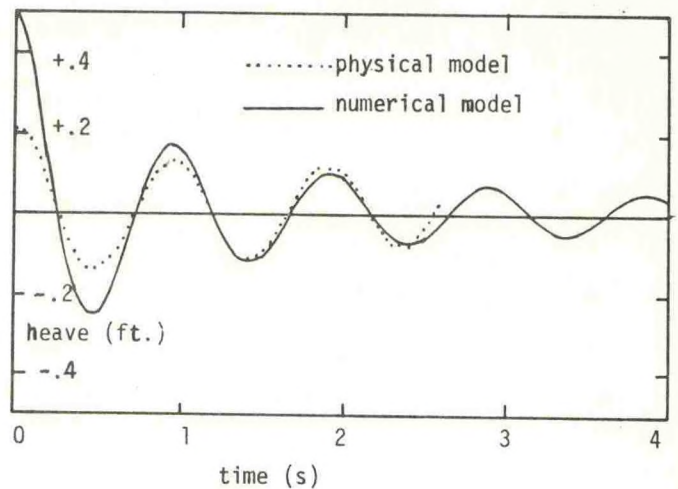


Fig. 2 Heave impulse response. Spherical buoy.

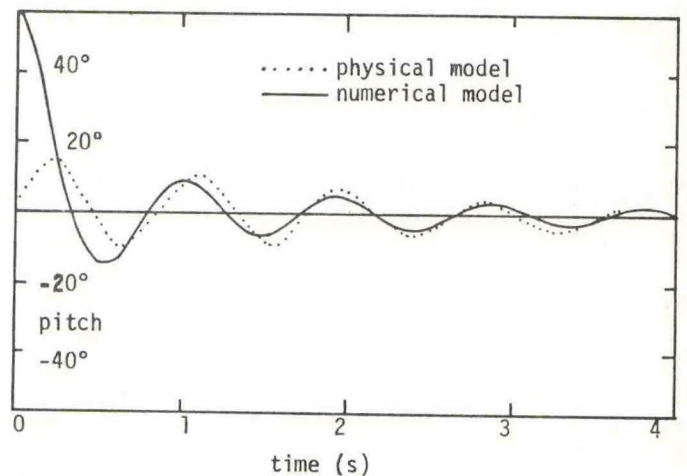


Fig. 3 Pitch impulse response. Spherical buoy.

Table 2 Natural Periods (seconds)

Buoy	Heave				Pitch			
	Numerical		Physical		Numerical		Physical	
	Freq. resp.	Imp. resp.	Imp.Res. OSU	Imp.Res. CSC	Freq. resp.	Imp. resp.	Imp.Res. OSU	Imp.Res. CSC
Spar	1.10	1.09	1.06	1.11	1.94	2.18	---	2.15
Sphere	.97	.94	.91	.93	.90	.94	.89	.92
Discus	1.00	.88	.87	.90	--- ( $\rightarrow \pi$ )	.67	.62	.64

The frequency response period from the laboratory tests - not shown.



2) Frequency response tests were made wherein the buoy was placed at the up-wave extremity of the background grid and about three feet from the wave flume wall. Super 8 mm movies were made of the buoy as it drifted across the grid. Again, time lapse analysis of the films were made to determine the maximum pitch and heave conditions for the buoy. The results were nondimensionalized and are plotted on Figs. 4 through 9. Superimposed on the figures are the results from the axisymmetric Green's function program. It should be kept in mind that the axisymmetric program does not account for viscous damping. Some small perturbations were created from waves reflecting from the buoy. However, these were very small in amplitude with respect to the amplitude of the incident wave.

A comparison was made from the results of the Green's function program with those published in (7) for a sphere floating with the water line at its mid section. Table 3 shows the results agree quite well. Comparison was made in the heave direction only.

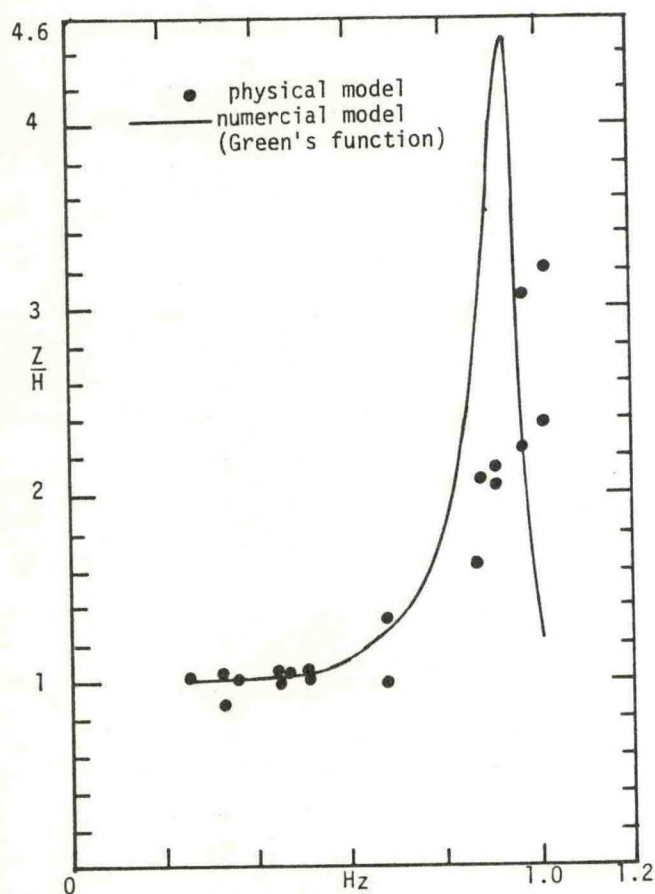


Fig. 4 Heave frequency response. Spar buoy.

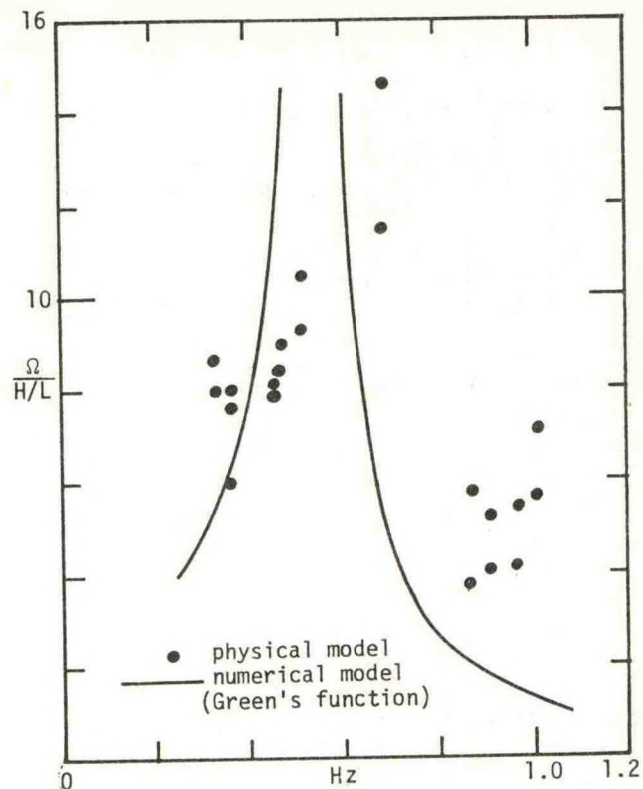


Fig. 5 Pitch frequency response. Spar buoy

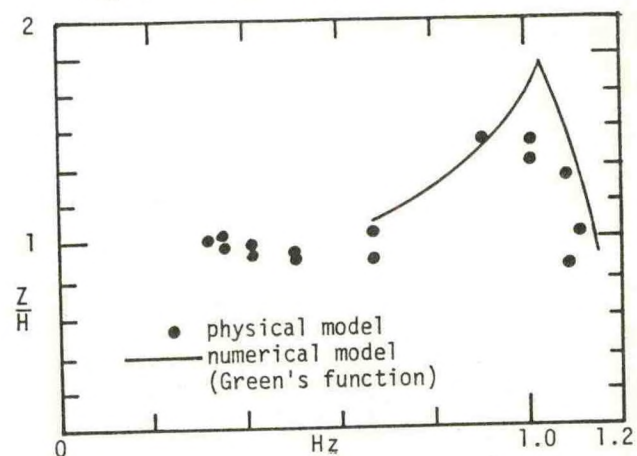


Fig. 6 Heave frequency response. Spherical buoy.

Table 3 Green's function program vs. Fig. 6.24 in (7). For sphere in heave.

Coeff.	Gf	Newman (7)	% diff.
$A_{22}$	.42	.43	2.3
$N_{22}$	.239	.246	2.9



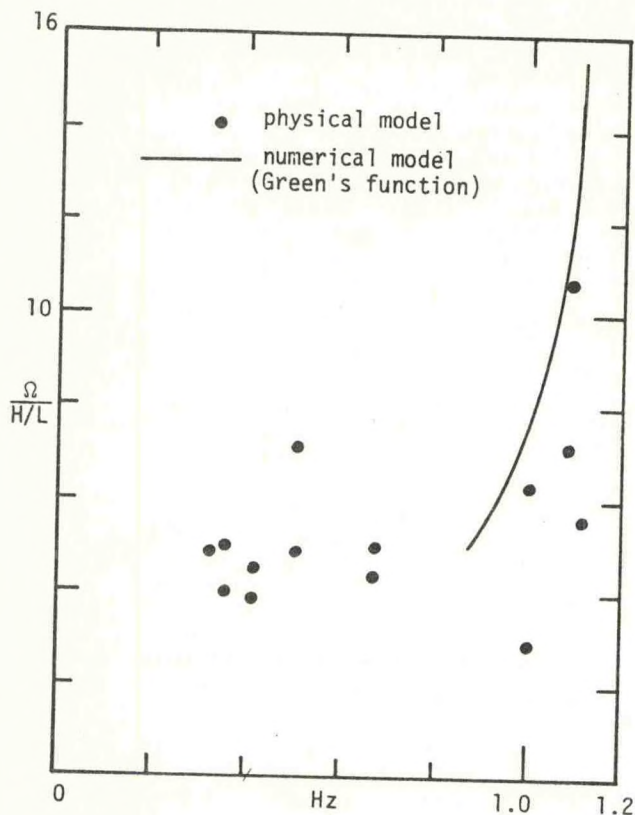


Fig. 7 Pitch frequency response. Spherical buoy.

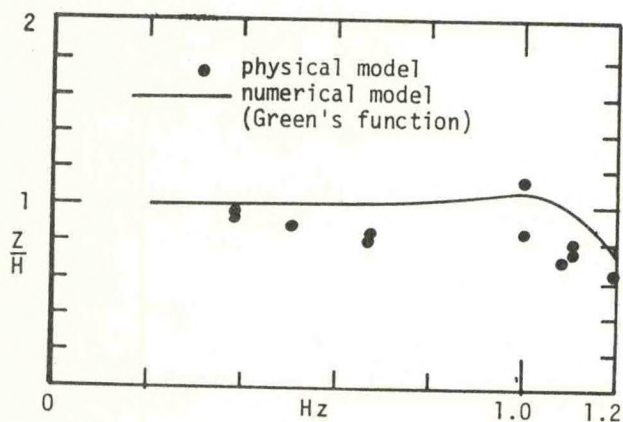


Fig. 8 Heave frequency response. Discus buoy.

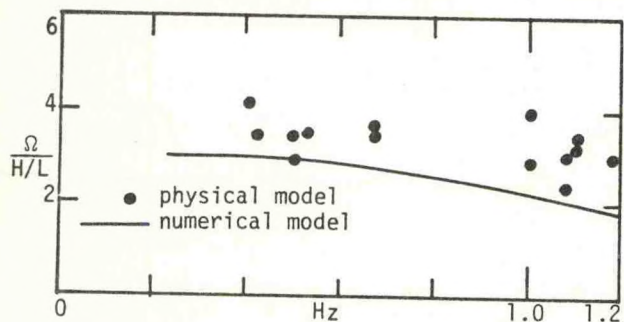


Fig. 9 Pitch frequency response. Discus buoy.

3) Drift tests were made wherein the buoy was placed at a position in the wave flume and a series of periodic waves were generated. After an apparent steady state condition was achieved, a marker was placed upon the side of the wave flume, directly opposite the buoy when the buoy was at the crest of a wave. At the same time, a stop watch was started and the buoy drift was timed for an appreciable period, sometimes until it had drifted 75 or 100 feet. When the buoy again reached the crest of a wave at the end of the test, the stop watch was stopped and the distance of drift was measured. In most cases, the distance of the drift was quite large with respect to errors that could have occurred due to the wall markers not being directly opposite to the buoy. In some cases, however, the buoy drifted only a very small amount due to the physics of the condition and that error could have been appreciable. Thus, slow drift speeds are not likely to be as accurate as the faster drift speeds. However, repeat tests were made and reproduction was fairly good. A wind anemometer was mounted at the wave flume to measure the wind. At first the wind speed was taken into account in reducing the drift speed of the buoy. However, too much scatter still entered into the data and those runs were discarded. Finally, the runs could only be made on a windless day, so that the testing stretched out over a few weeks time in November and December, utilizing the relatively windless hours of the morning.

The results of the drift tests were non-dimensionalized and are plotted in Figs. 10 through 12. Figure 10 is for the spherical buoy. The numbers alongside the plotted point refers to the wave steepness,  $H/L$ . The plotted point also represents the decimal point. The symbol,  $C$ , is the phase speed of the wave and  $V$  is the drift speed of the buoy. Approximate contours have been interpolated from the plotted values so that comparison can be made with the other models. It is obvious that more data are needed in order to firmly establish the contour positions. However, that which is presented here is the best that could be done in the time available up to now.

Figure 11 clearly shows the spar buoy drifted faster than the discus buoy. For  $h/L > .4$  to  $.6$  the spar buoy also generally drifted faster than the spherical buoy. On the average, the discus buoy drifts slightly slower than the spherical buoy.

For Fig. 12 a braided rope, 8 ft. long, was attached as a drogue to the spherical buoy. A three pound weight was attached to the bottom of the approximately 2.1 inch diameter rope. The very limited data indicate the rope slowed the drift speed except for the range  $1.5 < h/L < 2.2$ . Because of the limited data the results are inconclusive.

An important feature of these plots is their format for comparing drift speeds as a function of wave nonlinearity, i.e.  $h/L$  and  $H/L$ . They also show what percent of the phase speed of the wave is imparted to the buoy.



At the time of writing of this paper the numerical model has not been exercised to duplicate these drift test runs.

#### 4. CONCLUSIONS

The axisymmetric Green's function program gives excellent results for determining the added mass and radiation damping coefficients for the three degrees of freedom system of the buoy in two-dimensional motion, as evidenced by the impulse response and frequency response tests. The efficacy of the buoy motion program for the buoy on waves is still to be determined at the writing of this paper.

Nondimensional plots of the laboratory results of buoy drift as a function of the wave period and wave steepness show fairly clearly the relative drift speeds of the buoys as functions of wave frequency.

#### 5. ACKNOWLEDGEMENTS

The authors wish to thank Mr. Edmund Kerut and Mr. Brett Wilson for their helpful suggestions and endorsement of this work. Laboratory and computational assistance were provided by Clay Baumgartner, Ming-Kuang Hsu and Chung-Chu Teng. Their dedication to assisting most effectively to this study is much appreciated.

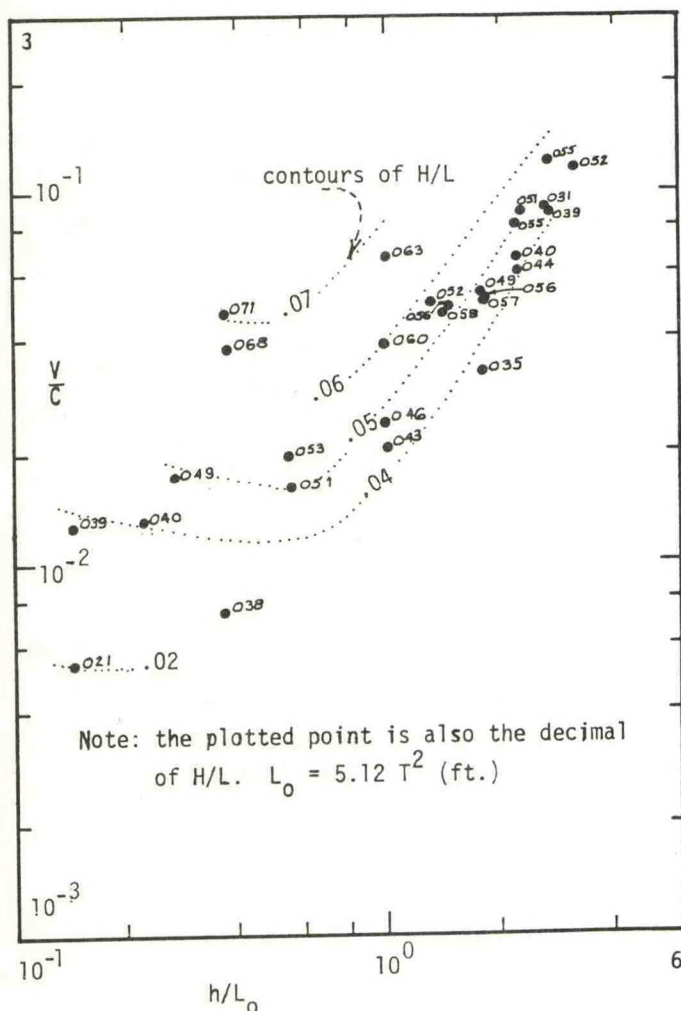


Fig. 10 Drift speed in periodic waves as a function of wave period and steepness. Spherical buoy.

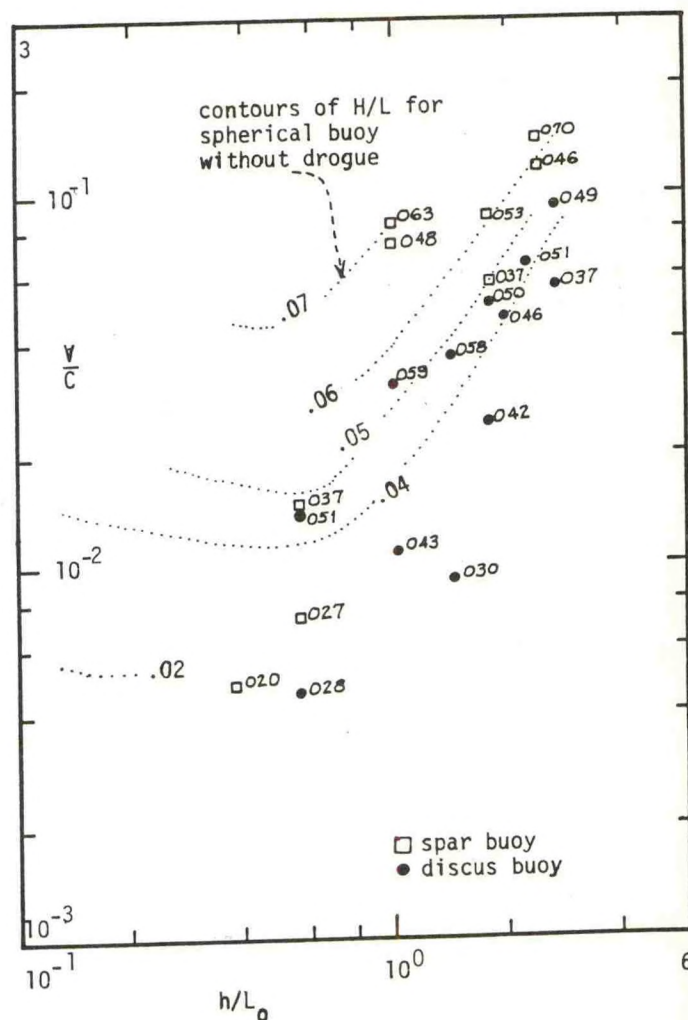


Fig. 11 Drift speed in periodic waves. Spar and discus buoys.



# REFERENCES

1. Atkinson, K. E., 1978, An Introduction to Numerical Analysis, John Wiley & Sons, New York, NY, pp. 471-481.
2. Chertock, G., 1971, "Integral Equations Methods in Sound Radiation and Scattering from Arbitrary Surfaces," Naval Ship Research and Development Center, Report 3538, 57 p.
3. Crandall, S. H., 1956, Engineering Analysis, McGraw-Hill Book Co., Inc. New York, NY, pp. 39-47.
4. Fenton, J. D., 1978, "Wave Forces on Vertical Bodies of Revolution," Journal of Fluid Mechanics, Vol. 85, pp. 241-255.
5. Garrison, C. J., 1974, "Hydrodynamics of Large Objects in the Sea, Part I: Hydrodynamic Analysis," Journal of Hydronautics, Vol. 8, No. 1, pp. 5-12.
6. Isaacson, M. St. Q., 1982, "Fixed and Floating Axisymmetric Structures in Waves," Journal of Waterway, Port, Coastal and Ocean Division, ASCE, Vol. 108, No. WW2, May, pp. 180-199.
7. Newman, J. N., 1977, Marine Hydrodynamics, The MIT Press, Cambridge, MA, pp. 285-311.
8. Thresher, R. W. and Nath, J. H., "Anchor-Last Deployment Simulation by Lumped Masses," Journal of Waterway, Port, Coastal and Ocean Division, ASCE, November 1975.
9. Wehausen, J. V. and Laitone, E. V., 1960, "Surface Waves," Handbook of Physics, Fluid Dynamics III, Vol. IX, Springer-Verlag, pp. 446-667.

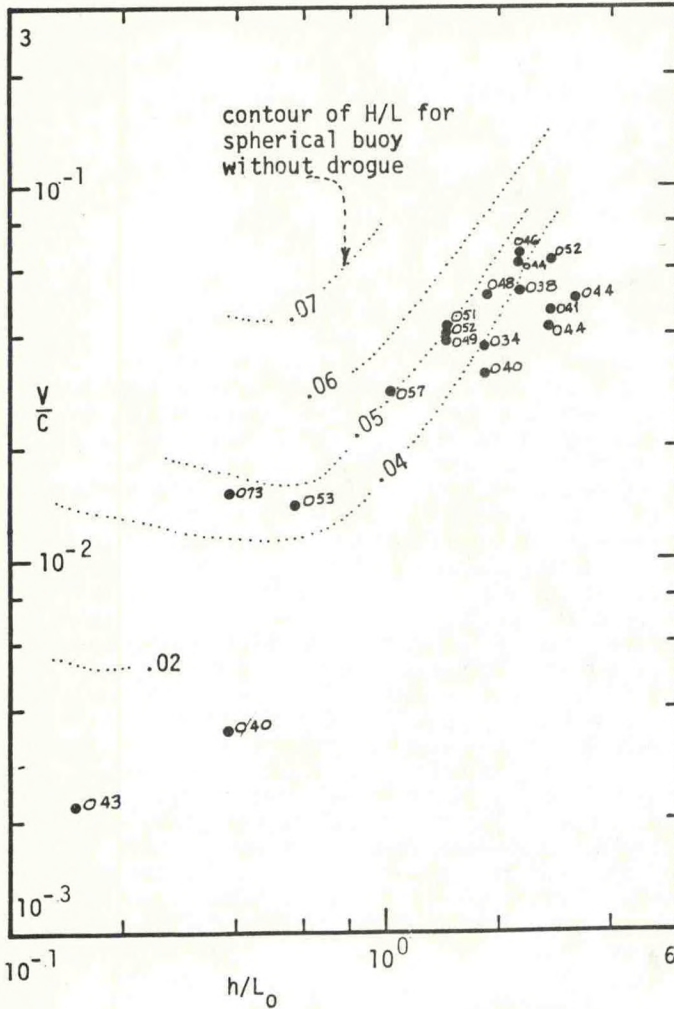


Fig. 12 Drift speed in periodic waves. Spherical buoy with rope drogue.



# THE ADDED MASS COEFFICIENTS OF SEVERAL VERTICALLY AXISYMMETRIC DRIFTING BUOYS

Jieh Lee

Computer Sciences Corporation  
National Space Technology Laboratories  
NSTL Station, MS 39529

## ABSTRACT

Numerical and experimental results are given for the added mass of several vertically axisymmetric drifting buoys. Buoy geometries of interest are a family of spheroids and a family of spar-type drifting buoys with various dimensions. Empirical data were extracted from experiments of free heave and pitch oscillations in calm water conducted in the towing tank of the National Space Technology Laboratories, Mississippi.

Numerical results for the added mass coefficients of the spheroidal buoys were calculated using a numerical model developed by Dr. J. H. Nath. Both the numerical and experimental results can be used in connection with ocean buoy motions associated with resonant conditions.

The present study is a part of an ongoing effort to validate the numerical models for drifting buoy motions developed by Dr. Nath and used extensively at NDBC. In particular, the results for the spheroidal hulls have found direct application in a project now under way at NDBC to design a Lagrangian effectiveness buoy.

## INTRODUCTION

A systematic drifting buoy design approach must rely heavily on appropriate analyses both in statics and dynamics. While limited knowledge is available specifically for buoys, the information and techniques already established for many types of ships and floating structures can be referenced. Since the hull forms of drifting buoys are, generally, much simpler than those of ships, static analysis in drifting buoy design is quite straightforward. The dynamic analysis, however, is much more complicated as a result of the complexity of applying both the hydrodynamic theory and the environmental model. The present state of the art in dynamic analysis of drifting buoys at the NOAA Data Buoy Center (NDBC) is based primarily on the time-domain numerical models (References 1 and 2), which are basically applications of the single wave design approach. In applying hydrodynamic theories, proper choice of the hydrodynamic coefficients, i.e. the added mass coefficients and damping coefficients, associated with the design environments is essential for satisfactorily simulating the buoy responses. This paper deals with the experimental determination of the added mass coef-

ficients in heave for several NDBC spar-type drifting buoys and the comparison between experimental and numerical results of the added mass and added mass moment of inertial coefficients for a family of spheroidal drifting buoys. The spar-type drifting buoys consists of FGGE (The First GARP Global Experiment) drifting buoys, STREX (The Storm Transfer and Response Experiment) drifting buoys, and a series of geometric variations. The buoy geometric variations are listed in Table 1, while the FGGE and STREX drifting buoys are shown in Figure 1. Five spheroidal buoy hulls with different vertical-axis-to-horizontal-axis ratios, i.e. 4.0, 2.0, 1.0, 0.5 and 0.25, were studied and their configurations are shown in Figure 2. All the experimental data were extracted from experiments of free heave and pitch oscillations in calm water, which were considered to be reliable for this study. Numerical models employed for calculation of the added mass coefficients were those described in References 1 and 2 for the spar-type and spheroidal drifting buoys, respectively. Both of the numerical programs were developed by Dr. J. H. Nath of Oregon State University.

Table 1. Spar Buoy Variations

GEOMETRY BUOY	CONE ANGLE (DEGREES)	SPAR DIAMETER (INCHES)	SPAR LENGTH (FEET)
STREX	25.8	8	5
FGGE	26.9	8	5
BUOY 1	30	8	5
BUOY 2	40	8	5
BUOY 3	20	8	3
BUOY 4	20	8	7
BUOY 5	20	4	5
BUOY 6	20	12	5

## BACKGROUND

The equations of motion for drifting buoys employed in the numerical models of References 1 and 2 were based on Newton's second law. A general descriptive formulation can be written as Virtual Mass  $\cdot$  Acceleration = Gravity + Hydrostatic Force + Radiation Damping Force + Viscous Drag + Wave-Exciting Force + Tether Tension (1) where each term is in matrix form. The virtual mass in the left hand side of equation 1 is the sum of the actual buoy mass and the added mass. The introduction of the added mass in the equations of motion allows for



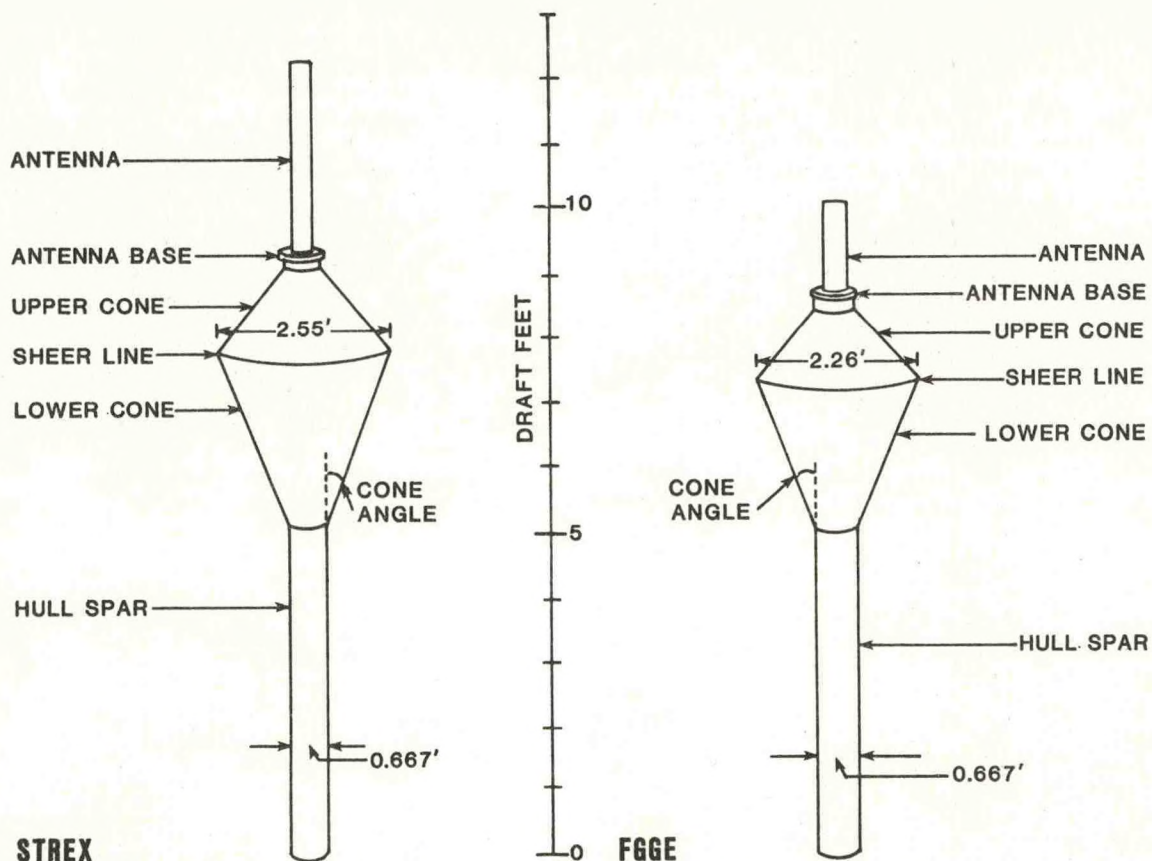


Figure 1. STREX and FGGE Buoy Configurations

the participation of the ambient fluid in the buoy dynamic response. The added mass can be calculated theoretically by considering the motion of the fluid field around the drifting buoys. Small oscillatory motions of an inviscid, incompressible fluid with a free surface can be described by a boundary value problem governed by Laplace's equation with appropriate boundary conditions on the free surface, on the bottom of the fluid, on the drifting buoy body surface, and at infinity if the fluid field is large enough. As a part of the solution, the added mass clearly depends not only on the flow pattern but also on the boundaries of the flow field. If the bottom of the fluid is a rigid impermeable plane and the radiation condition holds at infinity, the added mass should be a function of the drifting buoy body form and wave frequency. In another approach, the added mass can also be obtained from experiments. Owing to viscosity, bodies accelerated in real fluids experience other effects, and measured values of added mass may differ somewhat from those predicted by theory which assumes an ideal fluid, i.e., one which is inviscid and incompressible. For a long spar-type drifting buoy, the viscous effects may become important and reduce the accuracy of the added mass values calculated from hydrodynamic theories. Hence, it is convenient to consider the actual added mass in a real fluid, i.e., including the viscous effects, rather than the added mass simply from hydrodynamic theory for spar-type drifting buoys. The numerical model in Reference 1 was designed so that empirical added mass coefficients have to be input to the program, and there is

no subroutine to calculate added mass from hydrodynamic theory. A number of experiments were conducted to determine these types of added mass coefficients for several spar-type drifting buoys, and the results are given in the next section.

For spheroidal buoys, the numerical model in Reference 2 provides a systematic way to calculate the added mass coefficients through the hydrodynamic theory. Green's function method was employed in the program, which was based on the fact that the velocity potential associated with the flow about a floating body can be described by either a simple source or doublet distribution over the surface of the body. The added mass coefficients obtained by this approach do not consider the deviation caused by real fluid effects. However, frequency dependence is clearly described by this approach. A series of experiments was conducted to validate the Green's function program in Reference 2, and the results will be discussed in the next section.

From a theoretical consideration, the natural period in heave of a drifting body is a function of body mass, added mass, density of the fluid, gravity and waterplane area, while the natural period in pitch of a drifting buoy is a function of body mass moment of inertia, added mass moment of inertia, body mass, gravity, and metacentric height. A direct relationship exists between natural period in heave and added mass if other variables are kept constant. The same situation holds for the added mass moment of inertia and natural period in pitch. These simple relationships make the comparison



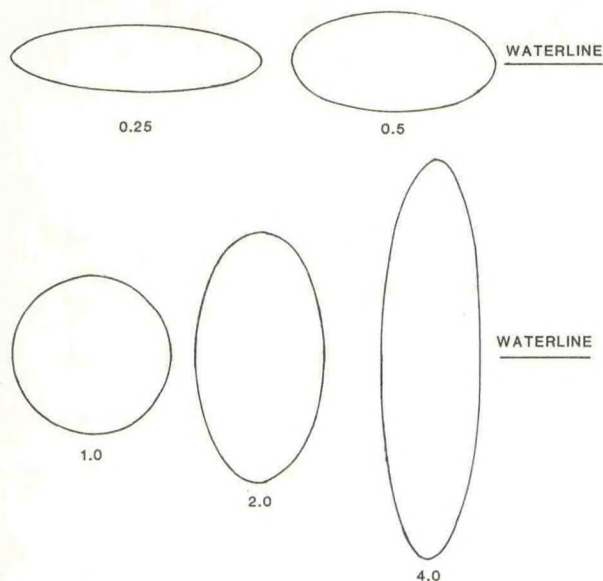


Figure 2. Spheroidal Buoy Configurations

between the experimental and numerical results straightforward in determining the added mass and added mass moment of inertia coefficients. All the tests conducted for both the spar-type and spheroidal drifting buoys were free heave and pitch oscillations in calm water. Since the damping forces were generally small for both the heave and pitch motions of those buoys, the natural periods in heave or pitch could be considered to be equal to the periods of free heave or pitch oscillations. The desired added mass coefficients were obtained by adjusting the input values of the added mass coefficients in the numerical models until the experimental natural periods were achieved. The experimental heave and pitch responses were measured by an accelerometer mounted on the top of the buoys and recorded in the form of graphical voltage variations on a strip chart. The periods could be easily read from the oscillatory curves on the charts.

## RESULTS

The final values of the added mass coefficients in heave for spar-type drifting buoys are shown in Figures 3, 4, and 5 with respect to the various geometric changes in the buoy hull, i.e. cone angle, spar diameter, and spar length, respectively. Increases in dimensions of these buoy characteristics cause increases in added mass coefficients. Figure 3 shows the relationship between the added mass coefficients in heave and buoy cone angle (definition in Figure 1), and a curve can be drawn through the data points. Although not enough reliable data were available, general trends of the added mass changes with respect to the changes in spar diameter and spar length can still be found in Figures 4 and 5, respectively. The frequency dependence was not studied for spar-type drifting buoys. If the wave frequency is not too small, e.g., approaching zero, no significant changes in added mass due to frequency changes will be expected. Since there was uncertainty in determining

the added mass moment of inertia, it will not be presented in this paper.

Close agreement was found between experimental and theoretical results for the added mass coefficients in heave for spheroidal drifting buoys. Figure 6 shows both the numerical and experimental results of the added mass coefficients in heave with respect to the vertical slenderness ratio, i.e., the ratio of the vertical buoy axis to the horizontal buoy axis. The relationships between added mass moment of inertia and vertical slenderness ratio are shown in Figure 7. Close agreement between experimental and numerical results exist for almost all the buoys except the spar-like buoys. This can be explained that, when the buoy becomes slender, the real fluid effect appears to become important, and measured values of added mass coefficients may differ somewhat from the values calculated from the ideal fluid theory.

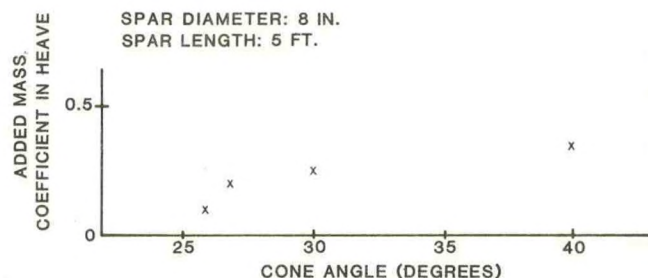


Figure 3. Relationship between Added Mass in Heave and Cone Angles for Spar-Type Buoys

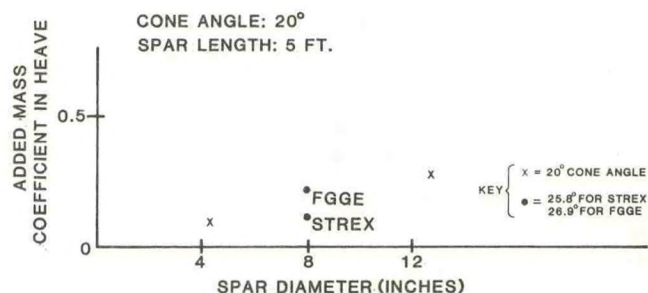


Figure 4. Relationship between Added Mass in Heave and Spar Diameter for Spar-Type Buoys

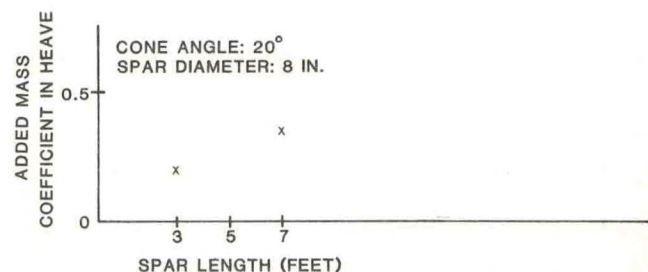


Figure 5. Relationship between Added Mass in Heave and Spar Length for Spar-Type Buoys



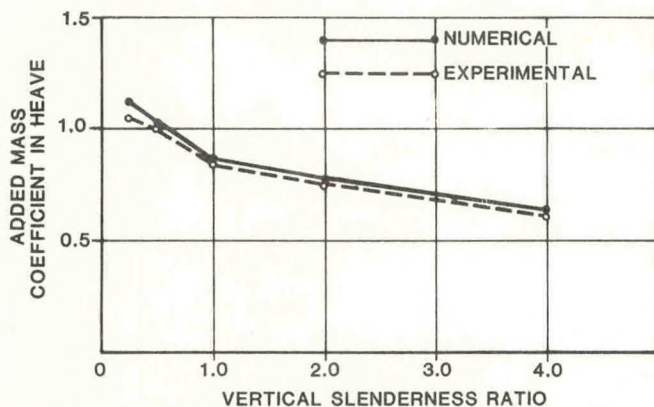


Figure 6. Relationship between Added Mass Coefficients in Heave and Buoy Slenderness for Spheroidal Buoys

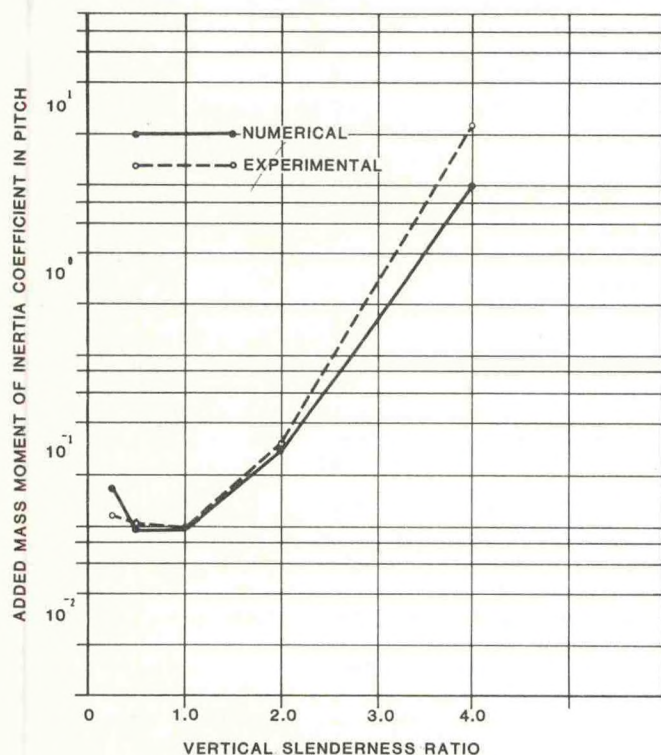


Figure 7. Relationship between Added Mass Moment of Inertia in Pitch and Buoy Slenderness for Spheroidal Buoys

## CONCLUSIONS

The experimental recordings of this study were considered to be satisfactory enough for comparison purposes. The changes of the added mass coefficients in heave for spar-type drifting buoys were plotted versus the changes in hull geometric dimensions, such as spar length, cone angle, and spar diameter. Although exhaustive information cannot be obtained from the graphs because of a lack of data resulting from the limited number of experimental cases, general trends can still be drawn from the graphs. The added mass coefficients for the spar-type buoys account for the actual added masses in a real fluid and are considered to be adequate for actual design purposes. For spheroidal buoys, the added mass coefficients in heave and the added mass moments of inertia in pitch were plotted versus the vertical slenderness ratio, i.e., the ratio of the vertical axis to the horizontal axis of the buoys. Close agreement was found for the added mass coefficients in heave and the added mass moments of inertia in pitch. The experimentally measured value of the added mass moment of inertia of the most spar-like buoy (slenderness ratio 4.0) differs somewhat from the numerically predicted value which assumes an ideal fluid. It can be concluded that viscous effects become important when the buoy is slender. Generally, the added mass and added mass moment of inertia coefficients calculated from ordinary hydrodynamic theory are sufficient for the design of spheroidal drifting buoys provided that the buoy slenderness ratio is not too large.

## ACKNOWLEDGEMENT

The author is grateful to Mr. W. B. Wilson and D. Dexter for helping in arranging and conducting all the experiments.

## REFERENCES

1. Nath, J. H., "Final Report - Task B PRL Buoy with Appendage Arm," Contract NA-81-QA-C-117, NDBO, January 1982.
2. Nath, J. H., "Final Report - Task A: Spheroid Buoy," Contract NA-81-AQ-C-117, Oregon State University, July 1982.



SLIPPAGE ERRORS AND DYNAMIC RESPONSE OF  
FOUR DROGUED BUOYS MEASURED AT SEA

by

John M. Dahlen and Narender K. Chhabra

The Charles Stark Draper Laboratory, Inc., Cambridge, MA

ABSTRACT

Four drogued buoy configurations were tested off the shore of Bermuda to measure and compare their slippage errors, tether line tensions, and drogue orientations and accelerations. In the moderate wind and sea conditions encountered slippage errors fell in the range 1-8 cm/s. The Polar Research Lab (PRL) Buoy/Holey Sock Drogue exhibited the smallest slippage and the greatest tension fluctuation. The commonly-used Scripps Institution of Oceanography (SIO) Buoy/Parachute Drogue exhibited the next smallest slippage and the least tension fluctuation. The SIO Buoy/Window Shade Drogue and the commonly-used PRL Buoy/Window Shade Drogue slipped somewhat more and experienced middle-range tension fluctuations.

TEST PLAN

Summary

Between 19 June and 3 July of 1978 The Charles Stark Draper Laboratory conducted a series of tests off the shore of Bermuda in order to find the slippage errors and measure the dynamics of important buoy/drogue configurations. The slippage error is the difference between the velocities of the buoy and the water mass to which it is drogued.

Figures 1 through 7 are drawings of the buoys and drogues which were tested. The following configuration pairs were used in each of three day-long tests:

- Test 1: SIO Buoy with Parachute Drogue and SIO Buoy with Window Shade Drogue.
- Test 2: SIO Buoy with Parachute Drogue and PRL Buoy with Window Shade Drogue.
- Test 3: SIO Buoy with Parachute Drogue and PRL Buoy with Holey Sock Drogue.

The buoys, drogues and tethers held force and motion sensing instruments called FVRs and OESE III. In addition, each test included a Waverider Buoy to measure wave height, a Surface Current Following (SCF) buoy, and a Subsurface Current Following (SSCF) buoy using a Holey Sock Drogue. The buoys were deployed, tended, and recovered from the R/V Erline, a 100-foot oceanographic vessel based at Bermuda. Surface wind observations were recorded aboard ship. During each test the Erline was tracked by the shore-based NASA C-Band Radar. Backup ship position was

recorded from the Erline's LORAN-C receiver. The buoys were located with respect to the ship by close-  
aboard range and bearing observations. All instruments provided 100% data return and the buoys were tracked successfully during all tests. We believe the data obtained provide a much-improved understanding of the drifting buoys tested and a contribution to the technology base needed for the achievement of better performance.

The SIO Buoy was developed by G. McNally at Scripps Institution of Oceanography. He and A.D. Kirwan at Texas A&M University deployed large numbers of these buoys with parachute drogues in various Pacific Ocean circulation studies. The PRL Buoy with Window Shade Drogue was developed by various investigators including W. Richardson at NOVA University, W. Vachon at Draper Lab, and Polar Research Lab (PRL) under contract to NDBO. It is marketed by PRL and used extensively by many scientists for Lagrangian circulation studies.

The SIO Buoy was also fitted with a Window Shade Drogue to help resolve the influences of the radically different drogues and buoys.

Finally the PRL Buoy was fitted with a Holey Sock Drogue. This new drogue promised to be more effective than the Window Shade, which was suspected of erratic rotational behavior and therefore reduced effectiveness as a water mass-locking device.

Approach

We designed the tests to provide, where practical, more than one route toward the objectives in case some data were lost or in case some data reduction scheme were to prove unmanageable.

- (1) Slippage of a drogued buoy was found in two ways:
  - (a) Comparison of the buoy's trajectory with that of the reference SSCF Buoy, which is believed to slip very little (an estimate of the reference drifter's slip is made and used to correct its velocity). The most serious uncertainty in the slip error found using this technique is due to the spatial separation between the buoys (usually less than 200 meters at the start and 500 meters at the end of each test).
  - (b) Measurement of the water drag force on the buoy's drogue. Using model test data on



drag force vs. slip velocity, we calculate slippage from measured drag. The most serious uncertainty in the slip error found using this technique is the assumption that steady flow model drag data can be applied to open ocean conditions.

These methods were the only practical techniques available to us considering financial limitations and rough open sea conditions.

- (2) Tether/Drogue force and motion measurements were made somewhat redundant by instrumenting each drogue with two Force Vector Recorders (FVRs) each of which contained a number of sensors including a tensiometer, a pressure transducer, accelerometers and magnetometers. These sensors enable us to determine drogue orientation and drag as well as wave-frequency fluctuations of tether line tension and drogue acceleration.
- (3) The performance of competitive configurations could usually be directly compared because they were put into the sea either side-by-side on the same day, or side-by-side with a standard configuration (the SIO Buoy with Parachute Drogue) on different days.

#### Trajectory Determination

The buoys were deployed approximately 5 miles off the west end of the south shore of Bermuda in 1000 fathoms. In this area the Erline, mounting a transponder on her mast, was reliably tracked by the NASA C-band radar located approximately 12 miles away at the east end of the south shore. Vessel position was also determined using LORAN-C, which was reported to be quite repeatable in this area due to the Coast Guard LORAN-C monitor station on the island. Each buoy was periodically located relative to the ship by maneuvering the Erline upwind to a stop with the buoy just under her bow, at which times gyro-compass bearing and transponder-buoy horizontal range were recorded. Radar reflectors were removed from all buoys after Test No. 1. Absolute buoy positions were found by adding the relative positions obtained to the absolute ship position from radar on Tests 1 and 2 and from LORAN on Test 3, when radar was unavailable. We estimate the overall buoy position error (relevant to velocity determinations) is less than 10 meters using the NASA radar and 100 meters using LORAN-C. Average buoy velocities found from smoothed fixes approximately 1 hour apart were thus accurate to within 0.3 to 3 cm/s using radar and LORAN, respectively.

#### Force Vector Recorders (FVRs)

The FVR is a self-contained instrument which digitally records the output of six sensors on a magnetic tape cassette. The FVR weighs 78 lb in air and 33 lb in water. Nineteen-in. diameter syntactic foam flotation shells were clamped around two of the four FVRs to render them neutrally buoyant.

The sensors used in an FVR include: linear accelerometers (SYSTRON-DONNER), single-axis magnetometers (INFINETICS), tensiometer (BLH), and pressure transducer (BLH). All sensors were sampled in a burst mode (sample period 0.52 s, burst duration 24.41 min. and burst repetition period 87.38 min.). All instruments used in any given test were precisely synchronized. The location and orientation of the sensors on the drogues and tethers is given in Figures 1, 3, and 4. The following is a brief rationale for the sensor arrangement used:

FVR 1 - on the parachute inner gimbal (see Figure 1). The balanced inner gimbal aligns itself with the parachute axis. The two pressure transducers, one in the FVR and one at the forward end of the inner gimbal, provide both depth and inclination of the parachute axis. A tensiometer at the negative Z-axis end measured the full force of the parachute. The X- and Z-axis magnetometers, an X-axis accelerometer and the differential pressure measurement enable us to calculate burst-averages of Euler angles and parachute force components. Unsmoothed pressure, accelerometer, and tensiometer signals provide wave frequency oscillation data. The weight of the FVR and gimbals provide the necessary ballast weight.

FVR 4 (w/flotation shell) - inserted in-line at the bottom of the tether (see Figure 1). Since this FVR is neutrally buoyant and under tension, it is aligned with the tether. The tensiometer at the negative Z-axis end measures tether tension. Accelerometers and magnetometers along the X- and Y-axes provide burst-averages of Euler angles and tether tension components. Unsmoothed accelerometer and tensiometer signals provide wave frequency oscillation data.

FVR 3 (w/flotation shell) - inserted in the rigid triangular bridle at the top of the Window Shade Drogue or Holey Sock Drogue (see Figures 3 and 4). This FVR is neutrally buoyant so as not to distort the drogue, and is mounted so it cannot rotate with respect to the triangular bridle. The tensiometer at the top (-Z-axis) measures tether line tension. The pressure transducer measures the depth of the tether/drogue junction. Accelerometers and magnetometers along the X- and Y-axes enable us to calculate the burst-average Euler angles of the triangular bridle and the burst-average tether tension components. Unsmoothed accelerometer, pressure transducer, and the tensiometer signals provide wave frequency oscillation data.

FVR 2 - inserted in the rigid triangular bridle at the bottom of the Window Shade Drogue or Holey Sock Drogue (see Figures 3 and 4). This FVR is not floated so that it may provide part of the required ballast weight. It cannot rotate with respect to the triangular bridle. The pressure transducer measures the depth of the bottom of the drogue. Accelerometers and magnetometers along the X- and Y-axes provide the burst-average Euler angles of the triangular bridle. Unsmoothed pressure transducer and accelerometer signals (including a Z-axis accelerometer) provide wave frequency oscillation data.



Balancing burst-average forces on the drogues, we can find the hydrodynamic force from the tether tension and weight forces. From this hydrodynamic force and published drogue drag coefficient data we can deduce an approximate slippage velocity for comparison with the directly-measured slip.

#### Ocean Environment Sensing Equipment (OESE) III

This is a version of OESE having eight data channels, presently occupied by 3 rate gyros, 3 accelerometers, and 2 magnetometers. The eight channels were sampled at a sampling period of 0.26 s. It complements the FVR, being especially suitable for sensing the high-frequency rotational oscillations of the surface buoys. OESE III was installed in one surface buoy during each of the three tests. The location and orientation of the sensors in the surface buoys is given in Figures 2 and 5.

#### Surface Current Measurement

A Surface Current Following (SCF) buoy, built at CSDL for earlier experiments, was used to track the surface current (see Figure 7). The SCF buoy is drogued to the upper 2 meters of water by its polyform flotation collar and its 59-inch long crossed vanes. The radar reflector shown in Figure 7 was not used after Test No. 1. In the data analysis, the wind forces and resulting slippage were estimated and combined with the buoy velocity to obtain a corrected surface current.

#### Wind Measurement

A hand-held wind speed and direction indicator was employed on the top deck in a location relatively free of interference from the vessel structure.

#### Subsurface Current Measurement

A Subsurface Current Following (SSCF) buoy was constructed at CSDL to track the subsurface current (see Figure 6). The radar reflector was removed from this buoy after Test No. 1. This rather small, low-windage buoy supported a large Holey Sock Drogue (see Figure 4), so we assumed this configuration would follow the subsurface current much better than the operational configurations we were evaluating. Furthermore, the slippage of this configuration was estimated from the wind and surface current measurements, so that a corrected SSCF buoy velocity was used as a reference or "ground truth" observation of subsurface current.

#### Wave Measurement

A common waverider buoy was provided by NDBO for wave height measurement. Data were telemetered to the ship where it was recorded on strip charts and magnetic tape recorders.

#### FORCE VECTOR RECORDER DATA

##### Time Histories

Typical time histories for Test No. 2 (SIO/Parachute vs. PRL/Windowshade) Burst No. 3, are given in

Figures 8-11. These data have not been edited. ACC means accelerometer output in units of the earth's surface gravity; MAG means magnetometer output in units of the earth's surface magnetic field (horizontal component, can be greater than 1 if input axis is not horizontal); P-INT is pressure in decibars where the FVR y-axis penetrates the FVR housing; P-EXT is pressure in decibars on the FVR1 +z-axis 1.41 m from center; and TENSION is given in pounds at the FVR -z-axis attachment. Selected burst-wide statistics are written on the plots. The reader is referred to our technical report<sup>1</sup> for a complete set of time histories, burst-wide statistics, tension histograms and tension PSDs. Pressure (depth), vertical acceleration, and tension data are readily interpreted. Note the large azimuthal oscillation of about one minute period experienced by the window shade midway through the burst.

#### Tether Tension - Comparisons and Conclusions

A summary of tether tension data is given in Figure 12. For the moderate test conditions (sea state 2-3, highest waves 2 m) prevailing during the tests some conclusions are apparent: Test No. 1 shows the parachute was somewhat easier on the tether than the window shade. The big difference between tension fluctuations on the two configurations in Test No. 2 shows the SIO buoy is much easier on the tether than the PRL buoy, probably because of its spar design. This observation is also apparent in the tension PSDs given for the two configurations in Figures 13 and 14. The sea state was somewhat milder in Test No. 3 (parachute tether tension fluctuations less than half what they were in Test No. 2), yet the Holey Sock tether experienced tension fluctuations as large as those on the window shade tether in Test No. 2. Hence we conclude the Holey Sock is hardest on the tether, which is not surprising in view of its large surface drag area and entrapped water mass. Extrapolation of these results to severe sea conditions would be impossible without the aid of a dynamic model. We believe tether tension fluctuation is a strong function of configuration and the critical length ratios involving wavelength, tether length, wave height, and drogue length.

#### Computation of Tension Vectors and Drogue Orientation

Each accelerometer (more appropriately called a specific force sensor) measures one component of the vector difference between acceleration and gravity. In our experiment the gravity vector was much larger than the acceleration vector, so for the purpose of computing "instantaneous" FVR orientation, we assumed zero acceleration (equivalent to assuming an on-board pendulum always points straight down). Each data frame (every 0.52 seconds) the accelerometers thus defined the gravity vector and the magnetometers defined the earth's magnetic field vector. From these vectors we computed the "instantaneous FVR-axes (x,y,z) unit vectors in earth coordinates (East, North, Up). In the case of FVR1, we used the difference between P-EXT and P-INT in place of ACC-Z. Instantaneous tension



components were found by multiplying the instantaneous tension magnitude by the instantaneous FVR-axes unit vectors. These instantaneous vectors have a significant error due to the aforementioned assumption of zero acceleration, so we averaged them over the entire burst to get average FVR orientation and tension. These average vectors approximate the true average vectors. This approximation has been tested in a computer simulation of wave-buoy-drogue dynamics and found to be reasonably accurate. More accurate measurements of orientation would involve much larger and more expensive instrumentation.

The mathematics of FVR attitude resolution and the complete set of results are given in our technical report.<sup>1</sup> The results for Burst No. 3, Test 2 are written on Figures 8 through 11.

The FVR1 tension components tell us the parachute hung down 35° below horizontal. This was a consistent trait except for a brief period after deployment when it tilted up, perhaps due to attached air bubbles. In Test 3, Burst 4, it hung down 65°. FVR4 components tell us the parachute tether was inclined 7°. FVR3 components indicate the window shade tether was inclined 10°, while FVR2 shows us the bottom of the window shade was inclined 7°. FVR2 and 3 components also show the window shade was twisted 7°.

Computation of Hydrodynamic Forces on the Drogues

Newtons Law applied to any drogue is

$$\vec{T} + \vec{H} + \vec{W} = M\vec{A}$$

where T is tension, H is the hydrodynamic force, and W is the net weight (weight minus static buoyancy).

Averaged over a burst,  $\vec{A}$  is zero, hence using burst averages

$$\vec{H} = -\vec{T} - \vec{W}$$

$\vec{T}$  is calculated from the FVR data in the manner described above, and  $\vec{W}$  was measured, so computation of  $\vec{H}$  was straightforward. In the case of the Parachute, FVR1 and FVR4 provided alternative computations. Results are tabulated in Table I. The subscripts n, e, u denote north, east, and up respectively. Note the significant values for  $H_u$ ! On the Window Shade and Holey Sock,  $H_u$  is much larger than the horizontal component; and it is down under the SIO Buoy while it is up under the PRL Buoy! This nonlinear dynamical system has given us some unexpected results. The FVR4 data in Test No. 1 is not tabulated because the instrument was not properly installed. In getting  $\vec{H}$  from FVR4 data, hydrodynamic force on the gimbal assembly was neglected. The data have not been rounded off to reflect measurement errors.

## Trajectory Data

NASA radar had vastly superior accuracy to LORAN, so for Tests 1 and 2, only NASA radar data was used. During Test 3, NASA radar was unavailable, so LORAN data was used. We averaged the LORAN data over a one minute window in order to reduce the effects of apparently random noise of 2 and 3 bits peak-to-peak. The resulting buoy trajectories are shown in Figures 15 through 17. Average velocities during the FVR data bursts are given in Table II. SSCF buoy velocities were in the range 16 to 25 cm/s. Buoy displacements with respect to the SSCF buoy are plotted in Figures 18 through 20. Buoy velocities with respect to the SSCF buoy, the simplest measure of slip, were in the range 1 to 9 cm/s. Complete data are given in our technical report.

## SLIPPAGE ANALYSIS

In our velocity notation, the first subscript denotes the reference frame ( $E \equiv$  earth,  $W_{ss} \equiv$  sub-surface water, etc); the second subscript identifies the moving body ( $d \equiv$  drogue,  $w_s \equiv$  surface water, etc); and the third subscript denotes the component ( $n \equiv$  north,  $e \equiv$  east).

Procedure 1: Assume SSCF buoy does not slip

$$(\vec{V}_{E(SSCF)} \equiv \vec{V}_{Ew_{ss}})$$

In this simplest procedure we find the slippage of a drogue equal to the vector difference between its velocity and the SSCF buoy velocity

$$\vec{V}_{w_{ss}d} = \vec{V}_{Ed} - \vec{V}_{E(SSCF)}$$

Results are given in Table III.

Procedure 2: Estimate slippage of SSCF buoy

In this procedure we first calculated the wind force on the SCF buoy during each burst and then its slippage through the surface water due to this force. This slippage was subtracted from the SCF buoy velocity to obtain an estimate of the surface current. See Table IV. Having the wind, the surface current, and the SSCF buoy velocities, we next calculated the forces on the SSCF buoy and the slippage of its Holey Sock drogue necessary for force balance. Of necessity all the above-mentioned force calculations used average velocities and drag coefficients. Drag coefficients and equations were taken from Nath<sup>2,3</sup> and Horner<sup>4</sup>. The Holey Sock slippage was then subtracted from the SSCF buoy velocity to obtain a better estimate of the sub-surface current. The slippages of the other drogues were then recalculated using this new sub-surface current. Results are given in Table V.

Procedure 3: Calculate slippage from drogue forces

Using the average hydrodynamic forces derived from FVR data (Table I) we calculated the slip of the



drogues using the steady-state drag equations and coefficients reported by Nath<sup>2,3</sup>. The coefficients vary with Reynolds number and the equations determine both normal and tangential drag components. The equations require the average inclination angle of the drogues from the horizon. These angles were also found from FVR data and are included in Table VI which presents the results.

#### Comparisons and Conclusions

In order to facilitate a comparison of the results found by the three procedures, the average slippage of each buoy during each test is plotted in Figure 21. The wind and shear which force the slippage are also shown. The PRL/Window Shade and PRL/Holey Sock results from Procedures 2 and 3 agree quite well, a fact which gives us some confidence in the Window Shade and Holey Sock drag equations and in the reliability of Procedure 2. Since Procedure 2 and 3 results sharply disagree in the SIO/Parachute case we believe our parachute drag equation is at fault. This is not really surprising, since the parachute hung down between 35 and 65 degrees. We did visually verify proper inflation of the parachute on two tests, however. We cannot explain the disagreement in the SIO/Window Shade results but place more confidence in Procedure 2. The radar reflectors may have degraded the accuracy in Test No. 1. For the moderate wind and sea conditions of the tests (sea state 2-3) we would then be inclined to rank the configurations in the following order, least prone to slippage error at the top:

PRL/Holey Sock  
SIO/Parachute  
PRL/Window Shade - SIO Window Shade

This ranking is by no means certain. Significant errors are introduced by spatial variability and measurement limitations. Furthermore, our results cannot be extrapolated to significantly different sea conditions without the aid of an accurate dynamic model.

In fact, it would be very useful to apply the large amount of data gathered during the tests toward evaluating and improving dynamic models of the drifters.

#### ACKNOWLEDGMENT

Our ocean test activities were jointly funded by: Texas A&M University, A.D. Kirwan (TAMU) and G. McNally (SIO), Co-principal Investigators; and the NOAA National Data Buoy Office, E. Kerut, Program Director. Analysis of the ocean test results were funded by the University of Washington, D.J. Baker, Jr. (UW) and W.D. Nowlin, Jr. (TAMU), Co-principal Investigators.

A.D. Kirwan and G. McNally helped us plan the ocean tests and provided technical advice in the preparation and deployment of the SIO buoys and parachute drogues. Other CSDL members, notably R. Araujo, C. Martorella, J. McKenna, J. Scholten, E. Scioli, F. Siraco, and M. Soikkeli played key roles in the design and preparation of hardware, conduct of sea tests, and processing of data. D. Brooks, Sperry/NDBO, ably assisted us at sea. The staff of the U.S.N. Tudor Hill Laboratory, Bermuda, CDR Wilson, OIC, provided numerous support services. Finally, the crew of the R/V Erlene, R. Lambert, Master, demonstrated great competence in handling both our equipment and the vessel.

#### REFERENCES

1. Chhabra, N.K., J.M. Dahlen, and J.R. Scholten, Ocean Experiment to Find Slippage Errors and Measure Dynamics of Four Drogued Buoys, The Charles Stark Draper Laboratory, Inc., Report R-1607, November 1982.
2. Nath, J.H., "Laboratory Validation of Numerical Model Drifting Buoy - Tether-Drogue System," Engineering Report for NOAA Data Buoy Office, Bay St. Louis, MS, July 29, 1977.
3. Nath, J.H., "Laboratory Model Test of Drifting Buoy and Drogue," Ocean Engineering Wave Research Facility T.R. 2, School of Engineering, Oregon State University, Corvallis, Oregon, September 1977.
4. Hoerner, S.F., "Fluid-Dynamic Drag, Theoretical, Experimental and Statistical Information," published by the Author, Midland Park, N.J. 1965.







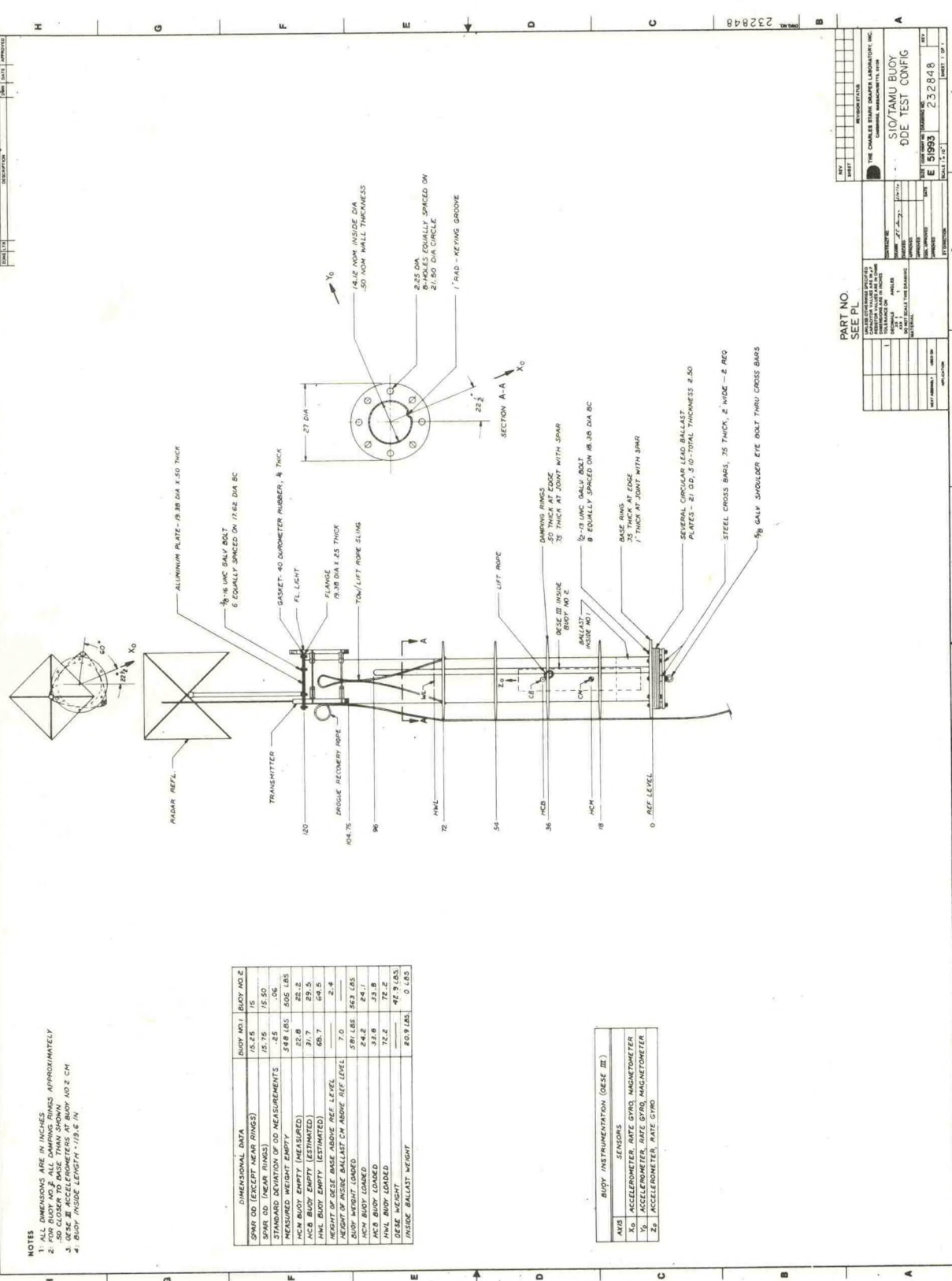


Figure 2.











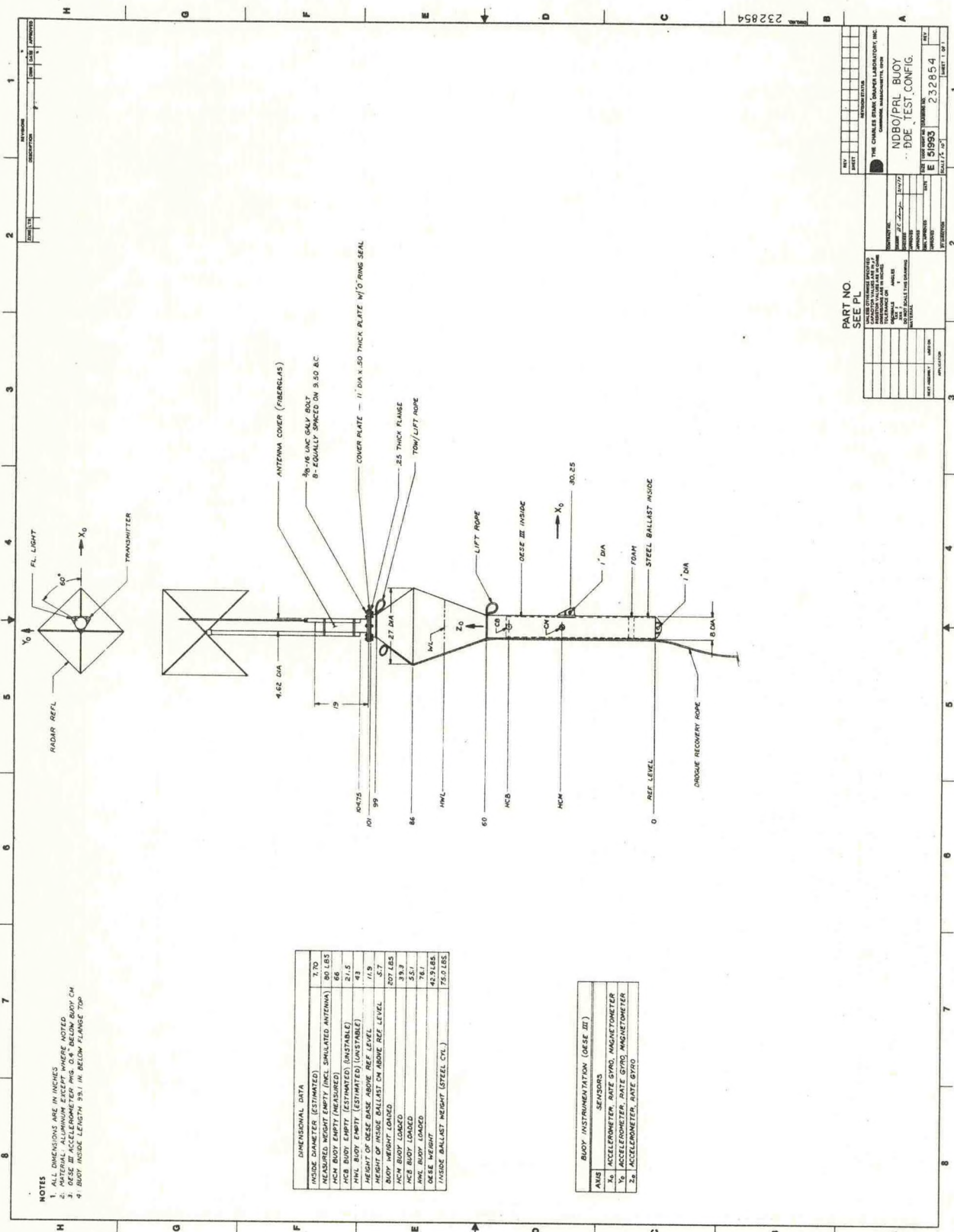


Figure 5.



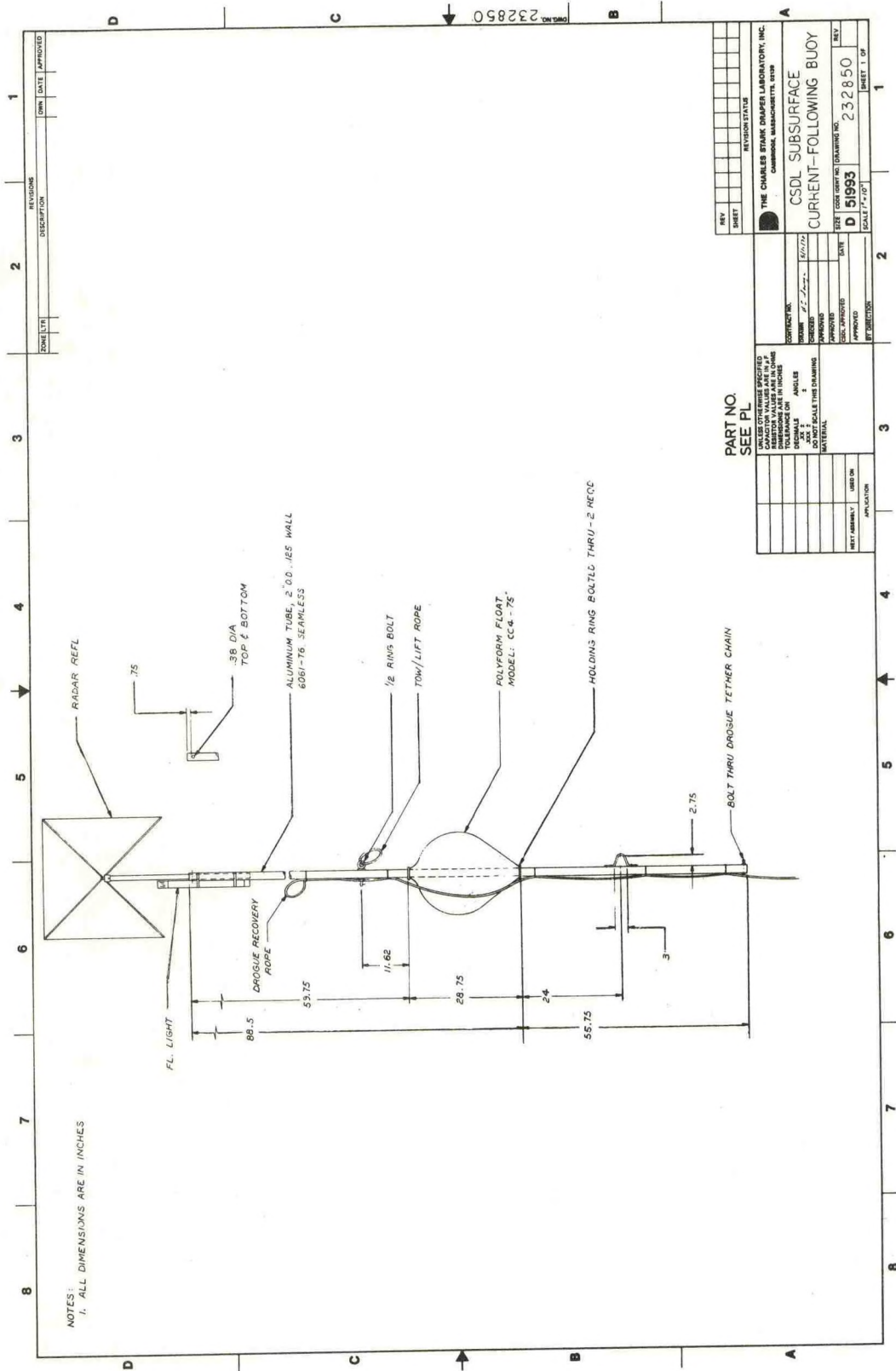


Figure 6.



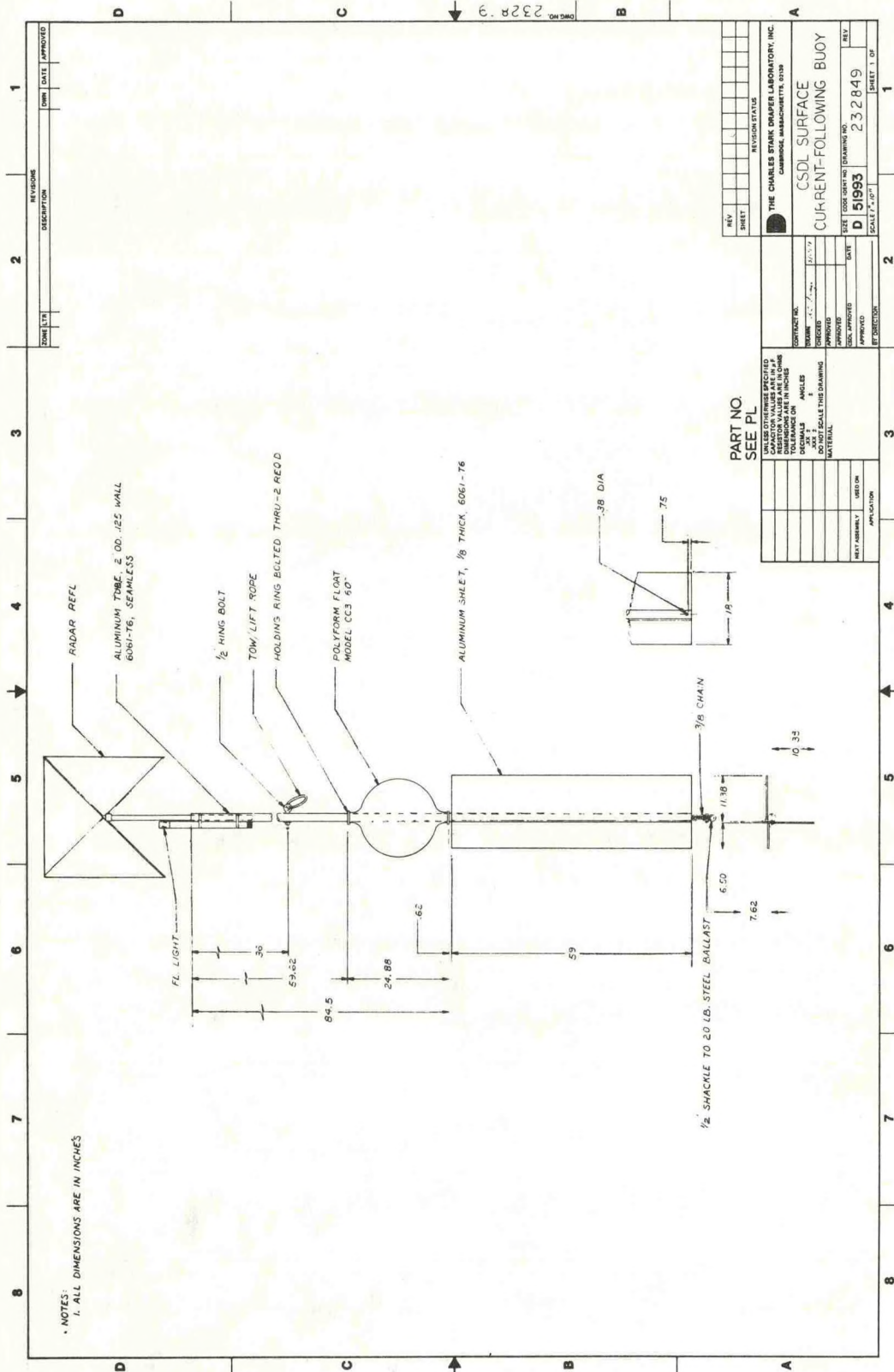


Figure 7.



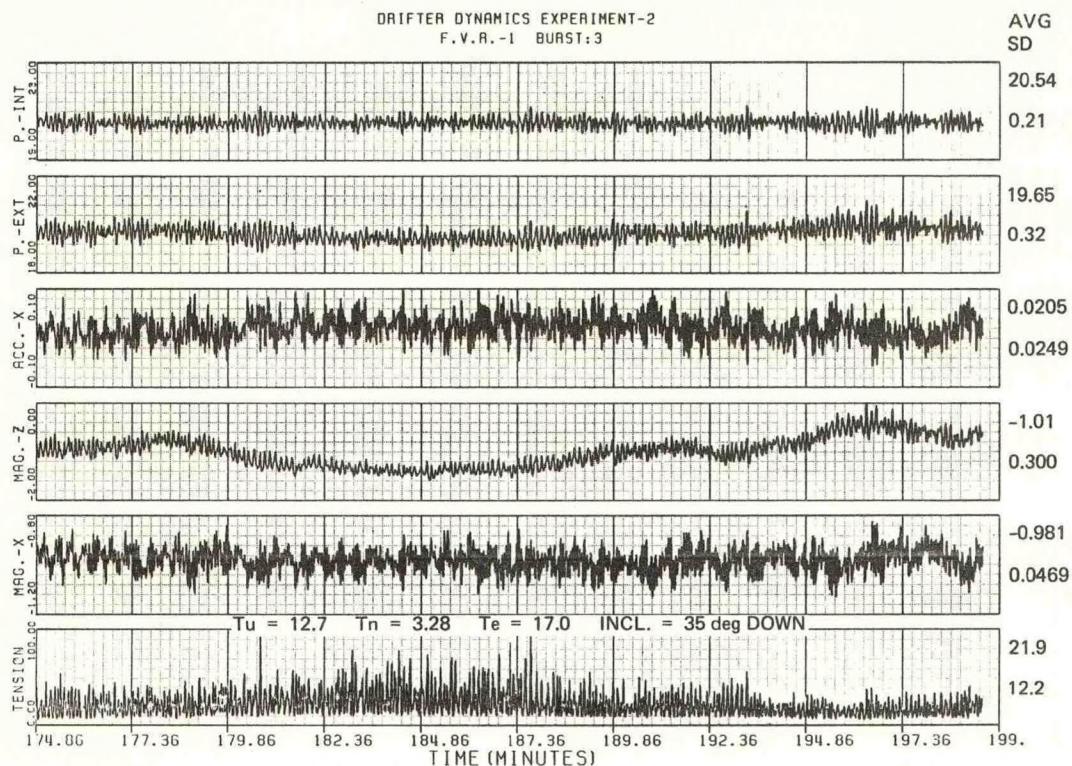


Figure 8. FVR sensor data, SIO/Parachute (gimbal).

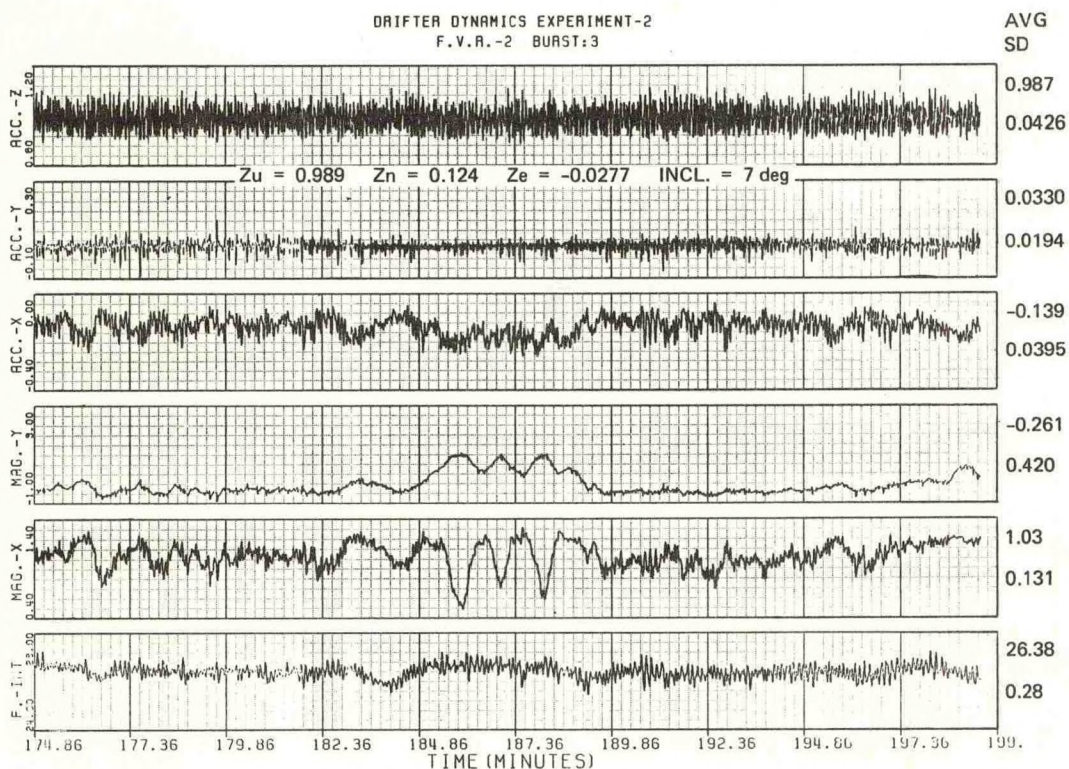


Figure 9. FVR sensor data, PRL/Window Shade (bottom).



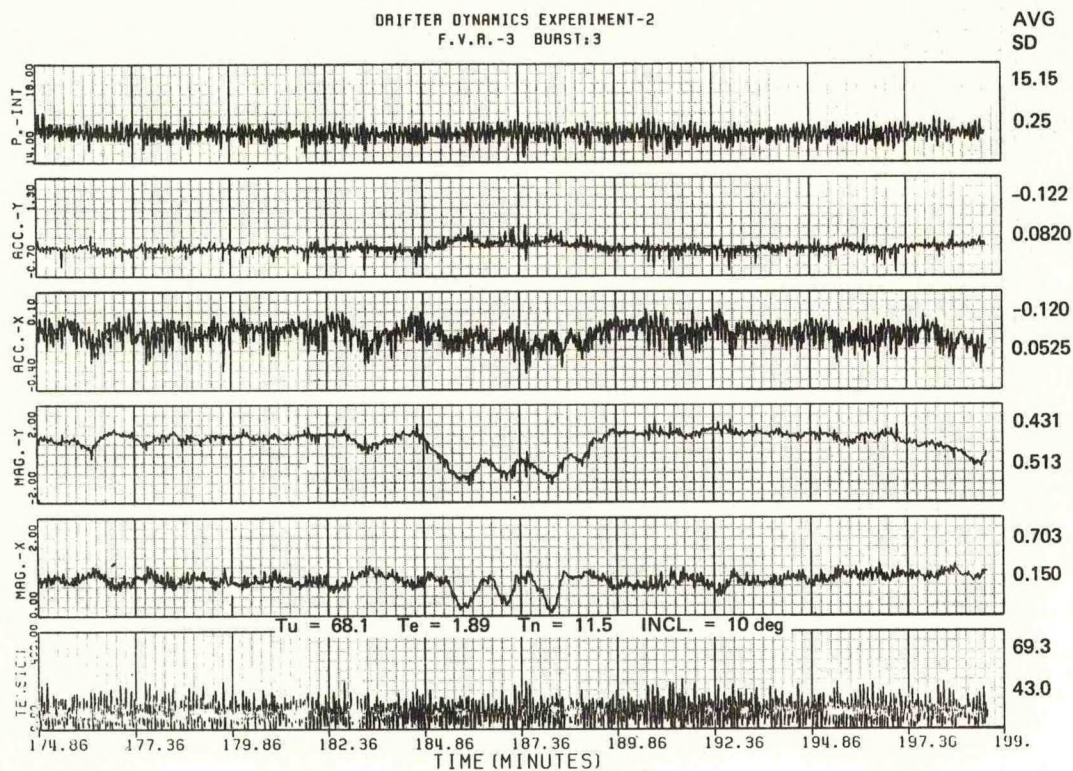


Figure 10. FVR sensor data, PRL/Window Shade (top).

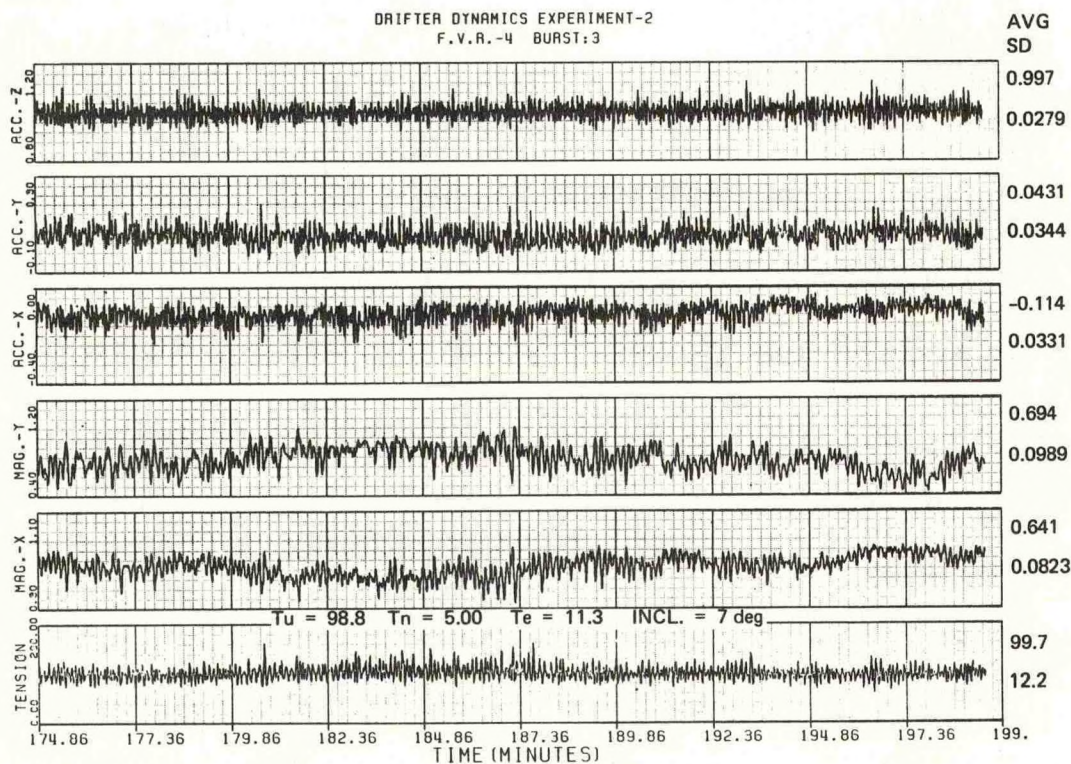


Figure 11. FVR sensor data, SIO/Parachute (tether).



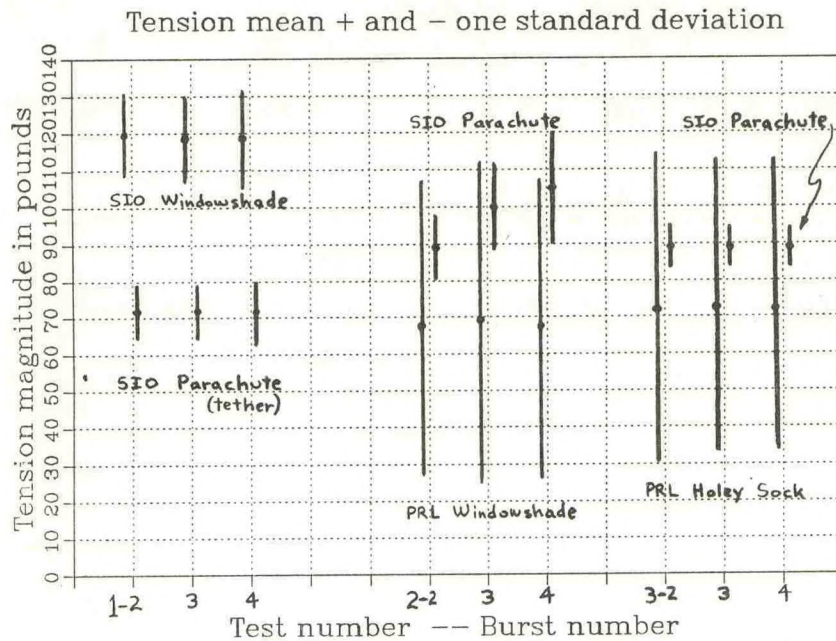


Figure 12.

DDE EXPT. 2: FVR 3 TENSION. BURST @ 10493 S.

Power Spectral Density

Average of 2 Runs of 2048 Spaced 750

Ramp removed? NO. Hanning window applied? NO.

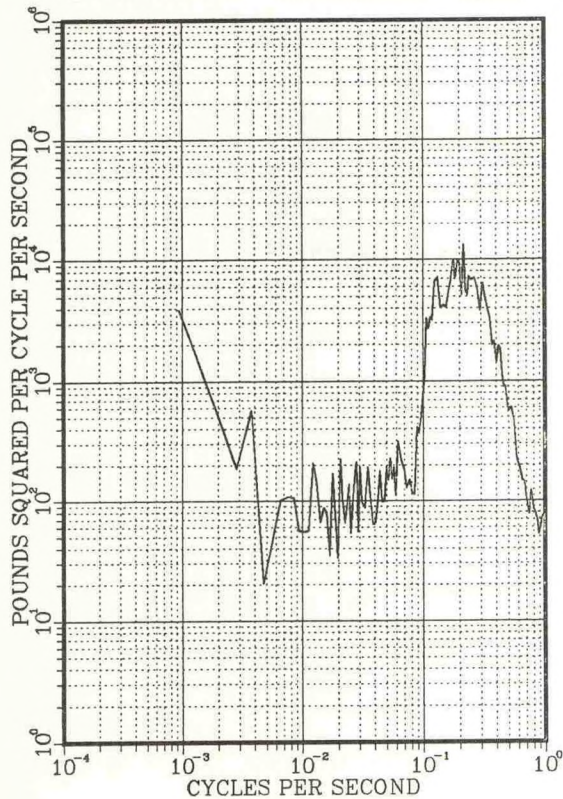


Figure 13.

DDE EXPT. 2: FVR 4 TENSION. BURST @ 10496 S.

Power Spectral Density

Average of 2 Runs of 2048 Spaced 750

Ramp removed? NO. Hanning window applied? NO.

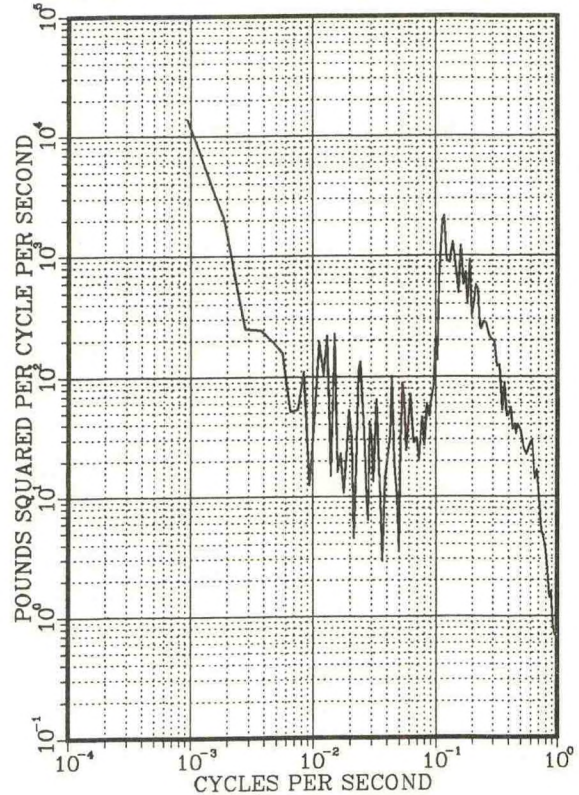


Figure 14.



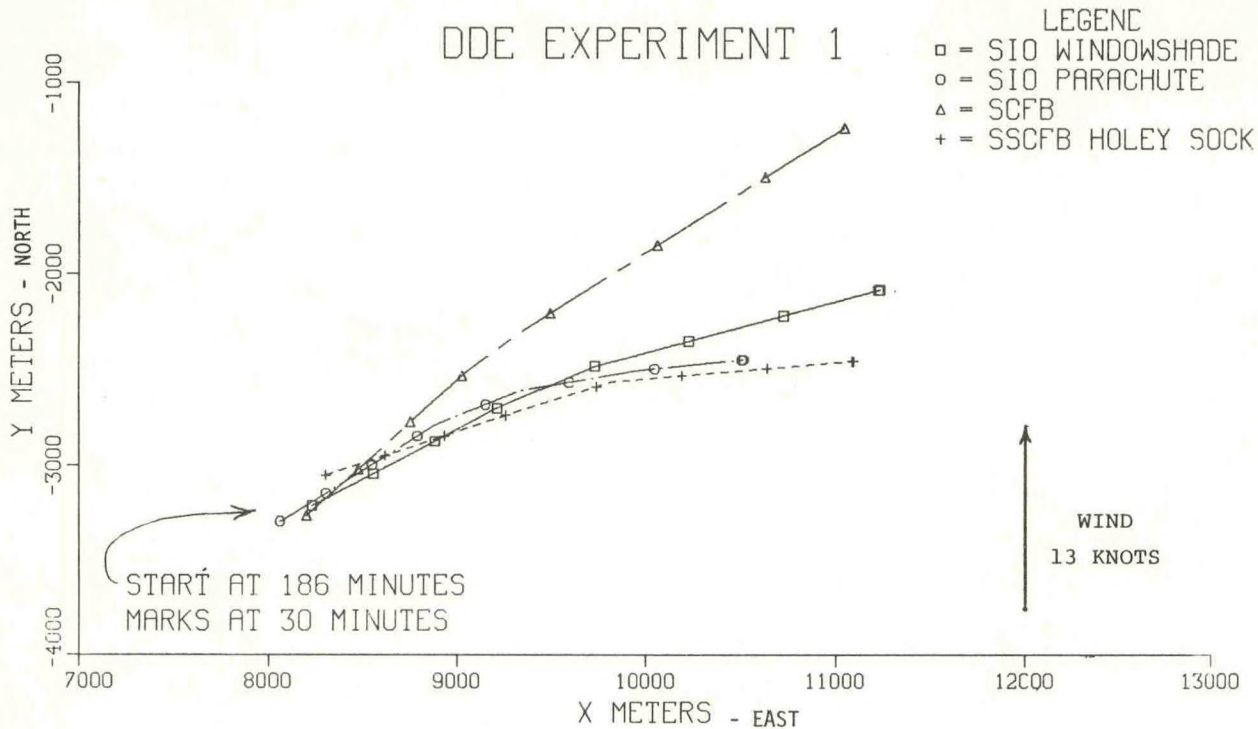


Figure 15. Trajectories of buoys.

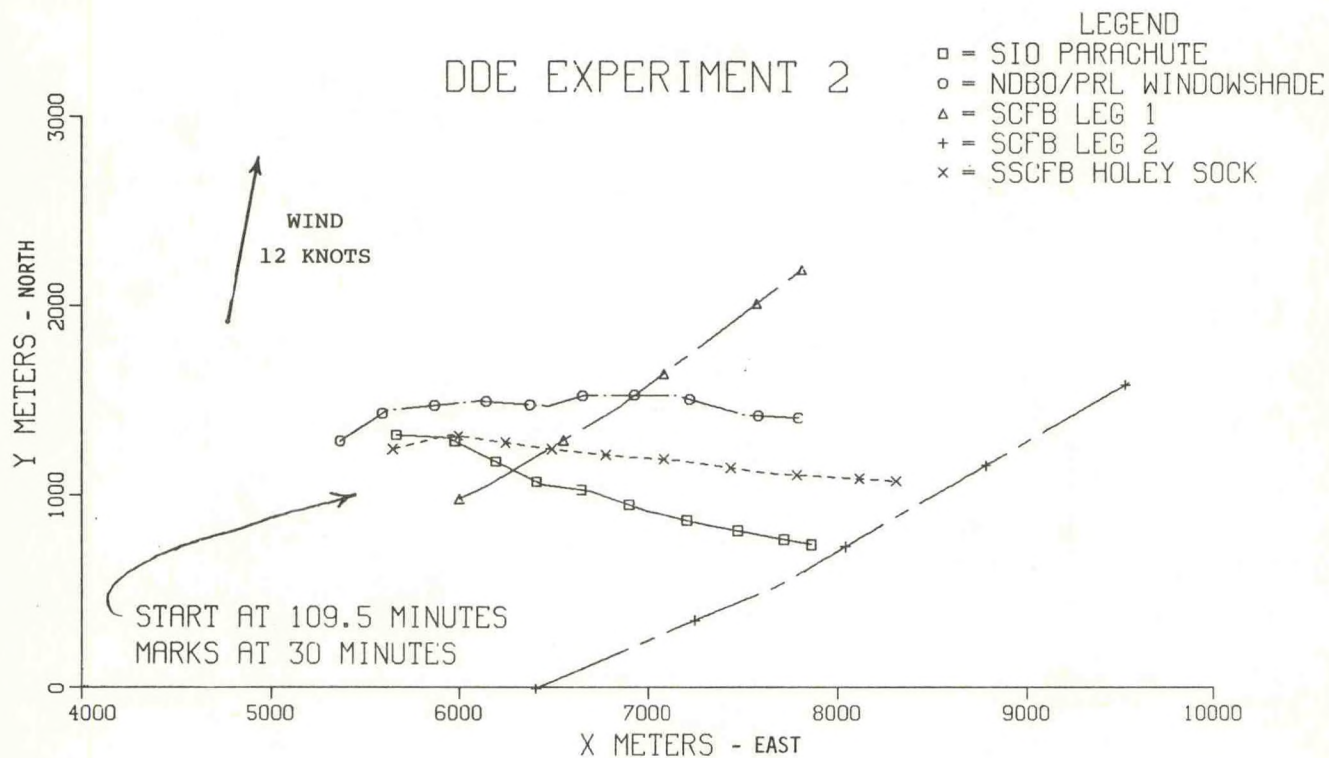


Figure 16. Trajectories of buoys.



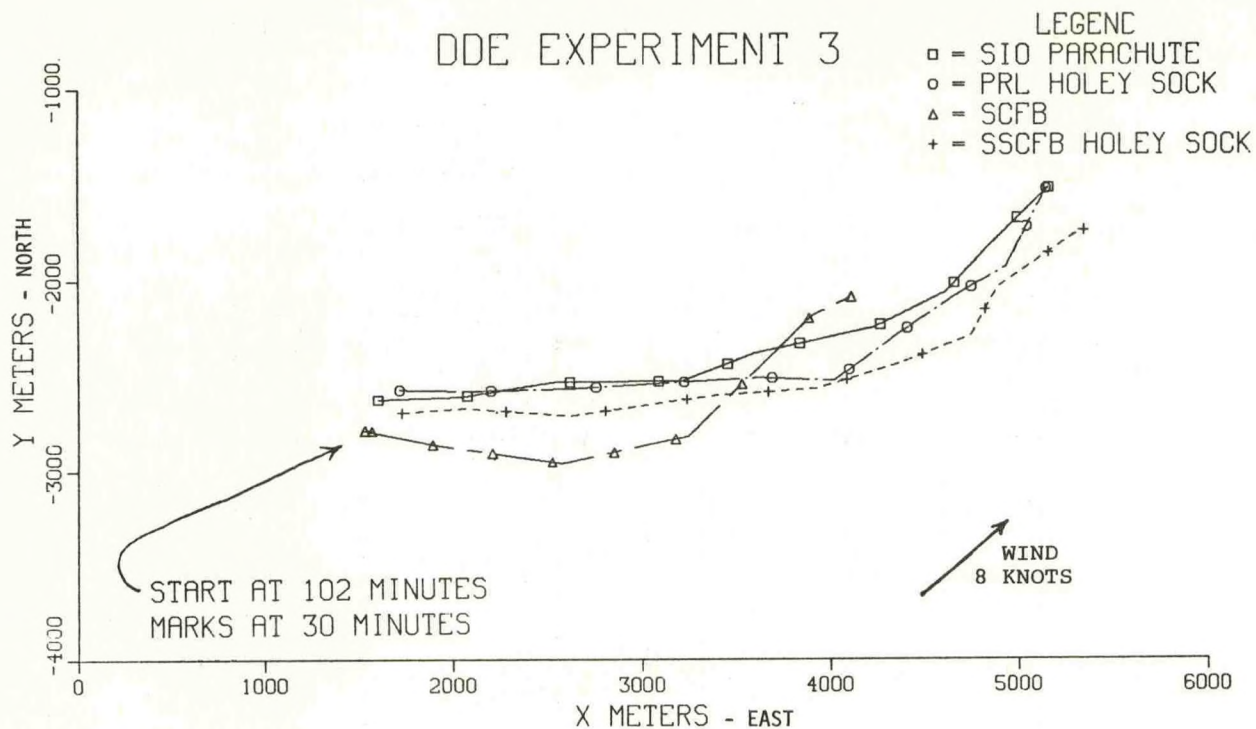


Figure 17. Trajectories of buoys.

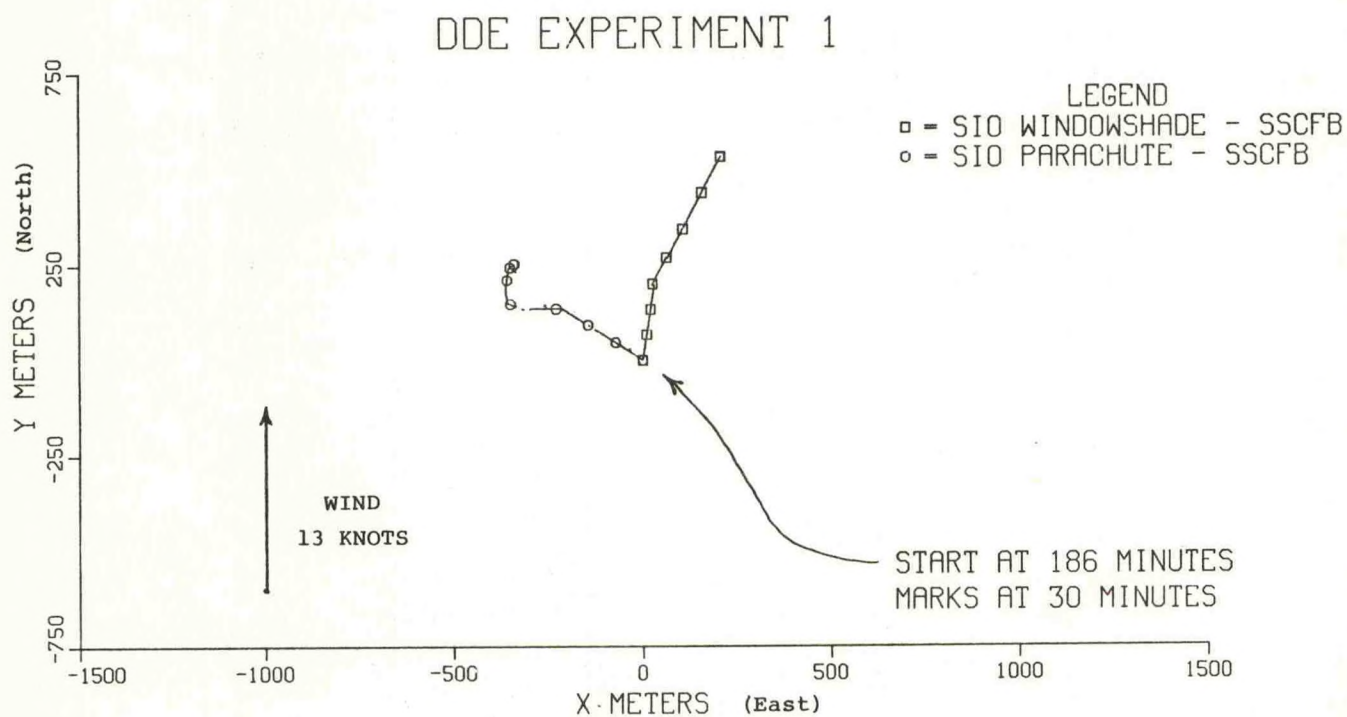


Figure 18. Displacements wrt subsurface current following buoy (SSCFB).



## DDE EXPERIMENT 2

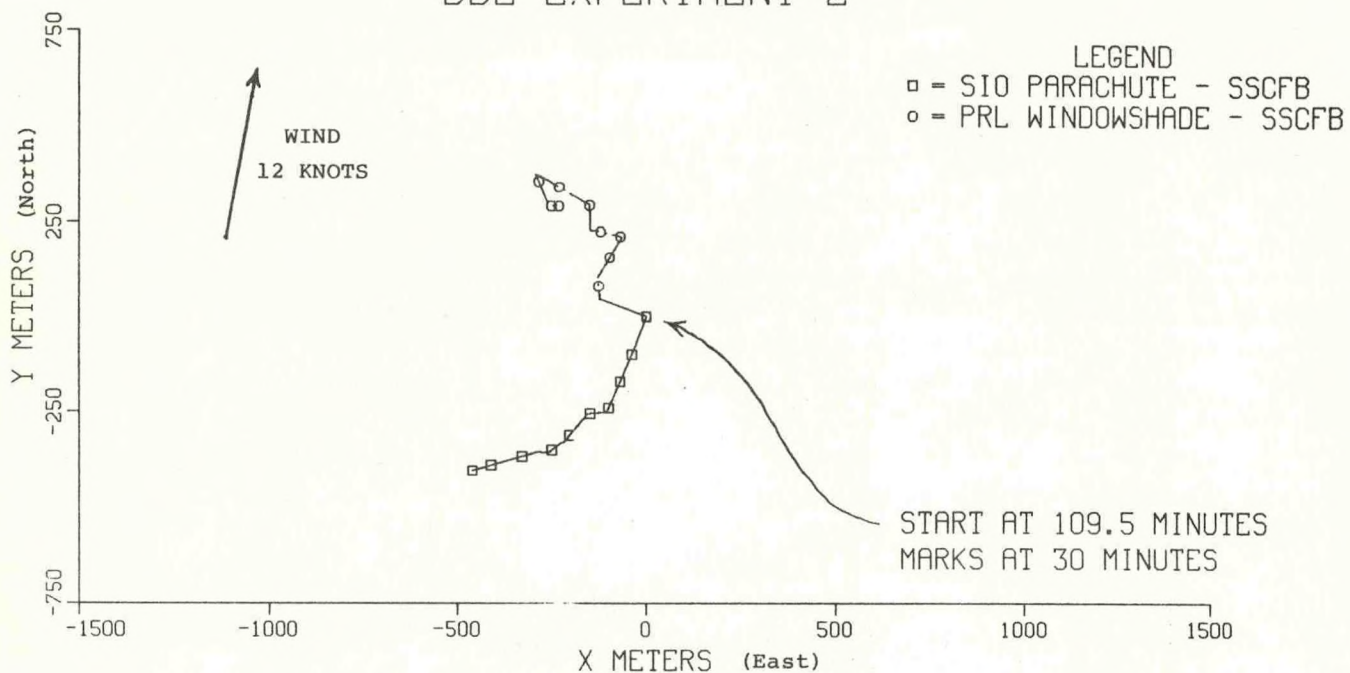


Figure 19. Displacements wrt subsurface current following buoy (SSCFB).

## DDE EXPERIMENT 3

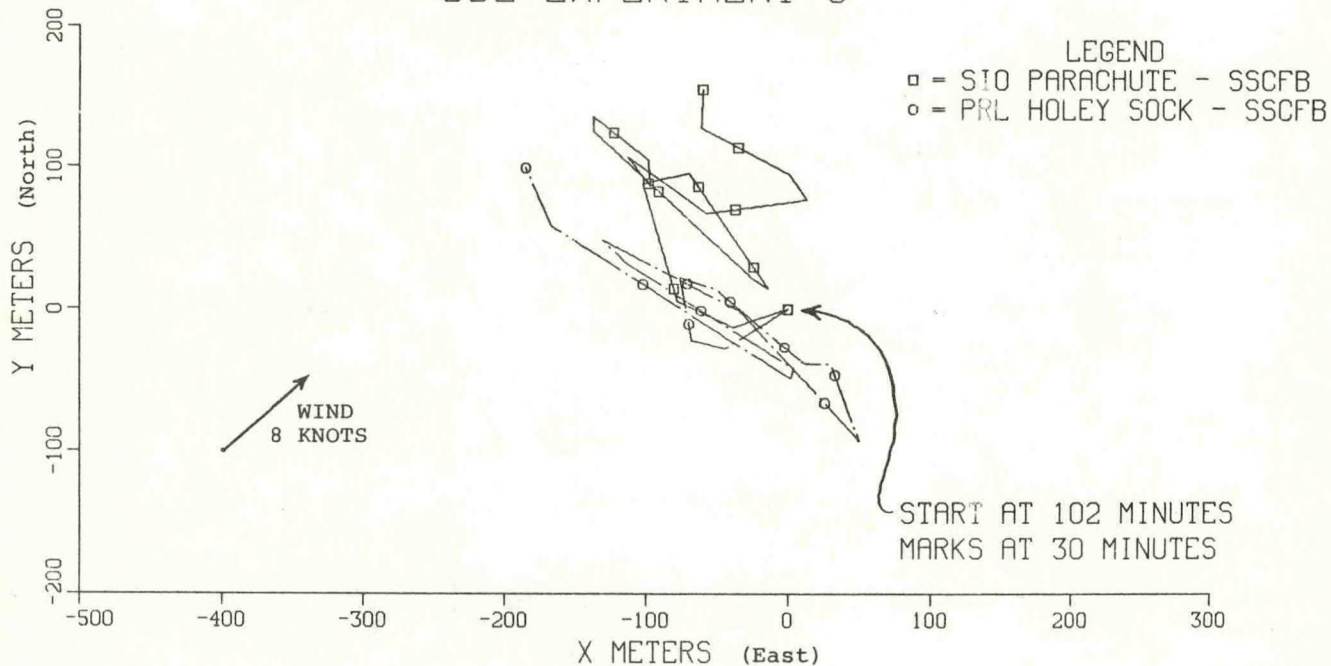


Figure 20. Displacements wrt subsurface current following buoy (SSCFB).



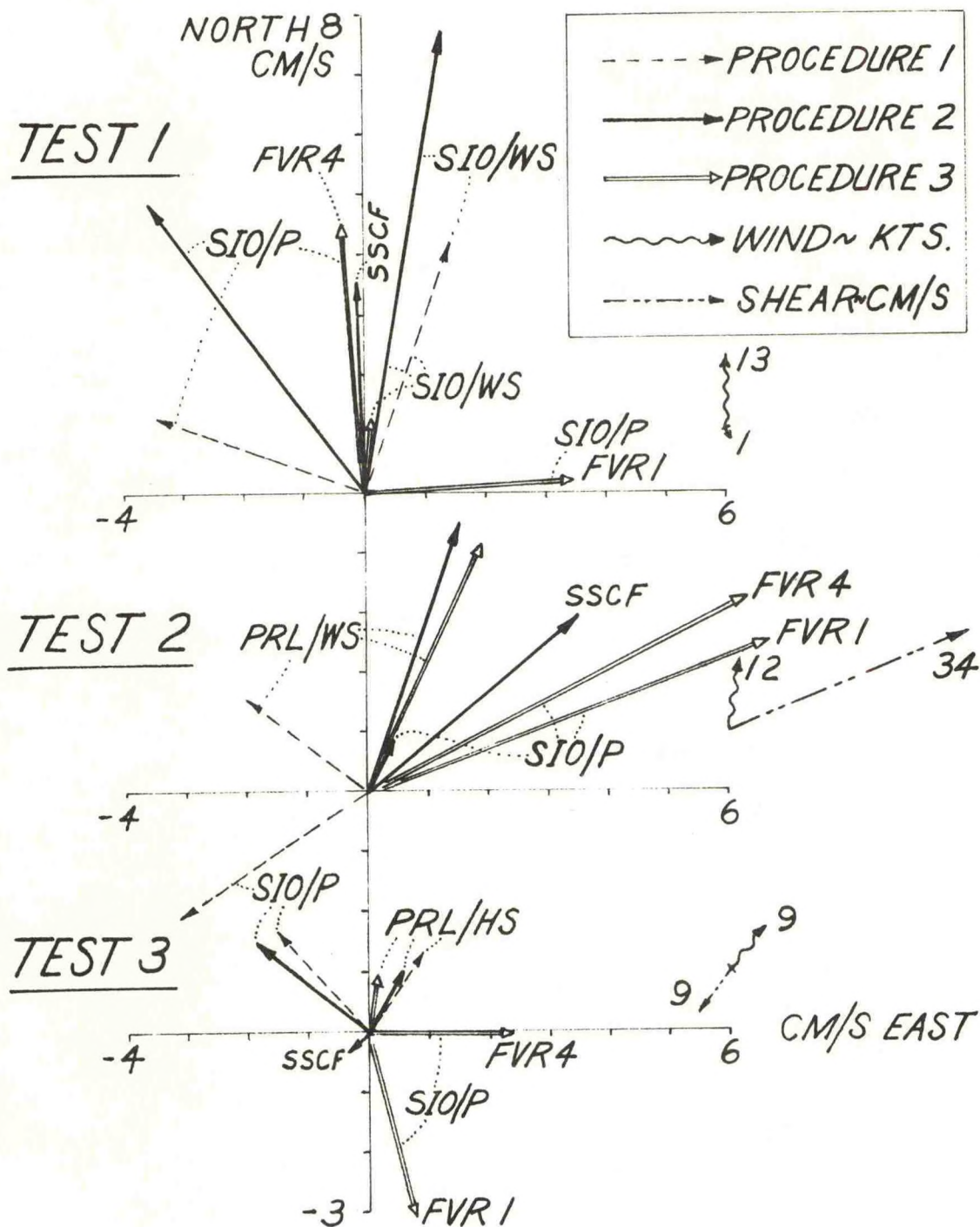


Figure 21. Slippage results.



Table I - Measured Droque Forces

Test No.	Burst No.	Hydrodynamic Force Measurements (lbs)											
		SIO Buoy/Parachute FVR#1 W = -1.4 lb			SIO Buoy/Parachute FVR#4 W = -80.2 lb*			SIO Buoy/Window Shade FVR#3 W = -81.3 lb*			PRL Buoy/Window Shade		
		$\bar{H}_e$	$\bar{H}_n$	$\bar{H}_u$	$\bar{H}_e$	$\bar{H}_n$	$\bar{H}_u$	$\bar{H}_e$	$\bar{H}_n$	$\bar{H}_u$	$\bar{H}_e$	$\bar{H}_n$	$\bar{H}_u$
1	2	-0.88	0.09	-0.33				-0.10	0.03	-38.19			
	3	-1.10	-0.06	-0.14				1.82	-1.71	-37.57			
	4	-1.95	-0.53	-0.26				-1.59	-2.02	-37.19			
2	2	-9.47	-10.07	3.86	-8.04	-8.44	-8.22	-5.52	-4.87	14.51			
	3	-12.45	-2.40	-8.02	-11.30	-5.00	-18.57	-1.89	-11.45	13.22			
	4	-17.90	-3.45	-12.32	-17.96	-5.80	-22.97	-2.65	-6.80	14.46			
3	2	2.32	0.53	-0.59	1.52	0.70	-8.52	0.71	-0.03	21.75			
	3	-0.79	0.89	-1.10	-1.04	0.01	-8.84	-0.61	-0.40	21.26			
	4	-0.63	1.27	-2.50	-1.28	-0.22	-9.69	-0.36	-1.04	21.03			
		PRL Buoy/Holey Sock**											

\*\* W = -94.7 lb\*

\* FVRs 3&4 weight = -5 lb, not zero as in Figures 1, 3, 4.



Table II Average buoy velocity components (e-east, n-north) as determined by tracking data. (cm/s)

Test No.	Burst No.	SIO Buoy/Parachute		SIO Buoy/Window Shade		SSCF Buoy/Holey Sock		SCF Buoy/Crossed Vanes	
		$\bar{V}_{Ebe}$	$\bar{V}_{Ebn}$	$\bar{V}_{Ebe}$	$\bar{V}_{Ebn}$	$\bar{V}_{Ebe}$	$\bar{V}_{Ebn}$	$\bar{V}_{Ebe}$	$\bar{V}_{Ebn}$
1	2	15.26	7.06	18.05	9.45	17.48	5.72	15.25	13.64
	3	13.42	8.35	22.86	10.76	22.02	7.08	17.84	14.86
	4	25.37	3.42	27.68	7.35	24.87	2.16	31.61	19.61
2	2	13.87	-4.44	PRL Buoy/Window Shade		15.74	0.05	31.29	18.49
	3	13.35	-2.27	13.57	5.85	15.83	-1.58	46.84	19.49
	4	13.64	-2.44	12.61	-0.91	18.56	-1.35	41.09	23.59
3	2	26.19	1.56	18.05	17.52	24.07	3.33	17.54	-2.57
	3	17.33	12.01	26.24	0.19	22.89	8.09	18.40	3.69
	4	17.03	12.48	23.40	6.69	18.05	9.05	25.42	11.84



Table III Drogue Slippage Errors (assuming that the SSCF Buoy has no slippage) - Procedure i. (cm/s)

Test No.	Burst No.	SIO Buoy/Parachute		SIO Buoy/Window Shade	
		$\bar{V}_{W_{ss} de}$	$\bar{V}_{W_{ss} dn}$	$\bar{V}_{W_{ss} de}$	$\bar{V}_{W_{ss} dn}$
1	2	-2.22	1.34	0.57	3.73
	3	-8.60	1.27	0.84	3.68
	4	0.50	1.26	2.81	5.19
	Average	-3.44	1.29	1.41	4.20
2				PRL Buoy/Window Shade	
	2	-1.87	-4.49	-2.17	5.80
	3	-2.48	-0.69	-3.22	0.67
	4	-4.92	-1.09	-0.51	-1.81
	Average	-3.09	-2.09	-1.97	1.55
3				PRL Buoy/Holey Sock	
	2	2.12	-1.77	2.17	-3.14
	3	-5.56	3.92	0.51	-1.40
	4	-1.02	3.43	0	8.47
	Average	-1.49	1.86	0.89	1.31



Table IV - Velocities of Wind (measured), SCFB (measured) and Surface Current (calculated). (cm/s)

Test No.	Burst No.	Wind Velocity		SCFB Velocity		Surface Current Velocity	
		$\bar{V}_{Eae}$	$\bar{V}_{Ean}$	$\bar{V}_{Ebe}$	$\bar{V}_{Ebn}$	$\bar{V}_{Ewe}$	$\bar{V}_{Ewn}$
1	2	0	669	15.25	13.64	15.62	-2.27
	3	-63	625	17.84	14.86	19.81	0.04
	4	71	685	31.61	19.61	30.66	3.46
2	2	91	572	31.29	18.49	34.82	20.28
	3	72	657	46.84	19.49	46.53	11.47
	4	98	557	41.09	23.59	40.37	16.87
3	2	291	307	17.54	-2.57	14.10	-6.46
	3	238	284	18.40	3.69	15.63	0.17
	4	359	428	25.42	11.84	21.22	6.60



Table V - Droque Slippage Errors and Estimate of the "True Subsurface Current" -  
Procedure 2. (cm/s)

Test No.	Burst No.	"True Subsurface Current" *		SIO Buoy/Parachute		SIO Buoy/Windowshade	
		$\bar{V}_{Ew\ e}$	$\bar{V}_{Ew\ n}$	$\bar{V}_{W\ de}$	$\bar{V}_{W\ dn}$	$\bar{V}_{W\ de}$	$\bar{V}_{W\ dn}$
1	2	17.69	2.22	-2.43	4.84	0.37	7.23
	3	22.65	3.78	-9.23	4.58	0.21	6.99
	4	24.41	-1.67	0.96	5.09	3.27	9.01
	Average	21.58	1.44	-3.57	4.84	1.28	7.74
2	2	12.94	-3.01	0.93	-1.43	0.63	8.86
	3	11.31	-4.18	2.04	1.91	1.30	3.27
	4	15.35	-4.54	-1.71	2.11	2.70	1.39
	Average	13.20	-3.91	0.42	0.86	1.54	4.51
3	2	25.37	4.53	0.82	-2.98	0.86	-4.34
	3	23.80	8.99	-6.47	3.02	-0.41	-2.30
	4	16.86	7.94	0.17	4.53	1.19	9.58
	Average	22.01	7.15	-1.83	1.52	0.55	0.98

\* Contrast with SSCFB/HS velocities tabulated in Table II.



Table VI - Drogue Slippage Calculated from Measured Forces - Procedure 3. (cm/s)

Test No.	Burst No.	Inclination from Horizon Degrees		DROGUE SLIPPAGE ERRORS cm/s							
				SIO Buoy/Parachute				SIO Buoy/Window Shade			
		FVR #1 & #2		FVR #1		FVR #4		FVR #3			
		Para-Chute*	Window-Shade	$\bar{V}_{W_{ss}de}$	$\bar{V}_{W_{ss}dn}$	$\bar{V}_{W_{ss}de}$	$\bar{V}_{W_{ss}dn}$	$\bar{V}_{W_{ss}de}$	$\bar{V}_{W_{ss}dn}$	$\bar{V}_{W_{ss}de}$	$\bar{V}_{W_{ss}dn}$
1	2	58.75	88.33	3.82	-0.39			0.52	-0.16		
	3	53.37	88.16	3.47	0.19			-1.93	1.82		
	4	38.60	87.95	3.03	0.82			1.66	2.11		
	Average			3.44	0.21			0.08	1.26		
2	2	15.29 (up)	82.08	4.10	4.36						
	3	35.44	80.45	7.26	1.40						
	4	35.54	81.73	8.72	1.68						
	Average			6.69	2.48						
3	2	34.49	88.60	-3.07	-0.70						
	3	53.75	88.85	2.43	-2.74						
	4	64.67	88.68	2.89	-5.82						
	Average			0.75	-3.09						

\* Down, except where noted



# UTILISATION OF WAVE ENERGY TO ENHANCE STATION KEEPING CAPABILITY OF FREE DRIFTING BUOYS

G DE F RETIEF

F P J MÜLLER

OCEAN ENGINEERING RESEARCH GROUP  
UNIVERSITY OF STELLENBOSCH

## ABSTRACT

Free drifting data buoys used for weather prediction purposes in the South Atlantic have been found to drift out of their deployment area fairly rapidly (approx. 800 km/month) as a result of prevailing wind and current conditions. This paper describes the model studies which were carried out on a device aimed at reducing drift rate by utilising wave power to propel the buoy against the prevailing wind, using wind direction for orientation.

The system, which is based on the principle of fishtail propulsion consists of a spring loaded foil which uses the relative motion between the buoy and surrounding water to produce a forward thrust. Reduction in drift rate using this device appears to possibly be as high as 40%.

## 1. INTRODUCTION

Free drifting satellite tracked buoys are used by the South African Weather Bureau for sensing wind, barometric pressure and sea temperature for weather prediction purposes in the South Atlantic Ocean.

Unfortunately, under the influence of the prevailing wind and current conditions, these buoys drift fairly rapidly (approximately 800 km/month) out of their deployment zone, which is the generating area of the cyclonic weather systems affecting South Africa (see Fig. 1). This study was aimed at testing the feasibility of reducing this eastward drift rate by means of a wave activated propulsion unit which would act against the wind and thereby minimise the need for costly redeployment of the buoys.

## 2. PRINCIPLE OF OPERATION

The proposed propulsion system is based on that of fish which rely on speed for their survival. As shown in Figures 2 and 3 a hydrodynamically shaped foil clamped on a standard weather buoy transverse to the direction of propulsion constitutes the "fishtail". Vertical oscillations of the foil are caused by the wave induced relative motion between the floating buoy and the surrounding water.

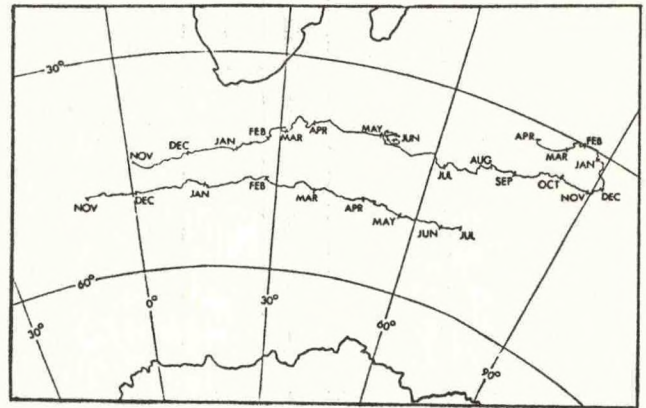


Fig. 1: Drift paths of two satellite tracked weather buoys. Positions are shown on first day of each month.

The four parameters effecting propulsion efficiency which were considered as variables in this investigation were: elasticity of the foil mounting, foil chord length, horizontal distance of foil from the buoy, depth of submergence of the foil. (The transverse span of the foil was chosen from practical considerations to be equal to the diameter of the buoy flotation chamber.)

### 2.1 Elasticity of mounting

Referring to fig. 4,  $V_r$  is the relative inflow velocity of the water with respect to the foil. If  $\alpha$  is the angle of attack, a lift force

$$L = C_L \cdot \rho / 2 \cdot V_r^2 \cdot A_F \quad \text{--- (1)}$$

and a drag force

$$D = C_D \cdot \rho / 2 \cdot V_r^2 \cdot A_F \quad \text{--- (2)}$$

are created, where

- $C_L$  = lift coefficient
- $C_D$  = drag coefficient
- $\rho$  = density of fluid
- $A_F$  = area of foil

$C_L$  and  $C_D$  are both functions of  $\alpha$ . (Ref. 1)



L and D result in the hydrodynamic force, R, with component, T, in the horizontal direction. Because T is the propelling force it should be as large as possible for a given inflow vector,  $V_r$ .

The dynamic moment,  $M_D$ , on the foil is balanced by the elastic moment,  $M_E$ , caused by the elastic mounting of the foil so that the foil will be in equilibrium when:

$$M_D = M_E$$

$$\therefore S_M \times R = C_E \times \theta$$

Where  $S_M$  is the lever arm of the dynamic moment and  $M_D$  is approximated by  $S_M \times R$ .  $C_E$  is the torsional coefficient of elasticity of the mounting. There is thus an optimum value for  $C_E$  which will allow the foil to take up a favourable angle,  $\theta$ , which will give a maximum value of T for a given  $V_r$ .

Because of the randomness of the sea and the resulting random movement of the buoy, the inflow vector,  $V_r$ , will vary in magnitude and direction in a complex manner. As it would be difficult to calculate a theoretical optimum value for  $C_E$ , an empirical approach was chosen.

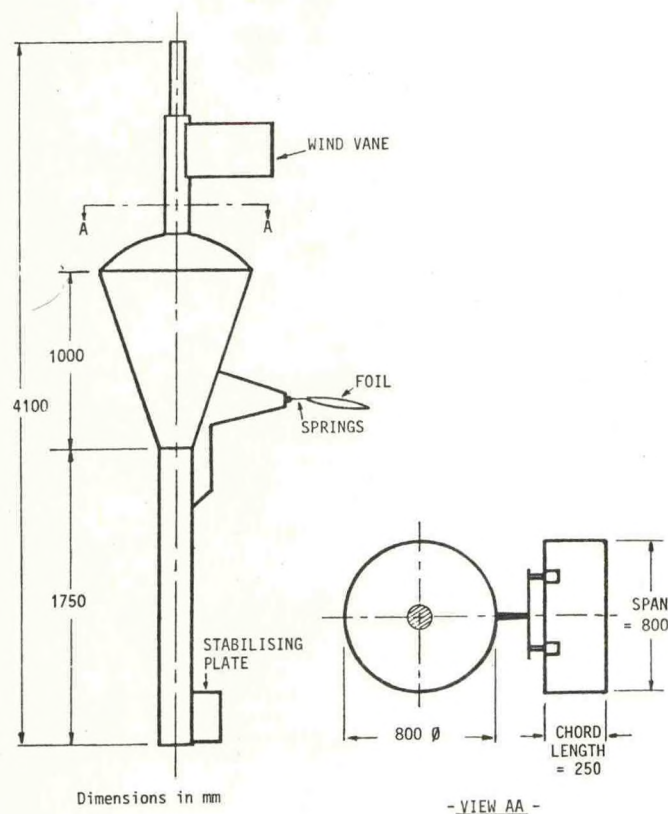


Fig. 2: Buoy configuration

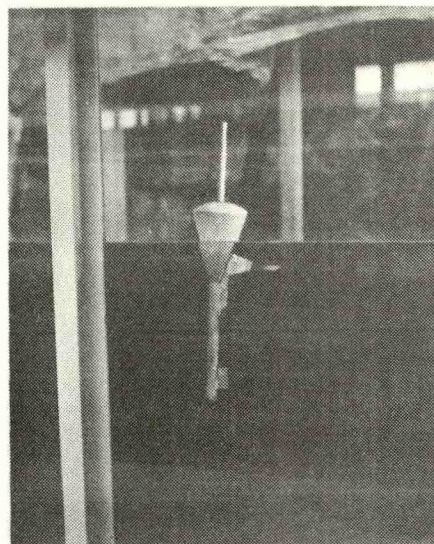


Fig. 3: Model buoy under test

## 2.2 Chord length

If the chord length,  $L_F$ , (see fig. 4) of the foil is increased, it will need a relatively larger vertical displacement of water to rotate the foil through a given angle,  $\theta$ . It will thus take longer to reach the optimum angle discussed above, or the angle may not be reached at all. On the other hand, decreasing the chord length reduces the area of the foil and hence, from eq. 1, the lift. The chord length should thus also be optimised for a given wave height.

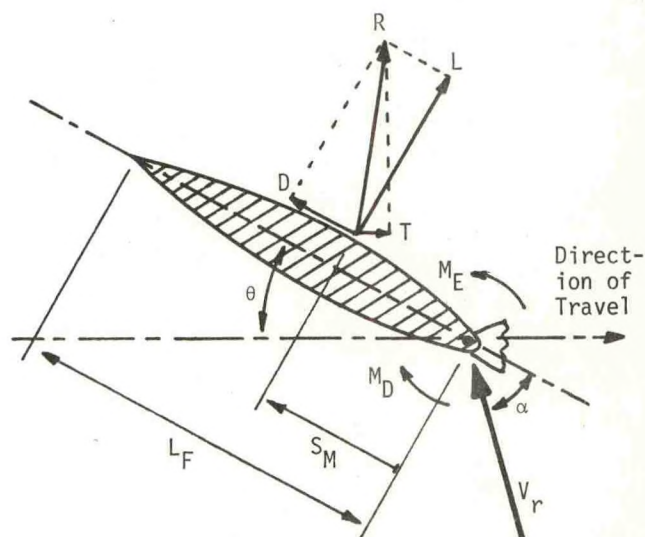


Fig. 4: Schematic vector diagram



### 2.3 Horizontal distance of foil from buoy

It can be expected that the relative vertical movement between the foil and water caused by the pitching of the buoy will increase as the horizontal lever arm is extended. There are however, structural limits to this length and a point may be reached where the buoy is displaced by the foil instead of vice versa.

### 2.4 Submerged depth of foil

The amplitude of orbital motion of water particles caused by wave action decreases exponentially with depth. As confirmed by the model tests it is thus advantageous to mount the foil as near as possible to the surface without the foil breaking surface and subjecting the mounting to impact loads.

## 3. MODEL TESTS WITH MONOCHROMATIC WAVES TO OPTIMISE FOIL PARAMETERS

To obtain the maximum possible propulsion effort from the foil, a one tenth scale Froude model of the buoy and wave propulsion device were tested under constant wave height conditions for a range of wave periods. Final tests were carried out under irregular waves as described in section 4. All tests were carried out in a 1 meter wide x 40 meters long flume (water depth 0,8 m) in the hydraulics laboratory of the University of Stellenbosch.

### 3.1 Frequency response

As can be seen from fig. 5 the buoy responded satisfactorily to wave periods between about 2,8 sec. and 5,0 sec. (prototype) with maximum propulsion at about 3,5 sec. where the pitching motion of the buoy reached a maximum. At longer periods the buoy merely followed the waterline with little or no pitching or relative movement. Shorter waves caused a heavy roll and directional instability.

### 3.2 Chord length and coefficient of elasticity

As discussed in section 2.1, the optimum coefficient of elasticity of the foil ( $C_E$ ) is determined amongst other things by the area of the foil and the magnitude of the relative inflow velocity (and thus wave height). Using a constant wave height of 0,5 meters and a foil width of 800 mm, the chord length was incremented in five steps from 150 mm to 350 mm. For each chord length a range of values for  $C_E$  between about 0,06 N.m/degree and 0,7 N.m/degree were used. Fig. 5 shows the results obtained with a chord length of 250 mm, for which  $C_E = 0,16$  N.m/degree gave the best results.

The  $C_E$ -values that gave the best results for each of the five different chord lengths are shown in Table 1. Fig. 6 shows the buoy velocity-frequency curves for each of these five cases. From these graphs it can be concluded that for a 800 mm wide foil and a wave height of 0,5 meter, a chord length of about 250 mm and a  $C_E$ -value of about 0,16 N.m/degree will provide maximum propulsion.

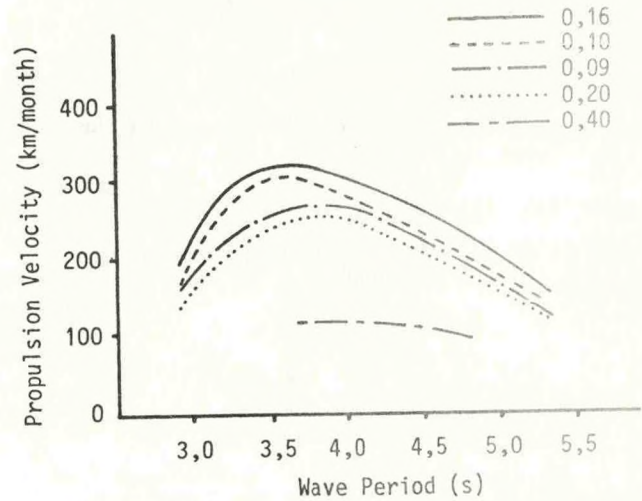


Fig. 5: Propulsion velocity vs wave period at various elasticity values (in N.m/degree) and constant chord length of 250 mm.

Chord Length (mm)	$C_E$ (N.m/degree)
150	0,06
200	0,08
250	0,16
300	0,16
350	0,24

Table 1: Optimum coefficient of elasticity ( $C_E$ ) for different chord lengths

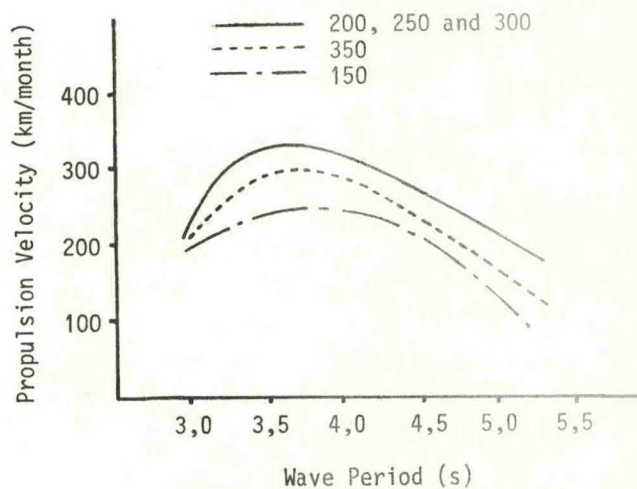


Fig. 6: Propulsion velocity vs wave period for different chord lengths (in mm) each at optimum elasticity value



## 2.2 Span of foil

Although an increase in foil span will produce an increase in propulsion velocity, as mentioned above, for structural and practical reasons the span was maintained at 800 mm.

## 3.4 Alternative configurations

Various other foil mounting configurations which were investigated included:

- a second foil to seaward of the buoy
- a split foil in order to try and utilise the buoy's rolling motion
- a vertical foil at the base of the buoy's spar
- a fixed vertical plate at the base of the spar to minimise the side roll of the buoy.

The first three alternatives did not produce any significant improvement in propulsion efficiency. In fact, the forward mounted foil completely removed the buoy's directional characteristics. The fixed plate at the base of the spar, on the other hand, made a dramatic improvement to the response of the system to shorter waves, as can be seen in Fig. 7.

## 4. TESTS WITH IRREGULAR WAVES

With the foil parameters optimised for regular waves, tests were then carried out under irregular conditions.

The energy density-frequency function of the waves in the study area were described by a Pierson-Moscowitz spectrum (Ref. 2) which peaks at a frequency of 0,1 Hz ( $T_{\text{peak}} = 10$  s).

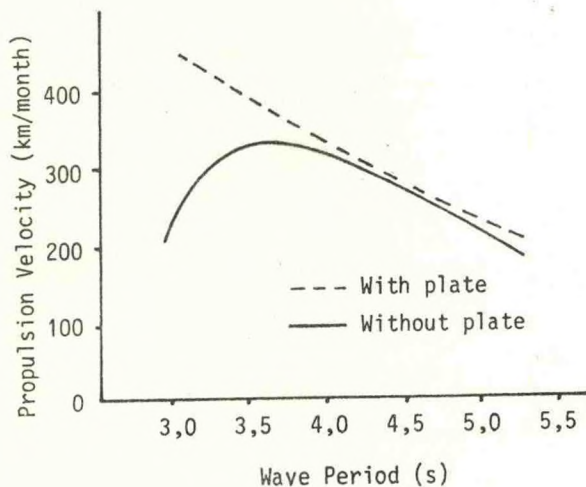


Fig. 7: Propulsion velocity vs wave period with and without damping plate for  $L_F = 250$  mm and  $C_E = 0,16$  N.m/degree

As the available irregular wave generators could not generate the full spectrum at a one tenth scale, only that portion indicated in Fig. 8 to which the propulsion system would respond was generated (i.e. from about 1,8 s to 5,0 s). To do this the total spectrum,  $S_T$ , of random waves was synthesised on a computer and the lower frequencies which were not required, were filtered out digitally in the frequency domain. The resulting partial energy density spectrum,  $S_P$ , still represented a random time function as indicated in Fig. 9.

The ratio between the significant wave height of the total spectrum,  $S_T$ , and the partial spectrum,  $S_P$ , was determined as follows:

$$H_{ST} = H_{MoT} = 4 \sqrt{\int_0^{\infty} S_T df} = 4 \sqrt{\text{Area under } S_T} \quad (\text{Ref. 3})$$

$$H_{SP} = H_{MoP} = 4 \sqrt{\int_0^{\infty} S_P df} = 4 \sqrt{\text{Area under } S_P}$$

$$\therefore \frac{H_{ST}}{H_{SP}} = \sqrt{\frac{\text{Area under } S_T}{\text{Area under } S_P}}$$

$$\approx 3,27 \text{ from Fig. 8.}$$

The significant wave height of the total spectrum is thus 3,27 times larger than that of the partial spectrum generated in the model.  $H_S$ -values tested for the truncated frequency band, ranged from 0,4 to 1,1 meters representing an  $H_S$  of between 1,3 and 3,6 meters for the full spectrum.

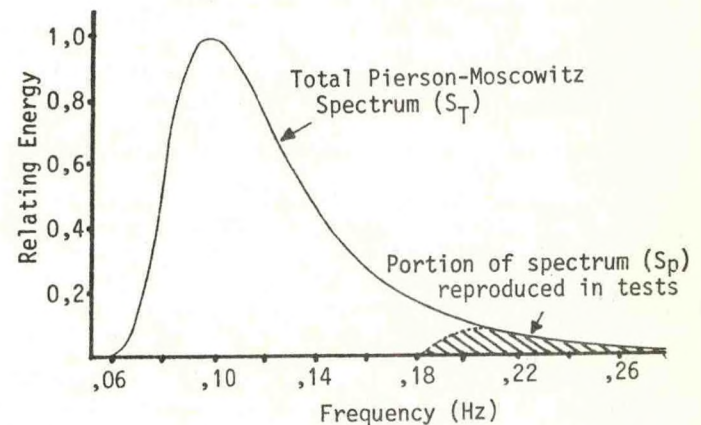


Fig. 8: Portion of Pierson-Moscowitz spectrum used for buoy tests.

Fig. 10 shows the propulsion velocity expressed in km/month plotted against the significant wave height of the total spectrum of irregular waves.  $C_E$  in this case, was 0,18 N.m/degree (prototype). Table 2 shows a typical distribution of wave heights for the study area (Ref. 4). From these results it was concluded that the buoy would on average be propelled at about 340 km/month (against the current) which would constitute a drift reduction of between 40% and 45%.



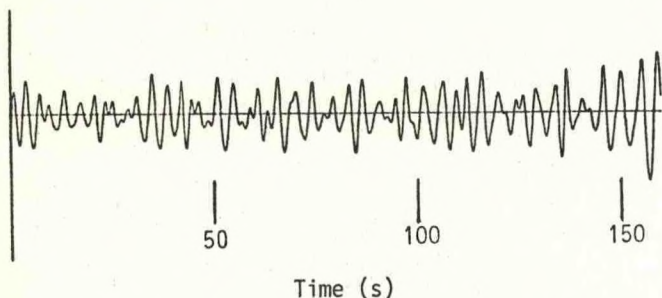


Fig. 9: Example of time domain function of partial spectrum ( $S_p$ )

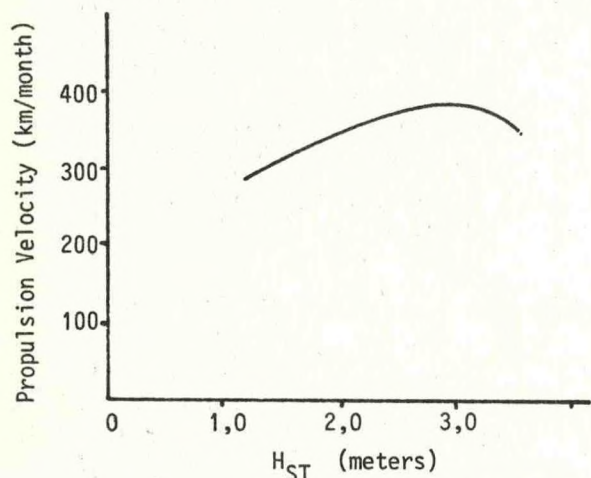


Fig. 10: Propulsion velocity vs significant wave height ( $H_{ST}$ ) of total spectrum for  $C_E = 0,18 \text{ N.m/degree}$

## 5. DISCUSSION AND CONCLUSION

The results presented above are based on a limited number of laboratory tests using a two dimensional irregular sea state. The effect of wind drag on the oscillatory motion of the buoy was not investigated and the assumption is made that a wind vane mounted at the top of the spar will successfully align the buoy into prevailing seas. The precise angle of the vane between wind direction and required propulsion direction (to accommodate Coriolis acceleration) will also probably only be found by full-scale experimentation. As the cost of fitting a trial unit to a buoy will be negligible the decision has been made to proceed with a full-scale test-run in lieu of more sophisticated and refined laboratory tests.

Although the work carried out on the proposed drift reduction system is of a preliminary nature, the results appear to be very promising. In the light of the high redeployment costs involved in maintaining a viable weather buoy array, 40% reduction in the drift rate can be considered a useful contribution to the Weather Bureau's programme. Steps are thus presently being taken to deploy a buoy fitted with a prototype propulsion unit.

Wave Height ( $H_{ST}$ )	% Occurrence
1,0 - 1,4	2,45
1,5 - 1,9	15,99
2,0 - 2,4	24,64
2,5 - 2,9	17,87
3,0 - 3,4	12,25
3,5 - 3,9	11,53
4,0 - 4,4	6,77
4,5 - 4,9	5,19
5,0 - 5,4	1,30
5,5 - 5,9	1,44
6,0 - 6,4	0,58

Table 2: Typical distribution of wave heights for study area (Ref. 4)

No attention was given in this study to improvements in hull shape and work in this direction (i.e. reduction of the buoy's drag coefficient) may well prove fruitful.

## 6. ACKNOWLEDGEMENTS

This study has been done in close co-operation with the National Research Institute for Oceanology of the South African CSIR and the Weather Bureau who supplied valuable information and assistance.

## 7. REFERENCES

- 1) Hoppe, KG. The Dynamo-elastic oscillating foil propeller, Dept. of Mechanical Engineering, University of Stellenbosch. (In print)
- 2) Ocean Wave Spectra. Proceedings of a conference sponsored by the U.S. Naval Oceanographic Office and others, Easton, Maryland, May 1-4, 1961, Prentice Hall, 1963.
- 3) U.S. Army Coastal Engineering Research Center, Shore Protection Manual, Vol. 1, 1977, U.S. Government Printing Office, Washington.
- 4) Van Schaik, C. Collection of wave data on the weather ship, South African Weather Ship, Technical Report No 1, December 1973.



# ADVANCES IN DRIFTING BUOY TECHNOLOGY UTILIZING A FLEXIBLE DESIGN APPROACH

John O. Anderson and Walter P. Brown

Polar Research Laboratory, Inc.  
123 Santa Barbara Street  
Santa Barbara, CA 93101

## ABSTRACT

The ARGOS system currently carried aboard polar orbiting satellites NOAA 6 and 7 provides a convenient means for investigators of many disciplines to collect data by telemetry from automatic stations or buoys in remote areas. Polar Research Laboratory, Inc. (PRL) has been developing and building buoys and other remote stations for this or similar satellite systems since 1975. A flexible design approach has been taken, allowing physical configuration, microprocessor programming and sensor suite to be varied readily to support the measurement requirements of a broad section of the scientific community. Development of buoys and supporting equipment is carried on as a continuing process because of the number of needs to be met. This paper provides examples of the flexible design philosophy in action, describing a variety of systems recently completed or still under development.

## INTRODUCTION

Polar Research Laboratory has been developing and building data collection buoys and platforms using satellite telemetry since 1975. Early systems used the Random Access Measurement System (RAMS) aboard the NIMBUS 6 polar orbiting satellite. In 1978, the telemetry systems were redesigned to work with the ARGOS system aboard the TIROS and NOAA series polar orbiting satellites. The first buoys developed were deployed on the Arctic ice cap prior to the launch of NIMBUS 6 and successfully measured barometric pressure and underice ambient noise for more than a year. A large number of stations have been built since that time, encompassing open ocean buoys, buoys for operating in ice covered seas and land or shipboard stations. The general design philosophy has been to provide flexibility of deployment techniques, maximum use of satellite link data capacity by use of on-board processing and flexibility of station and sensor suite configuration to support measurement requirements of a broad section of the scientific community.

The paper provides examples of the design philosophy in action, highlighting some of the

more unusual recent developments. These include the following:

### SUBSURFACE TEMPERATURE MEASUREMENT BUOY

The drifting buoy provides a relatively inexpensive means for gathering ocean related environmental data. A drifter family has been developed that carries meteorological and/or subsurface sensors. The most recent addition to this sensor family is a drifter compatible thermistor string with interface electronics to couple it to the standard in-buoy microprocessor. The parachute deployable version of this system is shown in Figure 1. The early development on this string was carried out by PRL under contract to the NOAA Data Buoy Office (NDBO) and tested in NDBO, NCAR and ONR (Arctic) programs.

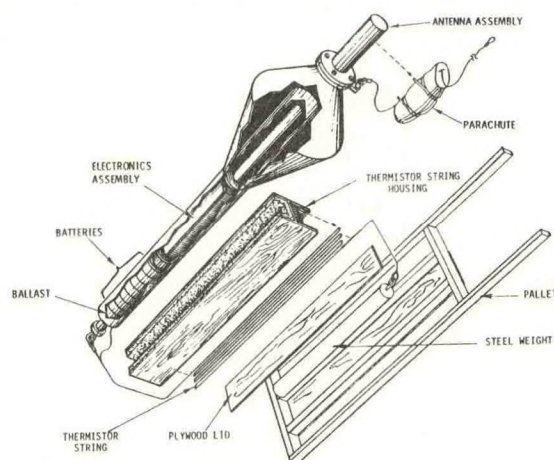


Fig. 1 Drifting Buoy With Thermistor String  
Packaged For Air Drop

No problems were experienced in the ice suspended strings used in the Arctic, but severe failures were encountered both in a group of six buoys deployed in the winter North Pacific as part of the STREX program and three buoys air deployed in the Gulf of Mexico. Five of the six STREX buoys were recovered after about eight months by NCAR/NDBO, allowing a detailed failure analysis to be made. A major problem with these strings was that a "hair fairing" had been included to increase the transverse drag of the string and



more closely couple it to horizontal currents. An unforeseen side effect, which is obvious in retrospect, is that the longitudinal drag is also increased. In high seas, the string must traverse vertically through the water column a considerable distance as the buoy rises and falls. The added fairing drag reduces the free fall rate of the string, tending to cause the string to slacken. The slack string is then subjected to sharp bends in the rotating currents generated by the waves and also led to high shock loads as the string snaps taut. Elimination of the slack problem and overall improvement of the design eliminated the failure problems in the next group of strings built which were again deployed for the North Pacific storm season.

Strings with 3 pressure (depth) sensors and 12 thermistors or up to 18 thermistors with no pressure sensors, can be accommodated by the existing design. The microprocessor offers a great deal of flexibility in data handling. In addition to providing instantaneous samples, other information can be included in the data format such as average readings and variance over selectable time periods, sampling at synoptic times, temporary storage of data on board, etc.

#### MET ADAP

The ARGOS Data Acquisition Platform (ADAP) is a portable self-contained data system designed for remote areas. It can handle a keypad input and/or up to 32 sensors and transmit the data via the satellite link. If multiple sensors are used in addition to the keypad, message length is usually more than 256 bits so that more than one transmission is required to relay the complete message. Keypad data is displayed in decimal form in four liquid crystal display windows (one eight bit data word per window) and up to 32 words of keypad entered data can be reviewed and edited under keypad control prior to transmitting the data. This configuration has proven to be useful in many applications that require manually entered data transmission and position from ships or remote sites.

Recently a special configuration has been developed for the use of shipboard meteorologists. This configuration allows entry of a four digit identifier code plus 12 groups of data with five digits each matching the standard World Meteorological Organization (WMO) format. The transmitted data is formatted so that System ARGOS can transfer it directly to the Global Telemetry System (GTS) for world wide dissemination. The liquid crystal display on this unit permits simultaneous viewing of all five digits in a group and allows scanning and editing of the entire message prior to transmitting it. A search and rescue message that can be triggered with a simple code can also be included. This unit is packaged in a briefcase for easy transportation.

#### AIR DROP WEATHER STATION

The ARGOS system provides a convenient means for gathering remote area meteorological data,

particularly in the high latitudes. PRL has applied the ARGOS PTT to a variety of weather stations tailored to meet specific needs for both land and on-ice applications.

A system currently being developed under NSF/ONR/PRL funding, initially for Antarctic use, is designed to be parachute dropped either from side door or rear door aircraft. It folds into a compact five foot long by two foot diameter package weighing about 225 pounds, including sensors, electronics and batteries. The system will drop with a terminal vertical velocity of about 20 ft/sec and will be decelerated on impact by an energy absorber. It falls over on ground contact because of the horizontal component of motion which is equal to surface wind speed. The system then erects itself using electric motor driven ball screws to operate the legs. The leg positions are controlled by a micro processor based system that uses two orthogonal single degree of freedom pendulums as vertical references. After erection, the instrument mast is automatically raised to the three meter level. A "brass board" version of the system has been built to test the various mechanisms used and this performs very well. The next phase in the development is the cleanup and simplification of the design of the various structural elements prior to air drop testing.

#### LOW COST MINI DRIFTER

Some applications do not require a full size buoy for simple drifter applications. A relatively low cost mini-drifter (Figure 2) was developed that can be ship deployed or paraded from side or rear door aircraft. The drifter weighs 72 to 100 pounds with length ranging from 53 to 71 inches depending on whether a 6 month or 12 month battery pack is selected. The buoy's small wind drag profile reduces the required drogue size, and the present version carries a 2-1/2 foot by 12 foot long window shade drogue.

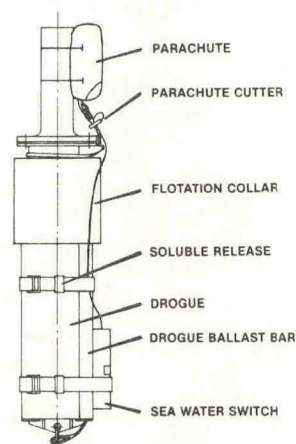


Fig. 2 Low Cost Mini Drifter



ARGOS LOCAL USER TERMINAL (LUT)

\_\_\_\_\_

The NOAA 6 and 7 satellites contain VHF beacon

To provide as complete an ARGOS system support

A block diagram of the LUT is shown in



INDEX

In an attempt to improve this situation, a

It is provided with an RS232 printer port so

POLAR BEAR TRACKER

1990-1991

An isometric drawing of the Polar Bear Tracker



tracker are 5.25 inches wide by 9 inches long by 6.1 inches deep. The depth includes a bracket that was needed to fit the Polar Bear Collar. The actual depth could be as little as 4 inches. With a suitable lithium battery pack, the Polar Bear Tracker could be adapted as a self-contained external position marker for moored buoys on other vehicles.

#### AMBIENT NOISE BUOY

In another application of the micro processor based electronics, a micropower, automatic data collection system was developed for obtaining synoptic acoustic ambient noise data in ice-covered seas for periods exceeding one year. The system samples and averages noise data in eleven selectable one third octave bands. The electronics are based in a tube inserted in a hole in the ice. Synoptic data samples are stored in a 24-hour memory under microprocessor control and relayed by once per minute burst transmissions to the ARGOS system. Buoy positions are determined to within a circular probability error (50%) of a few hundred meters by doppler measurements made on the transmitted signal using specially selected oscillators to control the transmitted frequency. Twenty-eight SYNoptic ARGOS (SYNARGOS) ambient noise measurement buoys have been used successfully in the Arctic. Development of the SYNARGOS System was sponsored by ONR (Code 425 ARCTIC).

Experiments were begun recently to determine whether the SYNARGOS concept could be used with free drifting buoys in open water. The difficulty in this approach is that hydrophones suspended from a surface float have to be nearly totally isolated from wave induced vertical motions because these motions produce tremendous pressure variations (relative to acoustic signals) which contaminate low frequency measurements. Two buoys were built using a small, near neutrally buoyant auxillary float tethered to the standard hull by a line supported by net floats. This float ducked under the waves and isolated the hydrophone somewhat from the wave motion, but significant contamination was still present at the lower frequencies. The next step will be to eliminate the auxillary float altogether and replace it with buoyancy distributed over a significant length of the tether line. This effectively acts as a long spar buoy and had been used successfully in early Navy experiments in which a fire hose was filled with positively buoyant fluid to form the distributed buoyancy. Other more recent large systems have been built using this approach and it appears that it can be scaled to drifting buoys. Some of the sonobuoy techniques that are compatible with the longer life required by the drifting buoy system can be used to further enhance performance.

#### PTT ELECTRONICS

The ARGOS Platform Transmit Terminal (PTT) used in the buoys is fabricated in a modular form to allow the maximum flexibility in user requirements. A block diagram of the electronics

is shown in Figure 5 and the physical description of the modules is shown in Figure 6.

A minimum configuration consists of four modules: the transmitter, oscillator, digital encoder and regulator timer. The minimum configuration is suitable for position only and serial digital requirements. An interface for a barometer and two temperature sensors (FGGE) or 8 to 32 analog input channels can be supplied by a single additional sensor interface box. Signal conditioning for nonstandard sensors can be handled by additional signal conditioning modules (not shown). A typical example of a signal conditioning module that is available would be a module capable of linearizing 10 non-linear thermistors and conditioning 3 bridge type pressure sensors. This module is contained in the same size box as the sensor interface.

The modules can be supplied with various length harnesses to allow the modules to be placed in the most convenient locations in a buoy.

The digital encoder is microprocessor based and thus allows a variety of data collection problems to be handled.

Typical data collection scenarios that can be accommodated are as follows:

1. Synoptic sampling at one or three hour intervals with 24 hour storage.
2. Averaging of data over minutes, hours or days with storage of many sample periods.
3. Statistical or variance calculations on the data before transmission.
4. Multiple transmitted repetition rates and ID's to allow ARGOS data processing cost savings. As an example, once each seven days a repetition period of 40 to 60 seconds would be used with one ID for location. The other 6 days, a repetition period of 180 to 200 seconds would be used with a second ID for data collection only.
5. Adaptive processing of data on board the buoy depending on measured parameters.

A third generation PTT is now in the design process which will incorporate the minimum configuration in one module slightly larger than the transmitter. This design should result in a lower cost smaller unit for position only and serial digital applications, but will lose some of the flexibility of the larger system.



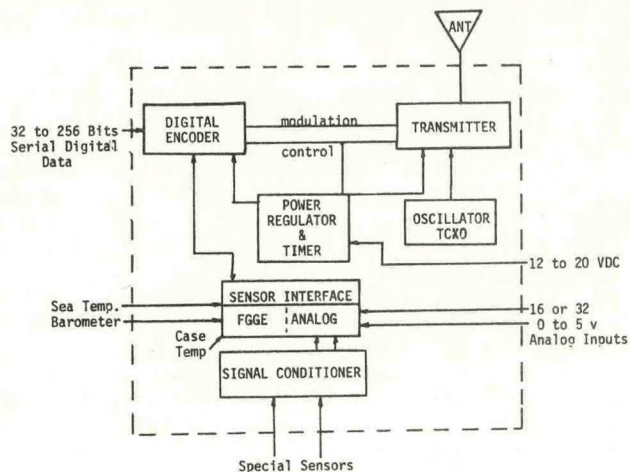


Fig. 5 Platform Transmit Terminal (PTT) Block Diagram

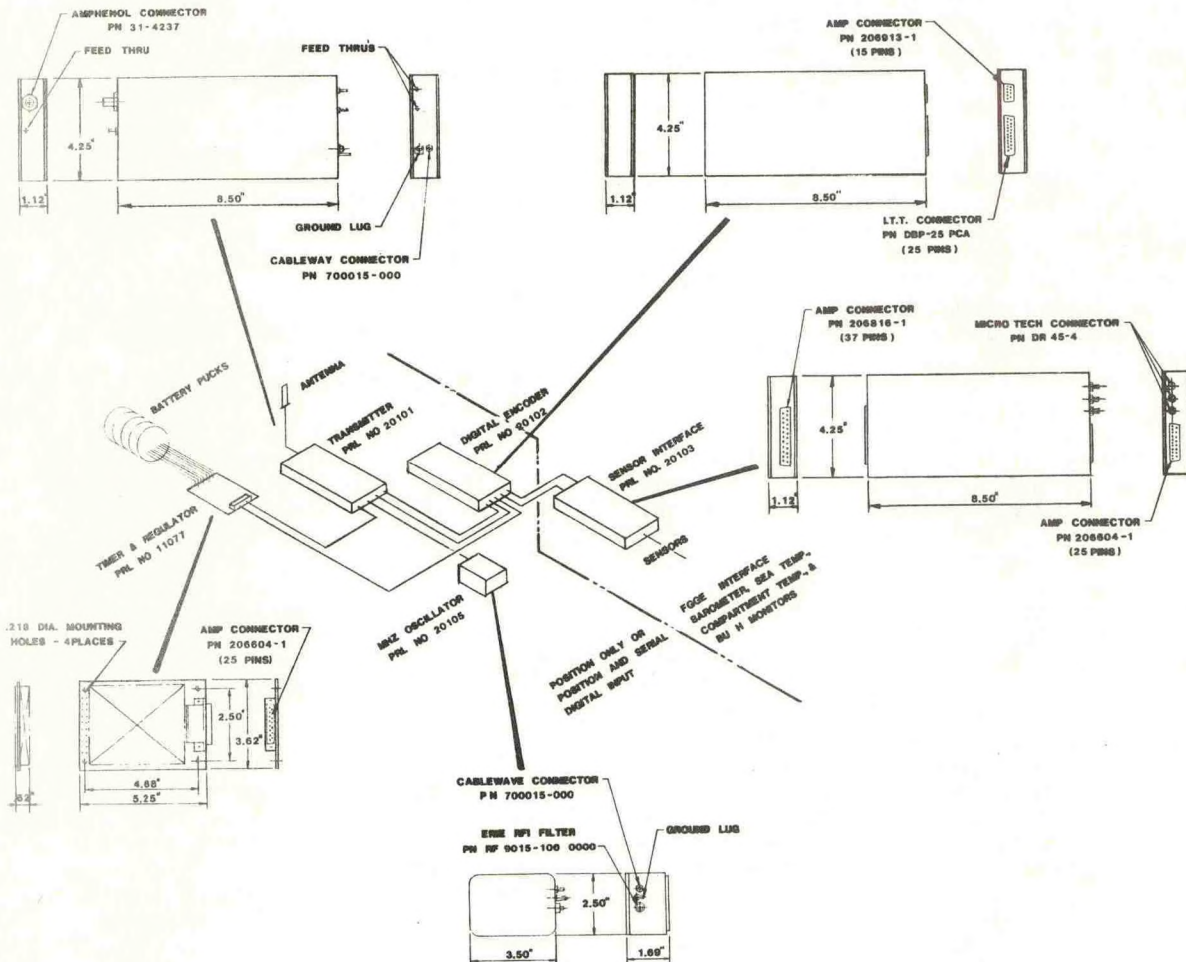


Fig. 6 PTT Physical Configuration



## ACKNOWLEDGEMENTS

We are indebted to Mobil North Sea for logistic support on and around the Beryl Alpha production platform. The work is supported by the Natural Environment Research Council and the Department of Energy and is published with the approval of the Director of the Institute of Geological Sciences (NERC).

## REFERENCES

- Avedik, F. and Renard, V., 1973. Seismic refraction on Continental shelves with detectors on sea floor, *Geophys. Prospecting*, 21, pp. 220-228.
- Browitt, C.W.A., 1979. Seismograph networks of the Institute of Geological Sciences, UK, *Phys. Earth and Planet. Interiors*, 18, pp. 127-134.
- Cranford, M.D., Johnson, S.H., Bowers, J.E., McAlister, R.A. and Brown, B.T., 1976. A direct-recording ocean-bottom seismograph, *Bull. seism. Soc. Am.*, 66, pp. 607-615.
- Francis, T.J.G., Porter, I.T., Lane, R.D., Osborne, P.J., Pooley, J.E. and Tomkins, P.K., 1975. Ocean bottom seismograph, *Marine Geophys. Res.*, 1, pp. 195-213.
- Higley, P.D. and Joyal, A.B., 1978. New mooring design for a telemetering off-shore oceanographic buoy, *Oceans '78*, Washington DC, Marine Tech. Soc., pp. 10-17.
- Houliston, D.J., 1978. A frequency multiplexing transmission system, *Inst. Geol. Sci.*, GSU Report No. 95.
- Myatt, J., Penn, A.W. and Poole, M.J., 1971. Isotope powered thermoelectric generators, Fourth United Nations International Conference on the Peaceful Uses of Atomic Energy, Geneva, 1971, A/CONF. 49/P/487, pp. 1-7.
- Rusby, J.S.M., Hunter, C.A., Kelley, R.F., Wall, J. and Butcher, J., 1978. The construction and offshore testing of the UK Data Buoy (DB1 Project), *Oceanology International*, 1978, pp. 64-80.
- Sinha, M.C., 1978. Stresses and deformations in cylindrical pressure vessels, Department of Geodesy and Geophysics Univ. Cambridge Report, pp. 1-15.
- Smith, W.A. and Christie, P.A.F., 1977. A Pull-Up Shallow Water Seismometer, *Marine Geophys. Res.*, 3, pp. 235-250.
- Sutton, G.H., Kasahara, J., Ichinose, W.N. and Byrne, D.A., 1977. Ocean bottom seismograph development at Hawaii Institute of Geophysics, *Marine Geophys. Res.*, 3, pp. 153-177.
- Turbitt, T., Browitt, C.W.A., Morgan, S.N., Newmark, R. and Petrie, D.L., 1983. Instrumentation for North Sea seismic data acquisition. In: A.R. Ritsema and A. Gurbinar (eds.), *Seismicity and Seismic Risk in the Offshore North Sea Area*, pp. 155-157.



All buoys basically drifted east turning south between 130 and 140°W. Also included in Fig. 6 are the more recent tracks of two subsequent AES buoy deployments in June and Sept. of 1982.

This pattern of eastward, then southward, flow was not unexpected for the AES buoys, but was a complete surprise for the southern two PRL buoys. In strong contrast buoys deployed earlier just south of and near the same longitude as the present deployment, all turned north into the Gulf of Alaska some becoming trapped in the Alaskan Gyre (Fig. 7). Other buoys deployed in the Alaskan Gyre tended to make at least one transit of the gyre. Previous buoy tracks that had reached the southerly latitudes, attained by the PRL buoys, (Fig. 8) had all started out substantially to the south of 40°N. Thus the set of drifter tracks from 1981-1982 appears to contradict earlier lagrangian results.

A closer look at the two southernmost PRL buoy tracks reveals that they are extremely well correlated both in overall trend and in detail. In addition a third buoy (3852), which was deployed at 53.5°N turned south and east after moving west, to retrace many of the features exhibited by the southernmost PRL buoys. Late in 1982 all three of these buoys turned north and moved quite rapidly. Unfortunately, buoy 3851 stopped transmitting after a couple of weeks of northward flow. Its partner 3850 continued northward along the west coasts of California, Oregon, and Washington and was recovered just off the west coast of Vancouver Island. During this coastal transit the buoy reached speeds of 100 cm/s.

Buoy 3852 turned north into the Gulf of Alaska and moved rapidly along the west coast of Alaska at speeds up to 150 cms-1. Late in March, 1983, the buoy ran aground on Kodiak Island (Fig. 6) before it could complete a cyclonic loop. It is interesting how buoy 3852 appears to follow the track of 3850 between 145 and 160°W, even though it crosses 160°W six months later. East of 145°W buoy 3852 appears to shift northward, making an anticyclonic loop just west of the Queen Charlotte Islands on its way in toward the coast. Close to the coast it moved rapidly (> 100 cm/s) parallel to the continental shelf break slowing down at around 148°W before going aground on Kodiak Island.

#### Statistical Comparisons

In order to evaluate the degree to which the tracks of buoys 3850 and 3851 were correlated an average latitude and longitude, for each buoy's track, was subtracted from the individual positions. The longitude difference, plotted as a function of time (day from deployment) in Fig. 9, shows the detailed similarity between the positions of these buoys. Also included in Fig. 9 is a similar longitude difference for buoy 3852 starting from the time when it crossed 160°N. A difference in average longitude for buoy 3852 results in an offset of this track from the other two but it is surprising how many of the smaller features are traced out by the track of buoy 3852

travelling through the area 6-7 months later. The first day of each month is indicated at the top of Fig. 9 for buoys 3850 and 3851 while the numbers at the bottom correspond to the start of each month for 3852.

The similarities between all three tracks is emphasized if the average longitude is calculated only for the region where the tracks overlap. The resulting longitude differences (Fig. 10) clearly demonstrate the close correspondence between these three buoy tracks. Although not shown here similar calculations, using latitude, yield the same results. These comparisons suggest that two buoys deployed at the same time but 200km apart (north-south) appeared coupled in space as they drifted east over a period of 12 months. In addition a third buoy, travelling the same region 6 months later, traced out many of the features indicated by the tracks of the earlier buoys.

To better quantify this relationship cross-correlations were computed, using a 30-day moving sample, between the positions of each of the three buoys. For longitude (Fig. 11a) the correlations between buoys 3850 and 3851 were generally near 1.0 over more than 80% of the record. Major departures occur in Oct. 1981, April 1982 and June-July of 1982. After Oct. 1982, when the buoys start to turn north, the correlation drops to become and remain negative.

Buoy 3852 is correlated with buoy 3850 in Fig. 11b and the correspondence in longitude is much lower than in Fig. 11a. There are, however, significant periods where the correlation is indeed near 1.0. Similar periods of high correlation can be seen in the values for buoys 3851 and 3852 plotted in Fig. 11c. Many, but not all, positive peaks in the former series correspond to high plus values in the latter. Examples are the peaks at 50, 90, 120, 190, and 300 dys. Counter examples can be found at 75, 105, and 135 days where the two series are apparently out-of-phase. Most of the high correlations in Figs. 11b, c occur over intervals of high correlation in Fig. 11a. (The change in scale should be noted).

Similar results were found for latitude (Figs. 12 a-c) with buoys 3850 and 3851 being highly correlated over most of the record. There is some correspondence between Figs. 11a and 12a suggesting that deviations in both latitude and longitude occurred simultaneously. Some events of lower correlation do not occur at the same time. Turning to Figs. 12b and c it appears that correlations between buoys 3850 and 3852 are similar for latitude and longitude, while correlations for latitude and longitude are often out-of-phase for correlations between buoys 3850 and 3851.

All of these comparisons suggest that the driving mechanisms, providing the buoy displacements, were relatively coherent over a space of at least 200 km and a period of 6 to 12 months. Thus the important question then is what are the buoys responding to; what are the forcing mechanisms responsible for this unusual oceanic behaviour?



### Geostrophic Flow

Due to the early pattern similarity between geostrophic currents, mapped by the CTD survey, and the buoy tracks, along with the agreement between geostrophic and buoy speeds, it was suggested that the buoy drifts indicate the baroclinic flow. Unfortunately monthly CTD surveys are not available to map the geostrophic flow in the eastern North Pacific. Instead an effort was made to produce maps of upper-level geostrophic flow from all available expendable bathy thermograph (XBT) data from an individual month. Using ship XBT data reported by radio message, 0/200 db dynamic topography was computed by inferring salinity from the climatological curves reported by Emery and Dewar (1982). The map for November 1981 is presented in Fig. 13 along with the corresponding buoy tracks for that month.

It should first be noted that the general pattern is similar to, and consistent with the climatological 0/200 db dynamic topography for November. The flow is slightly weaker than normal but the primary trend at 45°N is northeastward into the Gulf of Alaska. By comparison the buoy tracks trend eastward across the lines of dynamic topography. A similar lack of agreement can be seen in the map for May 1982 (Fig. 14). During this time the buoys were turning south between 45 and 50°N while the geostrophic flow should have taken them northward up into the Gulf of Alaska. Again the May 1982 map is representative of the climatological 0/200 db geostrophic flow. While it may be said that the November 1981 map was based on relatively few XBT measurements the May 1982 data coverage was more than adequate.

Comparisons between other months reveal the same results. The buoy tracks, in general, do not follow the pattern of 0/200 db geostrophic flow. This is in contrast to the results of McNally et al. (1983) who found overall agreement between their buoy tracks and climatological maps of dynamic topography.

### Atmospheric Pressure

McNally et al. (1983) also found a good correspondence between the tracks of drogued drifting buoys and climatological maps of mean monthly atmospheric pressure. The atmospheric pressure map for November 1981 is shown in Fig. 15 along with the corresponding buoy tracks. The agreement is striking between the isobaric contours and the general trends of the buoy trajectories. Once again the coherence between buoys 3850 and 3851 is apparent. The correspondence between buoy tracks and monthly mean atmospheric pressure continued throughout the period of drifter life. Another graphic example is in May 1982 (Fig. 16) when the buoys turned south in response to the atmospheric pressure pattern. It should be noted that a southward turn, north of 45°N was very anomalous.

A correspondence between buoy tracks and atmospheric pressure was characteristic not only of

these recent tracks but also of the earlier drifter data. For example Fig. 17 shows the monthly mean atmospheric pressure for January 1977 with a corresponding set of drifter tracks superimposed. Once again the tracks follow the contours, in this case turning sharply north up into the Gulf of Alaska. Note the relatively stronger atmospheric pressure gradients as compared to the November 1981 and May 1982 maps.

A dramatic difference in both isobaric patterns and pressure gradients can be seen between this January map from 1977 (Fig. 17) and a similar map for January 1982 (Fig. 18). In 1982 the isobars shift from running north into the Gulf to a somewhat weaker pattern tending eastward around a small low pressure cell. Once again the buoy tracks follow along the isobaric contours.

Plotting all of the available buoy tracks for January on a map of the climatological mean January atmospheric pressure (Fig. 19) emphasizes the year-to-year differences. Each track is marked with the appropriate year. As the climatological pattern is similar to the pattern in 1977 the 1977-78 tracks appear to parallel the contours. In strong contrast most of the 1982-83 buoy tracks cross the isobars as they transit eastward. The 1983 tracks of the three easternmost buoys, that turned north, also appear to follow the isobars suggesting that the circulation had once again returned to the climatological norm.

The buoy tracks and pressure maps, presented above, reveal the anomalous character of both from the fall of 1981 through the fall of 1982. It should be noted that these unusual patterns occurred just prior to the onset of equatorial warming now being considered a major El Niño event much like that which occurred in 1957. The rapid northward buoy motions along the west coast and in the Gulf of Alaska, which took place in early 1983, are consistent with the increase in coastal sea-level (Sus Tabata, pers. comm.) and associated stronger alongshore northward flow. The extremely high buoy velocities ( $\sim 100$  cm/s), during this period, suggest the anomalous character of this northward current.

It is interesting to note the overall lack of agreement between the buoy tracks and the mean monthly 0/200 db dynamic topography maps. Perhaps the reason why McNally et al. (1983) found rather general agreement between buoy tracks, and dynamic topography, was that the atmospheric pressure pattern, during the period of their observations (1977) was similar to the climatological pressure pattern which parallels the pattern of mean dynamic topography. In sharp contrast the atmospheric pressure patterns, during our measurement period (1982), were anomalous and crossed, rather than followed, contours of both climatological and mean monthly dynamic topography.

Thus in agreement with McNally et al. (1983) the strongest correspondence is found between buoy motion and the distribution of atmospheric pressure. There may be many physical mechanisms



linking these two such as the upper layer Ekman current or the effect of wave induced Stokes drift. It should be remembered that the surface wind does not parallel the isobars but rather flows some 20-40° to the left of the contours (Northern Hemisphere). The oceanic upper layer Ekman response would produce a current to the right of the wind bringing the flow back in line with the isobars. In addition, the Stokes drift would be in line with the wave propagation travelling before and parallel to the wind.

Under this interpretation it is curious to note the surprisingly coherent behaviour between buoys 3850, 3851, and 3852. The similarities between the tracks of 3850 and 3851 suggest a 200 km north-south coherence in the atmospheric pressure and its effect on buoy displacements. The persistence of this relationship is suggested by buoy 3852 transiting the region 6 months later and repeating some of the earlier behaviour of buoys 3850 and 3851.

Perhaps the best explanation of these events is that in comparison to previous years the wind driven upper ocean flow, in the region, was relatively weak and therefore coherent in space and time. In other words, relatively small changes in weak gradients of atmospheric pressure could possibly have led to the observed coherent variations in the buoy tracks. Under more vigorous atmospheric conditions fluctuations are spatially less coherent as evidenced by the buoy tracks from January, 1977 (Fig. 17).

The 6 month permanence of the anomalous flow conditions, suggested by the repeat track of buoy 3852, relates to the long duration of this anomalous event. As was true for the 1957 warming (Tully et al. 1960) abnormal conditions persisted for a long duration allowing weak, but quasi-stationary, circulation patterns to continue for some time. In this more recent event both the atmospheric pressure, and the buoy tracks were anomalous for over a year. The return to stronger-than-normal atmospheric flow was signalled by the turn of the buoy tracks to the north coupled with higher than normal velocities.

#### Acknowledgements

We would like to thank Dolly Dieter, relief captain Bill King and the crew of the R/V Alpha Helix for their assistance in carrying out the August 1981 field work. The atmospheric pressure data were acquired from the Fleet Numerical Ocean Center in Monterey, California. We also want to thank the Canadian Atmospheric Environment Service for providing us with their buoy data. The efforts of G. McNally and other investigators in sending their buoy tracks is gratefully acknowledged. Pat Lust and Paul Nowlan carried out the many calculations and produced the plots. This research was supported by the U.S. National Science Foundation under its grant #OCE-8018386 to the Institute of Marine Science, University of Alaska.

#### References

- Dodimead, A.J., F. Favorite and T. Hirano, 1963: Review of Oceanography of the Subarctic Pacific Region, International North Pacific Fisheries Commission, Bulletin No. 13, 195 pp.
- Emery, W.J. and J.S. Dewar, 1982: Mean temperature-salinity, salinity-depth and temperature-depth curves for the North Atlantic and the North Pacific. *Prog. Oceanog.*, 11, pp. 219-305.
- Favorite, F., 1967: The Alaskan Stream, *Bull. 21, Int. North Pac. Fish. Comm.*, 20 pp.
- McNally, G.J., W.C. Patzert, A.D. Kirwan, Jr., A.C. Vastano, 1983: The near-surface circulation of the North Pacific using satellite tracked drifting buoys. (Sub. to *J. Geophys. Res.*)
- Tully, J.P., A.J. Dodimead and S. Tabata, 1960: An anomalous increase of temperature in the ocean off the Pacific Coast of Canada through 1957 and 1958. *J. Fish. Res. Bd. Canada*, 17, 61-80.

#### List of Figures

1. Schematic diagram of the circulation in the Subarctic North Pacific. Numbers indicate volume transport ( $m^3/sec \times 10^6$ ) referred to 1000m. (From Favorite, 1967)
2. Schematic diagram of surface circulation relative to 1000db. (From Dodimead et al., 1963)
3. Cruise track for August 1981. Dots are CTD stations while circles indicate drogued buoy deployments.
4. Dynamic topography 0/1000db from the CTD stations in Fig. 3 along with the first two months of positions from the drogued buoys (dashed lines).
5. Salinity at 100m from the CTD stations in Fig. 3.
6. Tracks of all drifting buoys deployed after August 1981. Northernmost five are PRL buoys deployed as shown in Fig. 3. For these five dots indicate daily positions.
7. Tracks of all drifting buoys, deployed before August 1981, that travelled north of 52°N.
8. Tracks of all drifting buoys, deployed before August 1981, that travelled south of 45°N.
9. Longitude difference for buoys 3850, 3851, and 3852. Monthly time marks are given at the top for 3850, 3851 and at the bottom for 3852.
10. As in Fig. 9 except using mean longitudes for the overlap period only.
11. a. 30 day sample cross correlations between longitudes for buoys 3850 and 3851.



- b. 30 day sample cross correlations between longitudes for buoys 3850 and 3852.
  - c. 30 day sample cross correlations between longitudes for buoys 3851 and 3852.
- 12. a-c. As in Fig. 11 a-c except for latitude.
  - 13. Mean monthly 0/200 db dynamic topography inferred from TS/SZ curves for November 1981; superimposed are the Nov. 1981 tracks of drifting buoys.
  - 14. As in Fig. 13 for May 1982.
  - 15. Mean monthly sea level atmospheric pressure (mb) for November 1981 along with the corresponding tracks of drifting buoys.
  - 16. As in Fig. 15 except for May 1982.
  - 17. As in Fig. 15 except for January 1977.
  - 18. As in Fig. 15 except for January 1982.
  - 19. Mean monthly sea level, atmospheric pressure (mb) climatology for January along with appropriate drifting tracks for all years. Each track is labelled by year.



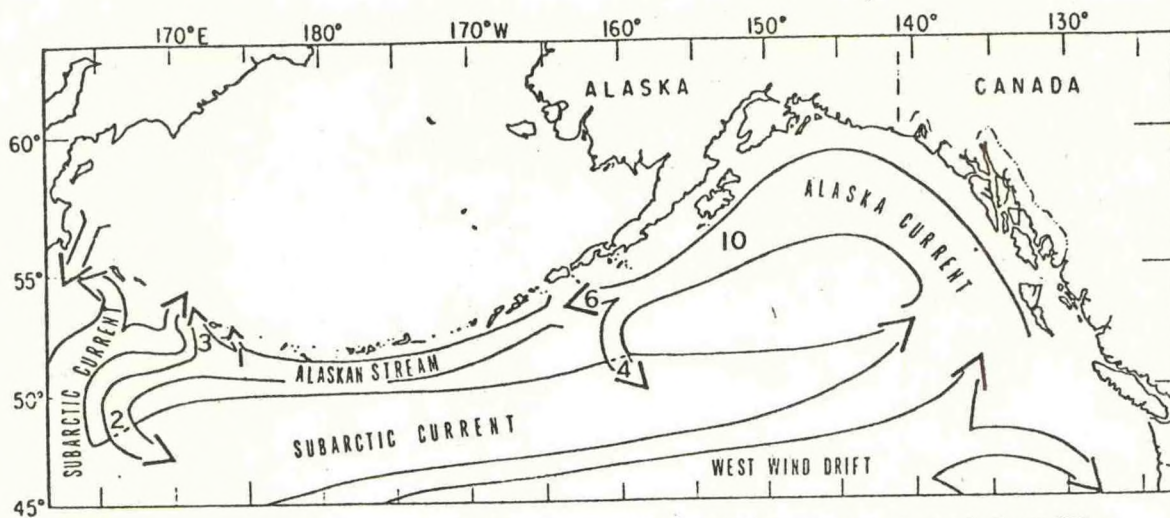


FIGURE 1 Schematic diagram of the Alaskan Stream. Numbers indicate volume transport ( $\text{m}^3/\text{sec} \times 10^6$ ) referred to the 1000-m level.

FIGURE 1.

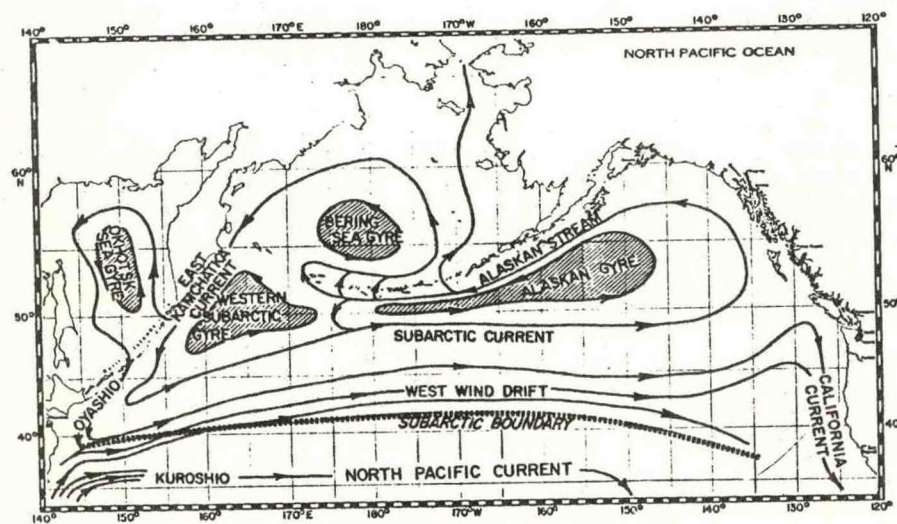


FIGURE 2 Schematic diagram of surface circulation relative to 1000 decibars.

FIGURE 2



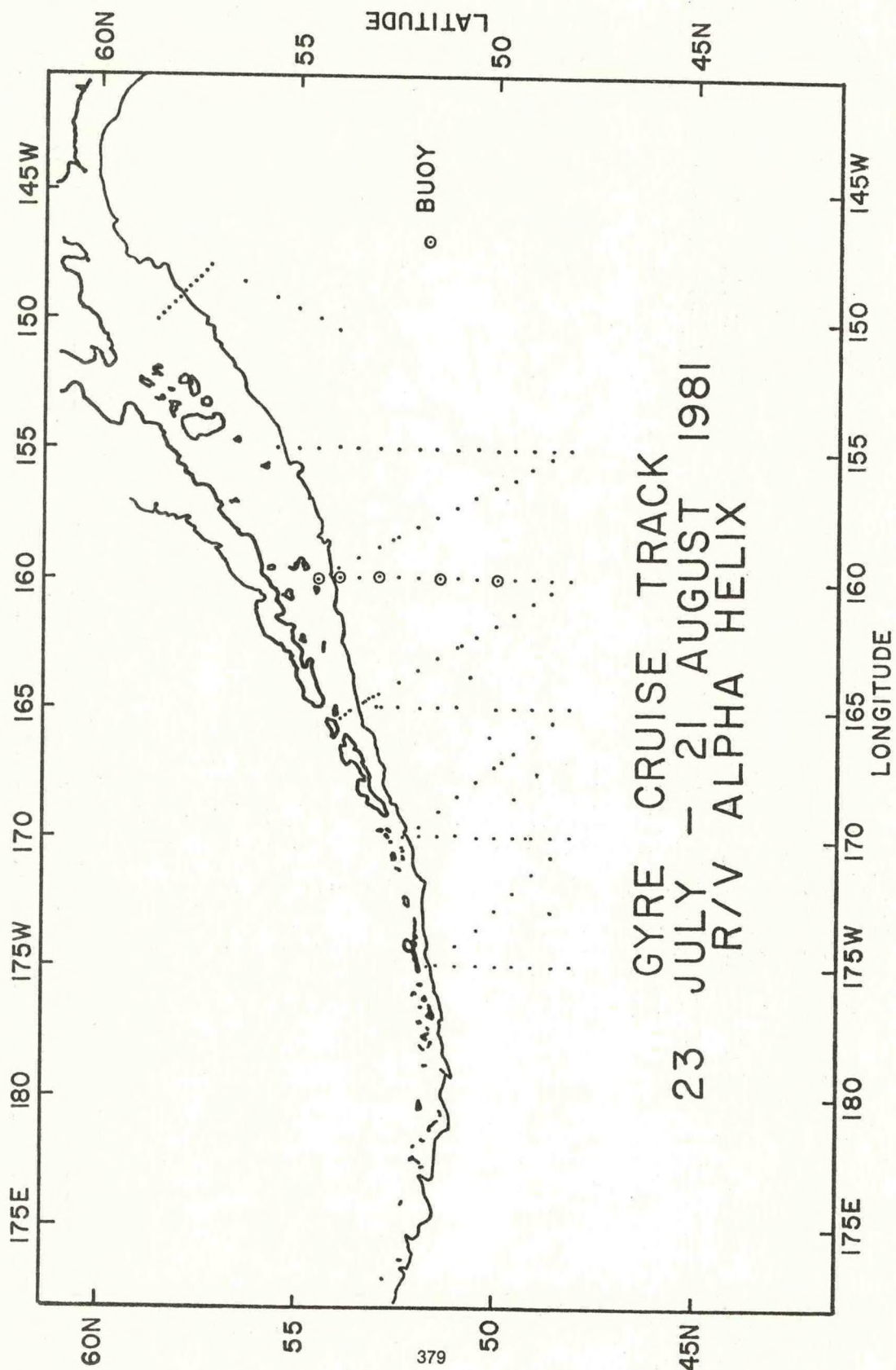


FIGURE 3



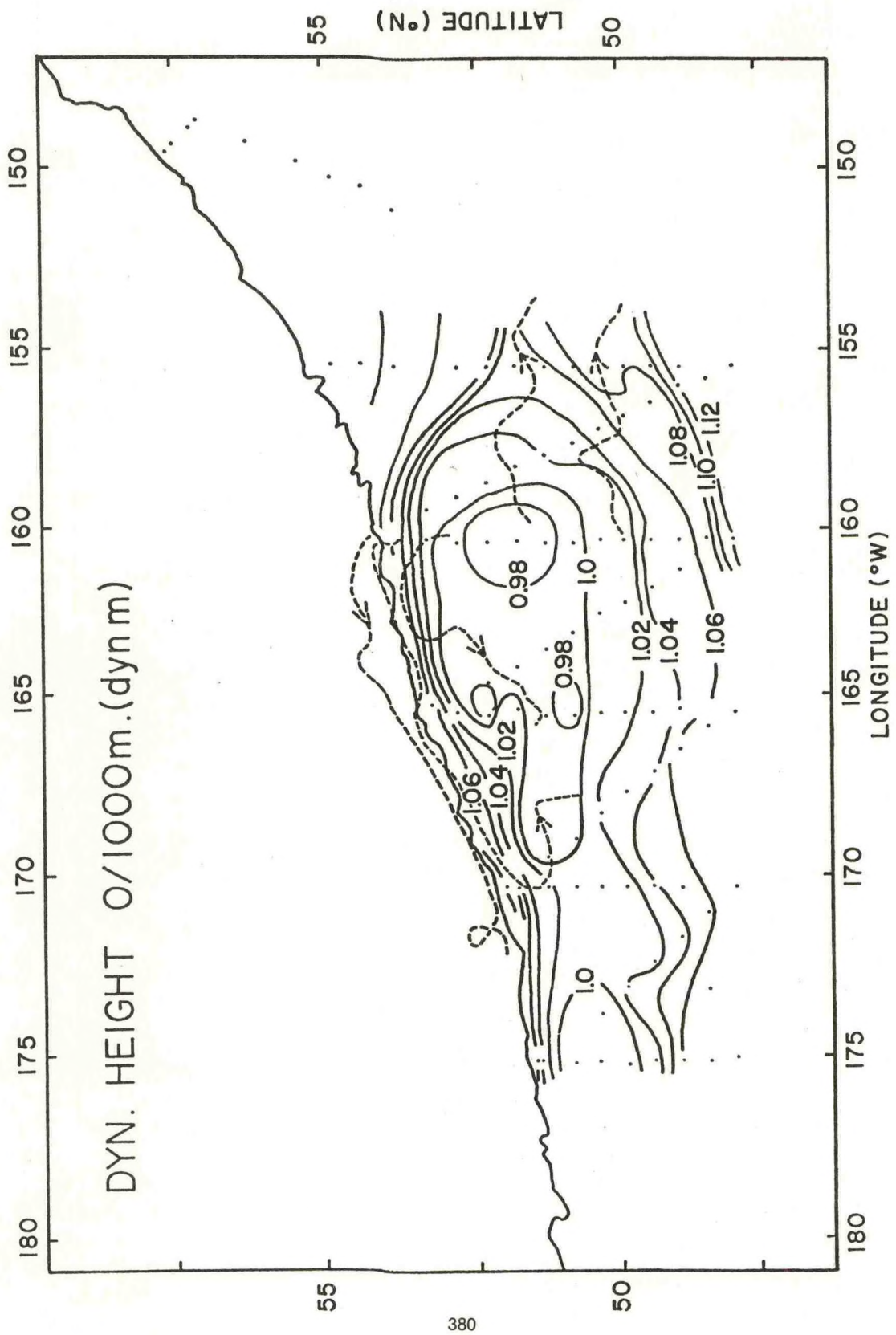


FIGURE 4



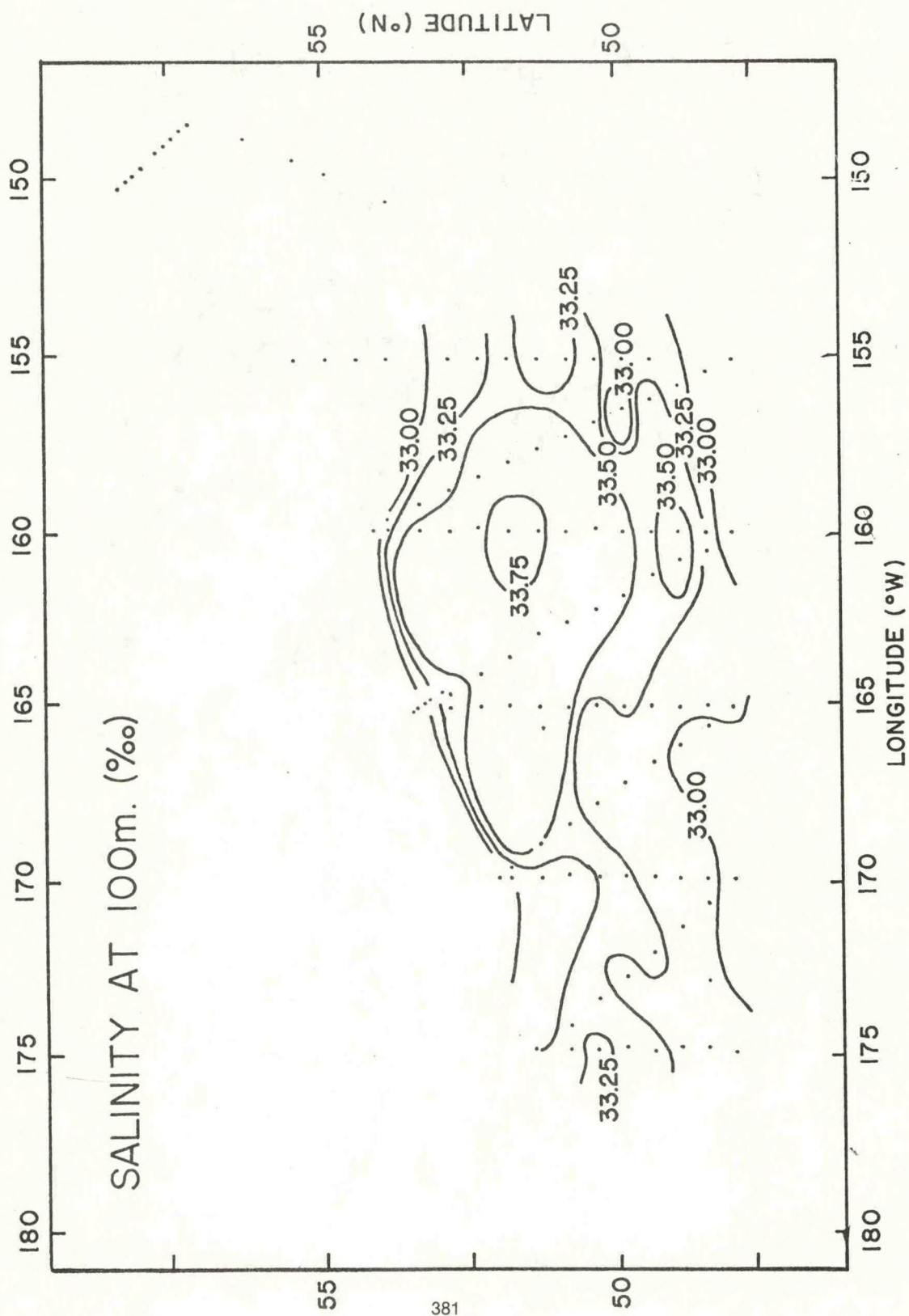


FIGURE 5



# ARGOS AND AES BUOY TRACKS TO MARCH 31, 1983

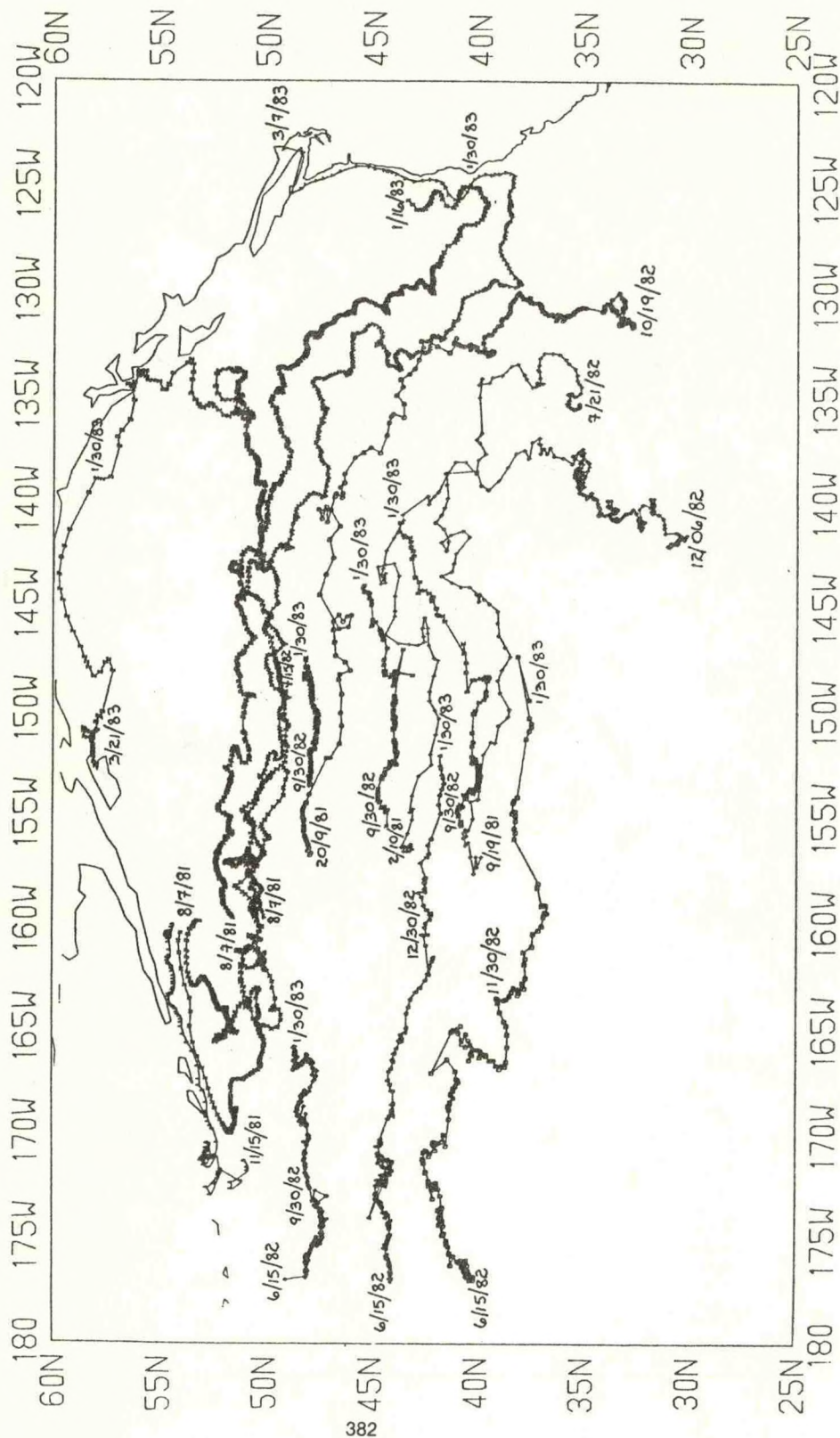


FIGURE 6



# ALL BUOYS PRE 1981 NORTH OF 52°N

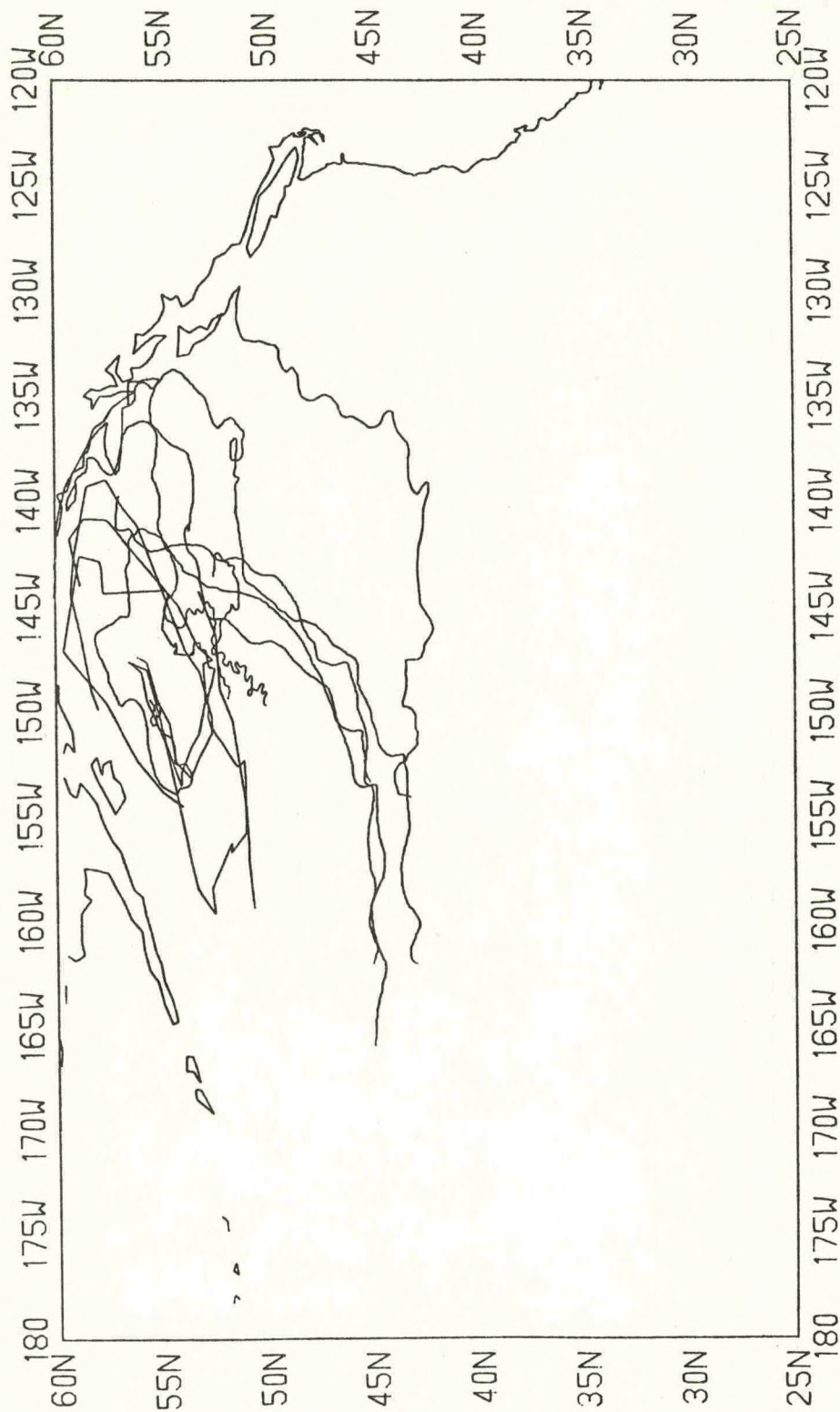


FIGURE 7



# ALL BUOYS PRE 1981 SOUTH OF 45 N

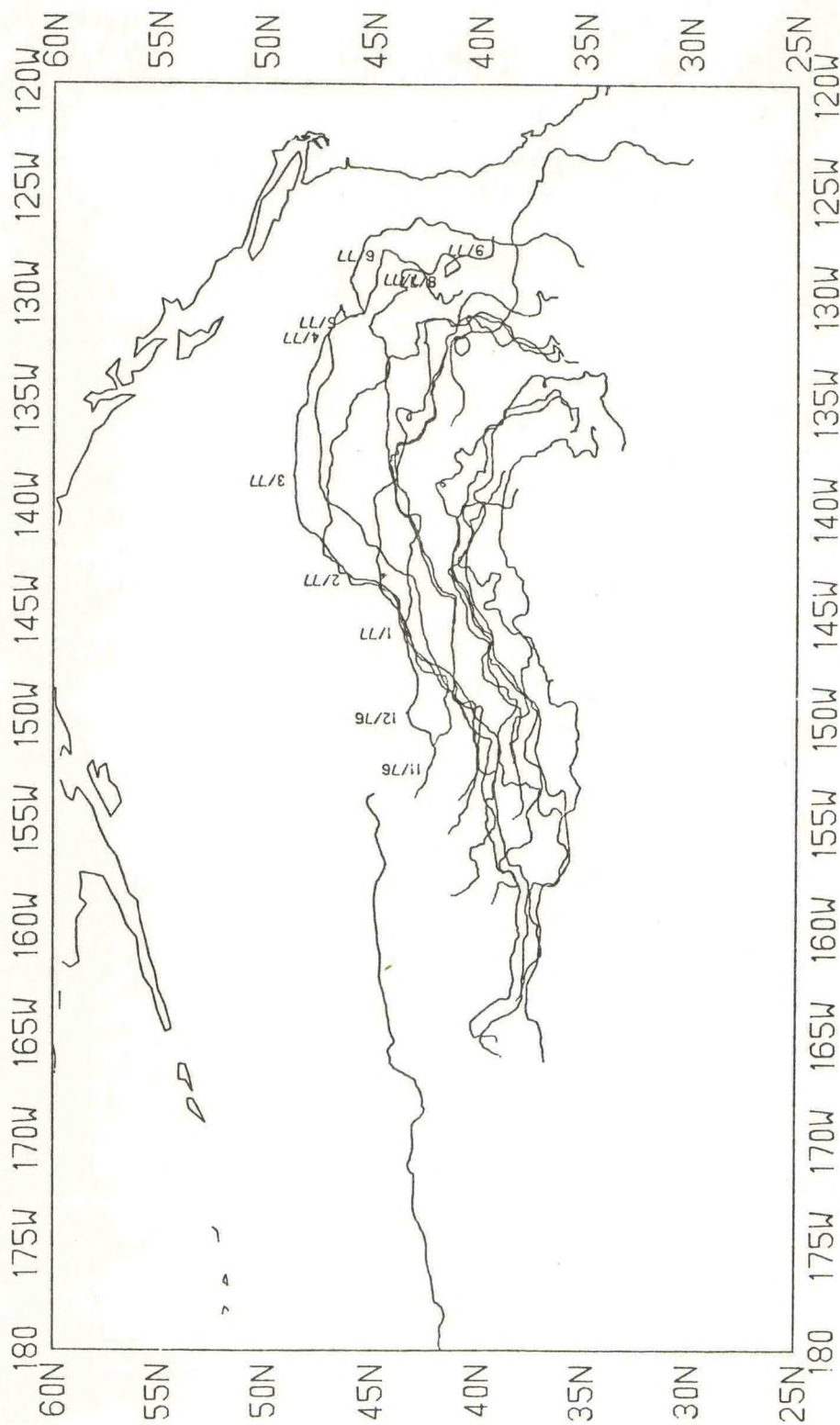


FIGURE 8



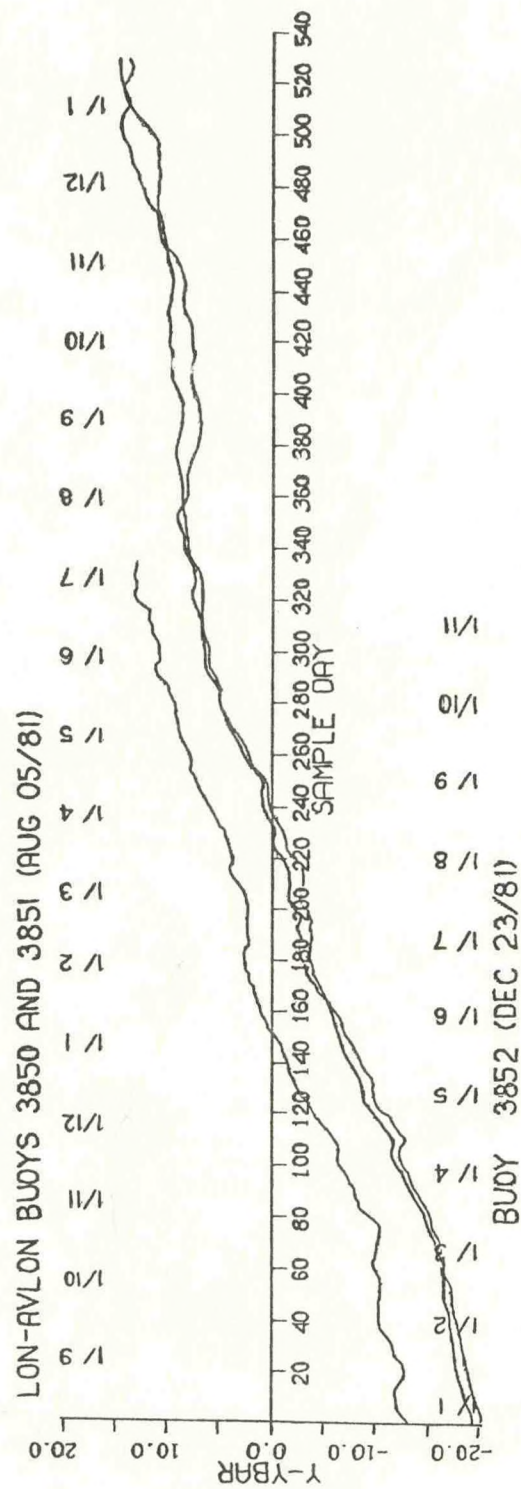


FIGURE 9



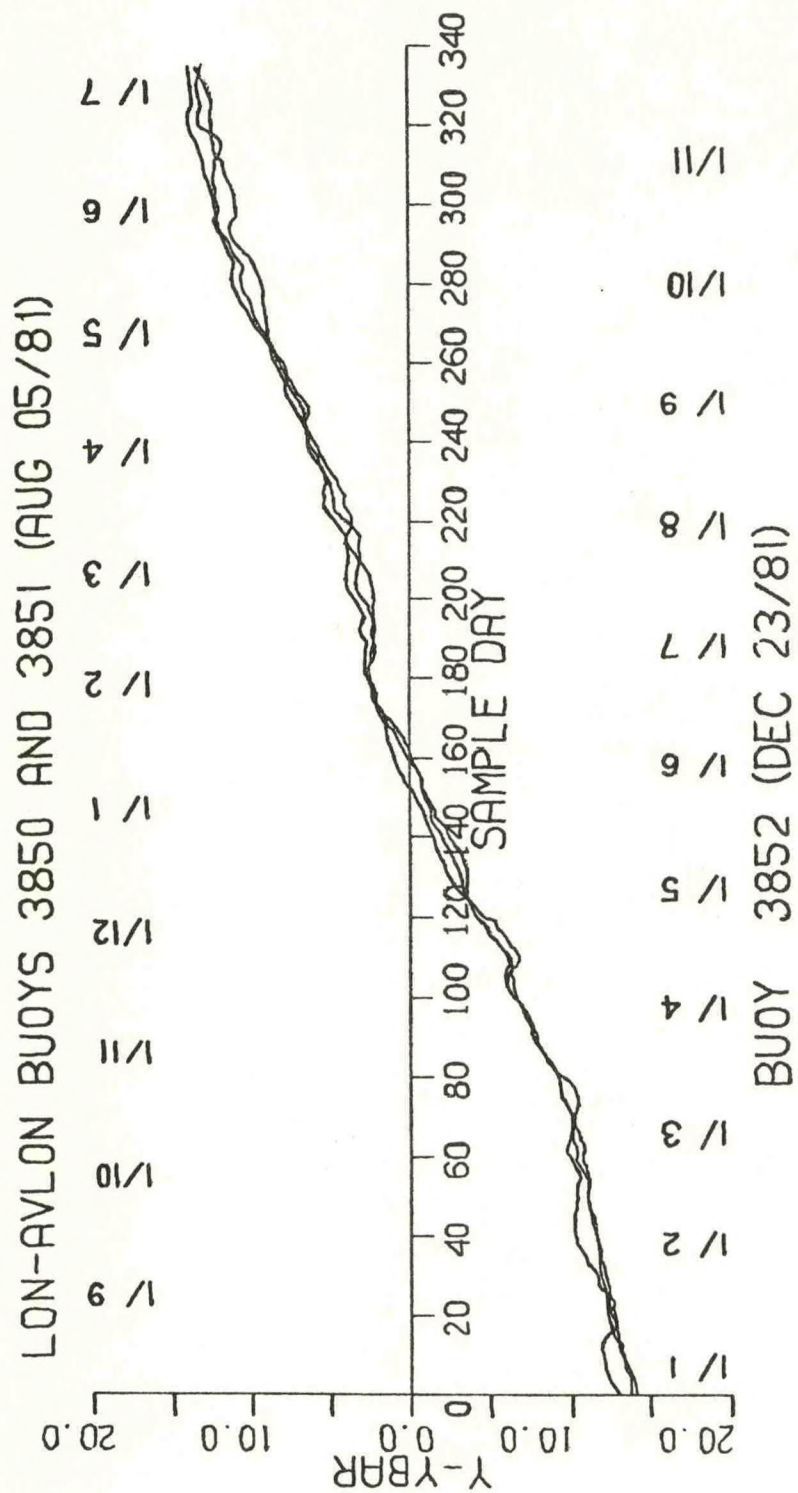


FIGURE 10



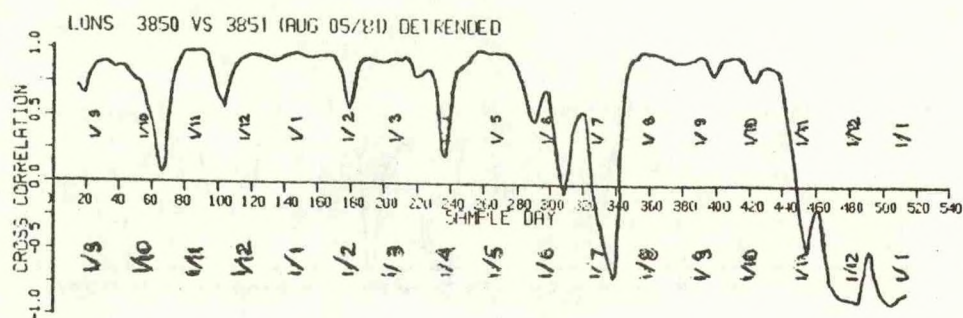


FIGURE 11. a

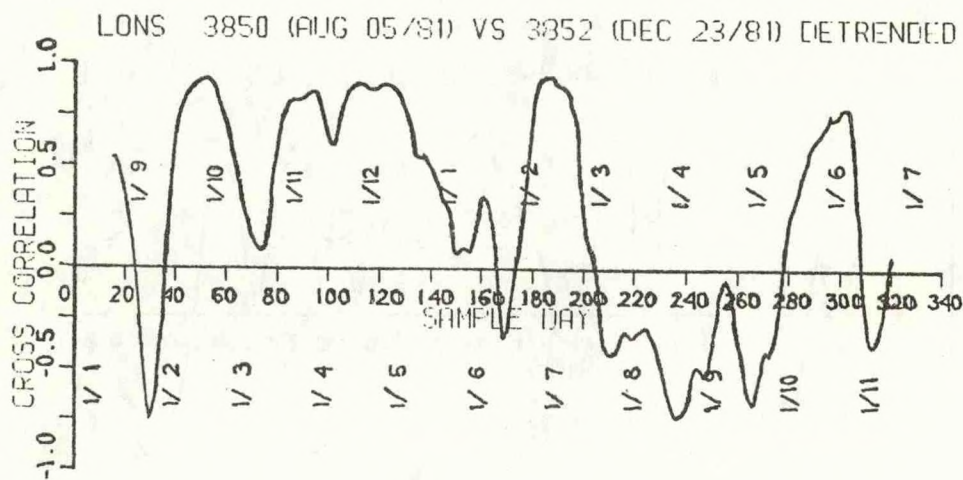


FIGURE 11. b

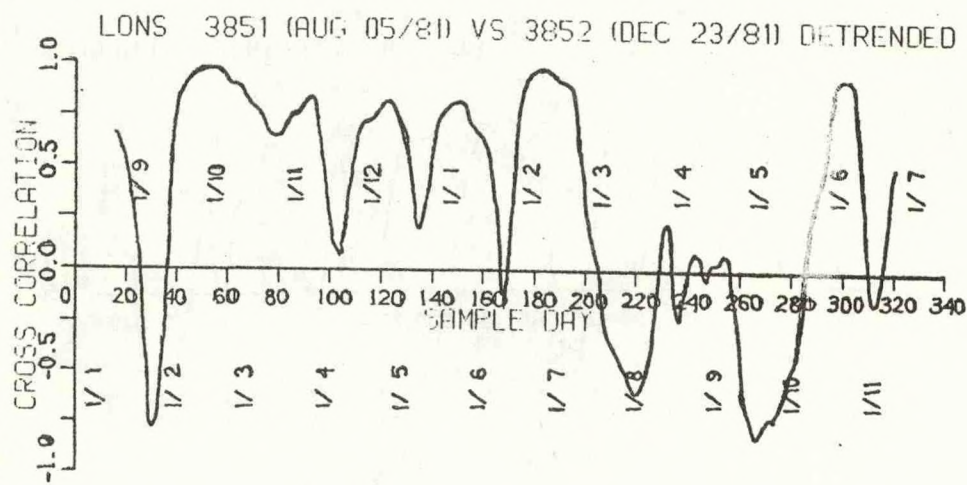


FIGURE 11. c



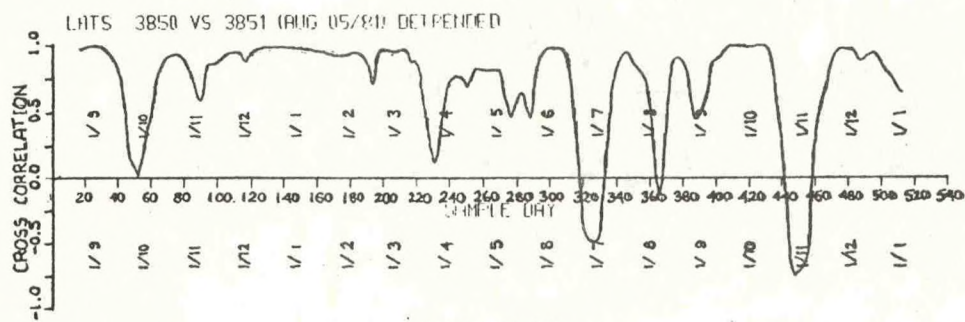


FIGURE 12. a

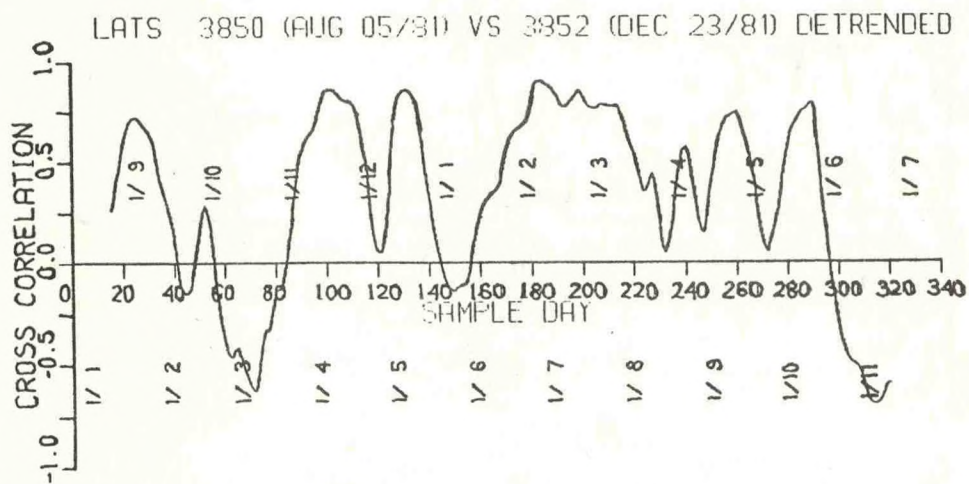


FIGURE 12. b

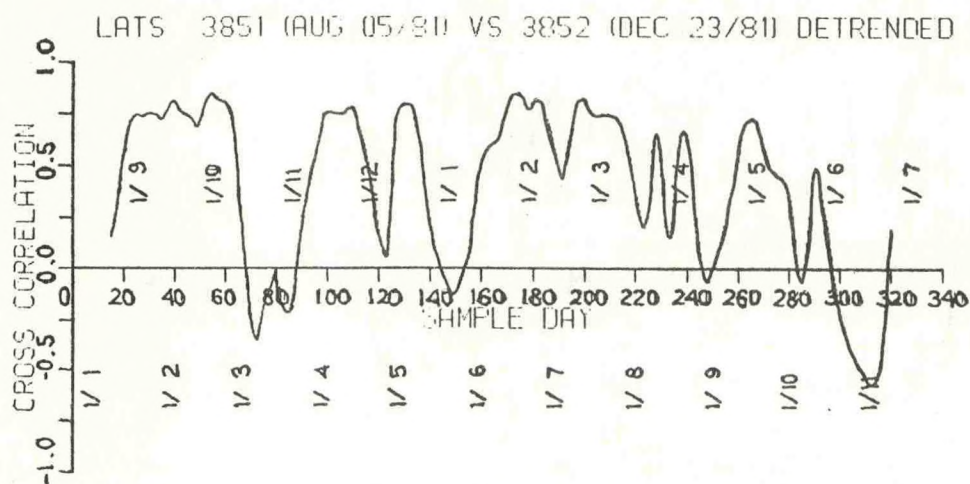
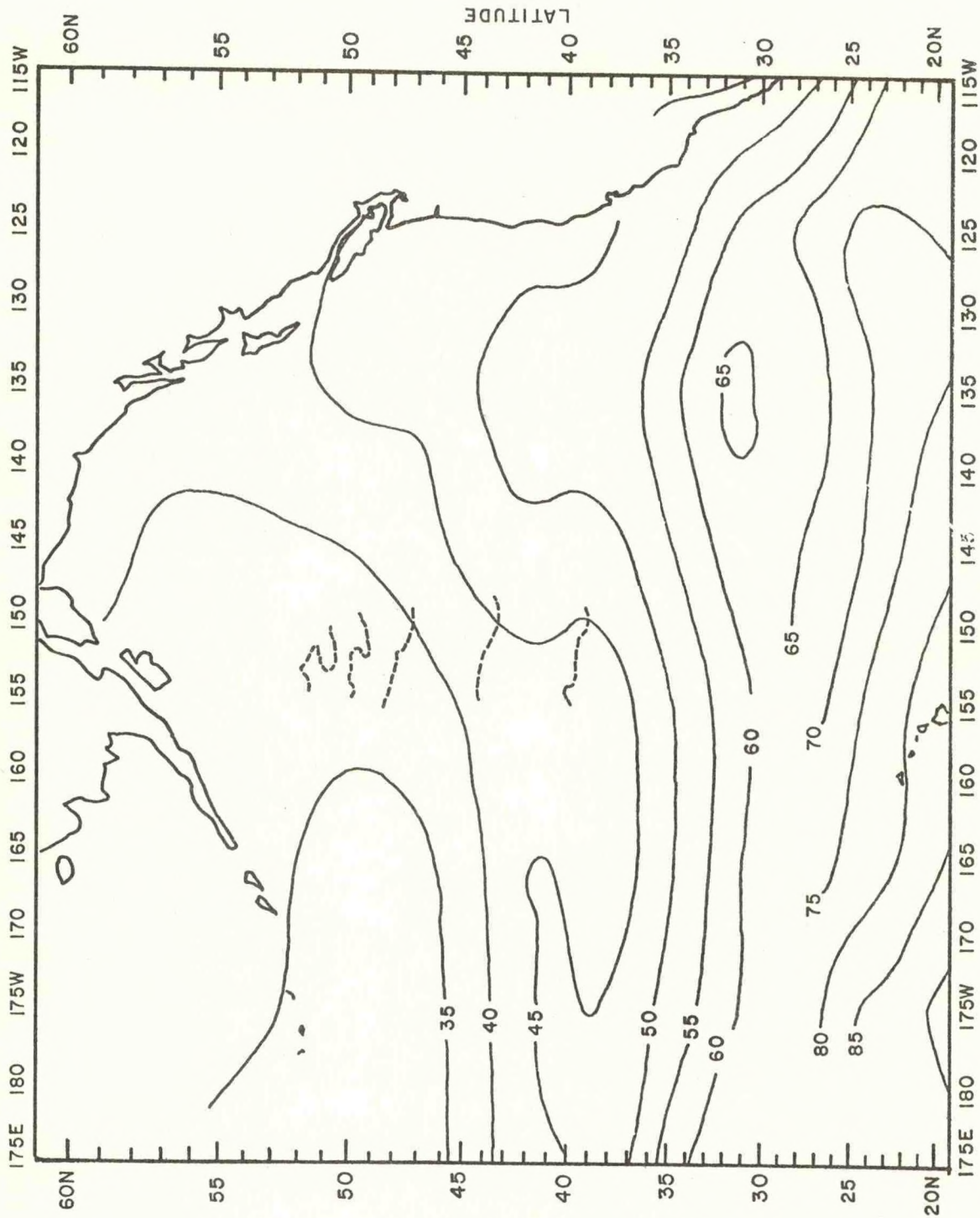


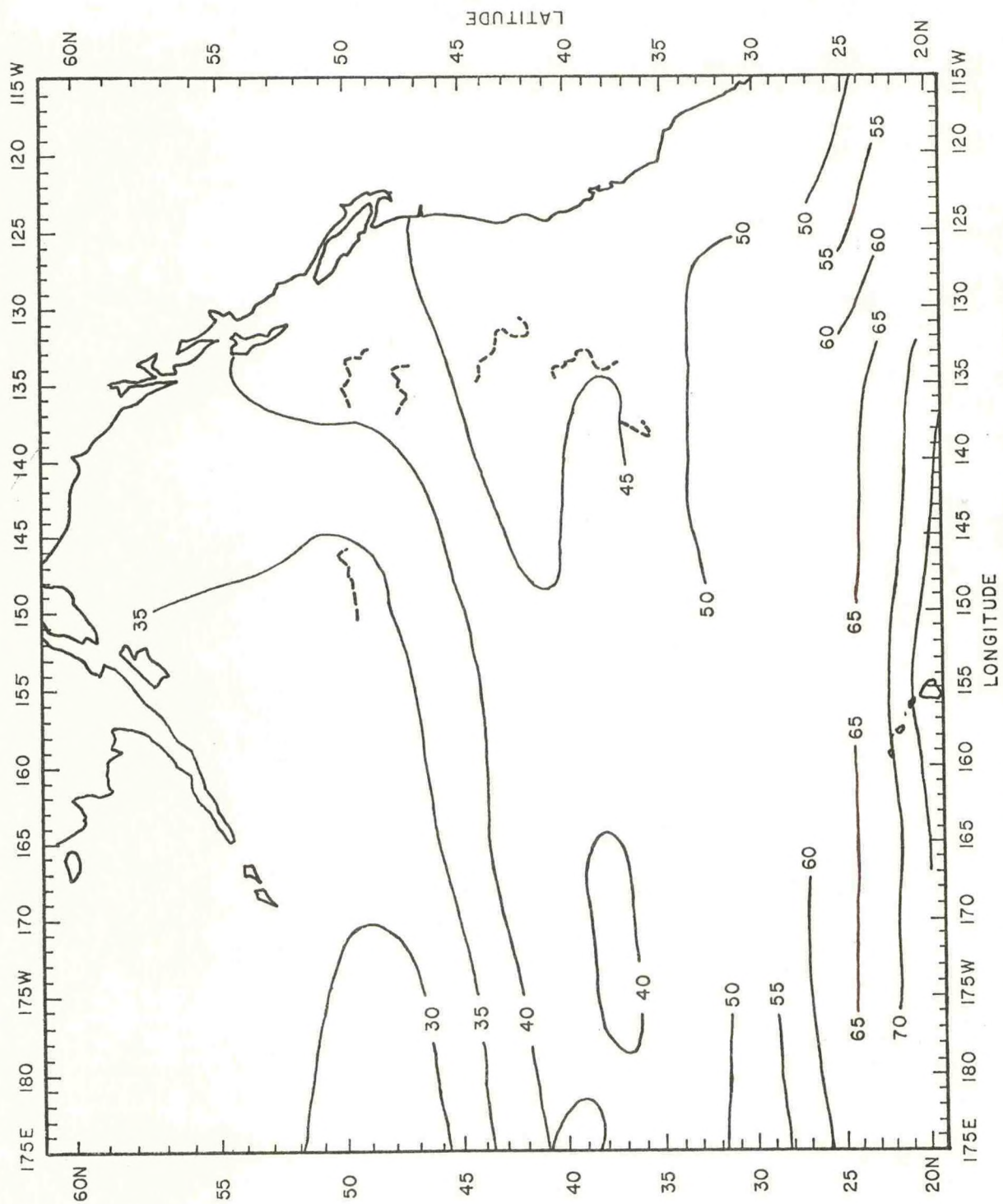
FIGURE 12. c





NOV 81 MONTHLY: DYNAMIC HEIGHT (DYN CM : 0/200 db)  
FIGURE 13





MAY 82 MONTHLY: DYNAMIC HEIGHT (DYN CM : 0/200 db)  
FIGURE 14



SEA LEVEL ATMOSPHERIC PRESSURE FOR NOVEMBER 1981

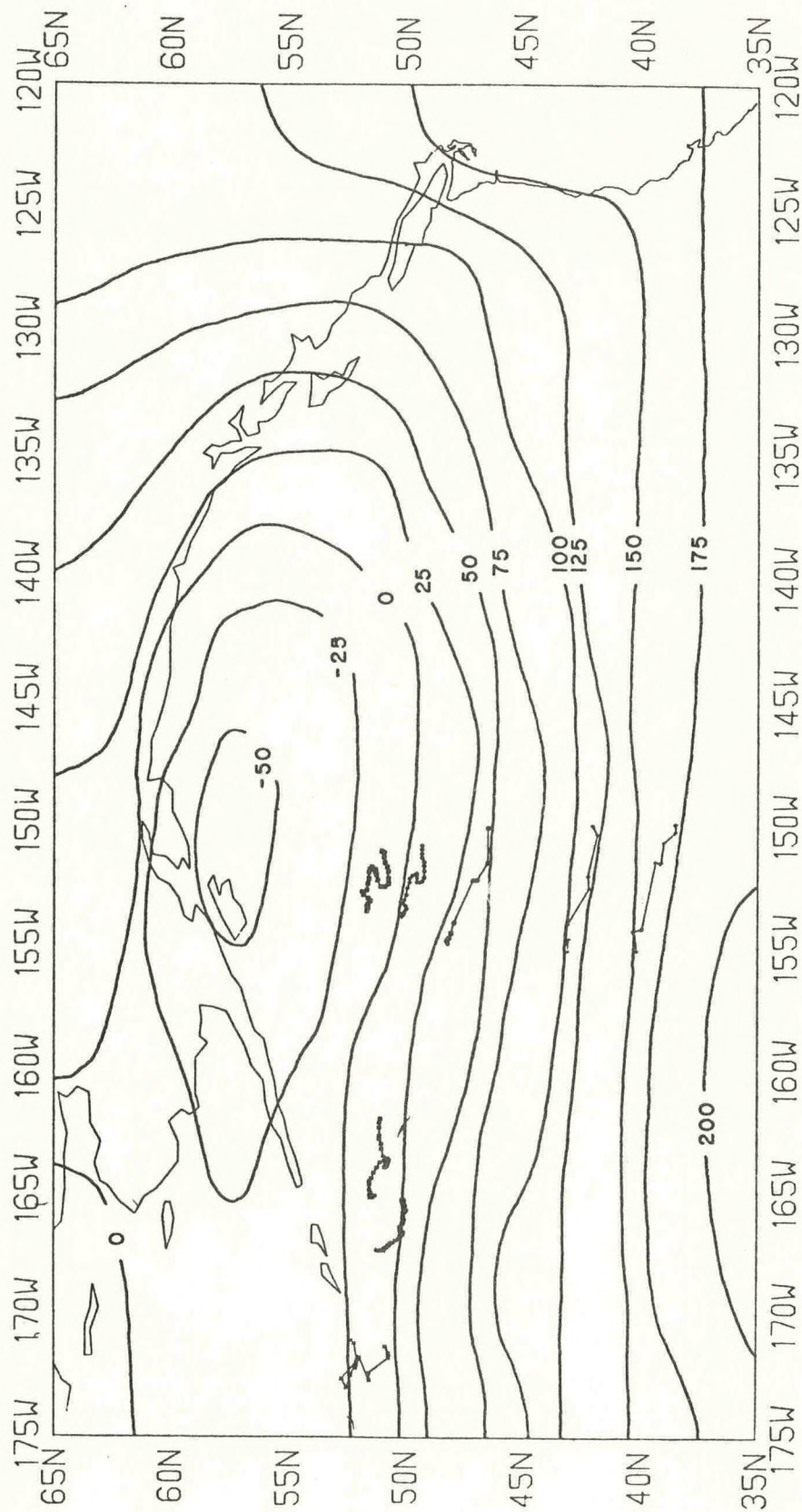


FIGURE 15



# SEA LEVEL ATMOSPHERIC PRESSURE FOR MAY 1982

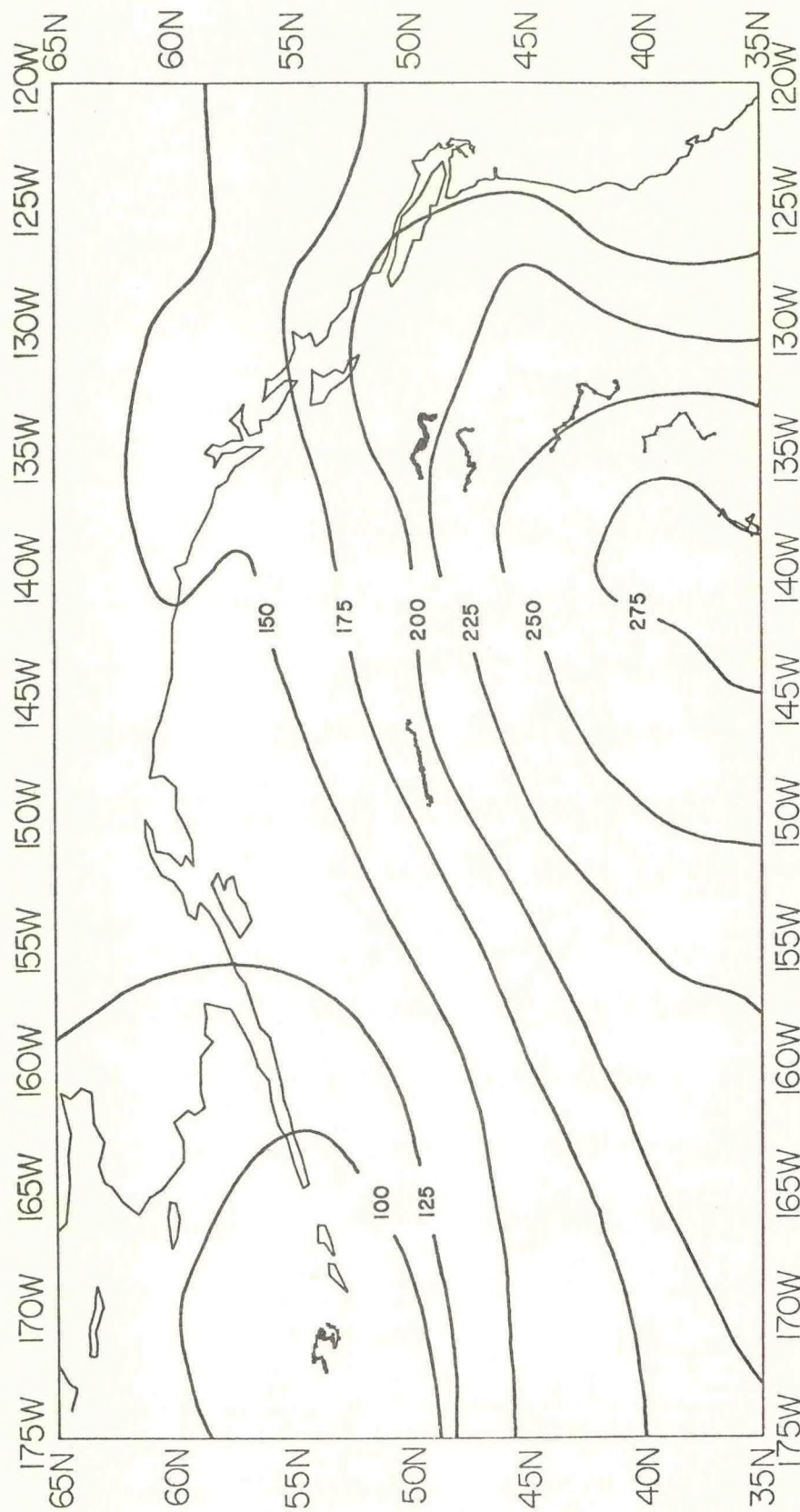


FIGURE 16



# SEA LEVEL ATMOSPHERIC PRESSURE FOR JANUARY 1977

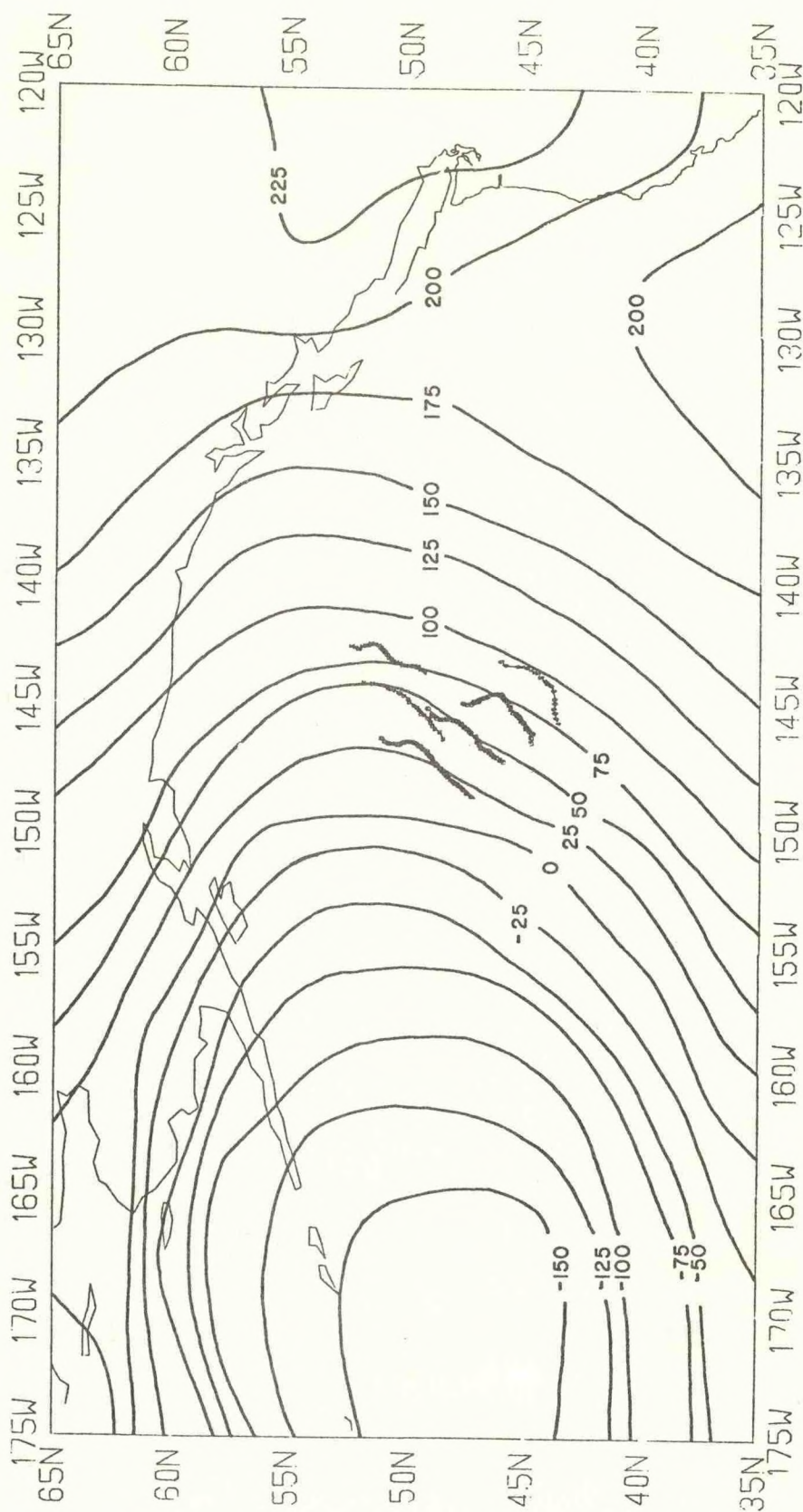


FIGURE 17



# SEA LEVEL ATMOSPHERIC PRESSURE FOR JANUARY 1982

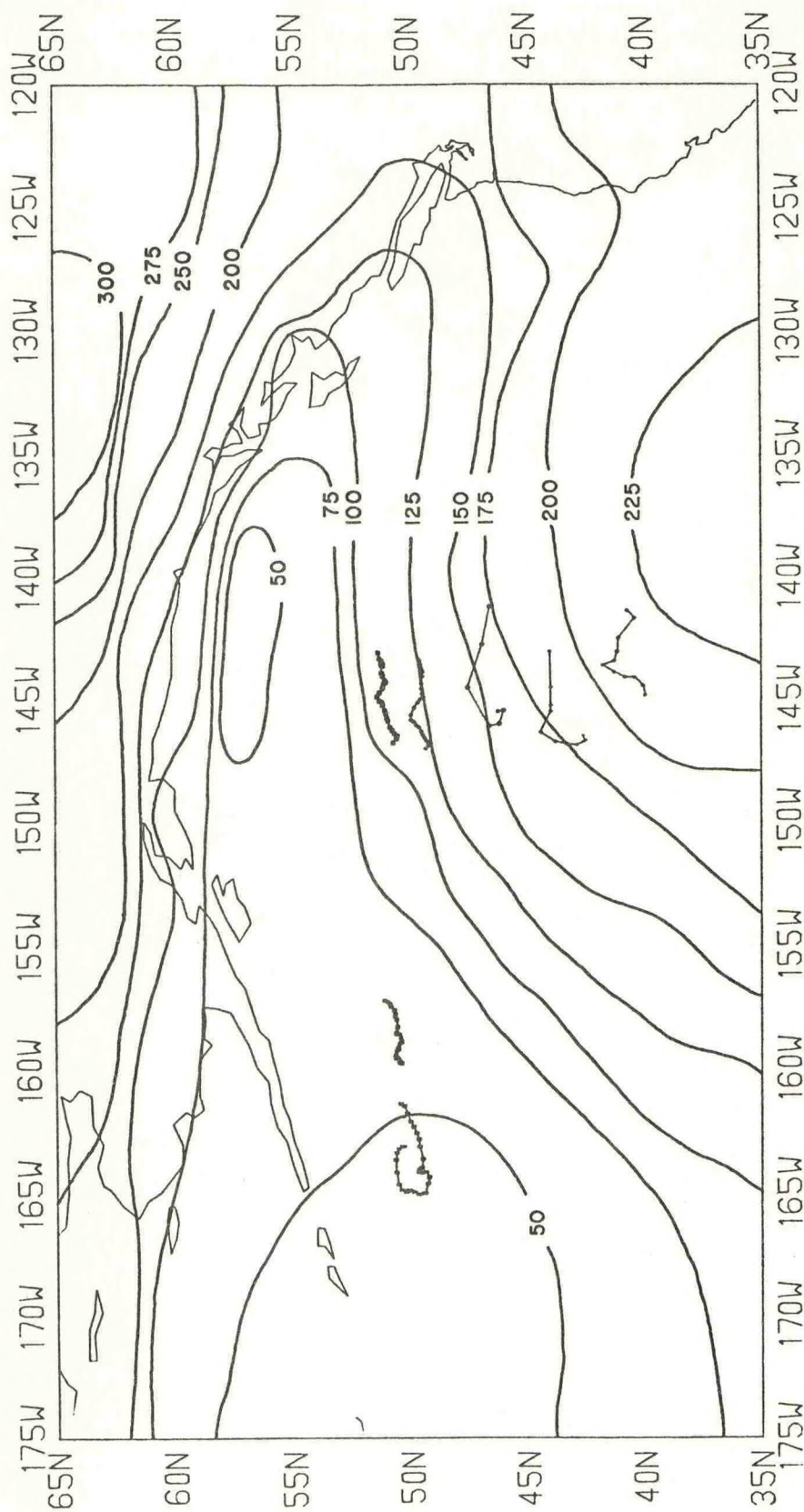
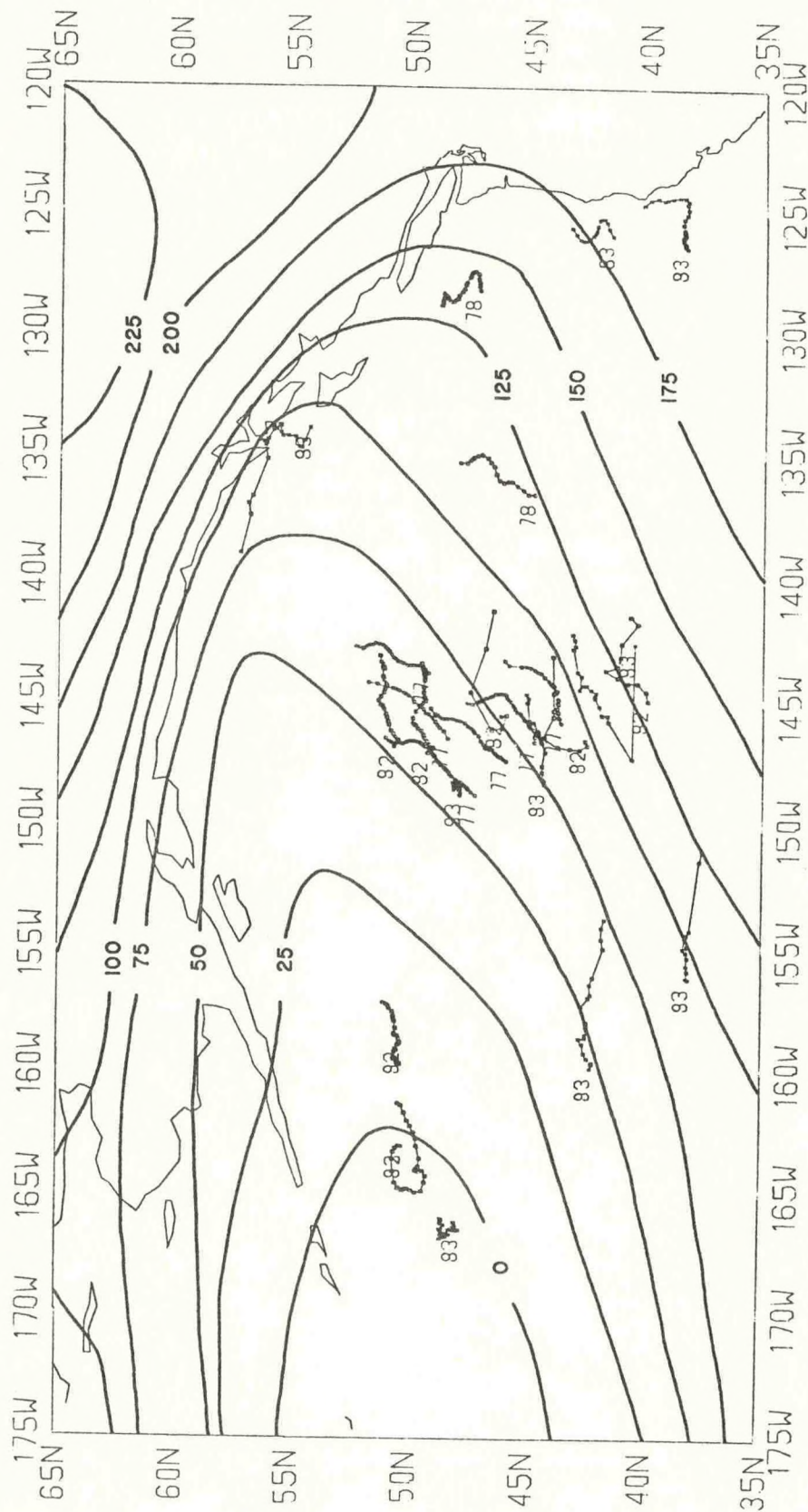


FIGURE 18



# SEA SURFACE ATMOSPHERIC PRESSURE CLIMATOLOGY FOR JANUARY









## **PAPERS SUBMITTED BUT NOT PRESENTED**

### **"COHERENT RECEPTION OF HF DRIFTING BUOY SIGNALS"**

**Zhengxu Qian**

**Institute of Oceanology, Academia Sinica  
Qingdao, China**

### **"CALCULATION OF STATICS OF SUBSURFACE MOORED BUOY SYSTEM"**

**Song Minghang**

**Institute of Oceanographic Instrumentation  
National Bureau of Oceanography  
Tianjin, China**







# COHERENT RECEPTION OF HF DRIFTING BUOY SIGNALS

Zhengxu Qian

Institute of Oceanology, Academia Sinica  
7 Nan Hai Rd, Qingsdao, China

## ABSTRACT

A homodyne phase-locked receiver can recover a signal deeply embedded in noise but will, when there is interference such as CW or broadcasting signals in the nearby frequency band, lose its locked condition or even be locked by the the interference. The jamming could be rejected by a HF synchronous integrator, a tracking matched comb filter as suggested by the author. A coherent receiver based on such a filter and PLL has been suggested and discussed. The buoy's signal should be changed to accommodate the technology by using a phase-modulated signal instead of a CW.

## 1. INTRODUCTION

As a simple and low cost tool, the HF drifting buoy is useful in the coastal and continental shelf zone for telemetering data of current, water temperature, wave etc. The effective working period after launching is about several months, which is matched with the time scale of a medium scale oceanographic phenomena and it could be used to monitor the eddy and loop too. The potential use is simply mooring it as a simplest buoy system, which is especially fit for observing the phenomena of the ocean surface, such as the light albedo just below the surface. The HF drifting buoy has been developing in recent years as has been the satellite linked drifting buoy.

The communication traffic of HF drifting buoy is a problem worth to study, since the existing CW buoy signal is simple but has never been the best for the failure of signal and losing of bearing by jamming. In a previous paper<sup>1</sup> a homodyne phase-locked receiver was suggested by the author, which can handle high level additive noise but is not suitable for use in the coastal area of China, since there exists serious interference of CW and broadcasting signals in the nearby standard international buoy frequency band, the receiver failed to lock with the buoy signal and sometime was even locked by the jamming signals. This paper gives fur-

ther discussion of coherent reception and introduces a HF synchronous integrator as a tracking narrow band matched filter for rejecting the jamming signals as the prestage of a coherent receiver. The existing CW buoy signal should be changed to phase modulated signal for best result.

## 2. COHERENT RECEPTION

Coherent or synchronous reception was first discussed using a phase-locked loop by de Bellescize<sup>2</sup> in 1932, which was sometime called homodyne reception. The theory and technology was fully developed during the recent decades especially since the development of space technology, where coherent receiver was widely used for space communication. A homodyne receiver was constructed for HF drifting buoy signal reception by Qian<sup>1</sup> in 1981 as shown in block diagram in fig.1. There is a slight difference from

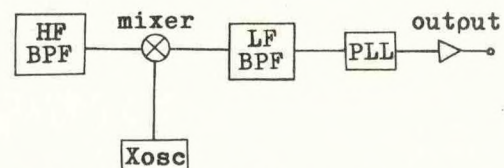


Fig.1. The homodyne receiver

the usual coherent receiver, the frequency  $f_l$  of local oscillator was not controlled by the phase-locked loop which was locked by  $f_s = f_c - f_l$  instead, where  $f_l$  is the buoy signal and  $f_s$  is a low frequency. It is considered that  $f_l$  will have slight changes in an ocean environment and  $f_l$  will be stable enough during the period of reception, then locking with  $f_s$  is equal to locking with  $f_l$ , and the former will be easier to implement. The bandwidth was determined by the parameters of the low pass filter within the phase-locked loop, the noise bandwidth  $B_n$  was determined by the loop bandwidth  $\omega_n$  as

$$B_n = \omega_n (\gamma + 1/4\gamma) / 2$$

for a second-order loop, and  $\gamma$  was the damping factor. The  $B_n$  can be made as small as required by  $\omega_n$ .

Although simpler in technology there exists a channel through which the image frequency  $f_l + 2f_s$  can jam, since the HF



bandpass amplifier do not have such high  $Q$  to reject the image when  $f_s$  is a small fraction of  $f_t$ . This was the reason for the failure of homodyne receiver in practical use.

### 3. SYNCHRONOUS INTEGRATOR

Inserting a very narrow band filter before mixer is an effective way to reject image frequency, but the high  $Q$  crystal filter is not suitable for any drift of the filter center frequency to the  $f_t$  will be a complete failure in reception. The synchronous integrator as a comb filter with its controllable tracking characteristic is an excellent filter for the purpose.

The first paper about synchronous integrator was published by Frater<sup>3</sup> in 1965. A diagram of the principle of synchronous integrator is shown in fig.2.

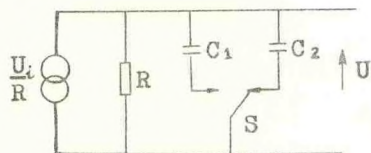


Fig.2. The synchronous integrator

The capacitors  $C_1$  and  $C_2$  are grounded one after another by switch  $S$  with a frequency  $f_c$  and charged in each half of a cycle. It is like two accumulators with programmable routine to store charges, the time constant  $\tau$ , usually much larger than  $1/f_c$ , determines the period of accumulating, which governs the ability of noise rejection. Ratio  $n$ ,  $n = \tau f_c$ , represents how many times the signals have been accumulated, the larger the number of  $n$ , the more energy of signal with the same frequency as  $f_c$  was stored while the noise and any other frequency signals were cancelled by itself. The process is much more like in a synchronous demodulator but its output is a DC voltage instead of a square wave in the synchronous integrator.

Tang<sup>4</sup> gave a theoretical analysis of the synchronous integrator, some of them are outlined here:

- Controlled by the synchronous frequency, a synchronous integrator is a matched filter for square wave with integration constant  $\tau = 2RC$  and bandwidth  $2/\tau$  as illustrated in fig.3.
- The amplitude  $\hat{U}$  of output square wave is
  - $\hat{U} = (\hat{U}_i \cos \varphi) / \pi$  when  $f_i = f_c$ ,  $\varphi$  is the phase difference.
  - $\hat{U} = \hat{U}_i \cos(\Delta \omega \tau + \varphi) / \pi \sqrt{1 + (2RC \Delta \omega)^2}$  where  $\Delta f = f_i - f_c$ , when  $\Delta f$  is small.
- The synchronous integrator could be used in cascade, its transfer function is simply the multiplication of each stage.

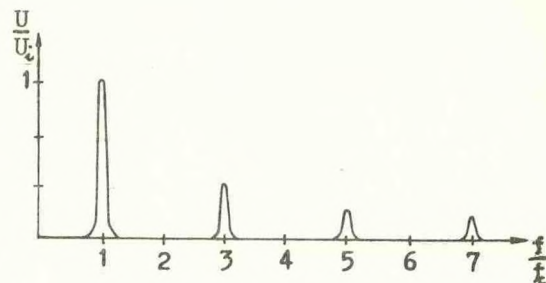


Fig.3. The filter characteristic of synchronous integrator

The effective noise bandwidth will reduce 3db for two cascaded stages with the same  $\tau$ .

### 4. HF SYNCHRONOUS INTEGRATOR

Both Frater and Tang's synchronous integrator can only be used in DC to low frequency range, for the leakage of the control voltages from the synchronous switch has the same frequency of signal. The leakage, which increases rapidly as the frequency increases, will become a spurious signal and cause false locking and detection. Tang suggested a better FET switch but leakage still remained.

A balanced switch has negligible leakage even in the VHF band. The balanced phase detector is such a good switch by assuming the open and close of a switch being multiplied by 0 and 1. Its differential outputs could be used to charge the two integrators. Excellent matching can be made by carefully adjusting the external components of the chips. For convenience, the fig.2 is rearranged in fig.4 as a HF synchronous integrator.

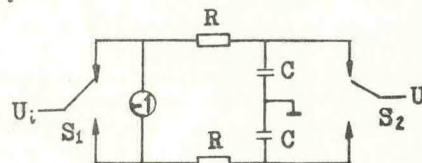


Fig.4. The HF synchronous integrator

The two integrators are in parallel and controlled by two switches  $S_1$ ,  $S_2$ . Parallel connecting will give better balance in HF than the serial connection in fig.2. The inverter connected between the inputs of two integrators will be discussed later. Synchronous integration will be performed in two steps with balanced phase detectors.  $S_1$  and two integrators with same constant  $RC$  as shown in fig.5a), accumulates the signals by storing its energy in phase in the two capacitors, and b) will output a square wave modulated by the signal amplitude as the second step. The  $S_1$  consists of  $M_1, M_2$  and  $S_2$  by  $M_3, M_4$ . The applied control voltage causes the  $M_1$ ,  $M_3$  conducting in



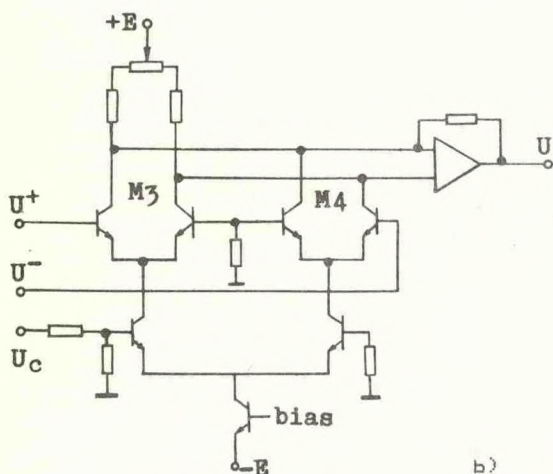
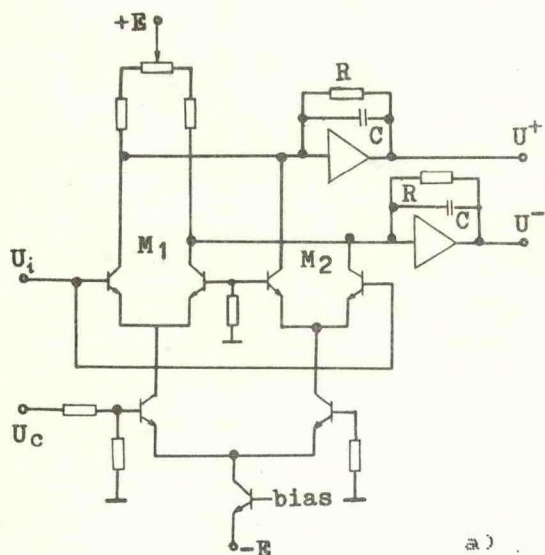


Fig. 5. a) Input switch and integrators, b) output switch of HF synchronous integrator

the positive half cycle and M2, M4 in the negative half hence the capacitors will be charged alternatively as done in fig. 2. The differential pairs M1, M2 and M3, M4 will cancel the transit as they are excellently matched. The differential output cause an inverter connected between the inputs of the integrators. Owing to the inverter, every one of the integrators will now be charged during the two half cycles instead of only one half cycle as Frator's. The time constant is changed from  $2RC$  to  $RC$ , but other parameters will remain the same as Tang's.

## 5. COHERENT RECEIVER

The signals of a HF drifting buoy usually have the form of:

$$U_t = \frac{1}{2} \dot{U} \left( 1 + \frac{4}{\pi} \sum_{n=0}^{\infty} \frac{1}{2n+1} \sin(2n+1)\Omega t \right) \sin \omega_c t \quad (1)$$

which is a amplitude modulated CW wave with modulating frequency  $\Omega$  and carrier frequency  $f_c$ , amplitude  $\dot{U}$ . A coherent receiver of fig. 6 can be used to handle this kind of signal.

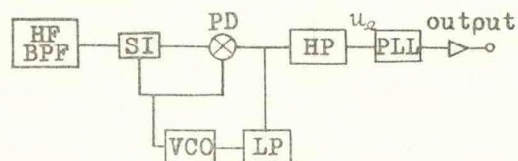


Fig. 6. The coherent receiver for HF drifting buoy

After the HF bandpass filter and synchronous integrator only the frequency band  $f_c \pm 4f$  could reach the phase detector, where  $4f$  is a bandwidth determined by  $\Omega$ ,  $\Omega$  has a low value as the slow varying oceanographic data. The time constants of the synchronous integrators have to fit with the necessary bandwidth of  $4f$ . The rejecting of interferences beyond the frequency bandwidth  $f_c \pm 4f$  will improve the working condition of phase-locked loop to track up the  $f_c$  and prevent it from being saturated by jammings.

The output of the phase detector as a multiplier is:

$$U_{PD} = U_t \frac{4}{\pi} \sum_{n=0}^{\infty} \frac{1}{2n+1} \sin(2n+1)\omega_c t \quad (2)$$

substituting (1) to (2) will get a long expression. The low and high pass filters after the phase detector select the DC and  $\Omega$  parts from the complex output to control the VCO with the DC error signal and the second PLL with  $U_{\Omega}$ . Since now  $f_c$  is equal to  $f_t$  (with a negligible phase error) the channel for image frequency no longer exists, the backwards in fig. 1 too. The  $U_{\Omega}$  will be:

$$U_{\Omega} = \dot{U} \cdot k / \pi \quad (3)$$

$k$  is the total gain of successive stages.

The experimental results of this coherent receiver and synchronous integrator will be published in another paper. The main results are as follow:  $f = 6.246 \text{ MHz}$ ,  $\Omega = 11 \text{ Hz}$ ,  $\Delta f = 55 \text{ Hz}$  variable to  $5.5 \text{ Hz}$ ,  $\tau = 18 \text{ ms}$  variable to  $180 \text{ ms}$ , noise bandwidth  $55 \text{ Hz}$  to  $5.5 \text{ Hz}$ .

## 6. THE COMMUNICATION TRAFFIC OF HF DRIFTING BUOY

The square wave amplitude modulated buoy signal was not the best communication traffic for the coherent receiver, since during half of the cycle of  $\Omega$  drops occurred for there is no  $f_c$  appeared on the receiver, especially when  $\Omega$  and S/N are low. If a  $180^\circ$  phase modulated signal is used then  $U_{\Omega}$  will be: (Tang's)

$$U_{\Omega} = 2\dot{U} \cdot k / \pi \quad (4)$$

its value will be two times greater than (3) with doubled RF power and no dropout



will occur by the continuity of the signals. It is obviously interesting since the power of transmitter will increase four times for the same  $U_0$  as in the square wave amplitude modulated signals.

A new HF drifting buoy equipped with Omega signal processing electronics is now in development in China with the idea suggested above.

## 6. CONCLUSION

The discussion of coherent reception of HF drifting buoy in this paper will lead to the following conclusions:

1. The HF synchronous integrator is a controlled tracking narrow band filter suitable for coherent reception to improve the S/N to a reasonable range for locking up PLL to a signal embedded deeply in the interference.
2. The leakage of control voltage in the synchronous integrator is solved by using balanced phase detector as the synchronous switch.
3. Cascading of HF synchronous integrators can reject very serious jamming in the nearby frequency band.
4. The  $180^\circ$  phase modulated signal will have a doubled  $U_0$  than ordinary CW signal.

## REFERENCES

1. Qian Z., 'A wave sensing drift buoy and its homodyne receiver', OCEANS, pp 437-441, 1981.
2. de Bellescize H., 'La reception synchrone', ONDE ELECTR., VOL. 11, PP 230-240, June 1932.
3. Frater R.H., 'Synchronous integrator and demodulator', REV. SCI. INST., Vol 36, No.5, pp 634-637, 1965
4. Tang H., 'Synchronous integrator--a method of extracting weak signal from noise'(IN CHINESE), J. NANKING UNIV. (natural sciences edition) No.1, pp 81-98, 1979.
5. Tang H., 'A method of suppressing correlation jamming at the frequency of reference signal'(IN CHINESE), J. Nanking Univ. (natural sciences edition) No.3, pp 639-645, 1982.



# CALCULATION OF STATICS OF SUBSURFACE MOORED BUOY SYSTEM

Song Minghang

Institute of Oceanographic Instrumentation  
National Bureau of Oceanography  
Tianjin, China

## ABSTRACT

A set of methods for the calculation of the statics of a single point taut subsurface moored buoy system is described for engineering design. Equations for the calculation of the statics of each components on the system such as instrument packages, mooring line, connecting hardware and floats are specifically given. Simple analyses and comparisons of some of the calculation methods are also presented.

## INTRODUCTION

The emphasis of this paper is laid on the methods for the calculation of the statics of a single point taut subsurface moored buoy system. It is well known that calculation of statics of a buoy system is the base of its design. A typical single point taut subsurface moored buoy system is depicted in Fig.1. It consists of a subsurface buoy, shackle assemblies (shackle-"o" ring-shackle), swivel assemblies (shackle-"o" ring-swivel-"o" ring-shackle), chain, steel wire ropes, current meters, chain-glass ball assemblies (chain with parallelly installed glass balls), acoustic release, damping nylon rope and

anchor. To calculate the statics of such a system means to calculate the static parameters of each components of the system. The main parameters are tension, fluid drag, tilt angle, length, depth and the horizontal displacement of the component from the anchor. The practical calculation is quite complicated because it is fulfilled iteratively using recurrence method.

Sea surface

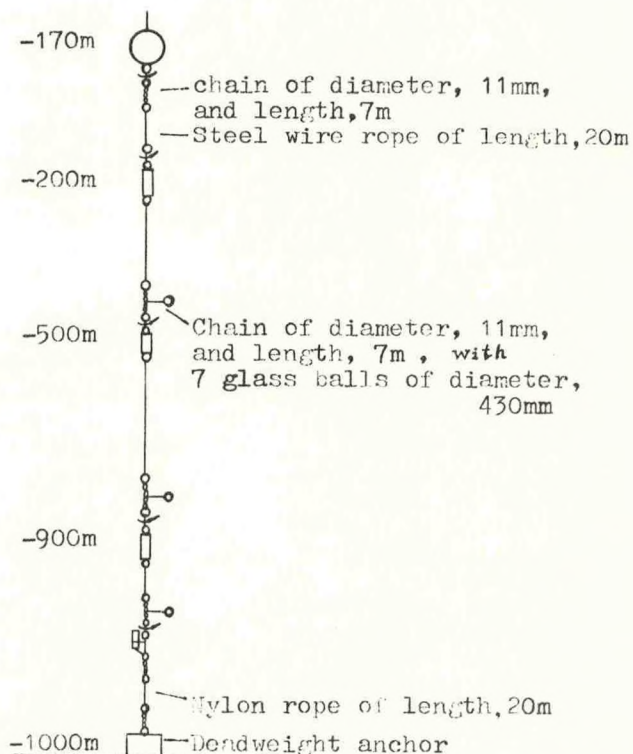



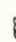
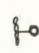

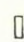




Fig.1 Single point taut subsurface moored buoy system



## LEGEND

	---buoy
	---shackle assembly
	---swivel assembly
	---chain
	---chain-glass ball assembly
	---steel wire rope, nylon rope
	---current meter
	---acoustic release
	---deadweight anchor

It is important for the designer to find an appropriate calculation method which is simple and can meet the operational requirements. This paper introduces a complete set of methods for the calculation of the statics of a single point taut subsurface moored buoy system in term of engineering design. Calculation by these methods, as the author regards, would be quite simple even without the help of a computer. In order to shorten the article, the deduction and some data comparisons are omitted and only the used methods are introduced in the paper.

## THEORETICAL PRESUMPTION

All calculations are based on the statics and the tangential component of drag of current is neglected. The environment for a subsurface moored buoy system is relatively favorable, because it is under the surface at a certain depth and is independent of the effects of surface waves and strong currents. Therefore it is possible to use a method of static equilibrium to calculate the characteristics and to obtain satisfactory approximation. In order

to ensure normal operation of the measuring instruments and the acoustic release and to obtain expected data, it is necessary to keep the taut subsurface mooring system maintaining a desired attitude (the tilt angle from the vertical for the current meters and the acoustic release should not exceed  $15^{\circ}$ ). Under the above mentioned condition the tangential drag coefficient is much smaller than the normal one, therefore the force applied to the system due to the current is chiefly normal.<sup>(3)</sup>

To simplify the calculation it is also assumed that the current speed decreases linearly with depth, and the current is at the same two-dimensional plane as the buoy system. Assume that the current is parallel to the horizontal plane. The two-dimensional plane is expressed as a Cartesian coordinate where abscissa  $X$  is the horizontal and ordinate  $Y$  is the vertical. A downward direction of  $Y$  is considered as positive. The elastic and structural elongation of all components on the system are negligible. The elongation of the steel wire rope and nylon rope is taken into account when they are being cut for preparing the mooring line. It is also assumed that the buoy system does not transfer moments.

## CALCULATION METHOD

### 1. Mathematic model of the current speed $V$

To calculate the statics of the buoy system is in the final analysis to calculate the tension and the fluid drag of the system. Current is the predominant factor that affects the statics of the system, especially the tilt angle. That is why building a mathematic model of the current speed is put as the first item of calculation.

What we should do is to determine the speed function, i.e., the variation of



current speed with depth and to determine the calculation depth for the current with averaged speed in a thin layer, when the variable current layer is divided into many thin layers of uniform current. It is appropriate to use a linear function to describe the variation of current speed in certain depth. Then current speed  $V$  can be expressed as

$$V = Ky + b \quad (1)$$

where  $y$  -- depth

$k$  -- proportionality coefficient

$b$  -- constant

Suppose current speed at sea surface is  $V_0 = 2$  knots, current speed at the depth of 1000m is  $V_{1000} = 0.5$  knot, then when the current speed decreases linearly with depth the equation of current speed is

$$V = -0.0007716y + 1.0288 \text{ m/s}$$

where  $y$  is in meters.

In practical calculation the middle point of each layer is taken as the calculation depth for that layer. The thickness of layers ( $\Delta y$ ) can be determined according to the need of the calculation. Thus the averaged current speed in each layer  $\bar{V}$  can be calculated. For a component of given shape, weight and length,  $\Delta s$ , situated between points  $i$  and  $i+1$  (see Fig.2), the calculation depth for the current with averaged speed  $\bar{V}$  in relevant speed layer can be calculated by the following equation:

$$y_i = \sum_1^{i-1} \Delta y + \frac{1}{2} \Delta s \cdot \sin \phi_i \quad (2)$$

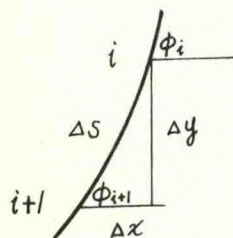


Fig.2 Calculation depth of current speed for steel wire rope

## 2. Calculation of the statics of subsurface buoy

The subsurface buoy is a major component

which provides a positive buoyancy for the whole system. Calculating its drag and tension provides an initial tension and tilt angle for calculating the static parameters of other components. The drag, tension and tilt angle from the horizontal of a sphere buoy (see Fig.3) are respectively given by

$$R_1 = \frac{1}{2} C_B \cdot \rho \pi r_B^2 \cdot V^2 \quad (3)$$

$$T_1 = (T_{1,y}^2 + T_{1,x}^2)^{\frac{1}{2}} \quad (4)$$

$$\phi_1 = \tan^{-1} \frac{T_{1,y}}{T_{1,x}} \quad (5)$$

where  $C_B$  -- drag coefficient of the buoy

$r_B$  -- radius of the buoy

$\rho$  -- density of sea water

$T_{1,y}$  -- net buoyancy of the buoy

$T_{1,x}$  -- drag of the buoy,  $T_{1,x} = R_1$

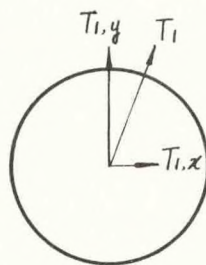


Fig.3. Force applied to the buoy

## 3. Calculation of the statics of the chain, shackle assemblies, swivel assemblies and chain-glass ball assemblies

Compared with the whole system, the above mentioned components are relatively small in dimension and large in quantity. To calculate their statics it is necessary to calculate the fluid drag. As hydromechanics shows, drag of a body of certain shape depends on its drag coefficient under certain condition when its flowward area is known. In the mean time drag coefficient depends on the angle of the body with current direction, so it is difficult to determine the drag coefficient of a body at any angle with current. As we have mentioned before, the taut subsurface moored system does not tolerate a significant tilt from the vertical, a slightly tilt system can be simply



regarded as a vertical system and the current thus will affect the components vertically. After such a presumption, drag can be calculated directly by the normal drag coefficient and can be considered as an one-variable function of current speed. Thus we can determinate the equation for calculating the drag of a component of certain shape. For example, the drag of a section of chain of weight in water per unit length (see Fig.4 )Pis

$$R_c = C_c \cdot \rho \cdot d \cdot \bar{V}^2 \cdot \Delta S = K \bar{V}^2 \quad (6)$$

where  $C_c$  -- normal drag coefficient of the chain

$\bar{V}$  -- averaged current speed

$\Delta S$  -- length of the section

$d$  -- diameter of the chain

$K$  --  $C_c \cdot \rho \cdot d \cdot \Delta S$

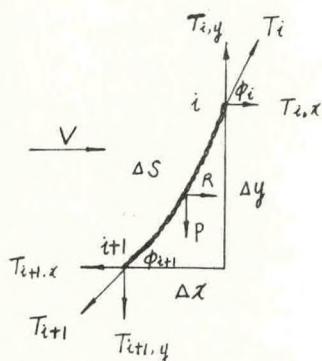


Fig. 4 .  
Force applied to the chain

As it should be, there are other methods for calculating the drag, for example, method using the normal drag or method using the projection of the normal drag on the X direction. However it is appropriate to use the simplified method as mentioned above since the drags  $R$  of those components are relatively small compared with tension on them and they affect the statics of the system slightly.

The tension and the tilt angle from the horizontal of a section of chain at the point of  $i+1$  can be calculated by the following equations:

$$T_{i+1} = (T_{i+1,y}^2 + T_{i+1,x}^2)^{\frac{1}{2}} \quad (7)$$

$$T_{i+1,y} = T_{i,y} - P \cdot \Delta S \quad (8)$$

$$T_{i+1,x} = T_{i,x} + R_c \quad (9)$$

$$\phi_{i+1} = \tan^{-1} \frac{T_{i+1,y}}{T_{i+1,x}} \quad (10)$$

$$\Delta y = \Delta S \cdot \sin \phi_{i+1} \quad (11)$$

$$\Delta x = \Delta S \cdot \cos \phi_{i+1} \quad (12)$$

The calculation methods for the shackle assembly and swivel assembly are the same as those for the chain.

It should be noted that the statics of the chain-glass ball assembly is also calculated by the same method as that for the chain, shackle assembly and swivel assembly. It is because the chain with glass balls can be considered approximately as a straight line since it is tautened by the buoyancy of the buoy. On the other hand, when the effect of the chain-glass ball assembly on the statics of the whole system is being considered, it is sufficient to take into account of only the resultants of buoyancies and drags of the chain and glass balls calculated respectively. The drag of the chain-glass ball assembly  $R$  can be calculated by a uniform equation:

$$R = P \cdot \bar{V}^2 \cdot \left( \frac{1}{2} C_g \cdot N \pi r_g^2 + C_c \cdot d \cdot \Delta S \right) \quad (13)$$

where  $C_g$  -- drag coefficient of the glass ball

$r_g$  -- radius of the glass ball

$N$  -- number of the glass balls

$C_c$  -- normal drag coefficient of the chain

$d$  -- diameter of the chain

$\Delta S$  -- length of the chain

Other parameters of the chain-glass ball assembly can be calculated by equations (7) -- (12).

4. Calculation of the statics of the current meters and the acoustic release  
The tension, tilt angle and other parameters of the current meters and the acoustic release can also be calculated by equations



(6)---(13). It should be emphasized that the tilt angle at the upper end of the instrument is different from that at the lower end after the instrument has been attached to the mooring system. It is shown in Fig.5 that the tilt angle of the instrument is expressed as the angle included between its central axis and the horizontal (abscissa X ).

$$\phi = \tan^{-1} \frac{T_{i,y} - \frac{P}{2}}{T_{i,x} + \frac{R}{2}} \quad (14)$$

where  $T_{i,y}$ ,  $T_{i,x}$  -- vertical and horizontal tension at the upper end of the instrument respectively

$P$  -- weight in water of current meter or release

$R$  -- drag of current meter or release  
The tilt angle can also be calculated by equation (15), since the difference between the tilt angles at upper and lower ends  $\phi_i$ ,  $\phi_{i+1}$  is generally not notable.

$$\phi = \frac{\phi_i + \phi_{i+1}}{2} \quad (15)$$

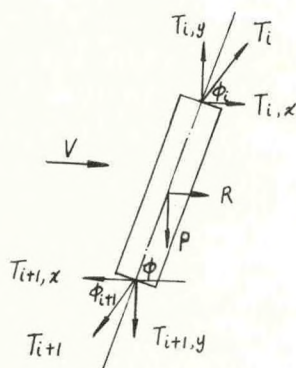


Fig.5. Tilt angle of the current meter or acoustic release

## 5. Calculation of statics of steel wire ropes

Steel wire ropes in plastic jackets are the longest component in the buoy system. Their static characteristics have a great influence on the statics of other components of the system. It is common knowledge that the

equations of static equilibrium for a section of steel wire rope of diameter,  $d$ , and length,  $ds$ , ( see Fig. 6) is given by<sup>(1)</sup>

$$T d\phi = (D + P \cos \phi) ds \quad (16)$$

$$dT = (P \sin \phi - F) ds \quad (17)$$

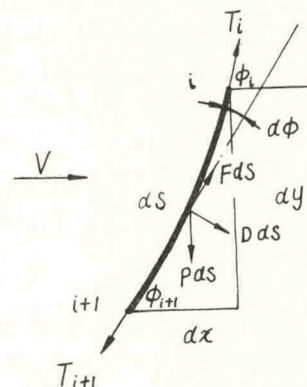


Fig.6. Force applied to element  $ds$  of steel wire rope

$T_i$  --tension of point  $i$

$T_{i+1}$  --tension of point  $i+1$

$\phi_i$  --tilt angle at point  $i$

$\phi_{i+1}$  --tilt angle at point  $i+1$

$P$  --weight in water per unit of length of steel wire rope

$D$  --normal drag per unit of length of steel wire rope

$F$  --tangential drag per unit of length of steel wire rope

$V$  --current speed

$dx, dy$  --projections of  $ds$  on axes  $X$  and  $Y$

If tangential component of drag  $F$  is neglected, an analytical equation for calculating the tension of steel wire rope at point  $i+1$  can be deduced as

$$T_{i+1} = T_i \exp \frac{P}{R} \cdot \frac{-2}{\sqrt{(-\frac{P}{R})^2 + 4}} \left( \tanh^{-1} \frac{2 \cos \phi_{i+1} - \frac{P}{R}}{\sqrt{(\frac{P}{R})^2 + 4}} - \tanh^{-1} \frac{2 \cos \phi_i - \frac{P}{R}}{\sqrt{(-\frac{P}{R})^2 + 4}} \right) \quad (18)$$

where  $R = \frac{1}{2} C_{DN} \cdot \rho \cdot d \cdot V^2$ , the drag per unit of length of steel wire rope when the rope is perpendicular to the current;  $C_{DN}$  -- normal drag coefficient of the rope.

It is obvious that it is very complicated to calculate the tension of the steel wire



rope using equation (18). Neglecting the tangential component of drag, we can obtain an equation from (17):

$$dT = p \cdot \sin \phi \cdot ds = p \cdot dy \quad (19)$$

Thus

$$\begin{aligned} T_{i+1} &= T_i - p \cdot \Delta y \\ &= T_i - p \cdot \sin \phi_{i+1} \cdot \Delta S \end{aligned} \quad (20)$$

That means the tension of steel wire rope is absolutely independent of current speed after tangential component of drag has been neglected and we can simply use equation (20) to calculate the tension of the steel wire rope. By the way, equation (20) is one of the formulas in the Catenary method for tension calculation.<sup>(2)</sup>

It is necessary to use different methods for calculating the tilt angle  $\phi_{i+1}$  of the steel wire rope depending on its length and diameter and the current magnitude. To calculate the static parameters of a short steel wire rope it is possible to use equations (6) -- (12) as those for the chain because the drag on the rope is much smaller than the tension on it. If the rope is long and thick or the current is strong, then

$$\Delta \phi = \frac{180^\circ}{\pi} \cdot \frac{R \sin^2 \phi_i + p \cos \phi_i}{T_i} \cdot \Delta S \quad (21)$$

$$\phi_{i+1} = \phi_i - \Delta \phi \quad (22)$$

are used. When the rope is thin and the current is weak, we can simplify the equations as

$$T_{i+1,x} = \sum_i T_{i,x} + R \cdot \Delta S_{i,i+1} \quad (23)$$

$$\phi_{i+1} = \cos^{-1} \frac{T_{i+1,x}}{T_{i+1}} \quad (24)$$

In a large range, the simplified equation for the tilt angle yields a large error. For instance, a comparison has been made for simple subsurface moored buoy systems of 1000m depth with ropes of different diameters and different current speeds ( see

Fig.7 ) using equations (21), (22) and (23), (24) respectively.

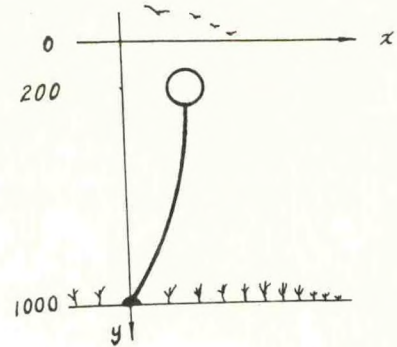


Fig.7. Simplified subsurface moored buoy system

Suppose that the surface current speed is  $V_0 = 2$  knots, at the depth of 1000m near the bottom the speed is  $V_{1000} = 0.5$  knot. The subsurface buoy of diameter  $r = 0.68$ m is submerged at the depth of 200m and provides net buoyancy of 840kg. For a steel wire rope of diameter,  $d = 12$ mm, and weight in water per unit of length, 0.26 kg/m, the maximum error of tilt angle calculated by two equations is  $\Delta \phi_{max} = 2^\circ$ . For another steel wire rope of diameter,  $d = 7$ mm, and weight in water per unit of length, 0.11 kg/m, the maximum error is  $\Delta \phi_{max} = 0.34^\circ$ . However, if the current speed increases, for example,  $V = 2$  knots within the depth range of 1000m, the calculation error of the tilt angle is considerable even the rope is thin ( $d = 7$ mm). It may reach  $\Delta \phi_{max} = 4.75^\circ$ . Therefore it is necessary for a designer to pay attention to the condition of using the simplified equations, especially when a strict restriction is laid on the tilt angle of the system.

#### 6. Calculation of static parameters of a nylon rope

A nylon rope of length, 20m, connecting the acoustic release and the anchor is included to reduce and absorb the momentary energy of impact on the system. Since the nylon



rope can be considered as a rope of neutral buoyancy with uniform tension at any point, its static parameters can thus be calculated by (see Fig.8 ):

$$T_{i+1} = T_i \quad (25)$$

$$T_{i+1,x} = T_{i,x} + \frac{1}{2} C_n \rho \cdot d_n \cdot \bar{V}^2 \quad (26)$$

$$\phi_{i+1} = \cos^{-1} \frac{T_{i+1,x}}{T_{i+1}} \quad (27)$$

$$T_{i+1,y} = T_{i+1} \cdot \sin \phi_{i+1} \quad (28)$$

$$(\text{or } T_{i+1,y} = (T_{i+1}^2 - T_{i+1,x}^2)^{\frac{1}{2}})$$

$$\Delta y = \Delta S \cdot \sin \phi_{i+1}$$

$$\Delta x = \Delta S \cdot \cos \phi_{i+1}$$

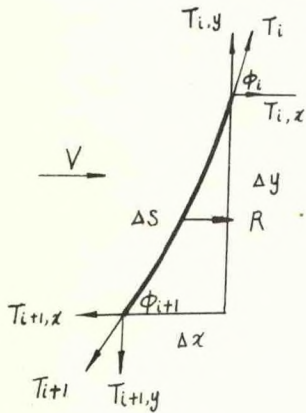


Fig.8. Force applied to the nylon rope

#### 7. Calculation of the necessary weight of the deadweight anchor

The weight of anchor in water  $P_w$  can be determined only after the static parameters of all components installed above the anchor have been calculated. Accumulating respectively the vertical and horizontal tension  $T_y$  and  $T_x$  of all components and neglecting the slope of the sea bottom,  $P_w$  is given by

$$P_w = \sum T_y + \frac{\sum T_x}{\mu} \quad (29)$$

where  $\mu$  is the friction factor between the anchor and sea bottom.

If the anchor is made of steel, the weight of anchor in air  $P_a$  is given by

$$P_a = \frac{P_w}{0.87} \quad (30)$$

The tilt angle  $\phi_m$  of the mooring line at

the anchor and the depth  $y$  where the anchor located can be calculated by

$$\phi_m = \tan^{-1} \frac{\sum T_y}{\sum T_x} \quad (31)$$

$$y = \sum \Delta y \quad (32)$$

#### CONCLUSION

Methods for the calculation of the statics of all components on the single point taut subsurface moored buoy system have been introduced. Those static parameters which can not meet the technical requirements (for instance, tilt angle or depth) can be corrected by adjusting the length of the steel wire rope or the number of glass balls. Calculation and adjustment should not be stopped until the technical requirements have been met.

The author has designed a subsurface moored buoy system of 1000m depth using the above mentioned methods. The results are satisfactory.

#### REFERENCE

- 1, H.O.Berteaux "Buoy Engineering" John Wiley & Sons, Inc. 1976
- 2, G.N.Ivanov-Frantskevich "Linearized Differential Equations of Static Equilibrium of A Catenary Line" "Oceanology" Vol.2, 1979
- 3, Chen Jiaqing, Zhang Nianfang, Yuan Yizhi "Calculation of the Statics of the Catenary Line in Uniform Current" 1978
- 4, W.H.Bell "Static Analysis of Single-point Moorings" 1977







\*1983 SYMPOSIUM ON BUOY TECHNOLOGY\*

April 27 - 29, 1983  
New Orleans, Louisiana

PARTICIPANTS LIST

\*\*\*\*\*

ADAMO, Louis C. Louis C. Adamo, Inc. 236 N. Acacia Avenue Solana Beach, CA 92075	BALLARD, Ronald Hq. Armament Div./Y1 Eglin AFB, FL 32542	BOND, Charles Computer Sciences Corp. Building 1100 NSTL, MS 39529
AINSLIE, A. R. Marex Cowes, Isle of Wight ENGLAND PO317AW	BANCHERO, Louis A. NORDA Building 1105 NSTL, MS 39529	BRADLEY, Albert Woods Hole Oceanographic Inst. Smith 201 Woods Hole, MA 02543
ALLEN, Alan Geophysical Service, Inc. P.O. Box 225621, MS 3977 Dallas, TX 75265	BARNES, Miles J. NAVOCEANO Building 8100 NSTL, MS 39529	BRAINARD, Edward C. Endeco, Inc. 312 Delano Road Marion, MA 02738
ALLEN, Robert G. Computer Sciences Corp. Building 2204 NSTL, MS 39529	BARRICK, Donald Ocean Surface Research 1131 Cranbrook Court Boulder, CO 80303	BRIGGS, Thomas H. U.S. Coast Guard Research and Development Center Shannock Hill Road Caroline, RI 02812
ALLENSWORTH, Ton Ferranti O.R.E., Inc. P.O. Box 709 Falmouth, MA 02541	BEACHT, William NOAA Data Buoy Center Building 1100 NSTL, MS 39529	BRISTOL, Richard G. Radar Devices, Inc. 4013 N. Ocean Dr., #303 Lauderdale By The Sea, FL 33308
ANDERSON, Iain Commander Third Coast Guard Dist. Bldg: 125, Rm. 317 Governors Island, NY 10004	BEDARD, Philip University of Miami 4600 Rickenbacker Cswy. Miami, FL 33149	BRODIE, Byron Environment Canada 301 Tulip Crescent Orleans, Ontario CANADA K1E 2A9
ANDERSON, John O. Polar Research Lab 123 Santa Barbara St. Santa Barbara, CA 93101	BELCHER, Michael Transport Canada, Canadian Coast Guard Place De Ville A-6 Ottawa, Ontario CANADA K1A 0N7	BROWITT, Chris Institute of Geological Sciences Murchison House Westmains Road Edinburgh EH9 3LA UNITED KINGDOM
ASHWORTH, Charles Cubic Corp. 9233 Balboa Ave. San Diego, CA 92123	BERGIN, Mark NORDA Code 331 NSTL, MS 39529	BROWN, Andrew Computer Sciences Corp. Building 2204 NSTL, MS 39529
BAARDA, J. P. Ministry of Transport and Public Works Director of Shipping and Maritime Affairs PB 5817 2280 HV Rijswijk THE NETHERLANDS	BERTEAUX, H. O. Woods Hole Oceanographic Inst. Woods Hole, MA 02543	BROWN, Walter P. Polar Research Lab 123 Santa Barbara St. Santa Barbara, CA 93101
BAER, Ledolph NOAA/NOS 1010 Executive Blvd. Rockville, MD 20852	BLOUCH, Pierre Direction De La Meteorologie C.O.B. EERM/CMM B.P. 337 F29273 Brest Cedex FRANCE	BURDETTE, Ernest L. Triton Systems, Inc. 109 E. Scenic Drive Pass Christian, MS 39571



# Participants List

Page 2

\*\*\*\*\*

CANADA, Raymond  
NOAA Data Buoy Center  
Building 1100  
NSTL, MS 39529

CAR, Martial  
NAVOCEANO  
Building 1002  
NSTL, MS 39529

CASAGRANDE, Chris  
General Oceanics  
1295 NW 163rd St.  
Miami, FL 33169

CASE, B. F.  
Computer Sciences Corp.  
Building 3203  
NSTL, MS 39529

CHANG, Ming-Houng  
Computer Sciences Corp.  
Building 2204  
NSTL, MS 39529

CHHABRA, Narender  
Charles Stark Draper Lab  
355 Technology Square  
Cambridge, MA 02139

CHRISTENSEN, Robert  
NAVOCEANO  
Building 1002  
NSTL, MS 39529

CIESLUK, Al  
Woods Hole Oceanographic  
Inst.  
Smith Building  
Woods Hole, MA 02543

CLARK, Larry  
National Science Foundation  
Oceanographic Facilities  
Support  
Washington, DC 20550

CLAUSNER, Jim  
Coastal Engineering Research  
Cntr.  
Waterways Experiment Station  
P.O. Box 631  
Vicksburg, MS 39180

CLAY, Peter  
Woods Hole Oceanographic Inst.  
Woods Hole, MA 02543

CLAYTON, Larry  
Computer Sciences Corp.  
Building 2204  
NSTL, MS 39529

COCHRANE, Douglas A.  
Cochrane Subsea Acoustics, Inc.  
147 Industrial Parkway  
Lafayette, LA 70508

COLBURN, Ted  
U.S. Coast Guard  
USCGC Storis Cogard Suprtcew  
Kodiak, AK 99619

COOLIDGE, Hank  
Computer Sciences Corp.  
Building 2204  
NSTL, MS 39529

COUGHLIN, Tom  
Preformed Marine, Inc.  
3644 Westchase Dr.  
Houston, TX 77084

CRANE, Alvin  
The Rochester Corp.  
P.O. Box 312  
Culpeper, VA 22701

CRESWELL, George R.  
Csiro Oceanography  
Hobart Tas  
AUSTRALIA

DAHLEN, John  
Charles Stark Draper Lab  
355 Technology Square  
Cambridge, MA 02139

DAMAN, Hendrik  
Computer Sciences Corp.  
Building 1100  
NSTL, MS 39529

D'AMICO, Angela  
ODSI Defense Systems, Inc.  
6110 Executive Blvd.  
Rockville, MD 20852

DAUBIN, Scott  
Daubin Systems Corp.  
104 Crandon, #315  
Key Biscayne, FL 33149

DAVIS, Don  
E G & G Sea-Link Systems  
2818 Towerview Road  
Herndon, VA 22071

DAVIS, Douglas  
NOAA/NWS  
819 Taylor Street  
Fort Worth, TX 76102

DEXTER, Dennis  
Computer Sciences Corp.  
Building 2204  
NSTL, MS 39529

DHEJNE, Rolf  
Protrade  
P.O. Box 6273  
S-40062 Gothenburg  
SWEDEN

DIAL, K. G.  
NORDA  
Code 521  
NSTL, MS 39529

DREVER, R.  
Applied Physics Lab  
Univ. of Washington  
1013 NE 40th  
Seattle, WA 98105

DUFILHO, Hal  
NAVOCEANO  
Code 6212  
NSTL, MS 39522

DUNN, George  
Computer Sciences Corp.  
Building 3203  
NSTL, MS 39529

EARLE, Marshall  
Marine Environments Corp.  
10629 Crestwood Dr.  
Manassas, VA 22110

ELKINS, J. H.  
NORDA  
Code 350  
NSTL, MS 39529

EMERY, Bill  
Univ. of British Columbia  
Oceanography Dept.  
Vancouver, BC  
CANADA V6T 1W5

ERICHSEN, Robert  
NOAA Data Buoy Center  
Building 1100  
NSTL, MS 39529



Participants List  
Page 3

\*\*\*\*\*

FENNER, Don  
NORDA  
Code 501  
NSTL, MS 39529

FOLEY, Edward  
David Taylor Naval Ship  
Research & Development Cntr.  
Bethesda, MD 20084

FRITTS, Roland  
Magnavox Electronic  
Systems Co.  
1010 Production Rd.  
Fort Wayne, IN 46808

FRYE, Dan  
Ferranti O.R.E., Inc.  
P.O. Box 709  
Falmouth Heights Road  
Falmouth, MA 02541

GAULD, Harry  
Cubic Corp.  
9233 Balboa  
San Diego, CA 92123

GAUTIER, Walt  
Computer Sciences Corp.  
Building 3203  
NSTL, MS 39529

GIES, Donald  
Gies Industries  
1112 N. Overhill Court  
Wilmington, DE 19810

GREEN, A. W.  
NORDA  
Building 1105  
NSTL, MS 39529

GULARDE, Ronald  
VSE  
2550 Huntington Ave.  
Alexandria, VA 22303

GUPTILL, Fred  
Hermes Electronics Ltd.  
40 Atlantic St.  
Dartmouth, Nova Scotia  
CANADA B2Y 4A1

HAAS, Frank J.  
Cordage Consultants, Inc.  
P.O. Box 321  
Skaneateles, NY 13152

HAMILTON, Glenn  
NOAA Data Buoy Center  
Building 1100  
NSTL, MS 39529

HAMILTON, Jim  
Dept. of Fisheries and Oceans  
Bedford Inst. of Oceanography  
P.O. Box 1006  
Dartmouth, Nova Scotia  
CANADA B2Y 4A2

HANNON, James  
Sippican Ocean Systems, Inc.  
7 Barnabas Road  
Marion, MA 02738

HECKER, Stanley  
MS/AL Sea Grant Consortium  
Caylor Building  
Ocean Springs, MS 39564

HEINMILLER, Robert  
Omnet, Inc.  
70 Tonawanda Street  
Boston, MA 02124

HILDER, Fred  
NORDA  
Building 1105  
NSTL, MS 39529

HILL, Winfield  
Sea Data Corp.  
One Bridge Street  
Newton, MA 02158

HOLLMAN, Rudolph  
NORDA  
Building 1100  
NSTL, MS 39529

HOLMES, John  
Computer Sciences Corp.  
NSTL, MS 39529

HORN, Harald  
IKU  
P.O. Box 1883  
Trondheim  
NORWAY 7001

HOWE, Don  
Magnavox Government &  
Industrial Electronics  
1313 Production Road  
Fort Wayne, IN 46808

HSU, Yuan-Huang L.  
Computer Sciences Corp.  
Building 2204  
NSTL, MS 39529

HUTCHINSON, William  
Computer Sciences Corp.  
Building 3203  
NSTL, MS 39529

JACKSON, Robert L.  
Sea Operations Engr.  
Western Electric Co., Inc.  
P.O. Box 20046  
Greensboro, NC 27420

JOHNSON, Charles L.  
The Johns Hopkins Univ.  
Johns Hopkins Road  
Laurel, MD 20707

KELLEY, E. J.  
U. S. Navy  
1501 Hollindale Drive  
Alexandria, VA 22306

KERUT, Edmund  
NOAA Data Buoy Center  
Building 1100  
NSTL, MS 39529

KIES, Phillip  
CG DET/NOAA Data Buoy Cntr.  
NSTL, MS 39529

KIRK, Bob  
NASA-Goddard  
GSFC-912  
Greenbelt, MD 20771

KLAUS, Vádislav  
Direction De La  
Météorologie  
CNRM, Avenue Eisenhower  
Toulouse  
FRANCE 31057

KOZAK, Ronald  
NOAA Data Buoy Center  
Building 1100  
NSTL, MS 39529

KOZIARA, Michael  
National Weather Serv.,  
NOAA  
1120 Old Spanish Trail  
Slidell, LA 70458



# Participants List

Page 4

\*\*\*\*\*

KUTMAN, Art  
MSE Engineering Systems  
265 Canarctic Drive  
Downsview, Ontario  
CANADA M32 2N7

LANZA, Marco  
Sea Data Corp.  
One Bridge Street  
Newton, MA 02158

LARGE, W. G.  
National Center for  
Atmospheric Research  
P.O. Box 3000  
Boulder, CO 80307

LAU, Joseph C.  
Computer Sciences Corp.  
Building 1100 3/F  
NSTL, MS 39529

LAZANOFF, Sheldon  
Science Applications, Inc.  
205 Montecito Ave.  
Monterey, CA 93908

LEE, Jieh  
Computer Sciences Corp.  
Building 1100  
NSTL, MS 39529

LeMAISTRE, P. Andre  
Yale Cordage, Inc.  
Old Sparhawk Mill  
Yarmouth, ME 04096

Le ROUX, Piet  
South African Weather Bureau  
Private Bag X97  
Pretoria 0001  
SOUTH AFRICA

LEVIN, Stan  
Blake Wire and Cable Corp.  
19505 Pacific Gateway Dr.  
Torrance, CA 90502

LEWIS, James K.  
Science Applications, Inc.  
4348 Carter Creek Pkwy.  
Suite 101  
Bryan, TX 77801

LUCKIANOW, Brian  
Dept. of Energy  
P.O.S.S.I.  
850 S. Clearview Pkwy.  
New Orleans, LA 70123

MAHAR, Dennis  
NOAA Data Buoy Center  
Building 1100  
NSTL, MS 39529

MARSHALL, Frank  
Naval Air Development Center  
P.O. Box 111  
Penns Park, PA 18943

MARTIN, M. S.  
Marex  
Cowes  
Isle of Wight  
ENGLAND PO317AW

MASTERSON, John  
National Center for  
Atmospheric Research  
P.O. Box 3000  
Boulder, CO 80307

MAY, Douglas  
Computer Sciences Corp.  
Building 1100  
NSTL, MS 39529

MAY, Jenny T.  
Engineering Service Assoc., Inc.  
12 Heritage Lane, Apt. 46  
New Orleans, LA 70114

MELLINGER, Ed  
Woods Hole Oceanographic Inst.  
Woods Hole, MA 02543

McCALL, Jerry  
NOAA Data Buoy Center  
Building 1100  
NSTL, MS 39529

McCLURE, Alan  
Alan C. McClure Assoc., Inc.  
2600 S. Gessna  
Suite 504  
Houston, TX 77063

McWILLIAMS, James  
National Center for  
Atmospheric Research  
P.O. Box 3000  
Boulder, CO 80307

MICHELENA, Eduardo  
NOAA Data Buoy Center  
Building 1100  
NSTL, MS 39529

MOOERS, Christopher  
Dept. of Oceanography  
Naval Postgraduate  
School  
Monterey, CA 93940

MOORE, D. J.  
Computer Sciences Corp.  
Building 1100  
NSTL, MS 39529

MULLER, F. P. J.  
Univ. of Stellenbosch  
Dept. of Civil Engr.  
Stellenbosch 7600  
REPUBLIC OF SOUTH AFRICA

MURPHY, Donald  
U.S.C.G. Research &  
Development Center  
Avery Point  
Groton, CT 06340

MURPHY, J. E.  
Univ. of New Orleans  
New Orleans, LA 70148

NATH, John  
Oregon State Univ.  
Dept. of Civil Engr.  
Corvallis, OR 97331

NEELY, Patrick  
Computer Sciences Corp.  
Building 1100  
NSTL, MS 39529

NIILER, Peter  
Scripps Inst. of  
Oceanography  
A-030  
La Jolla, CA 92093

OVERKIRCH, Joe  
NOAA Data Buoy Center  
Building 1100  
NSTL, MS 39529

O'BOYLE, Thomas  
FPO-1  
CHESNAVFACENGCOM  
Bldg. 200  
Washington, DC 20374

OLIVER, Sidney  
Research Triangle Inst.  
137 Markham Dr.  
Long Beach, MS 39560



# Participants List

Page 5

\*\*\*\*\*

ORR, Charles  
NAVOCEANO  
Building 8100  
NSTL, MS 39529

OWEN, Wadsworth  
Univ. of Delaware  
700 Pilottown Road  
Lewes, DE 19958

PALMER, Robert S.  
NOAA Data Buoy Center  
Building 1100  
NSTL, MS 39529

PARTRIDGE, Ray  
NOAA Data Buoy Center  
Building 1100  
NSTL, MS 39529

PATTERSON, Steven  
Dept. of Oceanography  
Texas A & M  
College Station, TX 77843

PAYNE, Richard  
Woods Hole Oceanographic Inst.  
Woods Hole, MA 02543

PERKINS, Henry  
NORDA  
Building 1105  
NSTL, MS 39529

PETRIE, George  
Hoffman Maritime Cons., Inc.  
9 Glen Head Road  
Glen Head, NY 11545

PETTIFER, Richard  
Meteorological Office/Cost 43  
Beaufort Park, Easthampstead  
Wokingham Berks  
UNITED KINGDOM

PICKETT, Robert Lee  
Great Lakes Research Lab  
2300 Washtenaw Avenue  
Ann Arbor, MI 48105

PIERSON, Cory  
Buoy Technology Inc.  
7 S. State Street  
Concord, NH 03301

PILLSBURY, Dale  
Oregon State Univ.  
School of Oceanography  
Corvallis, OR 97331

PRINE, George  
Computer Sciences Corp.  
Building 1100  
NSTL, MS 39529

QUAYLE, Robert  
National Climatic  
Data Center  
Asheville, NC 28801

RAFFA, Stan  
NAVOCEANO  
Building 8100  
NSTL, MS 39529

RAINNIE, William  
NOAA Data Buoy Center  
Building 1100  
NSTL, MS 39529

RANKIN, David  
Hermes Electronics, Ltd.  
P.O. Box 1005  
Dartmouth, Nova Scotia  
CANADA B2Y 4A1

REH, F. John  
Oceanographic Services, Inc.  
25 Castician Drive  
Goleta, CA 93117

REMOND, Frank  
Computer Sciences Corp.  
NSTL, MS 39529

REYNOLDS, Michael  
NOAA-PMEL  
3711 15th Ave., NE  
Seattle, WA 98105

RICHARDS, David  
Rope Services  
4910 Wright Road  
Suite 190  
Stafford, TX 77477

RIENECKER, Michele  
Naval Postgraduate School  
Dept. of Oceanography  
Monterey, CA 93940

ROSSO, Raymond  
Service Argos  
18th Ave., Eduard Belin  
31055 Toulouse Cedex  
FRANCE 31055

ROY, F. E.  
Environment Canada  
National Water Research  
Inst.  
P.O. Box 5050  
867 Lakeshore Road  
Burlington, Ontario  
CANADA L7R 4A6

SAUNDERS, Kim D.  
NORDA  
Code 331  
NSTL, MS 39529

SCALLY, Douglas  
NOAA Data Buoy Center  
Building 1100  
NSTL, MS 39529

SEILEY, John  
Computer Sciences Corp.  
6565 Arlington Blvd.  
Falls Church, VA 22046

SERSTAD, Bill  
Magnavox  
1313 Production Road  
Fort Wayne, IN 46808

SHAMP, Richard  
Marine Technology Society  
1500 Mass. Ave.  
Washington, DC 20005

SHIELDS, David  
Naval Civil Engineering  
Lab  
1755 Coachman Drive  
Camarillo, CA 93010

SMALL, Cyrus  
Computer Sciences Corp.  
Building 3203  
NSTL, MS 39529

SMITH, Paul Ferris  
Ferranti O.R.E., Inc.  
Falmouth Heights Road  
Falmouth, MA 02541

SMOKE, Clinton H.  
CG/DET/NOAA Data Buoy Cntr.  
NSTL, MS 39529

STEELE, Kenneth  
NOAA Data Buoy Center  
Building 1100  
NSTL, MS 39529



Participants List

Page 6

\*\*\*\*\*

STRAHLE, William  
U.S. Geological Survey  
Quissett Campus  
Woods Hole, MA 02543

STROEMME, Jan A.  
Bergen Ocean Data  
Fantoft Veggen 38  
5036 Fantoft  
Bergen  
NORWAY

STUART, J. C.  
Western Electric Co.  
P.O. Box 20046  
Greensboro, NC 27420

STYER, Fred  
Cochrane Acoustics  
147 Industrial Parkway  
Lafayette, LA 70508

SU, Ming-Yang  
NORDA  
Building 1105  
NSTL, MS 39529

SUMMY, Alan  
Commander  
Third Coast Guard District  
Building 125, Room 317  
Governors Island, NY 10004

SWENSON, Rick  
NAVOCEANO  
Building 8100  
NSTL, MS 39529

SYMONDS, Graham  
Atlantic Oceanographic Lab  
Bedford Inst. of Oceanography  
P.O. Box 1006  
Dartmouth, Nova Scotia  
CANADA

TIMPE, Gerald  
NOAA Data Buoy Center  
Building 1100  
NSTL, MS 39529

TOWLES, Terry  
Computer Sciences Corp.  
Building 1100  
NSTL, MS 39529

VADUS, Joseph  
NOAA  
8500 Timber Hill Lane  
Potomac, MD 20854

VAN DIJK, W. C. M.  
Ministry of Transport and  
Public Works  
van Alkemadeaan 400  
Den Haag,  
THE NETHERLANDS

VERBAAN, A.  
Ministry of Transport and  
Public Works  
P.O. Box 5817  
2280 HV Rijswijk  
THE NETHERLANDS

VOCKEROTH, Bob  
Atmospheric Environment  
Service  
4905 Dufferin St.  
Downsview, Ontario  
CANADA M3H 5T4

VOOHRES, Jan  
Marine Technology Society  
1730 "M" Street NW  
Washington, DC 20036

WALDEN, Robert  
Woods Hole Oceanographic Inst.  
Woods Hole, MA 02543

WARREN, Richard  
Hq AD/YIC  
Hq. Armament Div./YI  
Eglin AFB, FL 32542

WHITE, Douglas  
MacLaren Plansearch  
Suite 1020-Cogswell Tower  
2000 Barrington Street  
Halifax, Nova Scotia  
CANADA

WILEM, Frank  
Triton Systems, Inc.  
109 E. Scenic Drive  
Pass Christian, MS 39571

WILSON, Brett  
Computer Sciences Corp.  
Building 1100  
NSTL, MS 39529

WINCHESTER, James  
NOAA  
Office of the Administrator  
Washington, DC 20230

WOOD, Emerson  
NOAA/PMEL  
7600 Sand Point Way, NE  
Seattle, WA 98115

YALE, Thomas  
Yale Cordage Inc.  
Old Sparhawk Mill  
Yarmouth, ME 04096

ZERENER, John  
Aanderaa Instruments, Inc.  
30 F. Commerce Way  
Woburn, MA 01801



3 8398 1010 6188 9



NOAA CENTRAL LIBRARY

PRADA/14

